

0

The Origin of Bioelectrochemistry: An Overview

Pierre Bianco
BIP – CNRS, Marseille, France

0.1	Electrokinetic Phenomena	5
0.2	Membrane Phenomena	6
0.3	Electron Transfer Reactions in Biological Compounds	6
0.4	Transmission of Information in Living Organisms	8
	References	8

Electrical phenomena known in antiquity were lightning, the attraction of light bodies, and the discharges delivered by the torpedo fish. No relation among these seems to have been suspected at the time. Maybe the most intriguing natural phenomenon further related to bioelectrochemistry was the production of electricity by a living organism such as a fish (not only the torpedo fish but also the gymnotus, or eel of Surinam, and the electric catfish living in the Nile waters). Nevertheless, no attempts to explain electrical phenomena were undertaken during the long period that extends from antiquity to the beginning of the modern era, that is, the seventeenth century. It is accepted that the science of electricity began in 1600 with the treatise *De Magnete* by William Gilbert. The first “electric machine” producing electricity on demand was devised by Otto von Guericke in 1672; the first “condensers” known as *Leyden jars* were constructed by Ewald Georg von Kleist and Pieter van Musschenbroeck in the middle of the eighteenth century. At that time, electricity was considered a “fluid” that flowed within living organisms like water in pipes.

The earliest observations on the chemical effects produced by electricity were reported by Beccaria (ca. 1750), who observed gas evolution on passing electric

sparks through water placed in a tube. The first experiments on the effect of electric currents on living organisms were perhaps described by Johann Georg Sulzer at the same time. Sulzer found that when a plate of lead and another of silver laid on the tongue touched one another, a “vitriolic taste” was perceived by the experimenter. Unfortunately, Sulzer did not connect the observed phenomenon with electricity. The possibility of using Leyden jars opened new ways for investigating the effects of electricity on living organisms. In 1752, Leopoldo Caldani, an Italian physiologist from Bologna, concluded from his experiments on the crural nerves of various animals that “electric matter is the most effective of stimulating agents” in living organisms. From the rapidity of the muscular responses to repetitive stimuli via the nervous system, it became generally accepted that a “nerval fluid” or “animal spirit” must exist in living organisms, rapidly identified as “animal electricity”. In October 1786, Luigi Galvani, then professor of anatomy in Bologna, gave an account about his famous experiments on the muscular contractions that convulsed frog’s legs when touched with a metallic arc, or better a composite (iron + copper or silver) arc (Fig. 1). Galvani supposed that the observed phenomena was due to the “animal electricity”, the interior and

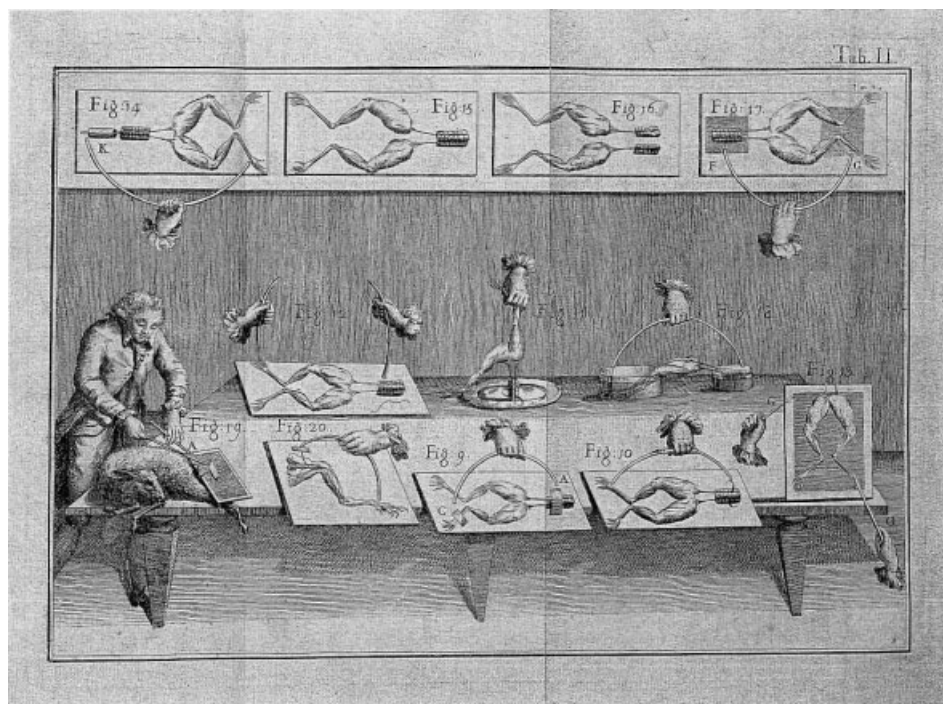


Fig. 1 The first experiments on “animal electricity” by Luigi Galvani described in *De Viribus Electricitatis in Motu Musculari Commentarius* (published in 1792).

exterior muscles of the frog’s legs forming a kind of small Leyden jar, and the nerve behaving as a conductor for the jar.

Volta, then professor of physics at the University of Pavia, first shared Galvani’s views. During 1790 to 1792, he carried out a series of careful experiments dealing with the effect of the electric discharges on the convulsion of frog’s legs, varying the nature and the combination of metals by using rather sophisticated heterogeneous metallic arcs. In 1794, he took a different stance, concluding that the “galvanism [...] is nothing but an artificial electricity set in motion by the contact of heterogeneous conductors”. In conclusion, he claimed that there was only one type of electricity. The construction of the “pile” (1799) derives, in fact, from Volta’s experiments on contact between metals.

This discovery can be regarded as the real foundation of the science of electrochemistry and, indirectly, of bioelectrochemistry, considered as an “affiliate” of electrochemistry. In reality, the controversies that have arisen from the different interpretations given by Galvani and Volta – the existence of an animal electricity and the assignment of muscular contraction to the contact potential difference between unlike metals, partly right and partly wrong, respectively – highlighted an undeniable feature, that is, that both assumptions were incomplete. Of course, there exists one type of electricity resulting from the movement of electrons but Galvani and Volta are pardonable because they were unaware of the electron concept. Nevertheless, Volta wrongly supposed that the contact of the two metals was also the

source of current, the production of which would be, as he himself said, a “perpetual motion”. A relatively satisfactory explanation was suggested by Johann Wilhelm Ritter (ca. 1800) who claimed that the contact potential difference between unlike metals could not be a source of energy: the source of energy required to contract the muscles of the frog’s legs should originate from chemical reactions providing the necessary energy.

Volta’s breakthrough stimulated a high level of research activity on the effect of the electric current. Davy spoke of the voltaic battery as “an alarm-bell to experimenters in every part of Europe”. The development of electrochemistry progressed throughout the nineteenth and twentieth centuries, thus allowing several fundamental as well as applied aspects to be investigated, leading to highly valuable discoveries and theories. Three main avenues were opened, including studies on new power supplies (development of cells and batteries), the problem of the transmission of charge through solutions, and the transfer of charge at metal–solution interfaces (Faraday’s laws). During this time, bioelectrochemistry developed more slowly, without striking discoveries compared to those that have marked the evolution of “mother” electrochemistry. It has benefited, however, from increasing knowledge in different areas covering biochemistry, membrane phenomena, electrophysiology, medical diagnosis, and so on. All these investigations have contributed to revealing of the electrochemical nature of a large variety of biological phenomena. Though it is not possible to encompass the totality of the numerous advances resulting from research in the field of bioelectrochemistry, we propose to examine the most important branches and experimental implementations gained

from the encounter between “pure” electrochemistry and biological and physiological phenomena. Progress in the understanding of biological and physiological processes using electrochemistry can be examined on the basis of two distinct sets of phenomena related to (1) the existence of potential differences at phase boundaries and (2) the electrical polarization and the electron-exchange process.

0.1

Electrokinetic Phenomena

At the end of the nineteenth century, research was undertaken on electrocapillary and electrokinetic phenomena that arise from matter in motion. Three related effects were distinguished, namely, electroosmosis, streaming potentials, and electrophoresis.

The existence of electroosmosis was confirmed experimentally shortly after the discovery of the decomposition of water by means of electric current. It is one of the earliest-known electrochemical effects. Studying the effect of electroosmosis has proven to be useful for the understanding of the metabolism of cells. For example, it was established by Blinks in the middle of the last century [1] that true electroosmosis is negligible compared to osmotic pumping in some large plant cells of fresh water and marine algae.

Streaming potentials are produced by a flow of liquid forced through a capillary system. In 1943, Miller and Dent [2] presented experimental evidence that streaming potentials are the cause of the wave portions of an electrocardiogram. Later, several experimenters attempted to correlate electrocardiogram profiles with different physiological events, such as the effect of the pulsatile flow of saline electrolytes

that can generate electrokinetic potentials remarkably similar to in vivo electrocardiograms (e.g. Findl and Kurtz, [3]).

Electrophoresis is concerned with the migration of particles under the influence of an external field. First, electrophoretic velocities were measured by the same experimental methods as those used by Hittorf (around 1853) for transport numbers. The method was remarkably developed and refined by Tiselius (1937, Nobel Prize in 1947). Since then, there have been a large number of applications in biology and medicine, in particular in the analysis of sera and the separation of amino acids and proteins. Recently, the technique was improved by coupling capillary electrophoresis to an electrochemical detector (CEEC) that can be implanted in vivo for studying microdialysis [4].

0.2

Membrane Phenomena

Membrane phenomena cover an extremely broad field. Membranes are organized structures especially designed to perform several specific functions. They act as a barrier in living organisms to separate two regions, and they must be able to control the transport of matter. Moreover, alteration in transmembrane potentials can have a profound effect on key physiological processes such as muscle contraction and neuronal activity. In 1875, Gibbs stated the thermodynamic relations that form the basis of membrane equilibria. The theory of ionic membrane equilibrium was developed later by Donnan (1911). From theoretical considerations, Donnan obtained an expression for the electric potential difference, commonly known as the membrane potential between two phases.

Results from Scatchard in 1953 [5] have indicated that ion-exchange membranes may be useful as electrodes at which there is no reduction or oxidation and no restriction to special classes of ions except size. The first ion-selective electrodes were constructed in 1936 and then largely developed in the 1960s, when Eisenman [6] established the relationship giving the electrical potential difference between two aqueous solutions separated by an ion-exchange membrane. Of particular interest for measurements in biological media was the construction of ion-selective electrodes capable of detecting calcium ions. In human serum and other biological fluids, calcium is partly bound to substances such as proteins. The detection of free calcium became possible by using a calcium-selective electrode. Afterward, other membrane electrodes were constructed (e.g. the urea electrode, by Guilbault and Montalvo, [7]).

Electric fields have been shown to influence the conformation of various natural and synthetic polynucleotides in solution. In 1958, Hill [8] calculated that high electric fields could bring about separation of the two molecule chains of nucleotides in DNA. It has even been suggested that the electric fields and their variations at biological interfaces might act as the trigger for division of genetic material in the cell prior to self-duplication. On the basis of the analogy between a cell surface–biological fluid interface and an electrode–solution interface, investigations were carried out around the 1970s using differential capacitance measurements (ac polarographic method) in conjunction with ellipsometry measurements. The dependence on applied potential of the adsorption of several biomolecules on mercury electrodes was investigated, thus giving insights into the different orientations and bindings

of biological molecules at solid–solution interfaces (1977; e.g. [9]).

0.3

Electron Transfer Reactions in Biological Compounds

Curiously, it is also from the study of capillary phenomena (developed by Lippman in 1873) that a new field of research was opened up toward the study of electron transfer reactions through the discovery of polarography by Heyrovsky in 1927 (Nobel Prize in 1959). This popular technique provided an extraordinary amount of data. To the question “What can electrochemical studies tell one about biological electron transfer and related processes?”, Dryhurst [10] replies by giving a definite set of similarities between electrochemical and biological reactions, comparing the interface electrode–solution to the interface enzyme–solution working in very similar conditions of pH, ionic strength, and temperature.

A large series of compounds of biological interest have been investigated through the second and third quarter of the last century using polarographic methods, for example, purines, pyrimidines, vitamin B₁₂ and related cobalamines, nucleic acids, pteridines, flavins and flavin nucleotides, porphyrins, cytochromes, and so on. As a practical example, the tests for cystine and proteins introduced by Brdička (1933) [11], which are of importance in clinical analysis, deserve to be mentioned. Brdička observed that catalytic activity existed not only for cystine but also for proteins containing –SH and –S–S– groups together with amino groups. These catalytic waves could be detected in solutions of cobalt(II) but were virtually absent in solutions of cobalt(III). The great merit of the catalytic

double wave detected in ammoniacal solutions containing cobalt(II) and cobalt(III) was based on the fact that the number of active groups that govern the height of the catalytic double wave differs from normal to pathological sera. Such a test has been shown to be efficient for detecting hepatitis cases and possible cancers in more than 90% of proved cases.

During the second half of the twentieth century, electroanalysis has enjoyed a renaissance because of the development of several new technologies (e.g. single and cyclic voltammetry, pulse voltammetry, etc.) resulting from an enormous exploratory effort in the theory and methodology of electrochemical techniques served by progress in electronics. Bioelectrochemistry has benefited from these new technologies that allowed other (e.g. solid) macro- and microelectrodes to be used. Microelectrodes were pioneered in the 1940s to measure oxygen concentrations inside biological tissues [12]. In 1969, Adams, a pioneer in the field of solid electrodes wrote [13]: “There is every reason to believe that the current interest in solid electrode voltammetry will continue and perhaps increase in the near future.” It was more than a vision for bioelectrochemistry where solid electrodes have been extensively used for several decades, in particular for direct observations in vivo. As an example, cyclic voltammetry at the platinum electrode has been shown to be suitable for analyses in blood serum by Koryta [14]. The measurement of the time dependence of ascorbic acid concentration in the cortex of an isolated kidney gave information about circulation within the organ (1973). Adams succeeded in probing the concentration of neurotransmitters by directly implanting microelectrodes inside the living brain of a rat [15]. Thereafter, microelectrodes were miniaturized to ultramicroelectrodes to be

used to probe chemical reactions inside even single biological cells [16].

Another major success for bioelectrochemistry was achieved in the field of redox protein electrochemistry. The first work using this approach was reported in 1965 by Griggio and Pinamonti [17]; concerning cytochrome *c*. In the 1980s, reports on different families of metalloproteins were published concomitantly by several groups [18–24], thus demonstrating that the direct electrochemistry of redox proteins could be observed provided that well-defined experimental conditions were fulfilled. A new avenue was thus opened toward the understanding of electron transfer processes throughout electron-carrier chains using the electrochemical model.

0.4

Transmission of Information in Living Organisms

This is, perhaps, the most complicated and sophisticated approach that has been tempted as a challenge for bioelectrochemistry: several reactions are involved in the overall process controlling the transmission of information in living organisms, including electron transfer, ion transport through membranes, and so on. One of the most important mechanisms consists of electrical signals transmitted after elaboration to the organs, which have to perform the required action. Various kinds of electrical conduction are involved in the overall process. Several approaches have contributed to unravel such a complicated process, for example, the work of Koryta [25], who studied a series of macrocyclic ligands with alkali metals and their properties in regard to membrane transport and phosphorylation uncoupling.

An – even shorter – overview on the development of bioelectrochemistry through its two centuries of existence illustrates well the kinds of biological and physiological problems that are being studied using electrochemical concepts and techniques. Several avenues have been opened toward the study of electron transfer processes in living organisms, the analysis of biological fluids, the control of the composition of the intracellular medium (as established by Neher and Sakmann, Nobel Prize winners in 1991), the electrochemical detection of immunological reactions, the construction of biosensors (which constitute a significant portion of the total effort), and so on. From the examination of the number of papers that have been published in the last ten years, it can be concluded that bioelectrochemistry is thriving with increasing vitality.

References

1. T. Shedlovsky, *Electrochemistry in Biology and Medicine*, John Wiley & Sons, New York, 1955.
2. J. R. Miller, R. F. Dent, *Lab. Clin. Med.* **1943**, *28*, 168.
3. E. Findl, R. J. Kurtz in *Electrochemical Studies of Biological Systems*, ACS Symposium Series (Ed.: D. T. Sawyer), American Chemical Society, Washington, DC, 1977, p. 180.
4. R. Weinberger, *Practical Capillary Electrophoresis*, Academic Press, New York, 1993.
5. G. Scatchard, *J. Am. Chem. Soc.* **1953**, *75*, 2883.
6. S. Ciani, G. Eisenman, G. Szabo, *J. Membr. Biol.* **1969**, *1*, 1.
7. G. G. Guilbault, J. Montalvo, *J. Am. Chem. Soc.* **1969**, *91*, 2164.
8. T. L. Hill, *J. Am. Chem. Soc.* **1958**, *80*, 2142.
9. H. Kinoshita, S. D. Christian, M. H. Kim et al. in *Electrochemical Studies of Biological Systems*, ACS Symposium Series (Ed.: D. T. Sawyer), American Chemical Society, Washington, DC, 1977, p. 118.
10. G. Dryhurst, *Electrochemistry of Biological Molecules*, Academic Press, New York, 1977.

11. R. Brdička, *Collect. Czech. Chem. Commun.* **1933**, 5, 148.
12. P. W. Davies, F. Brink, *Rev. Sci. Instrum.* **1942**, 13, 524.
13. R. N. Adams, *Electrochemistry at Solid Electrodes*, Marcel Dekker, New York, 1969.
14. J. Pradac, J. Koryta, *Ber. Bunsen-Ges. Phys. Chem.* **1973**, 77, 808.
15. R. N. Adams, *Prog. Neurobiol.* **1990**, 35, 297.
16. J. B. Chien, R. A. Wallingford, A. G. Ewing, *J. Neurochem.* **1990**, 54, 633.
17. L. Griggio, S. Pinamonti, *Atti dell'Istituto Veneto di Scienze, lettere ed Arti* **1965**, 124, 15.
18. P. Yeh, T. Kuwana, *Chem. Lett.* **1977**, 1145.
19. M. J. Eddowes, H. A. O. Hill, *J. Chem. Soc., Chem. Commun.* **1977**, 771.
20. K. Niki, T. Yagi, H. Inokuchi et al., *J. Electrochem. Soc.* **1977**, 124, 1889.
21. P. Bianco, J. Haladjian, *Biochim. Biophys. Acta* **1979**, 545, 86.
22. E. E. Bancroft, H. N. Blount, F. M. Hawkrige, *Biochem. Biophys. Res. Commun.* **1981**, 101, 1331.
23. I. Taniguchi, K. Toyosawa, H. Yamaguchi et al., *J. Chem. Soc., Chem. Commun.* **1982**, 1032.
24. F. A. Armstrong, H. A. O. Hill, N. J. Walton, *FEBS Lett.* **1982**, 145, 241.
25. J. Koryta, *Chem. Listy* **1973**, 67, 897.

1

Voltammetry of Proteins

Fraser A. Armstrong
Department of Chemistry, Oxford University, Oxford, UK

1.1	Introduction	13
1.2	Electrodes for Proteins	14
1.3	Voltammetric Methods	16
1.3.1	Protein Sample Contained in Solution	16
1.3.2	Protein Sample Confined to Electrode	18
1.3.3	General	19
1.4	Case Studies	19
1.4.1	Observing Active Sites	19
1.4.1.1	Iron-sulfur Clusters	19
1.4.1.2	Flavins	21
1.4.1.3	Highly Oxidizing Intermediates: Fe(IV)=O	22
1.5	Resolving Complex Reactions	23
1.5.1	Coupled and Gated Electron Transfer	23
1.5.2	Catalysis	26
1.6	Conclusion	28
	References	28

1.1 Introduction

Direct electrochemical methods for studying redox-active centers in proteins are those in which the exchange of electrons with an electrode is direct and does not involve electroactive mediators. To be useful, the interaction between the protein and the electrode should fulfill the following criteria: (1) interfacial electron transfer should be fast (reversible), which requires small reorganization energy requirements and good electronic coupling between the active site and the electrode surface; (2) the protein should not become denatured, and characteristic properties such as catalytic activity should not be impaired. Voltammetric methods offer some important advantages over potentiometry, which is the traditional method for measuring the electrochemical properties of redox cofactors in proteins.

Compared with potentiometry, voltammetric methods provide more rapid and direct measurements of redox properties, and a wide range of electrode potentials can be applied, often extending well beyond the thermodynamic limits of water (< -0.4 V and > 0.8 V vs the Standard Hydrogen Electrode (SHE), at pH 7). Active sites having very high or very low potentials may be difficult to study by

potentiometric methods, either because they are themselves very reactive in their highly oxidized or reduced states and thus decompose water, or the titrants or mediators that are used to elicit their redox chemistry also react with water. These problems can be overcome by direct electrochemical methods [1–3]. As outlined below, examples include the highly oxidizing catalytic intermediates of heme-containing peroxidases that exhibit reduction potentials higher than 0.75 V, and reduced states of certain Fe-S clusters that have reduction potentials below -0.55 V. (The term “reduction potential” defines the potential for a half-cell reaction written in the order $O + ne^- = R$, in which O and R are oxidized and reduced forms of the redox couple, respectively. Although this potential is commonly referenced against the SHE (as the other half cell), the nonstandard conditions under which biological systems are studied makes it appropriate to refer instead to a *formal* potential, denoted $E^{\circ'}$ and qualified for a particular set of conditions, where the temperature, pH, ionic strength, and specific ions present are specified.) The technical problems of measuring how reduction potentials vary over a wide temperature range, and the effects of high pressure can each be accommodated through voltammetric experiments [4]. Voltammetry can be used even if the different redox

states of an active site lack a spectroscopic handle, such as a strong and characteristic electronic transition or unpaired electrons; instead, the current peaks represent signals that can be used to label species and monitor the reactions of species that have been identified independently by spectroscopic techniques [2].

Importantly, and unlike potentiometry, voltammetric methods are dynamic and give information on kinetics, that is, rates of electron transfer and coupled (EC) reactions: the latter include those in which electron transfer drives a reaction such as ion/proton transfer, or is “gated”, that is, the case in which the electron-transfer event is controlled by a preceding chemical process. Redox reactions can be quantified in both the potential and time domains, and these may be separated and resolved: for example, steady-state catalytic studies of adsorbed enzymes reveal how catalytic electron transport varies as a function of potential, which can be important if the rate is sensitive to the oxidation state of a particular site in the molecule [1].

Direct electrochemical methods can often be integrated with spectroscopy. This is commonly carried out using an optically transparent cell (such as an OTTLE), which views the light absorbed by species in solution close to a gold mini-grid or conducting glass electrode. To cite an example, the intense Soret absorption band (390–450 nm), which is a key characteristic of heme groups, provides a good marker for studying cytochromes [5]. Improvements in sensitivity are making possible studies on proteins that are bound tightly (adsorbed) at the electrode – a good example being potential (AC)-modulated electroreflectance spectroscopy [6]. More specific information on the structural changes that accompany electron transfer can be obtained with techniques such

as surface-enhanced Raman spectroscopy (SERS) and surface-enhanced resonance Raman spectroscopy, particularly for heme proteins adsorbed on bare and modified Ag electrodes [7].

1.2

Electrodes for Proteins

Success in protein voltammetry depends critically upon the electrode and how it is prepared and modified. The current response may stem from protein molecules free in solution and undergoing a reaction upon diffusing to the electrode surface, or it may stem from molecules that are already bound tightly (adsorbed) to the electrode. Quasi-reversible diffusion-controlled electrochemistry has been documented for a wide range of proteins, mostly the smaller variety (molecular mass <15 kDa) that function as mobile electron carriers [3]. Diffusion-controlled electrochemistry requires that the protein interacts with the electrode in a transient manner, that is, weakly, so that the electrode does not become blocked. Increasingly, however, attention has turned to electrodes that bind protein molecules tightly, so that the sample is studied as a stable monolayer that typically comprises less than a picomole [1].

Since the pioneering studies of Hill [8] and Kuwana [9], the most successful electrodes for proteins have been noble metals (Au or Ag) modified with various adsorbates, or materials such as carbon or metal oxides that have natural surface functionalities [10–18]. Conducting metal oxides are often optically transparent, and thus provide additional possibilities for spectral studies, while a further development has been the modification of electrode surfaces with surfactant films [19–21]. Examples of

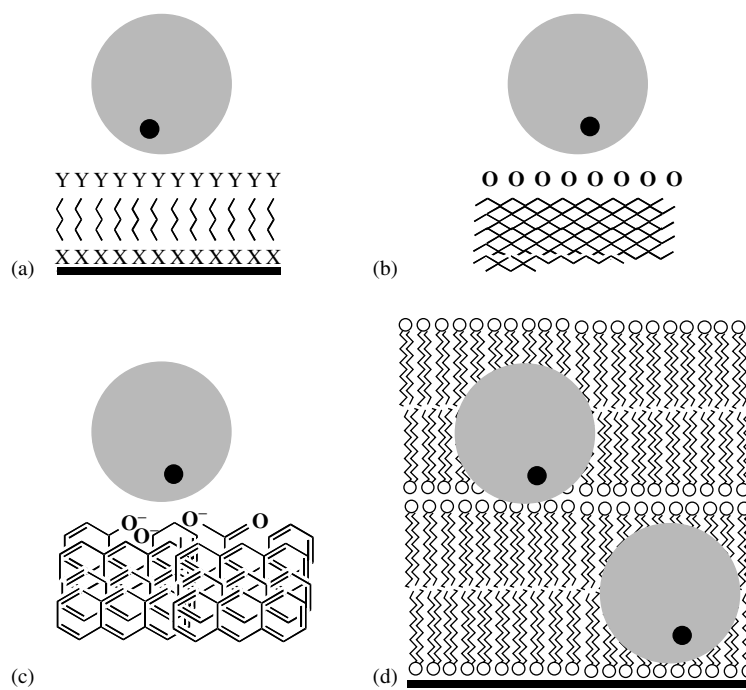


Fig. 1 Electrodes for protein voltammetry: (a) noble metals (Au, Ag) modified with a SAM. Group X is typically sulfur, while Y is a functionality, such as $-\text{CH}_3$, COO^- , CH_2OH , the variety and mixture of which can be designed to optimize the interaction with the protein. Examples are described in Refs. [10–13]; (b) a metal oxide electrode. Examples are described in Refs. [9, 15–18]; (c) a carbon electrode, typically pyrolytic graphite with the “edge” surface projected to the solution. Protein adsorption is often optimized by inclusion of polycations. Examples are described in Refs. [1, 14]; (d) An electrode coated with a surfactant layer within which the protein is confined. Examples are described in Refs. [19–21].

the electrodes that have been used successfully for protein studies are depicted in Fig. 1. It is important that the electrode binds the protein in an orientation suitable for fast electron transfer and that it does not cause the protein to denature; also it should not adsorb other molecules that block the surface. A problem with commonly used metal electrodes, such as Ag, Au, Pt, and Hg, is that they lead to denaturation and irreversible adsorption of the resulting inactive protein, and they are easily fouled by contaminants (the water molecules that are normally bound

at the electrode/electrolyte interface are easily displaced). This is demonstrated by the observation that an unmodified “pristine” Ag surface, prepared by treatment with a hydrogen flame, gives a reversible but short-lived voltammetric response with cytochrome *c* [22].

Many of the adsorbates used to modify metal electrodes produce self-assembled monolayers (SAMs), in which the terminal functional groups provide good binding sites for proteins. For example, cytochrome *c*, which is positively charged and contains an excess of lysine residues

in the region surrounding the heme edge, forms a stable electroactive layer at an Au electrode modified with a monolayer of *n*-alkanethiols that terminate in COO^- or mixtures of COO^- and OH [11]. This interaction is weakened if the ionic strength is raised. Likewise, the “blue” Cu protein azurin, in which the surface over the active site consists of a patch of hydrophobic amino acids, forms a stable electroactive layer at alkane thiols terminating in CH_3 groups, which is stable at high ionic strength [12, 13]. One pertinent question that can be addressed is how electrochemical ET rates depend upon the nature of these terminal groups or the length of the $(\text{CH}_2)_n$ spacer. For cytochrome *c*, an exponential variation of rate constant (k_0) with distance is observed for medium-to-long chain SAMs, as expected from theory; however, reports suggest that as the chain length is shortened, the electron-transfer rate becomes limited by other factors. It is not yet established why this should occur, but one explanation proposed by Niki and coworkers is that the protein is rarely in the right orientation for fast electron transfer and must first reorganize to achieve this [23]. Another interesting observation is that SAMs composed of mixtures of spacers or end functional groups yield protein layers that exhibit faster ET rates [11].

Metal oxide electrodes have been used with or without modification [9, 15–18]. Tin oxide and indium oxide are semiconductors, while ruthenium dioxide is a metallic conductor. All of these yield direct electrochemistry of cytochrome *c*, while modification with amine groups produces a positively charged surface that can be used for negatively charged proteins, such as the small Fe-S proteins known as ferredoxins [18].

Carbon (pyrolytic graphite or glassy carbon) is a very convenient electrode material for a wide range of proteins. The simple act of polishing with abrasives, such as alumina and diamond paste, generates hydrophilic surface oxide groups so that there is some similarity with conducting metal oxide electrodes [14]. Oxide formation is enhanced if the electrode is oriented so that the “edge” plane contacts the surface (pyrolytic graphite “edge”; PGE). The surface of PGE is rough and can be modified further, either by covalent attachment of functionalities or by adsorption of agents (coadsorbates) that assist the binding of protein molecules. For proteins with negatively charged surfaces, polycations are often effective: these range from simple metal cations to organic molecules such as aminocyclitols, polymyxin and polylysine, and they probably form cross-linkages between the protein and electrode surface, and between adjacent protein molecules [1].

Surfactant films accommodate proteins in a more hydrophobic environment. These films seem to stabilize many proteins, and often enhance their electron-transfer and catalytic properties. Surfactant films have been effective for proteins ranging from myoglobin to large membrane-bound systems such as the photosynthetic reaction center [19–21].

1.3 Voltammetric Methods

1.3.1

Protein Sample Contained in Solution

The most widely used method is DC cyclic voltammetry, although others such as square-wave voltammetry present useful advantages for particular problems. The disadvantages of cyclic voltammetry

are its relative lack of sensitivity and the frequent appearance of broad ill-defined waves from which potential values are difficult to ascertain. The reason for the poor response with proteins does not necessarily stem from poor electrode kinetics, but from the manner in which the protein diffuses between bulk solution and interaction sites on the electrode. This is illustrated in Fig. 2. In cyclic voltammetry, the commonly held belief is that the current response should be a pair of peaks, separated by $59/n$ mV (where n is the number of electrons transferred in the electrode reaction) whose amplitude varies as the square root of scan rate; however, this is true only for a uniform planar surface at which diffusion is linear and

is not the case if conditions are such as to provide a steady state current [24, 25]. The natural selectivity that proteins exhibit for their biological reaction partners is expected to extend to electrode interactions, and it may be that only certain zones on an electrode produce active encounters. As shown in Fig. 2, if these zones are small or widely separated, the electrode will behave instead like a microelectrode array: diffusion to isolated sites on the electrode then gives rise to steady state voltammetry having a sigmoidal waveform. The familiar peaklike voltammograms appear only at scan rates that are sufficiently slow to allow diffusion fields to overlap. Figure 2 also shows voltammograms obtained for solutions of cytochrome *c* obtained at

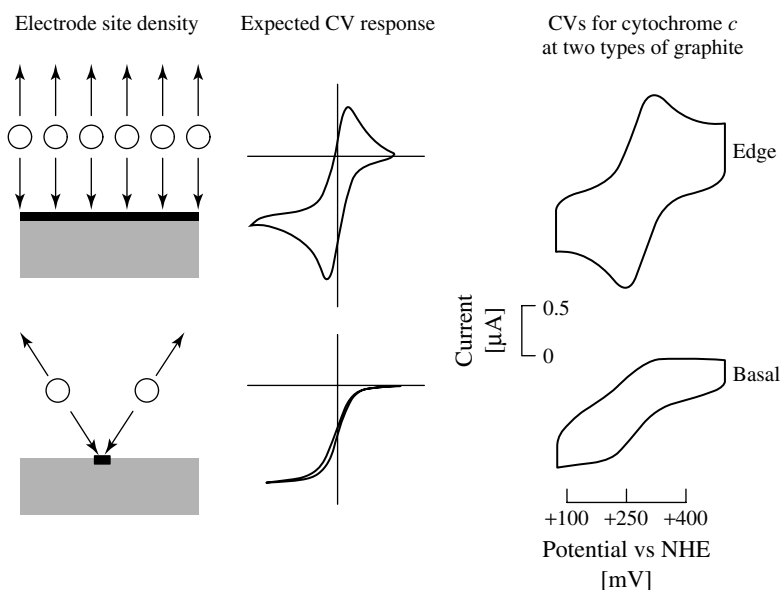


Fig. 2 Reversible voltammograms for: (top row) a diffusing redox couple reacting at a planar macroelectrode at which the entire surface is interactive; (bottom row) a diffusing couple reacting at a microelectrode, or a macroelectrode at which most of the surface is blocked to protein interaction. Theoretical voltammograms are shown at the center, while the right hand side shows actual results obtained for cytochrome *c* at a polished pyrolytic graphite edge plane (top) or basal plane electrode, (bottom) showing the effect of the density of interactive sites on the electrode.

electrodes differing greatly in their density of interaction sites [14, 24]. The effect of microscopic domains does not arise for protein molecules that are adsorbed (or for thin-layer voltammetry) but can still become important for enzymes if a catalytic current is being measured that is due to turnover of substrates diffusing from solution to isolated enzyme molecules adsorbed on the electrode [26].

By contrast, SW and DP voltammetries, aside from being inherently more sensitive than cyclic voltammetry, produce a peaklike current response regardless of the electrode conditions and diffusional geometry. Caution should be used, however, since the “pleasing” results that can be obtained often mask important mechanistic information and do not provide such immediate visualization of EC reactions as cyclic voltammetry. However, they do offer the means to drive reactions more effectively by providing large potential perturbations; thus, as well as being useful

for probing the driving force dependence of electron transfer, inherently slower reactions may be detected [27, 28].

1.3.2

Protein Sample Confined to Electrode

Redox-active species that are immobilized on the electrode and undergo simple reversible electron transfer give rise to a peak-type cyclic voltammetry response that is not influenced by diffusion effects, but which is, instead, much more sensitive to the characteristic properties of the protein [1]. Provided the sample is homogeneous and there are no interactions between molecules in the layer, the peaks for oxidation and reduction should have the Nernstian characteristics defined by Laviron; that is, they comprise finite passed charge with no tailing current, with a peak separation close to zero [29]. This is depicted in Fig. 3(a), where the capacitive background that is observed in real experiments is not shown. The peak widths

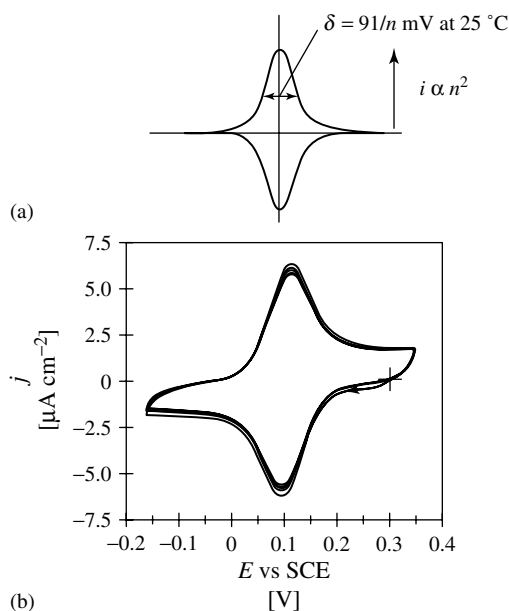


Fig. 3 Electrochemistry for a protein sample adsorbed on an electrode: (a) theoretical reversible cyclic voltammogram; (b) voltammograms (scan rate 2 V s^{-1}) of a film of azurin adsorbed on an Au electrode modified with a decane-thiol SAM, recorded on the fiftieth, hundredth, two-hundredth, and three-hundredth cycles, showing that the electrochemistry is stable (Q. J. Chi, J. D. Zhang, J. E. T. Andersen et al., *J. Phys. Chem. B* **2001**, *105*, 4669–4679, with permission of the American Chemical Society). In the system studied, k_0 is 290 s^{-1} . Rate constants over 2000 s^{-1} have been measured for azurin adsorbed on a PGE electrode, at which the ET distance is much shorter.

at half height (δ) should be $91/n$ mV at 25°C (or $84/n$ mV at 0°C) and the peak currents should vary as n^2 ; thus redox centers undergoing a cooperative two-electron reaction (such as flavin in many proteins) will appear particularly prominent in the voltammogram. Having the protein molecules already arranged at the electrode means that the response is not influenced by sluggish diffusion, so that much faster reactions can be studied. This includes coupled “EC” reactions in which the chemical process is usually the one of interest. For an enzyme, analysis of the catalytic electron-transport kinetics is aided by rotation of the electrode to control mass transport of substrate. It is also possible to transfer the coated electrode into a cryosolvent, and hence study electron transfer and coupled reactions at low temperatures [30].

For cyclic voltammetry, kinetic information can be obtained from the behavior of the peaks as the scan rate is increased. In square-wave voltammetry, the variable parameters are pulse height and frequency, and kinetics are extracted from appropriate models [27, 28]. Staircase cyclic voltammetry combines the attributes of potential-step (digital) methods with the visual qualities of cyclic voltammetry, which conventionally involves a linear (analogue) potential ramp [31]. Electron-transfer kinetics can be analyzed either in terms of the Butler-Volmer model (which yields values of k_0 , the electron exchange constant) or in terms of the Marcus theory, in which the system is defined by the parameters λ (reorganization energy) and k_{max} (the limiting rate constant at high overpotential). The Butler-Volmer model resembles the limit of the Marcus theory as $\lambda \rightarrow \infty$. Figure 3(b) shows voltammetry of a film of azurin adsorbed on an Au electrode modified with a decane-thiol SAM. The scans were taken at different times, showing

that the layer is stable, whereas scanning tunneling microscopy on the same system shows clearly discernable protein molecules that are well ordered [12]. The exchange rate constant k_0 is 290 s^{-1} for the decane thiol SAM/Au electrode, while rate constants over 2000 s^{-1} have been measured for azurin adsorbed on a PGE electrode, at which the ET distance is much shorter.

1.3.3

General

Other methods that have been applied to protein electrochemistry include chronoamperometry, which records the time course of the decaying current produced following a step in potential, and AC impedance methods, which can measure the rate of electron exchange at low driving force. AC-potential-modulated impedance has been used to measure k_0 values $>10^4\text{ s}^{-1}$ in the case of cytochrome *c* adsorbed at short chain-length SAMs on Au [23]. The electron-transfer reaction of cytochrome *c* at bare and SAM-modified Ag electrodes has also been studied by time-resolved surface-enhanced resonance Raman spectroscopy, monitoring the changes in characteristic spectral features of oxidized and reduced heme groups following a potential jump [32].

1.4

Case Studies

1.4.1

Observing Active Sites

1.4.1.1 Iron-sulfur Clusters

Iron-sulfur (Fe-S) clusters are among the most common redox-active cofactors in Biology, yet they lack a distinctive chromophore that enables them to be

observed under ambient conditions and in “real” time. The established methods for studying Fe-S clusters are Electron Paramagnetic Resonance Spectroscopy (EPR) [including ENDOR (electron-nuclear double resonance) and ESEEM (electron spin echo envelope modulation spectroscopy)], Mössbauer, and MCD, all of which require cryoscopic temperatures, whereas CD and NMR have been used with varying success to examine clusters at ambient temperatures. Another problem is that Fe-S clusters tend to have very negative reduction potentials, so that potentiometric titrations lasting several hours must be carried out under rigorously anaerobic conditions. Each of these problems can be overcome by voltammetry [33]. Once a particular cluster has been identified, its voltammetry provides both a measure of the reduction potential and a “handle” for the different reactions that the cluster may undergo.

Figure 4 shows the voltammetry of a small protein (a ferredoxin) that contains a [3Fe-4S] and a [4Fe-4S] cluster [34]. By correlation with spectroscopic studies, the two redox signals that are observed at higher potential have been assigned to

the well-established $[3\text{Fe-4S}]^{+/0}$ and $[4\text{Fe-4S}]^{2+/+}$ redox couples. The third signal at more negative potential is only observed in proteins containing a [3Fe-4S] cluster, and inspection of the peak shapes and pH dependence show the reaction to involve two electrons in a cooperative manner coupled to the uptake of at least two protons. This signal is, therefore, assigned to the couple $[3\text{Fe-4S}]^{0/2-}$, which produces an unusual “hyper-reduced” cluster in which all Fe atoms are formally in the 2^+ oxidation state. Consequently, a [3Fe-4S] cluster in a protein can be identified by the appearance of two signals; one at modest potentials corresponding to the $[3\text{Fe-4S}]^{+/0}$ couple, and another much sharper signal at more negative potentials corresponding to the hyper-reduction reaction involving $[3\text{Fe-4S}]^{0/2-}$.

In many proteins, clusters can interconvert between different structures, for example, between [3Fe-4S] and [4Fe-4S] forms. These transformations may be important physiologically since they produce changes in reduction potentials, ligand binding, and catalytic activities; and importantly, they depend on the particular oxidation

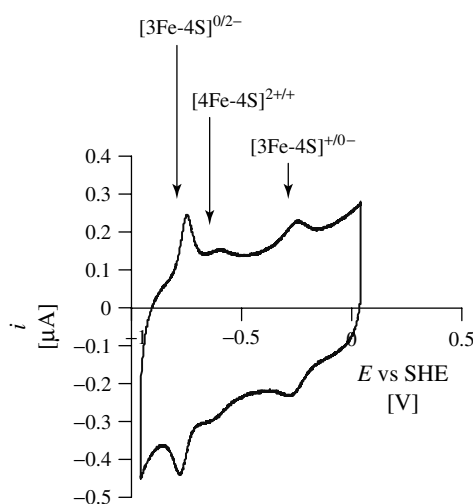


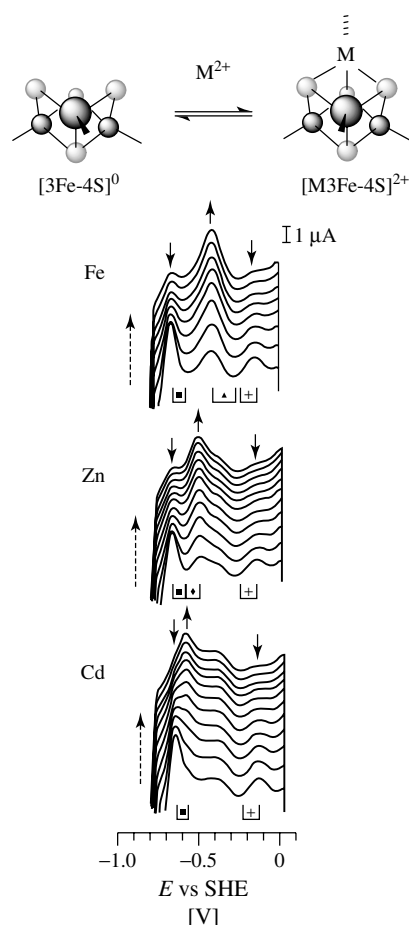
Fig. 4 Cyclic voltammogram of a film of ferredoxin that contains one [4Fe-4S] and one [3Fe-4S] cluster. The three redox couples observable in *Sulfolobus acidocaldarius* 7Fe ferredoxin have been assigned on the basis of other evidences, mostly spectroscopy. See Ref. [34].

levels of the clusters and, therefore, on the potential that is applied. Voltammetry, particularly of a film of protein adsorbed on an electrode, allows these reactions to be visualized and controlled. Metals other than Fe may be incorporated, resulting in heterometal clusters $[M3Fe-4S]$, and Fig. 5 shows the use of voltammetry to follow the fast reaction of a $[3Fe-4S]$ cluster with Fe^{2+} , Zn^{2+} , and Cd^{2+} to form $[4Fe-4S]$, $[Zn3Fe-4S]$, and $[Cd3Fe-4S]$ clusters respectively [35, 36]. This particular example, ferredoxin III isolated from a sulfate reducing bacterium *Desulfovibrio africanus*, contains two Fe-S clusters, a $[4Fe-4S]$ cluster that is inert and a $[3Fe-4S]$ cluster that is reactive and has a high affinity for various metal ions. The protein is adsorbed on a PGE electrode in the presence of polymyxin, and on addition of metal ions (M^{2+}) the reaction is observed simply by cycling the potential. By employing periods of time in which the electrode is polarized at different potentials, it is possible to determine the stabilities and metal ion affinities of different oxidation levels. A number of different heterometal derivatives $[M3Fe-4S]$ ($M^{2+} = Zn, Cd, Co, Cu, Pb$; and $M^+ = Tl$ and Cu) have been prepared “on the electrode” in adsorbed proteins and their stabilities, and redox properties have been compared [33, 35, 36].

Fig. 5 Reaction of a $[3Fe-4S]$ cluster with metal ions, as observed by voltammetry of a film of ferredoxin from *Desulfovibrio africanus*. Only the oxidative sweep is shown. The scan rate is 200 mV s^{-1} . Note the decrease in intensity (\downarrow) of the two signals from $[3Fe-4S]^{+/0}$ and $[3Fe-4S]^{0/2-}$ redox couples, while the signal due to $[M3Fe-4S]^{2+/+}$ grows (\uparrow). (J. N. Butt, F. A. Armstrong, J. Breton et al., *J. Am. Chem. Soc.* **1991**, 113, 6663–6670, with permission of the American Chemical Society.)

1.4.1.2 Flavins

Flavins (FAD and FMN) are important cofactors in enzymes, where they often occur together with various metal centers. In many cases, they undergo cooperative two-electron transfers (the semiquinone radical is usually unstable) so that in a protein that is adsorbed on an electrode they can be distinguished by a much sharper signal than that displayed by one-electron sites [37–39]. This is illustrated in Fig. 6, which shows the result obtained for a film of *E. coli* fumarate reductase (molecular mass 93 kDa) that contains an FAD cofactor and three Fe-S clusters. From the



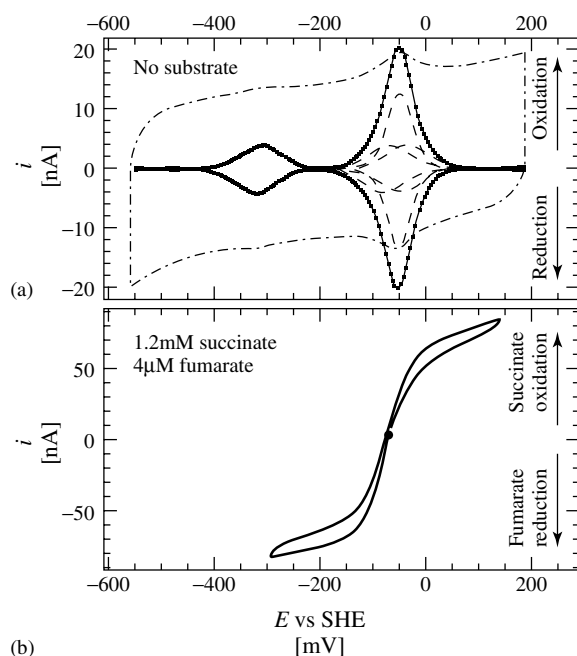


Fig. 6 Voltammetry of *E. coli* fumarate reductase: (a) voltammogram in the absence of substrate; (b) voltammogram obtained in the presence of fumarate and succinate. Note that the oxidation and reduction currents are equal when the succinate/fumarate ratio is 300. (C. Léger, K. Heffron, H. R. Pershad et al., *Biochemistry* **2001**, *40*, 11 234–11 245, with permission of the American Chemical Society.)

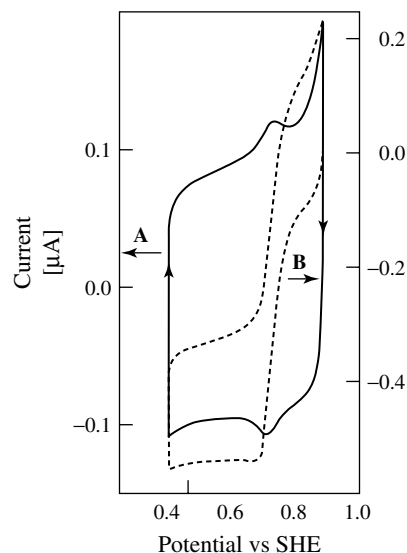
areas under the signals, the electroactive coverage is approximately equivalent to a monolayer. The signal due to the FAD is clearly observable and can be followed even at a scan rate of 100 V s^{-1} , which is fast enough to outrun catalysis when a substrate molecule is bound [38, 39].

1.4.1.3 Highly Oxidizing Intermediates: Fe(IV)=O

Fe(IV) is an important intermediate in such heme enzymes as cytochrome *c* oxidase and cytochrome P450, as well as the nonheme enzymes methane monooxygenase and ribonucleotide reductase. Voltammetric studies on yeast cytochrome

c peroxidase and various mutant forms have provided insight into the redox properties of the catalytic intermediate (Compound I) that contains the ferryl group (Fe(IV)=O) and a cation radical. When adsorbed at a PGE electrode, cytochrome *c* peroxidase catalyzes reduction of hydrogen peroxide at potentials ($>0.7 \text{ V}$) that are much higher than required for the natural electron donor, cytochrome *c* (0.26 V) [26]. The pyrolytic graphite electrode can be taken to quite high potentials without excessive water oxidation or surface degradation. An example is shown in Fig. 7. In the absence of substrate, a reversible redox couple is observed, the half-height

Fig. 7 Voltammetry of a film of yeast cytochrome *c* peroxidase adsorbed on a pyrolytic graphite edge electrode. (A) Voltammogram obtained in the absence of substrate, after adsorbing the enzyme from dilute solution at 0 °C. Both reduction and oxidation peak widths are below 84 mV. (B) In the presence of H₂O₂: the electrode is rotating at 400 rpm, but note that the reduction current in the negative direction still retains a peaklike feature, suggesting that the rotation rate is not high enough to ensure steady state conditions. (M. S. Mondal, H. A. Fuller, F. A. Armstrong, *J. Am. Chem. Soc.* **1996**, *118*, 263–264, with permission of the American Chemical Society.)



peak widths of which (both oxidation and reduction) are significantly narrower than the one-electron value. This suggests that the two-electron transition between Fe(III) and Compound I is a cooperative process [31, 40]. The potential at pH 5 is 760 mV for WT and 880 mV for a mutant W51F in which a distal-pocket tryptophan has been replaced by phenylalanine [41]. On addition of H₂O₂, the peaks transform to an amplified catalytic wave (dashed line), which also commences at high potential (see later). Voltammetry is, therefore, useful in determining the factors that stabilize Fe(IV) and in relating the redox energetics to catalytic activity.

1.5 Resolving Complex Reactions

1.5.1 Coupled and Gated Electron Transfer

The heme groups in many enzymes can adopt five- and six-coordinations, with the five-coordinate center being available for

substrate binding and turnover. Small proteins, including cytochrome *c* and site-directed variants, provide good examples of redox-dependent changes in axial ligation that are relevant to the larger enzymes, and which are “EC” reactions particularly suited to study by voltammetry. In mitochondrial cytochrome *c*, the Fe is axially ligated by a histidine and a methionine thioether. However, oxidation at high pH is followed by a ligand exchange (the methionine dissociates, to be replaced by a nearby lysine), which can be observed by cyclic voltammetry. The “high pH” form has a much lower reduction potential, as expected because the methionine stabilizes the Fe(II) form. The interconversion is quite slow, and can be studied with cytochrome *c* solutions that yield reversible ET at modified Au electrodes [42]. A particularly good example is a variant of yeast cytochrome *c*, in which phenylalanine-82, a ligand close to the axial ligand methionine-80, is replaced by a histidine [43]. Upon oxidation to Fe(III), methionine-80 is displaced spontaneously by histidine-82,

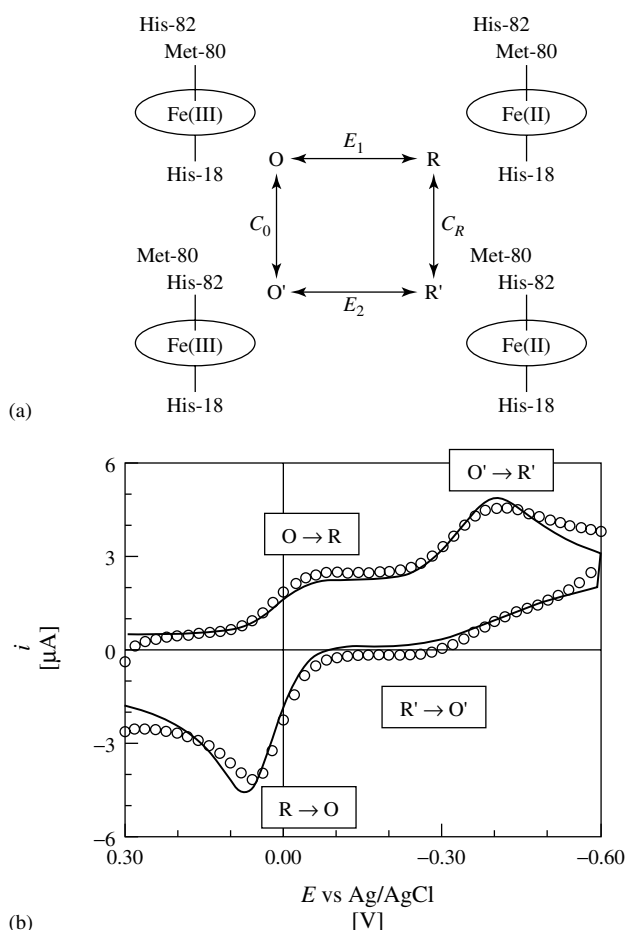


Fig. 8 (a) square scheme depicting redox-coupled ligand exchange at a mutant form of yeast cytochrome *c* (F82H), in which a phenylalanine residue close to the Fe has been replaced by a histidine. In the oxidized state (Fe(III)) the new ligand competes effectively with methionine-80 that normally ligates the Fe; (b) voltammogram of a solution of F82H cytochrome *c* reacting at an Au electrode modified with a layer of bis(4-pyridyl) disulfide. Scan rate is 50 mV s⁻¹. (B. A. Feinberg, X. Liu, M. D. Ryan et al., *Biochemistry* **1998**, 37, 13 091–13 101 with permission of the American Chemical Society.)

while reduction is followed by spontaneous recombination with methionine-80. The reactions are represented by a square scheme, which is shown along with the resulting EC voltammetry in Fig. 8. At a scan rate of 50 mV s⁻¹, the oxidation peak

appears at high potential, while reduction is seen at low potential. From the way that the voltammetry changes with scan rate, the rate constants for the ligand exchange reactions can be determined. In this case the reactions are quite slow.

Various coupled reactions occurring at Fe-S clusters have been investigated. As an example, a detailed study of proton transfer has been carried out on the well-characterized 7Fe ferredoxin from *Azotobacter vinelandii*, which is structurally defined to 1.4 Å resolution, and exhibits fast electron transfer at a PGE electrode, similar to that shown in Fig. 4 [44, 45]. In many proteins, [3Fe-4S] clusters bind a proton in their one-electron reduced states, a scheme for which is shown in Fig. 9. The oxidized form is a very weak base, expected to have a very high reduction potential, so it can be ignored. In *Azotobacter vinelandii* ferredoxin, the [3Fe-4S] cluster is buried below the surface, and the proton must transfer through an “anhydrous” barrier. How this transfer occurs, and the nature by which long-range proton transfer is coupled with

electron transfer are both relevant to the wider question of the mechanism of enzymes known as proton pumps. A mutant (D15N) in which proton transfer is retarded provides an example of the detection and quantitative investigation of “gating”. In this case, electron transfer to the cluster draws a proton into the protein, whereas the reoxidation process is gated by proton release. In D15N, an aspartate residue whose carboxylate is exposed to the surface above the [3Fe-4S] cluster has been replaced by asparagine.

Figure 9 shows plots of the positions of oxidation and reduction peaks observed when the pH of the contacting electrolyte is *above* and *below* the pK of the reduced cluster. Under the conditions $\text{pH} \gg \text{pK}$, the electrode reaction involves only electron transfer; therefore, the peaks separate as

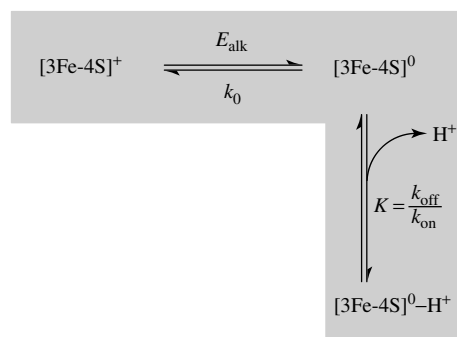
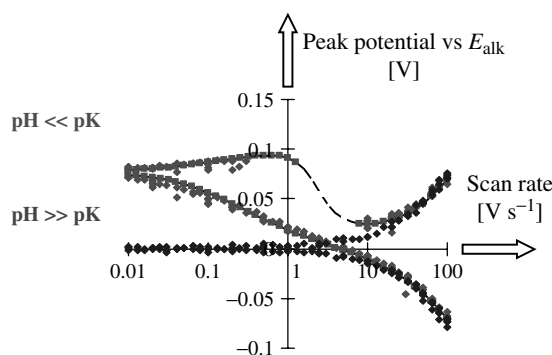


Fig. 9 Plots of peak positions against scan rate for the redox reaction of the buried [3Fe-4S] cluster in a D15N mutant of ferredoxin I from *Azotobacter vinelandii*. Under solution conditions $\text{pH} > \text{pK}$, only an electron is transferred; by contrast, for $\text{pH} < \text{pK}$, proton transfer also occurs, but at a rate that is sufficiently slow so that it becomes uncoupled at high-scan rates and proton release gates the oxidation process (no peak is observed) at intermediate scan rates. See Refs. [44 and 45].



the scan rate is raised, giving rise to a approximately symmetrical trumpet-shaped plot. Analysis of this plot in terms of the Butler-Volmer model gives a standard rate constant of 550 s^{-1} . By contrast, at low pH, three distinct regions of the plot are observed. First, at slow scan rates, the oxidation and reduction peak positions are close together; but at a much higher potential, as expected since the reduction potential increases as the pH is lowered. Second, at fast scan rates, the peak positions overlay those observed at high pH: this is because (commencing the cycle from the oxidative potential limit) the electron exchange occurs in both directions before the proton can transfer to the cluster. Finally, in the intermediate region, no oxidation peak is observed because the proton now has time to arrive at the cluster, but on the return scan the electron is trapped (species $[3\text{Fe-4S}]^0\text{-H}^+$) until the proton has been removed; the electron transfer is thus “gated” by the release of the proton ($k = 2.5 \text{ s}^{-1}$). The plot, therefore, divides the EC reaction into three distinct time domains. The native protein exhibits more complex kinetics, in which the rate constants k_{on} and k_{off} are much higher, assisted by the mobile aspartate side chain that binds a proton reversibly and serves as a courier.

1.5.2

Catalysis

For enzymes adsorbed on an electrode, both nonturnover and catalytic studies can be carried out. Nonturnover measurements are essentially the same as mentioned earlier, and focus on the active site redox transitions occurring in the absence of substrate. Addition of the substrate to the electrolyte results in catalytic

activity, which can be studied under transient or steady state conditions. Provided electron transfer is faster than turnover, the transformation to nonturnover voltammetry as the scan rate is increased (to a time domain too short to allow turnover to occur) provides information on the redox properties of the enzyme-substrate complex. For fumarate reductase (and other flavoenzymes), the prominence of the FAD signal over the other centers in the enzyme enables its oxidation and reduction peak positions to be observed, even at 100 V s^{-1} ; so that the reduction potential can be measured in the absence or presence of substrate [38, 39].

In steady-state voltammetry experiments, enzyme activity is viewed in the “potential domain” that can pinpoint the role of centers as electron relays, or reveal the presence of internal control mechanisms, such as a redox transformation that causes the enzyme to “switch off” at a certain potential. Such studies can also reveal and quantify how an enzyme is “redox-biased” to favor catalysis in a particular direction. Figure 6(b) shows the voltammetry of a film of fumarate reductase obtained in the presence of a low concentration of fumarate and a high concentration of succinate, from which it is easily seen how the catalytic activity of the enzyme is biased heavily in the direction of fumarate reduction [38]. This experiment has been carried out with a rotating disc electrode. The current for succinate oxidation is independent of rotation rate, while that for fumarate reduction is very sensitive because the reaction is diffusion controlled.

Figure 10 shows the catalytic voltammetry of a film of nitrate reductase, a membrane-bound enzyme that contains a Mo active site and Fe-S clusters [46]. The enzyme is adsorbed on a PGE electrode;

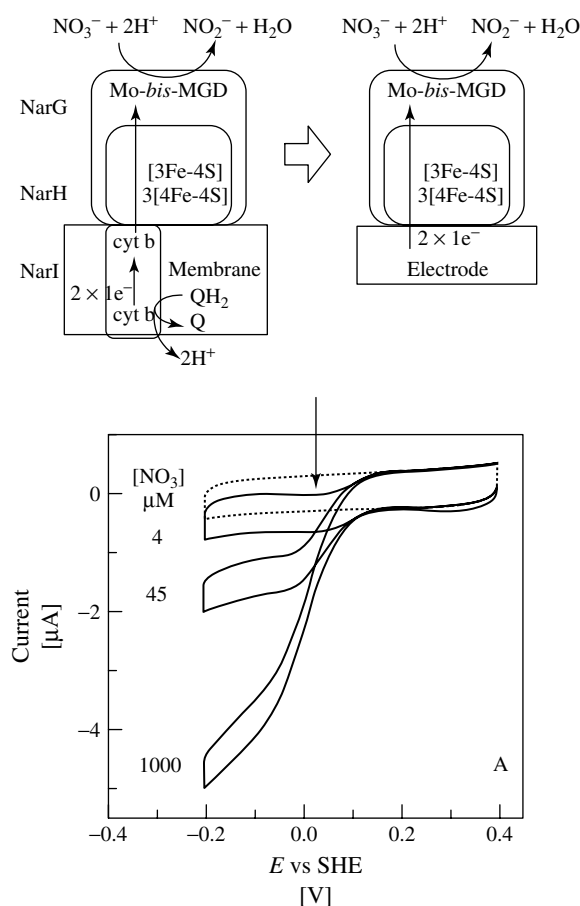


Fig. 10 Catalytic voltammetry of a film of nitrate reductase: (a) cartoon showing the membrane-extrinsic sub-complex NarGH bound to the membrane-intrinsic NarI (left), and adsorbed instead on an electrode (right); (b) catalytic voltammetry of a film of NarGH adsorbed on a PGE electrode in the presence of different concentrations of nitrate (voltammogram without substrate is also shown). Note (arrowed) that the catalytic current for the experiment at low nitrate concentration passes through a maximum. (L. J. Anderson, D. J. Richardson, J. N. Butt, *Biochemistry* **2001**, *40*, 11 294–11 307, with permission of the American Chemical Society.)

although in this case, unlike that for fumarate reductase, the electroactive coverage is too low to observe signals under non-turnover conditions. An interesting observation is that for low levels of nitrate the

activity (reduction current) passes through a maximum value at a particular potential, below which it decreases even though the driving force is raised. It is known that during the catalytic cycle, the Mo

center operates between Mo(VI), Mo(V), and Mo(IV) oxidation states, and one interpretation is that substrate binds more tightly to the intermediate Mo(V) form than to Mo(IV). This idea is supported by extensive measurements of the substrate and pH dependencies of voltammograms, and correlations with EPR-potentiometric data [46]. Applying a more negative potential causes the activity to drop, so that nitrate reductase is an example of an enzyme that displays a potential dependent “switch”. Similar properties are observed for another Mo enzyme, DMSO reductase from *E. coli* [47] and for succinate dehydrogenase from beef heart or *E. coli* [48]. These effects are difficult to observe by conventional experiments, but are easily detected by voltammetry and may be important physiologically in the regulation of metabolism.

1.6

Conclusion

The study of protein molecules at surfaces is a field in its infancy, for which dynamic electrochemical methods already play an important role. Contrary to the beliefs once held, protein molecules do “talk” to electrodes. Unique insight is being gained into complex problems of fundamental interest, and new technological applications are being identified. The methodology is interactive: electron transfer and coupled reactions are induced under precise conditions; and then, simultaneously, these reactions can be monitored, deconvoluted, and quantified. Future efforts are expected to focus more on larger and more complex enzymes, particularly those that exist, in vivo, associated with membranes. The problem of designing membrane-mimetic enzyme systems

on electrodes while retaining fast electron transfer will provide important challenges for the future.

References

1. F. A. Armstrong, H. A. Heering, J. Hirst, *Chem. Soc. Rev.* **1997**, 26, 169–179.
2. F. A. Armstrong in *Bioelectrochemistry of Biomacromolecules: Bioelectrochemistry: Principles and Practice* (Eds.: G. Lenaz, G. Milazzo), Birkhauser Verlag, Basel, 1997, pp. 205–255.
3. F. A. Armstrong, G. S. Wilson, *Electrochim. Acta* **2000**, 45, 2623–2645.
4. L. D. Gilles de Pelichy, E. T. Smith, *Biochemistry* **1999**, 38, 7874–7880.
5. A.-E. Nassar, Z. Zhang, N. Fu et al., *J. Phys. Chem. B* **1997**, 101, 2224–2231.
6. Q. Feng, S. Imabayashi, T. Kakiuchi et al., *J. Electroanal. Interfacial Electrochem.* **1995**, 394, 149–154.
7. S. Lecompte, H. Wackerbarth, T. Soulimane et al., *J. Am. Chem. Soc.* **1998**, 120, 7381–7382.
8. M. J. Eddowes, H. A. O. Hill, *J. Chem. Soc. Chem. Commun.* **1977**, 771–772.
9. P. Yeh, T. Kuwana, *Chem. Lett.* **1977**, 1145–1148.
10. P. M. Allen, H. A. O. Hill, N. J. Walton, *J. Electroanal. Interfacial Electrochem.* **1984**, 178, 69–86.
11. A. El-Kasmi, J. M. Wallace, E. F. Bowden et al., *J. Am. Chem. Soc.* **1998**, 120, 225–226.
12. Q. J. Chi, J. D. Zhang, J. E. T. Andersen et al., *J. Phys. Chem. B* **2001**, 105, 4669–4679.
13. L. J. C. Jeuken, F. A. Armstrong, *J. Phys. Chem. B* **2001**, 105, 5271–5282.
14. F. A. Armstrong, P. A. Cox, H. A. O. Hill et al., *J. Electroanal. Interfacial Electrochem.* **1987**, 217, 331–366.
15. E. F. Bowden, F. M. Hawkridge, H. N. Blount, *J. Electroanal. Interfacial Electrochem.* **1984**, 161, 355–376.
16. M. A. Harmer, H. A. O. Hill, *J. Electroanal. Interfacial Electrochem.* **1985**, 189, 229–246.
17. I. Taniguchi, K. Watanabe, M. Tominaga, F. M. Hawkridge, *J. Electroanal. Interfacial Electrochem.* **1992**, 333, 331–338.
18. I. Taniguchi, Y. Hirakawa, K. Iwakiri et al., *J. Chem. Soc. Chem. Commun.* **1994**, 953–954.
19. J. F. Rusling, *Acc. Chem. Res.* **1998**, 31, 363–369.

20. J. L. Kong, Z. Q. Lu, Y. M. Lvov et al., *J. Am. Chem. Soc.* **1998**, 120, 7371–7372.
21. P. J. Farmer, R. Lin, M. Bayachou, *Comments Inorg. Chem.* **1998**, 20, 101–120.
22. D. E. Reed, F. M. Hawkridge, *Anal. Chem.* **1987**, 59, 2334–2339.
23. A. Avila, B. W. Gregory, K. Niki et al., *J. Phys. Chem. B* **2000**, 104, 2759–2766.
24. F. A. Armstrong, A. M. Bond, H. A. O. Hill et al., *J. Phys. Chem.* **1989**, 93, 6485–6493.
25. F. A. Armstrong, A. M. Bond, H. A. O. Hill et al., *J. Am. Chem. Soc.* **1989**, 111, 9185–9189.
26. F. A. Armstrong, A. M. Bond, F. N. Buchi et al., *Analyst* **1993**, 118, 973–978.
27. T. M. Saccucci, J. F. Rusling, *J. Phys. Chem. B* **2001**, 105, 6142–6147.
28. L. J. C. Jeuken, J. P. McEvoy, F. A. Armstrong, *J. Phys. Chem. B* **2002**, 106, 2304–2313.
29. E. Laviron in *Electroanalytical Chemistry* (Ed.: A. J. Bard), Marcel Dekker, New York, 1982, pp. 53–157, Vol. 12.
30. J. P. McEvoy, F. A. Armstrong, *J. Chem. Soc. Chem. Commun.* **1999**, 1635–1636.
31. H. A. Heering, M. S. Mondal, F. A. Armstrong, *Anal. Chem.* **1999**, 71, 174–182.
32. D. H. Murgida, P. Hildebrandt, *J. Am. Chem. Soc.* **2001**, 123, 4062–4068.
33. F. A. Armstrong in *Advances in Inorganic Chemistry* (Eds.: A. G. Sykes, R. Cammack), Academic Press, New York, 1993, pp. 117–163, Vol. 38.
34. J. L. C. Duff, J. L. J. Breton, J. N. Butt et al., *J. Am. Chem. Soc.* **1996**, 118, 8593–8603.
35. J. N. Butt, F. A. Armstrong, J. Breton et al., *J. Am. Chem. Soc.* **1991**, 113, 6663–6670.
36. J. N. Butt, S. E. J. Fawcett, J. Breton et al., *J. Am. Chem. Soc.* **1997**, 119, 9729–9737.
37. A. Sucheta, R. Cammack, J. Weiner et al., *Biochemistry* **1993**, 32, 5455–5465.
38. C. Léger, K. Heffron, H. R. Pershad et al., *Biochemistry* **2001**, 40, 11 234–11 245.
39. A. K. Jones, R. Camba, G. A. Reid et al., *J. Am. Chem. Soc.* **2000**, 122, 6494–6495.
40. M. S. Mondal, H. A. Fuller, F. A. Armstrong, *J. Am. Chem. Soc.* **1996**, 118, 263–264.
41. M. S. Mondal, D. B. Goodin, F. A. Armstrong, *J. Am. Chem. Soc.* **1998**, 120, 6270–6276.
42. P. D. Barker, A. G. Mauk, *J. Am. Chem. Soc.* **1992**, 114, 3264–3619.
43. B. A. Feinberg, X. Liu, M. D. Ryan et al., *Biochemistry* **1998**, 37, 13 091–13 101.
44. J. Hirst, J. L. C. Duff, G. N. L. Jameson et al., *J. Am. Chem. Soc.* **1998**, 120, 7085–7094.
45. K. Chen, J. Hirst, R. Camba et al., *Nature* **2000**, 405, 814–817.
46. L. J. Anderson, D. J. Richardson, J. N. Butt, *Biochemistry* **2001**, 40, 11 294–11 307.
47. K. Heffron, C. Leger, R. A. Rothery et al., *Biochemistry* **2001**, 40, 3117–3126.
48. H. R. Pershad, J. Hirst, B. Cochran et al., *Biochim. Biophys. Acta* **1999**, 1412, 262–272.

2 Single Cell Electrochemistry

Jonathan M. Cooper
University of Glasgow, Glasgow, United Kingdom

Sung-Kwon Jung
Biocurrents Research Center, Woods Hole, Massachusetts

2.1	Introduction	33
2.2	Advantages of Microelectrodes in Single Cell Studies	35
2.3	Fabrication of Planar Microelectrodes Using Photolithography	36
2.3.1	Functional Three-dimensional Micromachined Electrochemical Devices	38
2.3.2	Advantages of Using Three-dimensional Microstructures	39
2.3.3	Biosensors, Microfluidics, Microarrays, and Lab-on-a-Chip	40
2.4	Self-referencing Microelectrodes	41
2.4.1	Ion-selective Microelectrodes	43
2.4.2	Self-referencing Amperometric Microelectrodes	43
2.5	Scanning Probe Microscopy and Single Cell Measurement	44
2.6	Semiconductor Devices for Biological Sensing	46
2.7	Corroborative Measurements for Single Cell Electrochemistry	47
2.8	Future Prospects	47
	References	48

2.1 Introduction

There is a huge diversity of cell types available for the biologist to study, ranging in size from a few microns in diameter to several tens of centimeters in length. The variation in size is only matched by the diversity of structure, illustrated by eukaryotic animal cells (enveloped by a cell membrane) and plant cells (enclosed by a robust cell wall). The greatest interest in single cell study has resulted from its relevance to human medicine and has included examples from the prokaryotes (such as the bacteria) and from the eukaryotes (e.g. mammalian cells). As the smallest unit of sustainable life, the single cell has provided a unique understanding of more complex biological systems. Analysis of metabolic events at this level has provided fundamental information about a wide range of important processes including cell signaling, cell–drug interactions, and disease mechanisms (including ischemia and cell death). There is now not only the possibility of obtaining data concerning biochemical processes, but also detail on physiological functionality, including for example, the generation of the action potential in neurons and the propagation of cell contraction in myocytes.

In terms of understanding complex biological systems, the study of the single cell has provided a number of clear advantages, particularly the deconvolution of signaling and metabolic events without the need to be concerned by the history, distribution, integrity, and activity of neighboring cells. In order to provide suitable analytical tools there has been extensive research into a variety of optical and electrochemical techniques with a correspondingly large literature. In the field of optical sensing, both natural and synthetic fluorescent probes have been introduced into cells through molecular biology, electroporation, and absorption in order to study both fundamental and applied aspects of the cellular physiology and biochemistry, as well as disease processes and drug activity. Generally, such fluorescent probes are “environmentally sensitive” such that their emission properties change as either the intracellular or the local conditions change (e.g. pH, ionic concentration). More recently, the genes for a variety of naturally occurring fluorochromes (such as green fluorescent protein) have been introduced at strategic points in the cell’s genome, such that it is now possible to tell if proximal genes have been activated (e.g. by the deliberate addition of a drug). Single cell fluorescence has also been greatly enhanced by advances

in organic chemistry (in producing new fluors), in the production of ultrasensitive imaging devices (most notably the charge coupled device, CCD) and new forms of microscopy, such as confocal imaging and near field scanning optical microscopy.

As an alternative to electroanalytical methods optical sensing have been developed over the last 20 years and are still used extensively in research and industry [1–3]. One important technique, known as patch clamping or voltage clamping, involves drawing a glass microcapillary and using it to capture a portion of the cell membrane, close to a potentiometric (ion) sensor. Preferably, a single ion channel is trapped within the low volume of the capillary, while the cell maintains its integrity and viability. As a method, it is able to detect quantal events in ion transport, resulting from the opening and closing of single channels. Although this chapter does not focus in detail on either patch clamping or fluorescence, both techniques are referred to again, later, as they provide important corroborative techniques, when used in conjunction with new electroanalytical methods.

Despite the predominant use of fluorescence and/or patch clamp techniques in single cell measurements, there has been a steady increase in the demand for new electroanalytical tools applicable to single cell studies [4]. Traditionally, such methods have been confined to the development and production of hand crafted sensors including the aforementioned glass capillaries [1–3] for patch clamping, as well as conical microelectrodes for scanning electrochemical microscopy (SECM) [5, 6] and carbon fiber microelectrodes to measure for example, the release of neurotransmitter from single neurons [7, 8].

More recently, techniques adapted directly from the semiconductor industry [9–13] have been used to manufacture sensors with more closely defined physical characteristics. In this context, the single cell, as a subject of study is of a comparable size to a variety of Bio-microelectromechanical systems (Bio-MEMS) devices that can now be produced through microfabrication and micromachining. Indeed, despite the small size of the single cell, relatively large signals can be readily obtained, ranging from several tens or hundreds of picoamperes in case of amperometric measurements, and across several decades of millivolts in the case of intracellular membrane potential measurements. In the latter cases, there is often the need to functionalize the electrode with an enzyme, thus creating a microbiosensor. One result of this, which presents a difficulty in making robust measurements, is that current densities tend to be smaller, often a result of the low catalytic activity of the enzyme and the small fluxes of analyte, either within or proximal to the cell.

In all cases, when low volume, single cell electrochemical measurements are being made on single cells, care must be taken to consider the fate of all species involved both in the electrochemical and the cell reactions (including the availability of oxygen, the levels of potentially toxic byproducts of cell metabolism; the buffering capacity of the system; the availability of nutrients; and the gradients of protons, either at the working or counter electrodes). In this latter context, Lab-on-a-Chip methods, described later may be used to create a microincubator system to constantly replenish the cell in culture.

In this chapter, we set out to review the current state of the art in single

cell electrochemical techniques, dating from early techniques that involved the direct electrochemical measurement of dopamine and the catecholamines [7, 8]. More recently, there have been a variety of methods [9–11], in which enzyme assays have been linked to electrochemical measurements, to provide a degree of specificity and enabled the determination of purines and lactate [13, 14]. While the use of Bio-MEMS methods has significantly lowered the absolute detection limit through minimal analyte dilution [9–11, 13, 14], the self-referencing technique, which is based on a difference measurement between two locations in a gradient, has permitted determination of real-time flux values with minimal impact of sensor drift or noise [15–19]. This latter approach belongs to a family of techniques employing position modulation of microprobes in order to enhance detection. The methods aim to negate small but irregular drift, which often compromises electrochemical measurements at the single cell level, by assuming the time-dependent drift is common to both physical locations of the sensor. Thus, the detection limit can be further reduced by two orders of magnitude below typical applications of microelectrodes. The chapter finally concludes with a brief review of aspects of probe microscopy in cell analysis.

2.2 Advantages of Microelectrodes in Single Cell Studies

In general, the advantages of using microelectrodes in electroanalysis (in which one physical dimension is below 100 μm) are already well documented [11, 13, 14,

20–28]. Most significantly, in all cases miniaturization of the electrode changes the nature of the profile of the diffusion gradient of the analyte between the bulk solution and the sensor surface (where often the process of measurement is changing the redox nature of the species under investigation). The exact nature of the diffusion profile is critically dependent on the precise geometry of the microelectrode, and may most often be approximated as a point, a disc, a cylinder, or a band. Regardless of the exact dimensions or geometry, a microelectrode benefits from more efficient transport of analyte to the sensor surface, resulting in higher fluxes of redox species and faster response times to achieve steady state equilibrium. There is a consequent improvement in ratio of the Faradaic current (the signal) to the non-Faradaic charging current (the latter decreasing as the double layer capacitance of the sensor falls as a function of the reduced surface area). Improvements in amplifiers, and their ready incorporation into instrumentation, now make low noise measurements routine, although clearly both proper shielding and grounding remain essential. Measurements of picoampere currents (typically equivalent to measurement of submicrovolt sized voltages) are commonplace, and at the state of the art, tens of nanovolts can be resolved.

In principle, both the spatial resolution of the measurement (i.e. the ability to position the electrode) and the signal to noise of the analytical signal will both improve with further miniaturization of the probe. While both of these attributes should be of significant importance in single cell measurements, there are, however, practical limits to the size of sensor, which ultimately defines the

ease with which the electrode can be fabricated and manipulated. The dimension of the microelectrode will also determine its mechanical robustness, and the size of the absolute signal being recorded. Static “probe” microelectrodes have generally been limited to a diameter of ca. 10 μm [7, 8, 20–22, 25–28], while “nanodes” (in which one dimension $<1\ \mu\text{m}$) have been mounted and rastered across a surface to produce very high-resolution two-dimensional maps (or micrographs) of ion- and redox fluxes, a technique more generally termed scanning electrochemical microscopy.

Thus electrochemical microelectrodes, providing good spatial and fast temporal resolution can be easily positioned at a predefined distance from either a confluent cell culture or a single cell. As long ago as the mid-1970s Wightman used single carbon fiber amperometric microelectrodes implanted (via a cannula) to measure dopamine release from rats *in vivo* [7]. Since then, similar methods have been used to determine a variety of electroactive extracellular species such as tryptophan and the catecholamines [8]. These sensors can also be positioned in conjunction with an optical fiber close to the cell to obtain electrochemical measurements, while simultaneously measuring changes in ion fluxes, such as calcium, using fluorescent indicator dyes [28]. Similar electroanalytical approaches have been used very successfully to monitor cellular oxidative bursts from single human fibroblasts [20, 22], including for example, the measurement of superoxide and peroxynitrite. In related work, peptides secreted from melanocytes and serotonin secreted from pancreatic β -cells have been monitored by electrochemical detection at a carbon fiber microelectrode [29, 30].

2.3

Fabrication of Planar Microelectrodes Using Photolithography

Whether considering a *static* or a *scanned* “probe” electrode, the size of the signal, and hence the interpretation of the data, critically depends on being able to faithfully reproduce the active measurement area. For hand crafted electrodes, the fabrication procedures for these electrodes are often labor-intensive and when the size becomes less than 10 μm , calibration is required because of the irregularity in size. In order to fabricate identical microelectrodes, methods are being adapted from the electronics industry in order to process devices with high throughputs and low costs. By using photolithography [9–11, 13, 14, 31] (literally *writing with light*), it is possible to precisely control the deposition of both metals and insulators on a surface, and hence define planar microelectrode arrays, Fig. 1. The technique makes use of a mask, a (UV) light source and a spun photoactive polymer (or *photoresist*) to transfer the pattern (from the mask) onto a surface, as a template for the subsequent deposition of metals or dielectrics. For example, metals such as gold or platinum, which provide suitable electroanalytical surfaces, can be readily deposited over the template and the geometry of the device revealed by dissolving the polymer using a technique known as “lift-off”. The process, which involves a number of sequential steps, can be repeated many times to reproduce identical microstructures.

At the center of the microfabrication procedure is the need to make a very accurate representation of the microelectrode (as the mask), for it is this “original” that will determine the quality of all subsequent devices. In addition, in order to ensure a faithful reproduction, careful

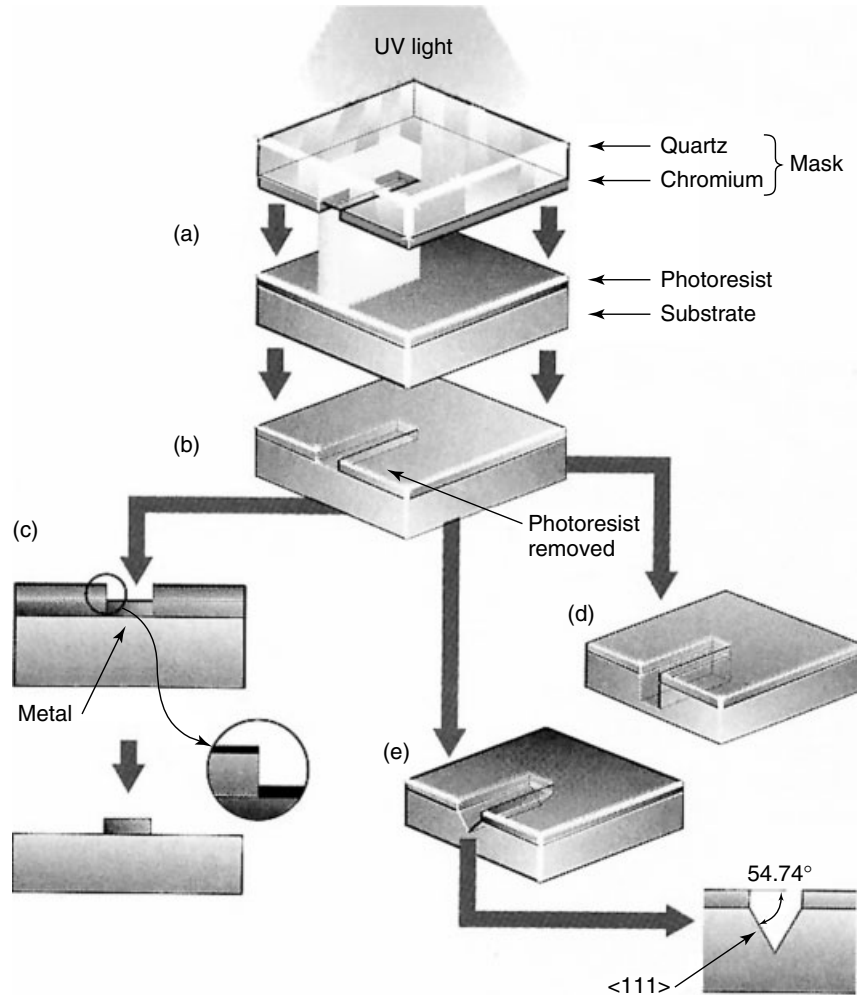


Fig. 1 Schematic of the fabrication processes used in planar microfabrication. The methods have been adapted to micromachining of surfaces to produce microstructured sensors, particularly those involved in producing gold planar microelectrodes on glass, used in electronic Petri dishes. (The schematic is reproduced from Ref. [31], although more details of the processes involved can be found in Ref. [9].)

consideration has to be given to the length of the exposure, the thickness of the polymer, the size of features on the mask, and the optical arrangement used. In the same manner in which metals can be patterned, dielectrics (insulators), including silicon nitride, photoactive glasses,

and thin and thick film polymers can also be deposited likewise, and used to isolate wires and delineate an active sensing area.

The process of photolithography and lift-off is highly reproducible, and is readily capable of defining sensor surface area

with feature sizes of ca. 2 μm . The limit of a feature, which can be fabricated by photolithography is a consequence of the wavelength of the light used in pattern transfer and the quality of the optics. Feature sizes as small as 150 nm, can be fabricated, although, in practice the cost of the instrumentation and the yield of production limit the size. Although the detailed methods of planar microfabrication technologies used in producing devices for bioanalysis are essentially the same as the core technology used in the microelectronics industry, there are a number of important differences in the materials used [31]. As there often is a need to view the cell(s) under a microscope, the “substrate” on which devices are fabricated is most often glass, which is optically transparent. Likewise, noble metals, particularly gold, are used throughout the device to prevent corrosion and provide a suitable electrode surface. Finally packaging, including encapsulation of active electronics or wires from corrosive biological solutions is required. The result is that a device made by photolithographic patterning of metals, and packaged provides a means for the production of a wide variety of two- or three-dimensional electrode arrays, which can be presented

in a similar manner to that shown in Fig. 2.

2.3.1

Functional Three-dimensional Micromachined Electrochemical Devices

One further application of planar, two-dimensional microfabrication is that the methods can be used as the foundation to develop three-dimensional structures, a methodology known as micromachining. By providing a volume above the electrode array there is the possibility of being able either to constrain the cell in a fixed volume, so preventing analyte dilution into the “bulk”, or of creating networks of fluidic channels to enable either the cell or the fluid to be moved relative to each other (ultimately comprising Lab-on-a-Chip and microfluidic techniques, see following discussion).

Micromachining has been used in the production of electroanalytical structures that have ultralow volumes, typically in the subnanoliter range [10, 11, 13, 14], and are thereby compatible with single cell methods. Broadly speaking, two different methods have been described for producing such picoliter-scale devices: embossing (or stamping) of microstructures

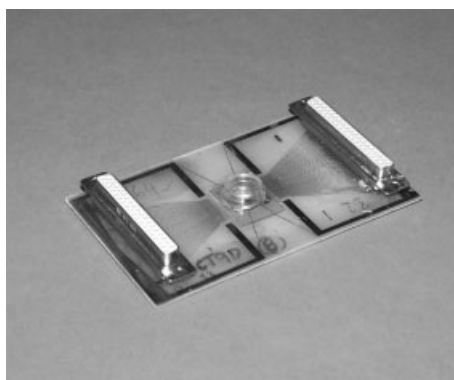


Fig. 2 A planar 64-microelectrode array, similar to those used in the development of the electronic Petri dish, with a series of connectors allowing electrical signals to be obtained from the central cellular playground. The device was produced using the methods shown in Fig. 1 in order to develop structures of the type shown in Fig. 3.

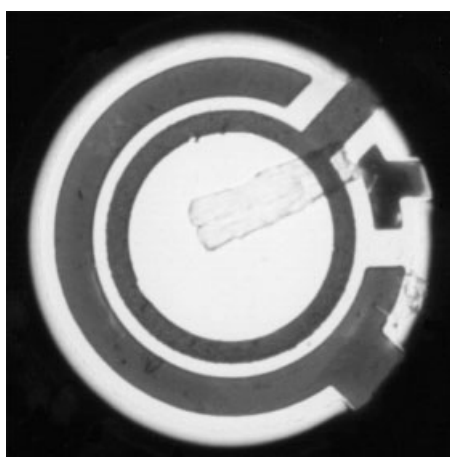
into plastics [10]; or incorporating sensors within a low volume chamber made from thick (40 μm) photoactive polymers [11, 13, 14]. In the latter case, the additional fabrication step of using a thick film layer, such as polydimethylsiloxane (PDMS) or SU8 [13], has enabled planar microelectrodes to be integrated into micromachined chambers in order to perform a variety of single cell analyses. For example, such devices with volumes in the range of 100 pL to 1 nL, have enabled detailed single heart cell analyses to be performed [13, 14]. In this work, the principle has been to use a cascade of solution-phase enzyme-linked assays to determine femtomole amounts of the purines, including adenosine and inosine [11, 14], and lactate [13], Fig. 3. More detailed studies can involve introduction of chemicals to affect the disruption of the cell membrane using detergents (to measure intracellular concentrations), or the addition of respiratory uncouplers, in order to simulate ischemia. Typically, the cell measurement device, Fig. 2, with detail in Fig. 3, will be mounted on a microscopic setup to enable measurements, Fig. 4.

2.3.2

Advantages of Using Three-dimensional Microstructures

Apart from providing new formats, to make novel measurements, such miniaturized devices offer additional electroanalytical advantages. For example, traditionally, one perceived disadvantage of single cell analysis has been the difficulty of mitigating for biological variation, resulting in the need to repeat the measurement on many different individual cells. Micromachining and microfabrication offer the possibility of developing array technologies and the ability to collect data from multiple single cell sensing sites. More systematic advantages, which occur directly from miniaturization within a three-dimensional chamber include greatly reduced amounts of material used in each assay (with reduction in costs) as well as the ability to constrain the volume surrounding the cell. In this latter case, although the flux of ions or metabolites from single cells may be small, the diffusion distance to the electrode is short (10–100 μm). The result is that responses

Fig. 3 A single heart cell within a picoliter-scale microchamber, see Refs. [11, 13, 14] for more details, which has been used for the ultrasensitive amperometric measurement of purines (the cell is ca. 120 μm in length). The view is a plane, with the three electrodes of the amperometric device, fabricated on a glass microscope slide. The photograph shows clearly the large outer counter electrode, the inner, concentric working electrode (at which the active sensing process occurs), and finally the small (white) Ag/AgCl reference electrode, against which the working potential is measured. The cell is placed by micropipette into the chamber. The device operates as a miniaturized Clark electrode, measuring hydrogen peroxide produced as a consequence of an enzyme cascade, in solution. Purine and lactate release can be detected in real time from the single cell in femtomolar amounts [11, 13, 14].



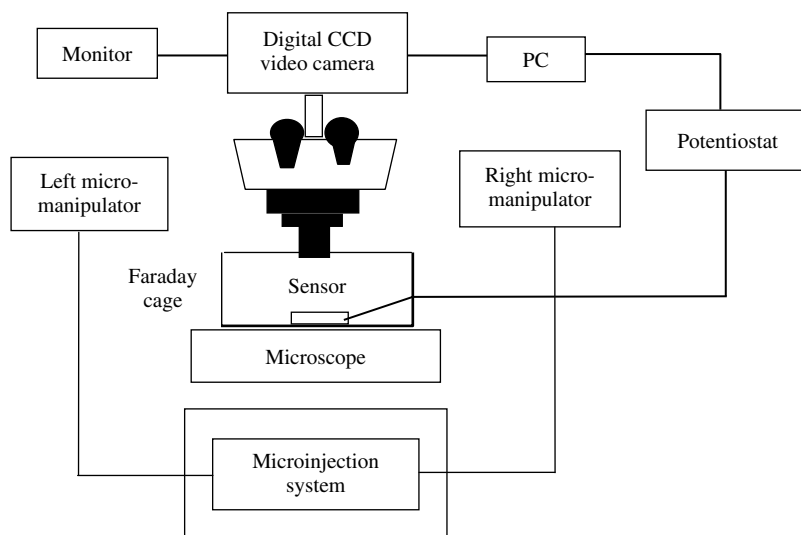


Fig. 4 High-sensitivity electrical measurements can be made by designing analytical instrumentation with suitable electrical shielding close to the single cell measurement chamber. The device shown has an integrated single cell analytical chamber, similar to the type shown in Fig. 3, together with shielded amplifiers and a PC interface. The setup is common to the measurements from a family of single sensors, currently being produced in the author's laboratories.

are fast (typically less than 10 s). For example, employing the Einstein equation, where l is distance; D , diffusion coefficient; and t , time:

$$l = (2Dt)^{1/2} \quad (1)$$

It takes only ~ 1.9 and ~ 7.5 s for oxygen and glucose, respectively, to diffuse $100\ \mu\text{m}$ within such a device, with none of the analyte lost to the bulk solution. Indeed, historically, one approach for single cell measurements has been to enhance mass detection limit by minimizing the analyte dilution, a technology that resulted in the development of the Cartesian divers for the measurement of oxygen consumption in pancreatic islet cells [32]. One future advantage of a reduced electrochemical path length is that the solution resistance falls correspondingly, and the measurements

of fast electrochemical reactions such as heterogeneous or homogeneous reaction become feasible.

2.3.3

Biosensors, Microfluidics, Microarrays, and Lab-on-a-Chip

The application of enzyme-linked assays with low-volume devices is analogous to the development of a microbiosensor, and has the ability to greatly extend the range of metabolites that can be measured from single cells [13, 14]. A further example of the use of enzyme assays involves the oxidase-linked enzyme-catalyzed oxidation of glucose in the presence of molecular oxygen by the flavoprotein, glucose oxidase [33] from groups of isolated kidney cells. As elsewhere [13, 14], the measurement procedure involves a Clark type oxygen (or

hydrogen peroxide electrode) “biosensor”, using an anode (or cathode), poised against a suitable reference electrode, enabling the determination of glucose flux as a function of distance from a free-standing microelectrode. Such studies illustrate the wide variety of both oxidase and dehydrogenase enzymes, which can now be readily linked to electrochemical assays. This offers the prospect of being able to perform whole cell analyses, using enzyme-linked assays, measuring different metabolites, at different stages of the cell cycle, a technique that was recently named “metabolomics”.

With recent advancement of micro-fabrication technologies in semiconductor industry, the construction of three-dimensional devices with electrodes incorporated within chambers and channels that can be used to constrain low volumes (typically nanoliters or below), and provide flow rates of less than microliters per minute. This technology, which has become synonymous with the term Lab-on-a-Chip, enables a variety of analytical measurements, including sample preparation, chromatographic separation, and detection (including electrochemical analysis) to be performed on the same device [34]. The technology provides the possibility of fast, cheap, and integrated analysis within closed fluidic systems. Fluids or cells can be moved by micropumps, or through a variety of techniques associated with electrochemical phenomena, including electroosmosis and dielectrophoresis, the latter being capable of moving fluids and different cell types independently of each other.

As an alternative to the closed fluidic systems described earlier, open microarrays structures can enable parallel measurements in which multiple manipulations are required for high throughput

cell-based assays and screens. Under such circumstances, it may be more realistic to introduce analytes and/or biological reagents by micropipetting, either manually [10, 11, 14] or by using either balanced pressure [13] or piezoelectric “ink-jet” systems [35]. In either case, there is the ability to dispense volumes of less than 10 pL (although there are significant differences in throughput). In these open-array experiments, in which the volume to be analyzed is <1 nL, there is an associated problem because of the loss of solvent by evaporation [10, 11, 14] (which can rapidly alter the effective concentration in a microchamber by an order of magnitude). The use of humidified environments and the ability to dispense and aspirate fluids through a layer of mineral oil have both been used to overcome such problems. At the limit of miniaturization, in order to explore diffusion as well as both electronic and chemical cross talk, 10 independently fabricated planar devices with volumes as low as ~4 pL have been used to provide possible insights into the limits of three-dimensional electroanalytical arrays [36].

2.4

Self-referencing Microelectrodes

Cells constantly, either actively or passively, transport chemicals across the plasma membrane and communicate with surrounding cells, generating chemical diffusion gradients around them. Measurement of such activities within gradients enables a better understanding of the cellular transport mechanisms. For example, calcium is regulated to nanomolar values in the cytosol by a complex interaction of cellular and plasma membrane pumps, reporters, channel activity, regional sequestration, and chemical

buffering. Such changes in ionic flux, although small, can have significant effects in the context of time-dependent drift of a local reference electrode. In order to overcome this, the technique of self-referencing microelectrodes [15–19] has been developed and applied to a number of

single cell methods. Central to the method is the need to use translational motion control systems comprising translation stages arranged in an orthogonal array and driven by linear stepper motors [37], thereby providing nanometer resolution of the microelectrode relative to the cell.

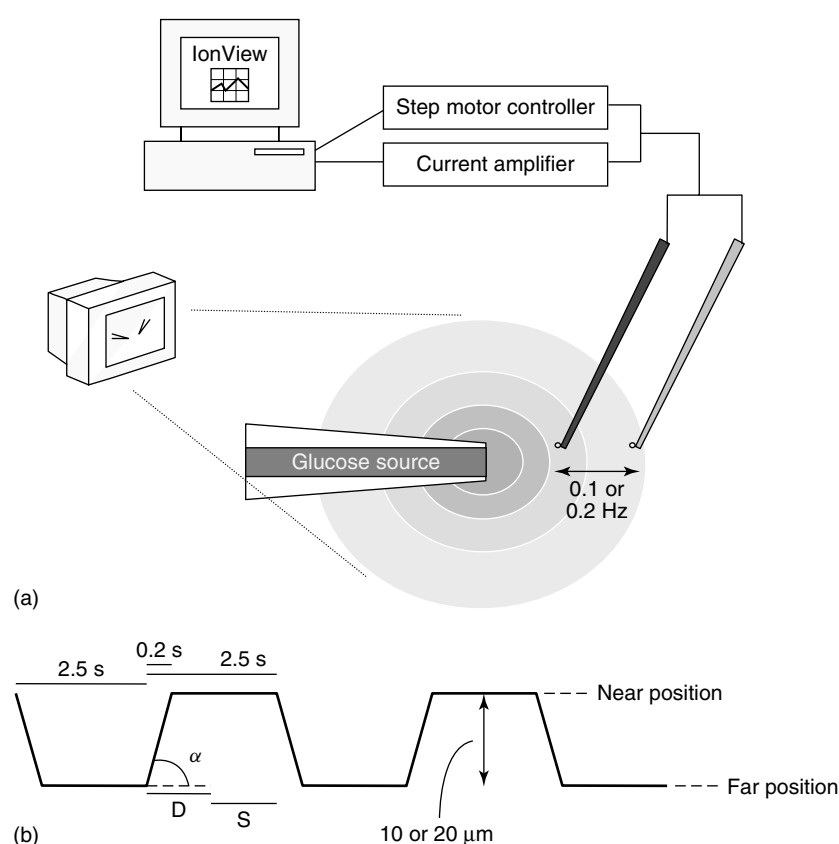


Fig. 5 (a) Illustration of the operation of the self-referencing glucose microsensor. A personal computer precisely controls the translational square wave frequency of sensor positioning allowing IonView software to report current changes referred to sensor movements in a gradient. The positioning of the sensor and its motion relative to the target site of interest is guided by observation with a video camera and a monitor. (b) Illustration of time-dependent sensor location and data processing in IonView software. The time corresponds to a translational square wave frequency of 0.2 Hz and an excursion distance of 10 μm . IonView automatically subtracts current values obtained at far position from those at near position. Whereas the first half of the values (denoted as D) at each position is discarded to eliminate the artifact from sensor motion and sensor response time, the second half (denoted as S) is sampled for mathematical subtraction. The speed of sensor movement is set by angle, α , and optimized to be $50 \mu\text{m s}^{-1}$.

In the self-referencing mode, the microelectrode is laterally oscillated between two points 5–20 μm apart at a square wave frequency of 0.1–0.3 Hz and data are collected at 100 Hz. The system setup and data processing are illustrated in Fig. 5 [15–19]. Data are reported as differences of voltage or current at two positions. The convention of the difference value is defined as $[(V, i_{\text{near}}) - (V, i_{\text{far}})]$, where (V, i_{near}) and (V, i_{far}) are the voltages or the currents at the near and far pole, respectively, from the cell. The difference values are directly related to fluxes, which is discussed later.

2.4.1

Ion-selective Microelectrodes

Ionic gradients can be measured potentiometrically with ion-selective microelectrodes [37–39] using, for example, a borosilicate capillary of 2–4- μm diameter, functionalized with an ionophore cocktail. The self-referencing ion-selective electrode reports differential voltages measured between two known positions. This information can be used to calculate the flux by employing Fick's first law, as

$$J = -D \left[\frac{C_{\text{av}} 10^{(C_f S \Delta V)} - C_{\text{av}}}{\Delta x} \right] \quad (2)$$

where S is the inverse of the Nernst slope in $(\text{mV})^{-1}$, C_{av} is the average concentration between two positions, ΔV is the difference in sensor response (mV), and x is the distance between the position of the two measurements. In a steep gradient generated from an artificial ion source, it is possible to observe a consistent disparity between concentration ratio and ΔV , which is because of the bandwidth of the system, particularly with regard to gradient reestablishment. This disparity

can be compensated for to obtain the values consistent with those obtained from stationary electrodes.

Self-referencing ion-selective electrodes have seen attractive applications in a diversity of medical problems. For example, the vacuolar-type H^+ -ATPase has been shown to play an important role in the acidification of the lumen of the proximal vas deferens, part of the male reproductive system. An acidic luminal fluid is required for the maintenance of sperm quiescence and for the prevention of premature activation of acrosomal enzymes during their storage in the epididymis and vas deferens. Proton secretion in the proximal vas deferens has been measured with the self-referencing technique (Fig. 6) [40]. Likewise, altered potassium homeostasis is indicative of dying cells, as the transplasma membrane potential is no longer maintained, as measured in both viable and nonviable embryos [41].

2.4.2

Self-referencing Amperometric Microelectrodes

The principle of the self-referencing technique can be easily applied to the measurements of redox active molecules. As the relationship between signal and concentration is mostly linear with amperometric microelectrodes, their fluxes around cells are calculated as follows:

$$J = -D \frac{C_f \Delta i}{S \Delta x} \quad (3)$$

where Δi is the difference current between two self-referencing positions and S is the sensitivity of a microelectrode in pA mM^{-1} , whereas other notations are the same as in Eq. (2). Self-referencing oxygen electrodes have been used for measurements in single pancreatic HIT

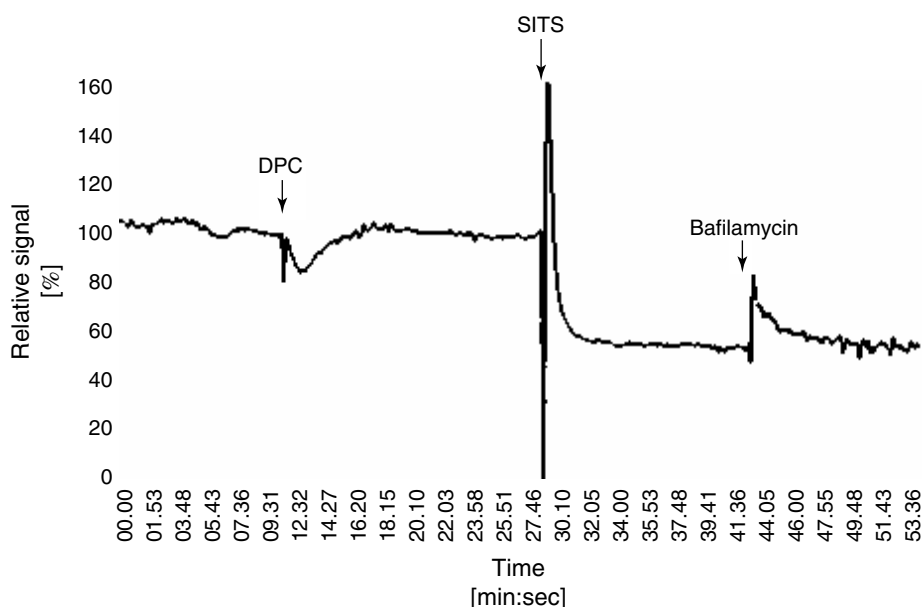


Fig. 6 Representative trace showing effects of diphenylamine-2-carboxylate (DPC), 4-acetamido-4'-isothiocyanostilbene-2,2'-disulfonic acid (SITS), and bafilomycin on rate of proton secretion. Addition of 0.5 mM DPC had no effect, and 1 mM SITS strongly inhibited

proton secretion to a level that was not further reduced by 1 μ M bafilomycin. An initial disturbance of proton gradient resulted from addition of SITS. Signal is expressed relative to control value.

cells [15, 16], shown in Fig. 7, as well as single neurons and single plant cells [17–19], and individual mouse embryos [42]. Most recently, using a size exclusion-based carbon fiber microelectrode, nitric oxide effluxes from single macrophages and damaged neural tissue have been measured [18].

The self-referencing technique can also be further expanded to the measurement of electrochemically dormant molecules, if enzymes are suitably incorporated within the microelectrodes, as biosensors. Oxidase enzymes are of special interest because the enzymes produce, in the presence of oxygen, hydrogen peroxide, which can be readily detected at an electrode. Under such circumstances, a glucose microelectrode should respond rapidly to

changing glucose concentrations when operated in a self-referencing mode [33]. Information about glucose consumption by pancreatic cells is of great medical importance because insulin secretion is metabolically driven in the pancreas, which is responsible for glucose homeostasis (e.g. using pancreatic HIT cell clusters [44]).

2.5

Scanning Probe Microscopy and Single Cell Measurement

The principle of rastering a microsensor across the surface and collecting high-resolution data is one which is now familiar, and is reviewed in detail in Volume X.

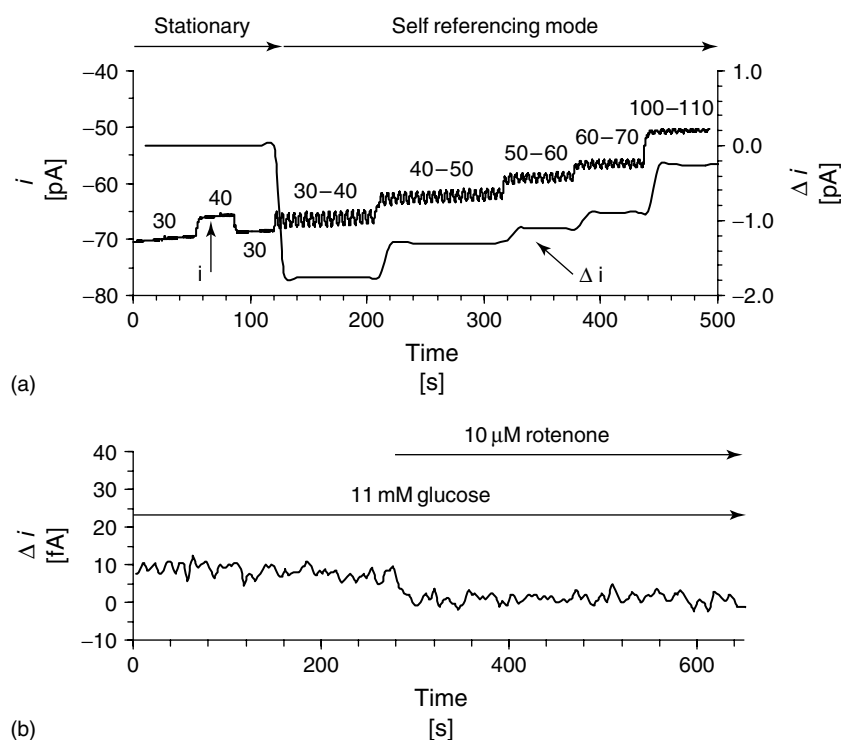


Fig. 7 (a) Real-time trace (i) and difference current (Δi) of oxygen current as a function of distance from an oxygen source (diameter $\sim 10 \mu\text{m}$) measured with a stationary and a self-referencing oxygen microsensor. In the self-referencing mode, the oxygen sensor was oscillated over a distance of $10 \mu\text{m}$ at a frequency of 0.2 Hz . The numbers are the relative distances from the oxygen source in microns. (b) Influence of rotenone on oxygen consumption by a single pancreatic HIT cell. The trace is an average representative of five measurements. The oxygen sensor was positioned $10 \mu\text{m}$ from the plasma membrane of the cell and oscillated in a square wave between 10 and $40 \mu\text{m}$ at a frequency of 0.2 Hz . Addition of rotenone significantly inhibited the mitochondrial respiration. A potential of -600 mV versus Ag/AgCl was applied to the oxygen sensor in a modified HEPES (4-(2-hydroxyethyl)-1-piperazine-ethane-sulphonic acid) buffer at 37°C . (Data from Ref. [43].)

Information concerning topology, heat, light, or the nature of the ionic species present can be readily obtained. The characterization and imaging of single cells with electrochemistry, known as SECM has recently been reviewed extensively [45] in order to explore the application of nanodes (or ultramicroelectrodes) in microscopy. In addition, there have been a variety of references to work that has

looked at model systems, to help interpret the results [46]. The technique of SECM is able to explore the flux and hence, concentration of a redox species by exploring the oxidation or the reduction current at a fixed distance (z) above the source (in this case, the cell or cells). The electrode is then scanned in the x and y directions in order to obtain a chemical image. Clearly additional data can be obtained by repeating

the scan while changing the distance (z) above the redox source. A variety of studies have looked at redox changes according either to their consumption of oxygen, where the tip acts as a Clark electrode; for example, Ref. [47], where it is possible to relate the consumption of oxygen with individual cell size, and cell growth within an embryo. Such work can be readily adapted and expanded in order to include mediators that are able to probe the transmembrane potential of bacteria [48].

In an alternative iteration of SECM, scanning ion-conductance microscopy (SICM) has also been used in order to image living cells in aqueous environments, using a microcapillary in order to probe ion flux [43, 49–51]. In such experiments, it is possible to gather information on the topology of the cell (as a function of its distance, z) from the microcapillary, leading to very high z -spatial resolution of the mouse melanocyte [43]. Such a technique readily leads to the possible estimation of the volume of individual cells including kidney, heart muscle, and cancerous breast cells [49]. In addition, small cellular structures, such as lamellipodia, dendrites, and microvilli have been resolved. The technique can readily be corroborated [50] by its use with simultaneous high-resolution optical microscopy involving scanned near field optical microscopy, SNOM (that operates as evanescent field imaging, below the limits of the diffraction limitation). Under such circumstances, it is possible to sarcomeric striations of the cardiomyocyte, indicating micron-scale resolution of subcellular organelles. This technique has recently been extended, such that when a single myocyte was patch-clamped [1–3] and imaged using SICM, it was possible to image a single ion channel, within a single cell [51].

2.6

Semiconductor Devices for Biological Sensing

In addition to using free-standing or scanned ion-selective electrodes based upon capillaries for ion measurements, as described earlier, photolithographic techniques have been used to adapt silicon devices (such as field-effect transistors) for use in biological measurements [9]. The techniques differs from those described for three-dimensional micromachining, in so much as silicon is being used as an active sensor. The vast majority of such devices are based upon the field-effect transistor, which are subsequently adapted as either ion-selective field-effect transistors (ISFETs) and light-addressable potentiometric sensors (LAPS). They are used to measure extracellular ion fluxes either in cell culture systems or clinical diagnostic tests [52–54]. Both ISFET and LAPS technologies have their strengths in the generic nature of their measurement systems (which also enable them to be used in the wider context of chemical imaging) and in the compatibility of their fabrication methods with industry standards. Devices used for cell screening either involve simple measurement of ions, or in a rather more complex manner, by measuring metabolic condition as a function of proton flux in LAPS technology [52–54]. As an alternative method, adapted metal oxide semiconductor field-effect transistors (MOSFETs), with the gate removed, have been used as a method to probe signaling in a variety of single cells, including both invertebrate and mammalian systems [55–58]. In a series of elegant experiments it has proved possible to use capacitive measurements to probe changes in the

cell's charged state, providing a method not only to stimulate but also collect information across real (in vitro) neural networks.

2.7

Corroborative Measurements for Single Cell Electrochemistry

In many cases, there is a need or a desire to be able to corroborate the single cell electrochemical measurement by use of an associated technique that can produce independent biological information. In some cases, this may be simple direct observation, so that events such as cell death or rigor (e.g. in the heart cell) that can be related directly to observed metabolic events [11, 13, 14]. Alternatively, fluorescence measurements involving the use of an optical fiber have been used for the measurement of ions, while simultaneous electrochemical measurements have greatly enhanced the biological information [28]. The marriage of oxygen or glucose microelectrodes to calcium fluorescence measurement in pancreatic islets has been observed [33]. The self-referencing electrochemical technique can also be linked to fluorescence measurements or used in conjunction with patch clamp [55–58]. Alternatively, the voltage clamping of a cell has been combined SICM to provide evidence for the spatial location of individual ion channels in the cell membrane, while the cell is held under electrochemical control [51]. Sub-single cell information has also been resolved using either SNOM [50] and subsequently related to electrochemical measurements of comparable resolution. Likewise, SECM data has been closely related to the topology of the observed cell structures [45].

2.8

Future Prospects

The further miniaturization of the electroanalytical sensors within chambers is inevitable. In future assays volumes of 10–500 pL will become more routine, and ultimately, the volume in an analytical chamber may be reduced sufficiently such that it may be possible to implement the application of single molecule electrochemical detection [59, 60] within these structures. Reduction in the size of the analytical chamber [11, 13, 14] and introduction of a variety of self-referencing techniques [15, 16, 18] have made it possible to make reliable single cell measurements, which carry forward the basic concepts from patch clamping [1–3], but enable a variety of metabolites to be measured. Volumes have been greatly reduced [36, 61] in such measurement systems, thereby enabling increasingly sensitive absolute measurements to be made. By reducing the time base between measurement pulses within the microsecond regime, it will be possible in the future to constrain the effective diffusion length within the solution, and thereby make measurements in volumes as small as 20 fL [62].

Coupled to the development of smaller sensors using nanotechnology, with increased functionality using biosensors, and with the development of methods for constraining lower volumes, the present challenge is the integration of fast, high-bandwidth, high-sensitivity instrumentation close to the sensors, for parallel recording from single cells. In this respect silicon may provide one possible route forward [55–58]. Undoubtedly, in the future, the greatest challenges will involve the development of techniques that combine miniaturization and molecular counting with integration of microfluidics

and biosensor technology and hence the automation of ultrasensitive single cell assays. Such technology would have significant impact in drug discovery and biotechnology as a whole, in providing a method to probe metabolic profiles of single cells in a high throughput format.

References

- O. P. Hammill, A. Marty, E. Neher et al., *Pflugers Arch.* **1981**, 391, 85–100.
- B. S. Khakh, X. R. Bao, C. Labarca et al., *Nat. Neurosci.* **1999**, 2, 322–330.
- B. Sakmann, E. Neher, *Annu. Rev. Physiol.* **1984**, 46, 455–472.
- D. M. Cannon Jr., N. Winograd, A. G. Ewing, *Annu. Rev. Biophys. Biomol. Struct.* **2000**, 29, 239–263.
- K. McCormack, R. Davies, *Pain* **1996**, 68, 5–11.
- C. Kranz, G. Wittstock, H. Wohlschlager et al., *Electrochim. Acta* **1997**, 42, 3105–3111.
- R. M. Wightman, E. Strope, P. M. Plotsky et al., *Nature* **1976**, 262, 145–147.
- R. M. Wightman, *Anal. Chem.* **1981**, 53, A1125–A1134.
- M. Lambrechts, W. Sansen, *Biosensors: Microelectrochemical Devices*, Institute of Physics Publications, New York.
- R. A. Clark, P. B. Hietpas, A. G. Ewing, *Anal. Chem.* **1997**, 69, 259.
- C. D. T. Bratten, P. H. Cobbold, J. M. Cooper, *Anal. Chem.* **1997**, 69, 253–258.
- D. O. Wipf, A. J. Bard, *Anal. Chem.* **1992**, 64, 1362–1367.
- X. Cai et al., *Anal. Chem.* **2002**; accepted.
- C. D. T. Bratten, P. H. Cobbold, J. M. Cooper, *Anal. Chem.* **1998**, 70, 1164–1170.
- S. -K. Jung, K. Hammar, P. J. S. Smith, *Biol. Bull.* **2000**, 199, 197–198.
- D. M. Porterfield, R. F. Corkey, R. H. Sanger et al., *Diabetes* **2000**, 49, 1511–1516.
- D. M. Porterfield, J. D. Laskin, S. -K. Jung et al., *Am. J. Physiol.* **2001**; in press.
- S. C. Land, D. M. Porterfield, R. H. Sanger et al., *J. Exp. Biol.* **1999**, 202, 211–218.
- S. M. Kumar, D. M. Porterfield, K. J. Muller et al., *J. Neurosci.* **2001**, 21, 215–220.
- C. Amatore, S. Arbault, D. Bruce et al., *Faraday Discuss.* **2000**, 116, 319–333.
- R. M. Wightman, D. O. Wipf in *Electroanalytical Chemistry* (Ed.: A. J. Bard), Marcel Dekker, New York, 1989, pp. 267–353, Vol. 15.
- S. Arbault, P. Pantano, J. A. Jankowski et al., *Anal. Chem.* **1995**, 67, 3382.
- Y. Y. Lau, T. Abe, A. G. Ewing, *Anal. Chem.* **1992**, 64, 1702–1705.
- G. Chen, D. A. Gutman, S. E. Zerby et al., *Brain Res.* **1996**, 733, 119–124.
- Q. Xin, R. M. Wightman, *Brain Res.* **1997**, 776, 126–132.
- M. A. Bunin, C. Prioleau, R. B. Mailman et al., *J. Neurochem.* **1998**, 70, 1077–1087.
- P. A. Garriss, J. R. C. Christensen, G. V. Rebec et al., *J. Neurochem.* **1997**, 68, 152–161.
- Q. Xin, R. M. Wightman, *Anal. Chem.* **1998**, 70, 1677–1681.
- C. D. Paras, R. T. Kennedy, *Electroanalysis* **1997**, 9, 203–208.
- C. A. Aspinwall, L. Huang, J. R. T. Lakey et al., *Anal. Chem.* **1999**, 71, 5551–5556.
- G. T. A. Kovacs, K. Petersen, M. Albin, *Anal. Chem.* **1996**, 68, 407A–412A.
- C. Hellerstrom, *Endocrinology* **1967**, 81, 105–112.
- S.-K. Jung, L. M. Kauri, W.-J. Qian et al., *J. Biol. Chem.* **2000**, 275, 6642–6650.
- J. Harrison et al., *Anal. Chem.*, submitted.
- A. V. Lemmo, J. T. Fisher, H. M. Geysen et al., *Anal. Chem.* **1997**, 69, 543–551.
- P. Yu, G. S. Wilson, *J. Chem. Soc., Faraday Discuss.* **2000**, 116, 305–317.
- P. J. S. Smith, K. Hammar, D. M. Porterfield et al., *Microsc. Res. Tech.* **1999**, 46, 398–417.
- P. J. S. Smith, J. R. Trimarchi, *Am. J. Physiol. Cell Physiol.* **2001**, 280, C1–C11.
- P. J. S. Smith, R. H. Sanger, L. F. Jaffe, *Methods in Cell Biology*, Academic Press, New York, 1994, pp. 115–134, Vol. 40.
- S. Breton, K. Hammar, P. J. S. Smith et al., *Am. J. Physiol.* **1998**, 275, C1134.
- J. R. Trimarchi, L. Liu, D. M. Porterfield et al., *Zygote* **2000**, 8, 15–24.
- J. R. Trimarchi, L. Liu, D. M. Porterfield et al., *Biol. Reprod.* **2000**, 62, 1866–1874.
- Y. E. Korchev, M. Milovanovic, C. L. Bashford et al., *J. Microsc.* **1997**, 188, 17–23.
- S.-K. Jung, R. H. Sanger, P. J. S. Smith et al., *Anal. Chem.* **2001**; in press.
- T. Yasukawa, T. Kaya, T. Matsue, *Electroanalysis* **2000**, 12, 653–659.
- C. A. Wijayawardhana, G. Wittstock, H. B. Halsall et al., *Anal. Chem.* **2000**, 72, 333–338.

47. H. Shiku, T. Shiraishi, H. Ohaya et al., *Anal. Chem.* **2001**, 73, 3751–3758.
48. C. Cai, B. Liu, M. V. Mirkin et al., *Anal. Chem.* **2001**; accepted in press.
49. Y. E. Korchev, J. Gorelik, M. Lab et al., *Biophys. J.* **2000**, 78, 451–457.
50. Y. E. Korchev, M. Raval, M. Lab et al., *Biophys. J.* **2000**, 78, 2675–2679.
51. Y. E. Korchev, Y. A. Negulyaev, C. R. W. Edwards et al., *Nat. Cell Biol.* **2000**, 2, 616–619.
52. P. Skladal, *Electroanalysis* **1997**, 9, 737–745.
53. A. Fanigliulo, P. Accossato, M. Adami et al., *Sens. Actuators, B* **1996**, 32, 41–48.
54. H. Uchida, W. Y. Zhang, T. Katsube, *Sens. Actuators, B* **1996**, 34, 446–449.
55. P. Fromhertz, A. Offenhauser, T. Vetter et al., *Science* **1991**, 252, 1290, 1293.
56. D. Braun, P. Fromhertz, *Phys. Rev. Lett.* **2001**, 86, 2905–2908.
57. G. Zeck, P. Fromhertz, *Proc. Natl. Acad. Sci. U.S.A.* **2001**, 98, 10 457–10 462.
58. S. Vassanelli, D. Fromhertz, *J. Neurosci.* **1999**, 19, 6767–6773.
59. F. F. Fan, J. Kwak, A. J. Bard, *J. Am. Chem. Soc.* **1996**, 118, 9669–9675.
60. F. F. Fan, A. J. Bard, *Science* **1995**, 267, 871–874.
61. O. Shirihai, P. Smith, K. Hammar et al., *Glia* **1998**, 23, 339–348.
62. M. M. Collison, R. M. Wightman, *Science* **1995**, 268, 1883–1885.
63. Y. T. Kim, D. M. Scarnulis, A. G. Ewing, *Anal. Chem.* **1986**, 58, 1782–1786.
64. R. Nuccitelli, Vibrating probe technique for studies of ion transport in *Noninvasive Techniques in Cell Biology* (Eds.: J. K. Foskett, S. Grinstein), Wiley-Liss, New York, 1990, pp. 273–310.
65. P. J. Kinlen, V. Menon, W. Ding, *J. Electrochem. Soc.* **1999**, 146, 3690–3695.
66. C. A. Siedlecki, R. E. Marchant, *Biomaterials* **1998**, 19, 441–454.

3 Bioelectronics

Christiane Ziegler
Department of Physics, University of Kaiserslautern, Kaiserslautern, Germany

3.1	Scope	53
3.2	Brief Summary of Electronic Signal Transduction in the Neural System	53
3.3	Biology Meets Electronics: Applications	57
3.3.1	Bioelectronic Noses	57
3.3.1.1	Comparison between Biological and Electronic Noses	57
3.3.1.2	Specific Example: Neural Network Biosensors	59
3.3.2	Biocomputer	64
3.3.3	Short Summary of In Vivo Applications	65
	References	65

3.1 Scope

No overall accepted definition for bioelectronics exists so far. In Ref. [1], one can find the following list of topics that may be related to bioelectronics:

- Biological materials for electronics;
- Biological-inorganic hybrids of relevance for electronics;
- Biocompatible electronic devices such as pacemakers and other electronic implants;
- In vivo sensors and other sensors for biologically relevant processes;
- Sensors based on biological materials or biological processes;
- Artificial sensing devices such as eyes, ears, noses, and so on;
- Materials for electronics synthesized by biological processes rather than by conventional synthesis;
- Materials inspired by biology and useful for electronics;
- Algorithms inspired by biology;
-

Often, only the first two – and sometimes, additionally, biosensors based on nerve cells or nerve cell tissues – are included in the definition. In this short review article, bioelectronics will be restricted to in vitro electronic devices

in which neural cells are involved as biological component, that is, the coupling of an electronically active biological system to an artificial electronics. After a short summary of the basics of electronic signal transduction in the nervous system (Sect. 3.2), applications such as natural neural network sensors and computer devices (Sect. 3.3) are discussed.

3.2 Brief Summary of Electronic Signal Transduction in the Neural System

Signals from the outer world are perceived by animals through the nervous system. Receptor cells in the sensing organs (eye, ear, nose, tongue, skin) convert outside signals (i.e. light, noise, odorant molecules, taste, pressure, temperature) into electrical signals, which are transported by neural cells to the brain (sensory system). From the brain, electrical signals are then transmitted to muscle cells through the motor nervous system.

The nervous system is divided into two parts: the central nervous system (CNS), which comprises the brain and the spinal cord, and the peripheral nervous system (PNS), which includes the rest of the nervous tissue.

Neural cells consist of four distinct regions: the cell body, the dendrites, the axon, and the synapses (Fig. 1). The cell body is the metabolic center of the cell, that is, it keeps the cell living

and functioning. The dendrites are small branches extending from the cell body and are the main receptive part of the cell. The axon is a long tube (up to 1 m in humans), sometimes covered by

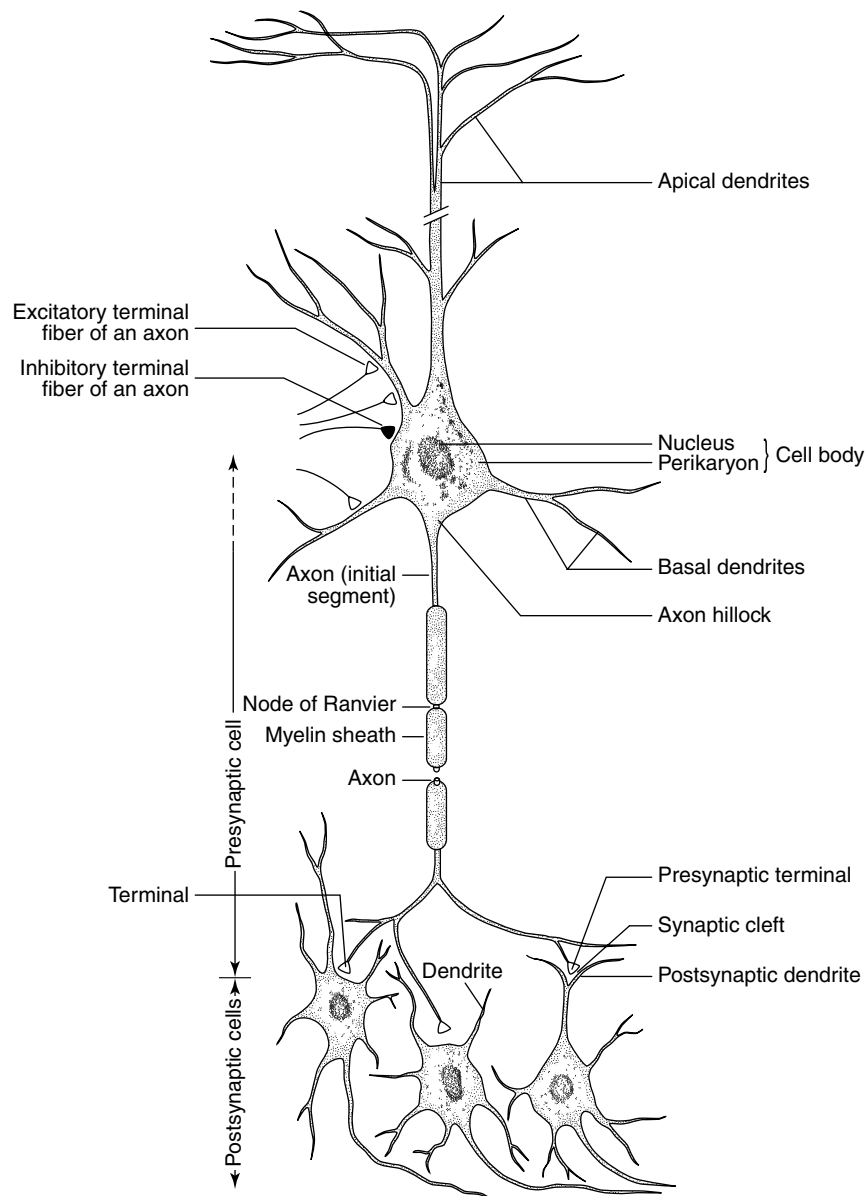


Fig. 1 Schematic view of the morphology of a typical neuron and its functional regions [2].

an insulating myelin sheath, which is regularly interrupted by the so-called nodes of Ranvier in which almost all of the ion channels (see the following text) are located. The synapses extend from the end of the axon and form the connections to other nerve or to muscle cells. In the membrane of the neural cell, there are proteins forming membrane-spanning ion channels for Na^+ , K^+ , Ca^{2+} , and Cl^- , which are either voltage- or ligand-gated. Voltage-gated means that changes in potentials over the membrane cause conformational changes in the protein structure and hence to an opening or closing of an inner transport channel (pore). Ligand-gated channels do the same upon binding a molecule, the ligand, to its receptor site.

The ion concentrations inside and outside the cell are vastly different for the single species. The K^+ concentration is much higher inside the cell, whereas the Na^+ concentration is much lower. Although there is electroneutrality inside the cell as well as outside, these different concentrations and also the different permeabilities through the membrane lead to an electrochemical potential across the membrane. For an exact calculation of the membrane potential, the concentrations and permeabilities of all ions as well as the diffusion currents have to be taken into account. The resting potential (i.e. when all channels are closed and hence no signal is transported along the axon) is -60 to -70 mV between the inner and outer cell compartment. This potential is near the resting potential for K^+ alone, that is, without taking the potentials of the other ions into account, because of the high permeability of the membrane for K^+ .

Because of a signal, from the outer world or from another nerve cell, (see in following text) a so-called action potential can

be initiated at the axon hill near the cell body (Fig. 2). During this action potential, the membrane potential is switched to around $+30$ to $+40$ mV for a short time (1 ms). This is generated because voltage-gated Na^+ channels (see in following text) open for a short time and therefore positive sodium ions can flow into the cell (along its concentration gradient), which raises the membrane potential. Because of this voltage change, the Na^+ channels close again and K^+ channels open up, which cause potassium to flow out of the cell (along the concentration gradient for K^+), which restores the negative inner potential. This action potential acts on other voltage-gated Na^+ channels located further down the axon where the next action potentials are generated in the same way with a frequency of about 1 kHz. The myelin sheath serves as an electrical isolation and prevents the potential from dying out due to membrane leakage. Therefore, in particular, long axons are covered by a myelin sheath. As soon as the action potential reaches the synapses, voltage-gated Ca^{2+} channels are opened. This leads to the excretion of membrane vesicles containing small chemical substances, the neurotransmitters, into the synaptic cleft between the (presynaptic) nerve cell and the next (postsynaptic) cell. These neurotransmitters diffuse through the cleft and bind to receptors that are usually located on the dendrites of the postsynaptic cell. Ligand-gated Na^+ channels open and lead to a membrane potential. If several of such channels are open, the membrane potential can become large enough to generate an action potential through opening of voltage-gated Na^+ channels (see preceding text). There are not only excitatory synapses, as described above, but also inhibitory ones that do not transmit, but block action potentials between

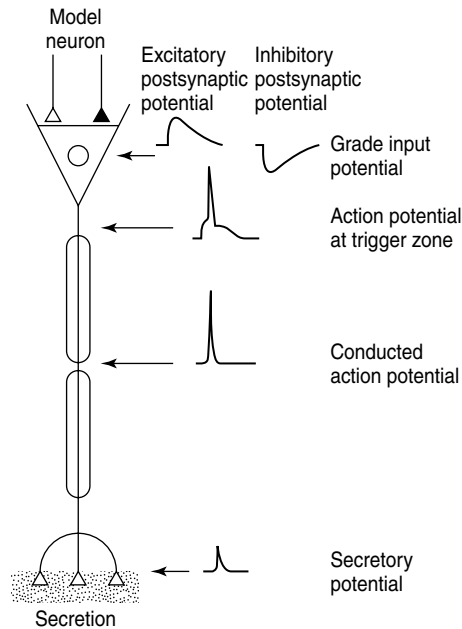


Fig. 2 Signals arising along the functional regions of a neuron [2].

two cells through the generation of a negative membrane potential. This inhibition is important to filter the information flooding between our sensing organs and our brain. All information coming from the different synapses is integrated by the cell. This means that there are two types of electrical signals by which information can be coded and transported: There are graduated membrane potentials building up near the synapses or at receptor cells. Graduated means that they can have any potential, which results from an addition of all positive (excitatory) or negative (inhibitory) potentials formed at the synapses. If a certain threshold potential is reached, the voltage-gated Na^+ channels at the axon hill can open and an action potential is initiated. The action potentials themselves are relatively stereotypic, that is, they exhibit always the same shape. Information is only coded

in the number and frequency of action potentials.

Details of signal transduction by neural cells can be found in a large variety of textbooks [2].

Nerve cells do not divide, and cut interconnections between nerve cells in the CNS are not able to regenerate, which leads to dysfunctions after brain or spinal cord injuries. This makes it also difficult to utilize these cells in technical devices because no cell lines can be established. This means that only primary cell cultures, that is, cells that come directly from a living animal, can be used. There are some neuron-like cell lines in which hybridoma cells between a type of cancer cells and a neural cell are used. Cancer cells divide easily and hence cell lines can be established. However, these hybridoma cell lines do not easily form synaptic junctions. Because without synapses there

is no signal transduction between cells, such single cells are limited in their use in bioelectronic applications. All applications that are referred to in Sect. 3.3 are therefore based on primary cell cultures.

3.3

Biology Meets Electronics: Applications

3.3.1

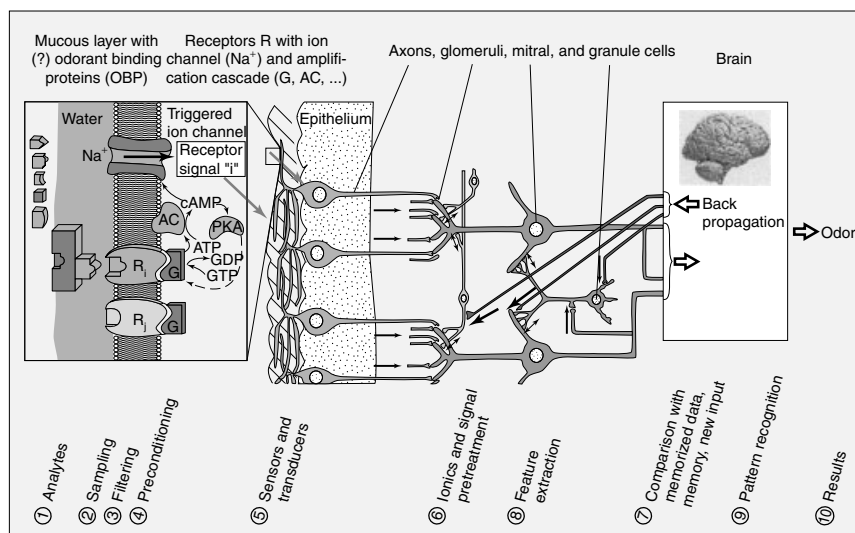
Bioelectronic Noses

3.3.1.1 Comparison between Biological and Electronic Noses

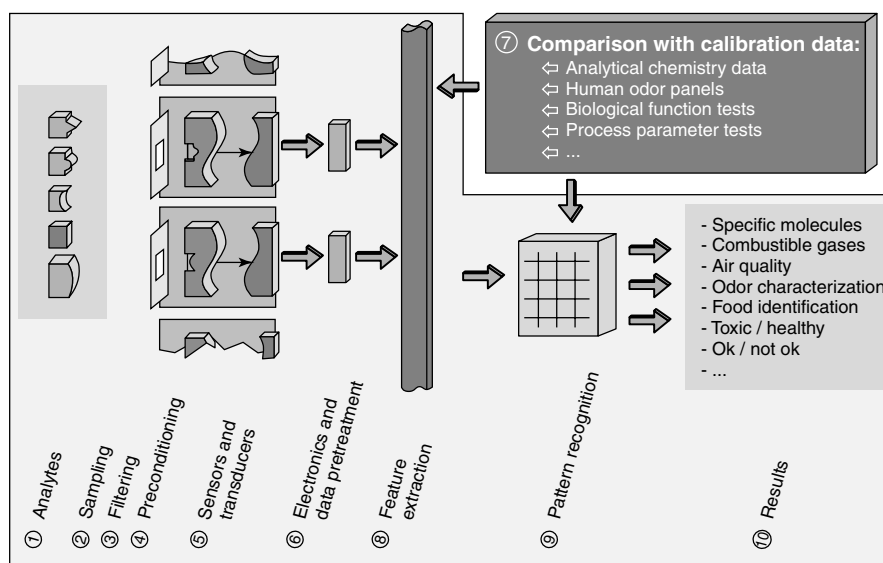
Our sense of smell is able to recognize and discriminate, with great sensitivity and accuracy, thousands of volatile molecules of diverse structure. Odorant stimuli at concentrations as low as a few parts per trillion can be detected. The general sensation of odors in biology, however, not only includes human odor sensation but also the odor sensation of animals in air and in water with their completely different sensitivity and selectivity patterns to detect chemical species in the gas and liquid state. Since we do not know details of odor perception in the various animals, the most general definition of a nose is as a detection system to sense any molecule in the gas or liquid state. The odor patterns generated by such odorant-detector systems evidently depend on their biological and biochemical architecture (see schematic Fig. 3a). These also depend on the individual training, learning, and preconditioning of the systems, on the environment, and so on.

In the first step of odor sensation, the gaseous analytes ①, which are typically small, mostly hydrophobic molecules with masses up to 300 amu, reach the olfactory region at the posterior of the nose. Sampling ② is done by inhalation with

different speeds. Dust and other particles are filtered ③ in the nostrils. A second step of filtering and sampling is performed by the mucous membrane, which is covered with a thin film of water. The hydrophobic odorants have to pass this barrier, which is probably promoted by so-called odorant binding proteins to reach the surface of an olfactory signal cell in the epithelium. The interaction with the odorant binding proteins may also lead to some preconditioning ④, because different interactions may occur. The following steps all happen on the surface or in the olfactory cell. The odorant molecules will interact specifically with (in humans) about 800 different receptor proteins embedded in the membrane of the 6 million neurons. This molecular recognition can be depicted as the essential step of sensing ⑤. The binding of the odorants triggers complex intracellular signal cascades, which can lead to action potentials. This step can be described as a transduction ⑤ of the former chemical information into an ionic, that is, an electrical information. In the further data treatment, the signals coming from this huge number of different olfactory cells must be guided by their axons to the so-called glomeruli in which a large number of axons meet. This is a kind of signal pretreatment ⑥, because the signals coming from one type of receptors are sent only to one (or two) of the different glomeruli. Or, in other words, axons of one type of receptor meet in one glomerulus. (This means that the number of glomeruli reflects the number of different receptors in a specific animal.) The feature extraction ⑧ is done by a backpropagation from the human brain by special centrifugal fibers, manipulating all steps of signal processing. The comparison with memorized data ⑦, for example, with



(a)



(b)

Fig. 3 (a) Schematic representation of the signal cascade in the human nose, which is involved in recognizing odor molecules (adapted from Ref. [3]). (b) Schematic representation of electronic nose systems, which are realized by modular sensor systems (adapted from Ref. [3]).

previously obtained odor sensations, and the pattern recognition ⑨ is done in the brain. This leads to a perception of the odor as the final result ⑩, which should

be related directly to the molecules at the beginning of the odor sensation process. (For a more detailed review, see Ref. [3] and references therein.)

An “electronic nose” is a technical chemical sensor system, which shows the same 10 principal steps of odor recognition (Fig. 3b). However, although general similarities may be seen, any more detailed view illustrates drastic differences between the biological and the technical system (see Refs. [4, 5] and references therein).

The most important part is the single sensor element, which consists of a chemically sensitive coating enabling molecular recognition and of transducers enabling signal conversion. The specific recognition site on a certain transducer is the key component of the total sensor system. Evidently, a large amount of different materials with different recognition sites can be utilized already today for chemical and biochemical sensor systems. The simpler the structure of these materials is, the easier it is to optimize their long-term stability. The design of bioelectronic noses, which utilize biological function units, is evidently more complex. Usually, their stabilities are limited and hence time-dependent signal outputs cause serious problems in calibration procedures. As a result, corresponding systems are not yet commercially available. Significant progress is expected by screening systematically new materials with stabilized biological functions that may be either biomimetic recognition sites or biological systems and by screening systematically new materials, which interface the biological function units with inorganic transducer substrates. So far it is not clear whether biomimetic structures with their enhanced stability will be superior to the evolutionary optimized biological structures that, however, rely on self-repair of their inherently unstable molecules.

Commonly used transducers monitor chemical compositions by monitoring phenomenological sensor properties such as

changes in mass, conductivity, capacity, optical parameters, or temperature. Examples include interdigital structures (for complex impedance measurements), thermopiles (for temperature measurements), piezoelectric oscillators based upon bulk, surface, or plate waves (for mass measurements), optics components (for optical measurements), multielectrode arrays (for electrochemical measurements or for electrical connections to axons in nerve systems), or arrays of capacitive sensor elements.

Table 1 illustrates, very schematically, the hierarchy in the description of bioelectronic noses with an increasing complexity concerning structures and functions. A bioelectronic nose will not compete with our human nose but will fulfill dissimilar functions: The detection of molecules that are toxic, of molecules that do not smell, and, most importantly, an odor detection that is independent of individual influences on a living being. On the other hand, a bioelectronic nose (if compared to an electronic nose with simple inorganic or organic recognition structures) can take advantage of some of the properties of the biological system if it utilizes living cells, in particular the amplification of small signals and self-repair mechanisms. This makes the use of cells superior to the use of single biomolecules, however, at the expense of an enhanced complexity of the system. In the following section, one specific example will be shown, which is a bioelectronic system even in a narrow definition of bioelectronics (cf. Sect. 3.1).

3.3.1.2 Specific Example: Neural Network Biosensors

A real biohybrid nose would consist of odorant receptor cells coupled to an electronic read-out unit. However, owing to the difficulties in establishing highly stable

Tab. 1 Molecular hierarchy in the complexity of structures and functions, which may be used in the design of bioelectronic noses. The respective parts of the biological nose are given in *italics*

-
- inorganic structures and organic molecules
 - biomimetic recognition sites
 - biological recognition sites
 - odorant binding proteins*
 - olfactory receptors*
 - recognition sites embedded in biological membranes
 - olfactory receptors in cilia*
 - recognition sites in membranes with subsequent signal amplification
 - whole cells
 - olfactory cells*
 - cell arrays
 - neural tissue
 - olfactory mucosa*
 - neural tissue with subsequent signal processing step
 - olfactory mucosa and olfactory bulb*
 - brain
 - olfactory mucosa, olfactory bulb, and olfactory cortex*
 - animals
 - humans
 - odor sensation of distinguished test persons*
-

odorant receptor cell cultures, nonsensory nerve cells have to be used today as an alternative. Although, with some exceptions, no specific odor response can be expected by such networks, also nonsensory neurons are very sensitive to a large variety of neuroactive compounds added to the culture medium [6]. Neuroactive compounds can be defined as water-soluble molecules that can influence the sensitive electrophysiological mechanisms of nerve cells [7]. Neuroactivity can have a variety of reasons because all the steps of action potential generation and transduction as described in Sect. 3.2 may be influenced. Furthermore, changes in the metabolism of the cell, which are brought about not only by chemicals but also physical parameters

like the temperature, can cause changes in the electrical activity of the neuron. Many interesting neuroactive compounds either act as ion channel blocker or block receptors in the synaptic cleft, mimicking neurotransmitters.

Nerve cells from the CNS of mammalian embryos grown in culture on microelectrode arrays [8–11] or on field-effect transistors [12] show spontaneous native activity patterns (i.e. action potential generation) after several days in culture. These neurons from embryos still have the ability to form synaptic connections (cf. Sect. 3.2) and can form nerve cell networks.

The effects of an altered environment can be studied by detecting changes in the spontaneous native action potential patterns. These changes are often substance and concentration specific (see below) and, most importantly, histiotypic.

As in nature, networks are relatively fault tolerant concerning, for example, changes in synaptic connections. All these effects can be measured by the change of membrane potential during an action potential (cf. Sect. 3.2). This potential has a direct influence on the gate of a field-effect transistor, or, in another device, it influences the capacity between a microelectrode and the axon, which can be measured with a.c.-coupled amplifiers with high input impedances. All measurement conditions have to be chosen so that *no* electrochemical reaction takes place at the electrode surface in order to avoid the formation of poisoning chemicals.

The contact between the cells and these electrodes is one of the very crucial points in such devices. Neural cells do not form a direct contact to metals or to silicon. These technical surfaces have therefore to be coated with a biocompatible overlay. There are different concepts that include positive charges provided by amino

silanes [13], artificial amino acids such as poly-D-lysine, or biological molecules such as laminin, which is an anchor protein in the extracellular matrix of cells. Because a tight contact of the cell to the electrode is advantageous as it minimizes signal loss into the electrolyte, new concepts aim at using only the short active amino acid sequences, the so-called epitopes, of laminin [14, 15] or even simpler molecules [16]. Such molecules can be used as derivatives with an electropolymerizable group such as hydroxyphenyl or pyrrol. In this case, such adhesion molecules can be immobilized directly at the electrode surfaces by applying a potential, therefore restricting the nerve cells onto the regions of measurement. However, there is still a huge amount of work to be done because each type of cell may react differently to the artificial environment so that no general concept for neural cell adhesion is at hand today. And restricting the adhesion area is, in most cases, not stable over a longer period, that is, the cells overgrow other regions of the substrate.

As it is now possible to maintain neural networks in electrophysiologically active and pharmacologically responsive states for over 9 months *in vitro* [17, 18], such systems have become reliable candidates for the detection and characterization of biologically significant effects of a great variety of chemical substances. An overview of tests performed till 1997 is given in Refs. [7, 18], a recent example (testing of cannabinoid agonists) can be found in Ref. [19]. Although still at an experimental stage, instruments for extracellular recording are commercially available [20–22]. Reported applications are fundamental aspects of cell networks [23], as well as pharmacological [18, 19] and toxicological response studies [18, 24], qualitative [7, 8], and even quantitative biosensing purposes

if artificial neural networks (ANNs) are used to evaluate the data from the natural neural network [25, 26]. Pharmacological response has also been studied in heart muscle cells, which give larger signals as compared to neural cells and are hence easier to study [27].

Some examples shall illustrate the concept of using natural neural networks for an analytical purpose. Figure 4 shows the toxicological effects of two neurotoxins, trimethyltin chloride (TMTC), and lead acetate (PbAc) [18]. The presented data are two different variables that can be derived from the measured voltage spikes of the network in percent of the value of the native network without any added neurochemicals. These variables are the total spike activity (corresponding to the number of action potentials) and the burst rate (i.e. the number per minute of so-called bursts, in which high spike activity is recorded, for details of signal processing, see Refs. [7, 18]). The activity of the network is completely inhibited after addition of 4 μM of TMTC or 2 mM of PbAc, but is restored after washing. This clearly shows that these chemicals act reversibly at these concentrations in the nervous system. Such studies are of general interest when new substances are developed, which can come into contact with the human nervous system, such as pharmaceuticals, body care products, but also pesticides and others.

Figure 4 also shows that taking different aspects (variables) of the network activity into account, one may get fingerprints of the different substances because they show different concentration dependencies.

The same holds for other neurochemicals. Bicuculline and strychnine both block inhibitory receptors in the synaptic cleft (see Sect. 3.2). This induces a

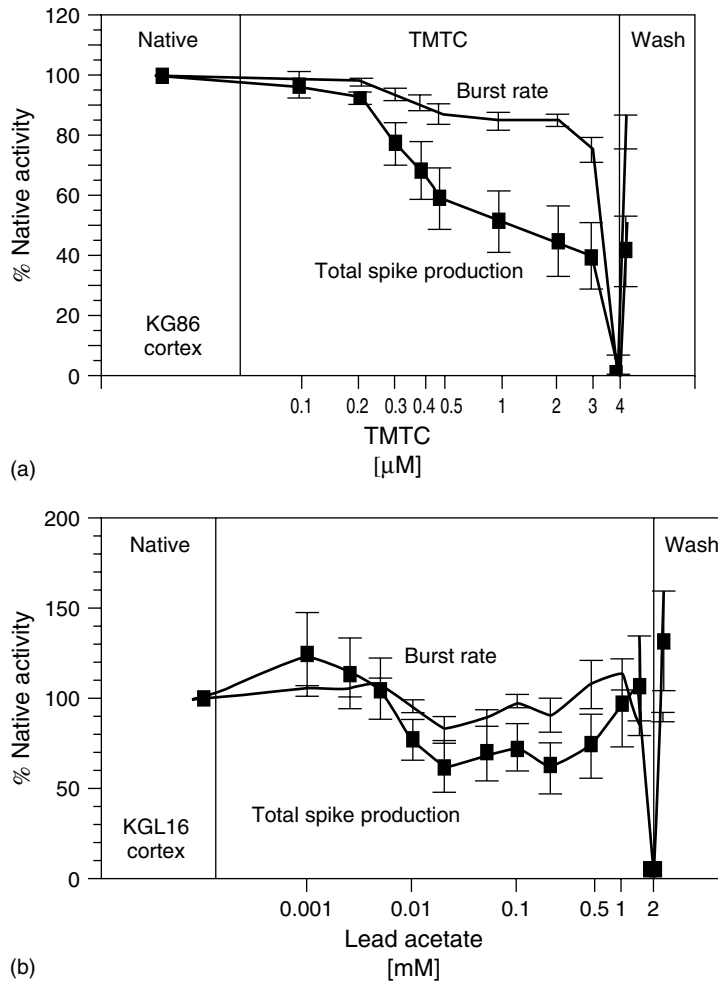
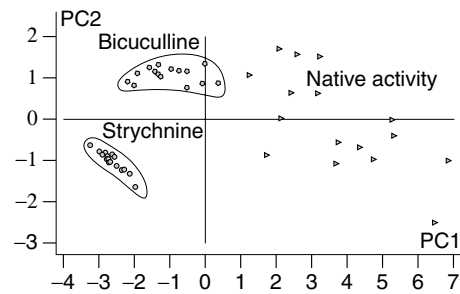


Fig. 4 Different recordings from networks of auditory cortex tissue upon application of trimethyltin (TMTc) (a) and lead acetate (b). For details, see text and Ref. [16].

higher network activity (because the inhibition does not work properly) at low concentrations and an oscillatory network response (similar to an epileptic attack) at higher concentrations. However, the oscillation starts at different absolute concentrations for the two substances and also the concentration dependency of the different measurable variables is different. Such differences can be evaluated in a

variety of data-processing methods, for example, in a so-called principal component analysis [28]. In the principal component analysis, a problem of high dimensionality is projected to only two dimensions so that a visualization of the results is possible. This means here that instead of an 11-dimensional coordinate system [11 different measurement variables (such as the number of action potentials per minute)

Fig. 5 Principal component analysis PCA of data recorded on embryonic mice spinal cord cultures in the native state, upon application of 60- μM bicuculline and, after a washing cycle, of 25- μM strychnine. PC1,2 are the principal components 1 and 2. Classification of data is best if data points are close together within one cluster and clusters are well separated. For details, see text and Ref. [25].



for both neurochemicals, measured at a fixed concentration] only 2 coordinates are used. Each of the coordinates contains information of all of the 11 variables. As can be seen from Fig. 5, all data points coming from one substance cluster in a small area that can clearly be distinguished from the area in which the data points of the other substance cluster. The native activity before addition of the neurochemicals, however, was widespread. Therefore, the two substances can easily be distinguished. Or, simplified: If a data point of a new measurement (which either contains

strychnine or bicuculline) falls within the cluster of the strychnine measurements, this sample contained strychnine.

The quantitative analysis of strychnine is presented in Fig. 6. Here, the different concentration dependencies of the different variables were evaluated by an ANN. In a neural network analysis, in a first step, the algorithm calculating the results has to be trained for the specific task. This is done by feeding data into the network and telling the system the correct result. The ANN calculates a result with the input variables, getting a completely false result at

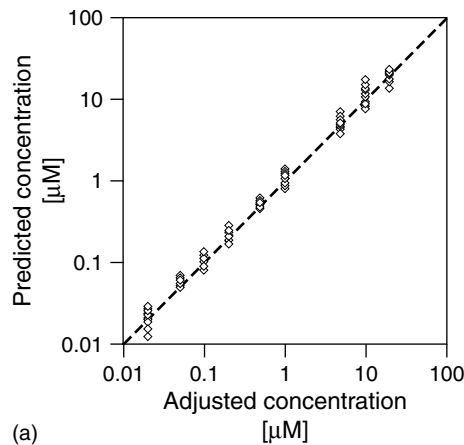
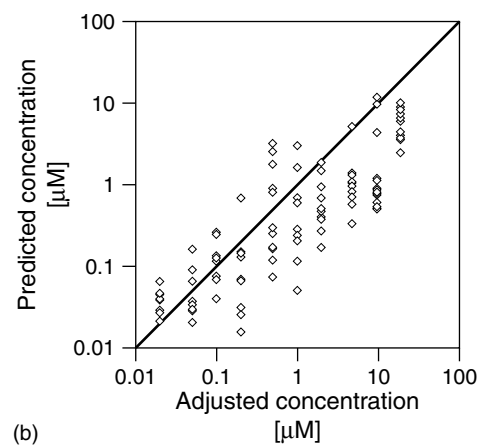


Fig. 6 Predicted vs. adjusted (real) concentration of strychnine in embryonic mice spinal cord cultures, evaluated with a backpropagation artificial neural network [22, 23, 25]. (a) The net was trained with 2/3 of the data



and tested with the remaining 1/3 of the data and (b) training was performed with data from a first concentration series, test with data from a subsequent series performed 30 min after the first.

the very beginning of the training phase. By changing the weights of different parts of the calculation, the network trains itself to reproduce the correct result. If later on, new, that is, unknown data are fed into the ANN, it is able to predict the correct answer by using the now optimized calculation parameters.

Shown in Fig. 6 is the correlation of real concentrations of strychnine and those concentrations that are predicted by the ANN analysis of experimental data of strychnine exposure [25, 26]. In the left part of the figure, the good correlation within the same experiment is shown. This means that a part of the data of one experiment was chosen to train the ANN, whereas the other data of the same experiment was used as the independent test data.

However, for real biosensor applications, the calibration and training of the ANN is done in a first, independent step. In a second step, that is, after days or weeks, an unknown analyte is studied. The result of such an experiment is shown on the right side of Fig. 6. Although still correlated, the prediction error is now large. In this experiment, the results used for training were obtained immediately before the sensor test was performed. One reason for the deviations is therefore certainly the poisoning of the network by the high strychnine concentrations and a too short recovery time between the training and analysis sequences. But these results show that, in principle, a quantification of biosensor data based on natural neural networks after evaluation by ANNs will be possible.

One trend in neuron-based biosensors concerns the utilization of whole tissue. Tissue may be even more organo-typic than in vitro grown cell networks. This is particularly important for drug tests

in the pharmaceutical industry. However, tissue cultures are in most cases difficult to keep for longer time, although new culture techniques may help promote longevity [29, 30].

Taking whole animals or at least complete sensory organs such as insect antenna comprises another relatively new trend, which was introduced by Rechnitz and coworkers in 1986 [31]. New experiments on potato beetles or their antenna show a sensitive response to broken green leaves [32], diseased potato tubers [33], or smouldering odorants [34]. These examples are nearest to a bioelectronic nose in its original sense.

3.3.2

Biocomputer

Parallel computing will be a feature of particular importance for future computer architectures. However, the trend towards massively parallel computers, that is, with thousands and more computing elements, such as in the connection machine, has lost impetus because of several problems inherent to silicon devices on the hardware and the software level. These problems include the connectivity problem, the complexity of an appropriate routing, and the difficulty to write parallel codes. On the other hand, parallel processing is performed in a very efficient way in biological systems, far superior to existing silicon-based devices. The other feature that one may overcome with biocomputers is the fact that silicon computers need absolutely correct input data to find the correct solution. One can hope that a biological computer will arrive at the correct answer based on partial information by filling in the gaps by itself. Therefore, the combination of natural neurons with silicon technology could lead

to bioelectronic circuits with fascinating new data processing properties. However, like in neural network-based biosensors, a tremendous amount of work has to be done before one can think of a real “biocomputer”.

A recent example in this direction was demonstrated by Ditto and coworkers with the so-called leech-ulator, in which two leech neurons were used for a simple mathematical addition [35]. Leech neurons are used because they have been extensively studied and are well understood. The neurons are electrically stimulated by inserted microelectrodes. Each neuron has its own electrical activity and responds in its own way to the electrical stimulus. These features can be used to make each neuron represent a number. Calculations are then performed by linking up the individual neurons. Using principles of chaos theory, the two neurons are selectively stimulated. From the signal cascade that follows, the PC can extract the correct answer to a simple addition problem.

Because the leech neurons are able to form their own connections from one to another, the biological computer works out its own way of solving the problem. This approach to computing is particularly suited to pattern recognition tasks such as reading handwriting, which would take enormous amounts of power to be performed on a conventional computer.

However, intracellular electrodes reduce the longevity of the neurons to extremely short periods, which limits the use of this approach for practical applications. The concept of extracellular detection described in Sect. 3.1 has therefore to be used for a real device. In particular, the use of CMOS devices in which data preprocessing can be performed in

the direct vicinity of the cells may be promising, hence reducing the problem of the still bad signal-to-noise ratio of extracellular recording devices [36].

3.3.3

Short Summary of In Vivo Applications

In vivo applications of bioelectronic devices, such as artificial limbs, cochlear or retina implants, will not be stressed here in detail. Many of the problems that have to be solved for in vitro devices, such as a stable neuron/electrode contact, do also matter for in vivo applications. However, for the latter, much more difficult requirements have to be met, such as biocompatibility not only against the neural cells but the whole body, including resistance to body reactions against the foreign device such as inflammation or scar formation, mechanical stability in a moving system (muscle, eye, . . .), long-term stability over years, as well as practical requirements such as easy implantation. Despite all these difficulties, there are systems such as pacemakers and cochlear implants already on the market [37]. Retina implants are under development [38]. And first studies are made with intelligent artificial limbs. Therefore one can hope that in the twenty-first century many of the above-mentioned problems will be solved.

References

1. S. Roth, *One-Dimensional Metals*, Wiley-VCH, Weinheim, Germany, 1995.
2. E. R. Kandel, J. H. Schwartz, *Principles of Neural Science*, 3rd ed., Elsevier, New York, 1991.
3. W. Göpel, Ch. Ziegler (coordinating authors), H. Breer, D. Schild (biological section), R. Apfelbach, J. Joerges, R. Malaka, (contributing authors), *Biosens. Bioelectron.* **1998**, *13*, 479–493.

4. Ch. Ziegler, W. Göpel (coordinating authors), H. Hämmerle, H. Hatt, G. Jung, L. Laxhuber, H.-L. Schmidt, S. Schütz, F. Vögtle, A. Zell (contributing authors), *Biosens. Bioelectron.* **1998**, *13*, 539–571.
5. W. Göpel, *Sens. Actuators, B* **1998**, *52*, 125–142.
6. Ch. Ziegler, *Fresenius Z. Anal. Chem.* **2000**, *366*, 552–559.
7. G. W. Gross, A. Harsch, B. K. Rhoades et al., *Biosens. Bioelectron.* **1997**, *12*, 373–393.
8. G. W. Gross, B. K. Rhoades, R. J. Jordan, *Sens. Actuators* **1992**, *6*, 1–8.
9. G. W. Gross, H. M. E. Azzazy, M.-C. Wu et al., *Biosens. Bioelectron.* **1995**, *12*, 373–393.
10. U. Egert, B. Schlosshauer, S. Fennrich et al., *Brain Res. Protocols* **1998**, *2*, 229–242.
11. S. M. Potter, Distributed processing in cultured neuronal networks in *Advances in Neural Population Coding* (Ed.: M. A. L. Nicolelis), Progress in Brain Research, Elsevier, New York, 2001, pp. 49–62, Vol. 130.
12. P. Fromherz, A. Offenhäuser, Th. Vetter et al., *Science* **1991**, *252*, 1290–1293.
13. J. J. Hickmann, D. A. Stenger, Interactions of cultured neurons with defined surfaces in *Enabling Technologies for Cultured Neural Networks* (Eds.: D. A. Stenger, T. M. McKenna), Academic Press, New York, 1994, pp. 51–76.
14. J. Graf, Y. Iwamoto, M. Sasaki et al., *Cell* **1987**, *48*, 989–996.
15. P. Heiduschka, W. Göpel, W. Beck et al., *Chem. – Eur. J.* **1996**, *2*, 667–672.
16. A. Blau, C. Weinl, J. Mack et al., *J. Neurosci. Methods* **2001**, *112*, 65–73.
17. G. W. Gross, Internal dynamics of randomized mammalian neuronal networks in culture in *Enabling Technologies for Cultured Neural Networks* (Eds.: D. A. Stenger, T. M. McKenna), Academic Press, New York, 1994, pp. 277–317.
18. G. W. Gross, S. Norton, K. Gopal et al., *Cellul. Eng.* **1997**, *2*, 138–147.
19. S. I. Morefield, E. W. Keefer, K. D. Chapman et al., *Biosens. Bioelectron.* **2000**, *15*, 383–396.
20. <http://www.multichannelsystems.com>.
21. <http://www.cnns.org/>.
22. http://www.panasonic.com/medical_industrial/medsys.asp.
23. <http://www.caltech.edu/~pinelab/steve.html>.
24. A. Gramowski, D. Schiffmann, G. W. Gross, *NeuroToxicology* **2000**, *21*, 331–342.
25. A. Harsch, Ch. Ziegler, W. Göpel, *Biosens. Bioelectron.* **1997**, *12*, 827–835.
26. A. Harsch, Ch. Ziegler, W. Göpel, *Sens. Actuators, B* **2000**, *65*, 160–162.
27. A. Mohr, W. Finger, K. J. Föhr et al., *Sens. Actuators, B* **1996**, *34*, 265–269.
28. A. Harsch, Ph.D. Thesis, University of Tübingen, Germany, 1997.
29. H. Kamioka, Y. Jimbo, P. J. Charley et al., *Cellul. Eng.* **1997**, *2*, 148–153.
30. P. Thiébaud, C. Beuret, M. Koudelka-Hep et al., *Biosens. Bioelectron.* **1999**, *14*, 61–65.
31. S. Belli, G. Rechnitz, *Anal. Lett.* **1986**, *19*, 403–416.
32. P. Schroth, M. J. Schöning, P. Kordos et al., *Biosens. Bioelectron.* **1999**, *14*, 303–308.
33. S. Schütz, B. Weißbecker, U. T. Koch et al., *Biosens. Bioelectron.* **1999**, *14*, 221–228.
34. S. Schütz, B. Weißbecker, H. E. Hummel et al., *Nature* **1999**, *398*, 298–299.
35. <http://www.neuro.gatech.edu/acl/>.
36. INPRO (Information Processing by Natural Neural Networks), European Union Project IST-2000-26463, for more information contact the author.
37. <http://www.medizin.uni-tuebingen.de/hno/cochlearimplant.htm> and links given there.
38. <http://www.uak.medizin.uni-tuebingen.de/subret> and <http://www.nero.uni-bonn.de/projekte/ri/ri-index-en.htm> and links given there.

4

Electrochemistry of NAD(P)⁺/NAD(P)H

Lo Gorton

Department of Analytical Chemistry, Lund University, Lund, Sweden

Elena Domínguez

*Department of Analytical Chemistry, Faculty of Pharmacy,
University of Alcalá, Madrid, Spain*

4.1	Introduction	69
4.1.1	NAD(P) ⁺ /NAD(P) in Living Systems	69
4.1.2	Formal Potential of the NAD ⁺ /NADH Redox Couple	72
4.1.3	Focus and Scope of the Chapter	73
4.2	Direct Electrochemical Oxidation of NAD(P)H	76
4.2.1	General Observations	76
4.2.2	Effect of Adsorption	76
4.2.3	Mechanism and Kinetics	78
4.3	Homogeneous Oxidation of NAD(P)H by Oxidizing Redox Compounds	81
4.3.1	One-electron No-proton Acceptors	82
4.3.2	Two-electron-proton Acceptors	84
4.3.2.1	<i>o</i> -quinones and <i>p</i> -quinones	84
4.3.2.2	Aromatic Diimines	88
4.4	Electrocatalytic Oxidation of NAD(P)H at Mediator-modified Electrodes	89
4.4.1	General Remarks of CMEs	89
4.4.1.1	<i>o</i> -Quinones and Phenylenediimine Derivatives	89
4.4.2	Other Mediating Functionalities and Metal-coated Electrodes	115
4.4.3	Catalytic NADH Oxidation at CMEs Based on Polymers	116
4.4.4	Mechanistic and Kinetic Aspects	118
4.5	CMEs Based on NADH-oxidizing Enzymes	123

4.6	Amperometric Biosensors Based on NAD(P)-dependent Dehydrogenase Enzymes	124
4.7	Direct Electrochemical Reduction of NAD(P)^+	124
4.7.1	General Observations	124
4.7.2	Adsorption Phenomena	126
4.7.3	Mechanism and Kinetics	127
4.8	Electrocatalytic Reduction of NAD(P)^+	131
4.8.1	Nonenzymatic Electroreduction of NAD(P)^+	131
4.8.2	Enzymatic Electroreduction of NAD(P)^+	133
	Acknowledgment	134
	References	134

4.1 Introduction

4.1.1 NAD(P)⁺/NAD(P) in Living Systems

The pyridine nucleotides, NAD (nicotinamide adenine dinucleotide) and NADP (nicotinamide adenine dinucleotide phosphate), are ubiquitous in all living systems as they are required for the reactions of more than 400 oxidoreductase-denoted dehydrogenases (250 of these depend on NAD and around 150 on NADP). This number represents 17% of all classified enzymes and consequently, these nucleotides are responsible for more enzymatic reactions than any other coenzyme [1]. Largely, the role of these nonproteinaceous coenzymes in enzyme-catalyzed reactions is to serve as the acceptor/donor of what is equivalent to a hydride ion (H^-) from the substrate in a reversible manner, thus playing a key role in biological electron transport [2]. This means that they have necessarily evolved to be specific in their redox reactions. It is of utmost importance for the functioning of the living cell system that these redox coenzymes are inherently fastidious in their choice of redox partners and therefore recognize and undergo rapid reaction with their desired redox partners

and at the same time, do not react at any appreciable rate with thermodynamically favorable but undesirable side reactions. Unlike many other oxidoreductases depending on other redox cofactors, such as flavin nucleotides, pyrroloquinoline quinone (PQQ), heme, and iron-sulfur clusters, in the nicotinamide-dependent dehydrogenases, the cofactor is not permanently bound within the enzyme but acts as a soluble cosubstrate, that is, there exists a 1:1 stoichiometric relationship between the cofactor and the substrate. It should be noted that a few other nonredox enzymes, such as adenosylhomocysteinase (EC 3.3.1.1), urocanate hydratase (EC 4.2.1.49), or myo-inositol-1-phosphate synthase (EC 5.5.1.4), contain very tightly bound NAD with no net change at the end of the reaction, but acting as a true coenzyme and serving catalytically as the hydrogen acceptor and donor for the intermediates in the reaction sequence [3].

There are two different forms of the nicotinamide coenzymes: β -NAD⁺ and β -NADP⁺. They have closely related structures, both revealed in Fig. 1, and unique electrochemical properties. In solution, NAD⁺ acquires a folded conformation as suggested from circular dichroism [4], fluorescence spectroscopy [5], NMR [6–8], and X-ray crystallography [9] experiments,

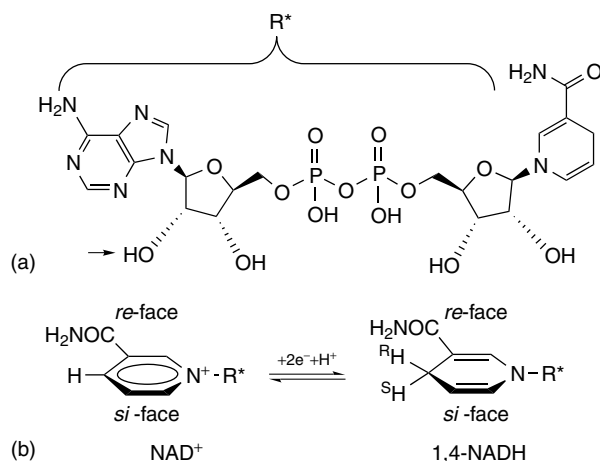
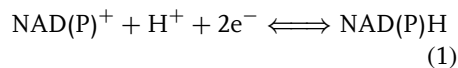


Fig. 1 (a) Formulas of enzymatically active 1,4-NADH (i.e. β -NAD reduced form). The isomer, an α -glycosidic nicotinamide-ribose linkage, is not enzymatically active. In the phosphorylated coenzyme, a $\text{PO}(\text{OH})_2$ group replaces the indicated H; (b) stereospecific redox reaction between NAD(P)^+ and NAD(P)H .

and also confirmed by molecular dynamics simulation [10]. While a consensus atomic-level model has not emerged from these data, and the interpretation of some NMR data have been questioned [11], NAD^+ in solution is thought to be a mixture of folded and unfolded forms with the aromatic rings in close proximity in the folded form. However, the nature and extent of the interaction between the aromatic rings in the folded position still remains controversial. Some groups have proposed that parallel-ring stacking with an interring distance of less than 0.39 nm is the hallmark of the folded form of NAD^+ [4, 12–14], while others have proposed a less restrictive [6, 7] conformation of the folded form with an interring distance greater than 0.45 nm and the aromatic rings not perfectly stacked in parallel [8]. Molecular dynamics calculations, consistent with NMR relaxation data, result in a conformation with an average interring distance of 0.52 nm, an average interring

angle of 148° , nearly parallel glycosyl bond vectors, and the nicotinamide *si* side facing the adenine [10]. Additional discrepancy is also observed in the relative proportions reported for the extended and folded conformation. A range within 15% and 60% has been reported for the folded conformation [14–16]. Regardless of how compact the folded conformation is in solution, this clearly contrasts with the extended unfolded configuration that NAD^+ offers when attached to an enzyme [17].

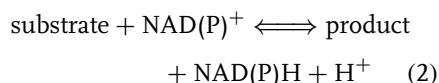
The redox reaction between the oxidized and reduced forms involves two electrons and one proton and can formally be considered as a hydride (H^-) transfer;



As in the case of biological systems, the hydride transfer takes place at the C-4 position of the nicotinamide ring and thus, a basic understanding of the electrochemical behavior of the $\text{NAD(P)}^+/\text{NAD(P)H}$

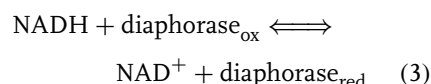
redox pair may lead to a more comprehensive overview of biological electron transfer mechanisms. Equally unique and one of the most stringently conserved properties of NAD(P) is the absolute stereospecificity of the dehydrogenases for these coenzymes. Some of them can only transfer the *R* hydrogen from the dihydronicotinamide to their substrates or the *S* hydrogen (sometimes also denoted as A and B), and the same stereospecificity is kept for the reduction of NAD(P)⁺ introducing the hydrogen either to the *re*-face of the trigonal C-4 or to the *si*-face, respectively, (Fig. 1b). Additionally, most NAD(P)-linked enzymes are also stereospecific for the hydrogen transfer of the substrate allowing stereochemical choices in biosynthetic work. The stereospecific mechanism of these reactions was clearly elucidated in the early 1950s by the group of Westheimer at the University of Chicago. This was made possible by the use of deuterated forms of coenzymes and substrates [18–21].

The basic redox reaction catalyzed by a NAD(P)-dependent dehydrogenase follows according to reaction (2):



However, more complex reaction schemes prevail, for example, the redox interconversion of L-glutamate and α -ketoglutarate catalyzed by L-glutamate dehydrogenase. Most of these dehydrogenases are specific to either NAD⁺ or NADP⁺; however, some can make use of both, although usually with different reaction rates. As a rule of thumb, the NAD⁺-dependent dehydrogenases are involved in catabolic reactions, whereas the NADP⁺-dependent ones are involved in anabolic reactions in conjunction with, for instance, photosynthesis [22].

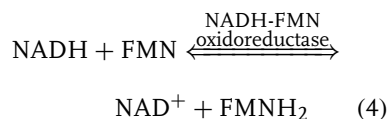
NAD⁺/NADH or NADP⁺/NADPH also participate in a number of other enzyme-catalyzed redox reactions, which do not involve dehydrogenases in the classical sense as described earlier. These redox enzymes contain bound cofactors such as flavins, heme, and iron-sulfur clusters. One group of these enzymes is usually denoted diaphorase (DI) when used in analytical systems and includes both flavin-containing lipoamide and lipoyl dehydrogenases (EC 1.8.1.4).



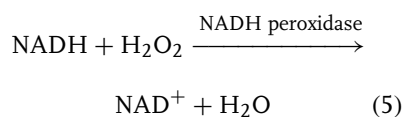
Both flavin adenine dinucleotide (FAD) and flavin adenine mononucleotide (FMN)-containing DIs are found, some specific for NAD, whereas others for NADP. They have been used for staining dehydrogenase-rich tissues and in attempted applications for the regeneration of the cofactor such as in bioelectroanalytical devices and flow systems (see following text) and in bioorganic synthetic reactions.

Examples of other redox enzymes include:

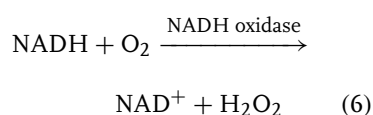
1. NADH-FMN oxidoreductase (or cytochrome *c* reductase, EC 1.6.99.3) catalyzing the reduction of FMN by NADH,



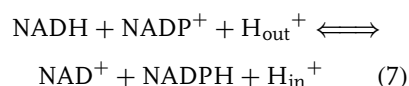
2. NADH peroxidase (EC 1.11.1.1) catalyzing the reduction of hydrogen peroxide by NADH,



3. NADH and NADPH oxidase (EC 1.6.99.1), a flavin enzyme using oxygen as electron acceptor for the oxidation of NADH with the production of hydrogen peroxide,

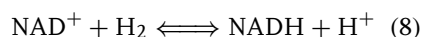


4. Proton translocating transhydrogenase (EC 1.6.1.1) found in bacteria and animal mitochondria that couples the transfer of reducing equivalents between NAD(H) and NADP(H) to the translocation of protons across the membrane, the equilibrium being shifted toward the inner transport



This enzyme is believed to play an important role in the redox balance of NADPH in the cell.

5. Hydrogenases containing iron-sulfur clusters (EC 1.12.1.2) and produced by a few microorganisms catalyze the reduction of NAD^+ into NADH by molecular hydrogen,



In biological electron-transfer pathways, such as the respiratory chain in the mitochondria, there is a switch between charge-transfer reactions involving one or two electrons. In the respiratory chain, the starting point is the donation of a hydride equivalent from cytosolic NADH to a membrane-bound flavoprotein (NADH dehydrogenase), which in turn delivers its charge to an iron-sulfur cluster containing protein, and then via ubiquinone through the cytochrome chain to cytochrome oxidase, and finally to molecular oxygen. The

charge-transfer reactions taking part prior to the reduction of NAD^+ to NADH in the cytosolic solution involve two electrons, whereas those occurring within the respiratory chain between the flavoprotein and cytochrome oxidase are one-electron reactions [22]. It has therefore been and still is of great interest and great controversy how the charge transfer occurs between NADH and the oxidized flavin within the flavoprotein NADH dehydrogenase as somewhere from NADH to ubiquinone, the reaction switches from being a two-electron- to a one-electron-transfer reaction. Similarly, but in the reverse order, the photosynthetic electron-transfer pathway starts with a series of one-electron-transfer reactions and ends up with a two-electron one-proton reduction of NADP^+ to NADPH.

4.1.2

Formal Potential of the NAD^+/NADH Redox Couple

The generally accepted formal potential, $E^{\circ'}$, of the NAD^+/NADH redox couple at pH 7.0 (25 °C) is -315 mV versus normal hydrogen electrode (NHE) (-560 mV vs. saturated calomel electrode (SCE) [23, 24]. From thermal data and the equilibrium constants of the ethanol/acetaldehyde and 2-propanol/acetone reactions catalyzed by alcohol dehydrogenase, a value of -320 mV was calculated, which was later recalculated to be -315 ± 5 mV versus NHE by Clark [23]. Through direct potentiometric titrations using several different mediators and xanthine oxidase as catalyst, Rodkey [25, 26] obtained an $E^{\circ'}$ value of -311 mV versus NHE (25 °C) and a temperature variation of the $E^{\circ'}$ of -1.31 mV/°C in the range of 20 to 40 °C. A variation of the $E^{\circ'}$ with pH of -30.3 mV/pH (30 °C) was found, which

is in good agreement with the theoretical value of -30.1 mV/pH . Rodkey and Donovan [27] also investigated the $E^{\circ'}$ of $\text{NADP}^+/\text{NADPH}$ and found that this redox couple at pH 7 is very close to that of NAD^+/NADH with a maximum difference at the same pH of 4 mV and the variation with pH being the same as that of the NAD^+/NADH redox couple. The $E^{\circ'}$ of the NAD^+/NADH redox couple remains more negative than the $E^{\circ'}$ of the many substrate/product couple depicted in reaction (2), being obvious that the catalytic oxidation of NADH into NAD^+ is thermodynamically favored, unless a second reaction (catalytic, chemical, or electrochemical) takes place making the reduction of NAD^+ virtually favorable.

The inherent nature of the redox reaction makes it natural to couple these dehydrogenase-catalyzed reactions to electrochemical methods. The transfer of electron(s) from a substrate to an electrode (or the reverse) may then take place via electrochemical redox reactions of the coenzymes, as depicted in Fig. 2. The utility of combining enzymes and electrochemical methods for electroanalytical applications was predicted by Clark and Lyons by an enzyme electrode [28] and by Shaw in energy production by a biofuel cell anode [29] in the early 1960s.

NAD(P) in either redox form is poorly dissolved in nonaqueous solutions. A series of NAD^+/NADH -model

compounds have therefore additionally been chemically and electrochemically investigated in both protic and aprotic media. Some of the commonly studied are nicotinamide, nicotinamide mononucleotide (NMN^+), 1-methyl-3-carbamoylpyridinium ion (MCP^+), 1-benzyl-3-carbamoylpyridinium ion (BNA^+), 10-methylacridinium (MA^+), 1-benzyl-3-cyanoquinolinium (BQCN^+), 1-benzyl-3-carbamoylquinolinium (BQA^+), and the corresponding 1,4-dihydro forms and dimers [30–71]. Some of these analogues are presented in Fig. 3. Biomimetic analogues of NAD^+ , comprising a nicotinamide functionality coupled via an atrazine ring to a dibenzenesulphonic acid unit, have demonstrated their potential use as artificial and stable coenzymes with different dehydrogenases [72, 73] with re-oxidation of the reduced biomimetic coenzyme by *N*-methylphenazinium [74].

4.1.3

Focus and Scope of the Chapter

The basic direct electrochemistry of $\text{NAD(P)}^+/\text{NAD(P)H}$ has been studied since the early 1960s [75] and is summarized. Overall, this chapter covers the charge-transfer reactions of both redox forms occurring not only at naked but also at chemically modified electrodes (CMEs) facilitating the interconversion of one redox form into the other. Following the

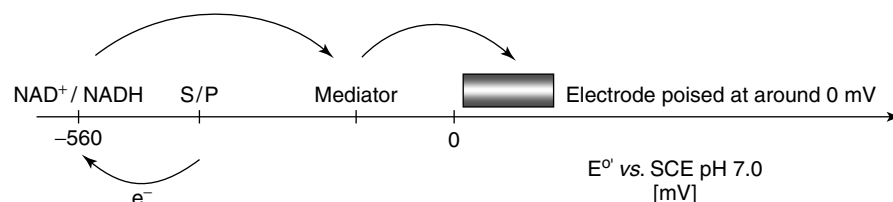
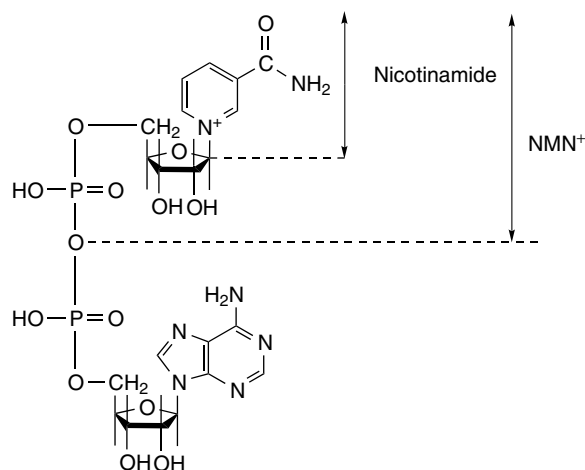


Fig. 2 Electron-transfer pathway in dehydrogenase-catalyzed reactions coupled to electrodes via electrochemical redox reactions of the coenzymes. Electron fluxes represent the oxidation of the substrate (e.g. Pyruvate/Lactate $E^{\circ'} = -435 \text{ mV}$ vs. SCE, pH 7.0).

Fig. 3 Formulas of some NAD^+/NADH analogues.Tab. 1 Summary of the main reactions in the electrochemistry of NAD^+/NADH

Overall redox process	
$\text{NAD}^+ + \text{H}^+ + 2\text{e}^- \rightleftharpoons \text{NADH}$	
Electrochemical oxidation of NADH Simple Electron Transfer (ECE mechanism)	Electrochemical reduction of NAD^+
$\text{NADH} \xrightarrow{-\text{e}^-} \text{NADH}^{\bullet+} \xrightarrow{-\text{H}^+} \text{NAD}^{\bullet} \xrightarrow{-\text{e}^-} \text{NAD}^+$	$\text{NAD}^+ \xrightarrow{+\text{e}^-} \text{NAD}^{\bullet} \xrightarrow{+\text{H}^+ + \text{e}^-} \text{NADH}$
Disproportionation $\text{NADH}^{\bullet+} + \text{NAD}^{\bullet} \rightleftharpoons \text{NADH} + \text{NAD}^+$	
Dimerization $2 \text{NAD}^{\bullet} \rightleftharpoons (\text{NAD})_2$	
Simple One Step Hydride Transfer $\text{NADH} + \text{Q} \longrightarrow \text{NAD}^+ + \text{QH}^-$ $\text{NAD}^+ + \text{RH} \longrightarrow \text{NADH} + \text{R}$	
Sequential Hydride Transfer within a complex (pathway I) $\text{NADH} + \text{Q} \rightleftharpoons [\text{NADH}^{\bullet+}\text{Q}^-] \longrightarrow [\text{NAD}^+\text{QH}^-] \longrightarrow \text{NAD}^+ + \text{QH}^-$	
Sequential Hydride Transfer within a complex (pathway II) $\text{NADH} + \text{Q} \longrightarrow [\text{NAD}^{\bullet}\text{QH}^{\bullet}] \longrightarrow [\text{NAD}^+\text{QH}^-] \longrightarrow \text{NAD}^+ + \text{QH}^-$	
Electrocatalytic oxidation through the formation of a charge transfer complex $\text{NADH} + \text{Med}_{\text{ox}} \rightleftharpoons [\text{CT}] \longrightarrow \text{NAD}^+ + \text{Med}_{\text{red}}$	
In detail: $\text{NADH} + \text{Med}_{\text{ox}} \rightleftharpoons [\text{NADH} - \text{Med}] \rightleftharpoons [\text{NADH}^{\bullet+}\text{Med}^{\bullet-}] \longrightarrow$ $[\text{NAD}^+\text{MedH}^{\bullet}] \longrightarrow \text{NAD}^+ + \text{MedH}^-$	
Electrocatalytic oxidation through a charge transfer-complex with innersphere electron transfer* $\text{PyH}_2 + \text{Q} \rightleftharpoons [\text{PyH}_2\text{Q}] \rightleftharpoons [\text{PyH}_2^{\bullet+}\text{Q}^{\bullet-}] \longrightarrow [\text{PyH}^+\text{QH}^{\bullet}] \longrightarrow \text{PyH}^+ + \text{QH}^-$	

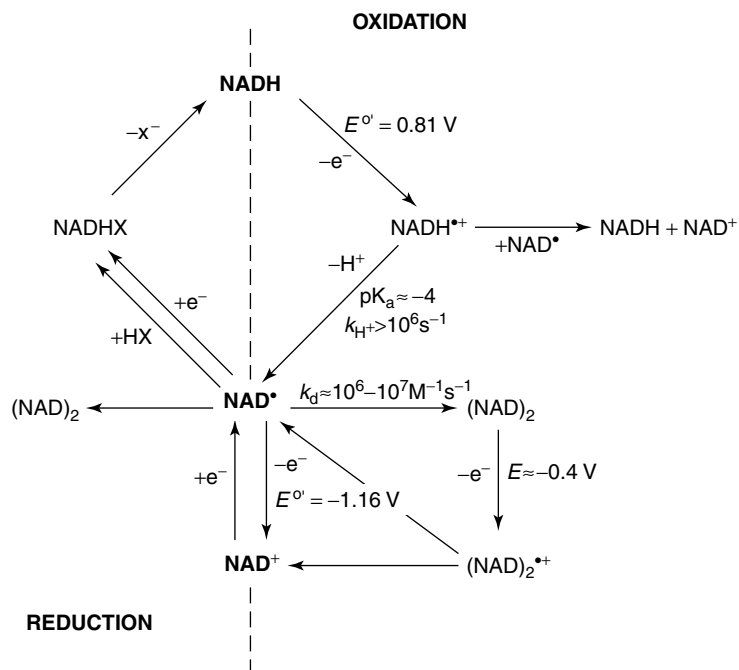
* PyH_2 corresponds to dihydropyridine compounds.

authors' view, the description of electrodes modified with inorganic and organic mediators and biochemical catalysts is also given. The homogeneous charge-transfer reactions with other redox compounds as the basis for the understanding of the reaction sequence occurring at electrodes chemically modified with compounds similar to those used as modifiers are also discussed. A summary of the main reactions described in this chapter is presented in Table 1. Sch. 1 depicts the electrochemical pathways for the oxidation and reduction of NADH and NAD^+ , respectively.

Much of the driving force for these studies has been, and still is, with the hope to increase the fundamental understanding of biological electron-transfer reactions, and also with the hope that the electrochemical reactions of $\text{NAD(P)}^+/\text{NAD(P)H}$ could be used for practical applications

such as in (electro)analytical chemistry [75] including amperometric biosensors [76, 77] and biofuel cells [78–80] and in electroorganic chiral synthesis [24, 81–84].

The general chemistry of NAD(P)^+ and NAD(P)H will not be covered or further commented on in this chapter, except that NAD(P)H is relatively stable in aqueous solutions at pHs more alkaline than pH 7 and NAD(P)^+ at pHs more acidic than pH 7. The stability is very much dependent on the buffer constituents and ionic strength. The pH where both redox forms together exhibit minimal destruction due to acid/base decomposition is found between pH 7 and 8, depending on whether the aqueous medium is unbuffered and when buffered, on the buffer constituents. In general, the stability of NADPH is less dependent on the buffer than is that of NADH. The reader is advised to refer to



Scheme 1 Pathways for the electrochemistry of NAD^+/NADH redox pair.

excellent books and reviews [24, 85–88] for further information.

4.2

Direct Electrochemical Oxidation of NAD(P)H

4.2.1

General Observations

Studies on the electrochemical oxidation of NADH have been made using cyclic voltammetry (CV), potential step chronoamperometry, constant electrode potential coulometry, and rotating disk electrode (RDE) methodology. Most commonly, a variety of carbonaceous electrode materials have been used including glassy carbon (GC) and pyrolytic graphite (PG) [75, 89–99], and carbon fibers [100–105]. Of the metal electrodes, platinum (Pt) [30, 75, 91, 94, 96, 98, 106–109] and gold (Au) electrodes [98, 110–115] are the most common electrode materials, although other metals, for instance, silver [116, 117], have also been used.

A poorly defined oxidation wave of NADH at a Pt electrode around 1 V versus NHE was observed in an initial study by Burnett and Underwood [118] reflecting the large over voltage of the electrochemical NADH oxidation. The electrode material has a significant effect on the over voltage. The oxidation of NADH in an aqueous solution, seen as a single peak in CV, takes place at potentials of ≈ 0.4 , ≈ 0.7 , and ≈ 1 V at C, Pt, and Au electrodes, respectively [75, 90, 97, 98]. As a common observation of all bare electrode materials, it was early recognized, as in the case of the reduction of NAD^+ (see in the following text), that the electrochemical reaction results in electrode fouling, necessitating careful pretreatment and conditioning of the electrodes to obtain reproducible

results between runs [30, 90, 94, 109]. CV often gives values of the number of electrons participating in the electrochemical process (n) close to the expected value of two, while lower values of n are usually found in coulometric studies. In continued coulometric studies by Coughlin and coworkers [106, 107] and by Jaegfeldt and coworkers [108], the investigators found a recovery of 99.3% enzymatically active NAD^+ , using low concentrations of the co-factor, a pretreated fast rotating Pt gauze electrode to minimize the adsorption, and correcting the decomposition of the coenzyme in solution [24]. From the fact that the major product of the electrochemical oxidation of NADH in aqueous solution was NAD^+ in combination with the fact that n is equal to two, it follows that the net reaction can be summarized as [90, 91, 119–121]:



4.2.2

Effect of Adsorption

It was early recognized that the electrochemical oxidation of NADH suffered from severe effects of adsorption. Early investigations at C and Pt electrodes showed that the adsorption of NAD^+ and possibly other unknown species occur at positive potentials [89–91, 93–95, 109], with indications of the desorption of NAD^+ from GC electrodes at a potential of 0 V [93]. In a thorough investigation by Samec and Elving, the oxidation of NADH at GC, Pt, and Au electrodes was studied and the results obtained at the different electrode materials with CV and RDE were compared [98]. The influence of the preadsorption of NAD^+ , NADH, NMN^+ , NMNH , nicotinamide, adenine, and adenosine before investigating the electrochemistry of

NADH, pointed to the fact that both the adenine and nicotinamide moieties are involved in adsorption at Pt and Au electrodes. NADH was also shown to adsorb onto C, Pt, and Au electrodes. This was demonstrated with electrodes exposed to NADH solutions at open circuit, followed by extensive cleaning with water and buffer. Then, CV experiments with these electrodes in buffers not containing NADH revealed anodic waves because of the oxidation of the adsorbed NADH. It was concluded that one of the major differences between the three electrode materials arises because of differences in the adsorption of the coenzyme at the electrode surface. At Pt and Au electrodes, NADH was strongly adsorbed, whereas at GC, it was the oxidation product NAD^+ that was most strongly adsorbed. Additionally, it was also observed at the Pt and Au electrodes, in parallel with the two-electron oxidation, there is a further oxidation process of the adsorbed NADH leading to unspecified products and presumably, poisoning the metal surface. RDE investigations with GC, Pt, and Au electrodes at concentrations of NADH below 2 mM revealed that the limiting current was linearly dependent on the square root of the angular velocity ($\omega^{1/2}$) and independent of scan direction. However, at higher concentrations, deviations from linearity were noticed for all the three-electrode materials, reflecting the influence on electrode fouling by the concentration of NADH in the solution.

The adsorption of NAD^+ on Au has been further studied during recent years using fourier transform surface-enhanced Raman scattering (FT-SERS) [113–115]. The surface-enhanced Raman scattering (SERS) of NAD^+ shows a strong potential dependence in the non-Faradaic regions. Either the adenine or the nicotinamide

moiety may change its adsorption state during the potential scanning process. In regions of positive electrode potential, only the bands responsible for the adenine and nicotinamide moieties can be observed. In contrast, with a negative shift of the potential, several additional strong bands representing the ribose and phosphate moieties are also evident. The stacked NAD^+ molecule is considered to be opened to some extent on an electrically charged electrode. Specifically, under sufficiently negative potential, the NAD^+ molecule appears to exist in a well-extended state on the gold electrode, leading to the tight adsorption of the entire NAD^+ molecule on the electrode.

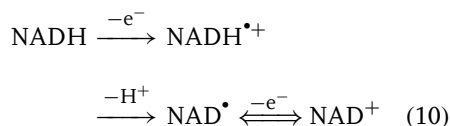
In a work from the 1980s, Blankespoor and Miller investigated the influence of the adsorption of NAD^+ on the electrode surface on the electrochemistry of NADH. Potential step chronoamperometry [99] of 1.0 mM NADH at pretreated GC electrodes with preadsorbed NADH (same as in [96]) was performed. At long timescales ($t > 0.1$ s), the current showed Cottrell behavior for a two-electron process. At short timescales ($t < 0.1$ s), however, the current was significantly less than that expected for a two-electron process and approached the Cottrell behavior for a one-electron process. If the same experiment was performed in the presence of 8 mM NAD^+ in the contacting solution even at very short times (≈ 2 ms), linear Cottrell behavior for a two-electron process was achieved. For pretreated uncoated GC with no NAD^+ in the contacting solution at times less than 7 ms, the current was even greater than expected for a two-electron process. The investigators found clear evidence that NAD^+ formed as the product when oxidizing NADH at carbon electrodes is adsorbed on the electrode surface and inhibits further oxidation of NADH. It

is also known that when oxidizing NADH at clean GC electrodes, a prewave appears on the NADH oxidation because of the weak adsorption of NADH and the strong adsorption of NAD^+ [97]. The normal NADH anodic wave appears at concentrations of NADH exceeding 0.1 mM. The prewave can be eliminated by first saturating the electrode surface with NAD^+ , for instance, by adding NAD^+ to the solution and waiting, or by electrolytically generating NAD^+ [94, 95]. At high concentrations of NAD^+ (19 mM) in the contacting buffer, reproducible cyclic voltammograms of NADH oxidation could be obtained [99].

4.2.3

Mechanism and Kinetics

To shed further light on the mechanism of NADH oxidation, Blaedel and Haas [30] oxidized NADH model compounds in acetonitrile and observed two main oxidation steps in the absence of a base, clearly demonstrating the stepwise oxidation of NADH-analogues. When oxidizing NADH in aqueous solutions, as mentioned earlier, only a single wave is observed and no waves due to the rereduction of intermediates have been observed in CV even at fast sweeps (30 V/s) [91], indicating a high chemical irreversibility of the reaction. A potential variation (E_p or $E_{1/2}$) with pH for the overall electrochemical NADH oxidation of -30 mV/pH may be expected if the limiting reaction involves a proton-transfer step, but has not been observed. Various results have been reported such as -17 [90], -11 [91], $+35$ mV/pH [106], and no pH dependence at all [120]. An electrochemical-chemical-electrochemical (ECE) mechanism for the electrochemical oxidation has therefore been proposed in several studies [30, 96, 97, 99, 109, 120, 122].

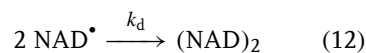


However, different views of the rate of the individual steps in the reaction mechanism and influences of the concurrent reactions have been discussed.

A key detail in the NADH oxidation pattern is the deprotonation step and its relation to the initial potential-determining electron-transfer step. Kinetic studies on the electrochemical oxidation of NADH were presented by Moiroux and Elving [96] and Jaegfeldt [109] almost simultaneously. Jaegfeldt reported the involvement of second-order pH dependence for which there is still no satisfactory explanation. Moiroux and Elving estimated the rate constant of the second step, k_{H^+} , in reaction (10)



to be 60 s^{-1} at NAD^+ -covered GC electrodes, assuming the rate to be initially comparable with the overall rate-limiting first step. The possibility of a dimerization of NAD^\bullet radicals has also been suggested as known to occur when electrochemically reducing NAD^+ [75, 123],



with a very high dimerization rate constant, k_d , in the order of 10^6 – $10^7 \text{ M}^{-1} \text{ s}^{-1}$ [98, 124–126], followed by the formation of NAD^+ from the oxidation of the dimer:

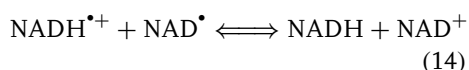


However, as the oxidation occurs positive to 0.2 V (oxidation of $(\text{NAD})_2$ to NAD^+

starts already at ≈ -0.4 V [75]), oxidation of NAD^\bullet to NAD^+ (last step in reaction (10)) would be sufficiently rapid to outrun the dimerization, so that practically no dimer is produced.

Blankespoor and Miller [99] later reexamined the results and demonstrated that NAD^+ is an inhibitor of the oxidation process and that the oxidation is of first order in NADH in the presence of a large excess of NAD^+ . Investigations by pulse radiolysis [127] indicated a deprotonation rate of $\text{NADH}^{\bullet+}$, reaction (11), much higher than the value estimated by Moiroux and Elving and greater than 10^6 s^{-1} , a value later confirmed by Matsue and coworkers to be $6 \cdot 10^6 \text{ s}^{-1}$ [128].

An extension of reaction (10) has been further suggested by also taking the disproportionation reaction into account.



A chemical one-electron oxidation by ferrocenium salts in buffered aqueous propanol [129, 130] (see also following text) gave an estimated value of the formal potential, E^0 , for the $\text{NADH}^{\bullet+}/\text{NADH}$ redox couple of 0.81 V. This value was later reexamined by Matsue and coworkers who found it to be 0.78 V versus SCE (at pH 7) [128]. Although reaction (14) is highly energetically favorable ($E_{\text{NAD}^+/\text{NAD}^\bullet}^0 = -1.16$ V), Blankespoor and Miller referred to studies by Amatore and Savéant [131], who used relatively comparable parameters in a theoretical treatment of a concurrent ECE and disproportionation mechanism, suggesting that more than 95% of the product is formed through the ECE pathway.

The high over-potential observed in the direct electrochemical oxidation of NADH is thus caused by the very high potential of the $\text{NADH}^{\bullet+}/\text{NADH}$ redox couple (first

reaction in the reaction sequence outlined earlier, reaction 10).



Thus, in light of an initial rate-limiting electron-transfer step and the knowledge of the E^0 of the produced radical (0.78 V vs. SCE) [128–130], its fast deprotonation rate ($6 \cdot 10^6 \text{ s}^{-1}$) [127, 128, 130] and its estimated high acidity ($\text{p}K_a \approx -4$) [39], a pH dependence of the oxidation of NADH , could not be observed. Thus, the reaction paths suggested by Elving and coworkers [96, 97] assuming an ECE mechanism, reaction (10), and further supported by experiments by Blankespoor and Miller [99] and calculations by Amatore and Savéant [131] may be supplemented as the most probable reaction sequence occurring (Sch. 1). However, there still remain unanswered questions that are able to give a full satisfactory explanation to all the observed results.

With strong support that the major route for direct oxidation of NADH occurs according to an ECE mechanism as outlined in reaction (10) and in Sch. 1, some results remain unexplained. In Ref. [93], Samec and Elving argue that in the reaction sequence $\text{NADH} \xrightarrow{-\text{e}^-} \text{NADH}^{\bullet+} \xrightarrow{-\text{H}^+} \text{NAD}^\bullet \xrightleftharpoons{-\text{e}^-} \text{NAD}^+$ the first reaction $\text{NADH} \xrightarrow{-\text{e}^-} \text{NADH}^{\bullet+}$ can be assumed to be rate-determining. As the oxidation occurs positive to +0.2 V, oxidation of NAD^\bullet to NAD^+ would be sufficiently rapid to outrun the dimerization, so that practically no dimer is produced. Under these circumstances, a single anodic two-electron wave should be observed at a potential that corresponds to the initial irreversible one-electron NADH oxidation and that is independent of the nature of the electrode material, NADH

concentration, and solution pH as well. However, as all three effects are, at least to some extent, involved in NADH oxidation at solid electrodes, modification of the mechanism outlined is required. The effect of electrode material is obviously significant and it may underlie the effects of both NADH concentration and solution pH. The correspondence between the rate of NADH oxidation at solid electrodes and the state of the electrode surface can be reasonably explained on the basis of intimate involvement of surface oxygen species in the rate-determining step of the overall reaction. Samec and Elving [97, 98] suggested in line with the work by Blaedel and Jenkins [90], that surface oxygen species are implicated in the reaction assisting in carbon hydrogen bond cleavage (Fig. 4). Even at electrodes not covered with adsorbed NAD^+ , the initial step in the NADH oxidation proceeds to at least some extent through redox mediator systems located close to the electrode surface such as the redox couples formed by oxygen adsorbed at Au and Pt surfaces, for example, $\text{OH}_{\text{ads}}^{\bullet}/\text{H}_2\text{O}$ and $\text{O}_{\text{ads}}/\text{OH}_{\text{ads}}^{\bullet}$ and by organic functionalities resulting from oxidation of a carbon surface, such as for instance, quinone/semiquinone/hydroquinone systems. The possible involvement of two surface oxygen redox systems in the first stage of the NADH oxidation is schematically depicted in Fig. 5 [97]. The electron transfer path involves electron exchange between energy levels located at the surface atom and in the electrode, coupled with electron exchange between energy levels of the surface oxygen atom and the

NADH molecule. The proton transfer path involves transfer of the proton bound to C(4) of NADH to a third species, which is the proton acceptor, for instance, a water molecule, with possible intermediate formation of a bond to the surface oxygen atom (Fig. 4).

These findings suggest that the pretreatment of the electrode surface in some way increases the number of surface oxygen groups causing the oxidation reaction to become kinetically more rapid. Studies in this direction have been carried out, however, mainly on carbon electrodes, where the effect is most pronounced [90, 132–137], both with electrochemical pretreatment and with other means such as radio frequency oxygen plasma treatment. Although the existence of functional oxides on carbon is well established, the type and quantity of functional groups varies greatly with carbon material and pretreatment

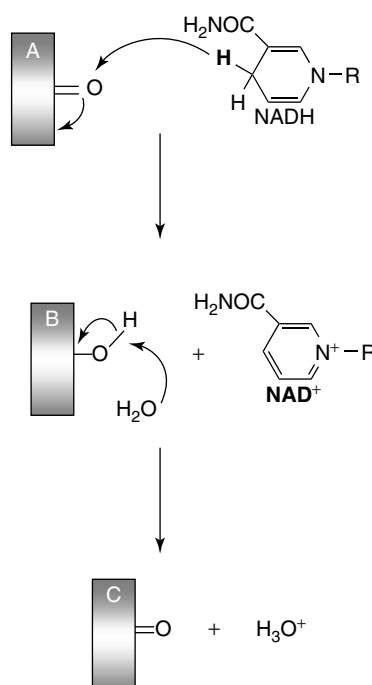


Fig. 4 Proton transfer path on oxidation of NADH involving movement of H at the C4 of the nicotinamide ring to a proton acceptor such as H_2O [97, 98].

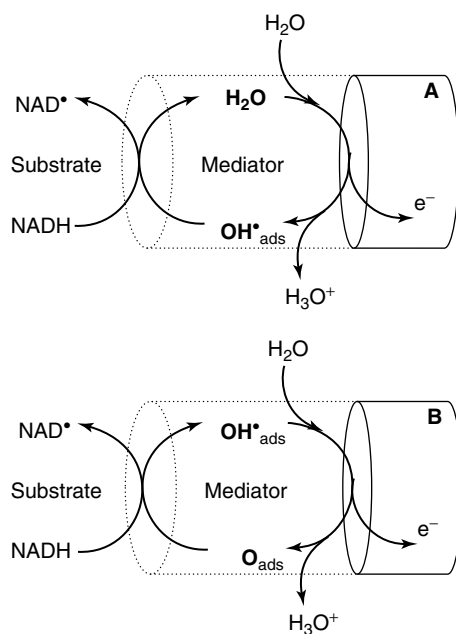


Fig. 5 Schematic representation of possible surface oxygen redox systems as mediators in the oxidation of NADH at solid electrodes [97, 98].

compared with an untreated carbon surface. However, the long-term stability of the electrocatalytic effect of these electrodes for continued NADH oxidation is very restricted, probably as a result of blocking by NADH oxidation products at the electrode surface (see also following text under CMEs for NADH oxidation).

On the basis of recent findings by Tuñón-Blanco and coworkers [139], one could also speculate that the adenine moiety of adsorbed NAD⁺ may undergo an oxidative reaction at high anodic potentials, forming a strongly mediating functionality on the electrode surface and thus facilitating the oxidation of NADH at potentials below the $E^{\circ'}$ of the NADH^{•+}/NADH redox couple, (Fig. 6).

history [138]. Oxygen functional groups on carbon have been studied and identified by infrared and Raman spectroscopy, wet chemical analysis, electron spectroscopy for chemical analysis (ESCA), and so forth. Most probably, the presence of quinones on the carbon electrode surface causes a rather drastic decrease in the over voltage

4.3 Homogeneous Oxidation of NAD(P)H by Oxidizing Redox Compounds

As mentioned earlier, the pyridine cofactors have critical positions in

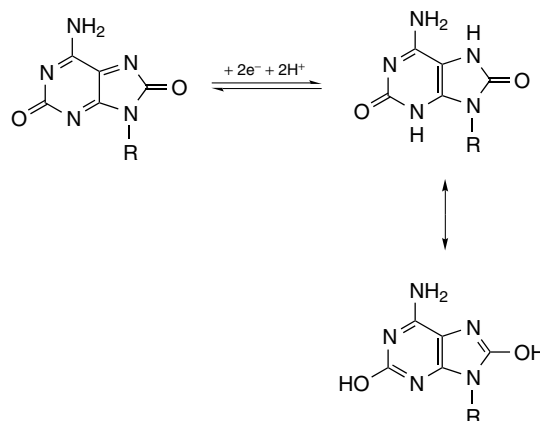


Fig. 6 Proposed structural formulas and redox reaction of the electrooxidized adenine moiety of NAD⁺ acting as an efficient mediator for NADH oxidation [139].

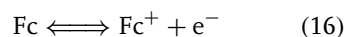
biological electron-transfer pathways located at the switching point between one and two electron reactions. It is therefore of great scientific interest to find evidence of either of the two reaction pathways when studying the oxidation of NAD(P)H or the reduction of NAD(P)^+ in model reactions either occurring directly at an electrode surface or between the NAD(P) counterpart and another redox molecule in solution. Many investigations have therefore been pursued with the objective of elucidating this important redox reaction proceeding in either direction. Experiments have been performed on NADH and NADPH in aqueous solutions and also on a great number of model compounds in both protic and aprotic media with organic and inorganic oxidants. Today there is still no general agreement on the true nature of the charge transfer reaction. These investigations are also of great importance for the understanding of the reaction sequence occurring at mediator-modified electrodes studied for the possible practical applications of catalytic NADH oxidation. A brief discussion of some of the most important investigations in this direction follows.

4.3.1

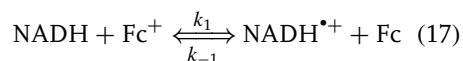
One-electron No-proton Acceptors

An extensive investigation of the reaction mechanism and kinetics between NADH and a series of ferrocenium hexafluorophosphate derivatives was made by Miller and coworkers [129, 130]. This investigation was pursued because the reaction between NADH and one-electron no-proton acceptors is abnormal in comparison with most biological reactions with NADH where a net transfer to the oxidizing agent of a hydride equivalent from

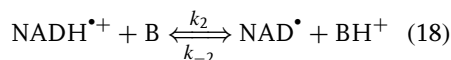
the four-position of the dihydropyridine ring occurs. With one-electron no-proton acceptors, the four-hydrogen from NADH is transferred to the solvent, not to the oxidant, and in this respect, it mimics the reaction occurring at a naked electrode surface. The reaction sequence when studied with CV proceeds as follows. In a first electrochemical step, ferrocene (Fc) is oxidized to ferrocenium (Fc^+);



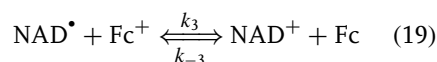
which in turn is then followed by the abstraction of the first electron from NADH to ferrocenium;



In the following reaction, the acid proton is donated to a component of the solvent (B).



Finally, the second electron is donated to a second ferrocenium



Miller and coworkers found that the reaction was first order with respect to both $[\text{Fc}^+]$ and $[\text{NADH}]$ (second order overall) and independent of pH, added NAD^+ , or Fc . In the reaction, two equivalents of Fc^+ and one equivalent of NADH , both reactants, were completely consumed and Fc and enzymatically active NAD^+ were isolated in greater than 75% yield.

In addition, they investigated a possible isotope effect with NADH deuterated in the four-position. As no primary isotope effect was found, it was thus established that for one-electron no-proton acceptors, the reaction proceeds with the first-electron donation as the rate-limiting step

(k_1) (c.f. above the direct oxidation at naked electrodes), and therefore, H^- , H^+ , or H^\bullet are not involved in the rate-limiting step. This was further supported by the observation that changes in pH or buffer concentration did not affect the rate of oxidation of NADH by Fc^+ . Thus, they could conclude that all their observations were consistent with rate-limiting one-electron transfer from NADH to Fc^+ . They further concluded that $k_2[B]$ must be greater than $k_{-1}[Fc]$ for the reaction to be rate-limited by the first electron donation.

The investigation was performed in an aqueous one-propanol solution in the presence of perchlorate, which affects the $E^{o'}$ of the ferrocenes and the reaction rate with NADH. To be able to draw kinetic-thermodynamic conclusions, values for the second-order rate constant, k_{obs} , and the $E^{o'}$ values were extrapolated to a perchlorate concentration equal to zero. The $E^{o'}$ s of the investigated ferrocenium/ferrocene derivatives range between +0.203 and 0.371 V versus SCE. Plots of $\log k_{obs}$ versus $E^{o'}$ revealed a straight line for the ferrocene derivatives with less positive $E^{o'}$ -values with a slope of 16.0 V^{-1} close to that predicted 16.6 V^{-1} for a process limited by the separation of the reactants, whereas for the most oxidative ferrocenes, deviations from linearity were observed. The interpretation given is that within the initial one-electron transfer, there are actually three processes that occur, namely, (1) the reactants must diffuse together to form an encounter complex, (2) an electron can then hop within the complex, and (3) finally, there must be diffusional separation of the products. For the weakest oxidizing ferrocenes, the actual rate-limiting process is therefore the separation of the $Fc/NADH^+$ pair, whereas for the ferrocenes with more positive $E^{o'}$ s,

the electron hopping is the rate-limiting process.

In this investigation, an approximate value of the $E^{o'}$ of the $NADH^{\bullet+}/NADH$ redox couple was also evaluated. Extrapolating the linear $\log k_{obs}$ versus $E^{o'}$ relationship to the diffusion-controlled rate-limited region, a value equivalent to 0.808 V versus SCE was estimated for this solvent. Recalculating the $E^{o'}$ value for aqueous solution, a value of 0.688 V versus SCE could be given. With this value in mind, the authors stated that the very positive potential found is indicative of the instability of $NADH^{\bullet+}$. Only very powerful one-electron oxidants will be able to oxidize NADH by a mechanism pathway involving one-electron transfer. Pulse radiolysis and laser flash photolysis studies [42, 127] further support this as $NADH^{\bullet+}$ is completely deprotonated within 1 μs , suggesting that $k_2[B]$ is greater than 10^6 s^{-1} at pH 7 in aqueous solution. In addition, the pK_a for $NADH^{\bullet+}$ could be estimated to be -3.5 , which is in agreement with that estimated from photochemical data in acetonitrile equal to -4 [39]. The value for deprotonation has later been determined to be $6 \cdot 10^6 \text{ s}^{-1}$ by Matsue and coworkers [128] who used pure aqueous buffers instead of a mixture of water and one-propanol. These authors evaluated the $E^{o'}$ of the $NADH^{\bullet+}/NADH$ to be 0.78 V versus SCE.

From these data, it is clear that the equilibrium of reaction (17) favors the left-hand side, but the existence of the fast irreversible reaction (18) allows reaction (17) to proceed in the forward direction. Reaction (19) is a homogeneous electron-transfer reaction. It proceeds irreversibly as the potential of the NAD^\bullet/NAD^+ couple is at least 1.3 V more negative [140] than that of the Fc^+/Fc couple, which in turn indicates that the equilibrium constant for reaction (19) is less than equal to 10^{-20} .

4.3.2

Two-electron-proton Acceptors4.3.2.1 ***o*-quinones and *p*-quinones**

Miller and coworkers have also investigated in a series of papers the homogeneous reaction with two-electron-proton acceptors, quinones and quinoneimines, both with electrochemistry and spectroscopy [141–143]. Initially, they started by reporting on the reaction between NADH and quinoneimines with electrochemical techniques (see in the following text). The UV/vis spectroscopy was also employed to examine the reaction kinetics and mechanism between NADH and 7 different *o*-quinones and 14 *p*-quinones in a pH interval between 6 and 8 [143]. As these two-electron-proton acceptors are capable of both electron transfer and hydride routes, the hope was to find evidence for either of the two basically different reaction pathways. Experiments run with deaerated and oxygen-saturated solutions yielded the same results revealing that molecular oxygen did not affect the reaction at all. They also compared the reaction rate with α - and β -NADH and two different quinones and found it to be in agreement with earlier investigations [144] that α -NADH has a higher reaction rate with these mediators than β -NADH, attributed to differences in conformation between α - and β -NADH. In summary, the reaction of NADH with all quinones investigated was first order in each reactant with a stoichiometry of 1 : 1. Using singly or doubly deuterated NADH, no reduced quinone was found with a deuterium incorporated onto a hydroquinone carbon; however, there was a primary isotope effect and a substantial substitution effect on the rate. Thus, there is strong evidence that the hydrogen is being exchanged between carbon (NADH) and oxygen (hydroquinone).

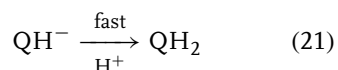
To answer the question whether the reaction between NADH and quinone type acceptors occurs according to a single step 1H^- transfer or sequentially either as $\text{H} - 1\text{e}^-$ or as $1\text{e}^- - \text{H}^+ - 1\text{e}^-$, has not been easy to resolve. Miller and coworkers [143] found that in general, the *o*-quinones reacted about 100 times more rapidly than *p*-quinones with comparable $E^{\circ'}$ -values. No variation of the second-order reaction rate constant (k_{obs}) with pH could be found. However, there was a linear correlation between $\log k_{\text{obs}}$ and the $E^{\circ'}$ value of the Q/QH^- redox couple at pH 7, $E^{\circ'}_{\text{Q}/\text{QH}^-, \text{pH}7}$, rather than with the Q/QH_2 redox couple for both *o*- and *p*-quinones. The slopes of the $\log k_{\text{obs}}$ versus $[\text{NADH}]$ for the two groups of quinones were close to identical (*o*-quinones; 16.4 V^{-1} , *p*-quinones; 16.9 V^{-1}), reflecting that when the reaction in both cases (*o*- and *p*-quinones) becomes more exothermic, one-half of the change in the thermodynamic value is reflected in the activation free energy, which in using electrochemical terms is equal to $\alpha = 0.5$. This could explain why no variation of the reaction rate was found with pH as the $E^{\circ'}$ s of both NAD^+/NADH and the Q/QH^- redox couples will move with 30 mV/pH-unit and thus the thermodynamic driving force will remain constant with a change in pH. Thus, strong evidence was presented showing that the initial step was not electron transfer generating NADH^+ or proton transfer to solution but rather transfer of the NADH hydrogen to the quinone oxygen in the rate-limiting step. However, the investigation did not decide whether the charge transfer occurred in a single one-hydride step or in a stepwise mode within an intermediate charge-transfer complex.

At pH 7, the simple one-step hydride transfer would occur according to the following. In the first step, the hydride

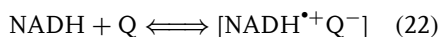
is transferred from NADH to the quinone yielding NAD^+ and QH^- .



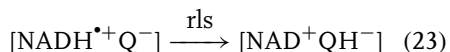
This is followed by rapid protonation of QH^- .



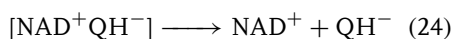
A net hydride transfer could also occur sequentially but within a complex according to two alternative reaction pathways proposed. In the first one [reactions (22)–(24)], the reaction starts with complex formation and donation of the first electron



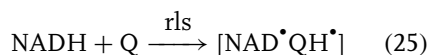
which is followed in a rate-limiting step by the transfer of the hydrogen atom



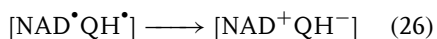
and finally, by the dissociation of the complex;



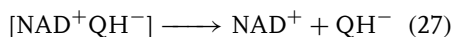
In an alternative pathway [reactions (25)–(27)], the formation of the complex is followed immediately by the transfer of a hydrogen atom



followed by the transfer within the complex of the second electron



and finally, the formation of the products

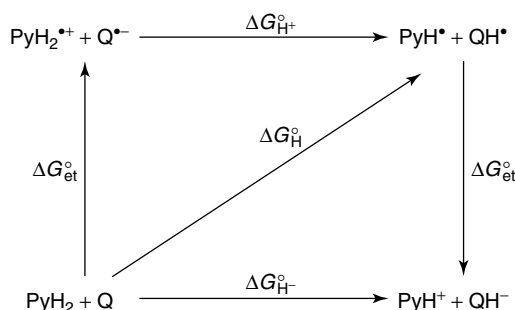


The general conclusion drawn by Miller and coworkers is that the charge transfer from NADH to the two-electron-proton acceptors does not occur according to an outer sphere stepwise

one-electron-transfer reaction but rather according to a hydride transfer mechanism. However, as there is definite proof for an intermediate charge transfer complex being formed between the two reactants (see the following text), the hydride equivalent can be transferred stepwise within the complex and rate-limiting hydrogen atom transfer followed by electron transfer (H, e^-) could not be ruled out.

In another series of detailed reports, Fukuzumi and coworkers [43–45, 47, 48, 50, 55] have tried to find evidence for an $\text{e}^- - \text{H}^+ - \text{e}^-$ sequence occurring between NADH analogues and quinones. They investigated the reaction between a great number of dihydropyridine compounds (PyH_2), being NADH model compounds, with *p*-benzoquinone derivatives (Q) in acetonitrile in the presence and absence of Mg^{2+} . In their investigations, they have proven that when PyH_2 reacts with Q, a charge transfer complex is formed [145,146]. Such complexes have been isolated and also their spectra have been detected. The investigated NADH model compounds could be divided into two separate groups: those equal to 1-(substituted benzyl)-1,4-dihydronicotinamide (X-BNAH) derivatives and *N*-methylacridan (AcH_2). Several possible reaction steps were examined that would yield the strongest correlation between the evaluated second-order rate constant, k_{obs} , and the ΔG through linear ($\log k_{\text{obs}}$ vs. ΔG) relationships. This necessitated the calculation of ΔG for a number of possible reaction steps.

In Sch. 2, possible reaction steps are revealed for which expressions for ΔG needed to be found. The ΔG_{et}^0 denotes the Gibbs free energy change for the transfer of the first electron, $\Delta G_{\text{H}^+}^0$ for the transfer of the proton, $\Delta G_{\text{et}'}^0$ for the transfer of the second electron, ΔG_{H}^0 for the transfer



Scheme 2 Proposed reaction pathways between dihydropyridine compounds (PyH₂) used as NADH model compounds and quinone derivatives.

of the hydrogen atom, and ΔG_{H-}° for the transfer of the hydride. The expressions relating these parameters are given below:

$$\frac{\Delta G_{et}^{\circ}}{F} = E^{\circ'} \left(\frac{\text{PyH}_2^{\bullet+}}{\text{PyH}_2} \right) - E^{\circ'} \left(\frac{\text{Q}}{\text{Q}^{\bullet-}} \right) \quad (28)$$

$$\frac{\Delta G_{et'}^{\circ}}{F} = E^{\circ'} \left(\frac{\text{PyH}^+}{\text{PyH}^{\bullet}} \right) - E^{\circ'} \left(\frac{\text{QH}^{\bullet}}{\text{QH}^-} \right) \quad (29)$$

$$\Delta G_{H+}^{\circ} = 2.3RT \left[\text{p}K_a \left(\frac{\text{PyH}_2^{\bullet+}}{\text{PyH}^{\bullet}} \right) - \text{p}K_a \left(\frac{\text{QH}^{\bullet}}{\text{Q}^{\bullet-}} \right) \right] \quad (30)$$

The $E^{\circ'}$ values of the $\text{PyH}_2^{\bullet+}/\text{PyH}_2$ and $\text{PyH}^+/\text{PyH}^{\bullet}$ were determined by CV, whereas the $E^{\circ'}$ values for $\text{Q}/\text{Q}^{\bullet-}$ and $\text{QH}^{\bullet}/\text{QH}^-$ were taken from the literature data. The addition of Mg^{2+} was motivated as these ions can form complexes with either PyH_2 and/or Q , thus affecting the oxidation potential of PyH_2 ($\text{PyH}_2^{\bullet+}/\text{PyH}_2$) or reduction potential of ($\text{Q}/\text{Q}^{\bullet-}$). Necessary $\text{p}K_a$ values could also be calculated. The final missing ΔG values, ΔG_H° and ΔG_{H-}° for correlations for hydrogen atom and single hydride transfer can then easily be calculated:

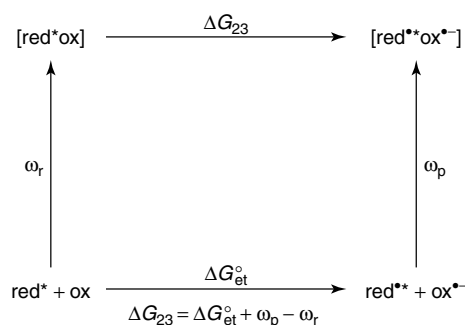
$$\Delta G_H^{\circ} = \Delta G_{et}^{\circ} + \Delta G_{H+}^{\circ} \quad (31)$$

$$\Delta G_{H-}^{\circ} = \Delta G_{et}^{\circ} + \Delta G_{H+}^{\circ} + \Delta G_{et'}^{\circ} \quad (32)$$

When plotting $\log k_{\text{obs}}$ versus ΔG_{H-}° (equivalent to a hydride transfer), two linear relationships were found with different intercepts: one for the X-BNAH derivatives and another for AcH_2 . The slopes of these straight lines were almost equal and show that as the reaction becomes more exothermic, about half of the change in ΔG_{H-}° is reflected in the activation barrier of the hydride-transfer reaction, that is, $\alpha = 0.5$, which is in accordance with the results of Miller and coworkers (see preceding text). On the other hand, when plotting $\log k_{\text{obs}}$ versus ΔG_H° , only one single straight correlation was found for all investigated X-BNAH derivatives including AcH_2 . The slope was larger by a factor of 2 than the slopes for the $\log k_{\text{obs}}$ versus ΔG_{H-}° plots, indicating that the change in ΔG_H° is directly reflected in the activation barrier of the hydride-transfer reactions, that is, α is close to unity (0.91). Thus, a single correlation of $\log k_{\text{obs}}$ versus ΔG_H° for both all X-BNAH derivatives and AcH_2 , in combination with the different intercepts between X-BNAH and AcH_2 in the plots of $\log k_{\text{obs}}$ versus ΔG_{H-}° ($= \Delta G_H^{\circ} + \Delta G_{et'}^{\circ}$), reveals that the activation barrier of the hydride-transfer reactions from PyH_2 to Q is dependent on only ΔG_H° and thereby independent of $\Delta G_{et'}^{\circ}$; the different correlations of the $\log k_{\text{obs}}$ versus ΔG_{H-}° plots between X-BNAH and AcH_2 are caused mainly by the

difference in the reduction potentials between X-BNAH/X-BNAH[•] (−1.08 V) and AcH/AcH[•] (−0.43 V). The apparent correlation of $\log k_{\text{obs}}$ versus $\Delta G_{\text{H}^-}^{\circ}$ may hold, provided that $\Delta G_{\text{et}}^{\circ}$ is correlated with $\Delta G_{\text{H}}^{\circ}$ in a homologous series of reactions. Thus, as $\Delta G_{\text{H}}^{\circ}$ consists of $\Delta G_{\text{et}}^{\circ}$ and $\Delta G_{\text{H}^+}^{\circ}$, the mechanistic question is reduced to (I) a direct transfer of a hydrogen atom from PyH₂ to Q, followed by an exothermic electron transfer from PyH[•] to QH[−] or (II) an electron transfer from PyH₂ to Q in the activation process and the subsequent proton transfer from PyH₂^{•+} to Q^{•−}, followed by an exothermic electron transfer from PyH[•] to QH[•]. To answer that question, Fukuzumi and coworkers investigated whether there were primary kinetic isotope effects ($k_{\text{H}}/k_{\text{D}}$) as they may provide useful information on whether an actual transfer of hydrogen nucleus occurs as a form of proton or hydrogen atom. Indeed, primary isotope effects were found. In the case of the electron-transfer activation mechanism, a kinetic isotope effect is expected to be attributed only to the proton transfer from PyH₂^{•+} to Q^{•−} as it is not expected for the electron-transfer process from PyH₂ to Q or from PyH[•] to QH[•]. Strong linear correlation was found between $\log (k_{\text{H}}/k_{\text{D}})$ and $(\Delta G_{\text{H}^+}^{\circ}/F)^2$ in agreement with the Marcus equation, whereas no linear correlation was found between $\log (k_{\text{H}}/k_{\text{D}})$ and $(\Delta G_{\text{H}}^{\circ}/F)^2$, indicating that the primary isotope effect was not correlated with $\Delta G_{\text{H}}^{\circ}$. A hydride transfer would require that $k_{\text{H}}/k_{\text{D}}$ should remain constant with a linear change in $\Delta G_{\text{H}^-}^{\circ}$ for the case where $\alpha = 0.5$. It could thus be concluded that an actual transfer of hydrogen nucleus occurs as a form of proton and the electron-transfer activation mechanism seems to be the most plausible one to explain both the variation of the rate constants and

the primary kinetic isotope effects in the hydride-transfer reactions from PyH₂ to Q. Furthermore, it was shown that a single correlation between $\log k_{\text{obs}}$ and $\Delta G_{\text{et}}^{\circ}/F$ for different X-BNAH, AcH₂, and NADH (whether in acetonitrile or water) in the absence and presence of Mg²⁺ prevails indicating that the activation barrier of the hydride-transfer reactions is well correlated with the energetics of the electron transfer $\Delta G_{\text{et}}^{\circ}$. However, the investigation also included studies of one-electron nonproton acceptors and the results from previous investigations on the use of such oxidants were also used for calculations. As a general remark, comparing the values of k_{obs} obtained for one-electron-nonproton acceptors and for the quinones (hydride acceptors) with similar $E^{\circ'}$ values, one finds that it is greater for the quinones. This fact has been used as evidence against an electron-transfer process involvement in the hydride-transfer reaction by assuming that the work term, ω_{p} , of the radical ion pair produced upon electron transfer can be neglected. However, as the reaction between NADH and its analogues occurs within a CT-complex through an inner sphere electron-transfer mechanism, the work term, ω_{p} , of the radical ion pair of opposite charges is expected to be much larger than for an outer sphere reaction mechanism and thus cannot be neglected. Sch. 3 reveals the difference between an outer sphere and an inner sphere reaction mechanism and also the relationship between $\Delta G_{\text{et}}^{\circ}$ and ΔG_{23}° , that is, the free energy change for the initial electron transfer occurring within the CT-complex, the second step in reaction (33). ω_{p} and ω_{r} are the work terms required to bring the products (red^{•+} and ox^{•−}) and the reactants (red^{*} and ox) together to the mean separation in the activated complex, which are largely coulombic. ω_{r} may be neglected

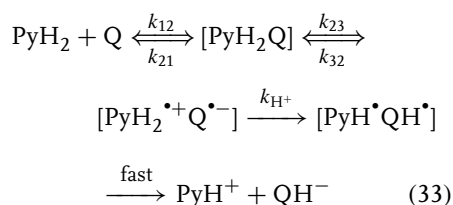


Scheme 3 Reaction mechanisms and relationship between the $\Delta G_{\text{et}}^{\circ}$ and ΔG_{23}° within the CT-complex.

as the reactants in the investigations included neutral species.

An expression for the rate constant, k_{obs} , based on these assumptions could thus be derived and when compared with experimental values, a good correlation was found.

The authors thus concluded that the most plausible reaction path would be accordingly what is outlined in reaction (33):



Miller and Valentine [147] in a later paper were sceptical of all the conclusions drawn by Fukuzumi and coworkers [47] and suggested that an appropriate and challenging view is that one-step hydride transfer should not be replaced by the more complicated three-step electron-proton-electron inner sphere mechanism until such evidence appears that unequivocally discriminates between the two pathways.

4.3.2.2 Aromatic Diimines

In addition to the extensive investigations of the reaction between NADH and various quinones and one-electron acceptors in solution, Miller and coworkers also

investigated the reaction between NADH and 14 diaminobenzenes and 7 diaminopyrimidines [141, 142]. These investigations were performed in aqueous solutions and with GC electrodes. The background and interest lie in the expected high reactivity of oxidized diamines as iminium ions are known to be better hydride acceptors than ketones and the mechanism has analogy in the flavin oxidation of NADH. The investigation concluded that the number of electrons transferred was equal to two, that 1,2-diimines are faster oxidants for NADH than 1,4-diimines, and that the transfer of the 4-hydrogen of NADH occurs to a protonated diimine. No real correlation could, however, be found between $\log k_{\text{obs}}$ and the $E^{\circ'}$ for these mediators. Also of significance is the finding that protonated diimines (i.e., positively charged) are more reactive than the corresponding neutral diimines. This is the first instance of positively charged mediators that are demonstrated superior to the neutral ones having otherwise the same catalytic functionality and $E^{\circ'}$.

It is thus possible to come up with some general remarks on the reactivity of possible oxidants for NADH. Two-electron-proton acceptors are better oxidants than one-electron-nonproton acceptors, aromatic diimines are better than quinones and oxidized aminophenols, oxidants with the catalytic functionality

located at the 1,2-position seem better than the corresponding ones having the catalytic functionality located in 1,4-position, and finally, positively charged mediators are better than neutral ones.

The need to be able to catalyze the electrochemical reactions of both NAD^+ and NADH at substantially lower applied potentials than at naked electrodes and with less or preferably no side reactions for any practical applications (analysis, fuel cells, electroorganic synthesis) has put focus on finding catalytic redox molecules (mediators) that can accomplish this goal. The use of mediators in bioelectrochemistry is today well established both for fundamental and applied purposes [23, 148–150]. One can in principle, divide the group of redox mediators into two separate groups: one-electron-nonproton acceptors/donors and two-electron-proton acceptors/donors. In recent years, in applied aspects of bioelectrochemistry, for example, in enzyme-based amperometric biosensors, focus has been on the use of the one-electron acceptors/donors rather than on the two-electron-proton acceptors/donors to facilitate shuttling of the electrons from/to the cofactor of redox enzymes and electrodes for the following reasons [150]: (1) as no protons participate in their redox conversion, the $E^{\circ'}$ remains constant with a change in pH and (2) there are no radical intermediates in the redox reaction prone to abortive side reactions. In contrast, the two-electron-proton acceptors/donors suffer from both of these two drawbacks in aqueous solutions. Thus, it is easily seen in the Marcus expression [151, 152] that a change in pH can greatly affect the second-order rate constant (k_{ET}) between the redox mediator of the two-electron-proton type and the enzyme cofactor, which in turn would in the case of an enzyme-based biosensor,

affect the response signal.

$$k_{\text{ET}} = \exp^{-\beta(d-d_0)} \exp^{-(\Delta G^{\circ} + \lambda)/4RT\lambda} \quad (34)$$

where β is the attenuation factor, d is redox-to-redox center distance, d_0 is equal to 3.6 Å, λ is the reorganization factor, and ΔG° the free energy change between the two reactants (in this case, between mediator and NAD^+ or NADH). However, neither the mediated oxidation of NADH nor the mediated reduction of NAD^+ (see in the following text) can be accomplished rapidly and continuously with redox compounds catalyzing a simple electron-transfer reaction in contrast to, for instance, flavin-containing oxidases and dehydrogenases, where the radical intermediates of the bound flavin molecule are stabilized within the protein globule by adjacent amino acid residues. Thus, for both electrocatalytic NADH oxidation and NAD^+ reduction, one has to look for redox mediators, which are able to accept/donate a hydride equivalent, either in one single reaction step or sequentially with the cofactor, and moreover, are able to be electrochemically converted into a sequential mode ($\text{e}^- - \text{H}^+ - \text{e}^-$) with the electrode and the contacting solution as the electrode is not likely to provide or to consume the proton. However, surface functionalities may facilitate proton transfer, see Fig. 4.

4.4 Electrocatalytic Oxidation of NAD(P)H at Mediator-modified Electrodes

4.4.1

General Remarks of CMEs

4.4.1.1 *o*-Quinones and Phenylenediimine Derivatives

The use of mediators as “depolarizing catalysts” in electrochemistry goes back to

the beginning of this century. The driving force to study the electrocatalytic oxidation reactions of NAD(P)H at electrodes intentionally modified, starting in the late 1970s, was based on several observations. The deliberate immobilization of compounds on electrode surfaces so that after immobilization, the electrode not only possesses its original properties but also those of the immobilized species was a relatively new area of research [153]. Bioelectrochemistry and electrochemistry in biology/medicine also experienced a dramatic increase in interest derived from the concept of enzyme-based amperometric biosensor in the 1960s. In 1977, the first two publications on efficient direct electron-transfer reactions with a small redox protein, cytochrome *c*, were reported [154, 155], rapidly followed by indirect electrochemical observation of direct electron transfer also with larger redox proteins with enzyme activity, lactase [156, 157], and HRP (horseradish peroxidase) [158] and the simultaneous interest in and increased knowledge of redox mediators to study biological redox systems [148]. It is therefore not surprising that during the same period, the first CME that was able to drastically reduce the large over voltage for electrochemical NADH oxidation appeared [159]. Since then, it has been the topic of many reports summarized in a number of review papers [76, 77, 149, 160–166]. Table 2 summarizes the extensive work done on CMEs for electrocatalytic NAD(P)H oxidation.

The first paper on a CME for electrocatalytic NADH oxidation reported by Tse and Kuwana in 1978 [159] was based on two primary amine containing *o*-quinone derivatives, dopamine or 3,4-dihydroxybenzylamine, that could be covalently immobilized onto the surface of cyanuric chloride-activated GC electrodes forming a monolayer on the electrode

surface. When immobilized, these redox compounds revealed from CV, $E^{\circ'}$ values of around +0.160 V versus SCE at pH 7 and the anodic peak potential in the presence of NADH at around +0.2 V. Thus, the over voltage could be reduced by some 0.4 V. When running CV, an ECE mechanism was shown for the electrocatalytic reaction. What was also important in their study was that they could confirm that enzymatically NAD^+ was produced as the product of the electrocatalytic reaction. The electrode also showed a high catalytic efficiency for the electrooxidation of ascorbate. However, there was a substantial difference in the stability of the surface-tethered *o*-quinone when catalyzing the oxidation of NADH or the oxidation of ascorbate. For NADH , the electrocatalytic property vanished after a few cycles, whereas for ascorbate, it seemed stable for a long term.

In a follow-up paper from Kuwana's group [167], an *o*-quinone derivative attached to a larger aromatic derivative (4-(2-(1-pyrenyl)vinyl)catechol) that strongly adsorbed on graphite was studied. When the mediator was kept in its reduced state (catechol), it was virtually stable for a long term. When kept in its oxidized state (*o*-quinone), some minor deactivation occurred with time, whereas when kept at a potential close to the $E^{\circ'}$, a much more rapid loss of electroactivity was noticed, explained by abortive side reactions caused by an initial reaction between catechol and *o*-quinone. In the presence of NADH , an even much faster deactivation process occurs, presumably caused by an intermediate semiquinone assumed to react with a radical intermediate of the coenzyme, $\text{NADH}^{\bullet+}$, to give an inactive compound, which poisons and blocks off the surface (Fig. 7).

Since the first paper by Tse and Kuwana, there have been numerous publications

Tab. 2 Chemically modified electrodes for electrocatalytic NAD(P)H oxidation based on inorganic and organic mediators

Mediating scheme	E^0/N vs. ref.	Immobilization	Rate constant $M^{-1} s^{-1}$	Sensitivity $\mu A\text{ } mM^{-1} cm^{-2}$	References
CARBON ELECTRODES					
Quinones	0–0.25 V vs. SCE, pH 7	Oxidized graphite, glassy carbon	800		132, 134–137, 169–174
Quinones	0.2–0.4 V vs SCE	Pretreated carbon fiber			101–105, 175
Sol-gel derived, ceramic-carbon electrodes	0.15 V vs. Ag/AgCl/KCl (satd.), pH 7.3				176
Alcohol dehydrogenase (ADH)- NAD ⁺ -modified carbon black	–0.04 V vs. SCE, pH 7.6	ADH + NAD ⁺ adsorbed on carbon black			177, 178
o-QUINONES					
3,4-Dihydroxybenzylamine (eugenol)	0.17 V vs. SCE, pH 7	Covalent on glassy carbon	$7.7 \cdot 10^4$ (homogeneous)		159, 179
Dopamine	0.13 V vs. SCE, pH 7	Covalent on glassy carbon			159
Dopamine	0.19 V vs. Ag/AgCl, pH 7	Electrochemical immobilization on glassy carbon	$3.6 \cdot 10^4$ (homogeneous)		180
Dopamine	0.2 V vs. Ag/AgCl, pH 7	Incorporated in lipid film cast onto glassy carbon			181
Imine derived from 3,4-dihydroxybenzaldehyde and 4-aminopyridine	0.34 V vs. Ag/AgCl, pH 7	Adsorption-self assembly on Pt		0.2 mM to 2.0 mM	182
Dopamine/3,4-dihydroxybenzoic acid	0.15 V vs. SCE, pH 7	Covalently bound to self-assembled cysteamine monolayers on Au		0.1 mM to 1.0 mM	183, 184

(continued overleaf)

Tab. 2 (continued)

Mediating scheme	E°/N vs. ref.	Immobilization	Rate constant $M^{-1} s^{-1}$	Sensitivity $\mu A\text{ } mM^{-1} cm^{-2}$	References
Poly(methacryloyl chloride) with dopamine	0.160 V vs. SCE, pH 6.35	Cast on glassy carbon			185
Poly(acryloyl chloride) or poly(methacryloyl chloride) with dopamine	0.17 V vs. SCE, pH 7	Cast on glassy carbon			186
Dopamine containing polymer	0.17 V vs. SCE, pH 7	Cast on glassy carbon		Diffusion controlled	187
Poly(3,4-Dihydroxybenzaldehyde) poly(2,3-DHB)	0.12–0.17 V vs. SSCE, pH 7	electropolymerized on GC, carbon felt/epoxy composite, effect of Mg^{2+} , Ca^{2+}	4.3 10^3 (3,4-DHB, pH 7) 1.3 10^3 (3,4-DHB, pH 8.5) 6.2 10^3 (3,4-DHB, pH 8.5, 20 mM Mg^{2+}) 10.2 10^3 (3,4-DHB, pH 8.5, 20 mM Mg^{2+})	0.01–1.2, 0.01–0.9 mM	188–192
4-Methyl-o-quinone	0.07 V vs. SCE, pH 8.2	Adsorbed on screen printed carbon			193
<i>p</i> -(4-Vinylpyridyl)- <i>N</i> -(3,4-dihydroxybenzylidene)aminobenzene	0.31 V vs. SCE, pH ~9.2.	Incorporated into the mercaptan monolayer on the electrode		0.1–2 mM	194
Chlorogenic acid (1,3,4,5-tetrahydroxycyclohexane-carboxylic acid 3-(3,4-dihydroxycinnamate))	0.223 V vs. Ag/AgCl, pH 7	Electrodeposited on GC	8.5 10^3 (0.05 mM NADH)	0.1–1.0 mM	195

4-[2-(2-Naphthyl)vinyl]catechol 4-[2-(9,10-ethanoanthracen-9-yl)vinyl]catechol	0.17 V vs. SCE	Adsorbed on graphite	$2 \cdot 10^6$	196
4-[2-(1-Pyrenyl)vinyl]catechol, 4-[2-(1-pyrenyl)ethano]catechol	0.10 V vs. SCE	Adsorbed on graphite	$1 \cdot 10^4$	167
1,2-Naphthoquinone	-0.15 V vs. SCE	Mixed with carbon paste		197
2,3-Dichloro-1,4-naphthoquinone covalently bound to N-substitutes pyrrole	-0.15 V vs. SCE, pH 7	Electropolymerized on carbon		164, 198
Mercaptohydroquinone	pH 6.35	Electropolymerized onto glassy carbon		199
Pyrroloquinoline quinone (PQQ)	-0.15 V vs. SCE	Covalent binding to cysteamine modified gold/N ϵ -2,4-dinitrophenyl lysine on gold	$2.3 \cdot 10^2$ (no Ca^{2+})	200–203
PQQ	-0.15 V vs. SCE, pH 7	PQQ-spiropyran monolayer on Au	$3.4 \cdot 10^4$ (20 mM Ca^{2+})	204, 205
PQQ	~0 V vs. SCE, pH 8.1	Immobilization of PQQ in electropolymerized films of aminobenzene isomers on gold, platinum and carbon		206

(continued overleaf)

Tab. 2 (continued)

Mediating scheme	E° / N vs. ref.	Immobilization	Rate constant $M^{-1} s^{-1}$	Sensitivity $\mu A\text{ } mM^{-1} cm^{-2}$	References
PQQ- NAD^+	-0.16 V vs. SCE, pH 8	Covalent attachment of PQQ to a cystamine monolayer on Au, followed by covalent linkage of N -(2-aminoethyl)- NAD^+			203, 207–209
Transition metal complexes containing 1,10-Phen- anthroline-5,6-dione Ligands [Re(phen-dione) (CO) ₃ Cl] and [Fe(phen-dione) ₃](PF ₆) ₂	0 V vs. SCE	Adsorbed on glassy carbon	$(6.2 \pm 0.6) 10^3$		210
	-0.05 V vs. SSCE, pH 8,	Mixed with carbon paste			211
	-0.03 V vs. SSCE, pH 8				
Os(4,4'-dimethyl-2,2'-bipyridine) ₂ (1,10-phenanthroline-5,6- dione)	0.032 V vs. Ag/AgCl, pH 7	Adsorbed on graphite	$1.9 \cdot 10^3$, at pH 6.1		212
Os(4,4'-dimethyl-2,2'-bipyridine) ₂ (1,10-phenanthroline-5,6- dione)	0 V vs. SCE, pH 6	Mixed with carbon paste		$140 \mu A\text{ } cm^{-2}$ $l\text{ } mmol^{-1}$	213
Homoleptic catechol-pendant terpyridine complexes [M(L2) ₂] ²⁺ (M = Co, Cr, Fe, Ni, Ru, and Os, and L2 = 4'-(3,4-dihydroxyphenyl)- 2,2' : 6',2''-terpyridine)	~0.1–0.3 V vs. Ag/AgCl, pH 7	Electrodeposition on GC and Pt			214

		<i>p</i>-QUINONE		
Chloranil		+0.050 V vs. SCE, pH 7	Covalent on graphite	164, 215
Chloranil covalently bound to <i>N</i> -substituted pyrrole		+0.1 V vs. SCE	Electropolymerization on carbon	164, 198
<i>p</i> -Benzoquinone		+0.115 V vs. Ag/AgCl, pH 7.3	Immobilized on graphite	216
<i>p</i>-PHENYLENEIMINE				
<i>p</i> -Phenylenediamine, <i>N,N,N',N'</i> - tetramethyl- <i>p</i> - phenylenediamine Variamine blue B		0.10 V vs. SCE	Mixed into carbon paste	217
Meldola blue		0.095 V vs. Ag/AgCl, pH 7	Adsorbed onto paraffin impregnated graphite	218
Meldola blue		−0.175 V vs. SCE	Adsorbed on graphite	160, 219–225
Meldola blue		−0.12 V vs. Ag/AgCl, pH 7	Adsorbed onto paraffin impregnated graphite	218
Meldola blue		−0.132 V vs. Ag/AgCl, pH 7.4	Immobilized as diamminetetra (isothio- cyanato)chromates (Reineckates) in graphite-epoxy composite electrodes	226
Meldola blue		−0.07 V vs. SCE, pH 7	Mixed into carbon paste	227, 228
Meldola blue		−0.14–−0.085 V vs. Ag/AgCl pH 7.5	Immobilized in electropolymerized films of polypyrrole with enzyme (ADH, LDH) and NAD ⁺	229, 230
Meldola blue		−0.05 V	Thick-film carbon electrode	231, 232

(continued overleaf)

Tab. 2 (continued)

Mediating scheme	E^0/V vs. ref.	Immobilization	Rate constant $M^{-1} s^{-1}$	Sensitivity $\mu A\text{ mM}^{-1} cm^{-2}$	References
Meldola blue	$-0.03\text{ V vs. SCE, pH } 7$	Immobilized on titanium phosphate coated onto a silica gel surface mixed with carbon paste		$1.0 \cdot 10^{-5} - 5.0 \cdot 10^{-5}\text{ M}$	233
Meldola blue	$\sim -0.1\text{ V vs. SCE}$	Immobilized in titania-, zirconia-sol-gel carbon composite electrodes		$2 \cdot 10^{-6} - 1 \cdot 10^{-3}$	234
Meldola blue	$0.11\text{ V vs. Ag/AgCl, pH } 7.3$	Immobilized in sol-gel, mixed into carbon paste		$0.5 - 10\text{ mM}$	176
Meldola blue	$-0.09 - 0.05\text{ V vs. SCE, pH } 7$	Adsorbed on Zr-phosphate mixed with carbon paste		39 mA M^{-1} ($10 - 200\text{ }\mu\text{M}$)	235
Random block methyl-siloxane polymer containing Meldola blue	$-0.15\text{ V vs. SCE, pH } 7$	Cast onto graphite		$40\text{ }\mu\text{A cm}^{-2}\text{ mM}^{-1}$	162, 236, 237
3-Anilino-Meldola blue	$-0.36\text{ V vs. SCE, pH } 7$	Adsorbed on graphite	$3 \cdot 10^3$		224
Azure I	$-0.225\text{ V vs. Ag/AgCl, pH } 7$	Adsorbed onto paraffin impregnated graphite	$0.63 \cdot 10^4$		218
Azure A	$\sim -0.01\text{ V vs. Ag/AgCl, pH } 7$	Covalently bound onto cystamine and cysteine modified gold			238
Azure A	$0.21\text{ V vs. Ag/AgCl, pH } 7$	Covalent bound to self-assembled monolayer of 3,3'-dithiobis(succinimidylpropionate) on Au	$5.5 \cdot 10^4$		239

Poly(Azure A) / poly(Azure I)	0.01 V vs. Ag/AgCl, pH 7/0.04 V vs. Ag/AgCl, pH 5.4	Electropolymerized on GC	0.3 A M ⁻¹	240–242
Azure II	–0.220 V vs. Ag/AgCl, pH 7	Adsorbed onto paraffin impregnated graphite	0.64 10 ⁴	218
Azure C	0.23 V vs. Ag/AgCl, pH 7	Covalent bound to self-assembled monolayer of 3,3'-dithiobis(succini- midylpropionate) on Au	9.5 10 ⁴	239
Methylene green	–0.115 V vs. Ag/AgCl, pH 7	Adsorbed on graphite/Adsorbed onto paraffin impregnated graphite	1.9 10 ⁴	218, 243
Methylene green Methylene green	–0.1 V vs. SCE 0.12 V vs. SCE, pH 7	Mixed into carbon paste Adsorbed on Zr-phosphate mixed into carbon paste		228, 241, 242 235
Poly(Methylene green)	0.112 V vs. Ag/AgCl, pH 5.4	Electropolymerized on GC	1.1 A M ⁻¹	241, 242, 244
Nile blue	–0.420 V vs. SCE, pH 7	Adsorbed on GC/ graphite/adsorbed on Ag	10	160, 221, 224, 245–247
Nile blue	–0.405 V vs. Ag/AgCl, pH 7	Adsorbed onto paraffin impregnated graphite	0.034 10 ⁴	218
Nile blue	–0.02 – –0.04 V vs. SCE, pH 7 (Zr), –0.03 V vs. SCE, pH 7	Adsorbed on Zr-, Ti-phosphate mixed into carbon paste	11 mA M ⁻¹ (10–120 μM)	235, 248–250

(continued overleaf)

Tab. 2 (continued)

Mediating scheme	$E^{\circ'}/V$ vs. ref.	Immobilization	Rate constant $M^{-1} s^{-1}$	Sensitivity $\mu A\text{ } mM^{-1} cm^{-2}$	References
Nile blue	~ -0.12 V vs. Ag/AgCl, pH 7	Covalently bound onto cystamine and cysteine modified gold			238
3- β -Naphthoyl-nile blue	-0.220 V vs. SCE, pH 7	Adsorbed on graphite	$5 \cdot 10^4$		164, 224, 245, 251–254
Bis(3,3-nile blue)-terephthoyl	-0.20 V vs. SCE, pH 7	Adsorbed on graphite	$2 \cdot 10^4$		255, 256
Poly(nile blue)	-0.07 V vs. SCE, pH 6.8	Electropolymerized on GC	$6.3 \cdot 10^2$		257
3- α -Pyrenylidene-nile blue	0.28 V vs. Ag/AgCl, pH 7	Adsorbed on graphite			255
Phenothiazine	-0.285 V vs. SCE, pH 7	Adsorbed onto paraffin impregnated graphite	$0.71 \cdot 10^4$		218
Toluidine blue O		Adsorbed on graphite/anodized glassy carbon/wax			221, 224, 245, 258–260
Toluidine blue O	-0.21 V vs. Ag/AgCl, pH 7	Adsorbed onto paraffin impregnated graphite	$1.01 \cdot 10^4$		218
Toluidine blue O	$-0.06 - 0.04$ V vs. SCE, pH 7 (Zr), -0.06 V vs. SCE, pH 7 (Ti)	Adsorbed on Zr-, Ti- phosphate mixed with carbon paste		$12\text{ mA } M^{-1}$	235, 249, 250, 261, 262
Toluidine blue O	-0.25 V vs. SCE, pH 7	Covalently bound onto carbon fibre		$(10 - 200\text{ }\mu M)$ $4.0 \cdot 10^{-5}$ – $1.5 \cdot 10^{-3}\text{ M}$	263

Toluidine blue O	~ -0.2 V vs. SCE, pH 7	Mixed into carbon paste		0.05–1.25 mM	264, 265
Toluidine blue O	Monomer: -0.125 V vs. Ag/AgCl, pH 7 (dimer: +0.135 V vs. Ag/AgCl, pH 7)	Covalently bound onto gold			238, 266/200
Poly(toluidine blue o)	0.05 V vs. Ag/AgCl, pH 5.4	Electropolymerized on GC/graphite			241, 242, 267, 268
Polymer containing covalently bound toluidine blue O	-0.1 ± 0.1 V vs. SCE, pH 7	RVC, graphite, mixed into carbon paste			269–277
3-β-Naphthoyl-toluidine blue O	-0.135 V vs. SCE, pH 7	Adsorbed on graphite	1.4 10 ⁴		224, 245
Methylene blue	-0.21 V vs. Ag/AgCl, pH 7	Adsorbed on paraffin impregnated graphite	0.8 10 ⁴		218
Methylene blue	0.08–0.1 V vs. SCE, pH 7 (Zr),	Adsorbed on Zr, Ti-phosphate mixed with carbon paste		28 mA M ⁻¹	235, 248, 249
Poly(methylene blue)	0.02 V vs. SCE, pH 7 (Ti)			(10–200 μM)	
	0.25 V vs. SCE, pH 7	Coelectropolymerized with pyrrole on GC		NADH 2.5 × 10 ⁻⁸ NADPH 4.0 × 10 ⁻⁸	278
Poly(methylene blue)	-0.04 V vs. SCE, pH 7	Electropolymerized onto a laponite gel			279
Poly(methylene blue)	0.015 V vs. Ag/AgCl, pH 5.4	Electropolymerized on GC		0.6 A M ⁻¹	241, 242

(continued overleaf)

Tab. 2 (continued)

Mediating scheme	E°/N vs. ref.	Immobilization	Rate constant $\text{M}^{-1} \text{s}^{-1}$	Sensitivity $\mu\text{A mM}^{-1} \text{cm}^{-2}$	References
Poly(methylene blue)	0.1 V vs. SCE, pH 9	Electropolymerized on screen printed gold			280
Brilliant cresyl blue	-0.34 V vs. SCE, pH 7	Adsorption on graphite			224, 259
Brilliant cresyl blue	-0.280 V vs. Ag/AgCl, pH 7	Adsorbed on paraffin impregnated graphite	$0.024 \cdot 10^4$		218
Brilliant cresyl blue	-0.02 V vs. SCE, pH 7 (Zr), -0.130 V vs. SCE, pH 7 (Ti)	Adsorbed on Zr-, Ti-phosphate mixed with carbon paste			235, 249
Brilliant cresyl blue	~ -0.035 V vs. Ag/AgCl, pH 7	Covalently bound onto cystamine and cysteine modified gold			238
Poly(brilliant cresyl blue)	0.048 V vs. Ag/AgCl, pH 7.4	Electropolymerized on GC		0.2 A M^{-1}	241, 242, 281
3- β -Naphthoyl-brilliant cresyl blue	-0.180 V vs SCE, pH 7	Adsorbed on graphite	$3 \cdot 10^4$		224
3- β -Naphthoyl-brilliant cresyl blue	0 V vs. SCE	Mixed with carbon paste			282
Methylene violet	0.005-0.02 V vs. SCE, pH 7	Adsorbed on Zr-phosphate mixed with carbon paste			235

Thionine	−0.02 V vs. SCE, pH 7 (Zr), 0.08 V vs. SCE, pH 7 (Ti)	Adsorbed on Zr-, Ti-phosphate mixed with carbon paste	235, 249
Thionine	0.14 V vs. SCE, pH 7	Covalently bound to self-assembled cysteamine monolayer	283, 284
Thionine	0.24 V vs. Ag/AgCl, pH 7	Covalent bound to self-assembled monolayer of 3,3'-dithiobis(succinimidypropionate) on Au	239
Crosslinked thionine	0.07 V vs. Ag/AgCl, pH 7	Reaction of thionine with toluene diisocyanate (triisocyanate) on glassy carbon/graphite	285, 286
Poly(thionine)	0 V vs. Ag/AgCl, pH 7	Electropolymerized on graphite/gold/glassy carbon/In-Sn oxide conducting glass	287–290
Methyl violet	0.02 V vs. SCE, pH 7 (Zr), 0.03 V vs. SCE, pH 7 (Ti)	Adsorbed on Zr-, Ti-phosphate mixed with carbon paste	235, 249
Resorufin	−0.26 V vs. SCE, pH 7	Adsorbed on graphite	160
Gallocyanine	−0.2 V vs. SCE, pH 7	Adsorbed on graphite	160
Methyl capri blue	−0.3 V vs. SCE, pH 7	Adsorbed on graphite	160

(continued overleaf)

Tab. 2 (continued)

Mediating scheme	E°/N vs. ref.	Immobilization	Rate constant $\text{M}^{-1} \text{s}^{-1}$	Sensitivity $\mu\text{A mm}^{-1} \text{cm}^{-2}$	References
Ethyl capri blue	$-0.31 \text{ V vs. SCE, pH } 7$	Adsorbed on graphite	10		160
N-methylphenazinium	$-0.16 \text{ V vs. SCE, pH } 7$	<i>o</i>-PHENYLENEDIIMINE (Electro)adsorbed onto graphite			291–295
N-ethylphenazinium	$-0.21 \text{ V vs. SCE, pH } 7$				
1-Methoxy-N-methylphenazinium	-0.15 V vs. SCE	Adsorbed onto paraffin impregnated graphite Immobilized as diamminetetra(isothiocyanato)chromates (Reineckates) in graphite-epoxy composite electrodes	$0.42 \cdot 10^4$		218
N-methyl-phenazinium	$-0.110 \text{ V vs. Ag/AgCl, pH } 7$				
1-methoxy-N-methylphenazinium	$-0.12 \text{ V vs. Ag/AgCl, pH } 7.4$		$3 \cdot 10^3$ (NMP ⁺) $6.5 \cdot 10^3$ (M-NMP ⁺)	$0.5 \mu\text{M} - 3 \text{ mM}$	226
N-methyl-phenazinium	-0.1 V vs. SCE	Immobilized in electropolymerized 1,2-, 1,3-, 1,4-diaminobenzene (DAB), pyrrole-2-carboxylic acid (PY-2-COOH) and 4,4'-dihydroxybenzophenone (DHB) on Au, Pt, carbon electrodes		$10^{-6} - 10^{-2} \text{ M}$	296

N-methylphenazinium + HRP + polyvinyl pyridine complexed [Os(bpy) ₂ Cl] ^{3+/2+} -polymer	0–0.1 V vs. SCE, pH 7		1 A cm ⁻² M ⁻¹ , 1 10 ⁻⁷ –2 10 ⁻⁴ M	297
Poly(o-phenylenediamine) (PPD)	0 V vs. SCE	Electropolymerized on carbon paste		264, 298, 299
p-AMINOPHENOL				
2,6-Dichlorophenol-indophenol	0.055 V vs. Ag/AgCl, pH 6.5	Adsorption onto graphite electrode and onto graphite electrodes pretreated with La(NO ₃) ₃ or Th(NO ₃) ₄	0.008–0.2 mM	300
9H-benzophenoxazin-9-one	–0.2 V vs. SCE, pH 7	Adsorbed on graphite	1.1 10 ³	160, 301
Poly(o-aminophenol) (PAP)	0 V vs. SCE			264, 298
Poly(aniline)-poly(vinylsulfonate)	0.1 V vs. SCE, pH 7	Electropolymerized on GC		302
Poly(indole-5-carboxylic acid)		Glassy carbon		303
Poly(phenosafrafranine)	–0.4– –0.2 V vs. Ag/AgCl, pH 7	Electropolymerized on graphite		304
FLAVIN				
Riboflavin	–0.430 V vs. Ag/AgCl, pH 7	Adsorbed onto paraffin impregnated graphite	0.083 10 ⁴	218
Riboflavin	–0.220 V vs. SCE, pH 7 (Zr), –0.33 V vs SCE, pH 7 (Ti)	Adsorbed on Zr-, Ti-phosphate mixed with carbon paste	8 10 ²	235, 249, 305, 306
FAD	–0.43 V vs. SCE, pH 7	Covalently bound to GC		307
FAD and FMN	–0.250 V vs. SCE, pH 7	Adsorbed on TiO ₂ modified carbon fibers	1–8 mM	308, 309

(continued overleaf)

Tab. 2 (continued)

Mediating scheme	E°/N vs. ref.	Immobilization	Rate constant $M^{-1} s^{-1}$	Sensitivity $\mu A\text{ } mM^{-1} cm^{-2}$	References
10-(3'-Methylthiopropyl)- isoalloxazinyl-7-carboxylic acid	-0.36 V vs. Ag/AgCl, pH 7	Adsorbed on Au	No catalysis		310
OTHER CATALYSTS					
Naphthol green B	-0.05 V vs. SCE, pH 7	Electropolymerized on glassy carbon	$9 \cdot 10^2$		311
2,7-Dinitro-9-fluorenone, 2,4,7-trinitro-9-fluorenone, 2,4,5,7-tetranitro-9-fluorenone	-0.05 V vs. Ag/AgCl, pH 8	Electrochemical reduction of adsorbed X-nitro-9-fluorenone on GC yields the hydroxylamine	$5.2 \cdot 10^4$	5 μM - 2 mM	312
2,4,7-Trinitro-9-fluorenone, 2,5,7-trinitro-9-fluorenone-4- carboxylic acid	-0.045 V vs. Ag/AgCl, pH 8 (-0.7 V vs. Ag/AgCl, 0.2 M Ca^{2+})	Electrochemical reduction of adsorbed X-nitro-9-fluorenone on GC yields the hydroxylamine			313
5,5'-Dithiobis(2-nitrobenzoic acid)	-0.04 V vs. SSCE, pH 7	Electrochemical reduction of adsorbed 5,5'- dithiobis(2-nitrobenzoic acid) on Au yields the hydroxylamine			314
NAD^+	0.13 V vs. Ag/AgCl, pH 7	Electropolymerization of NAD^+ mixed with carbon paste	$2.5 \cdot 10^5$	$1 \cdot 10^{-6}$ - $1 \cdot 10^{-5} M$	139

Various benzimidazole, 2-benzimidazolinone, 1,2,3,4-tetrahydroquinoxalinone-2, 1,5-benzodiazepine derivatives	~0.1 V vs. Ag/AgCl, pH 7	Adsorbed on pretreated carbon or Pt	315
Tetrathiofulvalene (TTF)	0.3 V vs. Ag/AgCl, pH 7.8	Mixed with carbon paste	316–318
Tetracyanoquinodimethan (TCNQ)	0.38 V vs. SCE	Adsorption on graphite	319, 320
	0.36 V vs. SCE	Electroadsorption on graphite	
TCNQ	0.22 V vs. SCE, pH 7.5	Mixed with carbon paste	316–318, 321
CONDUCTING SALTS			
NMA ⁺ TCNQ ⁻	+0.3 V vs. Ag/AgCl, pH		322
NMP ⁺ TCNQ ⁻	-0.2–+0.07 V vs. Ag/AgCl, pH 7	Deposition of conducting salt on glassy carbon or mixed with carbon paste	322–329
TTF:TCNQ	0.1–0.4 V vs. SCE, pH 7	Deposition of conducting salt on glassy carbon or mixed with carbon paste	327, 330
Hexamethylenetetratellurafulvalene tetracyanoquinodimethane (HMTTeF-TCNQ)			330, 331
OTHER MEDIATORS			
Mn ^{III} -meso-terraphenylporphine	-0.67 V vs.	Adsorption	332
Poly(metallophthalocyanine) Ni, Co, Zn	0.01 V vs. SCE, pH 7.4	Electropolymerized on glassy carbon	333

(continued overleaf)

Tab. 2 (continued)

Mediating scheme	E°/V vs. ref.	Immobilization	Rate constant $M^{-1} s^{-1}$	Sensitivity $\mu A\text{ mM}^{-1} cm^{-2}$	References
Tetraruthenated cobalt-porphyrin complex	0.7 V vs. Ag/AgCl	Films		ppb NADH	334
NaNiFe(III)(CN)_6	+0.2 V vs. Ag/AgCl pH 7.5	Electrodeposition on Ni			335
CoFe(II)(CN)_6	0.42 V vs.				336
Highly boron-doped conductive diamond electrodes	0.58 V vs. SCE, pH 7.1	Electrodeposition on Au		0.5–6.0 mM 0.1–0.5 μM	337, 338
<i>p</i> -Ferrocenylaniline films	0.25 V vs. Ag/AgCl, pH 7.2	Electrodeposited and adsorbed on carbon		0.25	339
Dimethylferrocene	0.3 V vs. Ag/AgCl, pH 7.8	Mixed with carbon paste			316, 317
Poly(3-methylthiophene)	0.45 V vs. Ag/AgCl, pH 7	Electrodeposition on Pt		10 ppb	340, 341
Os(bpy)_2 (PVI) $_{10}\text{Cl}$ polymer-	0.23 V vs. Ag/AgCl, pH 7	Polymer modified carbon fiber			342
Metallized carbon	0–0.2 V vs. SCE, pH 7				343–346

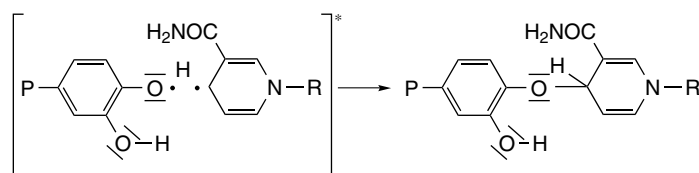


Fig. 7 Deactivation mechanism proposed for an adsorbed mediator of the *o*-quinone type and NADH [167].

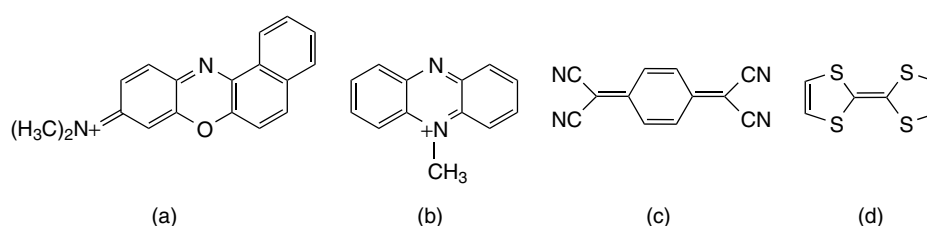


Fig. 8 Structural formulas of some commonly used mediators for catalytic NADH oxidation: (a) Meldola blue (*p*-phenylenediimine) [220, 252]; (b) *N*-methylphenazinium (*o*-phenylenediimine) [291]; (c) TCNQ [319]; and (d) TTF [316].

on CMEs for electrocatalytic NADH oxidation (Table 2). The structural formulas of the most common mediators are presented in Fig. 8. Analyzing these CMEs, a number of principally different evolution lines can be identified: (1) Search for a catalytic functionality other than a neutral *o*-quinone derivative that could further reduce the over voltage and at the same time, serve as a long-term stable catalyst. (2) Immobilization chemistry other than covalent binding to the electrode surface based on functionalization of solid electrodes. (a) Mediator derivatives that form strong interactions with the electrode surface such as adsorption of extended aromatic ring systems on carbon (graphite) and mediator-thiol derivatives forming self-assembled monolayers on gold. (b) Mediator derivatives that can be electropolymerized or trapped within electropolymerized layers onto the electrode surface. (c) Covalent introduction of

the mediator molecule into a polymeric backbone that can be cast onto solid electrodes. Other alternatives have been the mixing of monomeric or polymeric mediators into composite electrodes such as carbon paste [168] or the use of NAD(P)H-oxidizing enzymes immobilized on the electrode surface (Table 3).

The demands on the perfect mediator are very high. A successful transducer has to meet a number of demands. 1) The major object has been (and still is) to be able to substantially reduce the over voltage but at the same time, retain an acceptable reaction rate with at least a second-order rate constant of 10^6 to $10^7 \text{ M}^{-1} \text{ s}^{-1}$, preferentially higher, approaching a diffusion-controlled process. For sensor purposes, it would be highly desirable to be able to apply a potential of the electrode between 0 V and $\approx -0.2 \text{ V}$, that is, within “the optimal potential range”, where contributions to the response from

Tab. 3 Chemically modified electrodes for electrocatalytic NAD(P)H oxidation based on enzymes

Substrate Enzyme and mediator	Applied potential and pH	Immobilization	Linear response range	References
NADH Diaphorase	Direct electron transfer with electrode, 0 V vs. Ag/AgCl, pH 7.5–10.5	Entrapped on the surface of C paste and glassy C electrodes by covering with dialysis membranes.	10–80 μM	347
NADH Diaphorase + ferrocene	0.25 V vs. SCE, pH 7	Aminoferrocene, 2-aminoethylferrocene, or alkyl ferrocene- $\text{CH}_2\text{NH}(\text{CH}_2)_n\text{NH}_2$, ($n = 4-12$) was bonded with diaphorase onto poly(acrylic acid) film coated graphite felt electrode	0.01–0.1 mM	348–351
NADH Diaphorase + ferrocenemethanol	0.25 V vs. SCE, pH 7.5	Immobilized at the monolayer level at a Au electrode self-assembled with 2-aminoethanethiol		352
NADH Diaphorase + 2-ferrocenylethanol (2-FEA) or vitamin K3		Enzyme immobilized on electrode		353
NADH Diaphorase + hexacyanoferrate(III)	0.3 V vs. SCE, pH 9			354

NADH	–0.15–0 V vs. Ag/AgCl, pH 7–8.5	Enzyme on top of NAD ⁺ and mediator containing carbon paste	355–359
Diaphorase + ferrocene, <i>para</i> -benzoquinone, catechol, <i>para</i> -aminophenol, hexacyanoferrate, dichlorophenol-indophenol, anthraquinone sulfonate, vitamin K ₃ , flavines,			
NADH	0.4 V vs. SCE, pH 8	Immobilized on gold-plated polyester cloth	360
Diaphorase + ferrocenylmethanol			
NADH	0.2 V vs. SCE, pH 7	Immobilized on electrode	361
Diaphorase + ferrocenylmethanol			
NADH	0 V vs. SCE, pH 7	Immobilization of diaphorase within a laponite gel adsorbed on electrode surface	362
Diaphorase + electropolymerised methylene blue			
NADH	0.3 V vs. SCE, pH 7	Immobilized using PVA-SbQ on cylindrical carbon or Pt microelectrode	363
Diaphorase + ferricyanide			
NADH	0–0.25 V vs, SCE, pH 7.3	Enzyme and mediator mixed with carbon paste	228
Diaphorase + methylene green or Meldola blue		Meldola blue: 0.20 mA mM ^{–1} cm ^{–2} Methylene green: 0.24 mA mM ^{–1} cm ^{–2}	

(continued overleaf)

Tab. 3 (continued)

Substrate Enzyme and mediator	Applied potential and pH	Immobilization	Linear response range	References
NADH Diaphorase + Co(phen)_3^{3+}		Polypyrrole diaphragm electrode coated with diaphorase and Co(phen)_3^{3+}		364
NADH Diaphorase + ferricyanide	0.25 V vs. SCE, pH 7.5/0.3 V vs. SCE	Enzyme held behind a dialysis membrane – entrapped in a photocrosslinkable PVA bearing styrylpyridinium groups/Immobilized on NAD^+ modified carbon paste		365–368/369
NADH Diaphorase + cytochrome <i>c</i>	–0.2 V vs. SCE	Diaphorase electrostatically bound to cytochrome <i>c</i> immobilized $\text{In}_2\text{O}_3/\text{SnO}_2$ (ITO) electrode coated with polyglutamic acid derivatives		370
NADH Lipoamide dehydrogenase (diaphorase) + ferrocene	0.4 V vs. Ag/AgCl, pH 6–7	Redox gel formed from copolymerization of vinylferrocene with acrylamide and <i>N, N'</i> -methylenebisacrylamide and enzyme on ferrocene mixed with carbon paste	? –3 mM 0.67 $\mu\text{A mM}^{-1}$	371
NADH dehydrogenase + Ferrocenylmethanol, ferrocenecarboxylic acid, ferrocenebutyric acid	0.1 V vs. SCE, pH 6.8	Entrapped in a polypyrrole membrane on GC, direct ET with polypyrrole		372

NADH Salicylate hydroxylase + tyrosinase	−0.5 V vs. Ag/AgCl, pH 7.4	Enzymes mixed into carbon paste	1–50 μM	373, 374
NADH	0.15 V vs. SCE, pH 7	Dialysis membrane		375
NADH oxidase + 1',3'-dimethylferrocene ethanolamine				
NADH oxidase, $\text{RuCl}_6^{2-}/\text{RuCl}_6^{3-}$	0.15 V		1–10 mM NADH	376
NADH NADH oxidase + HRP + Os-PVP	−0.1–0 V vs. Ag/AgCl, pH 7	Redox gel formed on electrode	25 nM–10 μM	377
NADPH Ferrodoxin-NADP reductase	Direct electron transfer, −0.5–0 V vs. Ag/AgCl, pH 7.5	Adsorbed on glassy C, Au, or Ag electrodes	10–40 μM	347
NADPH Glutathione reductase + ferrocene	0.4 V vs. Ag/AgCl, pH 6–7	Redox gel formed from copolymerization of vinylferrocene with acrylamide and N, N'-methylenebisacrylamide and enzyme on ferrocene mixed with carbon paste	?–3 mM 1.05 $\mu\text{A mM}^{-1}$	371
NADH, NADPH	−0.1 V vs. SCE, pH 7	Electropolymerization of enzyme with amphiphilic pyrrole on electrode	29 $\text{mA M}^{-1} \text{ cm}^{-2}$, 0.2 μM (NADH), 15.8 $\text{mA M}^{-1} \text{ cm}^{-2}$, 0.4 μM (NADPH)	378–380
Flavin reductase + riboflavin				

easily oxidizable species, for example, ascorbate, urate, and acetaminophen, are negligible, where molecular oxygen is not electrochemically reduced, and where the potential of zero charge is found for most electrode materials resulting in low background currents and noise. In biofuel cell applications, the $E^{\circ'}$ of the mediator should approach that of NAD^+/NADH , so as not to lose any energy. 2) The mediator electrode should reveal long-life stability (weeks to months). The immobilization of the mediator should be irreversible. The chemical stability of the mediating functionality (hydrolysis, light decomposition, chemical oxidation), the electrochemical stability, and the stability in the presence of NADH (no radical side reactions) should be very high. 3). All reaction rates should be very high, and fast electron transfer rate between the electrode and the immobilized mediator, fast charge-transfer rate within the film (the latter applying to polymeric and multilayer coatings), fast reaction rate between NADH and the immobilized mediator should prevail. The mediator should be preferentially selective for NAD(P)H oxidation, have a well-defined stoichiometry with NAD(P)H , and finally, yield enzymatically active NAD^+ as the end product. In line with the work on homogeneous oxidation of NADH with oxidants referred to earlier, most work on CMEs for NADH oxidation has focused on the use of two-electron-proton acceptors. However, some work has been devoted to the use of one-electron-nonproton acceptor type mediators (Table 2). As anticipated, CMEs based on such types of mediators have been less successful in decreasing the over-voltage in reaching high reaction rates with NADH, and currently, there are no reports on the products formed as a result of the catalytic oxidation.

In agreement with the findings by Miller and coworkers [141], mediators incorporating a positively charged phenylenediimine functionality have shown some very promising properties. Monomeric phenylenediimines are neither for a long term chemically nor electrochemically stable, they cannot be easily immobilized onto an electrode surface, and the $E^{\circ'}$ is too high for any real applications. However, when introduced into a larger aromatic nucleus, the chemical and electrochemical stability is much increased and at the same time, the $E^{\circ'}$ is decreased by several hundred millivolts. Extended aromatic molecules are also strongly adsorbed onto carbon electrodes, especially onto graphite. Representative examples of such mediators are *N*-methylphenazinium (NMP^+ , “phenazine methosulfate”) incorporating a positively charged *o*-phenylenediimine functionality and 7-dimethylamino-1,2-benzophenoxazininium (“Meldola blue”), a positively charged *p*-phenylenediimine functionality (Fig. 8). These molecules have been studied since the early 1980s as electrode modifiers for NADH oxidation on the basis of their strong adsorption onto graphite [220, 252, 291]. In contrast to the earliest work on CMEs for NADH oxidation based on *o*-quinone modified electrodes, these modifiers allowed catalysis of NADH oxidation much below -100 mV versus SCE at pH 7 and with equal or even higher reaction rates with NADH than the *o*-quinones (Table 2). However, three- to four-membered aromatic ring systems such as NMP^+ and Meldola blue have restricted adsorption stability on graphite, and these mediators do suffer from chemical instability, NMP^+ being light-sensitive and easily demethylated and Meldola blue decomposing at pHs above 7.5 as it is underivatized in position 3. Numerous commercially available phenoxazine and

phenothiazine derivatives (common dyes, for example, Nile blue, methylene blue, and thionine) are derivatized in both position 3 and 7 with amine functionalities (at least one of which is a primary amine) making them alkaline-stable. However, as a result of the two “competing” *p*-phenylenediimine functionalities within these dyes, the positive charge is delocalized over the entire molecule with the result that the $E^{\circ'}$ is too low to result in high reaction rates with NADH. However, by coupling the primary amine functionality at position 3 or 7 of the commercially available phenoxazine and phenothiazine derivatives with, for example, an aromatic aldehyde or acid chloride, several beneficial new properties are donated to the original dye. The $E^{\circ'}$ of the original molecule at pH 7 is increased to a value close to that of Meldola blue (-175 mV vs. SCE, pH 7) as a result of the localization of the *p*-phenylenediimine functionality within the molecule and the number of aromatic rings can be increased, thereby stabilizing the CME [160, 219, 224, 245, 255, 256]. Still, these synthesized derivatives suffer from having pK_a values around

8 to 9, transferring the positively charged mediator into a neutral one at pHs higher than the pK_a (see Fig. 9), with the result that the reaction rate drastically drops, as also the long-term stability in the presence of NADH [162, 224]. The reason for this has not been elucidated but it could be speculated to be of the same origin as that of the *o*-quinones (Fig. 7).

A further support to the belief that positively charged mediators are superior to neutral ones with respect to reaction rate was shown in a work by Katz and coworkers [200]. PQQ (Fig. 10), was covalently immobilized onto a thiol derivative–modified gold electrode. The PQQ incorporates an *o*-quinone functionality and when immobilized, has an $E^{\circ'}$ value at pH 7 of -0.125 V versus SCE. In the presence of NADH, immobilized PQQ shows some moderate catalytic activity for NADH oxidation. However, when Ca^{2+} was added to the contacting solution, a much higher (≈ 10 times) catalytic activity was revealed by CV, although the addition of Ca^{2+} had virtually no effect on the $E^{\circ'}$ of PQQ; thus, the thermodynamic driving force ($\Delta E^{\circ'}$) remained constant. Addition of Ca^{2+} has also a

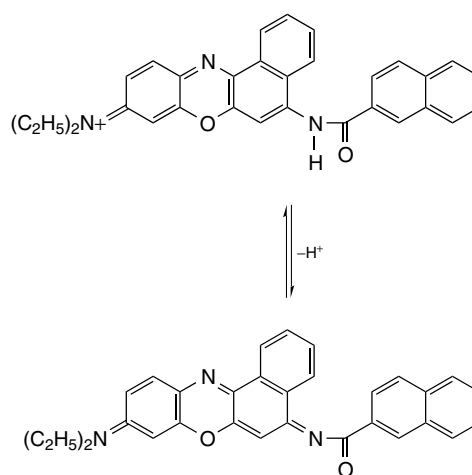


Fig. 9 Structural formulas of 3- β -naphthoyl-Nile blue (with a positively charged catalytic functionality having high reaction rate with NADH) and its imino form (with a neutral catalytic functionality having low reaction rate with NADH) [224].

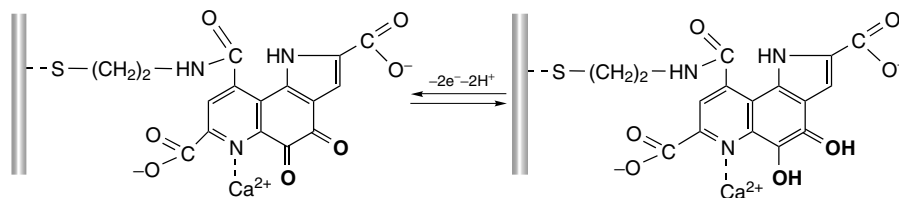


Fig. 10 Interaction of added Ca^{2+} ions with (PQQ) mediator covalently attached onto a thiol derivative gold electrode. The catalytic activity for NADH oxidation is increased ≈ 10 times with no effect on the E° of PQQ [200].

positive effect on the electron-transfer rate between the modifier and the electrode, increasing the rate constant from 3.3 to 18.7 s^{-1} . Other divalent metal ions such as Mg^{2+} and Ba^{2+} were also shown to have a positive effect on the reaction rate with NADH. Immobilized PQQ in the presence of Ca^{2+} have been used in a variety of biosensor prototypes. Of special interest is the further covalent binding of the surface-tethered PQQ with an enzymatically active NAD-derivative to form a coenzyme-mediator arrangement directly at the electrode surface [202, 203, 207–209].

Other *o*-quinone derivatives have also shown a drastic increase of the reaction with NADH in the presence of Ca^{2+} or Mg^{2+} . Electrodeposited 3,4-dihydroxybenzaldehyde on GC was shown to have a $\text{p}K_a$ of around 7 [190]. At pHs higher than the $\text{p}K_a$ value, the predominant form of the reduced form of the mediator is then QH^- , whereas below the $\text{p}K_a$, it is QH_2 . Additions of Mg^{2+} or Ca^{2+} were shown to increase the reaction rate with NADH only at pHs above the $\text{p}K_a$, reflecting the binding of the divalent ion only for the QH^- but not for the QH_2 form of the mediator.

Other larger aromatic ring systems incorporating *o*-quinone functionalities have also been investigated, especially 1,10-phenanthroline-5,6-dione. This compound has the ability to form strong and

stable complexes with a wide variety of transition metal ions such as Fe, Ru, Co, Cr, Ni, and Os, thus making the mediator molecule positively charged. Immobilization on carbon electrodes has been on the basis of adsorption [212], electropolymerization [210], or mixing with carbon paste [213]. The resulting CMEs showed good electrocatalytic properties for NADH oxidation.

One of the main drawbacks with the best modifiers for NADH oxidation is as mentioned earlier: the variation of the E° of the mediator with pH. However, in the last few years, some reports have been published where a variety of quinoic type mediators (phenoxazines, phenothiazines, phenazines, flavins) have been chemisorbed onto finely dispersed Zr- and Ti-phosphates, followed by mixing the resulting mediator-transition metal ion-phosphate complex into carbon paste electrodes [233, 235, 248–250, 261, 305, 306]. The resulting electrodes revealed high electrochemical activity of the bound mediator. The E° of the bound mediators did not or to a very low extent vary with the pH of the contacting solution. Although the E° remained constant with a change in pH, the E° value of the immobilized mediator could be somewhat (50–100 mV) influenced by the buffer constituents. When comparing the E° values of all bound mediators with their

$E^{\circ'}$ values in solution at pH 7, drastic shifts in the positive direction varied from about 50 to over 400 mV, thereby drastically increasing the reaction rate between the mediator and NADH (see also the following text).

4.4.2

Other Mediating Functionalities and Metal-coated Electrodes

Until a few years ago, most studied and efficient mediators used to incorporate either a *o*-quinone or a *p*-phenylenediimine functionality. There are, however, some other types of mediating structures known to have high reaction rates with NADH, for example, tetrathiafulvalene (TTF) and tetracyanoquinodimethane (TCNQ) (Fig. 8 and Table 2). Electrode materials based on acceptor/donor radical salts such as *N*-methylphenazinium tetracyanoquinodimethane (NMP-TCNQ) attracted much attention in the early 1980s. The conductivity of these materials is similar to that of

graphite and they have a working potential window of a few hundred millivolt around 0 V versus SCE. Oxidation of NADH on NMP-TCNQ radical salt electrodes was observed at -0.2 V [322–324], and thus the half-wave potential on the organic salt is shifted toward more negative potentials by 0.4 to 0.6 V as compared with carbon or platinum electrodes. The reaction rate for NADH oxidation was estimated to be close to that of Meldola blue and therefore, it would fall on the upper linear relationship in Fig. 11 (see further discussion). There has been some controversy regarding the reaction mechanism for NADH oxidation as to whether it occurs directly at the solid NMP-TCNQ (or TTF-TCNQ) electrode surface or is caused by the dissolution of some minor NMP^+ (or TTF^+) known as efficient oxidants for NADH.

In 1998 to 1999, some new efficient mediator functionalities were published. Aromatic molecules derivatized with nitro substituents can be electrochemically reduced to form hydroxylamine groups,

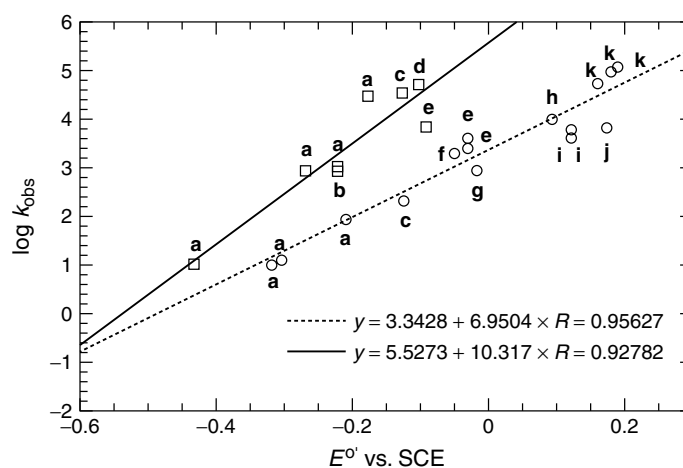


Fig. 11 Dependence of $\log k_{\text{obs}, [\text{NADH}] = 0}$ on the $E^{\circ'}$ at pH 7.0 for surface-immobilized mediators. Values taken from (a) [160], (b) [305], (c) [200], (d) [312], (e) [210] (pH 7.2), (f) [290], (g) [212], (h) [167], (i) [191], (j) [195] (calculated), (k) [239].

which in turn can be oxidized to nitroso groups by a two-electron-two-proton process [311–314]. In analogy to the quinone/hydroquinone system, the catalytic cycle involves the nitroso/hydroxylamine couple, as outlined in Fig. 12. Currently reported mediators show high reaction rates with NADH at low potentials (Table 2). The positive effect on the reaction rate in the presence of Ca^{2+} (up to 5 times) was also shown for some of these new types of mediators [313].

A drastic oxidation of carbon electrodes will introduce in a rather unselective way, oxygen-containing functionalities on its surface [90, 132–137, 172, 381–383]. Base-pretreated GC electrodes have been used to decrease the overpotential to around 350 mV, allowing LC-EC detection at 0.5 V versus Ag/AgCl with NADH limit of detection in the order of fmol [173]. Carbon-fiber microelectrodes, after electrochemical pretreatment [101–105, 175], have been used for NADH detection using fast scan (100 V/s) conditions to discriminate between NADH and other compounds that are also oxidized. The long-term stability of the pretreated carbon electrode surface is, however, far from great.

Various metal coatings on carbon electrodes have also been used to reduce the overvoltage for NADH oxidation [343–346]; however, the reduction of the overpotential is usually not selective for NADH but a general phenomenon for several other electrochemical reactions suffering from high overvoltages. Coating of porous titanium with binary Pt-Pd or ternary Pt-Pd-Rh/Ir alloys has also been reported to decrease the overvoltage for NADH oxidation at pH 9 [384]. Recently, it was reported that diamond electrodes [337, 338, 385] show much higher stability compared with other types of carbon electrodes for NADH oxidation, although the applied potential is rather high.

4.4.3

Catalytic NADH Oxidation at CMEs Based on Polymers

Polymer-coated electrodes for NADH oxidation can be divided into three major groups: those made from electropolymerization of monomers with no mediating properties, electropolymerization of monomers with mediating properties, and premade polymers into

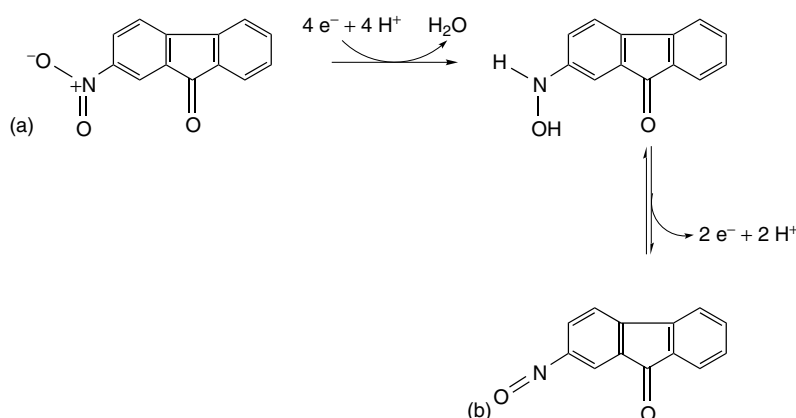


Fig. 12 Structural formulas of 2,4,7-trinitro-9-fluorenone (a) and electrochemical formation of its catalytic active form (b) [312].

which mediating functionalities are covalently bound.

Electrodes modified by electrodeposition of poly(3-methylthiophene) [340] and poly(indole-5-carboxylic acid) films [376] show a rather nonselective catalytic effect for NADH with concomitant oxidation of, for example, dopamine, epinephrine, and acetaminophen. However, the sensitivity for NADH is increased up to 10 times and interferences such as ascorbate could be minimized by charge-selective membranes. Also, poly(aniline)-poly(vinylsulfonate) coated GC electrodes were shown to give stable and reproducible electrocatalytic responses to NAD(P)H in citrate-phosphate buffer at pH 7 [302].

A number of *o*-quinone [164, 180, 188–192, 195, 198, 199], phenoxazine, and phenothiazine derivatives [229, 230, 240–242, 244, 257, 267] have been electropolymerized onto electrodes with varying degrees of success for practical applications (Table 2). The electropolymerization process leads in many cases to better stability of the modified layer and, of course, to a high loading of catalytic groups on the electrode surface. Electropolymerization has, in general, not largely affected the $E^{\circ'}$ of the *o*-quinone derivatives as compared with their monomer counterparts as they are based on a bifunctional monomer; one moiety contains the *o*-quinone and another the electropolymerizable moiety, whereas for the phenoxazines and phenothiazines, a drastic shift to the positive direction is usually registered. As mentioned above, many of the phenoxazine and phenothiazine dyes contain primary or secondary amine groups both in position 3 and 7, and are thus prone to electrochemical oxidation to form radicals. This process leads to the formation of a polymer and also causes localization of the positive charge to one of the remaining amine groups, thus

shifting the $E^{\circ'}$ value to a more positive region, with the result that a much higher reaction rate with NADH is obtained. The drawback is, however, that NADH does not readily penetrate and diffuse into the polymer making the response at these CMEs rather low.

The introduction of the mediating molecule into a polymeric backbone that could be cast onto a solid electrode or mixed into a composite electrode would in principle, be very beneficial as the surface concentration on the electrode surface can be much higher than that based on adsorption or covalent binding [153, 386]. The success, however, of this approach very much depends on several factors such as the partition coefficient of the analyte between the aqueous solution and the polymer phase, the diffusion coefficient of the analyte and the possible necessary counterions within the polymer film, and the redox self-exchange between adjacent redox sites within the polymer. In comparison with the progress that has been obtained with polymers incorporating one-electron-transfer mediators/donors that have shown great progress for redox enzymes with bound cofactors [150], the corresponding progress for mediator containing polymers for catalytic NADH oxidation has been less successful. The first attempts in this direction from Miller and coworkers based on *o*-quinones [185–187] showed that the redox propagation within the polymer was very sluggish and that NADH did not really penetrate the polymer bulk. The variation of the response current to NADH with the thickness of the deposited film at such electrodes showed that only for an initial increase in the coverage, there was an increase in the response. A continued increase in polymer deposition was followed by a decrease in response reflecting the low partition

coefficient and the low diffusion coefficient of NADH within the polymer film. The choice of *o*-quinone was also neither beneficial for the decrease in overvoltage nor for the stability of the mediator in the presence of NADH, as commented on earlier. Further attempts in this direction have been made with improved catalytic functionalities, for example, phenoxazine and phenothiazine derivatives [162, 236, 237, 269, 270, 272–274], but in principle, facing the same problems with redox self-exchange restrictions within the film, such as partition coefficient for NADH, and diffusion coefficient of NADH within the film. The polymer best suited for NADH penetration is based on a hydrophilic, permeable film of HRP covalently bound to a three-dimensional epoxy network having polyvinyl pyridine (PVP)-complexed $[\text{Os}(\text{bpy})_2\text{Cl}]^{3+/2+}$ redox centers. However, this approach suffers from the necessity of adding a soluble quinoid compound that in a first reaction is reduced by NADH and then in turn is reoxidized by molecular oxygen to form the hydrogen peroxide that in turn can start the reaction sequence with the covalently bound HRP and $[\text{Os}(\text{bpy})_2\text{Cl}]^{3+/2+}$ redox centers resulting in the response current [292].

4.4.4

Mechanistic and Kinetic Aspects

The decrease in overvoltage is closely related to the $E^{o'}$ of the mediator on the electrode surface. In principle, this means that the lower the $E^{o'}$ of the mediator is, the more is the overvoltage decreased. This decrease is usually measured either as the difference between the peak potential of cyclic voltammograms (E_p) or the difference between the half wave potential ($E_{1/2}$) of RDE scans for the catalyzed and uncatalyzed waves. For the simplest case

(monolayer coverage) where only the mass transport of NADH and/or the second-order rate constant (k_{obs}) between NADH and the mediator can limit the reaction, E_p and $E_{1/2}$ for the catalyzed waves are given by Eqns. (35) and (36).

$$E_p = E^{o'} + \frac{RT}{nF} \left[0.78 + \ln \left(\frac{D_{\text{NADH}}^{1/2}}{k_{\text{obs}} \Gamma} \right) + \ln \left(\frac{nF\nu}{RT} \right)^{1/2} \right] \quad (35)$$

$$E_{1/2} = E^{o'} + \frac{RT}{nF} \ln \left(1 + \frac{i_k}{i_{d(L)}} \right) \quad (36)$$

where

$$i_k = nFAk_{\text{obs}}\Gamma C_{\text{NADH}} \quad (37)$$

and

$$i_{d(L)} = 0.620nFAD_{\text{NADH}}^{2/3}\nu^{-1/6}C_{\text{NADH}}\omega^{1/2} \quad (38)$$

and where D_{NADH} is the diffusion coefficient, Γ the surface coverage of the mediator, A the electrode surface area, ν the sweep rate used for CV, C_{NADH} the bulk concentration of NADH, ν the kinematic viscosity, and ω the angular velocity of the RDE.

As can be seen, factors other than $E^{o'}$ affect the effective decrease in overvoltage, for example, sweep rate (ν), coverage (Γ), rotational speed (ω), and so forth. The picture becomes even more complicated when all other steps that may contribute to the kinetics of the charge transport between the NADH in solution and the electrode are considered.

It is of course of importance that the electron transfer rate between mediator and the electrode (k_s) does not set a limit to the rate of the overall reaction. The apparent electron transfer rate (k_s) of a surface-immobilized redox compound can

be evaluated in CV from the variation of the peak potentials of the oxidation and reduction waves with the sweep rate [254, 387, 388]. However, variations of the peak potential with sweep rate can also be caused by a number of other factors such as uncompensated resistance, local pH changes, and movements of counter ions [388]. The sweep method will therefore only give the lowest value of the rate constant. Typical reported values are 1 s^{-1} for oxidized carbon black [136], 4 to 17 s^{-1} for adsorbed phenoxazines and phenothiazines, depending on pH [220, 243, 254, 301], 3 to 6 s^{-1} for adsorbed *o*-quinones [167, 196], 3.3 s^{-1} for covalently bound PQQ on gold [200], 22 to 65 s^{-1} for electrodeposited dihydroxybenzaldehydes on GC [190, 191], 70 s^{-1} for 2-nitro-9-fluorenone on GC [312], 450 and 600 s^{-1} for 5,5'-dithiobis(2-nitrobenzoic acid) and 5,5'-dithiobis(2-nitropyridine), respectively, on gold [314].

When the mediator is adsorbed or covalently tethered in multilayers, or when incorporated into a polymeric backbone or film, the charge propagation in the film may contribute to the rate-limiting kinetics in the catalytic cycle of a CME [153, 386, 389–391]. The combined effects of electron and counterion transport as well as conformational changes and solvent molecule movements in the film during an electrochemical cycle are collectively denoted charge transport. For instance, in redox polymer-coated electrodes, the charge transport usually obeys Fick's law of diffusion and hence can be defined by a diffusion coefficient. The partition coefficient of NADH between the contacting solution and the polymer film, the diffusion coefficient of NADH in the polymer, and the reaction rate between NADH and the mediator in the film may also contribute to the rate-limiting kinetics.

The rate constant of the chemical reaction between NADH and the surface-attached mediator (k_{obs}) can be evaluated by CV [392] but is more appropriately done when a rotating electrode is used [153]. The situation is straightforward at CMEs bearing monolayers or less of immobilized mediator. The general equation for the catalytic current (i_{cat}) is, if Γ is less than equal to the monolayer and the applied stationary potential is greater than equal to 0.12 V more positive than the $E^{\circ'}$ of the mediator,

$$i_{\text{cat}} = \frac{nFAk_{\text{obs}}\Gamma C_{\text{NADH}} D_{\text{NADH}}^{2/3} \omega^{1/2}}{D_{\text{NADH}}^{2/3} \omega^{1/2} + 1.61 v^{1/6} k_{\text{obs}} \Gamma} \quad (39)$$

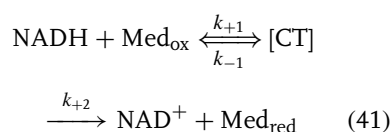
Equation (39) reverts to the Levich equation for an irreversible reaction when the heterogeneous rate constant k_f is replaced by $k_{\text{obs}}\Gamma$. Inversion of Eq. (39) thus gives the corresponding Koutecky-Levich equation,

$$\frac{1}{i_{\text{cat}}} = \frac{1}{nFAk_{\text{obs}}\Gamma C_{\text{NADH}}} + \frac{1}{0.620nFAD_{\text{NADH}}^{2/3} v^{1/6} C_{\text{NADH}}} \frac{1}{\omega^{1/2}} \quad (40)$$

Equation (40) shows that a plot of $1/i_{\text{cat}}$ versus $1/\omega^{1/2}$, extrapolating to $1/\omega^{1/2} \rightarrow 0$, gives the electrocatalytic rate from the intercept expressed as the product $k_{\text{obs}}\Gamma$. The coverage is evaluated from the integration of the area of the anodic or cathodic wave of a cyclic voltammogram. Care must be taken when evaluating the surface coverage as the effective area under the voltammetric wave can be largely influenced by the sweep rate if the electron transfer rate, k_s , has a limited value [254].

For many CMEs used for the electrocatalytic oxidation of NAD(P)H, it has been postulated that a charge transfer complex (CT) is formed in the reaction sequence

between NAD(P)H and the mediator because k_{obs} was found to decrease in a distinct pattern with an increase in the bulk concentration of NAD(P)H [160, 200, 212, 220, 224, 235, 245, 249, 301, 305]. This is also in agreement with the findings of the homogeneous reaction between NAD(P)H and its analogues with various electron acceptors [145, 146] (see preceding text).



Combination of the rate constants k_{+1} , k_{-1} , and k_{+2} yields (c.f. Michaelis-Menten kinetics)

$$K_M = \frac{k_{-1} + k_{+2}}{k_{+1}} \quad (42)$$

Now, the overall second-order rate constant, k_{obs} , can be expressed as

$$k_{\text{obs}} = \frac{k_{+2}}{K_M + C_{\text{NADH}}} \quad (43)$$

Inversion of Eq. (43) gives

$$\frac{1}{k_{\text{obs}}} = \frac{K_M}{k_{+2}} + \frac{C_{\text{NADH}}}{k_{+2}} \quad (44)$$

and substitution of k_{obs} , Eq. (44), into Eq. (40) gives

$$\begin{aligned} \frac{1}{i_{\text{cat}}} &= \frac{1}{n\text{FA} \left(\frac{k_{+2}}{K_M + C_{\text{NADH}}} \right) \Gamma C_{\text{NADH}}} \\ &+ \frac{1}{0.620n\text{FAD}_{\text{NADH}}^{2/3} v^{-1/6} C_{\text{NADH}}} \frac{1}{\omega^{1/2}} \end{aligned} \quad (45)$$

or

$$\begin{aligned} \frac{1}{i_{\text{cat}}} &= \frac{1}{n\text{FA}k_{+2}\Gamma} + \left(\frac{K_M}{n\text{FA}k_{+2}\Gamma} \right. \\ &\left. + \frac{1.61v^{1/6}}{n\text{FAD}_{\text{NADH}}^{2/3}\omega^{1/2}} \right) \frac{1}{C_{\text{NADH}}} \end{aligned} \quad (46)$$

If this assumption of a charge-transfer complex holds true, plots of $1/k_{\text{obs}}$ versus C_{NADH} and $1/i_{\text{cat}}$ versus $1/C_{\text{NADH}}$ would result in straight lines. Moreover, the intercept of Eq. (46) should be independent of C_{NADH} and ω . Experimental results from many different laboratories confirm Eqs. (44) to (46) [160, 200, 210, 212, 218, 220, 235, 239, 249, 301, 305] and it can be looked upon as a general observation with concluding evidence that a charge-transfer complex is formed between NAD(P)H and the mediator.

The rate constant, k_{obs} , can thus be obtained either through the use of CV or the use of a RDE. The close agreement between the results obtained with both CV or RDE [210, 312] further support the mechanism given in reaction (41).

If k_{obs} in Eq. (40) is replaced by $k_{+2}/(K_M + C_{\text{NADH}})$ from Eq. (43), then

$$i_{\text{cat}} = \frac{n\text{FA}[(k_{+2}/(K_M + C_{\text{NADH}})) \times \Gamma C_{\text{NADH}} D_{\text{NADH}}^{2/3} \omega^{1/2}]}{D^{2/3} \omega^{1/2} + 1.61v^{1/6} \times [k_{+2}/(K_M + C_{\text{NADH}})] \Gamma} \quad (47)$$

This equation tells us that for a constant C_{NADH} (up to about K_M), i_{cat} will vary linearly with Γ for small coverages and will be independent of Γ for high coverages. Experimental evidence has been reported [220]. This means that if the initial surface coverage of the mediator is sufficiently high, some inactivation or decomposition of the mediator will pass unnoticed with regard to the response current.

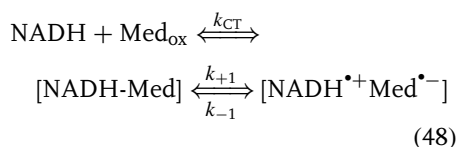
By 1986 [160], it was noticed that for a number of adsorbed phenoxazine derivatives, there exists a linear correlation between the experimentally evaluated $\log k_{\text{obs}}$ and the $E^{\circ'}$ of the immobilized mediator. Actually, it was found that obviously there existed two different linear correlations, one with mediators with higher

reaction rates and another with lower reaction rates. In Fig. 11 is shown $\log k_{\text{obs}}$ versus $E^{\circ'}$ plots of reliable values found so far in the literature. It is obvious that what was indicated in Ref. [160] still holds true, that is, there exists two different linear correlations. It is interesting to note that for immobilized PQQ [200], the evaluated k_{obs} falls on the lower line but in the presence of Ca^{2+} ions increasing the reaction rate of PQQ with NADH about 10 times, this k_{obs} falls on the upper line. Katz and coworkers [200] analyzed in detail the effect of Ca^{2+} on k_{+2} and K_{M} and surprisingly, equal values of k_{+2} were obtained in the absence and presence of Ca^{2+} , whereas the K_{M} value was very much affected by Ca^{2+} . In the absence of Ca^{2+} , the K_{M} value was 109 mM, whereas in the presence of 20 mM Ca^{2+} , the K_{M} value was lowered to 0.73 mM. This means that with Ca^{2+} addition, the equilibrium between NADH and PQQ is shifted dramatically to the intermediate complex formation but the decay rate of the CT-complex leading to the formation of NAD^+ is not changed at all. Therefore, the $[\text{Ca}^{2+} \cdots \text{PQQ}]$ complex initially formed (Fig. 10) has a much higher affinity for NADH than PQQ itself. Probably, the positive charge caused by the complex formation of Ca^{2+} with PQQ functioning as promoters for the NADH oxidation provide a favorable orientation of the NADH molecules for this redox process. It is also interesting to note that the highest k_{obs} value evaluated for the upper line, $5.2 \cdot 10^4 \text{ M}^{-1} \text{ s}^{-1}$, was obtained with a new type of mediator having a nitroso/hydroxylamine catalytic functionality (Fig. 12) with an $E^{\circ'}$ value at pH 7 of -0.05 V versus Ag/AgCl. Similar or even higher values of k_{obs} were found for some phenothiazines (thionine, Azure C, and Azure A) covalently bound to thiol derivative-modified gold electrodes [239],

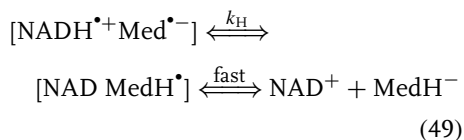
however, at much higher applied potentials ($\approx +210\text{--}230 \text{ mV}$ vs. Ag/AgCl). Thus, these mediators fall on the lower linear line. The perfect mediator for analytical purposes has not yet been identified, but some guidelines for future work can, however, be seen. One should focus on trying to make new mediator derivatives falling on the upper curve but having a higher E° value. To be able to reach a k_{obs} value of $10^7 \text{ M}^{-1} \text{ s}^{-1}$, the $E^{\circ'}$ at pH 7 should be around $+100 \text{ mV}$ versus SCE.

It has been found that k_{obs} is very much a function of pH. It is still not clear whether this is a result of the direct influence of pH on reaction kinetics or whether the $E^{\circ'}$ values of both the NAD^+/NADH and the mediator vary with pH. As an example, Meldola blue, k_{obs} increased from $3 \cdot 10^4$ at pH 7 to $8 \cdot 10^4 \text{ M}^{-1} \text{ s}^{-1}$ at pH 6, indicating that pH must have an effect on the reaction rate as the $E^{\circ'}$ of Meldola blue moves 30 mV per pH unit and thus $\Delta E^{\circ'}$ should be constant as the $E^{\circ'}$ of NAD^+/NADH also shifts 30 mV per pH unit. A similar increase in reaction rate with a decrease in pH was found for another benzophenoxazine derivative (9H-benzophenoxazin-9-one) adsorbed on graphite [301] and for 3,4-dihydroxybenzaldehyde electrodeposited on GC [191]. However, for both these mediators, the $E^{\circ'}$ will move below pH 7 at 60 mV per pH unit resulting in an increased $\Delta E^{\circ'}$ with a change in pH to more acidic values. For 9H-benzophenoxazin-9-one, both k_{+2} and K_{M} increased for lower pHs, although with a net increase in k_{obs} , whereas for 3,4-dihydroxybenzaldehyde, a decrease in pH led to a slight increase in k_{+2} but a more drastic decrease in K_{M} , thus causing a net increase in k_{obs} . Further investigations are indeed needed to be able to come up with a more detailed explanation for such findings.

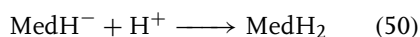
The lower reaction rate at higher pH in conjunction with less stable mediator properties have been discussed [160, 162, 301] in relation to the mechanism occurring in the solution proposed by Fukuzumi and coworkers [44, 145, 393]. In a first reaction step, NADH forms a CT-complex with the mediator. Next, the first electron is donated to form $[\text{NADH}^{\bullet+} \text{Med}^{\bullet-}]$.



The major reaction route would then be that the acid proton of $\text{NADH}^{\bullet+}$ within the complex should be transferred to the mediator part within the complex ($\text{Med}^{\bullet-}$), followed by a rapid transfer of the second electron, and finally, a decay of the complex and the release of enzymatically active NAD^+ and reduced mediator.

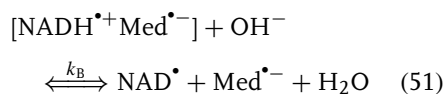


Depending on whether the mediator is a one- or two-proton acceptor, a possible follow-up process can then occur



which in a protic medium should be very fast.

At high pH, hydroxyl ions could possibly influence the reaction in a similar mode as was proposed in aprotic media when a base was added. Then, a reaction competing with reaction (49) could take place



leading to free radicals, which in turn may cause abortive side reactions, with the result that the mediator slowly decomposes, possibly followed by electrode fouling. No investigations so far have been made with rotating ring-disk electrodes trying with electrochemical means to identify the reaction products formed at CMEs. Such investigations should be done in the future to possibly shed further light into the reaction mechanism.

From a fundamental point of view, the reaction between NADH and flavin is the most interesting. As free flavins have at pH 7 $E^{\circ'}$ values around -0.43 V versus SCE, the resulting $\Delta E^{\circ'}$ between NADH and the flavin will not allow the reaction to be studied with electrochemical means as the resulting currents are too small. When adsorbed or covalently immobilized onto ordinary solid electrodes, flavin derivatives more or less retain their solution values [307, 394]. Recently, however, it was reported that when immobilizing riboflavin onto Zr- or Ti-phosphate, followed by mixing with carbon paste [235, 249, 305, 306], the $E^{\circ'}$ for riboflavin was found to be around -0.2 V versus SCE and virtually independent of pH. Thus, the reaction rate with NADH was substantially increased. It could be confirmed that for riboflavin too the reaction occurs in a CT-complex [305]. In the presence of Ca^{2+} or Mg^{2+} , a further shift in the $E^{\circ'}$ value of riboflavin was noticed, as also a drastic increase in the reaction rate with NADH. The possibility of changing the $E^{\circ'}$ of adsorbed riboflavin with the composition of the contacting solution [235, 305] for a constant pH and to change the pH of the solution while keeping the $E^{\circ'}$ of adsorbed riboflavin constant gives possibly a unique possibility to separately investigate the influence of pH and the influence of the difference in $E^{\circ'}$ values

between NADH and the flavin on the reaction rate between these two compounds. Moreover, a basic understanding of the interaction between quinoid-type mediators and Zr- and Ti-phosphate may lead to the fact that tailored modified electrodes can be designed for biosensor purposes, where the previous drawback with using electron-proton acceptor/donor type mediators having pH-dependent E^0 values will be circumvented. A similar effect on the E^0 value of immobilized flavins was found for TiCl_4 -treated carbon fibers [309]. The treatment causes the formation of a TiO_2 layer on the carbon fiber surface, which has a strong affinity for phosphate groups. Both FAD and FMN strongly bind to these electrodes, revealing E^0 values close to -0.2 V versus SCE at pH 7 with only a slight variation with pH and clear catalytic oxidation currents in the presence of NADH.

4.5 CMEs Based on NADH-oxidizing Enzymes

A number of CMEs for biocatalytic NADH and NADPH oxidation have also been described in the literature (Table 3). Most commonly, various preparations of DI have been used for NADH. Direct electron transfer between DI and electrodes seems possible [347], although the efficiency of direct electron transfer between the reduced enzyme and the electrode (either carbon paste or GC) is not very efficient. However, the electron transfer from reduced DI to the electrode can be mediated using both one-electron-nonproton and two-electron-proton acceptors (Table 3). The potential at which NADH is oxidized is therefore very much dependent on the mediator employed. A thermostable DI has been intensively studied by Ikeda

and coworkers [358, 359] and was used to oxidize NADH electrocatalytically, during which a variety of quinone compounds and several kinds of flavins were studied as mediators. The DI-catalyzed electrolytic oxidation, that is, bioelectrocatalytic oxidation of NADH, proceeds very rapidly with quinones and flavins as mediators. Analysis of the bioelectrocatalytic current by the theory of steady-state catalytic currents reveals that the bimolecular reaction rates between the enzyme and the quinones whose redox potentials are more positive than -0.28 V versus Ag/AgCl at pH 8.5 are as high as $10^8 \text{ M}^{-1} \text{ s}^{-1}$, suggesting the reactions to be diffusion-controlled. The redox potential of DI was determined to be more positive than NAD^+/NADH by 42 mV at pH 8.5 using a spectroscopic method. By changing the pH of the solution to more alkaline values, the E^0 of DI will be more negative than that of NAD^+/NADH , making it possible to run the reaction backward, that is, the bioelectrocatalytic reduction of NAD^+ is predicted to be favorable under alkaline conditions (see in the following text).

The electrochemical oxidation of NADH catalyzed by NADH dehydrogenase entrapped in a polypyrrole (PPy) membrane on an electrode surface has also been investigated [372]. The results suggest that direct electron transfer occurs between the enzyme and PPy without the aid of small mediators.

The NADH oxidase has also been used to oxidize NADH. The reaction can be based on mediated electron transfer from reduced NADH oxidase to the electrode [375, 376]. The reaction can also be based on the formation of hydrogen peroxide, which in turn, reacts with HRP covalently bound within an Os-containing hydrogel that efficiently mediates the reduction of reduced peroxidase [377].

For NADPH, efficient catalytic oxidation has been reported using three different redox enzymes, namely, ferredoxin-NADP-reductase [347], glutathione reductase [371], and flavin reductase [378, 379], using different types of mediators.

4.6

Amperometric Biosensors Based on NAD(P) -dependent Dehydrogenase Enzymes

Given the difficulties associated with the catalytic reduction of NAD^+ , all amperometric biosensors studied on the basis of NAD -dependent dehydrogenases have been focused on measuring NADH, usually its production, but in some instances, also its consumption, in conjunction with a dehydrogenase [76, 77]. However, for a successful approach, one must keep in mind that most of the reactions catalyzed by these dehydrogenases have $E^{\circ'}$ values more positive than that of the NAD^+/NADH redox couple. Only for a few reactions, for example, the oxidation of monosaccharides (glucose, galactose) or aldehydes by their corresponding dehydrogenases, does the equilibrium of the reaction (reaction (2), see preceding text) actually favor the production of NADH because the $E^{\circ'}$ s of these reactions have lower values than that of the NAD^+/NADH redox couple. To be able to construct a biosensor on the basis of a dehydrogenase by measuring the production of NADH, it is very essential that the initial NADH formed be instantaneously consumed by the mediator (or possibly directly at the electrode surface); otherwise, equilibrium in reaction (2) will be reached and further production of NADH will cease. The reduced mediator in turn must also be reoxidized rapidly to regenerate its active

oxidized form. In essence, this means that all three reaction steps (the enzymatic, the mediated, and the electrochemical) need to occur very close in space for a successful approach. This is outlined in Fig. 2 where it is shown that in the initial step, the electrons have to move against the thermodynamic driving force through an intimate coupling with the mediator and the electrode in order to realize a net thermodynamic driving force for NADH production. It is therefore very important that the mediated reaction is as rapid as possible motivating further search for finding the optimal mediator. Any biosensor based on an NAD -dependent dehydrogenase with the ambition of reaching the market must resolve the problem of immobilization of sufficient amounts of NAD^+ within the biosensor format. A very elegant approach has been suggested by Willner and coworkers through their covalent coupling of an enzyme-active NAD^+ analogue with a mediator (PQQ), which in turn is tethered to a gold electrode [202, 203, 208, 209]. However, in light of the restricted lifetime of both NAD^+ and NADH because of their susceptibility to decomposition in aqueous environment [24], a surplus of cofactor seems necessary and suggested coimmobilization of NAD^+ into composite electrodes [168] or in electropolymerized layers [229] together with mediator and enzyme may be a promising approach to solve this problem.

4.7

Direct Electrochemical Reduction of NAD(P)^+

4.7.1

General Observations

Studies on the electrochemical reduction of NAD^+ have been made using normal

DC polarography and phase-selective AC polarography at dropping-mercury electrodes, CV at the hanging-mercury drop electrode, potential-step chronoamperometry, constant electrode potential coulometry, and RDE methodology. Platinum, gold, PG, and GC electrodes have also been used.

The electrochemical reduction of NAD⁺ in aqueous solutions is well documented including studies on the adsorption of product, intermediates, and NAD⁺ itself on electrode surfaces [75, 97, 118, 124, 125, 395, 396]. In an initial polarographic study by Kaye and Stonehill [397], the reduction of NAD⁺ at the mercury electrode was observed as a single wave with an $E_{1/2}$ of ≈ -0.9 V in neutral aqueous solution. Burnett and Underwood [118] resolved this single wave into two cathodic waves, a first one at $E_{1/2} \approx -1.1$ V and a second at $E_{1/2} \approx -1.7$ V, by recording the polarogram in an alkaline buffer pH 9 to 10 to minimize the hydrogen evolution and chemical decomposition of the nucleotide and in the presence of tetraalkylammonium salt to depress adsorption of NAD⁺ and related species. Appropriate conditions, including ionic strength and surface activity of the background electrolyte and initial potential and potential scan rate, have to be chosen to diminish the adsorption effects [118], ascribed to be mainly caused by the adenine moiety [75, 124, 396, 398, 399] of the species participating in the overall reduction of NAD⁺ (see the following text).

The polarographic patterns of both waves have been extensively discussed by Elving and coworkers [75] including NAD⁺ and analogues (Fig. 3). A similar pattern is observed for all the one-substituted nicotinamides, including NAD⁺, showing the two well-separated $1e^-$ waves at alkaline pHs, the intensity

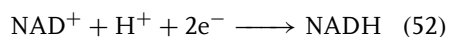
of the second wave being less than 10% of the first. Contrary to this pattern, nicotinamide shows, between pH 3 and 7, two adjacent cathodic waves of equal height, closely followed by a hydrogen discharge wave. Regardless of this different pattern, the first wave corresponds to a reversible $1e^-$ charge transfer (see following text), followed by an irreversible chemical dimerization of the radical formed, which is uncharged in the case of NAD^{•+} (NAD, reaction 12) but negatively charged for the nicotinamide [400]. Exhaustive controlled electrolysis of the one-substituted nicotinamides has provided an insight of the species involved [75]. In brief, after electrolysis at a potential corresponding to the first wave plateau (-1.25 V), both cathodic waves disappear and an anodic wave corresponding to the neutral dimer of the first wave product appears at ≈ -0.4 V (reaction 13). By comparison of the faradaic currents and the spectral characteristics of the final products of this electrolysis with the obtained under conditions of favored adsorption, Elving and coworkers demonstrated that the number of electrons in both cases is very close to 1 (0.96 ± 0.01) and that adsorption has very little effect on the nature of the electrolysis products. If potential is then shifted to -1.8 V, no further current flow is observed, indicating that the final product of the first wave is neither an intermediate in the formation of the second wave, nor is it further reduced to a different product. However, a small cathodic wave has also been reported to appear [401], which has been attributed to the free nicotinamide present as an impurity and slight NAD⁺ decomposition during extensive electrolysis at alkaline conditions. After exhaustive electrolysis at -1.80 V, the average value for n results to be very close to 2 (1.98 ± 0.11) [401] and no waves

are seen at mercury electrodes because, as already described, oxidation of the dihydropyridine product occurs at more positive potentials than that for the oxidation of mercury [75]. On PG electrodes, after electrolysis of MCP^+ (1-methyl-3-carbamoylpyridinium ion) at -1.80 V, a large anodic peak is observed at -0.04 V as a result of the oxidation of the $2e^-$ product; subsequent potential sweep toward more negative regions produces a cathodic peak at -1.18 V corresponding to the reduction of the MCP^+ formed during the anodic scan. Finally, if the potential is then scanned in the positive region, the expected dimer oxidation is seen at -0.34 V, followed by the peak at -0.04 V [75].

Taking into account these considerations and the appearance of the second wave at a potential where the dimer is not reduced (see following text), in addition to the high dimerization rate (reaction 12 and Sch. 1), and cyclic voltammetric patterns, Elving and coworkers concluded that the second electron transfer has to be faster than the dimerization and thus, NAD^+ is directly reduced to the dihydropyridine at the second wave in an overall $2e^-$ process. The rationale for involvement of a proton in the overall NAD^+ -reduction process derives from the formation of enzymatically active NADH . Two different sequences were thus postulated by these authors: (1) e^-, e^-, H^+ or (2) e^-, H^+, e^- . If protonation of the free radical formed on addition of the first electron is very rapid, as compared with its dimerization rate constant, either sequence could be competitive with the dimerization reaction in producing the dihydropyridine derivative; otherwise, the first sequence would be more likely [75]. This uncertainty was clearly solved by the fact that the neutral radical NAD^\bullet is not further reduced in aprotic media and thus, protonation

occurs prior to or concurrent with charge transfer [400].

Overall, the cathodic reduction of NAD^+ to NADH at mercury electrodes proceeds through two discrete $1e^-$ steps, well separated in potential, and through the protonation of the free radical produced on the first step prior to or concurrent with the second electron transfer (Sch. 1).



4.7.2

Adsorption Phenomena

Special attention has been paid to the importance of adsorption and conformation factors in the one-electron reduction of NAD^+ on different electrode surfaces [97, 124]. On mercury electrodes, the area occupied per NAD^+ molecule reaches an experimental limiting value of 130 \AA^2 , which calls for a folded configuration of the coenzyme with the nicotinamide and adenine rings parallel and close to each other and with the adenine ring flat on the electrode surface. This assumption is based on the theoretical areas for an extended or folded NAD^+ configuration as the minimum calculated areas result in 190 \AA^2 for the extended configuration and 125 \AA^2 and 85 \AA^2 for the folded configurations (parallel and perpendicular to the electrode surface, respectively) [97]. The theoretical areas have been deduced from projections of CPK space-filling models of NAD^+ for monolayer coverage. The folded parallel configuration at the electrode/solution interface calls then for an electron-transfer pathway from the electrode through the adenine ring to the nicotinamide moiety [97]. The possibility of adenine serving as a mediator for nicotinamide reduction has been demonstrated by pulse

radiolysis, fluorescence, and electrochemical experiments [399, 402]. Similarly, as previously described, the mediation of adenine for NADH oxidation has been suggested [134]. On GC electrodes, NAD⁺ covers an area of 90 Å² per molecule and most probably, a perpendicular configuration can be assumed, which agrees well with the proposed adsorption sequence for NAD⁺ produced by anodic NADH oxidation at clean GC electrodes [95]. Under such conditions, NAD⁺ is rapidly adsorbed in a parallel orientation, followed by a relatively slow reorientation to a perpendicular orientation where the adsorbate is more tightly bound than the planar-oriented adsorbate [95]. On PG electrodes, a parallel orientation of folded NAD⁺ may be favored because of the observed 110 Å² occupied per molecule and the planar-oriented hexagonal rings of these surfaces [97]. Negligible NAD⁺ adsorption is observed at platinum electrodes in the faradaic regions. Similar studies to the previously described using FT-SERS in gold electrodes are not possible in the faradaic region because all changes on the SERS bands occur or begin in the non-faradaic regions [113–115].

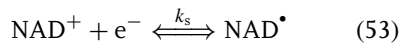
As previously discussed, NAD⁺ in solution is partially in a folded configuration [14–16]. It then seems clear that the folded conformation is preferentially adsorbed within the faradaic region, and differences may remain in the specific orientation, either parallel or perpendicular at the electrode/solution interface, depending on the electrode material.

4.7.3

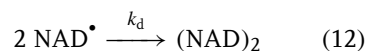
Mechanism and Kinetics

The first electron transfer to NAD⁺ is claimed to be reversible based on a log *i*-E plot [118] and cyclic voltammetric

curves [126]. However, unequivocal reversibility was further demonstrated by Schmamel and coworkers [401]. In their investigations, the slope of the first NAD⁺ wave was greater than that for a reversible 1e[−] transfer and *E*_{1/2} became more positive with the increase in concentration or drop time. These observations and the case of a reversible electrode process in the absence of adsorption are indicative of an irreversible dimerization subsequent to charge transfer, which was further supported by the difference in the cyclic voltammetric patterns at slow and rapid scan rates and the increase in the *i*_{pa}/*i*_{pc} ratio with increasing scan rate. Additionally, the 60-mV separation of peak potentials further supports the reversible 1e[−] nature of the redox couple [401, 75]. The heterogeneous rate constant, *k*_s, of this reaction:



has been estimated to exceed 1 cm s^{−1} and an *E*^{o'} of −1.155 V at pH 9.1 (25 °C) was found for the NAD⁺/NAD[•] couple [125]. The reversibility of reaction (53) is thus virtual because it is coupled to a fast dimerization reaction already described under the section of direct electrochemical oxidation of NADH.



Different values of *k*_d have been derived from electrochemical measurements, for example, 2 10⁶ [401], 3 10⁶ [124], 8 10⁶ [126], and 8 10⁷ M^{−1} s^{−1} [125]. Because of the rather complex mechanism of NAD⁺ reduction including a rapid follow-up chemical reaction and adsorption processes depending on experimental conditions (see following text), this constant should only be calculated under conditions in which the electron transfer

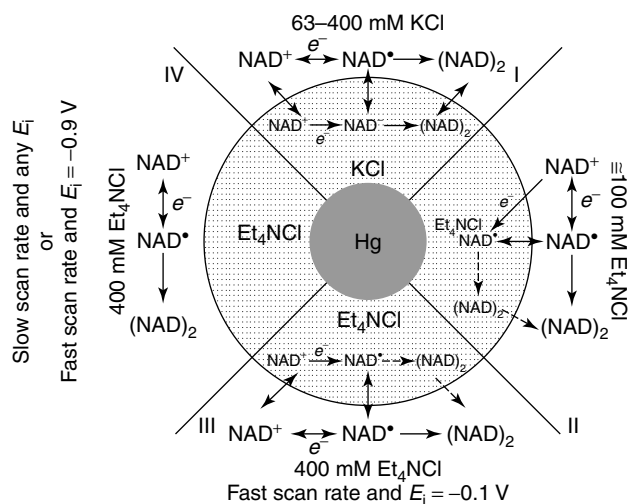
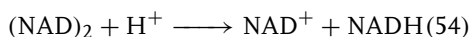


Fig. 13 Mechanistic pathways for the first charge transfer in NAD^+ reduction under different experimental conditions. Et_4NCl , tetraethylammonium chloride; E_i , initial scan potential. Shaded area around Hg corresponds to the adsorbed layer. (Redrawn from W. T. Bresnahan, P. J. Elving, *J. Am. Chem. Soc.* **1981**, *103*, 2379–2386.)

is strictly diffusion-controlled. A range of $k_d = 6 - 8 \cdot 10^7 \text{ M}^{-1} \text{ s}^{-1}$ [402, 403] was obtained from pulse radiolysis and spectrophotometric measurements. The dimer is not further reduced in the potential range down to -1.8 V (foot of the discharge current for hydrogen on mercury). However, when the potential is shifted into the background discharge region (-1.85 to -1.90 V), slow increase of absorption at 340 nm is observed, suggesting indirect reduction of the dimer to the dihydropyridine by interaction of the dimer with reduction products of background discharge such as hydrogen radicals. Alternatively, NAD dimers decompose at slightly alkaline conditions in the absence of oxygen to NAD^+ , which can be directly reduced in a $2e^-$ process at -1.8 V to dihydropyridines [75]. On the contrary, the oxidation of the dimer to NAD^+ is clearer starting at a potential of $\approx -0.4 \text{ V}$ [75].



A disproportionation reaction of the dimer resulting in NAD^+ and NADH has been also reported [404], which is at least formally analogous to the disproportionation of a semiquinone [97]:



From a mechanistic point of view, the reduction of NAD^+ to NAD^\bullet includes: (1) competing adsorption, (2) the timescale of the experiment, (3) the initial state of the electrode surface, and (4) the background solution ionic strength and surface activity [124]. The nature of the buffer is not expected to affect this first wave because its pH independence is above $\text{pH } 5$ [401]. A general overview of the mechanistic first-reduction pathway depending on experimental conditions is depicted in Fig. 13. In the absence of

surfactant, NAD⁺ undergoes both adsorption and diffusion-controlled reduction in KCl solutions. The former predominates on the timescale of fast-scan CV experiments, whereas diffusion-controlled currents are observed on slow timescale such as DC polarography and slow scan rate CV. The absence of pre- or postprocesses is ascribed to nearly equal adsorption of NAD⁺ and NAD[•]. The dimer is also adsorbed and it only desorbs at potentials more negative than -1.20 V and -1.32 V in 63 mM and 400 mM KCl solutions, respectively. Oxidation of adsorbed NAD[•] is not expected because the shape of the anodic peak on fast-scan CV indicates that it is diffusion-controlled. In the presence of low surfactant concentration (≈ 100 mM), two processes are seen on both slow and fast scan rates; one process involves reduction to soluble products of NAD⁺ as it diffuses to the electrode and the other to products that are adsorbed at the interface. As it remains uncertain whether NAD[•] dimerizes in the interphase or in the solution, the dashed arrows in Fig. 13 indicate that dimerization in the interphase would be followed by rapid desorption. In the presence of high surfactant concentration (≈ 0.4 M), NAD⁺ can be reduced under adsorption and diffusion control depending on both initial potential and scan rate. At starting potentials in which NAD⁺ is not adsorbed (-0.9 V), only diffusion-controlled currents are observed on both slow and fast scan rates. On the contrary, starting at -0.1 V, where NAD⁺ is adsorbed, and on rapid scan rate, reduction occurs under both adsorption and diffusion control. The former situation remains rather similar to that observed in the presence of KCl with the adsorption of both NAD⁺ and NAD[•] but with the adsorption of (NAD)₂, at most transient, as no AC tensammetric peak appears [124].

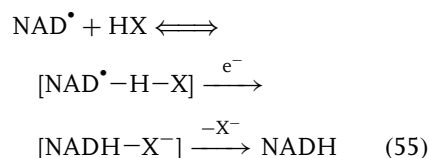
The formation of the dimer is not stereospecific [75, 123, 395]. Solutions of NAD⁺, electrolyzed at -1.1 V with mercury electrode produced a dimer mixture in a 90% yield consisting of two sets of stereoisomers, 4,4'-dimers (90%) and 4,6'-dimers (10%), where each set consisted of three different stereoisomers [123]. The relative abundance of the dimers was independent of pH (7–10) and no 6,6'-dimers could be indentified by high-performance liquid chromatography (HPLC) and NMR studies. This contrasts with the predominant formation of 6,6'-dimers in the electrochemical reduction of NAD analogues, particularly with small (e.g. H or CH₃) one-substituents or in the presence of DMSO (dimethyl sulfoxide) or acetonitrile [400]. When solutions of NAD⁺ were reduced at -1.8 V, that is, at the limiting current plateau of the second wave, the result was the formation of 1,4-NADH (50–60%), 1,6-NADH (15–30%), and dimers (10–20%) [75, 123]. The obtained amount of 1,4-NADH increased when pH was decreased from 10 to 7 [123]. Consequently, and unlike enzymatic reduction where stereoselectivity is inherent with the addition of hydrogen at the 4 position of the pyridine ring and from only one face of the plane of the ring (either *re* or *si* face), electrochemical reduction is not stereospecific.

The oxidation of the dimer (reaction 13) has been thermodynamically and kinetically studied with synthetic analogues of NAD dimers at gold and platinum electrodes [405] because (NAD)₂ shows interest as a potential two-electron donor acting with no involvement of proton transfer, and its oxidation may provide a way of generating the NAD[•] radical under milder conditions than that depicted in Sch. 1. Additionally, (NAD)₂ may be able to participate in enzymatic reactions [406–408].

The NAD^+ and $(\text{NAD})_2$ analogs form a chemically reversible redox couple but with a large separation (0.7 – 1.2 V) between the electrochemical reduction of NAD^+ and the oxidation of $(\text{NAD})_2$. It has been suggested that the reason for this peak separation lies in the different rate-limiting step for both processes. In fact, the reduction of NAD^+ to $(\text{NAD})_2$ requires the irreversible radical–radical dimerization of two NAD^\bullet radicals, whereas the oxidation of $(\text{NAD})_2$ into 2NAD^+ demands the cleavage of the dimerization radical $(\text{NAD})_2^{\bullet+}$ into NAD and NAD^+ (Sch. 1). The reduction of NAD^+ is kinetically controlled by the dimerization of the NAD^\bullet radicals, while the oxidation of $(\text{NAD})_2$ involves mixed kinetic control by electron transfer and cleavage of the $(\text{NAD})_2^{\bullet+}$ radical or total kinetic control by electron transfer [405].

The reduction at the second polarographic wave, resulting in the formation of NADH from NAD^+ by the net transfer of two electrons and a proton, is not as clearly understood as the first wave. Studies in organic media, acetonitrile, and DMSO that are poor proton donors have been carried out to elucidate the second reduction step. Two well-defined waves are only observed with nicotinamide as a model compound, while NAD^+ shows a $1e^-$ wave at $E_{1/2} \approx -1.0$ V in DMSO. A second wave only appears in the presence of a proton donor at -1.99 V, the intensity of which can be equal to the first wave when increasing proton concentration [75, 400]. In aqueous media, the pH range over which this second wave can be studied is restricted to pH 7 to 10, as a result of the background discharge current and hydrolysis of the coenzyme. Within this range, the difference found between the empirical variation of potential with pH, in the order of 20 mV, and

the theoretical value of 59 mV indicates that H_3O^+ is not the only proton donor and/or buffer compounds must also act as proton donors [97]. This is closely related to the very weak base character of the free radical NAD^\bullet , initially produced in the first wave, which is not protonated at pH 0.4 [409]. The reaction sequence for this second wave has been suggested as [97]:



where HX is a proton donor. The last step, which is a rapid first-order chemical reaction, may involve rearrangement of an initial dihydro product to 1,4- NADH and some 1,6- NADH , similar to the observation with NAD analogues [410]. The character of the proton donor strongly influences the NAD^\bullet reduction as it has been demonstrated by replacing K^+ ions in the background electrolyte by NH_4^+ at pH 9 [97]. Two possible explanations have been described: first, the positive charge in the nicotinamide moiety for the $\text{NAD}^\bullet - \text{NH}_4^+$ adduct favors radical reduction in contrast to the noncharged $\text{NAD}^\bullet - \text{H}_2\text{O}$, and second, the stronger acid character of NH_4^+ ($\text{p}K_a$ 9.2) versus H_2O ($\text{p}K_a$ 15.7) would favor the last dissociation step of Eq. (55), shifting the equilibrium towards NADH formation [97].

Complete electrochemical conversion of NAD^+ into NADH has been reported using electrochemically produced potassium amalgam in a specially designed reactor (10 M KOH , 1.5 A) and by electrochemically oxidizing NADH and undesirable produced species, mainly NAD dimers, back to active NAD^+ via a nickel foam anode [411]. However, the reduced coenzyme

proved to be only 70% biologically active owing to the presence of species other than the desired 4-dihydro-isomer (27% 6-dihydro, 1% 2-dihydro, and 2% mixed dimers) [412]. Higher yields, up to 95% in the absence of O_2 , are obtained by constant-current electrolysis (0.3 mA) of NAD-alginic acid covalent adducts [413, 414]. An anion-charged membrane has been used to divide an electrochemical cell into two compartments where electrolysis at -0.9 V versus Ag/AgCl yielded 85% conversion in 5 h [415]. As previously reported [413, 414], the activity of the resulting NADH is strongly dependent on the cathodic overpotential owing to the favored dimerization rather than the formation of inactive NADH isomers. Dimerization is claimed to be hindered at cholesterol-modified gold amalgam electrodes, but the turnover value for NAD^+ remains below 0.5 h^{-1} [416] or at electrodes modified with a cholesteryl oleate layer in the presence of divalent cations with approximately 100% conversion into 1,4-dihydro isomers [417].

4.8 Electrocatalytic Reduction of NAD(P)^+

The complications involved in the direct electrochemical reduction of NAD^+ has led to different mediated attempts based on nonenzymatic electrocatalysis and bioelectrocatalysis for the regeneration of enzymatically active NADH. However, one-electron mediators face the same limitations as described for direct reduction. Dimerization can be only prevented if an additional regeneration enzyme is used that is able to accept two electrons in two steps from the mediator, and then to transfer one electron pair to NAD^+ [418].

4.8.1

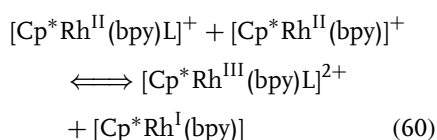
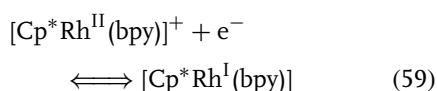
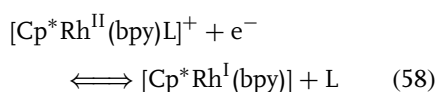
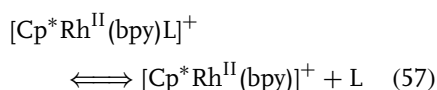
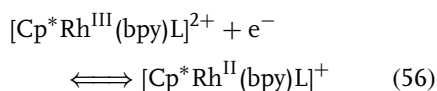
Nonenzymatic Electroreduction of NAD(P)^+

Just as with NADH oxidation with mediators, there has been a great controversy as to whether the reduction of NAD^+ occurs in a single one-hydride step or sequentially.

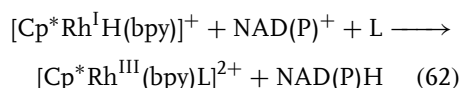
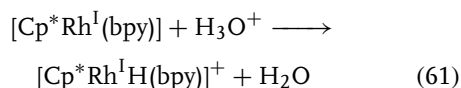
Photochemical enzyme-free methods have been reported for the reduction of NAD(P) [419–421]. The $\text{Rh}(\text{bpy})_3^{3+}$ derivatives have been successfully used as reduction catalysts, enabling electrochemical reduction [421–423]. The better stability of the bis-(tridentate) ligand $\text{Rh}(\text{terpy})_2^{3+}$ allowed a mechanistic study of the photoinduced reduction of NAD^+ , which seems to proceed by a hydride-transfer route according to the dependence of NAD^+ reduction on pH [424]. The intermediate Rh hydride complex was identified by ^1H NMR spectroscopy [422]. A similar conclusion is drawn when the process is studied at modified electrodes with electropolymerized pyrrole-substituted Rh(III) complexes in which hydrogenation involves the formation of an electrogenerated hydride complex, followed by the insertion of NAD^+ in the metal–hydride bond [425, 426]. Electrochemical and spectroscopic studies have demonstrated that Rh(III) complexes are more efficient than the Co(II) or Ir(III) partners for hydride transfer catalysis [427].

The electrochemical pathway for the mediated reduction of NAD(P)^+ through a hydride transfer mechanism with (pentamethylcyclopentadienyl)-2,2'-bipyridine chloro) rhodium(III), $(\text{Cp}^*\text{Rh}^{\text{III}}(\text{bpy})\text{L})^{2+}$, has been described in detail [418, 422, 425]. The rhodium(III) complex is reduced to rhodium(II) and (I) with the concomitant loss of one monodentate ligand that greatly

facilitates the disproportionation of the intermediary Rh(II) [428, 429]:



The Rh(I) complex can then incorporate a proton into its ligand sphere resulting in the hydrido complex that can transfer its hydride ($2\text{e}^- + \text{H}^+$) to NAD(P)^+ as follows [418, 425]:



The regioselective hydride transfer from $[\text{Cp}^*\text{Rh}(\text{bpy})\text{H}]^+$ to NAD^+ to give 1,4-NADH has been appointed to the ability of the amide group to coordinate to the ring-slipped Cp^*Rh metal center [70].

Similar requirements to those previously enumerated for the mediated oxidation of NADH apply to the reduction of NAD^+ . In general, redox catalysts for the electrochemical reduction of NAD^+ should be

selective, stable (both chemically and electrochemically), with high reaction rates and a redox potential that such direct cathodic reduction of NAD^+ leading to NAD dimers does not take place. Most of the nonenzymatic electrocatalytic reduction of NAD^+ is based on the mentioned rhodium (III) chemistry as two electron or hydride transfer selective mediators because direct hydride transfer to carbonyl groups of dehydrogenase substrates is always much slower than the transfer to the NAD(P)^+ [418] and additionally, they also show regioselectivity at the 4-position at ≈ -0.7 V versus SCE [430, 431]. The efficiency of these catalysts for the continuous regeneration of NADH is demonstrated by the enzymatic reduction of pyruvate to D-lactate in homogeneous conditions producing an enantiomeric excess of 94% [430, 432], which compares very well with direct dehydrogenase-based catalytic reduction of NAD^+ (reaction 2). Similar results are obtained with poly[pentamethylcyclopentadienyl-2,2'-bipyridine-chloro-rhodium(III)] modified graphite foil electrodes [431] or PPy $\text{Rh}(\text{terpy})_2^{3+}$ reticulated vitreous carbon electrodes [433]. However, the reaction rate in these systems remains rather low with a maximum turnover for NAD^+ of 2 h^{-1} , whereas strictly catalytic and homogeneous turnover rates easily reach values of 2000 h^{-1} [434, 435].

The only exception to the rhodium chemistry for the nonenzymatic electrocatalytic reduction of NAD^+ recalls the structure of flavins and it was demonstrated with aminopteridone derivatives [436]. In the same line, the low formal potential of neutral red (NR) and the possibility of electropolymerization resulted in poly(NR)-modified electrodes able to regenerate NADH at -0.6 versus Ag/AgCl and pH 6 [437].

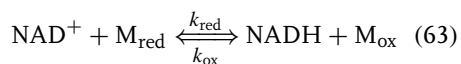
4.8.2

Enzymatic Electroreduction of NAD(P)⁺

As previously mentioned (reaction 8), hydrogenases catalyze the reduction of NAD⁺ with molecular hydrogen achieving maximum turnover values of 150 h⁻¹ in strictly catalytic redox systems [438–441]. Direct electrocatalytic reduction of NAD⁺ by two different *Alcaligenes eutrophus* species and *Desulfovibrio vulgaris* hydrogenases was simultaneously suggested by three groups in 1992 in GC [442], Pt grids containing 10% rhodium [443], and basal plane PG electrodes [444]. More recently, direct electron communication of *Alcaligenes eutrophus* H16 hydrogenase has also been reported [445].

More efficient systems can be designed by mediated bioelectrocatalysis that involve ferredoxin-NADP⁺ reductase (FNR) [81, 446–448], FMN-reductase [448], DI or lipoamide dehydrogenase [82, 358, 359, 447, 449–452], viologen-accepting pyridine nucleotide oxidoreductase [362, 453], enoate reductase [454], formate dehydrogenase [448, 455], and hydrogenase as biocatalysts [442, 456]. Even though for some of these enzymes direct electron transfer with electrode surfaces is successful to some extent (DI [347, 457]) different artificial or natural electron donors have been used as electron transfer mediators to increase the charge transfer efficiency. Quinones [358, 359, 447], methyl or propyl viologen derivatives [81, 362, 442, 446, 450–453, 456], dithiothreitol [82], and flavins [358, 359, 448, 449, 455] are used as electron donors.

The overall equation can be depicted as:



where the rate of NAD⁺ reduction, R_{red} , can be given by:

$$R_{\text{red}} = \frac{k_{\text{cat,red}}[\text{E}]}{1 + \frac{K_{\text{M,NAD}^+}}{[\text{NAD}^+]} + \frac{K_{\text{M,M}_{\text{red}}}}{[\text{M}_{\text{red}}]}} \quad (64)$$

Being $k_{\text{cat,red}}$ the catalytic constant for the NAD⁺ reduction, [E] the enzyme concentration, [NAD⁺], $K_{\text{M,NAD}^+}$ and [M_{red}], $K_{\text{M,M}_{\text{red}}}$, the concentrations and Michaelis-Menten constants of NAD⁺ and mediator in the reduced form, respectively. As previously described, some NAD(P)-related flavoenzymes (e.g. DI, FNR) can also catalyze the oxidation of NAD(P)H and a similar expression can also be applied. In the mediated bioelectroreduction of NAD(P)⁺, M_{red} shuttles electrons from the oxidized enzyme (E_{ox}) to electrodes obeying a ping-pong mechanism and then, M_{ox} is electrochemically reduced to M_{red} at appropriate electrode potentials. The electron transfer from DI to NAD⁺ is thermodynamically unfavorable because the $E^{\circ'}$ of the flavoenzyme remains 42 mV more positive at pH 8.5 than the $E^{\circ'}$ of NAD⁺ [358], see also above under Sect. 4.5. Redox couples with $E^{\circ'}$ sufficiently lower than that of the NAD(P)⁺/NAD(P)H pair could be efficient electron donors to drive the reaction toward NAD(P)⁺ reduction. Some quinones (e.g. adriaycin or alizarin red S) [358, 359, 447] and reduced methyl viologen derivatives (MV^{•+}) [451] render reaction rates sufficiently high to produce measurable electrocatalytic currents on the usual timescale of CV. This rate constant has been reported in the range of 7 · 10³ M⁻¹ s⁻¹ [452]. The redox kinetics between DI and the mediators has been expressed by a Butler-Volmer type equation, indicating a nonspecific and relatively simple electron transfer where the $\log(k_{\text{cat,red}}/K_{\text{M,M}_{\text{red}}})$ or $\log(k_{\text{cat,ox}}/K_{\text{M,M}_{\text{ox}}})$ versus $E_{\text{M}}^{\circ'}$ plots follow a linear Gibbs energy relationship, at least from -0.7 to -0.25 V versus Ag/AgCl [359].

Special attention should be given to the use of flavin-based mediators for the bioelectrocatalytic reduction of NAD(P)^+ . In fact, FAD or FMN spontaneously oxidizes NAD(P)H in living systems according to the standard Gibbs energy variation at pH 7.0 between NADH and FAD, $\Delta G^\circ = -20.3 \text{ kJ mol}^{-1}$. The reverse reaction is then rather forbidden and according to the Gibbs energy variation for the reduction of NAD^+ by FADH_2 :

$$\Delta G^\circ = 60.8 - 5.79\text{pH} + RT \ln \frac{[\text{FAD}][\text{NADH}]}{[\text{FADH}_2][\text{NAD}^+]} \quad (65)$$

the ratio $[\text{FAD}][\text{NADH}]/[\text{FADH}_2][\text{NAD}^+]$ should be lower than $3 \cdot 10^{-4}$ at pH 7.0 in order to make the reaction thermodynamically favorable [455]. This has only been achieved in thin-layer electrochemical experiments with a large electrode surface area in relation to the cell volume [455]. Reduction of NAD(P)^+ by FADH_2 or FMNH_2 in the presence of formate dehydrogenase, ferredoxin-NADP $^+$ -reductase, and FMN-reductase has been demonstrated under these experimental conditions [448, 455, 458]. Obviously, other alternatives to drive this unfavorable equilibrium is the coupling of a dehydrogenase-based reaction to remove NADH in the vicinity of the electrode surface. In fact, steady state electrocatalytic currents with flavin nucleotides and DI for the reduction of NAD^+ have been only demonstrated electrochemically in the presence of lactate dehydrogenase and an excess of pyruvate [359, 449].

Acknowledgment

Lo Gorton and Elena Domínguez thank The Swedish Natural Science Research Council (NFR) and The Spanish Ministry of Science and Technology, respectively,

for financial support and Prof. George S. Wilson, University of Kansas, Lawrence, KS, USA for valuable discussions.

References

1. H. B. White, III *Evolution of Coenzymes and the Origin of Pyridine Nucleotides*, Academic Press, New York, 1982.
2. F. H. Westheimer, H. F. Fisher, E. E. Conn et al., *J. Am. Chem. Soc.* **1951**, 73, 2403–2408.
3. K.-S. You, *CRC Crit. Rev. Biochem.* **1985**, 17, 313–451.
4. D. W. Miles, D. W. Urry, *J. Biol. Chem.* **1968**, 243, 4181–4188.
5. S. F. Velick, *J. Biol. Chem.* **1958**, 233, 1455–1467.
6. A. P. Zens, T. J. Williams, J. C. Wisowaty et al., *J. Am. Chem. Soc.* **1975**, 97, 2850–2857.
7. R. M. Riddle, T. J. Williams, T. A. Bryson et al., *J. Am. Chem. Soc.* **1976**, 98, 4286–4290.
8. A. P. Zens, T. A. Bryson, R. B. Dunlap et al., *J. Am. Chem. Soc.* **1976**, 98, 7559–7564.
9. J. J. Tanner, S.-C. Tu, L. J. Barbour et al., *Protein Sci.* **1999**, 8, 1725–1732.
10. P. E. Smith, J. J. Tanner, *J. Am. Chem. Soc.* **1999**, 121, 8637–8644.
11. J. Jacobus, *Biochemistry* **1971**, 10, 161–164.
12. R. H. Sarma, V. Ross, N. O. Kaplan, *Biochemistry* **1968**, 7, 3052–3062.
13. N. J. Oppenheimer, L. J. Arnold, N. O. Kaplan, *Proc. Natl. Acad. Sci. U.S.A.* **1971**, 68, 3200–3205.
14. G. McDonald, B. Brown, D. Hollis et al., *Biochemistry* **1972**, 11, 1920–1930.
15. O. Jardetzky, N. G. Wade-Jardetzky, *J. Biol. Chem.* **1966**, 241, 85–91.
16. R. H. Sarma, R. J. Mynott, *J. Am. Chem. Soc.* **1973**, 95, 7470–7480.
17. C. E. Bell, T. O. Yeates, D. Eisenberg, *Protein Sci.* **1997**, 6, 2084–2096.
18. H. F. Fisher, E. E. Conn, B. Vennesland et al., *J. Biol. Chem.* **1953**, 202, 687–692.
19. F. A. Loewus, F. H. Westheimer, B. Vennesland, *J. Am. Chem. Soc.* **1953**, 75, 5018–5021.
20. F. A. Loewus, P. Offner, H. F. Fisher et al., *J. Biol. Chem.* **1953**, 202, 699–706.
21. B. Vennesland, F. H. Westheimer in *The Mechanisms of Enzyme Action* (Eds.: W. D.

- McElroy, B. Glass), Johns Hopkins Press, Baltimore, 1954, pp. 357–410.
22. G. Dryhurst, K. M. Kadish, F. Scheller et al., *Biological Electrochemistry*, Academic Press, New York, 1982.
 23. W. M. Clark, *Oxidation-Reduction Potentials of Organic Systems*, Robert E. Krieger Publishing, Huntington, 1972.
 24. H. K. Chenault, G. M. Whitesides, *Appl. Biochem. Biotechnol.* **1987**, 14, 147–197.
 25. F. L. Rodkey, *J. Biol. Chem.* **1955**, 213, 777–786.
 26. F. L. Rodkey, *J. Biol. Chem.* **1959**, 234, 188–190.
 27. F. L. Rodkey, J. A. Donovan, *J. Biol. Chem.* **1959**, 234, 677–680.
 28. L. C. Clark, C. Lyons, *Ann. N.Y. Acad. Sci.* **1962**, 102, 29–45.
 29. I. M. Shaw, *Biochemical Fuel Cells*, Proc. Am. Power Sources Conf. (1963) 17, pp. 53–56.
 30. W. J. Blaedel, R. G. Haas, *Anal. Chem.* **1970**, 42, 918–927.
 31. D. Thévenot, G. Hammouya, *Experientia, Suppl.* **1971**, 18, 631–645.
 32. H. Hanschmann, *Stud. Biophys.* **1974**, 45, 183–194.
 33. I. Carelli, M. E. Cardinali, M. G. Bonicelli, *Annali di Chimica* **1977**, 67, 89–96.
 34. F. M. Martens, J. W. Verhoeven, R. A. Gase et al., *Tetrahedron* **1978**, 34, 443–446.
 35. A. Kitani, K. Sasaki, *Nippon Kagaku Kaishi* **1978**, (6) 817–821.
 36. Y. Ohnishi, M. Kitami, *Bull. Chem. Soc. Jpn.* **1979**, 52, 2674–2677.
 37. I. Carelli, M. E. Cardinali, F. M. Moracci, *J. Electroanal. Chem.* **1980**, 107, 391–404.
 38. K. Sasaki, A. Kitani, A. Kunai et al., *Bull. Chem. Soc. Jpn.* **1980**, 53, 3424–3429.
 39. F. M. Martens, J. W. Verhoeven, *Recl. Trav. Chim. Pays-Bas* **1981**, 100, 228–236.
 40. M. Miller, B. Czochralska, D. Shugar, *Bioelectrochem. Bioenerg.* **1982**, 9, 287–298.
 41. M. F. Powell, T. C. Bruice, *J. Am. Chem. Soc.* **1982**, 104, 5834–5836.
 42. F. M. Martens, J. W. Verhoeven, C. A. G. O. Varma et al., *J. Photochem.* **1983**, 22, 99–113.
 43. S. Fukuzumi, K. Hironaka, N. Nishizawa et al., *Bull. Chem. Soc. Jpn.* **1983**, 56, 2220–2227.
 44. S. Fukuzumi, Y. Kondo, T. Tanaka, *J. Chem. Soc., Perkin Trans.* **1984**, (2) 673–680.
 45. S. Fukuzumi, Y. Kondo, T. Tanaka, *J. Chem. Soc., Chem. Commun.* **1985**, (15) 1053–1054.
 46. N. W. Koper, S. A. Jonker, J. W. Verhoeven, *Recl. Trav. Chim. Pays-Bas* **1985**, 104, 296–302.
 47. S. Fukuzumi, S. Koumitsu, K. Hironaka et al., *J. Am. Chem. Soc.* **1987**, 109, 305–316.
 48. S. Fukuzumi, M. Ishikawa, T. Tanaka, *J. Chem. Soc., Perkin Trans.* **1989**, 2, 1811–1816.
 49. S. Fukuzumi, S. Mochizuki, T. Tanaka, *J. Am. Chem. Soc.* **1989**, 111, 1497–1499.
 50. S. Fukuzumi, S. Mochizuki, T. Tanaka, *Inorg. Chem.* **1990**, 29, 653–659.
 51. J. C. Leprêtre, D. Limosin, G. Pierre et al., *J. Electroanal. Chem.* **1990**, 286, 63–74.
 52. J. Klippenstein, P. Arya, D. D. M. Wayner, *J. Org. Chem.* **1991**, 56, 6736, 6737.
 53. M. Okamura, T. Kashiwagi, Y. Mikata et al., *Tetrahedron Lett.* **1991**, 32, 1475–1478.
 54. M. Okamura, T. Kashiwagi, Y. Mikata et al., *Chem. Lett.* **1992**, (7) 1247–1250.
 55. S. Fukuzumi, Y. Tokuda, *Chem. Lett.* **1992**, (9) 1721–1724.
 56. J. C. Leprêtre, D. Limosin, G. Pierre, *J. Electroanal. Chem.* **1992**, 324, 115–125.
 57. V. Glezer, J. Stradins, B. Turovska et al., *Electrochim. Acta* **1992**, 37, 277–279.
 58. A. Anne, P. Hapitot, J. Moiroux et al., *J. Am. Chem. Soc.* **1992**, 114, 4694–4701.
 59. A. Anne, J. Moiroux, J. M. Savéant, *J. Am. Chem. Soc.* **1993**, 115, 10 224–10 230.
 60. M. Angulo, R. Marin Galvin, M. Ruiz Montoya et al., *J. Electroanal. Chem.* **1993**, 348, 303–315.
 61. A. Anne, J. Moiroux, *Can. J. Chem.* **1995**, 73, 531–538.
 62. A. Anne, S. Fraoua, P. Hapiot et al., *J. Am. Chem. Soc.* **1995**, 117, 7412–7421.
 63. I. Prieto, M. Angulo, J. M. Rodríguez Mellado, *J. Electroanal. Chem.* **1995**, 399, 135–139.
 64. M. Angulo, I. Prieto, J. M. Rodríguez Mellado, *J. Electroanal. Chem.* **1995**, 399, 141–146.
 65. T. Kajiki, N. Tamura, T. Nabeshima et al., *Chem. Lett.* **1995**, (11) 1063–1064.
 66. E. Exposito, M. R. Montoya, M. Angulo et al., *J. Electroanal. Chem.* **1996**, 402, 211–215.
 67. A. Anne, S. Fraoua, V. Grass et al., *J. Am. Chem. Soc.* **1998**, 120, 2951–2958.
 68. J. C. Leprêtre, D. Limosin, G. Pierre et al., *Eur. J. Org. Chem.* **1998**, (10) 2237–2243.
 69. A. G. Rosales, M. R. Montoya, R. M. Galvin et al., *Electroanalysis* **1999**, 11, 32–36.

70. H. C. Lo, O. Buriez, J. B. Kerr et al., *Angew. Chem. Int. Ed. Engl.* **1999**, 38, 1429–1432.
71. S. Yasui, M. Okamura, M. Fujii, *Rev. Heteroatom Chem.* **1999**, 20, 145–165.
72. R. J. Ansell, D. A. P. Small, C. R. Lowe, *J. Mol. Catal. B: Enzyme* **1997**, 3, 239–252.
73. R. J. Ansell, D. A. P. Small, C. R. Lowe, *J. Mol. Recognit.* **1999**, 12, 45–56.
74. R. J. Ansell, C. R. Lowe, *Appl. Microbiol. Biotechnol.* **1999**, 51, 703–710.
75. P. J. Elving, C. O. Schmakel, K. S. V. Santhanam, *Crit. Rev. Anal. Chem.* **1976**, 6, 1–67.
76. I. Katakis, E. Domínguez, *Mikrochim. Acta* **1997**, 126, 11–32.
77. M. J. Lobo, A. J. Miranda, P. Tuñón, *Electroanalysis* **1997**, 9, 191–202.
78. B. Persson, L. Gorton, G. Johansson et al., *Enzyme Microb. Technol.* **1985**, 7, 549–552.
79. B. Persson, L. Gorton, G. Johansson, *Bioelectrochem. Bioenerg.* **1986**, 16, 479–483.
80. G. Palmore, R. Tayhas, H. Bertschy et al., *J. Electroanal. Chem.* **1998**, 443, 155–161.
81. R. DiCosimo, C.-H. Wong, L. Daniels et al., *J. Org. Chem.* **1981**, 46, 4622–4623.
82. Z. E. Shaked, J. J. Barber, G. M. Whitesides, *J. Org. Chem.* **1981**, 46, 4100–4101.
83. L. G. Lee, G. M. Whitesides, *J. Am. Chem. Soc.* **1985**, 107, 7008–7018.
84. W. Hummel, M. R. Kula, *Eur. J. Biochem.* **1989**, 184, 1–13.
85. J. Everse, B. Anderson, K.-S. You, *The Pyridine Nucleotide Coenzymes*, Academic Press, New York, 1982.
86. D. Dolphin, R. Poulson, O. Avramovic, *Coenzymes and Cofactors*, Wiley & Sons, New York, 1987.
87. D. Dolphin, R. Poulson, O. Avramovic, *Pyridine Nucleotide Coenzymes: Chemical, Biochemical, and Medical Aspects, Part A*, Wiley & Sons, New York, 1987.
88. D. Dolphin, R. Poulson, O. Avramovic, *Pyridine Nucleotide Coenzymes: Chemical, Biochemical, and Medical Aspects, Part B*, Wiley & Sons, New York, 1987.
89. W. J. Blaedel, R. A. Jenkins, *Anal. Chem.* **1974**, 46, 1952–1955.
90. W. J. Blaedel, R. A. Jenkins, *Anal. Chem.* **1975**, 47, 1337–1343.
91. R. D. Braun, K. S. V. Santhanam, P. J. Elving, *J. Am. Chem. Soc.* **1975**, 97, 2591–2598.
92. M. A. Jensen, P. J. Elving, *Bioelectrochem. Bioenerg.* **1978**, 5, 526–534.
93. J. Moiroux, P. J. Elving, *Anal. Chem.* **1978**, 50, 1056–1062.
94. J. Moiroux, P. J. Elving, *Anal. Chem.* **1979**, 51, 346–350.
95. J. Moiroux, P. J. Elving, *J. Electroanal. Chem.* **1979**, 102, 93–108.
96. J. Moiroux, P. J. Elving, *J. Am. Chem. Soc.* **1980**, 102, 6533–6538.
97. P. J. Elving, W. T. Bresnahan, J. Moiroux et al., *Bioelectrochem. Bioenerg.* **1982**, 9, 365–378.
98. Z. Samec, P. J. Elving, *J. Electroanal. Chem.* **1983**, 144, 217–234.
99. R. L. Blankespoor, L. L. Miller, *J. Electroanal. Chem.* **1984**, 171, 231–241.
100. M. F. Suaud-Chagny, F. G. Gonon, *Anal. Chem.* **1986**, 58, 412–415.
101. P. Pantano, W. G. Kuhr, *Anal. Chem.* **1993**, 65, 623–630.
102. W. B. Nowall, W. G. Kuhr, *Anal. Chem.* **1995**, 67, 3583–3588.
103. W. B. Nowall, W. G. Kuhr, *Electroanalysis* **1997**, 9, 102–109.
104. M. A. Hayes, E. W. Kristensen, W. G. Kuhr, *Biosens. Bioelectron.* **1998**, 13, 1297–1305.
105. M. A. Hayes, W. G. Kuhr, *Anal. Chem.* **1999**, 71, 1720–1727.
106. M. Aizawa, R. W. Coughlin, M. Charles, *Biochim. Biophys. Acta* **1975**, 385, 362–370.
107. R. W. Coughlin, M. Aizawa, B. F. Alexander et al., *Biotechnol. Bioeng.* **1975**, 17, 515–526.
108. H. Jaegfeldt, A. Torstensson, G. Johansson, *Anal. Chim. Acta* **1978**, 97, 221–228.
109. H. Jaegfeldt, *J. Electroanal. Chem.* **1980**, 110, 295–302.
110. K. Takamura, A. Mori, F. Kusu, *Bioelectrochem. Bioenerg.* **1981**, 8, 229–238.
111. A. Silber, C. Braeuchle, N. Hampp, *J. Electroanal. Chem.* **1995**, 390, 83–89.
112. X. Xing, M. Shao, C.-C. Liu, *J. Electroanal. Chem.* **1996**, 406, 83–90.
113. Y. J. Xiao, J. P. Markwell, *Langmuir* **1997**, 13, 7068–7074.
114. Y. J. Xiao, T. Wang, X. Q. Wang et al., *J. Electroanal. Chem.* **1997**, 433, 49–56.
115. Y. J. Xiao, Y.-F. Chen, X. X. Gao, *Spectrochim. Acta, A, Mol. Biomol. Spectrosc.* **1999**, 55, 1209–1218.
116. G. Li, J. Zhu, H. Fang et al., *J. Electrochem. Soc.* **1996**, 143, L141, L142.
117. G. Li, Q. Gu, C. Fan et al., *Anal. Lett.* **1998**, 31, 1703–1715.

118. J. N. Burnett, A. L. Underwood, *Biochemistry* **1965**, *4*, 2060–2064.
119. P. Leduc, D. Thévenot, *J. Electroanal. Chem.* **1973**, *47*, 543–546.
120. P. Leduc, D. Thévenot, *Bioelectrochem. Bioenerg.* **1974**, *1*, 96–107.
121. R. W. Coughlin, B. F. Alexander, *Biotechnol. Bioeng.* **1975**, *17*, 1379–1382.
122. J. Ludvik, J. Volke, *Anal. Chim. Acta* **1988**, *209*, 69–78.
123. H. Jaegfeldt, *Bioelectrochem. Bioenerg.* **1981**, *8*, 355–370.
124. W. T. Bresnahan, P. J. Elving, *J. Am. Chem. Soc.* **1981**, *103*, 2379–2386.
125. M. A. Jensen, P. J. Elving, *Biochim. Biophys. Acta* **1984**, *764*, 310–315.
126. A. J. Cunningham, A. L. Underwood, *Biochemistry* **1967**, *6*, 266–271.
127. J. Grodowski, P. Neta, B. W. Carlson et al., *J. Phys. Chem.* **1983**, *87*, 3135–3138.
128. T. Matsue, M. Suda, I. Uchida et al., *J. Electroanal. Chem.* **1987**, *234*, 163–173.
129. B. W. Carlson, L. L. Miller, *J. Am. Chem. Soc.* **1983**, *105*, 7453–7454.
130. B. W. Carlson, L. L. Miller, P. Neta et al., *J. Am. Chem. Soc.* **1984**, *106*, 7233–7239.
131. C. Amatore, J. M. Savéant, *J. Electroanal. Chem.* **1981**, *123*, 189–201.
132. J. F. Evans, T. Kuwana, M. T. Henne et al., *J. Electroanal. Chem.* **1977**, *80*, 409–416.
133. J. Scheurs, J. Van den Berg, A. Wonders et al., *Recl. Trav. Chim. Pays-Bas* **1984**, *103*, 251–259.
134. L. Falat, H. Y. Cheng, *J. Electroanal. Chem.* **1983**, *157*, 393–397.
135. N. Cenas, J. Rozgaite, A. Pocius et al., *J. Electroanal. Chem.* **1983**, *154*, 121–128.
136. N. Cenas, J. Kanapienienė, J. Kulys, *J. Electroanal. Chem.* **1985**, *189*, 163–169.
137. K. Ravichandran, R. P. Baldwin, *J. Liq. Chromatogr.* **1984**, *7*, 2031–2050.
138. R. L. McCreery in *Electroanalytical Chemistry* (Ed.: A. J. Bard), Marcel Dekker, New York, 1991, pp. 221–374.
139. M. I. Alvarez-González, S. B. Saidman, M. J. Lobo-Castañón et al., *Anal. Chem.* **2000**, *72*, 520–527.
140. W. T. Bresnahan, J. Moiroux, Z. Samec et al., *Bioelectrochem. Bioenerg.* **1980**, *7*, 125–152.
141. A. Kitani, Y.-H. So, L. L. Miller, *J. Am. Chem. Soc.* **1981**, *103*, 7636–7641.
142. A. Kitani, L. L. Miller, *J. Am. Chem. Soc.* **1981**, *103*, 3595–3597.
143. B. W. Carlson, L. L. Miller, *J. Am. Chem. Soc.* **1985**, *107*, 479–485.
144. J. Hajdu, D. S. Sigman, *Biochemistry* **1977**, *16*, 2841–2846.
145. S. Fukuzumi, N. Nishizawa, T. Tanaka, *J. Org. Chem.* **1984**, *49*, 3571–3578.
146. S. Fukuzumi, T. Tanaka, *Chem. Lett.* **1982**, (10) 1513–1516.
147. L. L. Miller, J. R. Valentine, *J. Am. Chem. Soc.* **1988**, *110*, 3982–3989.
148. R. Szentrimay, P. Yeh, T. Kuwana in *Electrochemical Studies of Biological Systems* (Ed.: D. T. Sawyer), ACS, Washington, D. C., 1977, pp. 143–169.
149. P. N. Bartlett, P. Tebbutt, R. G. Whitaker, *Prog. React. Kinet.* **1991**, *16*, 55–155.
150. A. Heller, *J. Phys. Chem.* **1992**, *96*, 3579–3587.
151. R. A. Marcus, *Angew. Chem. Int. Ed. Engl.* **1993**, *32*, 1111–1121.
152. R. A. Marcus, N. Sutin, *Biochim. Biophys. Acta* **1985**, *811*, 265–322.
153. R. W. Murray in *Electroanalytical Chemistry* (Ed.: A. J. Bard), Marcel Dekker, New York, 1984, pp. 191–368.
154. M. J. Eddowes, H. A. O. Hill, *J. Chem. Soc., Chem. Commun.* **1977**, (21) 771–772.
155. P. Yeh, T. Kuwana, *Chem. Lett.* **1977**, (10) 1145–1148.
156. I. V. Berezin, V. A. Bogdanovskaya, S. D. Varfolomeev et al., *Dokl. Akad. Nauk SSSR (in Russian)* **1978**, *240*, 615–618.
157. M. R. Tarasevich, A. I. Yaropolov, V. A. Bogdanovskaya et al., *Bioelectrochem. Bioenerg.* **1979**, *6*, 393–403.
158. A. I. Yaropolov, V. Malovik, S. D. Varfolomeev et al., *Dokl. Akad. Nauk. SSSR (in Russian)* **1979**, *249*, 1399–1401.
159. D. C.-S. Tse, T. Kuwana, *Anal. Chem.* **1978**, *50*, 1315–1318.
160. L. Gorton, *J. Chem. Soc., Faraday Trans. 1* **1986**, *82*, 1245–1258.
161. L. Gorton, E. Csöregi, E. Domínguez et al., *Anal. Chim. Acta* **1991**, *250*, 203–248.
162. L. Gorton, B. Persson, P. D. Hale et al., *ACS Symp. Ser.* **1992**, *487*, 56–83.
163. P. N. Bartlett in *Biosensor, Fundamentals and Applications* (Eds.: A. P. F. Turner, I. Karube, G. S. Wilson), Oxford Science Publishing, Oxford, 1987, pp. 211–246.
164. W. Schuhmann, H.-L. Schmidt in *Advances in Biosensors* (Ed.: A. P. F. Turner), JAI Press, London, 1992, pp. 79–130.

165. W. Schuhmann, J. Huber, H. Wohlschlaeger et al., *J. Biotechnol.* **1993**, 27, 129–142.
166. E. Lorenzo, F. Pariente, L. Hernandez et al., *Biosens. Bioelectron.* **1998**, 13, 319–332.
167. H. Jaegfeldt, T. Kuwana, G. Johansson, *J. Am. Chem. Soc.* **1983**, 105, 1805–1814.
168. L. Gorton, *Electroanalysis* **1995**, 7, 23–45.
169. R. C. Engstrom, V. A. Strasser, *Anal. Chem.* **1984**, 56, 136–141.
170. R. C. Engstrom, *Anal. Chem.* **1982**, 54, 2310–2314.
171. K. Ravichandran, R. P. Baldwin, *Anal. Chem.* **1984**, 56, 1744–1747.
172. J. Wang, T. Peng, *Anal. Chem.* **1986**, 58, 1787–1790.
173. E. J. Eisenberg, K. C. Cundy, *Anal. Chem.* **1991**, 63, 845–847.
174. G. Palleschi, H. S. Rathore, M. Mascini, *Electroanalysis* **1989**, 1, 199–203.
175. W. G. Kuhr, V. L. Barrett, M. R. Gagnon et al., *Anal. Chem.* **1993**, 65, 617–622.
176. S. Sampath, O. Lev, *J. Electroanal. Chem.* **1998**, 446, 57–65.
177. E. A. Yastrebova, I. V. Osipov, S. D. Varfolomeev et al., *Zhur. Anal. Khim. (Engl. Transl.)* **1982**, 37, 1278–1283.
178. E. A. Yastrebova, S. D. Varfolomeev, I. V. Osipov et al., *Dokl. Akad. Nauk. SSSR (Engl. Transl.)* **1982**, 266, 681–684.
179. C. Ueda, D. C.-S. Tse, T. Kuwana, *Anal. Chem.* **1982**, 54, 850–856.
180. R. S. Deinhammer, M. Ho, J. W. Anderegg et al., *Langmuir* **1994**, 10, 1306–1313.
181. Z. Wu, W. Jing, E. Wang, *Electrochem. Commun.* **1999**, 1, 545–549.
182. E. Lorenzo, L. Sanchez, F. Pariente et al., *Anal. Chim. Acta* **1995**, 309, 79–88.
183. J.-J. Sun, J.-J. Xu, H.-Q. Fang et al., *Bioelectrochem. Bioenerg.* **1997**, 44, 45–50.
184. J.-J. Sun, H.-Q. Fang, H.-Y. Chen, *Chem. Res. Chin. Univ.* **1998**, 14, 96 100.
185. C. Degrand, L. L. Miller, *J. Am. Chem. Soc.* **1980**, 102, 5728–5732.
186. M. Fukui, A. Kitani, C. Degrand et al., *J. Am. Chem. Soc.* **1982**, 104, 28–33.
187. A. N. K. Lau, L. L. Miller, *J. Am. Chem. Soc.* **1983**, 105, 5271–5277.
188. F. Pariente, E. Lorenzo, H. D. Abruña, *Anal. Chem.* **1994**, 66, 4337–4344.
189. F. Pariente, E. Lorenzo, F. Tobalina et al., *Anal. Chem.* **1995**, 67, 3936–3944.
190. F. Pariente, F. Tobalina, M. Darder et al., *Anal. Chem.* **1996**, 68, 3135–3142.
191. F. Pariente, F. Tobalina, G. Moreno et al., *Anal. Chem.* **1997**, 69, 4065–4075.
192. F. Tobalina, F. Pariente, L. Hernández et al., *Anal. Chim. Acta* **1998**, 358, 15–25.
193. M. J. Batchelor, M. J. Green, C. L. Sketch, *Anal. Chim. Acta* **1989**, 221, 289–294.
194. M. Kunitake, K. Akiyoshi, K. Kawatana et al., *J. Electroanal. Chem.* **1990**, 292, 277–280.
195. H. R. Zare, S. M. Golabi, *J. Electroanal. Chem.* **1999**, 464, 14–23.
196. H. Jaegfeldt, A. Torstensson, L. Gorton et al., *Anal. Chem.* **1981**, 53, 1979–1982.
197. K. Ravichandran, R. P. Baldwin, *J. Electroanal. Chem.* **1981**, 126, 293–300.
198. W. Schuhmann, R. Lammert, M. Haemmerle et al., *Biosens. Bioelectron.* **1991**, 6, 689–697.
199. G. Arai, M. Matsushita, I. Yasumori, *Nippon Kagaku Kaishi* **1985**, (5) 894–897.
200. E. Katz, T. Loetzbeyer, D. D. Schlereth et al., *J. Electroanal. Chem.* **1994**, 373, 189–200.
201. E. Katz, I. Willner, *J. Electroanal. Chem.* **1996**, 418, 67–72.
202. I. Willner, A. Riklin, *Anal. Chem.* **1994**, 66, 1535–1539.
203. A. Bardea, E. Katz, A. F. Bückmann et al., *J. Am. Chem. Soc.* **1997**, 119, 9114–9119.
204. M. Lion-Dagan, E. Katz, I. Willner, *J. Am. Chem. Soc.* **1994**, 116, 7913,7914.
205. E. Katz, B. Willner, I. Willner, *Biosens. Bioelectron.* **1997**, 12, 703–719.
206. A. Curulli, I. Carelli, O. Trischitta et al., *Biosens. Bioelectron.* **1997**, 12, 1043–1055.
207. E. Katz, S. V. Heleg, A. Bardea et al., *Biosens. Bioelectron.* **1998**, 13, 741–756.
208. I. Willner, E. Katz, B. Willner et al., *Biosens. Bioelectron.* **1997**, 12, 337–356.
209. I. Willner, E. Katz, B. Willner, *Electroanalysis* **1997**, 9, 965–977.
210. Q. Wu, M. Maskus, F. Pariente et al., *Anal. Chem.* **1996**, 68, 3688–3696.
211. F. Tobalina, F. Pariente, L. Hernández et al., *Anal. Chim. Acta* **1999**, 395, 17–26.
212. I. C. Popescu, E. Domínguez, A. Narváez et al., *J. Electroanal. Chem.* **1999**, 464, 208–214.
213. M. Hedenmo, A. Narváez, E. Domínguez et al., *Analyst* **1996**, 121, 1891–1895.
214. G. D. Storrer, K. Takada, H. D. Abruña, *Inorg. Chem.* **1999**, 38, 559–565.
215. H. Huck, H. L. Schmidt, *Angew. Chem. Int. Ed. Engl.* **1981**, 20, 402,403.

216. A. S. N. Murthy, J. Sharma, *Talanta* **1998**, 45, 951–956.
217. K. Ravichandran, R. P. Baldwin, *Anal. Chem.* **1983**, 55, 1586–1591.
218. Q.-J. Chi, S.-J. Dong, *J. Mol. Catal. A: Chem.* **1996**, 105, 193–201.
219. H. Huck, *Fresenius' J. Anal. Chem.* **1982**, 313, 548–552.
220. L. Gorton, A. Torstensson, H. Jaegfeldt et al., *J. Electroanal. Chem.* **1984**, 161, 103–120.
221. V. Laurinavicius, B. Kurtinaitiene, V. Gureviciene et al., *Anal. Chim. Acta* **1996**, 330, 159–166.
222. G. Nagy, I. Kapui, L. Gorton, *Sens. Actuators, B* **1995**, B24, 323–327.
223. G. Nagy, I. Kapui, L. Gorton, *Anal. Chim. Acta* **1995**, 305, 65–73.
224. B. Persson, L. Gorton, *J. Electroanal. Chem.* **1990**, 292, 115–138.
225. S. A. Wing, J. P. Hart, *Analyst* **1992**, 117, 1215–1229.
226. B. Gruendig, G. Wittstock, U. Ruedel et al., *J. Electroanal. Chem.* **1995**, 395, 143–157.
227. G. Bremle, B. Persson, L. Gorton, *Electroanalysis* **1991**, 3, 77–86.
228. J. Kulys, G. Gleixner, W. Schuhmann et al., *Electroanalysis* **1993**, 5, 201–207.
229. S. Yabuki, H. Shinohara, Y. Ikariyama et al., *J. Electroanal. Chem.* **1990**, 277, 179–187.
230. Y. Ikariyama, T. Ishizuka, H. Sinohara et al., *Denki Kagaku* **1990**, 58, 1097–1102.
231. S. D. Sprules, J. P. Hart, S. A. Wring et al., *Analyst* **1994**, 119, 253–257.
232. S. D. Sprules, J. P. Hart, R. Pittson et al., *Electroanalysis* **1996**, 8, 539–543.
233. L. T. Kubota, F. Gouvea, A. N. Andrade et al., *Electrochim. Acta* **1996**, 41, 1465–1469.
234. J. Wang, P. V. A. Pamidi, M. Jiang, *Anal. Chim. Acta* **1998**, 360, 171–178.
235. L. T. Kubota, L. Gorton, *Electroanalysis* **1999**, 11, 719–728.
236. P. Hale, H.-S. Lee, Y. Okamoto, *Anal. Lett.* **1993**, 26, 1073–1085.
237. B. Persson, H. S. Lee, L. Gorton et al., *Electroanalysis* **1995**, 7, 935–940.
238. D. D. Schlereth, E. Katz, H. L. Schmidt, *Electroanalysis* **1995**, 7, 46–54.
239. M. Ohtani, S. Kuwabata, H. Yoneyama, *J. Electroanal. Chem.* **1997**, 422, 45–54.
240. C.-X. Cai, K.-H. Xue, *J. Electroanal. Chem.* **1997**, 427, 147–153.
241. A. A. Karyakin, E. E. Karyakina, W. Schuhmann et al., *Electroanalysis* **1999**, 11, 553–557.
242. A. A. Karyakin, E. E. Karyakina, H. L. Schmidt, *Electroanalysis* **1999**, 11, 149–155.
243. J.-L. Han, A.-M. Yu, H.-Y. Chen, *Huaxue Xuebao (Acta Chim. Sinica)* **1995**, 53, 362–368.
244. D.-M. Zhou, H.-Q. Fang, H.-Y. Chen et al., *Anal. Chim. Acta* **1996**, 329, 41–48.
245. B. Persson, *J. Electroanal. Chem.* **1990**, 287, 61–80.
246. F. Ni, H. Feng, L. Gorton et al., *Langmuir* **1990**, 6, 66–73.
247. H. X. Ju, L. Dong, H. Y. Chen, *Chem. J. Chin. Univ. (in Chinese)* **1995**, 16, 1200–1203.
248. C. A. Pessoa, Y. Gushikem, L. T. Kubota et al., *J. Electroanal. Chem.* **1997**, 431, 23–27.
249. L. T. Kubota, F. Muteanu, A. Roddick-Lanzilotta et al., *Química Analítica* **2000**, 19 (Suppl. 1), 15–27.
250. A. Malinauskas, T. Ruzgas, L. Gorton, *J. Electroanal. Chem.* **2000**, 448, 55–63.
251. H. Huck, A. Schelter-Graf, J. Danzer et al., *Analyst* **1984**, 109, 147–150.
252. H. Huck, *Fresenius' J. Anal. Chem.* **1982**, 313, 548–552.
253. H. Huck, A. Schelter-Graf, H. L. Schmidt, *Bioelectrochem. Bioenerg.* **1984**, 13, 199–209.
254. H. Huck, *Phys. Chem. Chem. Phys.* **1999**, 1, 855–859.
255. L. Gorton, B. Persson, M. Polasek, G. Johansson in *Contemporary Electroanalytical Chemistry (ElectroFinnAnalysis)* (Eds.: A. Ivaska, A. Lewenstam, R. Sara), Plenum Publishing, New York, 1991, pp. 183–189.
256. M. Polasek, L. Gorton, R. Appelqvist et al., *Anal. Chim. Acta* **1991**, 246, 283–292.
257. C. X. Cai, K. H. Xue, *Anal. Chim. Acta* **1997**, 343, 69–77.
258. L. I. Boguslavsky, L. Geng, I. Kovalev et al., *Biosens. Bioelectron.* **1995**, 10, 693–704.
259. Q. Chi, S. Dong, *Electroanalysis* **1995**, 7, 147–153.
260. Q. Shi, Q. Cheng, P. Zhang, *Fenxi Huaxue* **1997**, 25, 690–692.
261. A. Malinauskas, T. Ruzgas, L. Gorton et al., *Electroanalysis* **2000**, 12, 194–198.
262. A. Malinauskas, T. Ruzgas, L. Gorton, *J. Colloid Interface Sci.* **2000**, 224, 325–332.
263. H. X. Ju, L. Dong, H. Y. Chen, *Talanta* **1996**, 43, 1177–1183.

264. M. J. Lobo-Castanon, S. L. Alvarez-Crespo, M. I. Alvarez-Gonzalez et al., *Sci. Pap. Univ. Pardubice, Ser. A* **1998**, 3, 17–29.
265. C. Ramirez Molina, M. Boujtita, N. El Murr, *Anal. Chim. Acta* **1999**, 401, 155–162.
266. D. D. Schlereth, E. Katz, H. L. Schmidt, *Electroanalysis* **1994**, 6, 725–734.
267. C.-X. Cai, K.-H. Xue, *Talanta* **1998**, 47, 1107–1119.
268. D.-M. Zhou, J.-J. Sun, H.-Y. Chen et al., *Electrochim. Acta* **1998**, 43, 1803–1809.
269. Y. Okamoto, T. Kaku, R. Shundo, *Pure Appl. Chem.* **1996**, 68, 1417–1421.
270. F. Torabi, K. Ramanathan, P.-O. Larsson et al., *Talanta* **1999**, 50, 787–797.
271. V. U. Spohn, *Nova Acta Leopold., Suppl.* **1998**, 15, 155–175.
272. B. Persson, H. L. Lan, L. Gorton et al., *Biosens. Bioelectron.* **1993**, 8, 81–88.
273. Z. Huan, B. Persson, L. Gorton et al., *Electroanalysis* **1996**, 8, 575–581.
274. E. Domínguez, H. L. Lan, Y. Okamoto et al., *Biosens. Bioelectron.* **1993**, 8, 167–175.
275. E. Domínguez, H. L. Lan, Y. Okamoto et al., *Biosens. Bioelectron.* **1993**, 8, 229–237.
276. H.-C. Shu, B. Mattiasson, B. Persson et al., *Biotechnol. Bioeng.* **1995**, 46, 270–279.
277. H.-C. Shu, L. Gorton, B. Persson et al., *Biotechnol. Bioeng.* **1995**, 46, 280–284.
278. Q. Chi, S. Dong, *Analyst* **1994**, 119, 1063–1066.
279. S. Cosnier, K. Le Lous, *J. Electroanal. Chem.* **1996**, 406, 243–246.
280. A. Silber, N. Hampp, W. Schuhmann, *Biosens. Bioelectron.* **1996**, 11, 215–223.
281. Y. Wang, D.-M. Zhou, H.-Y. Chen, *Chem. Res. Chin. Univ.* **1997**, 13, 276–281.
282. L. Gorton, G. Bremle, E. Csoeregi et al., *Anal. Chim. Acta* **1991**, 249, 4354.
283. J. J. Xu, H. Q. Fang, H. Y. Chen, *Chem. J. Chin. Univ. (in Chinese)* **1997**, 18, 706–710.
284. H.-Y. Chen, D.-M. Zhou, J.-J. Xu et al., *J. Electroanal. Chem.* **1997**, 422, 21–25.
285. K. Hajizadeh, H. T. Tang, H. B. Halsall et al., *Anal. Lett.* **1991**, 24, 1453–1469.
286. A.-M. Yu, J.-L. Han, K.-S. Yang et al., *Gaodeng Xuexiao Huaxue Xuebao (Chem. J. Chin. Univ.) (in Chinese)* **1995**, 16, 1204–1206.
287. K. Tanaka, S. Ikeda, N. Oyama et al., *Anal. Sci.* **1993**, 9, 783–789.
288. K. Tanaka, S. Ikeda, N. Oyama et al., *Anal. Sci.* **1993**, 9, 783–789.
289. C.-X. Cai, H.-X. Ju, H.-Y. Chen, *Gaodeng Xuexiao Huaxue Xuebao (Chem. J. Chin. Univ.) (in Chinese)* **1995**, 16, 368–372.
290. T. Ohsaka, K. Tanaka, K. Tokuda, *J. Chem. Soc., Chem. Commun.* **1993**, (3) 222–224.
291. A. Torstensson, L. Gorton, *J. Electroanal. Chem.* **1981**, 130, 199–207.
292. Y. Kimura, K. Niki, *Anal. Sci.* **1985**, 1, 271–274.
293. O. Miyawaki, T. Yano, *Enzyme Microb. Technol.* **1992**, 14, 474–478.
294. O. Miyawaki, T. Yano, *Enzyme Microb. Technol.* **1993**, 15, 525–529.
295. I. Carelli, I. Chiarotto, A. Curulli, *Curr. Top. Electrochem.* **1994**, 3, 141–157.
296. A. Curulli, I. Carelli, O. Trischitta et al., *Talanta* **1997**, 44, 1659–1669.
297. M. Vreeke, R. Maidan, A. Heller, *Anal. Chem.* **1992**, 64, 3084–3090.
298. M. J. Lobo, A. J. Miranda, J. M. Lopez-Fonseca et al., *Anal. Chim. Acta* **1996**, 325, 33–42.
299. M. J. L. Castañón, A. J. M. Ordieres, P. Tuñón Blanco, *Biosens. Bioelectron.* **1997**, 12, 511–520.
300. A. B. Florou, M. I. Prodromidis, M. I. Karayannis et al., *Electroanalysis* **1998**, 10, 1261–1268.
301. L. Gorton, G. Johansson, A. Torstensson, *J. Electroanal. Chem.* **1985**, 196, 81–92.
302. P. N. Bartlett, P. R. Birkin, E. N. K. Wallace, *J. Chem. Soc., Faraday Trans.* **1997**, 93, 1951–1960.
303. M. Somasundrum, J. V. Bannister, *J. Chem. Soc., Chem. Commun.* **1993**, (21) 1629–1631.
304. K. Tanaka, K. Tokuda, T. Ohsaka, *J. Chem. Soc., Chem. Commun.* **1993**, (23) 1770–1772.
305. L. T. Kubota, L. Gorton, *J. Solid State Electrochem.* **1999**, 3, 370–379.
306. A. Malinauskas, T. Ruzgas, L. Gorton, *Bioelectrochem. Bioenerg.* **1999**, 49, 21–27.
307. O. Miyawaki, L. B. Wingard, *Biochim. Biophys. Acta* **1985**, 838, 60–68.
308. H. Shinohara, *Proc. SPIE-Int. Soc. Opt. Eng.* **1996**, 2716, 177–182.
309. L. T. Kubota, L. Gorton, A. Roddick-Lanzilotta et al., *Bioelectrochem. Bioenerg.* **1998**, 47, 39–46.
310. K. J. Stine, D. M. Andrauskas, A. R. Khan et al., *J. Electroanal. Chem.* **1999**, 472, 147–156.
311. C. X. Cai, K. H. Xue, *Microchem. J.* **1998**, 58, 197–208.

312. N. Mano, A. Kuhn, *J. Electroanal. Chem.* **1999**, 477, 79–88.
313. N. Mano, A. Kuhn, *Electrochem. Commun.* **1999**, 1, 497–501.
314. E. Casero, M. Darder, K. Takada et al., *Langmuir* **1999**, 15, 127–134.
315. V. Laurinavicius, B. Kurtinaitiene, V. Li-
auksminas et al., *Monatshefte für Chemie*
1999, 130, 1269–1281.
316. P. C. Pandey, S. Upadhyay, B. C. Upadhyay
et al., *Anal. Biochem.* **1998**, 260, 195–203.
317. P. C. Pandey, *Trans. Indian Inst. Met.* **1998**,
51, 319–325.
318. P. C. Pandey, S. Upadhyay, H. C. Pathak
et al., *Anal. Lett.* **1998**, 31, 2327–2348.
319. A. S. N. Murthy, Anita, *Bioelectrochem.*
Bioenerg. **1994**, 33, 71–73.
320. A. S. N. Murthy, Anita, R. L. Gupta, *Anal.*
Chim. Acta **1994**, 289, 43–46.
321. P. C. Pandey, *Anal. Biochem.* **1994**, 221,
392–396.
322. J. Kulys, *Biosensors* **1986**, 2, 3–13.
323. J. Kulys, *Enzyme Microb. Technol.* **1981**, 3,
344–352.
324. W. J. Albery, P. N. Bartlett, *J. Chem. Soc.,*
Chem. Commun. **1984**, (4) 234–236.
325. W. J. Albery, P. N. Bartlett, A. E. G. Cass
et al., *J. Chem. Soc., Faraday Trans. 1* **1986**,
82, 1033–1050.
326. W. J. Albery, P. N. Bartlett, A. E. G. Cass
et al., *J. Electroanal. Chem.* **1987**, 218,
127–134.
327. K. McKenna, S. E. Boyette, A. Brajter-Toth,
Anal. Chim. Acta **1988**, 206, 75–84.
328. J. J. Kulys, U. Bilitewski, R. D. Schmid,
Anal. Lett. **1991**, 24, 181–189.
329. C. J. Stanley, R. B. Cox, M. F. Cardosi et al.,
J. Immunol. Methods **1988**, 112, 153–161.
330. S. Zhao, U. Korell, L. Cuccia et al., *J. Phys.*
Chem. **1992**, 96, 5641–5652.
331. S. Zhao, R. B. Lennox, *J. Electroanal. Chem.*
1993, 346, 161–173.
332. J. Wang, T. Golden, *Anal. Chim. Acta* **1989**,
217, 343–351.
333. F. Xu, H. Li, S. J. Cross et al., *J. Electroanal.*
Chem. **1994**, 368, 221–225.
334. L. Angnes, C. M. N. Azevedo, K. Araki et al.,
Anal. Chim. Acta **1996**, 329, 91–96.
335. B. F. Yon Hin, C. R. Lowe, *Anal. Chem.*
1987, 59, 2111–2115.
336. C.-X. Cai, K.-H. Xue, Y.-M. Zhou et al.,
Talanta **1997**, 44, 339–347.
337. T. N. Rao, I. Yagi, T. Miwa et al., *Anal.*
Chem. **1999**, 71, 2506–2511.
338. A. Fujishima, T. N. Rao, E. Popa et al.,
J. Electroanal. Chem. **1999**, 473, 179–185.
339. A. D. Ryabov, V. S. Kurova, V. N. Goral
et al., *Chem. Mater.* **1999**, 11, 600–604.
340. N. F. Atta, A. Galal, E. Karagozler et al.,
J. Chem. Soc., Chem. Commun. **1990**, (19)
1347–1349.
341. N. F. Atta, A. Galal, A. E. Karagozler et al.,
Biosens. Bioelectron. **1991**, 6, 333–341.
342. H. Ju, D. Leech, *Anal. Chim. Acta* **1997**, 345,
51–58.
343. J. Wang, F. Lu, L. Angnes et al., *Anal. Chim.*
Acta **1995**, 305, 3–7.
344. J. Wang, Q. Chen, M. Pedrero et al., *Anal.*
Chim. Acta **1995**, 300, 111–116.
345. J. Wang, P. V. A. Pamidi, C. L. Ren-
schler et al., *J. Electroanal. Chem.* **1996**, 404,
137–142.
346. C. J. McNeil, J. A. Spoors, J. M. Cooper
et al., *Anal. Chim. Acta* **1990**, 237, 99–105.
347. D. Kobayashi, S. Ozawa, T. Mihara et al.,
Denki Kagaku **1992**, 60, 1056–1062.
348. H. Ukeda, M. Imabayashi, K. Mat-
sumoto et al., *Agric. Biol. Chem.* **1989**, 53,
2909–2915.
349. M. J. Green, H. A. O. Hill, *J. Chem. Soc.,*
Faraday Trans. 1 **1986**, 82, 1237–1243.
350. Y. Kashiwagi, T. Osa, *Chem. Lett.* **1993**, (4)
677–680.
351. Y. Kashiwagi, Q. Pan, Y. Yanagisawa et al.,
Denki Kagaku oyobi Kogyo Butsuri Kagaku
1994, 62, 1240–1246.
352. T. Sawaguchi, T. Matsue, I. Uchida,
Bioelectrochem. Bioenerg. **1992**, 29, 127–133.
353. H. C. Chang, A. Ueno, H. Yamada et al.,
Denki Kagaku oyobi Kogyo Butsuri Kagaku
1990, 58, 1211–1212.
354. M. Comtat, M. Galy, P. Goulas et al., *Anal.*
Chim. Acta **1988**, 208, 295–300.
355. K. Miki, T. Ikeda, S. Todoriki et al., *Anal.*
Sci. **1989**, 5, 269–274.
356. S. Todoriki, K. Miki, T. Ikeda et al., *Denki*
Kagaku oyobi Kogyo Butsuri Kagaku **1990**,
58, 1089–1096.
357. S. Ozawa, T. Ikeda, M. Senda, *Anal. Sci.*
1991, 7, 1689–1692.
358. Y. Ogino, K. Takagi, K. Kano et al.,
J. Electroanal. Chem. **1995**, 396, 517–524.
359. K. Takagi, K. Kano, T. Ikeda, *J. Electroanal.*
Chem. **1998**, 445, 211–219.
360. S. Kunugi, K. Ikeda, T. Nakashima et al.,
Polym. Bull. **1990**, 24(2), 247–250.
361. H. C. Chang, A. Ueno, H. Yamada et al.,
Analyst **1991**, 116, 793–796.

362. S. Cosnier, K. LeLous, *Talanta* **1996**, *43*, 331–337.
363. I. Karube, K. Yokoyama, E. Tamiya, *Biosens. Bioelectron.* **1993**, *8*, 219–228.
364. Y. Miwa, M. Nishizawa, T. Matsue et al., *Denki Kagaku oyobi Kogyo Butsuri Kagaku* **1994**, *62*, 1256,1257.
365. M. Montagne, H. Durliat, M. Comtat, *Anal. Chim. Acta* **1993**, *278*, 25–33.
366. T. Noguer, J. L. Marty, *Enzyme Microb. Technol.* **1995**, *17*, 453–456.
367. M. Montagne, H. Erdmann, M. Comtat et al., *Sens. Actuators, B* **1995**, *B27*, 440–443.
368. T. Noguer, J. L. Marty, *Anal. Chim. Acta* **1997**, *347*, 63–69.
369. J. Katrlík, A. Pizzariello, V. Mastihuba et al., *Anal. Chim. Acta* **1999**, *379*, 193–200.
370. T. Suzuki, K. Yamamoto, Y. Tanaka et al., *Maku* **1989**, *14*, 319–328.
371. H.-Z. Bu, S. R. Mikkelsen, A. M. English, *Anal. Chem.* **1998**, *70*, 4320–4325.
372. T. Matsue, N. Kasai, M. Narumi et al., *J. Electroanal. Chem.* **1991**, *300*, 111–118.
373. T. Huang, A. Warsinke, T. Kuwana et al., *Anal. Chem.* **1998**, *70*, 991–997.
374. G. de Oliveira Neto, J. Rover, L. T. Kubota, *Electroanalysis* **1999**, *11*, 527–533.
375. C. J. McNeil, J. A. Spoors, D. Cocco et al., *Anal. Chem.* **1989**, *61*, 25–29.
376. M. Somasundrum, J. Hall, J. V. Bannister, *Anal. Chim. Acta* **1994**, *295*, 47–57.
377. Z. Liu, O. Niwa, T. Horiuchi et al., *Biosens. Bioelectron.* **1999**, *14*, 631–638.
378. S. Cosnier, M. Fontecave, D. Limosin et al., *Anal. Chem.* **1997**, *69*, 3095–3099.
379. S. Cosnier, M. Fontecave, C. Innocent et al., *Electroanalysis* **1997**, *9*, 685–688.
380. S. Cosnier, J.-L. Decout, M. Fontecave et al., *Electroanalysis* **1998**, *10*, 521–525.
381. J. M. Laval, C. Bourdillon, J. Moiroux, *J. Am. Chem. Soc.* **1984**, *106*, 4701–4706.
382. J. Wang, M. S. Lin, *Anal. Chem.* **1988**, *60*, 499–502.
383. J. Wang, E. González-Romero, *Electroanalysis* **1993**, *5*, 427–430.
384. L. Campanella, T. Ferri, M. P. Sammartino et al., *J. Mol. Catal.* **1987**, *43*, 153–159.
385. A. Fujishima, E. Popa, Z. Wu et al. in *Novel Trends in Electroorganic Synthesis* (Ed.: F. Torii), Springer, Tokyo, 1998, pp. 421–424.
386. R. W. Murray, *Molecular Design of Electrode Surfaces*, Wiley-Interscience, New York, 1992.
387. E. Laviron, *J. Electroanal. Chem.* **1979**, *101*, 19–28.
388. E. Laviron in *Electroanalytical Chemistry* (Ed.: A. J. Bard), Marcel Dekker, New York, 1982, pp. 53–151.
389. W. Albery, A. R. Hillman, *J. Electroanal. Chem.* **1984**, *170*, 27–49.
390. C. P. Andrieux, J. M. Dumas-Bouchiat, J. M. Savéant, *J. Electroanal. Chem.* **1984**, *169*, 9–21.
391. C. P. Andrieux, J. M. Savéant, *J. Electroanal. Chem.* **1984**, *171*, 65–93.
392. C. P. Andrieux, J. M. Savéant, *J. Electroanal. Chem.* **1978**, *93*, 163–168.
393. S. Fukuzumi, N. Nishizawa, T. Tanaka, *J. Chem. Soc., Perkin Trans. 2* **1985**, 371–378.
394. L. Gorton, G. Johansson, *J. Electroanal. Chem.* **1980**, *113*, 151–158.
395. A. L. Underwood, J. N. Burnett in *Electroanalytical Chemistry* (Ed.: A. J. Bard), Marcel Dekker, New York, 1973, pp. 1–85.
396. M. A. Jensen, W. T. Bresnahan, P. J. Elving, *Bioelectrochem. Bioenerg.* **1983**, *11*, 299–306.
397. R. C. Kaye, H. I. Stonehill, *J. Chem. Soc.* **1952**, *56*, 3244–3247.
398. J. Moiroux, S. Deycard, T. Malinski, *J. Electroanal. Chem.* **1985**, *194*, 99–108.
399. C. O. Schmakel, M. A. Jensen, P. J. Elving, *Bioelectrochem. Bioenerg.* **1978**, *5*, 625–634.
400. K. S. V. Santhanam, P. J. Elving, *J. Am. Chem. Soc.* **1973**, *95*, 5482–5490.
401. C. O. Schmakel, K. S. V. Santhanam, P. J. Elving, *J. Am. Chem. Soc.* **1975**, *97*, 5083–5092.
402. E. J. Land, A. J. Swallow, *Biochim. Biophys. Acta* **1968**, *162*, 327–337.
403. B. H. J. Bielski, P. C. Chan, *J. Am. Chem. Soc.* **1980**, *102*, 1713–1716.
404. W. T. Bresnahan, P. J. Elving, *Biochim. Biophys. Acta* **1981**, *678*, 151–156.
405. A. Anne, P. Hapiot, J. Moiroux et al., *J. Electroanal. Chem.* **1992**, *331*, 959–970.
406. B. Czocharalska, M. Szwedkowska, D. Shugar, *Arch. Biochem. Biophys.* **1980**, *199*, 497–505.
407. V. Carelli, F. Liberatore, A. Casini et al., *Bioorg. Chem.* **1980**, *9*, 342–351.
408. L. Avigliano, V. Carelli, A. Casini et al., *Biochim. Biophys. Acta* **1983**, *723*, 372–375.
409. E. M. Kosower, A. Teuerstein, H. D. Burrows et al., *J. Am. Chem. Soc.* **1978**, *100*, 5185–5190.

410. Y. Ohnishi, Y. Kikuchi, M. Kitami, *Tetrahedron Lett.* **1979**, 3005–3008.
411. F. G. Drakesmith, *A Process and Apparatus for the Electrochemical Regeneration of Co-enzymes*; Eur. Pat. Appl. 275649, A1, 1988.
412. F. G. Drakesmith, B. Gibson, *J. Chem. Soc., Chem. Commun.* **1988**, (22) 1493–1494.
413. M. Aizawa, R. W. Coughlin, M. Charles, *Biochim. Biophys. Acta* **1976**, 440, 233–240.
414. M. Aizawa, R. W. Coughlin, M. Charles, *Biotechnol. Bioeng.* **1976**, 18, 209–215.
415. S.-E. Yun, M. Taya, S. Tone, *Biotechnol. Lett.* **1994**, 16, 1053–1058.
416. S. H. Baik, C. Kang, C. Jeon et al., *Biotechnol. Tech.* **1999**, 13, 1–5.
417. M. Aizawa, S. Suzuki, M. Kubo, *Biochim. Biophys. Acta* **1976**, 444, 886–892.
418. E. Steckhan, *Top. Curr. Chem.* **1994**, 170, 83–111.
419. D. Mandler, I. Willner, *J. Am. Chem. Soc.* **1984**, 106, 5352, 5353.
420. P. Cuendet, M. Graetzel, *Photochem. Photobiol.* **1984**, 39, 609–612.
421. R. Wienkamp, E. Steckhan, *Angew. Chem. Int. Ed. Engl.* **1983**, 22, 782, 783.
422. E. Steckhan, S. Herrmann, R. Ruppert et al., *Organometallics* **1991**, 10, 1568–1577.
423. Y. Shimizu, A. Kitani, S. Ito et al., *Denki Kagaku* **1994**, 62, 1233, 1234.
424. K. Umeda, A. Nakamura, F. Toda, *Bull. Chem. Soc. Jpn.* **1993**, 66, 2260–2267.
425. E. Hofer, E. Steckhan, B. Ramos et al., *J. Electroanal. Chem.* **1996**, 402, 115–122.
426. C. Caix, S. Chardon-Noblat, A. Deronzier et al., *J. Organomet. Chem.* **1997**, 540, 105–111.
427. W. Kaim, R. Reinhardt, E. Waldhor et al., *J. Organomet. Chem.* **1996**, 524, 195–202.
428. U. Kölle, M. Grützel, *Angew. Chem. Int. Ed. Engl.* **1987**, 26, 567–570.
429. U. Koelle, A. D. Ryabov, *Mendeleev Commun.* **1995**, (5) 187–189.
430. R. Ruppert, S. Herrmann, E. Steckhan, *Tetrahedron Lett.* **1987**, 28, 6583–6586.
431. S. Cosnier, H. Gunther, *J. Electroanal. Chem.* **1991**, 315, 307–312.
432. R. Ruppert, M. Franke, S. Herrmann et al., *DEHEMA-Monogr.* **1989**, 112, 13–23.
433. M. Beley, J. P. Collin, *J. Mol. Catal.* **1993**, 79, 133–140.
434. A. Nakamura, H. Minami, I. Urabe et al., *J. Ferment. Technol.* **1988**, 66, 267–272.
435. M. Persson, M. O. Mansson, L. Bulow et al., *Bio-Technology* **1991**, 9, 280–284.
436. S. Kwee, H. Lund, *Bioelectrochem. Bioenerg.* **1974**, 1, 87–95.
437. A. A. Karyakin, O. A. Bobrova, E. E. Karyakina, *J. Electroanal. Chem.* **1995**, 399, 179–184.
438. B. Danielsson, F. Winqvist, J. Y. Malpote et al., *Biotechnol. Lett.* **1982**, 4, 673–678.
439. K. Otsuka, S. Aono, I. Okura, *Chem. Lett.* **1987**, (10) 2089–2090.
440. M. Takeuchi, I. Okura, F. Hasumi, *J. Mol. Catal.* **1991**, 68, L21–L23.
441. Q. H. Wong, L. Daniels, W. H. Orme-Johnson et al., *J. Am. Chem. Soc.* **1981**, 103, 6227, 6228.
442. D. D. Schlereth, V. M. Fernández, M. Sánchez-Cruz et al., *Bioelectrochem. Bioenerg.* **1992**, 28, 473–482.
443. J. Cantet, A. Bergel, M. Comtat et al., *J. Mol. Catal.* **1992**, 73, 371–380.
444. T. Sagara, H. Hirayama, K. Akutsu et al., *Bioelectrochem. Bioenerg.* **1992**, 28, 191–204.
445. K. Delecouls, P. Saint-Aguet, C. Zaborosch et al., *J. Electroanal. Chem.* **1999**, 468, 139–149.
446. M. Ito, T. Kuwana, *J. Electroanal. Chem.* **1971**, 32, 415–425.
447. K. Kano, K. Takagi, Y. Ogino et al., *Chem. Lett.* **1995**, (7) 589–590.
448. A. Bergel, M. Comtat, *Bioelectrochem. Bioenerg.* **1992**, 27, 495–500.
449. K. Takagi, K. Kano, T. Ikeda, *Chem. Lett.* **1996**, (1) 11–12.
450. T. Matsue, H. C. Chang, I. Uchida et al., *Tetrahedron Lett.* **1988**, 29, 1551–1554.
451. H. C. Chang, T. Matsue, I. Uchida et al., *Chem. Lett.* **1989**, (7) 1119–1122.
452. D. D. Schlereth, V. M. Fernández, *Biotechnol. Tech.* **1990**, 4, 201–204.
453. H. Günther, A. S. Paxinos, M. Schulz et al., *Angew. Chem. Int. Ed. Engl.* **1990**, 29, 1053–1055.
454. H. Simon, H. Günther, J. Bader et al., *Angew. Chem. Int. Ed. Engl.* **1981**, 20, 861–863.
455. A. Bergel, M. Comtat, *J. Electroanal. Chem.* **1991**, 302, 219–231.
456. D. D. Schlereth, V. M. Fernández, *Biotechnol. Lett.* **1989**, 11, 407–410.
457. T. Larsson, A. Lindgren, T. Ruzgas, *Bioelectrochemistry* **2001**, 53, 243–249.
458. A. Bergel, A. Courteix, J. Cantet et al., *Recents Prog. Genie Procédés* **1993**, 7, 231–236.

5 Electrochemical Immunoassay

C. Ajith Wijayawardhana, H. Brian Halsall, and William R. Heineman
University of Cincinnati, Cincinnati, Ohio

5.1	Introduction	147
5.2	Enzyme Electrochemical Immunoassays	148
5.2.1	Electrochemical Detection	148
5.2.2	The E-S-P System	158
5.2.3	Heterogeneous Enzyme Immunoassay	159
5.2.4	Ultrasensitive Heterogeneous Enzyme Assays in Small Volumes . . .	161
5.2.5	Homogeneous Enzyme Immunoassay	163
5.3	Nonenzyme Electrochemical Immunoassays	164
5.3.1	Nonenzyme Homogeneous Immunoassays	164
5.3.2	Heterogeneous Nonenzymatic Immunoassays	164
5.4	Electrochemical Immunosensors	166
5.5	Applications	170
5.6	Conclusion	170
	References	171

5.1

Introduction

The development of immunoassay is one of the great success stories in bioanalytical chemistry. Its success is due largely to the extraordinarily selective and versatile reagent provided by nature in the form of antibody (Ab). As part of the immune defense system in animals, antibodies with high specificity can be synthesized in reasonable quantity by an organism within weeks of being injected with a foreign species called an antigen (Ag). It is estimated that an animal can synthesize up to 10^7 to 10^8 antibodies of different specificities [1, 2]. This variability is the source of the remarkable versatility of immunoassay in detecting a broad range of analytes.

Traditionally, antibodies for immunoassays have been obtained from the antisera of animals immunized with the Ag of interest. Such antisera contain a collection of different antibodies called polyclonal antibodies, each specific for a different site (epitope) of the Ag. An Ag typically needs to be greater than approximately 1500 Daltons (Da) to elicit efficient Ab formation [1]. However, antibodies for smaller molecules, such as therapeutic drugs, can be obtained by covalently attaching the smaller molecule (hapten) to

some carrier Ag, usually a large protein or a multiple antigenic peptide (MAP) [3]. The resulting conjugate elicits the formation of antibodies, some of which are directed toward the hapten. Use of polyclonal antibodies, however, is complicated by the inconsistency in the polyclonal antisera from different animals or even among different batches from the same animal. This led to the development of monoclonal antibodies [4], which have a known, reproducible specificity and affinity. Monoclonal antibodies are obtained in large quantities from cell cultures grown from cells retrieved from the immunized animal and selected for producing the desired Ab. The more recently developed recombinant antibodies using molecular engineering methods are also expected to be widely used in the future because of their low cost and improved or novel specificities [5, 6].

The origins of using Ab electrochemical immunoassay (ECI) can be traced to the pioneering efforts of Breyer and Radcliff, who in 1951 used polarography to follow the interaction of azo-labeled protein with specific antiserum [7]. Although this predated radioimmunoassay – commonly misperceived to be the first type of immunoassay – by several years, it took more than a quarter of a century for developments in biochemistry, electronics, immunology, and analytical techniques to

fuse into a methodology now capable of almost unrivaled sensitivity. Also, ECI is free from the potentially hazardous radioactive labels used in radioimmunoassays, and can be applied directly to colored and/or turbid samples that are difficult for immunoassays with optical detection. Another advantage of ECI is the ability to work with extremely small samples because electrochemistry is an interfacial process where the important electrode processes occur at the electrode interface, not in bulk solution. This can be very important in situations where minimizing the sample volume is critical, as in the clinical testing of neonates, the blood analysis of ill or seriously injured patients, and the testing of cerebral and spinal fluids [8, 9]. Also, working in small volumes is of paramount importance in enzyme immunoassays, the most common type of immunoassay, because the enzymatic product is brought to detectable levels faster in small volumes where product dilution is restricted. This has been exploited in immunoassays in microcapillaries where analyte amounts of a few zeptomoles (10^{-21} moles) have been detected [10].

In this chapter, we first present the different formats used in ECI according to the type of label used. Since enzymes are by far the most common label type, we organize this in two parts according to whether an enzyme label is used or not. Each of these is further divided as *heterogeneous*, which refers to assays that require the separation of the Ab-bound Ag from the free Ag, and *homogeneous*, which refers to assays with no separation. Because of their importance to ECI, the different enzyme-substrate-product (E-S-P) systems and their properties are tabulated in Table 1. The sections on assay formats are followed by a discussion on the implementation of ECI in the form of miniaturized

and simple-to-use systems called electrochemical immunosensors. Next, a brief discussion on applications of ECI in clinical, pharmaceutical, environmental, and food analysis is given with the aid of the summary Table 2. The chapter concludes with an outlook to the future.

5.2

Enzyme Electrochemical Immunoassays

In enzyme ECI, the Ag or a second Ab is labeled with an enzyme that catalyzes the production of an electrochemically detectable product and the rate of product formation is used to quantitate Ag. Therefore, enzyme ECI relies on the Ab for specificity and the enzyme label for sensitivity through chemical amplification. Chemical amplification here refers to passing a substance through a catalytic, cycling, or multiplication mechanism to generate a relatively large amount of product [96, 97]. In this way, a trace concentration of analyte may result in significantly higher product concentration, which for analytical purposes can be more easily measured than the analyte itself. Before describing the different assay formats, we choose to discuss two key issues of enzyme ECI, electrochemical detection and the choice of E-S-P system.

5.2.1

Electrochemical Detection

The vast majority of electrochemical-detection techniques in immunoassay are based on voltammetry, the branch of electroanalysis that involves applying a potential to an electrochemical cell and measuring the current that results from oxidation or reduction at the electrode [98]. Of the many techniques of voltammetry,

Tab. 1 Common E-S-P systems in ECI

Enzyme label	Substrate	Product	Detection method	Limit of detection	Reference
Alkaline phosphatase (ALP)	4-Aminophenyl phosphate (PAPP)	4-Aminophenol (PAP)	FIA-EC, GC, 0.30 V vs. Ag/AgCl	E: 25 fM (500 zmole), T = 60 min E': 4 amole	11
	"	"	FIA-EC, GC, 0.325 V vs. Ag/AgCl	P: 9 nM	12
	"	"	IDA	P: 1 μM^2	13
	"	"	RDE, GC, 0.3 V vs. Ag/AgCl	E': 347 amole ² , T = 20 s P: 5 nM ²	14
	1-Naphthyl phosphate	1-Naphthol	FIA-EC, GC, 0.55 V vs. Ag/AgCl	E: 5.1 fM, T = 20 min P: 300 pM	15
	"	"	DPV, SPE immunosensor, 0.275 V vs. Ag pseudo ref.	E: 51 fM (770 zmole), T = 20 min P: 100 nM	16
	Glucose-6-phosphate	Glucose	Glucose sensor, 0.60 V vs. Ag/AgCl	E: ~ 0.02 IU, T = 30 min	17
	4-Hydroxynaphthyl-1-phosphate (HNP)	Dihydroxy naphthalene	FIA-EC, GC, 0.30 V vs. Ag/AgCl	E: 300 fM (6 amole), T = 20 min	18
	3-Indoxyl phosphate	Indigo blue	ACV, C paste immunosensor, -0.4 V vs. Ag/AgCl	P: 50 nM	19
	Phenyl phosphate	Phenol	LC-EC, C paste immunosensor, 0.85 V vs. Ag/AgCl	P: 10 nM	20
5-Bromo-4-chloro-3-indolyl phosphate ester		H ₂ O ₂	HRP-modified C immunosensor, 0.0 V vs. Ag/AgCl	550 fM, T = 5 min	21
6-(N-ferrocenylamino)2,4-dimethylphenyl phosphate		6-(N-ferrocenylamino)-2,4-dimethylphenol	Nafion-modified GC, 0.6 V vs. Ag/AgCl	E: 6.3 pM, T = 15 min	22

(continued overleaf)

Tab. 1 (continued)

Enzyme label	Substrate	Product	Detection method	Limit of detection	Reference
ALP + bienzymatic biosensor (tyrosinase & GDH)	Phenyl phosphate	Phenol ¹	Bienzyme catalytic biosensor with a Clark O ₂ electrode, 0.60 mV vs. Ag/AgCl	E: 3.2 fM (320 zmole), T = 57 min	23
ALP + bienzymatic system (NADH oxidase & alcohol dehydrogenase (ADH))	NADP ⁺	NAD ⁺ ¹	Membrane-covered Pt electrode, 0.60 V vs. Ag/AgCl	E: 50 amole, T > 20 min	24
HRP	3,3',5,5'-TMB	TMB (ox)	FIA-EC, GC, 0.10 V vs. Ag/AgCl	E: 85 fM, T = 15 min	25
	Hydroquinone	Benzoquinone	FIA-EC, GC, -0.25 V vs. Ag/AgCl	E: 1.7 pM, T = 15 min	25
	Redox Os ²⁺ -based polymer	Os ³⁺	Redox polymer-coated immunosensor	E: 0.01 µg mL ⁻¹	26
Glucose-6-phosphate dehydrogenase	NAD ⁺ + glucose-6-phosphate	NADH	LC-EC, C paste electrode, 0.8 V vs. Ag/AgCl	P: 0.1 µM	27
Galactosidase	4-aminophenyl-beta-D-galactopyranoside (PAPG)	PAP	FIA-EC, GC, 0.20 V vs. Ag/AgCl	E: 100 fM, T = 2 h P: 50 nM	28

Note: HRP: Horseradish peroxidase; TMB: Tetramethylbenzidine; ACV: Alternating-current voltammetry; amole: 1e-18 moles; DPV: Differential pulse voltammetry; E: Detection limit for unconjugated enzyme; E': Detection limit for conjugated (Ab/Ag) enzyme; FIA-EC: Flow-injection analysis with electrochemical detection; GC: Glassy carbon; LC-EC: Liquid chromatography with electrochemical detection; P: Detection limit for final enzymatic product; P': Detection limit for standards of P; RDE: Rotating disk electrode; SPE: Screen-printed electrode; SQV: Square-wave voltammetry; zmole: 1e-21 moles.

¹ Follow-up amplification step/s involving recycling enzymes.

² Unoptimized detection limit.

Tab. 2 Applications of Electrochemical Immunoassay

Analyte	Assay type	Label & substrate	Detection scheme	Limit of detection and/or range	Reference
Biomedical and pharmaceutical analysis					
ALP	He,E	ALP/PP	FIA-EC	40–500 U L ⁻¹	29
Amphetamine	Ho,N,C	Cobaltocenium ion	Nafion-modified electrode	2.5 nM–1.0 μM	30
Apolipoprotein E	He,E,S,I	ALP/PAPP	Membrane immunosensor	50–1000 μg L ⁻¹	21
Biotin	Ho,E,C,I	ALP/PAPP	Microporous Au-immunosensor	1 nM	31
”	He,E,C,I	”wired” HRP/H ₂ O ₂	”Wired”-enzyme immunosensor	10 nM–1 mM	26
Carcinoembryonic Ag	He,E,S	HRP/H ₂ O ₂ /ferrocenylmethanol (FMA)	SECM	~10 ⁴ molecules	32
Cocaine	He,E,N	ALP/PP	Benzymatic recycling biosensor with FIA- immunocolumn	380 pM (38 fmole)	33
”	Ho,E,C,I	HRP/H ₂ O ₂	Graphite-immunosensor	0.1–10 μM	34
Cortisol	Ho,E,C,I	HRP/H ₂ O ₂	Membrane-O ₂ electrode-immunosensor	0.1 μM	35
Digoxin	Ho,E,C	ALP/PAPP	Microporous Au- immunosensor	100 pM	31
”	He,E,C	ALP/PP	FIA-EC	50 pg mL ⁻¹	36
Digoxin	He,E,S	ALP/PAPP	Capillary-FIA-EC	10–1000 pg L ⁻¹	37
Digitoxin	He,E,C	ALP/PAPP	Microporous Au-immunosensor	10 nM	31
Estriol	Ho,N,C	Electroactive – NO ₂ groups	Differential pulse polarography	0.02–2.2 μg mL ⁻¹	38
Factor VIII	He,E,C,I	HRP/hydroquinone/H ₂ O ₂	GC-immunosensor	1 μg mL ⁻¹	39
”	He,E,C	ALP/glucose-6-phosphate	Glucose electrode	1.56–100 U mL ⁻¹	17

(continued overleaf)

Tab. 2 (continued)

Analyte	Assay type	Label & substrate	Detection scheme	Limit of detection and/or range	Reference
Fatty acid-binding protein	He,E,S,I	ALP/PAPP	Graphite-immunosensor	5–30 $\mu\text{g mL}^{-1}$	40
Hepatitis-B surface Ag	HeE,S	HRP/o-phenylenediamine	Linear-sweep polarography	0.1–5 ng mL^{-1}	41
"	He,E,S,I	GOx/glucose	Membrane-O ₂ electrode-immunosensor	0.1–100 $\mu\text{g mL}^{-1}$	42
Granulocyte macrophage colony-stimulating factor (GM-CSF)	He,E,C,I	ALP/PAPP	SPE immunosensor	0.10 $\mu\text{g mL}^{-1}$, 1–30 $\mu\text{g mL}^{-1}$	43
Human alpha-fetoprotein	He,E,C,I	Catalase/H ₂ O ₂	Membrane-O ₂ electrode-immunosensor	0.05–50 ng mL^{-1}	44
"	He,E,S	ALP/PAPP	FIA-EC	0.163 $\mu\text{g L}^{-1}$, 0.316–100 $\mu\text{g L}^{-1}$	45
Human chorionic gonadotropin (HCG)	Ho,E,S	ALP/PAPP	Microporous Au-immunosensor	2.5 units L^{-1}	46
"	He,E,C,I	Catalase/ H ₂ O ₂	Membrane-O ₂ electrode-immunosensor	0.02–100 IU mL^{-1}	47
Human IgG	He,E,C,S	Urease	Impedance measured on polymer-coated electrode	0.0001–100 $\mu\text{g mL}^{-1}$	48
Human-IgM	He,E,S,I	HRP/I ₂	Dispersed carbon material-immunosensor	1 nM	49
Human luteinizing hormone	Ho,E,S,I	HRP/H ₂ O ₂	"Enzyme-channeling" immunosensor	1 ng mL^{-1}	50
Human serum albumin (HSA)	He,M,C,I	Bi ³⁺	SPE immunosensor	0.2 $\mu\text{g L}^{-1}$ (90 fmole), 0.3–30 $\mu\text{g mL}^{-1}$	51
"	He,M,C	Cu ²⁺ (catalyst)/o-phenylenediamine	Linear-sweep polarography	10–500 ng mL^{-1}	52
"	He,M,C	Ni ²⁺	Differential pulse polarography	333 nM	53

Hydroxycoumarin (umbelliferone)	He,E,C,I	HRP/hydroquinone/ H ₂ O ₂	GC-Immunosensor	24 µM	54
"	He,E,C,I	HRP, H ₂ O ₂ , Fe(CN) ₆ ⁴⁻	Renewable immunosensor	20–1000 µM	55
Isoenzyme lactate dehydrogenase-1 (LDH-1)	Ho,E,I	LD-1/Lactate/ NAD ⁺	Membrane immunosensor	0.005–0.12 U mL ⁻¹	56
Lidocaine	Ho,E,C,I	GOx/glucose/mediator	Au-based immunosensor	5–50 µM	57
"	Ho,E,C,	Glucose-6-phosphate dehydrogenase/NAD ⁺	Assay kit, Pt electrode	1–10 ng mL ⁻¹	58
Mouse IgG	He,E,S	ALP/PAPP	IDA electrode	10–1000 ng mL ⁻¹	13
"	He,E,S	ALP/PAPP	FIA-EC	0.81 pg mL ⁻¹ , 6 orders magnitude	59
"	He,E,S	ALP/PAPP	RDE	50–5000 ng mL ⁻¹	60
"	He,E,S	ALP/PAPP	SECM	5–2500 ng mL ⁻¹	61
Orosomucoid (OMD, α ₁ -acid glycoprotein)	He,E,C	ALP/PP	LC-EC (carbon paste electrode)	1.0–10.0 ng mL ⁻¹	20
Phenobarbital	He,E,C	ALP/PAPP	Capillary-FIA-EC	30–3000 µg L ⁻¹	62
Phenytion	Ho,E,C	Glucose-6-phosphate dehydrogenase/ NAD ⁺ /2,6-dichloroindophenol (DCIP)	FIA-EC	2.5–30 µg mL ⁻¹	63
"	Ho,N,C	Cobaltocenium	Nafion-loaded C paste electrode	50–800 nM	64
"	He,E,C	ALP/(N-ferrocenyl)-6-amino-2,4- dimethyl phosphate	Nafion film modified electrode	10 nM	22
PSA	He,E,S	ALP/PAPP	FIA-EC	0.008 µg mL ⁻¹ , 0.02–1 µg mL ⁻¹	65
"	Ho,E,S	ALP/PAPP	Microporous Au-immunosensor	0.8–20 µg mL ⁻¹	46

(continued overleaf)

Tab. 2 (continued)

Analyte	Assay type	Label & substrate	Detection scheme	Limit of detection and/or range	Reference
Rabbit IgG	He,E,C,I	ALP/PP	Immunosensor with conductive biocomposites	0–14 $\mu\text{g mL}^{-1}$	66
"	He,E,S,	ALP/PP	Capillary-FIA-EC	5600 molecules	10
"	Ho,E,S,I	Choline oxidase/HRP/Choline	"Wireless"-enzyme immunosensor	2–1000 ng mL^{-1}	50
"	He,E,S	ALP/naphthyl phosphate	Sol-gel based immunosensor	50–5000 ng mL^{-1}	67
Red blood cells (Human)	He,E,S,I	HRP/ H_2O_2 / $\text{Fe}(\text{CN})_6^{4-}$	FIA-immunosensor	(1–30) 10^8 cells mL^{-1}	68
Theophylline	Ho,E,C	Glucose-6-phosphate dehydrogenase/ NAD^+ /2,6-DCIP	FIA-EC	2.5–40 mg mL^{-1}	69
"	He,E,C,I	ALP/PAPP	FIA-EC	25 ng mL^{-1}	70
Thyroid stimulating hormone(TSH)	He,E,S	ALP/PAPP	FIA-EC	0.02–100 mIU L^{-1}	71
"	He,E,S,I	ALP/NADP ⁺	Membrane immunosensor	0.2–100 mIU L^{-1}	24
Multianalyte detection in biomedical and pharmaceutical analysis					
Follicle stimulating hormone (FSH) and luteinizing hormone (LH)	He,E,S,I	HRP/ H_2O_2 /ferrocene	Chronoamperometry	2.1, 1.8 U L^{-1} ; FSH, LH	72
HCG and human placental lactogen	He,E,S	HRP/ H_2O_2 /ferrocenylmethanol	SECM	0.1 IU mL^{-1} ; 3 ng mL^{-1} ; HCG, HPL	73
HCG and PSA	He,E,S	ALP/PAPP	Microporous Au-immunosensor	0.4, 0.5 $\mu\text{g mL}^{-1}$; PSA, HCG	46
HSA and human IgG	He,M,C	Bi^{3+} and In^{3+}	Anodic stripping voltammetry (ASV)	1.8, 0.6 $\mu\text{g mL}^{-1}$; HAS, IgG	74

Spatially separated mouse IgG	He,E	ALP/PAPP	Chronoamperometry	NA	75
Environmental testing					
Alachlor	He, C, L, Ho,E,C,I	Liposome-ferrocyanide GOx/HRP/glucose	FIA-EC	25–300 $\mu\text{g mL}^{-1}$	76
Atrazine	He,E,C	ALP/PAPP	SPE immunosensor	12 ng L^{-1}	77
	He,E,C	GOx/glucose/ H_2O_2	Capillary-FIA-EC	0.10–10.0 $\mu\text{g L}^{-1}$	78
2,4-Dichlorophenoxyacetic acid (2,4-D)	He,E,C,I	GOx/glucose/ H_2O_2	SPE immunosensor	0.21 ppm	79
"	He,E,C,I	Acetylcholinesterase/ acetylcholine	SPE immunosensor	10 ng L^{-1}	80
"	He,E,C	ALP/phosphoric ester of [[[(4-hydroxyphenyl)amino]carbonyl] cobaltocenium hexafluorophosphate	Nafion-coated SPE	0.01–100 $\mu\text{g L}^{-1}$	81
"	He,E,C	β galactosidase/p-AP– β galactosidase	Bienzymatic recycling biosensor	5 pg mL^{-1} (5 amol), 0.02–100 ng mL^{-1}	82
"	He,E,C	ALP/PP	Bienzymatic recycling biosensor	0.001–1000 $\mu\text{g L}^{-1}$	23
Indole-3-acetic acid	He,E,C	ALP/PAPP	Capillary-FIA-EC	3 $\text{pg }\mu\text{L}^{-1}$	83
PCBs	He,E,C	ALP/1-naphthyl phosphate	SPE immunosensor	0.01–10 $\mu\text{g mL}^{-1}$	16
"	He,E,C	HRP/ferroceneacetic acid/ H_2O_2	FIA-EC	0.1–50 $\mu\text{g mL}^{-1}$	84
Food chemistry					
<i>Escherichia coli</i>	He,E,S,I	HRP/ H_2O_2	FIA-immunosensor	50–200 cells mL^{-1}	85
"	He,E,S	ALP/1-naphthyl phosphate or PAPP	Magnetized C electrode	4700 cells mL^{-1}	86
"	He,E	Glucose/Krebs glycolysis cycle/mediator	FIA-EC	10^5 – 10^8 cfu mL^{-1}	87
Luteinizing hormone (chicken)	He,E,S	ALP/PAPP	FIA-EC	2.5 pg mL^{-1}	12

(continued overleaf)

Tab. 2 (continued)

Analyte	Assay type	Label & substrate	Detection scheme	Limit of detection and/or range	Reference
Progesterone	He,E,C,I	ALP/PAPP	SPE immunosensor	5 ng mL ⁻¹	88
"	He,E,C,I	ALP/naphthyl Phosphate	SPE immunosensor	0–50 ng mL ⁻¹	89
Salmonella	He,E,S,I	ALP/PAPP	GC-immunosensor	5000 cells mL ⁻¹	90
"	He,E,S	ALP/NADP ⁺ /ADH/ Diaphorase/ferricyanide	Pt electrode	1000 cfu mL ⁻¹	91
"	He,E,S,I	HRP/H ₂ O ₂	FIA-Immunosensor	50–200 cells mL ⁻¹	85
<i>Staphylococcus aureus</i> (protein A-bearing)	He,E,S	ALP/NADP/ADH/ diaphorase	Pt electrode	10 pg mL ⁻¹ protein A	92
"	Ho,E,C,I	HRP/H ₂ O ₂	"Enzyme-channeling" immunosensor	1000 cells mL ⁻¹	93
<i>Miscellaneous</i>					
African swine virus (I)	He,E,C	HRP/H ₂ O ₂ /hydroquinone	FIA-EC	1–80 ng mL ⁻¹	94
Aleutian disease (Mink autoimmune disease)	Ho,E,C,I	Cholinesterase/butylthiocholine	Hg-film electrode	1–7 nM, specific Ab	95

Note: PCBs: Polychlorinated biphenyls; C: Competitive assay; GDH: Glucose dehydrogenase; GOx: Glucose oxidase; He: Heterogeneous; Ho: Homogeneous; I: Immunosensor; L: Liposomal; N: Nonenzyme; PP: Phenyl phosphate; PSA: Prostate-specific antigen; SECM: Scanning electrochemical microscopy; IDA: Interdigitated array.

amperometry has been the most popular with ECI. In amperometry, the electrode is held at a fixed potential and the current produced from a redox event at the electrode surface is measured. If detected in a convective media, as when using an RDE or a flow-through electrochemical cell, the method is termed *hydrodynamic chronoamperometry*. These are very sensitive methods, with typical detection limits in the nanomolar levels. Because detection can be done in very small sample volumes (less than 10 μL), the absolute amount of analyte in sample can be as low as 10^{-14} moles or less [99].

In amperometry, the optimum electrode potential for detection is chosen by obtaining the current response produced by the analyte as a function of the applied potential. This current response for an electroactive species in solution usually has three distinctive regions of behavior,

as shown by Curve A in Fig. 1. One, a region of potential where the compound is not electroactive and current is negligible. Two, a region of rising current response defined by the Nernst equation, if the system is reversible. Third, a limiting current plateau that is independent of potential. The best potential for detection is along this limiting current plateau where analyte is being electrolyzed at the limit of mass transport to the electrode and small changes in the applied potential do not significantly affect the current measurement. The current response at the limiting plateau is directly proportional to the analyte concentration and is given by the equation $I = nFADC^0/d$, where I is the current, n the number of electrons involved in the redox reaction, F the Faraday constant, A the electrode surface area, D the diffusion coefficient, C^0 the bulk analyte concentration, and d the thickness of the diffusion layer.

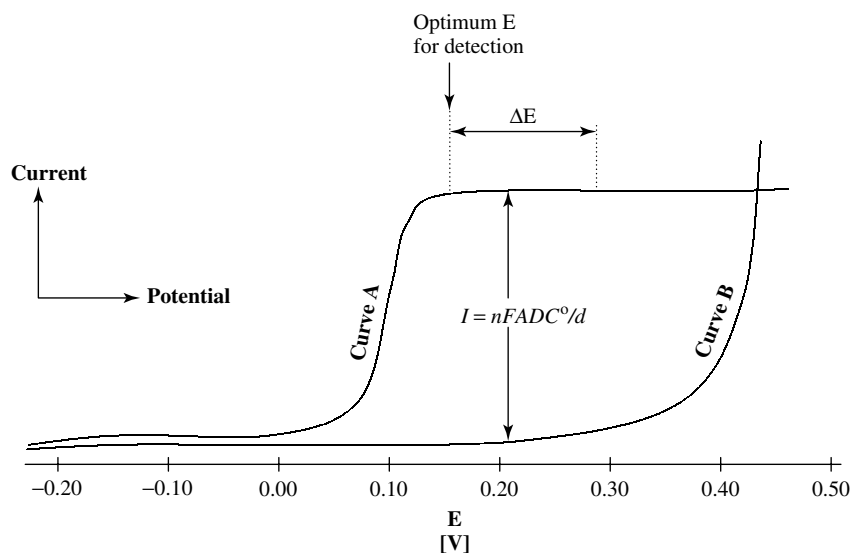


Fig. 1 A hypothetical hydrodynamic voltammogram for enzyme substrate (Curve B) and product (Curve A). The plateau current for product is given by $I = nFADC^0/d$ (see Sect. 5.2.1 for details).

5.2.2

The E-S-P System

The choice of the E-S-P system is a critical factor in enzyme ECI. It is important that the enzymatic reaction be rapid and that the substrate S be redox inactive over some potential range where the product P is active. This potential window for the hypothetical redox curves of P and S in Fig. 1 is denoted by ΔE . The optimum potential for detection within ΔE is at its low end where deleterious effects on the detection limit caused by the background noise and interferences from electroactive impurities are minimal. For the same reason, it is also always advantageous to have a P that reaches the limiting current plateau at a smaller E value. Reversibility of P, which had not been important in most applications thus far, is likely to become important with the growing interest in using recycling electrodes such as the IDA electrodes for enhanced sensitivity [13, 100].

Many of the E-S-P systems used in ECI and the detection limits obtained are given in Table 5.1. The most commonly used enzyme label of these is ALP. In the early days of ECI, PP was used as a substrate [20], but high oxidation potentials and electrode poisoning effects of P (phenol) have limited its use. The most popular enzyme-substrate (E-S) pair currently is ALP-PAPP, used first in ECI by Tang and coworkers in 1988 [101]. Its enzymatic product PAP has a low oxidation potential (i.e. 0.18 V vs. Ag/AgCl at a GC electrode in pH 7 buffer) and causes no electrode poisoning. Its reversibility has been very successfully exploited in electrochemical detection with IDA electrodes [13, 100]. A detection limit of 500 zeptomoles for ALP, the lowest reported for any single E-S pair for ECI

applications, was obtained with the ALP-PAPP pair [11]. The disadvantages of PAPP are its high cost, instability at pH 7, and nonenzymatic hydrolysis during substrate incubation [102]. Where low sensitivity is adequate, the less costly and more stable ALP substrate 1-naphthyl phosphate has been used [15, 103]. This E-S pair has shown to be especially good with screen-printed electrode-based immunosensors discussed in Sect. 5.4. Other enzymes used in ECI include HRP [26, 104], galactosidase [28], glucose-6-phosphate dehydrogenase (G6PDH) [27, 63], catalase [47], and acetylcholinesterase [80]. Of these, HRP has been used recently with separation-free immunosensors (Sect. 5.4) and galactosidase used to catalyze the formation of PAP from a substrate less prone to nonenzymatic hydrolysis than PAPP [28].

Although using a single E-S pair is the most common practice in enzyme immunoassays, there has been some interest lately in using multienzyme systems to further enhance assay sensitivity. This is best illustrated in a recent report where a bienzymatic biosensor was used to detect phenol produced in the reaction involving ALP and PP [23]. The detection scheme, as shown in Fig. 2a, involves using tyrosinase to oxidize phenol first to catechol and then to o-quinone. o-Quinone becomes a mediator in the enzymatic dehydrogenation of glucose and is reconverted to catechol. Quantitation of ALP is done indirectly by measuring the loss of O_2 in the oxidation of phenol. The bienzymatic recycling resulted in a 350-fold signal amplification, thus enabling the detection of 320 zeptomoles of ALP. Similarly, the E-S pair ALP-NADP⁺ has been used with bienzymatic recycling of the product NAD⁺ using ADH and either NADH oxidase [24] or diaphorase [92], as shown in Fig. 2(b).

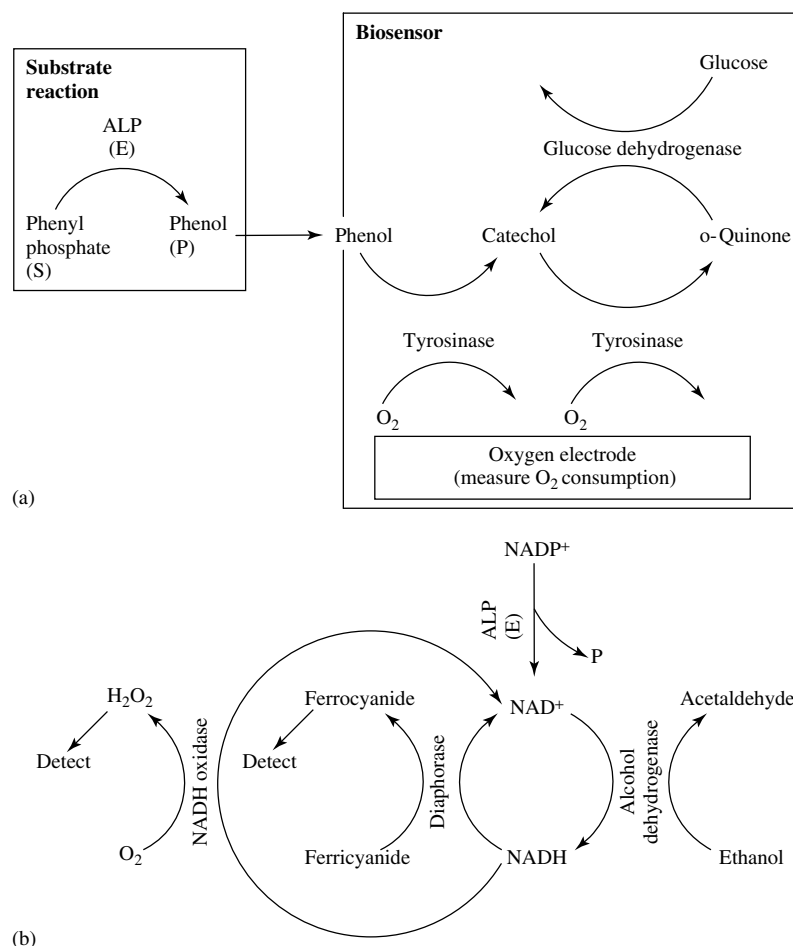


Fig. 2 Multienzyme cycling for enhanced assay sensitivity using (a) phenol recycling biosensor (b) NAD⁺-NADH cycling.

5.2.3

Heterogeneous Enzyme Immunoassay

Heterogeneous enzyme immunoassay is by far the most common assay format used in ECI. Most of the heterogeneous assays are based on the enzyme-linked immunosorbent assay (ELISA) technique where Ab is immobilized on the walls of small (<500 μ L) microtiter wells or cuvettes [105]. The general procedure of heterogeneous immunoassay is outlined

in Fig. 3 for determining Ag, which represents the analyte in this and other examples of enzyme ECI. The reaction surface, say the inside walls of a cuvette, is first prepared by attaching specific Ab to the walls by passive adsorption or covalent bonding. The cuvettes are then rinsed with a nonionic surfactant such as Tween 20 and a “blocker” protein such as bovine serum albumin [105], casein [106], or gelatin [107] to cover any exposed surface between Ab molecules to which proteins can bind

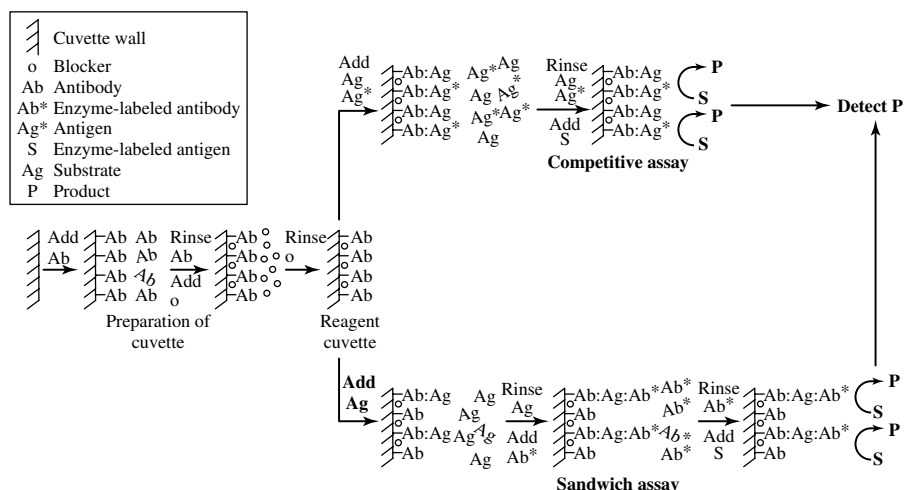


Fig. 3 General protocol for heterogeneous enzyme immunoassay.

nonspecifically (see Sect. 5.2.4). Cuvettes thus prepared are used in either competitive or sandwich immunoassays.

In competitive immunoassays, a standard of enzyme-labeled Ag^* is added to the sample for competitive equilibration with the Ab. Depending on the analyte and the configuration of the reaction vessel used, equilibration can take several minutes to hours, but adequate results may be obtainable before this. The unbound Ag and Ag^* are then rinsed from the tubes and the enzyme substrate S added. At a fixed time, the sample is analyzed for the electroactive product (P), whose concentration shall be proportional to the Ag^* in the well if the enzymatic reaction is carried out under substrate saturation conditions. Because of the competitive binding, a typical standard plot of the current versus the concentration of Ag has an inverse, linear relationship. The assays of this type in Table 2 are denoted by E (enzyme) and C (competitive) under the assay type.

The sandwich immunoassay is the other widely used form of heterogeneous enzyme immunoassay. As shown in Fig.3,

this assay derives its name from the fact that the analyte is “sandwiched” between two different antibodies, one of which is enzyme-labeled. It can be applied only to molecules that are sufficiently large and have an appropriate topographical distribution of epitopes to accommodate two antibodies simultaneously. The Ab specific for Ag is first immobilized on the cuvette walls, and the sample is then added and incubated to allow Ag binding. Following this, the cuvette is washed with buffer and a second antibody, Ab^* , also specific for Ag and labeled with an enzyme label, is added. After its incubation, the unbound Ab^* is rinsed from the cuvette and S added for electrochemical detection of P. Because more Ab^* is retained in the well at high concentrations of Ag, the signal due to P here is directly proportional to the concentration of Ag. In Table 2, the sandwich assays are denoted by E (enzyme) and S (sandwich) under assay format.

Electrochemical detection in a heterogeneous immunoassay, whether competitive or sandwich, can be done either directly in the container in which the assay was

done or in an external electrochemical cell by transferring an aliquot to it. Although the former has been done [90, 92], it involves the tedious process of transferring the electrodes from one cuvette to another with rinsing in between. More common, therefore, is the latter, and its most common form is FIA-EC. FIA, a powerful microanalytical method in batch analysis, involves introducing a sample to a mobile phase buffer via an injection valve and measuring the analyte at a detector downstream [108]. The rapidly moving buffer in FIA allows nearly instantaneous detection, and because of its favorable hydrodynamic profiles, amperometric detection with FIA is one of the most sensitive electroanalytical methods [109]. These properties make FIA ideal for immunoassays where there are usually several μL -volume samples to test, and its popularity in ECI is evident by the number of FIA-EC-based assays in Table 2. Where necessary, a liquid chromatography column can be added to the FIA system to remove substances that may interfere in the detection. Such systems are denoted in Table 2 by LC-EC. In most of the FIA-based ECI, a thin-layer electrochemical cell consisting of a glassy carbon working electrode operated amperometrically has served as the detector.

An adaptation of FIA for ECI is to use an in-line immunocolumn, with the column effluent allowed to pass through an electrochemical cell for detection. The first of this type, reported by Wilson and coworkers, used a high-performance chromatography column where Ab was immobilized for a competitive enzyme assay [110]. The immunocolumn was renewed in preparation for the next sample by passing acidic buffer through it to displace bound Ag and Ag*. In a slightly different design, a protein A immunocolumn was used to bind the Ab for an assay of theophylline [70]. Because

protein A can bind to most immunoglobulins with high affinity, this system can, in principle, be adapted for a variety of assays. However, these types of assays are generally time-consuming, and often, the harsh conditions used to renew the immunocolumn decrease its lifetime. Recently, Scheller and coworkers reported a noncompetitive immunoassay for cocaine using an immunocolumn where these problems were significantly reduced [33]. The immunocolumn contained a perfusion chromatography carrier modified by a large number of cocaine molecules. The sample was introduced into the column after mixing it with an excess of Ab* containing ALP. The excess Ab* was bound by cocaine in the column, but not the Ag-Ab* whose Ab* binding sites are occupied and unavailable for further binding. The Ag-Ab* was collected in the effluent, the enzyme substrate PP added, and the product phenol detected at a bienzymatic biosensor identical to the one described earlier. By packing the column with a large excess of cocaine, more than 200 assays were performed before the column required regeneration.

5.2.4

Ultrasensitive Heterogeneous Enzyme Assays in Small Volumes

Minimizing the reaction cell volume has a profound effect on the sensitivity and speed of an assay [99, 111]. This is due mainly to the fact that in smaller volumes, where the dilution of P is less, the P concentration can be brought to detectable levels more rapidly than would be possible otherwise. Another way that small volumes affect ECI is by shortening the diffusional distances that species in solution have to travel to react at the surface. Shorter diffusional distances result in reduced

incubation times and hence, to a reduced total assay time. However, minimizing the reaction cell volume has to be done with as little loss of the total surface area as possible in order to maintain an adequate number of binding sites. Microcapillaries, with their high surface-area-to-volume ratio, provide just that type of reaction cell. However, when using capillaries and other large surface area formats, nonspecific adsorption (NSA) of proteins becomes an issue of paramount importance. As noted earlier, rinsing with a simple mixture of a detergent and a blocker protein can reduce NSA to required levels when working with cuvettes or wells. In capillaries, on the other hand, where high assay sensitivity is sought and the high surface-area-to-volume ratio leads to a correspondingly high NSA, more sophisticated blocking techniques are called for. Halsall and coworkers have found that NSA in capillaries can be drastically reduced using a reagent mixture consisting of Tween 20 and a blocker protein as above to minimize NSA arising from hydrophobic forces, and ion-pairing reagents to minimize NSA arising from electrostatic forces [10]. The capillaries were also treated to yield an amino group-rich surface for attaching the Ab using carbodiimide coupling. The capillaries thus prepared and incorporated into FIA systems have enabled some of the most sensitive assays in immunoassay [10, 37]. A detection limit of 5600 molecules and a linear range of four orders of magnitude were reported for a sandwich assay of rabbit IgG in human serum in 70- μ L capillaries [10]. Similarly, 260 attomoles of digoxin have been detected using a 20- μ L capillary [37]. Capillary immunoassays have also been used in competitive enzyme immunoassays to detect indole-3-acetic acid in tomato embryos [83], phenobarbital

in serum [62], and atrazine [78] in river water.

Minimizing the reaction cell volume, however, can also be counterproductive to the assay sensitivity in situations where there is significantly more available sample than can be tested in the reaction volume. For example, say a 1-ml sample, which in fact contains 100 zeptomoles of Ag, is available for a sandwich assay. If a 20- μ L capillary were used, only two zeptomoles of enzyme label will at best remain in the capillary for detection. If, however, the full sample could be assayed while keeping the final detection volume at 20 μ L, the challenge would be less daunting with 100 instead of 2 zeptomoles of enzyme labels to detect. One way to optimize the assay sensitivity in terms of both the sampling capacity and the enzyme substrate incubation volume is to use an immunoreceptor that can be dispersed during sampling, but concentrated in a small volume for substrate incubation and detection. Paramagnetic microimmunobeads, sold by a number of companies [112], hold much promise for such ultrasensitive assays. These beads, typically 1 to 3 μ m in diameter, can be dispersed by gentle shaking during sampling, and separated and held against the reaction cell with a magnet for the various rinsing and washing steps of an assay. More importantly, the beads can be transferred to and mixed in an electrochemical cell. This provides much flexibility in choosing what enzyme substrate volume to mix in as well as the type of electrochemical detection method to use. Recently, we exploited this concept using an RDE in an assay for mouse IgG [14, 60]. In this work, RDE amperometry was adapted to place the rotating electrode directly on a microdrop of enzyme substrate to minimize product dilution. The excellent sensitivity of RDE amperometry

and the thorough mixing of the beads provided by the electrode enabled the detection of 413 attomoles of mouse IgG in less than 10 seconds [60]. This detection time is 30- to 120-fold faster than in capillary assays. Considering that NSA was the main factor in determining the detection limit in the bead-based assay and that no special treatment of the beads was done to minimize NSA, it is likely that even lower detection limits could be attainable with proper NSA blocking and using longer incubation times if necessary.

5.2.5

Homogeneous Enzyme Immunoassay

Homogeneous enzyme immunoassays use a competitive assay format that relies on a reduction in the rate of enzyme catalysis of Ag^* as it binds to the Ab. The general equilibrium scheme for homogeneous immunoassays, which also holds true for the nonenzymatic ones discussed later, is shown in Fig. 4. The

strength of the homogeneous assay lies in its ability to distinguish between Ag^* and $\text{Ab}:\text{Ag}^*$, which simplifies an assay by making a separation step unnecessary.

The first homogenous enzyme ECI was developed by Heineman and coworkers for phenytoin using glucose-6-phosphate dehydrogenase (G-6-PD) as the enzyme label and NAD^+ as the substrate [27]. The product, NADH, was determined by oxidation using LC-EC with a thin-layer cell containing a GC electrode held at 0.75 V versus Ag/AgCl. A reversed-phase C-18 LC precolumn was necessary to remove other proteins in the sample that would otherwise have passivated the electrode at such a high potential. The use of an LC column, however, was avoided in later work by allowing NADH to react with 2,6-DCIP mixed into the sample, and detecting the product DCIPH₂ at the much lower electrode potential of 0.20 V versus Ag/AgCl [63]. This improved assay protocol was applied to the detection of theophylline in whole blood [113] as well

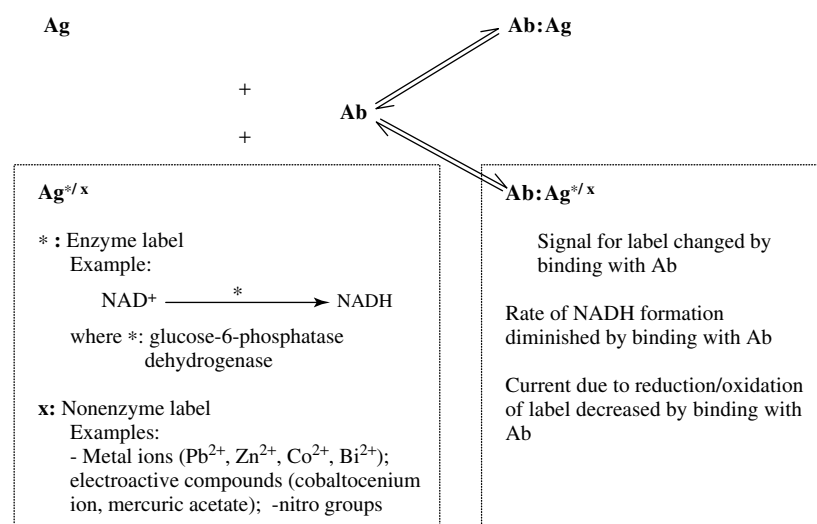


Fig. 4 General reaction scheme for both enzyme and nonenzyme homogeneous immunoassay.

as in hemolyzed, lipemic, and icteric serum samples [69]. The ability to perform immunoassays directly on such samples marks a significant advantage over assays based on optical detection where detection is severely hampered by spectral interferences due to turbidity and/or the intense color of the sample [114]. Homogeneous enzyme assays in Table 2 are denoted by E (enzyme) and Ho (homogeneous) under assay type. Another important area of ECI where homogeneous immunoassays are becoming very important is in electrochemical immunosensors discussed later.

5.3

Nonenzyme Electrochemical Immunoassays

A second class of ECI involves labeling an Ag with a nonenzymatic electroactive label. We shall denote this kind of conjugate by Ag^x to differentiate it from Ag^* , the enzyme-labeled Ag. Nonenzyme immunoassays developed thus far have been based on competitive binding of Ag and Ag^x to Ab. Electrochemical detection of the label is done while it is conjugated or after its release by adding a suitable cleaving reagent. Detection in virtually all these assays has been done at a Hg electrode. Although Hg electrodes have lost some popularity because of the toxicity of Hg, under proper handling Hg electrodes can give excellent sensitivity in electroanalysis [115]. This is particularly true for ASV in which the metal ion is preconcentrated in the Hg electrode prior to detection. Detection limits in the nanomolar range are obtained routinely with ASV. Modern advances, both in the design of Hg electrodes and in the automation of systems using Hg electrodes, are making it possible to use Hg electrodes safely [116].

5.3.1

Nonenzyme Homogeneous Immunoassays

As described in Sect. 5.2.5, homogeneous assays are based on the competitive binding of Ag and the labeled Ag to a limited amount of Ab. The labels that have been used in nonenzyme homogeneous assays are metal ions and electroactive functionalities or molecules. These immunoassays are based on the reduction of the electroactivity of the label, as measured by a drop in the current when Ag^* binds to Ab. It is believed that this drop is due to the decrease in the diffusion coefficient (see Sect. 5.2.1) of Ag^* as it binds to Ab and/or to the sequestration of Ag^* in the binding pocket of Ab, making it less available to the electrode [117]. Therefore, these assays are best suited for smaller Ags where the fractional change in the diffusion coefficient and/or the sequestration is greater upon binding to Ab.

This approach was first demonstrated using the electroactive functionality mercuric acetate in an assay for estriol [118]. Since then, assays for estriol using NO_2 groups [38], morphine using ferrocene [119], and HSA using metal ions Pb^{2+} [120], Co^{2+} [121], and Zn^{2+} [122] have been reported. However, homogeneous assays of this kind have not shown any significant advantage over other types, and their use is rare. Assays of this type in Table 2 are denoted by N (nonenzyme) and He (heterogeneous) under assay type.

5.3.2

Heterogeneous Nonenzymatic Immunoassays

The assays in this class have for the most part used electroactive metal ions for labels. The first such immunoassay was reported by Heineman and Halsall for the analyte HSA using the label

In^{3+} [53]. The Ag^x was made by coupling In^{3+} to Ag molecules using the bifunctional chelate diethylenetriamine pentaacetic acid (DTPA). Because In^{3+} is not found in human tissue, interference from the clinical sample itself is avoided. The assay protocol used is outlined in Fig. 5. Following competitive equilibration of Ag and Ag^x with Ab (adsorbed to insolubilized protein A), the Ab- Ag^x complex was separated by centrifugation. The In^{3+} label of Ag^x was then released by acidification and determined by differential pulse anodic stripping voltammetry (DP-ASV). The

peak height of the stripping wave for In^{3+} was shown to be inversely proportional to the HSA in the sample, as expected from a competitive assay.

An exciting possibility of heterogeneous immunoassay with ASV detection is its extension to multianalyte detection using multiple metal labels. This concept was successfully applied by Hayes and coworkers in the simultaneous detection of HSA and human IgG in perhaps what is the first multianalyte ECI [74]. Because ASV is an extremely sensitive method that can detect up to about six metals simultaneously, it

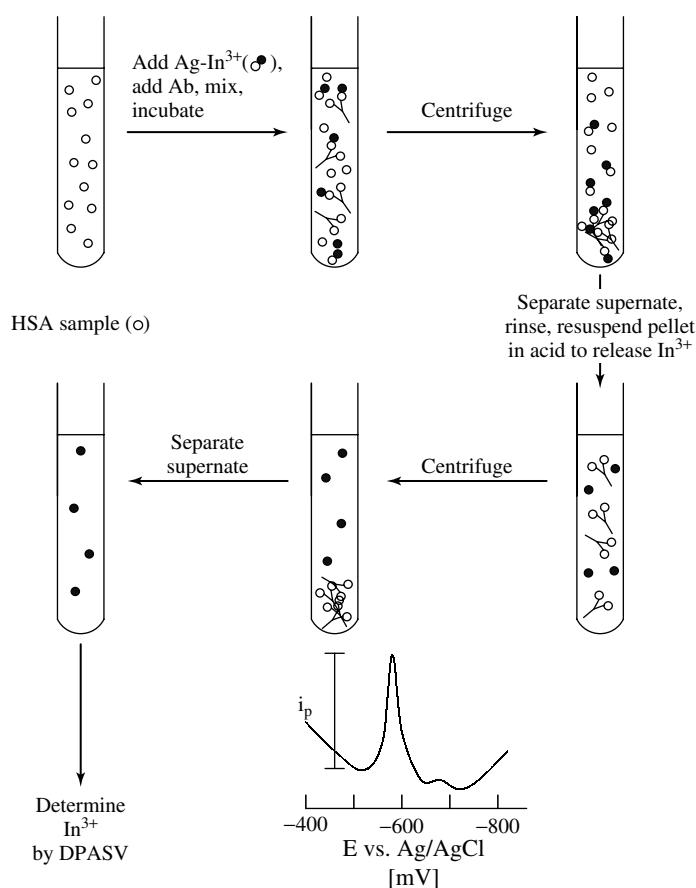


Fig. 5 Heterogeneous nonenzyme assay protocol for determining HSA with releasable In^{3+} label by ASV.

is possible to detect as many analytes, in principle [116].

Two other types of nonenzymatic heterogeneous immunoassay have been reported. One uses liposomes containing the electroactive marker ferrocyanide as a label [76]. Following the competitive binding of Ag^x in an immunocolumn, ferrocyanide is released by flushing with detergent, and detected at a downstream electrode. An alternative to the direct measurement of a metal ion was reported recently in a competitive immunoassay for HSA where Cu^{2+} catalyzed the conversion of o-phenylenediamine to the electroactive product 2,3-diaminophenaline, which was detected with linear-scan polarography [52]. Nonenzyme heterogeneous assays in Table 2 are denoted by N (nonenzyme) and He (heterogeneous) under assay type.

5.4 Electrochemical Immunosensors

The immunoassay techniques discussed so far have all been best suited for a lab environment because of both the type of equipment required and the experimental conditions used. In many instances, including virtually all clinical applications, this is not a problem since the tests need to be done in a lab environment anyway for a host of other reasons. However, methodology for less complicated and “on-the-spot” testing is finding an increasingly important niche in immunoassay [123]. This is particularly true for field-testing in environmental applications, home-based diagnostic kits, and testing in emergency situations, as in an ambulance or an operation theater. To adapt ECI to a system for “on-the-spot” analysis, the system must

be small, easy to handle and operate, capable of working without additional reagents, and renewable where use in a disposable manner is prohibitively expensive. The development of such systems is the focus of the rapidly developing area of ECI loosely termed *electrochemical immunosensors*, which is discussed in this section.

To the best of our knowledge, the ideal reagent-free electrochemical immunosensor for “on-the-spot” analysis has yet to be developed. Systems reported in the literature as electrochemical immunosensors, some of which are listed and denoted by I under assay type in Table 2, are based primarily on one factor: the immobilization of the sensing Ab or Ag directly on the electrode [124, 125]. The schematic of an electrochemical immunosensor, thus defined, is shown in Fig. 6. It should be noted that electrochemical immunosensors are often categorized as electrochemical biosensors, which covers any type of electrochemical sensor consisting of a biorecognition element placed directly over or in close proximity to the electrode [126].

The earliest works in electrochemical immunosensors were directed at using simple electrodes with passively adsorbed Ab to detect Ag based on any changes in the electrode potential due to Ag binding [127]. Their promise for simple, label-free, and direct immunosensors, however, was short-lived because of poor sensitivity due to nonspecific binding. Since then, potentiometric immunosensors using ion- and gas-sensing electrodes for enzyme assays [128, 129], pH electrodes, and field-effect transistors (FETs) [130] have been reported. These immunosensors too have had limited success because of poor selectivity due mainly to NSA [124, 131]. In contrast, a far greater degree of success has been achieved with amperometric immunosensors.

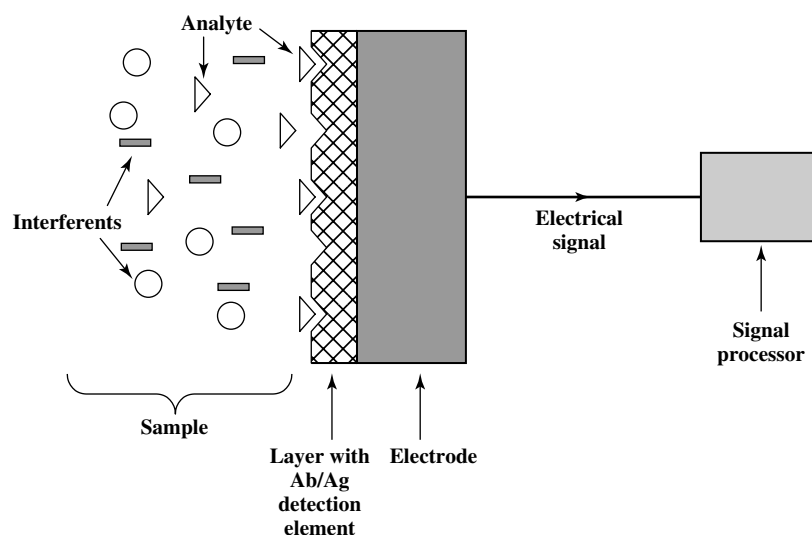


Fig. 6 The basic design of an electrochemical immunosensor.

The first amperometric immunosensor developed by Aizawa in 1979 for detecting HCG [47] consisted of an oxygen probe covered with a membrane coated with Ab. Detection was based on a competitive format using catalase to decompose H_2O_2 and the oxygen probe to measure the product O_2 as it diffused through the membrane. Similar membrane-based electrochemical immunosensors have been used to detect human α -fetoprotein [44], thyrotropin [24], and hepatitis-B surface antigen (HBsA) [42]. However, replacement of the membranes with each use is a disadvantage. The alternative of renewing the sensor surface by cleaving the Ab–Ag bond in acidic media has been applied to glassy carbon-based immunosensors [54, 68], but this too is tedious and renewability is never total. Such problems greatly hampered the growth of electrochemical immunosensors until the early 1990s when technologies to make disposable immunosensors were developed. For immunosensors to be disposable, they must

be inexpensive, made reproducibly in large numbers, and in this regard, the development of screen printed electrodes (SPEs) has been very important for electrochemical immunosensors.

SPEs, fabricated with thick-film technology [132] using a graphite powder-based ink to print electrodes on a polystyrene surface, are adapted for immunosensors chiefly by passive adsorption of antibodies to the electrode surface. SPE-based immunosensors have been used in a number of applications including the detection of the herbicide 2,4-D [79, 81, 133], PCBs [134], the biochemical messenger GM-CSF [43], and the hormone progesterone [87, 88, 135]. All these applications use enzyme labels in a heterogeneous assay format. An exception to using an enzyme is an SPE immunosensor for HSA reported recently by Wang and coworkers where a competitive and metal ion label format similar to the one described in Sect. 5.3.2 was used [51]. The mercury electrode necessary for stripping

electroanalysis was formed by in situ deposition of Hg^{2+} on a SPE carbon electrode. SPE immunosensors have also been used in semi-homogeneous enzyme assays, which are discussed shortly.

Two other recent technologies applied to electrochemical immunosensors, one based on thin-film technology (lithography) [136] and the other on the concept of “wired” redox enzyme electrodes [137, 138], are also likely to become important in the future. There has been much interest in using photolithographically patterned IDA electrodes in immunoassay following the first report by Heineman and coworkers [13]. Recently, a dual-analyte immunosensor made by thin-film technology was used to detect FSH and LH using a sandwich assay format [72]. The Ab immobilization was done on a thiol-modified gold electrode treated with avidin-photobiotin. Photolithography was applied to activate photobiotin in defined patterns for binding Neutravidin conjugated antibodies.

The concept of “wired” enzymes, borrowed from electrochemical biosensors [126], was recently applied to make an immunosensor for HRP [26]. Here, rabbit Ab for HRP was co-immobilized with the redox polymer $[\text{Os}(\text{bipyridyl})_2\text{poly-4-vinylpyridine}]_{10}\text{Cl}]\text{Cl}$ onto a GC electrode. Upon capture at the immunosensor surface, the redox centers of the HRP molecules become electrically wired to the electrode surface via the redox polymer. Therefore, when H_2O_2 is added to the immunosensor following the sample incubation and wash, the HRP that is oxidized during catalysis can be electrochemically reduced (and detected) to its original form by the wired electrode. The detection of HRP in this way was shown to have the classical features of a fast redox couple strongly bound to an electrode surface.

The immunosensors described thus far all use a heterogeneous assay format in contrast to the ideal “on-the-spot,” reagent-free, disposable or reusable, and one-step analysis envisioned with immunosensors. To the best of our knowledge, no present system is capable of all these, but the “separation-free” immunosensors that have appeared in the literature recently come a step closer toward this goal. These immunosensors are simpler to use because they do not require the separation of the enzyme-labeled Ab/Ag in the bulk from the surface-bound. One approach taken in doing this involves immobilizing the enzyme label along with the Ab in making the immunosensor [34, 35]. The electrochemical detection was based on the enzyme inhibition that follows Ag binding. For more sensitive assays, however, it is necessary to work with enzyme-labeled Ag or Ab in solution, and a method has to be devised to differentiate the enzyme labels in the bulk from the surface-bound. Meyerhoff and coworkers described an elegant method to do this, in which a microporous nylon membrane coated on one side with gold served to immobilize Ab as well as act as an electrode [46]. After incubation for the competitive binding of the enzyme-labeled Ag (Ag^*), the enzyme substrate was added from the backside of the porous membrane. Because of proximity and flow effects, the enzymatic product formed at the immunosensor surface was preferentially detected, thus differentiating it from the product formed in the bulk and allowing a separation-free assay. Another approach to discriminating the product formed in the bulk has been proposed where a reagent is added to scavenge the product formed in the bulk but not that formed near the electrode surface, which

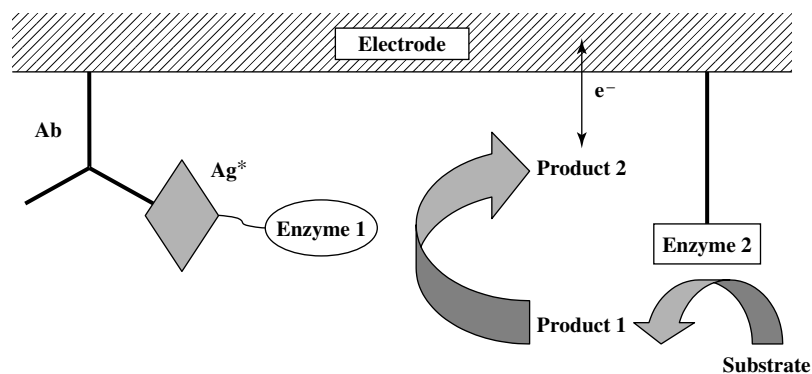


Fig. 7 The principle of enzyme-channeling immunoassay using an electrode-bound enzyme to make the substrate for the enzyme label on the Ag^* .

is oxidized by the electrode sooner than could be scavenged [77].

Enzyme-channeling immunoassay introduced by Litman and coworkers [139] gives another promising way to make separation-free immunosensors. The basic principle of enzyme channeling is illustrated in Fig. 7. As shown, the substrate for the enzyme label of Ag^* is produced *in situ* by a second enzyme co-immobilized with Ab on the immunosensor surface. Because of the distances involved, the enzymatic product of the second enzyme is “channeled” to the Ab-bound Ag^* , and hardly any to that in the bulk. In the area of ECI, enzyme channeling was first exploited by Brown and coworkers in 1991 to develop a potentiometric immunosensor [140]. Since then, Rishpon and coworkers have developed amperometric immunosensors based on enzyme channeling for *Staphylococcus aureus* [93], rabbit IgG, and human LH [50]. For these applications, GOx was used as the second enzyme and HRP as the Ag^* enzyme label. Hydrogen peroxide, the by-product in the oxidation of glucose at the second enzyme, becomes a co-substrate with iodide in the enzyme catalysis at Ag^* , and its product

I_2 is detected at the electrode. Recently, Heller and coworkers used the same principle with an osmium-containing redox hydrogel where choline oxidase was used for the second enzyme to catalyze the oxidation of choline to produce betaine aldehyde and H_2O_2 [141]. The H_2O_2 produced is channeled to the HRP labels on the Ab^* where it is reduced. Because of the hydrogel, the HRP labels are “wired” to the electrode and detected as in the earlier example.

The development of electrochemical immunosensors has increased rapidly over the last five years, and as the technologies that made this possible keep evolving, we can expect even more growth in the future. With respect to other types, electrochemical immunosensors can easily be miniaturized, and being insensitive to light, they can be used in opaque or turbid media. Also, since the signal transducer is electrical, it needs no signal conversions as with optical transducers. However, for their use as one-step and “on-the-spot” immunosensors, it will be necessary to find a way to incorporate all the reagents in the immunosensors in some way.

5.5

Applications

In Table 2, we give a comprehensive list of ECI applications. The table is arranged in three parts: biomedical and pharmaceutical analysis, environmental analysis, and food chemistry. Each entry in the table is further categorized according to the assay type, label and substrate, detection scheme, and the limit of detection and/or range obtained. Assay type tells whether it is homogeneous or heterogeneous, if an enzyme label is involved, and whether the assay is done using an immunosensor or not. The detection limits (and units) are given as reported in the original publications.

5.6

Conclusion

Electrochemical immunoassay has advanced greatly over the last two decades. Some of the most sensitive assays in immunoassay have been obtained with ECI. Being insensitive to the color and to a large degree the turbidity of the sample, ECI has a significant advantage over immunoassay with optical detection for direct applications to samples. The other asset of ECI likely to play a key role in the future is its easy adaptability to miniaturized immunoassays. Such assays are obviously important where minimizing sample volume is crucial as in the testing of neonates and critically injured patients. Furthermore, there has been much interest lately in miniaturized assays for multianalyte detection using a platform of densely patterned arrays of antibodies [8, 9]. Several technologies for patterning biochemically active arrays have been developed in the last ten years including ink-jet technology [142], screen printing [143],

photoresist/lift-off methodology [144], microcontact printing [145], and local photochemical activation of preimmobilized coupling agents [146]. There have already been some successes in multianalyte ECI [72, 73, 75], and as the earlier-mentioned technologies advance and become more accessible, we can expect research in this area to grow significantly. SECM, the tool of choice for probing the microscale electrochemistry of surfaces [147], might become very useful in multianalyte detection because it can address different regions of a surface by scanning it in two dimensions, thus making the use of multiple electrodes unnecessary. The feasibility of SECM for multianalyte detection in enzyme immunoassay has already been successfully demonstrated [32, 61, 73, 148, 149]. Micrototal analysis systems (μ TAS) [150], where the goal is a “lab-on-a-chip” that integrates microfabricated parts including control electronics for total analysis in a miniaturized sensor, is another technology likely to play a key role in the future of ECI. If successful, μ TAS can revolutionize ECI with miniaturized immunosensors used in a host of applications ranging from field-deployed sensors that continuously monitor air or water quality to implantable sensors that monitor various physiological conditions of the human body. Because of its amenability to miniaturization, ECI arguably has the best chance of immunoassay types to exploit these technologies. As noted in the introduction, ECI lay dormant for nearly 30 years before developments in technology and fundamental science could catapult it to the popular bioanalytical method it has become. Perhaps the earlier-mentioned technologies of today may usher a second growth of ECI with a whole set of new possibilities.

References

1. I. Roit, *Essential immunology*, 4th ed., Blackwell Scientific, Boston, 1980.
2. C. P. Price, D. J. Newman (Eds.), *Principles and Practice of Immunoassay*, 2nd ed., Macmillan, London, 1997.
3. D. N. Posnett, J. P. Tan, *Methods Enzymol.* **1989**, 178, 739–746.
4. G. Kohler, C. Milstein, *Nature* **1975**, 256, 495–497.
5. G. Winter, C. Milstein, *Nature* **1991**, 349, 293–299.
6. A. J. T. George, in *Principles and Practice of Immunoassay* (Eds.: C. P. Price, D. J. Newman), 2nd ed., Macmillan, London, 1997, pp. 65–98.
7. B. Breyer, R. Radcliff, *Nature* **1951**, 167, 79–81.
8. L. J. Kricka, *Clin. Chem.* **1998**, 44/9, 2008–2014.
9. P. R. Ekins, *Clin. Chem.* **1998**, 44/9, 2015–2030.
10. S. H. Jenkins, H. B. Halsall, W. R. Heinemann, *J. Clin. Immunoassay* **1990**, 13, 99–104.
11. R. Q. Thompson, M. Porter, C. Stuver et al., *Anal. Chim. Acta* **1993**, 271, 223–229.
12. Y. Qu, L. R. Berghman, F. Vandesande, *Anal. Biochem.* **1998**, 259, 167–175.
13. O. Niwa, Y. Xu, H. B. Halsall et al., *Anal. Chem.* **1993**, 65, 1559–1563.
14. C. A. Wijayawardhana, S. Purushothama, M. A. Cousino et al., *J. Electroanal. Chem.* **1999**, 468, 2–8.
15. M. Cardosi, S. Birch, J. Talbot et al., *Electroanalysis* **1991**, 3, 169–176.
16. M. Del Carlo, I. Lioni, M. Taccini et al., *Anal. Chim. Acta* **1997**, 342, 189–197.
17. R. Renneberg, W. Schössler, F. Scheller, *Anal. Lett.* **1983**, 16, 1279–1289.
18. M. Masson, T. Haruyama, E. Kobatake et al., *Anal. Chim. Acta* **1999**, 402, 29–35.
19. C. Fernández-Sánchez, *Anal. Chim. Acta* **1999**, 402, 119–127.
20. M. J. Doyle, H. B. Halsall, W. R. Heinemann, *Anal. Chem.* **1984**, 56, 2355–2360.
21. W. O. Ho, D. Athey, C. J. McNeil, *Biosens. Bioelectron.* **1995**, 10, 683–691.
22. A. La Gal Lal Salle, B. Limoges, C. Degrand, *Anal. Chem.* **1995**, 67, 1245–1253.
23. C. G. Bauer, A. V. Eremenko, E. Ehrenreich-Förster et al., *Anal. Chem.* **1996**, 68, 2453–2458.
24. D. Athey, C. J. McNeil, *J. Immunol. Methods* **1994**, 176, 153–162.
25. G. Volpe, D. Compagnone, R. Draisci et al., *Analyst* **1998**, 123, 1303–1307.
26. B. Lu, E. I. Iwuoha, M. R. Smyth et al., *Anal. Chim. Acta* **1997**, 345, 59–66.
27. H. M. Eggers, H. B. Halsall, W. R. Heinemann, *Clin. Chem.* **1982**, 28/29, 1848–1851.
28. M. Masson, Z. Liu, T. Haruyama et al., *Anal. Chim. Acta* **1995**, 304, 353–359.
29. S. D. Jackson, H. B. Halsall, A. J. Pesce et al., *Fresenius J. Anal. Chem.* **1993**, 346, 859–862.
30. B. Limoges, C. Degrand, P. Brossier et al., *Anal. Chem.* **1993**, 65, 1054–1060.
31. M. W. Ducey Jr., A. M. Smith, X. Guo et al., *Anal. Chim. Acta* **1997**, 357, 5–12.
32. C. A. Wijayawardhana, G. Wittstock, H. B. Halsall et al., *Anal. Chem.* **2000**, 72, 339–342.
33. C. G. Bauer, A. V. Eremenko, A. Kühn et al., *Anal. Chem.* **1998**, 70, 4624–4630.
34. A. A. Suleiman, Y. Xu, *Electroanalysis* **1998**, 10, 240–243.
35. Y. Xu, A. A. Suleiman, *Anal. Lett.* **1997**, 30, 2675–2689.
36. K. R. Wehmeyer, H. B. Halsall, W. R. Heinemann et al., *Anal. Chem.* **1986**, 58, 135–139.
37. N. Kaneki, Y. Xu, A. Kumari et al., *Anal. Chim. Acta* **1994**, 287, 253–258.
38. K. R. Wehmeyer, H. B. Halsall, W. R. Heinemann, *Clin. Chem.* **1982**, 28, 1968–1972.
39. F. Manning, C. O’Fagain, R. O’Kennedy et al., *Anal. Proc. Anal. Commun.* **1994**, 31, 13–15.
40. G. Key, A. Schreiber, R. Feldbrügge et al., *Clin. Biochem.* **1999**, 32, 229–231.
41. J. Xu, J. Song, W. Guo, *Anal. Lett.* **1996**, 29, 565–573.
42. J. L. Boitieux, D. Thomas, G. Desmet, *Anal. Chim. Acta* **1984**, 163, 309–313.
43. E. Crowley, C. O’Sullivan, G. G. Guibault, *Anal. Chim. Acta* **1999**, 389, 171–178.
44. M. Aizawa, A. Morioka, S. Suzuki, *Anal. Chim. Acta* **1980**, 115, 61–67.
45. Y. Xu, H. B. Halsall, W. R. Heinemann, *Clin. Chem.* **1990**, 36/11, 1941–1944.
46. M. W. Ducey Jr., A. M. Smith, X. Guo et al., *Anal. Chim. Acta* **1997**, 357, 5–12.
47. M. Aizawa, A. Morioka, S. Suzuki et al., *Anal. Biochem.* **1979**, 94, 22–28.

48. C. J. McNeil, D. Athey, M. Ball et al., *Anal. Chem.* **1995**, 67, 3928–3935.
49. C. A. Wijayawardhana, G. Wittstock, H. B. Halsall et al., *Electroanalysis* **2000**, 12, 640–644.
50. D. Ivnitski, J. Rishpon, *Biosens. Bioelectron.* **1996**, 11, 409–416.
51. J. Wang, B. Tian, K. R. Rogers, *Anal. Chem.* **1998**, 70, 1682–1685.
52. W. Guo, J. Song, M. Zhao et al., *Anal. Biochem.* **1998**, 259, 74–79.
53. M. J. Doyle, H. B. Halsall, W. R. Heineman, *Anal. Chem.* **1982**, 54, 2318–2322.
54. B. Deasy, E. Dempsey, M. R. Smyth et al., *Anal. Chim. Acta* **1994**, 294, 291–297.
55. B. Lu, M. R. Smyth, J. Quinn et al., *Electroanalysis* **1996**, 8, 619–622.
56. S. Kelly, D. Compagnone, G. Guilbault, *Biosens. Bioelectron.* **1998**, 13, 173–179.
57. K. Di Gleria, H. A. Hill, C. J. McNeil et al., *Anal. Chem.* **1986**, 58, 1203–1205.
58. G. A. Broyles, G. A. Rechnitz, *Anal. Chem.* **1986**, 58, 1241–1245.
59. Y. Xu, H. B. Halsall, W. R. Heineman, *J. Pharm. Biomed. Anal.* **1989**, 7, 1301–1311.
60. C. A. Wijayawardhana, H. B. Halsall, W. R. Heineman, *Anal. Chim. Acta* **1999**, 399, 3–11.
61. G. Wittstock, K. Yu, H. B. Halsall et al., *Anal. Chem.* **1995**, 67, 3578–3582.
62. J. Zhang, W. R. Heineman, H. B. Halsall, *J. Pharm. Biomed. Anal.* **1999**, 19, 145–152.
63. H. T. Tang, H. B. Halsall, W. R. Heineman, *Clin. Chem.* **1991**, 37/2, 245–248.
64. S. Rapicault, B. Limoges, C. Degrand, *Anal. Chem.* **1996**, 68, 930–935.
65. S. F. Chen, Y. Xu, M. Po-Chee, *Clin. Chem.* **1997**, 43/8, 1459–1461.
66. M. Santandreu, F. Cespedes, S. Alegret et al., *Anal. Chem.* **1997**, 69, 2080–2085.
67. J. Wang, P. V. A. Pamidi, K. R. Rogers, *Anal. Chem.* **1998**, 70, 1171–1175.
68. B. Lu, M. R. Smyth, R. O’Kennedy et al., *Anal. Chim. Acta* **1997**, 340, 175–180.
69. H. Yao, S. H. Jenkins, A. J. Pesce et al., *Clin. Chem.* **1993**, 39/7, 1432–1434.
70. D. A. Palmer, T. E. Edmonds, J. J. Seare, *Anal. Lett.* **1993**, 26, 1425–1439.
71. Z. Yu, Y. Xu, M. P. C. Ip, *J. Pharm. Biomed. Anal.* **1994**, 12, 787–793.
72. D. J. Pritchard, H. Morgan, J. M. Cooper, *Anal. Chim. Acta* **1995**, 310, 251–256.
73. H. Shiku, Y. Hara, T. Matsue et al., *J. Electroanal. Chem.* **1997**, 438, 187–190.
74. F. J. Hayes, H. B. Halsall, W. R. Heineman, *Anal. Chem.* **1994**, 66, 1860–1865.
75. Y. Ding, L. Zhou, H. B. Halsall et al., *J. Pharm. Biomed. Anal.* **1999**, 19, 153–161.
76. A. J. Edwards, R. A. Durst, *Electroanalysis* **1995**, 7, 838–845.
77. R. W. Keay, C. J. McNeil, *Biosens. Bioelectron.* **1998**, 13, 963–970.
78. T. Jiang, H. B. Halsall, W. R. Heineman, *J. Agric. Food. Chem.* **1995**, 43, 1098–1104.
79. S. Kröger, S. J. Setford, A. P. F. Turner, *Anal. Chem.* **1998**, 70, 5047–5053.
80. T. Kalb, P. Skládal, *Electroanalysis* **1997**, 9, 293–297.
81. M. Dequaire, C. Degrand, B. Limoges, *Anal. Chem.* **1999**, 71, 2571–2577.
82. F. F. Bier, E. Ehrentreich-Förster, C. G. Bauer et al., *Fresenius J. Anal. Chem.* **1996**, 354, 861–865.
83. H. Gao, T. Jiang, W. R. Heineman et al., *Fresenius J. Anal. Chem.* **1999**, 364, 170–174.
84. M. Del Carlo, M. Mascini, *Anal. Chim. Acta* **1996**, 336, 167–174.
85. A. G. Gehring, J. D. Brewster, P. L. Irwin et al., *J. Electroanal. Chem.* **1999**, 469, 27–33.
86. F. G. Perez, M. Mascini, I. E. Tothill et al., *Anal. Chem.* **1998**, 70, 2380–2386.
87. R. M. Pemberton, J. P. Hart, J. A. Foulkes, *Electrochim. Acta* **1998**, 43, 3567–3574.
88. R. M. Pemberton, J. P. Hart, P. Stoddard et al., *Biosens. Bioelectron.* **1999**, 14, 495–503.
89. J. D. Brewster, A. D. Gehring, R. S. Mazenko et al., *Anal. Chem.* **1996**, 68, 4153–4159.
90. J. L. Brooks, B. Mirhabibollahi, R. G. Kroll, *J. Appl. Bacteriol.* **1992**, 73, 189–196.
91. I. Abdel-Hamid, D. Ivnitski, P. Atanasov et al., *Anal. Chim. Acta* **1999**, 399, 99–108.
92. J. L. Brooks, B. Mirhabibollahi, R. G. Kroll, *Appl. Environ. Microbiol.* **1990**, 56, 3278–3284.
93. J. Rishpon, D. Ivnitski, *Biosens. Bioelectron.* **1997**, 12, 195–204.
94. M. Steine, U. Bilitewski, *Analyst* **1997**, 122, 155–159.
95. S. S. Babkina, E. P. Medyantseva, H. C. Budnikov et al., *Anal. Chim. Acta* **1993**, 273, 419–424.
96. W. R. Heineman, H. B. Halsall, *Anal. Chem.* **1985**, 57, 1321A–1331A.
97. W. J. Blaedel, R. C. Boguslaski, *Anal. Chem.* **1978**, 50, 1026–1032.

98. W. R. Heineman, P. T. Kissinger, in *Laboratory Techniques in Electroanalytical Chemistry*, (Eds.: P. T. Kissinger, W. R. Heineman), 2nd ed., Marcel Dekker, New York, 1996, pp. 51–123.
99. M. A. Cousino, T. B. Jarbawi, H. B. Halsall et al., *Anal. Chem.* **1997**, 69, 544A–549A.
100. U. Wollenberger, M. Paeschke, R. Hintsche, *Analyst* **1994**, 119, 1245–1249.
101. H. T. Tang, C. E. Lunte, H. B. Halsall et al., *Anal. Chim. Acta* **1988**, 214, 187–195.
102. I. Rosen, J. Rishpon, *J. Electroanal. Chem.* **1989**, 258, 27–39.
103. M. Del Carlo, I. Lioni, M. Taccini et al., *Anal. Chim. Acta* **1997**, 342, 189–197.
104. G. Volpe, D. Compagnone, D. Draisci et al., *Analyst* **1998**, 123, 1303–1307.
105. B. R. Clark, E. Engvall, in *Enzyme Immunoassay*, (Ed.: E. T. Maggio), CRC Press, Boca Raton, 1981, pp. 167–179.
106. R. F. Vogt Jr., D. L. Phillips, L. O. Henderson et al., *J. Immunol. Methods* **1987**, 101, 43–50.
107. K. Kato, Y. Umedo, F. Suzuki et al., *Clin. Chim. Acta* **1980**, 102, 261–265.
108. J. Ruzicka, E. H. Hansen, *Flow Injection Analysis*, Wiley & Sons, New York, 1981.
109. H. B. Halsall, W. R. Heineman, *J. Int. Fed. Clin. Chem.* **1990**, 2, 179–187.
110. G. S. Sittampalam, G. S. Wilson, *Trends Anal. Chem.* **1984**, 3, 96–99.
111. G. Wittstock, S. H. Jenkins, H. B. Halsall et al., *Nanobiology* **1998**, 4, 153–162.
112. The companies include Dynal Inc., of Norway and Bangs Inc., of Indiana, USA.
113. H. Yao, H. B. Halsall, W. R. Heineman et al., *Clin. Chem.* **1995**, 41/4, 591–598.
114. S. G. Thompson, in *Clinical Chemistry*, (Eds.: L. A. Kaplan, A. J. Pesce), Mosby, St. Louis, 1989, pp. 191–206.
115. J. Wang, *Stripping Analysis*, VCH, Deerfield Beach, 1985.
116. J. Wang, in *Laboratory Techniques in Electroanalytical Chemistry*, (Eds.: P. T. Kissinger, W. R. Heineman), 2nd ed., Marcel Dekker, New York, 1996, pp. 719–737.
117. Y. Xu, H. B. Halsall, W. R. Heineman, in *Immunochemical Assays and Biosensor Technology for the 1990s*, (Eds.: R. M. Nakamura, Y. Kasahara, G. A. Rechnitz), American Society for Microbiology, Washington, D.C., 1992, pp. 291–309.
118. W. R. Heineman, C. W. Anderson, H. B. Halsall, *Science* **1979**, 204, 865–866.
119. S. G. Weber, W. C. Purdy, *Anal. Lett.* **1979**, 12, 1–9.
120. I. A. Alam, G. D. Christian, *Fresenius Z. Anal. Chem.* **1982**, 15, 1449–1456.
121. I. A. Alam, G. D. Christian, *Fresenius Z. Anal. Chem.* **1984**, 318, 33–36.
122. I. A. Alam, G. D. Christian, *Fresenius Z. Anal. Chem.* **1985**, 320, 281–284.
123. C. L. Morgan, D. J. Newman, C. P. Price, *Clin. Chem.* **1996**, 42/2, 193–209.
124. P. Skládal, *Electroanalysis* **1997**, 9, 737–745.
125. P. Treloar, J. Kane, P. Vadgama, in *Principles and Practice of Immunoassay*, (Eds.: C. P. Price, D. J. Newman), 2nd ed., Macmillan, London, 1997, pp. 483–509.
126. B. R. Eggins, *Biosensors: an Introduction*, Wiley-Tubner, New York, 1996.
127. J. Janata, *J. Am. Chem. Soc.* **1975**, 97, 2914–2916.
128. L. Engel, W. Baumann, *Fresenius J. Anal. Chem.* **1993**, 346, 745–751.
129. N. Yamamoto, Y. Nagasawa, M. Sawai et al., *J. Immunol. Methods* **1978**, 22, 309–313.
130. M. Gotoh, E. Tamiya, M. Suzuki et al., *J. Mol. Catal.* **1989**, 53, 285–289.
131. C. L. Morgan, D. J. Newman, C. P. Price, *Clin. Chem.* **1996**, 42/2, 193–209.
132. H. D. Goldberg, R. B. Brown, D. P. Liu et al., *Sens. Actuators, B* **1994**, 21, 171–183.
133. T. Kaláb, P. Skládal, *Anal. Chim. Acta* **1995**, 304, 361–368.
134. M. D. Carlo, M. Mascini, *Field Anal. Chem. Technol.* **1999**, 3, 179–184.
135. J. P. Hart, R. M. Pemberton, R. Luxton et al., *Biosens. Bioelectron.* **1997**, 12, 1113–1121.
136. C. J. Zhong, M. D. Porter, *Anal. Chem.* **1995**, 67, 709A–715A.
137. A. Heller, *Acc. Chem. Res.* **1990**, 23, 128–148.
138. I. Katakis, A. Heller, in *Frontiers in Biosensors 1*, (Eds.: F. W. Scheller, F. Schubert, J. Fedrowitz), Birkhäuser Verlag, Boston, 1997, pp. 229–241.
139. D. J. Litman, T. M. Hanlon, E. F. Ullman, *Anal. Biochem.* **1980**, 106, 223–229.
140. D. V. Brown, M. E. Meyerhoff, *Biosens. Bioelectron.* **1991**, 6, 615–622.
141. C. N. Campbell, T. de Lumley-Woodyear, A. Heller, *Fresenius J. Anal. Chem.* **1999**, 364, 165–169.
142. J. D. Newman, A. F. P. Turner, G. Marrazza, *Anal. Chim. Acta* **1992**, 262, 13–17.

143. J. P. Hart, S. A. Wring, *Electroanalysis* **1994**, 6, 617–624.
144. P. Connolly, *TIBTECH* **12**, **1994**, 123–127.
145. J. Lahiri, E. Ostuni, G. M. Whitesides, *Langmuir* **1999**, 15/5, 2055–2060.
146. D. J. Pritchard, H. Morgan, J. M. Cooper, *Angew. Chem., Int. Ed. Engl.* **1995**, 34, 91–93.
147. Section 9.10 discusses the applications of SECM in bioelectrochemistry. Also, the reader is referred to the original paper on SECM, A. J. Bard, R.-R. F. Fan, D. T. Pierce et al., *Science* **1991**, 254, 68–74.
148. H. Shiku, T. Matsue, I. Uchida, *Anal. Chem.* **1996**, 68, 1276–1278.
149. A. L. Ghindilis, R. Krishnan, P. Atanasov et al., *Biosens. Bioelectron.* **1997**, 12, 415–423.
150. A. van der Berg, P. Bergveld (Eds.), *Micrototal Analysis Systems*, Kluwer Academic Press, Boston, 1995.

6

Electrochemistry of Metalloporphyrins in Nonaqueous Media

Karl M. Kadish^a and Eric Van Caemelbecke^{a,b}

^aUniversity of Houston, Houston, Texas

^bHouston Baptist University, Houston, Texas

6.1	Introduction	177
6.1.1	Porphyrin Electrochemistry in the Early 1960s and the 1970s	178
6.1.2	Porphyrin Electrochemistry in the 1980s and the 1990s	179
6.1.3	Selection of Appropriate Solvent and Supporting Electrolyte	179
6.1.4	Selection of Appropriate Supporting Electrolyte	180
6.2	Effect of Macrocycle Structure on Potentials	181
6.3	Effect of Axial Ligation	186
6.4	Periodic Table of Metalloporphyrins	191
6.4.1	Groups 1–4	191
6.4.2	Groups 5 and 6	192
6.4.3	Group 7	193
6.4.4	Group 8	195
6.4.4.1	Ruthenium	195
6.4.4.2	Osmium	196
6.4.4.3	Iron	196
6.4.4.3.1	Reaction of Heme-thiolate Proteins	203
6.4.4.3.2	Mechanism of Electron-transfer in Peroxidases	204
6.4.4.3.3	Reactions of Nitrite Reductions	205
6.4.4.3.4	Reactions of Nitric Oxide Reductases	205
6.4.5	Group 9	206
6.4.6	Group 10	209
6.4.7	Group 11	211
6.4.8	Group 12	213
6.4.9	Group 13	214
6.4.10	Group 14	215
6.4.11	Group 15	216

6.5	Concluding Statement	218
	Acknowledgments	218
	References	218

6.1 Introduction

Thousands of different metalloporphyrins have been electrochemically investigated in close to three dozen different nonaqueous solvents over the last three decades. These include compounds with hundreds of different macrocycles and coordinated axial ligands, and 70 different metal or nonmetal ions, of which some have been shown to exist in three or four different oxidation states (see the “Periodic Table of Metalloporphyrins” in Fig. 1 and *The Porphyrin Handbook*, Volumes 1–10 [1]).

Despite a large variety of known compounds, or perhaps because of it, previous reviews on metalloporphyrin electrochemistry have concentrated for the most part on describing the behavior of “simple” model compounds with octaethylporphyrin (OEP) or tetraphenylporphyrin (TPP) [2–10] macrocycles, and were most often arranged according to a specific element (Fe, for example), group of elements, the Periodic Table of the elements or the nature of the metal–ligand bond; examples in the latter case include porphyrins with metal–carbon bonds [3, 4, 11, 12] and those with metal–metal bonds [4, 11, 13]. Unfortunately, these approaches and perspectives are truly useful only if the reader is made aware of how changes in structure

and reactivity of a given compound may be related to the well-studied OEP and TPP derivatives via linear free energy relationships. This point was elucidated in a major review by Kadish, Van Caemelbecke, and Royal [7], which recently appeared in the literature.

This present review will not attempt to provide a comprehensive description of all known porphyrin electrochemistry in nonaqueous media, but will concentrate in part on specific types of porphyrin macrocycles, in part on specific groups of metalloporphyrins, and in part on guiding the reader through the vast array of electron-transfer mechanisms that can exist for a related series of compounds under a given set of experimental conditions. It is hoped that this approach will answer the majority of the reader’s questions as to what has been done in the past, while at the same time enabling the reader to utilize the data in the literature to predict what might be observed in future studies involving the electrochemistry of yet-to-be synthesized metalloporphyrin complexes.

Our current discussion will, therefore, begin with a brief historical overview of metalloporphyrin electrochemistry and a list of previously utilized nonaqueous solvents and supporting electrolytes, which have been used in porphyrin studies. It will be followed by a general description

1																	18
H	2											13	14	15	16	17	He
Li	Be											B	C	N	O	F	Ne
Na	Mg	3	4	5	6	7	8	9	10	11	12	Al	Si	P	S	Cl	Ar
K	Ca	Sc	Ti	V	Cr	Mn	Fe	Co	Ni	Cu	Zn	Ga	Ge	As	Se	Br	Kr
Rb	Sr	Y	Zr	Nb	Mo	Tc	Ru	Rh	Pd	Ag	Cd	In	Sn	Sb	Te	I	Xe
Cs	Ba	La	Hf	Ta	W	Re	Os	Ir	Pt	Au	Hg	Tl	Pb	Bi	Po	At	Rn
Fr	Ra	Ac															
Lanthanides	Ce	Pr	Nd	Pm	Sm	Eu	Gd	Tb	Dy	Ho	Er	Tm	Yb	Lu			
Actinides	Th	Pa	U	Np	Pu	Am	Cm	Bk	Cf	Es	Fm	Md	No	Lr			

Fig. 1 Periodic Table of metalloporphyrins. Shaded elements indicate specific elements that have been incorporated into a given porphyrin macrocycle. Extensive tabulations of redox potentials may be found in Ref. [21].

of metalloporphyrin redox behavior, arranged first according to the type of macrocycle and then according to the type of central metal or nonmetal ion in the complex. We will not include in this review a detailed discussion of solvent or substituent effects on metalloporphyrin redox reactions since both topics have recently been covered in great detail [7].

6.1.1

Porphyrin Electrochemistry in the Early 1960s and the 1970s

The electrochemistry of metalloporphyrins at the start of the 1960s involved, in large part, measurements of standard redox potentials for naturally occurring complexes in aqueous buffered media [14]. The choice of an aqueous solvent was often dictated by the biological relevance of the compounds available for study, while the choice of the measurement technique (potentiometry or polarography at a dropping mercury electrode) was necessitated by the type of available electrochemical instrumentation, virtually all of which was homemade and

limited almost exclusively to electrochemical laboratories. However, the situation began to change in the mid-1960s due to three main factors. The first was the publication of relatively easy-to-understand papers on cyclic voltammetric theory [15, 16], which led to the popularization of this technique as a rapid and efficient method for obtaining reversible redox potentials. The second was the increased use of nonaqueous solvents for studying electrochemical reactions [17–20], and the third was the increased “availability” of easily synthesized tetraphenyl and octaethylporphyrins with a wide variety of different central ions.

By the beginning of the 1970s, the majority of electrochemical studies on synthetic metalloporphyrins was being carried out in nonaqueous media using the technique of cyclic voltammetry. However, most utilized instrumentation was still homemade and only a handful of laboratories were actually making the measurements. An overview of the situation at this period is provided in several independent reviews [2, 6, 7, 9, 21].

6.1.2

Porphyrin Electrochemistry in the 1980s and the 1990s

A number of papers on the electrochemistry of synthetic porphyrins in the 1980s were involved with the following topics: (1) porphyrins with metal–carbon and metal–metal bonds [11–13, 22], (2) porphyrins with unusual structures, (3) porphyrins with central metal ions in very high [23] or very low oxidation states, (4) porphyrins able to react with small molecules and (5) porphyrins able to carry out a specific catalytic function [24–26].

A number of porphyrins with new and/or “unusual” macrocycles were synthesized in the 1980s and 1990s and the redox properties of these compounds were often compared to potentials for the oxidation or reduction of analogous compounds containing the same metal ion and the well-known TPP or OEP macrocycle. Examples include, but are not limited to, highly halogenated metalloporphyrins [27–39], metalloporphyrins with highly distorted macrocycles [37, 40–45], and metalloporphyrins linked to one or more other porphyrins or to different redox active molecules [46].

The Periodic Table of Metalloporphyrins, presented first by Buchler [47] and then by Kadish [2], was expanded in the 1980s to include most of the Main Group, lanthanide, and actinide elements, as well as a number of the Group 15 nonmetals. At the same time, the range of known metal or nonmetal oxidation states that could be accommodated by a given metalloporphyrin was expanded in part by the use of “novel” axial ligands or macrocycles, in part by the use of different solvents or solvent conditions (i.e. low temperature), and in part by the application of

new instrumental techniques that were able to identify previously unobserved or unreported transient intermediates in the various redox reactions.

The electrochemistry of metalloporphyrins in the 1980s and 1990s was no longer limited by the need to construct appropriate instrumentation, which had become commercially available at relatively low cost and was becoming standard analytical equipment in a large number of nonelectrochemical laboratories around the world. The reporting of redox potentials for newly synthesized porphyrins thus became routine and, more often than not, most studies of metalloporphyrin electrochemistry had as their main focus the use and application of electrochemical techniques toward the solving of chemical problems. Several key areas of chemical problems that were examined in recent years include (1) the effect of macrocycle distortion on porphyrin redox potentials [30, 42, 45, 48], (2) quantitating relationships between structure and chemical or electrochemical reactivity with the use of linear free energy relationships, that is, substituent effects, (3) the use of metalloporphyrins to activate small molecules [24–26], (4) the elucidation of relationships between redox potentials and catalytic properties of a given metalloporphyrin or group of metalloporphyrins [24], (5) the study of donor–acceptor interactions between two linked porphyrins or between a metalloporphyrin and another redox active center (e.g. such as a fullerene [46]).

6.1.3

Selection of Appropriate Solvent and Supporting Electrolyte

The earliest electrochemical studies of metalloporphyrins in aprotic media

utilized dimethylformamide (DMF) or dimethylsulfoxide (DMSO) for reductions and benzonitrile (PhCN), acetonitrile (CH₃CN) or butyronitrile (BuCN) for oxidations. Electrochemical data are now available in close to three dozen different nonaqueous solvents with the majority of data appearing in the nonbinding solvent dichloromethane (CH₂Cl₂) [21]. One advantage of CH₂Cl₂ is its large cathodic and anodic potential range, which can span from -1.9 to $+1.9$ V vs a saturated calomel electrode (SCE), thus enabling one to examine both oxidations and reductions of a given compound under the same single set of solution conditions.

Table 1 lists the most common nonaqueous solvents that have previously been utilized for the electrochemistry of metalloporphyrins. Purification procedures, potential limits and physical characteristics of these solvents are given in the literature [17–20, 49, 50].

The selection of a specific nonaqueous solvent from the list in Table 1 was based in many cases only on the “habit” of the individual laboratory, but in others it very much depended on the requirements of the individual experiment. The first requirement is, of course, solubility and the electrochemical parameters that one is investigating. One must also consider ease of purification, the chemical reactivity of the solvent, its ability to stabilize π -anion or π -cation radicals, and its overall potential range for both oxidation and reduction, the latter of which will depend in part on the type of electrode material (Hg for example cannot be used for oxidations, while Ag and Au both have a limited positive range in solvents containing some anions.). Other practical factors include the cost of the solvent, its toxicity, and its general ease of handling.

Tab. 1 List of solvents used in electrochemical studies of metalloporphyrins

Solvent abbreviation	Name
1,1,1-TCE	1,1,1-Trichloroethane
1,2-DBE	1,2-Dibromoethane
1,2-DME	1,2-Dimethoxyethane
2-MeTHF	2-Methyltetrahydrofuran
C ₆ H ₅ Cl	Chlorobenzene
C ₂ H ₂ Cl ₂	Dichloroethane
C ₂ H ₂ Cl ₄	1,1,2,2-Tetrachloroethane
C ₆ H ₄ Cl ₂	1,3-Dichlorobenzene
C ₆ H ₆	Benzene
CH ₂ Br ₂	Dibromomethane
CH ₂ Cl ₂	Dichloromethane (methylene chloride)
CHCl ₃	Trichloromethane
Cl-Naph	1-Chloronaphthalene
DMA	<i>N, N</i> -Dimethylacetamide
DMF	<i>N, N</i> -Dimethylformamide
DMSO	Dimethylsulfoxide
EtOH	Ethanol
EtONa	Sodium ethoxide
HMP	Hexamethylphosphoramide
HQ	Hydroquinone
Me ₂ CO	Acetone
Me ₂ NH	Dimethylamine
MeCN	Acetonitrile
MeCO ₂ Et	Ethyl acetate
Me-Naph	1-Methylnaphthalene
MeNO ₂	Nitromethane
NMA	<i>N</i> -Methylacetamide
NMF	<i>N</i> -Methylformamide
PC	Propylene carbonate
PhCN	Benzonitrile
PrCN	<i>n</i> -Butyronitrile
Py	Pyridine
THF	Tetrahydrofuran

6.1.4

Selection of Appropriate Supporting Electrolyte

A list of the supporting electrolytes that have been used for studies of metalloporphyrin electrochemistry is given in Table 2 [21]. The majority of electrochemical studies involving metalloporphyrins in

Tab. 2 List of supporting electrolytes used in metalloporphyrin studies arranged by size of the cation

Electrolyte abbreviation	Name
KCN	Potassium cyanide
LiBr	Lithium bromide
LiCl	Lithium chloride
LiClO ₄	Lithium perchlorate
NaClO ₄	Sodium perchlorate
NH ₄ PF ₆	Ammonium hexafluorophosphate
TMACl	Tetramethylammonium chloride
TMAP	Tetramethylammonium perchlorate
TMAPF ₆	Tetramethylammonium hexafluorophosphate
TEABF ₄	Tetraethylammonium tetrafluoroborate
TEACl	Tetraethylammonium chloride
TEAP	Tetraethylammonium perchlorate
TEAPF ₆	Tetraethylammonium hexafluorophosphate
TPrABF ₄	Tetra- <i>n</i> -propylammonium tetrafluoroborate
TPrAP	Tetra- <i>n</i> -propylammonium perchlorate
TPrASO ₃ CF ₃	Tetra- <i>n</i> -propylammonium trifluoromethylsulfonate
TBABF ₄	Tetra- <i>n</i> -butylammonium tetrafluoroborate
TBABr	Tetra- <i>n</i> -butylammonium bromide
TBACl	Tetra- <i>n</i> -butylammonium chloride
TBAOH	Tetra- <i>n</i> -butylammonium hydroxide
TBAOTeF ₅	Tetra- <i>n</i> -butylammonium pentafluorooxotellurate
TBAP	Tetra- <i>n</i> -butylammonium perchlorate
TBAPF ₆	Tetra- <i>n</i> -butylammonium hexafluorophosphate
TBASO ₃ CF ₃	Tetra- <i>n</i> -butylammonium trifluoromethylsulfonate
THAP	Tetra- <i>n</i> -hexylammonium perchlorate
THASbF ₆	Tetra- <i>n</i> -hexylammonium hexafluoroantimonate(V)

nonaqueous media have utilized tetraalkylammonium salts as supporting electrolytes, the most common of which have been the tetrabutylammonium perchlorates and tetraethylammonium perchlorates (abbreviated TBAP and TEAP). Several studies have also utilized tetraalkylammonium salts of BF₄[−] or PF₆[−], (i.e. TBABF₄ or TBAPF₆). The selection of one supporting electrolyte over another may depend on the cost and ease of purification, or it may have been the need for a laboratory to select a salt that had a minimum or a maximum coordination ability with the investigated porphyrin in its neutral, electrooxidized or electroreduced form. Usually, ClO₄[−], BF₄[−] and PF₆[−] can be considered as nonbinding or very weakly binding anions and this sometimes has been a major factor in their selection for studies of electrooxidation processes.

Finally, there is the question of supporting electrolyte concentration. Most measurements have been made in solutions containing 0.1 M TBAP (the most often utilized salt), but others have utilized solutions with 0.2 M supporting electrolyte, especially in the case of spectroelectrochemical measurements. Attention should be paid to this fact since redox potentials measured in solutions of 0.1 M TBAP are not always identical to those measured with TBAP concentrations of 0.01 or 1.0 M. The experimentally obtained differences in potential may amount to several hundred millivolts and will vary as a function of the specific metalloporphyrin and the specific electrode reaction examined [21].

6.2 Effect of Macrocycle Structure on Potentials

All known metalloporphyrins are electroactive (see summary of selected redox

potentials [21]), and virtually all are able to undergo three or more electron-transfer reactions in nonaqueous media, with the exact number of processes depending on the potential range of the utilized electrochemical solvent, the type of macrocycle, the type of central metal ion, and/or the type of axially coordinated ligands.

The first synthetic porphyrins whose electrochemistry was studied in nonaqueous solvents were largely those with TPP or OEP macrocycles. The electrochemical behavior of the TPP and OEP complexes are generally similar to each other, but the more basic OEP derivatives are almost always easier to oxidize and harder to reduce than the TPP complexes containing the same central metal ion and the same set of axial ligands as shown in Fig. 2(a) for (TPP)Zn and (OEP)Zn.

The absolute potential difference between half-wave potentials for oxidation and reduction of a given (OEP)M or (TPP)M complex was initially claimed to be a constant value of 2.25 ± 0.15 V [51, 52], but there are now many examples in the literature where this is not the case.

Several important trends in the electrochemical behavior of synthetic metalloporphyrins have been pointed out over the last 35 to 40 years. The first is that metalloporphyrins can be reduced by two, and only two, electrons at the conjugated macrocycle to give porphyrin π -anion radicals and dianions. The same compounds can also be oxidized by two, and only two, electrons at the conjugated macrocycle to give π -cation radicals and dications. The porphyrins may also undergo one or more metal-centered reactions, some of which have been unambiguously assigned as involving the metal orbitals and others of which are open to continuing

debate as to the site of electron transfer. Most metal-centered redox processes have been reported to occur at potentials that are located between $E_{1/2}$ for formation of the porphyrin π -cation and π -anion radical, although examples have been reported where this seems not to be the case.

Early electrochemical studies on metalloporphyrins containing OEP or TPP macrocycles have led to often-quoted diagnostic criteria for differentiating reactions, which occur at the π -conjugated macrocycle as opposed to those that occur at the central metal ion [51, 52]. These include a constant HOMO-LUMO gap (2.25 ± 0.15 V [51, 52]) (highest occupied molecular orbital-lowest unoccupied molecular orbital) independent of the metal oxidation state and a constant difference between $E_{1/2}$ for the two stepwise reversible one-electron reductions or two stepwise reversible one-electron oxidations at the porphyrin π -ring system. However, more recent investigations of porphyrins with macrocycles other than OEP or TPP have shown that those diagnostic criteria are not always followed, and in many cases, the values of $\Delta E_{1/2}$ seem to be related to the planarity of the macrocycle, the nature of the metal ion, and/or the presence or absence of specific axially coordinated axial ligands, which preferentially stabilize one oxidation state over the other.

A schematic representation of several porphyrin macrocycles, which have been studied with regard to their electrochemical properties in different metallated forms, is given in Fig. 3 and abbreviations for a much larger group of investigated compounds is given in Table 3.

The electrochemistry of (TMP)M, (R₈TPP)M, (DPP)M, (Br₈TPP)M, (Br₈TMP)M,

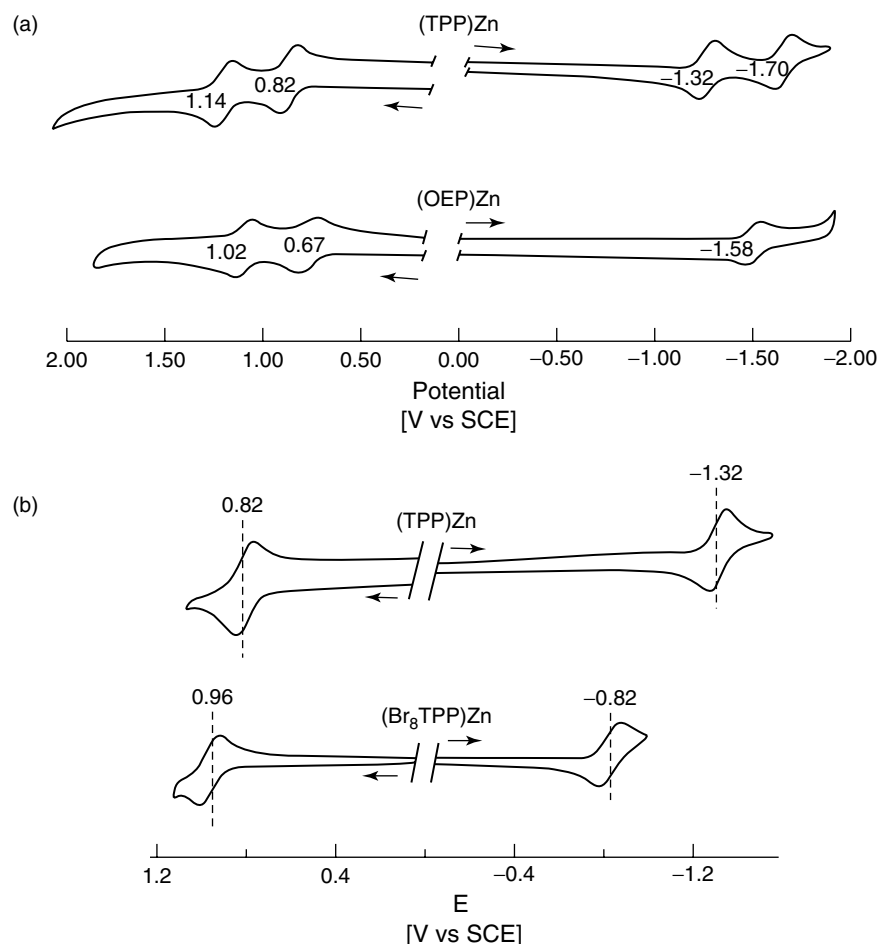


Fig. 2 Cyclic voltammograms of (a) (TPP)Zn and (OEP)Zn and (b) (TPP)Zn and (Br₈TPP)Zn.

(F₂₀TPP)M, and other macrocycles described in Fig. 3 has been discussed in a recent review [7]. All of the porphyrins exhibit reductions and oxidations at the π -conjugated macrocycle, but the potential at which these redox reactions are located will depend on the planarity and basicity of the macrocycle that can effect each oxidation and reduction to a different degree, thus leading to substituent effects that can differ substantially depending on the specific site of electron transfer.

For example, the oxidation, but not the reduction, of porphyrins with highly distorted macrocycles, such as R₈TPP (R = an alkyl group), DPP, Br₈TPP, and F₂₀Br₈TPP, are all generally easier (occur at a more negative potential) than is observed in the case of analogues having an OEP or a TPP macrocycle, and the same metal ion/axial ligand combination [7]. The easier oxidation has been explained theoretically as resulting from a destabilization of the HOMO due to

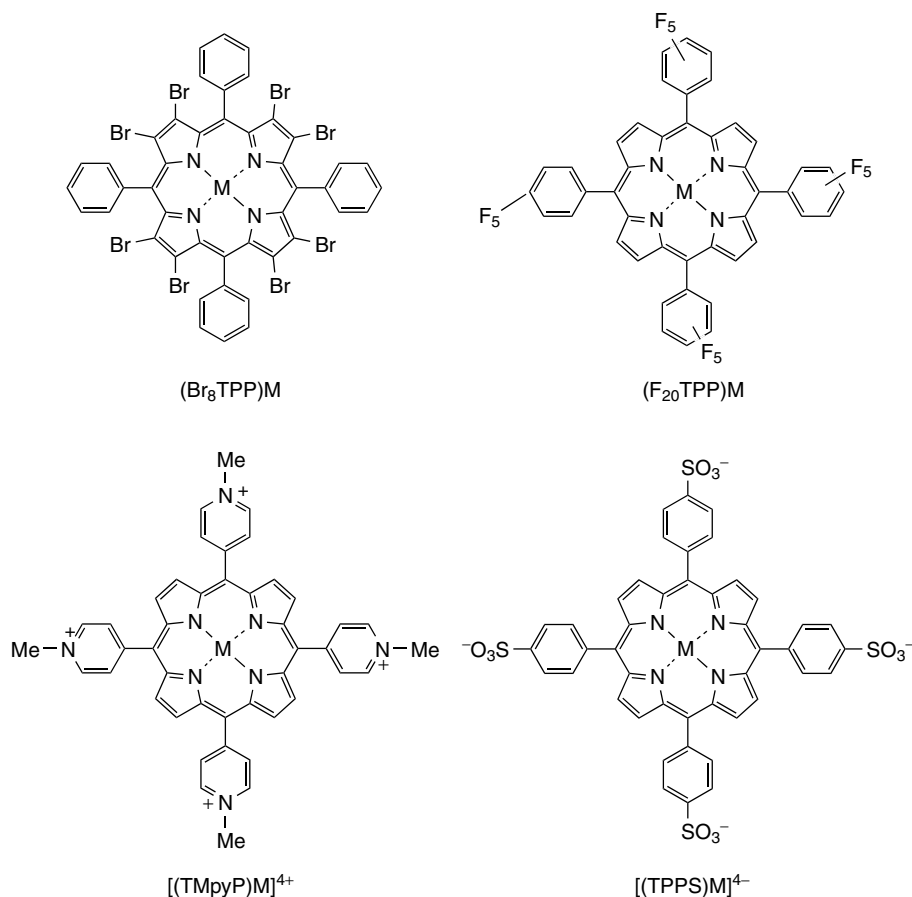


Fig. 3 Selected porphyrin macrocycles.

macrocycle distortion [35, 42, 43]. In the case of (Br₈TPP)M and (Br₈TMP)M, there is a systematic anodic shift in $E_{1/2}$ for the reduction upon going from TPP to Br₈TPP [29, 30, 35, 36] or from TMP to Br₈TMP [7] as a macrocycle, and this contrasts with much smaller differences between $E_{1/2}$ for the first oxidation of the same compounds or series of compounds. This is illustrated in Fig. 2(b), which compares cyclic voltammograms of (TPP)Zn and (Br₈TPP)Zn under the same solution conditions. As seen in this figure, the difference in reduction potentials amounts

to 500 mV, while the oxidations are separated by only 140 mV, thus leading to a substantially reduced HOMO-LUMO gap in the case of (Br₈TPP)Zn.

Also, it should be pointed out that some (Br₈TPP)M derivatives sometimes undergo additional electroreductions that are not observed for (TPP)M, and these involve, in at least one case, a stepwise elimination and electroreduction of the Br groups on the porphyrin macrocycle [34].

Porphyrins with F₂₀TPP macrocycles are all easier to reduce and more difficult to oxidize than the same compounds

Tab. 3 List of selected porphyrin macrocycles (see Fig. 3 for selected structures of these macrocycles)

Abbreviation	Common name
TPP	Tetraphenylporphyrin
OEP	Octaethylporphyrin
TMP	Tetramesitylporphyrin
TBP	Tetrabenzoporphyrin
Br ₈ TPP	Octabromotetraphenylporphyrin
T(F ₅)PP	Tetrakis-(pentaphenyl)porphyrin
DPP	Dodecaphenylporphyrin
Me ₈ TPP	Octamethyltetraphenylporphyrin
T(<i>p</i> -Me)PP	Tetrakis-(<i>p</i> -methylphenyl)porphyrin
triPh((<i>o</i> -NH ₂)Ph)P	5-(<i>o</i> -Aminophenyl)triphenylporphyrin
(NO ₂)TPP	2-Nitro-tetraphenylporphyrin
(2-O)OEP	Oxophlorin
(5-NO ₂)OEP	5-Nitro-octaethylporphyrin
T(CF ₃)P	Tetrakis(perfluoromethyl)porphyrin
TPPS(4)	Tetrakis(<i>p</i> -(sodiumsulfonato)phenyl)porphyrin
[(TMpy(4)P)] ⁴⁺	5,10,15,20-Tetrakis(1-methylpyridinium-4-yl)porphyrin
(<i>N</i> -Ph)TPP	(<i>N</i> -Phenyl)-tetraphenylporphyrin
DPIXDME	Deuterioporphyrin IX dimethyl ester
Etio	Etioporphyrin
HPIXDME	Hematoporphyrin IX dimethyl ester
MPIX	Mesoporphyrin IX
MPIXDME	Mesoporphyrin IX dimethyl ester
PPIX	Protoporphyrin IX
PPIXDME	Protoporphyrin IX dimethyl ester
T(<i>o</i> -piv)PP	<i>Meso</i> - α , α , α , α -tetrakis(<i>o</i> -pivamidophenyl)porphyrin
TPP(a-(C12) ₂ -CT)	α -5, α -15, β -10, β -20-Bis[2,2'-dodecane-diamidodiphenylene]porphyrin

with a TPP macrocycle, and potential differences of 440 to 570 mV have been reported between compounds in these two series [7, 21].

Several porphyrins with Br₈F₂₀TPP, Cl₈F₂₀TPP or Me₈F₂₀TPP macrocycles have been investigated for their electrochemical properties [7, 21, 44] and, as expected on the basis of the highly electron-withdrawing halogen groups, differences of up to 800–900 mV have been reported between $E_{1/2}$ for reduction of the (TPP)M and (X₈F₂₀TPP)M complexes with the same metal ion. The electron-withdrawing halogen groups on the porphyrin macrocycles of Br₈F₂₀TPP

and Cl₈F₂₀TPP not only induce a positive shift in the potentials but also sometimes lead to a merging of the two one-electron ring-centered oxidations, thus giving what appears to be a single overall two-electron-transfer process. Details of this interesting electrochemical feature have been presented in the literature [7]. A now well-known, but perhaps unusual, electrochemical behavior is seen for porphyrins having positively charged macrocycles, as in the case of the TMpyP derivatives (see structure in Fig. 3). The reduction of most (TMpyP)M^{II}, (TMpyP)M^{III} and (TMpyP)M^{IV} complexes in nonaqueous media generally occurs in

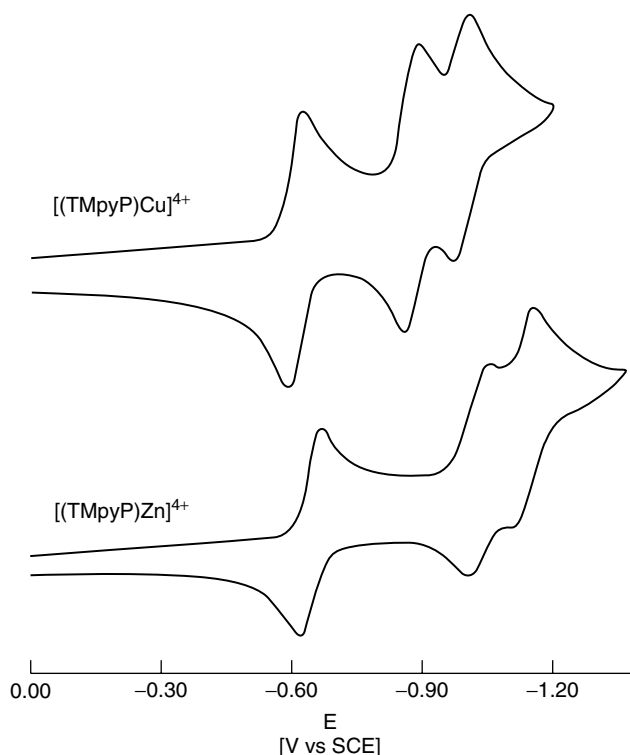


Fig. 4 Cyclic voltammograms of $[(\text{TMpyP})\text{M}]^{4+}$ where $\text{M} = \text{Cu}(\text{II})$ or $\text{Zn}(\text{II})$ in DMF, 0.1 M TBAP. (Adapted from K. M. Kadish, C. Araullo, G. B. Maiya, D. Sazou, J.-M. Barbe, R. Guillard, *Inorg. Chem.* **1989**, 28, 2528–2533.)

multiple overlapping two-electron-transfer steps [53–55] (Fig. 4) and a discussion of the electron-transfer mechanism has recently been reviewed [7].

6.3 Effect of Axial Ligation

A large number of different axial ligands have been complexed to metalloporphyrins, and 252 examples taken from the literature are summarized in Table 4 [21]. Each ligand has been bound to one or more complexes in nonaqueous media and a summary of potentials, along with

abbreviations of the ligands is found in Ref. [21].

Metalloporphyrins containing different σ -bonded alkyl or aryl groups [3, 45, 56–64] or the diatomic molecules NO [27, 65–77] or CO (see following sections) have been electrochemically investigated and several reviews of the general electrochemical behavior of these compounds have been published [7, 12, 78]. Metalloporphyrins with 29 different central ions are now known to form carbon σ -bonded complexes (see Fig. 5) [12] and the electrochemical behavior of these compounds has been shown to depend on the central metal ion.

Tab. 4 List of axial ligands which have been coordinated to metalloporphyrins

$:\text{CH}=\text{CHPh}^-$	$(:\text{CH}_2\text{CH}_2\text{Ph})^-$	$-(\text{CH}_2\text{Ph})\text{CH}-$
$(\text{CO})_2$	$(\text{CO})_3$	$(\text{NPh})_2^{2-}$
$:\text{C}(\text{NHCH}_2\text{Ph})_2$	$:\text{CHCH}_2\text{Ph}$	$1-(\text{MeCO})\text{Im}$
1,2-Me ₂ Im	1-MeIm	2-CNPy
2-MeIm	3-(MeCO)Py	3-(NH ₂)Py
3-(OH)Py	3-(OMe)Py	3,4-Me ₂ Py
3,5-Cl ₂ Py	3-BrPy	3-ClPy
3-CNpy	3-MePy	4-(Me ₂ N)Py
4-(MeCO)Py	4-(MeO)Py	4-(NH ₂)Py
4-(NMe ₂)Py	4-(OMe)Py	4,4'-bipy
4-CNPy	4-MeIm	4-MePy
4-NH ₂ py	4-OH-pip	4-PhIm
4-PhPy	5,6-Me ₂ BzIm	acac ⁻
AuCl ₄ ⁻	azpy	BF ₄ ⁻
biPy	Br ⁻	Bu
BuCN	BzIm	$\text{C}=\text{C}(p\text{-C}_6\text{H}_4\text{Cl})_2$
$\text{C}=\text{CPh}_2$	$\text{C}=\text{CPh}_2$	$\text{C}_2\text{H}_2\text{Ph}$
$\text{C}_2\text{H}_2\text{Ph}$	C_2H_3	$\text{C}_2\text{H}_3\text{O}_2^-$
C_2Ph	$\text{C}_3\text{H}_6\text{Br}$	$\text{C}_3\text{H}_6\text{Cl}$
$\text{C}_3\text{H}_6\text{I}$	$\text{C}_4\text{H}_8\text{Br}$	$\text{C}_4\text{H}_8\text{Cl}$
$\text{C}_4\text{H}_8\text{I}$	$\text{C}_5\text{H}_{10}\text{Br}$	$\text{C}_5\text{H}_{10}\text{Cl}$
$\text{C}_5\text{H}_{10}\text{I}$	C_5H_{11}	$\text{C}_6\text{F}_4\text{H}$
C_6F_5	C_6H_{11}	$\text{C}_6\text{H}_{12}\text{I}$
C_6H_{13}	$\text{C}_6\text{H}_4\text{CN}$	$\text{C}_6\text{H}_4\text{Me}$
$\text{C}_6\text{H}_4\text{SO}_3^-$	C_8H_{13}	cat^{2-}
CCl_3	$\text{CH}=\text{C}(p\text{-C}_6\text{H}_4\text{Cl})_2$	$\text{CH}=\text{CPh}_2$
CH_2Br	CH_2Cl	CH_2I
CH_2Ph	CH_2Ph	CHCl_2
CHI_2	CHMe_2	CHO_2^-
Cl_3	Cl^-	ClO_4^-
CMe_3	cMU	CN^-
CNCH_2Ph	CO	$\text{Co}(\text{CO})_4$
CO_2Et	COEt	COMe
COPr	$\text{Cr}(\text{CO})_3\text{Cp}$	CS
CSe	dabco	DMF
DMS	DMSO	dppe
Et	EtNH ₂	EtOH
F ⁻	facam ⁻	Fc
$\text{Fe}(\text{CO})_4$	H ⁻	HSO_4^-
I ⁻	Im	$m\text{-(OH)C}_6\text{H}_4\text{NH}_2$
$m, m\text{-C}_6\text{F}_2\text{H}_3$	Me	Me ₂ NH
MeCN	$\text{Mn}(\text{CO})_5$	$\text{Mo}(\text{CO})_3\text{Cp}$
N_3^-	$\text{N}_4(\text{CH}=\text{CH}_2)$	$\text{N}_4(\text{CH}=\text{CHCN})$
$\text{N}_4\text{C}(\text{CH}=\text{CH}_2)$	$\text{N}_4\text{C}(\text{CH}=\text{CHCN})$	$\text{N}_4\text{C}(\text{CMe}_3)$
$\text{N}_4\text{C}(m\text{-C}_6\text{H}_4\text{Me})$	$\text{N}_4\text{C}(p\text{-C}_6\text{H}_4(\text{NO}_2))$	$\text{N}_4\text{C}(p\text{-C}_6\text{H}_4\text{Me})$
$\text{N}_4\text{C}_2(\text{CO}_2\text{Me})_2$	N_4CEt	N_4CMe
NCS^-	NH_2OH	NH_3
NHMe_2	NMe_3	NO
NO_2^-	NO_3^-	NPh_2^-

(continued overleaf)

Tab. 4 (continued)

NS	<i>o, m, p</i> -C ₆ H ₂ F ₃	<i>o, o, p</i> -C ₆ H ₂ F ₃
O ₂ ^{•-}	O ₂ ²⁻	O ₂ ²⁻
O ₂ C(3-ClC ₂ H ₄) ⁻	O ₂ C(<i>o</i> -C ₆ H ₃ Cl) ⁻	O ₂ CCCl ₃ ⁻
O ₂ CCF ₃ ⁻	O ₂ CCH ₂ Cl ⁻	O ₂ CCH ₂ Ph ⁻
O ₂ CCHCl ₂ ⁻	O ₂ CCMe ₃ ⁻	O ₂ CEt ⁻
O ₂ CH ⁻	O ₂ C- <i>m</i> -C ₆ H ₃ NO ₂ ⁻	O ₂ CMe ⁻
O ₂ CPr ⁻	OBu ⁻	OC ₂ F ₅ ⁻
OC ₃ HF ₆ ⁻	OC ₆ H ₂ (NO ₂) ₃ ⁻	<i>o</i> -C ₆ H ₄ Et
OCH ₂ Ph ⁻	OCMe ₃	OCN ⁻
O ₂ CPh ⁻	<i>o</i> -cresol ⁻	OEt ⁻
OH ⁻	OH ₂	<i>O-m, m</i> -Bu ₂ , <i>o</i> -(OH)C ₆ H ₂ ⁻
<i>O-m, p</i> -C ₆ H ₃ Me ₂ ⁻	OMe ⁻	<i>O-o, p</i> -C ₆ H ₃ (NO ₂) ₂ ⁻
<i>O-o, p</i> -C ₆ H ₃ Me ₂ ⁻	<i>O-p</i> -C ₆ H ₃ CN ⁻	<i>O-p</i> -C ₆ H ₃ NO ₂ ⁻
<i>O-p</i> -C ₆ H ₄ Me ⁻	<i>O-p</i> -C ₆ H ₄ NO ₂ ⁻	OPh ⁻
OPh ⁻	<i>O-p</i> -PhO- <i>o, p</i> -(NO ₂) ₂ Ph ⁻	<i>O-p</i> -PhO- <i>p</i> -(NO ₂)Ph ⁻
OPr ⁻	OPr ⁻	OTeF ₅ ⁻
P(OEt) ₃	P(OMe) ₃	<i>p</i> -C ₆ H ₄ Br
<i>p</i> -C ₆ H ₄ Me	<i>p</i> -C ₆ H ₄ Cl	<i>p</i> -C ₆ H ₄ F
<i>p</i> -C ₆ H ₄ NO ₂	<i>p</i> -C ₆ H ₄ OMe	<i>p</i> -cresol ⁻
PEt ₃	PF ₃	PF ₆ ⁻
Ph	Ph	PhCH ₂ NH ₂
PhNH ₂	pip	PPh ₂ Me
PPh ₃	PPhMe ₂	Pr
PrOH	Py	Pyan
Pyen	PyPh	Pyrazole
pyz	Quinine	Quinuclidine
Re(CO) ₅	S(CH ₂) ₄	S ₂ ⁻
SbF ₆ ⁻	SC ₆ F ₄ H ⁻	SCN ⁻
Se ²⁻	SH ⁻	SnPh ₃ ⁻
<i>S-o</i> -(CF ₃ CONH)C ₆ H ₄	<i>S-o, o</i> -C ₆ H ₃ (CF ₃ CONH) ₂	SO ₃ CF ₃ ⁻
SO ₃ (<i>p</i> -Me)C ₆ H ₄ ⁻	SO ₃ Me ⁻	SO ₃ Ph ⁻
SO ₄ ²⁻	<i>S-p</i> -C ₆ H ₄ Me ⁻	SPh ⁻
tdt ²⁻	THF	THF
tMU	<i>trans</i> -1,2-(4-py) ₂ C ₂ H ₂	W(CO) ₃ Cp

For example, σ -bonded porphyrins with Rh, P, As, or Sb central ions undergo reversible oxidations and reductions at the π -conjugated macrocycle and there is little effect of the σ -bonded axial ligand on the porphyrin electrochemical behavior [12, 21]. However, derivatives with Al, Ga, In or Tl central metals all undergo a rapid cleavage of the metal-carbon bond after a one-electron oxidation of the compound. In contrast, the Fe, Ru, and Co σ -bonded metalloporphyrins (see further sections of the review) will undergo a metal-centered

oxidation followed by a migration of the axial ligand to one of the four nitrogens of the porphyrin macrocycle.

The σ -bonded Fe and Co complexes are generally unstable upon reduction at the metal center and this electrode reaction may be followed by a cleavage of the metal-carbon bond [12]. This is not the case for the osmium sigma-bonded complex (OEP)Os(Ph)₂, which undergoes both oxidations and reductions at the metal center without loss of the axial ligand [79].

1																	18
H	2																He
Li	Be																
Na	Mg																
K	Ca	Sc	Ti	V	Cr	Mn	Fe	Co	Ni	Cu	Zn	Ga	Ge	As	Se	Br	Kr
Rb	Sr	Y	Zr	Nb	Mo	Tc	Ru	Rh	Pd	Ag	Cd	In	Sn	Sb	Te	I	Xe
Cs	Ba	La	Hf	Ta	W	Re	Os	Ir	Pt	Au	Hg	Tl	Pb	Bi	Po	At	Rn
Fr	Ra	Ac															

Fig. 5 Periodic Table of sigma-bonded metalloporphyrins. All 27 shaded elements have been synthesized but only the 16 lightly shaded ones have been electrochemically investigated.

A significant number of nitrosyl metalloporphyrins has been synthesized over the past two decades [78, 80]. (see Periodic Table of nitrosyl porphyrins in Fig. 6) and the most well-characterized of these complexes have been those with Fe(II) [5, 66, 67, 71, 76, 77, 81–89] or Co(II) [27, 67, 70, 90–93] central metal ions.

Porphyrin-nitrosyl complexes with six other metal ions are also known, and all but one of which has been electrochemically investigated. These are: Ru [69, 73, 94–96], Os [5], Rh [97], Cr [98], Mo [99] and Mn [100]. Some nitrosyl metalloporphyrins can be reversibly reduced or oxidized by one or two electrons without loss of the NO ligand and this generally occurs when the electrode reactions involve the π -conjugated macrocycle; in the case of a metal-centered reduction or oxidation, however, the electron-transfer reactions will most often be accompanied by a loss of the NO ligand, resulting in an irreversible oxidation as shown in Fig. 7 for the case of (TPP)Cr(NO) and (TPP)Mn(NO) in CH_2Cl_2 .

In this regard, it should be noted that the loss of NO may be sufficiently slow so that the electrode reaction appears reversible on the cyclic voltammetry and/or thin-layer

timescales of 0.1 to 15 s but not on the bulk-electrolysis timescale, which could be as long as 20–30 minutes depending on the design of the utilized electrochemical cells. The stability of the metal-NO bond may be related to the site of electron addition or electron abstraction (ring, metal or NO axial ligand) but it may be also related to the nature of the electrochemical solvent (bonding *vs* nonbonding) that will compete with NO for an axial coordination position on the metal.

The actual site of electron transfer upon reduction or oxidation of porphyrins with bound NO groups has not been well established except for compounds with Fe(II) or Co(II) central metals, where an oxidation of the former complex involves the Fe(II)/Fe(III) redox couple and an oxidation of the latter involves electrogeneration of a Co(II) porphyrin π -cation radical [7].

Several types of metalloporphyrins with carbonyl ligands have been electrochemically investigated. The first is represented by (P)[Rh(CO)₂]₂ [101] and (P)[Ir(CO)₂]₂ [102] where P = TPP or OEP, but the ones most often studied for their electrochemistry have been the air-stable porphyrins with a single CO axial ligand such as (P)M^{II}(CO) and (P)M^{II}(CO)(L) where L is a

1																	18
H	2											13	14	15	16	17	He
Li	Be											B	C	N	O	F	Ne
Na	Mg	3	4	5	6	7	8	9	10	11	12	Al	Si	P	S	Cl	Ar
K	Ca	Sc	Ti	V	Cr	Mn	Fe	Co	Ni	Cu	Zn	Ga	Ge	As	Se	Br	Kr
Rb	Sr	Y	Zr	Nb	Mo	Tc	Ru	Rh	Pd	Ag	Cd	In	Sn	Sb	Te	I	Xe
Cs	Ba	La	Hf	Ta	W	Re	Os	Ir	Pt	Au	Hg	Tl	Pb	Bi	Po	At	Rn
Fr	Ra	Ac															

Fig. 6 Periodic Table of nitrosyl metalloporphyrins. All 9 shaded elements have been synthesized but only the 7 lightly shaded ones have been electrochemically investigated.

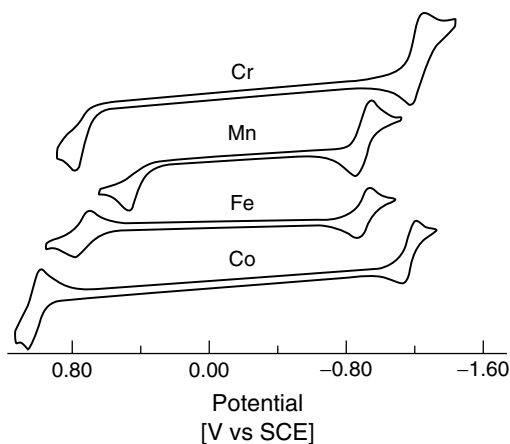


Fig. 7 Cyclic voltammograms of (TPP) $M^{II}(\text{NO})$ ($M = \text{Cr, Mn, Fe or Co}$) in CH_2Cl_2 containing 0.1 M TBAP. (Adapted from S. L. Kelly, D. Lançon, K. M. Kadish, *Inorg. Chem.* **1984**, 23, 1451–1458.)

nitrogenous base or solvent molecule and $M = \text{Ir}$ [103] or Ru [92, 104–113]. A third class of porphyrins with carbonyl ligands are those that coordinate CO molecules after *in situ* electrogeneration of the porphyrin in a specific metal oxidation state. Examples in this category include derivatives of $(\text{P})\text{Fe}^{II}(\text{CO})_x$ and $[(\text{P})\text{Co}^{III}(\text{CO})_x]^+$ where $x = 1$ or 2 [36, 114, 115].

The porphyrins with nonlabile CO axial ligands undergo almost exclusively macrocycle-centered reductions and oxidations, which is not the case when there is a metal-centered reaction as is observed for $(\text{P})\text{Fe}^{II}(\text{CO})_x$ and $[(\text{P})\text{Co}^{III}(\text{CO})_x]^+$. For instance, $\text{Fe}(\text{II})$ porphyrins coordinate one or two CO molecules, but no coordination

is seen for the $\text{Fe}(\text{III})$ and $\text{Fe}(\text{I})$ forms of the porphyrin. In a similar manner, $\text{Co}(\text{III})$ porphyrins coordinate either one or two CO ligands depending on the solution conditions, but neither the $\text{Co}(\text{II})$ nor $\text{Co}(\text{I})$ forms of the porphyrin bind CO. Thus, the $\text{Fe}(\text{II})$ and $\text{Co}(\text{III})$ porphyrin carbonyl complexes lose their axial CO molecules when converted electrochemically to another oxidation state.

Electrogenerated $\text{Ni}(\text{I})$ porphyrins have also been proposed to bind CO [116] but a stable product has never been isolated in the solid state.

Finally, it should be noted that $\text{Rh}(\text{II})$ porphyrins with PF_3 [117] or thiocarbonyl axial ligands [118] have also been

examined and the electrochemical data for these complexes have been compared to the results for related (P)Rh(CO) derivatives under similar experimental conditions.

6.4 Periodic Table of Metalloporphyrins

Most free-base porphyrins that have been investigated to date undergo two reversible one-electron oxidations and two reversible one-electron reductions, but in some cases the electrogeneration of a monoanion or dianion is also accompanied by addition of protons on the macrocycle [119, 120]. The electrochemistry of metalloporphyrins with metals from Group 1 through 15 of the Periodic Table has recently been reviewed [7], and only a brief summary of the most important results will be given in the present chapter.

6.4.1 Groups 1–4

No electrochemistry of Group 1 porphyrins has yet been reported in the literature. The Group 2 porphyrins usually exhibit electrode reactions that involve formation of π -cation radicals and dications upon oxidation and π -anion radicals and dianions upon reduction. However, in some cases the second reduction is shifted beyond the negative potential limit of the solvent, thus precluding observation of this reaction.

With the exception of the Sc(III) complexes, the electrochemistry of Group 3 metalloporphyrins is limited in large part to double- and triple-decker derivatives of the type (P)₂M, (P)(Pc)La and (P)La(Pc)M(P), where Pc represents a phthalocyanine and M = Gd(III), Y(III) or Lu(III) [121–126]. These species all

have a rich electrochemistry that was recently reviewed by Buchler and Ng [7]. The electrochemically examined mononuclear Sc(III) porphyrins are represented by (OEP)Sc(OH), which shows straightforward redox behavior involving the porphyrin macrocycle [52, 128].

The Group 4 porphyrins, represented by complexes with M = Ti, Zr, and Hf, have been studied in detail, but again, with the exception of the Ti complexes, most of these porphyrins exist as (P)₂M and (P)(Pc)M complexes, where P = OEP or TPP and M = Zr or Hf [127]. A number of Ti porphyrins with oxo, peroxy [129–132], halogen [133–134] or chalcogen [135–137] axial ligands have been synthesized and many of these compounds have been studied as to their electrochemical properties. The Ti porphyrins can exist with the metal ion in a +4, +3 or +2 oxidation state, and in most cases, other than for the titanyl porphyrins, the electrode reactions of these compounds are accompanied by chemical reactions involving a loss of the axial ligand [7].

The electrochemistry of (P)₂Zr involves the conjugated π -ring system. The two macrocycles interact with each other through the bridging Zr ion and the half-wave potentials for their oxidation and reduction occur at different half-wave potentials [7, 127], as is expected when a molecule contains two equivalent and interacting redox centers. The (P)₂Zr complexes should, in principle, show up to four reductions and four oxidations (assuming that the redox reactions of the two macrocycles occur at different half wave potentials as a result of the interacting equivalent redox centers), but fewer redox processes are actually observed within the potential window of the solvent/supporting electrolyte system, which

ranges in the most optimal of cases between +2.0 V and –2.0 V versus SCE in one or more solvents.

6.4.2

Groups 5 and 6

The most studied of the Group 5 porphyrins have been compounds with vanadyl and niobium metal ions; no electrochemical data have yet been reported for tantalum porphyrins. Vanadium porphyrins have been synthesized as both V(IV) and V(II) complexes. The vanadyl derivatives, represented as (P)VO, generally undergo well-defined reduction and oxidation reactions involving the porphyrin, macrocycle; the lower oxidation state V(II) complexes have been prepared as (P)V^{II}(L) and (P)V^{II}(L)₂ derivatives, where P = T(*p*-Me)PP or OEP and L = THF or PPhMe₂, but these species have not been examined as to their electrochemical properties [7].

The synthesis of several niobium porphyrins has been described in the literature, but the electrochemistry of these compounds is limited to mononuclear derivatives of (P)Nb^{VO}(O₂CMe) and (P)NbO, where P = OEP or TPP [138–140] and dinuclear derivatives of [(P)Nb]₂O₃ where P = T(*p*-CH₃)PP or OEP [141].

Porphyrins with all of the Group 6 metals have been investigated as to their electrochemistry, but most data have been obtained for the Cr and Mo complexes [7]. The only porphyrins with a tungsten metal ion whose electrochemistry has been reported are the oxo/hydroxo derivatives (P)WO(OH) [52, 142]. Both metal and ring-centered processes are observed upon reduction of these W(V) porphyrins, and a similar electrochemical behavior has generally been reported for most Cr(V)

and Mo(V) porphyrins having the same set of axial ligands.

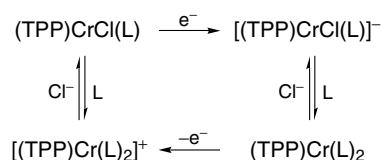
The earliest electrochemistry of chromium porphyrins involved Cr(III) derivatives with anionic axial ligands and/or coordinated nitrogeneous bases, but a number of studies have since been carried out with complexes having Cr(II), Cr(IV) or Cr(V) central metal ions. The latter series of compounds are exemplified by the oxo-Cr(IV), oxo-Cr(V), and nitrido-Cr(V) [143–147] derivatives. Cr(IV) μ -oxo dimers are also known [148, 149].

A one-electron oxidation of the oxo-Cr(IV) porphyrin will lead to an oxo-Cr(V) species, and this result contrasts with the nitridochromium(V) porphyrins [150], all of which exhibit only macrocycle-centered electron transfers upon oxidation.

Solvent effects on the redox potentials and electroreduction mechanisms of (TPP)CrCl have been discussed by Basolo and Hoffman [151, 152], as well as by Bottomley and Kadish [153]. The former research group demonstrated that (TPP)CrCl can readily coordinate with Lewis bases containing oxygen, sulfur or nitrogen donor atoms to form six-coordinate Cr(III) species of the type (TPP)CrCl(L), while the latter group indicated that the Cr(III)/Cr(II) process was accompanied by chemical reactions coupled with reversible electron transfers. The current-voltage curves led the authors to propose the electron-transfer mechanism shown in Sch. 1.

The redox reactions of (TPP)CrClO₄, (TPP)CrClO₄(L) and [(TPP)Cr(L)₂]⁺ were also investigated and correlations between $E_{1/2}$ for reduction of (TPP)CrClO₄ and the Gutman solvent donor number [154], as well as between $E_{1/2}$ for reduction of (TPP)CrClO₄ or (TPP)Cr^{II} and the solvent dielectric constant, were also examined [98].

Scheme 1 “Box mechanism” for the first reduction of (P)CrX(L), where X is a halide and L a solvent molecule or a nitrogeneous base.



Molybdenum porphyrins containing metal ions in +2, +4 or +5 oxidation states are known, but only the complexes with a +4 or +5 metal oxidation state have been investigated as to their electrochemical properties. Electrochemically examined porphyrins with Mo(IV) ions have been of the type (P)MoO(X), where X = F[−], Cl[−], Br[−], NCS[−], OH[−], OMe[−] or ClO₄[−] and P = OEP or TPP [155, 156], while the Mo(VI) porphyrins are represented by *bis*-peroxo complexes of the type (P)Mo(O₂)₂, where P = T(*p*-Me)PP, T(*m*-Me)PP and TPP [157]. The first type of molybdenum porphyrins have been shown to undergo only macrocycle-centered reductions, but both macrocycle- and metal-centered redox processes were reported for oxidation of the same compounds. Detailed electrochemical studies of oxomolybdenum(V) porphyrins have been reported in the literature [2, 7], and potentials of the Mo(V)/Mo(IV) couple were shown to vary with the nature of the anionic axial ligands on (P)MoO(X) as well as with the covalent character of the Mo^V-X bond. The *bis*-peroxomolybdenum(VI) porphyrins of the type (P)Mo(O₂)₂ were studied for their electrochemical properties in CH₂Cl₂ 0.1 M TBAP, and the compounds were shown to undergo one macrocycle-centered oxidation and two metal-centered reductions [157].

Cis-dioxomolybdenum(VI) porphyrins have also been examined after the addition or abstraction of electrons. The reduction [158] of (TPP)Mo(O)₂

yields (TPP)MoO, while oxidation of the compound [159] leads to [(TPP)MoO]⁺.

6.4.3

Group 7

The most extensively studied of the Group 7 porphyrins are the manganese complexes that can exist in up to four different oxidation states [23]. In fact, no electrochemistry of technetium porphyrins has yet been reported, and the electrochemistry of rhenium porphyrins has been limited to compounds of the type (P)HRe(CO)₃ and (P)[Re(CO)₃]₂ where P = TPP, TMTAA or TAA [160–162].

Although manganese porphyrins have been characterized as stable derivatives with metal oxidation states of +2, +3, +4 and +5, most electrochemistry has been carried out with the Mn(III) derivatives containing anionic axial ligands [7]. High valent porphyrins containing manganese with a +4 or +5 oxidation state have been described for their spectroscopic [23] and catalytic properties [24], but relatively little electrochemical data have been published due to the high reactivity of these compounds.

All Mn(III) porphyrins examined to date are easily reduced to their Mn(II) form, and this electrode reaction is usually followed at more negative potentials by the formation of a Mn(II) π -anion radical and dianion, the latter of which may or may not be observed depending on the cathodic potential window of the solvent and basicity of the porphyrin macrocycle. The Mn(III)

porphyrins can be oxidized at the metal center or at the porphyrin π -conjugated system with the exact site of electron transfer depending on the nature of the axial ligands. Either a Mn(IV) porphyrin or a Mn(III) porphyrin π -cation radical is generated in the first oxidation of the Mn(III) complex. The formation of an Mn(IV) porphyrin should be followed at more positive potentials by oxidation of the macrocycle to give a Mn(IV) porphyrin π -cation radical (assuming that the Mn(IV) form of the porphyrin does not react with the solvent or an added component), whereas the formation of a Mn(III) porphyrin π -cation radical is generally followed at more positive potentials by a second electron abstraction from the macrocycle to give a Mn(III) porphyrin dication.

The specific pathway by which a Mn(III) porphyrin is oxidized will depend on the type of macrocycle and the specific set of axial ligands. The site of electron transfer and the potentials for oxidation may also be a function of the porphyrin ring basicity or its planarity, the nature of the solvent, the type of counterion on Mn(III), and the basicity and/or steric effects of any bound axial ligands [7, 24]. A summary of the possible reactions that might occur are illustrated in Sch. 2.

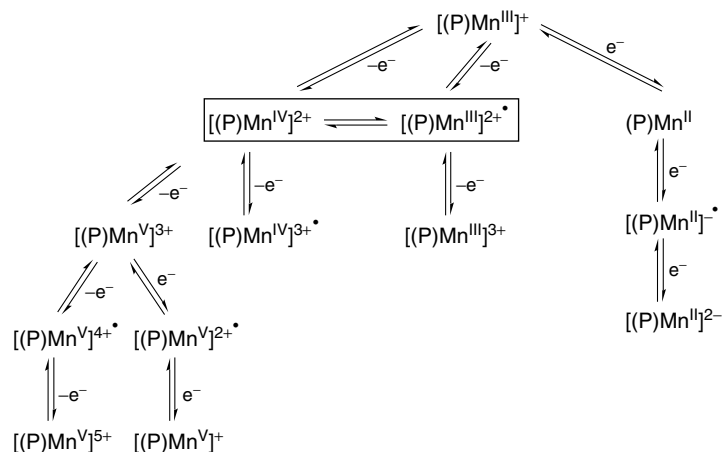
Five major types of manganese porphyrins have been electrochemically characterized to date. These are (1) (P)Mn^{III}X, where X is a halide ion or an anionic species such as C₂H₅O₂⁻, N₃⁻, OCN⁻, OH⁻ or SCN⁻, (2) (P)Mn^{III}(N₄CR) where N₄CR is a tetrazolato axial ligand [163], (3) (P)Mn^{II}(NO) [100], (4) oxo-Mn(IV) complexes, (P)Mn^{IV}O [23, 164, 165], and (5) bimetallic (P)Mn complexes with μ -nitrido bridges.

The first type of porphyrins have been characterized for their Mn(III)/Mn(II)

electrode reactions under a variety of different solution conditions [7, 21]. Early electrochemical studies by Boucher and Garber focused on $E_{1/2}$ values of the Mn(III)/Mn(II) reaction as a function of the porphyrin macrocycle [167], and this work was followed several years later by studies of electrochemical substituent effects on a series of (T(*p*-X)PP)MnCl complexes [166]. The effect of counterion [168] and the effect of solvent and/or supporting electrolyte [166] on the Mn(III)/Mn(II) reaction has also been reported. The Mn(II) porphyrins formed upon reduction of (P)Mn^{III}X are usually stable under a nitrogen atmosphere, but this may not be the case in the presence of oxygen that may bind to the metal center.

Manganese porphyrins containing non-planar macrocycles such as DPP and F_x DPP ($x = 4, 8, 20$ or 28), T(2,6-(OMe)₂, 3, 5-Cl₂)PP have been synthesized [169] and investigated electrochemically [170, 171], as have Mn(III) complexes with a positively charged macrocycle [53] such as in the case of [(TMpyP)MnCl]⁴⁺. The DPP derivatives show electrochemical behavior similar to manganese porphyrins with planar macrocycles (such as TPP), but the stability of the reduced and oxidized forms of the porphyrins as well as the potentials at which they are electrogenerated will vary with the type, number, and position of the added substituents.

Manganese porphyrins with a nitrosyl axial ligand have also been examined for their electrochemical properties. The oxidation of (TPP)Mn(NO) to its Mn(III) form is accompanied by a loss of the NO ligand (Fig. 7). However, the two reductions of the compound are reversible and stepwise generate a Mn(II) nitrosyl porphyrin π -anion radical and a nitrosyl porphyrin dianion at more negative potentials [100]. High valent manganese porphyrins have



Scheme 2 Electron-transfer reactions of manganese(III) porphyrins.

been used as oxidation catalysts [24, 172, 173], and studies [174] have focused on the formation of these species via an electrochemical oxidation of the Mn(III) complex. The substitution of Cl^- by OH^- as a counterion on the manganese porphyrin can lead to a Mn(IV) species as the singly oxidized product and a similar site of electron transfer may be seen upon oxidation of $(\text{P})\text{Mn}^{\text{III}}\text{Cl}$ complexes with specific types of porphyrin macrocycles (such as DPP or substituted DPP), or when the electrochemistry of the porphyrin is carried out at low temperature [174]. A Mn(IV) species has also been proposed for the singly electrooxidized product of the μ -nitrido dimer $(\text{TPP})\text{Mn-N-Fe}(\text{Pc})$ in CH_2Cl_2 [175].

6.4.4

Group 8

6.4.4.1 Ruthenium

The first ruthenium porphyrins studied were of the type $(\text{P})\text{Ru}^{\text{II}}(\text{CO})$. The electron-transfer mechanism for reduction and oxidation of these compounds has been examined under different solution conditions [104, 105], and the nature of the

singly reduced or singly oxidized product has been shown to depend on the solvent in which the electrochemistry was investigated. For example, a Ru(I) porphyrin was proposed as a reduction product of $(\text{OEP})\text{Ru}(\text{CO})$ in MeCN, PhCN or PrCN, but a Ru(II) porphyrin π -anion radical was generated upon reduction of the same compound in DMSO or Py [176]. Ruthenium porphyrins of the type $(\text{P})\text{Ru}(\text{L})$ or $(\text{P})\text{Ru}(\text{L})_2$, where L is a thioether, sulfoxide or benzoate axial ligand have also been examined for their electrochemical properties [177]. Those compounds usually undergo two one-electron oxidations and a single one-electron reduction. The first oxidation was proposed to be metal-centered, while the second oxidation was shown to involve the porphyrin macrocycle. A few examples of *trans*-dioxoruthenium(VI) porphyrins containing TMP, OEP, TPP, $\text{T}(p\text{-Cl})\text{PP}$, $\text{T}(p\text{-Me})\text{PP}$, or $(\text{T}(p\text{-OMe})\text{PP})$ macrocycles have been reported and studies of these compounds have shown that the compounds usually undergo one oxidation and one reduction [178, 179]. The oxidation was proposed to involve the porphyrin π -ring system while the reduction,

which was irreversible, was assigned as involving a conversion of Ru(VI) to Ru(V).

The electrochemistry of ruthenium porphyrins coordinated to small molecules, such as CS [118], PF₃ [117], NO [69, 72, 73, 96], or bound by a σ -bonded alkyl or aryl group [57, 180–182], has also been documented in the literature. The electroreduction of (T(*p*-Me)PP)Ru^{II}(CS)(L) where L = EtOH, CN, Im or Py has been studied in THF, DMF or Et₂Cl₂, and a mechanism involving a two-electron-transfer processes, accompanied by an uptake of protons, has been proposed by Latos-Grazynski and coworkers [118]. Kadish and coworkers [117] reported the electrochemistry of (P)Ru(PF₃), where P = TPP, T(*p*-Br)PP, T(*p*-Me)PP, T(*p*-Et)PP or OEP. The authors pointed out similarities between the electrochemistry of the CO and PF₃ derivatives in CH₂Cl₂, but differences in electrochemical behavior were observed in other nonaqueous solvents.

The electrochemistry of ruthenium nitrosyl porphyrins has been investigated by several research groups [69, 72, 73, 96]. The electrochemistry of sigma-bonded ruthenium(III) porphyrins [57, 180–182] parallels that reported for sigma-bonded iron(III) porphyrins [12]. A migration of the axial ligand follows the one-electron, or in some cases, two-electron oxidation of the sigma-bonded iron(III) complex [2, 12, 45, 56, 183, 184]; and a migration of the axial ligand from the metal of the singly oxidized porphyrin to one of the four nitrogens of the macrocycle has also been observed for σ -bonded Ru(III) porphyrins [12].

6.4.4.2 Osmium

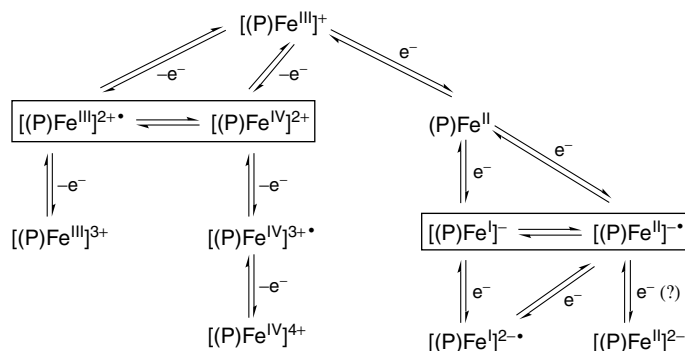
Osmium porphyrins can exist with the metal ion in one of several different oxidation states and derivatives of Os(II), Os(III), Os(IV), Os(V), or Os(VI) have

been studied for their electrochemical properties [7]. (OEP)Os^{II}(CO)(Py) can be converted to its Os(III) form upon an initial one-electron oxidation and to its Os(III) porphyrin π -cation radical form after the abstraction of a second electron at more positive potentials [110]. Osmium(III) derivatives can be reduced and oxidized at the metal center [5, 110, 185]. The first oxidation of Os(IV) porphyrins or the first reduction of Os(V) porphyrins of the type (P)Os(L)₂ where P = MPIXDME, TPP, OEP, T(*p*-OMe)PP, T(*p*-Me)PP, or T(*p*-Cl)PP and L = OEt[−], OMe[−], OiPr[−], OPh[−], SPh[−], SC₆F₄H[−], SC₆H₄Me[−], Br[−] or Ph are also metal-centered [79, 186]. A summary of the various redox mechanisms and half-wave potentials for selected redox reactions is given in the literature [7, 21].

6.4.4.3 Iron

The electrochemistry of iron porphyrins in nonaqueous media has been discussed in several reviews [2, 7, 10, 12], and only a few of the major trends of iron porphyrin electrochemistry will be summarized in the current paper. Both high and low oxidation states of the metal ion can be accessed upon reduction or oxidation of iron porphyrins and the overall electron-transfer mechanism of these metalloporphyrins is shown in Sch. 3, where [(P)Fe^{III}]⁺ represents the initial compound in the absence of an associated anionic ligand.

In general, most synthetic iron porphyrins are able to undergo three or four electron-transfer reactions in a variety of nonaqueous solvents, with the exact number of redox reactions depending on the type of porphyrin macrocycle, the type of axial ligands, and the solvent/supporting electrolyte mixture used



Scheme 3 Electron-transfer reactions of iron(III) porphyrins.

to make the electrochemical measurement. (TPP)FeX, where X is a halide ion, undergoes three well-defined reductions and two well-defined oxidations in most solvents [187], while (TPP)Fe(NO) [68] and (TPP)Fe(C₆H₅) [188] show two reductions and two oxidations, respectively. The electrode reactions of these compounds are generally all reversible and all involve either the conjugated macrocycle or the central metal ion to give porphyrins in Fe(IV), Fe(III), Fe(II) or Fe(I) oxidation states.

The type of axial ligand(s) coordinated to the iron center will determine not only the redox potentials, rates and mechanisms for electron transfer but will also strongly influence the oxidation state and spin state of the central iron ion and the associated chemistry of the neutral, electrooxidized, and electroreduced forms of the porphyrin. Virtually, all monomeric iron porphyrins with halide or perchlorate axial ligands contain Fe(III) in their air-stable form, but a conversion of Fe(III) to Fe(II) is readily accomplished at potentials generally located between +0.12 and -0.5 V vs SCE.

The Fe(III)/Fe(II) electrode reactions of synthetic (P)FeX complexes have been extensively investigated over the last 30 years and have been the subject of several detailed reviews [2, 7, 10]. The effect of

solvent and counterion on half-wave potentials of iron porphyrins was examined by several research groups between 1975 and 1981, but the most systematic study of how solvent and axially coordinated monovalent anions will affect the redox potentials was undertaken by Bottomley and Kadish, who characterized reductions of (TPP)FeX with five different anions in 12 different nonaqueous solvents [187]. The results of this study showed that the binding strength of the counterion to the Fe(III) porphyrin in CH₂Cl₂ increased in the order: ClO₄⁻ < Br⁻ < Cl⁻ < N₃⁻ < F⁻. A similar stabilization of Fe(III) over Fe(II) by the counteranion was also observed in PhCN and DMF, but the effect was less pronounced in the latter two solvents.

The half-wave potentials for the Fe(III)/Fe(II) reaction of (TPP)FeX varied little as a function of the counteranion in DMSO or Py, and this was accounted for by a displacement of the halide axial ligand by a bound solvent molecule leading to [(TPP)Fe^{III}(S)₂]⁺ and (TPP)Fe^{II}(S)₂ in solution, where S = DMSO or Py. The effect of solvation on the Fe(III)/Fe(II) reaction of (TPP)FeX was quantitated by Bottomley and Kadish who correlated *E*_{1/2} values for reduction with the Gutmann solvent donor number [187]. Half-wave potentials

for reduction of Fe(II) porphyrins are also relatively insensitive to the counterion on the Fe(III) form of the complex, with the only exceptions being compounds with $X = \text{OH}^-$ or OMe^- , where $E_{1/2}$ is shifted negatively (from compounds with Cl^- or ClO_4^- counterions) as a result of an enhanced stabilization of the Fe(II) form of the porphyrin, which maintains the anion as a bound axial ligand [189, 190].

Fe(III) and Fe(II) porphyrins may be four, five, or six coordinate in solution and will contain a high, intermediate or low-spin iron center depending on the type of axial ligand [80]. Most six-coordinate Fe(III) porphyrins with axially coordinated nitrogenous bases are low spin, whereas most six-coordinate Fe(III) porphyrins coordinated with oxygen donor ligands are high spin. A variety of electron-transfer mechanisms is possible upon conversion of the initial Fe(III) complex to its Fe(II) form, and selected examples that are most often observed are summarized in Sch. 4.

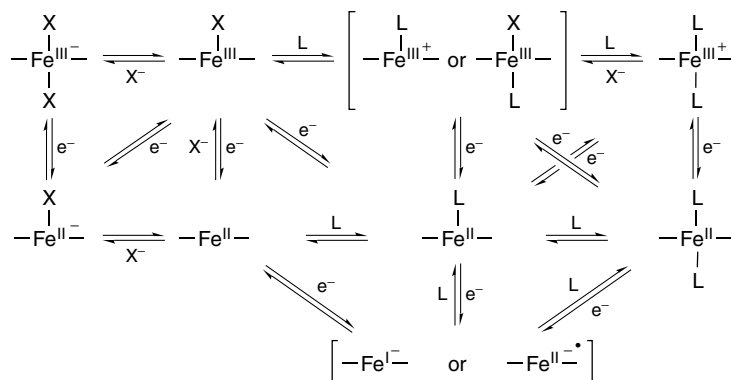
The relationship between ligand-binding strength of different nitrogenous bases to iron(II) or iron(III) porphyrins and $E_{1/2}$ for reduction of these compounds was reported in independent studies by Constant and Davis [191] and Kadish and Bottomley [192, 193]. Iron(II) complexes of the form $(\text{TPP})\text{Fe}(\text{L})_2$, where L was one of eleven different substituted Pys were electrochemically investigated by Bottomley and Kadish, who showed that $E_{1/2}$ for the Fe(II)/Fe(I) reaction was directly proportional to the aqueous $\text{p}K_a$ value of the Py ligand [192, 193]. The thermodynamics of ligand addition to Fe(II) porphyrins, as measured by electrochemical techniques, has also been reported [194, 195].

The effect of *ortho* phenyl substituents on the spectroscopic, redox properties and axial ligand binding constants for a series

of iron(III) substituted TPPs was examined by Walker and coworkers [196]. The authors concluded that the *ortho*-halogens or *ortho*- CF_3 groups were electron donating as a result of a direct overlap between the electron cloud of the substituents and the π system of the porphyrin. Several theoretical papers have discussed the influence of substituents at the *meta*, *para*, and *ortho* positions of the meso-phenyl groups on the ionization potentials of *ortho*, *meta*, and *para*-substituted TPPs [197–200]. Other studies have examined the electron-transfer rate constants of iron porphyrins and looked at relationships between rate constants and axial coordination [2, 10].

The effect of substituents on electron-transfer rate constants has also been reported [201], and a summary of these studies have been given in several reviews [2, 7, 10]. The previously open-to-question assignment of the Fe(II) reduction product as an Fe(I) species or an Fe(II) porphyrin π -anion radical [202] now seems definitive in many cases [203, 204], but the exact site of electron transfer will vary as a function of the solution conditions as well as the porphyrin macrocycle.

The reduction of Fe(II) porphyrins appeared from most early studies to be relatively insensitive to changes in solvent [187], and this was due to the weakly complexing nature of the Fe(II) form of the porphyrin with virtually all utilized electrochemical solvents except for Py. However, the complete lack of solvent binding by Fe(I) porphyrins was less than clear-cut and it is now known that some singly reduced iron(II) porphyrins can bind a Py molecule at low temperature under certain solution conditions [204]. Recent electrochemical studies on nonplanar iron(III) porphyrins of the type $(\text{F}_x\text{DPP})\text{FeCl}$ [203], where $x = 0, 12, 20, 28$ or 36 and $(\text{T}(\text{C}_3\text{F}_7)\text{P})\text{FeCl}$ or



Scheme 4 Electroreduction of iron(III) porphyrins in coordinating media.

($\text{T}(\text{C}_3\text{F}_7)\text{P})\text{Fe}(\text{py})_2$ [205], have revealed that the site of reduction in iron(II) porphyrins will depend not only on the specific porphyrin macrocycle but also on the type of axial ligation to iron(II).

Some iron(III) porphyrins can be oxidized at the metal center to give an iron(IV) species [23], while others are oxidized at the porphyrin π -conjugated system to produce an iron(III) porphyrin π -cation radical. Early studies involving solvent and/or counterion effects of iron porphyrins indicated that compounds of the type $(\text{P})\text{FeX}$, where $\text{P} = \text{OEP}$ or TPP , were oxidized at the porphyrin ring [187, 206, 207], and similar conclusions were also reached by the groups of Goff and Reed [208–211] on the basis of IR spectroscopy. Several iron(III) porphyrins bound to weak-field ligands, such as ClO_4^- , SO_3CF_3^- or $\text{C}(\text{CN})_3^-$, were also examined as to their electrochemical properties and both $(\text{TPP})\text{FeClO}_4$ and $(\text{TPP})\text{FeSO}_3\text{CF}_3$ were proposed to produce iron(III) porphyrin π -cation radicals upon oxidation [212].

Fuji examined a series of $(\text{P})\text{FeCl}$ complexes containing Cl groups at either the meso or the β -pyrrole positions of the macrocycle [213]. All of the compounds

were oxidized at the porphyrin macrocycle and $E_{1/2}$ values for these electrode reactions were located between 1.08 and 1.45 V, depending on the specific porphyrin macrocycle. The half-wave potentials were shifted toward more positive potentials with increase in the electron-withdrawing affinity of the substituents on the macrocycle, but the magnitude of the shift in $E_{1/2}$ was larger for those compounds that had substituents at the meso positions than for those that were substituted at the β -pyrrole positions of the macrocycle.

Most iron(III) porphyrins with axially bound halide groups such as Cl^- are initially oxidized at the porphyrin π -ring system, independent of the type of porphyrin macrocycle. However, a switch in the electron-transfer site from the ring to the metal may occur when iron(III) porphyrins are axially bound by hydroxy, methoxy, or σ -bonded groups such as C_6H_5 , or $\text{C}_6\text{F}_4\text{H}$ [7, 12].

The direct electrochemical oxidation of an iron(III) porphyrin to give an iron(IV) complex has been observed on a number of occasions, but the high oxidation state product is often quite reactive [23, 24, 26, 189, 214–218]. Thus, the oxidations

of (TMP)Fe(OH) and (TMP)Fe(OMe) are irreversible at room temperature (due to a chemical reaction involving the Fe(IV) species), but both oxidized products were formulated as Fe(IV) derivatives at low temperature [189, 214, 215, 217, 218]. The reaction was shown to involve an EC process in which the electrochemical step is the oxidation of the macrocycle and the chemical step the elimination of HClO₄ and the following rearrangement of the molecule to its oxo form (Sch. 5) [214].

Iron(IV) porphyrins can be generated upon oxidation of σ -bonded iron(III) porphyrins [7, 12, 62, 184, 188, 219] with the stability of the electrooxidized product, depending in large part on the porphyrin macrocycle and the type of σ -bonded axial ligand [12]. The chemical or electrochemical oxidation of a *bis*-fluoro Fe(III) complex, [(T(*p*, *m*-F₂)PP)Fe(F)₂][−], has been examined by Nanthakumar and Goff [220, 221] and the iron oxidation state was assigned as Fe(III) or Fe(IV), on the basis of NMR and UV-visible spectroscopy.

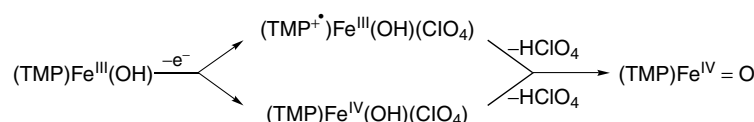
Kadish and coworkers examined the effect of porphyrin ring distortion on the redox potentials of (Br_{*x*} TPP)FeCl, where *x* varied from 0 to 8 [7, 29, 30]. The first reduction of the compounds varied linearly with the number of Br groups on the macrocycle, but not the first oxidation (Fig. 8).

A nonlinear relationship between *E*_{1/2} for oxidation of (Br_{*x*} TPP)FeCl and *x* was obtained and was interpreted in terms of two opposite effects; one was the electron-withdrawing effect of the Br substituents,

which stabilized the HOMO, and the other was the increased nonplanarity of the macrocycle, which resulted in a destabilization of the HOMO [29]. Similar effects of macrocycle distortion on the electrochemistry of other nonplanar porphyrins have been reported [7, 37, 42, 45, 170, 171, 184, 219, 222–225]. Several picket fence and basket-handle porphyrins have also been investigated for their electrochemical properties [226–236].

Several iron porphyrins bound to diatomic molecules, such as CO, NO, CS, CSe, and O₂, have also been examined as to their electrochemistry in nonaqueous media. Fe(II) porphyrins can coordinate CO to give *mono*- and *bis*-CO derivatives [237–239], and the electrooxidation of these species by cyclic voltammetry results in irreversible waves because of a rapid loss of CO upon formation of Fe(III) [7, 30, 240]. Studies of (TPP)FeCl and (TPP)FeClO₄ in Py and CH₂Cl₂/Py mixtures under a CO atmosphere indicated that the following five types of iron(II) porphyrins could be formed: (TPP)Fe, [(TPP)FeCl][−], [(TPP)Fe(CO)Cl][−], (TPP)Fe(py)₂, and (TPP)Fe(CO)(py), and that these could be electrochemically converted into two types of iron(I) porphyrins, namely [(TPP)Fe][−] and [(TPP)Fe(CO)(py)][−] [240].

Studies of (Br_{*x*} TPP)FeCl under a CO atmosphere revealed that the number of CO molecules bound to the iron(II) form of the porphyrin depends on the number of Br groups on the macrocycle [30]. Plots of *v*_{CO} vs *x* were constructed



Scheme 5 Electrooxidation of hydroxyiron(III) porphyrins.

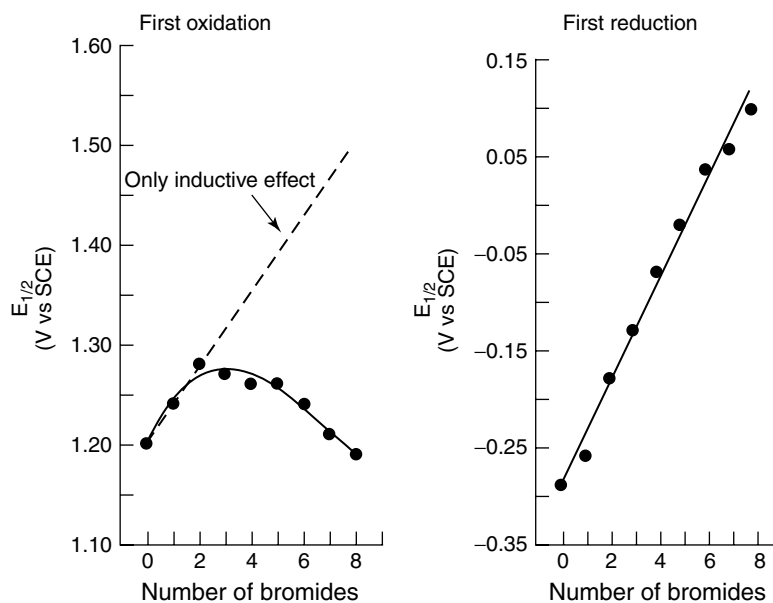


Fig. 8 Plot of $E_{1/2}$ versus number of Br groups on $(\text{Br}_x\text{TPP})\text{FeCl}$ in PhCN, 0.1 M TBAP. (Adapted from K. M. Kadish, F. D'Souza, A. Villard, M. Autret, E. Van Caemelbecke, P. Bianco, A. Antonini, P. Tagliatesta, *Inorg. Chem.* **1994**, 33, 5169, 5170.)

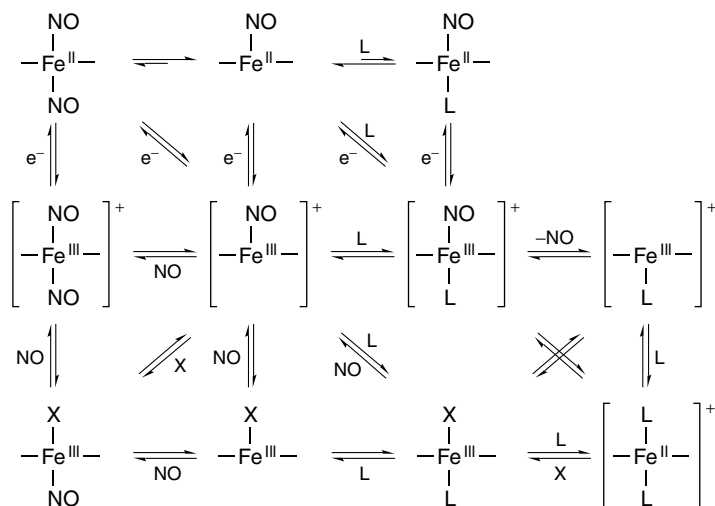
and the resulting nonlinear correlation interpreted in terms of two competing effects, one of which was the electron-withdrawing effect of the Br substituents, and the other the nonplanarity of the macrocycle [30].

Stable Fe(II) porphyrins complexed with NO have been characterized as $(\text{P})\text{Fe}(\text{NO})$, $(\text{P})\text{Fe}(\text{NO})_2$, and $(\text{P})\text{Fe}(\text{NO})(\text{L})$ [80], although the original formulation of $(\text{P})\text{Fe}(\text{NO})_2$ has now been called into question in favor of an $(\text{P})\text{Fe}(\text{NO})(\text{ONO})$ assignment [76, 77]. Lançon and Kadish investigated the electrochemistry of $(\text{P})\text{Fe}(\text{NO})$ and $(\text{P})\text{Fe}(\text{NO})(\text{L})$ in 10 different electrochemical solvents [68]. The electrooxidation of $(\text{P})\text{Fe}(\text{NO})$ reversibly leads to $[(\text{P})\text{Fe}(\text{NO})]^+$ in a nonbinding solvent, whereas the electroreduction reversibly leads to $[(\text{P})\text{Fe}(\text{NO})]^-$. The initial oxidation of $(\text{P})\text{Fe}(\text{NO})$ was proposed (on the

basis of IR and electron spin resonance (ESR) spectroscopy) to give the bis-nitrosyl complex $[(\text{P})\text{Fe}(\text{NO})_2]^+\text{ClO}_4^-$ under an NO atmosphere [83], but more recent studies by Lorkovic and Ford suggest the formation of $(\text{P})\text{Fe}(\text{NO})(\text{ONO})$ [76, 77]. Ryan and coworkers [66] reported that $(\text{P})\text{Fe}(\text{NO})$ ($\text{P} = \text{TPP}$ or OEP) undergoes three one-electron reductions in nonaqueous solvents and the products of the first two one-electron reductions were characterized by UV-visible spectroelectrochemistry.

A large number of redox processes may occur for iron nitrosyl complexes in binding solvents such as DMSO or Py, and examples of several pathways, which have been characterized or proposed are summarized in Sch. 6.

The reversible half-wave potentials for oxidation of iron(II) porphyrins bound to



Scheme 6 Electrooxidation of nitrosyl iron(II) porphyrins.

NO, CS, and CSe are shifted positively with respect to the values of $E_{1/2}$ for reduction of the same porphyrin in the absence of the axial ligand [241]. The product formed after electrochemical oxidation of (OEP)Fe(O₂) has been identified as an η_2 -dioxygen adduct [7]. Fe(II) porphyrins complexed by CS, CSe, and NO show no loss of the diatomic molecule upon oxidation. Six-coordinate (P)Fe(CS)(py) [242] and (P)Fe(CS)(py) [243] are reversibly oxidized by one electron at $E_{1/2} = 0.73$ and 0.70 V, respectively, in CH₂Cl₂, and these potentials may be compared to an $E_{1/2} = 0.52$ V for oxidation of (P)Fe(NO)(py) [71] under the same solution conditions.

Two iron porphyrins may be bridged through a single bridging atom X to form a binuclear metalloporphyrin of the type (P)Fe-X-Fe(P), and the electrochemistry of these compounds where X = O, N, or C has been recently reviewed [7]. The formal oxidation states of the two iron atoms are +3 for the μ -oxo complexes, +3.5 for the μ -nitrido compounds and

+4 for the μ -carbido derivatives, but none of these assignments is unambiguous, given the existing spectroscopic data. On the other hand, the electrooxidation of μ -oxo, μ -nitrido, and μ -carbido porphyrins is relatively straightforward, and with one exception [244], has been shown to occur in multiple reversible single-electron-transfer steps, in which each of the two porphyrin macrocycles is oxidized at a separate half-wave potential consistent with an interaction of the two macrocycles through the bridging ligand. The μ -oxo porphyrin dimer [(T(*p*-Et₂N)PP)Fe]₂O can be oxidized by a total of four electrons in CH₂Cl₂ [244]. Two one-electron oxidations of the compound occur at $E_{1/2} = 0.34$ and 0.47 V, while a subsequent two-electron oxidation step is seen at $E_{1/2} = 0.76$ V. The oxidation of one porphyrin macrocycle in [(P)Fe]₂O is more difficult than the oxidation of the other, and the difference in $E_{1/2}$ can be accounted for by an electrostatic interaction between the two electroactive sites of the molecule.

The μ -nitrido complex, $[(\text{TPP})\text{Fe}]_2\text{N}$, is stable in CH_2Cl_2 , benzonitrile or Py, and up to four electrons can be abstracted from the compound without a loss of the nitrido-bridged structure [245]. A nitrido-bridged $\text{Fe(IV)}\text{-Fe(IV)}$ dimer was proposed for the singly oxidized compound while the doubly oxidized product was described as a μ -nitrido $\text{Fe(IV)}\text{-Fe(IV)}$ π -cation radical.

$[(\text{TPP})\text{Fe}]_2\text{C}$ in CH_2Cl_2 can be oxidized by four electrons in four successive one-electron-transfer steps, but the number of oxidations varies with the nature of the nonaqueous solvent [246]. Neutral $[(\text{TPP})\text{Fe}]_2\text{C}$ was shown to contain two Fe(IV) units by Mössbauer spectroscopy [247], and the four redox processes of this porphyrin most likely correspond to a stepwise oxidation of the π -ring system to form initially two individual π -cation radicals (one on each macrocycle) and then two porphyrin dication at more positive potentials [246].

A comprehensive review of σ -bonded iron porphyrin electrochemistry has recently been published [12], and results on these compounds will not be discussed in the present paper. Several reviews have been published on the redox tuning of iron porphyrins over the last 20 years [2, 7, 10, 192] and this topic will also not be covered in the present paper. The exact potential for the $\text{Fe(III)}/\text{Fe(II)}$ reaction will depend on the type of axial ligand coordinated to the Fe(III) or Fe(II) forms of the porphyrin. Axial ligands such as NO, C_6H_5 and ClO_4^- will change drastically the potential at which the $\text{Fe(III)}/\text{Fe(II)}$ redox couple is observed, but shifts of $E_{1/2}$ for this redox reaction will occur upon solvent binding to the Fe(III) and/or Fe(II) form of the compound. The basicity of the porphyrin macrocycle will also influence $E_{1/2}$ for the $\text{Fe(II)}/\text{Fe(III)}$ electrode process.

The $\text{Fe(III)}/\text{Fe(II)}$ reactions are not the only porphyrin redox processes, which may be tuned by a change in the macrocycle, and half-wave potentials for the ring-centered redox reactions will also vary with the planarity of the macrocycle [42]. For example, $(\text{Et}_8\text{TPP})\text{FeCl}$, which has a nonplanar macrocycle [21], is oxidized to its Fe(III) π -cation radical form at $E_{1/2} = 0.66$ V [21], but the same electrode reactions of $(\text{TPP})\text{FeCl}$ and $(\text{OEP})\text{FeCl}$ (two porphyrins with planar macrocycles) occur at $E_{1/2} = 1.14$ and 1.08 V, respectively [21]. The $\text{Fe(III)}/\text{Fe(II)}$ reaction of $[(\text{P})\text{Fe}(\text{HIm})_2]^+\text{X}^-$ shifts in potential owing to hydrogen bonding of the bound imidazole, and several studies of these hydrogen binding interactions as they apply to redox potentials, have been reported in the literature [286–289].

6.4.4.3.1 Reaction of Heme-thiolate Proteins

In their resting states, the P450s and NOSs exist as a mixture of a hexacoordinated low-spin state Fe(III) species with a water molecule *trans*- to one proximal cysteinate ligand and a pentacoordinated high-spin state species with only cysteinate as an axial ligand [248]. The proteins can be reduced to their iron(II) states and transfer electrons to particular substrates as well as bind various ligands such as CO or O_2 . The binding of O_2 will yield an $\text{Fe(II)}\text{-O}_2$ species that is a very poor oxidizing agent, except toward particularly reactive substrates. The next step in the catalytic activation of the substrate by the P450s or NOS involves a one-electron reduction of the $\text{Fe(II)}\text{-O}_2$ species and the formation of several intermediates that are less well characterized [249]. The first product is a ferric peroxo complex of the type $\text{Fe(II)}\text{-O-O}^-$ that can be protonated to yield $\text{Fe(III)}\text{-O-OH}$. The last intermediate in the cycle is obtained via a heterolytic

cleavage of the O–O bond after protonation of the terminal O(H) atom and a loss of H₂O [250–252]. This high valent iron-oxo porphyrin has been described as an Fe(IV)=O porphyrin radical, an Fe(V)=O species or a Fe(IV)-O[•] species and should react with electron-rich centers of the substrate. All of the reactive states from Fe(II) to the high valent oxo species are involved in the catalytic cycle of substrate monooxygenation by the P450s and NOSs; their function in biological systems has recently been reviewed [248].

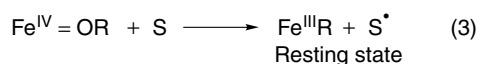
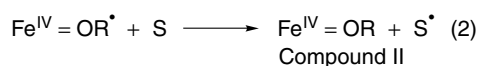
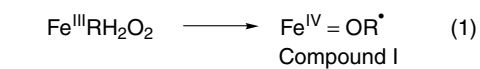
Heme-thiolate proteins have been reported to catalyze a large number of reactions, including diverse types of oxidations, reductions, isomerizations and dehydrations [248]. The nature and mechanism of these reactions have been discussed in detail [248], and the reactions have been shown to be associated with various reactive states under which the heme-thiolate protein can exist. The nature of the iron porphyrin intermediate in the protein that is involved in the activation of a substrate will depend on the reactivity of the substrate. It has recently been shown [253, 254] that in the mutant P450s, the ratio between different reactions that occur on the same substrate will be a function of the rates of proton delivery to the active site of P450, suggesting that the presence of distal amino acid residues also affects the rate of transformation of Fe(II)-O₂ to Fe(III)-OO⁻ and Fe(V)=O.

6.4.4.3.2 Mechanism of Electron-transfer in Peroxidases Peroxidases have been divided into three categories [255]. These are Class I, the intercellular peroxidases, Class II, the extracellular peroxidases and Class III, the well-known extracellular plant peroxidases. The peroxidases in Class I, II, and III differ in the number of disulfide bonds and bound calcium ions,

but all of the peroxidases use the catalytic cycle described in Sch. 7 [256].

The first step of the cycle [Sch. 7, (1)] involves the removal of two electrons from the protein, one coming from the metal ion and the other usually coming from the porphyrin moiety, which contains the iron [257]. The intermediate thus generated is known as Compound I. This species that contains two oxidizing equivalents of the protein can oxidize two substrate molecules. The first step, which is described in Eq. (2) of Sch. 7, involves formation of Compound II via reduction of the porphyrin π -cation radical, while the second step leads to the resting state of the protein via a reaction between Compound II and a second substrate molecule [Sch. 7, (3)]. Both Compounds I and II are sufficiently stable so that several spectral methods have been used to determine the electronic structure of these species [258–262]. Kinetic studies for formation of these compounds have also been carried out [263–269]. The rate-limiting step under steady state conditions is most often the reduction of Compound II [266–271], a result that is accounted for by an easier reduction of the porphyrin radical as compared with the Fe(IV) center in Compound II. Traditional substrates for peroxidases are phenols and other aromatic dyes, although in cytochrome c peroxidase the substrate is ferro-cytochrome c [272, 273].

Electron transfer between the porphyrin radical and the substrate is readily achieved, while the aromatic substrate is unable to transfer directly an electron to the iron because of steric hindrance within the active site pocket, thus slowing down the third electrode reaction described in Sch. 7. Further details on the electron-transfer reactions of peroxidases, including cytochrome and

Scheme 7 Mechanism of electron-transfer in Peroxidases.

their enzyme-substrate complexes, have been reported in a recent review [256].

involve a switch in the nature of the axial ligand.

6.4.4.3.3 Reactions of Nitrite Reductions

Two major pathways have been shown to exist in nitrite reduction [274]. In the first pathway, nitrite is reduced to NO, while in the second there is a direct conversion of nitrite to NH₃ or NH₄⁺. Two classes of nitrite reductase (NIR), namely the cytochromes cd [274], and the copper nitrite reductase [274], have been identified for the first pathway and two classes of enzyme, namely the siroheme nitrite reductase and cytochrome c nitrite reductase, have been proposed to follow the second pathway. The mechanism of these four enzymes has been recently reviewed [274], and only a brief summary of the electron-transfer reactions of cytochrome cd nitrite reductase will be given here. The initial step in the conversion of NO₂ to NO involves a binding of the nitrite ion to the metal of the reduced heme. This first step is followed by the uptake of two protons and the loss of one water molecule to yield an electrophilic ferrous Fe²⁺-NO⁺ species, also formulated as a Fe³⁺-NO[•] complex. The dissociation of NO from this species produces the ferric heme d, which is in turn reduced back to its original state by heme c. Why the enzyme does not reduce the nitrosyl species, Fe^{II}-NO⁺ or Fe^{III}-NO to its Fe^{II}-NO form, prior to dissociation of NO in the heme, has been discussed in the literature [274], and may

6.4.4.3.4 Reactions of Nitric Oxide Reductases

The bacterial nitric oxide reductase (NOR) is able to reduce NO to N₂O during bacterial denitrification [275–278]. A review on the topic has recently been published [274] and only the electron-transfer mechanism of the enzyme is discussed in the present review.

NOR has been suggested to contain a heme c and two heme b groups [279–285], so that this type of enzyme has been defined as a cytochrome cbb_{NO} complex with the heme b_{NO} at a binuclear catalytic site along with a nonheme iron [276]. It has been proposed [281], by similarities between NOR and the family of cytochrome oxidase, that the catalytic site for NO binding and activation is the dinuclear high spin heme b and the nonheme containing iron (III), and that low-spin hemes are used as electron sinks.

In the first step of the reaction, two electrons from two low-spin hemes are provided to the catalytic site, and the reduction of both the heme b and the nonheme Fe is accompanied by a release of a water molecule [274]. In the next step, two molecules of NO and one proton are added to the active site to yield two Fe^{II}-NO complexes, one from the heme b and the other from the nonheme. In the last step of the mechanism, one molecule of N₂O is produced by the active site. The first

step in the catalytic cycle is also proposed to be accompanied by axial ligation of the proximal histidine to the Fe(III) form of the heme b, but this ceases when NO coordinates to the Fe^{II} center of heme b.

6.4.5

Group 9

Iridium porphyrins have been the least-studied among the Group 9 metalloporphyrins. Only a few types of iridium porphyrins have been investigated for their electrochemical properties, including (P)Ir(CO)Cl [102], (P)Ir(CO)₃ [103] and [(P)IrCl₂]dppe [290], where P = OEP or TPP. Metal-centered and ring-centered processes are observed for (P)Ir(CO)₃ [102], while (P)Ir(CO)Cl and [(P)IrCl₂]dppe are characterized by only macrocycle-centered processes.

A number of studies have been carried out on the air-stable Rh(III) porphyrins represented by (P)Rh(R), (P)RhX and (P)RhX(L), where R is an alkyl group, X a halide ion, and L a nitrogenous base [183, 291–301]. A few air-stable monomeric Rh porphyrins of the type (P)Rh(NO) and (P)Rh(NO)₂ have also been electrochemically characterized [298].

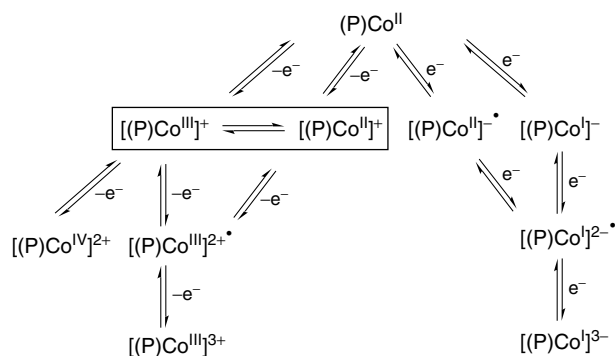
The electrooxidation of Rh(III) porphyrins is relatively straightforward and consists for the most part of two successive one-electron transfers, both of which involve the porphyrin π -ring system. An assignment of the electron-transfer site has often been made on the basis of ESR and/or UV-visible spectra of the singly oxidized products. Other types of rhodium porphyrins, which have been electrochemically examined include [(TPP)Rh(L)₂]⁺Cl[−] and (TPP)Rh(L)Cl, where L = NMe₂, both of which were proposed to form a dimeric Rh(II) species after an initial one-electron

reduction at the Rh(III) center [295]. However, more recent studies by the group of Savéant [300, 301] suggested that the reaction proceeds via a more complicated multielectron transfer and conversion to [(P)Rh^I][−].

(TPP)Rh(COMe) was shown to undergo two one-electron reductions, the first of which was proposed to be macrocycle-centered on the basis of UV-visible data [296]. (TPP)Rh(O₂) also exhibits two reductions with the product depending on the type of utilized solvent [302]. A Rh(II) porphyrin dimer was electrogenerated in PhCN or THF, but a σ -bonded product, (P)Rh^{III}(CH₂Cl), was formed in CH₂Cl₂.

Cobalt porphyrins have been by far the most well-studied of the Group 9 porphyrins. The electrochemistry of cobalt porphyrins is characterized by both metal- and ring-centered electrode processes. The most often characterized metal-centered processes have been the Co(III)/Co(II) and Co(II)/Co(I) transitions, which occur at potentials easily accessible in most nonaqueous electrochemical solvents. The two ring-centered redox processes are only observed for easily reducible complexes (usually those with multiple electron-withdrawing groups on the macrocycle, such as in the case of CN₄TPP or Br₈TPP) and involve the conversion of a Co(I) porphyrin to its Co(I) π -anion radical form followed at more negative potentials by a conversion of the Co(I) π -anion radical to its dianionic form. Oxidation of the Co(III) complexes will give a Co(III) porphyrin π -cation radical and then a dication at more positive potentials. A summary of these electrode processes is shown in Sch. 8.

As shown in Sch. 8, the oxidation of cobalt(II) porphyrins can also proceed via the initial formation of a Co(II) π -cation radical (as opposed to a Co(III) species), and this has been shown to



Scheme 8 Electron-transfer reactions of cobalt(II) porphyrins.

occur for (TPP)Co in dry noncoordinating solvents. An oxidation of the sigma-bonded (P)Co^{III}(R) complexes to their Co(IV) form has also been proposed for derivatives containing an alkyl axial ligand [303].

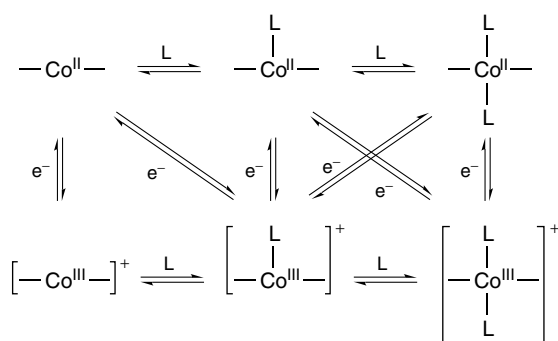
Cobalt porphyrins with several types of macrocycle have been electrochemically investigated, but the most often and most well-studied of the cobalt porphyrins has been (TPP)Co, which was initially characterized in the mid-1960s [51, 304] and has since been cited and reexamined in literally hundreds of publications over the next three decades [7, 21]. A large number of electrochemical studies have focused on the effect of solvent, axial ligation, and supporting electrolyte or counterion on the redox reactions of (P)Co and (P)CoCl. Sch. 9 summarizes several possible electron-transfer pathways, which can occur for the Co(II)/Co(III) transition.

Cobalt(II) porphyrins can be tetra-, penta- or hexacoordinated, while the Co(III) complexes are generally 5- or 6-coordinate, depending on the solution conditions. Basolo and coworkers showed that the potential for oxidation for a Co(II) porphyrin or related macrocycle could be related linearly to the base strength of the bound axial ligand [305, 306], and a similar relationship has been observed between

$E_{1/2}$ for the Co(II)/Co(III) reaction of the complex and the coordinating ability of the aprotic solvent in which the electrochemistry was carried out [2, 307, 308]. Oxidation potentials of Co(II) porphyrins also depend on the type and concentration of the supporting electrolyte, with the most difficult oxidations occurring in solutions of TBABF₄ and the easiest in solutions of TBACl [307, 309, 310].

(TPP)Co in a low dielectric constant such as toluene or benzene [311] undergoes two one-electron reductions and only two oxidations are seen as opposed to three in most other solvents. The first oxidation under these conditions involves the simultaneous abstraction of two electrons from (TPP)Co to give [(TPP)Co]²⁺, while the first reduction leads to a stable Co(I) complex formulated as [(TPP)Co]⁻. Other studies relating to the effect of counterion and solvent binding on the (P)CoX electrochemistry [310] have been discussed in a recent review [7].

The type of porphyrin macrocycle will influence both the half-wave potentials and the overall redox behavior of cobalt porphyrins [34, 55, 308, 312–314]. Porphyrins with macrocycles, which vary substantially in basicity and planarity have been studied, including T(*p*-X)PP, (CN)_x TPP, Br_x TPP,



Scheme 9 Electrooxidation of cobalt(II) porphyrins in coordinating media.

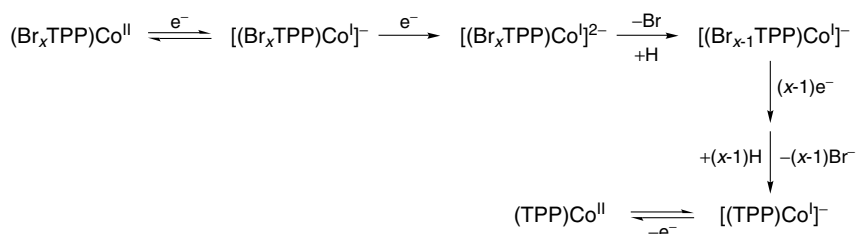
TMpyP, and TMP (see Table 3 for macrocycle abbreviations and Fig. 3 for structures of selected macrocycles).

The Co(III)/Co(II) and Co(II)/Co(I) reactions of (T(*p*-X)PP)Co were investigated in butyronitrile, and plots of $E_{1/2}$ for these two electrode reactions versus 4σ (the substituent constant) gave linear relationships with slopes of 0.034 and 0.041 V, respectively [308]. The electron-withdrawing effect of substituents on $E_{1/2}$ was also evaluated for ((CN) $_x$ TPP)Co [312, 313], where $x = 1$ to 4 and the largest effect was seen for ((CN) $_4$ TPP)Co, where the first reduction was 0.55 V more positive than the analogous metal-centered reduction of (TPP)Co [313]. The electrochemical and spectroelectrochemical properties of ((CN) $_4$ TPP)Co were investigated in several different nonaqueous solvents [313], and three well-defined one-electron reductions were generally observed within the potential range of each solvent. The first

one-electron reduction was proposed to occur at the porphyrin π -ring system [313] (as opposed to the metal center that occurs for the case of (TPP)Co), while the second and third one-electron reductions were proposed to involve the stepwise formation of a Co(I) π -anion radical followed by a Co(I) dianion at more negative potentials.

(Br $_x$ TPP)Co complexes with $x = 0$ to 8 were shown to undergo three one-electron oxidations and up to nine one-electron reductions in PhCN containing TBAP as supporting electrolyte [34]. The conversion of the compounds to their cobalt(I) forms was reversible, but the second electron addition, which should produce the cobalt(I) π -anion radical form of these compounds, was shown to be coupled with a stepwise elimination of Br groups as shown in Sch. 10.

Araullo-McAdams and Kadish investigated the electrochemistry of [(TMpyP)



Scheme 10 Electroreduction of (Br $_x$ TPP)Co^{II}.

$\text{Co}^{\text{II}}]^{4+}$ (see Fig. 3 for structure of the TMpyP macrocycle) in DMF, DMSO, and Py [55]. A single oxidation and up to four reductions were observed; some reactions were shown to be metal-centered and involved only a single electron, while others were centered at the porphyrin π -conjugated system or the four 1-methyl-4-pyridyl substituents and involved two electrons.

One important characteristic of cobalt porphyrins is their ability to bind or react with small molecules, such as NO [27, 67, 70, 91, 93, 100], CO [36, 114, 115], O_2 [314–320], or CO_2 [321], and several studies have focused on the chemical and/or electrochemical reactivity of (P)Co toward these small molecules. The interaction of cobalt porphyrins with NO and the electrochemical properties of the resulting cobalt-nitrosyl porphyrins have been investigated by several research groups [7]. (TPP)Co(NO) exhibits two oxidations and three reductions at a micro-electrode in CH_2Cl_2 [90]. The NO group remains coordinated after electrooxidation and the initial electron abstraction from (TPP)Co(NO) was proposed to involve the porphyrin π -ring system. Other electrode reactions were accompanied by a dissociation of NO from the compound and the site of electron transfer could not be determined.

(OEP)Co(NO) was shown by Fajer and coworkers to be oxidized to its π -cation radical form without a loss of NO [67] and the oxidized product was assigned as an a_{2u} type radical on the basis of IR spectroscopy [70]. The electrochemistry of (P)Co(NO) has been reported in several coordinating media and these results have been discussed in a recent review [7]. Derivatives of (T(*p*-X)PP)Co(NO) have also been electrochemically investigated [70, 93] and an

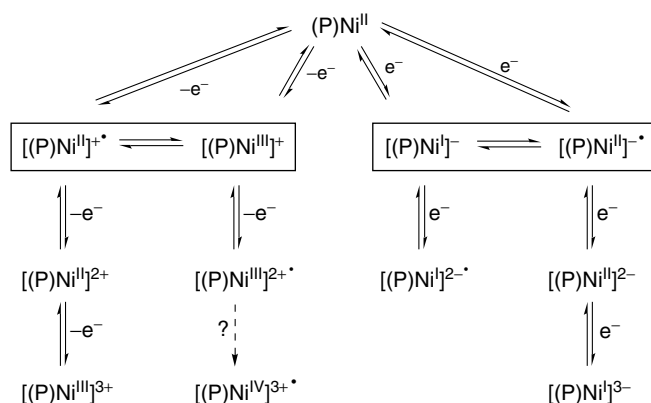
electron-transfer mechanism similar to that of (TPP)Co(NO) [91] or (OEP)Co(NO) was observed. (TPPBr₄NO₂)Co(NO) was also electrochemically investigated [27] and showed what was proposed to be a transient Co(I)-nitrosyl complex.

The electrochemistry of cobalt porphyrins has been examined under both CO [36, 114, 115] and O_2 atmospheres. The studies under O_2 were to examine the application of cobalt porphyrins as electrocatalysts for the four-electron reduction of O_2 to H_2O [314, 316, 317, 322]. The oxidation of (P)Co under a CO atmosphere has been reported for P = TPP [115], OEP [114] and Br_{*x*}TPP (*x* = 0 to 8) [29]. (OEP)Co is converted to [(OEP)Co^{III}(CO)]⁺ in CH_2Cl_2 under CO [114] and these results contrast with what was observed for oxidation of the same compound under N_2 , where a Co(II) porphyrin π -cation radical was proposed as the singly oxidized product. The electrooxidation of (Br_{*x*}TPP)Co under CO leads to both *mono* and *bis*-CO complexes in solution with the ratio of *mono*/*bis* adducts depending on the number of Br groups on the porphyrin macrocycle [29].

6.4.6 Group 10

Very little electrochemistry has been published on Pt or Pd porphyrins. In contrast, the electrochemistry of nickel porphyrins with numerous different macrocycles has been reported in the literature and the most commonly observed electron-transfer mechanisms that occur upon reduction or oxidation of the Ni(II) derivatives are shown in Sch. 11.

The air-stable form of the neutral porphyrins contain Ni(II). In some cases, derivatives with Ni(I) or Ni(III) central metal ions can be electrogenerated, but in others only Ni(II) π -cation radicals and



Scheme 11 Electron-transfer reactions of nickel(II) porphyrins.

dications or Ni(II) π -anion radicals and dianions are observed as electron-transfer products [116, 323–326]. The exact site of electron transfer will depend in part on the specific porphyrin macrocycle, in part on the presence or absence of any coordinated axial ligands, in part on the properties of the solvent and in part on the type of supporting electrolyte as well as on the temperature of the measurement [7].

Some nickel(II) porphyrins are converted to a Ni(II) porphyrin π -dication in two well-separated one-electron-transfer steps [7], while other Ni(II) porphyrins exhibit two, closely spaced and often overlapped one-electron-transfer steps upon oxidation [7]. The occurrence or absence of overlapped one-electron oxidations will depend on both the solution conditions and the type of porphyrin macrocycle, but in most cases the final oxidation product can be described as a $[(P)Ni^{III}]^{3+}$ species.

Nickel porphyrins with Me_8TPP , TC_6TPP , Et_8TPP or DPP macrocycles (see macrocycle abbreviations in Table 2) have all been examined for their electrochemical behavior [7, 21] and, in

agreement with theoretical calculations, the nonplanar nickel porphyrins are usually easier to oxidize than the complexes with a planar macrocycle [42]. The electrochemistry of $[(TMpyP)Ni]^{4+}$ in DMF differs significantly from the other nickel(II) porphyrins, in that both the neutral and reduced forms of the compound have been shown to exist in a monomer-dimer equilibrium [327]. The two electron oxidation product of $(TpivPP)Ni$ was proposed to contain a Ni(IV) π -cation radical [328], but a later study by Savéant and coworkers suggested an oxidation of the picket fence [234].

Both low and high oxidation states of nickel porphyrins are easily accessible in many nonaqueous solvents and the exact site of electron transfer (metal vs ring) upon reduction or oxidation has been the topic of numerous studies [7]. Bocian and coworkers [325], as well as Connich and Macor [326], showed that a Ni(II) porphyrin π -cation radical can be converted to a Ni(III) porphyrin in binding solvents such as Py, THF or MeCN. The type of Ni(II) porphyrin π -cation radical, that is, a_{1u} or a_{2u} , will depend on the type of porphyrin macrocycle and a Ni(II) π -cation

radical with a mixed a_{1u} and a_{2u} character has been described in the literature [329].

The electroreduction of Ni(II) porphyrins and related macrocycles was investigated by the groups of Stolzenberg [330–332], Fajer [333], Kadish [116, 323, 328, 334, 335], Savéant [324] and more recently, by Fajer, Mansuy and coworkers [336], who showed that the very electron-deficient $((NO_2)_7T(oxo-Cl_2)PP)Ni$ was reduced in three reversible one-electron reductions. Earlier work had shown that Ni(II) chlorins or isobacteriochlorins could be reduced to their Ni(I) state [330, 331, 333], as opposed to porphyrins, where a Ni(II) porphyrin π -anion radicals was generally formed upon reduction [7]. However, the singly reduced products of Ni(II) porphyrins have been described as Ni(I) porphyrins, Ni(II) porphyrin π -anion radicals or Ni(II) porphyrin π -anion radicals with some Ni(I) character [116]. The exact site of electron transfer and formulation of the reduction product will depend on several factors, two of which include the solution conditions and the nature of the porphyrin macrocycle [7].

Several fluorine-substituted (DPP)Ni derivatives (see Fig. 9) have also been investigated as to their electrochemical properties in nonaqueous solvents and a summary of the data has been discussed in a recent review that compared the electrochemical behavior of planar and nonplanar Ni(II) porphyrins [7].

Nickel porphyrins with nonplanar macrocycles had a smaller to slightly smaller HOMO-LUMO gap than nickel porphyrins with planar macrocycles (such as TPP), but the difference in HOMO-LUMO gap on going from a planar to a nonplanar macrocycle varies with the type of substituents on the nonplanar macrocycle. For example, the HOMO-LUMO gap of $(Et_8F_{20}TPP)Ni$ is 60 mV smaller than that of (TPP)Ni, but

the HOMO-LUMO gap of $(Br_8F_{20}TPP)Ni$ is 410 mV smaller than that of (TPP)Ni [7]. The absolute potential separation between the first and second oxidations of the substituted (DPP)Ni derivatives increases on changing the supporting electrolyte from TBAP to TBAPF₆ [7]. This result can be accounted for by a stronger axial binding of ClO_4^- over PF_6^- to $[(P)Ni]^+$, along with a larger binding constant of ClO_4^- to doubly oxidized $[(P)Ni]^{2+}$ as compared with singly oxidized $[(P)Ni]^+$.

6.4.7

Group 11

Copper and silver porphyrins exist as stable M(II) complexes, while gold porphyrins contain a M(III) metal oxidation state in their air-stable form. The Ag(II) porphyrins can be oxidized to their Ag(III) form before formation of a π -cation radical and dication at more positive potentials [337, 338]. Reduction of these compounds involves formation of a Ag(I) porphyrin, followed by electrogeneration of a π -anion radical and dianion at more negative potentials [337]. However, the latter two ring-centered processes are most often not observed because of demetalation of the electrogenerated Ag(I) porphyrin [339–341].

The electrochemistry of $(P)Cu^{II}$ involves macrocycle-centered electrode reactions in nonaqueous media, although a $Cu(II)/Cu(I)$ reaction has been proposed for a few complexes, most notably $((CN)_4TPP)Cu$ [342] and $(N-CH_3TPP)CuCl$ [343]. The electrochemical generation of a Cu(I) porphyrin in the case of $((CN)_4TPP)Cu$ occurs only after formation of the dianionic form of the complex [342].

Several Cu(II) porphyrins with nonplanar macrocycles have been examined for their electrochemical properties, one

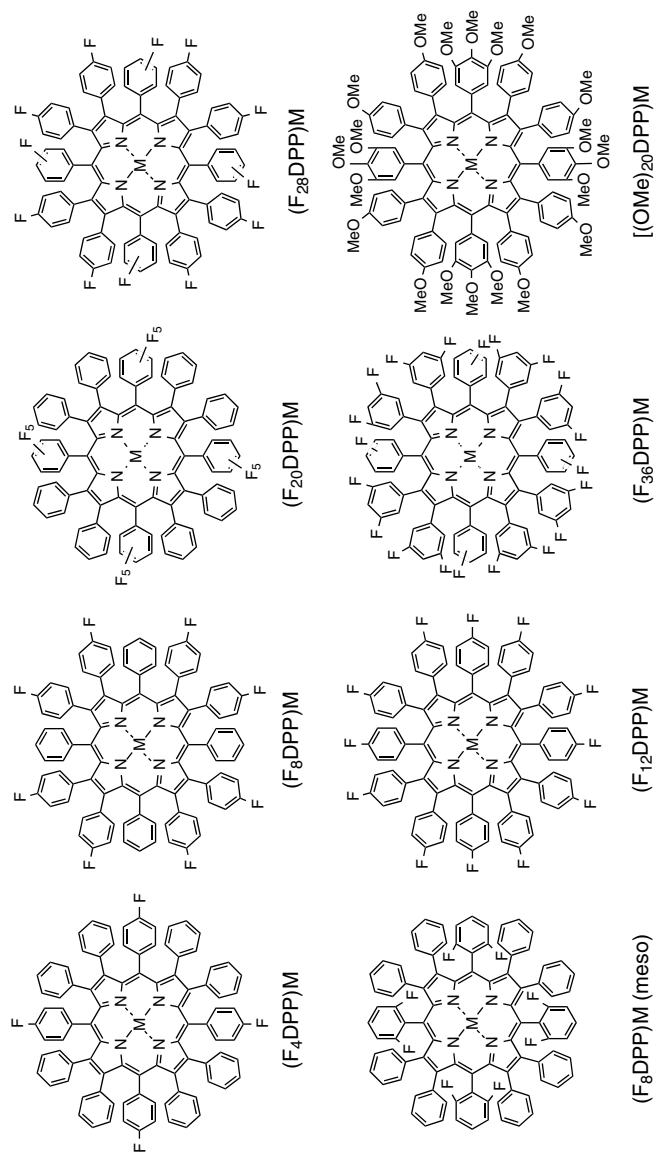


Fig. 9 Structures of fluorinated substituted DPP.

of which is (Et₈TPP)Cu, which exhibits two reversible one-electron oxidations in nonaqueous media [344, 345]; the singly oxidized product, [(Et₈TPP)Cu]⁺, was formulated as an a_{2u} porphyrin π -cation radical on the basis of its IR spectrum [344] and this formulation was also confirmed by resonance Raman studies [345]. Another nonplanar porphyrin, (DPP)Cu, was shown to undergo two successive ring-centered one-electron reductions and two successive ring-centered one-electron oxidations [346]. Both oxidations of the compound were easier (occurred at more negative potentials) than the respective oxidations of (TPP)Cu and this result was accounted for by a destabilization of the HOMO owing to the nonplanarity of the macrocycle.

The electrochemistry of gold porphyrins has been limited to [(TPP)Au]⁺AuCl₄⁻, MPIX dimethylester, and Etio Au(II) complexes [347a]. The compounds were oxidized via a single one-electron-transfer step to their π -cation radical form and were reduced by three steps, the first of which was proposed to generate an Au(III) π -anion radical. However, more recent studies by the groups of Kadish, Fukuzumi and Crossley show the unambiguous formation of a Au(II) porphyrin in the first electron addition [347b].

6.4.8

Group 12

The electrochemistry of zinc, cadmium, and mercury porphyrins is uncomplicated and only macrocycle-centered electrode reactions are observed in nonaqueous solvents [7, 21]. Metalloporphyrins with this type of metal ion have been studied in some detail, but the best characterization of the electrochemical reaction products has been obtained with zinc porphyrins

whose site of electron transfer is very well defined [2, 7]. In fact, (P)Zn complexes have been used as standard for comparison with other oxidized or reduced metalloporphyrins, especially the iron(III) porphyrins that can undergo either metal- or ring-centered electrode processes [7].

Most electrochemical studies on zinc porphyrins have involved planar compounds such as (OEP)Zn or (TPP)Zn, but some electrochemical data on nonplanar zinc porphyrins such as (X₈F₂₀TPP)Zn, where X = F [32], Br [44], Cl [44] or Me [44] have also been published. The first and second oxidations of (TPP)Zn and (OEP)Zn are well separated in potentials in most nonaqueous solvents, and both [(TPP)Zn]⁺ and [(OEP)Zn]⁺ have been examined by ESR spectroscopy [348–350]. A dimerization of [(OEP)Zn]⁺ was proposed [348, 349], but no evidence of dimer formation was found in the case of [(TPP)Zn]⁺ or other [(P)Zn]⁺ complexes.

The oxidative behavior of (TPP)Zn has been examined in the presence of nitrogenous bases by Kadish and coworkers [351, 352], and an electrochemical study of (TPP)Zn and [(TPP)Zn(L)]⁺ yielded the first quantitative measurements of nitrogenous base addition to porphyrin π -cation radicals.

Only a few nonplanar zinc porphyrins have been electrochemically examined [7, 21]. The electrochemical behavior of these compounds resemble that of the planar compounds in that two ring-centered one-electron reductions and two ring-centered one-electron oxidations are obtained. However, in the case of (X₈F₂₀TPP)Zn, (X = Cl, Br, Me) [44] the two oxidations of the nonplanar compounds are overlapped in potential giving what appears to be a single two-electron-transfer process.

6.4.9

Group 13

The first electrochemistry of metalloporphyrins with a Group 13 metal ion involved OEP derivatives of the type (OEP)M(OH), where M = Al, Ga, In or Tl [52]. These studies were later followed by an electrochemical characterization of (P)MCl, (P)MClO₄, (P)Tl(O₂CCF₃), and (P)M(R), where P = OEP or TPP [7, 353–356].

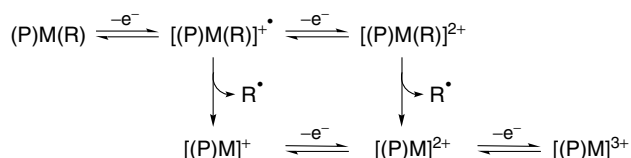
Four classes of Group 13 metalloporphyrins have thus far been characterized for their electrochemical properties in nonaqueous media. These include (1) compounds with anionic axial ligands, represented as (P)MX, where X is usually a halide or ClO₄[−], (2) compounds with carbon sigma-bonded ligands, represented as (P)M(R), where R is an alkyl or an aryl group [12], (3) metal–metal bonded complexes of the type (P)MM'(L), where M is the metal ion within the porphyrin and M'(L) the metalate axial ligand represented in some cases by Re(CO)₅, Mn(CO)₅ or Fe(CO)₄ and in others by M'(CO)₃Cp where M' = Cr, Mo or W [13], (4) compounds with a tetrazolato or a triazolato axial ligand represented as (P)In(N₄CR) and (P)In(N₃CR) [357, 358].

The porphyrins in groups (1) and (2) above have been characterized with Al(III), Ga(III), In(III), and Tl(III) metal ions, while those in groups (3) are limited to compounds with In(III) and Tl(III) metal ions. The triazolato and tetrazolato

compounds have been mainly those with In(III) metal ions [358, 359]. The electrochemistry of metal–metal bonded [13] and Group 13 sigma-bonded [12] porphyrins has been discussed in a recent review and the present chapter will only summarize the most important electrochemical behavior of the compounds.

The Group 13 porphyrins usually show similar electrochemical behavior upon going down the Periodic Table, although differences do exist in the stability of the oxidized and reduced forms of the compounds upon going from Al(III) to Tl(III). All complexes of the type (P)MX, where M = Al(III) [360], Ga(III) [355], In(III) [356], or Tl(III) [353], and P = TPP or OEP are oxidized at the porphyrin macrocycle to give π -cation radicals and dication, and all but those in the thallium series [353] are converted to their π -anion radicals and dianions upon reduction. The Tl(III) complexes undergo what appears in many cases to be a metal-centered two-electron reduction prior to demetallation [339].

The σ -bonded porphyrins of the type (P)M(R) are characterized by two reversible macrocycle-centered reductions for compounds with M = Al, Ga, In, or Tl central ions, but as shown in Sch. 12, the oxidation pathway and stability of the electrogenerated species will depend on both the specific metal ion and the type of σ -bonded axial ligand. Further details for the electrochemistry of these compounds



Scheme 12 Electrooxidation of (P)M(R), where R is an alkyl or aryl group and M is an element from Group 13 of the Periodic Table.

and other types of porphyrins with Group 13 metal ions have been discussed in a recent review [12].

6.4.10

Group 14

Most electrochemical data on Group 14 metalloporphyrins involves compounds with Ge(IV) [58, 64, 361, 362], Sn(IV) [363–365] or Sn(II) [366] metal ions and only a few examples of Si(IV) [59] and Pb(II) [367] porphyrin electrochemistry have been reported.

The characterized Si complexes are represented as (P)Si(R)₂, (P)Si(R)X, and (P)SiX₂, where P = TPP, OEP or T(*p*-Me)PP, R = Ph or Me and X = OH[−], ClO₄[−], F[−], Cl[−] or O₃SCF₃[−], while the electrochemistry of Pb porphyrins has most often been described for (OEP)Pb^{II} [52, 367] and (TPP)Pb^{II} [52, 59, 368, 369].

The electroreduction of Si porphyrins involves reactions at the π -ring system [51, 304]. Si porphyrins with an OEP macrocycle have been shown to undergo one or more coupled chemical reactions following electrooxidation [59], while Si porphyrins with a TPP or substituted TPP macrocycle exhibit two reversible one-electron oxidations centered at the conjugated macrocycle [368].

A number of Ge(IV), Sn(II) and Sn(IV) porphyrins has been investigated for their electrochemical properties. The Ge porphyrins are represented as (P)Ge(R)₂ and (P)Ge(R)X [58], where P = TPP or OEP, R = Me, CH₂C₆H₅ or C₆H₅ and X = Cl[−], OH[−] or ClO₄[−]. The Sn(II) porphyrins [365, 366] are represented as (P)Sn, where P = OEP, T(*p*-Me)PP, T(*m*-Me)PP or TMP, while the Sn(IV) porphyrins are represented as (P)Sn(L), where P = TPP, T(*m*-Me)PP, T(*p*-Me)PP or OEP

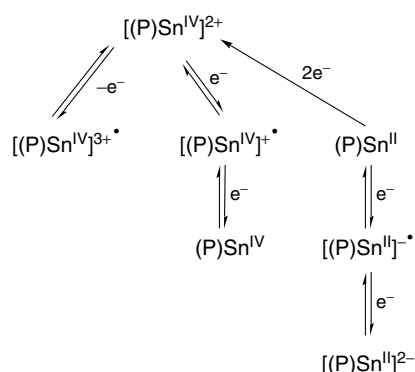
and L = S^{2−} or Se^{2−} or (P)SnX₂, where P = T(*p*-Me)PP or T(*m*-Me)PP and L = ClO₄[−], Br[−], Cl[−], F[−] or OH[−]. A few Sn(IV) porphyrins with carbon σ -bonded axial ligands have also been examined for their electrochemistry [365] and these are of the type (P)SnMeI, where P = OEP, T(*p*-Me)PP, T(*m*-Me)PP or TMP.

The electrochemistry of (P)Ge(R)₂ and (P)Ge(R)X are characterized by one or two reversible single-electron additions leading to porphyrin π -anion radicals and dianions. The compounds also undergo two oxidations, the first of which is always reversible in the case of the (P)Ge(R)₂ complexes [58]. A rapid cleavage of the Ge-carbon bond was proposed to follow electron transfer and the final product of the oxidation was formulated as (P)Ge(R)(ClO₄) [58].

The mechanism for electroreduction of (P)GeX₂ was shown to depend on the type of bound anion [362]. (P)Ge(OH)₂ is reduced in two successive reversible one-electron transfers involving the porphyrin π -ring system and a similar site of electron transfer was proposed for the electroreduction of (P)Ge(ClO₄)₂; the reduced ClO₄[−] complex is unstable and reacts with water in the solvent or water molecules bound to the compound to give (P)Ge(OH)(ClO₄) during the timescale of the measurement.

(P)Sn^{II} can be converted electrochemically to [(P)Sn^{IV}]²⁺, but the reduction of Sn(IV) to Sn(II) has not been observed, and the overall electrochemical behavior of the monomeric species [(P)Sn^{IV}]²⁺ occurs as shown in Sch. 13 [366].

The reduction of Sn(IV) porphyrins occur at the π -ring system and are usually reversible, while the oxidation usually involve the axial ligand and are irreversible on the cyclic voltammetry timescale. For example, (P)SnS [363], (P)SnSe [363] and (P)SnFe(CO)₄ [370, 371], where P =



Scheme 13 Electron-transfer reactions of tin(IV) porphyrins.

TPP, T(*m*-Me)PP, T(*p*-Me)PP or OEP all undergo two reversible one-electron reductions centered at the porphyrin macrocycle, but only a single irreversible oxidation [363, 372]. In each case, the irreversibility of the oxidation was accounted for by a cleavage of the tin-axial ligand bond following electron transfer.

The electrochemical properties of Sn(II) porphyrins in coordinating media have been discussed in a recent review [7]. The compounds were proposed to undergo two reversible one-electron macrocycle-centered reductions and an irreversible transfer of two electrons upon oxidation. The oxidation yielded ultimately a product formulated as $[(P)Sn^{IV}(X)S]^+$, where $S = py$, THF or PhCN and $X = PF_6^-$ or ClO_4^- .

6.4.11

Group 15

Most examined Group 15 porphyrins contain a M(V) ion, but derivatives with a +3 metal ion are also known and conversion between the M(V) and M(III) form of the porphyrin via a stable or transient M(IV) species has been reported in the literature [373–375]. The P(V), As(V), and Sb(V) porphyrins can be divided into three groups according to the nature of their axial ligands [7]. One group contains

two σ -bonded axial ligands (such as CH_3 or C_6H_5), another contains two anionic axial ligands (such as Cl^- , OH^- or OMe^-), and the third contains one σ -bonded axial ligand and one anionic axial ligand. The M(V) porphyrins contain an overall charge of +1 in their $[(P)M(R)_2]^+$, $[(P)M(R)(X)]^+$ or $[(P)M(X)_2]^+$ oxidation states, and thus each complex must be associated with another anion in the solid state or in solution [7].

The majority of electrochemical data for Group 15 porphyrins has been for compounds with a phosphorus [376–380] or antimony [373] ion. The electrochemistry of arsenic [381] and bismuth [382] porphyrins is limited to $[(OEP)As(R)(R')]^+$, $[(OEP)As(R)(X)]^+$ and $[(OEP)As(X)(X')]^+$ (R and R' are sigma-bonded ligands, X and X' are anionic axial ligands) in the arsenic series and $(P)Bi(X)$, where $P = TPP$, TMP , $T(p\text{-Me})PP$ or OEP and $X = NO_3^-$ or $SO_3CF_3^-$ for the bismuth porphyrins.

The As(V) complexes undergo two oxidations and two reductions, all of which initially occur at the porphyrin π -ring system [7]. An additional electrode process is seen for $[(OEP)As(F)_2]^+PF_6^-$, which is associated with reduction of an As(III) porphyrin species formed in solution after generation of the As(V) porphyrin dianion.

The bismuth porphyrins studied by the groups of Kadish and Guillard undergo two macrocycle-centered oxidations, and unlike what is observed for the other Group 15 porphyrins, none of the bismuth porphyrins shows evidence for conversion from the M(III) to the M(V) form of the complex. The authors pointed out that the oxidation potentials of (P)Bi(SO₃CF₃) were rather insensitive to the type of porphyrin macrocycle.

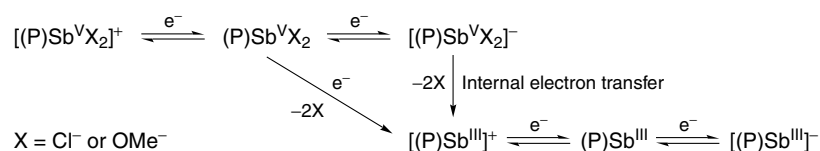
The electrochemically examined phosphorus porphyrins are represented by [(P)P^V(L)₂]⁺X[−], where P = TPP, OEP or T(*p*-Me)PP; L = OH[−], OR[−] or Cl[−] and X[−] = Cl[−] or OH[−], while the antimony porphyrins, which have been studied for their electrochemical properties are (OEP)Sb and (OEP)SbClO₄ for derivatives with a Sb(III) ion and are represented by (P)Sb(X)(X'), (P)Sb(R)(R') and (P)Sb(R)(X), where P = TPP, OEP or T(*p*-Me)PP, R or R' is a sigma-bonded ligand such as CH₃ and X or X' is an anionic axial ligand such as OH[−], OMe[−], Cl[−] or F[−] for those porphyrins that contain a Sb(V) central ion.

Earlier electrochemical investigations of [(TPP)P(Cl)₂]⁺Cl[−] showed that the compound could be reduced in two one-electron-transfer steps, both of which occur at the porphyrin π -ring system. The reduced products were relatively unstable and a mechanism involving an internal electron transfer between the π -ring system and the central ion was suggested to account for the electrochemical behavior of this compound as well

as those of the type (P)P(X)₂, where X = OMe[−] or Cl[−]. The electrochemistry of [(P)P(OR)₂]⁺OH[−], where OR[−] is a phenoxide or substituted phenoxide anion, was characterized by two successive one-electron-transfer steps centered at the porphyrin macrocycle [383].

Antimony porphyrins have been prepared with central ions in both +5 and +3 oxidation states, but most electrochemical data on these compounds have been obtained for derivatives containing Sb(V). The Sb(V) porphyrins are all extremely easy to reduce with the first reduction occurring at $E_{1/2} = -0.26$ V for [(TPP)Sb(Cl)₂]⁺ and at -0.42 V for [(TPP)Sb(OMe)₂]⁺. The mechanism for electroreduction of Sb(V) porphyrins has been discussed [7] for compounds of the type [(T(*p*-Me)PP)Sb(X)₂]⁺Cl[−], where X = OMe[−] or Cl[−]. Each compound undergoes two one-electron reductions on the cyclic voltammetry timescale to give porphyrin π -anion radicals and dianions, but the stability of the electroreduced products varies with the nature of the axial ligand [373, 374]. The compounds with X = OMe[−] were relatively stable after reduction, but the compounds with X = Cl[−] were shown to undergo a series of chemical reactions following electron transfer. The ultimate stable porphyrin product of the reduction was proposed to contain a Sb(III) ion. The electroreduction mechanism of [(P)Sb(X)₂]⁺ is illustrated in Sch. 14.

As shown in this scheme, the internal charge transfer from the porphyrin ring to



Scheme 14 Electroreduction of [(P)Sb^VX₂]⁺ where X = Cl[−] or OMe[−].

the central Sb ion occurs after reduction of the compounds by one or two electrons and is accompanied in each case by a loss of the two axial ligands.

A few antimony(V) porphyrins with one of two sigma-bonded ligands (CH_3 or C_2H_5) have been electrochemically investigated. The compounds are usually extremely stable and are characterized by facile reductions coupled with chemical reactions involving a loss of the axial ligands. The $[(\text{P})\text{Sb}(\text{Me})(\text{X})]^+$ complexes undergo one reversible oxidation within the positive potential limit of the solvent, and $E_{1/2}$ for these reactions were found to be directly related to the strength of the axial ligand *trans*- to the Me group [373].

6.5

Concluding Statement

The present review describes the electrochemistry of synthetic metalloporphyrins in nonaqueous media. This work does not include metalloporphyrin electrochemistry in aqueous media and discusses only briefly the electrochemistry of some iron porphyrins in real biological systems. We have not included the electrochemistry of porphyrin-like complexes such as metallocorroles, metalloporphycenes and metallochlorins, or the electrochemistry of pigments of biological relevance, such as vitamin B12 derivatives. For a coverage of these topics, the reader is referred to recent major reviews in *The Porphyrin Handbook*.

Acknowledgments

K. M. K. acknowledges support of the Robert A. Welch foundation for continuous support of his research on porphyrin electrochemistry over the last 25 years under Grant E-680.

References

1. K. M. Kadish, R. Smith, Guillard, *The Porphyrin Handbook*, Academic Press, San Diego, 2000, Vol. 1–10.
2. K. M. Kadish, *Prog. Inorg. Chem.* **1986**, *34*, 435–605.
3. K. M. Kadish in *Redox Mechanisms and Interfacial Properties of Molecules of Biological Importance*, (Eds.: G. Dryhurst, K. Niki), Plenum Press, New York, NY, 1988, pp. 27–45.
4. K. M. Kadish, R. Guillard, *Chem. Rev.* **1988**, *88*, 1121–1146.
5. J. W. Buchler, W. Kokisch, P. D. Smith, *Struct. Bonding* **1978**, *34*, 79.
6. D. G. Davis in *The Porphyrins*, (Ed.: D. Dolphin), Academic Press, New York, 1978, Vol. 5.
7. K. M. Kadish, E. Van Caemelbecke, G. Royal, Electrochemistry of Metalloporphyrins in Nonaqueous Media, in *The Porphyrin Handbook*, (Eds.: K. M. Kadish, K. Smith, R. Guillard), Academic Press, San Diego, 2000, pp. 1–114, Vol. 8.
8. J.-H. Fuhrhop in *Porphyrins and Metalloporphyrins*, (Ed.: K. Smith), Elsevier, New York, 1975.
9. R. H. Felton in *The Porphyrins*, (Ed.: D. Dolphin), Academic Press, New York, 1978, Vol. 3.
10. K. M. Kadish in *Iron Porphyrins*, (Eds.: A. B. P. Lever, H. B. Gray), Addison Wesley, Reading, 1983, pp. 161–249, Vol. 2.
11. R. Guillard, C. Lecomte, K. M. Kadish, *Struct. Bonding* **1987**, *64*, 205–268.
12. R. Guillard, E. Van Caemelbecke, A. Tabard, K. M. Kadish, Synthesis, Spectroscopy and Electrochemical Properties of Porphyrins with Metal-Carbon Bonds, in *The Porphyrin Handbook*, (Eds.: K. M. Kadish, K. Smith, R. Guillard), Academic Press, San Diego, 2000, pp. 295–345, Vol. 3.
13. J.-M. Barbe, R. Guillard, Synthesis, Spectroscopic and Structural Studies of Metal-Metal-bonded Metalloporphyrins, in *The Porphyrin Handbook*, (Eds.: K. M. Kadish, K. Smith, R. Guillard), Academic Press, San Diego, 2000, pp. 211–244, Vol. 3.
14. J. E. Falk, *Porphyrins and Metalloporphyrins*, Elsevier Publishing, New York, 1964.
15. R. S. Nicholson, I. Shain, *Anal. Chem.* **1964**, *36*, 706.
16. R. S. Nicholson, *Anal. Chem.* **1965**, *37*, 1351.

17. C. K. Mann in *Electroanalytical Chemistry*, (Ed.: A. J. Bard), Marcel Dekker, New York, 1969, Vol. 3.
18. C. K. Mann, R. K. Barnes, *Electrochemical Reactions in Nonaqueous Systems*, Marcel Dekker, New York, 1970, Vol. 3.
19. D. T. Sawyer, J. L. Roberts, *Experimental Electrochemistry for Chemists*, John Wiley & Sons, New York, 1974.
20. D. T. Sawyer, A. Sobkowiak, J. L. Roberts, *Electrochemistry For Chemists*, 2nd ed., John Wiley & Sons, New York, 1995.
21. K. M. Kadish, E. Van Caemelbecke, G. Royal, Metalloporphyrins in Nonaqueous Media: Database of Redox Potentials, in *The Porphyrin Handbook*, (Eds.: K. M. Kadish, K. Smith, R. Guilard), Academic Press, San Diego, 2000, pp. 1–219, Vol. 9.
22. K. M. Kadish, R. Guilard, *Comments Inorg. Chem.* **1988**, 7, 287–305.
23. R. Weiss, A. Gold, A. X. Trautwein, J. Turner, High-Valent Iron and Manganese Complexes of Porphyrins and Related Macrocycles, in *The Porphyrin Handbook*, (Eds.: K. M. Kadish, K. Smith, R. Guilard), Academic Press, San Diego, 2000.
24. B. Meunier, A. Robert, G. Pratviel, J. Bernadou, Metalloporphyrins in Catalytic Oxidations and Oxidative DNA Cleavage, in *The Porphyrin Handbook*, (Eds.: K. M. Kadish, K. Smith, R. Guilard), Academic Press, San Diego, 2000, pp. 121–187, Vol. 4.
25. K. S. Suslick, Shape-selective Oxidation by Metalloporphyrins, in *The Porphyrin Handbook*, (Eds.: K. M. Kadish, K. Smith, R. Guilard), Academic Press, San Diego, 2000, pp. 41–63, Vol. 3.
26. J. T. Groves, K. Shalyaev, J. Lee, Oxometalloporphyrins in Oxidative Catalysis, in *The Porphyrin Handbook*, (Eds.: K. M. Kadish, K. Smith, R. Guilard), Academic Press, San Diego, 2000, pp. 17–40, Vol. 3.
27. K. M. Kadish, Z. Ou, X. Tan, T. Boschi, D. Monti, V. Fares, P. Tagliatesta, *J. Chem. Soc., Dalton Trans.* **1999**, 10, 1595–1602.
28. P. Ochsenbein, K. Ayougou, D. Mandon, J. Fischer, R. Weiss, R. N. Austin, K. Jayaraj, A. Gold, J. Turner, J. Fajer, *Angew. Chem., Int. Ed. Engl.* **1994**, 33, 348–350.
29. K. M. Kadish, F. D'Souza, A. Villard, M. Autret, E. Van Caemelbecke, P. Bianco, A. Antonini, P. Tagliatesta, *Inorg. Chem.* **1994**, 33, 5169, 5170.
30. P. Tagliatesta, J. Li, M. Autret, E. Van Caemelbecke, A. Villard, F. D'Souza, K. M. Kadish, *Inorg. Chem.* **1996**, 35, 5570–5576.
31. T. Wijesekera, D. Dupre, M. S. R. Cader, D. Dolphin, *Bull. Soc. Chim. Fr.* **1996**, 133, 765–775.
32. E. K. Woller, S. G. DiMagno, *J. Org. Chem.* **1997**, 62, 1588–1593.
33. M. Autret, Z. P. Ou, A. Antonini, T. Boschi, P. Tagliatesta, K. M. Kadish, *J. Chem. Soc., Dalton Trans.* **1996**, 2793–2797.
34. F. D'Souza, A. Villard, E. Van Caemelbecke, M. Franzen, T. Boschi, P. Tagliatesta, K. M. Kadish, *Inorg. Chem.* **1993**, 32, 4042–4048.
35. F. D'Souza, M. E. Zandler, P. Tagliatesta, Z. Ou, J. Shao, E. Van Caemelbecke, K. M. Kadish, *Inorg. Chem.* **1998**, 37, 4567–4572.
36. K. M. Kadish, J. Li, E. Van Caemelbecke, Z. P. Ou, N. Guo, M. Autret, F. D'Souza, P. Tagliatesta, *Inorg. Chem.* **1997**, 36, 6292–6298.
37. M. W. Grinstaff, M. G. Hill, E. R. Birnbaum, W. P. Schaefer, J. A. Labinger, H. B. Gray, *Inorg. Chem.* **1995**, 34, 4896–4902.
38. G. Hariprasad, S. Dahal, B. G. Maiya, *J. Chem. Soc., Dalton Trans.* **1996**, 3429–3436.
39. J. G. Goll, K. T. Moore, A. Ghosh, M. J. Therien, *J. Am. Chem. Soc.* **1996**, 118, 8344–8354.
40. M. Ravikanth, D. Reddy, A. Misra, T. K. Chandrashekar, *J. Chem. Soc., Dalton Trans.* **1993**, 1137–1141.
41. D. Reddy, M. Ravikanth, T. K. Chandrashekar, *J. Chem. Soc., Dalton Trans.* **1993**, 3575–3580.
42. M. Senge, Highly Substituted Porphyrins, in *The Porphyrin Handbook*, (Eds.: K. M. Kadish, K. Smith, R. Guilard), Academic Press, San Diego, 2000, pp. 240–347, Vol. 1.
43. J. A. Schelnutt, X.-Z. Song, J.-G. Ma, S.-L. Jia, W. Jentzen, C. J. Medforth, *Chem. Soc. Rev.* **1998**, 27, 31–41.
44. J. A. Hodge, M. G. Hill, H. B. Gray, *Inorg. Chem.* **1995**, 34, 809–812.
45. K. M. Kadish, E. Van Caemelbecke, F. D'Souza, C. J. Medforth, K. M. Smith, A. Tabard, R. Guilard, *Inorg. Chem.* **1995**, 34, 2984–2989.
46. D. Gust, Intermolecular Photoinduced Electron-Reactions of Metalloporphyrins, in *The Porphyrin Handbook*, (Eds.: K. M. Kadish,

- K. Smith, R. Guilard), Academic Press, San Diego, 2000, pp. 153–205, Vol. 8.
47. J. W. Buchler in *Porphyrins and Metalloporphyrins*, (Ed.: K. Smith), Elsevier, New York, 1975.
48. J. A. Shelnutt, X.-Z. Song, J.-G. Ma, S.-L. Jia, W. Jentzen, C. J. Medford, *Chem. Rev.* **1998**, 27, 31–41.
49. D. D. Perrin, W. L. F. Armarego, D. R. Perrin, *Purification of Laboratory Chemicals*, Pergamon Press, New York, 1980.
50. J. F. Coetzee, *Recommended Methods for Purification of Solvents and Tests for Impurities*, Pergamon Press, New York, 1982.
51. R. H. Felton, H. Linschitz, *J. Am. Chem. Soc.* **1966**, 88, 1113–1116.
52. J.-H. Fuhrhop, K. M. Kadish, D. G. Davis, *J. Am. Chem. Soc.* **1973**, 95, 5140–5147.
53. E. Van Caemelbecke, W. Kutner, K. M. Kadish, *Inorg. Chem.* **1993**, 32, 438–444.
54. K. M. Kadish, C. Araullo, G. B. Maiya, D. Sazou, J.-M. Barbe, R. Guilard, *Inorg. Chem.* **1989**, 28, 2528–2533.
55. C. Araullo-McAdams, K. M. Kadish, *Inorg. Chem.* **1990**, 29, 2749–2757.
56. K. M. Kadish, E. Van Caemelbecke, E. Gueletii, S. Fukuzumi, K. Miyamoto, T. Suenobu, A. Tabard, R. Guilard, *Inorg. Chem.* **1998**, 37, 1759–1766.
57. J. W. Seyler, C. R. Leidner, *J. Chem. Soc., Chem. Commun.* **1989**, 794.
58. K. M. Kadish, Q. Y. Xu, J.-M. Barbe, J. E. Anderson, E. Wang, R. Guilard, *J. Am. Chem. Soc.* **1987**, 109, 7705–7714.
59. K. M. Kadish, Q. Y. Xu, J.-M. Barbe, *Inorg. Chem.* **1988**, 27, 1191–1198.
60. K. M. Kadish, Q. Y. Xu, J. E. Anderson, *ACS Symp. Ser.* **1988**, 378, 451–465.
61. K. M. Kadish, F. D'Souza, E. Van Caemelbecke, A. Villard, J.-D. Lee, A. Tabard, R. Guilard, *Inorg. Chem.* **1993**, 32, 4179–4185.
62. D. Lançon, P. Cocolios, R. Guilard, K. M. Kadish, *Organometallics* **1984**, 3, 1164–1170.
63. G. B. Maiya, B. C. Han, K. M. Kadish, *Langmuir* **1989**, 5, 645–650.
64. Q. Y. Xu, J. M. Barbe, K. M. Kadish, *Inorg. Chem.* **1988**, 27, 2373–2378.
65. R. Guilard, G. Lagrange, A. Tabard, D. Lançon, K. M. Kadish, *Inorg. Chem.* **1985**, 24, 3649–3656.
66. I. K. Choi, D. Feng, K. J. Paeng, M. D. Ryan, *Inorg. Chem.* **1991**, 30, 1832–1839.
67. E. Fujita, C. K. Chang, J. Fajer, *J. Am. Chem. Soc.* **1985**, 107, 7665–7669.
68. K. M. Kadish, D. Lançon, P. Cocolios, R. Guilard, *Inorg. Chem.* **1984**, 23, 2372, 2373.
69. K. M. Kadish, V. A. Adamian, E. Van Caemelbecke, Z. Tan, P. Tagliatesta, P. Bianco, T. Boschi, G. B. Yi, M. A. Khan, G. B. Richter-Addo, *Inorg. Chem.* **1996**, 35, 1343–1348.
70. A. D. Kini, J. Washington, C. P. Kubiak, B. H. Morimoto, *Inorg. Chem.* **1996**, 35, 6904–6906.
71. D. Lançon, K. M. Kadish, *J. Am. Chem. Soc.* **1983**, 105, 5610–5617.
72. I. M. Lorkovic, K. M. Miranda, B. Lee, S. Bernhard, J. R. Schoonover, P. C. Ford, *J. Am. Chem. Soc.* **1998**, 120, 11 674–11 683.
73. I. M. Lorkovic, P. C. Ford, *Inorg. Chem.* **1999**, 38, 1467–1473.
74. M. Hoshino, K. Yasufuku, S. Konishi, M. Imamura, *Inorg. Chem.* **1984**, 23, 1982.
75. L. E. Laverman, M. Hoshino, P. C. Ford, *J. Am. Chem. Soc.* **1997**, 119, 12 663–12 664.
76. I. Lorkovic, P. C. Ford, *J. Am. Chem. Soc.* **2000**, 122, 6516–6517.
77. I. Lorkovic, P. C. Ford, *Inorg. Chem.* **2000**, 39, 632, 633.
78. L. Cheng, G. Richter-Addo, Binding and Activation of Nitric Oxide by Metalloporphyrins and Heme, in *The Porphyrin Handbook*, (Eds.: K. M. Kadish, K. Smith, R. Guilard), Academic Press, San Diego, 2000, pp. 219–290, Vol. 4.
79. W. H. Leung, T. S. M. Hun, K. Y. Wong, W. T. Wong, *J. Chem. Soc., Dalton Trans.* **1994**, 2713–2718.
80. W. R. Scheidt, Systematics of the Stereochemistry of Porphyrins and Metalloporphyrins, in *The Porphyrin Handbook*, (Eds.: K. M. Kadish, K. Smith, R. Guilard), Academic Press, San Diego, 2000, pp. 49–112, Vol. 3.
81. D. S. Bohle, C.-H. Hung, *J. Am. Chem. Soc.* **1995**, 117, 9584, 9585.
82. K. M. Kadish, *J. Electroanal. Chem.* **1984**, 168, 261–274.
83. L. W. Olson, D. Schaeper, D. Lançon, K. M. Kadish, *J. Am. Chem. Soc.* **1982**, 104, 2042–2044.
84. B. B. Wayland, L. W. Olson, *J. Am. Chem. Soc.* **1974**, 96, 6037–6041.
85. I. K. Choi, M. D. Ryan, *Inorg. Chim. Acta* **1988**, 153, 25–30.

86. X. H. Mu, K. M. Kadish, *Inorg. Chem.* **1990**, 29, 1031–1036.
87. J. W. Buchler, W. Kokisch, P. D. Smith, *Z. Naturforsch. B* **1978**, 33b, 1371.
88. E. Fujita, J. Fajer, *J. Am. Chem. Soc.* **1983**, 105, 6743–6745.
89. M. K. Ellison, W. R. Scheidt, *J. Am. Chem. Soc.* **1997**, 119, 7404, 7405.
90. K. M. Kadish, X. H. Mu, *Inorg. Chem.* **1990**, 29, 1031–1036.
91. K. M. Kadish, X. H. Mu, X. Q. Lin, *Inorg. Chem.* **1988**, 27, 1489–1492.
92. K. M. Kadish, X. H. Mu, *Pure Appl. Chem.* **1990**, 62, 1051–1054.
93. G. B. Richter-Addo, S. J. Hodge, G.-B. Yi, M. A. Khan, T. Ma, E. Van Caemelbecke, N. Guo, K. M. Kadish, *Inorg. Chem.* **1996**, 35, 6530–6538.
94. D. S. Bohle, C.-H. Hung, B. D. Smith, *Inorg. Chem.* **1998**, 37, 5798–5806.
95. D. S. Bohle, P. A. Goodson, B. D. Smith, *Polyhedron* **1996**, 15, 3147–3150.
96. D. S. Bohle, C.-H. Hung, A. K. Powell, B. D. Smith, S. Wocadlo, *Inorg. Chem.* **1997**, 36, 1992–1993.
97. B. B. Wayland, R. A. Newman, *Inorg. Chem.* **1981**, 20, 3093–3097.
98. S. L. Kelly, K. M. Kadish, *Inorg. Chem.* **1984**, 23, 679–687.
99. T. Diebold, M. Schppacher, B. Chevrier, R. Weiss, *J. Chem. Soc., Chem. Commun.* **1979**, 693, 694.
100. S. L. Kelly, D. Lançon, K. M. Kadish, *Inorg. Chem.* **1984**, 23, 1451–1458.
101. C.-L. Yao, J. E. Anderson, K. M. Kadish, *Inorg. Chem.* **1987**, 26, 2725–2727.
102. K. M. Kadish, Y. J. Deng, C.-L. Yao, J. E. Anderson, *Organometallics* **1988**, 7, 1979–1983.
103. C. Swistak, J.-L. Cornillon, J. E. Anderson, K. M. Kadish, *Organometallics* **1987**, 6, 2146–2150.
104. K. M. Kadish, D. Chang, *Inorg. Chem.* **1982**, 21, 3614–3618.
105. K. M. Kadish, D. J. Leggett, D. Chang, *Inorg. Chem.* **1982**, 21, 3618–3622.
106. K. M. Kadish, J. L. Cornillon, C.-L. Yao, T. Malinski, G. Gritzner, *J. Electroanal. Chem.* **1987**, 235, 189–207.
107. S. Takagi, T. K. Miyamoto, M. Hamagushi, Y. Sasaki, *Inorg. Chim. Acta* **1990**, 173, 215–221.
108. E. R. Birnbaum, W. P. Schaefer, J. A. Labin-ger, J. E. Bercaw, H. B. Gray, *Inorg. Chem.* **1995**, 34, 1751–1755.
109. K. M. Kadish, P. Tagliatesta, Y. Hu, Y. J. Deng, X. H. Mu, L. Y. Bao, *Inorg. Chem.* **1991**, 30, 3737–3743.
110. G. M. Brown, F. R. Hopf, T. J. Meyer, D. G. Whitten, *J. Am. Chem. Soc.* **1975**, 97, 5385–5390.
111. G. M. Brown, F. R. Hopf, J. A. Ferguson, T. J. Meyer, D. G. Whitten, *J. Am. Chem. Soc.* **1973**, 95, 5939–5942.
112. T. Boshi, G. Bontempelli, G.-A. Mazzochin, *Inorg. Chim. Acta* **1979**, 37, 155–160.
113. D. P. Rillema, J. K. Nagle, L. F. Barringer, T. J. Meyer, *J. Am. Chem. Soc.* **1981**, 103, 56–62.
114. Y. Hu, B. C. Han, L. Y. Bao, X. H. Mu, K. M. Kadish, *Inorg. Chem.* **1991**, 30, 2444–2446.
115. X. H. Mu, K. M. Kadish, *Inorg. Chem.* **1989**, 28, 3743–3747.
116. K. M. Kadish, M. M. Franzen, B. C. Han, C. Araullo-McAdams, D. Sazou, *J. Am. Chem. Soc.* **1991**, 113, 512–517.
117. K. M. Kadish, Y. Hu, P. Tagliatesta, T. Boschi, *J. Chem. Soc., Dalton Trans.* **1993**, 1167–1172.
118. K. Rachlewicz, M. Grzeszczuk, L. Latos-Grazynski, *Polyhedron* **1993**, 12, 821–829.
119. G. Peychal-Heiling, G. S. Wilson, *Anal. Chem.* **1971**, 43, 545–550.
120. G. Peychal-Heiling, G. S. Wilson, *Anal. Chem.* **1971**, 43, 550–556.
121. D. Chabach, A. De Cian, J. Fischer, R. Weiss, M. E. Bibout, *Angew. Chem., Int. Ed. Engl.* **1996**, 35, 898, 899.
122. J. W. Buchler, P. Hammerschmitt, I. Kaufeld, J. Löffler, *Chem. Ber.* **1991**, 124, 2151–2159.
123. J. W. Buchler, B. Scharbert, *J. Am. Chem. Soc.* **1988**, 110, 4272–4276.
124. J. K. Duchowski, D. F. Bocian, *Inorg. Chem.* **1990**, 29, 4158–4160.
125. J. W. Buchler, M. Kihn-Botulinski, J. Löffler, B. Scharbert, *New J. Chem.* **1992**, 16, 545–553.
126. D. Chabach, M. Tahiri, A. De Cian, J. Fischer, R. Weiss, M. E. Bibout, *J. Am. Chem. Soc.* **1995**, 117, 8548–8556.
127. J. Buchler, D. K. P. Ng, Metal Tetrapyrrole Double- and Triple-Deckers with Special Emphasis on Porphyrin Systems, in *The Porphyrin Handbook*, (Eds.: K. M. Kadish, K. Smith, R. Guilard), Academic Press, San Diego, 2000, pp. 246–294, Vol. 3.

128. J. W. Buchler, G. Eikermann, L. Puppe, K. Rohbock, H. H. Schneehage, D. Weck, *Liebigs Ann. Chem.* **1971**, 745, 135–151.
129. T. Malinski, D. Chang, J. M. Latour, J.-C. Marchon, M. Gross, A. Giraudeau, K. M. Kadish, *Inorg. Chem.* **1984**, 23, 3947–3955.
130. A. R. Miksztal, J. S. Valentine, *Inorg. Chem.* **1984**, 23, 3548–3552.
131. P. Friauf, J. Goulon, J. Fischer, L. Ricard, M. Schappacher, R. Weiss, M. Momenteau, *Nouv. J. Chim.* **1985**, 9, 33–40.
132. R. Guillard, J.-M. Latour, C. Lecomte, J.-C. Marchon, J. Protas, D. Ripoll, *Inorg. Chem.* **1978**, 17, 1228–1237.
133. J.-M. Latour, J. C. Marchon, N. Nakajima, *J. Am. Chem. Soc.* **1979**, 101, 3974–3976.
134. M. Nakajima, J.-M. Latour, J. C. Marchon, *J. Chem. Soc., Chem. Commun.* **1977**, 763.
135. C. Ratti, P. Richard, A. Tabard, R. Guillard, *J. Chem. Soc., Chem. Commun.* **1989**, 69–70.
136. R. Guillard, C. Ratti, A. Tabard, P. Richard, D. Dubois, K. M. Kadish, *Inorg. Chem.* **1990**, 29, 2532–2540.
137. L. K. Woo, J. A. Hays, V. G. Young, C. L. Day, C. Caron, F. D'souza, K. M. Kadish, *Inorg. Chem.* **1993**, 32, 4186–4192.
138. P. Richard, R. Guillard, *J. Chem. Soc., Chem. Commun.* **1983**, 1454.
139. R. Guillard, P. Richard, M. El Borai, E. Laviron, *J. Chem. Soc., Chem. Commun.* **1980**, 516–518.
140. J. E. Anderson, Y. H. Liu, R. Guillard, J.-M. Barbe, K. M. Kadish, *Inorg. Chem.* **1986**, 25, 3786–3791.
141. J. E. Anderson, Y. H. Liu, R. Guillard, J.-M. Barbe, K. M. Kadish, *Inorg. Chem.* **1986**, 25, 2250–2255.
142. C. M. Newton, D. G. Davis, *J. Magn. Reson.* **1975**, 20, 446–457.
143. J. W. Buchler, C. Dreher, K.-L. Lay, Y. J. A. Lee, W. R. Scheidt, *Inorg. Chem.* **1983**, 22, 888.
144. J. W. Buchler, C. Dreher, *Z. Naturforsch. B.* **1984**, 39, 222.
145. L. A. Bottomley, F. L. Neely, *Inorg. Chem.* **1997**, 36, 5435–5439.
146. F. L. Neely, L. A. Bottomley, *Inorg. Chim. Acta* **1992**, 192, 147–149.
147. J. T. Groves, T. Takahashi, W. M. Butler, *Inorg. Chem.* **1983**, 22, 884–887.
148. P. J. Nichols, J. D. Fallon, B. Moubaraki, K. S. Murray, B. O. West, *Polyhedron* **1993**, 12, 2205.
149. K. A. Macor, T. G. Spiro, *J. Am. Chem. Soc.* **1983**, 105, 5601–5607.
150. L. A. Bottomley, F. L. Neely, *Inorg. Chem.* **1990**, 29, 1860–1865.
151. F. Basolo, R. D. Jones, D. A. Summerville, *Acta Chem. Scand.* **1978**, A32, 771.
152. D. A. Summerville, R. D. Jones, B. M. Hoffman, F. Basolo, *J. Am. Chem. Soc.* **1977**, 99, 8195–8202.
153. L. A. Bottomley, K. M. Kadish, *Inorg. Chem.* **1983**, 22, 342–349.
154. V. Gutmann, *The Donor-Acceptor Approach to Molecular Interactions*, Plenum Press, New York, 1978.
155. T. Malinski, P. M. Hanley, K. M. Kadish, *Inorg. Chem.* **1986**, 25, 3229–3235.
156. J. Topich, N. Berger, *Inorg. Chim. Acta* **1982**, 65, L131–L134.
157. K. M. Kadish, D. Chang, T. Malinski, H. Ledon, *Inorg. Chem.* **1983**, 22, 3490–3492.
158. H. Ledon, F. Varescon, T. Malinski, K. M. Kadish, *Inorg. Chem.* **1984**, 23, 261–263.
159. T. Malinski, H. Ledon, K. M. Kadish, *J. Chem. Soc., Chem. Commun.* **1983**, 1077–1079.
160. D. D. Axtell, G. R. Miller, T. H. Ridgway, M. Tsutsui, *J. Coord. Chem.* **1978**, 8, 113–115.
161. K. M. Kadish, D. Schaeper, L. A. Bottomley, M. Tsutsui, R. L. Bobsein, *J. Inorg. Nucl. Chem.* **1980**, 42, 469–474.
162. K. M. Kadish, L. A. Bottomley, D. Shaefer, M. Tsutsui, R. L. Bobsein, *Inorg. Chim. Acta* **1979**, 36, 219.
163. R. Guillard, N. Jagerovic, J.-M. Barbe, Y. H. Liu, I. Perrot, C. Naillon, E. Van Caemelbecke, K. M. Kadish, *Polyhedron* **1995**, 14, 3041–3050.
164. R. S. Czernuszewicz, Y. O. Su, M. K. Stern, K. A. Macor, D. Kim, J. T. Groves, T. G. Spiro, *J. Am. Chem. Soc.* **1988**, 110, 4158–4165.
165. J. T. Groves, M. K. Stern, *J. Am. Chem. Soc.* **1988**, 110, 8628–8638.
166. L. J. Boucher, H. K. Garber, *Inorg. Chem.* **1970**, 9, 2644–2649.
167. K. M. Kadish, M. M. Morrison, *Bioelectrochem. Bioenerg.* **1977**, 3, 480.
168. S. L. Kelly, K. M. Kadish, *Inorg. Chem.* **1982**, 21, 3631–3639.
169. K. Perie, J.-M. Barbe, P. Cocolios, R. Guillard, *Bull. Soc. Chim. Fr.* **1996**, 133, 697–702.

170. R. Guillard, K. Perie, J. M. Barbe, D. J. Nurco, K. M. Smith, E. Van Caemelbecke, K. M. Kadish, *Inorg. Chem.* **1998**, *37*, 973–981.
171. S. Fukuzumi, I. Nakanishi, J.-M. Barbe, R. Guillard, E. Van Caemelbecke, N. Guo, K. M. Kadish, *Angew. Chem., Int. Ed. Engl.* **1999**, *38*, 964–966.
172. R. D. Arasasingham, T. C. Bruice, *Inorg. Chem.* **1990**, *29*, 1422–1427.
173. R. D. Arasasingham, G.-X. He, T. C. Bruice, *J. Am. Chem. Soc.* **1993**, *115*, 7985–7991.
174. K. R. Rodgers, H. M. Goff, *J. Am. Chem. Soc.* **1988**, *110*, 7049–7060.
175. C. Ercolani, J. Jubbe, G. Pennesi, U. Russo, G. Trigiant, *Inorg. Chem.* **1995**, *34*, 2535–2541.
176. Y. J. Deng, X. H. Mu, P. Tagliatesta, K. M. Kadish, *Inorg. Chem.* **1991**, *30*, 1957–1960.
177. A. Pacheco, B. R. James, S. J. Retting, *Inorg. Chem.* **1995**, *34*, 3477–3484.
178. W. H. Leung, C. M. Che, *J. Am. Chem. Soc.* **1989**, *111*, 8812–8818.
179. C. Ho, W. H. Leung, C. M. Che, *J. Chem. Soc., Dalton Trans.* **1991**, 2933–2939.
180. J. W. Seyler, C. R. Leidner, *Inorg. Chem.* **1990**, *29*, 3636–3641.
181. J. W. Seyler, L. K. Safford, P. E. Fanwick, C. R. Leidner, *Inorg. Chem.* **1992**, *31*, 1545–1547.
182. J. W. Seyler, L. K. Safford, C. R. Leidner, *Inorg. Chem.* **1992**, *31*, 4300–4307.
183. R. Guillard, K. M. Kadish, *Chem. Rev.* **1988**, *88*, 1121–1146.
184. K. M. Kadish, E. Van Caemelbecke, F. D'Souza, C. J. Medforth, K. M. Smith, A. Tabard, R. Guillard, *Organometallics* **1993**, *12*, 2411–2413.
185. J. P. Collman, D. S. Bohle, A. K. Powell, *Inorg. Chem.* **1993**, *32*, 4004–4011.
186. C. M. Che, W. H. Leung, W. C. Chung, *Inorg. Chem.* **1990**, *29*, 1841–1846.
187. L. A. Bottomley, K. M. Kadish, *Inorg. Chem.* **1981**, *20*, 1348–1357.
188. D. Lançon, P. Cocolios, R. Guillard, K. M. Kadish, *J. Am. Chem. Soc.* **1984**, *106*, 4472–4478.
189. C. Swistak, X. H. Mu, K. M. Kadish, *Inorg. Chem.* **1987**, *26*, 4360–4366.
190. K. M. Kadish, R. K. Rhodes, *Inorg. Chem.* **1983**, *22*, 1090–1094.
191. L. A. Constant, D. G. Davis, *Anal. Chem.* **1975**, *47*, 2253–2260.
192. L. A. Bottomley, L. Olson, K. M. Kadish, *Adv. Chem. Ser.* **1982**, *201*, 279–311.
193. K. M. Kadish, L. A. Bottomley, *Inorg. Chem.* **1980**, *19*, 832–836.
194. K. M. Kadish, L. K. Thompson, D. Beroiz, L. A. Bottomley, *ACS Symp. Ser.* **1977**, *38*, 51.
195. K. M. Kadish, D. Schaeper, *J. Chem. Soc., Chem. Commun.* **1980**, 1273–1275.
196. R. Koerner, J. L. Wright, X. D. Ding, M. J. M. Nasset, K. Aubrecht, R. A. Watson, R. A. Barber, L. M. Mink, A. R. Tipton, C. J. Norvel, K. Skidmore, U. Simonis, F. A. Walker, *Inorg. Chem.* **1998**, *37*, 733–745.
197. A. Ghosh, *J. Phys. Chem.* **1994**, *98*, 11 004.
198. A. Ghosh, *J. Am. Chem. Soc.* **1995**, *117*, 4691–4699.
199. A. Ghosh, *Acc. Chem. Res.* **1998**, *31*, 189–198.
200. A. Ghosh, Quantum Chemical Studies of Molecular Structures and Potential Energy Surfaces of Porphyrins and Hemes, in *The Porphyrin Handbook*, (Eds.: K. M. Kadish, K. Smith, R. Guillard), Academic Press, San Diego, 2000, pp. 1–38, Vol. 7.
201. K. M. Kadish, M. M. Morrison, L. A. Constant, L. Dickens, D. G. Davis, *J. Am. Chem. Soc.* **1976**, *98*, 8387–8390.
202. C. A. Reed in *ACS Advances in Chemistry Series*, (Ed.: K. M. Kadish), American Chemical Society, Washington, D.C., 1982, Vol. 201.
203. K. M. Kadish, E. Van Caemelbecke, F. D'Souza, M. Lin, D. J. Nurco, C. J. Medford, T. P. Forsyth, B. Krattinger, K. M. Smith, S. Fukuzumi, I. Nakanishi, J. A. Shelnutt, *Inorg. Chem.* **1999**, *38*, 2188–2198.
204. R. J. Donohoe, M. Atamian, D. F. Bocian, *J. Am. Chem. Soc.* **1987**, *109*, 5593–5599.
205. K. T. Moore, J. T. Fletcher, M. J. Therien, *J. Am. Chem. Soc.* **1999**, *121*, 5196–5209.
206. M. A. Phillippi, E. T. Shimomura, H. M. Goff, *Inorg. Chem.* **1981**, *20*, 1322–1325.
207. A. Wolberg, *Isr. J. Chem.* **1974**, *12*, 1031–1035.
208. C. A. Reed, T. Mashiko, S. P. Bentley, M. E. Kastner, W. R. Scheidt, K. Spartalian, G. Lang, *J. Am. Chem. Soc.* **1979**, *101*, 2948–2958.
209. H. M. Goff, M. A. Phillippi, A. D. Boersma, A. P. Hansen, *Electrochemical and Spectroscopic Studies on Biological Redox Components*, ACS Advances in Chemistry Series, American Chemical Society, Washington, D.C., 1982, pp. 357–376, Vol. 201.

210. M. A. Phillippi, H. M. Goff, *J. Am. Chem. Soc.* **1982**, *104*, 6026–6034.
211. T. E. Shimomura, M. A. Phillippi, H. M. Goff, W. F. Scholz, C. A. Reed, *J. Am. Chem. Soc.* **1981**, *103*, 6778–6780.
212. A. D. Boersma, H. M. Goff, *Inorg. Chem.* **1984**, *23*, 1671–1676.
213. H. Fujii, *J. Am. Chem. Soc.* **1993**, *115*, 4641–4648.
214. J. T. Groves, J. A. Gilbert, *Inorg. Chem.* **1986**, *25*, 123–125.
215. T. S. Calderwood, W. A. Lee, T. C. Bruice, *J. Am. Chem. Soc.* **1985**, *107*, 8272, 8273.
216. J. T. Groves, Z. Gross, M. K. Stern, *Inorg. Chem.* **1994**, *33*, 5065–5072.
217. T. S. Calderwood, T. C. Bruice, *Inorg. Chem.* **1986**, *25*, 3722–3724.
218. W. A. Lee, T. S. Calderwood, T. C. Bruice, *Proc. Natl. Acad. Sci. U.S.A.* **1985**, *82*, 4301–4305.
219. S. Fukuzumi, I. Nakanishi, K. Tanaka, T. Suenobu, A. Tabard, R. Guillard, E. Van Caemelbecke, K. M. Kadish, *J. Am. Chem. Soc.* **1999**, *121*, 785–790.
220. A. Nanthakumar, H. M. Goff, *J. Am. Chem. Soc.* **1990**, *112*, 4047–4049.
221. A. Nanthakumar, H. M. Goff, *Inorg. Chem.* **1991**, *30*, 4460–4464.
222. L. D. Sparks, C. J. Medforth, M. S. Park, J. R. Chamberlain, M. R. Ondrias, M. O. Senge, K. M. Smith, J. A. Shelnutt, *J. Am. Chem. Soc.* **1993**, *115*, 581–592.
223. R.-J. Cheng, P. Y. Chen, P.-R. Gau, C.-C. Chen, S.-M. Peng, *J. Am. Chem. Soc.* **1997**, *119*, 2563.
224. R. A. Sheldon, (Ed.), *Metalloporphyrins in Catalytic Oxidations*, Marcel Dekker, New York, 1994.
225. M. W. Grinstaff, M. G. Hill, J. A. Labinger, H. B. Gray, *Science* **1994**, *264*, 1311.
226. D. Lexa, P. Maillard, M. Momenteau, J. M. Savéant, *J. Am. Chem. Soc.* **1984**, *106*, 6321–6323.
227. C. Gueutin, D. Lexa, J.-M. Savéant, D.-L. Wang, *Organometallics* **1989**, *8*, 1607–1613.
228. D. Lexa, J. Mispelter, J.-M. Savéant, *J. Am. Chem. Soc.* **1981**, *103*, 6806–6812.
229. D. Lexa, J.-M. Savéant, D. L. Wang, *Organometallics* **1986**, *5*, 1428–1434.
230. D. Lexa, M. Momenteau, J.-M. Savéant, F. Xu, *Inorg. Chem.* **1985**, *24*, 122–127.
231. C. Gueutin, D. Lexas, M. Momenteau, J.-M. Savéant, F. Xu, *Inorg. Chem.* **1986**, *25*, 4294–4307.
232. D. Lexa, M. Momenteau, P. Rentien, G. Rytz, J.-M. Savéant, F. Xu, *J. Am. Chem. Soc.* **1984**, *106*, 4755–4765.
233. D. Lexa, M. Momenteau, J. M. Savéant, F. Xu, *J. Am. Chem. Soc.* **1986**, *108*, 6937–6941.
234. A. El-Kasmi, D. Lexa, P. Maillard, M. Momenteau, J.-M. Savéant, *J. Am. Chem. Soc.* **1991**, *113*, 1586–1595.
235. J. H. Cameron, S. C. Turner, *Polyhedron* **1993**, *12*, 1675–1680.
236. J. H. Cameron, S. C. Turner, *J. Chem. Soc., Dalton Trans.* **1993**, 1941–1945.
237. S. H. Strauss, R. H. Holm, *Inorg. Chem.* **1982**, *21*, 863–868.
238. D. V. Stynes, B. R. James, *J. Chem. Soc., Chem. Commun.* **1973**, 325.
239. B. B. Wayland, L. F. Mehne, J. Swartz, *J. Am. Chem. Soc.* **1978**, *100*, 2379–2383.
240. C. Swistak, K. M. Kadish, *Inorg. Chem.* **1987**, *26*, 405–412.
241. D. Dolphin, B. R. James, H. C. Welborne, *ACS Adv. Chem. Ser.* **1983**, *201*, 563.
242. L. A. Bottomley, M. R. Deakin, J.-N. Gorce, *Inorg. Chem.* **1984**, *23*, 3563–3571.
243. J.-N. Gorce, L. A. Bottomley, *Inorg. Chem.* **1985**, *24*, 1431–1436.
244. D. Chang, P. Cocolios, Y. T. Wu, K. M. Kadish, *Inorg. Chem.* **1984**, *23*, 1629–1633.
245. K. M. Kadish, R. K. Rhodes, L. A. Bottomley, H. M. Goff, *Inorg. Chem.* **1981**, *20*, 3195–3200.
246. D. Lançon, K. M. Kadish, *Inorg. Chem.* **1984**, *23*, 3942–3947.
247. D. R. English, D. N. Hendrickson, K. S. Suslick, *Inorg. Chem.* **1983**, *22*, 367, 368.
248. D. Mansuy, P. Battioni, Diversity of Reactions Catalyzed by Heme-Thiolate Proteins, in *The Porphyrin Handbook*, (Eds.: K. M. Kadish, K. M. Smith, R. Guillard), Academic Press, San Diego, 2000, pp. 1–15, Vol. 4.
249. P. R. O. de Montellano, (Ed.), *Cytochrome P450: Structure, Mechanism and Biochemistry*, Plenum Publishing, New York, 1995.
250. J. T. Groves, Y. Z. Han in *Cytochrome P450: Structure, Mechanism, and Biochemistry*, (Ed.: P. R. O. de Montellano), 2nd ed., Plenum Publishing, New York, 1995, p. 3.
251. P. R. Ortiz de Montellano in *Cytochrome P450: Structure, Mechanism, and Biochemistry*, (Ed.: P. R. O. de Montellano), 2nd ed., Plenum Publishing, New York, 1995, p. 245.

252. E. J. Mueller, P. J. Loida, S. G. Sligar in *Cytochrome P450: Structure, Mechanism, and Biochemistry*, (Ed.: P. R. O. de Montellano), 2nd ed., Plenum Publishing, New York, 1995, p. 83.
253. A. D. N. Vaz, D. F. McGinnity, M. J. Coon, *Proc. Natl. Acad. Sci. U.S.A.* **1998**, 95, 3555.
254. A. D. N. Vaz, S. J. Pernecky, G. M. Raner, M. J. Coon, *Proc. Natl. Acad. Sci. U.S.A.* **1996**, 93, 4644.
255. K. G. Welinder, *Curr. Biol.* **1992**, 2, 388.
256. T. L. Poulos, Peroxidase and Cytochrome P450 Structures, in *The Porphyrin Handbook*, (Eds.: K. M. Kadish, K. M. Smith, R. Guilard), Academic Press, San Diego, 2000, pp. 189–218, Vol. 4.
257. D. Dolphin, A. Forman, D. C. Borg, J. Fajer, R. H. Felton, *Proc. Natl. Acad. Sci. U.S.A.* **1971**, 68, 614.
258. R. Rutter, M. Valentine, M. P. Hendrich, L. P. Hager, P. G. Debrunner, *Biochemistry* **1983**, 22, 4769.
259. B. Chance, L. Powers, Y. Ching, T. Poulos, G. R. Schonbaum, I. Yamazaki, K. G. Paul, *Arch. Biochem. Biophys.* **1984**, 235, 596.
260. V. Fulop, R. P. Phizackerley, S. M. Soltis, I. J. Clifton, S. Wakatuski, J. Erman, J. Hajdu, S. L. Edwards, *Structure* **1994**, 2, 201.
261. S. L. Edwards, H. X. Nguyen, R. C. Hamlin, J. Kraut, *Biochemistry* **1987**, 26, 1503.
262. P. Gouet, H. M. Jouve, P. A. Williams, I. Anderson, P. Andreoletti, L. Nussaume, J. Hajdu, *Nat. Struct. Biol.* **1996**, 3, 951.
263. H. B. Dunford in *Peroxidases in Chemistry and Biology*, (Eds.: J. Everse, K. E. Everse, M. B. Grisham), CRC Press, Boca Raton, 1991, pp. 1–24, Vol. 2.
264. H. K. Baek, H. E. Van Wart, *Biochemistry* **1989**, 28, 5714.
265. D. Job, H. B. Dunford, *Eur. J. Biochem.* **1976**, 66, 607.
266. H. B. Dunford, M. L. Cotton, *J. Biol. Chem.* **1975**, 250, 2920.
267. I. C. Kuan, K. A. Johnson, M. Tien, *J. Biol. Chem.* **1993**, 268, 20 064.
268. R. S. Koduri, M. Tien, *Biochemistry* **1994**, 33, 4225.
269. H. Wariishi, J. Huang, H. B. Dunford, M. H. Gold, *J. Biol. Chem.* **1991**, 266, 20 694.
270. J. E. Critchlow, H. B. Dunford, *J. Biol. Chem.* **1972**, 247, 3703.
271. J. E. Critchlow, H. B. Dunford, *J. Biol. Chem.* **1972**, 247, 3714.
272. A. M. Altschul, R. Abrams, T. R. Hogness, *J. Biol. Chem.* **1940**, 136, 777.
273. T. Yonetani, *Enzymes* **1976**, 13, 345.
274. L. Cheng, G. B. Richter-Addo, Binding and Activation of Nitric Oxide by Metalloporphyrins and Heme, in *The Porphyrin Handbook*, (Eds.: K. M. Kadish, K. M. Smith, R. Guilard), Academic Press, San Diego, 2000, pp. 189–218, Vol. 4.
275. B. A. Averill, *Chem. Rev.* **1996**, 96, 2951.
276. W. G. Zumft, H. Körner, *Antonie van Leeuwenhoek* **1997**, 71, 43.
277. B. C. Berks, S. J. Ferguson, J. W. B. Moir, *Biochim. Biophys. Acta* **1995**, 1232, 97.
278. T. C. Hollocher in *Nitric Oxide. Principles and Actions*, (Ed.: J. Lancaster Jr.), Academic Press, San Diego, 1996, pp. 289–344.
279. T. Fujiwara, Y. Fukumori, *J. Bacteriol.* **1996**, 178, 1866.
280. P. Girsch, S. de Vries, *Biochim. Biophys. Acta* **1997**, 202, 1318.
281. P. Moënné-Loccoz, S. de Vries, *J. Am. Chem. Soc.* **1998**, 120, 5147.
282. M. R. Cheesman, W. G. Zumft, A. J. Thomson, *Biochemistry* **1998**, 37, 3994.
283. N. Sakurai, T. Sakurai, *Biochemistry* **1997**, 36, 13 809.
284. N. Sakurai, T. Sakurai, *Biochem. Biophys. Res. Commun.* **1998**, 243, 400.
285. T. Sakurai, N. Sakurai, H. Matsumoto, S. Hirota, O. Yamauchi, *Biochem. Biophys. Res. Commun.* **1998**, 251, 248.
286. P. O'Brien, D. A. Sweigart, *Inorg. Chem.* **1985**, 24, 1405–1409.
287. M. M. Doeff, D. A. Sweigart, P. O'Brien, *Inorg. Chem.* **1983**, 22, 851–852.
288. R. Quinn, M. Nappa, J. S. Valentine, *J. Am. Chem. Soc.* **1982**, 104, 2588–2595.
289. R. Quinn, J. Mercer-Smith, J. N. Burstyn, J. S. Valentine, *J. Am. Chem. Soc.* **1984**, 106, 4136–4144.
290. K. M. Kadish, Y. J. Deng, J. D. Korp, *Inorg. Chem.* **1990**, 29, 1036–1042.
291. J. E. Anderson, C.-L. Yao, K. M. Kadish, *Inorg. Chem.* **1986**, 25, 718,719.
292. J. E. Anderson, C.-L. Yao, K. M. Kadish, *Organometallics* **1987**, 6, 706–711.
293. J. E. Anderson, C.-L. Yao, K. M. Kadish, *J. Am. Chem. Soc.* **1987**, 109, 1106–1111.
294. J. E. Anderson, Y. H. Liu, K. M. Kadish, *Inorg. Chem.* **1987**, 26, 4174–4179.
295. K. M. Kadish, C.-L. Yao, J. E. Anderson, P. Cocolios, *Inorg. Chem.* **1985**, 24, 4515–4520.

296. K. M. Kadish, J. E. Anderson, C. L. Yao, R. Guillard, *Inorg. Chem.* **1986**, *25*, 1277–1280.
297. K. M. Kadish, W. Koh, P. Tagliatesta, D. Sazou, R. Paolesse, S. Licoccia, T. Boschi, *Inorg. Chem.* **1992**, *31*, 2305–2313.
298. K. M. Kadish, Y. Hu, T. Boschi, P. Tagliatesta, *Inorg. Chem.* **1993**, *32*, 2996–3002.
299. V. Grass, D. Lexa, J.-M. Savéant, *J. Am. Chem. Soc.* **1997**, *119*, 7526–7532.
300. V. Grass, D. Lexa, M. Momenteau, J.-M. Savéant, *J. Am. Chem. Soc.* **1997**, *119*, 3536–3542.
301. D. Lexa, V. Grass, J.-M. Savéant, *Organometallics* **1998**, *17*, 2673–2676.
302. J. E. Anderson, C.-L. Yao, K. M. Kadish, *Inorg. Chem.* **1986**, *25*, 3224–3228.
303. S. Fukuzumi, K. Miyamoto, T. Suenobu, E. Van Caemelbecke, K. M. Kadish, *J. Am. Chem. Soc.* **1998**, *120*, 2880–2889.
304. A. Stanienda, G. Biebl, *Z. Phys. Chem.* **1967**, *52*, 254–275.
305. M. J. Carter, L. M. Engelhardt, D. P. Rillema, F. Basolo, *J. Chem. Soc., Chem. Commun.* **1973**, 810–812.
306. M. J. Carter, D. P. Rillema, F. Basolo, *J. Am. Chem. Soc.* **1974**, *23*, 392–400.
307. L. A. Truxillo, D. G. Davis, *Anal. Chem.* **1975**, *47*, 2260–2267.
308. F. A. Walker, D. Beroiz, K. M. Kadish, *J. Am. Chem. Soc.* **1976**, *98*, 3484–3489.
309. J. Huet, A. Gaudemer, C. Boucly-Goester, P. Boucly, *Inorg. Chem.* **1982**, *21*, 3413–3419.
310. K. M. Kadish, X. Q. Lin, B. C. Han, *Inorg. Chem.* **1987**, *26*, 4161–4167.
311. X. H. Mu, X. Q. Lin, K. M. Kadish, *Electroanalysis* **1989**, *1*, 113–116.
312. A. Giraudeau, H. J. Callot, J. Jordan, I. Ezhar, M. Gross, *J. Am. Chem. Soc.* **1979**, *101*, 3857–3862.
313. X. Q. Lin, B. Boisselier-Cocolios, K. M. Kadish, *Inorg. Chem.* **1986**, *25*, 3242–3248.
314. C. Shi, F. C. Anson, *Inorg. Chem.* **1998**, *37*, 1037–1043.
315. C. Shi, F. C. Anson, *Inorg. Chem.* **1992**, *31*, 5078–5083.
316. B. Steiger, C. Shi, F. C. Anson, *Inorg. Chem.* **1993**, *32*, 2107–2113.
317. M. Yuasa, F. C. Anson, *J. Porphyrins Phthalocyanines* **1997**, *1*, 181–188.
318. F. D'Souza, Y.-Y. Hsieh, G. R. Deviprasad, *J. Electroanal. Chem.* **1997**, *426*, 17–21.
319. F. D'Souza, Y.-Y. Hsieh, G. R. Deviprasad, *Chem. Commun. (Cambridge)* **1998**, 1027, 1028.
320. Y. Le Mest, C. Inisan, A. Laouenan, M. L'Her, J. Talarmin, M. El Kalifa, J.-Y. Saillard, *J. Am. Chem. Soc.* **1997**, *119*, 6095–6106.
321. M. Tezuka, M. Iwasaki, *Chem. Lett.* **1993**, *3*, 427–430.
322. H.-Z. Yu, J. S. Baskin, B. Steiger, F. C. Anson, A. H. Zewail, *J. Am. Chem. Soc.* **1999**, *121*, 484, 485.
323. K. M. Kadish, M. M. Franzen, B. C. Han, C. Araullo-McAdams, D. Sazou, *Inorg. Chem.* **1992**, *31*, 4399–4403.
324. D. Lexa, M. Momenteau, J. Mispelter, J.-M. Savéant, *Inorg. Chem.* **1989**, *28*, 30–35.
325. J. Seth, V. Palaniappan, D. F. Bocian, *Inorg. Chem.* **1995**, *34*, 2201–2206.
326. P. A. Connick, K. A. Macor, *Inorg. Chem.* **1991**, *30*, 4654–4663.
327. K. M. Kadish, D. Sazou, Y. M. Liu, A. Saoiabi, M. Ferhat, R. Guillard, *Inorg. Chem.* **1988**, *27*, 686–690.
328. K. M. Kadish, D. Sazou, G. B. Maiya, B. C. Han, Y. H. Liu, A. Saoiabi, M. Ferhat, R. Guillard, *Inorg. Chem.* **1989**, *28*, 2542–2547.
329. C. Y. Lin, S. Hu, T. Rush, III, T. G. Spiro, *J. Am. Chem. Soc.* **1996**, *118*, 9452, 9453.
330. A. M. Stolzenberg, M. T. Stershic, *Inorg. Chem.* **1987**, *26*, 3082, 3083.
331. A. M. Stolzenberg, M. T. Stershic, *J. Am. Chem. Soc.* **1988**, *110*, 6391–6402.
332. A. M. Stolzenberg, M. T. Stershic, *J. Am. Chem. Soc.* **1988**, *110*, 5397–5403.
333. M. W. Renner, L. R. Furenlid, K. M. Barkigia, A. Forman, H. K. Shim, D. J. Simpson, K. M. Smith, J. Fajer, *J. Am. Chem. Soc.* **1991**, *113*, 6891–6898.
334. K. M. Kadish, D. Sazou, Y. H. Liu, A. Saoiabi, M. Ferhat, R. Guillard, *Inorg. Chem.* **1988**, *27*, 1198–1204.
335. D. Chang, T. Malinski, A. Ulman, K. M. Kadish, *Inorg. Chem.* **1984**, *23*, 817–824.
336. K. Ozette, P. Leduc, M. Palacio, J. Bartoli, K. M. Barkigia, J. Fajer, P. Battioni, D. Mansuy, *J. Am. Chem. Soc.* **1997**, *119*, 6442, 6443.
337. K. M. Kadish, X. Q. Lin, J. Q. Ding, Y. T. Wu, C. Araullo, *Inorg. Chem.* **1986**, *25*, 3236–3242.
338. S. E. Jones, H. N. Po, *Inorg. Chim. Acta* **1980**, *42*, 95–99.

339. A. Giraudeau, A. Louati, H. J. Callot, M. Gross, *Inorg. Chem.* **1981**, 20, 769–772.
340. A. Kumar, P. Neta, *J. Phys. Chem.* **1981**, 85, 2830.
341. M. Krishnamurthy, *Inorg. Chem.* **1978**, 17, 2242–2245.
342. A. Giraudeau, A. Louati, M. Gross, H. J. Callot, L. K. Hanson, R. K. Rhodes, K. M. Kadish, *Inorg. Chem.* **1982**, 21, 1581–1586.
343. D. Kuila, A. B. Kopelove, D. K. Lavalley, *Inorg. Chem.* **1985**, 24, 1443–1446.
344. M. W. Renner, K. M. Barkigia, Y. Zhang, C. J. Medforth, K. M. Smith, J. Fajer, *J. Am. Chem. Soc.* **1994**, 116, 8582–8592.
345. S. A. Sibilia, S. Hu, C. Piffat, D. Melamed, T. G. Spiro, *Inorg. Chem.* **1997**, 36, 1013–1019.
346. J. Takeda, M. Sato, *Chem. Lett.* **1995**, 939, 940.
347. (a) M. E. Jamin, R. T. Iwamoto, *Inorg. Chim. Acta* **1978**, 27, 135–143. (b) K. M. Kadish, Wenbo E., Z. Ou, J. Shao, P. J. Sentic, K. Ohkubo, S. Fukuzumi, M. J. Crossley, *J. Chem. Soc. Dalton, Chem. Commun*, **2002**, 356–357.
348. J.-H. Fuhrhop, D. Mauzerall, *J. Am. Chem. Soc.* **1969**, 91, 4174–4181.
349. J. Fajer, D. C. Borg, A. Forman, D. Dolphin, R. H. Felton, *J. Am. Chem. Soc.* **1970**, 92, 3451–3459.
350. R. Felton, D. Dolphin, D. C. Borg, J. Fajer, *J. Am. Chem. Soc.* **1969**, 91, 196–198.
351. K. M. Kadish, L. R. Shiue, R. K. Rhodes, *Inorg. Chem.* **1981**, 20, 1274–1277.
352. K. M. Kadish, L. R. Shiue, *Inorg. Chem.* **1982**, 21, 3623–3630.
353. K. M. Kadish, A. Tabard, A. Zrineh, M. Ferhat, R. Guillard, *Inorg. Chem.* **1987**, 26, 2459–2466.
354. K. M. Kadish, J.-L. Cornillon, A. Coutsolelos, R. Guillard, *Inorg. Chem.* **1987**, 26, 4167–4173.
355. K. M. Kadish, B. Boisselier-Cocolios, A. Coutsolelos, P. Mitaine, R. Guillard, *Inorg. Chem.* **1985**, 24, 4521–4528.
356. K. M. Kadish, J.-L. Cornillon, P. Cocolios, *Inorg. Chem.* **1985**, 24, 3645–3649.
357. R. Guillard, I. Perrot, A. Tabard, P. Richard, C. Lecomte, Y. H. Liu, K. M. Kadish, *Inorg. Chem.* **1991**, 30, 27–37.
358. R. Guillard, N. Jagerovic, A. Tabard, C. Nailon, K. M. Kadish, *J. Chem. Soc., Dalton Trans.* **1992**, 1957–1966.
359. R. Guillard, N. Jagerovic, A. Tabard, P. Richard, L. Courthaudon, A. Louati, C. Lecomte, K. M. Kadish, *Inorg. Chem.* **1991**, 30, 16–27.
360. R. Guillard, A. Zrineh, A. Tabard, A. Endo, B. C. Han, C. Lecomte, M. Souhassou, A. Habbou, M. Ferhat, K. M. Kadish, *Inorg. Chem.* **1990**, 29, 4476–4482.
361. K. M. Kadish, Q. Y. Xu, J.-M. Barbe, *Inorg. Chem.* **1987**, 26, 2565–2566.
362. K. M. Kadish, Q. Y. Xu, J.-M. Barbe, J. E. Anderson, E. Wang, R. Guillard, *Inorg. Chem.* **1988**, 27, 691–696.
363. R. Guillard, C. Ratti, J.-M. Barbe, D. Dubois, K. M. Kadish, *Inorg. Chem.* **1991**, 30, 1537–1542.
364. K. M. Kadish, Q. Y. Xu, G. B. Maiya, J.-M. Barbe, R. Guillard, *J. Chem. Soc., Dalton Trans.* **1989**, 1531–1536.
365. K. M. Kadish, D. Dubois, S. Koeller, J.-M. Barbe, R. Guillard, *Inorg. Chem.* **1992**, 31, 3292–3294.
366. K. M. Kadish, D. Dubois, J.-M. Barbe, R. Guillard, *Inorg. Chem.* **1991**, 30, 4498–4501.
367. J. A. Ferguson, T. J. Meyer, D. G. Whitten, *Inorg. Chem.* **1972**, 11, 2767–2772.
368. C. R. Lorenz, H. D. Dewald, F. R. Lemke, *J. Electroanal. Chem.* **1996**, 415, 179–181.
369. K. M. Kadish, D. G. Davis, *Ann. N. Y. Acad. Sci.* **1973**, 206, 495–503.
370. K. M. Kadish, B. Boisselier-Cocolios, C. Swistak, J.-M. Barbe, R. Guillard, *Inorg. Chem.* **1986**, 25, 121–122.
371. K. M. Kadish, C. Swistak, B. Boisselier-Cocolios, J.-M. Barbe, R. Guillard, *Inorg. Chem.* **1986**, 25, 4336–4343.
372. R. Guillard, J.-M. Barbe, M. Fahim, A. Atmani, G. Moninot, K. M. Kadish, *New J. Chem.* **1992**, 16, 815–820.
373. K. M. Kadish, M. Autret, Z. P. Ou, K. Akiba, S. Masumoto, R. Wada, Y. Yamamoto, *Inorg. Chem.* **1996**, 35, 5564–5569.
374. Y. H. Liu, M. F. Benassy, S. Chojnacki, F. D'souza, T. Barbour, W. J. Belcher, P. J. Brothers, K. M. Kadish, *Inorg. Chem.* **1994**, 33, 4480–4484.
375. T. Barbour, W. J. Belcher, P. J. Brothers, C. E. F. Rickard, D. C. Ware, *Inorg. Chem.* **1992**, 31, 746–754.
376. C. A. Marrese, C. J. Carrano, *J. Chem. Soc., Chem. Commun.* **1983**, 1279.
377. S. Mangani, E. F. Meyer, D. F. Cullen, M. Tsutsui, C. Carrano, *Inorg. Chem.* **1983**, 22, 400.

378. C. A. Marrese, C. J. Carrano, *J. Chem. Soc., Chem. Commun.* **1982**, 1279.
379. C. A. Marrese, C. J. Carrano, *Inorg. Chem.* **1983**, 22, 1858–1862.
380. K.-y. Akiba, R. Nadano, W. Satoh, Y. Yamamoto, S. Nagase, Z. Ou, X. Tan, K. M. Kadish, *Inorg. Chem.*, **2001**, 40, 5553–5567.
381. K. M. Kadish, Z. Ou, X. Tan, W. Satoh, Y. Yamamoto, K. Akiba, manuscript in preparation.
382. L. Michaudet, D. Fasseur, R. Guillard, *J. Porphyrins Phthalocyanines* **2000**, 4, 261–270.
383. T. A. Rao, B. G. Maiya, *Inorg. Chem.* **1996**, 35, 4829–4836.

7

Electrochemical Measurements of Nitric Oxide in Biological Systems

Tadeusz Malinski
Ohio University, Athens, Ohio

7.1	Introduction	231
7.1.1	The Role of Nitric Oxide in Biological Systems	231
7.1.1.1	NO Release in Biological Systems	231
7.1.1.2	NO as a Regulator of the Cardiovascular System	233
7.1.1.3	NO in the Nervous System	234
7.1.1.4	NO as a Part of the Immune System	234
7.1.1.5	Pathology of NO Release	235
7.2	Electrochemical Methods for NO Detection	235
7.2.1	Electrochemical Oxidation of NO	235
7.2.2	Preparation of Porphyrinic Sensor	238
7.2.2.1	Operation Modes	242
7.2.3	Clark Probe for NO Detection	243
7.3	Measurement of NO in Biological Systems	244
7.3.1	Measurement of NO in a Single Cell	244
7.3.2	In vitro Measurement of NO in Tissue	246
7.3.3	In vivo Measurements of NO in the Kidney	248
7.3.4	In vivo Measurements of NO in the Beating Heart	249
7.3.5	Measurement of NO in the Brain	252
7.3.5.1	In vitro Measurement with Clark Probe	252
7.3.5.2	In vivo Measurement with Porphyrinic Sensor	252
7.3.6	Measurements of NO in Human Beings	255
	References	255

7.1

Introduction

7.1.1

The Role of Nitric Oxide in Biological Systems

Nitric oxide (NO) has been implicated in the pathogenesis of several diseases. A deficiency of NO may play a role in some diseases (hypertension, hyperglycemia, atherosclerosis, Parkinson's disease and Alzheimer's disease) whereas an increase of NO may participate in others (arthritis, reperfusion injury, cancer) [1–11]. Thus, from a biochemical as well as a medical perspective, it is important to quantify the details of NO production in abnormal and normal tissues, including direct measurements. NO is stable in oxygen-free and cell-free solutions. However, NO reacts rapidly with several components in vitro or in vivo, producing protein nitrosylation as well as reacting with hemoglobin and oxygen. In the presence of superoxide, NO is rapidly converted to peroxynitrite. Consequently, NO has a half-life of two to six seconds in vivo, and detection of NO in biological systems has been proven to be technically difficult [12, 13].

The currently used instrumental techniques for NO measurements are spectroscopic and electrochemical

methods [14, 15]. Mass spectrometry and gas chromatography have been used occasionally for NO detection but are much less sensitive. Spectroscopic methods are based on the detection of the products of NO oxidation: NO_2^- or NO_3^- (UV-visible spectroscopy, electron spin resonance (ESR) spectroscopy, or spin trapping). Electrochemical methods include voltammetry, amperometry, and coulometry. Electrochemical methods offer several features that are not available from analytical spectroscopic methods. Most important is the capability afforded by the use of microelectrodes for direct in situ measurements of NO in single cells near the source of NO synthesis (nitric oxide synthase NOS) [16–18]. Electrochemical methods detect NO directly and are based on electron exchange between NO and an electrode. All spectroscopic methods detect NO indirectly. Therefore, electrochemical methods are more suited than the spectroscopic methods for in situ, in vitro, and in vivo monitoring of NO concentration in biological systems.

7.1.1.1 NO Release in Biological Systems

Before 1987, NO biosynthesis was thought to be restricted to bacteria engaged in nitrification or denitrification reactions. However, we have recently learned that NO

can be released by many different cells in mammalian systems [19–21]. NO can play different physiological roles, depending on the place of its release. It can be a neurotransmitter when (for seconds) a small puff of it is generated by the neurons of central and peripheral nervous system. It can regulate blood pressure and inhibit blood coagulation when (for minutes) a larger burst of it is generated in the endothelium, a monolayer of cells lining the cardiovascular system. Also, NO can act as a cytostatic agent when (for hours) a continuous blast of it is biosynthesized by the immune system; its presence may halt the proliferation of cancer and pathogens [21].

NOS is the enzyme that biosynthesizes the cosubstrates L-arginine and O_2 into the coproducts NO and L-citrulline (Fig. 1) [22]. NOS generates NO by catalyzing the oxidation of a guanidine nitrogen on the amino acid L-arginine. The enzyme is stereospecific for the L-isomer, as D-arginine is not a substrate. This process is an overall five-electron oxidation of nitrogen with little or no chemical or biochemical precedence. Surprisingly, this multistep, odd-electron transfer is carried out by a single protein. There are two constitutive nitric oxide synthase (cNOS) isoforms, neuronal (nNOS), and endothelial (eNOS), and one inducible NOS isoform (iNOS). All three iso-enzymes are homodimers. Each monomer has a molecular weight ranging from 130 000 to 150 000

daltons, containing four prosthetic groups: flavin-adenine dinucleotide (FAD); flavin mononucleotide (FMN), (6R)-5,6,7,8-tetrahydrobiopterin (BH_4), and iron protoporphyrin IX (Heme) [23]. The turnover rate of NO production is about seven molecules of NO per eNOS monomer and about forty molecules of NO per nNOS. Since NO is hydrophobic (solubility in water is only 1.82 mmol/L) and somewhat lipophilic ($K_{ow} > 6.5$ at 37 °C), it diffuses rapidly through the hydrophobic environment of cell membranes like O_2 and N_2 . In the aqueous phase of the cytoplasm, the diffusion coefficient of NO is $3.6 \times 10^{-5} \text{ cm}^2 \text{ s}^{-1}$ [24]. Biosynthesized within the cell, NO may react with a select few types of molecules inside the cell, or outside (after free diffusion through the cell membrane). The most rapid scavenger of NO is superoxide (O_2^- , $k = 6.7 \times 10^9 \text{ M}^{-1} \text{ s}^{-1}$). The peroxynitrite ($OONO^-$) that is formed in the reaction between O_2^- and NO is quite stable, but when protonated ($pK_a = 6.8$), usually it quickly rearranges to H^+ and NO_3^- . Reaction of NO with O_2 is much slower and leads to production of NO^+/NO_2^- , followed by further oxidation to NO_3^- . NO may also react with a few metal ions (iron, copper or manganese), which are usually bound to proteins. The selective reactivity of NO with such proteins and its reaction with O_2^- and O_2 dominate the chemistry of NO in biological systems.

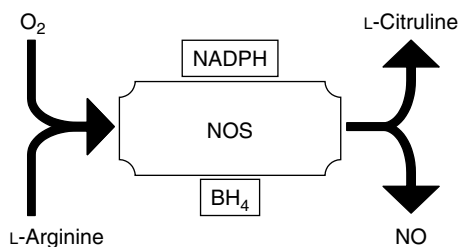


Fig. 1 NOS catalyzed production of NO from L-arginine. Tetrahydrobiopterin (BH_4) is an essential cofactor; NADPH acts as the source of electrons for oxygen reduction-activation.

To date, a cNOS and an iNOS have been found in many cell types in various parts of the body (Table 1). The monolayer of cells lining the cardiovascular system (the endothelium) contains mainly the eNOS and produces the largest amount of NO. The endothelium should be considered one of the largest specialized organs in the body; the total weight of eNOS cells in the human body is about 1.5 kg and is comparable with the weight of the liver. In the brain, NO is produced by both nNOS and eNOS. nNOS is also found in myocytes and in the skeletal muscles. NO can also act as a cytostatic agent in the immune system. NO from iNOS can be produced (after induction) by almost every cell in the human body, where it plays a primary role in host defense. In this role, NO may defend the body against invading bacteria, viruses, and even cancer.

7.1.1.2 NO as a Regulator of the Cardiovascular System

Vascular endothelial cells contain calcium-dependent constitutive eNOS. In order to maintain normal blood pressure, eNOS synthesizes NO in bursts lasting a few

minutes. The synthesis of NO is stimulated by chemical agonists such as bradykinin, acetylcholine, ATP, and several other agents that stimulate Ca^{2+} flux. However, physical agonists such as shear stress, flow, electrical current, light, and electromagnetic fields can also stimulate NO release in the cardiovascular system by causing the release of Ca^{2+} from internal stores of cytoplasm or by opening ion channels to allow the relatively large extracellular Ca^{2+} concentration into the cell [25]. After eNOS is turned on by Ca^{2+} flux and biosynthesizes NO for about a minute, it is turned off by the phosphorylation of one of its serine residues. The production of NO from eNOS is also inhibited by NO itself [26].

NO synthesized by eNOS cells, diffuses out in all directions. About 80 to 90% of NO released by the endothelium in the cardiovascular system is washed away by the blood, where it is used to prevent platelet aggregation and the subsequent formation of blood clots. The remaining amount of NO diffuses to the wall (smooth muscle) of arteries and veins and triggers a cascade of events leading to the production of cyclic GMP and smooth muscle relaxation. Relaxation of the smooth muscle allows the blood vessel to dilate (increase of vessel diameter), resulting in lowered blood pressure. The cardiovascular system maintains a constant level of NO at a given blood flow [27]. When blood flow increases, the endothelium releases more NO to maintain its constant concentration in the blood stream. When this normal level is not produced, either because production is blocked by administration of eNOS inhibitors or by pathological states such as deposition of cholesterol on the wall of the arteries (atherosclerosis), the vascular muscles do not relax to the

Tab. 1 NO synthases

Constitutive NOS	Inducible NOS
Vascular endothelium	Vascular endothelium
Brain	Vascular smooth muscle
Platelets	Macrophages
Adrenal glands	Kupffer cells
Peripheral nerves	Hepatocytes
Mast cells	Endocardium
Masangial cells	Masangial cells
Myocardium	Lymphocytes
Megakaryocytes	Chondrocytes
	Fibroblasts
	Neutrophils
	Megakaryocytes

appropriate degree, and vasoconstriction results [28, 29]. Vasoconstriction increases blood pressure, decreases flow, and is responsible for hypertension [30].

Platelets in the blood can also release NO [26]. One platelet can produce about 10^{-17} moles of NO in a single burst lasting a few minutes, when all its eNOS are activated. NO released by platelets prevents blood coagulation, formation of thrombi, and subsequent blockage of arteries. The pathology of this process leads to coronary thrombosis and is a major cause of stroke. The heart itself releases a significant amount of NO, on a beat-to-beat basis, during the systolic (compression) as well as the diastolic (decompression) period [10]. Under normal conditions NO is produced in the beating heart by eNOS cells, which are always located in close proximity 10 to 20 μm from cardiac muscle cells (myocytes). The basal concentration of NO in the heart is maintained at a relatively high level about 400 to 500 nmol/L, which changes gradually with the changing intensity of preload forces on the heart. Without the mechanical transduction of NO production, cardiac output would change abruptly as preload changed abruptly. Under conditions when heart has to provide extensive work (pumping blood under heavy stress, exercise, etc.), NO is produced by myocytes in addition to eNOS cells. Myocyte NO production is not stimulated by mechanical forces of the heart but by norepinephrine [27].

7.1.1.3 NO in the Nervous System

nNOS, like cNOS, is turned on by Ca^{2+} flux, but only produces NO for a few seconds before being shut off by the binding of NO to the heme in the active site; the nNOS then rests for a few minutes until the bound NO disassociates. NO generated by nNOS in certain neurons

in the peripheral nervous system serves as a neurotransmitter to help control the cardiovascular, respiratory and digestive systems [31–35].

In the central nervous system, NO acts as a neurotransmitter in the cerebellum. Its action resembles the interaction between eNOS cells and smooth muscle cells in a blood vessel. NO released from the postsynaptic neurons (in response to activation of receptor molecule *N*-methyl-D-aspartate) stimulates neighboring neurons to produce cyclic GMP. NO has also been implicated in another part of the brain – the hippocampus, which is involved in learning and the formation of memory. NO appears to be essential for establishing long-term potentiation memory but not short-term potentiation memory. In long-term potentiation, the strength of synaptic contact increases as a consequence of the frequent use of memory. Some recent findings support the possibility that NO can act as a retrograde messenger in this process. The inhibition of NO release in hippocampus prevents long-term potentiation and decreases learning capabilities.

7.1.1.4 NO as a Part of the Immune System

The role of NO in the immune system is much different from its role in the cardiovascular or the nNOS system [36–42]. In humans, almost every type of cell in the body can express iNOS. In contrast to nNOS and eNOS, the iNOS is calcium-independent. The signal to translate the DNA sequence for the iNOS into the amino acid sequence for the iNOS enzyme comes from certain cytokines, which are produced by the infected cells. Any kind of infection (including bacterium, viruses, or cancer) will lead to the production of cytokines. Cytokines carry the message of the infectious state to the surrounding cells,

which will start to produce iNOS. Immediately after translation is complete and prosthetic groups are in place, iNOS will continuously produce large amounts of NO for an extended period (several hours). The total NO production will therefore be much higher than that produced by eNOS.

iNOS produces a sufficient concentration of NO to locally inhibit ribonucleotide reductase, the enzyme that converts ribonucleotides to the deoxyribonucleotides necessary for DNA synthesis, hence the profound cytostatic effect of NO on the proliferation of rapidly dividing tumor cells or pathogens. In addition, DNA synthesis is a fundamental step in normal cell proliferation. Even normally high NO concentrations from cNOS can inhibit the ribonucleotide reductase, thus halting the proliferation of smooth muscles around major arteries and cardiac myocytes. NO is not toxic even at higher biological concentrations. Therefore, it is unlikely that NO can actually kill tumor cells but just limit their proliferation.

7.1.1.5 Pathology of NO Release

A pathology of NO production can lead to many diseases (Table 2). In most

Tab. 2 Pathology of NO release

<i>NO concentration</i>	
<i>Too low</i>	<i>Too high</i>
Hypertension	Septic shock
Atherosclerosis	Hypotension
Diabetes	Excessive bleeding
Ischemia (stroke, heart attack)	Meningitis
Alzheimer's disease	Rheumatoid arthritis
Parkinson's disease	
Fibrosis	
Cancer	

life-threatening diseases such as hypertension, atherosclerosis, and diabetes, the net concentration of NO is lower than in a healthy system. This does not necessarily mean that the expression of eNOS or nNOS is lower. In some of these diseases, eNOS expression is even higher (hypertension).

7.2

Electrochemical Methods for NO Detection

7.2.1

Electrochemical Oxidation of NO

Electrochemical methods for NO determination offer several features that are not available with spectroscopic approaches. Perhaps the most important is the capability of microelectrodes to directly measure NO in single cells in situ, in close proximity to the source of NO generation. Figure 2 shows sensors that have been developed for the electrochemical measurement of NO. One is based on the electrochemical oxidation of NO on a platinum electrode (the classical Clark probe for detection of oxygen) and operates in the amperometric mode [17]. The other is based on the electrochemical oxidation of NO on conductive polymeric porphyrin (porphyrinic sensor) [24]. The Clark probe uses a platinum wire as a working electrode (anode) and a silver wire serves as the counterelectrode (cathode). The electrodes are mounted in a capillary tube filled with a sodium chloride/hydrochloric acid solution separated from the analyte by a gas-permeable membrane. A constant potential of 0.9 V is applied, and direct current (analytical signal) is measured from the electrochemical oxidation of NO on the platinum anode. In the porphyrinic sensor, NO is catalytically oxidized on a polymeric metalloporphyrin

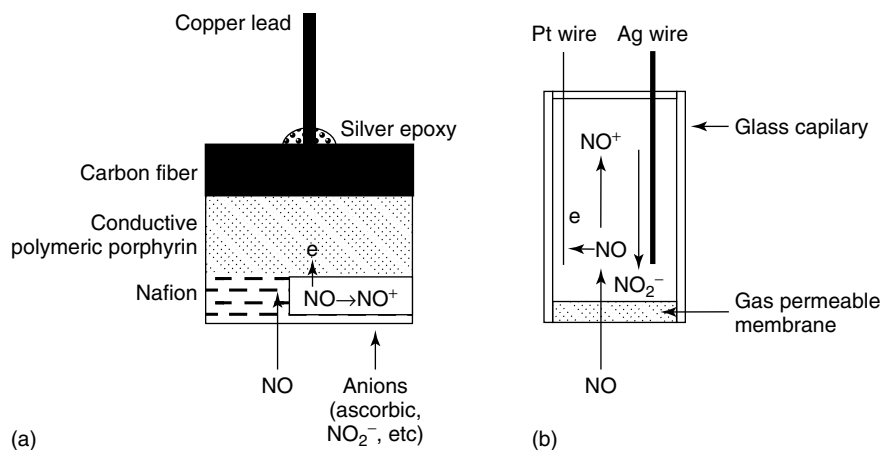
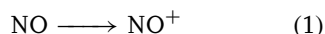


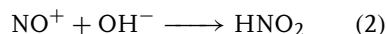
Fig. 2 Schematic diagram of the porphyrinic sensor (counterelectrode is not shown) (a) and Clark-type probes, as adopted for determination of NO (b).

(*n*-type semiconductor) on which the oxidation reaction occurs at 610 mV (versus a saturated calomel electrode (SCE)), that is, about 200 mV lower than the potential required for NO oxidation on platinum or carbon electrodes. The current efficiency for the reaction on porphyrinic film is much higher than on platinum or carbon, even at the physiological pH of 7.4.

Generally, the oxidation of NO on solid electrodes proceeds via “EC mechanisms”: electrochemical oxidation (1) followed by a chemical reaction (2) [24, 43, 44]. The first electrochemical step is a one-electron transfer from an NO molecule to the electrode, resulting in the formation of NO^+



NO^+ is a relatively strong Lewis acid and, in the presence of OH^- , is converted to nitrite (NO_2^-) in the fast, highly irreversible chemical step:



Since the oxidation potential of nitrite in an aqueous solution is only 60 to 80 mV, more positive than that of NO, oxidation of

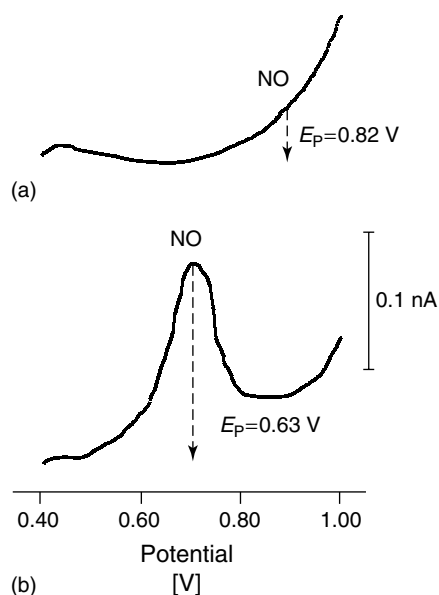
NO on solid electrodes utilizing scanned potentials, that is, with electrodes operated in the voltammetric mode, results in further oxidation of nitrite to nitrate, a process in which two additional electrons are transferred. Currents resulting from the one-electron oxidation of NO to NO_2^- , and two-electron oxidation of NO_2^- to NO_3^- , are highly overlapped.

Using a bare metal, carbon, or porphyrin electrode, it is impossible to differentiate nitrite produced electrochemically than from that derived from chemical NO oxidation. Therefore, a barrier has to be placed between the electrode and the analyte to prevent access of nitrite to the electrode surface. This has been achieved in the porphyrinic sensor by depositing a layer of cation exchanger (Nafion), which repels negatively charged species such as NO_2^- (Fig. 2a). Nafion also prevents the formation of NO_2^- in the film after one electron oxidation of NO to NO^+ . In the Clark-type probe, the analyte solution containing NO and nitrite are separated from the inner electrode solution by a gas-permeable membrane.

Fig. 3 DPV's obtained from oxidation of 0.1- μM NO on a carbon fiber electrode covered with Nafion and carbon fiber electrode covered with polymeric (TMHPP)Ni porphyrin and Nafion.

Oxidation of NO on classical conductive materials such as noble metals (platinum, gold, etc.) or carbon, which are used as electrodes, produces a relatively low current at neutral pH. This is due to a strong absorption of NO to the electrode surface and a slow rate of electron transfer between NO and the electrode. Typical differential pulse voltammograms (DPV) of NO on carbon fiber covered with Nafion, and carbon fiber covered with porphyrinic film and Nafion are shown in Fig. 3. There is about a 190 mV difference between the oxidation potential of NO on carbon fiber and porphyrinic film. A concentration of 0.1- μM NO produces a very small current on the carbon fiber electrode operating in the DPV mode (Fig. 3a). However, this same carbon fiber covered with a layer of polymeric porphyrin produces a much larger current (Fig. 3b) for NO oxidation. The current generated on polymeric porphyrin is mass transport controlled and is linearly proportional to the concentration of NO. The linearity is observed over four orders of magnitude of NO concentration [45].

The sensitivity and selectivity of the polymeric porphyrin depends not only on the potential of NO to oxidize but also on the fast process of electrochemical NO oxidation, which generates the high current. In addition, surface effects, axial ligation to the central metal in the porphyrin, nature of the central metal (iron \geq nickel > cobalt \gg zinc, copper), gas permeability through sensor layer(s), and fast removal of NO^+ by Nafion are all important in promoting fast and selective oxidation



of NO. Typical current density for NO oxidation on a porphyrinic sensor is 0.3 to 1.8 $\text{mA cm}^{-2} \mu\text{M}^{-1}$, and is at least four to seven times higher than that which can be obtained on activated carbon fiber covered with Nafion. Current density for NO oxidation on the porphyrinic sensor depends on film quality, and should be at least 0.4 $\text{mA cm}^{-2} \mu\text{M}^{-1}$ for measurements in biological environments. Sensors based on high-quality polymeric films will show current densities of 1.5–1.8 $\text{mA cm}^{-2} \mu\text{M}^{-1}$ and a detection limit approaching 10^{-9} M NO. A current density comparable to that of carbon fiber indicates poor quality (high impedance) of the porphyrinic film. Moreover, the design of the porphyrinic sensor results in a high selectivity for NO because the current generated by NO oxidation is usually several orders of magnitude higher than the current produced by other species oxidized at a similar potential. A typical example of such a potential interferant is dopamine, which can be oxidized on a carbon fiber covered with Nafion at a

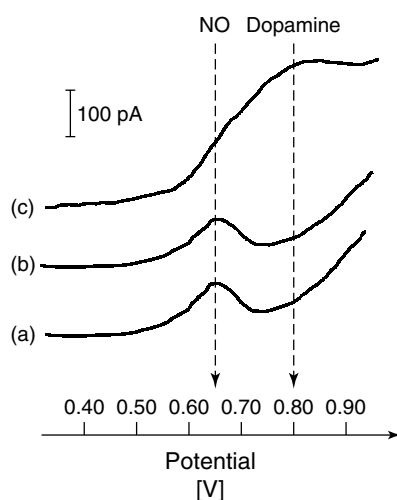


Fig. 4 DPV's of 50-nM NO solution recorded in the absence (a) and in the presence of 1 μ M of dopamine (b) and 0.2 mM of dopamine (c).

potential of 0.56 V. However, oxidation of dopamine on a porphyrinic sensor occurs at 0.80 V with the current density, which is about four orders of magnitude lower than that observed for the oxidation of NO (Fig. 4). Dopamine at a concentration of 0.1 μ M produces no measurable current, and at 0.2 mM produces the current comparable to that produced by the oxidation of 50 nM NO.

7.2.2

Preparation of Porphyrinic Sensor

Microsensors are produced by threading a carbon fiber (diameter 7 μ m) through the pulled end of a capillary tube with about 1 cm left protruding. Nonconductive epoxy is put at the glass–fiber interface. After the epoxy cement drawn into the tip of the capillary has cured, the carbon fiber is sealed in place. The carbon fiber is then sharpened by gradual burning (propane-air microburner, 1300–1400°). The sharpened fiber is immersed in melting wax-rosin (5 : 1) at a controlled temperature for 5 to 15 sec, and after cooling is sharpened again. The flame temperature

and the distance of the fiber from the flame need to be carefully controlled. The resulting electrode is a slim cylinder with a small diameter (0.5–2 μ m) rather than a short taper, a geometry that aids in implantation and increases the active surface area. The tip (length 2–6 μ m) is the only electroactive part of the carbon fiber. For the sensor to be implanted into a cell, this length must be less than the cell thickness. The unsharpened end of the fiber is attached to a copper wire lead with silver epoxy cement. The sharpened tip of the carbon fiber is covered with a film of conductive polymeric film (Fig. 5).

Molecules that undergo fast random polymerization on the electrode surface, like tetraphenylporphyrins with amino or pyrrole substituents on the phenyl ring, will form films with a well-developed surface but poor catalytic properties for NO oxidation and low electrical conductivity. Out of more than forty different porphyrinic and nonporphyrinic and organic and inorganic electrocatalysts tested for these properties, only three show the desired characteristics: tetrakis (3-methoxy-4-hydroxyphenyl)

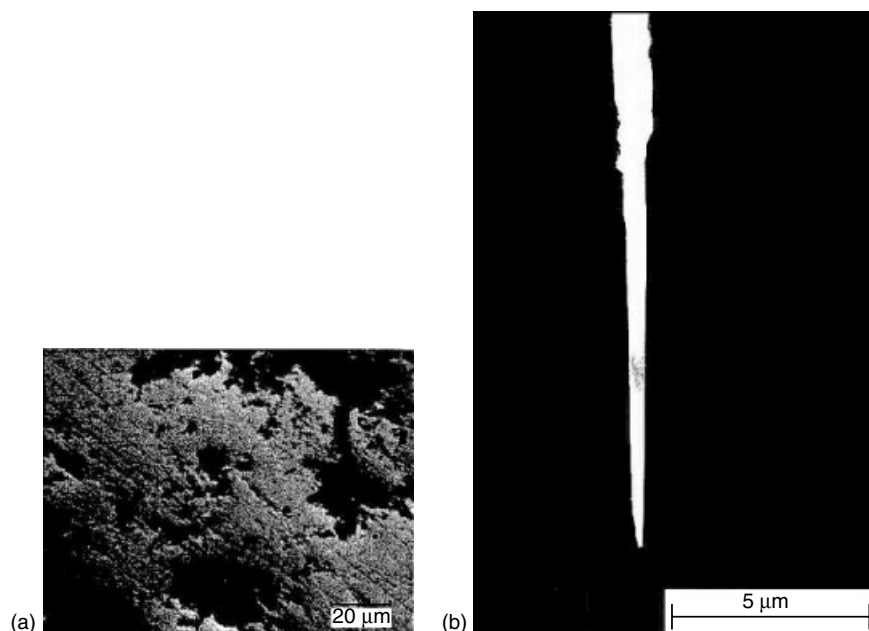


Fig. 5 Scanning electron micrograph of a thin film of polymeric (TMHPP)Ni (a) and the tip of a thermally pointed carbon fiber sensor covered with polymeric (TMHPP)Ni and Nafion film (b).

porphyrin (TMHPP), *meso*-tri (N-methyl-4-pyridinium)-*p*-phenylene-5'-O-2', 3'-O-isopropylideneuridine-porphyrin (PUP) and N, N'-bis[5-*p*-phenylene-10,15,20-tris(3-methoxy-4-hydroxyphenyl)-porphyrin]-1,10-phenanthroline-4,7-diamide ($H_2(1,10\text{-phen})(TMHPP)_2$), with Ni(II), Co(II) or Fe(II) as central metals [46–51]. The continuous-scan cyclic voltammograms showing formation of the films from (TMHPP)Ni and (PUP)Co are depicted in Fig. 6. The detection limit for NO depends on film quality and varies between 5×10^{-8} and 10^{-9} M. The best sensitivity is usually obtained using a PUP film. However, the stability of TMHPP films or $H_2(1,10\text{-phen})(TMHPP)_2$ film (about 60 days) is much better than the stability of PUP films (about 7 days).

As described previously, the porphyrinic film is covered with Nafion. This serves

to attract NO^+ from the underlying polymeric porphyrin surface and prevents its further oxidation to NO_2^- , as well as to prevent access of NO_2^- and other common biological anions such as ascorbate to the porphyrinic film. The current due to NO oxidation on polymeric porphyrin initially increases with thin Nafion coverage. However, thicker films ($>1 \mu m$) cause the NO current to decrease. In order to test the integrity of the Nafion film, the current due to the Ni(II)-Ni(III) reaction can be measured. Oxidation of Ni(II) to Ni(III) in the film occurs only if diffusion of the OH^- counterion into the film occurs. Because a Nafion film with sufficient thickness (without pinholes) will prevent OH^- diffusion, a lack of Ni(II)-Ni(III) conversion in the voltammogram (obtained in 0.1 M NaOH) is a good method for verifying film integrity. Figure 7 shows

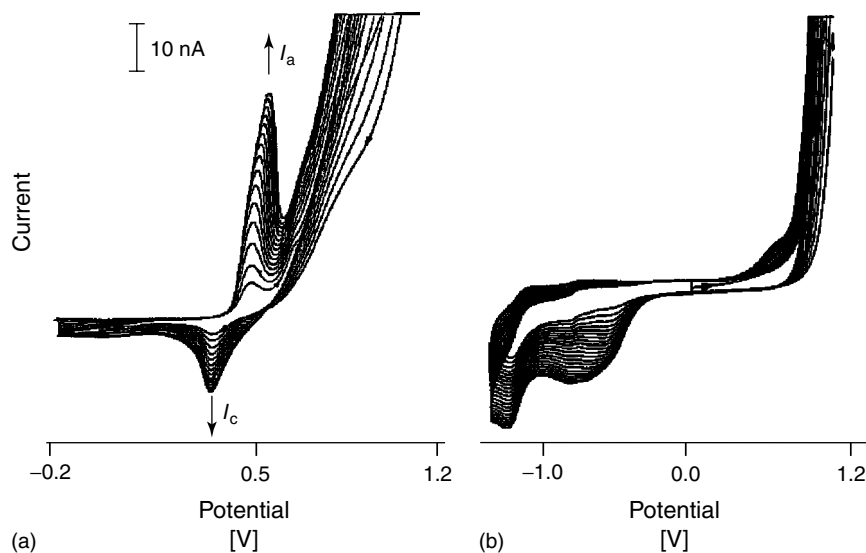


Fig. 6 Continuous-scan cyclic voltammograms obtained by a polymerization of (TMHPP)Ni (a) and (PUP)Co (b) on a carbon electrode.

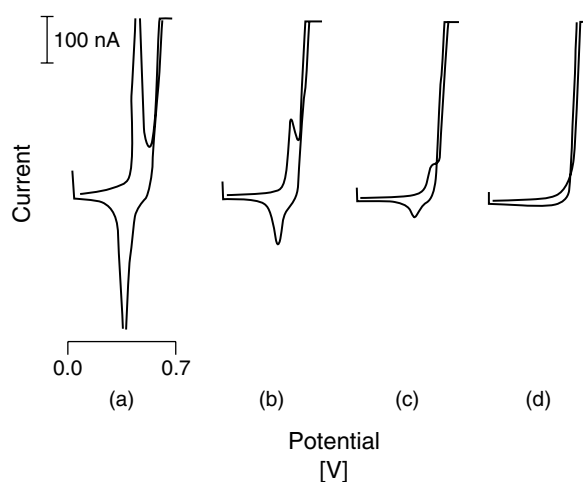


Fig. 7 Cyclic voltammograms of Ni(II)/Ni(III) couple recorded at the different coverage of (TMHPP)Ni film with Nafion.

cyclic voltammograms obtained for this same poly-(TMHPP)Ni film covered with Nafion films of different thickness, after sequential coating by dipping the carbon fiber for 5 s into a 1.25% ethanolic solution of Nafion. Each coat of Nafion decreases

Ni(II) and Ni(III) peaks by a factor of about three. The thickness of Nafion obtained after three coatings (total 15s) is sufficient to prevent diffusion of high concentrations of small anions. Sensors have to be further tested for their response to nitrite in a

buffer solution at pH 7.4. A lack of response to $20\text{-}\mu\text{M}$ NO_2^- , a concentration 1 to 2 orders of magnitude higher than that expected in plasma, indicates that Nafion coating is sufficient for NO measurements in this medium. It should be noted that NO_2^- concentrations of $\geq 10\text{ }\mu\text{M}$ are found in airway lining fluid and saliva, representing a potential problem. Nafion coatings, therefore, may need to be individualized for different biological systems.

Multiple porphyrinic electrodes (an electrode array) for studies of NO release in large cells and tissues can be constructed in the disk form using glass microcapillaries. A bundle of 2 to 6 fibers mounted in a glass capillary in a similar way to that described for a single fiber can be effective in many large cell or tissue experiments [6]. The use of large electrodes (diameter $> 100\text{ }\mu\text{m}$) does not improve the performance of the sensor. This is due to an increase of the background current (capacity current), and the inability to place the sensor at the site where the highest concentration of NO is to be expected (the cell membrane). This last limitation can be overcome by using a large surface sensor on which cells can

be grown directly. In this case, the sensor consists of vitreous carbon support covered with a polymeric film and Nafion (Fig. 8). The detection limit of this sensor is similar to that obtained from the carbon fiber sensor. This sensor provides a convenient way to measure NO release in cell cultures under various conditions.

Carbon fiber-based sensors are too fragile to be used in deep-tissue measurements. However, these sensors can be protected by insertion into an intravenous catheter, which can be implanted in tissues or blood vessels. To make the catheter-protected sensor, a bundle of (5–7) carbon fibers are mounted inside a truncated needle (Fig. 9). After curing, the shaft of the truncated needle is coated with a nonconducting epoxy. Then, conductive porphyrinic film and Nafion are deposited on the protruding carbon fiber. A puncture needle is used to place a Teflon catheter with a perforated tip deep inside the tissue of a blood vessel. The Teflon catheter's position is secured and the puncture needle is removed. Then, an NO sensor mounted at the end of a truncated needle shaft is inserted into the hollow Teflon catheter. The

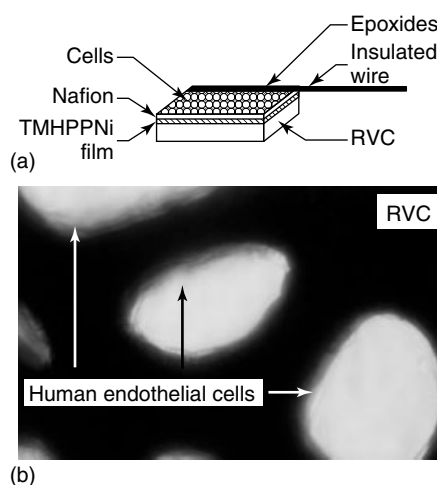


Fig. 8 Schematic diagram of a porphyrinic sensor adapted to detect NO released from cells grown directly on its surface (a); photograph of eNOS cells (human umbilical vein eNOS cells) grown directly on a porphyrinic sensor (b).

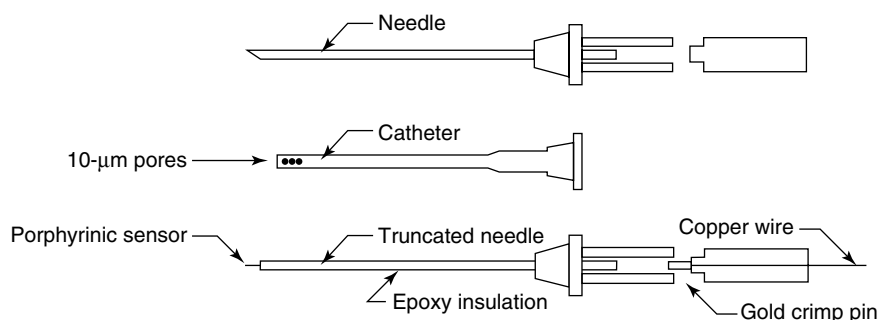
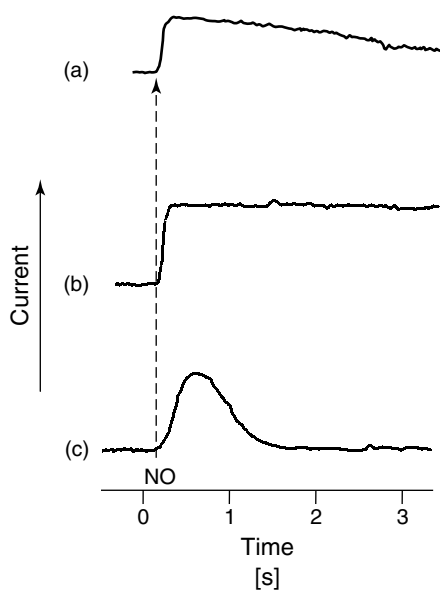


Fig. 9 Schematic diagram of an intravenous catheter-protected porphyrinic sensor for in vivo measurement.

NO sensor should be just short enough to fit inside the perforated catheter and protect the NO sensor tip from mechanical damage.

7.2.2.1 Operation Modes

DPV or chronoamperometry can be used to monitor analytical signals (current is linearly proportional to NO concentration). In DPV, a potential modulated with 40-mV rectangular pulses is linearly scanned



from 0.4 to 0.8 V. The resulting voltammogram (alternating current versus voltage plot), contains a peak due to NO oxidation. The peak current should be observed at a potential of 0.63 to 0.67 V (using 40-mV pulse amplitude), which is the characteristic potential for NO oxidation on a porphyrinic-Nafion sensor. In chronoamperometric measurements, a constant potential between 0.65 and 0.70 V is kept constant, and a plot of current versus time is recorded. This amperometric method (with a response time better than 0.1 ms), provides rapid quantitative response to minute changes in NO concentration. DPV, which also provides quantitative information but requires approximately 5 to 40 s for the voltammogram to be recorded, is used mainly for qualitative analysis (i.e. verification of specificity). Several other electroanalytic techniques, including normal pulse voltammetry, square wave voltammetry, and coulometry, can be used to measure NO with a porphyrinic sensor. Amperograms and voltammograms can be recorded with three-electrode systems. Such three-electrode systems consist

Fig. 10 Amperometric curves showing porphyrinic sensor responses to NO in homogenous static solution (a), homogenous flowing solution, and a heterogeneous flow solution (blood).

of (1) an NO sensor working electrode, (2) a platinum wire (0.25 mm) counter-electrode, and (3) a silver/silver chloride electrode or calomel electrode as the reference electrode. A typical amperometric response of the sensor under varying flow conditions is shown in Fig. 10. The current measured with both techniques is (at constant NO concentration) controlled by mass transport (laminar flow or diffusion) of NO to the electrode. Therefore, for accurate determination of NO concentration, the sensor has to be calibrated under mass transport conditions similar to those used for *in vivo* or *in vitro* measurements. The flow rate of blood at which the NO is monitored has to be measured or calculated based on the diameter of the blood vessel and the blood pressure. A flow system of the mimetic solution of blood (e.g. an aqueous solution of dextran, MW 70 000 with a viscosity of 2.8 cP at 37 °C) can be used to calibrate the NO sensor response outside a biological system.

7.2.3

Clark Probe for NO Detection

The Clark probe was originally designed for the detection of oxygen. The probe consists of a glass pipette whose opening is sealed with a thick, gas-permeable rubber membrane. Only gases readily diffuse into the glass pipette through the membrane and are then oxidized or reduced at the surface of the metal electrode (working electrode). In the Clark probe for oxygen detection, a working electrode (platinum) is polarized with a potential of -0.9 V versus the counter/reference electrode (silver), and a current due to the reduction of oxygen is observed. The reduction of oxygen involves a four-electron transfer yielding superoxide (O_2^-) and peroxide (O_2^{2-}) intermediates, with the final reduction

product being water. For the detection of NO with the Clark probe, the polarization of the electrodes should be $+0.9$ versus the silver electrode (*vis-à-vis* -0.9 for oxygen) [17]. A mixture of NaCl and HCl can be used as the electrolyte; the probe does not respond to NO in basic solution.

The Clark probe operates in the amperometric mode. As an analytical signal, current is measured at a constant potential of 0.9 V. For a Clark probe with a glass pipette diameter of $300\text{-}\mu\text{m}$ platinum anode ($50\text{-}\mu\text{m}$) and silver cathode ($200\text{-}\mu\text{m}$), the current is 3 to $100\text{ pA}/\mu\text{M}$. This current is relatively small because of the low NO concentration achieved within the glass pipette. The detection limit of the electrode is about 10^{-8} M when determined in a homogeneous solution, where a constant concentration of NO can be achieved on both sides of the gas-permeable membrane. However, when the probe is used for measurements of low concentrations of NO in a biological environment (heterogeneous NO solution), several problems may arise that limit this application.

The response of the electrode is relatively slow, with a half-rise time of 1.4 to 3.2 s. This is about three orders of magnitude slower than the typical response time of porphyrinic sensors. The slow response time is mainly due to the long diffusion distance to the electrode. Because of its relatively large size, the electrode cannot be placed exactly at the site where NO concentration is highest (e.g. membrane of the cell). Furthermore, a fraction of NO that reaches the probe chamber (capillary) may be lost inside due to reaction with oxygen, which also readily diffuses through the membrane. Thus, while the gas-permeable membrane will prevent diffusion of NO_2^- from the sample solution to the capillary chamber, it will not prevent the formation of NO_2^- and

NO_3^- in the chamber resulting from the reactions of NO with O_2 and O_2^- ; the latter is an intermediate product of electrodic reduction of oxygen in the silver cathode. Accordingly, the concentration of NO measured with a Clark probe in a biological medium will usually be one to two orders of magnitude lower than the concentration measured with a porphyrinic sensor. The highest sensitivity for NO is obtained at a potential of approximately 0.9 V.

7.3

Measurement of NO in Biological Systems

7.3.1

Measurement of NO in a Single Cell

By use of a manual or motorized computer-controlled micromanipulator with 0.2- μm x-y-z- resolution, the porphyrinic sensor can be implanted into a single cell, placed on the surface of the cell membrane, or kept at a controlled distance (0.2–10 μm) from an NO generating cell [16, 25, 52–58].

When the tip of the sensor touches the cell membrane, a transient small electrical noise is observed. This is a good indicator of zero distance from the cell, and from this point, the sensor can be moved out from the surface by 0.2-mm increments controlled by a computer. Injection of NOS agonists can be done with micro-, nano-, or femto injectors. Injection of larger volumes of agonists with a microinjector will cause a “jet effect,” and the initial release of NO will be due to a mechanical force agonist (shear stress). The shear stress peak of NO will be followed by an NO peak resulting from the effect of the chemical agonist of NOS. Injection of the agonist with a nano- or femto injector will reduce significantly the jet effect and subsequent NO release due to shear stress.

Figure 11 shows the pattern of NO release from a single human umbilical vein endothelial cell (HUVEC) isolated from the culture, and the pattern of NO release from a single cell still in the culture. The sensor was placed in close proximity to the cell membrane ($4 \pm 1 \mu\text{m}$). This

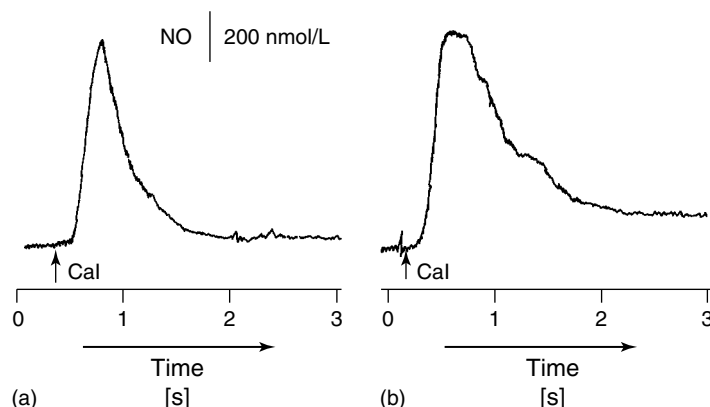


Fig. 11 Amperogram of NO recorded with porphyrinic sensor (diameter 0.75 μm) placed $4 \pm 1 \mu\text{m}$ from the surface of the isolated single eNOS cell (a) and placed $4 \pm 1 \mu\text{m}$ from the surface of single cell in the cell culture (6×10^6 cells) (b). NO release was stimulated from human umbilical vein eNOS cells with calcium ionophore (Cal).

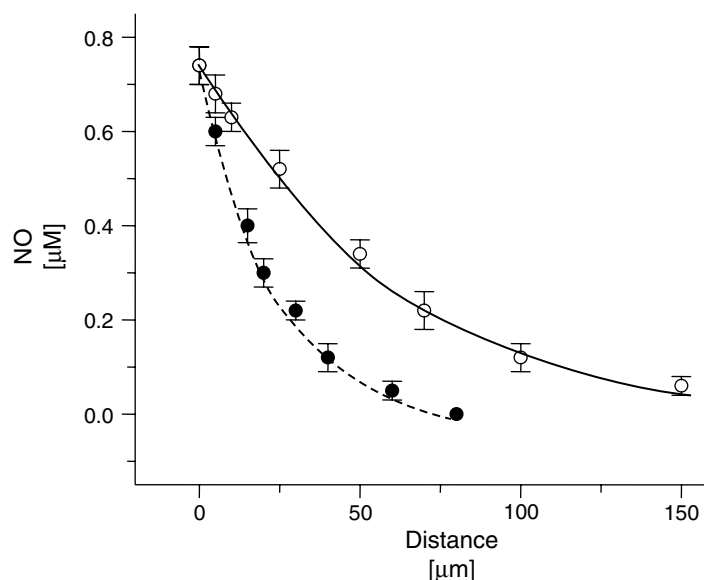


Fig. 12 Exponential decrease of NO concentration with increasing distance of porphyrin sensor from the membrane of a single isolated eNOS cell (solid line), a single eNOS cell in cell culture and a single eNOS cell in culture (3×10^4 cells). NO release was stimulated from HUVEC with Cal.

figure shows that the peak concentration of NO on the membrane of a single cell isolated from a given eNOS cell culture will be the same as the peak concentration of NO measured on the membrane of a single cell in the same culture. However, the duration of the plateau is significantly extended when measurements are done in a cell culture. This difference is due to the horizontal gradient in NO concentrations, which is much smaller in a cell culture. The depletion of NO from the membrane is slower when the cell is surrounded by other cells that release NO in a culture. In a single isolated cell, the gradient of NO concentration between the surface and bulk solution is high all around the cell. Therefore, the process of NO depletion is relatively rapid.

The height of the peak of NO release depends on the distance of porphyrinic

sensor from a membrane surface (Fig. 12). The highest NO concentration is observed on the HUVEC membrane (750 ± 20 nM), with concentration decreasing exponentially with the distance from the cell membrane. At about $60 \mu\text{m}$ from the cell membrane, the NO concentration was 80 nM (single isolated cell) and at a distance greater than $70 \pm 15 \mu\text{m}$ from the cell membrane, NO is not detectable by the porphyrinic sensor. The decrease of NO concentration from the cell surface is not as rapid when the cell is surrounded by another cell from cell culture. However, at a distance greater than 170 ± 15 nm from the cell membrane (in cell culture) NO is also not detectable by the porphyrinic sensor.

From an analytical standpoint, the detection of NO at the site of the highest concentration, the surface of the

eNOS cell membrane, is the most convenient and accurate method for measurement of endogenous NO. Because of the hydrophobic properties of NO (partition coefficient between nonaqueous/aqueous phase = 6.5), the membrane is a storage reservoir for NO [24]. Therefore, a small volume membrane develops a relatively high steady state concentration of NO within a short period of time after activation of NOS. During the diffusion of NO through the aqueous phase, significant dilution occurs. Thus, in situ measurement of NO released from a single isolated cell, from a group of tissue culture cells, or from an isolated artery, requires the positioning of the electrochemical porphyrinic sensor on the membrane surface of the endothelium or in close proximity. As can be seen in Fig. 12, NO decreased exponentially with distance from the eNOS cell; therefore, even under static conditions of eNOS cell culture medium, it would be impossible to detect NO by the sensor at a distance greater than 170 μm from the surface of endothelium. The diameter of the sensor (smaller than, or comparable to the diameter of the eNOS cell) allows its placement on or close to the membrane surface. These features of electrochemical detection with the sensor offer significant practical advantages over UV-visible spectroscopy, ESR spectroscopy, or biochemical assays in real-time detection of NO [15].

An additional feature of electrochemical detection is the direct measurement of net NO (biologically active) concentration and not a total concentration of NO produced by the endothelium, which includes its oxidation products NO_3^- , NO_2^- , or peroxynitrite (ONOO^-). The net NO concentration measured by the sensor is that concentration detectable after about a millisecond time (the response time of

the sensor). This concentration of NO has a real physiologic meaning as the NO can rapidly diffuse to smooth muscle cells and cause their relaxation.

7.3.2

In vitro Measurement of NO in Tissue

NO concentration can be measured with electrochemical sensors in tissue slices as small as 50 μm [9, 10, 28, 54, 59]. NO concentration was measured in vitro in the carotid artery of normotensive Wistar-Kyoto (WKY), spontaneously hypertensive rats (SHR), and spontaneously hypertensive rat-stroke prone (SHR-SP) using a porphyrinic sensor placed near the cell surface ($10 \pm 2 \mu\text{m}$). Amperometric curves showing the change of NO concentration with time were recorded in the absence and presence of membrane superoxide dismutase (SOD) with attached polyethylene glycol 400 (PEG-SOD activity 100 U ml^{-1}) (Fig. 13). Since PEG-SOD rapidly dismutates superoxide (O_2^-), this indirect approach was used to estimate production of O_2^- at the time of NO release. After addition of CaI, a rapid increase of NO concentration was observed. Peak NO concentration was higher for WKY than SHR and SHR-SP rats (530, 320, and 290 nM, respectively). In the presence of PEG-SOD, an increase of peak NO concentration was observed for both WKY and hypertensive rats. In the WKY strain, SOD treatment increased the peak NO release by 8%. However, for hypertensive rats the increase of NO peak concentration was much higher (40–60%) in the presence of PEG-SOD than for normotensive rats. This finding indicates that a significant concentration of O_2^- is generated in the carotid artery of hypertensive rats, and this O_2^- consumed a major portion of NO in a

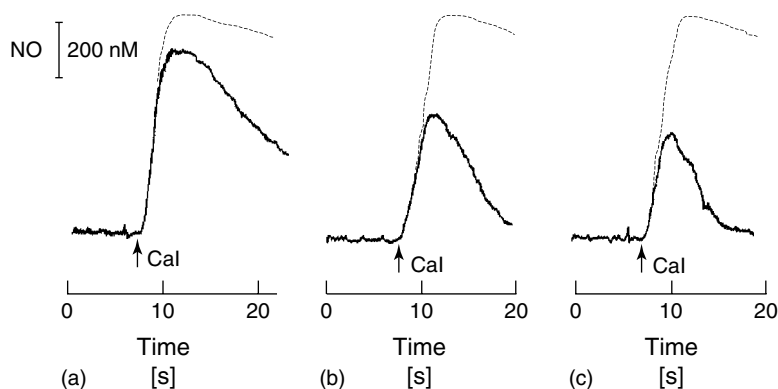


Fig. 13 Typical amperograms showing changes of NO concentration near the surface ($10 \pm 3 \mu\text{m}$) of the endothelium of the carotid artery of WKY rat (a) SHR-SP rats (b) and diabetic rats (c). NO was measured with a porphyrinic sensor (diameter $3 \mu\text{m}$) in the presence (dotted line) and absence (solid line) of PEG-SOD.

fast chemical reaction. This process leads to the decrease of the biologically active NO concentration, followed by vasoconstriction and hypertension.

This is a typical example of the unique application of the electrochemical sensor for the detection of NO release from normotensive and hypertensive rats [6, 29, 30, 55, 60–62]. It has been reported, based on spectroscopic measurements, that the endothelium of hypertensive rats produced more $\text{NO}_2^-/\text{NO}_3^-$ than the endothelium of WKY rats [63]. However, these reports were in contradiction to the data obtained on smooth muscle relaxation, hindered in hypertensive rats [62]. This means that the endothelium of hypertensive rats should produce less NO. Electrochemical measurements with the porphyrinic sensor clearly show that the biologically active net concentration of NO produced by the endothelium of hypertensive rats is lower than that produced by the endothelium of WKY rats. These results correlate well with previously reported smooth muscle relaxation data. Total production of NO by the endothelium of hypertensive rats is higher

than in WKY rats. However, the endothelium of hypertensive rats also generated significant amounts of superoxide, which rapidly reacts with NO to produce the stable product OONO^- . Therefore, the net NO concentration as detected by the porphyrinic sensor is much lower in hypertensive rats as compared with WKY rats. In the presence of membrane permeable PEG-SOD, an effective dismutation of O_2^- occurred, followed by a large increase of net NO concentration in SHR rats, finally exceeding that observed for WKY rats in the absence of PEG-SOD. Peroxynitrite when protonated ($\text{pK}_a = 6.8$) to HOONO usually undergoes isomerization ($t_{1/2} < 1 \text{ s}$) to form hydroxyl cation and nitrate anion [64]. However, at high concentrations of NO and O_2^- , large concentrations of HOONO can be formed. Under these conditions, HOONO may undergo cleavage to a hydroxyl free radical (OH^\bullet), a nitrogen dioxide free radical (NO_2^\bullet), or nitronium cation (NO_2^+) and hydroxide anion (OH^-). Three of these cleavage products (OH^\bullet , NO_2^- , NO_2^+) are among the most reactive and damaging species in biological

systems, and may be major contributors to the severe damage of the endothelium and the cardiovascular system occurring in hypertension. A similar increase in O_2^- production by dysfunctional endothelium is observed during endotoxemia.

7.3.3

In vivo Measurements of NO in the Kidney

Figure 14(a) shows the amperometric curve measured in vivo during endotoxemia with a porphyrinic sensor placed in the rat kidney. During administration of lipopolysaccharide (LPS), an increase of

NO production from its basal concentration was observed. The concentration of NO reached a peak of 210 nM after 240 s, persisting for 15 min before decaying at a rate of 0.7 nM s^{-1} . After 45 min, the NO concentration started to rise again, but at a much slower rate. A plateau of NO release was established $80 \pm 15 \text{ min}$ after LPS administration.

UV-visible spectroscopy (Griess reagent) was used to determine a change of NO_2^-/NO_3^- concentration in blood during endotoxemia [65]. Both NO_2^- and NO_3^- are the end products of NO oxidation in biological systems (Figure 14b). The concentration of NO_2^- and NO_3^-

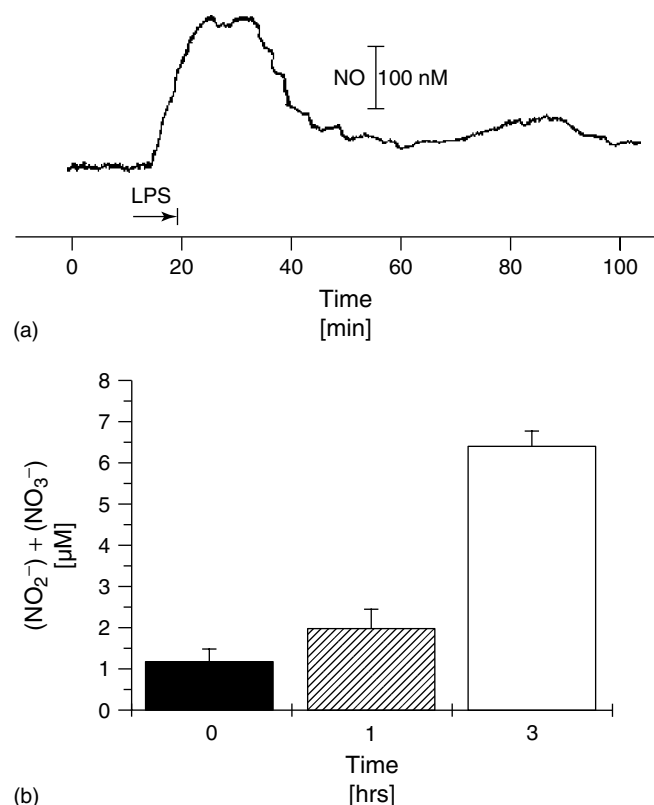


Fig. 14 (a) NO release recorded in the kidney of a rat during septic shock; (b) concentration of NO in the blood measured by UV-visible spectroscopy (Griess reagent) during septic shock.

significantly increased from basal 1.3 to 6.3 μM after 6 h of endotoxemia. The most dramatic rate of increase was observed after 3 h of endotoxemia. The concentration of O_2^- (measured in vitro during stimulation with A23187 using a chemiluminescence method) also increased significantly during endotoxemia [9]. During the first hour of endotoxemia, the O_2^- concentration increased threefold relative to the control.

Induction of iNOS by bacterial toxins directly or through cytokines leads to the generation of NO in arterial walls. Administration of toxin (LPS) also generated NO by calcium-dependent eNOS in the endothelium during endotoxemia. The high production of NO by the endothelium is observed only in the early acute phase of endotoxemia (first 20 min); however, it has a profound effect on the late chronic phase of endotoxemia when iNOS becomes the main generator of NO. The porphyrinic NO sensor measured only free NO; that is, the net NO concentration not consumed in the extremely fast chemical reaction with O_2^- and other redox centers in the tissue. This free NO, when measured intermittently, remained approximately the same during the second chronic phase of endotoxemia, in spite of high NO production by iNOS (after 45 min from LPS infusion), measured indirectly by assaying the accumulation of the NO decay products (NO_2^- ; NO_3^-) in blood plasma by the Griess method. NO measurement with the porphyrinic sensor clearly indicates that the net concentration of NO is only two times higher during the late chronic phase of endotoxemia, than the observed preendotoxemic basal concentration. This net NO concentration is much lower than the total NO produced during this period, but still sufficient to account for the coincident chronic hypotension observed. However,

low-net NO concentration cannot be accountable for the sudden death of animals after about 6 h of endotoxemia. Direct electrochemical measurements suggest that the dysfunction of eNOS cells eventually leading to the death of the animal is triggered by $\text{O}_2^-/\text{OONO}^-$, rather than by NO itself during endotoxemia.

7.3.4

In vivo Measurements of NO in the Beating Heart

Measurement of NO amidst the dynamic in vivo conditions of cyclic breathing and heart beating is a challenging task [10]. In order to overcome these potential interferences and to record a reliable NO signal, the catheter-protected porphyrinic sensor is slightly modified in two ways. First, the active sensor tip is shortened to 50 to 60 μm from 0.3 to 0.5 mm usually used for in vivo measurements. In addition, the truncated needle from which the active sensor tip emerges is cut 50- to 60- μm shorter than its protective catheter, so that the tip of the sensor is completely recessed within the ventilated catheter tip, rather than protruding from an unventilated catheter tip. The sensor has to be tested under different experimental conditions to ensure that the sensor did not generate an analytical signal when subjected to conditions of fluid pressure, mechanical deformation of the sensor tip, or intrinsic electrical activity within the heart.

In order to estimate potential piezoelectric interference due to mechanical deformation of the sensor tip, a micromanipulator can be used to deform the sensor tip at physiologically relevant frequency (1–3 Hz). As can be seen in Fig. 15, the deformation of the sensor generates small electrical perturbations, six to ten times smaller than the signal

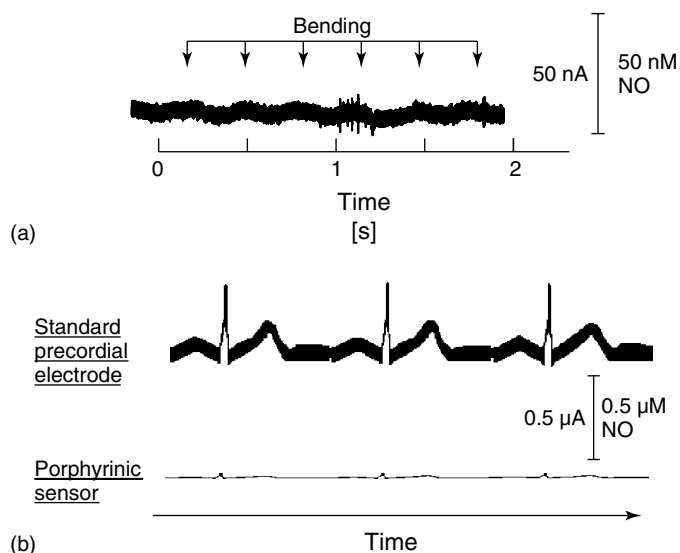


Fig. 15 Response of the catheter-protected porphyrinic sensor to mechanically bending the active tip of the sensor at a frequency of 3 Hz, and to an ECG signal. The vertical bars represent the equivalent current that would be generated by the porphyrinic sensor in the 50 nM NO [(a), lower tracing] or 0.5- μ M NO (b).

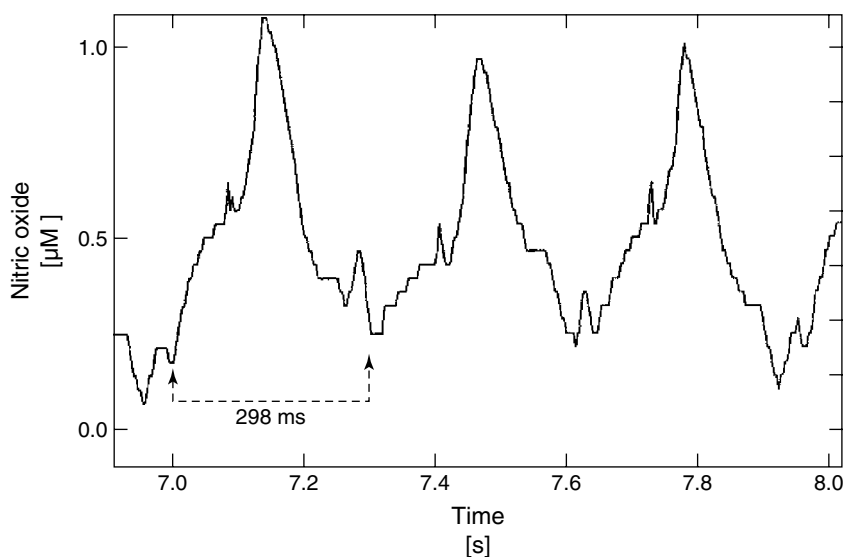


Fig. 16 Changes of NO concentration recorded in a beating heart. The porphyrinic sensor was implanted in the myocardium (left ventricle, rabbit).

recorded by the sensor at a low (20–50 nM) concentration of NO. To eliminate the possibility that the sensor might respond to the electrical current generated within the extensive cardiac conduction system or within the depolarizing myocardium, the sensor can be used as the exploring electrode connected to a standard electrocardiography (ECG). As is apparent from Fig. 15, when used in this manner, the porphyrinic sensor is barely able to detect the ECG signal. In these experiments, observing the analytic response of the sensor to potential piezoelectric or *in vivo* electrical current interferants, the measured peak of NO was at least 30 to 50 times larger and temporarily shifted from the conservatively estimated background noises.

An anesthetized rabbit was used to measure local fluctuations in NO concentration in the apical left ventricular myocardium. Rapid changes in cardiac NO concentration related to the cardiac cycle are observed (Fig. 16). In the rabbit heart (endocardium), each cardiac cycle (period about 300 ms) begins and ends with an intercycle NO concentration of about 100 nM. During early systole, NO concentration reaches a basal of 0.2 μM followed by a slow increase to a semi-plateau. Early diastolic filling is accompanied by a rapid increase of NO concentration with a peak diastolic about 1.1 μM that is attained at 240 ms into the cardiac cycle. After this peak, there is a sharp decay in the intercycle NO concentration. The NO signal recorded by the sensor disappears when monitored at a potential of 0.40 V (which is 230 mV below the peak potential of NO oxidation), clearly indicating that the signal measured at 0.67 V is due to NO,

not mechanical noises, which are independent of potential. To demonstrate the relationship between the ECG signal, left ventricular volume, and instantaneous NO concentration, simultaneous recordings of each of these were performed (Fig. 17).

During ischemia of the heart, a significant decrease of the mechanically stimulated NO release is observed (Fig. 18). After 240 s of ischemia, the peak of NO is 400 nM (about 60% lower than the control). NO is released in a pulsatile fashion from the beating heart and its synthesis is directly related to ventricular loading conditions *in vivo*. Direct measurements of NO with the porphyrinic sensor in the beating heart may help to explain

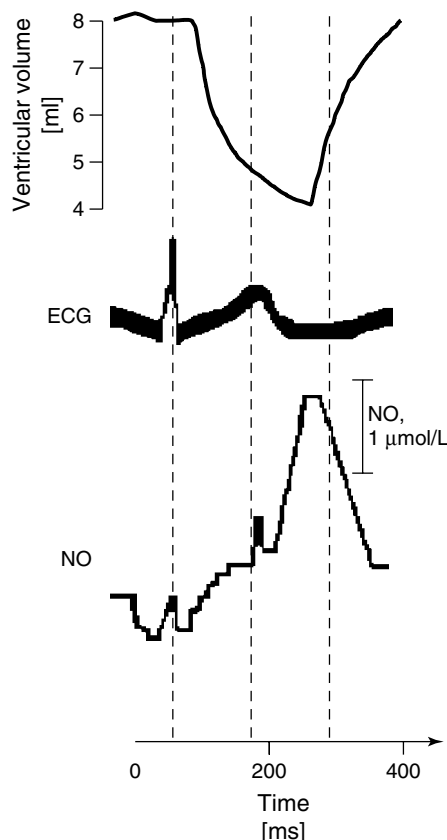


Fig. 17 NO signal, ECG signal, and ventricular volume recorded simultaneously in the left ventricle in the beating heart (rabbit).

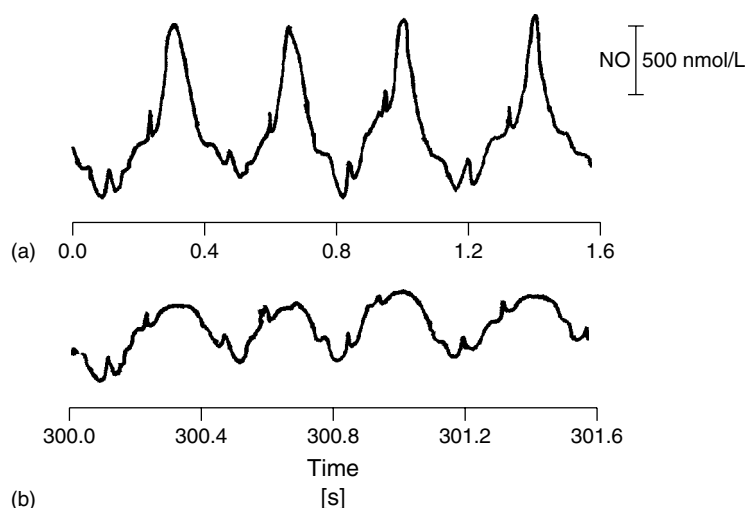


Fig. 18 NO concentration recorded in the wall of the left ventricle of the beating heart (rabbit) under normal (a) and ischemic conditions (b), (after 240 s of ischemia).

certain aspects of the beat-to-beat regulation of cardiac performance and also provide insight into the pathophysiology of diseases associated with increased myocardial distention, such as valvular heart disease or heart failure [10]. Cells within the heart are subjected to tremendous mechanical deformation during filling and beating. NO affects mechanical properties of cardiac myocytes by increasing cGMP to facilitate relaxation and to mediate an acetylcholine stimulated decrease in contractility. Amperometric detection with a porphyrinic sensor is the only analytical method currently available to measure NO concentration in the beating heart with sufficient time resolution and sensitivity.

7.3.5

Measurement of NO in the Brain

7.3.5.1 In vitro Measurement with Clark Probe

Figure 19 presents an amperometric curve obtained at different potentials for NO

released from the cellular layer of a rat's cerebellar slices [17]. The white matter was stimulated with biphasic pulse-trains (intensity $\pm 600 \mu\text{A}$, frequency 20 Hz, duration of pulse-train 5 s). The electrical stimulation of the white matter evoked increases in NO concentration between 20 and 75 nM. Figure 19(b) shows an amperogram obtained in the presence of 100-nM NO at different potentials. The applied potential results in current increases, which are maximal at a potential of about 0.9 V.

7.3.5.2 In vivo Measurement with Porphyrinic Sensor

Figure 20(a) presents a typical amperometric curve obtained from in vivo measurements of NO concentrations in a rat's brain during a middle cerebral artery occlusion (MCAO). The porphyrinic sensor was stereotactically implanted perpendicularly into the ipsilateral parietal cortex at coordinates 0.8-mm posterior and 4.5-mm lateral to the bregma, and 3 mm below dura. An increase in NO concentration (about

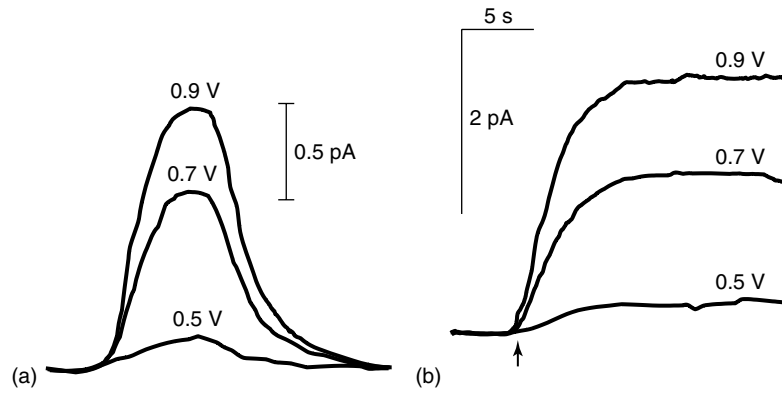


Fig. 19 NO release in the molecular layer of a rat's cerebellar slices measured during white-matter stimulation (20 Hz for 5 s); traces were recorded at different platinum anode potentials. (b) Currents measured in the presence of 100-nM NO at different potentials. (Reproduced from K. Shibuki et al., *Nature* **1991**, 349, 326, with permission.)

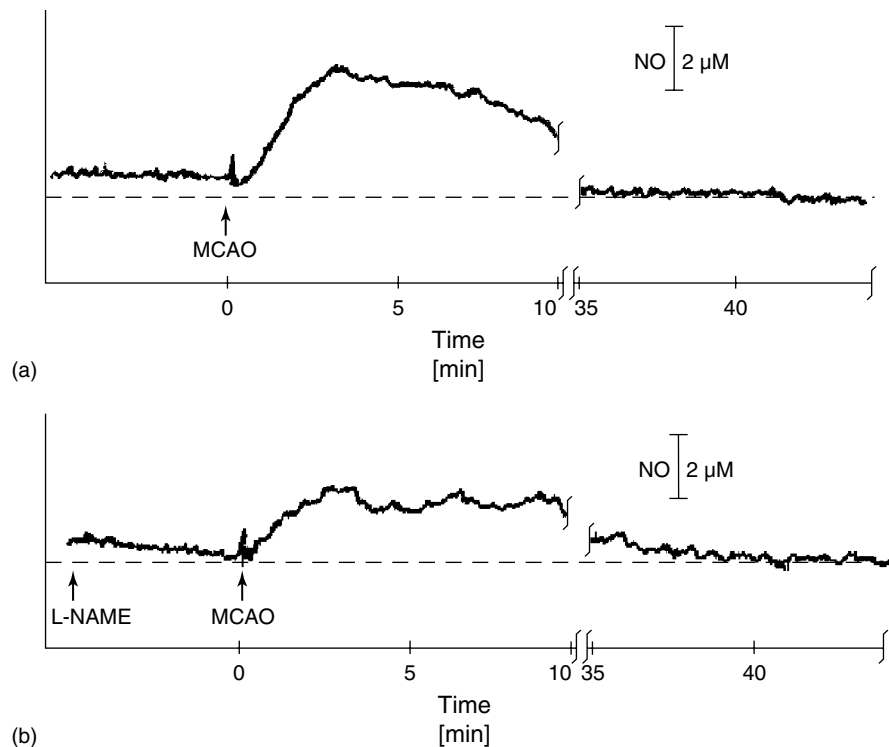


Fig. 20 Continuous recording of the changes of NO concentration in the ischemic brain (rat) in the absence (a) and in the presence of an NOS inhibitor (L-NAME).

2.2 μM) was established after 3 min. After 6 min of ischemia, NO concentration gradually decreased, after 20 min it decreased below basal level of 40 nM, and after 35 min was undetectable by the sensor. In the presence of L-NAME (cNOS inhibitor infused 5 min before MCAO), the NO concentration also increased but its maximum was 0.9 μM (about 60% lower than the control). After 40 min, the NO concentration

was slightly below (30 nM) the basal level and was detectable by the sensor. The kinetics of NO release and its concentration produced during ischemia is related to the brain damage. Initial high production of NO during the acute phase of ischemia plays a beneficial role in preventing brain damage [66]. However, after prolonged ischemia cNOS starts also to produce O_2^- , which consumes NO. The generation of

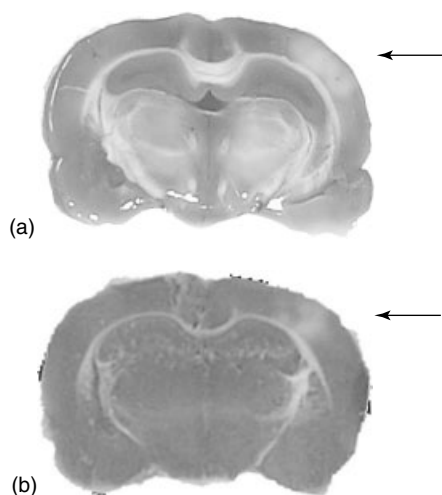


Fig. 21 Necrosis of ischemic brain; normal (a) and treated with L-NAME (b).

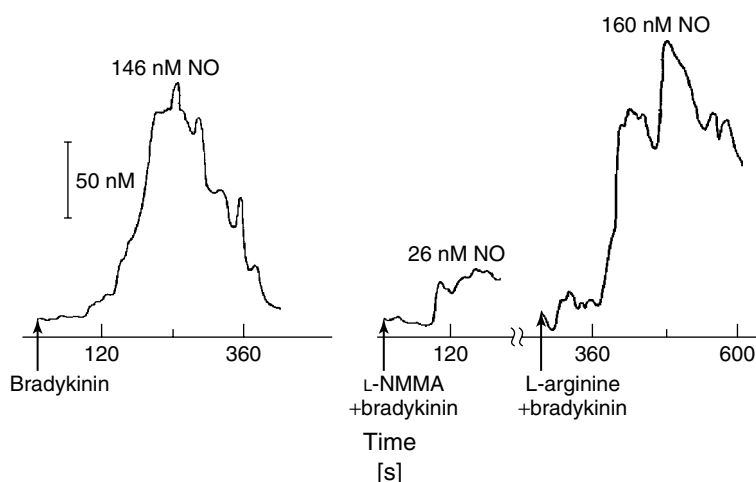


Fig. 22 In vivo measurement of NO concentration in human beings.

high concentration of ONOO initiates a cascade of events leading to the production of highly oxidative radicals (OH^\bullet , NO_2), and subsequent brain damage. The lowering of NO production during ischemia prevents the generation of O_2^- , ONOO^- , OH^\bullet and NO_2^\bullet , and mollifies ischemia damage (Fig. 21). The necrosis of the brain decreased significantly in the presence of L-NAME (control 7% of necrosis L-NAME 3% of necrosis).

7.3.6

Measurements of NO in Human Beings

Catheter-protected porphyrinic sensors can be sterilized with ethylene oxide and used for NO measurement in humans [67]. For measurements of NO in veins or arteries, an intervenous catheter is used. Two cannulae are inserted into a vein. A 24-G catheter is inserted retrogradely, and a 23 G butterfly needle is positioned anterogradely with its tip 10 to 15 mm from the end of the catheter. The catheter is flushed with 0.5-ml heparin (5000 U/ml), and a NO sensor is mounted on a 24-G needle and is placed so its tip protruded 1 to 2 mm beyond the end of the catheter. A platinum wire counter-electrode and silver/silver chloride reference electrode can be placed on the skin adjacent to the vein and covered with conductive gel. Heparin solution physiological saline or drugs can be infused continuously through the butterfly needle. Infusion of bradykinin causes a dose-dependent NO signal, attenuated by coinfusion of inhibitor of NOS L-NMMA (Fig. 22). Infusion of L-arginine with bradykinin restored NO concentration.

The detection of a signal for NO in response to bradykinin provides further

evidence in man that the endothelium-derived relaxing factor is NO. Functional studies suggest that the alteration in the L-arginine/NO pathway occurs in hypertension, diabetes, and hypercholesterolemia, and decreased production of NO might be a link between risk factors and atherogenesis [68]. The ability to assess local generation of NO with porphyrinic sensor should facilitate exploration of the role of this mediator in physiological or pathophysiological processes.

References

1. D. S. Bredt, *Free Radical Res.* **1999**, 31, 577.
2. V. L. Dawson, T. M. Dawson, *Proc. Soc. Exp. Biol. Med.* **1996**, 211, 33.
3. S. Grunfeld, C. A. Hamilton, S. Mesaros et al., *Hypertension* **1995**, 26, 854.
4. T. Malinski, M. Kapturczak, J. Dayharsh et al., *Biophys. Res. Commun.* **1993**, 194, 654.
5. J. P. Cooke, V. J. Dzan, *Circ. Res.* **1997**, 96, 379.
6. M. Tschudi, S. Mesaros, T. Luscher et al., *Hypertension* **1996**, 27, 1.
7. K. S. Christopherson, D. S. Bredt, *J. Clin. Invest.* **1997**, 100, 2424.
8. C. Ladecola, *Trends Neurosci.* **1997**, 20, 132.
9. R. J. Gryglewski, P. P. Wolkow, W. Uracz et al., *Circ. Res.* **1998**, 82, 819.
10. D. J. Pinsky, M. Kapturczak, E. Block et al., *Circ. Res.* **1997**, 81, 372.
11. N. Hill-Kapturczak, M. Kapturczak, E. R. Block et al., *C. J. Am. Soc. Nephrol.* **1999**, 3, 481.
12. J. S. Beckman, W. H. Koppenol, *Am. J. Phys.* **1996**, 271, C1424.
13. F. Kiechle, T. Malinski, *Ann. Clin. Lab. Sci.* **1996**, 26, 501.
14. T. Malinski, S. Mesaros, P. Tomboulion, *Methods Enzymol.* **1996**, 268, 58.
15. T. Malinski, E. Kubaszewski, F. Kiechle, *Methods Neurosci.* **1996**, 31, 14.
16. T. Malinski, Z. Taha, *Nature* **1992**, 358, 656.
17. K. Shibuki, O. Okada, *Nature* **1991**, 349, 326.
18. T. Malinski, E. Kubaszewski, F. Kiechle et al., *The Biology of Nitric Oxide*, Portland Press, London, 1994.
19. R. F. Furchott, J. V. Zawadzki, *Nature* **1980**, 288, 373.

20. R. M. J. Palmer, A. G. Ferrige, S. Moncada, *Nature* **1987**, 327, 524.
21. R. M. J. Palmer, D. S. Ashton, S. Moncada, *Nature* **1988**, 333, 664.
22. R. M. J. Palmer, E. A. Higgs, S. Moncada, *Pharm. Rev.* **1991**, 43, 1991.
23. C. Nathan, *J. FASEB* **1992**, 6, 3051.
24. T. Malinski, Z. Taha, S. Grunfeld et al., *Biochem. Res. Biophys. Res. Commun.* **1993**, 193, 1076.
25. L. A. Blatter, Z. Taha, S. Mesaros et al., *Circ. Res.* **1995**, 76, 922.
26. T. Malinski, M. Radomski, Z. Taha et al., *Biochem. Biophys. Res. Commun.* **1993**, 194, 960.
27. A. Kanai, H. C. Strauss, A. Truskey et al., *Circ. Res.* **1995**, 77, 284.
28. T. Malinski, M. Kapturczak, J. Dayharsh et al., *Biochem. Biophys. Res. Commun.* **1993**, 194, 654.
29. W. Linz, T. Jessen, R. H. A. Becker et al., *Circulation* **1997**, 96, 3164.
30. F. Cosentino, S. Patton, V. d'Uscio et al., *J. Clin. Invest.* **1998**, 101, 1530.
31. D. S. Bredt, S. H. Snyder, *Proc. Natl. Acad. Sci. U.S.A.* **1990**, 87, 682.
32. Z. G. Zhang, M. Chopp, F. Bailey et al., *J. Neurol. Sci.* **1995**, 128, 22.
33. L. J. Forman, P. Liu, R. G. Nagele, *Neurochem. Res.* **1998**, 23(2), 141–148.
34. P. Klatt, K. Schmidt, G. Uray et al., *J. Biol. Chem.* **1994**, 268, 14 781.
35. J. B. Hibbs, R. R. Traintor, Z. Vavrin, *Science* **1987**, 235, 473.
36. D. H. Stuehr, H. J. Cho, N. S. Kwon et al., *Proc. Natl. Acad. Sci. U.S.A.* **1991**, 88, 7773.
37. S. Archer, *FASEB L.* **1993**, 7, 349.
38. Y. -J. Sung, J. H. Hotchkiss, R. F. Austic et al., *Biochem. Biophys. Res. Commun.* **1992**, 184, 36.
39. L. R. Cantilena, R. P. Smith, S. Frasure, *J. Lab. Clin. Med.* **1992**, 51, 496.
40. R. F. Furchgott, P. M. Vanhoutte, *Faseb J.* **1987**, 3, 2007.
41. K. M. K. Rao, J. Padmanabhan, D. L. Kilby, *J. Leukocyte Biol.* **1992**, 51, 496.
42. R. G. Bogle, S. Mancada, C. D. Pearson et al., *E. Br. J. Pharmacol.* **1992**, 105, 768.
43. T. Malinski, Z. Taha, S. Grunfeld et al., *Anal. Chim. Acta* **1993**, 279, 135.
44. T. Stephane, F. Bediour, F. Devynek, *Talanta* **1996**, 43, 303.
45. S. Mesaros, S. Grunfeld, A. Mesarosova et al., *Anal. Chim. Acta* **1997**, 339, 265.
46. L. Czuchajowski, E. J. Bennett, S. Goszczynski et al., *J. Am. Chem. Soc.* **1989**, 111, 607.
47. J. E. Bennett, T. Malinski, *Chem. Mater.* **1991**, 3, 490.
48. T. Malinski, A. Ciszewski, J. Bennet et al., *J. Electrochem. Soc.* **1991**, 138, 2008.
49. T. Malinski, J. Bennett, *E. Redox Chemistry and Interfacial Behavior of Biological Molecules*, Plenum Press, New York, 1988, pp. 87–107.
50. J. R. Fish, E. Kubaszewski, A. Peat et al., *Chem. Mater.* **1992**, 4, 795.
51. T. Malinski, J. Bennet, F. Bailey et al., *Proceedings of the 12th international conference of the IEEE Engineering in Medicine and Biology Society*, IEEE, Philadelphia, 1990, Vol. 12, p. 1691.
52. F. L. Kiechle, T. Malinski, *Am. J. Clin. Pathol.* **1993**, 100, 567.
53. J. Balligand, D. Ungureanu-Lorgrois, W. Simmons et al., *J. Biol. Chem.* **1994**, 269, 27 580.
54. R. Cohen, F. Plane, S. Najibi et al., *Proc. Natl. Acad. Sci. U.S.A.* **1997**, 94, 4193.
55. G. Wiemer, B. Pierchala, S. Mesaros et al., *Endothelium* **1996**, 4, 119.
56. H. Heitsch, S. Brovkovich, T. Malinsky et al., *Hypertension* **2001**, 37, 72.
57. L. Vergnani, S. Hatrik, F. Ricci et al., *Circulation* **2000**, 101, 1261.
58. S. F. Silverton, O. A. Adebajo, B. S. Moonga et al., *Biochem. Biophys. Res. Commun.* **1999**, 259, 73.
59. V. Brovkovich, S. Patton, S. Brovkovich et al., *J. Phys. Pharm.* **1997**, 48 663.
60. G. Wiemer, B. Pierchola, S. Mesaros et al., *Endothelium* **1996**, 4, 119.
61. T. Malinski, M. Kapturczak, T. Dayharsh et al., *Biochem. Biophys. Res. Commun.* **1993**, 194, 654.
62. S. Grunfeld, C. A. Hamilton, S. Mesaros et al., *Hypertension* **1995**, 26, 1995.
63. L. Linder, W. Kiowski, F. Buhler et al., *Circulation* **1990**, 81, 1769.
64. J. S. Beckman, *Nitric Oxide: Principles and Actions*, Academic Press, San Diego, 1996.
65. H. J. Gyllenhammer, *Immunol. Methods* **1987**, 97, 209.
66. T. Malinski, F. Bailey, Z. G. Zhang et al., *J. Cereb. Blood Flow Metab.* **1993**, 13, 335.
67. P. Valance, S. Patton, K. Bhagat et al., *Lancet* **1995**, 345, 153.
68. R. G. Knowles, M. Palacios, R. M. J. Palmer et al., *Proc. Natl. Acad. Sci. U.S.A.* **1989**, 86, 5159.

8

Scanning Electrochemical Microscopy Applied to Biological Systems

Hitoshi Shiku, Hiroaki Ohya
Yamagata Public Corporation for the Development of Industry,
Yamagata 990-2473, Japan

Tomokazu Matsue
Department of Biomolecular Engineering, Graduate School of Engineering,
Tohoku University, Sendai 980-8579, Japan

8.1	SECM	259
8.1.1	Feedback Mode	259
8.1.2	Generation/Collection Mode	261
8.2	Applications to Biological Systems	262
8.2.1	Enzymes	266
8.2.2	Antigen–Antibodies	267
8.2.3	Local Fluxes Through Biological Materials	268
8.2.4	Liquid–Liquid Interfaces, Liquid–Air Interfaces	269
8.2.5	Planar BLMs	270
8.2.6	Cells, Tissues	271
	References	273

8.1 SECM

SECM (Scanning electrochemical microscopy) is a technique to characterize the local electrochemical nature of various materials by scanning a probe microelectrode [1, 2]. The spatial resolution of SECM is inferior to the conventional scanning probe microscopes such as scanning tunneling microscopy (STM) and atomic force microscopy (AFM) as the fabrication of the probe, microelectrode, with nanometer sizes is quite difficult and the faradaic current of the microprobe is very small (often picoamps or less). However, SECM has unique characteristics that cannot be expected for STM and AFM: SECM can image localized chemical reactions and it also can induce localized chemical reactions in a controlled manner.

SECM has been widely applied to numerous fields involving electrochemistry, such as electrode surfaces, polymers, biomaterials, and liquid–liquid interfaces [3–12]. The probe current reflects the electrochemical processes occurring in the small space surrounded by the probe and the substrate. The electron transfer at the probe and substrate (if conductive) and mass transfer across the solution affect the probe current. The probe current is also influenced if chemical reactions

or adsorption–desorption processes occur within the gap solution or at the electrode surface. Therefore, the phenomena in the “ultramicro electrochemical cell” can be quantitatively understood by analyzing the probe current response [13]. The volume of the small space and the transient time for a molecule to transfer from the probe to substrate are precisely controlled by changing the probe-sample separation, which offers new research fields for characterizing single molecules [14, 15] or highly reactive radical species [16, 17].

8.1.1 Feedback Mode

One of the most remarkable features of microelectrode measurements is that one can observe steady state redox currents in relatively short time domains. When the current response at a microelectrode is in a steady state, a hemispherical diffusion region of the electrogenerated species is formed around the microelectrode probe (Fig. 1a). The size of the diffusion region largely relies on the probe radius and the steady state current is expressed by the following equation:

$$i = 4nFDCa \quad (1)$$

where F is Faraday's constant, D and C are the diffusion coefficient and the bulk

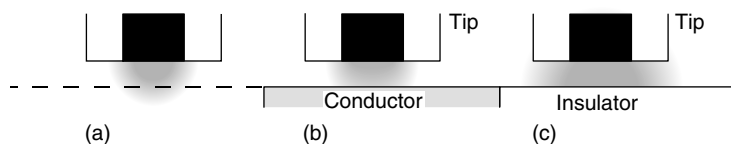


Fig. 1 Schematic illustration of the feedback mode SECM.

concentration of the reagent, and a is the radius of the microelectrode probe. If a planar wall exists within the hemispherical region, the distribution of the species changes due to geometrical perturbation.

When the wall is a conductor, the gradient becomes steeper compared with that in the bulk solution and therefore the probe current increases (Fig. 1b). The situation showing a larger faradaic current compared to the steady state current in the bulk solution is called a positive feedback mode [3–7]. For example, an electrode reaction at the probe converts a species in its oxidized state into the corresponding reduced species, which diffuses onto the conducting substrate to regenerate the oxidized species. This redox cycling between the probe and substrate increases the redox response at the probe. The opposite case is called the negative feedback mode. When the wall is an insulator, the current declines, reflecting the broader concentration profile at the probe surface (Fig. 1c). In the feedback mode, either positive or negative, the probe current largely depends on the probe-substrate distance. This is the most fundamental characteristic of SECM and therefore the probe can be precisely positioned at the desirable point by monitoring probe current. For both conductive and insulating samples, SECM can provide topographic information on the sample surfaces by scanning the microelectrode probe.

The feedback mode SECM is an experimental setup to measure faradaic current

profiles along the sample surface (x - y plane) or normal to the surface (z direction) by scanning the probe within the very small probe-sample separation where the probe current deviates from the steady state value. Voltammetry and chronoamperometry at fixed positions are also available. The currents reflect entire events including mass transfer, charge transfer, and chemical reactions (if any) in the small space between the probe and substrate. For all circumstances, the steady state current observed in the bulk solution is a very important parameter that is considered as a standard response for quantitative analysis.

However, it is not easy to calculate the exact relation between the probe current and the probe-sample distance in the feedback mode due to the geometric complexity in the experimental system. For quantitative analyses, digital simulation has been used in the feedback mode SECM both for conductor and insulator substrates [18]. Digital simulation is a powerful technique for analysis of relatively complicated electrochemical systems such as SECM. In the simulation, the space between the probe and the substrate are divided into small volume elements. Mass transfer based on diffusion for each volume element is calculated. If one chooses suitable initial and boundary conditions, the experimental situation including the mass transfer and various chemical reactions can be simulated. From the simulation, one can determine the heterogeneous rate

constants [19–21], homogeneous reaction constants [16, 17, 22–24], local fluxes, diffusion coefficients [25], and so forth. This quantitative analysis was introduced in 1989 for SECM studies and to date this is still a most reliable method to quantify various parameters in a specific experimental system.

8.1.2

Generation/Collection Mode

In the General/Collection (G/C) mode experimental set up, the potentials of the two working electrodes were controlled with a bipotentiostat [26]. A species electrogenerated at an electrode (the generator) surface diffuses into the solution and is detected at the other working electrode (the collector). This mode is applicable to the studied with rotating ring-disk electrodes or microarray electrodes. In 1986, Engstrom and coworkers [27–30] reported the G/C experimental systems with an amperometric ultramicroelectrode probe. They placed a probe microelectrode very close to a macrosized electrode and detected ferricyanide, which was generated at the large electrode. Gathering a set of transient current responses recorded at several probe-substrate distance, the concentration profiles near the generator electrode have been visualized with tens of ms time resolution [27]. In the same article, they demonstrated the capability of the experimental system to image surface reactivity with 20- μm spatial resolution and also detected short lifetime active species such as NAD^\bullet radical. They

successfully applied their experimental system to mapping of concentration profiles for epinephrine and determination of the second-order rate constant for the reaction between epinephrine quinone and leucoadrenochrome [28].

G/C mode experiments are basically topography independent in estimating local concentration profiles only if the probe-substrate distance is far enough from the sample surface. However, when the probe is placed very close to the sample surface, the geometrical influence of the microelectrode probe in the experiment system should be considered carefully. Figure 2 shows two typical situations in the G/C mode experiments, in which amperometric probe is inserted into the diffusion layer of the substrate electrode. In the first case shown in Fig. 2(a), the probe-sample separation is significantly large and there is no crossover of the diffusion regions from the probe and the sample surface. Local concentration can be directly estimated from the probe current by using Eq. (1), although the concentration around the probe is not exactly homogeneous. There are several studies [31, 32] done in the G/C mode to estimate the fluxes by recording the concentration profile around the substrate. In these studies, the surrounding concentration profile of the species was compared with theoretical ones calculated based on diffusion equations. The latter case shown in Fig. 2(b), the probe diffusion layer has reached the sample surface. This situation is more likely in the feedback mode. Eq. (1) cannot be used for estimation of the

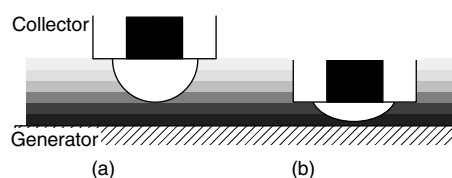


Fig. 2 Schematic illustration of the G/C mode SECM.

local concentration. The digital simulation technique mentioned earlier is still applicable [33, 34], but the calculation becomes much more complicated because the concentration profile formed at the substrate is wide spread. In addition, when the probe is laterally scanned for imaging, convolution of the topography and original concentration profile makes the interpretation of the images unclear. A study of two-dimensional mapping of the local fluxes has been reported [35].

There are several ways to avoid the feedback effect. One is to use transient techniques such as fast-scan cyclic voltammetry that have been vigorously carried out for monitoring single cell events by means of microelectrode [36]. A pure concentration profile will be obtained within a short time scale before the diffusion layer at the probe reached the sample surface. The other is to utilize potentiometric probes that have been already demonstrated in G/C mode SECM imaging [37–39]. As the potentiometric probe does not consume or generate electroactive species, original concentration profiles around the sample are less perturbed. There have been a lot of studies involving mapped concentration profiles of Cl^- , H^+ , Na^+ , K^+ , NH_4^+ , and so on. A study of mapping of local chemical reagent distribution by scanning a potentiometric probe was reported in 1972 [40].

8.2

Applications to Biological Systems

SECM is applicable to many surfaces that generate electroactive substances (G/C mode) or that regenerate the redox species consumed at the probe reaction (feedback mode). Therefore, SECM has high

potential to examine biological systems under physiological conditions with high spatial resolution. For instance, enzyme-catalyzed reactions, electron and ion transport through biomembranes, and chemical communication within a cell and between cells have been investigated with SECM. In the SECM studies focusing on biological systems, base substrates are basically not electrodes and therefore, the experimental setups are somewhat different from those in the standard SECM experiments. Typically, there are three types of sample configurations: (1) Biomaterials immobilized on solid supports. (2) Membranes or interfaces sandwiched by two liquid phases for analyzing flux through the boundary due to electron or mass transfer. (3) Living samples for intact observation.

The first category includes enzyme-catalyzed reactions or metabolic reactions at solid substrates. Table 1 is a list of the studies that characterize immobilized biomaterials by SECM. Glucose oxidase is a major enzyme used as a target to demonstrate various detection schemes. So far, imaging in the G/C and feedback modes, and the detection of the biocatalytic products with a specially fabricated probe have been reported [41–45]. Diaphorase is the only enzyme routinely visualized by the feedback mode SECM imaging at the monolayer surface coverage [46–48]. Alkaline phosphatase and HRP have been used for the labeled enzyme to characterize antigen–antibody binding [49–53]. Mitochondria and yeast have been visualized by SECM, on the basis of metabolic reactions catalyzed by enzymes existing in the samples. To date, all the experiments were carried out in excess enzyme substrate conditions.

Table 2 introduces studies for analyzing local fluxes due to electron transfer

Tab. 1 SECM studies on immobilized enzymes, immobilized biomaterials

<i>Sample</i>	<i>Monitoring reagents</i>	<i>Reference and notes</i>
Plant tissue containing enzymes	Norepinefrine, dopamine	41
Glucose oxidase	H ₂ O ₂	41 Collecting enzymatically generated electroactive species
	FcCOOH, Fe(CN) ₆ ⁴⁻ , HQ	42 Determining enzymatic kinetic parameters
	Hydroquinone	43 Imaging enzymatic activity and topography
	H ₂ O ₂	44 Probing with enzyme electrode
Glucose oxidase monolayer	H ₂ O ₂	45
Diaphorase monolayer	FcCH ₂ OH, Co(phen) ₃ ²⁺	46 Determining enzymatic kinetic parameters
	FcCH ₂ OH	47, 48
Mitochondria	TMPD	43
Urease, Yeast	H ⁺	37 Using potentiometric pH selective tip
	Fe ³⁺	41 Monitoring metal uptake
Algae	<i>p</i> -Aminophenol	49 By use of alkaline phosphatase labeled antigen
Anti-digoxin		50 By use of HRP labeled antibody
CEA	FcCH ₂ OH	51 Dual immunoassay
HCG, HPL	FcCH ₂ OH	52, 53 Multiimmunoassay
CEA, HCG, HPL, AFP	FcCH ₂ OH	

Notes: HRP, horseradish peroxidase; TMPD, *N,N,N',N'*-tetramethyl-*p*-phenylenediamine; CEA, carcinoembryonic antigen; HCG, human chorionic gonadotropin; HPL, human placental lactogen; AFP, α -fetoprotein.

or mass transfer through the boundary of porous membranes, liquid–liquid interfaces, liquid–gas interfaces, and planar bilayer lipid membranes (BLMs). Fluxes through porous biological membranes have been characterized in the G/C mode by SECM imaging. Hydrodynamic pressures, osmotic pressures, electric fields, and concentration gradients drive the fluxes [31, 35, 54–61]. Electron [62–68] and mass transfer [69–74] at liquid–liquid and liquid–air interface are characterized by the approach characteristics of a probe microelectrode to the interface. In Table 2, the microelectrode probe was placed in the left side of the liquid phase. The potential between the two

liquid phases is generally unbiased and two electrodes configuration is available. BLMs are formed in a pinhole made in the Teflon sheet where the membranes are oriented vertically [75–79] or horizontally [80].

Finally, studies on living samples such as cells or tissues are shown in Table 3. SECM imaging capability offers both topography of the sample surface and the distribution of a specific species generated from the cells or tissues [81–87]. Time course recording with a probe fixed very close to the sample is another important experimental setup [88–102]. The chronoamperometric responses are critically influenced by the probe-sample separation.

Tab. 2 Studies on analysis of local flux across membranes or interfaces

Sample	Monitoring reagents	Reference and notes
Characterization of local flux through biological materials		
Porous mica	$\text{Fe}(\text{CN})_6^{4-}$	31, 54
Hairless mouse skin	$\text{Fe}(\text{CN})_6^{4-}$	55–58 Driven by membrane potential
Dentine slice	$\text{Fe}(\text{CN})_6^{4-}$	59, 60 Driven by hydrostatic pressure
Laryngeal cartilage	$\text{Ru}(\text{NH}_3)_6^{3+}$, O_2	35 Driven by osmotic pressure
Human dentine	$\text{Fe}(\text{CN})_6^{4-}$	61 Driven by concentration gradient
Electron transfer at liquid–liquid interface		
R(water)/Fc(nitrobenzene)		62 R = FcCOO^- , $\text{Ru}(\text{bpy})_3^{3+}$ 63 R = InCl_6^{3-} , $\text{Fe}(\text{CN})_6^{3-}$, $\text{Fe}(\text{phen})_3^{2+}$, $\text{Mo}(\text{CN})_8^{4-}$
$\text{Fe}(\text{CN})_6^{3-}$ (water)/TCNQ(DCE)		64
Vitamin B ₁₂ (water)/DBCH(Benzonitrile)		65 Investigating surfactant effects
ZnPor (benzene)/ $\text{Ru}(\text{CN})_6^{4-}$ (water)		66
Electron transfer across monolayer at liquid–liquid interface		
ZnPor(benzene)/R (water)		67 Monolayer of saturated phosphocholine R = $\text{Ru}(\text{CN})_6^{4-}$, $\text{Mo}(\text{CN})_8^{4-}$, $\text{Fe}(\text{CN})_6^{4-}$, $[\text{Co}(\text{II})\text{sepulchrate}]^{2+}$, V^{2+} 68 Monolayer of a mixture of conjugated and saturated phospholipids R = $\text{Fe}(\text{CN})_6^{4-}$
Mass transfer through liquid/liquid or liquid–gas interface		
Water/heptane	Cu^{2+}	69
Water/DCE	Cu^{2+}	69 Cu^{2+} in DCE was chelated by oxyme
	O_2	70
	Br_2 , $\text{Fe}(\text{CN})_6^{4-}$	71 Double potential step chronoamperometry
	K^+	72 K^+ in DCE was transported with DB18C6 Utilizing a micropipette base electrode
Water/nitrobenzene	O_2	70
	FcCH_2OH , $\text{Co}(\text{phen})_3^{2+}$	73
Water/air	Br_2	71 Double potential step chronoamperometry
Mass transfer through monolayer at air–water interface		
Water/air	O_2	74
Mass and charge transfer through BLM		
BLM	H^+	75 Using potentiometric pH microelectrode
	H^+ , NH_4^+	76 Using NH_4^+ selective microelectrode

Tab. 2 (continued)

Sample	Monitoring reagents	Reference and notes
BLM incorporated alamethicin ion channel	H^+ , K^+ , Na^+ , Ca^{2+}	77 With double-barreled microelectrodes
	FcCH ₂ OH, FcCOOH/FcCOO [−]	78 Estimation of permeation coefficients
	$Ru(NH_3)_6^{3+}$, $Fe(CN)_6^{3-}$, I^-	79
	I^-	80 Study of charge transfer through BLM

Notes: TCNQ, 7,7,8,8-tetracyanoquinodimethane; DCE, 1,2-dichloroethane; Por, 5,10,15,20-tetraphenyl-210H,23H-porphine; DBCH, trans-1,2-dibromocyclohexane; DB18C6, dibenzo-18-crown-6.

Tab. 3 Studies on cells and tissues, including studies of extracellular time course recording with microelectrodes

Sample	Monitoring reagents	Reference
Lingstrum sinensis leaf	$Fe(CN)_6^{4-}$	81
	O_2	81
Elodea leaf	$O_2, Ru(NH_3)_6^{3+}$	81
Guard cells in <i>tradescantia fluminesis</i>	O_2	82
Algal protoplast	O_2	83, 84
	$O_2, Fe(CN)_6^{4-}$	85
	$Fe(CN)_6^{4-/3-}$, $Co(phen)_3^{2+}$, FcCH ₂ OH, HQ	86
	<i>p</i> -BQ, O_2	32
SW-480(epithelial-like)	O_2	87
Simian virus 40-transformed human fibroblast	H_2O_2, O_2	88
Pancreatic islet	O_2	89
Chinese hamster ovarian cancer cell	Doxorubicin	90
Detection of exocytosis at single cells		
Bovine adrenal medullary cell	Epinephrine, Norepinephrine	36, 91–97
PC12 (rat pheochromocytoma)	Dopamine	98
Mast cell	Serotonin	99
Pancreatic β -cell	Insulin	100, 101
Rat melanotrophs	α -Melanocyte stimulating hormone	102

BQ, benzoquinone; HQ, hydroquinone.

8.2.1

Enzymes

For SECM applications to biological systems, the two electrode configuration (with a working and an auxiliary electrode) is available and the sample substrates are generally unbiased. The basics for the SECM operation described in the previous section are valid and experiments are carried out in the feedback or the G/C mode. Typical characteristics for both modes can be seen through the studies on immobilized enzymes.

A kinetic analysis of immobilized enzymes has been carried out in the feedback mode SECM. Bard and coworkers studied kinetics between glucose oxidase and mediators at the enzyme-immobilized surfaces [42]. When the probe approaches the enzyme-immobilized surface in the presence of excess glucose, oxidation current for the mediator is enhanced due to the regeneration of the mediator at the surface. Utilizing digital simulation, approach curves reflecting catalytic current increase due to immobilized glucose oxidase were analyzed for a couple of mediators and for several immobilizing procedures. In the simulation, a Michaelis–Menten type equation expressing the reaction between the mediator and the enzyme was adopted for the boundary condition at the biocatalytic substrate surface. The equation was further simplified to two limiting cases: zero- and first-order electron-transfer kinetics for large and small mediator concentrations, respectively. In the literature, they indicated a detection limit criterion for feedback mode SECM [42, 43]:

$$J_{\text{med}} > 10^{-3} DC/a \quad (2)$$

where J_{med} is the flux for the mediator at the enzyme-immobilized substrate surface

under assumption of a zero-order heterogeneous enzymatic reaction, D and C are the diffusion coefficient and bulk concentration profiles of the reagent, and a is the radius of the probe microelectrode. This expression will be useful for judging the applicability of the feedback mode operation for the specific experimental circumstance. The expression (2) suggests that the smaller probe radius for high resolution imaging in the feedback mode SECM could be canceled out by the lower sensitivity for the local enzymatic activity. Lower mediator concentration is desirable to detect the catalytic enhancement originated from redox cycling between the probe and the immobilized enzyme.

Yamada and coworkers carried out characterization of a diaphorase monolayer at a glass surface in the same operation mode SECM [46]. Diaphorase purified from *Bacillus stearothermophilus* is a membrane protein, which catalyzes the oxidation of NADH in the presence of an electron mediator. Because of the high activity of diaphorase, a Michaelis–Menten type equation was applicable without further simplification for the boundary condition at the substrate surface. In the following studies [47], diaphorase patterns with monolayer-level coverage at flat glass substrates were visualized by feedback mode imaging.

Feedback mode SECM imaging was successfully employed to map metabolic activities with high spatial resolution. Heterogeneous distributions of active NADH cytochrome reductase within individual mitochondria membrane surfaces were visualized [43]. However, as suggested by Bard's group, this mode will not generally be accessible for surfaces with relatively lower enzymatic activities. On the other hand, the G/C mode may offer wider applicability for imaging biocatalytic reactions

at the sample surface. In fact, the first report on mapping of biocatalytic reactions at solid supports was done by the G/C mode procedure, in 1989 [41]. In this study, glucose oxidase and plant tissues containing enzymes were incorporated into carbon paste. Recently, a glucose oxidase coating on an alkanethiolate-gold substrate with monolayer-level coverage was visualized by monitoring the oxidation current of H_2O_2 continuously generated by the surface immobilized enzyme [45]. The resolution was improved by adding catalase, which effectively eliminates H_2O_2 in the bulk solution. Enzyme electrodes [44] or potentiometric pH probes [37] have been applied to observe enzymatically active regions in samples, that is another advantage of the G/C mode over the FB mode operation.

8.2.2

Antigen–Antibodies

Electrochemical detection in immunoassays has already been a great success by utilizing labeled enzymes to enhance signals originating from antigen–antibody binding. SECM strengthens the protocol due to its capability of two-dimensional visualization of the distribution of antigen–antibody complexes with high spatial resolution. Because of the small volume and small area required for an assay, total throughput can be drastically improved compared with the current assays running in a 96-well plate. A study characterizing antigen–antibody complexes on a solid support was reported by Wittstock and coworkers [49]. Alkaline phosphatase-labeled antigen was used for sensing antigen–antibody binding. The antigen-coated reaction zones were prepared at a glass substrate by

using the enzyme-labeled and the enzyme free antigen solutions. In aqueous solutions, the probe is laterally scanned along the substrate surface to detect oxidation current of *p*-aminophenol generated by the enzyme-catalyzed hydrolysis of *p*-aminophenyl phosphate. As the probe directly detects the enzymatic product, no incubation time for the enzyme reaction is necessary.

The combination of SECM with the enzyme-linked immunosorbent assay (ELISA) offers a novel assay system of biologically important materials. We have characterized CEA microspotted on a glass substrate [50]. The sample preparation was basically similar to a conventional sandwich method utilizing HRP-labeled antibody, but analyte solution containing CEA was microspotted in a 20- μm -radius region with a tapered glass capillary. In the presence of H_2O_2 and ferrocenylmethanol, the probe detected the reduction current of ferriciniummethanol produced by HRP-catalyzed reaction at the substrate. In a single SECM image of 400 $\mu\text{m} \times 500 \mu\text{m}$, ten spots for immobilized CEA were clearly visualized as the area of large reduction current and, as a result, as low as 10 000 CEA molecules per spot were detectable. We have extended this SECM/ELISA for multianalyte sensing system. In addition to CEA, HCG, HPL, and α -fetoprotein were applied for dual- and multianalyte immunoassays [51–53]. Figure 3 shows a set of SECM images taken in the dual-immunoassay of HCG and HPL [51]. On each substrate, anti-HCG and anti-HPL were microspotted at the spatially addressable reaction zone, namely, the left for anti-HCG and the right for anti-HPL. Then, an analyte solution containing HCG and/or HPL was dropped onto the substrate, and then the substrate was

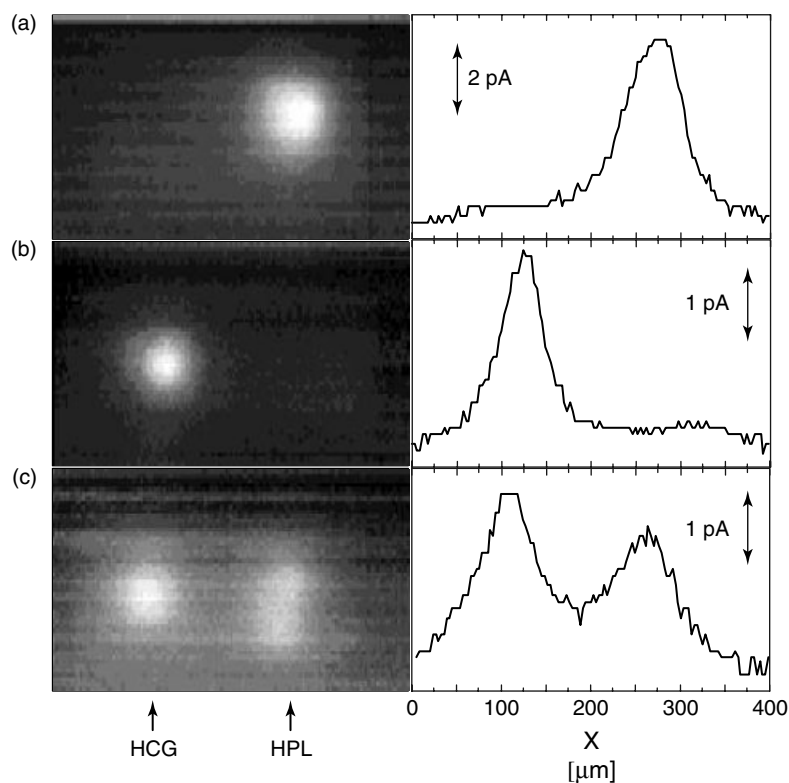


Fig. 3 SECM images and their cross-sections of the substrates for the dual-immunoassay. The substrate microspotted with anti-HCG (left arrow) and anti HPL (right arrow) were prepared with analyte solution containing HPL (a), HCG (b) or a mixture of HPL and HCG (c) (from ref. [51]. Copyright 1997 Elsevier Science.).

treated with a solution containing the two HRP-labeled antigens. The location of signal at the reaction zones (Fig. 3) indicates the type of antigen in the analyte solution. The calibration curves for both analytes were also shown in the literature. This assay protocol will be applicable to simultaneous detection of various biomolecules.

8.2.3

Local Fluxes Through Biological Materials

SECM affords a microscopic view of heterogeneous flux distribution across porous membranes. The probe senses a

particular redox species by choosing a suitable electrode potential and, moreover, the local flux can be quantitatively determined by analyzing SECM images. White and coworkers studied the SECM imaging of transport of redox species through porous membranes [31, 54–58]. They used a galvanostatic mode to maintain a steady state membrane current. The local fluxes of a particular redox species through the membrane pores were measured with a probe located close to the membrane surface. The G/C mode SECM imaging allows quantitative estimation of both the flux through individual pores and the pore size. The experimental data can

be fitted with those calculated based on semi-spherical diffusion equation to obtain fluxes. As samples, the hairless and nude mouse skin demonstrated measurement of the fluxes of ferrocyanide ion transfer through the pores by SECM [58]. The overall rate of ferrocyanide transport across the skin was analyzed by either inductively coupled plasma-mass spectroscopy or atomic adsorption spectroscopy. The ratio of the ferrocyanide ion transfer across the pores to that through the other part of the skin was discussed on the basis of solution compounds or surfactant effect [58].

Unwin and coworkers measured osmotically driven redox fluxes through porous laryngeal cartilage [35]. In their experiments, the probe-sample distance was significantly small to allow high spatial resolution mapping of the flux distribution, but, at the same time, the current profiles were affected by the probe-sample separation at each data point. Thus, the SECM image was a convolution of the local flux and topographical information at the sample surface. In a separate measurement, they imaged the same area without an osmotic driving force to obtain a pure topography. Then, the topographic image was subtracted from the original image to yield the two-dimensional flux distributions. One point should be mentioned, however, that their calculation was done under assumptions of the homogeneity of the flux at the sample surface within the area of probe size and the axial symmetry to the probe center.

8.2.4

Liquid–Liquid Interfaces, Liquid–Air Interfaces

Recently, electron transfer and mass transfer across liquid–liquid or liquid–air

interface have been vigorously studied by SECM [6, 7]. Bard and Mirkin and coworkers applied feedback mode SECM to analyze the electron transfer at the interface between two immiscible electrolyte solutions (ITIES) [62]. The potential between the two liquid phases is unbiased and controlled by changing the ratio of the concentration of supporting electrolyte in the two liquid phases. Because of the novel approach to direct detection of local reactions occurring at the interface, SECM/ITIES has made a remarkable impact overcoming traditional approaches.

Tsionski and coworkers extended the study to the electron transfer through a lipid monolayer at a benzene–water interface [67]. The electron transfer reactions between the oxidized form of zinc porphyrin (ZnPor^+) in a benzene phase and the reduced form of a metal complex (R , $\text{R} = \text{Ru}(\text{CN})_6^{4-}$, $\text{Mo}(\text{CN})_8^{4-}$, $\text{Fe}(\text{CN})_6^{4-}$, and so forth (Table 2)) in an aqueous phase have been surveyed. At the probe microelectrode surface, ZnPor^0 was oxidized to ZnPor^+ . When the probe is positioned close to the benzene–water interface, ZnPor^+ is reduced back to ZnPor^0 by accepting an electron from R in the aqueous phase at the liquid–liquid interface. In the experiment, the driving force was controlled with two parameters; the difference in standard potentials of the redox mediators in benzene and in water (ΔE^0), and the interfacial potential drop ($\Delta\phi_w^0$), which is controllable by varying the concentration ratio of a base electrolyte such as ClO_4^- in the two liquids. The driving force dependence on the electron transfer rate at the liquid–liquid interface has been shown in the literature in the absence and presence of the monolayer. The existence of the monolayer lowers the electron transfer

rate through the liquid–liquid interface. Interestingly, they observed an “inverted region” where electron transfer rate declines as the overpotential is increased, which may be explainable by Marcus theory.

Unwin and coworkers studied oxygen transfer across a monolayer dispersed at an air–water interface [74]. They have constructed an SECM measurement system in a Langmuir trough. A monolayer of 1-octadecanol was formed on the aqueous subphase containing potassium nitrate and the surface pressure of the monolayer was controlled with a compression barrier. A U-shaped microelectrode probe was placed in the aqueous solution and moved up to the air–water interface. When the probe approaches an air–water interface in the absence of the monolayer, the reduction current for O_2 is enhanced by positive feedback, due to fast translocation of O_2 from the gas phase to the solution. They recorded a set of approach curves while controlling the monolayer compression. A plot of the oxygen transfer rate as a function of the molecular area has been shown.

The same group also reported the first work that applied SECM for studying mass transport across an air–water interface [71]. By utilizing double potential step amperometry, bromine transfer through the air–water interface was investigated. An anodic pulse of 1.20 V versus AgQRE and 10-ms width was applied in a solution containing bromide anion to generate bromine at a probe–interface separation of 2.9 μm , then, the probe potential was stepped to 0.70 V to reduce bromine in the solution. On the basis of digital simulation analysis, the bromine transfer at the interface is diffusion controlled in the time scale of the experiment.

8.2.5

Planar BLMs

Because of the structural similarity to biomembranes, the planar BLM is an attractive experimental system to characterize ion and electron transport by measuring membrane potential or ion conductivity. The BLM is also used as a matrix for carriers and ion channels that promote highly selective and effective transport. The direct detection scheme of the SECM to probe local concentration shifts near the BLM supplements the information that conventional impedance measurements did not support. Antonenko and coworkers measured local pH changes near a BLM by means of a potentiometric pH microelectrode [75]. The pH profile evolves during the transport of weak bases such as ammonia through the BLM. Recently, they have elaborated on this study by utilizing an ammonium ion-selective microelectrode. The membrane permeability of ammonia was determined from the direct measurements of both H^+ and NH_4^+ concentration profiles perpendicular to the BLM surface [76]. Furthermore, double-barreled microelectrodes responsive to H^+ , K^+ , Na^+ , or Ca^{2+} were fabricated to simultaneously measure two cation concentrations within the unstirred layer face at the BLM surfaces [77]. Using a similar experimental procedure, they also studied permeation mediated by ion carriers such as nigericin or tributyltin across BLMs and estimated the exchange rates of K^+/H^+ and Cl^-/OH^- occurring near BLM surfaces [75].

Yamada and coworkers studied BLM permeation for hydrophobic ferrocene (Fc) derivatives by microvoltammetry [78]. Linear sweep voltammetry has been carried out with a microelectrode positioned close to the BLM. Two voltammograms for the

reduction of $\text{Ru}(\text{NH}_3)_6^{3+}$ and for the oxidation of ferrocenecarboxylic acid were recorded at the same probe-BLM separation. The deviation behavior of the voltammograms normal to that taken apart from the BLM has been found to be different. Namely, the reduction current for $\text{Ru}(\text{NH}_3)_6^{3+}$ evidently decreased compared with that taken far from the BLM surface. On the contrary, the decline of the oxidation current for ferrocenecarboxylic acid normal to that measured in the bulk solution was slight. The results obviously reflect the difference of the BLM permeability for the two redox species. Digital simulation was applied to analyze the permeation phenomena considering several processes including the transmembrane mass transfer and the diffusion in the vicinity of the BLM surface. The permeation coefficients for ferrocenecarboxylic acid were quantitatively estimated from the analysis. They also discussed the pH effect on BLM permeability for the ferrocenecarboxylic acid. Recently, the same experimental procedure has been applied to estimate permeability of several redox species through a cell membrane of an algal protoplast [86].

Matsue and coworkers studied ion transportation process across voltage-gated alamethicin ion channels incorporated

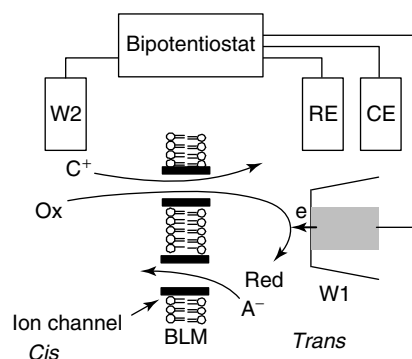
into a BLM [79]. Alamethicin, a polypeptide antibiotic, forms barrel-type ion channels penetrating through the BLM when the membrane potentials are applied. Figure 4 shows a schematic illustration of the experimental system. A redox species such as $\text{Ru}(\text{NH}_3)_6^{3+}$ was added in the cis side. A microelectrode (W1) soaked in the trans side was positioned close to the BLM incorporating alamethicin channels. Then a positive membrane potential pulse was applied at the working electrode 2 (W2), where the total ionic current was measured. Simultaneously, the probe microelectrode detected the reduction current for $\text{Ru}(\text{NH}_3)_6^{3+}$, which permeated from the cis to the trans side through the alamethicin ion channels. The chronoamperometric responses were recorded at the microelectrode and analyzed by digital simulation to obtain the permselectivity for several redox species through the channels. $\text{Fe}(\text{CN})_6^{4-}$ transportation through the channels have found to be restricted due to its negative charge compared with cationic $\text{Ru}(\text{NH}_3)_6^{3+}$.

8.2.6

Cells, Tissues

In this section, we note studies on monitoring of intact biological samples such as

Fig. 4 Schematic illustration of the experimental setup for characterization of the redox permeability across alamethicin ion channels in a planar bilayer lipid membrane (from ref. [79]. Copyright 1994 American Chemical Society.).



living cells or tissues. This application of SECM has been receiving a great deal of attention because it can afford vast knowledge, which has not been gained by the studies of living samples by means of microelectrodes [88–102]. Microelectrodes have been applied to *in vivo*, intra- and extra-cellular electrochemistry since 1970s that will be described elsewhere in this volume. The extracellular detection scheme shares its technical advantages and limitations with SECM technique [88–102]. The probe-sample separation is a critical parameter for spatial and temporal resolutions of the experimental systems. Preclusion due to the consumption of electrolysis at the microelectrode probe should be considered carefully.

Exocytotic secretion of catecholamines from a single adrenal medullary cell has been investigated [36, 91–97]. A carbon-fiber microelectrode positioned adjacent to the cell records a series of current spikes due to the oxidation of catecholamines released from individual vesicles after their fusion with the cell membrane. The spike-like responses were compared with the data obtained by fast-scan voltammetry [36]. The shape of the spikes also largely depends on the distance between the probe and the cell surface. The smaller probe-sample separation affords shorter time resolution and was found to resolve a rate-determining step in the secretion of catecholamines from the vesicle at the cell membrane. Spatially resolved current responses were obtained within the single cell surface by changing lateral position of a pair of microelectrodes [95]. To date, various studies characterized single cell responses by positioning a microelectrode very close to the surface have been reported [96–102].

SECM provides direct visual information on topography and local electrochemical activity of biological materials. The images of plant tissues have been reported in an early SECM study to demonstrate the capability of SECM to explore living samples [81]. Recently, intact leaves have been studied. SECM measurements exhibited the topography of stomata and images of O_2 evolution from stomata and a single stomatal complex [82]. Photosynthesis and respiration activities of single cells were quantitatively evaluated by monitoring the O_2 concentration profile around a single plant cell [83]. The O_2 consumption/generation rate of a single algal protoplast evidently depends on the illumination power of light irradiation. In the dark, the O_2 concentration profile declines when approaching the cell surface due to O_2 uptake by the respiration of the single cell. When light irradiated, the cell shows a positive gradient, due to O_2 evolution by photosynthesis. Oxygen evolution was saturated with light intensity of more than 15 klux. From the concentration profile around the single cell, the total consumption/evolution rate for oxygen was quantitated. The electron transfer from the photosynthetic electron-transport chain to an electron acceptor, known as the Hill reaction, was also studied. The influence of BQ on the respiratory and photosynthetic activity of a single protoplast was investigated in detail by using SECM. BQ interacts with the respiratory and photosynthetic electron-transport chains to accept electrons and, as a consequence, BQ itself is reduced to HQ. The analysis of localized concentrations of BQ and HQ yielded the fluxes. The intracellular redox reactions were discussed based on these fluxes and oxygen generation/consumption rates [32].

References

1. A. J. Bard, F.-R. F. Fan, J. Kwak et al., *Anal. Chem.* **1989**, 61, 132–138.
2. R. C. Engstrom, C. M. Pharr, *Anal. Chem.* **1989**, 61, 10 99A–11 04A.
3. A. J. Bard, G. Denuault, C. Lee et al., *Acc. Chem. Res.* **1990**, 23, 357–363.
4. A. J. Bard, F.-R. F. Fan, D. T. Pierce et al., *Science* **1991**, 254, 68–74.
5. M. Arca, A. J. Bard, B. R. Horrocks et al., *Analyst* **1994**, 119, 719–726.
6. M. V. Mirkin, *Anal. Chem.* **1996**, 68, 177A–182A.
7. A. L. Barker, M. Gonsalves, J. V. Macpherson et al., *Anal. Chim. Acta* **1999**, 385, 223–240.
8. L. A. Bottomley, *Anal. Chem.* **1998**, 70, 425R–475R.
9. L. A. Bottomley, J. E. Coury, P. N. First, *Anal. Chem.* **1996**, 68, 185R–230R.
10. R. M. Nyffenegger, R. M. Penner, *Chem. Rev.* **1997**, 97, 1195–1230.
11. H. Takano, J. R. Kenseth, S. Wong et al., *Chem. Rev.* **1999**, 99, 2845–2890.
12. <http://www.msstate.edu/Dept/Chemistry/dow1/secm/secm.bib.html>.
13. A. J. Bard, F.-R. F. Fan, *Faraday Discuss.* **1992**, 94, 1–22.
14. F.-R. F. Fan, A. J. Bard, *Science* **1995**, 267, 871–874.
15. F.-R. F. Fan, J. Kwak, A. J. Bard, *J. Am. Chem. Soc.* **1996**, 118, 9669–9675.
16. F. Zhou, A. J. Bard, *J. Am. Chem. Soc.* **1994**, 116, 393, 394.
17. D. A. Treichel, M. V. Mirkin, A. J. Bard, *J. Phys. Chem.* **1994**, 98, 5751–5757.
18. J. Kwak, A. J. Bard, *Anal. Chem.* **1989**, 61, 1221–1227.
19. D. O. Wipf, A. J. Bard, *J. Electrochem. Soc.* **1991**, 138, 469–474.
20. A. J. Bard, M. V. Mirkin, P. R. Unwin, *J. Phys. Chem.* **1992**, 96, 1861–1868.
21. M. V. Mirkin, T. C. Richards, A. J. Bard, *J. Phys. Chem.* **1993**, 97, 7672–7677.
22. P. R. Unwin, A. J. Bard, *J. Phys. Chem.* **1991**, 95, 7814–7824.
23. F. Zhou, P. R. Unwin, A. J. Bard, *J. Phys. Chem.* **1992**, 96, 4917–4924.
24. C. Demaille, P. R. Unwin, A. J. Bard, *J. Phys. Chem.* **1996**, 100, 14 137–14 143.
25. R. D. Martin, P. R. Unwin, *J. Electroanal. Chem.* **1997**, 439, 123–136.
26. A. J. Bard, L. R. Faulkner, *Electrochemical Methods*, Wiley & Sons, New York, 1980.
27. R. C. Engstrom, M. Weber, D. J. Wunder et al., *Anal. Chem.* **1986**, 58, 844–848.
28. R. C. Engstrom, T. Meaney, R. Tople et al., *Anal. Chem.* **1987**, 59, 2005–2010.
29. R. C. Engstrom, R. M. Wightman, E. R. Kristensen, *Anal. Chem.* **1988**, 60, 652–656.
30. R. C. Engstrom, B. Small, L. Kattan, *Anal. Chem.* **1992**, 64, 241–244.
31. B. D. Bath, R. D. Lee, H. S. White et al., *Anal. Chem.* **1998**, 70, 1047–1058.
32. T. Yasukawa, I. Uchida, T. Matsue, *Biophys. J.* **1999**, 76, 1129–1135.
33. R. D. Martin, P. R. Unwin, *Anal. Chem.* **1998**, 70, 276–284.
34. R. D. Martin, P. R. Unwin, *J. Chem. Soc. Faraday Trans.* **1998**, 94, 753–759.
35. J. V. Macpherson, D. O'Hare, P. R. Unwin et al., *Biophys. J.* **1997**, 73, 2771–2781.
36. R. M. Wightman, T. J. Schroeder, J. M. Finnegan et al., *Biophys. J.* **1995**, 68, 383–390.
37. B. R. Horrocks, M. V. Mirkin, D. T. Pierce et al., *Anal. Chem.* **1993**, 65, 1213–1224.
38. G. Denuault, M. H. T. Frank, L. M. Peter, *Faraday Discuss.* **1992**, 94, 23–35.
39. C. Wei, A. J. Bard, G. Nagy et al., *Anal. Chem.* **1995**, 67, 1346–1356.
40. H. S. Issacs, G. Kissel, *J. Electrochem. Soc.* **1972**, 119, 1628–1632.
41. J. Wang, L.-H. Wu, D. Li, *J. Electroanal. Chem.* **1989**, 272, 285–292.
42. D. T. Pierce, P. R. Unwin, A. J. Bard, *Anal. Chem.* **1992**, 64, 1795–1803.
43. D. T. Pierce, A. J. Bard, *Anal. Chem.* **1993**, 65, 3598–3604.
44. B. R. Horrocks, D. Schmidtke, A. Heller et al., *Anal. Chem.* **1993**, 65, 3605–3614.
45. G. Wittstock, W. Schuhmann, *Anal. Chem.* **1997**, 69, 5059–5066.
46. H. Yamada, H. Shiku, T. Matsue et al., *Bioelectrochem. Bioenerg.* **1994**, 33, 91–93.
47. H. Shiku, T. Takeda, H. Yamada et al., *Anal. Chem.* **1995**, 67, 312–317.
48. H. Shiku, I. Uchida, T. Matsue, *Langmuir* **1997**, 13, 7239–7244.
49. G. Wittstock, K. Yu, H. B. Halsall et al., *Anal. Chem.* **1995**, 67, 3578–3582.
50. H. Shiku, T. Matsue, I. Uchida, *Anal. Chem.* **1996**, 68, 1276–1278.
51. H. Shiku, Y. Hara, T. Matsue et al., *J. Electroanal. Chem.* **1997**, 438, 187–190.

52. H. Balets, W. Gopel, J. Hess, (Eds.), *Sensors Update*, vol. 6, Chap. 12, Wiley-VCH, Weinheim, **2000**.
53. H. Shiku, Y. Hara, T. Takeda et al., *ACS Symp. Ser.* **1997**, 656, 202–209.
54. E. R. Scott, H. S. White, *J. Membr. Sci.* **1991**, 58, 71–87.
55. E. R. Scott, H. S. White, *Solid State Ionics* **1992**, 53–56, 176–183.
56. E. R. Scott, H. S. White, J. B. Phipps, *Anal. Chem.* **1993**, 65, 1537–1545.
57. E. R. Scott, A. I. Laplaza, H. S. White et al., *Pharm. Res.* **1993**, 10, 1699–1707.
58. E. R. Scott, J. B. Phipps, H. S. White, *J. Invest. Dermatol.* **1995**, 104, 142–145.
59. J. V. Macpherson, M. A. Beeston, P. R. Unwin et al., *J. Chem. Soc. Faraday Trans.* **1995**, 91, 1407–1410.
60. J. V. Macpherson, M. A. Beeston, P. R. Unwin, *Langmuir* **1995**, 11, 3959–3963.
61. S. Nagues, G. Denuault, *J. Electroanal. Chem.* **1996**, 408, 125–140.
62. C. Wei, A. J. Bard, M. V. Mirkin, *J. Phys. Chem.* **1995**, 99, 16 033–16 042.
63. Y. Selzer, D. Mandler, *J. Electroanal. Chem.* **1996**, 409, 15–17.
64. T. Solomon, A. J. Bard, *J. Phys. Chem.* **1995**, 99, 17 487–17 489.
65. Y. Shao, M. V. Mirkin, J. F. Rusling, *J. Phys. Chem. B* **1997**, 101, 3202–3208.
66. M. Tsionsky, A. J. Bard, M. V. Mirkin, *J. Phys. Chem.* **1996**, 100, 17 881–17 888.
67. M. Tsionsky, A. J. Bard, M. V. Mirkin, *J. Am. Chem. Soc.* **1997**, 119, 10 785–10 792.
68. M.-H. Delville, M. Tsionsky, A. J. Bard, *Langmuir* **1998**, 14, 2774–2779.
69. C. J. Slevin, J. A. Umberes, J. H. Atherton et al., *J. Chem. Soc. Faraday Trans.* **1996**, 92, 5177–5180.
70. A. L. Barker, J. V. Macpherson, C. J. Slevin et al., *J. Phys. Chem. B* **1998**, 102, 1586–1598.
71. C. J. Slevin, J. V. Macpherson, P. R. Unwin, *J. Phys. Chem. B* **1997**, 101, 10 851–10 859.
72. Y. Shao, M. V. Mirkin, *J. Electroanal. Chem.* **1997**, 439, 137–143.
73. H. Yamada, S. Akiyama, T. Inoue et al., *Chem. Lett.* **1998**, 147–148.
74. C. J. Slevin, S. Ryley, D. J. Walton et al., *Langmuir* **1998**, 14, 5331–5334.
75. Y. N. Antonenko, A. A. Bulychiev, *Biochim. Biophys. Acta* **1991**, 1070, 279–282, 474–480.
76. Y. N. Antonenko, P. Pohl, G. A. Denisov, *Biophys. J.* **1997**, 72, 2187–2195.
77. P. Pohl, S. M. Saparov, Y. N. Antonenko, *Biophys. J.* **1998**, 75, 1403–1409.
78. H. Yamada, T. Matsue, I. Uchida, *Biochem. Biophys. Res. Commun.* **1991**, 180, 1330–1334.
79. T. Matsue, H. Shiku, H. Yamada et al., *J. Phys. Chem.* **1994**, 98, 11 001–11 003.
80. M. Tsionski, J. Zhou, S. Amemiya et al., *Anal. Chem.* **1999**, 71, 4300–4305.
81. C. Lee, J. Kwak, A. J. Bard, *Proc. Natl. Acad. Sci. U.S.A.* **1990**, 87, 1740–1743.
82. M. Tsionsky, Z. G. Cardon, A. J. Bard et al., *Plant Physiol.* **1997**, 113, 895–901.
83. T. Yasukawa, I. Uchida, T. Matsue, *Denki Kagaku* **1998**, 66, 660–661.
84. T. Yasukawa, T. Kaya, T. Matsue, *Chem. Lett.* **1999**, 975–976.
85. T. Yasukawa, T. Kaya, T. Matsue, *Anal. Chem.* **1999**, 71, 4637–4641.
86. T. Yasukawa, I. Uchida, T. Matsue, *Biochim. Biophys. Acta* **1998**, 1369, 152–158.
87. T. Yasukawa, Y. Kondo, I. Uchida, T. Matsue, *Chem. Lett.* **1998**, 767, 768.
88. S. Arbault, P. Pantano, J. A. Jankowski et al., *Anal. Chem.* **1995**, 67, 3382–3390.
89. S.-K. Jung, W. Gorski, C. A. Aspinwall et al., *Anal. Chem.* **1999**, 71, 3642–3649.
90. H. Lu, M. Gratzl, *Anal. Chem.* **1999**, 71, 2821–2830.
91. D. J. Leszczyszyn, J. A. Jankowski, O. H. Viveros et al., *J. Biol. Chem.* **1990**, 265, 14 736–14 737.
92. R. M. Wightman, J. A. Jankowski, R. T. Kennedy et al., *Proc. Natl. Acad. Sci. U.S.A.* **1991**, 88, 10 754–10 758.
93. K. T. Kawagoe, J. A. Jankowski, R. M. Wightman, *Anal. Chem.* **1991**, 63, 1589–1594.
94. T. J. Schroeder, J. A. Jankowski, K. T. Kawagoe et al., *Anal. Chem.* **1992**, 64, 3077–3083.
95. T. J. Schroeder, J. A. Jankowski, J. Senyshyn et al., *J. Biol. Chem.* **1994**, 269, 17 215–17 220.
96. R. H. Chow, L. von Ruden, E. Neher, *Nature* **1992**, 356, 60–63.
97. R. H. Chow, J. Klingauf, E. Neher, *Proc. Natl. Acad. Sci. U.S.A.* **1994**, 91, 12 765–12 769.
98. T. K. Chen, G. Luo, A. G. Ewing, *Anal. Chem.* **1994**, 66, 3031–3035.

99. G. Alvarez de Toledo, R. Fernandez-Chacon, J. M. Fernandez, *Nature* **1993**, 363, 554–558.
100. R. T. Kennedy, L. Huang, M. A. Atkinson et al., *Anal. Chem.* **1993**, 65, 1882–1887.
101. L. Huang, H. Shen, M. A. Atkinson et al., *Proc. Natl. Acad. Sci. U.S.A.* **1995**, 92, 9608–9612.
102. C. D. Paras, R. T. Kennedy, *Anal. Chem.* **1995**, 67, 3633–3637.

9 Ion-Selective Electrodes for Measurements in Biological Fluids

Eric Bakker
Auburn University, Auburn, Alabama

Mark E. Meyerhoff
The University of Michigan, Ann Arbor, Michigan

9.1	Zero-current Electrochemical Cells Incorporating Ion-selective Membranes	279
9.2	Selectivity of Potentiometric Membrane Electrodes	284
9.3	Glass Electrodes	286
9.4	Solid-state Electrodes	290
9.5	Liquid Membrane Electrodes	291
9.5.1	Ion-exchangers	292
9.5.2	Neutral Ionophores	293
9.5.3	Charged Ionophores	297
9.6	Gas-sensing Probes	298
9.7	Ion-selective Electrode-based Biosensors	302
	References	306

9.1 Zero-current Electrochemical Cells Incorporating Ion-selective Membranes

Ion-selective electrodes (ISEs) are relatively simple yet important electroanalytical devices that are now used routinely to quantitate a large number of different analytes in complex biological samples. In many instances, these sensors can be miniaturized to yield micrometer-sized sensing tips for intracellular sensing applications [1], for the mapping of chemical gradients [2], and for scanning probe electrochemical microscopy [3]. The time response of ISEs is often rapid (within milliseconds in some cases), and they are characterized as nonperturbing measurement devices because the analyte is normally not consumed in the course of the measurement. Further, they are among the very few analytical methods capable of measuring ion activities, rather than total concentrations [4].

Measurements with ISEs are carried out using an electrochemical cell similar to the basic design depicted in Fig. 1. The actual selective ion-sensing process is confined to the ion-selective membrane, which contacts the sample on one side and an internal filling solution on the other. In planar miniaturized systems, the latter often consists of a hydrophilic polymer

(hydrogel) doped with suitable electrolytes and saturated with water [5]. An internal reference electrode, usually silver–silver chloride, completes the measuring cell within the ion-selective electrode. A similar reference electrode also contacts the sample through a so-called bridge electrolyte, an aqueous solution or hydrogel with an electrolyte composition that is compatible with the sample to be measured. This junction between the bridge electrolyte and the sample phase yields a small, ideally invariant liquid junction potential as the sample composition is changed owing to differences in the mobilities of the ions on each side of this liquid–liquid junction [6, 7].

As Fig. 2 illustrates, the observed zero-current cell potential (electromotive force, emf) is a sum of each individual potential drop that occurs across the entire cell. Indeed, each vertical line in Fig. 2 represents an interface where a boundary potential develops. It is the potential across the ion-selective membrane that will be directly dependent on the ion composition of the sample and the contacting inner electrolyte. Therefore, all other potential contributions must be reversible and constant, so that observed cell potential (E_{cell}) changes can be attributed to changes in the membrane potential only, which in turn are indicative of changes in the ion activity in the sample phase.

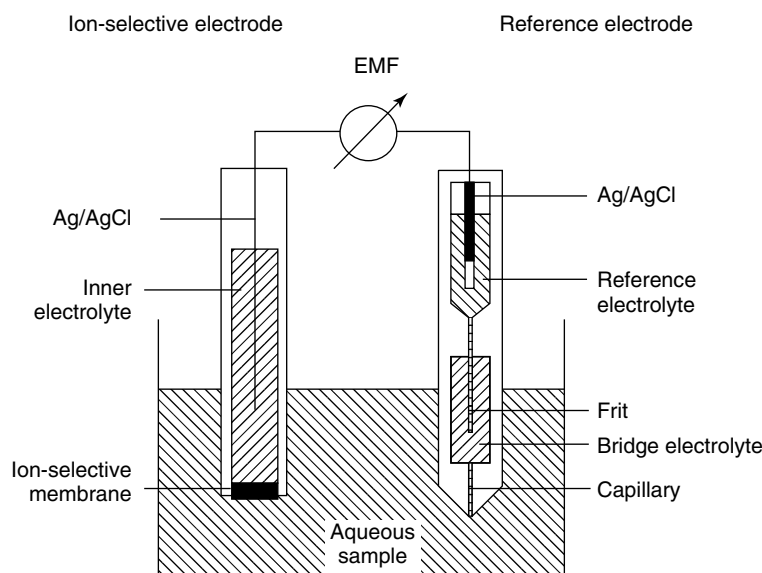


Fig. 1 Experimental assembly for measuring ISEs in a zero current galvanic cell.

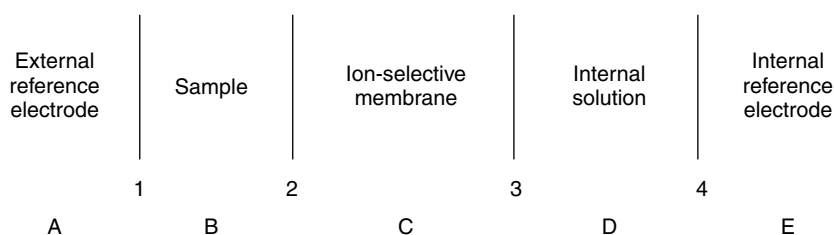


Fig. 2 Basic cell notation of ISE cell assembly. Numbers and vertical bars denote boundary potentials. The sum of all individual boundary potentials make up the observed cell potential.

The electrode that houses the ion-selective membrane, the inner electrolyte, and the inner reference electrode is called the indicator electrode or working electrode. If the external reference electrode contains an interchangeable bridge electrolyte, it is often termed a double junction reference electrode to indicate that two separate liquid junction potentials are present (one between the reference electrolyte and the bridge electrolyte, and the second between the bridge electrolyte and the sample solution). The use of combination pH glass

electrodes is commonplace (that is, indicator and reference electrode are combined into one housing), although two separate electrode housings are still often used when working with most other ISE indicator electrodes.

As mentioned earlier, the observed cell potential E_{cell} is the sum of all potential contributions in the cell. Therefore, according to Fig. 2, E_{cell} is written as a function of the Galvani potential differences between the individual solutions and electrode materials as follows:

$$\begin{aligned}
E_{\text{cell}} &= (\phi_E - \phi_D) + (\phi_D - \phi_C) \\
&+ (\phi_C - \phi_B) + (\phi_B - \phi_A) \\
&= E_4 + E_3 + E_2 + E_1 \quad (1)
\end{aligned}$$

If all potential changes are constant, with exception of the phase boundary potential E_2 , Eq. (1) simplifies to:

$$E_{\text{cell}} = K + E_2 \quad (2)$$

where $K = E_1 + E_3 + E_4$. The boundary potential E_3 between the ion-selective membrane and the inner electrolyte solution is typically constant as the ionic composition of this inner electrolyte does not change in most practical situations. The boundary potential at the membrane/sample interface, E_2 , is in ideal cases a direct function of the sample ion activity. It is assumed that sample ions can rapidly exchange with the ion-selective membrane material so that interfacial equilibrium must exist. Any ion will spontaneously partition in the space charge region according to its standard chemical potential difference and to its so-called free ion activity in each phase. Hydrophilic ions prefer the aqueous phase, whereas ions with a high affinity for the membrane material will rather distribute to the membrane phase. Since these ions carry a charge, this process spontaneously forms a space charge region, very locally at the interface, and yields a phase boundary potential that perfectly counterbalances the chemical tendency of each ion to partition into one or the other phase. In practice, therefore, each bulk phase remains essentially electroneutral. This process can be expressed mathematically as follows:

The electrochemical potential for ion I in the aqueous phase, $\tilde{\mu}_I$, is as:

$$\begin{aligned}
\tilde{\mu}_I(\text{aq}) &= \mu_I(\text{aq}) + zF\phi(\text{aq}) = \mu_I^0(\text{aq}) \\
&+ RT \ln a_I(\text{aq}) + zF\phi(\text{aq}) \quad (3)
\end{aligned}$$

and for the contacting ion-selective membrane phase:

$$\begin{aligned}
\tilde{\mu}_I(\text{mem}) &= \mu_I(\text{mem}) + zF\phi(\text{mem}) \\
&= \mu_I^0(\text{mem}) + RT \ln a_I(\text{mem}) \\
&+ zF\phi(\text{mem}) \quad (4)
\end{aligned}$$

where μ_I is the chemical potential of ion I (μ_I^0 under standard conditions), z is the charge, and a_I the activity of the uncomplexed ion I, ϕ is the electrical potential, and R , T , and F are the universal gas constant, the absolute temperature, and the Faraday constant. Since it is assumed that the interfacial ion transfer and complexation processes are fast and that, therefore, equilibrium holds at the interface, the electrochemical potentials for both phases must be equal. This leads to the following expression for the phase boundary potential E_{PB} (which is identical to E_2 shown in Eqs. 1 and 2):

$$\begin{aligned}
E_{\text{PB}} = \Delta\phi &= -\frac{\mu_I^0(\text{mem}) - \mu_I^0(\text{aq})}{zF} \\
&+ \frac{RT}{zF} \ln \frac{a_I(\text{aq})}{a_I(\text{mem})} \quad (5)
\end{aligned}$$

The term comprising the standard chemical potentials is often combined to the symbol k_I , that is, $k_I = \exp(\{\mu_I^0(\text{aq}) - \mu_I^0(\text{org})\}/RT)$. In this case, Eq. (5) simplifies to:

$$E_{\text{PB}} = \frac{RT}{zF} \ln \frac{k_I a_I(\text{aq})}{a_I(\text{mem})} \quad (6)$$

The concept of spontaneous interfacial ion distribution in the space charge region and its influence on the observed boundary potential is mathematically formulated in Eq. (6). Ions with a higher free energy of transfer from the sample to the membrane phase, a higher sample activity, and/or a lower membrane activity obviously lead to a more positive boundary

potential (when $I = \text{cation}$). This potential counteracts the tendency of the ions to further distribute unequally across the interface. Since $a_I(\text{mem})$ is usually constant, as is k_I , Eq. (2), taken together with Eq. (6) reduces to the well-known Nernst equation describing the response of the electrochemical cell toward ion I :

$$E_{\text{cell}} = E_I^0 + \frac{RT}{zF} \ln a_I(\text{aq}) \quad (7)$$

Note that in this equation all of the sample-independent emf contributions are included into one constant potential term (E_I^0). In practice, ISEs obey this equation when the ion-selective membrane interacts reversibly with the specific ion of interest; that is, a rapid ion transfer must occur between the sample and the sensing membrane (high exchange current density). On the other hand, this partitioning process must have no substantial effect on the chemical composition of the ion-selective membrane (that is, $a_I(\text{mem})$ must remain constant to obtain Nernstian response). Silver halide precipitate membranes, for example, can be used as ion-selective sensing materials as long as the surface composition remains intact and does not become fouled by other silver precipitates.

A Nernstian response to silver ions can be observed since silver can reversibly interact (precipitate and dissolve) with the membrane and the concentration of silver in the membrane is invariant (unit activity for solid phase). Analogous cases can be made for other suitable membrane materials.

As can be seen in Eq. (7), the observed potential change is proportional to the logarithm of the sample ion activity and to the absolute temperature and inversely proportional to the charge of the analyte ion. For measurements performed at 25 °C, Eq. (7) reduces to the following if potentials are measured in millivolts:

$$E_{\text{cell}}(\text{mV}) = E_I^0 + \frac{59.2}{z} \log a_I(\text{aq}) \quad (8)$$

The sensitivity of the analytical technique is therefore mainly dependent on the charge z of the analyte. For monovalent or divalent cations, for example, a 10-fold concentration change will yield +59.2 mV or +29.6 mV change in the observed cell potential. Anionic analytes (with negative z values) will induce negative potential changes. Figure 3 shows a typical calibration curve for a calcium-selective electrode based on a liquid membrane

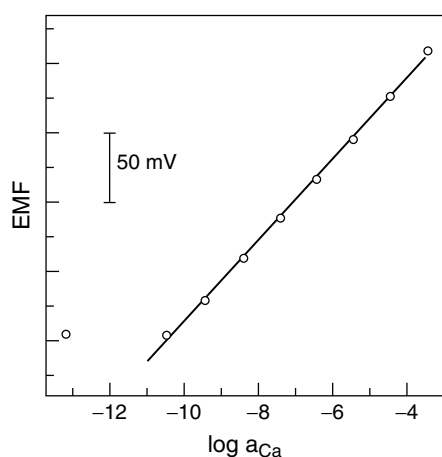


Fig. 3 Potentiometric response of a highly selective calcium electrode on the basis of the lipophilic calcium ionophore ETH 129 (see Ca^{2+} -1 in Fig. 4), measured in calcium buffered solutions with a physiological electrolyte background.

doped with the neutral ionophore ETH 129 (see structure $\text{Ca}^{2+}\text{-1}$ in Fig. 4) [8]. The samples containing low sample activities are buffered with the calcium chelator ethylenediamine tetraacetate (EDTA). This calcium buffer eliminates the influence of calcium ions leaching from the membrane

into the sample, which ordinarily dictates the lower detection limit. ISEs are capable of assessing free rather than total ion concentrations or activities. This experimental distinction between free and complexed forms of the analyte makes them quite useful for bioavailability studies.

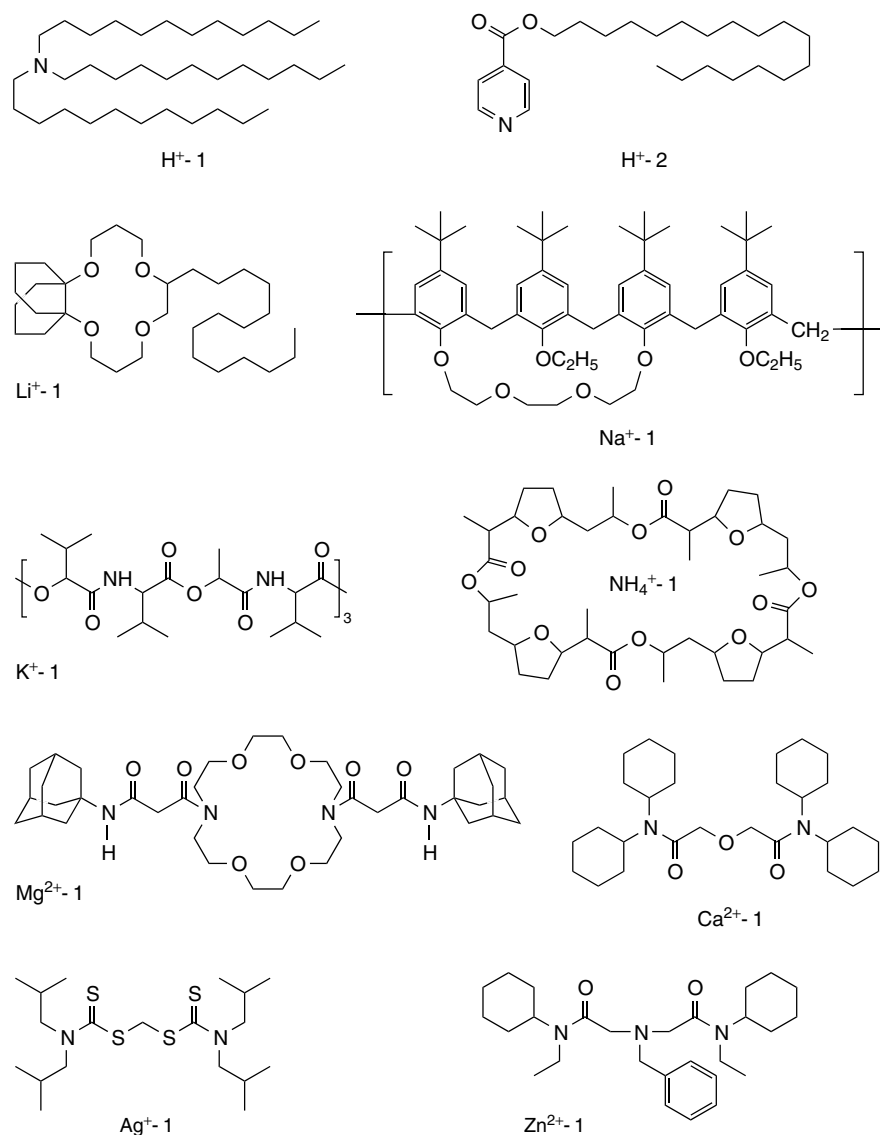


Fig. 4 Structures of typical cation-selective ionophores used in organic ISE membranes.

In routine blood analysis of electrolytes, where ISEs are used nearly universally, sometimes extremely small concentration changes are assessed with direct potentiometry. This requires potential stabilities and reproducibilities in the 10 to 100 microvolt range, which is achieved in temperature-controlled flow-through cells and with frequent, automated recalibrations between measurements. In batch mode benchtop analyses with ISEs, such a high precision is often not observed. In addition, accuracies are mainly limited by variations in the liquid junction potential between the calibration and sample phases and by interferences from other sample ions, temperature fluctuations, and if concentrations rather than activities are desired, variations in activity coefficients. The latter reflects the well-known relationship between the sample activity a_I and its concentration c_I :

$$a_I = \gamma_I c_I \quad (9)$$

where γ_I is the activity coefficient. Many possible experimental biases can be minimized in benchtop analysis by adding an ionic strength adjusting solution to the sample prior to measurement. ISEs are also routinely integrated into automatic titration instruments where they make up excellent endpoint indicators. In these cases, the accuracy and precision of the cell potential readings affect the accuracy of the analytical measurement to a much smaller extent than in direct potentiometry, where the observed E_{cell} is used to quantitate the analyte level in the sample phase.

9.2

Selectivity of Potentiometric Membrane Electrodes

For ISEs, interferences by other sample ions are mainly dictated by their

competitive partitioning into the ion-selective membrane phase. Often, therefore, ISEs are well understood in the sense that their response behavior is usually fully predictable from thermodynamic constants, such as the free enthalpies of transfer of the uncomplexed ions from the sample into the membrane. The selectivity can be characterized with one thermodynamically founded potentiometric selectivity coefficient K_{IJ}^{pot} for each interfering ion. It is obtained from the simple relationship, which directly relates the selectivity coefficient to the difference in the two E^0 values for both measured ions:

$$K_{IJ}^{\text{pot}} = \exp \left\{ \frac{E_J^0 - E_I^0}{RT} z_I F \right\} \quad (10)$$

where z_I is the charge of the so-called primary ion I and J is any interfering ion. The subscript IJ in the symbol K_{IJ}^{pot} describes the chosen primary and interfering ions. For example, the selectivity coefficient for a sodium-selective electrode over interfering calcium ions is characterized with the symbol $K_{\text{Na,Ca}}^{\text{pot}}$. Evidently, the selectivity coefficient is a direct function of the differences of the individual potentials extrapolated to 1-M activity for the ions I and J ($E_J^0 - E_I^0$); that is, the vertical shift between the single calibration curves at 1M sample activities. Correct K_{IJ}^{pot} values are obtained from adequate, unbiased E^0 measurements for each ion.

Historically, potentiometric selectivity coefficients were used to assess the extent of interference in a mixed sample by use of the so-called Nicolsky-Eisenman equation [9]:

$$E_{\text{cell}} = E_I^0 + \frac{RT}{z_I F} \ln \left(a_I + \sum K_{IJ}^{\text{pot}} a_J^{z_I/z_J} \right) \quad (11)$$

The activity term in the Nernst Eq. (7) is extended by a sum of selectivity-weighted activities of interfering ions. In essence, the selectivity coefficient must be as small as possible for each interferent ion so that Eq. (11) reduces toward Eq. (7). The Nicolsky-Eisenman equation has been extensively used in the literature for the past three decades. Unfortunately, it fails to give accurate mixed potential predictions if the charges of the primary and interfering ions are not identical [10, 11]. Nonetheless, it is still valuable to give rough estimates of the extent of interference, and is accurate for the response regions where only one ion is the predominant potential determining species. For liquid membrane electrodes (see following text), the following equation has been developed that offers more accurate predictions of the cell emf value in a sample containing a mixture of monovalent and divalent ions [12]:

$$E_{\text{cell}} = E_I^0 + \frac{RT}{F} \ln \left[\frac{1}{2} \sum_{i1} K_{I,i1}^{\text{pot}^{1/z_1}} a_{i1}(\text{aq}) \right] + \sqrt{\left(\frac{1}{2} \sum_{i1} K_{I,i1}^{\text{pot}^{1/z_1}} a_{i1}(\text{aq}) \right)^2 + \sum_{i2} K_{I,i2}^{\text{pot}^{2/z_1}} a_{i2}(\text{aq})} \quad (12)$$

The indices $i1$ and $i2$ under the sums in Eq. (12) indicate that only the sample activities of monovalent ($i1$) or divalent ions ($i2$) are summed. The summations involve all extractable ions, including the analyte ion I^{z_1} , in which case $K_{I,I}^{\text{pot}} = 1$. Equation (12) is valid for any number of monovalent and divalent ions in the sample. It has been extended to cover ions of higher valency as well [12].

In general, it is desired to use ion-selective electrode membranes in biological samples that exhibit very small selectivity coefficients to ensure accurate analytical results. Before one embarks on the optimization of ISE selectivity, however, it is crucial to evaluate the expected composition of the samples to be measured. Often, seemingly nonideal selectivities are irrelevant for a practical application if the primary ion is relatively concentrated and the interferent is dilute or virtually nonexistent. The following equation has been developed for liquid membrane ISEs to predict required maximum selectivity coefficients if any one interferent ion is not allowed to give a larger than 1% interference [10]:

$$K_{IJ}^{\text{pot}}(\text{required}) = \frac{a_I}{(100a_J)^{z_1/z_J}} \quad (13)$$

Consider, for example, the measurement of a sample that contains equal 1.0-mM activities of NaCl, KCl, and CaCl₂. According to Eq. (13), a sodium-selective electrode must show the following selectivity coefficients to reliably quantitate sodium in this sample: $K_{\text{Na,K}}^{\text{pot}} < 0.010$, and $K_{\text{Na,Ca}}^{\text{pot}} < 0.0031$. On the other hand, a calcium-selective electrode must only exhibit $K_{\text{Ca,Na}}^{\text{pot}} = K_{\text{Ca,K}}^{\text{pot}} < 0.10$. If the sample were to be diluted 10-fold, the requirements would change to $K_{\text{Na,K}}^{\text{pot}} < 0.010$, and $K_{\text{Na,Ca}}^{\text{pot}} < 0.0010$, and $K_{\text{Ca,Na}}^{\text{pot}} = K_{\text{Ca,K}}^{\text{pot}} < 1.0$. These examples show that required selectivity coefficients involving two ions of the same charge are simple to predict, but Eq. (13) must be used to predict cases with ions of different charges. The effect of sample dilution on the required selectivity coefficients can be easily understood. ISE responses to divalent ions show half the slope of monovalent ions (Eq. 8). Sample dilution will therefore decrease the

cell potential for the monovalent ion more strongly than for the divalent ion, thereby requiring a less selective electrode if the divalent ion is to be assessed.

Table 1 tabulates the normal measuring ranges of some common cations in blood, and required maximum selectivity coefficients of ISEs used to assess these ions in undiluted and diluted blood samples. Required K_{IJ}^{pot} are calculated according to Eq. (13) by using the minimum primary ion and maximum interfering ion activities shown in the Table.

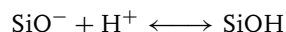
Analogous predictions can be made for other target samples, and the required selectivity coefficients form a basis for ISE evaluation and optimization.

As shown specifically in the following sections, different ion-selective membrane materials exhibit selectivities according to fundamentally different processes, including adsorption, precipitation, liquid-liquid partitioning, and complexation. These processes can be optimized to yield ISEs that satisfy a given analytical requirement.

9.3

Glass Electrodes

The most widely used ISE is, without doubt, the pH glass membrane electrode. Nearly one hundred years ago, Cremer reported its basic behavior [13]. pH glass electrodes have since evolved into highly reliable sensors as they show a wide dynamic measurement range, high selectivity, and good temperature resistance [14]. The pH response of glass electrodes arises from a hydrated surface layer that contains fixed SiO^- ion-exchanger sites that are highly selective to the hydrogen ion activity. pH glass electrodes often display extraordinary potentiometric selectivities for H^+ over other cations (Table 2), which is largely due to the favorable equilibrium for the primary equilibrium reaction occurring within the hydrated layer of the glass:



Interestingly, there are still some debates concerning the exact response

Tab. 1 Normal concentration range of some cations in blood and required maximum selectivity coefficients K_{IJ}^{pot} of ISEs for their reliable assessment by direct potentiometry in undiluted and 10-fold diluted blood samples, as calculated according to Eq. (13)

Ion I	$a_I(\text{min})$	$a_I(\text{max})$	$\text{Log}K_{IJ}^{\text{pot}}$ (required) in blood		
			Interferent J	Undiluted	10-fold diluted
Na^+	1.02×10^{-1}	1.12×10^{-1}	K^+	−0.6	−0.6
			Mg^{2+}	−0.2	−0.7
			Ca^{2+}	−0.3	−0.8
K^+	2.60×10^{-3}	3.70×10^{-3}	Na^+	−3.6	−3.6
			Mg^{2+}	−1.8	−2.3
			Ca^{2+}	−1.9	−2.4
Mg^{2+}	1.60×10^{-4}	2.80×10^{-4}	Na^+	−5.9	−4.9
			K^+	−2.9	−1.9
			Ca^{2+}	−2.4	−2.4
Ca^{2+}	3.40×10^{-4}	4.10×10^{-4}	Na^+	−5.6	−4.6
			K^+	−2.6	−1.6
			Mg^{2+}	−1.9	−1.9

Tab. 2 Membrane compositions and selectivities of important ISEs^a

Analyte	Membrane type	Membrane composition	$\text{Log}K_{ij}^{\text{pot}}$
H ⁺	Glass	72.2% SiO ₂ , 6.4% CaO, 21.4% Na ₂ O (mol%)	Na ⁺ : -11, K ⁺ : -11
H ⁺	Polymer	Tri- <i>n</i> -dodecylamine, KTpClPB, PVC, <i>bis</i> -2-ethylhexylsebacate	Na ⁺ : -10.4, K ⁺ : -9.8, Ca ²⁺ : <-11.1
H ⁺	Polymer	Octadecyl isonicotinate, KTpClPB, PVC, <i>ortho</i> -nitrophenyloctylether	Li ⁺ : -6.9, Na ⁺ : -5.6, K ⁺ : -4.4
Li ⁺	Polymer	7-tetradecyl-2,6,9,13-tetraoxa- tricyclo[12.4.4.0 ^{1.14}] docosane, KTpClPB, PVC, <i>bis</i> (benzylphenyl)adipate	Na ⁺ : -3.1, K ⁺ : -3.6, NH ₄ ⁺ : -3.8, Ca ²⁺ : <-5.0
Na ⁺	Glass	11% Na ₂ O, 18% Al ₂ O ₃ , 71% SiO ₂	K ⁺ : -2, Ag ⁺ : +2.6, NH ₄ ⁺ : -4.2, H ⁺ : 1 to 2.5
Na ⁺	Polymer	Calix[4]arenecrown-4 ionophore, KTpClPB, PVC, <i>ortho</i> -nitrophenyloctylether	Li ⁺ : -2.8, K ⁺ : -5.0, NH ₄ ⁺ : -4.4, Mg ²⁺ : -4.5, Ca ²⁺ : -4.4
K ⁺	Polymer	Valinomycin, NaTFPB, PVC, <i>bis</i> -2-ethylhexylsebacate	Na ⁺ : -4.5, Mg ²⁺ : -7.5, Ca ²⁺ : -6.9
NH ₄ ⁺	Polymer	Nonactin/Monactin, KTpClPB, PVC, <i>ortho</i> -nitrophenyloctylether	Li ⁺ : -2.9, Na ⁺ : -2.3, K ⁺ : -1.1, Mg ²⁺ : -4.0, Ca ²⁺ : -4.0
Mg ²⁺	Polymer	Double-armed dizazacrown ether ionophore (see Mg ²⁺ -1 in Fig.4), KTpClPB, PVC, <i>ortho</i> -nitrophenyloctylether	Li ⁺ : -3.7, Na ⁺ : -3.2, K ⁺ : -1.4, NH ₄ ⁺ : -2.0, Ca ²⁺ : -2.5
Ca ²⁺	Polymer	<i>N,N,N',N'</i> -tetracyclohexyl-3- oxapentanediamide (ETH 129), KTpClPB, PVC, <i>ortho</i> -nitrophenyloctylether	Na ⁺ : -8.3, K ⁺ : -10.1, Mg ²⁺ : -9.3
Ag ⁺	Solid-State	Ag ₂ S	Cu ²⁺ : -6, Pb ²⁺ : -6 to -9, H ⁺ : -5, Hg ²⁺ : -2
Ag ⁺	Polymer	Methylenebis(diisobutyldithiocarbamate), NaTFPB, PVC, <i>bis</i> -2-ethylhexylsebacate	Na ⁺ : -8.7, K ⁺ : -8.2, Ca ²⁺ : -11.0, Cu ²⁺ : -10.5, Pb ²⁺ : -10.3

(continued overleaf)

Tab. 2 (continued)

Analyte	Membrane type	Membrane composition	$\text{Log}K_{ij}^{\text{pot}}$
Zn^{2+}	Polymer	<i>N</i> -benzyliminodiacetic acid <i>bis</i> (<i>N</i> -ethyl- <i>N</i> -cyclohexylamide, KTpClPB, PVC, <i>ortho</i> -nitrophenyloctylether	Li^+ , Na^+ : -2.7, K^+ : -2.5, NH_4^+ : -3.1, Ca^{2+} : -2.8, Cd^{2+} : -3.6, Pb^{2+} : -2.1
F^-	Solid-State	Single LaF_3 crystal	OH^- : -1, Br^- : -4, Cl^- : -4, HCO_3^- : <-3
Cl^-	Polymer	2,7-di- <i>tert</i> -butyl-9,9-dimethyl-4,5- xanthenediamine, MTDDACl, PVC, <i>ortho</i> -nitrophenyloctylether	Sal^- : +1.8, SCN^- : +1.6, NO_3^- : +0.7, HCO_3^- : -2.6
I^-	Solid-State	50 mol% Ag_2S , 50 mol% AgI	Cl^- : -4, Br^- : -7, SCN^- : -4, S^{2-} : >10
S^{2-}	Solid-State	Ag_2S	Br^- : -25, I^- : -18, Cl^- : -30
HSO_3^-	Polymer	Guanidinium derivative ionophore, PVC, <i>ortho</i> -nitrophenyloctylether	ClO_4^- : -2.2, Cl^- : <-3.0, Sal^- : -2.3
SCN^-	Polymer	chloro[5,10,15,20-tetrakis[4-(hexyloxy- carbonyl)phenyl] porphyrinato] manganese(III), PVC, ETH 469	ClO_4^- : -2.0, I^- : -2.3, NO_3^- : -3.6, NO_2^- : -3.0, Cl^- : -3.4, HCO_3^- : -5.1
CO_3^{2-}	Polymer	<i>N</i> , <i>N</i> -dioctyl-4-trifluoroacetylbenzamide, MTDDACl, PVC, <i>bis</i> -2-ethylhexylsebacate	SCN^- : +1.0, NO_3^- : -1.6, Br^- : -3.5, Cl^- : -5.0, Sal^- : +3.3
NO_2^-	Polymer	2,9,16,23 tetra- <i>tert</i> -butylphthalocyanine)- cobalt(III), hexadecyltrioctylammonium iodide, PVC, dibutylphthalate	SCN^- : -1.0, I^- : -1.6, NO_3^- : -3.1, Cl^- : -3.5, Br^- : -2.9
Phosphate	Polymer	3-decyl-1,5,8-triazacyclodecane-2,4-dione, PVC, Dibutylsebacate	SCN^- : -2.3, NO_3^- : -2.8, Cl^- : -2.3, OAc^- : -3.2

(continued overleaf)

Tab. 2 (continued)

Analyte	Membrane type	Membrane composition	$\text{Log}K_{ij}^{\text{Pot}}$
Salicylate	Polymer	(2,9,16,23-tetra-tert-butylphthalocyanine) tin(IV), PVC, dinonyl sebacate	$\text{ClO}_4^-: -3.3$, $\text{SCN}^-: -2.9$, $\text{Cl}^-: -4.8$, $\text{OAc}^-: -3.4$

^asee [15, 16] and references cited therein. Abbreviations: KTpClPB, potassium tetrakis(4-chlorophenyl)borate; PVC, poly(vinyl chloride); NaTFPB, sodium tetrakis[3,5-bis(trifluoromethyl)phenyl]borate; MTDDACl, methyl tridodecyl ammonium chloride.

mechanism of the pH glass electrode. Some researchers favor viewing it as an adsorption process, rather than simple ion-exchange, responsible for the observed pH response [17].

A variety of optimized glass compositions exist that are suited for a variety of applications. The classical sodium-containing glass has been largely replaced by lithium glass. High content of Li_2O favors a low membrane resistance and low alkali error; that is, a larger measuring range. Today, glass electrodes that are small, have extremely large measuring ranges of pH 0 to 14, and show low resistances even with the relatively thick membranes required to achieve acceptable robustness can be manufactured. In the early years of pH glass electrode development, researchers tended to blow their own glass electrodes akin to Christmas tree bulbs. These electrodes were extremely fragile and had to be handled with great care. Today, glass membrane thicknesses can exceed 1 mm and can therefore be sufficiently strong to break a laboratory beaker without damaging the glass membrane itself. Glasses with extremely high Li_2O content, however, tend to crystallize easily and can therefore not be handled by a glass blower. Moreover, they have shorter lifetimes, corrode more easily, and are not suited for

high temperature applications (including the sterilization cycles for certain biological measurements; for example, monitoring the pH of cell cultures, etc.). Therefore, a variety of more rugged and extremely stable high temperature glasses are commercially available. Although they exhibit emf response over a reduced pH range, they function reliably at high temperature without the need for intermittent calibration.

Since pH glass membrane electrodes are used in a variety of applications, manufacturers of pH electrodes have devoted much effort in designing combination pH electrodes in many shapes and sizes, for use in NMR test tubes, with flat surfaces for paper and cheese pH measurements, pressure-resistant electrodes for reactor applications, and a large variety of laboratory pH electrodes. Beyond the type, size, and shape of the pH sensitive glass, an essential component of the combination pH electrode is the external reference electrode. Depending on the application of the pH electrode, one can choose from refillable electrolytes in single- and double-junction designs, as well as low viscosity maintenance-free solid polymers and gel electrolytes that can sustain high external pressures. In addition, available junction materials range from simple ceramic frits,

flat, circular ceramic frits for surface pH applications, Teflon sleeve junctions, free diffusion liquid junctions, and hole junctions for polymeric electrolytes. Some reference electrolytes can be pressurized in special chambers, while others are factory prepressurized or sustain high pressures without additional treatment. The excellent reliability, lifetime, and analytical performance of pH glass electrodes/reference combinations set an extremely high standard that few, if any other ISEs, can match.

Some specialized glass formulations have been found to be sensitive to ions other than H^+ as well. Glass membranes with a high content of Na^+ , for example, are known to be more Na^+ responsive [14]. While they are still selective for H^+ , they can be used to assess Na^+ activities in many biological samples because at physiological pH, the activity of H^+ is low compared to Na^+ levels (140 mM in blood), and thus does not contribute to the measured E_{cell} value. Indeed, such glass electrodes are still used today in a number of clinical blood analyzers, despite the availability of much more selective ionophore-based sodium electrodes (see following text). A different class of glass electrodes, chalcogenide glasses, has been found to respond to a variety of heavy metal ions, including lead and cadmium [18].

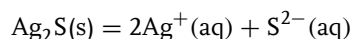
The main limitation of glass membrane electrodes in biological applications is their tendency to be fouled by strongly adsorbing proteins, and by the limited number of ions that can be sensed potentiometrically via glass membranes. Indeed, glass membranes cannot be utilized to sense anions, and thus do not provide a generic approach for ion sensing. While the protein adsorption problems can be reduced with repetitive washing cycles, difficulties in manufacturing miniaturized versions of glass electrodes to be used in conjunction

with other types of ISEs in planar sensor arrays, and so on have motivated significant research on different pH selective materials. Most notable are pH electrodes based on polymeric membranes doped with amine functional ionophores [19], and solid-state iridium oxide membrane materials [20].

9.4

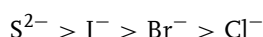
Solid-state Electrodes

ISEs based on solid-state membrane materials use sparingly soluble inorganic salts as the membrane matrix. Interesting examples of this family of electrodes include the silver precipitate-based membranes. Pressed pellets of silver sulfide (Ag_2S) are known to respond to silver ions because the membrane is a conductor for silver cations [21–23]. Interestingly, this membrane is also sensitive to sulfide ions because any change in the sample sulfide activity affects the available silver activity at the surface of the electrode membrane according to the following dissolution equilibrium:



This electrode shows a very high selectivity to both silver and sulfide (both ions cannot be present in solution in large quantities because of the small solubility product of Ag_2S). The only substantial interferent is the mercury(II) ion owing to the extremely low K_{sp} for HgS . The pressed pellet requires periodic polishing to remove surface adsorbates and other precipitates, but shows otherwise very long lifetimes. This principle has been extended to other silver salts, especially silver halides. Silver sulfide pellets doped with CuS will respond to Cu^{2+} because of the larger dissolution equilibrium of CuS relative to Ag_2S . A silver sulfide pellet doped with

AgBr will be bromide selective, and so on. The selectivity observed with such silver halide precipitates follows exactly the solubility product of the respective silver salt. Consequently, the following sequence is always observed for any given silver precipitate membrane:



A silver chloride precipitate membrane in prolonged contact with an I^{-} -containing solution will therefore eventually become an iodide-sensitive electrode since all surface bound chloride will exchange with iodide. However, this process can take some time in dilute solutions, during which the electrode remains essentially responsive to chloride [24]. Unfortunately, silver precipitate membranes are often unsuitable for use in biological samples as (1) thiol-containing molecules (proteins containing cysteines) may foul the surface of the ion-selective membrane and (2) the AgCl may dissolve because silver ions are complexed by protein amine functions [25]. Chloride measurements in such samples are therefore normally not performed with AgCl-based membranes. Analytical properties similar to pressed pellet membranes have also been observed with silver salts embedded in a silicone membrane, with ionophore-based silver-selective liquid membranes, and with silver–silver halide wires. The latter class is usually less preferred for practical measurements since any exposed metal may induce some redox species cross-sensitivity of the electrode, which does not usually occur with ion-conducting membrane-based indicator electrodes.

Another solid-state membrane of extremely high selectivity and applicability is the single crystal LaF_3 membrane electrode [26]. The crystal is doped with europium to lower its electrical resistance

and it acts as an effective pure F^{-} conductor. When used as a fluoride ion-selective electrode material, a large measuring range of about 6 orders of magnitude is observed (10^{-6} M to 1 M F^{-}), with Nernstian response slopes. The only significant interferent is hydroxide (due to the low solubility of $La(OH)_3$). Such electrodes are typically used under strict pH control between 5 and 6 to avoid hydroxide interference at higher pH and the formation of HF at lower pH, which would decrease the free activity of F^{-} . Suitable ionic strength adjustment buffers for fluoride measurements typically also contain complexing agents such as citrate to remove cations such as aluminum and iron from the sample that have a tendency to complex fluoride. The LaF_3 electrode has an extremely long lifetime under normal use. Its main disadvantage is its cost due to the necessity of using a polished single crystal.

9.5 Liquid Membrane Electrodes

Organic liquid membrane ISEs are certainly the most versatile group of ISEs, and have been especially successful for measurements in biological samples. Their response is dependent on liquid–liquid partitioning principles. The ion-selective membrane is either a highly plasticized hydrophobic polymer, a liquid organic phase, or a plasticizer-free polymer with a low glass transition temperature. With the first system, the plasticizer to polymer ratio is often large (2 : 1 by weight), and the main function of the polymer was originally to provide the membrane with required mechanical stability. The choice and concentration of plasticizer dictates to a large part the polarity of the membrane, membrane

selectivity, and diffusion coefficients of active components in the membrane. For biomedical applications, it is often more desirable to use systems without any leachable components, and plasticizer-free polymers are becoming increasingly available.

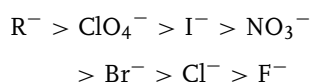
A variety of components are either freely dissolved in this hydrophobic matrix or covalently anchored onto the polymeric backbone of the membrane. These membrane components mediate the selective extraction of many analytes and also make sure that the ISE membrane exhibits ion-exchanger properties. Thus far, liquid/polymer membrane ISEs for more than five-dozen analytes have been described [15, 27, 28]. They are routinely used in clinical analysis for the direct potentiometric detection of many anions and cations, and their application is steadily broadening with the advent of more selective membrane materials, advances in miniaturization, and the availability of more rugged sensors. Two main classes of liquid membrane ISEs can be distinguished: one that contains an ion-exchanger without molecular receptor properties, and the other that is based on highly selective ionophores. While modern chemical research is mainly directed to the improvement of the second class, many commercial ISEs are still based on the first.

9.5.1

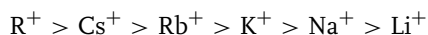
Ion-exchangers

Liquid or solvent polymeric membranes must exhibit ion-exchanger properties to properly function. It was mentioned previously that the concentration of analyte ion in the membrane phase must remain approximately invariant in the course of an experiment. In a classical two-phase partitioning experiment, however, a concentration increase of an electrolyte

in the sample would lead to a proportional increase in the organic phase. Therefore, according to Eq. (6) such a process would lead to no change in the phase boundary potential since the ratio $a_1(\text{aq})/a_1(\text{mem})$ is constant. Consequently, liquid membranes are routinely doped with a salt of a lipophilic ion, for example, tridodecylmethylammonium chloride for anion-selective electrodes and potassium tetrakis(4-chlorophenyl)borate for cation-selective electrodes. Numerous other ion-exchangers have been reported in the literature, but their main function is always the same. Prior to use, the liquid membrane is allowed to condition in a solution that contains a high concentration of the cation or anion to be measured. During this conditioning period, the hydrophilic counterion of the ion-exchanger in the membrane is replaced with the analyte ion of interest. The selectivity of such membranes is a direct function of the free energy of hydration of the measured ions. For anion-selective membranes (containing the anion salt of a quaternary ammonium ion, for example), the observed selectivity sequence always follows the so-called Hofmeister sequence:



where R^- denotes an organic anion. By complete analogy, the selectivity sequence for ion-selective membranes incorporating a cation-exchanger is:



Consequently, ion-exchanger-based ISEs have historically been used for the detection of perchlorate and nitrate, as well as a host of lipophilic organic ions including certain drugs and cationic/anionic surfactants. Indeed, the use of such electrodes for

rapid quantitation of charged organic drug species is the subject of a monograph and several reviews [29, 30]. Given the limited selectivity over other lipophilic ions (both organic and inorganic), such drug sensors are best used for monitoring the drug content of pharmaceutical formulations, where the presence of such interferent species are not typically present.

Another more recent application of ion-exchanger-based membrane electrodes relates to their utility for sensing polyionic species, including the anticoagulant heparin, and its antidote polycationic protamine [31]. With the appropriate choice of the organic ion-exchanger in the membrane (tridodecylmethylammonium chloride in the case of polyanion sensing, and dinonylnaphthalene sulfonate in the case of polycation sensing) $0.1\text{--}10\text{ }\mu\text{g mL}^{-1}$ levels of polyions can be sensed in biological samples. These new sensors, however, function via a nontraditional nonequilibrium response mechanism, based on the cooperative extraction of the polyion into the membrane to form strong ion-pairs with the lipophilic exchanger. Indeed, no useful potentiometric response is observed if the membrane is equilibrated with the given polyion for extended periods to completely convert the ion-exchanger to the polyion complex form. However, if operated always in a nonequilibrium mode, these ion-exchanger-based sensors can provide a simple means to measure certain high charge density polyions in samples as complex as whole blood.

Interestingly, anion-exchanger-based membrane electrodes are also used routinely to assess chloride in extracellular fluids. While there are some interferences from thiocyanate (for patients who smoke cigarettes) and bicarbonate, as well as from some large anionic molecules such as heparin, calibration in samples with

very similar background electrolytes can minimize these effects. In recent years, however, ionophore-based chloride sensors that offer potential advantages over the ion-exchanger-based system, most notably with respect to selectivity, have become available [15].

It is interesting to note that the listed selectivity sequences are thermodynamic and are not always observed under practical measuring conditions. If a strongly interfering ion is present but relatively dilute (typically at less than 10^{-4} M levels), its effect on the cell potential is often much smaller than predicted on the basis of the Nicolsky equation and its modifications [32]. Such low concentrations lead to a local depletion of these ions at the membrane surface and to an incomplete ion exchange, even if thermodynamically favored. For short exposure times, therefore, the electrode can often still reliably be used to assess the analyte. After prolonged contact with a sample containing a strong interferent, the electrode does, however, completely recondition and fails to respond to the primary analyte. These effects have historically been exploited for sensing applications in samples for which no thermodynamic selectivity was available. It requires careful reconditioning between measurements, and is not recommended if intrinsically better selectivity can be achieved with another ISE. This effect is perhaps an explanation as to why some manufacturers offer ion-exchanger-based ISEs for a variety of ions, although the basic membrane compositions are essentially identical.

9.5.2

Neutral Ionophores

Lipophilic, electrically neutral ionophores, also called ion carriers because of their

capability of selectively transporting ions across artificial membranes, are chemical components that are essential to achieving high-sensing selectivity with liquid or polymer membrane-based ISEs. Neutral carrier-based membranes also require the addition of a lipophilic ion-exchanger for proper functioning. The ion-exchanger forms the counterion of the complexed analyte in the membrane, and is typically less concentrated than the ionophore. For example, cation-selective membranes may contain the ionophore and the lipophilic tetraphenylborate derivative cation-exchanger potassium tetrakis(4-chlorophenyl)borate, while anion-selective membranes may be doped with tridodecylmethylammonium chloride as anion-exchanger in addition to the ionophore. While ionophore-free ion-exchanger-based membranes always show the same selectivity pattern that follows the hydration energies of the ions, ionophore-based membranes show selectivities that are significantly different. This stems from the formation of strong complexes between the extracted analyte ion and the ionophore in the membrane. Complex formation constants can vary widely, and have been reported to be around 10^8 M^{-1} for monovalent to about 10^{20} M^{-2} for divalent ions. Sensor selectivity is now dictated by the free energy of transfer of the ions from the aqueous to the membrane phase, the complex formation constants between the extracted ions and the ionophore, and the concentrations of ionophore and lipophilic ion-exchanger (also called ionic site) in the membrane. Because hydration energies are still important, given that an ion extraction process is involved, it is typically much more difficult to design ISEs for hydrophilic ions than it is for hydrophobic ones. On the other hand, it is often a challenge to design selective receptors for

extremely large, bulky ions. Consequently, ionophore-based ISEs for potassium were realized quite early on, while truly selective sensors for magnesium, lithium, sodium, and small anions such as chloride and phosphate have only been developed fairly recently and are still topics of current research. Ionophore-based ISEs for bulky anions such as perchlorate are virtually unknown.

Figures 4 (see earlier) and 5 illustrate the structures of a small selection of successful ionophores used to prepare liquid/polymeric membrane ISEs. Table 2 summarizes the typical membrane compositions of the corresponding ISEs and observed selectivity coefficients. Observed selectivities are in many cases extremely high, and contribute to the great success that such sensors have enjoyed for practical measurement applications in biological samples.

Ionophores can be developed on the basis of a variety of recognition principles. They include simple crown ethers, bis-crown ionophores, crowns with bulky side groups to prohibit intermolecular sandwich formation, noncyclic amide and thioamide ionophores, basket-shaped calix[4] arene and calix[6] arene ionophores, calixarenes with crown bridges, thiocarbamates, lipophilic amine bases as H^+ -ionophores, guanidinium derivatives, multitopic hydrogen bond-forming ionophores for selective anion recognition, metalloporphyrins, corrins, and phthalocyanines with different metal centers and a variety of axial ligands, and aromatic trifluoroacetyl derivatives for the recognition of hydrophilic nucleophiles. It should be noted that some of these ionophores are electrically charged in their uncomplexed form, and this special class of ion carriers is discussed separately later.

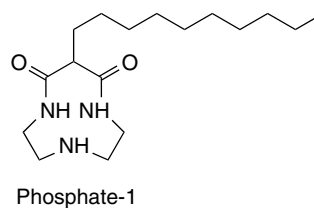
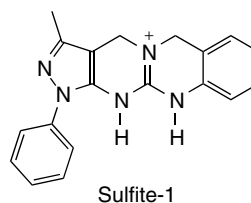
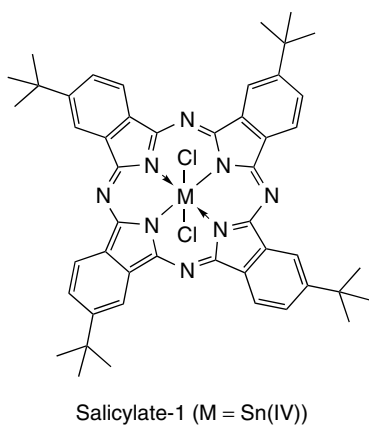
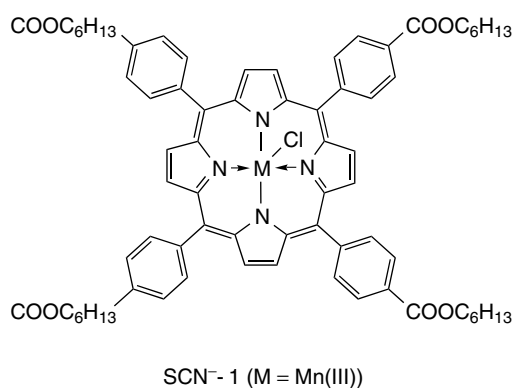
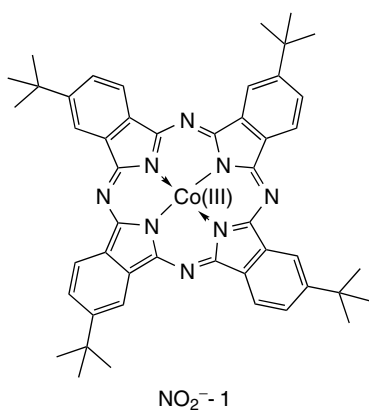
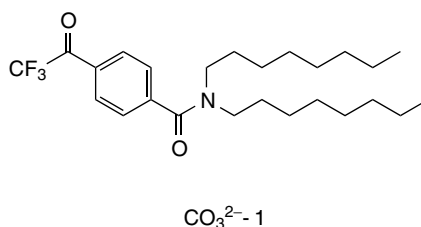
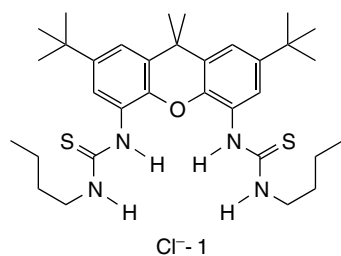


Fig. 5 Structures of typical anion-selective ionophores used in ion-selective electrode membranes.

To function properly in ion-selective membranes, ionophores typically share a number of important characteristics [33]. They should be highly lipophilic so that they are strongly retained within the

hydrophobic membrane phase to ensure a long lifetime of the sensor [34]. This is most often achieved by adding long alkyl chains, cyclohexyl or adamantyl substituents to the molecular backbone.

They should have a polar moiety or a set of polar functional groups that is responsible for the ion recognition process. The rest of the ionophore molecules should contain hydrophobic regions that are compatible with the surrounding membrane matrix. The historical argument that an ionophore molecule must also exhibit a certain mobility within the membrane has been largely disproved by the comparable analytical performance of a number of membrane materials where the ionophore is covalently anchored onto the polymeric backbone [35]. It seems beneficial, however, to at least either have mobile ionophores or mobile ionic sites to guarantee an acceptably low membrane resistance.

Membrane selectivities for any given ionophore can vary substantially. Membranes of relatively high polarity are typically preferred for the development of divalent ISEs and many anion-selective electrodes, while nonpolar membranes are generally more suited for monovalent cations. However, the role of membrane polarity on the membrane selectivity has been overrated in the past as there seems to be no direct correlation when a large

number of plasticizers are compared [36]. Indeed, many other parameters appear to influence selectivity equally as well, including the tendency to form ion pairs, the availability of functional groups on the plasticizer that can compete with the ionophore, and indirect variations of complex stoichiometries of the ionophore in different solvent environments. Therefore, optimization of ISE selectivity is to a large degree still an empirical process. However, if the complex stoichiometries are known, optimum membrane concentration ratios between ionophore and lipophilic ionic sites can be effectively predicted. A thermodynamic analysis of the correlation between expected selectivity coefficient and membrane composition reveals that selectivity maxima do indeed exist [37]. Table 3 shows the optimum concentration ratios for a select number of assumed complex stoichiometries and charges of the two compared ions. Since some ionophores are capable of forming mixed complexes, it is advisable to use these values as first guesses only and to evaluate the selectivity for a wide range of ionic site concentrations.

Tab. 3 Optimum concentration ratio of lipophilic anionic sites to neutral ionophore, giving highest selectivity for the analyte ion over an interfering ion. The optimum ratios are dependent on the charges of both ions and the respective complex stoichiometries (number of ligands per ion) in the membrane

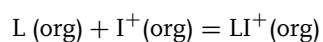
Charge of cation		Stoichiometry of ligand–ion complex		
<i>I</i> (analyte) z_i	<i>J</i> (interfering ion) z_j	<i>I</i> (analyte) n_i	<i>J</i> (interfering ion) n_j	Optimum ratio of sites to ionophore
2	2	1	2	1.41
2	2	2	3	0.77
2	2	3	4	0.54
2	1	1	1	1.62
2	1	2	2	0.73
2	1	3	3	0.46
1	1	1	2	0.71

Microelectrode forms of neutral carrier-based membrane electrodes with tip diameters of 1 μm or less have been used by physiologists for many years to probe the free concentration of potassium, calcium, sodium, and proton activity within single cells [38]. Such electrodes can be prepared conveniently by incorporating the appropriate membrane components (including required lipophilic sites) either in a wet organic liquid or polymer form, within the distal end of pulled glass pipet tips in which the inner walls at the distal end have been treated with an organosilane reagent to render them hydrophobic. The inner filling solution and Ag/AgCl wire complete the microelectrode assembly. For intracellular measurements, an external reference electrode can be placed outside the cell, provided that correction for the cell membrane potential is made via separate experiments with two Ag/AgCl electrode-based pipets filled with KCl, one inside and the other outside a separate cell bathed in the same solutions. Alternately, dual-barrel micropipets can be prepared, in which one barrel contains the ISE membrane and the other is filled with KCl (and a Ag/AgCl reference wire) to serve as the external reference within the biological cell being probed.

9.5.3

Charged Ionophores

Most ionophores used in liquid/polymer membrane ISEs today are electrically neutral in their uncomplexed form and assume the charge of the analyte ion when complexed. In the membrane, therefore, the following complexation equilibrium exists between ionophore L and the analyte I^+ :



Consequently, ISE membranes containing such ionophores must also contain a lipophilic ion-exchanger whose charge is opposite that of the analyte ion, which dictates the concentration of LI^+ complex in the membrane through the electroneutrality condition. However, Fig. 5 also shows the structures of a small selection of ionophores that are electrically charged in their uncomplexed form (see the metalloporphyrin and phthalocyanine structures in Fig. 5). With the exception of the successful dialkylphosphate calcium carriers [39], such ionophores have been somewhat neglected in the field since there has been evidence that the binding selectivity of the ionophore cannot be fully translated into a high-sensing selectivity for a corresponding ISE prepared with these compounds. In recent years, however, this view has been modified and electrically charged ionophores are being evaluated more aggressively, especially in the design of receptors for anionic species. An additional electrical charge on the coordinating functional group of the ionophore seems especially attractive to further strengthen otherwise weak complexes with additional coulombic forces, which can be particularly useful in the case of anion recognition.

Functional ISEs based on charged carriers can be fabricated with membranes that contain just the salt of a charged ionophore, since the ionophore has both ionophoric and ion-exchanger properties. However, it has been shown that the corresponding sensing selectivities are then often less than ideal [40]. Consider, for example, a membrane with a charged ionophore selective for a monovalent anion. The concentration of uncomplexed ionophore in the membrane is ordinarily small and dictated by the dissociation constant of the complex:

$$LA(\text{org}) = L^+(\text{org}) + A^-(\text{org})$$

If the ISE membrane were to be conditioned in a solution of an interferent whose complex with the ionophore is weaker, the concentration of uncomplexed ionophore in the membrane would be larger since the dissociation constant is now larger as well. In a mixed sample situation where both ions are present, an intermediate situation would be observed, that is, a higher interfering ion level would lead to a higher concentration of uncomplexed ionophore in the membrane. This dependency between sample composition and uncomplexed ionophore concentration is nonideal, since it effectively favors the formation of the complex with a weaker binding analyte. Optimum selectivities can be achieved by incorporating an ion-exchanger into the membrane that has the same charge as the analyte, and which forms the counterion of the uncomplexed ionophore L^+ . That concentration must now be invariant of the type of sample ion extracted, and theory predicts the ISE selectivity to be dependent on the binding selectivity of the charged ionophore in the very same way as for membranes containing neutral ionophores [40]. In effect, the presence of the lipophilic additive serves to maintain a fixed level of uncomplexed charged carrier L^+ , thereby buffering the

membrane phase with respect to the free primary ion activity in the membrane, which further serves to enhance selectivity.

Interestingly, suitable extensions of this theory have allowed researchers to explain other peculiar effects involving some charged carrier-based ISEs, for example, apparently super-Nernstian response slopes that are sometimes observed [41]. While the details of this effect are beyond the scope of this chapter, it should be emphasized that such behavior can be explained with thermodynamic processes occurring at the sample–membrane interface. Undoubtedly, charged carrier-based ISEs, especially for anions, will be a major research direction in years to come.

9.6

Gas-sensing Probes

Several of the ion-selective membrane electrodes described in the previous section can also be employed as transducers to devise highly selective potentiometric gas-sensing probes. As shown in Table 4, equilibrations of gases in aqueous solution yield ionic species. Hence, a number of relatively simple and analytically useful probes can be constructed by incorporating ISE-based electrochemical cells as detectors behind outer gas permeable membranes, and choosing appropriate

Tab. 4 Some potential analyte gases and their relevant solution phase equilibria that can be employed to devise potentiometric gas-sensing probes based on inner ion-selective membrane electrodes

Analyte gas	Equilibrium reactions	Inner ion electrode
CO ₂	CO ₂ + H ₂ O \longleftrightarrow H ⁺ + HCO ₃ [−]	H ⁺ , CO ₃ ^{2−}
SO ₂	SO ₂ + H ₂ O \longleftrightarrow H ⁺ + HSO ₃ [−]	H ⁺ , HSO ₃ [−] , SO ₃ ^{2−}
NO ₂	NO ₂ + H ₂ O \longleftrightarrow NO ₃ [−] + NO ₂ [−] + H ⁺	H ⁺ , NO ₂ [−] , NO ₃ [−]
HOAc (acetic acid)	HOAc \longleftrightarrow H ⁺ + OAc [−]	H ⁺ , OAc [−]
NH ₃	NH ₃ + H ₂ O \longleftrightarrow NH ₄ ⁺ + OH [−]	H ⁺ , NH ₄ ⁺

inner electrolyte solutions into which the analyte gas can equilibrate [42].

In 1958, Severinghaus and Bradley originally proposed the classical design for such devices [43] for the measurement of CO_2 in blood and this is shown in Fig. 6. The inner ion-selective membrane in this configuration is usually a pH-sensitive glass membrane, although other pH-sensitive ISEs including neutral carrier-based polymeric membrane electrodes can also be employed. The gas-sensing probe is designed in such a

way that the inner membrane electrode transducer presses tightly against an outer gas permeable membrane barrier, typically silicone rubber or microporous Teflon materials, creating a very thin layer of inner electrolyte between the inner ion-sensing membrane and outer gas-permeable film. Note that the external reference electrode for the ISE is also placed behind the gas-permeable membrane in the bulk of the inner filling solution; hence the entire electrochemical cell is confined to this filling solution, and thus the complete device

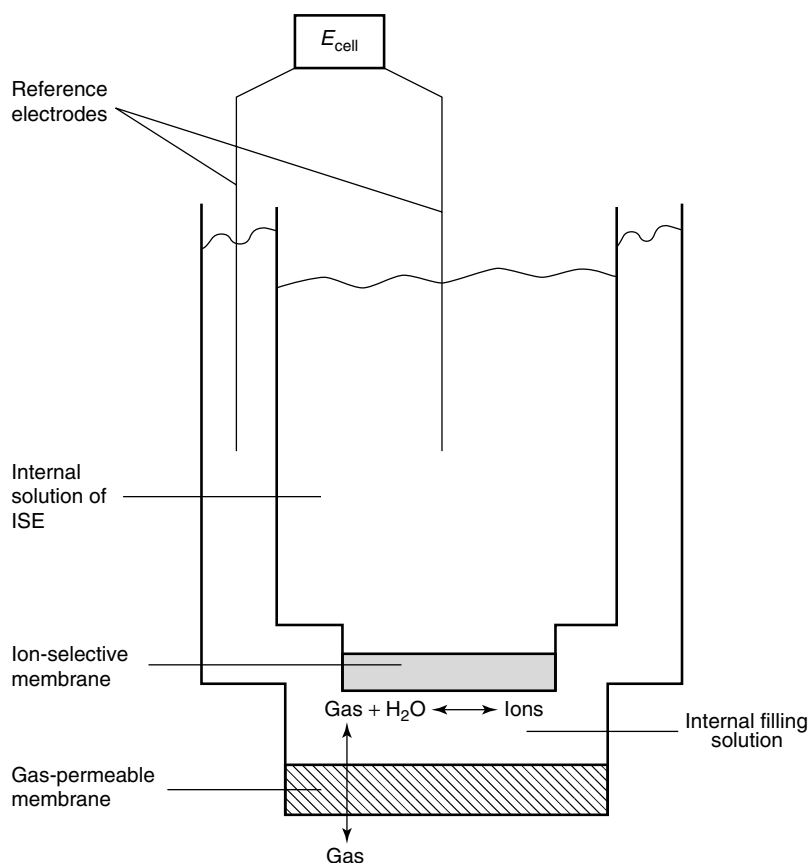


Fig. 6 Schematic of typical potentiometric gas-sensing probe. Inner electrode is a glass membrane pH sensor for a conventional Severinghaus style device. Other ISEs can be used in a similar geometric arrangement to detect ionic forms of gases within the thin layer of the inner filling electrolyte solution at the distal end of the probe.

should be termed a gas-sensing “probe” or “sensor,” not a gas-sensing “electrode.”

For the conventional Severinghaus style sensor, equilibration of analyte gas from the sample phase through the outer gas-permeable membrane determines the pH of the inner thin film of electrolyte at the distal end of the probe. For a CO₂ sensor, as an example, equilibration of the analyte in aqueous solution yields protons and bicarbonate ions (Table 4). Using a pH sensor as the inner transducer, the electrochemical potential of the cell can be written as:

$$E_{\text{cell}} = K + 0.059 \log a_{\text{H}^+}(\text{film}) \quad (14)$$

where a_{H^+} is the activity of hydrogen ions in the thin film of inner electrolyte, and K is the sum of all additional constant emf values of the cell, including the voltage of the inner reference electrode of the pH sensor and the external reference electrode. Note that there are no junction potentials considered within this K term, since the inner reference electrode, typically a bare Ag/AgCl contact, is in direct ionic contact with the same inner electrolyte solution as the ion-sensing membrane. The equilibrium constant for CO₂ equilibration can be written as:

$$K_{\text{CO}_2} = \frac{a_{\text{H}^+} \times a_{\text{HCO}_3}}{P_{\text{CO}_2}} \quad (15)$$

where P_{CO_2} is the partial pressure of CO₂. When the P_{CO_2} is equal on both sides of the gas-permeable membrane, the thin film of electrolyte is in complete equilibrium with the sample phase (e.g. blood) and the a_{H^+} within the thin film is directly proportional to the P_{CO_2} in the sample:

$$a_{\text{H}^+}(\text{film}) = \frac{K_{\text{CO}_2} P_{\text{CO}_2}}{a_{\text{HCO}_3}(\text{film})} \quad (16)$$

Substitution of $a_{\text{H}^+}(\text{film})$ from Eq. (16) into Eq. (14) yields an expression for the

voltage of the gas sensor as function of the P_{CO_2} in the sample phase:

$$E_{\text{cell}} = K + 0.059 \log \frac{K_{\text{CO}_2} P_{\text{CO}_2}}{a_{\text{HCO}_3}(\text{film})} \quad (17)$$

If the activity of bicarbonate is kept constant within the film, which can be achieved by using a fairly concentrated NaHCO₃ solution (0.1 M) as the inner filling solution (with added KCl or NaCl to poise the potential of the Ag/AgCl reference electrode in contact with the bulk of this solution, see Fig. 6), and given that K_{CO_2} is a constant, Eq. (16) can be rewritten as:

$$E_{\text{cell}} = K' + 0.059 \log P_{\text{CO}_2} \quad (18)$$

Thus, the gas-sensing probe responds like any ISE with a Nernstian slope toward the analyte gas.

By analogy [42], sensors for any of the other acidic analyte gases listed in Table 4 can be prepared by using a solution of the conjugate base anion as the inner filling solution (with added chloride salt). In each case, increasing the level of gas in the sample phase lowers the pH of the thin electrolyte film, which is sensed directly by the pH glass or other pH-sensitive membrane electrode. A sensor for ammonia gas can be prepared by using an NH₄Cl solution as the inner electrolyte. Here, the conjugate acid, NH₄⁺, is held constant, and the equation for the output voltage of the probe is:

$$E_{\text{cell}} = K' - 0.059 \log P_{\text{NH}_3} \quad (19)$$

It should be noted that the response of these gas-sensing probes is also directly proportional to the dissolved concentration of the analyte gas in accordance with Henry's law: $P_{\text{gas}} = H \times [\text{gas}]$, where H is Henry's constant for the given gas at a given temperature.

The response time of these gas-sensing probes is generally on the order of 3 to 5 min at very low dissolved concentrations of the analyte gas ($<10^{-4}$ M), and approx. 1 min at higher levels ($>10^{-3}$ M). Further, selectivity over ions in the sample phase is excellent because such ions cannot pass through the outer gas-permeable membrane and influence the output voltage of the inner potentiometric measurement cell. One could therefore measure low levels of ammonium ions in the presence of very high levels of potassium and/or sodium by adjusting the pH of the sample phase to a value greater than 11, where all ammonium will be in the form of free ammonia gas, and then determining this dissolved gas level with the ammonia gas-sensing probe. However, selectivity of these sensors is by no means absolute. Other volatile gases or neutral organic acids or bases that can permeate the outer “gas”-permeable membrane can yield significant interference problems [44]. For example, using the conventional Severinghaus design, measurement of CO_2 in the presence of SO_2 would be nearly impossible, since SO_2 is a stronger acid, and its diffusion into the inner electrolyte would also decrease the pH of the film of bicarbonate filling solution within the CO_2 sensor. In the case of NH_3 gas sensors, volatile amines, such as methylamine and ethylamine, pose similar interference problems.

One can enhance the selectivity of potentiometric gas sensors by using a buffered inner filling solution, and using an inner ISE detector that responds with selectivity toward an ionic form of the gas. For example, instead of using an inner pH sensor, an alternate design for an ammonia-sensing probe would make use of a nonactin-based (see compound NH_4^+ -1 in Fig. 4) polymer membrane type ISE as

the inner transducer in conjunction with highly buffered (at pH 7.0 or so) inner filling solution. Ammonia diffusion through the outer gas permeable membrane will result in the formation of ammonium ions within the thin film that can be sensed by the inner electrode. Although amines can also diffuse into the film, the nonactin-based sensor exhibits high selectivity for ammonium over these protonated amines, and hence little or no interference will be observed [45]. The disadvantage of this concept, relative to the conventional Severinghaus design, is that the resulting device has only a very limited dynamic measurement range where Nernstian response is observed. At increasing gas levels, the pH of the inner buffer solution will be altered, and the fraction of analyte gas in the ionic form at equilibrium will decrease, thereby yielding a significant nonlinear emf response as a function of increasing the gas level in the sample. Sensors of this type have also been demonstrated for determination of SO_2 , CO_2 and NO_2 using inner sulfite/bisulfite, carbonate, and nitrate–nitrite selective polymer membrane type ISEs, respectively.

Another alternate potentiometric gas-sensing design, specifically developed to measure P_{CO_2} in whole blood samples within modern point-of-care biomedical instruments [46], relies on a novel differential measurement approach, using two identical membrane electrodes. Figure 7 illustrates this configuration. The two identical polymeric membranes are doped with a neutral proton carrier (e.g. tridodecylamine; see compound H^+ -1 in Fig. 4), rendering these membranes pH selective but also gas permeable (owing to their polymeric nature). The electrodes only differ with respect to the composition of their inner reference electrolyte solutions, one being strongly buffered with

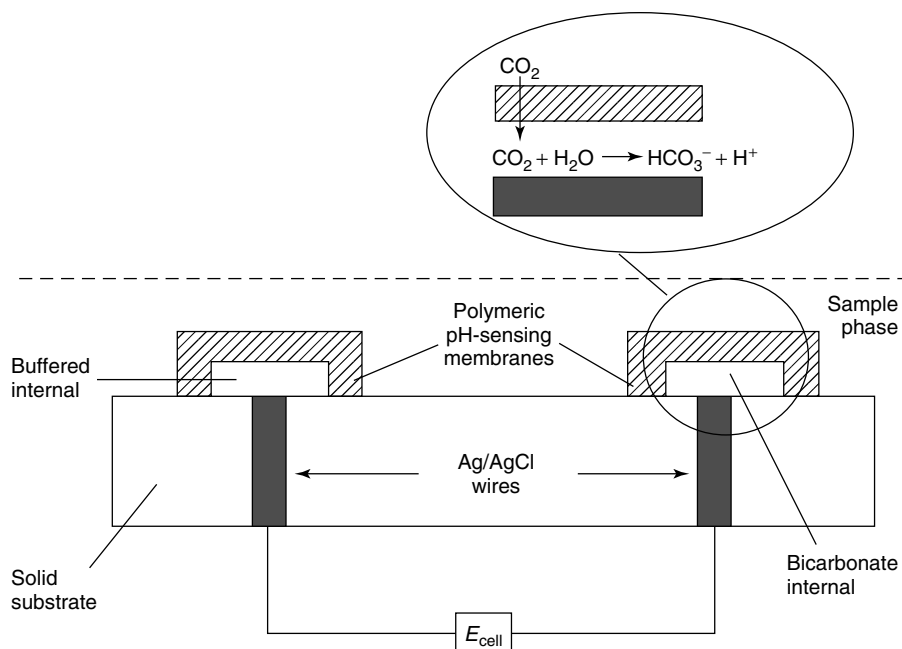


Fig. 7 Illustration of a differential sensor design for measuring carbon dioxide levels in biological fluids using two identical planar polymer membrane pH sensors with different internal solutions.

respect to pH, and the other composed of the typical $\text{NaHCO}_3/\text{NaCl}$ electrolyte employed as the inner filling solution within the conventional Severinghaus design. Measuring the cell voltage of the right electrode (without buffer) versus the left electrode (with buffer) will be insensitive to the pH of the sample, since the outer surfaces of both membranes will respond equally but in opposite directions to the proton activity in the sample phase (i.e. pH responses on the sample side of the membranes cancel each other). Carbon dioxide diffusion into the inner reference electrolyte of the left electrode does not change the pH of the buffer, but the equilibration of CO_2 within the right electrode alters the pH of the inner solution, yielding a change in the membrane potential. The net result is that such a differential design will yield

emf response to only P_{CO_2} in the sample via exactly the same expression as Eq. (18), except the voltage will become more negative rather than positive, with increasing CO_2 levels. In practice, as depicted in Fig. 7, these differential CO_2 sensors are constructed as thin layer films on inexpensive planar substrates (plastic, ceramic), creating essentially disposable chip type devices.

9.7

Ion-selective Electrode-based Biosensors

Beyond gas sensors, ISEs can also be utilized to devise novel biosensors, capable of detecting many important charged and neutral molecules in complex biological samples. The most widely studied and useful design for such biosensors is the

enzyme electrode [47], which couples the biological specificity of an enzyme catalyzed reaction with the inherent selectivity of the ISE to create a single probe capable of responding reversibly to biological molecules. Selectivity of the final analytical biosensor is controlled by the additive selectivities of these two components of the measurement system. Consequently, ionic interferences are often avoided by employing potentiometric gas-sensing probes as the underlying transducer for fabrication of such enzyme-based biosensors.

To fabricate an enzyme electrode, a given highly purified enzyme is immobilized either physically (entrapment behind semipermeable membrane) or chemically (e.g. crosslinked as a thin layer) at the surface of an appropriate ISE or gas sensor. For example, a sensor for urea can be prepared by immobilizing the enzyme urease at the surface of an ammonium ion-selective membrane electrode, prepared by incorporating the antibiotic nonactin (structure NH_4^+ -1 in Fig. 4) into a PVC or other polymeric membrane. Figure 8 illustrates such a device for measuring urea in whole blood samples. Urea (an analyte measured in blood to determine kidney function) diffuses from the blood sample into the thin layer of immobilized urease at the surface of the ion-sensing membrane. In this thin biocatalytic layer, the following reaction occurs: $\text{UREA} + \text{H}_2\text{O} \rightarrow 2\text{NH}_3 + \text{CO}_2$. At a physiological pH of 7.4, the vast majority of ammonia gas is in the form of protonated ammonium ions (NH_4^+) and CO_2 is in the form of bicarbonate ions (HCO_3^-). The ammonium ions generated within this layer can be detected potentiometrically by the polymeric membrane doped with nonactin. A steady state level of ammonium ions exists in this thin layer when the rate of ammonium ion generation from

the enzymatic reaction is equal to the rate that this product can diffuse away from the layer into the bulk of sample solution. An analogous urea sensor can be prepared using an ammonium selective glass membrane electrode as the transducer onto which the urease is immobilized. Using thin immobilized enzyme layers, response times for such devices can be 1 min or less at mM concentrations of urea.

Detection limits for enzyme-based potentiometric biosensors are governed by the innate detection limits of the membrane electrode toward the product of the enzyme reaction, as well as the kinetics of the enzymatic reaction (Michaelis-Menten constant and turnover number of the enzyme), and mass transfer rate of substrate into the enzymatic layer. Carr and Bowers developed in detail the theory of how such parameters affect the response curves of such sensors [48]. Generally, enzyme-based potentiometric biosensors respond to target substrates over the concentration range of 0.01 mM to 10 mM. In the case of the urea example mentioned earlier, limited selectivity of the nonactin-based ammonium membrane electrode over potassium ions ($K_{\text{NH}_4, \text{K}}^{\text{pot}} = 0.1$) influences not only the detection limits but the accuracy of urea measurements in samples containing significant levels of potassium. For measurement of blood urea levels, typically in the range of 3 to 10 mM, variations in background levels of potassium (normally 2 to 6 mM) can influence the emf value, and therefore reliable measurements can only be made by measuring K^+ levels separately with a K^+ -selective membrane electrode (usually based on valinomycin; see K^+ -1 in Fig. 4) and correcting the output voltage of the biosensor for these variations.

Another option for overcoming such ionic interferences is to immobilize the

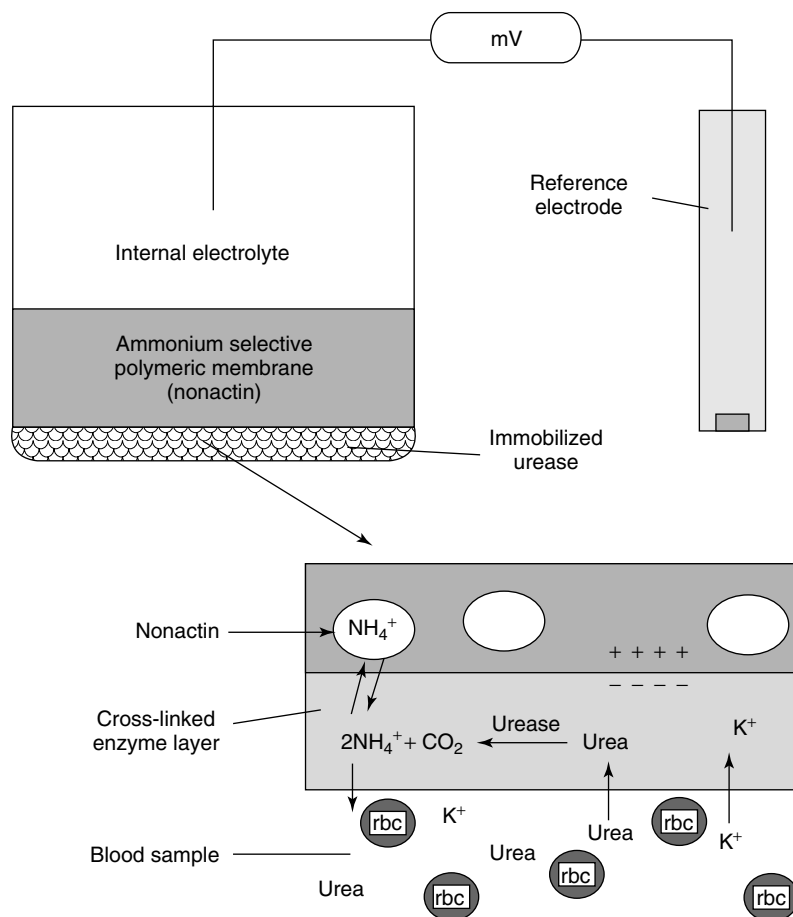


Fig. 8 Design of potentiometric urea sensor based on the immobilized enzyme urease on the surface of a polymer membrane type ammonium ISE.

enzyme at the surface of gas-sensing probes. For example, in the case of urea measurements, the problem of potassium interference can be eliminated completely by fabricating the biosensor with an ammonia gas sensor as the underlying transducer. Ammonia generated from urea diffusion into the enzyme layer, passes through the outer gas-permeable membrane of the gas sensor, increasing the pH of the thin film of inner NH_4Cl filling solution within such devices, which is detected by the inner glass electrode (if traditional

Severinghaus gas-sensor design is utilized). It should be noted that such devices will still function at physiological pH, even though the vast majority of total ammonia generated enzymatically under such conditions will be in the ammonium ion form. However, the 1% that is gas is still adequate to provide a significant response to the substrate in the 0.1- to 10-mM range. Biosensors based on decarboxylating enzymes that liberate carbon dioxide immobilized on CO_2 gas-sensing probes can be devised in analogous manner.

Tab. 5 Examples of some bioanalytically useful potentiometric enzyme-based biosensors that can be prepared for monitoring important biomolecules using appropriate immobilized enzymes and ISE or gas sensing detectors

Analyte	Enzyme	Reaction	ISE detectors
Urea	Urease	$\text{Urea} \longrightarrow 2\text{NH}_3 + \text{CO}_2$	NH_4^+ -glass or polymer NH_3 -gas sensor H^+ -glass or polymer
Creatinine	Creatininase	$\text{Creatinine} \longrightarrow \text{N-methylhydantoin} + \text{NH}_3$	NH_4^+ -glass or polymer NH_3 -gas sensor
L or D-amino acids	L or D amino acid oxidase	$\text{L (D) AA} \longrightarrow \text{RCOOH} + \text{NH}_3 + \text{H}_2\text{O}_2$	NH_4^+ -glass or polymer NH_3 -gas sensor
L-glutamine	Glutaminase	$\text{L-glutamine} \longrightarrow \text{glutamic acid} + \text{NH}_3$	NH_4^+ -glass or polymer NH_3 -gas sensor
Adenosine	Adenosine deaminase	$\text{Adenosine} \longrightarrow \text{inosine} + \text{NH}_3$	NH_4^+ -glass or polymer NH_3 -gas sensor
L-glutamate	Glutamate decarboxylase	$\text{L-glutamate} \longrightarrow \text{GABA} + \text{CO}_2$	CO_2 -gas sensor
Amygdalin	β -Glucosidase	$\text{amygdalin} \longrightarrow \text{HCN} + 2\text{C}_6\text{H}_{12}\text{O}_6 + \text{benzaldehyde}$	CN^- -solid-state
Glucose	Glucose oxidase	$\text{glucose} + \text{O}_2 \longrightarrow \text{gluconic acid} + \text{H}_2\text{O}_2$	H^+ -glass or polymer
Penicillin	Penicillinase	$\text{Penicillin} \longrightarrow \text{penicilloic acid}$	H^+ -glass or polymer

Many potentiometric enzyme electrodes for widely different analyte species can be prepared merely by choosing the appropriate ISE transducer and immobilized enzymatic reagent. Table 5 summarizes the enzymes and ISEs/gas sensors used to construct biosensors for a number of important biomolecules, ranging from urea and creatinine to amino acids, nucleotides, and even glucose and penicillin. In the

latter two cases, the relevant enzymes catalyze a reaction that generates acid products, resulting in pH changes within the thin film of immobilized biocatalyst. Hence, simple glass or polymeric membrane pH electrodes can be employed as transducers for such devices. However, detection of pH changes requires that the samples being analyzed possess the same level of buffering capacity

as the standards used to calibrate such sensors. Thus, practical application of the pH electrode-based biosensors normally mandates dilution of the sample with a defined buffer reagent before accurate measurements can be made.

In practice, potentiometric biosensors are used just like any other membrane electrodes or gas-sensing probe. Calibration plots are prepared using known standards of the biomolecule analytes (usually prepared in a given buffer), and exposing the sensors to these solutions until a steady state emf value can be recorded (usually in 1 to 2 minutes). Plots of emf versus log [substrate] are prepared and used to obtain concentration data for unknown samples (either diluted in buffer or nondiluted) that are exposed to the same sensor under exactly the same measurement conditions.

References

1. D. Ammann *Ion-Selective Microelectrodes*, Springer, Berlin, 1986.
2. M. A. Pineros, J. E. Shaff, L. V. Kochian, *Plant Physiol.* **1998**, 116, 1393.
3. B. R. Horrocks, M. V. Mirkin, D. T. Pierce et al., *Anal. Chem.* **1993**, 65, 1213.
4. W. E. Morf, *The Principles of Ion-Selective Electrodes and of Membrane Transport*, Elsevier, New York, 1981.
5. E. Lindner, V. V. Cosofret, R. P. Buck et al., *Electroanalysis* **1995**, 7, 864.
6. D. P. Brezinski, *Analyst* **1983**, 108, 425.
7. R. E. Dohner, W. E. Morf, W. Simon et al., *Anal. Chem.* **1986**, 58, 2585.
8. U. Schefer, D. Ammann, E. Pretsch et al., *Anal. Chem.* **1986**, 58, 2282.
9. G. G. Guilbault, R. A. Durst, M. S. Frant et al., *Pure Appl. Chem.* **1976**, 48, 127.
10. E. Bakker, R. K. Meruva, E. Pretsch et al., *Anal. Chem.* **1994**, 66, 3021.
11. W. E. Morf, W. Simon in *Ion-Selective Electrodes in Analytical Chemistry* (Ed.: H. Freiser), Plenum Press, New York, 1978.
12. M. Nägele, E. Bakker, E. Pretsch, *Anal. Chem.* **1999**, 71, 1041.
13. M. Cremer, *Z. Biol. (Munich)* **1906**, 47, 562.
14. G. Eisenman, (Ed.), *Glass Electrode for Hydrogen and Other Cations*, Marcel Dekker, New York, 1967.
15. P. Bühlmann, E. Pretsch, E. Bakker, *Chem. Rev.* **1998**, 98, 1593.
16. M. E. Meyerhoff, *Trends Anal. Chem.* **1993**, 12, 257.
17. C. Huang, Y. C. Jean, K. L. Cheng, F. C. Chang, *J. Electrochem. Soc.* **1995**, 142, L175.
18. A. E. Owen, *J. Non-Cryst. Solids* **1980**, 35, 36, 999.
19. U. Oesch, D. Ammann, Z. Brzózka et al., *Anal. Chem.* **1986**, 58, 2285.
20. S. A. M. Marzouk, S. Ufer, R. P. Buck et al., *Anal. Chem.* **1998**, 70, 5054.
21. E. Pungor, K. Toth, *Analyst* **1970**, 95, 625.
22. E. Pungor, K. Toth, *Pure Appl. Chem.* **1973**, 34, 105.
23. W. E. Morf, G. Kahr, W. Simon, *Anal. Chem.* **1974**, 46, 1538.
24. A. Hulanicki, T. Sokalski, A. Lewenstam, *Mikrochim. Acta* **1988**, 111, 119.
25. M. L. Hitchman, A. Aziz, D. D. H. Chingakule et al., *Anal. Chim. Acta* **1985**, 171, 141.
26. M. S. Frant, J. W. Ross, *Science* **1966**, 154, 1553.
27. E. Bakker, P. Bühlmann, E. Pretsch, *Electroanalysis* **1999**, 11, 915.
28. M. S. Frant, *Analyst* **1994**, 119, 2293.
29. V. V. Cosofret, R. P. Buck, *Pharmaceutical Applications of Membrane Sensors*, CRC Press, Boca Raton, 1992.
30. V. V. Cosofret, R. P. Buck, *Crit. Rev. Anal. Chem.* **1993**, 24, 1.
31. M. E. Meyerhoff, B. Fu, E. Bakker et al., *Anal. Chem.* **1996**, 68, 168A.
32. M. Maj-Zurawska, T. Sokalski, A. Hulanicki, *Talanta* **1988**, 35, 281.
33. E. Pretsch, M. Badertscher, M. Welte et al., *Pure Appl. Chem.* **1988**, 60, 567.
34. O. Dinten, U. E. Spichiger, N. Chaniotakis et al., *Anal. Chem.* **1991**, 63, 596.
35. E. J. R. Sudholter, P. D. Vanderwal, M. Skowronskaptasinska et al., *Anal. Chim. Acta* **1990**, 230, 59.
36. R. Eugster, T. Rosatzin, B. Rusterholz et al., *Anal. Chim. Acta* **1994**, 289, 1.
37. R. Eugster, P. M. Gehrig, W. E. Morf et al., *Anal. Chem.* **1991**, 63, 2285.
38. D. Ammann, *Ion-Selective Microelectrodes*, Springer, Berlin, 1986.
39. J. W. Ross, *Science* **1967**, 156, 1378.

40. U. Schaller, E. Bakker, U. E. Spichiger et al., *Anal. Chem.* **1994**, 66, 391.
41. S. Amemiya, P. Bühlmann, Y. Umezawa, *Anal. Chem.* **1998**, 70, 445.
42. J. W. Ross, J. H. Riseman, J. A. Krueger, *Pure Appl. Chem.* **1973**, 35, 473.
43. W. Severinghaus, A. F. Bradley, *J. Appl. Physiol.* **1958**, 13, 515.
44. R. K. Kobos, S. J. Parks, M. E. Meyerhoff, *Anal. Chem.* **1982**, 54, 1976.
45. Y. M. Fraticelli, M. E. Meyerhoff, *Anal. Chem.* **1981**, 53, 1857.
46. M. E. Meyerhoff, *Clin. Chem.* **1990**, 36, 1567.
47. G. G. Guilbault, *Analytical Uses of Immobilized Enzymes*, Marcel Dekker, New York, 1984.
48. P. Carr, L. D. Bowers, *Immobilized Enzymes in Analytical and Clinical Chemistry: Fundamentals and Applications*, Wiley & Sons, New York, 1980.

10 Electrochemistry in Bioanalysis

Susan R. Mikkelsen
University of Waterloo, Waterloo, Canada

10.1	Introduction	311
10.1.1	Bioanalysis	311
10.1.2	Electroanalytical Methods	311
10.2	Potentiometric Methods	312
10.2.1	Introduction	312
10.2.2	Zero-Current Potentiometry	313
10.2.2.1	ISEs in Bioanalysis	314
10.2.2.2	Enzymes, Antibodies, and Nucleic Acids with Zero-Current Potentiometry	315
10.2.3	Dynamic Potentiometry	316
10.2.4	Emerging Technology	317
10.2.5	Commercialization of Potentiometric Devices	318
10.3	Amperometric Methods	320
10.3.1	Introduction	320
10.3.2	Direct Amperometric Methods	321
10.3.3	Amperometric Measurements with Enzymes	323
10.3.4	Amperometric Immunoassays and Immunosensors	327
10.3.5	Amperometric Nucleic Acid Assays and Sensors	329
10.3.6	Emerging Technology	330
10.3.7	Commercialization of Amperometric Devices	330
10.4	Impedimetric Methods	332
10.4.1	Introduction	332
10.4.2	Impedimetric Assays and Sensors	333
10.4.3	Commercially Available Instruments for Impedance Measurements	334

10.5	Future Directions and Perspectives	334
	Acknowledgment	335
	References	335

10.1 Introduction

10.1.1 Bioanalysis

The American Association of Bioanalysts considers the field of bioanalysis to include qualitative and quantitative analytical methods in bacteriology (including mycobacteriology), mycology, parasitology, virology, immunology, haematology (including flow cytometry), chemistry (including urinalysis), endocrinology, toxicology, andrology, embryology, and clinical molecular biology. As diverse as these areas evidently are, they have at least one factor in common: analytes are always present in a complex biological matrix. Thus, special demands are placed on the selectivity of a method (i.e. its ability to discriminate analyte from possible interfering species), if the method is to be useful in practice. The electroanalytical methods detailed below achieve the required selectivity through the measurement method (see also Volume 3), through electrode surface modification (see also Volume 10), or by the addition of selective chemical or biochemical reagents to the assay mixture.

This chapter surveys applications of electroanalytical methods to practical

problems in bioanalysis and considers the state of commercialization of traditional and promising new methods and instrumentation. Every effort has been made to cite recent review articles, so that readers may readily find more detailed information. The subsections are organized according to the instrumental method; hopefully, the diversity of applications will stimulate further innovations in methodology and instrumentation for bioanalysis.

10.1.2 Electroanalytical Methods

Three broad classifications of electrochemical methods are used in this chapter. Potentiometric methods include zero-current potentiometry and methods in which current of controlled magnitude is applied to the working electrode, such as in potentiometric stripping analysis (PSA). Amperometric methods consider all techniques in which current is measured; these include constant-potential amperometry and amperometric measurements made in response to a variety of applied potential waveforms in voltammetric methods. Impedimetric methods comprise a final classification; in these methods, faradaic currents are generally absent, and impedance, conductance, or capacitance is the measured property.

Descriptions of the underlying principles and practical examples of these methods may be found in many textbooks. Excellent textbooks include the widely cited *Electrochemical Methods: Fundamentals and Applications* [1], and *Laboratory Techniques in Electroanalytical Chemistry* [2]. The novice may find the Analytical Chemistry by Open Learning series [3–5] and the primer *Electroanalysis* [6] particularly useful. More specialized texts that focus on bioanalytical electrochemistry [7–11] and biosensors [12, 13] are also available.

Volume 3 of this series may be consulted for a survey of electrochemical instrumentation and electroanalytical chemistry. In addition, several chapters in this volume contain detailed information on methods of importance to bioanalysis. In particular, Chapter 17 (mediated electron transfer), Chapter 7 (electrochemistry of nitric oxide), Chapter 12 (electrochemistry of nucleic acids), Chapter 13 (enzyme electrodes), Chapter 14 (*in vivo* electrochemistry), Chapter 5 (electrochemical immunoassays), Chapter 2 (single cell electrochemistry), and Chapter 9 (ion-selective electrodes) provide more details on the fundamental processes underlying the applications to bioanalysis that are described in this chapter.

10.2

Potentiometric Methods

10.2.1

Introduction

Potentiometry may be conducted at zero applied current or at controlled nonzero current values; in both cases, electrochemical potential is measured and related to analyte concentration. Under

ideal conditions, a metallic indicator electrode in contact with a solution containing its cation will have a potential described by the Nernst equation (Eq. 1):

$$E_{\text{cell}} = E - E_{\text{ref}} \\ = E^0 + \left(\frac{RT}{nF} \right) \times \ln[M^{n+}] - E_{\text{ref}}, \quad (1)$$

where E_{cell} is the measured cell potential, E is the indicator electrode potential, E_{ref} is the potential of the reference electrode, E^0 is the standard potential and R , T , n , and F have their usual meanings. If no current is applied to the cell, and if no chemical reaction involving M^{n+} occurs at the electrode surface, $[M^{n+}]$ represents the metal ion concentration in the bulk of the solution. When the experiment generates a different concentration of metal ion at the surface of the working electrode, either by current flow or by chemical reaction, $[M^{n+}]$ represents the metal ion concentration (actually an activity) at the electrode surface.

This general expression has been elaborated to describe the response of ion-selective electrodes (ISEs) in which an activity gradient exists for an ion, a , across a membrane that separates an external from an internal reference electrode:

$$E_{\text{cell}} = \text{constant} + \left(\frac{RT}{zF} \right) \\ \times \ln(A_{a,\text{external}}/A_{a,\text{internal}}), \quad (2)$$

where $A_{a,\text{external}}$ and $A_{a,\text{internal}}$ represent the activities of ion a in the external (sample) and internal (reference) solutions, respectively, and constant includes the difference in potentials of the two reference electrodes and their liquid junction potentials. In practice, activity coefficients are assumed equal in the external and

internal solutions and concentrations are substituted for activities.

When the electrode is selective for but not specific to the ion of interest (the principal ion), the Nicolsky–Eisenman equation applies (Eq. 3):

$$E = \text{constant} + \left(\frac{RT}{z_i F} \right) \times \ln \left(a_i + \sum K_{ij} a_j^{z_i/z_j} \right), \quad (3)$$

where E is the measured potential, R , T , and F have their usual meanings, z_i and z_j are the charges on the analyte and interfering ions, respectively, a_i and a_j are the activities of the analyte and interfering ions, respectively, and K_{ij} is the potentiometric selectivity coefficient [14]. This empirical equation is now known to be inaccurate when two ions of different charge

contribute significantly to the measured potential [15], and detailed procedures to overcome this problem have been suggested [16].

10.2.2

Zero-Current Potentiometry

Nonselective, metallic indicator electrodes have been used for potentiometric measurements in complex biological media, for example, Pt electrodes have been used to monitor the redox potential of fermentation broths as cultures grow [17]. However, zero-current potentiometry more often involves ISEs based on solid membranes, composed of a sparingly soluble salt of the ion of interest or liquid membranes, in which an ion-selective reagent is dissolved, with the membrane separating reference

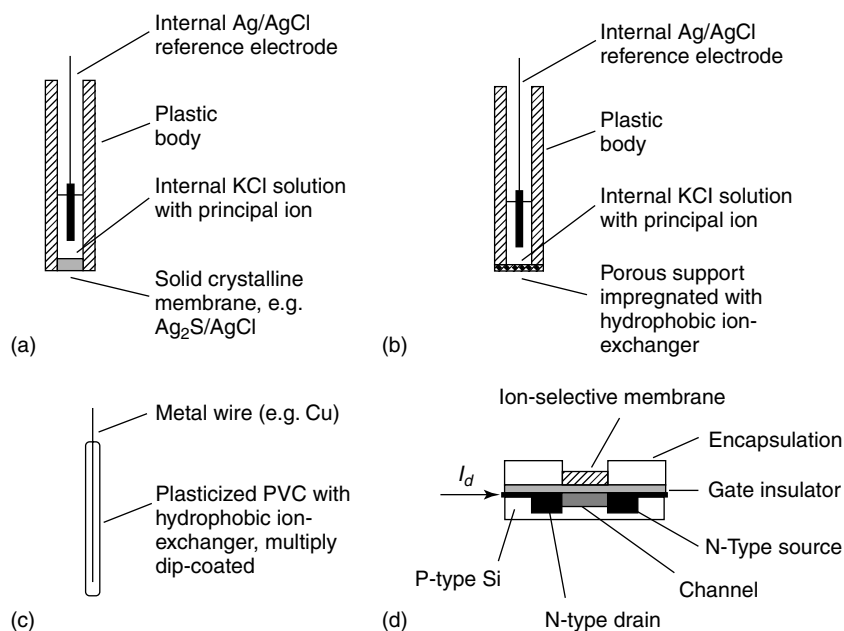


Fig. 1 ISEs: (a) The solid membrane; (b) liquid membrane; (c) coated-wire electrode; (d) field-effect transistor. The analyte solution is in contact with the ion-selective layers; potentials for A–C are measured using an external reference electrode, while the drain current, I_d , is monitored using a current-to-voltage converter in D.

from the analyte solutions; more recently, solid-state devices have been introduced that are based on coated metallic conductors or field-effect transistors (FETs). Examples of these potentiometric electrodes are shown in Fig. 1. An excellent introduction to the principles of their operation is given by Cunningham [13].

10.2.2.1 ISEs in Bioanalysis

Well-established potentiometric devices used in bioanalysis are based on macroscopic electrodes that use gas-permeable polymer, solid or liquid membranes selective to CO_2 , NH_3 , pH, or various alkali, alkaline earth, or halide ions [7]. The membranes separate the external analyte solution from the inner reference solution, and these electrodes are used in conjunction with an integral or external reference electrode. The selectivities of these membranes can be excellent, for example, the main interferent in the fluoride ISE that uses a solid $\text{LaF}_3/\text{EuF}_2$ membrane is hydroxide, with a $K_{\text{F}/\text{OH}}$ value of 0.1; thus, over the pH range 0–8.5, the electrode responds in a Nernstian fashion to fluoride concentrations above 10^{-6} M [9]. Solid Ag_2S membranes doped with AgX , where X is Cl^- , Br^- , I^- , CN^- , or SCN^- , are used for the determination of these anions.

The oldest clinical applications of potentiometry involved blood gas analysis, and this method is still used to quantify dissolved carbon dioxide: a glass pH electrode is housed behind a membrane permeable to CO_2 , and a thin solution layer of hydrogen carbonate separates the pH electrode from the membrane. This device, called the *Stow-Severinghaus electrode*, remains unchanged in principle from its original version reported in 1958 [18]. The measurement is based on the hydrolysis of CO_2 to HCO_3^- and H^+ in the thin solution

layer, and the measured local pH indicates the bulk pCO_2 values. The ammonia gas-sensing electrode is based upon similar measurement principles: ammonium ion formation causes a local decrease in pH in the intermembrane space; although ammonia itself is not clinically relevant, the ammonia gas-sensing electrode has been incorporated into enzyme-based sensors for other, clinically important analytes such as urea and creatinine [19].

ISEs for Li^+ , K^+ , Ca^{2+} , and Mg^{2+} have been developed on the basis of liquid membranes that contain ionophores: these are hydrophobic chelating agents that contain selective binding sites for the ion of interest. While the structures of ionophores used in commercially available devices are often proprietary, examples of well-studied ISE ionophores include 14-crown-4 ether for Li^+ [20] and valinomycin for K^+ [21]. Valinomycin is 5000 times more selective toward K^+ over Na^+ and 18 000 times more selective toward K^+ over H^+ .

Efforts to produce a phosphate-selective ISE have been hindered by its diverse speciation and lability in biological samples; a recent review describes various potentiometric and amperometric approaches to this problem [22]. Of the potentiometric approaches, selectivity is most often achieved using inorganic or organometallic extracting agents such as organotin compounds in liquid-membrane ISEs, cobalt complexes or metallic cobalt in coated-wire and metallic electrodes, respectively. Nickel phosphate, silver phosphate, and mixtures of lead precipitates have also been used in phosphate ISEs. All of these sensors suffer from limited selectivity. Enzyme-based sensors for phosphate have also been a topic of research; as yet, however, no commercial phosphate sensor exists [22].

The difference between free and total concentrations of ions can be significant in biological samples and is particularly important for calcium and magnesium [23]. ISEs are known to respond to free ion activity (Eq. 3), but it has recently been shown that direct potentiometric measurements can lead to total ionic concentrations of calcium if the composition of the inner solution induces a strong zero-current flux of the primary ion toward the inner compartment [24].

10.2.2.2 Enzymes, Antibodies, and Nucleic Acids with Zero-Current Potentiometry

Potentiometric electrodes have been used as transducers in biosensors in which a thin layer containing enzymes, antibodies, or whole cells separates the electrode surface from the analyte solution and provides selective recognition properties. Thin layers containing enzymes or cells catalyze reactions that cause the localized production or consumption of the species to which the electrode responds. Antibodies, incorporated into immunosensors, have been shown to cause small but measurable signals upon antigen binding, but usually require a label (such as an enzyme) that allows catalysis of a reaction that can be followed potentiometrically [13].

Potentiometric enzyme electrodes have been demonstrated for many clinically important analytes, including glucose, urea, creatinine, amino acids, uric acid, oxalate, and penicillin. Urea sensors, for example, have been developed that use immobilized urease to produce HCO_3^- and NH_4^+ , and this reaction has been detected using pCO_2 and pNH_3 gas-sensing electrodes, glass pH electrodes, glass- or liquid-membrane ammonium ISEs, and ion-selective FETs. Chapter 4 of Volume 6 concerns the grafting of molecular properties onto semiconductor surfaces. Reviews of

enzyme-based potentiometric biosensors are available [25–29], and detection limits for substrate are generally of the order of 10^{-5} M. Further examples include a glutamate sensor based on glutamate decarboxylase and a CO_2 gas-sensing electrode [30], a urea sensor using urease and a liquid-membrane ISE for ammonium ion that contains the ionophore nonactin [31], a disposable urea sensor based on urease and an ammonium-sensitive polymer matrix [32], an organophosphate sensor using a hydrolase enzyme in conjunction with a pH electrode [33], a lysine sensor using lysine oxidase and a solid-state ammonium electrode [34], a glucose-sensitive enzyme-modified FET coated with Nafion and applied to serum determinations [35], a cyanide sensor with a detection limit of 10^{-10} M based on enzyme inhibition at a peroxidase-modified FET coated with poly(4-vinylpyridine-co-styrene) [36]. Applications of enzyme-based potentiometric biosensors in flow injection analysis have revealed only millimolar detection limits for urea and penicillin [37]. Intact, viable cells of the *Hansenula polymorpha* (a source of alcohol oxidase) and *Gluconobacter oxidans* (containing a xylose dehydrogenase) were immobilized on pH-sensitive FETs in sensors for formaldehyde [38] and xylose [39], respectively.

Binding between antibodies or antigens, with one partner immobilized on a membrane, has been monitored potentiometrically; this kind of “direct” immunosensor was originally proposed by Janata and demonstrated by the binding of mannan to concanavalin A, a lectin [40]. Aizawa’s group showed potentiometric responses to antigen–antibody interactions on membranes [41, 42]. Baumann’s group has shown that solid-state coated-wire electrodes made of titanium or graphite can also be used to detect immunological

binding reactions directly [43, 44]. More recently, a chloride ISE based on Ag_2S has been modified with antibody to thyroid-stimulating hormone (TSH) in a nonlabeled immunosensor for TSH [45]. In all of these sensors, the change in potential that occurs with analyte concentration is small but reproducible. This topic has been reviewed by Bergveld [46].

Enzymes are commonly used as labels in potentiometric immunosensors to improve the detectability of the antibody–antigen interaction. The enzyme label is bound either to the analyte species and used as a reagent in a competitive immunoassay scheme, or to a second antibody, used to label antigen (analyte) that binds to a primary antibody immobilized on the transducer surface. Antibody-modified Langmuir-Blodgett films [47] and ion-selective polyvinylchloride (PVC) films [48] have been suggested for potentiometric immunosensor design. Urease [48–50], glucose oxidase [50], β -lactamase [51], and peroxidase [52] have been used as labels in immunosensors for model analytes such as human and rabbit IgG, antihuman IgG, *Salmonella typhimurium*., and α -2-interferon.

FETs have also been directly coupled to biological processes, in so-called BioFETs, to record electrical signals from surface-adherent mammalian hippocampal neurons on an array of 16 micro-FETs [53] and to monitor the response of intact insect antennae to the plant odor component, Z-3-hexen-1-ol [54].

Total DNA has been quantitated using a silicon light-addressable potentiometric sensor (LAPS) modified with a biotinylated nitrocellulose membrane to capture DNA labeled with streptavidin (through a DNA-binding protein) and urease (through

an anti-DNA antibody) [55]. Sequence-selective detection of polymerase chain reaction products has been carried out in a similar manner [56], and in both cases, the pH change due to reaction of the urease label is the measured signal.

10.2.3

Dynamic Potentiometry

PSA has been introduced as a method for the detection of trace metals and nucleic acid sequences in biological samples, and specialized instrumentation for PSA is commercially available (Radiometer). The method is based on monitoring potential changes at an electrode to which (a) constant current is applied [57] or (b) a chemical oxidant is introduced [58]; these have been described in more detail in a monograph [59]. Both methods have recently been applied to the determination of copper, zinc, and selenium in human plasma and urine, using a mercury film working electrode [60]; chemical stripping was effective for copper and zinc quantitation, using mercuric ions as the oxidant in both cases, whereas constant-current oxidation was used for the determination of selenium *via* oxidation to hydrogen selenide. Cadmium and lead have also been determined in blood using PSA [61]. Disposable, screen-printed electrodes for lead quantitation by PSA have been reported [62], and a model immunosensor has been proposed that uses screen-printed electrodes and PSA detection for monitoring the interaction of human serum albumin (HSA) with the HSA antibody, using Bi^{3+} as a marker ion [63].

PSA was introduced as a bioanalytical method for nucleic acid analysis by Wang [64], who showed that transition metal complexes that are reversibly bound

to an electrode-immobilized double-stranded (ds) DNA layer can be stripped by the application of a constant reducing current to the electrode surface. Peaks in the chronopotentiograms corresponding to the maximum differential potential change that occurs as the complexes are reduced can be correlated, by height or area, with the quantity of dsDNA on the electrode surface. A variety of carbon-based electrode materials, including carbon paste and screen-printed graphite inks for disposable sensors, were examined using an adsorptive DNA immobilization procedure. Peptide nucleic acids have been used instead of native sugar-phosphate backbone DNA to aid the detection of point mutations [65–67], and applications have included the detection of the human immunodeficiency virus and the point mutation in the p53 gene associated with cancer [68, 69].

Recently, Mascini's group has also used this method, in combination with disposable graphite screen-printed electrodes, initially for model DNA sequence detection [70] and more recently for the quantitation of human apolipoprotein E genotypes [71]; in both cases, daunomycin was used as an indicator species. Daunomycin is a DNA intercalant bearing both quinone and hydroquinone functionalities, and Mascini's group used constant-current oxidation of the hydroquinone moiety for detection. Their detection limit of $1 \mu\text{g mL}^{-1}$ target DNA resulted in the need for PCR amplification prior to DNA detection.

10.2.4

Emerging Technology

A fundamental breakthrough, first reported in 1992, has occurred in the measurement of polyions by potentiometry [72]. In principle (Eqs. 2 and 3),

the determination of analytes possessing high charge would be expected to proceed with extremely poor sensitivity, as the calibration slope RT/zF is inversely related to analyte ion charge. However, it has recently been shown that much more sensitive devices for heparin, a polyanion, and protamine, a polycation, can be constructed using PVC membranes doped with tridodecylmethyl-ammonium chloride, an anion exchanger, or dinonylnaphthalene sulfonate, a cation exchanger [73–75]. The selectivity and sensitivity of these membranes is truly remarkable: a potential difference of -50 mV was observed upon changing the porcine heparin ($z = -70$) concentration from 0.04 to $0.4 \mu\text{M}$, and even greater sensitivity was observed toward beef lung heparin, which possesses higher charge density, although Eq. (1) predicts a potential change of less than 1 mV with a tenfold concentration change of species possessing such high charge. The sensitivity and selectivity of these devices are believed to result from a nonequilibrium extraction process that leads to tight ion pairs with the exchanger in the PVC membrane, causing charge separation at the sample-membrane interface. Applications of polyion-selective electrodes to enzymatic assays (involving proteases and their inhibitors) and model immunoassays (involving the avidin-biotin reaction) have been reviewed [76].

Further recent advances in potentiometric bioanalysis include the invention of self-plasticizing ion-selective membranes, in which the ionophores are covalently immobilized and no leachable plasticizer is incorporated into the photocurable membranes; near-Nernstian responses were observed for potassium, sodium, calcium, and pH sensors constructed using commercially available ionophores [77].

Microfabrication [78], and now nanofabrication [79], of ISEs and FETs promises to enable multianalyte assays in continuous-readout implantable devices or for in vitro testing with immunosensor arrays.

10.2.5

Commercialization of Potentiometric Devices

Microfabrication has been the topic of a recent review in which thin-film ($<1\ \mu\text{m}$, based on vacuum evaporation, sputtering or chemical vapor deposition) and thick-film ($>10\ \mu\text{m}$, based on screen printing or lamination) technologies are described for the mass production of potentiometric sensors and sensor arrays [80]. Current challenges include the cost of fabrication, especially for thin-film devices, the control of physical dimensions of the sensing elements, the incorporation of liquid reservoirs, and the stability of the integrated reference electrodes.

Many ISEs based on solid or liquid membranes and ion-selective FETs possess sufficiently small K_{ij} values (Eq. 1) toward common interferents, and have been developed into commercial benchtop analyzers that allow the measurement of Na^+ , K^+ , Ca^{2+} , Cl^- , HCO_3^- , and other ions, in instruments that are designed solely for ISE measurements or in combination with other integrated devices (such as amperometric sensors and spectrophotometers) to measure other parameters [7]. Applications of these devices to blood gas analysis have been reviewed recently [81]. Companies that produce this instrumentation for clinical chemistry applications include Abbott Diagnostics, AVL, Bayer Diagnostics, Beckman Coulter, Nova Biomedical, Ortho-Clinical Diagnostics, Boehringer-Mannheim/Roche, and Radiometer [82]. Many instruments allow measurements to

be made directly on serum or whole blood, as these matrices possess relatively constant ionic strength (activity coefficients vary with ionic strength and temperature); urine samples are generally diluted with ionic strength buffer. Matrix effects have been a concern for ISEs that are used for whole blood assays, and the need for protein-containing quality control materials has been the topic of one recent review [83].

Clinical interest in Mg^{2+} has increased recently, with the commercialization of Mg^{2+} ISEs based on neutral carrier ionophores for benchtop clinical electrolyte instruments such as AVL and Nova [84]. Magnesium is important for neuronal activity, cardiac excitability, muscular contraction, and blood pressure, among other physiological roles; it exists bound to proteins or to small anions and as free Mg^{2+} , but has traditionally been measured as total Mg. The recent availability of ISEs combined with the known decrease in dietary magnesium intake in the western world has stimulated clinical research that may have important implications in cardiac care [85] and diabetes [86], as it is now known that “ionized Mg” (free Mg^{2+}) levels can vary, whereas total Mg remains constant.

Significant recent advances in microfluidics and sensor miniaturization have resulted in a new class of portable, point-of-care blood chemistry analyzer. The i-STAT Portable Clinical Analyzer is perhaps the most developed of these devices. Figure 2 shows a diagram of the i-STAT disposable cassette that contains thin-film potentiometric ISEs for sodium, potassium, chloride, ionized calcium, pH, pCO_2 , and urea (via urease and an ammonium ISE) in addition to amperometric sensors (discussed in Sect. 10.3) for oxygen and glucose (via glucose oxidase with hydrogen peroxide

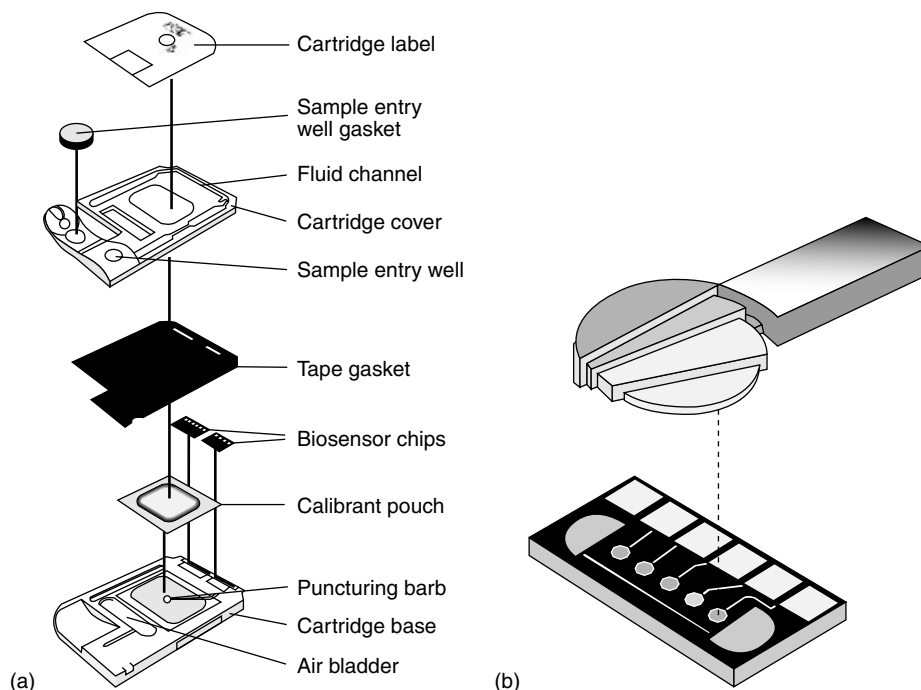


Fig. 2 Exploded view of an i-STAT Cassette (a) and the incorporated biosensor chips (b). Blood samples are introduced through the sample entry well gasket and flow through the fluid channel, where they pass over the sensing elements of the biosensor chips. These elements measure sodium, potassium, chloride, ionized calcium, pH, and $p\text{CO}_2$ using ISEs.

Enzyme-containing elements measure urea, which is hydrolyzed to ammonium ions that are measured potentiometrically, and glucose, which is measured amperometrically via enzymatic production of hydrogen peroxide. The $p\text{O}_2$ is measured amperometrically and hematocrit is determined conductometrically. (Reproduced from company literature.)

detection) and a conductometric sensor for hematocrit (see Sect. 10.4); once filled with whole blood, the cassette is connected to a hand-held, battery-operated unit containing measurement electronics, a liquid-crystal display (LCD) and, if desired, a small, detachable printer. This device has been tested for use in critical and neonatal care and in hemodialysis units with excellent results [87–89].

The LAPS represents another major advance in commercially available potentiometric bioanalysis [90]. In this device, a pH-sensitive silicon nitride insulator functions as a phototransistor gate.

Changes in pH at the gate-solution interface cause titration of surface hydroxyl and amino functions, causing a change in gate potential. Cellular metabolism causes acidification of the surrounding medium, and this device, commercialized as the Cytosensor Microphysiometer (Molecular Devices), has been used to monitor cellular metabolism via pH change under a variety of stressing situations. The Cytosensor, shown schematically in Fig. 3, has been used for the determination of compound toxicities [91], the study of recombinant adrenoceptor subtypes [92], and has been suggested for the determination of

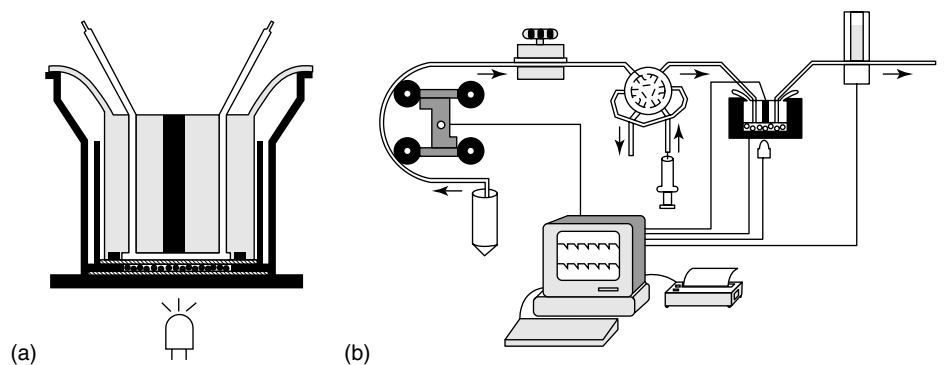


Fig. 3 The Cytosensor Microphysiometer. (a) Flow chamber containing cells retained in a disk-shaped region between two microporous polycarbonate membranes; the top of the sensing surface contacts the lower membrane and is illuminated by an LED; culture medium flows across the outer surface of the upper

membrane. (b) Instrumentation electronics control illumination and data acquisition, and the periodic flow of culture medium; a complete device contains eight flow chambers managed by one computer. (Reproduced from company literature.)

antibiotic susceptibilities [93]. A different LAPS device, also based on pH measurement, has been used in an immunosensor for the detection of pathogenic bacteria; in this device, antibodies are used to selectively detect *E. coli* O157 : H7 and to capture the organisms on a membrane; detection occurs via a urease label that causes acidification of the solution during reaction with urea [94].

10.3

Amperometric Methods

10.3.1

Introduction

Amperometric methods include all those in which current is the measured parameter. Arguably, the simplest of these methods uses the fuel cell in which no potential is applied: current is generated in response to a thermodynamically favorable overall cell reaction that involves two electrodes in a solution; although uncommon as an analytical method, the fuel cell approach

has been applied to the determination of biomass during cell cultivation for a variety of organisms, and detection limits below 10^5 cells mL^{-1} have been reported for *P. aeruginosa*, *F. arbuscens*, and *E. coli* [95, 96].

The most established amperometric methods for bioanalysis involve constant-potential amperometry, in which mass-transport-controlled oxidation or reduction is used to quantitate the product (or substrate) of an enzymatic reaction. For rapid (reversible) electrochemical reactions, Eq. (4) describes the current obtained at a planar working electrode:

$$i = \frac{(nFADC)}{\delta}, \quad (4)$$

where i is the limiting current, measured at a potential where all analyte is oxidized or reduced, n and F have their usual meanings, D is the diffusion coefficient of the electroactive species, C is its bulk solution concentration, and δ is the thickness of the stagnant layer immediately adjacent to the electrode surface (the Nernst

diffusion layer). If transport of analyte to the electrode surface occurs solely by diffusion, $\delta = (\pi Dt)^{1/2}$, and Eq. (4) becomes the well-known Cottrell equation. If the working electrode is rotated (or if the solution is stirred) at a fixed rate, δ becomes constant and the current is invariant with time.

Although time-dependent signals are inconvenient for bioassays that are not automated, commercial instruments commonly measure current at defined times or integrate current for a defined period (in chronocoulometry) following the application of the potential: in both cases, the magnitude of the resulting signal (current difference or charge) is directly proportional to the concentration of the redox-active species.

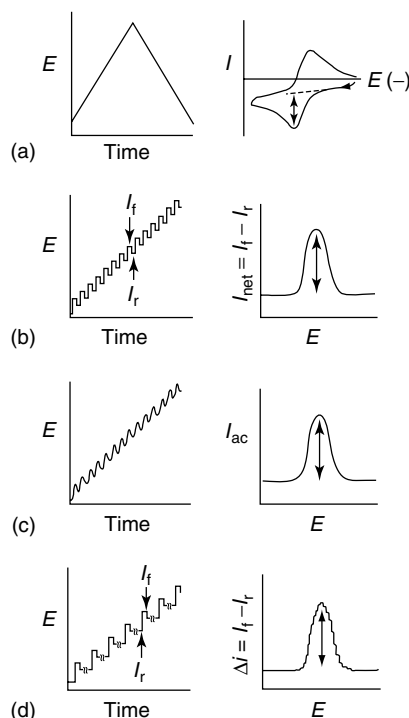
Cyclic, square wave, ac, and differential pulse voltammetry have also been used for bioanalysis, although commercialization of specialized bioassay instruments that exploit the increased selectivity of these methods has not yet occurred. Figure 4 shows the applied waveforms and (reversible) voltammetric responses for each of these techniques. Equations describing the peak currents may be found in most texts; of analytical importance is the direct proportionality between peak current magnitude and analyte concentration for all four techniques.

Fig. 4 Voltammetric waveforms and responses for a reversibly redox-active analyte: (a) cyclic voltammetry; (b) square wave voltammetry; (c) alternating current voltammetry; and (d) differential pulse voltammetry. The arrows in the waveforms represent times at which current is measured, while double-headed arrows in the response curves show the measured parameters that are directly proportional to analyte concentration.

10.3.2

Direct Amperometric Methods

This section considers analytes that may be directly quantitated via their selective oxidation or reduction under appropriate conditions. The amperometric quantitation of dissolved oxygen, the oldest bioanalytical application of amperometry, exploits a gas-permeable membrane for selectivity; oxygen diffuses across this membrane and is reduced at an unmodified, internal electrode held at constant potential [81]. The original Clark electrode used a polyethylene membrane and a Pt internal working electrode [97], and this device replaced Warburg manometry for routine oxygen quantitation. A historical review of biological oxygen measurements has been published [98], and this focuses mainly on the oxygen electrode.



These devices have been miniaturized and extensively studied for in vivo applications [99, 100]. The no-net-flux method of in vivo calibration has been introduced for sensors housed in microdialysis probes [100], but calibration is generally done before implantation and after explantation. Recently, the double potential step technique has been applied to the in vivo chronocoulometric quantitation of oxygen using a gold working electrode and an activated carbon reference electrode implanted in the venous bloodstream of animals (8 dogs, 1 sheep, and 1 pig); although the working electrodes were in direct contact with blood, this study found that some biofouling by blood proteins occurred over an implantation time of 4 years (9 of the 10 implanted electrodes showed no tissue overgrowth), but oxygen measurements were not affected when the electrodes were tested in buffer after the explantation [101].

Catecholamines and other neurotransmitters, such as dopamine, 5-hydroxyindole-3-acetic acid, homovanillic acid, dihydroxyphenylacetic acid, and 5-hydroxytryptophan (serotonin), are oxidizable at carbon electrodes. Over the past two decades, chromatographic and capillary electrophoretic techniques have been used in conjunction with electrochemical detection for the separation, identification, and quantitation of these compounds and their bioconjugates in body fluids and microdialysates [102–107, and references therein]. A recent advance includes the use of a redox-cycling electrochemical cell for high-performance liquid chromatography (HPLC) detection that, through repeated oxidation and reduction of the reversibly electroactive dopamine, allows detection limits of 116 pM to be achieved [106]. A carbon fiber working electrode, positioned at the outlet of a

30- μ m-diameter capillary, was electrically isolated from the electrophoretic separation using an integrated decoupler, which allowed nanomolar detection limits to be achieved for dopamine in brain microdialysate [107]. Capillary electrophoresis with electrochemical detection has allowed microsampling of neurotransmitters from single neurons of the pond snail *Planorbis corneus*, with which microelectrochemistry at single cells has also been done, using 5- to 10- μ m-diameter carbon fiber microelectrodes sealed in glass to expose only the tip, which is beveled flat at a 45° angle [108]. Carbon fiber working microelectrodes have also been used for the real-time in vivo detection of neurotransmission events [109]. Temporal resolution is provided by high-speed chronoamperometry or fast-scan cyclic voltammetry at electrodes coated with Nafion, a cation exchanger that rejects ascorbate, which is typically present at concentrations 2 to 3 orders of magnitude higher than those of dopamine, norepinephrine, and serotonin [109].

Exocytosis that results in the secretion of 5-hydroxytryptophan and insulin has been monitored from single pancreatic β -cells (human, porcine, canine, mouse, and cultured tumor cells), using 9- μ m-diameter carbon fiber electrodes [110]. Unmodified electrodes allowed 5-HT quantitation, while modification with a ruthenium oxide/cyanoruthenate film allowed selective quantitation of insulin at electrodes positioned 1 μ m away from cell surfaces.

An interdigitated gold microarray electrode coated with Nafion has recently been used to detect serotonin in human whole blood samples (20 μ L) to monitor allergic response, during which serotonin is secreted into the bloodstream [111]. Results showed excellent agreement between electrochemically monitored serotonin

levels and IgE levels determined by immunoassay.

Nitric oxide has been of considerable recent interest because of its signaling properties and its importance in pathophysiology [112, 113]. Methods for the electrochemical detection of NO have been reviewed [114, 115]. The two principal amperometric methods have recently been compared for in vivo NO detection: direct oxidation at Pt/Ir electrodes, with selectivity provided by membrane coatings, or oxidation at Ni-porphyrin modified carbon fiber microelectrodes coated with Nafion for anion rejection; of these, only the second method yielded signals that could be attributed to NO [116].

The redox behavior of nucleic acids, especially at mercury and carbon electrodes, has been studied for decades, and a variety of quantitative methods exist [117–120, and references therein]. Recently, derivatized nucleic acids in solution have been selectively quantitated by ac voltammetry at copper electrodes [121], while DNA bound to gold electrode surfaces via gold-thiol chemisorption has been quantitated by chronocoulometry using charge-compensating redox markers [122]. Derivative square wave voltammetry has been used to examine chemically induced DNA damage following reaction with styrene oxide [123].

Cyclic voltammetry at a graphite working electrode has been used directly on white and red blood cells from human bone marrow; one of the three irreversible anodic peaks observed with a bone marrow blood cell mixture was only present in leukemic patients [124]. Cyclic voltammetry has also been used directly on *E. coli*, rat jejunal mucosal tissue, and the enzyme lactate dehydrogenase to evaluate oxidative damage [125]. An earlier study showed that bacteria can be classified as gram-positive

or gram-negative on the basis of peak positions and currents in cyclic voltammograms performed at basal plane pyrolytic graphite electrodes; the voltammetric response is believed to result from coenzyme A oxidation [126].

10.3.3

Amperometric Measurements with Enzymes

Since the introduction of the Clark oxygen electrode more than four decades ago [97], measurements of oxidase enzyme activities and oxidase substrate concentrations have been performed using this device or a similar device in which the oxidase product, hydrogen peroxide, is reoxidized to molecular oxygen. It has also been shown that oxidase enzymes, although quite selective toward their electron-donating substrates (glucose, lactate, cholesterol), are not very selective toward oxygen as an electron-acceptor: rapid reduction of alternate species such as ferricyanide, ferrocene derivatives, quinone derivatives, and the phenoxazine/phenothiazine class of dyes also occurs if these species possess a formal potential that is more positive than that of the enzyme's active site [127–130]. These mediator compounds then act as shuttles to transfer electrons from the reduced enzyme to an amperometric electrode.

The first biosensor was reported in 1962 [131, 132], and consisted of glucose oxidase bound to a membrane covering an amperometric oxygen electrode. This was the first device that could be used to measure the concentration of an enzyme substrate without adding enzyme as a reagent to the analyte solution. The term biosensor now applies to any combination of transducer (electrochemical, optical, piezoelectric, thermoelectric)

with biological recognition agent (enzyme, antibody, chemoreceptor, nucleic acid) that results in a device for the selective measurement of an analyte species [133]. Chapters 4 and 6 of Volume 10 consider electrochemical biosensors and electrocatalysis at modified electrodes.

Several recent reviews have discussed the coupling of selective biological redox processes with amperometric electrodes. A review of bioelectrochemistry with emphasis on amperometric biosensors has been published as a section of the biannual review of dynamic electrochemistry [134], and reviews covering recent developments in clinical applications of electroanalysis and biosensors are also available [135–137]. A survey of the mechanistic aspects of amperometric biosensors has appeared [138]; this review considers direct electron transfer from enzyme to electrode, mediation by freely diffusing species such as ferrocenes, mediation by electron-hopping through redox-active gels, mediation through conducting polymers, mediator-modified enzymes and mediator-modified electrodes, and concludes that electrochemically deposited polymers are promising materials for inexpensive, reproducible mass production of miniaturized sensors and electrode arrays. Two recent reviews focus on electrosynthesized polymers as immobilization matrices for enzymes and other biomolecules [139, 140]. A very comprehensive review of immobilization techniques and mediation mechanisms has appeared that emphasizes communication between redox proteins and conducting supports for bioelectronic applications [141]; these authors focus on the advantages and implications of tailored, organized protein architectures in ordered and defined nanostructures with the aim of improving electronic coupling between redox proteins and

transducers (see also Chapter 9 of Volume 10). More specialized reviews of glucose sensors [142] and the application of biosensors as selective detectors for chromatographic and electrophoretic instruments [143] are also available.

Challenges facing the development of *in vitro* amperometric biosensors (interference rejection, rapid response, reproducibility, response range) have been met in many cases, and commercially available devices based on disposable test strips that incorporate miniature two- or three-electrode electrochemical cells are available for a variety of analytes (see Sect. 10.3.7). Thin-film and thick-film technology [80] have been used to mass-produce reproducible sensing elements, and amperometric detection in oxidase-based devices occurs by peroxide oxidation or the oxidation of freely diffusing mediators such as ferricyanide and ferrocene derivatives. The screen-printing process for disposable sensor preparation has also been reviewed [144].

New developments in this area include uric acid sensors based on the mediation of urate oxidase by a novel redox polymer, poly(*N*-methyl-*o*-phenylenediamine) [145], and by the freely diffusing mediator 1-methoxy-5-methylphenazinium [146], continued research on the direct amperometric detection of NADH [147] and the use of redox mediators [148] for dehydrogenase enzymes, to allow practical sensors that exploit this large class of enzymes, and the use of cytochrome P450-modified glassy carbon electrodes as drug metabolism biosensors [149].

The area of long-term, continuous, *in vivo* measurement using enzyme-based amperometric biosensors has encountered some unique challenges in addition to the problems of biocompatibility, miniaturization, and the need for

telemetric data transmission that have also been encountered during the development of *in vivo* amperometric oxygen sensors [150]. Implantable sensors must ideally be “reagentless”, that is, the addition of reagents, either enzymes or cosubstrates, is not possible once the devices have been implanted. Glucose sensors in which the enzyme layer can be recharged, or replaced every ten days, have been proposed [142, 151], but this is not ideal for the user and may result in non-compliance. In addition, chemicals from the sensor must not escape into the surrounding environment.

Two approaches to reagentless *in vivo* amperometric glucose sensors have emerged, and these devices are illustrated in Fig. 5. In the first, immobilized glucose oxidase catalyzes the oxidation of glucose with concomitant reduction of molecular oxygen; no artificial electron acceptors are used and the hydrogen peroxide is detected at a platinum [152] or platinum-iridium anode [153, 154]. Although this design has been criticized because of the inherently variable *in vivo* oxygen levels, Wilson’s group has shown that oxygen levels of 10 mm Hg and above yield sensor responses to 10 mM glucose that are 90% of those achieved with high oxygen levels; with 2 mM glucose, virtually no oxygen dependence was observed at 8 mm Hg and above [154]. The main advantage of this design is the absence of artificial mediators that could leach into the surrounding environment. However, peroxide oxidation requires an applied potential of 600 to 700 mV vs Ag/AgCl, and at these potentials, oxidation of interferences such as ascorbate and urate may occur. Membrane materials such as Nafion, a cation exchanger that prevents anion transport to the anode, combined with cellulose acetate, have been used to minimize this

kind of interference [154, 155]. Nafion has been shown to mineralize via deposition of calcium phosphate, both *in vitro* (cell culture medium) and *in vivo* in subcutaneous implants in rats [156], but in the glucose sensors, the Nafion-cellulose acetate interference rejection membranes are placed between the immobilized enzyme layer and the Pt/Ir anode to prevent direct contact with the biological environment [154, 155]. An outer layer of mixed polysiloxane and polyurethane is used to provide biocompatibility. With these devices, sensitivities of 3 to 4 nA mM⁻¹ are achieved [154].

The second approach employs artificial electron acceptors, and *in vivo* experiments have involved sensors that cross-link glucose oxidase in redox-active hydrogels used as coatings on gold anodes [157, 158]. These hydrogels are block copolymers formed by reaction of poly[(1-vinylimidazole)osmium(4,4'-dimethylbipyridine)₂Cl] with poly(ethylene glycol) diglycidyl ether 400 in the presence of glucose oxidase, and form the first of the three layers on the gold electrode surface; mediation occurs by the reduction of Os(III) by the enzyme, and electron-hopping through the hydrogel allows Os(III) regeneration by oxidation at the gold electrode. Interference rejection and glucose flux restriction occurs at the second layer, composed of Nafion and cellulose acetate, whereas the third layer is a biocompatible polyethylene oxide film. In air, these sensors show 2 to 3 nA mM⁻¹ sensitivity, but under argon, the sensitivity improves to 4 to 5 nA mM⁻¹ because the native reaction of glucose oxidase with oxygen can occur, but the peroxide produced by this reaction is not detected at the applied potential of 200 mV versus saturated calomel electrode (SCE) [157]. These sensors have been implanted in jugular veins of rats, where

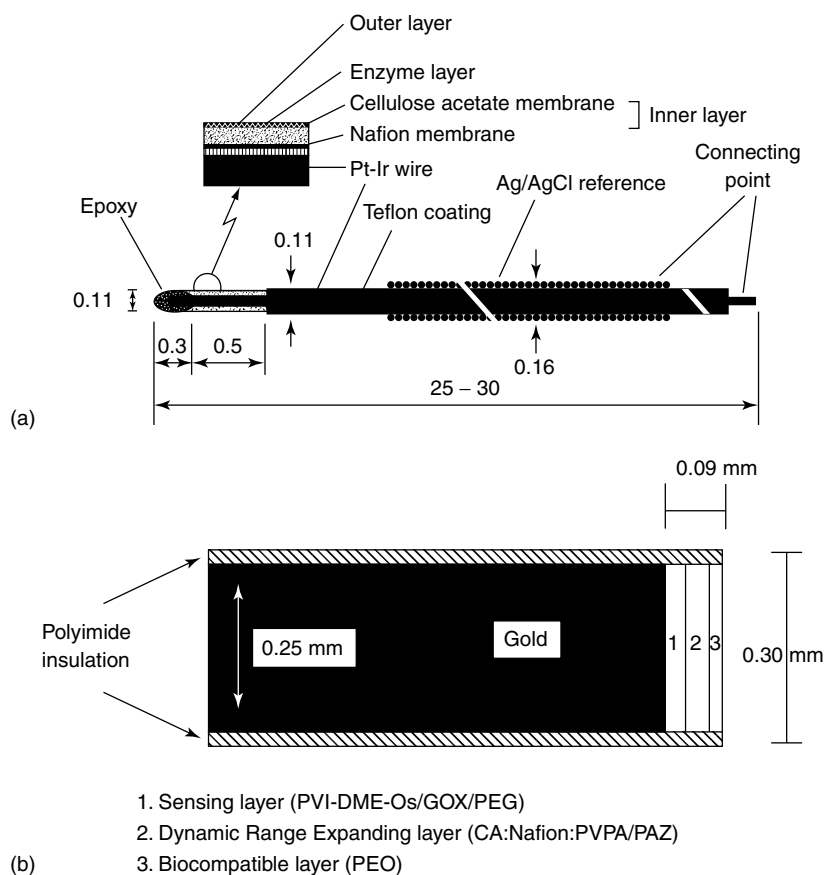


Fig. 5 The two main approaches to amperometric enzyme-based biosensors for in vivo measurements: (a) Wilson's group uses a Pt-Ir wire electrode coated with Nafion and cellulose acetate for interference rejection, followed by the enzyme layer and a biocompatible outer layer; the enzyme generates hydrogen peroxide, which is oxidized at the electrode (Reproduced from Y. Hu, G. S. Wilson, *J. Neurochem.* **1997**, 68, 1745–1752). (b) Heller's group uses a gold electrode modified first with an enzyme/mediator polymer layer, followed by a dynamic range expanding layer that also aids in interference rejection, and finally a biocompatible outer layer; once reduced by glucose, the enzyme glucose oxidase is reoxidized by Os(III), and the generated Os(II) is oxidized at the gold surface to yield the measured current. (Reproduced from J. G. Wagner, D. W. Schmidtke, C. P. Quinn et al., *Proc. Natl. Acad. Sci. U.S.A.* **1998**, 95, 6379–6382.)

oxygen concentrations are relatively low and invariant [157], and subcutaneously in chimpanzees [158]; comparison of the continuous in vivo sensor measurements with periodic in vitro blood glucose measurements was performed in response

to various stimuli, including insulin and glucose administration, and good agreement between these methods was observed.

Calibration of implanted devices remains an issue to be resolved. In research

trials, sensors are calibrated *in vivo* by comparison of sensor readings with accepted *in vitro* blood glucose measurements (e.g. finger-stick measurements), and can be calibrated *in vitro* before implantation and after explantation [150, 154, 157]. Long-term implants suffer from biofouling, and a continuous decrease in sensitivity occurs [159, 160]. New methods for *in vivo* calibration have been proposed [161, 162], and work is continuing in this area. Implants are ideally made subcutaneously, and analyte levels in the interstitial fluid, rather than blood or plasma levels, are measured. It has recently been shown, over a three-day trial in dogs, that subcutaneous amperometric peroxide-based glucose measurements parallel plasma glucose levels with only a slight delay (<10 min), occurring when blood levels fluctuate [163].

Further reports of importance to the area of *in vivo* sensing include the use of voltammetric waveforms for interference discrimination in amperometric glucose oxidase-modified, peroxide-based carbon fiber microelectrodes [164], the modification of carbon fiber microelectrodes with osmium-based redox polymer containing glutamate oxidase and ascorbate oxidase for *in vivo* rat brain glutamate and ascorbate measurements [165], the development of lactate oxidase-peroxide-based devices for *in vivo* lactate measurements in rat brain and subcutaneous tissue [166, 167], and the integration of lactate and glucose sensors onto a single silicon containment sensor [168].

10.3.4

Amperometric Immunoassays and Immunosensors

The use of antibodies as analytical reagents allows strong binding and selective recognition of analytes. Antibodies

are glycoproteins that possess two identical antigen-binding sites and have a molecular weight of about 150 kD. The antibody-antigen reaction itself is not easily monitored with readily available equipment, so a label is generally bound to either the antibody or the antigen. Either the antibody or the antigen may be the analyte species, but more commonly, it is the antigen; the antigen may be a small molecule (a hapten) or a large protein or glycoprotein in which an epitope, or surface structure, combines with one of the antibody paratopes or binding sites. Immunoassays are described as competitive, where analyte competes with a labeled analyte reagent for a limited number of binding sites, or noncompetitive, where quantitative binding of analyte to excess antibody is detected using a second labeled antibody. Typically, antibodies have antigen association constants between 10^5 and 10^{12} M^{-1} [169], so that, in principle, competitive immunoassays are capable of detecting picomolar concentrations of analytes, whereas noncompetitive assays are potentially capable of detecting concentrations that are several orders of magnitude lower [170]. In heterogeneous immunoassays, the labeled species react with binding partners that are immobilized on a solid support, such as a microtiter plate or an electrode surface, and excess labeled reagent is removed by a rinse step. Homogeneous assays rely on a change in the properties of the label that occurs upon binding between the labeled reagent and the binding partner; as the properties of the label change in a detectable manner, separation of the bound from the free labeled reagent is unnecessary.

Amperometric methods have been used to detect labels that are simple redox-active molecules or enzymes that generate

redox-active species as a reaction product. Enzymatic labels have the inherent benefit of amplification: a single enzyme label can produce thousands of detectable molecules. In this section, amperometric immunoassays and immunosensors are considered together because immunosensors are simply heterogeneous immunoassays in which the working electrode itself functions as the solid support. Recent reviews of electrochemical immunoassays [171], immunoassays [172], and immunosensors in clinical analysis [173] have been published; all of these have some discussion devoted to amperometric measurements. Advantages of amperometric measurements over more traditional absorbance or fluorescence measurements include speed, accuracy, precision, and the ability to make measurements on turbid or intensely colored samples.

One review focuses on methods for attaining zeptomole detection limits in amperometric immunoassays [174]. Enzymatic amplification schemes have been proposed for absorbance-based immunoassays in which a labeling enzyme, alkaline phosphatase, dephosphorylates NADP to begin a second amplification stage involving alcohol dehydrogenase and diaphorase; this “cascade” scheme was tested in a noncompetitive immunoassay for TSH and found to have a detection limit of 10 zmol with an intensely colored formazan product [175, 176]. Cascade schemes have also been tested in electrochemical immunoassays; detection limits in the picomolar to femtomolar ranges have been found [177, and references therein]. Enzymes that have now been tested in amperometric immunoassays include alkaline phosphatase [178–181], peroxidase [182–189], glucose oxidase [190–192], glucose-6-phosphate dehydrogenase [193], and

catalase [194]. The microporous gold electrode used by Meyerhoff's group allows substrate diffusion from the back side of the electrode, with the alkaline phosphatase label bound on the front side of the electrode; this scheme allows separation-free immunoassays because both product formation and detection occur at the surface of the electrode [180].

Chemical amplification schemes have also been tested in amperometric immunoassays. For example, Guo and coworkers used a copper ion label in a 6:1 ratio to the labeled species, HSA, in a heterogeneous competitive immunoassay format. Following the rinse step, Cu^{2+} was released into the solution by lowering the pH, and the increased temperature allowed the copper-catalyzed conversion of *o*-phenylenediamine to the electroactive product, 2,3-diaminophenazine, and the detection limit for albumin was lowered by two orders of magnitude to 7 ng mL⁻¹, compared with direct metal ion labeling [195].

Further methodological improvements have been shown using alkaline phosphatase as a labeling enzyme. Capillary electrochemical enzyme immunoassay, in which an inner capillary wall is used as the solid support and detection occurs downstream in an amperometric flow cell, has been introduced by Heineman's group and shown to have a 3-pmol detection limit for phenobarbital in serum [196]. Alternate substrates to replace 4-aminophenylphosphate have been investigated: 1-naphthylphosphate was shown to be preferred for the determination of progesterone in milk [197] and 3-indoxyl phosphate, which generates indigo dimer that is readily detected by ac voltammetry, yielded a detection limit for human IgG of 0.1 nM [198]. Immunoassay methods are not limited to

the detection of molecular analytes, and several amperometric immunoassays have now been reported for the detection of pathogens. The detection of *Salmonella* species is of importance in food processing, and amperometric enzyme-linked assays have been described for its quantitation at levels as low as 8000 cells mL⁻¹ [197, 199]. *Staphylococcus aureus* is also of interest in food production, and an amperometric immunosensor has been reported for its detection [200]. Enterohemorrhagic *Escherichia coli* O157:H7 has become a worldwide health problem, and amperometric filtration-capture [201] and immunomagnetic flow injection immunoassays [202] have been developed with detection limits of 5×10^3 and 1×10^5 cells mL⁻¹, respectively. Differential pulse voltammetry has been used in an enzyme-linked immunoassay for *Helicobacter pylori*-specific IgG; the substrate 3,3'-5, 5'-tetramethylbenzidine was used for the peroxidase label, and this method showed a sevenfold improvement in detection limit compared with spectrophotometric detection [203].

10.3.5

Amperometric Nucleic Acid Assays and Sensors

In 1987, Bard's group reported that the binding of small, redox-active transition metal polypyridine complexes with high molecular weight nucleic acids in solution can be studied by voltammetry; the decrease in the apparent diffusion coefficient that occurs upon binding led to significantly decreased voltammetric peak currents, allowing the determination of association constants [204]. Since then, several groups have studied electrode-bound nucleic acids and oligonucleotides in an effort to develop sequence-selective DNA

biosensors [205–213] and sensors for the study of small molecule interactions with DNA [214–216]. A short review of electrochemical DNA sensors was published in 1996 [217], and significant developments have occurred since that time.

Covalently immobilized calf thymus DNA on glassy carbon electrodes was detected using tris(2,2'-bipyridyl)cobalt(III) and tris(1,10-phenanthroline)cobalt(III), complexes that are reversibly electroactive at moderate applied potentials [205]. Immobilization using carbodiimide and N-hydroxysuccinimide reagents to generate NHS esters on the carbon surface occurs at the guanosine residues [206], and this allowed immobilization of short, single-stranded oligonucleotides possessing a (dG)_n tail [206, 207]. The two cobalt complexes associate selectively with the double-stranded form of DNA and bind only weakly to single-stranded forms; thus, the recognition of complementary DNA that results in the hybridization on the electrode surface between surface-bound probe and soluble target sequences yields in significantly higher voltammetric peak currents for the reduction of the cobalt complexes. The detection of a model sequence and the Δ F508 deletion sequence associated with cystic fibrosis have been accomplished with synthetic oligonucleotides [206, 207] and with 400-base PCR products amplified from human DNA [208].

Oligonucleotides modified with a terminal thiol group can be chemisorbed onto gold electrodes and, after hybridization with a soluble complementary sequence, detected voltammetrically using the redox-active bis (benzimidazole) dye Hoechst 33258 [209]. This group also showed that voltammetric peak potentials for acridine orange [210] and daunomycin [211]

could be used to distinguish surface-bound double- and single-stranded DNA.

Electrocatalytic oxidation of guanosine residues by electrogenerated tris(2,2'-bipyridyl)ruthenium(III) has recently been shown to provide a useful transduction mechanism in DNA biosensors [212]. Probe strands in which inosine was substituted for guanosine were immobilized on an electrode surface, and these hybridized selectively with targets that contained oxidizable guanosine residues; PCR-amplified genomic DNA from herpes simplex virus type II, *Clostridium perfringens*, and human immunodeficiency virus were detected by this method.

Recent work with DNA-modified gold electrodes has shown that single-base mismatches (point mutations) can be detected in immobilized double-stranded oligonucleotides using redox-active molecules that intercalate between the stacked base pairs [213]. In this work, charge transport from daunomycin, methylene blue, and an iridium polypyridine complex (all intercalators) through synthetic 15-base oligodeoxynucleotides was significantly attenuated when single-base mismatches were present at any of the three locations in the hybridization product; a nonintercalating DNA-binding complex, ruthenium pentamine chloride, showed unaffected voltammetric signals in the presence of the mismatches.

Voltammetry at modified electrodes has also been used to investigate the interactions of redox-active DNA-binding agents with immobilized DNA. Examples include the survey done by Hashimoto and coworkers [211], an investigation of methylene blue [214], a comparison of interactions of redox cations with surface-bound and solution DNA [215], and an investigation of the kinetics and mechanism of mitoxantrone

interaction with DNA immobilized on glassy carbon electrodes [216].

10.3.6

Emerging Technology

Several reviews of new materials for chemical and biochemical sensors have appeared recently [218–221]. New applications of sol-gels (see also Volume 1, Chapter 8), zeolites, organic polymers, and conducting composites to sensing devices include small inorganic ions, gases, small organic molecules, proteins, and DNA. Sensors and assays employing molecularly imprinted polymers have also been reviewed [222, 223]. Extensive fundamental research on alkanethiol self-assembled monolayers is expected to yield reproducibly fabricated enzyme electrodes in which control of molecular architecture is readily achieved [224].

Fabrication of sensors and sensor arrays is in a state of rapid development. The groups led by Kuhr [225, 226] and Heineman [227, 228] have made significant advances in microfabrication of sensor arrays for simultaneous multianalyte amperometric assays and sensors; both have applied their arrays to immunoassays [226, 227]. Further research efforts toward controlled-release microchip fabrication [229] and nanoscale chemical sensors [230] have also shown promise and will aid in the development of sensors and sensing arrays for in vitro and in vivo measurements.

10.3.7

Commercialization of Amperometric Devices

Biosensors based on hydrogen peroxide detection have been sold by Yellow Springs Instruments (YSI) for many years, and

the YSI 2700® is their most advanced instrument [231]. The YSI biosensors are based on a Pt electrode, covered with a cellulose acetate dialysis membrane, an enzyme layer, and a polycarbonate membrane that limits substrate diffusion, so that the enzyme itself does not limit the reaction rate. This instrument is marketed for food analysis and biotechnology and allows the following oxidase substrates to be determined: choline (to 450 mg L⁻¹), D-glucose (to 9 g L⁻¹ with one membrane and 25 g L⁻¹ with a second type), ethanol (to 3.2 g L⁻¹), galactose (to 25 g L⁻¹), hydrogen peroxide (to 600 mg L⁻¹), lactose (to 25 g L⁻¹), L-glutamate (to 10 mM), L-glutamine (to 8 mM), L-lactate (to 2.67 g L⁻¹), methanol (to 2.50 g L⁻¹), and sucrose (to 25 g L⁻¹). A simple flow injection system is used to transport analyte into the flow cell in which the biosensors are housed. Nova manufactures the BioProfile series, designed for cell culture applications, and allows hydrogen peroxide-based biosensor detection of glucose, lactate, glutamine, and glutamate. Many commercially available clinical laboratory analyzers that use ISEs for potentiometric blood gas and electrolyte quantitation also employ amperometric measurements for routine assays of dissolved oxygen, glucose, and lactate in blood, urine, and other body fluid samples [82].

Point-of-care testing has now become feasible with the introduction of the handheld i-STAT instrument and similar portable devices, such as the optically based Reflotron. The i-STAT (Fig. 2) contains both potentiometric and amperometric sensors integrated into sensor arrays that are included within disposable cassettes [87–89]. Eight tests are possible with the most advanced cassette, the EC₈₊, and these are sodium, potassium, chloride,

urea nitrogen, glucose, pH, pCO₂, and hematocrit (five additional values are calculated from these results, including bicarbonate, total carbon dioxide, base excess, anion gap, and hemoglobin).

Devices designed for use by individuals with no technical training have traditionally focused on the need for regular glucose measurements by diabetic patients. Since the first introduction of the ExacTech amperometric glucose-monitoring device by MediSense Inc. (which was taken over by Abbott in 1996), several other electrochemical glucose meters have been introduced. In 1998, the market for such devices was dominated by four companies: LifeScan (42%), Boehringer-Mannheim/Roche (18%), Abbott/MediSense (16%), and Bayer (12%); all others together held 12% of the total market [232]. Of the four main companies, all now market an amperometric glucose self-testing device. LifeScan recently introduced the *FastTake*, Boehringer-Mannheim/Roche provides the Accu-Chek Advantage and Accu-Chek Complete devices, Abbott produces the Precision Q.I.D. and the Precision Q.I.D. Pen (the ExacTech line is now sold only in Europe), and Bayer offers the Glucometer Elite. Clinical testing results for these devices have been reported [233–235].

The monitoring of blood lactate levels in high-performance athletics has led to the introduction of handheld devices, similar to the devices used for blood glucose monitoring by diabetics [236]. The Analox P-LM-5 (Analox Instruments, England) uses a 5-μL blood sample and produces a value within 20 s of application of the sample to the lactate oxidase/peroxide-based test strip. The Lactate Pro (Arkray Inc., Japan) is another lactate oxidase-based, amperometric, handheld device for lactate monitoring, and is marketed for athletes

who desire peak performance during competitions. These devices compete with the Roche Accusport, which is based on reflectance photometry, and are sold for about US \$400.

An exciting development in individual monitoring is occurring with the commercial introduction of subcutaneous implantable glucose sensors for continuous and long-term monitoring. It has been shown that subcutaneous glucose measurements reflect plasma glucose levels, but the subcutaneous implants do not cause the sensor fouling that has been observed with blood measurements. The MiniMed Continuous Subcutaneous Blood Glucose (CSBG) Monitoring System (Applied Medical Technology Co., UK) was approved for physician-supervised use by the US FDA in February, 1999. It is based on glucose oxidase/hydrogen peroxide detection technology and consists of a three-electrode cell housed in flexible polymer tubing with a side window to expose the active electrode area that is covered by a polyurethane membrane. The miniaturized sensor is embedded in a split 22-gauge needle that is removed after the sensor is inserted into the abdominal region. The sensor is connected to an external pager-sized meter by wires, allowing data collection every 10 s, and an average value calculated every minute [237]. A second CSBG instrument is being developed by Synthetic Blood International (Ohio) for similar applications; their device uses a silicone-sheathed Pt electrode with the glucose oxidase enclosed in a semipermeable cellulose acetate membrane, coupled with a titanium-encased battery and microprocessor [238].

Electrochemical DNA sensors and sensor arrays are being developed by at least three companies in the United States. Clinical Microsensors, Inc. (Pasadena CA) is

interested in direct electron transfer from ferrocene-labeled DNA to gold electrodes, while Xanthon, Inc. (Research Triangle Park, NC) is developing sensors on the basis of electrocatalytic guanine oxidation [239, 240]. AndCare Inc. (Durham, NC) is developing a multichannel electrochemical system for quantitative monitoring of PCR amplification using intermittent pulse amperometry and a labeling enzyme (peroxidase) mediated by tetramethylbenzidine [241].

10.4

Impedimetric Methods

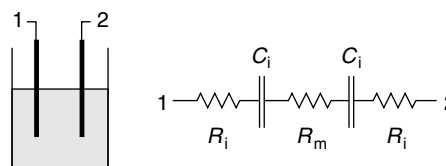
10.4.1

Introduction

Impedimetric measurements are based on the nonfaradaic response observed between two electrodes immersed in a sample solution when a high frequency (1 to 300 kHz) alternating potential is applied. The amplitude of the applied waveform is small, and this, combined with the high frequency relative to other electrochemical methods, effectively prevents faradaic reactions from occurring to any significant extent. In contrast to potentiometric and amperometric methods, impedimetric methods are not analyte-selective; instead, bulk properties of the solution and the electrode–solution interfaces are monitored.

The impedance cell can be thought of as a simple electrical circuit, composed of two capacitors, that represent the two electrode–solution interfaces, separated by a series of three resistors that symbolize the polarization resistance at each electrode surface, with the electrolyte (solution) resistance in the center, as shown in Fig. 6. The overall impedance of the cell Z consists of an overall capacitance C and a total

Fig. 6 Equivalent circuit representation of a typical impedance cell used in microbiology. The symbols R_i and C_i represent the interfacial resistances and capacitances, respectively, while R_m is the resistance of the medium separating the two electrodes.



resistance R , and depends on the angular frequency ω of the applied potential waveform, as shown in Eq. (5):

$$Z = \left(\frac{R^2 + 1}{C^2 \omega^2} \right)^{1/2}. \quad (5)$$

Instrumentation allows the measurement of capacitance, resistance, or its inverse, conductance, and is based on Wheatstone bridge electronics. The first commercial instrument for bioanalytical measurements consisted of a reference cell and a sample cell placed in opposing arms of the bridge; this device, the Strattometer, was used to study blood coagulation and microorganism growth in culture media [242].

10.4.2

Impedimetric Assays and Sensors

A review of the diverse food hygiene applications of impedance microbiology has recently been published [243]. The detection of *Enterobacteriaceae*, particularly *Salmonella* spp., the determination of total bacterial counts, and the examination of antibiotics and food additives for antimicrobiological effects are important. Another short review describes a model explaining the effects of microbial growth and metabolism on capacitance at electrode-medium interfaces [244].

Recently reported impedimetric assays also focus on the detection and enumeration of microorganisms: the detection of *E. coli* in potable water [245] and the

quantitation of bacterial content in milk samples [246]. Antimicrobial susceptibility testing has also been performed on gram-negative bacilli by an impedance assay [247]. Dielectric spectroscopy has been used to study the internal structures of cells [248], and has been used in conjunction with multivariate calibration and artificial neural networks to quantitate the metabolic substrates in biological cell suspensions [249].

Impedimetric measurements are inherently nonselective, but the modification of electrode surfaces with selective recognition agents has resulted in selective sensing devices based on impedimetric transducers. Reviews of immunosensors and cell-based biosensors include sections on impedance transduction [177, 250, and references therein]. A review of bioelectronic noses, devices intended to mimic the human olfactory system in detecting and identifying odors, includes interdigital structures for complex impedance measurements and arrays of capacitive sensor elements [251].

Hendji and coworkers studied interdigitated pairs of gold film electrodes prepared by micromachining [252]. This device records a differential signal between an enzyme-modified surface and a control surface modified with an inert protein; the studied enzymes included urease, glucose oxidase, and acetylcholinesterase. Darbon and coworkers [253] and Souteyrand and coworkers [254] studied antigen-antibody interactions, and this measurement method

was included in Bergveld's review [46]. Nucleic acids have also been detected by impedimetric methods, using single-stranded DNA-modified electrodes [255]. A self-assembled peptide monolayer has been used for the impedimetric detection of viruses [256].

Polymer membranes have shown great promise for impedimetric sensors. Sheppard and coworkers coated interdigitated platinum electrodes with a pH-sensitive hydrogel that swelled with a change in pH [257]. McNeil and coworkers exploited a polymer that dissolves at pH values above 7; in their urea sensor designed with a base transducer of screen-printed gold ink electrodes, urease was incorporated as an outer layer over this polymer, and the presence of urea in solution resulted in the dissolution of the inner polymer layer with very large concomitant impedance changes [258]. Screen-printed interdigitated carbon electrodes coated with a layer of poly(methylvinyl ether)/maleic anhydride modified by esterification with *n*-octanol were further modified with layers of urease or creatinine deaminase and then used to monitor urea or creatinine levels in serum [259]; in this work, alkaline pH caused ester hydrolysis, and this led to marked changes in capacitance.

10.4.3

Commercially Available Instruments for Impedance Measurements

At present, four companies provide specialized impedance measurement instrumentation for clinical microbiology or food hygiene applications. BioMérieux manufactures the Bactometer, which can monitor conductance, capacitance, or impedance in up to two temperature-controlled incubators, each containing 256 samples. Malthus Instruments produces

the System V, which monitors only conductance, but can handle up to 1200 samples. Don Whitley Scientific manufactures the "Rapid Automated Bacterial Impedance Technique" (RABIT) instrument, which is capable of measuring conductance in a maximum of 16 incubators, each containing 32 individually temperature-controlled electrode tubes. Sy-Lab offers the BacTrac, which monitors total impedance in 6 individually temperature-controlled incubators, each containing a maximum of 40 impedance tubes. All of these instruments monitor relative or absolute changes in impedance or conductance at regular intervals (e.g. every 6 min) [243].

10.5

Future Directions and Perspectives

Electroanalytical methods have become increasingly important for practical assays in complex biological media. The commercial promise of ISEs and electrochemical biosensors has now been realized for the *in vitro* quantitation of many clinically important analytes, and new devices for *in vivo* quantitation are being commercialized. Point-of-care and physician office laboratory testing is now a reality, but the fundamental problem of quality control must be addressed. The American Association of Bioanalysts recently conducted a large-scale comparison of clinical test results obtained from the physician office laboratories and specialized off-site clinical laboratories, and very large discrepancies were found [260]. Devices designed for this type of application, and for use by nonprofessionals, must be designed for user-independent results.

The i-STAT Portable Clinical Analyzer [87–89] is one example of the recent

trend toward the incorporation of electrochemical sensing elements into arrays for simultaneous multianalyte analysis. Other examples of this kind of microfabricated total analysis systems, or μ TAS devices, that incorporate electrochemical transducers such as ISEs and amperometric enzyme electrodes have been introduced and are expected to gain commercial importance in clinical settings [261, 262].

Acknowledgment

The Natural Sciences and Engineering Research Council of Canada is gratefully acknowledged for the ongoing financial support of the author's research program.

References

1. A. J. Bard, L. R. Faulkner, *Electrochemical Methods, Fundamentals and Applications*, 2nd Ed., Wiley & Sons, New York, 2001.
2. P. T. Kissinger, W. R. Heineman, *Laboratory Techniques in Electroanalytical Chemistry*, 2nd ed., Marcel Dekker, New York, 1996.
3. T. Riley, C. Tomlinson, *Principles of Electroanalytical Methods*, Wiley & Sons, New York, 1987.
4. A. Evans, *Potentiometry and Ion Selective Electrodes*, Wiley & Sons, New York, 1987.
5. T. Riley, A. Watson, *Polarography and Other Voltammetric Methods*, Wiley & Sons, New York, 1987.
6. C. M. A. Brett, A. M. O. Brett, *Electroanalysis*, Oxford University Press, Oxford, 1998.
7. G.-A. Junter, (Ed.), *Electrochemical Detection Techniques in the Applied Biosciences: Volume 1: Analysis and Clinical Applications*, Ellis Horwood, Chichester, 1988.
8. G.-A. Junter, (Ed.), *Electrochemical Detection Techniques in the Applied Biosciences: Volume 2: Fermentation and Bioprocess Control, Hygiene and Environmental Sciences*, Ellis Horwood, Chichester, 1988.
9. J. Wang, *Electroanalytical Techniques in Clinical Chemistry and Laboratory Medicine*, VCH Publishers, New York, 1988.
10. W. F. Smith, *Voltammetric Determination of Molecules of Biological Significance*, Wiley & Sons, New York, 1992.
11. J. P. Hart, *Electroanalysis of Biologically Important Compounds*, Ellis Horwood, Chichester, 1990.
12. D. G. Buerk, *Biosensors: Theory and Applications*, Technomic Publishing, Lancaster, 1993.
13. A. J. Cunningham, *Introduction to Bioanalytical Sensors*, Wiley & Sons, New York, 1998.
14. B. P. Nicolsky, M. M. Schultz, A. A. Beljustin in *Glass Electrodes for Hydrogen and Other Cations*, (Ed.: G. Eisenman), Marcel Dekker, New York, 1967.
15. E. Bakker, R. K. Meruva, E. Pretsch et al., *Anal. Chem.* **1994**, 66, 3021–3030.
16. E. Bakker, E. Pretsch, P. Buehlmann, *Anal. Chem.* **2000**, 72, 1127–1133.
17. M. J. Silva, J. L. Wong, *Bioelectrochem. Bioenerg.* **1995**, 37, 141–148.
18. J. W. Severinghaus, A. F. Bradley, *J. Appl. Physiol.* **1958**, 13, 515–520.
19. L. Campanella, M. P. Sammartino, M. Tomassetti, *Analyst* **1990**, 115, 827–830.
20. V. P. Y. Gadzekpo, J. M. Hungerford, A. M. Kadry et al., *Anal. Chem.* **1985**, 57, 493–495.
21. A. Malinowska, M. E. Meyerhoff, *Anal. Chem.* **1998**, 70, 1477–1488.
22. S. O. Engblom, *Biosens. Bioelectron.* **1998**, 13, 981–994.
23. B. M. Altura, B. T. Altura, *Scand. J. Clin. Lab. Invest.* **1996**, 56 (Suppl. 224), 211–234.
24. A. Ceresa, E. Pretsch, E. Bakker, *Anal. Chem.* **2000**, 72, 2050–2054.
25. I. Karube, K. Ikebukuro, Y. Murakami et al., *Ann. N.Y. Acad. Sci.* **1995**, 750, 101–108.
26. H. S. Yim, C. E. Kibbey, S. C. Ma et al., *Biosens. Bioelectron.* **1993**, 8, 1–38.
27. J. M. Kauffman, G. G. Guilbault, *Bioprocess Technol.* **1991**, 15, 63–82.
28. J. Janata, *Principles of Chemical Sensors*, Plenum Press, New York, 1989.
29. D. Monroe, *Crit. Rev. Clin. Lab. Sci.* **1989**, 27, 109–158.
30. G. V. Diaz, L. H. el-Issa, M. A. Arnold et al., *J. Neurosci. Methods* **1988**, 23, 63–69.
31. M. H. Gil, A. P. Piedade, S. Alegret et al., *Biosens. Bioelectron.* **1992**, 7, 645–652.
32. C. Eggenstein, M. Borchardt, C. Diekmann et al., *Biosens. Bioelectron.* **1999**, 14, 33–41.
33. A. Mulchandani, P. Mulchandani, I. Kaneva et al., *Anal. Chem.* **1998**, 70, 4140–4145.

34. J. Saurina, S. Hernandez-Cassou, S. Alegret et al., *Biosens. Bioelectron.* **1999**, *14*, 67–75.
35. S. V. Dzyadevich, Y. I. Korpan, V. N. Arkhipova et al., *Biosens. Bioelectron.* **1999**, *14*, 283–287.
36. V. Volotovskiy, N. Kim, *Biosens. Bioelectron.* **1998**, *13*, 1029–1033.
37. R. Koncki, I. Walcerz, E. Leszczynska, *J. Pharm. Biomed. Anal.* **1999**, *19*, 633–638.
38. Y. I. Korpan, M. V. Gonchar, A. A. Sibirny et al., *Biosens. Bioelectron.* **2000**, *15*, 77–83.
39. A. N. Reshetilov, M. V. Donova, D. V. Dovbnaya et al., *Biosens. Bioelectron.* **1996**, *11*, 401–408.
40. J. Janata, *J. Am. Chem. Soc.* **1975**, *97*, 2914, 2915.
41. M. Aizawa, A. Morioka, S. Suzuki et al., *Anal. Biochem.* **1979**, *94*, 22–28.
42. N. Yamamoto, Y. Nagasawa, M. Sawai et al., *J. Immunol. Methods* **1978**, *22*, 309–317.
43. U. Pfeifer, W. Bauman, *Fresenius J. Anal. Chem.* **1992**, *343*, 541–549.
44. L. Engel, W. Bauman, *Fresenius J. Anal. Chem.* **1994**, *349*, 447–450.
45. Z.-H. Lin, G.-L. Shen, Q. Miao et al., *Anal. Chim. Acta* **1996**, *325*, 87–92.
46. P. Bergveld, *Biosens. Bioelectron.* **1991**, *6*, 55–72.
47. T. Dubrovsky, S. Vakula, C. Nicolini, *Sens. Actuators, B* **1994**, *22*, 69–73.
48. R. Koncki, A. Owczarek, W. Dzwolak et al., *Sens. Actuators, B* **1998**, *47*, 246–250.
49. K. Dill, L. H. Stanker, C. R. Young, *J. Biochem. Biophys. Methods* **1999**, *41*, 61–67.
50. L. Campanella, R. Attioli, C. Colapicchioni et al., *Sens. Actuators, B* **1999**, *55*, 23–32.
51. T. A. Sergeyeva, A. P. Soldatkin, A. E. Rachkov et al., *Anal. Chim. Acta* **1999**, *390*, 73–81.
52. A. L. Ghindilis, P. Atanasov, E. Wilkins, *Sens. Actuators, B* **1996**, *34*, 528–532.
53. A. Offenhausser, C. Sprossler, M. Matsuzawa et al., *Biosens. Bioelectron.* **1997**, *12*, 819–826.
54. P. Schroth, M. J. Schoning, P. Kordos et al., *Biosens. Bioelectron.* **1999**, *14*, 303–308.
55. V. T. Kung, P. R. Panfili, E. L. Sheldon et al., *Anal. Biochem.* **1990**, *187*, 220–227.
56. J. D. Olson, P. R. Panfili, R. F. Zuk et al., *Mol. Cell. Probes* **1991**, *5*, 351–358.
57. D. Jagner, *Trends Anal. Chem.* **1983**, *2*, 53–56.
58. S. Bruckenstein, J. W. Bixler, *Anal. Chem.* **1965**, *37*, 786–790.
59. J. Wang, *Stripping Analysis: Principles, Instrumentation and Applications*, VCH, Deerfield Beach, 1985.
60. M. L. Gozzo, L. Colacicco, C. Calla et al., *Clin. Chim. Acta* **1999**, *285*, 53–68.
61. P. Ostapczuk, *Clin. Chem.* **1992**, *38*, 1995–2001.
62. J. Wang, B. Tian, *Anal. Chem.* **1993**, *65*, 1529–1532.
63. J. Wang, B. Tian, K. R. Rogers, *Anal. Chem.* **1998**, *70*, 1682–1685.
64. J. Wang, C. Xiaohua, G. Rivas et al., *Anal. Chim. Acta* **1996**, *326*, 141–147.
65. J. Wang, *Biosens. Bioelectron.* **1998**, *13*, 757–762.
66. E. Palecek, M. Fojta, M. Tomschik et al., *Biosens. Bioelectron.* **1998**, *13*, 621–628.
67. J. Wang, E. Palecek, P. E. Nielsen et al., *J. Am. Chem. Soc.* **1996**, *118*, 766–770.
68. J. Wang, X. Cai, G. Rivas et al., *Anal. Chem.* **1996**, *68*, 2629–2634.
69. J. Wang, G. Rivas, X. Cai et al., *Anal. Chim. Acta* **1997**, *344*, 111–118.
70. G. Marrazza, I. Chianella, M. Mascini, *Biosens. Bioelectron.* **1999**, *14*, 43–51.
71. G. Marrazza, G. Chiti, M. Mascini et al., *Clin. Chem.* **2000**, *46*, 31–37.
72. S. Ma, V. C. Yang, M. E. Meyerhoff, *Anal. Chem.* **1992**, *64*, 694–697.
73. B. Fu, E. Bakker, V. C. Yang et al., *Macromolecules* **1995**, *28*, 5834–5840.
74. J. H. Yun, V. C. Yang, M. E. Meyerhoff, *Anal. Biochem.* **1995**, *224*, 212–220.
75. L.-C. Chang, M. E. Meyerhoff, V. C. Yang, *Anal. Biochem.* **1999**, *276*, 8–12.
76. S. Dai, J. M. Esson, O. Lutze et al., *J. Pharm. Biomed. Anal.* **1999**, *19*, 1–14.
77. L. Y. Heng, E. A. H. Hall, *Anal. Chem.* **2000**, *72*, 42–51.
78. A. Uhlig, E. Lindner, C. Teutloff et al., *Anal. Chem.* **1997**, *69*, 4032–4038.
79. M. Versen, B. Klehn, U. Kunze et al., *Ultramicroscopy* **2000**, *82*, 159–163.
80. E. Lindner, R. P. Buck, *Anal. Chem.* **2000**, *72*, 336A–345A.
81. C. E. W. Hahn, *Analyst* **1998**, *123*, 57R–86R.
82. Internet addresses for these companies are: www.abbottdiagnostics.com, www.avlmed.com, www.bayerdiag.com, www.beckman.com, www.boehringer-mannheim.com, www.novabiomedical.com, and www.orthoclinical.com; a review of a recently-introduced point-of-care blood gas and electrolyte analyzer from Radiometer can

- be found in J. Lindemans, P. Hoefkens, A. L. van Kessel et al., *Clin. Chem.* **1999**, 45, 111–117.
83. B. Maas, R. Sprokholt, A. Maas et al., *Scand. J. Clin. Lab. Invest. Suppl.* **1996**, 224, 179–186.
 84. R. J. Elin, E. N. Hristova, S. A. Cecco et al., *Scand. J. Clin. Lab. Invest. Suppl.* **1996**, 224, 203–210.
 85. B. M. Altura, B. T. Altura, *Scand. J. Clin. Lab. Invest. Suppl.* **1996**, 224, 211–234.
 86. N. Mikhail, K. Ehsanipoor, *South Med. J.* **1999**, 92, 1162–1166.
 87. D. Bingham, J. Kendall, M. Clancy, *Ann. Clin. Biochem.* **1999**, 36, 66–71.
 88. J. N. Murthy, J. M. Hicks, S. J. Soldin, *Clin. Biochem.* **1997**, 30, 385–389.
 89. M. H. Gault, C. E. Harding, S. Duffett et al., *Nephron* **1998**, 80, 344–348.
 90. H. M. McConnell, J. C. Owicki, J. W. Parce et al., *Science* **1992**, 257, 1906–1912.
 91. D. Cooke, R. O’Kennedy, *Anal. Biochem.* **1999**, 274, 188–194.
 92. M. Pihlavisto, M. Scheinin, *Eur. J. Pharmacol.* **1999**, 385, 247–253.
 93. G. T. Baxter, L. J. Bousse, T. D. Dawes et al., *Clin. Chem.* **1994**, 40, 1800–1804.
 94. A. G. Gehring, D. L. Patterson, S. I. Tu, *Anal. Biochem.* **1998**, 258, 293–298.
 95. S. Nishikawa, S. Sakai, I. Karube et al., *Appl. Environ. Microbiol.* **1982**, 43, 814–818.
 96. H. P. Benetto, J. L. Stirling, K. Tanaka et al., *Biotechnol. Bioeng.* **1983**, 25, 559–568.
 97. L. C. Clark, *Trans. Am. Soc. Artif. Intern. Organs* **1956**, 2, 41–47.
 98. J. W. Severinghaus, P. B. Astrup, *J. Clin. Monitor.* **1986**, 2, 174–189.
 99. D. G. Buerk, A. G. Tsai, M. Intaglietta et al., *Microcirculation* **1998**, 5, 219–225.
 100. X. Z. Liang, Y. Zhang, C. E. Lunte, *J. Pharm. Biomed. Anal.* **1998**, 16, 1143–1152.
 101. N. Holmstroem, P. Nilsson, J. Carlsten et al., *Biosens. Bioelectron.* **1998**, 13, 1287–1295.
 102. J. Cummins, L. M. Matheson, J. F. Smyth, *J. Chromatogr.* **1990**, 528, 43–53.
 103. C. D. Forster, I. A. Macdonald, *Biomed. Chromatogr.* **1999**, 13, 209–215.
 104. C. Holmes, G. Eisenhofer, D. S. Goldstein, *J. Chromatogr., B* **1994**, 653, 131–138.
 105. P. Tuomainen, P. T. Mannisto, *Eur. J. Clin. Chem. Clin. Biochem.* **1997**, 35, 229–235.
 106. J. K. Cullison, J. Waraska, D. J. Buttaro et al., *J. Pharm. Biomed. Anal.* **1999**, 19, 253–259.
 107. J. Qian, Y. Wu, H. Yang et al., *Anal. Chem.* **1999**, 71, 4486–4492.
 108. B. B. Anderson, A. G. Ewing, *J. Pharm. Biomed. Anal.* **1999**, 19, 15–32.
 109. D. J. Michael, R. M. Wightman, *J. Pharm. Biomed. Anal.* **1999**, 19, 33–46.
 110. C. A. Aspinwall, L. Huang, J. R. T. Lakey et al., *Anal. Chem.* **1999**, 71, 5551–5556.
 111. M. Okochi, H. Yokouchi, N. Nakamura et al., *Biotechnol. Bioeng.* **1999**, 65, 480–484.
 112. L. Liaudet, F. G. Soriano, C. Szabo, *Crit. Care Med.* **2000**, 28, N37–N52.
 113. F. L. Kiechle, T. Malinski, *Am. J. Clin. Pathol.* **1993**, 100, 567–575.
 114. T. Malinski, S. Mesaros, P. Tomboulion, *Methods Enzymol.* **1996**, 268, 58–69.
 115. D. Christodoulou, S. Kudo, J. A. Cook et al., *Methods Enzymol.* **1996**, 268, 69–83.
 116. N. Villeneuve, F. Bedioui, K. Voituriez et al., *J. Pharmacol. Toxicol. Methods* **1998**, 40, 95–100.
 117. V. Brabec, *Biopolymers* **1979**, 18, 2397–2404.
 118. D. Krznavic, B. Cosovic, *Anal. Biochem.* **1986**, 156, 454–462.
 119. E. Palecek, *Anal. Biochem.* **1988**, 170, 421–431.
 120. C. Teijeiro, K. Nejedly, E. Palecek, *J. Biomol. Struct. Dyn.* **1993**, 11, 313–331.
 121. P. Singhal, W. Kuhr, *Anal. Chem.* **1997**, 69, 4828–4832.
 122. A. B. Steel, T. M. Herne, M. J. Tarlov, *Anal. Chem.* **1998**, 70, 4670–4677.
 123. J. Mbindyo, L. Zhou, Z. Zhang et al., *Anal. Chem.* **2000**, 72, 2059–2065.
 124. H.-N. Li, Y.-X. Ci, J. Feng et al., *Bioelectrochem. Bioenerg.* **1999**, 48, 171–175.
 125. R. Kohen, *J. Pharmacol. Toxicol. Methods* **1993**, 29, 185–193.
 126. T. Matsunaga, T. Nakajima, *Appl. Environ. Microbiol.* **1985**, 50, 238–242.
 127. A. E. G. Cass, G. Davis, G. D. Francis et al., *Anal. Chem.* **1984**, 56, 667–671.
 128. S. A. Jaffari, J. C. Pickup, *Biosens. Bioelectron.* **1996**, 11, 1167–1175.
 129. T. Kaku, H. I. Karan, Y. Okamoto, *Anal. Chem.* **1994**, 66, 1231–1235.
 130. M. L. Fultz, R. A. Durst, *Anal. Chim. Acta* **1982**, 140, 1–18.
 131. L. C. Clark, C. Lyons, *Ann. N.Y. Acad. Sci.* **1962**, 102, 29–45. A later version, using hydrogen peroxide oxidation, is described in (132).
 132. S. J. Updike, G. P. Hicks, *Nature* **1967**, 214, 986–988.

133. A. P. F. Turner, I. Karube, G. S. Wilson, (Eds.), *Biosensors: Fundamentals and Applications*, Oxford University Press, Oxford, 1987, pp. v–vii.
134. J. L. Anderson, L. A. Coury, J. Leddy, *Anal. Chem.* **1998**, *70*, 519R–589R.
135. J. Wang, *Anal. Chem.* **1999**, *71*, 328R–332R.
136. J. Wang, *J. Pharm. Biomed. Anal.* **1999**, *19*, 47–53.
137. E. Magner, *Analyst* **1998**, *123*, 1967–1970.
138. K. Habermueller, M. Mosback, W. Schuhmann, *Fresenius J. Anal. Chem.* **2000**, *366*, 560–568.
139. E. Palmisano, P. G. Zambonin, D. Centonze, *Fresenius J. Anal. Chem.* **2000**, *366*, 586–601.
140. S. Cosnier, *Biosens. Bioelectron.* **1999**, *14*, 443–456.
141. I. Willner, E. Katz, *Angew. Chem., Int. Ed. Engl.* **2000**, *39*, 1181–1218.
142. E. Wilkins, P. Atanasov, *Med. Eng. Phys.* **1996**, *18*, 273–288.
143. H. A. Fishman, D. R. Greenwald, R. N. Zare, *Annu. Rev. Biophys. Biomol. Struct.* **1998**, *27*, 165–198.
144. J. P. Hart, S. A. Wring, *Trends Anal. Chem.* **1997**, *16*, 89–103.
145. T. Nakaminami, S.-I. Ito, S. Kuwabata et al., *Anal. Chem.* **1999**, *71*, 1928–1934.
146. T. Nakaminami, S.-I. Ito, S. Kuwabata et al., *Anal. Chem.* **1999**, *71*, 4278–4283.
147. M. A. Hayes, W. G. Kuhr, *Anal. Chem.* **1999**, *71*, 1720–1727.
148. M. Mayer, M. Genrich, W. Kunnecke et al., *Anal. Chim. Acta* **1996**, *324*, 37–45.
149. E. I. Iwuoha, S. Joseph, Z. Zhang et al., *J. Pharm. Biomed. Anal.* **1998**, *17*, 1101–1110.
150. C. Henry, *Anal. Chem.* **1998**, *70*, 594A–598A.
151. P. Atanasov, S. Yang, C. Salehi et al., *Biosens. Bioelectron.* **1997**, *12*, 669–680.
152. W. K. Ward, J. E. Troupe, *ASAIO J.* **1999**, *45*, 555–561.
153. J. P. Lowry, M. Miele, R. D. O'Neill et al., *J. Neurosci. Methods* **1998**, *79*, 65–74.
154. Y. Hu, G. S. Wilson, *J. Neurochem.* **1997**, *68*, 1745–1752.
155. Y. Zhang, Y. Hu, G. S. Wilson et al., *Anal. Chem.* **1994**, *66*, 1183–1188.
156. R. C. Mercado, F. Moussy, *Biosens. Bioelectron.* **1998**, *13*, 133–145.
157. J. G. Wagner, D. W. Schmidtke, C. P. Quinn et al., *Proc. Natl. Acad. Sci. U.S.A.* **1998**, *95*, 6379–6382.
158. D. W. Schmidtke, A. Heller, *Anal. Chem.* **1998**, *70*, 2149–2155.
159. N. Wisniewski, F. Moussy, W. M. Reichert, *Fresenius J. Anal. Chem.* **2000**, *366*, 611–621.
160. V. Thome-Duret, M. N. Gangnerau, Y. Zhang et al., *Diabetes Metab.* **1996**, *22*, 174–178.
161. B. Aussedat, V. Thome-Duret, G. Reach et al., *Biosens. Bioelectron.* **1997**, *12*, 1061–1071.
162. J. P. Lowry, R. D. O'Neill, M. G. Boutelle et al., *J. Neurochem.* **1998**, *70*, 391–396.
163. K. Rebrin, G. M. Steil, W. P. Van Antwerp et al., *Am. J. Physiol.* **1999**, *277*, E561–E571.
164. L. I. Netchiporouk, N. F. Shram, N. Jaffrezic-Renault et al., *Anal. Chem.* **1996**, *68*, 4358–4364.
165. N. V. Kulagina, L. Shankar, A. C. Michael, *Anal. Chem.* **1999**, *71*, 5093–5100.
166. Y. Hu, G. S. Wilson, *J. Neurochem.* **1997**, *69*, 1484–1490.
167. D. Pfeiffer, B. Moeller, N. Klimes et al., *Biosens. Bioelectron.* **1997**, *12*, 539–550.
168. J. Perdomo, C. Sundermeier, H. Hinkers et al., *Biosens. Bioelectron.* **1999**, *14*, 27–32.
169. B. Harlow, D. Lane, *Antibodies: A Laboratory Manual*, Cold Spring Harbor Laboratory, Cold Spring Harbor, 1988.
170. R. Ekins, *Nature* **1989**, *340*, 256–258.
171. A. Warsinke, A. Benkert, F. W. Scheller, *Fresenius J. Anal. Chem.* **2000**, *366*, 622–634.
172. D. S. Hage, *Anal. Chem.* **1999**, *71*, 294R–304R.
173. R.-I. Stefan, J. F. K. van Staden, H. Y. Abdoul-Enein, *Fresenius J. Anal. Chem.* **2000**, *366*, 659–668.
174. M. A. Cousino, W. R. Heineman, H. B. Halsall, *Ann. Chim.* **1997**, *87*, 93–101.
175. C. J. Stanley, A. Johansson, C. H. Self, *J. Immunol. Methods* **1985**, *83*, 89–95.
176. A. Johannsson, D. H. Ellis, D. L. Bates et al., *J. Immunol. Methods* **1986**, *87*, 7–11.
177. A. L. Ghindilis, P. Atanasov, M. Wilkins et al., *Biosens. Bioelectron.* **1998**, *13*, 113–131.
178. R. Renneberg, W. Schoessler, F. Scheller, *Anal. Lett.* **1983**, *16*, 1279–1289.
179. S. H. Jenkins, H. B. Halsall, W. R. Heineman, *Anal. Biochem.* **1988**, *168*, 292–299.
180. M. W. Ducey, A. M. Smith, X. Guo et al., *Anal. Chim. Acta* **1997**, *357*, 5–12.
181. Y. Qu, L. R. Berghman, F. Vandesande, *Anal. Biochem.* **1998**, *259*, 167–175.

182. I. Abdel-Hamid, A. L. Ghindilis, P. Atanasov et al., *Anal. Lett.* **1999**, 32, 1081–1094.
183. J. Rishpon, D. Ivnitski, *Biosens. Bioelectron.* **1997**, 12, 195–204.
184. D. Ivnitski, T. Wolf, B. Solomon et al., *Bioelectrochem. Bioenerg.* **1998**, 45, 27–32.
185. J. M. F. Romero, M. Stiene, R. Kast et al., *Biosens. Bioelectron.* **1998**, 13, 1107–1115.
186. M. Santadreu, A. Alegret, L. Fabregas, *Anal. Chim. Acta* **1999**, 396, 181–188.
187. F. Wendzinski, B. Gruendig, R. Renneberg et al., *Biosens. Bioelectron.* **1997**, 12, 43–52.
188. A. F. Chetcuti, D. K. Y. Wong, M. C. Stuart, *Anal. Chem.* **1999**, 71, 4088–4094.
189. M. A. Lopez, F. Ortega, E. Dominguez et al., *J. Mol. Recognit.* **1998**, 11, 178–181.
190. G. A. Robinson, V. M. Cole, G. C. Forrest, *Biosensors* **1988**, 3, 147–160.
191. A. Benkert, F. Scheller, W. Schoessler et al., *Anal. Chem.* **2000**, 72, 916–921.
192. R. W. Keay, C. J. McNeil, *Biosens. Bioelectron.* **1998**, 13, 963–970.
193. D. Athley, C. J. McNeil, W. R. Bailey et al., *Biosens. Bioelectron.* **1993**, 8, 415–419.
194. B. Mirhabibollahi, J. L. Brooks, R. G. Kroll, *J. Appl. Bacteriol.* **1990**, 68, 577–585.
195. W. Guo, J.-F. Song, M.-R. Zhao et al., *Anal. Biochem.* **1998**, 259, 74–79.
196. J. Zhang, W. R. Heineman, H. B. Halsall, *J. Pharm. Biomed. Anal.* **1999**, 19, 145–152.
197. J. L. Brooks, B. Mirhabibollahi, R. G. Kroll, *J. Appl. Bacteriol.* **1992**, 73, 189–196.
198. C. Fernandez-Sanchez, M. B. Gonzalez-Garcia, A. Costa-Garcia, *Biosens. Bioelectron.* **2000**, 14, 917–924.
199. B. Mirhabibollahi, J. L. Brooks, R. G. Kroll, *J. Appl. Bacteriol.* **1990**, 68, 577–585.
200. A. G. Gehring, C. G. Crawford, R. S. Mazenko et al., *J. Immunol. Methods* **1996**, 195, 15–25.
201. R. S. Mazenko, F. Rieders, J. D. Brewster, *J. Microbiol. Methods* **1999**, 36, 157–165.
202. F. G. Perez, M. Mascini, I. E. Tothill et al., *Anal. Chem.* **1998**, 70, 2380–2386.
203. Y.-N. He, H.-Y. Chen, J.-J. Zheng et al., *Talanta* **1997**, 44, 823–830.
204. M. T. Carter, M. Rodriguez, A. J. Bard, *J. Am. Chem. Soc.* **1989**, 111, 8901–8911.
205. K. M. Millan, A. Spurmanis, S. R. Mikkelsen, *Electroanalysis* **1992**, 4, 929–932.
206. K. M. Millan, S. R. Mikkelsen, *Anal. Chem.* **1993**, 65, 2317–2323.
207. K. M. Millan, A. Saraullo, S. R. Mikkelsen, *Anal. Chem.* **1994**, 66, 2943–2948.
208. K. M. Millan, S. R. Mikkelsen, presented at ACS National Meeting, San Francisco, CA, April 15, 1997.
209. K. Hashimoto, K. Ito, Y. Ishimori, *Anal. Chem.* **1994**, 66, 3830–3833.
210. K. Hashimoto, K. Miwa, Y. Ishimori, *Supramol. Chem.* **1993**, 2, 265–268.
211. K. Hashimoto, K. Ito, Y. Ishimori, *Anal. Chim. Acta* **1994**, 286, 219–224.
212. M. E. Napier, C. R. Loomis, M. F. Sistare et al., *Bioconjugate Chem.* **1997**, 8, 906–913.
213. S. O. Kelley, E. M. Boon, J. K. Barton et al., *Nucleic Acids Res.* **1999**, 27, 4830–4837.
214. S. O. Kelley, J. K. Barton, *Bioconjugate Chem.* **1997**, 8, 31–37.
215. A. B. Steel, T. M. Herne, M. J. Tarlov, *Bioconjugate Chem.* **1999**, 10, 419–423.
216. A. M. Oliveira Brett, T. R. A. Macedo, D. Raimundo et al., *Biosens. Bioelectron.* **1998**, 13, 861–867.
217. S. R. Mikkelsen, *Electroanalysis* **1996**, 8, 15–19.
218. M. E. Tess, J. A. Cox, *J. Pharm. Biomed. Anal.* **1999**, 19, 55–68.
219. H. Mkuguruma, I. Karube, *Trends Anal. Chem.* **1999**, 18, 62–68.
220. F. Cespedes, S. Alegret, *Trends Anal. Chem.* **2000**, 19, 276–285.
221. F. Cespedes, E. Martinez-Fabregas, S. Alegret, *Trends Anal. Chem.* **1996**, 15, 296–304.
222. T. Takeuchi, J. Haginaka, *J. Chromatogr., B* **1999**, 728, 1–20.
223. K. Yano, I. Karube, *Trends Anal. Chem.* **1999**, 18, 199–204.
224. J. J. Gooding, D. B. Hibbert, *Trends Anal. Chem.* **1999**, 18, 525–533.
225. S. E. Rosenwald, N. Dontha, W. G. Kuhr, *Anal. Chem.* **1998**, 70, 1133–1140.
226. N. Dontha, W. B. Nowall, W. G. Kuhr, *J. Pharm. Biomed. Anal.* **1999**, 19, 83–91.
227. Y. Ding, L. Zhou, H. B. Halsall et al., *J. Pharm. Biomed. Anal.* **1999**, 19, 153–161.
228. C. A. Wijayawardhana, G. Wittstock, H. B. Halsall et al., *Anal. Chem.* **2000**, 72, 333–338.
229. J. T. Santini, M. J. Cima, R. Langer, *Nature* **1999**, 397, 335–338.
230. J. Kong, N. R. Franklin, C. Zhou et al., *Science* **2000**, 287, 622–625.
231. The internet address for Yellow Springs Instruments is www.ysi.com.
232. The marketing firm of Frost & Sullivan, San Jose, CA performed this research and published it on their website, www.frost.com.

233. M. E. Collison, P. J. Stout, T. S. Glushko et al., *Clin. Chem.* **1999**, 45, 1665–1673.
234. A. G. Glasmacher, W. Brennemann, C. Hahn et al., *Exp. Clin. Endocrinol. Diabetes* **1998**, 106, 360–364.
235. G. J. Kost, H.-T. Vu, J. H. Lee et al., *Crit. Care Med.* **1998**, 26, 581–590.
236. Internet addresses for Analox Instruments and Arkray Inc. are www.analox.com and www.arkray.co.jp. See also N. Shimojo, K. Naka, H. Uenoyama et al., *Clin. Chem.* **1993**, 39, 2312–2314, for a description of the Lactate Pro.
237. The internet address for Applied Medical Technology Co. is www.minimed.com. See also J. J. Mastrototaro, *J. Pediatr. Endocrinol. Metab.* **1999**, 12 (Suppl. 3), 751–758.
238. The internet address for Synthetic Blood International is www.sybd.com.
239. The internet addresses for Clinical Microsensors and Xanthon are www.microsensor.com and www.xanthoninc.com.
240. E. K. Wilson, *Chem. Eng. News* **1998**, 76, 47–49.
241. M. Wojciechowski, R. Sundseth, M. Moreno et al., *Clin. Chem.* **1999**, 45, 1690–1693.
242. G. A. Junter, in *Electrochemical Detection Techniques in the Applied Biosciences*, Vol. 1, (Ed.: G. A. Junter), Ellis Horwood, Chichester, 1988, pp. 139–156.
243. M. Wawerla, A. Stolle, B. Schalch et al., *J. Food Prot.* **1999**, 62, 1488–1496.
244. P. A. Noble, *J. Microbiol. Methods* **1999**, 37, 45–49.
245. K. O. Colquhoun, S. Timms, C. R. Fricher, *J. Appl. Bacteriol.* **1995**, 79, 635–639.
246. C. J. Felice, R. E. Madrid, J. M. Olivera et al., *J. Microbiol. Methods* **1999**, 35, 37–42.
247. A. H. Huang, J. J. Wu, Y. M. Weng et al., *J. Clin. Microbiol.* **1998**, 36, 2882–2886.
248. K. Asami, T. Yonezawa, H. Wakamatsu et al., *Bioelectrochem. Bioenerg.* **1996**, 40, 141–145.
249. A. M. Woodward, A. Jones, X.-Z. Zhang et al., *Bioelectrochem. Bioenerg.* **1996**, 40, 99–132.
250. C. Ziegler, *Fresenius J. Anal. Chem.* **2000**, 366, 552–559.
251. C. Ziegler, W. Goepel, H. Haemmerle et al., *Biosens. Bioelectron.* **1998**, 13, 539–571.
252. A. M. N. Hendji, N. Jaffrezic-Renault, C. Martelet et al., *Sens. Actuators, B* **1994**, 21, 123–129.
253. P. Darbon, V. Michel, F. Math et al., *Anal. Chem.* **1998**, 70, 5072–5078.
254. E. Souteyrand, J. R. Martin, C. Martelet, *Sens. Actuators, B* **1994**, 20, 63–69.
255. E. Souteyrand, J. P. Cloarec, J. R. Martin et al., *J. Phys. Chem. B* **1997**, 101, 2980–2985.
256. M. Knichel, P. Heiduschka, W. Beck et al., *Sens. Actuators, B* **1995**, 28, 85–94.
257. N. F. Sheppard, M. J. Lesho, P. McNally et al., *Sens. Actuators, B* **1995**, 28, 95–102.
258. C. J. McNeil, D. Athey, M. Ball et al., *Anal. Chem.* **1995**, 67, 3928–3935.
259. W. O. Ho, S. Krause, C. J. McNeil et al., *Anal. Chem.* **1999**, 71, 1940–1946.
260. J. Hurst, K. Nickel, L. H. Hilborne, *J. Am. Med. Assoc.* **1998**, 279, 468–471.
261. E. Pearson, A. Gill, P. Vadgama, *Ann. Clin. Biochem.* **2000**, 37, 119–145.
262. I. Poels, S. Picioreanu, L. J. Nagels et al., *Biomed. Chromatogr.* **2000**, 14, 30–31.

11 Interfacial Properties of Proteins/Spectroelectrochemical Studies

Katsumi Niki
Illinois State University, Normal, Illinois

11.1	Introduction	343
11.2	Methodologies	344
11.2.1	Surface-enhanced Resonance Raman Scattering Spectroscopy	344
11.2.2	Electroreflectance (Potential-Modulated UV-vis Reflectance) Spectroscopy	345
11.2.3	Infrared Reflection Absorption Spectroscopy	346
11.2.4	Absorption Linear Dichroism and Total Internal Reflection Fluorescence Spectroscopies	346
11.3	Redox Behavior of Heme- and Flavoproteins at Unmodified Electrode Surfaces	346
11.3.1	Gold Electrode	346
11.3.1.1	Cytochrome <i>c</i>	346
11.3.1.2	Cytochrome <i>c</i> ₃	347
11.3.2	Silver Electrode	347
11.3.2.1	Cytochrome <i>c</i>	347
11.3.2.2	Cytochrome <i>c</i> ₃	350
11.3.2.3	Cytochrome <i>c</i> ₅₅₂ (<i>Thermus thermophilus</i>)	351
11.3.2.4	Cytochrome <i>b</i> ₅ and Hemoglobin	351
11.3.2.5	Myoglobin	352
11.3.2.6	Flavoproteins	352
11.3.2.7	Cytochrome P-450	353
11.4	Electrode Reaction of Electron Transfer Proteins at Modified Electrodes	353
11.4.1	Cytochrome <i>c</i> at Pyridine Derivative-modified Electrodes	354
11.4.1.1	ER Spectroscopic Studies	354
11.4.1.2	SERRS Studies	356
11.4.1.3	Stability of Bis-(4pyridyl) Disulfide and 4-Mercaptopyridine at Gold Electrodes	357

11.4.2	Cytochrome <i>c</i> at ω -Functional Alkanethiol Modified Electrodes	357
11.4.3	Cytochrome <i>c</i> at Iodine-modified Electrodes	358
11.4.4	Cytochrome <i>c</i> ₃ at 4,4'-Bipyridyl and Carboxylic Acid-terminated Alkanethiol Modified Electrodes	358
11.4.5	Proteins Cast in Lipid Bilayer	359
11.5	Molecular Orientation of Proteins on Solid Substrates. Cytochrome <i>c</i> Immobilized on Self-assembled Monolayers	359
11.5.1	IRRAS Studies	359
11.5.2	Conformation of Cytochrome <i>c</i> on Carboxylic Acid-terminated SAM	359
11.6	Electron Transfer Kinetics of Electron Transfer Proteins at Electrode Surfaces	360
11.6.1	Electron Transfer Kinetics of Cytochrome <i>c</i> at Carboxylic Acid-terminated Alkanethiol SAM	360
11.6.2	Electron Transfer Kinetics of Cytochromes <i>c</i> and <i>c</i> ₅₅₂ at Silver Electrode	361
11.6.3	Electron Transfer Kinetics of Azurin at Methyl-terminated Alkanethiol Self-assembled Monolayers	362
	Recent review article related to this chapter	362
	References	362

11.1 Introduction

It is well known that there are electrostatic interactions between redox proteins in the physiological electron transfer (ET) chains. The initial step in the formation of a protein complex is a nonspecific association between two proteins, followed by a rotational diffusion on the molecular surface to reach a proper configuration for the ET reaction. Details of the molecular structure of such complexes and intermolecular ET reactions have not been fully understood by using physiological redox complexes because of the complexity of biological systems.

In electrochemical systems, on the other hand, electrodes act as both electron acceptors and electron donors, and are considered a simple model system for mimicking a charged interface of the physiological binding domain. The heterogeneous ET reactions between electrodes and various ET proteins in solutions have been extensively studied, as described in previous chapters. The electrode reactions of cytochrome *c* at mercury, platinum, silver, and gold electrodes have been reported to be irreversible. On the other hand, the electrode reactions of cytochromes *c*₃ (cyt. *c*₃) have

been found to exhibit a reversible electrode reaction at both mercury and solid electrodes without surface modifiers. The addition of 4,4'-bipyridyl leads to a reversible voltammetric behavior of horse cytochrome *c* (cyt. *c*: hereafter cyt. *c* represents horse heart cytochrome *c* unless otherwise stated) on gold and platinum electrodes. Since then, numerous surface modifiers that facilitate direct electrochemistry of various ET proteins have been proposed.

In this chapter, electrochemical properties of ET proteins at electrode interfaces studied by spectroelectrochemical techniques are described. In situ spectroelectrochemical techniques at well-defined electrode surfaces are sufficiently selective and sensitive to distinguish not only steady state structures and oxidation states of adsorbed species but also dynamics of reactants, products, and intermediates at electrode surfaces on a monolayer level. The spectroelectrochemical techniques used in studies of ET proteins include IR reflection-absorption, potential-modulated UV-vis reflectance (electroreflectance), surface-enhanced Raman scattering (SERS) and surface plasmon resonance, total internal reflection fluorescence, (TIRF) and absorbance linear dichroism spectroscopies.

11.2

Methodologies

Detailed account of experimental setups for spectroelectrochemistry can be found elsewhere. A brief summary is provided in this chapter.

11.2.1

Surface-enhanced Resonance Raman Scattering Spectroscopy

The technique of SERS spectroscopy is based on the enhancement of Raman signals for those species adsorbed on sub-microscopically roughened noble metal electrodes or colloids (particularly silver, gold and copper). The interaction of adsorbates with the metal surfaces results in a large enhancement of the Raman scattering cross section. The enhancement factor compared to the dissolved molecules can be up to six orders of magnitude. If the excitation line is in resonance with an electronic transition of the adsorbed molecules, the molecular resonance Raman and the surface-enhanced Raman effects can combine and sensitivity is further increased. The SERS observed under the resonance condition is called the surface-enhanced resonance Raman scattering (SERRS). The enhancements of vibrational signals of chromophores make resonance Raman attractive as a method of selective analysis of the chromophore within a peptide matrix on a monolayer or submonolayer level. In the cases of biological molecules, the advantages of high sensitivity and quenching of fluorescence by the metal surface are attractive. In addition, the small scattering cross section of water allows the observation of SERS (SERRS) of the adsorbates in aqueous solutions.

Cotton and coworkers were the first to demonstrate that SERS and SERRS

spectroscopies are applicable to obtaining structural-functional information on biological macromolecules (cyt. *c* and myoglobin, Mb) adsorbed on a silver electrode [1]. In the case of cyt. *c* adsorbed on the silver electrode, strong Raman bands originating from the heme chromophore were observed when the adsorbed cyt. *c* was irradiated by a laser excitation wavelength in the vicinity of the electronic transition energy in cyt. *c* [the Soret band (B band) at 410 nm, for both ferro- and ferri-forms and Q bands (α - and β -bands) at 550 nm and 520 nm for the ferro-form], whereas the Raman bands originating from the protein matrix remained too weak to be detected in the resonance Raman scattering (RRS) signals [2–5].

Argon ion (514.5, 488.0, 476.5, 496.5 nm), krypton ion (674.1, 530.9, 568.2 nm) and tunable dye lasers have commonly been used as excitation energy sources. The SERS spectra from gold electrodes are only obtainable with excitation energies smaller than 570 nm. The Raman scattering spectra are typically detected in one of two modes: A photodiode array or CCD camera enables us to measure a large frequency range in a short time, but generally lacks the spectral resolution required for detailed analysis [6]. A monochromatic detection (double monochromator and photon-counting system) is time-consuming to use because it requires scanning over the frequency range of interest. However, it offers much better resolution and can be easily extended to dual-channel Raman difference spectroscopy [7]. Degradation of cyt. *c* caused by a prolonged exposure to laser irradiation is prevented by using a rotating electrode, but photoreduction of ferri-cyt. *c* has been observed in some cases [8].

The retention of native conformations is confirmed by the comparison of SERRS

of the adsorbed species with RRS of the solution species and of the redox potentials in adsorbed with solution state [7, 9–18] or the enzymatic activity of the adsorbed species [19, 20].

11.2.2

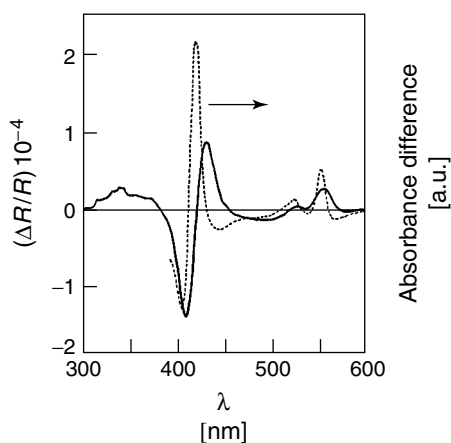
Electroreflectance (Potential-Modulated UV-vis Reflectance) Spectroscopy

Potential-modulated UV-vis reflectance spectroscopy, often referred to as electroreflectance (ER), was originally developed in solid-state physics to characterize surfaces and was applied to studies of the electronic band structure of semiconductors. The ER technique has also been used to characterize metal electrode surfaces in the absence and presence of adsorbates. The reflectivity of metal electrodes is a function of the surface charge density of the electrodes. ER technique has also been used to investigate electrode reactions of organic species adsorbed on the electrode surfaces. Several review articles on ER are available [21–24].

Hinnen and coworkers first applied the ER technique to elucidate the electrode reaction mechanism (formal potentials

of adsorbed species) of cyt. *c* and cyt. *c*₃ adsorbed on a gold electrode [25]. Sagara and coworkers [26] and Feng and coworkers [27] showed that the ER technique enabled one to measure the ET rates of the adsorbed species at electrode surfaces up to 10^4 s^{-1} , whereas traditional electrochemical techniques only enabled one to measure the ET rates up to several hundreds times per second. In the ER measurements, the electrode surface is covered by the adsorbed layer (monolayer or submonolayer coverage) of electrochemically active species, which undergoes a reversible (rapid) redox reaction and is regarded as a mirror in the wavelength range of interest. When the electrode potential is modulated by an ac potential in the vicinity of the formal potential of the adsorbed species, the spectrum of the reflected light (ER spectrum) corresponds to the difference spectrum between the oxidized and reduced forms of the adsorbed species [24, 26]. Figure 1 shows the ER spectrum of the cyt. *c*₃ adsorbed on the gold electrode in 30-mM phosphate solution at pH 7.0. The structure of the ER spectrum accords with the difference spectrum of cyt. *c*₃ in the solution (broken line).

Fig. 1 ER spectrum of cyt. *c*₃ adsorbed on gold electrode at its formal potential in 30-mM phosphate buffer solution at pH 7.0. $\Delta E_{ac} = 70 \text{ mV}$, $\omega = 90 \text{ s}^{-1}$. The broken line represents the difference spectrum of cyt. *c*₃ in solution phase. (This is not always true. The ER spectrum of dye molecules directly adsorbed on electrode surfaces is different from the difference spectrum of the solution species, but the signal intensities against electrode potential are Nernstian [27]).



When the electrode potential is scanned at the maximum of the ER spectrum ($\lambda = 420$ nm), an ER voltammogram is obtained with the peak at its formal potential. The ET rates of the adsorbed species can be calculated from the modulation frequency dependence of the peak heights (real and imaginary parts) [28].

11.2.3

Infrared Reflection Absorption Spectroscopy

The polarization-modulation Infrared Reflection Absorption Spectroscopy (IRRAS) technique at a high-incident angle of the parallel polarized IR beam is used to investigate the structures of cyt. *c* and surface modifiers at electrode interfaces. The electrical double-layer structure of the gold electrode covered by cyt. *c* with a surface modifier at the monolayer level remains the same when the electrode is emersed from the electrolyte solution at controlled potential. In *ex situ* IRRAS measurements, an interference by electrolytes at the emersed electrode can be minimized. Monolayers of adsorbates with a dipole moment perpendicular to the electrode surface can absorb on the order of 10^3 of the *p*-polarized IR radiation at high angles of incidence. The interaction of the adsorbate with the *s*-polarized IR radiation, on the other hand, is negligibly small. Thus, the absorption of radiation by the adsorbate at the electrode surface can be detected by measuring the intensity of the reflected *p*-polarized light with respect to the reflected *s*-polarized light (measuring intensities of the reflected *p*- and *s*-polarized components alternatively by using the polarization-modulation technique) [29].

11.2.4

Absorption Linear Dichroism and Total Internal Reflection Fluorescence Spectroscopies

It has been known that the configuration of protein layers at synthetic membranes such as self-assembled monolayers (SAM) at electrode surfaces play a crucial role in the ET characteristics at protein/membrane interfaces and biological functions of the protein molecules. Differences in molecular orientation give rise to differences in ET activities and biofunction of the protein layers. Saavedra and his coworkers reported a method for determining the dipole orientation distribution of molecules in a thin film using a combination of two techniques: absorption linear dichroism measured in a planar integrated optical waveguide-attenuated total reflection (IOW-ATR) geometry, and emission anisotropy, measured in a TIRF geometry [30, 31].

11.3

Redox Behavior of Heme- and Flavoproteins at Unmodified Electrode Surfaces

11.3.1

Gold Electrode

11.3.1.1 Cytochrome *c*

Cytochrome *c* in the solution often exhibits an irreversible voltammetric response at gold electrodes, with the exception of a carefully prepared gold electrode [32]. A strong adsorption of cyt. *c* on an electrode surface is considered to block the ET reaction of cyt. *c* in the solution. Hinnen and coworkers, and Hinnen and Niki measured the formal potential of horse heart cyt. *c* adsorbed on gold, ruthenium, and glassy carbon electrodes by

ER voltammograms and found that the formal potentials are around -0.25 V versus NHE (normal hydrogen electrode) in 20-mM KClO_4 , which depend on the supporting electrolyte but nearly independent of the electrode materials [25, 33]. The formal potential of horse heart cyt. *c* adsorbed on a polycrystalline gold electrode is estimated from the peak potential of the ER voltammogram to be -0.18 V in 30 mM phosphate buffer at pH 7.0, which is 0.44 V more negative than that of the native one [34]. It is interesting to note that cyt. *c* adsorbed directly on the gold electrode takes part in a reversible (rapid) ET process at its formal potential. The voltammetric reduction peak of cyt. *c* in the solution at the gold electrode agrees with the formal potential of the adsorbed cyt. *c*, but no reoxidation peak is observed [33]. The oxidation potential of the adsorbed ferro-cyt. *c* is so negative that it cannot mediate the reoxidation of ferro-cyt. *c* in the solution. The shift of the formal potential is probably due to an unfolding of the protein structure of cyt. *c* upon the adsorption on the gold electrode surface.

11.3.1.2 Cytochrome c_3

Cytochromes c_3 are C-type tetra hemeproteins isolated from the respiratory chain of sulfate reducing bacteria, *Desulfovibrio*, which contain about 110 amino acid residues in the molecule and their molecular weights range 13 to 14 kD. This class of proteins is distinguished from other C-type cytochromes by their unique structure and redox properties. The fifth and sixth axial ligands are imidazoles of the histidine residue and the hemes are covalently bound to a single peptide through thioether linkages. The formal potentials of four hemes in cyt. c_3 are closely spaced (spread in the range of 100–200 mV) and their average is about 0.5 V more negative

than that of mitochondrial cyt. *c* [35]. The formal potential of cyt. c_3 from *D. vulgaris*, Miyazaki strain, adsorbed on a polycrystalline gold electrode is determined to be -0.26 V versus NHE, which is practically the same as that of the native species [25]. The adsorbed cyt. c_3 mediates the ET reaction of cyt. c_3 in the solution, which can take place in a direct electrode reaction without ET mediators or surface modifiers.

11.3.2

Silver Electrode

11.3.2.1 Cytochrome *c*

Cotton and coworkers first reported that the surface-bounded horse heart cyt. *c* is reoxidized at 0.04 V versus NHE by SERRS measurements [1], which has a 0.22 V more negative potential than the formal potential of the native one [37]. Niki and coworkers showed from SERRS measurements that the formal potential of cyt. *c* adsorbed on a silver electrode is -0.05 V [38]. Hildebrandt and Stockburger have extensively studied the conformation and redox properties of horse heart cyt. *c* adsorbed on a silver electrode by using the SERRS technique [7, 9, 39–42]. Cytochrome *c* exhibits various conformational states upon adsorption on the silver electrode [39–42]. The RRS of ferro- (cyt. c^{2+}) and ferri-cyt. *c* (cyt. c^{3+}) in an aqueous solution at pH 7.0 and SERRS of cyt. c^{2+} and cyt. c^{3+} adsorbed on the silver electrode at -0.16 V versus NHE, and SERRS of cyt. c^{2+} and cyt. c^{3+} adsorbed on the silver electrode at 0.34 V are shown in Fig. 2 [41, 42].

Most of the SERRS bands are well correlated with the RRS bands obtained in an aqueous solution, in which cyt. *c* is present in the six-coordinate low spin (6cLS) configuration and the axial ligands are methionine and histidine in the native state. The marker bands ν_4 at 1360 cm^{-1}

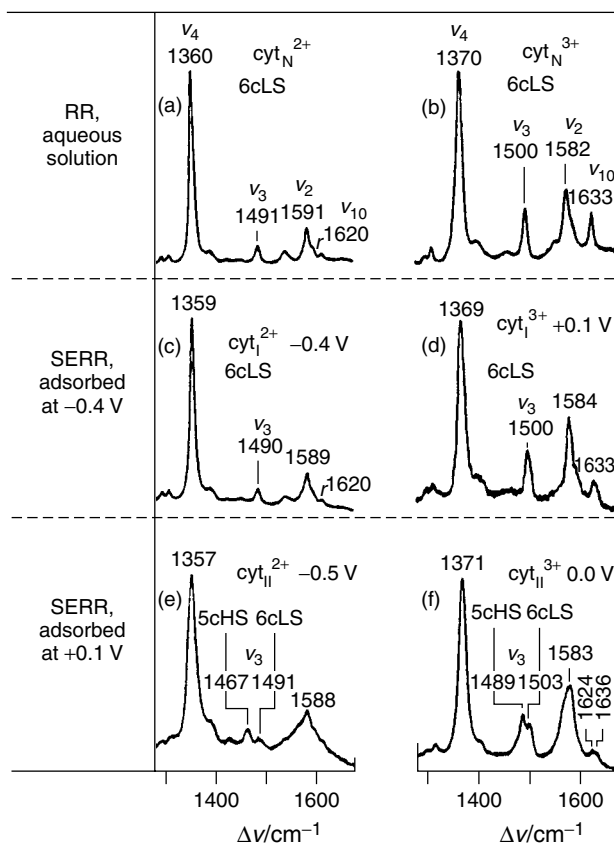


Fig. 2 RRS and SERRS spectra of cyt. *c* excited at 413 nm. (a) RRS of native cyt. c^{2+} in aq. solution. (b) RRS of native cyt. c^{3+} in aq. solution. (c) SERRS of cyt. c^{2+} measured at -0.4 V after adsorption at -0.4 V. (d) SERRS of cyt. c^{3+} measured at $+0.1$ V after adsorption at -0.4 V. (e) SERRS of cyt. c^{2+} measured at -0.5 V after adsorption at $+0.1$ V. (f) SERRS of cyt. c^{3+} measured at 0.0 V after adsorption at $+0.1$ V. The cyt. c_{II}^{3+} and cyt. c_I^{2+} contributions are subtracted from (d) and (e), respectively. Electrolyte: (0.05 M Na_2SO_4 , 0.05 M tris/cacodylic acid buffer at pH 7.0. Electrode potentials are given against saturated calomel electrode, which is 0.244 V versus NHE. (P. Hildebrandt, M. Stockburger, *Biochemistry*, **1989**, 28, 6710–6721, Fig. 2 in page 6712.)

(cyt. c^{2+}) and 1370 cm^{-1} (cyt. c^{3+}) or v_3 at 1491 cm^{-1} (cyt. c^{2+}) and 1500 cm^{-1} (cyt. c^{3+}) in Figs. 2(a) and (b) are the 6cLS configuration. The SERRS spectrum shown Fig. 2(c) was obtained from cyt. *c* adsorbed on the silver electrode at -0.16 V

and is very similar to the RRS spectrum of cyt. c^{2+} . When the electrode potential is shifted from -0.16 V to 0.34 V, the observed SERRS spectrum (Fig. 2d) is very similar to cyt. c^{3+} of the 6cLS state. However, the SERRS spectrum at 0.34 V

is time-dependent and the spectrum becomes essentially the same as that shown in Fig. 2(f) after about two hours. An adsorption-induced partial transformation from the 6cLS state to the five-coordinate high spin state (5cHS) is observed. The SERRS spectra of cyt. *c* on the silver electrode adsorbed at 0.34 V are shown in Figs. 2(e) and (f). The spin-state marker bands observed at 0.24 V appear as doublets (mixtures of the 6cLS and 5cHS states), for example, ν_3 at 1489 cm^{-1} (5cHS) and 1503 cm^{-1} (6cLS) or ν_{10} at 1624 cm^{-1} (5cHS) and 1636 cm^{-1} (6cLS) for cyt. c^{3+} [43]. When the electrode potential is shifted from 0.24 V to -0.26 V , cyt. c^{3+} is reduced to cyt. c^{2+} and the ν_3 bands are observed at 1467 cm^{-1} (5cHS) and 1491 cm^{-1} (6cLS), respectively, and the SERRS spectrum shown in Fig. 2(e) approaches that shown in Fig. 2(c) (6cLS state) after several hours. [41].

Hildebrandt and Stockburger found that there are two conformational states of cyt. *c* upon adsorption on a silver electrode [38–40]. Cytochrome *c* adsorbed on the silver electrode at negative potentials ($<0.04\text{ V}$) exhibits the state I (cyt. c_I) conformation and that adsorbed at positive electrode potentials ($>0.04\text{ V}$) exhibits the state II (cyt. c_{II}) conformation. The structure of the RR spectrum of cyt. *c* in the solution is fully maintained in the state I, which must be the same for the whole cyt. *c* molecules. In the state II, the spin state of the heme iron is in the mixed 5cHS and 6cLS conformation. The conformational states I and II are at potential-dependent equilibrium. The most stable species of ferro-cyt. *c* is the reduced form of state I (cyt. c_I^{2+}) in the electrode potential range, more negative than 0.2 V and that of ferri-cyt. *c* is the oxidized form of state II (cyt. c_{II}^{3+}) in the electrode potential range more positive

than 0.2 V . The stability of cyt. c_{II} depends on the composition and concentration of the supporting electrolyte. When the electrode potential is maintained at more negative potentials than -0.34 V , both cyt. c_I^{2+} and cyt. c_{II}^{2+} are considerably irreversibly denatured (cannot be reoxidized reversibly). The formal potential of cyt. $c_I^{2+/3+}$ is estimated to be 0.25 V , which is close to that of the native value in solution. On the other hand, the formal potentials of cyt. $c_{II}^{2+/3+}$ (5cHS) and cyt. $c_{II}^{2+/3+}$ (6cLS) are estimated to be -0.07 , which agrees with the results obtained by Niki and coworkers [11, 38], and -0.17 V , respectively. At potentials more positive than the point of zero charge (pzc) of the silver electrode (-0.41 V versus NHE) [44], the surface charge density in the double layer is negative in sign (more anions than cations) and a rapid change from the state I to II (denaturation or unfolding) is noted. These equilibria strongly depend on the properties of anions and the charge distribution at the silver electrode/electrolyte interface, suggesting that the changes in the structure of the heme moiety is induced by the electrostatic interactions between the electrode and cyt. *c*. At more positive potentials than the pzc, the interaction between the silver electrode and lysine residues of cyt. *c* may be weak because of the ionic association of excess anions in the double layer and the lysine residues. The overall reaction scheme of the potential induced transformation of cyt. *c* adsorbed on the silver electrode is shown in Fig. 3 [41].

In the state II, the axial Met-Fe bond is weakened, leading to a thermal equilibrium between the 6cLS and 5cHS configurations. These structural changes are induced by the electrostatic interactions between the basic protein and charged electrode surfaces. It was also

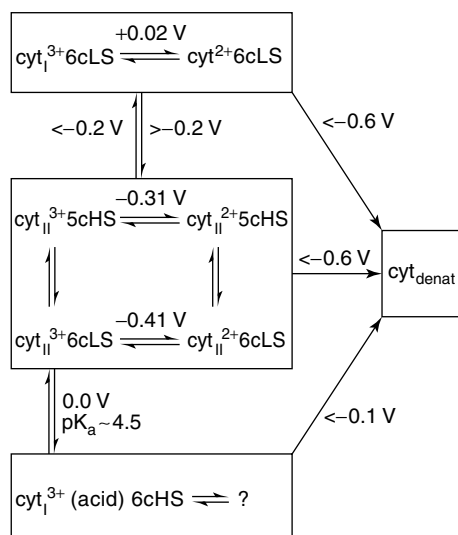


Fig. 3 Overall reaction scheme of the potential induced transformation of cyt. *c* adsorbed on silver electrode. Electrode potentials are given against saturated calomel electrode, which is 0.244 V versus NHE. (P. Hildebrandt, M. Stockburger, *Biochemistry*, **1989**, 28, 6710–6721, Fig. 15 in page 6719.)

demonstrated that similar conformational transition may occur at charged surfaces other than the electrode surface [7]. The docking of cyt. *c* onto the negatively charged binding domains of cyt. oxidase and cyt. reductase induces the formation of the conformational states I and II.

11.3.2.2 Cytochrome *c*₃

Niki and coworkers studied the redox properties of cyt. *c*₃ from *Desulfovibrio vulgaris*, Miyazaki and Hildenborough strains, and *Desulfovibrio desulfuricans*, Norway strain, adsorbed on a silver electrode by the SERRS technique [11]. The average formal potential of the hemes in cyts. *c*₃ adsorbed on a silver electrode is determined by voltammetric measurements and is nearly the same as that in the native state. On the other hand, the redox potentials of the adsorbed cyts. *c*₃ monitored by the shift of the oxidation state marker band of SERRS are about 100 mV more positive than those measured by voltammetry. The redox transition of the oxidation state marker

band takes place in the vicinity of the formal potential of the most positive redox site among the four hemes. This is probably due to the fact that cyts. *c*₃ are specifically adsorbed on the silver electrode through the lysine residues with the most positive formal potential surrounding the heme. The heme located closest to the electrode is only responsive to the excitation wavelength of 514.5 nm and the enhancement diminishes rapidly with distance from the electrode surface. In addition, the bonds that align in parallel with the surface field are selectively enhanced relative to the vibrations that are perpendicular to the surface field. Verma and coworkers demonstrated that cyt. *c*₃ from *D. vulgaris*, Miyazaki, adsorbed on a silver colloid (citrate-reduced) could be reduced by hydrogen in the presence of hydrogenase, physiological redox partner of cyt. *c*₃ [19]. These results showed that the enzymatic activity of cyt. *c*₃ is preserved even in its adsorbed state on a citrate-reduced silver colloid. An adsorption-induced partial transformation from the low-spin (LS) to the high-spin (HS) state is observed on the silver colloid. Eng and coworkers studied RRS and SERRS of cyt. *c*₃ isolated from *D. desulfuricans* [46]. A comparison of the protein in a solution with that on a silver colloid (citrate-reduced) shows that the native structure of cyt. *c*₃ is retained at the SERRS-active substrate. No indication of the HS state of the adsorbed cyt. *c*₃ was observed. The

difference between two research groups is probably due to the difference either in preparation of the silver colloid or in the cytochrome strain [19, 46].

Hobara and coworkers reported that the conformation of ferri-cyt. c_3 (*D. desulfuricans*, Norway strain) changes upon adsorption on a bare silver electrode from the 6cLS to the mixed 5cHS and 6cLS state [47]. The fraction of the 5cHS state increases upon reduction to the ferro-form. The change in the spin state between the ferri- and ferro-cyt. c_3 is reversible. The formal potentials of cyt. c_3 adsorbed on the bare silver electrode was monitored by the shift of the oxidation state marker band and is -0.12 V in the forward scan (reduction) and -0.07 V versus NHE in the reverse scan (reoxidation). These results are consistent with the formal potential of the heme in cyt. c_3 with the most positive potential, which is closest to the silver electrode surface and is therefore subject to the largest enhancement. The ER voltammogram of cyt. c_3 adsorbed directly on the bare silver electrode surface exhibits significant hysteresis and a low voltammetric signal on the reverse scan, probably because of a slow reorganization of the heme moiety of the adsorbed cyt. c_3 .

11.3.2.3 Cytochrome c_{552} (*Thermus thermophilus*)

The potential-dependent processes of the ET heme protein cyt. c_{552} from *Thermus thermophilus* adsorbed on a silver electrode is studied by using SERRS [48]. In the reduced state at -0.16 V versus NHE, the SERRS spectrum of cyt. c_{552} is very similar to the RRS spectrum in the solution, suggesting that the adsorbed cyt. c_{552} retains its native structure in the 6cLS state. When the electrode potential is changed from -0.16 to 0.24 V, the adsorbed cyt. c_{552} is oxidized to the

ferri-form and exists in the mixed 5cHS and 6cLS state, which is different from that of the ferri-form in the solution. When the adsorbed cyt. c_{552} is rereduced to the ferro-form at -0.16 V, no evidence for the formation of the HS state, that is, the conformational state of the adsorbed cyt. c_{552} , is reversible. The formal potential of the adsorbed cyt. c_{552} is determined by monitoring the intensity of SERRS signals to be 0.144 V for cyt. $c_{552}^{2+/3+}$ (6cLS), which is a little more negative than the value of the solution species (0.228 V) [49]. The discrepancy in the formal potentials between the native and adsorbed cyt. c_{552} and a non-Nernstian behavior of the adsorbed cyt. c_{552} can be attributed to the coupling of the ET reaction and conformational transitions.

11.3.2.4 Cytochrome b_5 and Hemoglobin

SERS spectra of cyt. b_5 and of oxyhemoglobin (HbO_2) adsorbed on a silver colloid (borohydride reduced) showed distinct changes relative to the solution RRS [50]. The reduced form of these proteins showed SERRS spectra similar to the solution RRS spectra, although some conversion to Fe^{III} was generally observed. In the case of deoxy Hb, the Fe-imidazole stretching band appears to shift from 215 to 200 cm^{-1} in the SERRS spectrum, suggesting some perturbation of the heme-protein linkage. These results indicate that the heme attraction to the silver surface is facilitated under an oxidizing condition, perhaps via increased surface charge on the silver surface.

De Groot and Hester demonstrated that the SERRS spectrum of oxyhemoglobin (HbO_2) gives no indication of the presence of the HS component (no μ -oxo dimer is present on the silver surface) on silver colloids (citrate-reduced) [51], in contrast to the results of Smulevich and

Spiro (on the borohydride reduced silver colloids) [50]. The presence of only LS heme strongly supports a retention of the native state on the silver surface. De Groot and coworkers demonstrated that the SERRS spectrum of hemoglobin (Hb) retains its native state on the citrate-reduced silver colloids and concluded that the difference between the two groups is due to the preparation of silver colloids [20].

11.3.2.5 Myoglobin

Commercially available Mb does not show well-defined cyclic voltammograms at any electrode. However, purified samples of both horse heart and sperm whale met-myoglobins have been found to show stable redox waves at a highly hydrophilic surface of In_2O_3 electrodes [52, 53].

Mb adsorbed on silver colloids (borohydride reduced) showed the same SERS characteristics as those of Hb. Met-aquo Mb showed facile μ -oxo dimer formation, whereas deoxy Mb did not, but its Fe-imidazole stretching band was lowered to 200 cm^{-1} , as in the case of deoxy Hb [50]. The correspondence between SERRS of the adsorbed Mb (whale) and RRS of the solution Mb for both oxidized and reduced forms is best if the values for the LS state Mb are used in the comparison [1]. However, Mb in solution is present in the HS aquamet Fe(III) state, which suggests that Mb undergoes a change in spin state upon adsorption on a silver electrode. Another possibility is that Mb retains its HS state but the frequencies are shifted because of a direct interaction of the heme group with the electrode. It is likely that the reduction of Fe(III) to Fe(II) occurs at -0.36 V versus NHE for Mb adsorbed on the silver electrode followed by its reoxidation at 0.04 V , suggesting that the formal potential of the adsorbed Mb on the silver

electrode is shifted toward a more negative potential than the formal potential of the solution Mb at $E^{\circ'}(\text{Mb}^{2+/3+}) = 0.055 \pm 0.003\text{ V}$ [50, 51]. The possibility of a loss of the heme or protein denaturation appears more probable in the case of Mb.

11.3.2.6 Flavoproteins

It was shown that there is one-to-one correspondence of all bands of SERS at silver colloids (borohydride reduced) and RRS in solution of a riboflavin-binding proteins, several of which show the same frequency and relative intensity in the two spectra [54]. The SERS spectra of riboflavin-binding proteins and glucose oxidase (GO_x) show very similar features but differ significantly from the RRS spectrum of the Ag^+ -complexed flavin. It was shown that the activity of GO_x adsorbed on silver colloid remained nearly intact. On the other hand, Lee and coworkers reported that the SERRS signals of the riboflavin-binding proteins on a colloidal silver (EDTA reduced) are shown to arise from free flavin extracted from the riboflavin-binding proteins. No spectra with the flavin incorporated in the proteins are observed [55]. Thus, the spectra are most probably due to free flavin as an impurity in the preparations.

Holt and Cotton concluded that a careful purification of GO_x results in extremely weak and, under some circumstances, undetectable SERRS spectra at a silver electrode [56, 57]. GO_x shows a gradual disruption of the protein matrix on the electrode surface as Flavin adenine dinucleotide (FAD) is released from the GO_x molecule onto the electrode surface and denaturation of the GO_x structure allows direct contact between FAD and the electrode surface. The flavoproteins suffer loss of flavin upon contact with SERS active silver surfaces in all cases

reported to date [58]. The flavin dissociated from GO_x tends to form a complex with Ag^+ , and this may be a factor leading to the loss of the prosthetic group.

SERRS of flavin mononucleotide (FMN) and flavodoxin (Fld) from *D. vulgaris*, Hildenborough strain, was recorded by depositing on silver colloids (borohydride reduced) [59]. The SERS signals are sensitive to the electrode potential and agree very well with those obtained at a silver electrode. The formal potentials of both FMN ($E^\circ = -0.245 \text{ V}$ versus NHE) and Fld (around -0.22 V) in the solution are close to those of adsorbed species evaluated from cyclic voltammograms at a basal plane graphite (BPG) electrode. The SERRS signal of FMN is very weak at a potential in the vicinity of -0.25 V because the reduced form is SERRS inactive (no resonance effect is involved). The SERRS intensities of the oxidized form of Fld are about one-tenth of those of FMN. This is probably due to the fact that the protein matrix of Fld prevents a direct interaction between the chromophore and a silver electrode. A slow dissociation of Fld takes place under an irradiation of the laser beam and generates monomeric FMN. The SERRS signals of Fld, which is adsorbed on BPG and covered by silver colloids, are almost the same as those observed on the silver electrode.

11.3.2.7 Cytochrome P-450

It was shown from the SERRS measurement on silver colloids (citrate-reduced) that drug-induced rat liver cyt. P-450 possesses different relative populations of the LS/HS character in their native states. Denaturation from the active form (P-450) to an inactive form (P-420) or loss of the heme on the silver colloid is prevented if careful control of pH and colloid preparation were made [10]. The ability of a particular colloid to support an active

enzyme is due to a layer of citrate ions, which forms a coating on the colloid surface, providing a spacer between the silver surface and the protein, and protecting it from silver-induced reactions [18]. The change from the LS to the mixed LS/HS state is observed in the SERRS spectra of cyt. P-450 LM2 (rabbit liver) upon the adsorption on silver colloids. Both substrate-induced spin-state changes in the oxidized P-450 and an effect of the thiolate ligand on the oxidation state marker band in the reduced P-450 were observed in the SERS spectra of the adsorbed enzyme [12]. These findings indicate that the protein structure near the substrate binding site and the coordination by thiolate are not affected by the interaction with the metal surface. It is assumed that the catalytic activity of the adsorbed enzyme is preserved.

The SERRS of P-450 (rat liver) adsorbed onto a phosphatidyl-choline/silver colloid (citrate-reduced) substrate leads to a low to high spin-state conversion. This spin-state marker band shift is ascribed to a strong interaction of P-450 with the phospholipid coating [17].

11.4

Electrode Reaction of Electron Transfer Proteins at Modified Electrodes

Since Eddowes and Hill first reported that 4,4'-bipyridyl (4,4'-bipy) modified gold and platinum electrodes, which facilitate a reversible (rapid) electrode reaction of cyt. *c*, numerous surface modifiers have been reported [60]. Among these surface modifiers, carboxylic acid-terminated alkanethiol SAM are most attractive for mimicking physiological ET partners with positively charged binding sites [61].

11.4.1

Cytochrome *c* at Pyridine**Derivative-modified Electrodes**11.4.1.1 **ER Spectroscopic Studies**

Hinnen and Niki [33], and Sagara and coworkers [34] studied the interfacial properties of cyt. *c* at a gold electrode in the presence of various surface modifiers by an ER technique and found that there are two types of surface modifiers. Cytochrome *c*

is immobilized on a bis(4-pyridyl) disulfide (4-PySSPy) or 4-mercaptopyridine (PySH) modified gold electrode and the electrode reaction of cyt. *c* takes place through the film formed by the surface modifier. Figure 4 shows the ER voltammograms (potential dependence at constant wavelength) and the differential capacity curves and voltammograms of cyt. *c* adsorbed on bare and 4-PySSPy modified gold electrodes. The same results

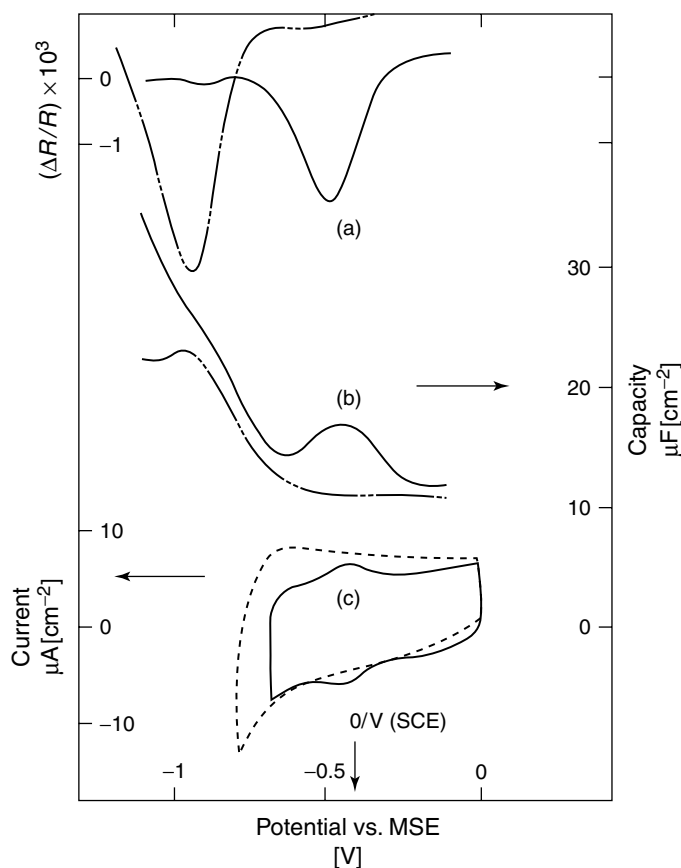


Fig. 4 (a) ER voltammograms at $\lambda = 405$ nm and (b) The differential capacity curves of cyt. *c* on bare (broken line) and 4-PySSPy modified (solid line) gold electrodes. (c) Cyclic voltammograms of 4-PySSPy modified (broken line) and cyt. *c* immobilized on 4-PySSPy modified (solid line) gold electrodes. Electrode potential is given against HgSO_4/Hg in saturated K_2SO_4 , which is 0.65 V versus NHE. (C. Hinnen, K. Niki, *J. Electroanal. Chem.* **1989**, 264, 157–165, Fig. 4 on page 162.)

are obtained with the PySH-modified gold electrode. The formal potential of cyt. *c* immobilized on the surface modifier is slightly more negative than that of the native one, which is about 450 mV more positive than that of cyt. *c* adsorbed on a bare gold electrode. Figure 5 shows the ER voltammogram of cyt. *c* adsorbed on the gold electrode in the presence of 4,4'-bipy

in the solution. The peak potential, which corresponds to the formal potential of cyt. *c* coadsorbed with 4,4'-bipy, is 0.03 V versus NHE. It is about 0.23 V more negative than that of the native one and 0.21 V more positive than the one adsorbed on the bare gold electrode. It is also interesting to note that the electrode reaction of cyt. *c* coadsorbed with 4,4'-bipy is reversible (a rapid

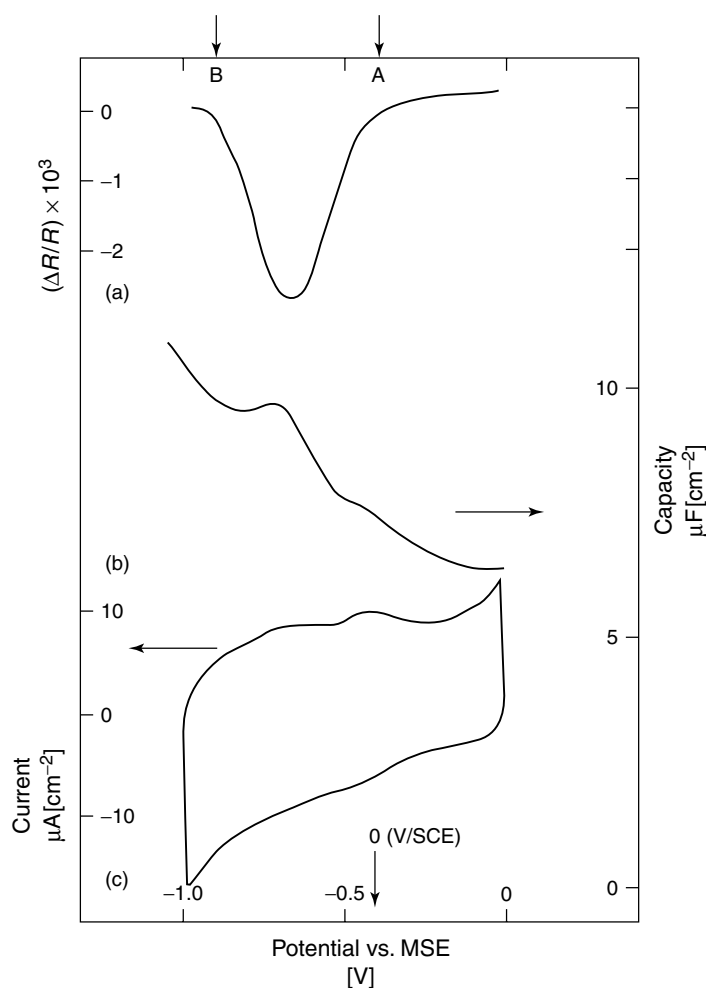


Fig. 5 (a) ER voltammogram at $\lambda = 405$ nm, (b) the differential capacity curve and (c) cyclic voltammogram of cyt. *c* at 4,4'-bipy modified electrode. Arrows A and B indicate the formal potentials of native cyt. *c* and cyt. *c* adsorbed on a bare gold electrode, respectively. Electrode potential is given against $HgSO_4/Hg$ in saturated K_2SO_4 , which is 0.65 V versus NHE.

electrode reaction). The ER voltammetric peak is shifted to -0.18 V after rinsing the electrode with the supporting electrolyte, which is identical to the formal potential of cyt. *c* on the bare gold electrode. These results suggest that 4,4'-bipy is washed out and cyt. *c* remained adsorbed on the gold electrode. The formal potential of cyt. *c* coadsorbed with 4,4'-bipy on the gold electrode is strongly dependent on the concentration of 4,4'-bipy in the solution and varies from -0.18 V (without 4,4'-bipy) to 0.03 V (saturated 4,4'-bipy solution) [62]. Models of the interfacial structure of cyt. *c* in the presence of surface modifiers are proposed as shown in Fig. 6 [34]. The type I represents cyt. *c* adsorbed directly on the gold electrode. The type II represents cyt. *c* coadsorbed with a surface modifier such as 4,4'-bipy on the gold electrode. The type III represents cyt. *c* immobilized on a surface modifier the gold electrode.

11.4.1.2 SERRS Studies

Taniguchi and coworkers studied the binding of surface modifiers on gold and silver electrodes using SERS (SERRS) [63–66].

It was shown that cleavage of the S–S bonding of 4-PySSPy takes place upon adsorption on both gold and silver electrodes, and a stable chemisorbed film is formed through sulfur to these electrodes [63, 65]. Cytochrome *c* adsorbed on a gold or silver electrode is displaced entirely by 4-PySSPy and the electrode reaction of cyt. *c* in the solution takes place through the PyS- film on the electrode surface [63, 64]. Added purine partially displaces cyt. *c* from a silver electrode surface and a mixed adsorbed layer of purine and cyt. *c* is formed, at which a reversible electrode reaction of cyt. *c* takes place [63].

Fan and coworkers studied using SERS the conformation of pyridine derivatives at a silver electrode in the presence of cyt. *c* [67]. When the 4,4'-bipy modified silver electrode is transferred in a cyt. *c* solution, 4,4'-bipy partially displaces cyt. *c* from the electrode and a mixed adsorbed layer of 4,4'-bipy and cyt. *c* is formed. The spin state of the coadsorbed cyt. *c* is a mixture of the 5cHS and 6cLS states. The formal potential of the coadsorbed cyt. *c* estimated from the shift of the oxidation

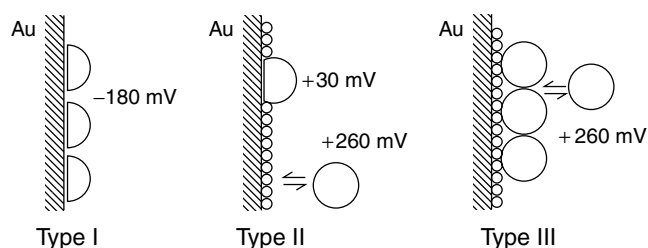


Fig. 6 Schematic representations of cyt. *c* at gold electrode in the absence and in the presence of surface modifier. Type I represents cyt. *c* adsorbed on a bare gold electrode. Type II represents cyt. *c* coadsorbed with the surface modifier such as 4,4'-bipy on a gold electrode. Type III represents cyt. *c* immobilized on the surface modifier on a gold electrode. The large and small circles represent cyt. *c* and surface modifier molecules, respectively. Semicircle represents an unfolded cyt. *c*. Electrode potentials are given against NHE. (T. Sagara, K. Niwa, A. Sone et al., *Langmuir*, **1990**, 6, 254–262, Fig. 12 in page 262.)

state marker band of SERRS is 0.05 V versus NHE, which is 0.21 V more negative than that of the native one and 0.20 V more positive than that of the adsorbed cyt. *c* on a bare silver electrode. 2,2'-Bipyridyl forms a silver chelate upon adsorption on a silver electrode. When the silver electrode covered by cyt. *c* layer is transferred into 2,2'-bipy solution, a slow displacement of cyt. *c* by 2,2'-bipy takes place and both molecules coexist at the electrode surface.

When the silver electrode covered by a cyt. *c* layer is transferred into 4-PySSPy solution, the SERRS signals of cyt. *c* disappear because cyt. *c* is completely displaced by 4-PySSPy. However, cyt. *c* is subsequently immobilized on top of the 4-PySSPy modified electrode and a rapid electrode reaction takes place at the formal potential of the native one. The adsorption of bis-(2-pyridyl) disulfide (2-PySSPy) and cyt. *c* is competitive. Bis-(2-pyridyl) disulfide coadsorbs with cyt. *c* on the silver electrode and the electrochemical function of this adsorbed layer is similar to that of the film formed by 4,4'-bipy coadsorbed with cyt. *c*.

An adsorbed layer of 1,2-Bis(4-pyridyl) ethylene (4-PyCH) on a silver electrode is stable and is hard to displace by cyt. *c*. Cytochrome *c* is not immobilized on the PyCH layer, but cyt. *c* in the solution undergoes a rapid electrode reaction through this layer.

The SERS signals of the cyt. *c*/4-PyS/Au electrode excited by 647.1-nm laser are almost identical to those of the 4-PyS/Au electrode, but the SERRS of the cyt. *c*/4-PyS/Ag excited by a 413.1-nm laser gives rise to the strong enhancement of the cyt. *c* signals without interference by the signals of the surface modifier [68, 69]. The spin state of cyt. *c* immobilized on the 4-PyS modified silver electrode is in the 6cLS state suggesting that cyt. *c* is in the

native configuration. This fact, together with a similarity of the low frequency region of the SERR spectrum to the Raman resonance spectrum of the protein in solution, provides strong evidence that the heme environment of cyt. *c* is unperturbed in the adsorbed state on the 4-PyS modified silver electrode. Photodegradation of cyt. *c* adsorbed on the 4-PyS-modified electrode is noticed after a prolonged irradiation of the sample at moderately high laser power.

11.4.1.3 Stability of Bis-(4pyridyl) Disulfide and 4-Mercaptopyridine at Gold Electrodes

A structural instability of the 4-PyS modified electrode prepared from the solutions of 4-PySSPy and 4-PySH has been reported [70]. This instability manifests itself as a decrease in the ability of the modified surfaces to facilitate the electrode reaction of cyt. *c* with an increase of immersion time in the precursor solutions. The modified surfaces spontaneously decompose to yield an adlayer composed largely of adsorbed atomic and oligomeric sulfur.

11.4.2

Cytochrome *c* at ω -Functional Alkanethiol Modified Electrodes

The SERRS spectrum of cyt. *c* immobilized on a carboxylic acid-terminated alkanethiol modified gold or silver electrode reveals that both oxidized and reduced forms of cyt. *c* are in the 6cLS state [68, 69] and its formal potential is 0.26 V versus NHE in 10-mM phosphate buffer solution at pH 7.0 [71, 72]. These results strongly support the retention of the native state of cyt. *c* on the carboxylic acid-terminated alkanethiol modified electrodes. Song and coworkers reported the formal potential of cyt. *c* of the system, cyt. *c*/HOOC(CH₂)_{*n*}S/Au (*n* = 5, 10 and

15), to be 0.215 V in 4.4-mM phosphate buffer solution at pH 7.0 [73].

11.4.3

Cytochrome *c* at Iodine-modified Electrodes

Cytochrome *c* is found to exhibit a quasireversible voltammetric response at an iodine-modified silver electrode. SERRS spectroscopy indicates that cyt. *c* immobilized on the iodine-modified silver electrode is in the 6cLS state [74, 75]. The shift of the oxidation state marker band was plotted against the electrode potential and the formal potential of cyt. *c* immobilized on the iodine-modified silver electrode is estimated to be 0.19 V versus NHE, which is somewhat negative relative to that of the native state. A similar shift is also seen when cyt. *c* interacts with mitochondrial membranes (50–60 mV) [76, 77]. It can be concluded that the SERRS results indicate that the adsorbed cyt. *c* is structurally similar to the native protein in solution. The SERRS spectrum of cyt. *c* adsorbed on the iodine-modified gold electrode is different from that on the iodine-modified silver electrode. The SERRS spectrum of cyt. *c* (ox) excited by 550 nm at open-circuit potential reveals that cyt. *c* is present in the mixed 5cHS and 6cLS state [78].

11.4.4

Cytochrome *c*₃ at 4,4'-Bipyridyl and Carboxylic Acid-terminated Alkanethiol Modified Electrodes

SERRS spectroscopic and ER voltammetric techniques were used to investigate the effect of surface modifiers, 11-mercaptoundecanoic acid (11-MUDA) and 4,4'-bipy, on the structure and redox properties of cyt. *c*₃ from *D. desulfuricans*, Norway strain, at a silver electrode [47]. The ER voltammograms of cyt. *c*₃ immobilized on

11-MUDA exhibit a small hysteresis between the forward and backward potential scans, suggesting that the redox process is reversible and that cyt. *c*₃ retains its native structure. The SERRS spectra of cyt. *c*₃ (both oxidized and reduced forms) immobilized on 11-MUDA clearly indicate that the hemes are in the 6cLS state. The formal potential of cyt. *c*₃ immobilized on the 11-MUDA modified silver electrode was monitored by the shift of the oxidation state marker band and is –0.20 V versus NHE, which is about 0.10 V more negative than that observed on a bare silver electrode [11].

The SERS bands attributable to both cyt. *c*₃ and 4,4'-bipy suggest that 4,4'-bipy is coadsorbed with cyt. *c*₃ on the silver electrode surface [47]. The spin state of ferri-cyt. *c*₃ is in the mixed 6cLS and 5cHS state, which is similar to that observed in the absence of 4,4'-bipy. The transformation from the oxidized form (the mixed spin state) to the reduced form (6cLS state) is completed at 0.0 V, which is 0.2 V more positive than the formal potential of the most positive redox site of the native cyt. *c*₃. The intensity of the SERRS spectrum of the cyt. *c*₃ coadsorbed with 4,4'-bipy in the low-frequency region (370–430 nm) is considerably weak compared with that of RRS in solution. This result supports the idea that 4,4'-bipy has a significant effect on the heme environment of the adsorbed cyt. *c*₃. The formal potential of cyt. *c*₃ coadsorbed with 4,4'-bipy is monitored by the shift of the oxidation state marker band that becomes more positive with increasing concentration of 4,4'-bipy. The shift of the formal potential can be explained in terms of the decrease in the heme exposure to the solvent by shielding the exposed heme edge by 4,4'-bipy molecules.

11.4.5

Proteins Cast in Lipid Bilayer

Rusling and his collaborators have obtained reversible voltammetric responses of cyt. P-450_{cam}, hemoglobin, Mb, cyt. *c*, and chlorella ferredoxin cast in liquid crystal films or composites of liquid crystal and Nafion [79–81] on gold electrodes. The structure of the cast films was characterized by low angle x-ray diffraction. The structures of Mb and cyt. P-450_{cam} in the cast film were characterized by UV-vis, Electron Spin Resonance (ESR), and reflectance Fourier Transform Infrared (FT-IR) spectroscopic techniques, and are shown to be similar to the native conformations. Visible linear dichroism and ESR anisotropy showed that Mb is specifically oriented in the static films. The orientation of the heme plane of Mb averaged 60° with respect to the normal to the film plane, and distributions are rather broad.

11.5

Molecular Orientation of Proteins on Solid Substrates. Cytochrome *c* Immobilized on Self-assembled Monolayers

As a result of the heterogeneous distributions of electrical charge and chemical functionalities present on the surface of most proteins, the adsorption of proteins to solid substrates of differing surface properties may produce different molecular orientations. The optical thickness of protein layers can be evaluated by using ellipsometry, surface plasmon resonance, or guided wave perturbation. When a chromophore of the protein is used as a probe, polarized spectroscopic techniques are found to be applicable to measure the tilt angle of the heme moiety in protein films. Macdonald and Smith used SERRS

spectroscopy to measure the conformation of cyt. *c* adsorbed on a citrate-coated silver colloid and found that the heme orientation was influenced by the surface coverage of protein [82].

11.5.1

IRRAS Studies

The IRRAS spectrum of a gold electrode emerged from the solution containing cyt. *c* and 4-PySSPy reveals that the 4-PySSPy molecules are oriented perpendicularly to the electrode surface (as PyS-), and that cyt. *c* is immobilized on the 4-PySSPy layer [83]. On the other hand, 4,4'-bipy adsorbed on a gold electrode gives rise to weak IRRAS signals, suggesting that the dipole moment of the adsorbed 4,4'-bipy molecule is parallel to the electrode surface. The amount of cyt. *c* coadsorbed with 4,4'-bipy is estimated from the intensity of the IRRAS signals of cyt. *c* to be about 70% of those observed at the gold electrode with monolayer coverage. The amount of the coadsorbed cyt. *c* with 4,4'-bipy-measured voltammetry is estimated to be about 50% of a monolayer.

11.5.2

Conformation of Cytochrome *c* on Carboxylic Acid-terminated SAM

Edmiston and coworkers studied the orientation distribution of the heme group in the protein films by using a combination of absorption linear dichroism and fluorescence anisotropy [30, 31, 84]. Electrostatic adsorption of the positively charged protein to the negatively charged head group of archidic acid deposited on a Langmuir-Blodgett film produces a narrow orientation distribution of the heme (a tilted angle from *z*-axis is $46 \pm 6^\circ$).

11.6 Electron Transfer Kinetics of Electron Transfer Proteins at Electrode Surfaces

11.6.1

Electron Transfer Kinetics of Cytochrome *c* at Carboxylic Acid-terminated Alkanethiol SAM

The charging current of the electrical double layer at the electrode interface limits the electrode reaction rate measurements by traditional electrochemical techniques. The potential-modulated ER spectroscopic technique, on the other hand, involves the measurement of the faradaic current as a difference in the spectrum between oxidized and reduced forms at the electrode surface generated by an ac modulation of the electrode potential. This technique enables the measurement of electrode reaction rates up to approximately 10^4 s^{-1} because the effect of the double-layer charging current can be minimized [28].

The ET reaction rates between cyt. *c* (horse heart) and a gold (111) electrode through the carboxylic acid-terminated alkanethiol, $\text{HOOC}(\text{CH}_2)_n\text{SH}$, SAM are measured by the ER technique as a function of the chain length of alkanethiols ($n = 2-11$) [71, 72, 85]. The ET reaction

rate constant decreases exponentially with the chain length as shown in Fig. 7, and the exponential decay factor given by the Marcus theory is 1.09 ± 0.02 per methylene group ($0.71 \pm 0.01 \text{ \AA}^{-1}$).

The ET rates through the long alkanethiol SAM are controlled by the ET rates through the alkanethiol bonds. The ET reaction rates through the short-chain alkanethiol monolayers, on the other hand, are nearly independent of the chain length. It is assumed that there is a configurational rearrangement of cyt. *c* on the SAM prior to the ET reaction: a thermodynamically stable adsorbed structure of cyt. *c* (ox) (I), which is formed upon the adsorption of cyt. *c* from the solution to the carboxylate termini, resulting in a configurational rearrangement to cyt. *c* (ox) (II), at which the most efficient ET reaction takes place. The ET reaction is followed by a second configurational rearrangement given by Eq. (3) to form a thermodynamically stable binding state, cyt. *c* (red)(I). The rate-controlling step of the ET reaction through a short alkanethiol chain is very likely to be the configurational rearrangement of cyt. *c* on the SAM surface given by Eq. (1) and the transformation rate constant k_1 of the forward reaction is estimated

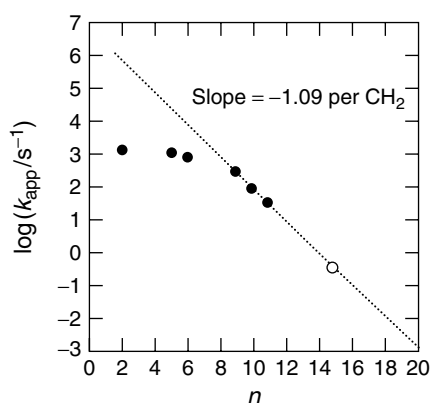
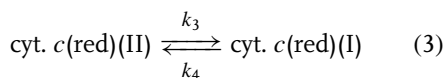
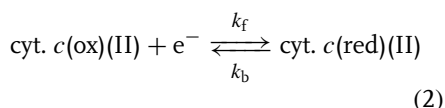
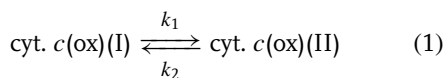


Fig. 7 Logarithmic plots of the apparent standard rate constant of cyt. *c* as a function of a number of methylene groups of alkanethiol SAM. (●) obtained by ER technique and (○) obtained by ac impedance technique. (Z.-Q. Feng, S. Imabayashi, T. Kakiuchi et al., *J. Chem. Soc., Faraday Trans.* **1997**, 93, 1367–1370, Fig. 3 on page 1369.)

to be $2.6 \times 10^3 \text{ s}^{-1}$.



The ET rate through longer chain alkanethiols decreases with increasing ionic strength or decreasing pH of the solution and is markedly suppressed with increasing the solution viscosity [83]. The rate-limiting ET step through short alkyl chains results from a configurational rearrangement process of cyt. *c* from a stable binding form on the carboxylic acid terminus to a configuration that facilitates the most efficient ET pathway represented by Eq. (1) [85]. The ET rate on the mixed SAM, which was formed in the mixed solution of $\text{HS}(\text{CH}_2)_{10}\text{COOH}$ and $\text{HS}(\text{CH}_2)_9\text{CH}_3$, reaches a maximum when the solution contains 20% $\text{HS}(\text{CH}_2)_9\text{CH}_3$ and is about six times faster than that on the SAM of the single component [86]. Collinson and coworkers measured the ET rate of cyt. *c* covalently attached to the carboxylic acid-terminated alkanethiol (16-mercaptohexadecanoic acid)-modified gold by cyclic voltammetry and found that the ET rate is similar to that of cyt. *c* immobilized electrostatically on the same electrode [87]. The cyclic voltammetric peak broadening of cyt. *c* immobilized electrostatically on the carboxylic acid-terminated alkanethiol SAM was explained in terms of inhomogeneity in the formal potential and kinetics of cyt. *c* on the SAM [88–90].

Cytochrome *c* extracted from yeast (iso-1 cyt. *c*) exhibits a different kinetic

behavior from that of horse heart cyt. *c* on the carboxylic acid-terminated alkanethiol modified gold electrode. The exponential decay factor of the ET rates through longer alkyl chains ($n = 7$ and 10) is similar to that of horse heart cyt. *c*, but the ET rates are about three orders of magnitude smaller [90]. The ET rates through the mixed SAM formed in the 1 : 1 mixed solution of $\text{HS}(\text{CH}_2)_{10}\text{COOH}$ and $\text{HS}(\text{CH}_2)_7\text{OH}$ (or $\text{HS}(\text{CH}_2)_8\text{OH}$) are 2000 to 2500 times faster than those through pure carboxylic acid-terminated SAM. On the contrary, the ET rate of horse heart cyt. *c* through the mixed SAM is five times faster than that through the pure carboxylic acid-terminated SAM [90].

Ruzgas and coworkers measured the ET reaction rate of cyt. *c* at a gold electrode through *N*-acetylcysteine SAM by the ER technique and proposed a modified approach to evaluate the ET rate constants [91]. However, the kinetic results obtained are unreasonably small.

11.6.2

Electron Transfer Kinetics of Cytochromes *c* and *c*₅₅₂ at Silver Electrode

Both traditional electrochemical and ER techniques cannot provide insight into molecular processes at the electrode interface, which includes conformational transformations of the electroactive species coupled with the ET reactions as has been reported for cyt. *c* [71, 72, 85]. SERRS can provide both structural and kinetic information on the ET process of cyt. *c* at an electrode surface. The time-resolved SERRS technique was developed to elucidate the heterogeneous ET rate of cyt. *c* with different conformations at a silver electrode surface by monitoring the change in the SERRS intensity with time after applying a potential step [92, 93]. The

time dependence of the SERRS signals of iso-1 cyt. *c* adsorbed on the silver electrode were measured in a time domain between 45 and 175 ms after a potential step from 0.16 to +0.29 V versus NHE by using a rotating electrode to avoid photodegradation. Both the ET reaction and the conformational transition rates of cyt. *c* at the silver electrode have been measured to be 10.3 s^{-1} and 4.3 s^{-1} , respectively. The dynamics of cyt. *c*₅₅₂ from *Thermus thermophilus* at the silver electrode was also measured by time-resolved SERRS [94].

11.6.3

Electron Transfer Kinetics of Azurin at Methyl-terminated Alkanethiol Self-assembled Monolayers

Ulstrup and his coworkers showed that azurin can be assembled directly on gold (111) by adsorption via the surface disulfide group [95, 96]. The copper redox center is located opposite to the electrode in this orientation so that the distance of the ET pathway is too large to exhibit a well-defined voltammogram (the ET rate is very slow). On the other hand, the immobilization of azurin is achieved through hydrophobic interactions between the hydrophobic area around the copper redox center and methyl-terminus of alkanethiol SAMs. Gaigalas and coworkers showed that the blue copper protein, azurin, can be immobilized on the methyl-terminated hexanethiol SAM and azurin exhibits quasi-reversible electron exchange with gold electrode through the SAM [97]. Ulstrup and his coworkers measured the distance dependence of the ET rate by using alkanethiols with different chain lengths. The ET rate is almost independent of the chain length up to ca. 9 methylene units but follows exponential distance

decay with a decay constant (β) of 1.03 ± 0.02 per CH_2 unit at longer chain lengths [98].

Recent review article related to this chapter

Extensive review article was published on the redox reaction of cyt. *c* through SAM on electrodes [99].

References

1. T. M. Cotton, S. G. Schultz, R. P. Van Duyne, *J. Am. Chem. Soc.* **1980**, *102*, 7960–7962.
2. T. M. Cotton in *Spectroscopy of Surfaces* (Eds.: R. J. H. Clark, R. E. Hester), Wiley & Sons, New York, 1988, pp. 91–153.
3. T. M. Cotton, J.-H. Kim, G. D. Chumanov, *J. Raman Spectrosc.* **1991**, *22*, 729–742.
4. T. M. Cotton, J.-H. Kim, R. E. Holt, *Adv. Biophys. Chem.* **1992**, *2*, 115–147. (JAI Press).
5. P. Hildebrandt in *Cytochrome c: Multidisciplinary Approach* (Eds.: R. A. Scott, A. G. Mauk), University Science Books, Sausalito, 1996, pp. 285–314.
6. P. Hildebrandt, G. J. Pielak, R. J. P. William, *Eur. J. Biochem.* **1991**, *201*, 211–216.
7. P. Hildebrandt, M. Stockburger, *Biochemistry* **1989**, *28*, 6722–6728.
8. P. Hildebrandt, K. A. Macor, R. C. Czernuszewicz, *J. Raman Spectrosc.* **1988**, *19*, 65–69.
9. P. Hildebrandt, M. Stockburger, *J. Phys. Chem.* **1986**, *90*, 6017–6024.
10. K. Kelley, B. N. Rospendowski, W. E. Smith et al., *FEBS Lett.* **1987**, *222*, 120–124.
11. K. Niki, Y. Kawasaki, Y. Kimura et al., *Langmuir* **1987**, *3*, 982–986.
12. P. Hildebrandt, R. Greinert, A. Stier et al., *FEBS Lett.* **1988**, *227*, 76–80.
13. C. R. Wolf, J. S. Miles, S. Seilman et al., *Biochemistry* **1988**, *27*, 1597–1603.
14. T. M. Cotton, V. L. Schlegel, R. E. J. Holt et al., *Proc. SPIE-Int. Soc. Opt. Eng.* **1989**, *1,055*, 263–270.
15. T. M. Cotton, B. N. Rospendowski, V. L. Schlegel et al., *Proc. SPIE-Int. Soc. Opt. Eng.* **1991**, *1,403*, 93–96.
16. S. Hashimoto, R. Nakajima, I. Yamazaki et al., *FEBS Lett.* **1989**, *248*, 205–209.

17. B. N. Rospendowski, V. L. Schlegel, R. E. Holt et al., in *Charge and Field Effects in Biosystems-2* (Eds.: A. M. J. Allen, S. F. Clearry, F. M. Hawkridge), Plenum Press, New York, 1989, pp. 43–58.
18. B. N. Rospendowski, K. Kelley, C. R. Wolf et al., *J. Am. Chem. Soc.* **1991**, *113*, 1217–1225.
19. A. L. Verma, K. Kimura, T. Yagi et al., *Chem. Phys. Lett.* **1989**, *159*, 189–192.
20. J. de Groot, R. E. Hester, S. Kaminaka et al., *J. Phys. Chem.* **1988**, *92*, 2044–2048.
21. D. M. Kolb in *Spectroelectrochemistry: Theory and Practice* (Ed.: R. J. Gale), Plenum, New York, 1988, pp. 78–188.
22. W. Plieth in *Spectroscopic and Diffraction Techniques in Interfacial Electrochemistry* (Eds.: C. Gutierrez, C. Melendres), Kluwer Academic Publishing, The Netherlands, 1990, pp. 223–260.
23. W. Plieth, W. Kozlowski, T. Twomey in *Adsorption of Molecules at Metal Electrodes* (Eds.: J. Lipkowski, P. N. Ross), VCH, New York, 1992, pp. 239–284.
24. T. Sagara, *Recent Res. Dev. Phys. Chem.* **1998**, *2*, 159–173.
25. C. Hinnen, R. Parsons, K. Niki, *J. Electroanal. Chem.* **1983**, *147*, 329–337.
26. T. Sagara, S. Igarashi, H. Sato et al., *Langmuir* **1991**, *7*, 1005–1012.
27. T. Sagara, J. Iizuka, K. Niki, *Langmuir* **1992**, *8*, 1018–1025.
28. Q. Feng, T. Sagara, K. Niki, *Anal. Chem.* **1995**, *67*, 3564–3570.
29. O. Hofmann, K. Doblhofer, H. Gerischer, *J. Electroanal. Chem.* **1984**, *161*, 337–344.
30. P. L. Edmiston, L. L. Wood, J. E. Lee et al., *J. Phys. Chem.* **1996**, *100*, 775–784.
31. P. L. Edmiston, J. E. Lee, S.-S. Cheng et al., *J. Am. Chem. Soc.* **1997**, *119*, 560–570.
32. E. F. Bowden, F. M. Hawkridge, H. N. Blount, *J. Electroanal. Chem.* **1984**, *161*, 355–376.
33. C. Hinnen, K. Niki, *J. Electroanal. Chem.* **1989**, *264*, 157–165.
34. T. Sagara, K. Niwa, A. Sone et al., *Langmuir* **1990**, *6*, 254–262.
35. K. Niki, Y. Kobayashi, H. Matsuda, *J. Electroanal. Chem.* **1984**, *168*, 275–286.
36. F. M. Hawkridge, T. Kuwana, *Anal. Chem.* **1973**, *45*, 1021–1027.
37. W. R. Heineman, B. J. Norris, J. F. Goelz, *Anal. Chem.* **1975**, *47*, 70–84.
38. K. Niki, Y. Kawasaki, C. Hinnen et al. in *Frontiers of Bioinorganic Chemistry* (Ed.: A. V. Xavier), VCH, Weinheim, 1983, pp. 622–630.
39. P. Hildebrandt, M. Stockburger in *Spectroscopy of Biological Molecules: Proceedings of the First European Conference on Spectroscopy of Biological Molecules* (Eds.: A. J. P. Alix, L. Bernard, M. Manfait), John Wiley & Sons, Chichester, 1985, pp. 25–30.
40. P. Hildebrandt, M. Stockburger in *Raman Spectroscopy: Sixty Years On Vibrational Spectra and Structure*, (Eds.: H. D. Bist, J. R. Durig, J. F. Sullivan), Elsevier Science Publishing, The Netherlands, 1989, pp. 443–446, Vol. 17A.
41. P. Hildebrandt, M. Stockburger, *Biochemistry* **1989**, *28*, 6710–6721.
42. P. Hildebrandt, *J. Mol. Struct.* **1991**, *242*, 379–395.
43. N. Parthasarathi, C. Hansen, S. Yamaguchi et al., *J. Am. Chem. Soc.* **1987**, *109*, 3865–3871.
44. G. Valette, A. Hamelin, *J. Electroanal. Chem.* **1973**, *45*, 301–319.
45. P. Hildebrandt, T. Heimburg, D. Marsh, *Eur. Biophys. J.* **1990**, *18*, 193–201.
46. L. H. Eng, V. Schlegel, D.-L. Wang et al., *Langmuir* **1996**, *12*, 3055–3059.
47. D. Hobara, K. Niki, T. M. Cotton, *Biospectroscopy* **1998**, *4*, 161–170.
48. S. Lecomte, H. Wackerbarth, P. Hildebrandt et al., *J. Raman Spectrosc.* **1998**, *26*, 687–692.
49. K. Hon-Nami, T. Oshima, *J. Biochem. (Tokyo)* **1977**, *82*, 769–776.
50. G. Smulevich, T. G. Spiro, *J. Phys. Chem.* **1985**, *89*, 5168–5173.
51. J. de Groot, R. E. Hester, *J. Phys. Chem.* **1987**, *91*, 1693–1696.
52. I. Taniguchi, K. Watanabe, M. Tominaga et al., *J. Electroanal. Chem.* **1992**, *333*, 331–338.
53. M. Tominaga, T. Kumagai, S. Takita, *Chem. Lett.* **1993**, 1771–1774.
54. R. A. Copeland, S. P. A. Fodor, T. G. Spiro, *J. Am. Chem. Soc.* **1984**, *106*, 3872–3874.
55. N.-S. Lee, Y.-Z. Hsieh, M. D. Morris et al., *J. Am. Chem. Soc.* **1987**, *109*, 1358–1363.
56. R. E. Holt, T. M. Cotton, *J. Am. Chem. Soc.* **1987**, *109*, 1841–1843.
57. R. E. Holt, T. M. Cotton in *Redox Chemistry and Interfacial Behavior of Biological Molecules* (Eds.: G. Dryhurst, K. Niki), Plenum Press, New York, 1988, pp. 217–228.
58. R. E. Holt, T. M. Cotton, *J. Am. Chem. Soc.* **1989**, *111*, 2815–2821.

59. V. Brabec, K. Niki, *Chem. Lett.* **1988**, 1445–1448.
60. M. A. Eddowes, H. A. O. Hill, *J. Chem. Soc. Chem. Commun.* **1977**, 771, 772.
61. M. J. Tarlov, E. F. Bowden, *J. Am. Chem. Soc.* **1991**, *113*, 1847–1849.
62. T. Sagara, H. Murakami, S. Igarashi et al., *Langmuir* **1991**, *7*, 3190–3196.
63. I. Taniguchi, M. Iseki, T. Eto et al., *Bioelectrochem. Bioenerg.* **1984**, *13*, 373–383.
64. I. Taniguchi, M. Iseki, H. Yamaguchi et al., *J. Electroanal. Chem.* **1984**, *175*, 341–348.
65. I. Taniguchi, M. Iseki, H. Yamaguchi et al., *J. Electroanal. Chem.* **1985**, *186*, 299–307.
66. I. Taniguchi in *Redox Chemistry and Interfacial Behavior of Biological Molecules* (Eds.: G. Dryhurst, K. Niki), Plenum Publishing, New York, 1988, pp. 113–123.
67. K.-J. Fan, I. Satake, K. Ueda et al. in *Redox Chemistry and Interfacial Behavior of Biological Molecules* (Eds.: G. Dryhurst, K. Niki), Plenum Publishing, New York, 1988, pp. 125–138.
68. D. Hobara, K. Niki, T. M. Cotton, *DENKI KAGAKU* **1993**, *61*, 776, 777.
69. D. Hobara, K. Niki, C.-I. Zhou et al., *Colloids Surf. A: Physicochem. Eng. Aspects* **1994**, *93*, 241–250.
70. B. D. Lamp, D. Hobara, M. D. Porter et al., *Langmuir* **1997**, *13*, 736–741.
71. Z.-Q. Feng, S. Imabayashi, T. Kakiuchi et al., *J. Electroanal. Chem.* **1995**, *394*, 149–154.
72. Z.-Q. Feng, S. Imabayashi, T. Kakiuchi et al., *J. Chem. Soc., Faraday Trans.* **1997**, *93*, 1367–1370.
73. S. Song, R. A. Clark, E. F. Bowden et al., *J. Phys. Chem.* **1993**, *97*, 6564–6572.
74. C.-I. Zhou, T. M. Cotton, X.-G. Qu et al. in *Redox Mechanisms and Interfacial Properties of Molecules of Biological Importance* (Eds.: F. A. Schultz, I. Taniguchi), The Electrochemical Society of Pennington, New Jersey, 1993, pp. 63–74.
75. T.-H. Lu, X.-J. Yu, S.-J. Dong et al., *J. Electroanal. Chem.* **1994**, *369*, 79–86.
76. P. L. Dutton, D. F. Wilson, C.-P. Lee, *Biochemistry* **1970**, *9*, 5077–5082.
77. J. Vanderkooi, M. Erecinska, B. Chance, *Arch. Biochem. Biophys.* **1973**, *157*, 531–540.
78. D. Hobara, K. Niki, G. Chumanov et al., unpublished results.
79. J. F. Rusling, *Interface* **1997**, *6*(4), 26–31.
80. J. F. Rusling, *Acc. Chem. Res.* **1998**, *31*, 363–369.
81. Y. M. Lvov, Z.-Q. Lu, J. B. Schenkman et al., *J. Am. Chem. Soc.* **1998**, *120*, 4073–4080.
82. I. D. G. Macdonald, W. E. Smith, *Langmuir* **1996**, *12*, 706–713.
83. K. Niwa, M. Furukawa, K. Niki, *J. Electroanal. Chem.* **1988**, *245*, 275–285.
84. J. E. Lee, S. S. Saavedra, *Langmuir* **1996**, *12*, 4025–4032.
85. A. Avila, W. Gregory, K. Niki et al., *J. Phys. Chem. B* **2000**, *104*, 2759–2766.
86. S. Arnold, Z.-Q. Feng, T. Kakiuchi et al., *J. Electroanal. Chem.* **1997**, *438*, 91–97.
87. M. Collinson, E. F. Bowden, M. J. Tarlov, *Langmuir* **1992**, *8*, 1247–1250.
88. T. M. Nahir, E. F. Bowden, *J. Electroanal. Chem.* **1996**, *410*, 9–13.
89. R. A. Clark, E. F. Bowden, *Langmuir* **1997**, *13*, 559–565.
90. A. E. Kasmi, J. M. Wallace, E. F. Bowden et al., *J. Am. Chem. Soc.* **1998**, *120*, 225–226.
91. T. Ruzgas, L. Wong, A. K. Gaigalas et al., *Langmuir* **1998**, *14*, 7298–7305.
92. S. Lecomte, H. Wackerbarth, T. Soulimane et al., *J. Am. Chem. Soc.* **1998**, *120*, 7381–7382.
93. H. Wackerbarth, U. Klar, W. Günther et al., *Appl. Spectrosc.* **1999**, *53*, 283–291.
94. S. Lecomte, P. Hildebrandt, T. Soulimane, *J. Phys. Chem. B* **1999**, *103*, 10 053–10 064.
95. A. K. Gaigalas, G. Niaura, *J. Colloid Interface Sci.* **1997**, *193*, 60–70.
96. Q. Chi, J.-D. Zhang, E. P. Friis, J. E. T. Andersen, J. Ulstrup, *Electrochem. Commun.* **1999**, *1*, 91–96.
97. Q. Chi, J.-D. Zhang, J. U. Nealsen, E. P. Friis, Ib. Chorkendorff, G. W. Canters, J. E. T. Andersen, J. Ulstrup, *J. Am. Chem. Soc.*, **2000**, *122*, 4047–4055.
98. Q. Chi, J.-D. Zhang, J. E. T. Andersen, J. Ulstrup, *J. Phys. Chem. B*, **2001**, *105*, 4669–4679.
99. M. Fedurco, *Coordin. Chem. Rev.*, **2000**, *209*, 263–331.

12

Electrochemical Analysis of Nucleic Acids

Emil Paleček, Miroslav Fojta, František Jelen, and Vladimír Vetterl
Institute of Biophysics, Brno, Czech Republic

12.1	Introduction	369
12.1.1	History	369
12.1.2	Nucleic Acid Samples	370
12.2	Electrochemical Behavior of NA Components	370
12.2.1	Adsorption/Desorption Behavior	370
12.2.1.1	Mercury Electrodes	370
12.2.1.1.1	Oligonucleotides	374
12.2.1.2	Solid Electrodes	375
12.2.2	Reduction and Oxidation	375
12.2.3	Microanalysis of Nucleic Acid Components by Stripping Techniques	376
12.2.3.1	Principles	376
12.2.3.2	Reactions of Pyrimidine and Purine Bases with the Electrode Mercury	376
12.2.3.3	Unusual Bases and Nucleosides	377
12.2.3.3.1	5-Ribosyluracil (pseudouridine)	377
12.2.3.3.2	Methylated Adenines	378
12.2.3.3.3	5-Fluorouracil (5-FU)	378
12.2.3.4	Sparingly Soluble Compounds of Nucleic Acid Components with Copper	379
12.3	Adsorption/Desorption Behavior of NAs	379
12.3.1	Mercury Dropping Electrode	379
12.3.1.1	Adsorption of Double-stranded (Native) DNA	381
12.3.1.2	Adsorption of Single-stranded (Denatured) DNA	381
12.3.2	Adsorption Kinetics at Mercury Dropping and Hanging Electrodes	381
12.3.3	Electrochemical Impedance Spectroscopy (EIS)	382
12.3.3.1	Other Techniques	384
12.3.4	Adsorption of NAs on Other Electrodes	384
12.3.4.1	DNA Adsorption to Charged Lipid Membranes	385

12.4	Reduction and Oxidation of NAs on Different Electrodes	385
12.4.1	Mercury Electrodes	385
12.4.1.1	Reduction of Adenine and Cytosine Residues	385
12.4.1.2	Anodic Signal of Guanine Residues	386
12.4.2	Carbon Electrodes	387
12.4.3	Other Solid Electrodes	389
12.4.4	Analysis of NAs by Different Electrochemical Techniques	389
12.5	Relations Between Structures and Electrochemical Responses of DNA	391
12.6	DNA Structure on Electrode Surfaces	393
12.6.1	Dependence of the dsDNA Signals at the HMDE on Potential Scanning Direction	394
12.6.2	Opening of the DNA Double Helix Around -1.2 V (Region U)	395
12.6.2.1	Opening of dsDNA at Acid pHs in a Wider Potential Range T	398
12.7	Interactions of NAs with Small Molecules	399
12.7.1	Reversible (Noncovalent) Interactions	399
12.7.1.1	Inorganic Cations and Simple Metal Complexes	400
12.7.1.2	Organic Metal Chelates	400
12.7.1.3	Other Noncovalent DNA Binders	401
12.7.2	Covalent Interactions	403
12.7.2.1	Electroactive Markers of NAs	403
12.7.2.2	Other Nucleic Acid Modifications	405
12.8	DNA Conductivity	406
12.8.1	Application of Electrodes in DNA Conductivity Studies	406
12.9	Analytical Applications	407
12.9.1	Sensors for DNA Hybridization	407
12.9.1.1	Immobilization of DNA on the Electrode	408
12.9.1.2	Detection of the Hybridization Event	408
12.9.1.3	Redox Indicators Covalently Bound to DNA	410
12.9.1.4	Indicator-free Detection Systems. Intrinsic Electroactivity of DNA	410
12.9.1.5	Changes in Interfacial Properties and DNA Conductivity	410
12.9.1.6	Blocking and Interfacing the Transducer	411
12.9.1.7	Electrocatalytic Reactions	412
12.9.1.8	Detection of Point Mutations	412
12.9.2	Sensors for DNA Damage	412
12.9.2.1	Detection of DNA Strand Breaks	413
12.9.2.2	Damage to DNA Bases	413
12.9.2.3	Detection of Damaging Agents Specifically Interacting with DNA	414
12.9.2.4	DNA Cleavage Controlled by Electrochemical Reactions	414
12.9.3	Other Determinations	415

12.9.3.1	Determination of ssDNA in an Excess of dsDNA	415
12.9.3.2	Determination of RNA Traces in DNA Solutions	415
12.9.3.3	Determination of Proteins	416
12.10	Conclusion	417
	Addendum	418
	Acknowledgment	418
	References	419

12.1

Introduction

12.1.1

History

To our knowledge, the first paper dealing with electrochemical analysis of nucleic acids (NAs) was published by Berg in 1957 [1]. He used a supporting electrolyte containing cobalt ions to determine proteins in RNA and DNA samples, and under the given conditions, found that NAs were polarographically inactive species. The ability of DNA and RNA to yield reduction and oxidation signals upon interaction with electrodes was discovered by Paleček in 1958 and in the years [2–5]. It was the so-called oscillographic polarography at controlled a.c. (OP) [6] that proved to be better suited for the analysis of NAs than the d.c. polarography popular at that time. Using OP, it was shown that in addition to the reduction of adenine (A) (whose reduction at dropping mercury electrode (DME) in strongly acidic medium was described already in 1945 [7]); cytosine (C) was also reducible at a DME at neutral pH [2, 8], and that guanine (G) produced a specific anodic signal, later explained by the oxidation of the DNA reduction product formed at highly negative potentials [2, 3, 9]. A, C, and G residues yielded their signals, not

only in nucleosides and nucleotides but also in RNA and DNA [2–5]; and NA signals were strongly influenced by the NA structures [4, 5, 10].

In the following decade, electrochemical techniques, and particularly differential pulse polarography (DPP), produced early evidence of DNA premelting and polymorphism of the DNA double helix (reviewed in [11]). The results of conventional electrochemical analysis of NAs with mercury or carbon electrodes immersed in the NA solution during the electrochemical measurements were thoroughly reviewed [4, 5, 10–18]. In the last 15 years, new trends appeared oriented toward the immobilization of the NA at the electrode surface. It was found that DNA and RNA could be easily immobilized at mercury and carbon electrodes, simply by immersing the electrode in a drop of NA solution for a short time. As a result of strong adsorption of DNA or RNA a stable layer was formed at the electrode surface; the electrode was then washed and electrochemical measurements were performed in solutions not containing any NA. By this method, the volume of the analyte was reduced by 2 to 3 orders of magnitude. The technique was called adsorptive transfer stripping voltammetry (AdTSV). Development of sensors (detectors) for DNA hybridization and for DNA damage applying adsorptive

or covalent immobilization of DNA at the electrode (transducer) to create recognition layers at their surfaces, became popular in the years that followed.

12.1.2

Nucleic Acid Samples

Currently, an electrochemist can analyze a number of different kinds of highly purified synthetic and natural DNA and RNA molecules. In addition to highly polymerized chromosomal DNA samples that were available even 50 years ago, better defined plasmid DNAs and viral DNAs and RNAs have become available (Fig. 1). Shorter or longer DNA fragments can be prepared by cleavage of the viral and plasmid DNAs by restriction endonucleases. Amplification of pieces of any DNA can be performed by the Polymerase Chain Reaction (PCR) from minute amounts of NAs. Biosynthetic polynucleotides with monotonous or random nucleotide sequences, as well as synthetic oligonucleotides, whose nucleotide sequence can be programmed at the automatic synthesizer, are commercially available. RNA oligonucleotides are, however, more expensive than oligodeoxyribonucleotides (ODNs). Oligonucleotides with chemically modified bases and/or the sugar-phosphate backbone, as well as end-labeled DNAs, can be prepared or purchased.

In this paper, we briefly summarize the basic electrochemical properties of NAs and their components, and survey the recent trends in the electrochemical analysis of NAs, including labeling of NAs with electroactive markers, covalent and noncovalent immobilization of NA at the electrode surfaces, and development of sensors for DNA hybridization and DNA damage. We wish to show that electrodes are important tools, useful in biochemical

analysis, which may help solve some specific biological problems and contribute to better understanding of NA interactions with electrically charged surfaces.

12.2

Electrochemical Behavior of NA Components

12.2.1

Adsorption/Desorption Behavior

12.2.1.1 **Mercury Electrodes**

The encounter of molecules at biological interfaces, such as cell membranes and nuclear matrix, is the initial step in biomolecular processes and a prerequisite for the manifestation of biological effects of biopolymers in living cells [19–21]. It has been known that electric fields having magnitudes equivalent to those existing at a charged cell surface/biological fluid interface affect the conformation of DNA in solution [22–24]. As a rough model of a biological surface/biological fluid interface, an electrolyte solution/electrode interface can be employed to study the interfacial behavior of NAs. Mercury electrodes, which have an atomically smooth surface, the charge of which can easily be changed and controlled in a relatively wide range, have proved to be well suited for such experiments [25].

NAs, as well as NA bases, nucleosides, and nucleotides, are strongly adsorbed at the mercury electrodes [26–63]. Among bases, G is most strongly adsorbed at these electrodes [28]. The adsorption can be followed by measurement of the impedance and/or differential capacitance of the electrode double layer [26, 27, 31, 32, 34–39, 41, 42, 47]. In 1965, it was found by one of us (VV) [26, 27] that NA bases possess an extraordinarily high ability of

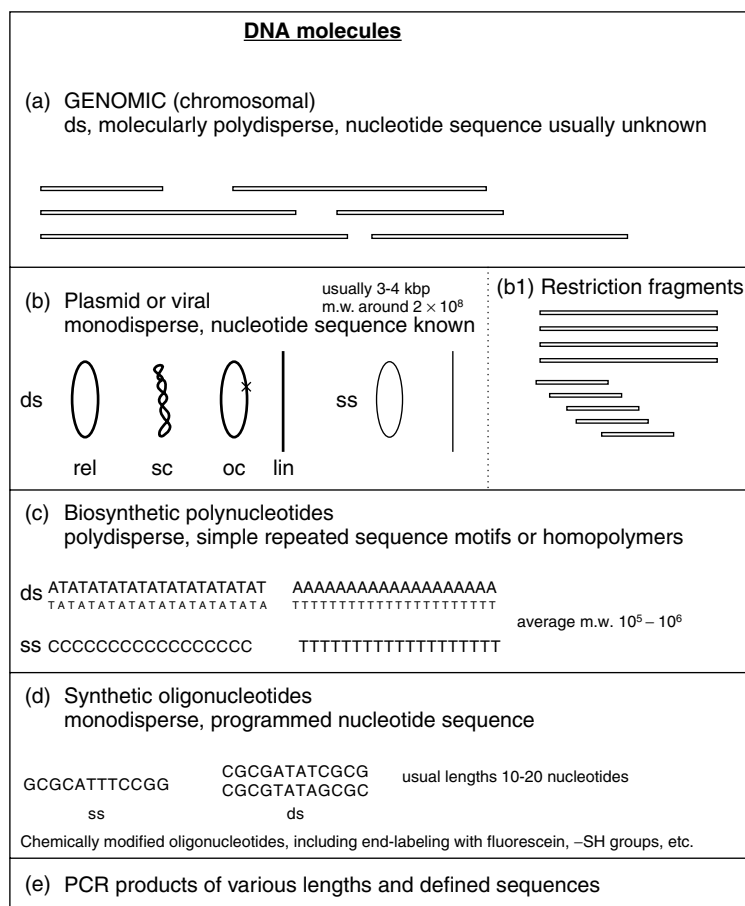


Fig. 1 Nucleic acid samples available for electrochemical experiments. (a, b) naturally occurring DNAs; (b1) dsDNA fragments of defined lengths and nucleotide sequences can be conveniently prepared by cleavage with restriction endonucleases; (c) NAs (both DNA and RNA) synthesized by enzymes; (d) fully synthetic DNAs and RNAs of limited lengths; (e) PCR, can amplify the desired DNA segment from template DNA. ds, double-stranded; ss, single-stranded, kbp, kilobase pairs. Covalently closed circles of sc, supercoiled and rel, relaxed DNA. oc, open circular DNA (containing at least one interruption of the sugar-phosphate backbone); lin, linear DNA. See text for more details.

self-association at the electrode surface and undergo a two-dimensional (2-D) condensation forming a monomolecular layer (self-assembled monolayer (SAM), a compact film). By this high condensation ability, NA bases differ from most of the other purine and pyrimidine derivatives,

which currently do not occur in NAs. The two-dimensional condensation was also observed in some of the halogen-, aza-, and methyl derivatives of common NA bases [28–31] and in most of the nucleosides [41, 43–46] and nucleotides [47–49, 64] commonly occurring in NAs.

The formation of a compact film at the electrode is characterized by the appearance of a well-defined capacitance “pit” on the capacitance-potential (C-E) curves (Fig. 2).

The orientation of bases and nucleosides in the compact film [50–52, 54–56], the effect of ions of the solvent and substituents of bases on the film formation [28–31, 34, 50–52, 54, 55, 65, 66], the energy of the interaction between bases in the compact film [34, 54, 55, 67, 68], and the kinetics of the two-dimensional condensation of bases at the electrode surface [43, 46, 54, 57–59, 65, 69–83] were investigated. In neutral bases the capacitance pit is usually observed near the potential of the electrocapillary maximum (potential of zero charge, p.z.c.), with the exception of bases with a large electric permanent dipole

moment [84] like C, which forms the pit at negative potentials [27, 47, 57, 85–87]. The halogen ions can induce a new potential region of condensation with C [86] and with A [59].

We have studied the effect of bromine substituents on the two-dimensional condensation of C, U, and uridine. The potential of maximum adsorption, and thus the potential of the capacitance pit, depends on the mutual competition between the electrostatic and nonelectrostatic adsorption forces and the forces that repulse the adsorbed molecules from the electrode surface. In neutral bases and nucleosides, the nonelectrostatic adsorption usually prevails and the pit appears near the p.z.c. With C at pH 5.0, the electrostatic adsorption on the negatively charged electrode surface via the positive charge on *N*-3

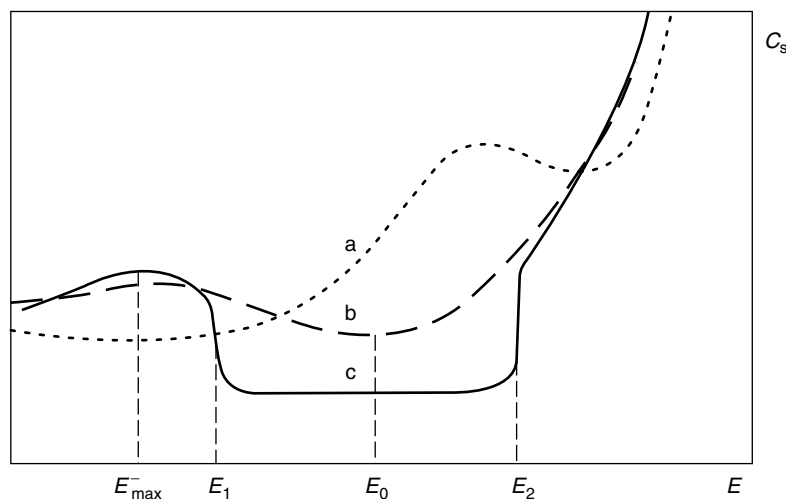


Fig. 2 Dependence of differential capacitance C_s on the electrode potential E . (a) capacitance curve of the background electrolyte measured at hanging mercury drop electrode (HMDE) in the absence of surface active substances, (b) capacitance curve of electrolyte solution with surface active substance, (c) capacitance curve characteristic for the two-dimensional condensation of adsorbed molecules on the electrode. E_{\max}^- , potential of cathodic tensammetric maximum. Between the potentials E_1 and E_2 , a compact film is formed on the electrode. (a) background electrolyte: 2 M NaCl, pH 7; (b) 20 mM thymine (T), pH 7, 40 °C; (c) 20 mM T, pH 7, 17 °C. [V. Drazan and V. Vetterl, unpublished].

and positive end of the permanent dipole moment prevails over the nonelectrostatic adsorption, and the pit appears at very negative potentials. The bromine substituent increases the polarizability of C and thus increases the nonelectrostatic dispersion forces between the C molecule and the electrode surface. With 5-Br-C the nonelectrostatic adsorption is stronger than the electrostatic one and the pit occurs near the p.z.c [31, 88]. The bromine substituent usually decreases the solubility of bases or nucleosides and increases the standard free energy of adsorption. Thus the bromine substituent can either decrease the tendency to two-dimensional condensation due to the lower solubility of the substituted derivative as was observed with 5-bromouracil [31], or can increase the 2D-condensation ability due to the higher adsorption energy of the substituted derivative as observed with 5-Br-uridine.

We have shown that the capacitance pit corresponding to the compact layer formed at the electrode surface is observed in the C solutions in 0.5 M NaCl at pH 5.5, but not at pH 7.0 [31, 85, 86]. The two-dimensional condensation of C molecules at the mercury electrode surface is thus obviously supported by protonation of a part of the C molecules. Ab initio quantum chemical calculations have proved that protonation significantly increases the stabilization energy of both stacked and hydrogen-bonded C dimers, which may support the two-dimensional condensation [89].

From the temperature dependence of the capacitance pit or electrocapillary measurements, the surface concentration of the adsorbed molecules and the area *A* required for an adsorbed molecule at the electrode surface can be determined [34, 43–45, 50–52, 55]. Using data obtained for the crystal structure of bases the area that would be occupied by one

adsorbed molecule in different surface orientations can be evaluated and compared to the experimentally determined area *A*. From these calculations, it has been concluded that at low surface concentrations (the so-called dilute adsorption region) the adsorbed bases lie flat at the electrode surface. In the compact layer, the adsorbed bases seem to adopt a perpendicular surface orientation [50, 60]. Similar reorientation from flat to perpendicular position at higher surface concentrations has been observed with several nucleosides and nucleotides [48, 51, 52, 54, 61]. Some nucleosides, such as adenosine, can probably adopt two different perpendicular orientations at the electrode surface [29, 41, 42, 50, 62, 63]. De Levie and Wandlowski [90] have suggested that the compact film of U is a planar array of hydrogen-bonded molecules, similar to that found in the solid state. The adsorption energy and the energy of the lateral interactions between bases in the compact layer can be estimated, either from the course of adsorption isotherms [27, 28, 50, 60–62] or from the temperature dependence of the capacitance pit [34, 54, 55, 91]. For A in a neutral solvent this energy was -4.7 kJ mol^{-1} [55].

Direct observation of an ordered phase of NA bases on solid electrodes by techniques, such as scanning tunneling microscopy (STM) and atomic force microscopy (AFM), may help determine the orientation of the molecules in the compact film [83, 92–98]. These techniques were also recently applied to the surface of mercury [99–101]. It was found that cationic detergent benzalkonium chloride (BAC), used for DNA spreading on mica in scanning force microscopy, forms a condensed film at the mercury electrode surface. The corresponding pit on C-E curves resembled the pits of bases and

nucleosides [102]. A similar cationic detergent cetyl-dimethyl-benzylammonium chloride formed capacitance pits on C-E curves as well [103].

12.2.1.1.1 Oligonucleotides Adsorption of oligonucleotides on mercury electrodes was studied by a.c. polarography [48, 49, 104, 105], surface tension measurements [106], DPP, and adsorptive stripping cyclic voltammetry (CV) [107]. The self-complementary decamer d(CCAGGCCTGG) produced cathodic and anodic signals. By measuring the anodic peak G (resulting from G residues), it was possible to detect the decamer at subnanomolar concentrations [107]. With oligoriboadenylates, it was found that the shorter molecules (dinucleotides and trinucleotides) were adsorbed with all A residues oriented flat at the electrode surface and with all sugar or sugar-phosphate residues close to the surface. The tetranucleotides and longer oligomers seemed to be adsorbed with a maximum of three A rings directly anchored to the electrode surface [106].

Impedance measurements of peptide nucleic acid (PNA) and DNA decamers (GTAGATCACT and complementary sequences) were performed at HMDE [108] (Fig. 3). From the calculated degree of the electrode coverage by adsorbed PNA and DNA decamers it was found that with DNA decamers the degree of the maximum coverage was reached near the potential (potentials are given against the saturated calomel electrode, if not stated otherwise) of -0.6 V, where the electrode surface is neutral and the decamers are adsorbed via their hydrophobic bases. The dependence of the electrode coverage degree by PNA molecules on the potential showed two maxima, at -1.2 V and -0.5 V. At -1.2 V, the electrode had a negative charge, and the PNA decamers were not electrostatically repulsed from the electrode as DNA decamers (in contrast to DNA the PNA backbone is electrically neutral [109, 110]). The second maximum at -0.5 V corresponded to the PNA adsorption by its hydrophobic bases [108]. Prolonged exposure of PNA to highly negative potentials did not result in PNA

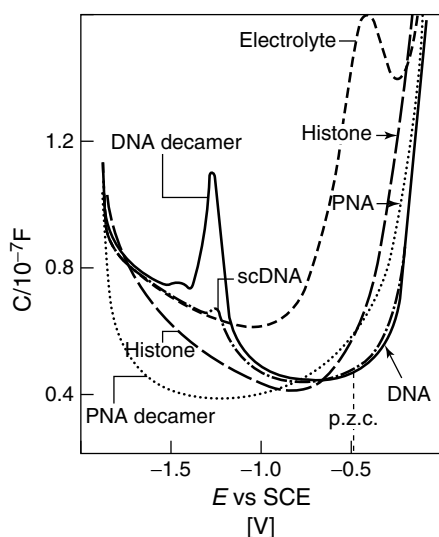


Fig. 3 AC impedance response of PNA and DNA decamers (nucleotide sequence GTAGATCACT), sc plasmid DNA (scDNA) and a histone at HMDE. Concentrations: DNA and PNA decamers $10 \mu\text{g ml}^{-1}$, pUC19 DNA $110 \mu\text{g ml}^{-1}$, histone $30 \mu\text{g ml}^{-1}$; The samples were adsorbed under conditions securing full coverage of the electrode at neutral pH and room temperature. (Adapted from M. Fojta, V. Vetterl, M. Tomschik et al., *Biophys. J.* **1997**, 72, 2285–2293.)

desorption, whereas almost all of the DNA was removed from the surface at these potentials.

12.2.1.2 Solid Electrodes

Recently, the use of solid electrodes [43, 50, 64, 72, 93, 94, 96, 111–127], instead of mercury, has opened new perspectives for the understanding of the factors that govern the formation of self-organized monolayers at the electrochemical interface and widened the experimental field, namely by STM and AFM imaging [64, 83, 93–96, 112, 113, 116–118, 126, 127]. Single crystal gold electrodes have been increasingly used in electrochemical studies so that reliable results are obtained on a well-defined surface structure, which now allows a correct assessment of the surface specificity of interfacial processes [124]. It was shown that U and uridine may form condensed layers, not only at the mercury electrode interface [31, 43, 46, 71] but also at a gold single crystal interface [72, 112]. Gold electrodes have been selected because they display a broad double layer region and have been the object of many investigations [114, 119–122]. Recently it was found that C and cytidine form condensed layers at the single crystal gold electrode as well [116, 128]. Both PNA and DNA oligomers displayed a strong adsorption onto the carbon electrode [129]. Potential-controlled release of DNA from solid electrodes has been utilized in the development of gene carriers for future gene therapies [130, 131].

12.2.2

Reduction and Oxidation

Among simple NA constituents, A and C (and their nucleosides and nucleotides) can be reduced at mercury electrodes

in aqueous solutions. Both bases produce well-developed pH-dependent polarographic waves involving base protonation (reviewed in [132, 133]). G is reduced at the mercury electrode at highly negative potentials close to background discharge, yielding 7,8-dihydrogen G [134, 135] (Fig. 4). This reaction is chemically reversible. Oxidation of the G reduction product can be observed in cyclic or in anodic stripping modes if the electrode is shortly exposed to highly negative potentials prior to scanning to positive potentials [136–138]. The mechanism of electroreduction of inosine (nucleoside of hypoxanthine, a deamination product of A) was recently studied using elimination polarography [139]. Reduction of T and U at a mercury electrode can be observed in nonaqueous media [140, 141]. At carbon electrodes, purine bases produce well-defined oxidation peaks within a wide pH range (0–12.5) [142, 143]. Purine nucleosides and nucleotides are oxidized at potentials more positive than the parent bases [144]. Signals corresponding to the oxidation of purine bases, nucleotides, and nucleotides have also been obtained using chemically modified carbon electrodes [145, 146] (for more details see Sect. 12.4.3). Recently, Cai and coworkers [147] proposed a method for trace A determination using an electrochemically/chemically modified (in alkaline sodium nitrate solution) carbon paste electrode (CPE). Pyrimidines are considered to be electroinactive on carbon electrodes; however, Oliveira-Brett and Matysik recently reported [148] specific anodic peaks observed in solutions of T and C bases (but not their nucleosides). Sugar components of nucleotides can be oxidized at copper electrodes [149].

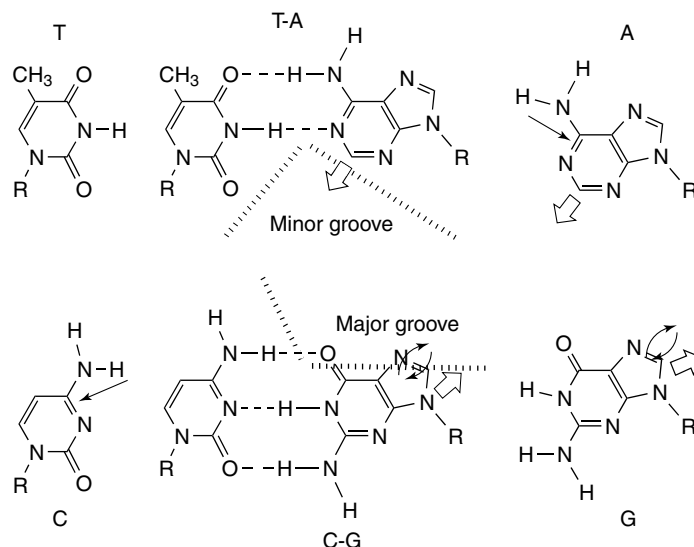


Fig. 4 Scheme of electroactive sites in NA bases. Adenine (A) and cytosine (C) are reducible at mercury electrodes. Guanine (G) undergoes a chemically reversible reduction at the mercury electrodes, yielding an anodic peak G due to oxidation of its reduction product. A and G can be oxidized at carbon electrodes. Watson–Crick base pairs TA and CG are shown without the reduction sites involved in hydrogen bonding. Arrows indicate schematically electrode reduction or oxidation: (\longrightarrow), reduction at mercury electrodes; (\rightleftharpoons), oxidation at carbon electrodes; (\circlearrowright), chemically reversible reduction/oxidation of G at mercury electrodes; for more details see the text.

12.2.3

Microanalysis of Nucleic Acid Components by Stripping Techniques

12.2.3.1 Principles

Cathodic stripping voltammetry (CSV) can be used to determine low concentrations of substances that form sparingly soluble compounds with mercury of the electrodes [150–152]. The process of deposition (first step) can be generally expressed as production of mercury ions and formation of a sparingly soluble film. The second step (stripping) takes place in a negative-going potential scan, reducing the deposited salt back into the solution, stripping the film. The

relations between the peak potential at equilibrium on one side, and the pH, anion concentration and solubility on the other, were published [152–154]. In general, the peak potential becomes more negative with increasing pH, increasing anion concentration and decreasing solubility of the compound, and more positive with the higher association constant of the acid.

12.2.3.2 Reactions of Pyrimidine and Purine Bases with the Electrode Mercury

It was first shown by Revenda [155] that some inorganic anions form sparingly soluble salts with mercury to produce anodic polarographic waves. Later, it

was found that similar anodic currents were produced by sulfur-containing organic substances [156], and by organic compounds such as derivatives of barbituric acid, including U [157, 158]. Depolarization of the mercury electrode with all DNA bases was demonstrated by Paleček [2, 9], using the OP method. All NA bases produced in an alkaline medium indentation on the OP curves dE/dt against E , probably caused by formation of compounds with the electrode mercury. At the time, these findings were little exploited for analytical purposes because of a low sensitivity of the available methods. At millimolar concentrations, it was, however, possible to detect changes in the indentations of T, U, 5-hydroxymethyluracil and other bases because of UV-irradiation of their solutions [159]. Later, we showed that pyrimidine and purine bases commonly occurring in NAs (U, T, C, A, G) and a number of their derivatives yielded similar anodic waves using DC polarography (DCP) and normal pulse-polarography (NPP), and peaks using DPP [160, 161]. These signals appeared close to 0 V because of the formation of sparingly soluble compounds with mercury. The behavior of NA bases was studied at various concentrations of the bases, pH values, pulse amplitudes, and so on, by NPP and DPP. The DPP behavior of C was similar to that of U; detection limit of C was about 5 μ M. Differences between the behavior of U and T were large at higher concentrations at which the electrode was fully covered [160]. DPP rendered it possible to determine A and G at concentrations of 1 to 10 μ M [161].

Earlier, it was assumed that the use of CSV in organic analysis is limited mainly to sulfur-containing substances [162–164]. Using the HMDE, it was demonstrated that pyrimidine and

purine bases, and their derivatives, can be deposited on a mercury electrode and then stripped out by scanning to negative potentials [160, 161, 165, 166]. Using DPCSV, purine and pyrimidine bases were analyzed at very low concentrations (Table 1). The sensitivity of the determination depended on several parameters, such as the potential and time of deposition, electrode size and scan rate. Pyrimidine bases could be determined at concentrations down to 10 to 100 nM, and purine bases at concentrations as low as 1 to 10 nM (the limit of A detection was about 2 nM at 6 min waiting time) [161, 166]. Nucleosides and nucleotides derived from pyrimidine bases were inactive and did not substantially interfere with the determination of bases [160].

For CSV analysis of purine and pyrimidine bases, we also applied the transfer step (Sect. 12.4.4.) to find out whether the layers of mercury compounds were sufficiently stable to remain on the electrode after its washing and transfer to another solution. (This method was called cathodic transfer stripping voltammetry CTSV). We found that A yielded a well-developed peak whose height only slightly decreased as a result of medium exchange [167]. In contrast to A, C produced no CTSV signal while showing a peak in conventional CSV. This result suggested that by using CTSV it would be possible to analyze some mixtures of bases that differ in their ability to undergo transfer of their deposited layers.

12.2.3.3 Unusual Bases and Nucleosides

12.2.3.3.1 5-Ribosyluracil (pseudouridine)

5-Ribosyluracil (pseudouridine) is one of the family of unusual nucleosides contained in transfer ribonucleic acid (tRNA), and its determination in urine

Tab. 1 The ability of pyrimidine and purine derivatives to form sparingly soluble compounds with the electrode mercury

<i>Pyrimidine derivatives</i>			<i>Purine derivatives</i>		
Cytosine	+	[160,166]	Adenine	+	[161,166]
Thymine	+	[160,166]	Guanine	+	[161,166]
Uracil	+	[160,166]	Xanthine	+	[161]
Cytidine	–	[160]	Hypoxanthine	+	[161]
Thymidine	–	[160]	Adenosine	+	[161]
Uridine	–	[160]	Guanosine	+	[161]
Pseudouridine	+	[169]	Xanthosine	+	[161]
5-Bromouracil	+	[166,176]	Inosine	+	[161]
5-Chlorouracil	+	[166,176]	1-Methyladenine	+	[170]
5-Fluorouracil	+	[166,176]	3-Methyladenine	+	[170]
5-Acetyluracil	+	[176]	6-Methyladenine	+	[170]
5-Formyluracil	+	[176]	2-Aminopurine	+	[166]
5-Nitrouracil	+	[176]	8-Oxyadenine	+	[166]
5-Azauracil	+	[176]	6-Benzyladenine	+	[166]
6-Azauracil	+	[176]	Uric acid	+	[170]
6-Chlorouracil	+	[166]			
6-Methylthymine	+	[176]			
2-Thiouracil	+	[166]			
Orotic acid	+	[166]			

Sparingly soluble compound with the electrode mercury is produced (+), not produced (–).

and blood is used in cancer diagnostics [168]. Pseudouridine as well as uridine and deoxyuridine were investigated by DCP, DPP, and NPP [169]. Among these U nucleosides, only pseudouridine yielded anodic polarographic currents in alkaline medium, whereas uridine and deoxyuridine were inactive under the same conditions [169]. The inactivity of these substances was caused by substitution of the base residue at position N1 by the sugar, while in the case of the uridine isomer, pseudouridine and the ribose residue were bound to C5 of the pyrimidine ring. Using DPCSV in connection with a HMDE, it was shown that pseudouridine could be determined in concentrations down to 20 to 60 nM.

12.2.3.3.2 Methylated Adenines Adenine and its methylated derivatives (1-CH₃-Ade,

N-CH₃-Ade and *N,N'*-diCH₃-Ade) were studied in alkaline solutions using several electrochemical methods, including CSV [170]. Some of these substances represent rare NA constituents. It was shown that the 6-aminogroup of A is the mercury binding site, and CSV could be used for the determination of methylated As. The detection limit for *N*-CH₃-Ade was comparable to that for A [170]. Methyl substituents affected the adsorption and two-dimensional condensation of A [30].

12.2.3.3.3 5-Fluorouracil (5-FU) 5-Fluorouracil (5-FU) is frequently used in the treatment of a wide variety of carcinomas. It is well known that many anticancer drugs are toxic to the treated organism and that the actual dosage must be carefully controlled. It was demonstrated that 5-FU reacts with the mercury electrode

[forming a sparingly soluble compound] and can be determined by CSV at low concentrations [166]. Later, it was found that in a slightly alkaline medium 5-FU could be monitored [171] at pH 10 (borate buffer) or at pH 7.6 (borax with 0.1 M KNO_3) [172], at concentrations down to 50 nM. CSV was also applied to determine 5-FU in human serum with the previous solvent extraction procedure to prevent the interference of other electrochemically active substances. The limit of detection was 5 μM and mean recovery 43% [171]. Recently, CSV and DPCSV studies of determination of 5-FU in urine [173] and in blood serum [174] were published. Using DPCSV, and following a simple pretreatment procedure with trichloroacetic acid, 5-FU was determined with almost 100% recovery [175, 176]. It was also shown that a flow-injection system with mercury electrode as a detector could provide sensitive CSV determination of 5-FU [177, 178].

12.2.3.4 Sparingly Soluble Compounds of Nucleic Acid Components with Copper

In the presence of A and adenosine, the copper(II)/copper(Hg) couple split to the copper(II)/copper(I) and copper(I)/copper(Hg) couples [179, 180]. Sparingly soluble compounds of copper(I) with A and its ribonucleoside were accumulated on the electrode, either by reduction of the Cu(II) ions or by oxidation of the copper amalgam electrode. The copper(I) A deposit was stripped either cathodically or anodically. The stripping peaks obtained for copper complexes had higher detection limits, but appeared over a wider range of pH and at more negative potentials than the peaks related to mercury compounds [161]. It was shown that in addition to A, other purine bases, such as G, hypoxanthine, xanthine, and their nucleosides (guanosine and inosine) [181–183],

as well as pyrimidine base C and cytidine [66] produced similar effects in the presence of copper; these compounds were detectable at low concentrations by stripping techniques.

12.3

Adsorption/Desorption Behavior of NAs

On interacting with electrodes, DNA and RNA are usually strongly adsorbed, undergoing charge transfer reactions in their adsorbed states and sudden desorption in narrow potential ranges, resulting in tensammetric signals [10, 12, 14]. Both the faradaic and tensammetric signals can provide information, not only about the kind and about the concentration of the analyzed NA but also about the changes in the NA structure, and about the interaction of the NAs with various compounds. Studies of DNA and RNA adsorption/desorption properties are, therefore, of importance for a better understanding of different types of interactions of these biomacromolecules with electrodes. Miller measured the differential capacitance of the DME in 1961 and showed that ss and dsDNA as well as RNA are adsorbed in a potential range of about 0 to -1.1 V [37, 38].

12.3.1

Mercury Dropping Electrode

The adsorption of NAs can be followed by a number of physical and electrochemical methods such as voltammetry [184], a.c. polarography [31, 40, 185–187], measurements of the surface tension [40, 188, 189], and of the impedance and/or differential capacitance of the electrode double layer [31, 37, 38, 88]. Differential capacitance C of the electrode double layer is a sensitive indicator of the adsorption. When the NAs are adsorbed at the

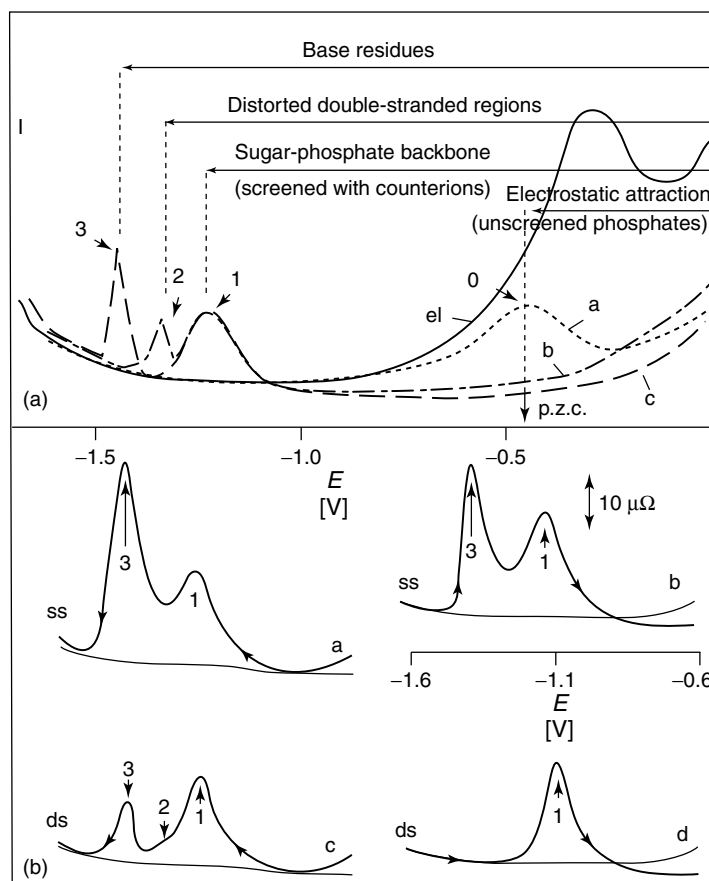


Fig. 5 Adsorption/desorption behavior of double- or single-stranded DNA at mercury electrodes (at weakly alkaline pH's). (a) scheme of AC polarographic curves of DNA obtained with DME. (a) dsDNA, low ionic strength; (b) dsDNA, moderate ionic strength; (c) ssDNA; (el) background electrolyte; p.z.c. See text for more details. (b) AC admittance curves measured at HMDE. (a, b) ssDNA; (c, d) dsDNA; (a, c) initial potential -0.5 V, potential scanned from positive to negative values; (b, d) initial potential -1.7 V, potential scanned from negative to positive values [F. Jelen and P. Belusa, unpublished]; see text for more details.

electrode surface, they remove from the surface the molecules and ions of the solvent and lower the value of the differential capacitance of the electrode double layer, because the solvent has usually much higher dielectric permittivity than the NAs. The potential of maximum adsorption of NAs is usually close to the p.z.c.

At desorption potentials the adsorption-desorption (tensammetric) peaks appear on the C-E curves, resulting from sudden changes of the surface charges and/or surface coverage within a narrow potential range.

It was shown [184, 186, 190–197] that all types of residues—purine and pyrimidine

bases, ribose and/or deoxyribose, and phosphoric acid participated in the adsorption of NAs. The extent of participation of these components in the adsorption of NAs depended on pH and ionic strength of the solvent and on the electric charge of the electrode surface given by the electrode potential E (Fig. 5). At neutral pH and moderate ionic strength, at the electrode potentials close to the p.z.c., hydrophobic bases were adsorbed most strongly. At low ionic strengths and on the positively charged electrode surface the NAs were adsorbed electrostatically by their negatively charged phosphate groups.

12.3.1.1 Adsorption of Double-stranded (Native) DNA

At moderate ionic strengths ($\mu \sim 0.3$ M), the phosphate charges are screened and dsDNA is adsorbed as an electroneutral compound [186, 190], predominantly via the sugar-phosphate backbone. The tensammetric (adsorption/desorption) peak appears on a.c. polarograms and/or C-E curves at about -1.1 V and is denoted as peak 1 in Fig. 5. If dsDNA contains some ss or distorted regions in which the hydrophobic bases can come into contact with the electrode surface, another tensammetric peak 2 appears on C-E curves around a potential of -1.3 V. This peak corresponds to the desorption (reorientation) of distorted regions of dsDNA that are adsorbed firmly via bases (Fig. 5).

At low ionic strengths ($\mu < 0.1$ M) dsDNA is electrostatically adsorbed via charged phosphate groups at potentials corresponding to the positively charged electrode surface. Unscreened phosphate charges are repulsed [186, 198] from the negatively charged surfaces, and dsDNA can be only weakly adsorbed via bases (coming predominantly from the

molecule ends in shorter intact dsDNAs), if available. The corresponding tensammetric (reorientation) peak occurs around the p.z.c. and is denoted as peak 0 (Fig. 5).

12.3.1.2 Adsorption of Single-stranded (Denatured) DNA

In the range of ionic strengths 0.01 to 1.0 M single-stranded (ss) DNA is adsorbed as an apparently electroneutral molecule via sugar-phosphate backbone and (more strongly) via bases [10, 184, 186, 190–197]. The tensammetric peak at about -1.1 V corresponding to the desorption of sugar-phosphate backbone was denoted as peak 1. The peak around -1.4 V corresponding to the desorption of bases was denoted as peak 3 (Fig. 5).

12.3.2

Adsorption Kinetics at Mercury Dropping and Hanging Electrodes

Adsorption of DNA is diffusion-controlled [37]. If insufficient time is allowed for adsorption, the surface will only be partly covered and the amount adsorbed Γ_t (surface concentration) at a time t will be given by the Koryta expression [199]

$$\Gamma_t = kc\sqrt{Dt} \quad (1)$$

where $k = 0.745$ for the DME and $k = 1.13$ for the HMDE [200, 201], c is the bulk concentration, and D is the diffusion coefficient. The differential capacitance of the electrode double layer C depends on Γ_t and thus on concentrations c , if measurements are made at constant t . At low c Eq. (1) is valid and the dependence of the capacity C on c is a straight line. At high concentration c the surface concentration Γ_t reaches the saturated value Γ_s and the capacity C reaches almost constant value C_s . The intercept of the linear plot of

capacity C against concentration c for dilute solutions with the almost constant C_s values at high concentrations gives the limiting concentration c_s at which the surface becomes fully covered at the given time t . From the values c_s the saturated surface concentration Γ_s (fully covered surface) and the area A occupied per one nucleotide on the electrode surface $A = M/N\Gamma_s$ (M is the mean molecular weight of a nucleotide and N is the Avogadro number, $N = 6.023 \times 10^{23} \text{ g}^{-1} \text{ mol}^{-1}$) can be calculated [37]. Miller [37, 38] found that with herring sperm denatured DNA adsorbed at DME (dropping time $t = 14.5 \text{ s}$) the saturated value of the surface concentration Γ_s was reached at $c_s = 75 \mu\text{g ml}^{-1}$. From Eq. (1) it was calculated that $\Gamma_s = 6 \times 10^{-5} \text{ mg cm}^{-2}$. The corresponding area A occupied per one nucleotide on the electrode surface was $A = 93 \text{ \AA}^2$ [37]. Later, Janik and Sommer [191] found about 85 \AA^2 per nucleotide for poly(U) containing about 100 nucleotides; the area A decreased with the increasing length of the polynucleotide chain down to 75 \AA^2 (with polynucleotides of about 1500 nucleotides). Coverage of about 110 \AA^2 per molecule of tRNA (about 75 nucleotides) was observed [202]. These results suggest that in longer ss NA chains the ratio of three-dimensional loops/adsorbed segment trains may increase, allowing smaller fraction of the nucleotide residues to come into direct contact with the surface.

We studied the time dependence of the impedance of the electrode double layer around the potentials of the tensammetric peaks and around the potential of maximum adsorption of native and denatured calf thymus DNA ($100 \mu\text{g ml}^{-1}$ in 0.3 M NaCl with $0.05 \text{ M Na}_2\text{HPO}_4$, pH 8.6). At potentials of maximum adsorption (around -0.7 V) the differential

capacitance of the double layer decreased faster with denatured DNA than with native DNA as a result of the higher diffusion coefficient of denatured DNA (as shown in previous studies) [10, 203]. The final value of the differential capacity $11 \mu\text{F cm}^{-2}$ was reached with denatured DNA after about 4 s, with native DNA after 30 s [88]. Polyadenylic acid [poly(A)] can assume (depending on pH and ionic strength) either ss or ds form [186, 187, 204–206]. The more flexible ss poly(A) has a higher diffusion coefficient than the double-helical one [206] so that the diffusion transport to the electrode of ss poly(A) is faster than the adsorption of the ds one [194].

12.3.3

Electrochemical Impedance Spectroscopy (EIS)

Useful information about the adsorption kinetics, mobility of the adsorbed polynucleotide segments, and mechanism of electrode processes can be obtained by measurement of the frequency dependence of the impedance of the electrode double layer (EIS) [31, 88, 207–209]. If the adsorption/desorption process is slow with respect to the period of the a.c. potential used for the impedance measurement, the measured capacitance values decrease with increasing frequency (dispersion of the capacity). The frequency effect is most remarkable around the potentials of adsorption/desorption peaks. With more flexible ss polynucleotides, the frequency effect is larger than with the more rigid ds ones [210].

It was shown [91, 208, 211, 212] that for monomeric surface-active substances, diffusion to the surface is the slowest step and, therefore, the rate-determining factor in the adsorption mechanism at the

surface. Consequently, at high bulk concentration of the surface-active material, when the diffusion transport is fast as per Fick's First law, the height of the tensammetric peak depends less on frequency than at low bulk concentration (slow diffusion transport). On the other hand, the bulk concentration of a polymeric substance has sometimes no influence on the frequency dependence of tensammetric peaks. Complete lack of frequency dependence of the tensammetric peaks on the bulk concentration indicates that no significant diffusion of whole polymeric molecules takes place during the variation in potential of the imposed alternating voltage. Hence, the frequency effect must depend on the rate of migration of adsorbable segments from the surface phase into the adsorption layer and vice versa. Migration of segments can occur only in conjunction with rearrangement of the whole polymeric molecule; consequently, the temperature dependence of the dispersion is expected to be far stronger than in the case of unhindered diffusion of small molecules [211, 212].

The lack of any dispersion of the capacity in the peaks of polylysine [212] shows that the adsorption/desorption process that gives rise to the peaks is not diffusion controlled, in spite of the fact that the diffusion of the polymeric molecules to the surface is a relatively slow process, requiring times on the order of seconds to reach equilibrium at polylysine concentrations employed. This effect is explained by assuming that there exists at the interface a region of high polymer concentration, known as the surface phase, and that the peaks result from the adsorption and desorption of segments of the polymer from the surface phase. This process does not need to depend on the diffusion of whole polymer molecules from the solution, and

is fast enough at elevated temperatures to keep pace with a signal of low audio frequency [208, 212]. Similar behavior might be expected with other biopolymers, including DNA.

From the frequency dependence of the impedance of the electrode double layer represented in a complex impedance plot (the imaginary component Z'' is plotted against the real component Z' , Cole-Cole, or Nyquist plot), the electric equivalent circuit of the electrode covered with an adsorbed layer can be determined. From such a circuit, the physical parameters of the layer, such as the effective thickness and the degree of molecular order of the layer, can also be evaluated [213–221]. The complex plane impedance plots for DNA exhibited arc shapes, from which the apparent resistance R_2 of the layer and the solution resistance R_1 were determined. The resistance R_2 represents the dielectric losses of the capacitance of the electrode double layer, that is, the energy lost as heat, which arises because of the friction of charged DNA segments forced to move in a viscous solvent by an a.c. electric field [88]. It was found that with DNA solutions at the potentials where desorption takes place, the dielectric losses are higher (i.e. the resistance R_2 is lower) than at the potentials of maximum adsorption. Desorption of denatured ssDNA is accompanied by higher dielectric losses than desorption of native dsDNA. With denatured DNA desorption of more firmly bound bases is accompanied by higher dielectric losses than desorption of the sugar-phosphate backbone [88]. In the potential region of desorption the resistivity component of the impedance increases more steeply in ssDNA than in dsDNA. This can be explained by a higher flexibility of the denatured DNA compared with the dsDNA resulting in higher dielectric

losses during the adsorption/desorption process [88].

12.3.3.1 Other Techniques

The ellipsometric method was used to study adsorbed DNA for the first time by Humphreys and Parsons [222]. Since that time the sensitivity of this method has appreciably increased [223]. The measurement of x-ray reflection enabled studies of the structure of very thin layers (down to several Å) and the morphology of the interface [224].

12.3.4

Adsorption of NAs on Other Electrodes

Electrochemical techniques, scanning probe microscopy (STM, AFM), and ellipsometry can be used for the investigations of layers of NA bases, nucleosides, and polynucleotides adsorbed and/or deposited on metallic and semiconductor substrates. Hinnen and coworkers [225] studied the adsorption of ds and ssDNA on gold electrodes by CV and differential capacitance measurements. From the gold surface, the DNA was completely desorbed at -0.8 V. The ellipsometric observation [222] and impedance measurements [108] showed complete desorption of ssDNA from the Hg surface at about -1.6 V. Thus, the DNA on the Hg surface was still adsorbed at the potentials of reduction of base residues, while from the gold surface DNA was desorbed (at -0.8 V) before the reduction of base residues could take place [225]. For a potential step from -0.8 V to a potential near the p.z.c. (around 0 V), the time required to obtain a nearly constant value of differential capacitance using a gold electrode was about 7 min for native DNA and 2 min for denatured DNA; the final value of the differential capacity being about $12 \mu\text{F cm}^{-2}$

both for ds and ssDNA. The final value using a Hg electrode was $11 \mu\text{F cm}^{-2}$ and the time required to obtain this nearly constant value was shorter than with a gold electrode.

The adsorption of DNA on gold was also studied by STM and AFM techniques [226, 227]. NAs were adsorbed in a broad range of potentials on carbon and silver electrodes [126, 129, 188, 189, 228, 229]. Gold surfaces modified with thiol-derivatized DNA duplexes were studied as a function of potential using AFM [230]. The duplexes either stood up (up to about $+0.45$ V against a Ag wire) or were flat (at more positive potentials) on the gold surface, depending on the electrode potential relative to p.z.c. At open circuit monolayers of well-packed DNA helices with a film depth of about 45 Å corresponding to an average $\sim 45^\circ$ orientation of the helical axis with respect to the gold surface were formed. The voltage-induced morphology changes were reversible and constituted a nanoscale mechanical switch. New insight into the mechanism of biopolymer adsorption at charged surfaces can be obtained by the study of surface properties using optical methods [84, 223, 231–235] and x-ray reflection [224].

Adsorption of organic molecules on the surface of a semiconductor influences the region of the space charge in it. The effect of the internal electric field of the semiconductor on the optical properties of its surface is well established [236]. A number of significant studies of organic thin films have been carried out using ellipsometry [237], showing high sensitivity of this technique to the interfaces with organic species, and to very thin films of biological materials [234, 235, 237]. Ellipsometry has experienced a rapid evolution in the last two decades. The extension of the technique into the infrared region was

possible by coupling the ellipsometer to a Fourier-transform infrared spectrometer (FTIR) [223]. This combination provided significant advantages in studying the optical response of complex thin-film structures, such as high-temperature superconductors [232] or anisotropic materials [231, 233].

Adsorption of ssDNA on gallium arsenide (GaAs) surfaces was studied, and its reactions with complementary and noncomplementary strands probed [238]. The adsorption of DNA on GaAs surfaces was studied, both on a GaAs wafer and on the molecular controlled semiconductor resistor (MOCSEr) [239] using FTIR spectroscopy, X-ray Photoelectron Spectroscopy (XPS) measurements, and electrical measurements. It was found that DNA is bound directly to the GaAs surface through the phosphate group, without any modification of the surface or of the adsorbates. The hybridization process of the adsorbed ssDNA with its complementary strands was performed both on a GaAs wafer and on the MOCSEr and then compared to the reaction with the noncomplementary strands. Both the IR spectroscopy and the MOCSEr indicated selectivity in the reactions [238].

12.3.4.1 DNA Adsorption to Charged Lipid Membranes

The negatively charged phosphate groups along the DNA backbone strongly interact with cationic lipid membranes, to which DNA readily adsorbs forming highly ordered two-dimensional aggregates. These aggregates can be imaged with AFM. It was found that the DNA adsorption depends on the surface charge density and on the size of the cationic lipid bilayer areas [240]. A condensed phase of DNA on a lipid membrane was also observed by Spector [241] using AFM.

12.4

Reduction and Oxidation of NAs on Different Electrodes

NAs can be reduced and oxidized at electrodes yielding faradaic signals that can be useful in biochemical analysis (reviewed in [14, 15, 242]). Perhaps the largest number of results has been obtained with mercury and carbon electrodes.

12.4.1

Mercury Electrodes

In agreement with the electrochemical behavior of the monomeric units of the NAs (Sect. 12.2), A and C residues in single-stranded (ss) NAs were reducible at mercury electrodes (Figs. 4, 6). The presence of G in DNA and RNA was manifested by an anodic peak G in cyclic modes (Figs. 4, 6a). T and U residues were inactive in aqueous solutions; in nonaqueous solutions (such as dimethyl formamide with 0.1 M tetrabutyl ammonium perchlorate) reduction of U residues was observed in poly(U) [243]. With ssNAs, qualitatively similar results were obtained, both on the DME and on the HMDE; this was, however, not the case with dsNAs where significant (relatively slow) conformational changes took place at the HMDE surface under certain conditions (Sect. 12.6). Reduction of NAs on mercury electrodes involved protonation of the NA base residues [10], similar to protonation of free bases (Sect. 12.2).

12.4.1.1 Reduction of Adenine and Cytosine Residues

In contrast to free A, which is reduced at acid but not at neutral pHs, reduction of A residues in ssDNA and ssRNA can be observed even at neutral pH, when a

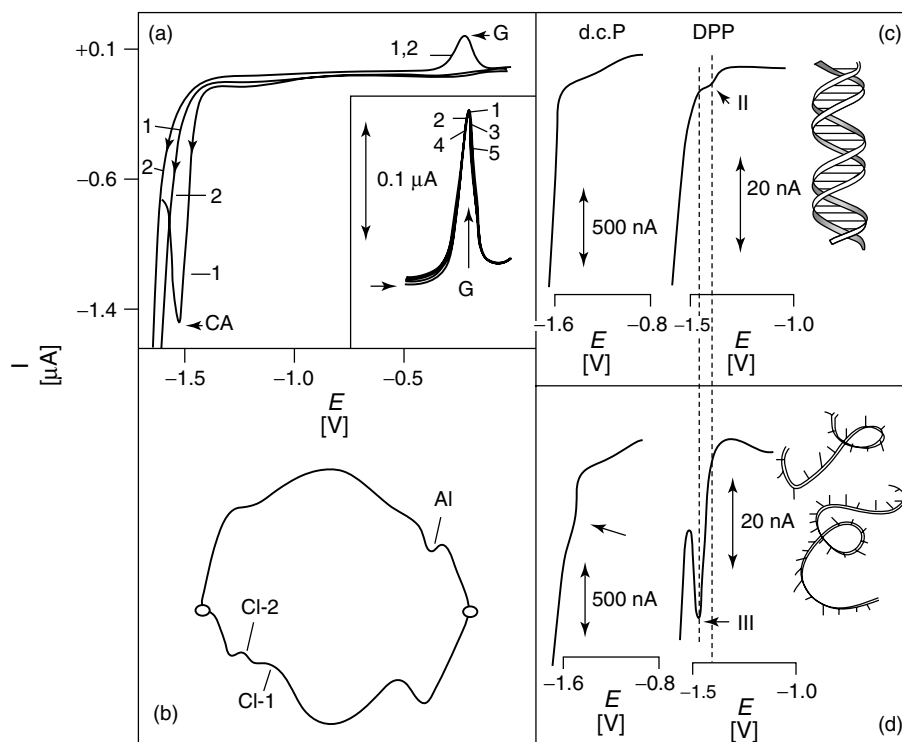


Fig. 6 Schemes of reduction and oxidation signals of DNA at mercury electrodes. (a) cyclic voltammograms of ssDNA obtained upon repeated potential cycling. (CA), peak due to reduction of C and A; (G), peak due to G; inset, detail of peak G; the succeeding scans are numbered. (b) OP at controlled AC: polarogram $dE/dt = f(E)$ of ssDNA. The indentations CI-2 and AI correspond to peak CA and peak G, respectively. (c, d), d.c. and DP polarograms of (c), ds or (d), ssDNA. DPP peak III corresponds to the CV peak CA. (Adapted from E. Paleček, in *Topics in Bioelectrochemistry and Bioenergetics* (Ed.: G. Milazzo), John Wiley & Sons, Chichester, 1983, pp. 65–155, Vol. 5; F. Jelen, E. Paleček, *Biophys. Chem.* **1986**, 24, 285–290; L. Havran, M. Fojta and E. Paleček, unpublished.)

suitable salt (such as 0.3 M CsCl or 0.3 M ammonium formate) efficiently screening the negatively charged phosphates of the NA (and facilitating the nucleic acid adsorption) is used in a buffered background electrolyte. Under these conditions, A and C residues in DNA and RNA are reduced in an adsorbed state, usually in a single peak (wave) at potentials close to -1.4 V. For more details, see previous reviews [4, 5, 10, 31] and references therein.

12.4.1.2 Anodic Signal of Guanine Residues

The ability of DNA and RNA to produce an anodic signal due to G residues was recognized about 40 years ago by means of OP [2, 3, 9] (Fig. 6b). It was shown that at highly negative potentials of the background electrolyte decomposition a G reduction product was formed, the oxidation of which was probably responsible for the observed anodic signal [245, 246]. Then, for almost two decades, this phenomenon

was little studied in connection with replacement of OP by differential (derivative) pulse polarography as a preferred method for the NA electrochemical analysis.

Application of CV to studies of G signals in guanosine [134, 135], synthetic polynucleotides [244], and DNA [135], as well as identification of the G reduction product by means of macroscale electrolysis [135], helped to understand better the electrode processes to which G residues were subjected on the mercury electrode and to find conditions suitable for the analysis of G-containing compounds [136]. It has been shown that ODNs [107, 247], synthetic polynucleotides, DNAs, and RNAs [136, 138] as well as PNA [247] containing G display in CV (or in other methods working in the cyclic mode) an anodic peak close to -0.3 V (peak G) (Fig. 6a), while NAs not containing G do not produce this peak. A condition for the appearance of peak G is the previous polarization of the mercury electrode to sufficiently negative potentials (around -1.8 V). At these potentials reduction of G residues takes place involving the 7,8 double bond of the imidazole ring in G as a primary reduction site (Fig. 4). In the anodic process reoxidation of the G reduction product back to G occurs. This chemically reversible process takes place even when a NA contains A and/or C residues in addition to G, where A and C reduction leads to the formation of products blocking the electrode surface (Fig. 6a) [244]. The electrode process of G residues involves protonation [135, 136], and close to neutral pH it requires the presence of some salts in the background electrolyte, such as 0.6 M ammonium formate, 0.1 M MgCl_2 , and $\text{Mg}(\text{ClO}_4)_2$ [136], to provide a well-developed peak G. Peak G is highly symmetric (suggesting involvement of adsorption in the electrode process), offering a better possibility for the

determination of NAs at concentrations below ppm (by stripping techniques) than the highly asymmetric reduction peak of C and A residues formed at potentials too close to the background discharge. Square wave voltammetric (SWV) stripping [248] and constant current chronopotentiometric stripping analysis (CPSA) [249] were applied to study peak G, at concentrations below 1 ppm both techniques produced a peak G better developed than that obtained with CV. In CPS and SWVs analyses, the electrode was exposed to negative potentials (around -1.8 V) for at least 1 s; prolonged contact of ssDNA at these potentials was favorable for the accumulation of the G reduction product. At these potentials a disturbance of the structure of dsDNA on the electrode surface may, however, take place (Sects. 12.5 and 12.6).

Recently mercury film electrodes (MFE) have been employed in NA analysis. Using mercury film on a silver electrode, cathodic signals of electroreducible nucleosides and high concentrations (hundreds of $\mu\text{g ml}^{-1}$) of denatured and degraded calf thymus DNA were obtained [250]. We used mercury film on a glassy carbon electrode (GCE) for the measurements of both redox and tensammetric response of DNA, RNA, synthetic polynucleotides, and PNA [251]. Yeast tRNA and calf thymus ssDNA were detected at concentrations of 50 and 100 ng ml^{-1} , respectively, at 180 s accumulation, when peak G was measured using CPSA at the MFE. Moreover, MFE (like the HMDE) was capable of detecting cleavage of DNA in solution and on the electrode surface [252] (Sect. 12.9).

12.4.2

Carbon Electrodes

Oxidizability of A and G residues (Fig. 4) in polynucleotides was demonstrated by

the end of the 70 s [243, 253]. Linear sweep voltammetric (LSV) signals were, however, poorly developed and the improvement achieved by application of DPV [253] was not sufficient to obtain sensitivity comparable to that obtained with mercury electrodes. Reports of well-developed peaks produced by ssDNA on GCE [254] were probably due to the presence of free purine bases released from DNA by treatment with concentrated perchloric acid [248].

Recently, application of CPSA with sophisticated baseline correction dramatically improved the sensitivity of the NA analysis on carbon electrodes [255–257]. Poorly developed peaks and inflections produced by NAs at concentrations of hundreds or tens of micrograms per ml with voltammetric techniques turned into well-developed peaks G^{ox} and A^{ox} (due to oxidation of G and A, respectively) detectable at concentrations 2 to 3 orders of magnitude lower (Fig. 7). It was shown that both the interfacial and redox properties of RNA and DNA are strongly dependent on the nature of the carbon electrode materials [258]. The trend in the sensitivity: CPE > pyrolytic graphite >

highly oriented pyrolytic graphite > carbon strip (showing detection limits for $(G)_{20}$ ODN of 20, 30, 40, and 50 ng per ml, respectively, using 5-min accumulation); at these ODN concentrations, no response was obtained with glassy carbon and carbon fiber electrodes. Careful searching for a suitable carbon fiber material in J. Wang's laboratory resulted in a finding that carbon fibers are suitable as microelectrodes for determination of NAs at high sensitivity in unstirred solutions at very low ionic strength [259]. CPSA of NAs with carbon electrodes now offers sensitivities comparable to those obtained with mercury electrodes [247, 257, 260]. Recent data suggest that even the voltammetric stripping on carbon electrodes can match the sensitivity of CPSA, if proper baseline correction is applied to compensate for the very high charging currents of carbon electrodes [247, 261]. Renewable graphite pencil electrodes were demonstrated to be an excellent material for trace measurements of NAs, showing low detection limits and good surface-to-surface reproducibility [262]. Membrane-covered electrodes were used for the analysis of

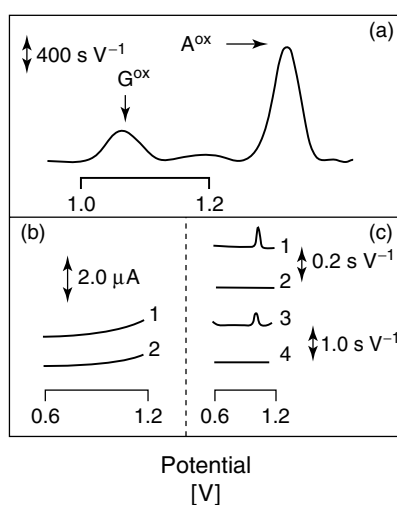


Fig. 7 CPSA of DNA and RNA at carbon electrodes. (a) ssDNA decamer AAAAGGAGAG at a relatively high concentration of 1 µg ml⁻¹ (310 nM) showing oxidation peaks of G (G^{ox}) and A (A^{ox}). Voltammetric (b), and chronopotentiometric (c) G (oxidation) stripping peaks of tRNA at concentrations of 10 ng ml⁻¹ at 5-min accumulation time (B1, C3,) and 5 ng ml⁻¹ (200 pM) at 10-min accumulation (C1). Corresponding background electrolytes (B2, C2 and C4). (Adapted from M. Tomschik, F. Jelen, L. Havran et al., *J. Electroanal. Chem.* **1999**, 476, 71–80; J. Wang, X. Cai, J. Wang et al., *Anal. Chem.* **1995**, 67, 4065–4070.)

short ODNs in the presence of long NA molecules [259, 263].

12.4.3

Other Solid Electrodes

Solid electrodes modified with various compounds have been used to improve DNA oxidation response. Siontorou and coworkers [264] obtained peaks A^{ox} and G^{ox} of degraded DNA at GCE modified with self-assembled bilayer lipid membrane. Using GCE modified with Nafion-ruthenium oxide pyrochlore, enhancement of oxidation peaks of both peaks, G^{ox} and A^{ox} , was achieved [145]. Thorp's group investigated DNA oxidation response at GC and indium-tin oxide (ITO) electrodes modified with self-assembled dicarboxylate monolayers [265], and with nitrocellulose and nylon membranes [266]. In these experiments, DNA was attached to the electrode either covalently or via adsorption forces in the modifier layer; bare ITO surface did not adsorb DNA. Oxidation of DNA was mediated by a redox metal chelate $[Ru(bipy)_3]$, which shuttled electrons to the electrode surface from DNA in solution or attached at the modifier film [265, 266]. Electrocatalytic oxidation of DNA was observed also when a redox mediator was immobilized on the electrode surface, for example, on ITO modified with electropolymerized poly $[Ru(bipy)_3]$ film [146].

Adsorption and electrooxidation of ss NAs on a silver electrode were studied by electrochemical methods and surface-enhanced Raman spectroscopy [189, 228]. Using the latter electrode, Fan and coworkers [229] observed an anodic signal in solutions of DNA. This signal was attributed to redox reactions of purine bases, and provided a convenient way to determine DNA. Oxidation of purine bases

on the gold electrode (where measurement of the respective anodic currents is complicated by simultaneous formation of gold oxide) was discussed by Hinnen and coworkers [225]. Pang and coworkers electrooxidized native and denatured DNA and purine nucleotides on a gold microelectrode [267]. A Copper electrode in connection with sinusoidal voltammetry was utilized by Singhal and Kuhr [149, 268] for determination of nucleotides, oligonucleotides, and DNA based on oxidation of the sugar moiety. This detection approach is universal to all types of nucleotides and is highly sensitive for both ss and dsDNA.

12.4.4

Analysis of NAs by Different Electrochemical Techniques

Various electrochemical methods have been applied for the analysis of NAs, including DPP [5, 11] and DPV [13, 269, 270], linear sweep and CV [13, 271] square wave [138] and a.c. voltammetry [272–274], and recently constant current chronopotentiometry [249, 255–257, 275, 276] and elimination voltammetry [139, 277–279]. DPP was applied for the analysis of DNA in 1966 [280], and in a short time, it replaced OP and d.c. polarography used in the early NA studies [4, 5]. The main advantage of DPP is its better sensitivity and resolution of peaks. Calf thymus ssDNA produced a well-developed DPP peak III (Fig. 6d) at concentrations of about 10 to 20 $\mu\text{g ml}^{-1}$, while dsDNA was inactive at the same concentration. At higher concentrations (hundreds of $\mu\text{g ml}^{-1}$), dsDNA produced peak II at potentials by about 70 mV more positive than peak III (Fig. 6c). For years, DPP was the most sensitive instrumental method of determination of traces of ssDNA in dsDNA samples [5].

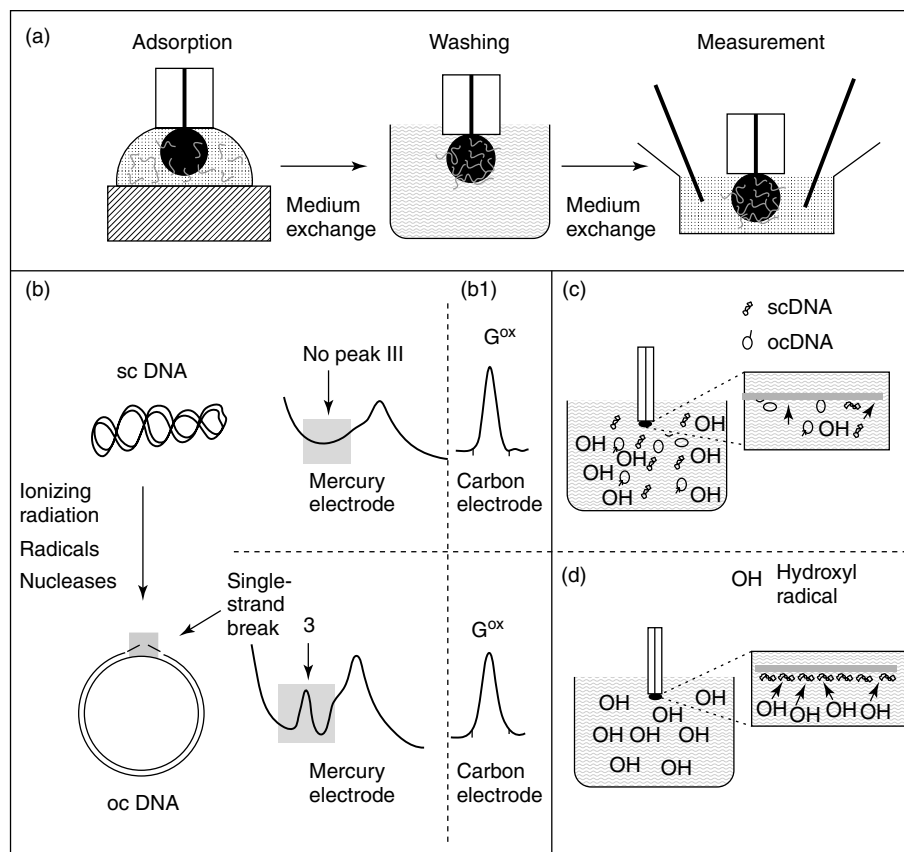


Fig. 8 (a) Schematic representation of the adsorptive transfer stripping procedure. NA (or protein) is strongly adsorbed at the electrode from a small (3–5 μ l) drop of solution. Then the DNA-modified electrode is washed, followed by transfer into a usual electrochemical cell with blank background electrolyte, where the measurement is performed. Multiple medium exchanges are possible, and this allows the study of interactions of surface-confined DNA with substances in solution. (b, c) Detection of DNA strand breaks (sbs) with DNA-modified mercury electrodes. (b) Scheme of AC voltammetric response of sc and open circular (oc) DNA at mercury electrodes. ScDNA does not yield

peak III. Introduction of a sb in scDNA results in a better accessibility of bases in the vicinity of the sb and in formation of peak III. (b1), Unlike mercury electrodes, carbon electrodes are little sensitive to formation of sb in DNAs. (c) Voltammetric detection of formation of DNA sb in solution. ScDNA is treated with a DNA-cleaving agent followed by DNA adsorption at the electrode. After washing, the electrode is transferred into a cell and DNA voltammetric response is measured. (c) Detection of DNA-damaging agent with scDNA-modified electrode. Intact scDNA adsorbed at the electrode serves as a sensitive layer of a sensor for DNA damage.

Tens to hundreds of micrograms of DNA, required for DPP and for other above mentioned polarographic and voltammetric techniques, were acceptable in the

analysis of chromosomal DNAs, but these DNA amounts were too large for the analysis of plasmid and viral DNAs, DNA fragments, and synthetic oligonucleotides,

whose preparation is laborious and/or expensive. Application of adsorptive stripping techniques in 1986 [203] helped to decrease bulk concentrations of DNA by about two orders of magnitude and to reduce the lowest amounts of the analyte to hundreds of ng of the NAs. Shortly afterward, these amounts were decreased by 2 to 3 orders of magnitude, using a simple way of preparation of DNA-modified electrode [281]. Instead of performing the voltammetric analysis with the HMDE immersed in the analyte, the DNA-modified electrode was prepared by immersing the electrode into a drop of the analyte (about 3–5 μl) for a short period of time (usually 30–300 s), during which the DNA was irreversibly adsorbed and firmly attached to the electrode (Fig. 8a). The HMDE was then washed and transferred to the background electrolyte (not containing any DNA) in which the voltammetric measurements were performed. This medium-exchange procedure was called AdTSV [13, 281–283].

DNA, RNA, and protein-modified electrodes can be prepared using both carbon and mercury surfaces [283]. Stability of immobilization of NAs at HMDE and graphite electrodes is very good [270]. AdTSV has been widely applied to various kinds of NA and protein studies [13, 15, 249, 270, 281, 284, 285]. Compared with conventional voltammetry, AdTSV has many advantages that are mainly due to the separation of the biomacromolecule adsorption from the electrode processes. These advantages include (1) reduction of the sample volume to 3 to 10 microliters, (2) elimination of interferences by low molecular mass substances that are washed off in AdTSV, (3) adsorption of the biomacromolecule on the electrode from media not suitable for the conventional voltammetric analysis, (4) in studies

of interactions of DNA immobilized at the electrode surface with other compounds in solution such as specific proteins. During the measurement, the results of AdTSV are influenced neither by the DNA interactions in the bulk of solution nor by transport of DNA to the electrode from the solution. More details about analytical applications and the use of NA-modified electrodes are given in Sects. 12.7 and 12.9.

12.5

Relations Between Structures and Electrochemical Responses of DNA

In early d.c. polarographic and OP studies, marked differences in the responses of native (double-stranded, ds) and denatured (single-stranded, ss) DNA were observed [4, 11] (Figs. 5, 6). Large signals of ssDNA as compared with much smaller or no signals produced by dsDNA were explained by decreased accessibility of the electroactive sites in dsDNA (Fig. 4) [4, 5, 10, 11, 14, 15]. The primary reduction sites of C and A (on mercury electrodes) are located in the interior of the DNA duplex structure, where they form a part of the Watson-Crick hydrogen bonding system (Fig. 4). The primary reduction site of G is located closer to the surface of the molecule in the major groove and it is not involved in the Watson-Crick hydrogen bonding. The primary oxidation sites (on carbon electrodes) are also not involved in this hydrogen bonding.

In agreement with the location of the A and C reduction sites in dsDNA, the DNA reduction signals (obtained with mercury electrodes) showed a high sensitivity to changes in the DNA structure. In the d.c. polarographic mode (with DME) at neutral pH-values the dsDNA

was inactive, while the ssDNA produced a polarographic reduction wave (Fig. 6d) at concentrations of hundreds of μg per ml [5]. DPP peak II produced by dsDNA was highly sensitive to small changes in the DNA structure induced by chemicals, enzymes, and radiations. In intact chromosomal dsDNA this peak was about a

hundred times smaller than peak III of ssDNA. Both ss and dsDNAs produced a DP (non-faradaic) peak I, which was less sensitive to changes in the DNA structure and was, therefore, not used in the DNA structure studies. At neutral pH, the DPP was capable of reflecting changes in the DNA structure in the bulk of solution

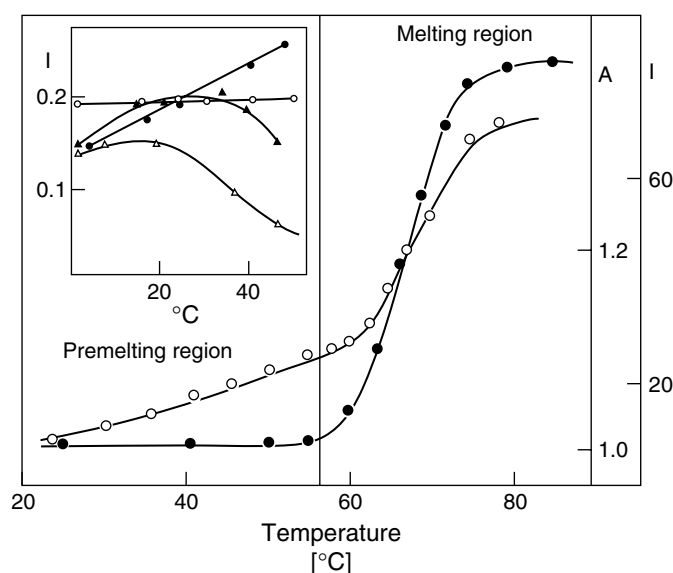


Fig. 9 Premelting changes in DNA conformation detected by UV-adsorption (●), and electrochemical methods (○). Temperature dependence of the heights of DPP peak II of dsDNA was measured in 4-M NaClO_4 , 0.05-M sodium phosphate, pH 6.5 at temperatures indicated in the graph; absorbance at 260 nm. Inset, temperature dependence of the heights of CV peak G of dsDNA obtained in 0.3-M ammonium formate, 0.05-M sodium phosphate, pH 6.9 by (▲), conventional voltammetry performed at the given temperatures; (△), AdTSV: (○, ●, △) DNA adsorption at the given temperatures, CV measurement at room temperature (after medium exchange); (△), adsorption at room temperature, measurement at the temperatures given in the graph; (○, ●, △), dsDNA; (○) ssDNA. Premelting changes in dsDNA conformation occurring at elevated temperatures (△, ▲) are fixed at the electrode surface and manifested by CV measurements at room temperature (●). No such changes occur in ssDNA (○). When CV measurements are performed at elevated temperatures, the height of peak G decreases with temperature because of the shift in potential of G reduction (at highly negative potentials). (Adapted from E. Paleček, *Bioelectrochem. Bioenerg.* **1988**, 20, 171–194; E. Paleček, I. Fric, *Biochem. Biophys. Res. Commun.* **1972**, 47, 1262–1269.)

(Fig. 9), and its results agreed well with those of optical methods [10, 11]. In addition, the non-faradaic capacity signals of DNA obtained by a.c. polarography (Fig. 5) were highly sensitive to changes in DNA structure. A.c. polarographic peak III provided information about accessibility of bases for interaction with the electrode surface and its changes were in most cases qualitatively similar to changes in faradaic signals. Strong influence of DNA structure on electrochemical signals made mercury electrodes suitable for studies of DNA structural transitions and detection of local conformational changes. Mercury electrodes sensitively reflected single strand interruptions in linear and circular DNA molecules [286], transition from right-handed B-DNA to left handed Z-DNA double-helix [287], and differences in the superhelix density of sc DNAs (Fig. 8) and superhelix density-dependent structural transitions in DNA [10, 273]; some examples are given in Sect. 12.9.

A comparison between the responses of ss and dsDNA, obtained by DPP (with DME) on one hand, and CV and SWV (with HMDE, at full and partial electrode coverages) on the other, is shown in Fig. 10(a, b). A qualitative difference between ss and dsDNA is observed only by DPP (ssDNA produces peak III while dsDNA yields peak II but not peak III). At the HMDE the faradaic responses differ only quantitatively and ssDNA always shows higher signals than the parent dsDNA. The difference between the ss and dsDNA signals is higher at a partial electrode coverage (faster diffusion of ssDNA contributes to this difference) and in cathodic signals (Fig. 10a). At full electrode coverage, peak G of calf thymus dsDNA (Fig. 10b) corresponded approximately to 50% of the height of this peak produced by ss form of this DNA. The

difference between the CV anodic peak G heights of ss and dsDNA was thus smaller (Fig. 10b) than in the cathodic peak CA, in agreement with the location of the G reduction site outside the hydrogen bonding system, close to the DNA molecule surface. On carbon electrodes the difference in the heights of the oxidation peaks of ss and dsDNAs (Fig. 10c) was even smaller, reflecting probably only the different flexibilities of ss and dsDNA molecules adsorbed at relatively rough carbon surfaces [31].

With polarographic methods working with large potential excursions during the drop lifetime or with voltammetric methods using HMDE the electrochemical responses have not always corresponded to the DNA structure in solution [10]. This problem, which is connected with slow processes involving dsDNA structure on the electrode surface, is discussed in the following section.

12.6 DNA Structure on Electrode Surfaces

A good correlation between polarographic responses (obtained with methods working with small potential excursions during the drop lifetime) and optical methods (Sect. 12.5) suggests that the structure of dsDNA is not significantly changed because of the adsorption of dsDNA at DME in the potential range of the measured DNA reduction signals (i.e. around -1.4 V). It is shown that in a narrow potential window, close to the potential of the a.c. polarographic peak I (Sect. 12.3), large changes in the interfacial properties of dsDNA may occur and involve major parts of the adsorbed DNA molecules.

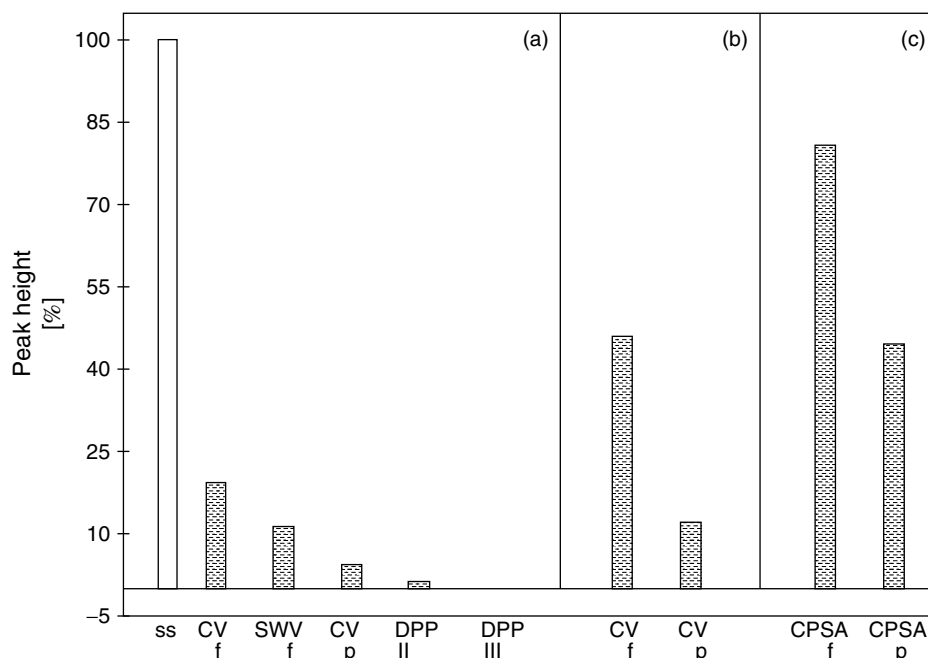


Fig. 10 Relative heights of faradaic peaks of calf thymus ss and dsDNAs at full (f) and partial (p) electrode coverage obtained by (a, b) cyclic voltammetric (CV) and SWV stripping analysis (at HMDE) and by (DPP at DME) at neutral pH and (c) by CPSA at pyrolytic graphite electrodes. (a, b). Signals of dsDNA are displayed relatively to the signals of ssDNA that were taken as 100% (for each given experimental conditions). At partial electrode coverage of HMDE ($10 \mu\text{g DNA ml}^{-1}$, 60 s waiting) the surface concentration of ssDNA was higher than that of dsDNA (the latter DNA has a lower diffusion coefficient). To obtain full electrode coverage dsDNA was at a concentration of $200 \mu\text{g ml}^{-1}$ and ssDNA at $40 \mu\text{g ml}^{-1}$. At HMDE some secondary changes in the structure of dsDNA may occur (Sect. 12.6) whose extent is influenced by the time for which dsDNA is exposed to potentials of the region U

(Fig. 11). These changes cannot influence the DPP signals of dsDNA (obtained with DME); consequently, the DPP peak III (characteristic for ssDNA) is completely absent in intact dsDNA (Figs. 4 and 6 for the location of the reduction sites in DNA and other details). (a) DPP peak II (about 70 mV less negative than peak III) is sensitive to damage of dsDNA. Signals obtained with HMDE: CA, cathodic peak (due to reduction of A and C residues) (b) G anodic peak (due to oxidation of the G reduction product). (a, b) Background electrolyte: 0.3 M ammonium formate, 0.05 M sodium phosphate, pH 6.9. (c) DNA was adsorbed from 0.2 M NaCl, 50 mM phosphate, pH 7 and CPSA performed in 0.2 M sodium acetate pH 5 after medium exchange; CPSA oxidation peak of G, G^{ox} is shown. ([10]; F. Jelen, L. Havran and E. Paleček, unpublished).

12.6.1

Dependence of the dsDNA Signals at the HMDE on Potential Scanning Direction

In 1961, Miller [37] concluded on the grounds of his differential capacity measurements (Sect. 12.3.) that in the region

of positive potentials partial unwinding of dsDNA took place on the mercury electrode. Later, Flemming [17, 290] did not confirm Miller's conclusion and assumed that DNA preserved its double-helical structure over the whole range of potentials. Flemming's [290] a.c.

voltammetric measurements of dsDNA (with the HMDE) agreed qualitatively with a.c. polarographic results (using DME), only if the potential was scanned from negative to positive values (Fig. 5b). When scanned in the opposite direction dsDNA yielded (at the HMDE) a “sharp peak” at about -1.5 V (corresponding to a.c. voltammetric peak III, characteristic for ssDNA) (Fig. 5b). On the other hand, ssDNA produced the “sharp peak” independently of the potential scanning direction. To explain his observations Flemming assumed that at potentials more positive than p.z.c., the dsDNA surface concentration (at full electrode coverage) was low, while at more negative potentials the concentration and thickness of the adsorption layer increased and intermolecular interactions between the dsDNA segments (extended into the solution) took place. Flemming speculated that the “round peak” (corresponding to peak I) is due to desorption of isolated dsDNA molecules and the “sharp peak” to desorption of associates of the dsDNA molecules [17, 18, 290]

Shortly afterward, it was shown [184, 197, 291] that keeping dsDNA on the mercury electrode at potentials around -1.2 V at neutral pH resulted in electrochemical responses characteristic for ssDNA; no difference whether (not clear) capacitive or faradaic signals were measured [10, 12]. These results suggested that formation of the capacitive “sharp peak” by dsDNA (when scanning to the negative potentials) could hardly be explained only by association of dsDNA molecules. To overcome this difficulty, Berg [18] suggested a complicated model for DNA adsorption and electron exchange based on a so-called potential induced π -state of dsDNA involving B-A transition at the surface and hypothetical changes of other DNA properties, as well as electron hopping

to bases inside the dehydrated parts of adsorbed DNA molecules. The idea of electron hopping in dsDNA is now being intensively studied and is discussed in Sect. 12.8. The experimental evidence presented by Berg [18] in support of his model was limited to the observation that the “sharp peak” decreased (“peak fading” in Berg’s terminology), either as a result of waiting at the potential of this peak (about -1.4 V) or due to scanning over this potential [18]. This phenomenon can, however, be explained by two well-known facts: (1) at about -1.4 -V reduction of A and C residues takes place, producing the DNA reduction product that blocks the electrode surface [184, 197, 244, 292] (Fig. 6, Sect. 12.4); such electrode blocking with intact dsDNA is negligible, but it may gain importance at longer waiting times if dsDNA is degraded or contaminated with ssDNA. (2) At the same potential the unreduced dsDNA should gradually desorb from the surface [108] (Sect. 12.3). Thus, no new special properties of DNA are necessary to explain the “peak fading.”

12.6.2

Opening of the DNA Double Helix Around -1.2 V (Region U)

Detailed studies based on both faradaic and capacitive DNA signals showed that at neutral and weakly alkaline pH-values the prolonged contact of dsDNA with the surface of the mercury electrode charged to potentials around -1.2 V (region U) resulted in striking changes in the electrochemical responses of DNA (Fig. 11). These changes, characteristic for ssDNA, were interpreted as the opening of the DNA double helix at the electrode surface [10, 15], and consequently, to an increased accessibility of bases for their

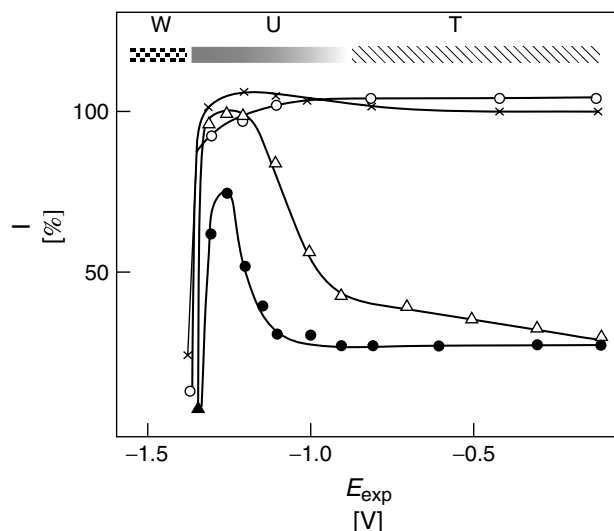


Fig. 11 Changes in the dsDNA structure at the HMDE surface at potentials around -1.25 V (region U) at neutral pH. The graph shows the dependence of relative heights of the cathodic peak CA of (\bullet , Δ) ds and (\circ , \times) ssDNA on the electrode potential. (Δ , \circ), conventional voltammetry (DNA was adsorbed at the electrode at the given potentials); (\bullet , \times), AdTSV (DNA was adsorbed at -0.1 V followed by medium exchange. Then, the surface-anchored DNA was exposed to the potentials E_{exp} given in the graph for 100 s, followed by CV scan). Heights of peak of ssDNA obtained by conventional voltammetry for accumulation potential -0.1 V was taken as 100%. The helix opening in the region U was relatively slow (about 1 min was necessary to open major portion of chromosomal dsDNA molecules). No structural changes were observed in the region W. No extensive DNA opening was taking place in the region T; fast opening limited to the vicinity of the DNA strand ends could, however, occur in this potential region. At acid pH's DNA opening in the region T gained importance and close to pH 5 the peak heights of dsDNA almost corresponded to those of ssDNA. See text for more details. (Adapted from E. Paleček, *Bioelectrochem. Bioenerg.* **1992**, 28, 71–83.)

interaction with the electrode. It was suggested ([10, 293] and referenced therein) that the opening of the dsDNA is due to strains in the DNA molecule, resulting from a strong repulsion of the negatively charged DNA phosphates from the electrode surface to which the DNA was firmly adsorbed via hydrophobic bases (provided for example by single-strand interruptions, the DNA molecule ends, and transiently

opened DNA regions) (Fig. 11). It was shown that the DNA opening was relatively slow (tens to hundreds of s were necessary to open about 90% of a chromosomal DNA on the electrode surface) and its rate increased with the potential shift to more negative values [293]. The duplex opening was partially irreversible [293, 294] and depended on the DNA nucleotide sequence [295]. With calf thymus DNA, both

AT and GC pairs were involved in the early stage of the opening process [293]. Opening of dsDNA on the mercury electrode at potentials of the region U was observed at ionic strengths between about 0.1 and 1.0. At low ionic strength, dsDNA was adsorbed at negative potentials of the mercury electrode very weakly [294] because of strong repulsion of the unscreened negative charges of the DNA phosphates from the electrode surface and because the above-mentioned phenomena could not come into play. In 10-mM KClO_4 , where probably only electrostatic interactions were involved, no differences in the differential capacity of ss and sonicated dsDNA were observed [225]. Under conditions of moderate ionic strengths at potentials positive (region T) or negative (region W) to the region U (Fig. 11), no extensive surface changes in DNA conformation (comparable to those observed in region U) were detected [10, 296].

It does not appear probable that the DNA opening on the electrode surface corresponds fully to the known DNA denaturation in solution; some special features and/or limitations of the opening process can be expected with the DNA immobilized at the surface. For example, formation of “ladder DNA” [12] or some other ds form in which bases are accessible for the interaction with electrode surface might also be compatible with the experimental data [10, 293, 295]. Increase in oxidation peaks of A and G were observed on graphite electrodes at sufficiently negative potentials (between -0.4 and -0.8 V) [31, 190]. These peak changes were larger in AT-rich DNAs and were interpreted in terms of DNA unwinding on a negatively charged graphite surface. More work with carbon electrodes will be necessary to better understand this phenomenon. Literature about the problem of DNA structure

on mercury electrodes was thoroughly reviewed [10, 12, 18, 31]. Further, we wish to limit ourselves mainly to more recent papers dealing with the subject.

Recent results obtained with a DNA-modified HMDE [293] unambiguously excluded the explanation offered by Flemming (reviewed in [17]). DsDNA was attached at the HMDE at potential $E_a - 0.1$ V (i.e. at a potential more positive than the p.z.c.); the electrode was washed and transferred to the background electrolyte not containing DNA and exposed to potentials E_{bx} (varying from -0.1 to -1.55 V) for 100 s prior the CV measurements [293]. In these experiments, a distinct region U was observed (showing a steep increase in peaks CA and G) similar to that obtained in a conventional way with the HMDE immersed in a DNA solution during the measurements. In experiments with the DNA-modified HMDE, the amount of DNA attached to the electrode surface could not increase (because there was no DNA in the bulk of solution to diffuse to the electrode and to reoccupy the empty surface resulting from reorientation of the DNA molecules), and the increase of CV peaks could not thus be due to a higher DNA surface concentration at negative potentials.

The irreversibility of the opening of dsDNA [293] is in agreement with the finding that the electrode tends to fix DNA in the spatial arrangement in which the molecule was adsorbed at the electrode surface [282, 283, 288]. For example, signals of dsDNA (but not of ssDNA) showed typical premelting changes when dsDNA was adsorbed at different temperatures (in an AdTSV experiment with the HMDE) and voltammetric measurements were carried out (after the medium exchange) at room temperature [288] (Fig. 9). Similarly, effects of composition and pHs of the medium from

which DNA was adsorbed effectively influenced the signals measured (in AdTSV) in the usual background electrolyte at neutral pH [282, 283, 288]. Our studies of a.c. voltammetric behavior of DNA complexes with intercalators [297] (Sect. 12.7.1) suggested that an altered DNA conformation may be conserved after DNA adsorption at the HMDE surface and the intercalator removal.

A strong support for opening of the DNA double helix in the region U has recently been obtained from our experiments with covalently closed circular (ccc) DNAs ([272, 284] (Fig. 8b)). These DNAs do not contain any molecular ends and strand interruption, and their extensive unwinding is prevented for topological reasons [298, 299]. Exposition of the cccDNAs (plasmid sc DNAs) to the potentials of the region U at the HMDE surface resulted in little or no detectable DNA opening, as indicated either by faradaic [284] or capacitive [272] signals, in agreement with the limitations in the duplex unwinding of these DNA molecules [298, 299]. Studies of DNA adducts with platinum drugs, such as bifunctional *cis*- and *trans*-diaminedichloroplatinum(II) and monofunctional diethylenetriaminedichloroplatinum(II) (dien-Pt), showed that the effects observed in region U are inhibited by interstrand crosslinks (produced by the bifunctional compounds), but not by other types of adducts formed in DNA by dien-Pt, in agreement with the concept of the DNA surface opening, which should be inhibited by the DNA inter-strand crosslinks [300].

12.6.2.1 Opening of dsDNA at Acid pHs in a Wider Potential Range T

Decrease of pH (from neutral) resulted in an increase of the reduction signals of dsDNA in the region T; at about pH 5

the signals of dsDNA were close to those of ssDNA and a distinct region U was no longer observable. This effect was explained by protonation of bases at acid pHs connected with destabilization of the DNA structure [10]. It was assumed that partially protonated DNA was adsorbed in the region T via protonated regions, with further protonation and destabilization taking place at the surface in the neighborhood of the adsorbed segments. This process was much faster as compared with DNA opening observed at neutral pH [10].

It has been shown above that the HMDE is a useful tool in the study of interfacial properties of DNA, including conformational changes of DNA occurring at the surface. In cases when such changes should be avoided, polarographic methods working with small voltage excursions during the (DME) drop lifetime should be applied [10]. Even in experiments with the HMDE, the surface changes in the DNA structure can be minimized by choosing proper conditions, including fast voltage scanning. The possibility of potential-controlled opening of dsDNA appears very attractive in connection with recent attempts to create DNA biotechnologies on chips involving fast DNA sequencing (Sect. 12.9).

Opening of the DNA double helix on the surface was recently observed with the atomic force microscope (AFM). Individual dsDNA molecules attached to an AFM tip and a gold surface were overstretched, and the mechanical stability of the DNA double/helix was investigated [301]. Stretching experiments with single DNA molecules revealed a highly cooperative transition, where the natural B-DNA was converted into a new overstretched conformation called S-DNA [302]. In λ -phage DNA the B-S transition at 65 piconewtons

(pN) was followed by a second conformational transition at 150 pN, during which the DNA double helix melted into two single strands [301]. On relaxation, the two single strands recombined to the ds conformation. Both the B-S and melting transitions occurred at significantly lower forces in poly(dA-dT), compared with poly(dG-dC) [303].

12.7

Interactions of NAs with Small Molecules

12.7.1

Reversible (Noncovalent) Interactions

A broad range of low-molecular mass inorganic and organic species interact reversibly with NAs. Basically, there are three different modes of small molecule binding to duplex DNA [304] (Fig. 12): (1) binding of cations along the outer surface of DNA double helix, primarily via electrostatic interactions with phosphate anions. This mode of binding is not restricted to dsDNA. In addition to nonspecific condensation-type interactions [305],

transition metals can also form site-specific complexes with base residues; (2) groove binding interactions involving direct contacts of the interacting molecules with inner surfaces of major or minor grooves of DNA double helix, including edges of base pairs in these grooves (depending on the nature of the interacting species, hydrogen bonding, electrostatic and/or van der Waals contacts may take part in this mode of binding); and (3) intercalation of planar condensed aromatic ring systems between adjacent base pairs, primarily involving stacking interactions. Interaction of DNA binders with DNA results in changes of electrochemical responses of the former substances due to altered mass transport and/or decreased accessibility of the binder electroactive moiety. In addition, alterations of DNA electrochemical behavior upon interaction with the ligands can be detected. Electrochemical techniques have been shown to be capable of determination of binding constants, binding modes as well as binding site sizes of association of DNA with ligands. Differential binding of some substances to ss and dsDNA can

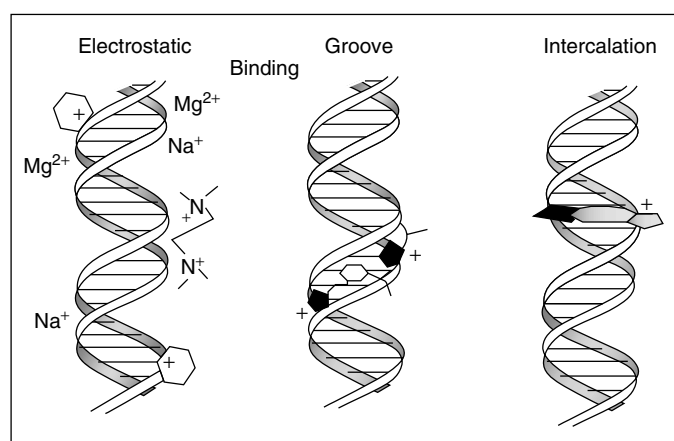


Fig. 12 Scheme of three general modes of interactions of dsDNA with small molecules. See the text for details.

be utilized in electrochemical detection of DNA hybridization or degradation [306] (Sect. 12.9).

12.7.1.1 Inorganic Cations and Simple Metal Complexes

Concentrations of monovalent (sodium, potassium, ammonium) ions significantly affect adsorption of DNA on an electrode (Sect. 12.3). This effect is related to shielding of negative charges of DNA sugar-phosphate backbone by the counterions. Interactions of magnesium ions with DNA (which play a unique role in many biological processes) were utilized by Maeda and coworkers [307] in a Mg^{2+} ion-selective electrode. Association of divalent transition metals (cadmium, lead) with DNA was studied by Sequaris and coworkers [308, 309], using cyclic and alternating current voltammetry and chronocoulometry at the HMDE. Enhanced adsorption of Pb^{2+} ions at the HMDE as a result of the presence of DNA, and compaction of DNA from an extended coil to a condensed state in the presence of lead ions were observed [309]. Assembly of silver ions along duplex DNA molecule, followed by chemical reduction of the metal, was used by Braun and coworkers [310] to create an electrically conductive nanowire. Differential behavior of large DNA molecules and smaller RNA ones upon interaction with trivalent $[\text{Co}(\text{NH}_3)_6]^{3+}$ complex was utilized by us in a method for RNA determination in DNA samples [269]. While long DNA molecules were precipitated by 50 mM cobalt complex, RNA molecules remained in solution and were detected using AdTSV (Sect. 12.9). Binding of $[\text{Ru}(\text{NH}_3)_6]^{3+/2+}$ complex to thiol-derivatized ODNs, anchored on gold electrodes [311, 312] or to DNA electrostatically immobilized at functionalized 4-thiopyridine monolayer

on gold surface [313], was employed for detection and quantification of DNA on the electrodes, and for detection of DNA hybridization [311]. On the DNA-modified electrode, reversibility of reduction of the positively charged ruthenium(III) complex (attracted to the surface-confined DNA) was enhanced relative to bare (DNA-free) electrode, while reversibility of reduction of negatively charged ferricyanide (repelled from the DNA) was lowered [311]. Some metal ions exhibited an ability to form a coordinate bond with oxygen and nitrogen atoms of base residues. Free DNA bases and purine nucleotides form sparingly soluble salts with mercury (Sect. 12.2). Accumulation of mercury (II) ions in polyuridylic acid adsorbed at the HMDE surface was reported by Johnston and coworkers [314]. Copper(I) ions were stabilized upon binding to purine or C bases and nucleosides, and resulted in the formation of insoluble species at the HMDE or GCE and in splitting of Cu^{2+} reduction at the HMDE into two one-electron steps [66, 183]. Purine bases, denatured and native DNA bound nickel(II) ions and catalyzed electroreduction of the metal at the mercury electrode [315].

12.7.1.2 Organic Metal Chelates

Organic metal chelates possess several advantages in studies of specific DNA interaction because of their well-pronounced (and often reversible) electrochemistry, and the possibility to control the mode of DNA binding by choosing the proper metal chelating ligands. Bard and coworkers [316, 317] observed that tris-chelated ruthenium, cobalt and iron complexes with 1,10-phenanthroline (phen) interacted with duplex DNA via intercalation. However, the mode of binding depended on the metal redox state, for (2+) ions exhibiting more favorable hydrophobic

interaction with DNA than for the (3+) ones. Analogous 2, 2'-bipyridine (bipy) chelates of ruthenium and osmium displayed predominantly electrostatic binding [317]. The cathodic and anodic CV peak potentials of the electrostatic binders (e.g. $[\text{Os}(\text{bipy})_3]^{3+/2+}$) shifted to more negative values, while a shift to more positive values was observed upon intercalative binding (e.g. $[\text{Co}(\text{phen})_3]^{3+/2+}$) [316, 318]. Normal pulse voltammetry on an ITO electrode was used to determine binding constants and distribution of (bipy)₃ and (phen)₃ metal chelates bound to DNA [319]. Association of $[\text{Ru}(\text{phen})_3]^{2+}$ or $[\text{Os}(\text{phen})_3]^{2+}$ with DNA was detected via the measurements of electrogenerated chemiluminescence (ECL) of the metal chelate in the presence of oxalate on gold, GC, or platinum electrodes [320, 321]. Intercalation of the ruthenium complex resulted in a stronger decrease of the ECL signal than external binding of the osmium chelate. On the other hand, an ECL signal appeared on association of $[\text{Ru}(\text{phen})_3]^{2+}$ with duplex DNA at aluminum(III)-alkanebisphosphonate thin film [318]. A microscale method for the study of the interactions of DNA with other redox-active molecules (e.g. intercalative cobalt chelates) based on DNA-modified gold electrodes was proposed by Pang and Abruña [322]. Selective binding of the Co, Os, or Ru (phen)₃ complexes to duplex NAs was utilized in discrimination between ss and dsDNA on the electrode, and detection of DNA hybridization [275, 323–326] (Sect. 12.9).

Single- and double-stranded DNA oligomers containing G displayed catalytic enhancement of the oxidation of ruthenium [265, 266, 327] or rhenium [328] complexes on carbon or ITO electrodes. These chelates were capable of one-electron oxidation of G residues [146, 265,

266, 327, 328]. Reduced forms of the complexes shuttled electrons from DNA to the electrode, where the oxidized form was electrochemically regenerated. Using this effect, Johnston and coworkers [329] studied solvent accessibility of nucleobases in ss and duplex DNA. Formation of DNA duplex precluded direct collision of $[\text{Ru}(\text{bipy})_3]^{3+}$, with the G residue and the electrons had to tunnel through a finite distance. This distance was lower when G was in a mismatch and the oxidation rate followed the trend $\text{G}(\text{single-strand}) > \text{GA} > \text{GG} > \text{GT} > \text{GC}$. $[\text{Os}(\text{bipy})_3]^{3+}$ exhibited analogous electrocatalytic effects in the presence of 8-oxo-G (8-OG), which has lower redox potential than G [330]. DNA interactions with metalloporphyrins (MPs) containing copper, nickel, zinc and cadmium ions were studied by Qu and Li [331], using CV on an HMDE. MPs lacking an axial ligand were capable of intercalating into DNA double helix, resulting in a deep decrease of the MP signal. MPs containing the axial ligand exhibited only outside DNA binding, resulting in a weaker current change. Binding constants of copper complexes with phen and a macrocyclic ligand tetrabenzo-[b,f,j,n] [1, 5, 9, 13]-tetraazacyclohexadecane were determined by means of CV at GCE [306]. These chelates caused DNA cleavage under aerobic conditions in the presence of reducing agents (Sect. 12.9).

12.7.1.3 Other Noncovalent DNA Binders

Specific interaction of a minor-groove binding dye, Hoechst 33258, with dsDNA on a gold electrode resulted in an enhancement of the dye oxidation signal. This effect was utilized by Hashimoto and coworkers [332] to detect DNA hybridization (Sect. 12.9). Wang and coworkers [333] studied interaction of daunomycin (DM) with DNA in solution

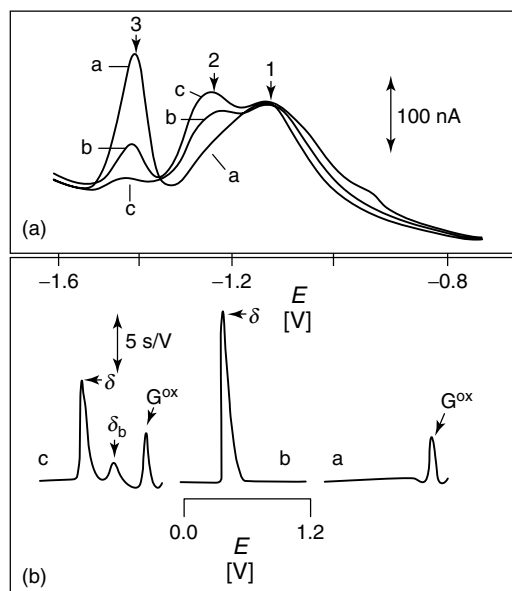


Fig. 13 Examples of electrochemical detection of reversible interactions of duplex DNA with small molecules. (A), AdTS AC voltammetric behavior of dsDNA adsorbed at HMDE in the presence of chloroquine (CQ). (a), no CQ; (b), 10 μ M CQ; (c), 50 μ M CQ. Upon binding of intercalators, DNA peak 2 increases while peak 3 decreases. (B), interaction of DNA with DM followed by CPSA at CPE. As a result of DM binding to DNA, peak δ corresponding to free DM decreases and peak δ_b attributed to the bound drug appears; (a), DNA; (b), DM; (c), DNA-DM. (Adapted from M. Fojta, L. Havran, J. Fulneckova et al., *Electroanalysis* **2000**, 12, 926–934; J. Wang, M. Ozsoz, X. H. Cai et al., *Bioelectrochem. Bioenerg.* **1998**, 45, 33–40.)

and on the electrode surface by means of CPSA at CPE (Fig. 13b). DNA-bound DM was oxidized at more positive potentials than the free drug. Moreover, low concentration of the drug in the bulk of solution induced conformational changes in DNA adsorbed on the electrode. Mascini's laboratory used DM as an electroactive indicator of polynucleotide duplex formation [334]. Using reversible electrochemistry of DM, site-specifically coupled to an ODN, Kelley and coworkers [335] studied long-range electron transfer through ds ODNs anchored on a gold electrode via end thiol groups. It was shown that perfectly matched DNA double helix effectively conducted electrons from DM bound to the ODN, at a distant site relative to the electrode surface. Disturbing effects of single-base mismatches on electron transfer through base stack (Sect. 12.8) could be detected by measuring voltammetric signals of DNA intercalators (DM, methylene blue or a metallointercalator), but not of groove or electrostatic binders [336]. Association

of another DNA-binding drug, distamycin, with a manganese porphyrin derivative and binding of the complex to DNA was followed by Rodriguez and Bard [337]. Pandey and Weetal [338] proposed a technique of electrochemical detection of DNA intercalation involving a photochemical reaction of anthraquinone derivatives. These intercalators were photochemically activated and then reduced by an electron donor, followed by electrooxidation of the reduction product at a modified CPE. In the presence of DNA, the anodic current decreased because of a limited transport of the DNA-bound anthraquinone to the electrode. Aromatic amines (vigorous carcinogens and important environmental pollutants) were sensitively detected using dsDNA-modified CPE. The technique proposed by Wang and coworkers [339] was based on selective accumulation of the analyte in the DNA sensing layer via intercalative binding. By measuring DNA AC voltammetric signals at an HMDE, we [297] monitored DNA conformational

changes induced by various intercalators (Fig. 13a). In the presence of chloroquine, doxorubicin, 9-amino acridine, and Co, or Ru metal chelates during DNA adsorption on the electrode and subsequent removal of these substances, changes in DNA peaks indicating distortions of the DNA double helix and a reduced ability of the DNA to be unwound at the HMDE surface (Sect. 12.6) were observed.

A sensor for DNA-binding drugs was developed by Maeda and coworkers [340, 341]. This technique is based on thiol-derivatized DNA-modified gold electrode. The DNA layer strongly suppressed CV response of the ferrocyanide/ferricyanide redox pair. On binding of cationic intercalative drug (e.g. quinacrine or acridine orange), electrostatic repulsion between surface-confined DNA and the anionic depolariser was decreased, and the electrode reaction became more feasible, displaying increasing current response with the drug concentration. Takenaka and coworkers studied electrochemical behavior of DNA complexes with bis-intercalators (e.g. a bis-9-acridinyl derivative with a viologen linker) [342] and threading intercalators (e.g., a ferrocenyl-modified naphthalene diimide) [343, 344]. Using the threading intercalator, a sensor capable of discrimination between single-stranded, duplex, and hairpin DNA on the gold electrode surface and a sensor for DNA hybridization [345] was proposed. The ferrocenyl naphthalene diimide derivative complexed with the surface-attached DNA facilitated electron transfer from glucose oxidase-catalyzed reaction to the electrode [346]. A fullerene derivative carrying a cationic intercalative moiety (pyridinium cation) exhibited a specific CV response on binding to duplex DNA [347]. Brett and coworkers [348–352] developed

a GCE-based DNA sensor, useful in studies of electrochemical behavior of drugs, such as metronidazole [348–350], nitroimidazoles [351] or mitoxantrone [352]. A natural quinoxaline antibiotic echinomycin (EM) was electrochemically active and yielded several CV signals applicable for its determination at submicromolar concentrations [F. Jelen, A. Erdem, and E. Paleček, unpublished]. Interaction of EM with dsDNA attached to the HMDE resulted in specific DNA and EM signals in agreement with the strong binding of EM to dsDNA by bis-intercalation. Under the same conditions, interaction of EM with ssDNA resulted in high DNA, but very small or no EM signals suggested only very weak binding of EM to ssDNA on the electrode surface. EM, thus, appears to be a good candidate for a redox indicator in electrochemical DNA hybridization sensors (Sect. 12.9.1).

12.7.2

Covalent Interactions

Derivatization and complexation procedures are commonly used in electrochemical analysis if the analyte is inherently not electroactive [16, 353]. Natural NAs are electroactive, but their oxidation and reduction on electrodes is electrochemically irreversible taking place at highly positive or highly negative potentials [10, 132, 353].

12.7.2.1 Electroactive Markers of NAs

Complexation (see the preceding paragraph) and derivatization of NAs has been used to obtain reversible electrode processes at less extreme potentials; catalytic signals can afford higher sensitivity and improved selectivity for the DNA structure. The first electroactive markers covalently bound to DNA were investigated in the beginning of the 1980s [242, 354–358]. They

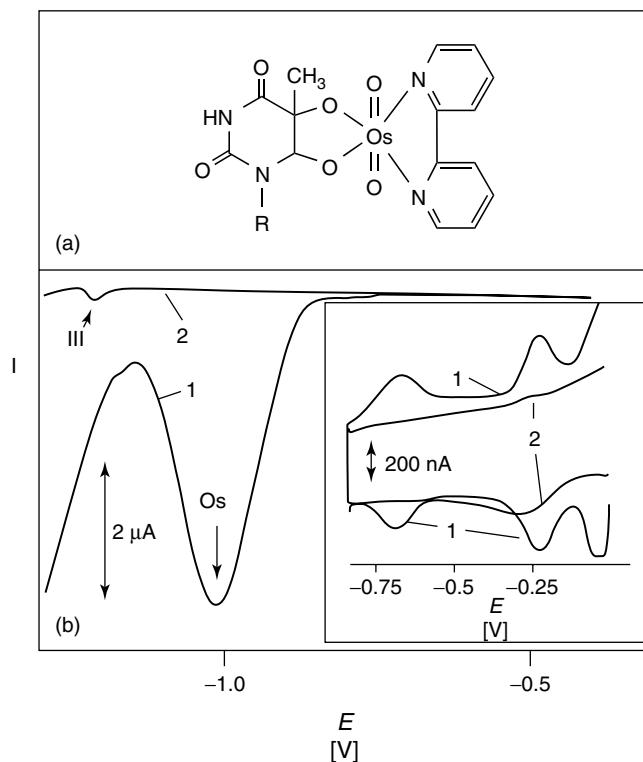


Fig. 14 DNA modified with osmium tetroxide, 2, 2'-bipyridine (Os, bipy). (A), structure of the Os,bipy adduct with T residue. (B), AdTSV DP voltammograms of (1), Os,bipy-modified DNA and (2), unmodified ssDNA; Os, catalytic peak yielded by the DNA adduct; III, peak due to reduction of A and C. Inset, cyclic voltammogram of the (1). modified and (2), unmodified DNA showing reversible faradaic peaks of the DNA-Os,bipy adduct. Background electrolyte: 0.3 M ammonium formate, 50 mM sodium phosphate, pH 6.9. ([242, 359]; R. Kizek, L. Havran, M. Fojta, and E. Paleček, *Bioelectrochemistry*, in press).

were based on osmium tetroxide complexes with nitrogen ligands (Os, L) and fulfilled all the above requirements [355, 356, 359]; they produced a reversible couple at about -0.6 V, yielded a catalytic signal at about -1.2 V on the mercury electrode (Fig. 14), and showed useful selectivity for ssDNA. Os,L binds to C5-C6 double bond of pyrimidines, showing a strong preference for Ts (Fig. 14). Osmium tetroxide, 2, 2'-bipyridine (Os,bipy), and

some other Os,L are highly selective for ssDNA [360, 361]; Os,bipy and other Os,L complexes have been widely applied as probes of the DNA structure, in vitro and in vivo, in connection with nonelectrochemical methods, including DNA sequencing techniques and immunoassays [299, 360, 362, 363]. Most of the DNA-Os,L adducts can be determined electrochemically at ppb concentrations [242]; in AdTSV experiments with 5- μ l analyte volume tens of

pg are thus sufficient (corresponding to several femtomoles of a ss 20-mer ODN).

Quite recently, in an attempt to develop a universal, sensitive, and convenient method of DNA or RNA detection, electroactive oligonucleotides were prepared by covalent linkage of a ferrocenyl group to the amino hexyl-terminated ODN [364]. Using HPLC equipped with an electrochemical detector, DNA and RNA were determined at femtomole level [364]. CV with a Pt disk electrode showed a reversible couple around 0.4 V [364] in 50 mM KCl, 50 mM MgCl₂ and 50 mM Tris-HCl (pH 8.0). To design a DNA biosensor Korri-Yousoufi and coworkers [365] synthesized an electroactive polypyrrole functionalized with ODN, which produced an oxidation peak at -0.2 V associated with the oxidation (or doping) of the polypyrrole chains (indicating that the ODN-substituted polypyrrole film was highly electroactive). (For further details Sect. 12.9). Functionalization of other conducting polymers-polythiophenes with individual nucleobases yielded selective nucleobase-responsive material potentially useful in the development of DNA hybridization sensors [366].

12.7.2.2 Other Nucleic Acid Modifications

Gold surfaces modified with thiol-derivatized ODNs were investigated by various methods [230, 311, 312, 367–370], mainly in connection with the development of the DNA hybridization sensors (Sect. 12.9). The purpose of end labeling of ODNs with thiol or disulfidic groups was not to introduce in DNA an electroactive marker but to attach DNA on gold via a sulfur-gold linkage. On mercury surfaces these groups can, however, produce specific signals and turn into efficient electroactive markers of DNA [E. Paleček and L. Havran, unpublished data]. Many

biologically important substances bind covalently to DNA [304]. In recent years electrodes were successfully applied in studies of DNA adducts with some anticancer drugs, such as mitomycin C and thiotepa, by Marin and coworkers [285, 371–374]. Great potentialities of electrochemical analysis in the research of a large number of DNA-drug adducts have been, however, little utilized.

Peptide (or polyamide) nucleic acid (PNA) is one of the candidates for diagnostic and therapeutic applications in medicine of the 21st century [375–377]. In PNA the entire sugar-phosphate is replaced by (*N*-(2-amino-ethyl) glycine units. In contrast to DNA and RNA (with negatively charged backbones), PNA has an electrically neutral backbone. Electrochemical responses of PNA were similar to DNA and RNA (i.e. A, C and G were reduced on mercury electrodes; G producing an anodic CV peak due to oxidation of the G reduction product; and A and G were oxidized on carbon electrodes) [247]. Peak potentials of ssPNA at the HMDE were shifted to negative values as compared with ssDNA. Differences in backbones of PNA and DNA were manifested by the different adsorption behavior of these two compounds, as detected by a.c. impedance [108] on mercury (Fig. 3), and by chronopotentiometric measurements on carbon electrodes [129]. At higher surface concentrations, association of PNA molecules on the mercury surface was observed; prolonged exposure of PNA to highly negative potentials did not result in PNA desorption under conditions, when almost all DNA molecules were removed from the surface. Adsorption of PNA increased with decreasing salt concentration; in contrast, adsorption of DNA decreased under the same conditions [108]. In DNA hybridization sensors,

PNA has proved to be a better probe than DNA [375] (Sect. 12.9).

12.8

DNA Conductivity

Studies of DNA conductivity have a long history [378–382]. Recent attempts to draw conclusions about DNA electron transfer from fluorescence quenching measurements on DNA strands containing donor and acceptor molecules have spurred a debate over the question of whether or not the DNA double helix is able to conduct electrical charges (reviewed in [383–386]). Other approaches, including application of electrodes [335, 387–393], have also been applied. Jortner and coworkers [394] and Okada and coworkers [395] suggested possible long-range carrier transport by a hopping mechanism. It was shown by Giese [396, 397] that when nucleobase radical ions were formed within the DNA duplex, a long-range charge transfer that required properly spaced G residues could occur. Importance of G residues, and particularly of GG steps, was demonstrated by Schuster and coworkers [398–401]. Okahata and coworkers [402] observed high anisotropic conduction in oriented, densely packed DNA helices along their longitudinal axis, but not in the plane perpendicular to it. Passage of electron or hole current through a cluster of dsDNA molecules with characteristics resembling those of a semiconductor was reported by Fink and Schöneberger [403].

12.8.1

Application of Electrodes in DNA Conductivity Studies

Berg [18] (Sect. 12.6) and Barker [389–391] were probably the first who attempted to

draw conclusions about the DNA conductivity from their polarographic/voltammetric studies. According to Barker [389–391], DNA loops extending to the solution from chromosomal ssDNA adsorbed on the mercury electrode may capture hydrated photoelectrons that migrate along the DNA strands by hopping. This process is pH-dependent and occurs at weakly alkaline pHs. Attachment of a thiol group to one end of an ODN made it possible to form SAMs of ds or ssDNAs on gold surfaces [230, 311, 312, 368, 370]. Redox properties of methylene blue intercalated in DNA helices attached to gold electrodes via 5'-end thiol-terminated linkers were investigated by Kelley and coworkers [369]. To locate exactly the redox center within the duplexes, DM was covalently bound to G residue in 15-mer DNA duplexes, and efficient reduction of DM on a gold electrode regardless of the DM position in the duplex was observed [335, 392]. CA mismatch between DM and the electrode surface completely abolished the electroreduction of DM. These results indicated that electron transfer was blocked by perturbation in base stacks induced by base mismatches, and supported the concept of the long-range (wire-like) charge transfer within the π -stack of the DNA duplex. It was shown by Heller and coworkers [388] that in contrast to a conducting polymer the disordered chromosomal dsDNA film was not able to “wire” the soybean peroxidase to induce electroreduction of H_2O_2 to water. On the other hand, in ordered solid 12-mer dsDNA film (aligned to the gold electrode via the end thiol) dsDNA displayed semiconductor characteristics that were disturbed by occurrence of mismatched base pairs in the DNA duplex and did not occur in ssDNA. It was concluded that randomly oriented dsDNA did not conduct electrons or holes.

The results of Heller and coworkers [388], Okahata and coworkers [402], and Fink and Schöneberger [403] appear to be consistent with a doped ionic semiconductor model, in which the cause of carrier mobility and donor ionization is the reduced difference between the static and high frequency longitudinal dielectric constants resolved in the direction of the long axes of the helices in aligned dsDNA films. Porath and coworkers [393] measured electrical transport through individual poly(dG)/poly(dC) molecules connected to two metal nanoelectrodes. They obtained, in air as well as in vacuum, nonlinear current-voltage curves that exhibited a voltage gap at low applied bias, indicating large-bandgap semiconductor behavior. In recent years, substantial progress in studies of the DNA conductivity has been made, but many questions remain unanswered. One of the most exciting discoveries is the change in the electrical properties of dsDNA on introduction of a base mismatch, demonstrated by a number of authors using different approaches [230, 275, 335, 375, 392, 397, 404–406]. This finding, as well as future elucidation of DNA conductivity, may have a tremendous impact on our understanding of many biological processes, including mutagenesis, carcinogenesis, and DNA repair, and can be utilized in biotechnologies for the construction of DNA sensors and various electronic devices.

12.9 Analytical Applications

12.9.1 Sensors for DNA Hybridization

DNA renaturation and hybridization, that is, the ability of DNA to reform its

double-helical structure from its complementary single strands, was discovered about 40 years ago by J. Marmur and P. Doty [407]. Shortly afterward, the ability of electroanalysis to follow DNA renaturation was demonstrated [11, 408]. The principle of DNA hybridization was utilized in many molecular-biological methods, including nucleotide sequencing. Rapid testing of nucleotide sequences is required in different fields, including diagnostics of various diseases, genetic testing, forensic medicine, rapid analysis of biological warfare agents, environmental testing, and so on. Development of an inexpensive, easy-to-use, fast response device remains the focus of interest for many scientists. Compared with devices based on optical transducers, the electrochemical devices are much cheaper, simpler, smaller, and more modest in their power requirements.

At present, the development of the electrochemical biosensors using ssDNA as a recognition layer is a rapidly developing field [327, 334, 361, 375, 387, 409–413]. In such a biosensor, a short ssODN (DNA probe) is immobilized on an electrode (transducer) to create the recognition layer. The probe-modified electrode is then immersed into a solution of target DNA to test its nucleotide sequence. When the sequence of target DNA exactly matches that of the probe DNA (based on the complementarity principle stating that A pairs with T and G with C), a hybrid (probe-target) duplex DNA is formed at the electrode surface. The following sections will focus on two most important steps in the detection of the DNA nucleotide sequence: the formation of the DNA recognition layer and hybrid duplex DNA, and the transformation of the latter event into an electrical signal.

12.9.1.1 Immobilization of DNA on the Electrode

Both non-covalent and covalent bindings of the probe to the electrode surface have been used. Adsorption forces were utilized for binding DNA to carbon [414–416], mercury [108, 281, 326], and gold [322, 417] surfaces. Very strong binding of DNA to mercury surfaces is due to hydrophobic interactions of bases with the surface, preventing under usual conditions, efficient DNA hybridization [326]. Electrostatic binding of DNA to the positively charged carbon electrode is sufficiently strong and bases are accessible for the specific interaction with target DNA [129, 275, 410, 418]. Marazza and coworkers [419] compared the probe immobilization by adsorption at controlled potential with avidin-biotin probe immobilization on disposable graphite screen-printed electrodes, using DM as a redox indicator. They concluded that simple adsorption is more reproducible than the avidin-biotin procedure and CPSA is more efficient than DPV. Rather high concentrations of target DNA were necessary for the analysis ($1\text{--}4\text{ }\mu\text{g ODN ml}^{-1}$).

Various kinds of covalent binding of DNA to carbon, gold, mercury, and ITO [146, 327] surfaces were used (Sect. 12.4). Random covalent binding of DNA to electrode surfaces involving chemical modification of bases [299] (such as with carbodiimide derivatives, applied for immobilization of the probe DNA to carbon and other electrodes [409]) may decrease the specificity of the recognition layer and thus cannot be recommended. Significantly, better results can be expected with immobilization of the probe via one end of the DNA molecule not involving damage to DNA bases (such as with thiolated ODNs which can easily be immobilized to the gold [230, 311,

312, 335, 367–370, 387, 392] and mercury [L. Havran and E. Paleček, unpublished] surfaces). Thiol-terminated aliphatic linkers are frequently used to place the probing sequence at a proper distance from the electrode surface. Covalently bound probes provide better possibilities for easy removal of non-specifically bound molecules. A microfabricated disposable DNA sensor, based on a gold electrode and a DNA probe with a mercaptohexyl group at the 5'-end, for the detection of hepatitis virus B DNA was introduced [420]. Hoechst 33258 was used as an indicator detecting 10^4 to 10^6 copies of DNA per ml. The sensor was applied for the analysis of DNA extracted from blood of patients. Various techniques of pretreatment of the gold electrode and thiol-linked probe immobilization involving tricky aspects have been employed in many papers [311, 332, 421–423]. Recently, a procedure based on treatment of the electrode with boiling KOH followed by concentrated nitric acid, has been developed and provides reportedly reproducible results [345].

12.9.1.2 Detection of the Hybridization Event

In the early studies, redox indicators interacting preferentially with dsDNA, such as simple intercalators (some metal intercalators, DM, etc.) and minor-groove binders (e.g. Hoechst 33258), were applied to differentiate between ds and ssDNA [420, 424, 425] (reviewed in [409, 410, 418]). These indicators interacted not only with dsDNA but also with ssDNA, and duplex formation was detected from the signal increase (compared to the probe alone). Redox indicators with higher selectivity for duplex DNA are currently being sought.

Bis-intercalators and threading intercalators are particularly interesting as redox indicators. The latter intercalator, which

has substituents on opposite sites of the intercalating aromatic ring system, must thread one of the substituents between the base pairs at the intercalation site. These types of molecules usually have high DNA binding constants, indicating that once the substituent slides between the base pairs, a very stable complex is formed. Natural and synthetic bis-intercalators have two intercalating rings covalently linked

with a connecting chain. Recently, electrochemical studies of the synthetic threading intercalator ferrocenyl naphthalene diimide [426] and the naturally occurring nogalamycin [427] and bis-intercalator EM (antibiotic and antitumor agent) were undertaken (Fig. 15). Both intercalator types bound to dsDNA more tightly than usual intercalators, showing almost no response with ssDNA-modified

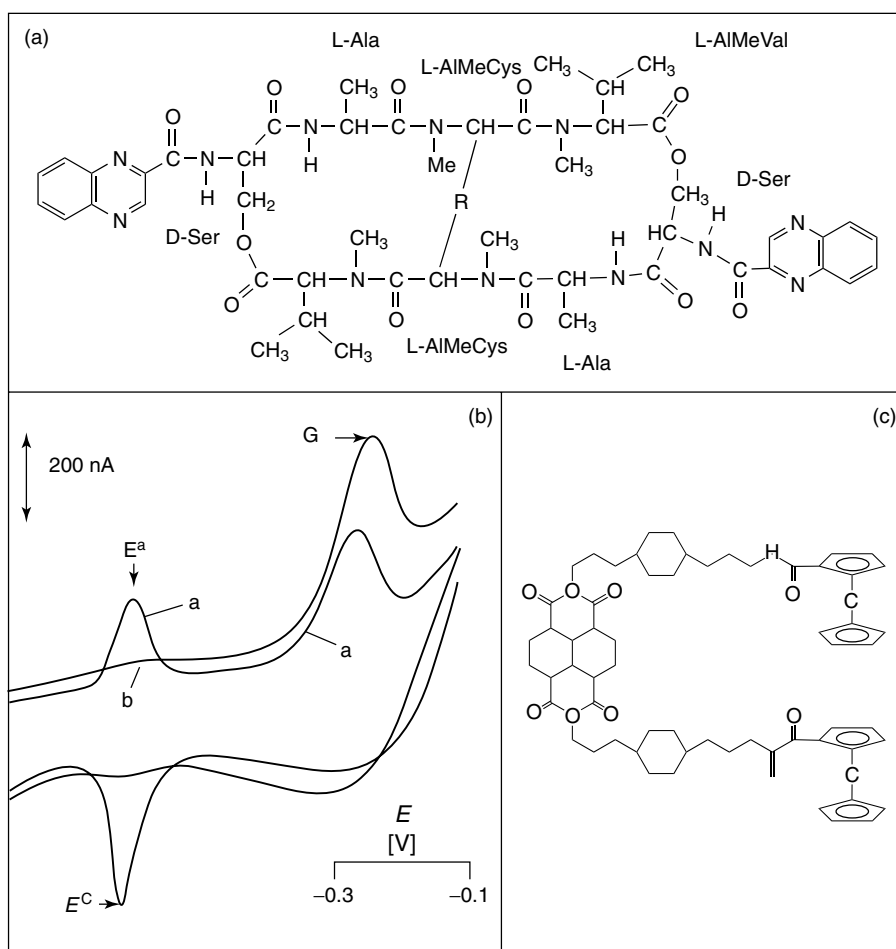


Fig. 15 Chemical structures of (a) a bis-intercalator EM; (c) a threading intercalator ferrocenyl naphthalene diimide; (b) sections of cyclic voltammograms of EM with DNA. (a) EM+dsDNA; (b) EM+ssDNA. In contrast to a mixture of EM with ssDNA, complex of EM with dsDNA yields a specific reversible pair of peaks (F. Jelen, A. Erdem and E. Paleček, *Bioelectrochemistry*, in press).

electrodes. Bis-9-acridinyl derivatives containing linker chains with one or more viologen linkers were synthesized [342, 343, 346] as potential electrochemical indicators of dsDNA. Ferrocenyl naphthalene diimide was used to detect (dT)₂₀, using (dA)₂₀ as a probe immobilized on the gold electrode via adsorption [417]. By this method, (dT)₂₀ was detected at sub-attomole levels. Even higher sensitivity was obtained with thiolated probe chemisorbed on a gold electrode using ferrocenyl naphthalene diimide (Fig. 15) as a redox indicator [345]. By this approach, it was possible to detect the yeast choline transport gene in plasmid DNA. Studies of the ability of this method to discriminate DNAs with one or more mismatches are under way.

12.9.1.3 Redox Indicators Covalently Bound to DNA

In principle, target DNA can be covalently end-labeled with a redox indicator producing a signal on binding the target DNA to the probe. It appears more convenient to bind a redox indicator to an ODN complementary to target DNA (reporter probe) on the site next to that hybridized to the probe [428]. Various kinds of covalent modifications of the target or reporter probe NAs can be used (Sect. 12.7) to detect the hybridization event through the signal of the electroactive marker. Electroactive markers producing catalytic signals may yield high sensitivity for the analysis, and thus appear very promising. ODNs labeled with ferrocene were used to detect DNA sequences by HPLC with electrochemical detection [429] at femtomole levels. Combination of this technique with PCR [430], using ferrocene-modified ODNs as primers, resulted in a sensitivity increase down to the sub-attomole level.

These principles can be utilized in DNA sensor development.

12.9.1.4 Indicator-free Detection Systems. Intrinsic Electroactivity of DNA

Any electrode can be used to distinguish the probe and the target DNAs if their base contents are sufficiently different. For example, the absence of an electroactive G in the probe, but not in the target, was used to detect DNA hybridization on ITO [146, 265, 266, 330, 431] and carbon electrodes [326, 327, 432]. To overcome the limitations of the probe sequences (absence of G), guanines in the probe sequence were substituted by hypoxanthine residues (pairing with C's) and the hybridization detected through the target DNA G signal [327, 432]. Such substitution may, however, decrease the stability of the duplex and the specificity of the hybridization.

12.9.1.5 Changes in Interfacial Properties and DNA Conductivity

Large differences between the interfacial properties of ds and ssDNAs observed earlier by capacitance measurements [10, 37] suggested that a.c. impedance measurements could be used to detect DNA hybridization on electrodes [433, 434] (Sect. 12.8.). A three-component ODN system on a gold electrode (involving avidin-biotin interactions) was used to detect specific DNA sequences by means of faradaic impedance spectroscopy [435]. Impedance spectroscopy does not seem, however, to be the most convenient method for the DNA biosensor; faster and simpler voltammetric or chronopotentiometric methods will probably be more convenient. Conductivity of the perfect DNA, contrasting with a loss of conductivity in duplexes with mismatched bases, may be of use in

the development of the DNA hybridization sensors (Sect. 12.8).

12.9.1.6 Blocking and Interfacing the Transducer

In contrast to model studies using ODNs as target DNAs, in experiments with real DNA samples, nonspecific interactions on the electrode surfaces (involving DNA impurities, long ssDNA chains, etc.) can obscure the hybridization signals. Efficient interfacing between the DNA system and the electrode surface is thus necessary. Thiols and conducting polymers have been used for this purpose.

Individual chains of organic conjugated polymers possess a high intrinsic conductivity [436, 437]. These conducting polymers can be synthesized chemically (for example, polyphenylenes) or electropolymerized as thin films onto an electrode (e.g. polythiophenes and polypyrroles). Experimentally obtained conductivities of conjugated polymers are between 1 and 10^4 S/cm, several orders of magnitude lower than those of metals, but sufficiently high to consider these macromolecular chains (several micrometers in length) as molecular wires [436]. Deposited as thin films on electrodes, the reversible redox processes in these polymers can be potential-controlled and cyclic voltammogram can provide an electrochemical signature of the given polymer. This signature is very sensitive to the nearby environment; any modification of the pendant groups along the chain is electrically transduced to the electrode and manifested by modified polymer electrochemical signature. Different functionalities can be inserted in the polymer known to show selectivity for solution species such as antibodies, enzymes, and NAs. Specific chemical recognition resembling affinity chromatography can thus be built through

proper functionalization of the conducting polymers.

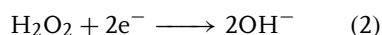
Conducting polymers, such as copolymer functionalized with an osmium complex [438–442], polyazines, polyanilines, polypyrroles [365, 413, 436, 443], and polythiophenes [366] (reviewed in [444–446]), may be used for blocking and interfacing the transducer, for modulation of the DNA interactions at surfaces and for generating signals resulting from such interactions. Conducting polypyrrole functionalized with bulky ODN remained electroactive in aqueous media; on interacting with the complementary but not the noncomplementary ODN, a decrease in the voltammetric current at -0.2 V was observed [365]. Adsorption of NAs on a polypyrrole-coated GCE was utilized for amperometric ODN detection in flowing streams [443]. Doping of the NA probes within electropolymerized polypyrrole films and monitoring the current changes provoked by the hybridization event appears to be a promising label-free biosensing strategy [447].

Two component films were prepared, containing in addition to a thiol-derived ssDNA probe a diluent thiol, mercaptohexanol, to prevent nonspecific adsorption of ssDNA on the gold surface [423]. The dielectric constant and thickness of the film were measured by two-color surface plasmon resonance and the amount of DNA tethered to the surface was quantified. The kinetics of hybridization and thermally induced dehybridization were measured, indicating a high efficiency of the hybridization process. Self-assembled monolayer containing a viologen group was formed on a gold electrode via gold-S bonds [448]. Binding of dsDNA to this layer resulted in a positive shift of the redox potential of the viologen centers, indicating hydrophobic interactions. Alkanethiol

monolayers can easily be assembled not only on gold but also at mercury surfaces [449–453].

12.9.1.7 Electrocatalytic Reactions

Electrode processes in experiments with redox indicators involved one or a few electrons and were, therefore, inherently low-yield reactions. Recently catalytic processes have been used to collect as many electrons as possible ([327, 454, 455]; E. Paleček, M. Fojta, and L. Havran, unpublished). Thorp [327] used a soluble mediator that moved close to G residues present only in target DNA (but absent in the probe) and shuttled electrons to the polymer-modified ITO electrode. The reduced form of the mediator $[\text{Ru}(\text{bipy})_3]^{2+}$ was oxidized by holding the electrode at a sufficiently positive potential. The oxidized form of the mediator removed electrons from G residues, generating reduced $[\text{Ru}(\text{bipy})_3]^{3+}$ and completing a catalytic cycle. About 100 electrons per hybridized G could be collected under favorable conditions. Horseradish peroxidase coupled to target DNA was applied to detect the hybridization by electrocatalytic reduction of hydrogen peroxide



The enzyme molecule turned over about 1800 times per second, producing about 3600 electrons in 1 s [456]. This approach was also used in connection with the detection of point mutations (see below).

12.9.1.8 Detection of Point Mutations

Many diseases are connected with a single base mutation (point mutation) at specific sites of the genome. Detection of a change in a single nucleotide in the DNA is rather difficult and requires highly specific methods. The first electrochemical

detection of a point mutation (single base mismatch) was achieved by using PNA probe instead of DNA [275]. This method was applied to detect the mutation hot spot in the p53 gene [406]. A relatively simple technique using a CPE and a simple redox indicator was used to obtain these results. Caruana and Heller [455] detected a single base mismatch in an 18-mer ODN, using a redox polymer-coated microelectrode and thermostable soybean peroxidase-labeled target DNA. They obtained excellent discrimination between a perfectly matched duplex and a single base mismatch at elevated temperature, while at room temperature such discrimination was not possible. Specificity and sensitivity are, perhaps, the most important features of a DNA hybridization sensor. Caruana and Heller [455] offered a method superior in both sensitivity and specificity, representing significant progress towards a practical DNA hybridization sensor.

12.9.2

Sensors for DNA Damage

DNA damage may cause serious disturbances of cell life. Chemical changes in the DNA bases may lead to alterations in base pairing followed by mutations [304]. Formation of DNA double-strand breaks frequently results in mitotic faults and chromosome aberrations. Accumulation of mutations and/or other kinds of DNA damage represents serious carcinogenic and teratogenic risks. Development and improvement of analytical techniques, capable of rapid and sensitive detection of various types of DNA damage (including DNA biosensors) is, therefore, the focus in many laboratories. The sensitivity of electrochemical methods to changes in DNA structure has been utilized in these investigations. Three basic approaches can

be distinguished: (1) detection of DNA sbs (Fig. 8), (2) detection of base damage, and (3) detection of substances that specifically interact with DNA (covalently and/or non-covalently) that are electroactive and yield specific electrochemical signals. Electrochemical detection is also frequently employed in methods of the determination of modified nucleobases (such as 8-OG or other adducts) based on DNA hydrolysis, followed by HPLC separation [457]; these approaches are, however, out of the scope of this chapter.

12.9.2.1 Detection of DNA Strand Breaks

Generally, DNA sb's are formed by the direct hydrolysis (enzymatic or chemical) of the phosphodiester bond, on damage to the deoxyribose moiety (usually after a radical attack), or as a consequence of some kinds of chemical damage to DNA bases followed by a destabilization of the DNA sugar-phosphate backbone [304]. In 1960s and 1970s we showed that DNA sb could be detected using DPP. The polarographic peak II (Sect. 12.4) increased markedly on treatment of dsDNA with DNase I [458], with ionizing radiation and/or with ultrasound [458, 459]. Later, voltammetric techniques, including LSV [460, 461] or a.c. voltammetry [462], were used to study electrochemical behavior of sonicated or γ -irradiated DNA. A highly sensitive DNA biosensor has been developed in our laboratory [272, 273, 276, 463, 464]. This sensor is based on qualitative differences between the behavior of sc DNA, and DNA molecules containing free ends (oc, see Fig. 8, or linear). On mercury electrodes, the latter DNAs produce non-faradaic (tensammetric) peak 3 and a well-developed faradaic peak CA (Sect. 12.4), because of partial unwinding of the double helix on the electrode surface in the vicinity of the strand ends (Sect. 12.6). On the contrary,

in scDNA lacking sbs, the nucleobases cannot interact with the electrode surface that results in the absence of peak 3 and in restricted electroreducibility of C and A at the HMDE (Sects. 12.3 and 12.4; Fig. 8). This method made possible the detection of a single chain interruption among 2.5×10^5 phosphodiesteric bonds [272]. The HMDE and MFE [252] modified with adsorbed scDNA have been used for the detection of hydroxyl radicals formed through Fenton chemistry in laboratory-prepared solutions, and in various samples of natural and industrial water or food [273]. ScDNA can also be cleaved at the HMDE surface enzymatically. Deoxyribonuclease I cleaved electrode surface-confined scDNA in a remarkably potential dependent manner [463]. On the contrary, measurements of peak G^{ox} on carbon electrodes exhibited no significant differences between the signals of sc and linear or oc DNAs [252, 257] (Fig. 8). A deep degradation of DNA due to acid hydrolysis [248] or oxidative damage mediated by copper complexes [306] was required to observe increased intensity of DNA signals on carbon electrodes. Such changes were also accompanied by a decreased binding of an intercalative redox indicator [306], suggesting a significant loss of double-stranded character of the DNA.

12.9.2.2 Damage to DNA Bases

Chemical damage to DNA base residues may change (or abolish) their intrinsic electroactivity (Sect. 12.4). Moreover, damaged bases can be released from DNA molecules, which may be monitored by transfer stripping techniques (Sect. 12.4) and/or by CSV (Sect. 12.2) [248]. Peak G measured at the HMDE (Sect. 12.4) was used as the transduction signal in systems detecting DNA alkylating or acylating agents. Methylation of the DNA G residues

by dimethyl sulfate resulted in a decrease of peak G [138]. ssDNA was modified, either in solution followed by AdTS (DNA was separated from the reaction mixture by washing the DNA-modified HMDE) or on the electrode surface (intact DNA was immobilized at the HMDE and the electrode was immersed in dimethyl sulfate for 20 to 30 min). Decrease of peak G was observed also in DNA interacting with mitomycin C, a drug attacking primarily G residues [285, 372, 374, 465], and in another antineoplastic drug thiotepa [371]. On the basis of a similar principle, the DNA-modified graphite electrode was used as a sensor for the detection of antitumor platinum drugs [466]. Using DNA-modified CPE, Wang and coworkers [467] developed a highly sensitive (at $\mu\text{g L}^{-1}$ levels) biosensor for the detection of hydrazine derivatives usable in environmental analysis. Interaction of the hydrazines with immobilized DNA resulted in a decrease of peak G^{ox} . Thorp and coworkers [330] utilized differences in the redox potentials of G and 8-OG (a highly abundant G oxidation product formed in vivo upon oxidative stress) in the development of a method for the detection of 8-OG. $[\text{Os}(\text{bipy})_3]^{3+}$ complex was capable of shuttling electrons from 8-OG (but not from unmodified G) to the ITO electrode, exhibiting electrocatalytic effect (Sect. 12.7). Changes in DNA electrochemical behavior due to damage to DNA bases by UV radiation were detected by DPP [468], and by CPSA using a screen-printed electrode-based DNA sensor [469]. Some kinds of base damage or abasic sites can be converted into sb or ssDNA regions by using DNA repair enzymes. We [M. Fojta and E. Paleček, unpublished] detected apurinic sites in DNA using *E. coli* exonuclease III, an enzyme that cleaves dsDNA at abasic sites followed by exonucleolytic degradation of one DNA strand. The

resulting ssDNA regions were sensitively detected by measuring AC voltammetric peak 3 (Sect. 12.3). To detect base damage, mismatch-sensitive DNA hybridization techniques can be used [329, 336, 405].

12.9.2.3 Detection of Damaging Agents Specifically Interacting with DNA

Covalent adducts and/or noncovalent complexes of DNA with some chemicals, including carcinogens or cytostatics, produce specific electrochemical signals. Appearance of specific peaks was observed on DNA interactions with mitomycin C, osmium tetroxide complexes, DM, aromatic amines, and a variety of other DNA binders (Sect. 12.7).

12.9.2.4 DNA Cleavage Controlled by Electrochemical Reactions

In vivo, many DNA-damaging processes involve redox reactions. For example, redox-active metals, such as copper, iron or manganese, can mediate reactions yielding reactive oxygen species that are vigorous DNA-damaging agents. Electrodes have been utilized to control redox states of the metals and to modulate subsequent DNA damage. Rodriguez and coworkers [470] electrochemically activated Mn(III) and Fe(III) complexes with a porphine derivative in the presence of oxygen. As a result, cleavage of scDNA present in the bulk of the solution took place, and was detected by means of gel electrophoresis. We [464] electrochemically modulated cleavage of scDNA adsorbed at the surface of the HMDE in the presence of iron or copper complexes and of chromium compounds, using in situ electrochemical detection of the DNA sbs formation (see above). Both laboratories [464, 470] detected a certain extent of DNA cleavage in the absence of the metal complexes, suggesting a role of oxygen reduction

products on the platinum and mercury electrodes. Thorp's group [328] generated both single-sbs and piperidine-labile sites by controlled-potential electrolysis of DNA (sc plasmid or an oligonucleotide, respectively) in the presence of trans-[Re(O)₂(4-OMe-py)₄]⁺. Piperidine cleavage revealed damage specifically to G residues, suggesting a primary mechanism of one-electron oxidation of G mediated by the metal complex (Sect. 12.7).

12.9.3

Other Determinations

12.9.3.1 Determination of ssDNA in an Excess of dsDNA

The specificity and high sensitivity of DP polarographic peak III to ss (denatured) DNA (Sect. 12.4) was utilized in methods of determination of trace amounts of ssDNA in an excess of ds (native) DNA [280]. An analogous approach was applied for the determination of ssRNA in excess of bacteriophage f2 sus 11 double-stranded RNA [471]. DPP measurements were able to detect <1% of ssDNA in dsDNA. Moreover, using DPP peak III intramolecular ss regions generated by exonuclease III (an enzyme degrading one strand of dsDNA) in dsDNA molecules were detected [472]. CV or AC voltammetric measurements following heat treatment of plasmid DNAs were employed to determine small amounts of the nicked (oc) form of the plasmid in excess of scDNA [272, 473]. At 92°C, only the nicked (or linear) molecules were irreversibly denatured, but not covalently closed sc circles. The amount of ocDNA was calculated from the amount of ssDNA (which appeared after the sample heating) manifested by an increase of CV peak G [473] or tensammetric peak 3 [272]. The same principle was applied,

for example, to monitor nicking of scDNA upon ionizing irradiation.

12.9.3.2 Determination of RNA Traces in DNA Solutions

DNA samples are usually contaminated by small portions of RNA and determination of the RNA content in DNA samples is frequently necessary. Optical methods used for this purpose have low sensitivity and specificity. Recently, highly sensitive and specific electrochemical methods have been proposed [269, 270]. Natural RNAs produced qualitatively the same redox response as DNA at the HMDE [271] (Fig. 16a), MFE [251], and carbon electrodes [255] at neutral and weakly acidic pH's. On the other hand, in weakly alkaline media RNAs yielded a single tensammetric peak R (at about -1.3 V, Fig. 16), whose potential differed from peak potentials of both DNA peaks (peak 1 at -1.2 V and peak 3 at -1.45 V; in the references [269–271], peak 1 and peak 3 are denoted as peak D1 and peak D2, respectively) [269–271] (Fig. 16b). This difference made it possible to detect simultaneously DNA and RNA in a mixture, and to determine traces of RNA in samples of DNA. Using AdTS DPV at the HMDE, picomole amounts of tRNA or total bacterial RNA were determined in almost 200-fold excess of native chromosomal or plasmid DNA [270]. Such a direct approach was, however, ineffective when RNA in more than tenfold excess of single-stranded DNA was to be determined (e.g. DNA of some viruses and bacteriophages such as M13 are naturally single-stranded). To overcome this limitation, we developed [269] a procedure combining selective precipitation of ss or dsDNA by [Co(NH₃)₆]³⁺ and AdTS DPV. Short molecules of RNA with globular tertiary structure (e.g. tRNAs) remained

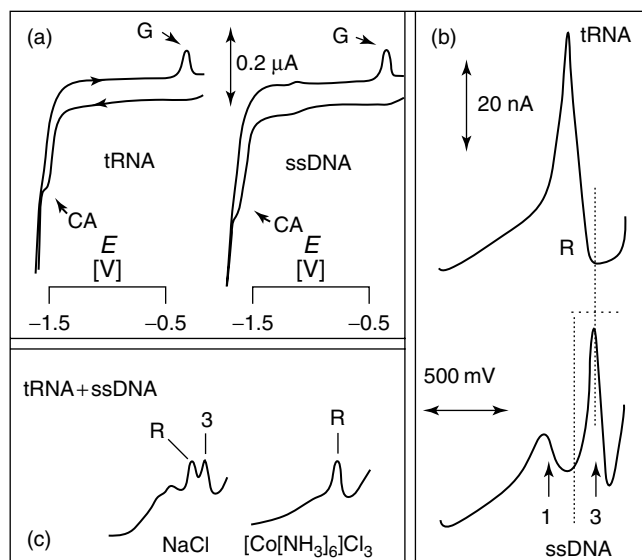


Fig. 16 (a) AdTS cyclic voltammograms of yeast transfer RNA (tRNA, left) and of ssDNA (right) obtained in 0.3 M ammonium formate, 50 mM sodium phosphate, pH 6.9. Potentials of peak CA and peak G of DNA and DNA do not differ. (b) AdTS DP voltammograms of tRNA (top) and ssDNA (bottom) obtained in 0.3 M sodium bicarbonate, pH 9.6; under these conditions, tRNA yields a single capacitive peak R at potential differing from those of DNA peaks 1 and 3. (c) AdTS DP voltammograms of a 1 : 8 (w/w) mixture of tRNA + ssDNA obtained at pH 9.6 after adsorption of the NAs from 0.2-M NaCl (left) or 50-mM [Co(NH₃)₆]Cl₃. DNA is selectively precipitated by the cobalt complex. (Adapted from M. Fojta, R. Doffkova, E. Paleček, *Electroanalysis* **1996**, *8*, 420–426; E. Paleček, M. Fojta, *Anal. Chem.* **1994**, *66*, 1566–1571; M. Fojta, C. Teijeiro, E. Paleček, *Bioelectrochem. Bioenerg.* **1994**, *34*, 69–76.)

in solution (yielding peak R), while long filamentous DNA molecules were precipitated on addition of the cobalt complex (Fig. 16c). Possible coprecipitation of polydisperse total cellular RNA was eliminated by partial degradation of RNA into short oligonucleotides prior to addition of [Co(NH₃)₆]³⁺ [269].

12.9.3.3 Determination of Proteins

Knowing the protein content is important in characterizing the purity of the

NA sample. DPP determination of cystine/cysteine containing proteins based on catalytic currents in cobalt solutions [474] was, for many years, one of the most sensitive nonradioactive methods of protein determination. Using this technique, it was possible to determine about 1% of protein in a few micrograms of DNA [475]. Recently described methods of protein determination, by means of CPSA on mercury [249] and carbon electrodes [476], will probably offer even better sensitivities.

12.10 Conclusion

Since its beginning by the end of the 1950s and thereafter for about two decades, electrochemical analysis of NAs developed as a typical basic research activity. In that time, fundamental information about the adsorption/desorption properties, as well as reduction and oxidation of DNA at the mercury and solid electrodes, was obtained [4, 5]. High sensitivity of mercury electrodes for changes in DNA structure was utilized in biochemical analysis [5, 11]. In the 1980s, this research was almost abandoned because the sensitivity of the conventional voltammetric analysis was too low to compete with methods such as gel electrophoresis, commonly used in the NA laboratories. In that decade, only a few laboratories continued their electrochemical studies of NAs. Nevertheless, it was during that period when new electrochemical approaches were designed, resulting in a tremendous increase in the sensitivity of the DNA electrochemical analysis, in the invention of the DNA-modified electrodes [281, 288], and in the introduction of the first electroactive markers into the DNA molecules [242, 354–358]. These new approaches represented the necessary background for development of DNA sensors. In the first half of the 1990s, more laboratories entered the field in an attempt to develop sensors for DNA hybridization [409]. Although some of the early papers suffered from a lack of knowledge of the DNA chemistry, they, nevertheless, represented an important stimulus in the development of the field. Since the mid-nineties, the creation of an electrochemical DNA hybridization sensor has become a reality, and in recent years we have witnessed an increased interest in biochemists and biotechnology companies

in DNA electrochemistry and sensor development [477–480]. Attempts to exploit the results of the basic research for commercial purposes represented, on one hand, another stimulation of DNA electrochemistry research; and on the other, resulted in delay in the publication of a few papers because of the patenting of new principles and procedures. At present, there are indications that the first simple electrochemical DNA hybridization sensor applicable for practical purposes might be available in the near future.

In recent years, attempts have been made to develop microfabrication technologies for integrated NA analysis [477–483]. Electrodes have been used, not only in the development of the DNA sensors but also in developing bioelectronic chips for sample preparation, and this may become a part of integrated systems for DNA hybridization. Using such a system, bacterial cells can be separated by means of dielectrophoresis and subjected to electronic lysis, followed by proteolytic digestion on a single bioelectronic chip [477, 483]. NAs released from the cells can then be tested on a separate DNA hybridization chip. Miniaturized DNA chips, incorporating a large number of oligomer probes or even longer DNAs (500 to 5000 nucleotides in length), to increase the accuracy and capacity of the sensor were created. High probe densities of small silicon chips were achieved up to approximately 10^5 sites cm^{-2} [436, 484]. In addition to silicon, glass, and some polymers with flat or porous surfaces were used as substrates. ODN probes were anchored on the solid substrates in various ways, including polyacrylamide gels; deposited as small dots on a glass substrate [485], and photochemically addressed as sensing dots, associated with in situ synthesis of the desired ODN probe [484, 486]. Potentialities of the DNA

chips have already been largely confirmed, but detection of the hybridization event still raises some questions. In fact, the currently used DNA chips require fixation of a fluorescence or radioactive tag to the target DNA, costing time and effort, and the subsequent reading of the chip requires expensive equipment. It is believed that application of electrochemical principles described in this review may offer a simple and effective solution to this problem.

Addendum

After finishing this paper an important progress in the development of the electrochemical DNA hybridization sensors was achieved [487–520] bringing the research closer to its goal, that is to the design of a new type of a DNA biosensor for the analysis of real DNA samples. This research is in part reflected in the special issue of *Talanta* devoted to electrochemistry of NA's and DNA biosensors [497]. Most of the papers on the development of the electrochemical DNA hybridization sensors discussed in Sect. 12.9.1 dealt with model systems using relatively short target ODNs, while experiments working with real DNA samples were rather rare because of problems with nonspecific adsorption of noncomplementary (and therefore nonhybridized) DNA. All systems relied on solid electrodes with immobilized short single-stranded probe DNA, on which both the hybridization and detection steps were performed [487]. Recently a new method has been proposed [488–490, 513] in which the DNA hybridization is performed at one surface (surface H, optimized for DNA hybridization; commercially available magnetic beads were used as surface H) and electrochemical detection on another surface, the detection electrode (DE). Owing to minimum nonspecific DNA adsorption

at the surface H very high specificity of the DNA hybridization can be reached. The DE can be chosen only with respect to the electrode process securing high sensitivity of the analysis. High sensitivity in the detection of relatively long target DNAs has been obtained (1) by using label-free methods, namely, cathodic stripping voltammetry at mercury or solid mercury amalgam electrodes for the determination of purine bases, released from DNA by acid treatment [488, 489] or oxidation of DNA guanine residues at carbon electrodes [491] and (2) by enzyme-linked immunoassay of target DNA modified by osmium tetroxide, 2, 2'-bipyridine (DNA-Os,bipy) at carbon electrodes [490] (3) by enzyme-linked sandwich assay based on streptavidin-biotin interactions [492] and (4) by direct determination of DNA-Os,bipy at mercury or carbon electrodes [493, 494], and (5) by precipitation of silver on gold nanoparticle tags followed by CPSA determination of the silver at carbon electrodes [495]. Studies of DNA hybridization kinetics on gold electrodes by optical surface plasmon resonance showed that the d.c. field can enhance or retard DNA hybridization and can also denature surface-immobilized DNA duplexes [496]. The latter phenomenon may correspond to the opening of the DNA duplexes summarized in Sect. 12.6 and can be utilized in the development of the DNA hybridization sensors. Incorporation of the above principles into a microfluidic system may soon result in a new device for the sequence analysis of long natural DNA molecules.

Acknowledgment

This work was supported by a grant of the Grant Agency of the Czech Republic No. 204/97/K084 (to E.P.), by grants of the Grant Agency of the Academy of

Sciences of the Czech Republic Nos. S5004107 (to V.V.), A4004801 (to M.F.), A4004901 (to F.J.), and A4004002 (to V.V.) and by institutional grants K4055109 and Z5004920. The authors are grateful to Drs. M. Heyrovsky and Z. Pechan for critical reading of the manuscript.

References

1. H. Berg, *Biochem. Z.* **1957**, 329, 274–276.
2. E. Paleček, *Naturwissenschaften* **1958**, 45, 186, 187.
3. E. Paleček, *Nature* **1960**, 188, 656, 657.
4. E. Paleček, in *Progress in Nucleic Acid Research and Molecular Biology* (Eds.: J. N. Davidson, W. E. Cohn), Academic Press, New York 1969, pp. 31–73, Vol. 9.
5. E. Paleček, in *Methods in Enzymology: Nucleic Acids, part D* (Eds.: L. Grossman, K. Moldave), Academic Press, New York, 1971, pp. 3–24, Vol. 21.
6. R. Kalvoda, *Techniques of Oscillographic Polarography*, Elsevier, New York, 1965.
7. J. Heath, *Nature* **1946**, 158, 23.
8. E. Paleček, B. Janik, *Arch. Biochem. Biophys.* **1962**, 98, 527.
9. E. Paleček, *Collect. Czech. Chem. Commun.* **1960**, 25, 2283–2289.
10. E. Paleček, in *Topics in Bioelectrochemistry and Bioenergetics* (Ed.: G. Milazzo), John Wiley & Sons, Chichester, 1983, pp. 65–155, Vol. 5.
11. E. Paleček, *Prog. Nucleic Acid Res. Mol. Biol.* **1976**, 18, 151–213.
12. H. W. Nurnberg, P. Valenta, in *Ions in Macromolecular and Biological Systems* (Eds.: D. H. Everett, B. Vincent), Sciencetechnica, Bristol, 1977, pp. 201–236.
13. E. Paleček, *Bioelectrochem. Bioenerg.* **1986**, 15, 275–295.
14. E. Paleček, in *Encyclopedia of Analytical Science* (Ed.: A. Townshend), Academic Press, London, 1995, pp. 3600–3609, Vol. 6.
15. E. Paleček, *Electroanalysis* **1996**, 8, 7–14.
16. J. M. Sequaris, in *Wilson and Wilson's Comprehensive Analytical Chemistry* (Eds.: G. Svehla, J. G. Vos), Elsevier, Amsterdam, 1992, pp. 115–156, Vol. XXVII.
17. H. Berg, in *Topics in Bioelectrochemistry Bioenergetics* (Ed.: G. Milazzo), John Wiley & Sons, London, 1976, pp. 39–104, Vol. 1.
18. H. Berg, in *Comprehensive Treatise of Electrochemistry of Biopolymers Vol. 10. Electrochemistry of Biopolymers* (Eds.: S. Srinivasan, Y. Chizmadzhev, J. Bockris et al.), Plenum, New York, 1985, pp. 189–229.
19. R. Berezney, D. S. Coffey, *Biochem. Biophys. Res. Commun.* **1974**, 60, 1410–1417.
20. E. Neumann, in *Ions in Macromolecular and Biological Systems* (Eds.: D. H. Everett, B. Vincent), Sciencetechnica, Bristol, 1978, pp. 170–191.
21. S. M. Gasser, U. K. Laemmli, *Cell* **1986**, 46, 521–530.
22. D. Porschke, M. Jung, *J. Biomol. Struct. Dyn.* **1985**, 6, 1173–1184.
23. E. Neumann, *Prog. Biophys. Mol. Biol.* **1986**, 47, 197–231.
24. E. Neumann, *Bioelectrochem. Bioenerg.* **1986**, 16, 565–567.
25. S. Trasatti, A. Petrii, *Pure Appl. Chem.* **1991**, 63, 711–734.
26. V. Vetterl, *Experientia* **1965**, 21, 9–11.
27. V. Vetterl, *Collect. Czech. Chem. Commun.* **1966**, 31, 2105–2126.
28. V. Vetterl, *Abhandlungen der DAW, Berlin* **1966**, 4, 493–500.
29. V. Vetterl, E. Kovarikova, R. Zaludova, *Bioelectrochem. Bioenerg.* **1977**, 4, 435–444.
30. J. Jursa, V. Vetterl, *J. Electroanal. Chem.* **1989**, 289, 237–244.
31. V. Brabec, V. Vetterl, O. Vrana, in *Experimental Techniques in Bioelectrochemistry* (Eds.: V. Brabec, D. Walz, G. Milazzo), Birkhauser Verlag, Basel, 1996, pp. 287–359, Vol. 3.
32. R. deLevie, *Chem. Rev.* **1988**, 88, 599–609.
33. B. Janik, P. J. Elving, *J. Am. Chem. Soc.* **1970**, 92, 235–243.
34. V. Drazan, V. Vetterl, *Collect. Czech. Chem. Commun.* **1998**, 63, 1977–1993.
35. M. S. Ibrahim, M. E. Ahmed, A. M. Kawde et al., *Analysis* **1996**, 24, 6–9.
36. M. E. Ahmed, M. S. Ibrahim, Y. M. Temerk et al., *Electrochim. Acta* **1996**, 41, 2883–2892.
37. I. R. Miller, *J. Mol. Biol.* **1961**, 3, 229–240.
38. I. R. Miller, *J. Mol. Biol.* **1961**, 3, 357–361.
39. M. Rueda, A. Mota, M. L. S. Goncalves et al., *J. Electroanal. Chem.* **1997**, 431, 257–267.
40. H. Jehring, *Elektrosorptionsanalyse mit der Wechselstrompolarographie.*, Akademie, Berlin, 1974.
41. V. Vetterl, *J. Electroanal. Chem.* **1968**, 19, 169–173.

42. V. Vetterl, *Biophysik* **1968**, 5, 255–260.
43. C. Buess-Herman, *Prog. Surf. Sci.* **1994**, 46, 335–375.
44. C. Buess-Herman, C. Franck, L. Gierst, *J. Electroanal. Chem.* **1992**, 329, 91–103.
45. J. Lipkowski, C. Buess-Herman, J. P. Lambert et al., *J. Electroanal. Chem.* **1986**, 202, 169–189.
46. M. Scharfe, C. Buess-Herman, *J. Electroanal. Chem.* **1994**, 366, 303–310.
47. V. Vetterl, J. Pokorny, *Bioelectrochem. Bioenerg.* **1980**, 7, 517–526.
48. D. Krznaric, P. Valenta, H. W. Nurnberg et al., *J. Electroanal. Chem.* **1978**, 93, 41–56.
49. P. Valenta, D. Krznaric, *J. Electroanal. Chem.* **1977**, 75, 437–454.
50. V. Brabec, S. D. Christian, G. Dryhurst, *J. Electroanal. Chem.* **1977**, 85, 389–405.
51. Y. M. Temerk, M. M. Kamal, M. E. Ahmed et al., *Bioelectrochem. Bioenerg.* **1986**, 16, 497–507.
52. C. Mousty, G. Quarin, *Electrochim. Acta* **1990**, 35, 1291–1302.
53. U. Retter, *J. Electroanal. Chem.* **1982**, 136, 164–167.
54. U. Retter, H. Lohse, *J. Electroanal. Chem.* **1982**, 134, 243–250.
55. U. Retter, V. Vetterl, J. Jursa, *J. Electroanal. Chem.* **1989**, 274, 1–9.
56. T. Wandlowski, M. Heyrovsky, L. Novotny, *Electrochim. Acta* **1992**, 37, 2663–2672.
57. U. Retter, *J. Electroanal. Chem.* **1980**, 106, 371–375.
58. R. Sridharan, R. deLevie, *J. Electroanal. Chem.* **1987**, 218, 287–296.
59. V. Vetterl, R. de Levie, *J. Electroanal. Chem.* **1991**, 310, 305–315.
60. V. Brabec, M. H. Kim, S. D. Christian et al., *J. Electroanal. Chem.* **1979**, 100, 111–133.
61. V. Brabec, S. D. Christian, G. Dryhurst, *Bioelectrochem. Bioenerg.* **1978**, 5, 635–649.
62. V. Brabec, S. D. Christian, G. Dryhurst, *Biophys. Chem.* **1978**, 7, 253–268.
63. G. Quarin, *Electrochim. Acta* **1984**, 29, 1707–1714.
64. N. J. Tao, Z. Shi, *J. Phys. Chem.* **1994**, 98, 7422–7426.
65. Z. A. Ahmed, M. E. Ahmed, M. S. Ibrahim et al., *Bioelectrochem. Bioenerg.* **1995**, 38, 359–365.
66. M. M. Correia dos Santos, P. M. P. Sousa, A. M. M. Modesto et al., *Bioelectrochem. Bioenerg.* **1998**, 45, 267–273.
67. R. Guidelli, M. L. Foresti, *J. Electroanal. Chem.* **1986**, 197, 103–121.
68. E. V. Stenina, B. B. Damaskin, *J. Electroanal. Chem.* **1993**, 349, 31–40.
69. L. Pospisil, M. Svestka, *J. Electroanal. Chem.* **1997**, 426, 47–53.
70. T. Wandlowski, L. Pospisil, *J. Electroanal. Chem.* **1989**, 258, 179–192.
71. H. Francois, M. Scharfe, C. Buess-Herman, *J. Electroanal. Chem.* **1990**, 296, 415–428.
72. M. Scharfe, A. Hamelin, C. Buess-Herman, *Electrochim. Acta* **1995**, 40, 61–67.
73. T. Wandlowski, R. de Levie, *J. Electroanal. Chem.* **1993**, 349, 15–30.
74. T. Wandlowski, G. B. Jameson, R. de Levie, *J. Phys. Chem.* **1993**, 97, 10 119–10 126.
75. T. Wandlowski, G. B. Jameson, R. de Levie, *J. Electroanal. Chem.* **1994**, 379, 215–222.
76. C. Donner, H. Baumgartel, L. Pohlmann et al., *Ber. Bunsen-Ges. Phys. Chem.* **1996**, 100, 403–412.
77. B. Kurtyka, R. de Levie, *J. Electroanal. Chem.* **1995**, 397, 311–314.
78. T. Wandlowski, M. Hromadova, R. de Levie, *Langmuir* **1997**, 13, 2766–2772.
79. F. David, H. Ouguenoune, A. Bolyos et al., *Anal. Chim. Acta* **1994**, 292, 297–304.
80. L. Pospisil, M. Svestka, *J. Electroanal. Chem.* **1994**, 366, 295–302.
81. L. Pospisil, S. Zalis, N. Fanelli, *J. Chem. Educ.* **1995**, 72, 997–1002.
82. A. Avranas, N. Papadopoulos, *Langmuir* **1992**, 8, 2804–2809.
83. R. Srinivasan, R. de Levie, *J. Electroanal. Chem.* **1986**, 206, 307–312.
84. V. Brabec, V. Kleinwachter, V. Vetterl, in *Bioelectrochemistry of Biomacromolecules* (Eds.: G. Lenaz, G. Milazzo), Birkhauser Verlag, Basel, 1997, pp. 1–104, Vol. 5.
85. V. Vetterl, *Bioelectrochem. Bioenerg.* **1976**, 3, 338–345.
86. J. Jursa, V. Vetterl, *Bioelectrochem. Bioenerg.* **1984**, 12, 137–146.
87. J. Jursa, V. Vetterl, *Studia Biophys.* **1986**, 114, 75–82.
88. V. Vetterl, N. Papadopoulos, V. Drazan et al., *Electrochim. Acta* **2000**, 45, 2961–2971.
89. J. Sponer, J. Leszczynski, V. Vetterl et al., *J. Biomol. Struct. Dyn.* **1996**, 13, 695–766.
90. R. de Levie, T. Wandlowski, *J. Electroanal. Chem.* **1994**, 366, 265–270.
91. V. I. Melik-Gaikazyan, *J. Phys. Chem. (USSR)* **1952**, 26, 560–580.

92. W. M. Heckl, D. P. Smith, G. Binnig et al., *J. Proc. Natl. Acad. Sci.* **1991**, 88, 8003–8005.
93. R. Srinivasan, J. C. Murphy, N. Pat-tabiraman, *Ultramicroscopy* **1991**, 42–44, 453–459.
94. R. Srinivasan, P. Gopalan, *J. Phys. Chem.* **1993**, 97, 8770–8775.
95. N. J. Tao, J. A. de Rose, S. M. Lindsay, *J. Phys. Chem.* **1993**, 97, 910–919.
96. N. J. Tao, Z. Shi, *J. Phys. Chem.* **1994**, 98, 1464–1471.
97. T. Wandlowski, D. Lampner, S. Lindsay, *J. Electroanal. Chem.* **1996**, 404, 215–226.
98. M. Holzle, T. Wandlowski, D. M. Kolb, *Surf. Sci.* **1995**, 335, 281–290.
99. C. Bruckner-Lea, J. Janata, J. Conroy et al., *Langmuir* **1993**, 9, 3612–3617.
100. J. Janata, C. Bruckner-Lea, J. F. T. Conroy et al., in *Interfacial Design and Chemical Sensing* (Eds.: T. E. Mallovk, D. J. Harrison), ACS, Washington DC, 1994, pp. 175–184.
101. J. F. T. Conroy, K. Caldwell, C. Bruckner-Lea et al., *Electrochim. Acta* **1995**, 40, 2927–2934.
102. F. Jelen, V. Vetterl, A. Schaper et al., *J. Electroanal. Chem.* **1994**, 377, 197–203.
103. S. Sotiropoulos, P. Nikitas, N. Papadopoulos, *J. Electroanal. Chem.* **1993**, 356, 225–243.
104. B. Janik, P. J. Elving, *J. Am. Chem. Soc.* **1973**, 95, 8495–8502.
105. D. Krznaric, P. Valenta, H. W. Nurnberg, *J. Electroanal. Chem.* **1975**, 65, 863–881.
106. V. Brabec, A. P. Kavunenko, *J. Electroanal. Chem.* **1987**, 237, 261–267.
107. E. Paleček, V. Kolar, F. Jelen et al., *Bioelectrochem. Bioenerg.* **1990**, 23, 285–299.
108. M. Fojta, V. Vetterl, M. Tomschik et al., *Biophys. J.* **1997**, 72, 2285–2293.
109. A. D. Mesmaeker, K.-H. Altmann, A. Waldner et al., *Curr. Opin. Struct. Biol.* **1995**, 5, 343–355.
110. P. E. Nielsen, M. Egholm, O. Buchard, *Bioconjugate Chem.* **1994**, 5, 3–7.
111. A. Popov, R. Naneva, N. Dimitrov et al., *Electrochim. Acta* **1992**, 37, 2369–2371.
112. T. Dretschkow, A. S. Dakkouri, T. Wandlowski, *Langmuir* **1997**, 13, 2843–2856.
113. T. Dretschkow, T. Wandlowski, *Electrochim. Acta* **1998**, 43, 2991–3006.
114. K. Takehara, S. Yamada, Y. Ide, *J. Electroanal. Chem.* **1992**, 333, 339–344.
115. H. Bare, C. Buess-Herman, *Physicochem. Eng. Aspects* **1998**, 134, 181–191.
116. T. Wandlowski, D. Lampner, S. M. Lindsay, *J. Electroanal. Chem.* **1996**, 404, 215–226.
117. M. Kasaya, H. Tabata, T. Kawai, *Surf. Sci.* **1995**, 342, 215–223.
118. M. Kasaya, H. Tabata, T. Kawai, *Surf. Sci.* **1998**, 406, 302–311.
119. K. Takehara, Y. Ide, *Bioelectrochem. Bioenerg.* **1992**, 27, 501–507.
120. K. Takehara, Y. Ide, *Bioelectrochem. Bioenerg.* **1992**, 29, 103–111.
121. K. Takehara, Y. Ide, *Bioelectrochem. Bioenerg.* **1992**, 27, 207–219.
122. B. Roelfs, E. Bunge, C. Schroter et al., *J. Phys. Chem. B* **1997**, 101, 754–765.
123. Z. Yang, I. Engquist, B. Liedberg et al., *J. Electroanal. Chem.* **1997**, 430, 189–195.
124. E. Lust, A. Janes, P. Miidla et al., *J. Electroanal. Chem.* **1997**, 425, 25–37.
125. Z. Yang, I. Enquist, M. Wirde et al., *Langmuir* **1997**, 13, 3210–3218.
126. G. M. Brown, D. P. Allison, R. J. Warmack et al., *Ultramicroscopy* **1991**, 38, 253–264.
127. R. Srinivasan, J. C. Murphy, N. Pattabiraman, *Ultramicroscopy* **1992**, 42, 453–459.
128. S. Hason, V. Vetterl, *Bioelectrochem.* **2001**, in press.
129. J. Wang, G. Rivas, X. H. Cai et al., *Electroanalysis* **1997**, 9, 120–124.
130. J. Wang, G. Rivas, X. Zhang et al., *Langmuir* **1999**, 15, 6541–6545.
131. J. Wang, X. Zhang, C. Parrado et al., *Electrochem. Commun.* **1999**, 1, 197–202.
132. B. Janik, P. J. Elving, *Chem. Rev.* **1968**, 68, 295–319.
133. J. W. Webb, B. Janik, P. J. Elving, *J. Am. Chem. Soc.* **1973**, 95, 991–1003.
134. L. Trnkova, M. Studnickova, E. Paleček, *Bioelectrochem. Bioenerg.* **1980**, 7, 644–658.
135. M. Studnickova, L. Trnkova, J. Zetek et al., *Bioelectrochem. Bioenerg.* **1989**, 21, 83–86.
136. E. Paleček, F. Jelen, L. Trnkova, *Gen. Physiol. Biophys.* **1986**, 5, 315–329.
137. E. Paleček, M. Tomschik, V. Stankova et al., *Electroanalysis* **1997**, 9, 990–997.
138. F. Jelen, M. Tomschik, E. Paleček, *J. Electroanal. Chem.* **1997**, 423, 141–148.
139. L. Havran, L. Trnkova, O. Dracka, *J. Electroanal. Chem.* **1998**, 454, 65–73.
140. T. E. Cummings, P. J. Elving, *J. Electroanal. Chem.* **1978**, 94, 123.
141. T. E. Cummings, P. J. Elving, *J. Electroanal. Chem.* **1979**, 102, 237–248.
142. G. Dryhurst, P. J. Elving, *J. Electrochem. Soc.* **1968**, 115, 1014–1022.

143. G. Dryhurst, G. F. Pace, *J. Electrochem. Soc.* **1970**, *117*, 1259–1265.
144. G. Dryhurst, *Anal. Chim. Acta* **1971**, *57*, 137–149.
145. J. M. Zen, M. R. Chang, G. Ilangoan, *Analyst* **1999**, *124*, 679–684.
146. A. C. Ontko, P. M. Armistead, S. R. Kircus et al., *Inorg. Chem.* **1999**, *38*, 1842–1846.
147. X. Cai, B. Ogorevc, K. Kalcher, *Electroanalysis* **1995**, *7*, 1126–1131.
148. A. M. O. Brett, F. M. Matysik, *J. Electroanal. Chem.* **1997**, *429*, 95–99.
149. P. Singhal, W. G. Kuhr, *Anal. Chem.* **1997**, *69*, 3552–3557.
150. K. Brainina, *Talanta* **1971**, *18*, 513–520.
151. K. Brainina, E. Neyman, *Electroanalytical Stripping Methods*, Wiley & Sons, New York, 1993.
152. T. M. Florence, *J. Electroanal. Chem.* **1979**, *97*, 219–236.
153. J. Heyrovsky, J. Kuta, *Principles of Polarography*, Czechoslovak Academy of Sciences, Prague, 1965.
154. F. Vydra, K. Stulik, E. Julakova, *Electrochemical Stripping Analysis*, Wiley & Sons, New York, 1973.
155. J. Revenda, *Collect. Czech. Chem. Commun.* **1934**, *6*, 453–467.
156. I. M. Kolthoff, C. Barnum, *J. Am. Chem. Soc.* **1940**, *62*, 3061–3066.
157. P. Zuman, J. Koryta, R. Kalvoda, *Collect. Czech. Chem. Commun.* **1953**, *18*, 350–365.
158. O. Manousek, P. Zuman, *Chem. Listy* **1955**, *49*, 668–678.
159. D. Kalab, *Chem. Zvesti* **1964**, *18*, 435–439.
160. E. Paleček, F. Jelen, *Collect. Czech. Chem. Commun.* **1980**, *45*, 3472–3481.
161. E. Paleček, *Anal. Biochem.* **1980**, *108*, 129–138.
162. M. R. Smyth, J. G. Osteryoung, *Anal. Chem.* **1977**, *49*, 2310–2314.
163. T. M. Florence, *J. Electroanal. Chem.* **1978**, *97*, 237–255.
164. Y. Vaneesorn, W. F. Smyth, *Anal. Chim. Acta* **1980**, *117*, 183–191.
165. E. Paleček, *Anal. Lett.* **1980**, *13*, 331–345.
166. E. Paleček, F. Jelen, M. A. Hung et al., *Bioelectrochem. Bioenerg.* **1981**, *8*, 621–631.
167. E. Paleček, F. Jelen, I. Postbieglova, *Studia Biophys.* **1989**, *130*, 51–54.
168. E. Borek, O. K. Scharma, T. P. Waalkes, in *Modified Nucleosides and Cancer* (Ed.: G. Nass), Springer-Verlag, Heidelberg **1983**, pp. 301–315.
169. E. Paleček, *Anal. Chim. Acta* **1985**, *174*, 103–113.
170. E. Paleček, J. Osteryoung, R. A. Osteryoung, *Anal. Chem.* **1982**, *54*, 1389–1394.
171. A. J. M. Ordieres, M. J. G. Gutierrez, A. C. Garcia et al., *Analyst* **1987**, *112*, 243–251.
172. J. Wang, S. M. Lin, V. Villa, *Analyst* **1987**, *112*, 247–251.
173. M. Khodari, M. Ghandour, A. M. Taha, *Talanta* **1997**, *44*, 305–310.
174. J. Yan, C. Zhu, G. Pu, *Bioelectrochem. Bioenerg.* **1993**, *29*, 347–355.
175. Y. Jiangli, Z. Chongjie, P. Guogong et al., *Bioelectrochem. Bioenerg.* **1993**, *29*, 347–355.
176. B. Bouzid, A. M. G. Mac Donald, *Anal. Chim. Acta* **1988**, *211*, 155–173.
177. B. Bouzid, A. M. G. Mac Donald, *Anal. Proc.* **1986**, *23*, 295–297.
178. B. Bouzid, A. M. G. Mac Donald, *Anal. Chim. Acta* **1988**, *211*, 175–193.
179. S. Glodowski, R. Bilewicz, Z. Kublik, *Anal. Chim. Acta* **1987**, *201*, 11–22.
180. S. Glodowski, R. Bilewicz, Z. Kublik, *Anal. Chim. Acta* **1986**, *186*, 39–47.
181. X. Zhao, W. R. Jin, Y. Wang, *Electrochim. Acta* **1996**, *41*, 887–893.
182. X. Zhao, W. R. Jin, J. Tang, *Electroanalysis* **1996**, *8*, 370–374.
183. M. M. Correia dos Santos, C. M. L. F. Lopes, M. L. Simoes-Goncalves, *Bioelectrochem. Bioenerg.* **1996**, *39*, 55–60.
184. P. Valenta, H. W. Nurnberg, P. Klahre, *Bioelectrochem. Bioenerg.* **1974**, *1*, 487–505.
185. E. Paleček, V. Vetterl, *Biopolymers* **1968**, *6*, 917–928.
186. V. Brabec, E. Paleček, *Biopolymers* **1972**, *11*, 2577–2589.
187. V. Brabec, E. Paleček, *Z. Naturforsch.* **1973**, *28c*, 685–692.
188. V. Brabec, G. Dryhurst, *J. Electroanal. Chem.* **1978**, *91*, 219–229.
189. V. Brabec, K. Niki, *Biophys. Chem.* **1985**, *23*, 63–70.
190. V. Brabec, V. Glezers, V. Kadysh, *Collect. Czech. Chem. Commun.* **1983**, *48*, 1257–1271.
191. B. Janik, R. G. Sommer, *Biopolymers* **1973**, *12*, 2803–2822.
192. H. Berg, G. Horn, J. Flemming, in *Dynamic Aspects of Biopolyelectrolytes and Biomembranes*, Elsevier Press, New York, 1982, pp. 181–184.
193. J. Flemming, *Biopolymers* **1973**, *9*, 1975–1988.

194. B. Janik, R. G. Sommer, *Bioelectrochem. Bioenerg.* **1976**, 3, 622–633.
195. B. Malfoy, J. M. Sequaris, P. Valenta et al., *J. Electroanal. Chem.* **1977**, 75, 455–469.
196. P. Valenta, P. Grahmann, *J. Electroanal. Chem.* **1974**, 49, 41–53.
197. P. Valenta, H. W. Nurnberg, *Biophys. Struct. Mech.* **1974**, 1, 17–26.
198. V. Brabec, *Biophys. Chem.* **1980**, 11, 1–7.
199. J. Koryta, *Collect. Czech. Chem. Commun.* **1953**, 18, 206.
200. J. Koryta, *Collect. Czech. Chem. Commun.* **1953**, 18, 206–213.
201. P. Delahay, I. Trachtenberg, *J. Am. Chem. Soc.* **1957**, 79, 2355–2362.
202. M. K. Kaisheva, M. Matsumoto, Y. Kita et al., *Langmuir* **1988**, 4, 762–765.
203. E. Paleček, P. Boublikova, F. Jelen, *Anal. Chim. Acta* **1986**, 187, 99–107.
204. W. Guschlbauer, V. Vetterl, *FEBS Lett.* **1969**, 4, 57–60.
205. V. Vetterl, W. Guschlbauer, *Arch. Biochem. Biophys.* **1972**, 148, 130–140.
206. W. Guschlbauer, *Nucleic Acid Structure*, Springer Verlag, New York, 1976.
207. C. M. A. Brett, A. M. O. Brett, *Electrochemistry. Principles, Methods, and Applications*, Oxford University Press, Oxford, 1993.
208. I. R. Miller, D. C. Grahame, *J. Am. Chem. Soc.* **1957**, 79, 3006–3012.
209. M. Sluyters-Rehbach, J. H. Sluyters, *J. Electroanal. Chem.* **1982**, 136, 39–58.
210. L. Hanak, V. Vetterl, *Bioelectrochem. Bioenerg.* **1998**, 46, 9–13.
211. A. N. Frumkin, B. B. Damaskin, in *Modern Aspects of Electrochemistry* (Eds.: J. O. M. Bockris, B. E. Conway), Butterworth, London, 1964, pp. 149–223.
212. I. R. Miller, D. C. Grahame, *J. Am. Chem. Soc.* **1956**, 78, 3577–3585.
213. E. Sabatani, J. Cohen-Boulakia, M. Bruening et al., *Langmuir* **1993**, 9, 2974–2981.
214. E. Sabatani, Y. Gafni, I. Rubinstein, *J. Phys. Chem.* **1995**, 99, 12 305–12 311.
215. R. P. Janek, W. R. Fawcett, A. Ulman, *J. Phys. Chem.* **1997**, 101, 8550–8558.
216. R. P. Janek, W. R. Fawcett, A. Ulman, *Langmuir* **1998**, 14, 3011–3018.
217. P. Diao, D. L. Jiang, X. L. Cui et al., *Bioelectrochem. Bioenerg.* **1998**, 45, 173–179.
218. P. Diao, D. L. Jiang, X. L. Cui et al., *Bioelectrochem. Bioenerg.* **1999**, 48, 469–475.
219. A. E. Vallejo, C. A. Gervasi, L. M. Gassa, *Bioelectrochem. Bioenerg.* **1998**, 47, 343–348.
220. H. O. Finklea, D. A. Snider, J. Fedyk et al., *Langmuir* **1993**, 9, 3660–3667.
221. X. Cui, D. Jiang, P. Diao et al., *J. Electroanal. Chem.* **1999**, 470, 9–13.
222. M. W. Humphreys, R. Parsons, *J. Electroanal. Chem.* **1977**, 75, 427–436.
223. A. Roeseler, *Infrared Spectroscopic Ellipsometry*, Akademie-Verlag, Berlin, 1990.
224. O. M. Magnussen, B. M. Ocko, M. Deutsch et al., *Nature* **1996**, 384, 250–252.
225. C. Hinnen, A. Rousseau, R. Parsons et al., *J. Electroanal. Chem.* **1981**, 125, 193–203.
226. T. Boland, B. D. Ratner, *Biophysics* **1995**, 92, 5297–5301.
227. R. M. Zimmerman, E. C. Cox, *Nucleic Acids Res.* **1994**, 22, 492–497.
228. E. Koglin, J.-M. Sequaris, in *Topics in Current Chemistry*, Springer-Verlag, New York, 1986, pp. 1–, Vol. 4.
229. C. Fan, H. Song, X. Hu et al., *Anal. Biochem.* **1999**, 271, 1–7.
230. S. O. Kelley, J. K. Barton, N. M. Jackson et al., *Langmuir* **1998**, 14, 6781–6784.
231. J. Humlicek, A. Roeseler, *Thin Solid Film* **1993**, 234, 332–336.
232. J. Humlicek, C. Thomsen, M. Cardona et al., *Physica C* **1994**, 222, 166–172.
233. J. Humlicek, *Philos. Mag. B* **1994**, 70, 699–710.
234. A. Rothen, C. Mathot, *Immunochemistry* **1969**, 6, 241–251.
235. A. Rothen, in *Surface and Membrane Science*, (Ed.: D. A. Cadonhead), Academic Press, New York, 1974, Vol. 8.
236. M. Cardona, *Modulation Spectroscopy*, Academic Press, New York, 1969.
237. R. M. A. Azzam, N. M. Bashara, *Ellipsometry and Polarized Light*, North-Holland, New York, 1977.
238. R. Artzi, Feinberg Graduate School, Weizmann Institute of Science, Rehovot, 1999.
239. A. Vilan, R. Ussyshkin, K. Gartsman et al., *J. Phys. Chem. B* **1998**, 102, 3307–3312.
240. H. Clausen-Schaumann, H. E. Gaub, *Langmuir* **1999**, 15, 8246–8251.
241. M. S. Spector, J. M. Schnur, *Science* **1997**, 275, 791–792.
242. E. Paleček, M. A. Hung, *Anal. Biochem.* **1983**, 132, 236–242.
243. V. Brabec, *Gen. Physiol. Biophys.* **1983**, 2, 193–199.
244. F. Jelen, E. Paleček, *Biophys. Chem.* **1986**, 24, 285–290.

245. B. Janik, E. Paleček, *Z. Naturforsch.* **1966**, 21b, 1117, 1118.
246. B. Janik, E. Paleček, *Elektrochemische methoden und prinzipien in der molekularbiologie, III. Jenaer symp.*, Academic-Verlag, Berlin, 1966, Abhandlungen der DAW, pp. 513–518.
247. M. Tomschik, F. Jelen, L. Havran et al., *J. Electroanal. Chem.* **1999**, 476, 71–80.
248. F. Jelen, M. Fojta, E. Paleček, *J. Electroanal. Chem.* **1997**, 427, 49–56.
249. M. Tomschik, L. Havran, M. Fojta et al., *Electroanalysis* **1998**, 476, 71–80.
250. J. Wu, Y. Huang, J. Zhou et al., *Bioelectrochem. Bioenerg.* **1997**, 44, 151–154.
251. T. Kubicarova, M. Fojta, J. Vidic et al., *Electroanalysis* **2000**, 12, 1390–1391.
252. T. Kubicarova, M. Fojta, J. Vidic et al., *Electroanalysis* **2000**, 12, 122–142.
253. V. Brabec, *Bioelectrochem. Bioenerg.* **1981**, 8, 437–449.
254. C. M. A. Brett, A. M. O. Brett, S. H. P. Serrano, *J. Electroanal. Chem.* **1994**, 366, 225–231.
255. J. Wang, X. Cai, J. Wang et al., *Anal. Chem.* **1995**, 67, 4065–4070.
256. J. Wang, X. Cai, C. Jonsson et al., *Electroanalysis* **1996**, 8, 20–24.
257. X. Cai, G. Rivas, P. A. M. Farias et al., *Bioelectrochem. Bioenerg.* **1996**, 401, 41–47.
258. C. Cai, G. Rivas, P. A. M. Farias et al., *Electroanalysis* **1996**, 8, 753–758.
259. J. Wang, X. Cai, J. Fernandez et al., *Anal. Chem.* **1997**, 69, 4056–4059.
260. J. Wang, *Anal. Chem.* **1995**, 67, R487–R492.
261. J. Wang, S. Bollo, J. L. L. Paz et al., *Anal. Chem.* **1999**, 71, 1910–1913.
262. J. Wang, A. N. Kawde, E. Sahlin, *Analyst* **2000**, 125, 5–7.
263. J. Wang, X. H. Cai, J. R. Fernandes et al., *Anal. Chem.* **1997**, 69, 4056–4059.
264. C. G. Siontorou, A. M. O. Brett, D. P. Nikolecis, *Talanta* **1996**, 43, 1137–1144.
265. M. E. Napier, H. H. Thorp, *Langmuir* **1997**, 13, 6342–6344.
266. M. E. Napier, H. H. Thorp, *J. Fluorescence* **1999**, 9, 181–186.
267. D.-W. Pang, Y.-P. Qi, Z.-L. Wang et al., *Electroanalysis* **1995**, 7, 774–776.
268. P. Singhal, W. G. Kuhr, *Anal. Chem.* **1997**, 69, 4828–4832.
269. M. Fojta, R. Doffkova, E. Paleček, *Electroanalysis* **1996**, 8, 420–426.
270. E. Paleček, M. Fojta, *Anal. Chem.* **1994**, 66, 1566–1571.
271. M. Fojta, C. Teijeiro, E. Paleček, *Bioelectrochem. Bioenerg.* **1994**, 34, 69–76.
272. M. Fojta, E. Paleček, *Anal. Chim. Acta* **1997**, 342, 1–12.
273. M. Fojta, V. Stankova, E. Paleček et al., *Talanta* **1998**, 46, 155–161.
274. M. Fojta, R. P. Bowater, V. Stankova et al., *Biochemistry* **1998**, 37, 4853–4862.
275. J. Wang, E. Paleček, P. E. Nielsen et al., *J. Am. Chem. Soc.* **1996**, 118, 7667–7670.
276. M. Fojta, L. Havran, E. Paleček, *Electroanalysis* **1997**, 9, 1033, 1034.
277. O. Dracka, *J. Electroanal. Chem.* **1996**, 402, 19–28.
278. L. Trnkova, O. Dracka, *J. Electroanal. Chem.* **1993**, 348, 265–271.
279. L. Trnkova, O. Dracka, *J. Electroanal. Chem.* **1996**, 413, 123–129.
280. E. Paleček, B. D. Frary, *Arch. Biochem. Biophys.* **1966**, 115, 431–436.
281. E. Paleček, I. Postbieglova, *J. Electroanal. Chem.* **1986**, 214, 359–371.
282. E. Paleček, *Anal. Biochem.* **1988**, 170, 421–431.
283. E. Paleček, F. Jelen, C. Teijeiro et al., *Anal. Chim. Acta* **1993**, 273, 175–186.
284. C. Teijeiro, K. Nejedly, E. Paleček, *J. Biomol. Struct. Dyn.* **1993**, 11, 313–331.
285. C. Teijeiro, P. Perez, D. Marin et al., *Bioelectrochem. Bioenerg.* **1995**, 38, 77–83.
286. M. Vojtiskova, E. Lukasova, F. Jelen et al., *Bioelectrochem. Bioenerg.* **1981**, 8, 487–496.
287. J. M. Sequaris, M. L. Kaba, P. Valenta, *Bioelectrochem. Bioenerg.* **1984**, 13, 225–227.
288. E. Paleček, *Bioelectrochem. Bioenerg.* **1988**, 20, 171–194.
289. V. Brabec, E. Paleček, *J. Electroanal. Chem.* **1978**, 88, 373–385.
290. J. Flemming, H. Berg, *Bioelectrochem. Bioenerg.* **1974**, 1, 459–465.
291. E. Paleček, *Collect. Czech. Chem. Commun.* **1974**, 39, 3449–3455.
292. H. W. Nurnberg, P. Valenta, *Croat. Chem. Acta* **1976**, 48, 623–641.
293. E. Paleček, *Bioelectrochem. Bioenerg.* **1992**, 28, 71–83.
294. V. Brabec, E. Paleček, *Studia Biophys.* **1976**, 60, 105–110.
295. F. Jelen, E. Paleček, *Gen. Physiol. Biophys.* **1985**, 4, 219–237.

296. E. Paleček, in *Proc. Electroanalysis in Hygiene, Environmental, Clinical and Pharmaceutical Chemistry* (Ed.: W. F. Smyth), Elsevier, Amsterdam 1980, pp. 79–99.
297. M. Fojta, L. Havran, J. Fulneckova et al., *Electroanalysis* **2000**, *12*, 926–934.
298. A. D. Bates, A. Maxwell, *DNA Topology*, Oxford University Press, Oxford, 1993.
299. E. Paleček, *Crit. Rev. Biochem. Mol. Biol.* **1991**, *26*, 151–226.
300. D. Kasparova, O. Vrana, V. Kleinwachter et al., *Biophys. Chem.* **1987**, *28*, 191–197.
301. H. Clausen-Schaumann, M. Rief, C. Tolksdorf et al., *Biophys. J.* **2000**, *78*, 1997–2007.
302. D. Bensimon, V. Simon, V. Croquette et al., *Phys. Rev. Lett.* **1995**, *74*, 4754–4757.
303. M. Rief, H. Clausen-Schaumann, H. E. Gaub, *Nat. Struct. Biol.* **1999**, *6*, 346–349.
304. M. G. Blackburn, M. J. Gait, *Nucleic Acids in Chemistry and Biology*, IRL Press, New York, 1990.
305. G. S. Manning, *Q. Rev. Biophys.* **1978**, *11*, 179–246.
306. J. Labuda, M. Buckova, M. Vanickova et al., *Electroanalysis* **1999**, *11*, 101–107.
307. M. Maeda, K. Nakano, S. Uchida et al., *Chem. Lett.* **1994**, 1805–1808.
308. J.-M. Sequaris, M. Esteban, *Electroanalysis* **1990**, *2*, 35–41.
309. J.-M. Sequaris, J. Swiatek, *Bioelectrochem. Bioenerg.* **1991**, *26*, 15–28.
310. E. Braun, Y. Eichen, U. Sivan et al., *Nature* **1998**, *391*, 775–778.
311. A. B. Steel, T. M. Herne, M. J. Tarlov, *Anal. Chem.* **1998**, *70*, 4670–4677.
312. A. B. Steel, T. M. Herne, M. J. Tarlov, *Bioconjugate Chem.* **1999**, *10*, 419–423.
313. M. Aslanoglu, A. Houlton, B. R. Horrocks, *Analyst* **1998**, *123*, 753–757.
314. R. F. Johnston, D. M. Lewis, J. Q. Chambers, *J. Electroanal. Chem.* **1999**, *466*, 2–7.
315. J. L. M. Alvarez, J. A. G. Calzon, J. M. L. Fonseca, *J. Electroanal. Chem.* **1998**, *457*, 53–59.
316. M. T. Carter, A. J. Bard, *J. Am. Chem. Soc.* **1987**, *109*, 7528–7530.
317. M. T. Carter, M. Rodriguez, A. J. Bard, *J. Am. Chem. Soc.* **1989**, *111*, 8901–8911.
318. X. H. Xu, A. J. Bard, *J. Am. Chem. Soc.* **1995**, *117*, 2627–2631.
319. T. W. Welch, H. H. Thorp, *J. Phys. Chem.* **1996**, *100*, 13 829–13 836.
320. M. Rodriguez, A. J. Bard, *Anal. Chem.* **1990**, *62*, 2658–2662.
321. M. T. Carter, A. J. Bard, *Bioconjugate Chem.* **1990**, *1*, 257–263.
322. D. W. Pang, H. D. Abruna, *Anal. Chem.* **1998**, *70*, 3162–3169.
323. A. Erdem, B. Meric, K. Kerman et al., *Electroanalysis* **1999**, *11*, 1372–1376.
324. K. M. Millan, A. Saraullo, R. Mikkelsen, *Anal. Chem.* **1994**, *66*, 2943–2948.
325. Y. Mishima, J. Motonaka, S. Ikeda, *Anal. Chim. Acta* **1997**, *345*, 45–50.
326. X. Cai, G. Rivas, H. Shiraishi et al., *Anal. Chim. Acta* **1997**, *344*, 64–76.
327. H. H. Thorp, *Tibtech* **1998**, *16*, 117–121.
328. D. H. Johnston, C.-C. Cheng, K. J. Campbell et al., *Inorg. Chem.* **1994**, *33*, 6388–6390.
329. D. H. Johnston, K. C. Glasgow, H. H. Thorp, *J. Am. Chem. Soc.* **1995**, *117*, 8933–8938.
330. P. A. Ropp, H. H. Thorp, *Chem. Biol.* **1999**, *6*, 599–605.
331. F. Qu, N.-Q. Li, *Electroanalysis* **1997**, *9*, 1348–1352.
332. K. Hashimoto, K. Ito, Y. Ishimori, *Anal. Chem.* **1994**, *66*, 3830–3833.
333. J. Wang, M. Ozsoz, X. H. Cai et al., *Bioelectrochem. Bioenerg.* **1998**, *45*, 33–40.
334. S. Palanti, G. Marrazza, M. Mascini, *Anal. Lett.* **1996**, *29*, 2309–2331.
335. S. O. Kelley, N. M. Jackson, M. G. Hill et al., *Angew. Chem., Int. Ed. Engl.* **1999**, *38*, 941–945.
336. S. O. Kelley, E. M. Boon, J. K. Barton et al., *Nucleic Acids Res.* **1999**, *27*, 4830–4837.
337. M. Rodriguez, A. J. Bard, *Inorg. Chem.* **1992**, *31*, 1129–1135.
338. P. C. Pandey, H. H. Weetall, *Anal. Chem.* **1994**, *66*, 1236–1241.
339. J. Wang, G. Rivas, D. B. Luo et al., *Anal. Chem.* **1996**, *68*, 4365–4369.
340. M. Maeda, Y. Mitsuhashi, K. Nakano et al., *Anal. Sci.* **1992**, *8*, 83, 84.
341. K. Nakano, M. Maeda, S. Uchida et al., *Anal. Sci.* **1997**, *13*(Suppl S), 455–456.
342. S. Takenaka, T. Ihara, M. Takagi, *J. Chem. Soc., Chem. Commun.* **1990**, 1485–1487.
343. S. Takenaka, Y. Uto, H. Saita et al., *Chem. Commun.* **1998**, 1111, 1112.
344. S. Takenaka, K. Yamashita, Y. Uto et al., *Denki Kagaku* **1998**, *12*, 1329–1334.
345. S. Takenaka, K. Yamashita, M. Takagi et al., *Anal. Chem.* **2000**, *72*, 1334–1341.
346. S. Takenaka, Y. Uto, M. Takagi et al., *Chem. Lett.* **1998**, 989–990.

347. S. Takenaka, K. Yamashita, M. Takagi et al., *Nucleic Acids Symp. Ser.* **1999**, 42, 149, 150.
348. A. M. O. Brett, S. H. P. Serrano, I. Gutz et al., *Bioelectrochem. Bioenerg.* **1997**, 42, 175–178.
349. A. M. O. Brett, S. H. P. Serrano, S. I. G. R. Gutz, *Electroanalysis* **1997**, 9, 110–114.
350. A. M. O. Brett, S. H. P. Serrano, I. Gutz et al., *Bioelectrochem. Bioenerg.* **1997**, 42, 1132–1137.
351. A. M. O. Brett, S. H. P. Serrano, I. Gutz et al., *Electroanalysis* **1997**, 9, 1132–1137.
352. A. M. Brett, T. R. Macedo, D. Raimundo et al., *Biosens. Bioelectron.* **1998**, 13, 861–867.
353. J. Kuta, E. Paleček, in *Topics Bioelectrochem. Bioenerg.* (Ed.: G. Milazzo), John Wiley & Sons, Chichester, London, 1983, pp. 1–63, Vol. 5.
354. E. Paleček, E. Lukasova, F. Jelen et al., *Bioelectrochem. Bioenerg.* **1981**, 8, 497–506.
355. E. Lukasova, F. Jelen, E. Paleček, *Gen. Physiol. Biophys.* **1982**, 1, 53–70.
356. E. Lukasova, M. Vojtiskova, F. Jelen et al., *Gen. Physiol. Biophys.* **1984**, 3, 175–191.
357. E. Paleček, M. Vojtiskova, F. Jelen et al., in *Charge and Field Effects in Biosystems* (Eds.: M. J. Allen, P. N. R. Usherwood), Abacus press, Tonbridge, 1984, pp. 397–404.
358. E. Paleček, M. Vojtiskova, F. Jelen et al., *Bioelectrochem. Bioenerg.* **1984**, 12, 135, 136.
359. F. Jelen, P. Karlovsky, P. Pecinka et al., *Gen. Physiol. Biophys.* **1991**, 10, 461–473.
360. E. Paleček, F. Jelen, E. Minarova et al., *Structural Tools for the Analysis of Protein-Nucleic Acid Complexes*, Birghauser Verlag, Basel, 1992, pp. 1–22.
361. J. M. Hall, J. Moore-Smith, V. Bannister et al., *Biochem. Mol. Biol. Int.* **1994**, 32, 21–28.
362. E. Paleček, *Methods Enzymol.* **1992**, 212, 139–155.
363. E. Paleček, in *Nucleic Acids and Molecular Biology* (Eds.: F. Eckstein, D. M. J. Lilley), Springer Verlag, Berlin, 1994, pp. 1–13, Vol. 8.
364. T. Ihara, Y. Maruo, S. Takanaka et al., *Nucleic Acids Res.* **1996**, 24, 4273–4280.
365. H. Korri-Yousoufi, F. Garnier, P. Srivastava et al., *J. Am. Chem. Soc.* **1997**, 119, 7388, 7389.
366. P. Bauerle, A. Emge, *Adv. Mater.* **1998**, 3, 324–330.
367. M. J. Tarlov, E. F. Bowden, *J. Am. Chem. Soc.* **1991**, 113, 1847–1849.
368. T. M. Herne, M. J. Tarlov, *J. Am. Chem. Soc.* **1997**, 119, 8916–8920.
369. S. O. Kelley, J. K. Barton, N. M. Jackson et al., *Bioconjugate Chem.* **1997**, 8, 31–37.
370. R. Levicky, T. M. Herne, M. J. Tarlov et al., *J. Am. Chem. Soc.* **1998**, 120, 9787–9792.
371. D. Marina, R. Valera, E. de la Red et al., *Bioelectrochem. Bioenerg.* **1997**, 44, 51–56.
372. D. Marin, P. Perez, C. Teijeiro et al., *Biophys. Chem.* **1998**, 75, 87–95.
373. D. Marin, C. Teijero, P. Perez et al., *Recent Res. Dev. Electrochem.* **1998**, 1, 31–43.
374. P. Perez, C. Teijeiro, D. Marin, *Chem. Biol. Interact.* **1999**, 117, 65–81.
375. J. Wang, *Biosens. Bioelectron.* **1998**, 13, 757–762.
376. E. Uhlmann, A. Peyman, G. Breipohl et al., *Angew. Chem. Int. Ed. Engl.* **1998**, 37, 2797–2823.
377. P. E. Nielsen, *Acc. Chem. Res.* **1999**, 32, 624–630.
378. D. D. Eley, D. I. Spivey, *Trans. Faraday Soc.* **1962**, 58, 411.
379. D. Dee, M. E. Baur, *J. Chem. Phys.* **1974**, 60, 541–560.
380. T. A. Hofmann, J. Ladik, *Adv. Chem. Phys.* **1964**, 7, 84.
381. S. Suhai, *J. Chem. Phys.* **1972**, 57, 5599–5603.
382. V. Mikac-Dadic, V. Pravdic, A. Rupprecht, *Bioelectrochem. Bioenerg.* **1974**, 1, 364–369.
383. T. J. Meade, in *Metal Ions in Biological Systems* (Eds.: A. Siegel, H. Siegel), Marcel Dekker, New York, 1996, pp. 453–478.
384. B. Norden, P. Lincoln, B. Akerman et al., in *Metal Ions in Biological Systems* (Eds.: A. Sigel, H. Sigel), Marcel Dekker, New York, 1996, pp. 177–252, Vol. 33.
385. E. Tuite, in *Organic and Inorganic Photochemistry* (Eds.: V. Ramamurthy, K. S. Schanze), Marcel Dekker, New York, 1998, pp. 55–74.
386. R. E. Holmlin, P. J. Dandliker, J. K. Barton, *Angew. Chem. Int. Ed. Engl.* **1997**, 36, 2714–2730.
387. S. O. Kelley, J. K. Barton, in *Metal Ions in Biological Systems. Interactions Between Free Radicals and Metal Ions in Life Processes* (Eds.: A. Sigel, H. Sigel), 1999, pp. 211–249, Vol. 36.
388. G. Hartwich, D. J. Caruana, T. deLumley-Woodyear et al., *J. Am. Chem. Soc.* **1999**, 121, 10803–10812.

389. G. C. Barker, *J. Electroanal. Chem.* **1986**, 214, 373–390.
390. G. C. Barker, *J. Electroanal. Chem.* **1987**, 226, 171–192.
391. G. C. Barker, A. W. Gardner, *Analyst* **1992**, 117, 1811–1828.
392. S. O. Kelley, J. K. Barton, *Science* **1999**, 283, 375–381.
393. D. Porath, A. Bezryadin, S. de Vries et al., *Nature* **2000**, 403, 635–638.
394. J. Jortner, M. Bixon, T. Langenbacher et al., *Proc. Natl. Acad. Sci.* **1998**, 95, 12 759–12 765.
395. A. Okada, V. Chernyak, S. Mukamel, *J. Phys. Chem. A* **1998**, 102, 1241–1251.
396. B. Giese, S. Wessely, M. Spormann et al., *Angew. Chem. Int. Ed. Engl.* **1999**, 38, 996–998.
397. E. Meggers, M. E. Michel-Beyerle, B. Giese, *J. Am. Chem. Soc.* **1998**, 120, 12 950–12 955.
398. B. Armitage, D. Ly, T. Koch et al., *Proc. Natl. Acad. Sci.* **1997**, 94, 12 320–12 325.
399. S. M. Gasper, G. B. Schuster, *J. Am. Chem. Soc.* **1997**, 119, 12 762–12 771.
400. Y. Kan, G. B. Schuster, *J. Am. Chem. Soc.* **1999**, 121, 11 607–11 614.
401. D. Ly, L. Sanii, G. B. Schuster, *J. Am. Chem. Soc.* **1999**, 121, 9400–9410.
402. Y. Okahata, T. Kobayashi, K. Tanaka et al., *J. Am. Chem. Soc.* **1998**, 120, 6165, 6166.
403. H.-W. Fink, C. Schonenberg, *Nature* **1999**, 398, 407–410.
404. T. de Lumley-Woodyear, D. J. Caruana, C. N. Campbell et al., *Anal. Chem.* **1999**, 71, 394–398.
405. J. Wang, P. E. Nielsen, M. Jiang et al., *Anal. Chem.* **1997**, 69, 5200–5212.
406. J. Wang, G. Rivas, X. H. Cai et al., *Anal. Chim. Acta* **1997**, 344, 111–118.
407. J. Marmur, R. Rownd, C. L. Schildkraut, in *Progress in Nucleic Acid Research* (Eds.: J. N. Davidson, W. E. Cohn), Academic Press, London, 1963, pp. 231–300, Vol. 1.
408. E. Paleček, *Die Polarographie in Chemotherapie, Biochemie und Biologie. I. Jenaer symp.*, Academic Verlag, Berlin, 1964, Abhandlungen der DAW, pp. 270–274.
409. S. R. Mikkelsen, *Electroanalysis* **1996**, 8, 15–19.
410. J. Wang, G. Rivas, X. Cai et al., *Anal. Chim. Acta* **1997**, 347, 1–8.
411. E. Paleček, M. Fojta, M. Tomschik et al., *Biosens. Bioelectron.* **1998**, 13, 621–628.
412. J. Wang, *Anal. Chem.* **1999**, 71, 328R–332R.
413. J. Wang, *Chem.-A Eur. J.* **1999**, 5, 1681–1685.
414. J. Wang, G. Rivas, X. H. Cai, *Electroanalysis* **1997**, 9, 395–398.
415. J. Wang, J. R. Fernandes, L. T. Kubota, *Anal. Chem.* **1998**, 70, 3699–3702.
416. J. Wang, G. Rivas, J. R. Fernandes et al., *Electroanalysis* **1998**, 10, 553–556.
417. K. Yamashita, S. Takenaka, M. Takagi, *Nucleic Acids Symp. Ser.* **1999**, 42, 185, 186.
418. J. Wang, X. H. Cai, G. Rivas et al., *Anal. Chem.* **1996**, 68, 2629–2634.
419. G. Marrazza, I. Chianella, M. Mascini, *Biosens. Bioelectron.* **1999**, 14, 43–51.
420. K. Hashimoto, K. Ito, Y. Ishimori, *Sens. Actuators* **1998**, 46, 220–225.
421. S. O. Rolley, J. K. Barton, N. M. Jackson et al., *Bioconjugate Chem.* **1997**, 8, 31.
422. Y. Okahata, Y. Matsunobu, K. Ijio et al., *J. Am. Chem. Soc.* **1992**, 114, 8299, 8300.
423. K. A. Peterlinz, R. M. Georgiadis, *J. Am. Chem. Soc.* **1997**, 119, 3401, 3402.
424. K. Hashimoto, K. Miwa, M. Goto et al., *Supramol. Chem.* **1993**, 2, 265–270.
425. K. Hashimoto, K. Ito, Y. Ishimori, *Anal. Chim. Acta* **1994**, 286, 219–224.
426. S. Takenaka, M. Takagi, Y. Uto et al., *Nucleic Acids Symp. Ser.* **1998**, 39, 107, 108.
427. S. Takenaka, M. Takagi, *Bull. Chem. Soc. Jpn.* **1999**, 72, 327–337.
428. T. Ihara, M. Nakayama, M. Murata et al., *Chem. Commun.* **1997**, 1609, 1610.
429. S. Takenaka, Y. Uto, H. Kondo et al., *Anal. Biochem.* **1994**, 218, 436–443.
430. Y. Uto, H. Kondo, M. Abe et al., *Anal. Biochem.* **1997**, 250, 122–124.
431. M. E. Napier, C. R. Loomis, M. F. Sistare et al., *Bioconjugate Chem.* **1997**, 8, 906–913.
432. J. Wang, G. Rivas, J. R. Fernandes et al., *Anal. Chim. Acta* **1998**, 375, 197–203.
433. C. Berggren, P. Stalhandske, J. Brundell et al., *Electroanalysis* **1999**, 11, 156–160.
434. E. Souteyrand, J. P. Cloarec, J. R. Martin et al., *J. Phys. Chem. B* **1997**, 101, 2980–2985.
435. A. Bardea, F. Patolsky, A. Dagan et al., *Chem. Commun.* **1999**, 21–22.
436. F. Garnier, in *Biomedical Chemistry: Applying Principles to the Understanding and Treatment of Disease* (Ed.: P. F. Torrence), John Wiley & Sons, Chichester, 2000, pp. 349–369.

437. T. A. Skotheim, *Handbook of Conducting Polymers*, Marcel Dekker, New York, 1986.
438. T. de Lumley-Woodyear, C. N. Campbell, A. Heller, *J. Am. Chem. Soc.* **1996**, *118*, 5504, 5505.
439. T. de Lumley-Woodyear, P. Rocca, J. Lindsay et al., *Anal. Chem.* **1995**, *67*, 1332–1338.
440. Y. Degani, A. Heller, *J. Phys. Chem.* **1987**, *91*, 1285–1289.
441. A. Heller, *Acc. Chem. Res.* **1990**, *23*, 128–134.
442. I. Katakis, A. Heller, in *Frontiers in Bioelectronics I. Fundamental Aspects* (Eds.: F. W. Scheller, F. Schubert, J. Fedrowitz), Birkhauser Verlag, Basel, 1997, pp. 229–241.
443. J. Wang, M. Jiang, B. Mukherjee, *Anal. Chem.* **1999**, *71*, 4095–4099.
444. S. Cosnier, *Biosens. Bioelectron.* **1999**, *14*, 443–456.
445. S. Cosnier, *Electroanalysis* **1997**, *9*, 894–902.
446. F. Palmisano, G. Zambonin, D. Centozze, *Fresenius' J. Anal. Chem.* **2000**, *366*, 586–601.
447. J. Wang, M. Jiang, A. Forbes et al., *Anal. Chim. Acta* **1999**, *402*, 7–12.
448. J. Li, G. Cheng, S. Dong, *Electroanalysis* **1997**, *9*, 834–837.
449. K. Slowinski, R. V. Chamberlain, R. Bilewicz et al., *J. Am. Chem. Soc.* **1996**, *118*, 4709–4710.
450. K. Slowinski, R. V. Chamberlain, C. J. Miller et al., *J. Am. Chem. Soc.* **1997**, *119*, 11 910–11 919.
451. D. Mandler, I. Turyan, *Electroanalysis* **1996**, *8*, 207–213.
452. N. Muskal, I. Turyan, D. Mandler, *J. Electroanal. Chem.* **1996**, *409*, 131–136.
453. N. Muskal, D. Mandler, *Electrochim. Acta* **1999**, *45*, 537–548.
454. T. Lumley-Woodyear, D. J. Caruana, C. N. Campbell et al., *Anal. Chem.* **1999**, *71*, 394–398.
455. (a) D. J. Caruana, A. Heller, *J. Am. Chem. Soc.* **1999**, *121*, 769–774; (b) E. Paleček, R. Kizek, L. Havran et al., *Anal. Chim. Acta* **2002**, in press.
456. T. Lumley-Woodyear, C. N. Campbell, A. Heller, *J. Am. Chem. Soc.* **1996**, *118*, 5504, 5505.
457. H. J. Helbock, K. B. Beckman, M. K. Shigenaga et al., *Proc. Natl. Acad. Sci.* **1998**, *95*, 288–293.
458. E. Paleček, *Biochim. Biophys. Acta* **1967**, *145*, 410–417.
459. J. Puranen, M. Forss, *Strahlentherapie* **1983**, *159*, 505–507.
460. J. M. Sequaris, P. Valenta, H. W. Nurnberg, *Int. J. Radiat. Biol. Related Stud. Phys. Chem. Med.* **1982**, *42*, 407–415.
461. J.-M. Sequaris, P. Valenta, H. W. Nurnberg et al., *Bioelectrochem. Bioenerg.* **1978**, *5*, 483–503.
462. D. Krznaric, B. Cosovic, J. Stuber et al., *Chem.-Biol. Interact.* **1990**, *76*, 111–128.
463. M. Fojta, T. Kubicarova, E. Paleček, *Electroanalysis* **1999**, *11*, 1005–1012.
464. M. Fojta, T. Kubicarova, E. Paleček, *Biosens. Bioelectron.* **2000**, *15*, 107–115.
465. R. Buresova, *Ph.D. Thesis*, Masaryk University, Brno, 1997.
466. V. Brabec, *Electrochim. Acta* **2000**, *45*.
467. J. Wang, M. Chicharro, G. Rivas et al., *Anal. Chem.* **1996**, *68*, 2251–2254.
468. M. Vorlickova, E. Paleček, *Int. J. Radiat. Biol.* **1974**, *26*, 363–372.
469. J. Wang, G. Rivas, M. Ozsos et al., *Anal. Chem.* **1997**, *69*, 1457–1460.
470. M. Rodriguez, T. Kodadek, M. Torres et al., *J. Bioconjugate Chem.* **1990**, *1*, 123–131.
471. E. Paleček, J. Doskocil, *Anal. Biochem.* **1974**, *60*, 518–530.
472. E. Lukasova, M. Vojtiskova, E. Paleček, *Bioelectrochem. Bioenerg.* **1980**, *7*, 671–684.
473. P. Boublikova, M. Vojtiskova, E. Paleček, *Anal. Lett.* **1987**, *20*, 275–291.
474. E. Paleček, Z. Pechan, *Anal. Biochem.* **1971**, *42*, 59–71.
475. M. Vorlickova, E. Paleček, *Biochim. Biophys. Acta* **1973**, *331*, 276–282.
476. X. Cai, G. Rivas, P. A. M. Farias et al., *Anal. Chim. Acta* **1996**, *332*, 49–57.
477. M. J. Friedrich, *Lab. Med.* **1999**, *30*, 181–189.
478. J. Hodgson, *Nat. Biotechnol.* **1998**, *16*, 725–727.
479. R. F. Service, *Science* **1998**, *282*, 396–399.
480. E. K. Wilson, *Chem. Eng. News* **1998**, *76*, 47–49.
481. W. Gopel, P. Heiduschka, *Biosens. Bioelectron.* **1994**, *9*, 3–13.
482. D. T. Burke, M. A. Burns, C. Mastrangelo, *PCR Methods Appl.* **1997**, *7*, 189–197.
483. J. Cheng, E. L. Sheldon, L. Wu et al., *Nat. Biotechnol.* **1998**, *16*, 541–546.
484. E. L. Sheldon, *Clin. Chem.* **1993**, *39*, 718–722.

485. G. Yershov, V. Barsky, E. Belgovskiy et al., *Proc. Natl. Acad. Sci.* **1996**, 93, 4913.
486. U. Maskos, E. M. Southern, *Nucleic Acids Res.* **1992**, 20, 1675–1684.
487. E. Paleček, M. Fojta, *Anal. Chem.* **2001**, 73, 74A–83A.
488. E. Paleček, S. Billova, L. Havran et al., *Talanta* **2002**, in press.
489. E. Paleček, M. Fojta, F. Jelen, *Bioelectrochem.* **2001**, in press.
490. E. Paleček, R. Kizek, L. Havran et al., *Anal. Chim. Acta* **2001**, in press.
491. J. Wang, A.-N. Kawde, A. Erdem et al., *Analyst* **2001**, 126, 2020–2024.
492. J. Wang, A. Xu, A. Erdem et al., *Talanta*, **2002**, in press.
493. R. Kizek, L. Havran, M. Fojta et al., *Bioelectrochem.* **2001**, in press.
494. M. Fojta, L. Havran, R. Kizek et al., *Talanta*, **2002**, in press.
495. J. Wang, R. Polsky, D. Xu, *Langmuir* **2001**, 17, 5739–5741.
496. R. J. Heaton, A. W. Peterson, R. M. Georgiadis, *Proc. Natl. Acad. Sci. USA* **2001**, 98, 3701–3704.
497. Electrochemistry of nucleic acids and development of electrochemical DNA sensors, *Talanta, Special issue* 2002.
498. L. Alfonta, A. K. Singh, I. Willner, *Anal. Chem.* **2001**, 73, 91–102.
499. P. M. Armistead, H. H. Thorp, *Anal. Chem.* **2000**, 72, 3764–3770.
500. P. M. Armistead, H. H. Thorp, *Anal. Chem.* **2001**, 73, 558–564.
501. L. Authier, C. Grossiord, P. Brossier, *Anal. Chem.* **2001**, 73, 4450–4456.
502. F. Azek, C. Grossiord, M. Joannes et al., *Anal. Biochem.* **2000**, 284, 107–113.
503. P. K. Bhattacharya, J. K. Barton, *J. Am. Chem. Soc.* **2001**, 123, 8649–8656.
504. G. Bidan, M. Billon, K. Galasso et al., *Appl. Biochem. Biotechnol.* **2000**, 89, 183–193.
505. E. M. Boon, D. M. Ceres, T. G. Drummond et al., *Nature Biotechnol.* **2000**, 18, 1096–1100.
506. A. Erdem, K. Kerman, B. Meric et al., *Anal. Chim. Acta* **2000**, 422, 139–149.
507. C. H. Fan, G. X. Li, Q. R. Gu et al., *Anal. Lett.* **2000**, 33, 1479–1490.
508. S. Hason, J. Dvorak, F. Jelen et al., *Talanta* **2002**, in press.
509. G. Marrazza, G. Chiti, M. Mascini et al., *Clin. Chem.* **2000**, 46, 31–37.
510. G. Marrazza, S. Tombelli, N. Mascini et al., *Clin. Chim. Acta* **2001**, 307, 241–248.
511. M. Mascini, I. Palchetti, G. Marrazza, *Fres. J. Anal. Chem.* **2001**, 369, 15–22.
512. D. T. Odom, J. K. Barton, *Biochemistry* **2001**, 40, 8727–8737.
513. E. Paleček, *Talanta* **2002**, in press.
514. F. Patolsky, A. Lichtenstein, I. Willner, *Angew. Chem. Int. Ed. Engl.* **2000**, 39, 940–943.
515. M. I. Pividori, A. Merkoci, S. Alegret, *Analyst* **2001**, 126, 1551–1557.
516. E. Souteyrand, C. Chen, J. P. Cloarec et al., *Appl. Biochem. Biotechnol.* **2000**, 89, 195–207.
517. S. Takenaka, K. Yamashita, M. Takagi et al., *Anal. Chem.* **2000**, 72, 1334–1341.
518. S. Takenaka, *Bull. Chem. Soc. Japan* **2001**, 74, 217–224.
519. A. Tani, A. J. Thomson, J. N. Butt, *Analyst* **2001**, 126, 1756–1759.
520. C. Xu, H. Cai, P. G. He et al., *Analyst* **2001**, 126, 62–65.

13 Enzyme Electrodes

*Frieder W. Scheller and Ulla Wollenberger
University of Potsdam, Golm, Germany*

13.1	Coupling of Enzyme-Catalyzed Reactions with Electrochemical Indication	433
13.2	Biochemical Fundamentals	433
13.2.1	Catalytic Action of Enzymes	433
13.2.2	Classification of Enzymes	435
13.2.2.1	Oxidoreductases	435
13.2.2.2	Transferases	435
13.2.2.3	Hydrolases	436
13.2.2.4	Lyases	436
13.2.2.5	Isomerases	436
13.2.2.6	Ligases	436
13.3	Configurations of Enzyme Electrodes	437
13.4	Immobilization of Enzymes on Electrode Surfaces	438
13.4.1	Methods of Immobilization	438
13.4.1.1	Adsorption	438
13.4.1.2	Gel Entrapment	438
13.4.1.3	Covalent Coupling	439
13.4.1.4	Crosslinking	439
13.4.2	Immobilization Effects in Enzyme Electrodes	439
13.5	Types of Enzyme Electrodes	441
13.6	Performance Parameters of Mono-Enzyme Electrodes [13]	446
13.6.1	Concentration Dependence of the Signal (Measuring Range)	446
13.6.2	pH Dependence	447
13.6.3	Temperature Dependence	447

13.7	Coupled Enzyme Reactions in Electrochemical Enzyme Sensors . . .	447
13.7.1	Sequential Enzyme Reactions	448
13.7.2	Enzyme Competition	451
13.7.3	Accumulation of Intermediate	452
13.7.4	Amplification by Analyte Recycling	452
13.7.4.1	Enzymatic Recycling	453
13.7.4.1.1	Linear Recycling	453
13.7.4.1.2	Exponential Recycling	456
13.7.4.2	Bioelectrochemical Recycling	456
13.7.5	Sequential Activation of Enzymes	456
13.8	Application	457
	References	458

13.1 Coupling of Enzyme-Catalyzed Reactions with Electrochemical Indication

Traditionally, *enzymes* are used as analytical reagents to measure substrate molecules by catalyzing the turnover of these species to detectable products. In addition, compounds modifying the rate of the enzyme reaction, such as activators, prosthetic groups, inhibitors and enzymes themselves, are accessible to the measurement [1]. Owing to their excellent chemical specificity, enzymes allow the determination of minute amounts in complex media and thus avoid the need of highly sophisticated instrumentation. Furthermore, when enzymes are employed as labels in binding assays using antibodies, binding proteins, lectins, and so on, the inherent chemical amplification properties of the enzyme's catalytic activity can be exploited to realize extremely sensitive assay methods (Table 1).

Finally, biologically related parameters, for example, taste, odor, fatigue substances, mutagenicity, and nutritivity are quantifiable by using multienzyme systems, intact organelles or cells [2, 3].

Electrochemical sensors are well-established tools in the determination of gases ion activities, and oxidizable and reducible organic substances down to

the submicromolar concentration range. The analysis of many other important substances by electrochemical sensors requires *the coupling with an enzymatic reaction* which involves an electroactive species (Table 2).

13.2 Biochemical Fundamentals

The electrodes determine mainly the output of the electroenzymatic process. In contrast, the analytical selectivity is determined by the specificity of the signal-producing interaction of the enzyme with the analyte. Moreover, the properties of the enzyme, such as its specific activity, influence the dynamic range, and the sensitivity of biosensors. In this respect, account has to be taken of the fact that enzymatic processes are susceptible to deviations from their optimal environmental conditions; in particular, their thermal and chemical stability is limited. These peculiarities decisively determine the limits of applicability of enzymes.

13.2.1 Catalytic Action of Enzymes

A prerequisite for the catalytic function of an enzyme is its native structure, which is

Tab. 1 Analytical potential of enzymes

<ul style="list-style-type: none"> • Efficient substrate conversion: up to 10^5 molecules per sec • Sensitivity for substrates: Millimolar–Nanomolar • Sensitivity for inhibitors: Millimolar–Picomolar • High chemical selectivity • Measurable substances: Substrates Cosubstrates Enzymes activity Prosthetic groups Inhibitors/Activators • Signal generation and amplification in binding assays Immunoassay DNA hybridization
--

Tab. 2 Coupling of enzymes with electrochemical sensors in enzyme electrodes

<i>Biocomponents</i>		
Oxidoreductases Dehydrogenases Oxidases Peroxidases Electron-transferases	Hydrolases: Proteases Esterases Glycosidases	
	Transferases: Kinases Transaminases	
	Indicated species	
	Cosubstrates: NAD(P)H O_2/H_2 Mediators	
	Products: Phenols Redox dyes	Products: H^+ HCO_3^- NH_4^+
Electrode type	Prosthetic groups: Heme PQQ FAD Cu^{2+}	I^- F^-
	Amperometric electrodes	Potentiometric electrodes

Note: PQQ: Pyrroloquinolinequinone tricarboxylic acid.

determined by the number and sequence of amino acids (primary structure) forming the molecule. Favored by hydrogen bonds, parts of the polypeptide chain exist in a α -helical or a β -sheet structure (secondary structure). Most enzymes are globular proteins, the tertiary structure of which may be fixed by disulfide bonds between cysteine residues.

In spite of these stabilizing interactions, the ordered three-dimensional structure is only stable below 50 °C and at medium pH. Exceptions are enzymes from microorganisms that have adapted to extreme environmental conditions, for example, temperatures up to 90 °C.

Within the mostly spherical, ellipsoidal, or kidney-shaped protein molecules a local cavity with a characteristic constitution and stereoconfiguration forms the catalytically active center, where a chemically and spatially congruent substrate ("lock-and-key principle") is converted to a product. To a limited extent, the protein structure is capable of adapting conformationally to the substrate.

Enzymes accelerate the equilibrium formation of chemical reactions by a factor of 10^8 – 10^{20} as compared with uncatalyzed reactions. Thus urea is hydrolyzed at pH 8 and 20 °C in the presence of urease about 10^{14} times faster than without catalysis, and the splitting of H_2O_2 is accelerated by a factor of 3×10^{11} in the presence of catalase [4].

13.2.2

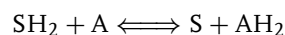
Classification of Enzymes

The roughly 3000 enzymes currently known are grouped into six main classes according to the type of the reaction catalyzed [5]. At present only a limited number are used for analytical purposes.

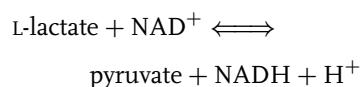
13.2.2.1 Oxidoreductases

(EC 1.X.X.X) catalyze oxidation and reduction reactions by transfer of hydrogen or electrons. The following are of analytical importance:

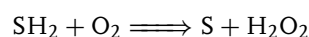
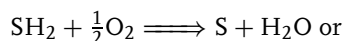
1. *dehydrogenases* catalyze hydride transfer from the substrate, S, to an acceptor, A (which is not molecular oxygen), or vice versa:



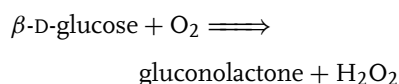
Example: lactate dehydrogenase (EC 1.1.1.27)



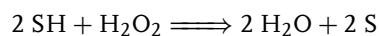
2. *oxidases* catalyze hydrogen transfer from the substrate to molecular oxygen:



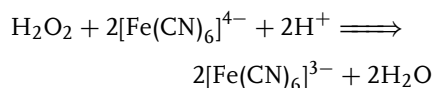
Example: glucose oxidase (EC 1.1.3.4)



3. *peroxidases* catalyze oxidation of a substrate by hydrogen peroxide:



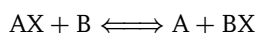
Example: horseradish peroxidase (EC 1.11.1.7)



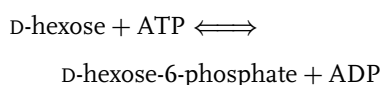
13.2.2.2 Transferases

(EC 2.X.X.X) transfer C-, N-, P-, or S-containing groups (alkyl, acyl, aldehyde,

amino, phosphate, glycosyl) from one substrate to another. Transaminases, transketolases, transaldolases and transmethy-lases belong to this class:



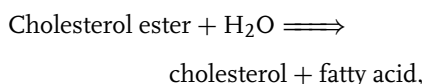
Example: hexokinase (EC 2.7.1.1)



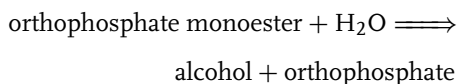
13.2.2.3 Hydrolases

(EC 3.X.X.X) catalyze cleavages or the reverse fragment condensation. According to the type of bond cleaved, a distinction is made between peptidases, esterases, glycosidases, phosphatases, and so on.

Examples: cholesterol esterase (EC 3.1.1.13)



alkaline phosphatase (EC 3.1.3.1)



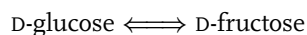
13.2.2.4 Lyases

(EC 4.X.X.X) nonhydrolytically remove groups from their substrates under formation of double bonds, or add groups to double bonds. Only a few enzymes of this class are used in analysis.

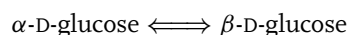
13.2.2.5 Isomerases

(EC 5.X.X.X) catalyze intramolecular rearrangements and are subdivided into racemases, epimerases, mutases, cis-trans-isomerases, and so on.

Examples: glucose isomerase (EC 5.3.1.5)



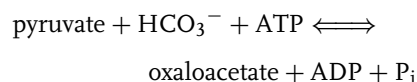
Mutarotase (aldose-1-epimerase) (EC 5.1.3.3)



13.2.2.6 Ligases

(EC 6.X.X.X) split C–C, C–O, C–N, C–S, and C-halogen bonds without hydrolysis or oxidation, mostly with the concomitant consumption of high-energy compounds like adenosine triphosphate (ATP) and other nucleoside triphosphates.

Example: pyruvate carboxylase (EC 6.4.1.1)



Several components are required for the catalytic process, which are either directly involved in catalysis or influence the formation of the enzyme-substrate complex. They are designated *coenzymes*, *prosthetic groups*, and *effectors*.

Coenzymes receive redox equivalents, protons, or chemical groups from the substrate during the enzymatic reaction. Since coenzymes readily dissociate from the enzyme they can act as group mediators between different enzyme molecules (e.g. coenzyme A). In case the factor is not reconverted to its original state by the same enzyme, it is called cosubstrate. An example would be cleavage of the energy-rich ATP to adenosine diphosphate (ADP) and phosphate during energy-consuming substrate conversion and the regeneration of the ATP by adenylate kinase. Many vitamin derivatives, such as coenzyme A, pyridoxal-phosphate, thiamine pyrophosphate, and cobalamine (Vitamin B₁₂) are coenzymes

of enzymatic reactions. Oxidative coenzymes with a defined redox potential serve as hydrogen or electron carriers during oxidoreduction reactions.

Prosthetic groups have the same function as coenzymes but are tightly bound to the enzyme. When they are split off, the protein is mostly denatured. Flavin nucleotides and heme are the most important prosthetic groups.

Effectors accelerate (activators) or block (inhibitors) the catalytic process. Many of them are metal ions, for example, Mg^{++} , Ca^{++} , Zn^{++} , K^+ , and Na^+ , which either form stoichiometric complexes with the substrate, stabilize an optimal protein conformation, or effect the association of subunits. These inorganic complements of enzyme reactions are frequently subsumed together with coenzymes as cofactors.

13.3 Configurations of Enzyme Electrodes

An enzyme electrode (Fig. 1) is a dense package of dialyzer, enzyme reactor, and detector. A typical example would be a

glucose or lactate electrode comprising the appropriate oxidase entrapped in or bound to a membrane that is fixed at an oxygen or hydrogen peroxide detecting electrode and covered by a semipermeable membrane [6].

The *membrane* directed towards the (usually ideally mixed or flowing) measuring solution fulfils a number of functions. Firstly, it provides the sensor with a certain degree of selectivity. The pore size and, perhaps, charge permits the exclusion of deleterious or interfering molecules, such as proteins or electroactive compounds and may provide useful partitioning of other compounds. Furthermore, the thickness and pore size permit us to affect the measuring range of the sensor by controlling the actual rate of reagents reaching the reaction layer.

After permeation of analyte, cosubstrates, and effectors through the membrane to the underlying *enzyme layer* the analyte is converted therein under formation or consumption of a detectable species. In the illustrated case this is the formation of reduced mediator or cosubstrate (e.g. hydrogen peroxide from oxygen) that is oxidized at the electrode

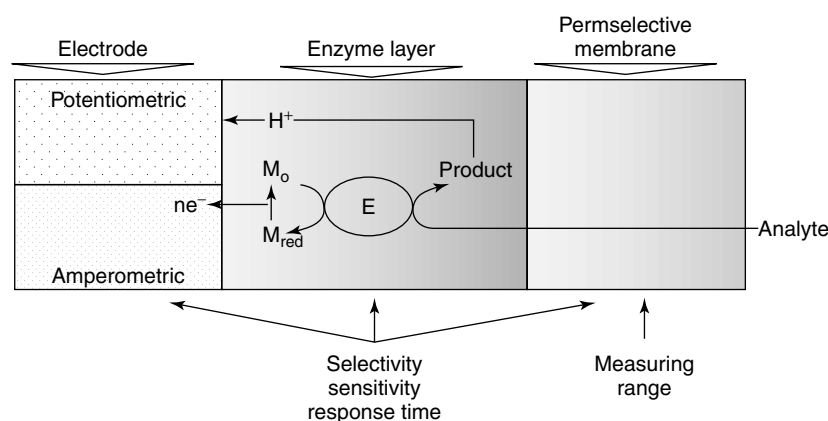


Fig. 1 Scheme of an enzyme electrode.

or the generation of protons. The enzyme membrane is characterized by an *enzyme loading* reflecting the interplay of enzyme kinetics and mass transport. The loading is crucial for the response characteristics and the stability of the sensor whereas the choice of enzyme determines the chemical selectivity of the measurement.

The choice of the *indicator electrode* is largely determined by the species involved in the sensing reaction. Oxygen and H_2O_2 , which are the cosubstrate and product of oxidases, as well as NAD(P)H, the cosubstrates of about 300 pyridine nucleotide-dependent dehydrogenases, can be determined amperometrically. Hydrolases are mostly coupled to ion selective electrodes. Based on these principles, many enzyme sensors have been developed and commercialized [2, 3].

13.4 Immobilization of Enzymes on Electrode Surfaces

13.4.1 Methods of Immobilization

For the repeated use of enzymes in analytical devices, numerous techniques for fixing them to carrier materials including membranes and electrode surfaces have been developed [3]. Immobilization brings about a number of further advantages for their application in analytical chemistry.

- In many cases the enzyme is stabilized;
- The immobilized enzyme may be easily separated from the sample;
- The stable and largely constant enzyme activity renders the enzyme an integral part of the analytical instrument.

The techniques for immobilizing enzymes comprise physical and chemical methods as well as combinations of both [7]. The main physical methods are adsorption to water-insoluble carriers or surfaces and entrapment in water-insoluble polymeric gels. Chemical immobilization is effected by covalent coupling to derivatized carriers or by intermolecular crosslinking of the biomolecules. The suitability of a method for a particular task is at present still being empirically elucidated. However, some generally valid aspects will be outlined below.

13.4.1.1 Adsorption

Adsorption of biomolecules at the electrode surface is the simplest method of immobilization. An aqueous solution of the biomolecules is contacted with the active surface for defined period. Thereafter the molecules that are not adsorbed are removed by washing.

Since the adsorption of a protein to a functionalized surface is a reversible process, changes of pH, ionic strength, substrate concentration, temperature, and so on may detach the biomolecule. In addition to the simplicity of the procedure, the advantage of adsorptive immobilization is that it does not need nonphysiological coupling conditions or chemicals potentially impairing enzyme or cell functions.

13.4.1.2 Gel Entrapment

Entrapment in polymeric gels prevents the biomolecules from diffusing from the reaction mixture. On the other hand, small substrate and effector molecules can easily permeate. Gel entrapment is a milder procedure than adsorption, that is, the biomolecules are not covalently bound to the matrix, membrane or to each other. The method is therefore

widely employed. The most important matrices used are hydrogels such as alginate, carageenan, collagen, cellulose triacetate, polyacrylamide, gelatin, agar, silicone rubber, and poly(vinyl alcohol).

13.4.1.3 Covalent Coupling

Covalently coupled enzymes are either reacted with the activated (e.g. functionalized) surface or copolymerized with a reactive monomer. The reaction should involve only groups that are not essential for the biological activity of the biomolecule. Chemically reactive sites of a protein may be amino groups, carboxyl groups, phenol residues of tyrosine, sulfhydryl groups or the imidazole group of histidine. The immobilization is conducted in three steps: activation of the carrier, coupling of the biomolecule, and removal of adsorbed but not covalently attached biomolecules. A disadvantage of covalent coupling is the frequently occurring loss of activity [8].

13.4.1.4 Crosslinking

Enzymes may be intermolecularly crosslinked by bi- or multifunctional reagents. The protein molecules may be crosslinked with each other or with another, functionally inert protein (e.g. albumin or gelatin). The biomacromolecules can also be adsorbed to a carrier or entrapped in a gel and then crosslinked. Among others, glutaraldehyde, biisocyanate derivatives, and bisdiazobenzidine are being used as bifunctional reagents [8].

The advantages of crosslinking are the simple procedure and the strong chemical binding of the biomolecules. Furthermore, the choice of the degree of crosslinking permits the physical properties to be influenced. The main drawback is the possibility of activity losses due to chemical

alterations of the catalytically essential sites of the protein.

13.4.2

Immobilization Effects in Enzyme Electrodes

Both for economic reasons and in order to achieve a high sensitivity and functional stability, immobilization methods having a high activity yield are desirable for biosensors [2, 8].

Whilst in homogenous solution the initial rate of substrate conversion rises linearly with enzyme concentration. With immobilized enzymes, the measured reaction rate depends also on substrate mass transfer.

In enzyme electrodes the biocatalyst and the signal transducer are spatially combined, that is, the enzyme reaction proceeds in a layer separated from the measuring solution. The substrates reach the membrane system of the biosensor by convective diffusion from the solution. The rate of this external transport process depends essentially on the degree of mixing. In the multilayer system in front of the sensor the substrates and products are transferred by diffusion. Slow mass transfer to and within the enzyme matrix leads to different concentrations of the reaction partners in the measuring solution and in the matrix. Diffusion and the enzyme reaction do not proceed independently of one another; they are coupled in a complex manner.

Usually in the operation of biosensors the flow conditions are adjusted to provide a mass transfer rate from the solution to the membrane system which is fast as compared with the internal mass transfer (exception: implanted sensors). On the other hand, variations of the diffusion resistance of the semipermeable

membrane are being used to optimize the sensor performance. A semipermeable membrane with a molecular weight cutoff of 10,000 and a thickness of 10 μm only slightly influences the response time and sensitivity. In contrast, thicker membranes increase the measuring time, but may also lead to an extension of the linear measuring range.

The ratio of the rate of the enzymatic reaction to that of diffusion indicates whether the process in an enzyme layer is determined by enzyme kinetics or by substrate diffusion. At low enzyme activity, the process is kinetically controlled. In this case the substrate concentration does not become zero in any part of the enzyme layer, that is, the enzyme sensor signal is mainly a function of the "active" enzyme concentration. Therefore, effectors (activators, inhibiting factors, including H^+ , and OH^-) and, the amount of enzyme in front of the transducer, as well as the time-dependent enzyme inactivation, may all directly effect the measuring signal.

At high enzyme loadings internal diffusion control is reached. Any substrate molecule diffusing into the enzyme layer is immediately converted therein; only part of the enzyme is acting catalytically. Diffusion controlled sensors exhibit the following characteristics as long as an enzyme reserve is present:

- the sensitivity remains constant;
- the sensitivity does not depend on inhibitors and pH variation;
- the temperature is of minor influence since the activation energy of diffusion ($\sim 2.5\%/\text{ }^\circ\text{C}$) is lower than that of the enzyme reaction ($10\%/\text{ }^\circ\text{C}$).

At high substrate concentration the enzyme reaction rate attains a limiting

value. Therefore the enzyme sensor signal reaches a concentration-independent value corresponding to the product concentration at the transducer surface.

From the analysis of the coupling of enzyme reaction and mass transfer, the following conclusions may be drawn for the design of biosensors. The substrate concentration at which deviations from the analytically usable linear measuring range occur depends on the extent of diffusion limitation. Under kinetic control, a linear dependence may only be expected for very low substrate concentrations. Under diffusion control, the decrease of substrate concentration in the enzyme layer caused by slow substrate diffusion results in an extended linear range. It has to be considered, however, that for two-substrate reactions deviations from linearity may also be produced by cosubstrate limitation.

At low substrate concentration, the sensitivity of kinetically controlled sensors increases linearly with the enzyme loading. When the amount of enzyme becomes sufficiently high as to provide complete substrate conversion the system passes over to diffusion control. Under these conditions, a decrease of the diffusion resistance by decreasing the layer thickness results in an increased sensitivity. Nevertheless, a membrane-covered enzyme electrode is only 10 to 50% as sensitive as a bare electrode for an analogous electrode-active substance.

The variation of the enzyme loading is a means of determining the minimum amount of enzyme required for maximum sensitivity. Furthermore, this test reveals the magnitude of the enzyme reserve of diffusion-controlled sensors.

Owing to the excess of enzyme in the membrane, a diffusion limited enzyme sensor has a higher functional stability than a kinetically controlled one. With

the former, 2000 to 10 000 measurements per enzyme membrane can be performed, while kinetically controlled sensors typically permit only 200 to 500 measurements.

The response time is determined by the mass transfer. Using fast-responding transducers in stationary measurements, a stable signal is obtained within one second up to a few minutes.

In summary, it may be concluded that optimal sensitivity and response time can be achieved by applying high enzyme activity in thin membranes [2].

13.5

Types of Enzyme Electrodes

The oxygen electrode according to Clark and its version modified for H_2O_2 detection are the most widely used transducers in biosensors [3]. The electrode potential is crucial for the selectivity of the sensor. Any electroactive substance being converted at lower potential contributes to the total current. Thus at an electrode potential of +600 mV for H_2O_2 measurement, ascorbic acid, uric acid, or paracetamol (acetaminophen) are oxidized as well.

A way to reduce interferences by cooxidizable sample constituents is by keeping the applied electrode potential as low as possible. Therefore, a reaction partner is chosen to be electrochemically indicated that is converted at low potential. For this purpose, the natural electron acceptors of many oxidoreductases have been replaced by redox-active dyes or other reversible *electron mediators*. Among them are the ferricyanide/ferrocyanide couple, *N*-methylphenazinium sulfate, ferrocenes, and benzoquinone. With these mediators an electrode potential around +200 mV can be applied, which decreases

electrochemical interferences and permits us to apply such enzymes coupled with electrodes in oxygen-free solution. In analogy to the natural cosubstrate the mediator is often added to the sample solution [3, 9]. However, homogeneous reaction of the mediators with endogenous electron acceptors such as ascorbate must be avoided.

The integration of redox enzymes at electrode surfaces together with such mediator compounds to act like electron transfer systems in biomembranes, enables a reagentless measuring regime. The covalent binding or adsorption of mediator and enzyme to the electrode or their integration into the electrode body itself, as in case of carbon paste electrodes, have been shown to be successful concepts that lead to functioning glucose sensors [9–11].

Adsorption of redox polymers at carbon electrodes result in the catalysis of the electron transfer by wiring the enzyme molecules to the electrode. In this manner sensors for glucose, hydrogen peroxide, and NAD(P)H were developed by wiring enzyme to glassy carbon electrodes, with an osmium complex. It was shown that such a network is capable of connecting FADH_2/FAD centers of glucose oxidase and pyrroloquinoline quinone centers of glucose dehydrogenase to the electrode [10, 11].

The rate of enzymatic reactions can also be established by potentiometric measurement of product formation using an ion selective electrode. The most important ion selective electrode is the glass electrode for pH measurement. Despite their outstanding selectivity for H^+ ions, glass electrodes are used only seldom in enzyme electrodes because their sensitivity is affected by the buffer capacity of the sample matrix or sensor filler solution.

Tab. 3 Mono-enzyme electrodes for some relevant analytes

Analyte	Enzyme	Indicated species				
		O ₂	H ₂ O ₂	Mediator	Prosthe- tic group	H ⁺ NAD(P)H Others
Acetylcholine, Carbamates, Organophosphates Alcohols	Acetylcholine esterase EC 3.1.1.7	X	X	X		X
	Alcohol oxidase EC 1.1.3.13	X	X	X		
	Alcohol dehydrogenase EC 1.1.3.13					X
	(NAD(P) ⁺ -dept.)					
D-Amino acids	D-Amino acid oxidase EC 1.4.3.3	X	X	X		
L-Amino acids	L-Amino acid oxidase EC 1.4.3.2	X	X	X		NH ₄ ⁺ I ⁻
Ascorbic acid	Ascorbate oxidase EC 1.10.3.3	X				
L-Asparagine	Asparaginase EC 3.5.1.1					X
Amygdalin	β -Glucosidase EC 3.2.1.21					CN ⁻
Bile acid	β -Hydroxysteroid dehydrogenase EC 1.1.1.51					X
Cholesterol	Cholesterol oxidase EC 1.1.3.6	X	X			

Tab. 3 (continued)

Analyte	Enzyme	Indicated species						
		O ₂	H ₂ O ₂	Mediator	Prosthe- tic group	H ⁺	NAD(P)H	Others
Hydrogen peroxide	Peroxidase EC 1.11.1.7			X	X			
	Catalase EC 1.11.1.6	X						
Isocitrate	Isocitrate dehydrogenase EC 1.1.1.42						X	
	Lactate oxidase EC 1.1.3.2	X	X	X				
Lactic acid	Cytochrome b ₂ EC 1.1.2.3			X	X			
	Lactate dehydrogenase EC 1.1.1.27						X	
Malate	(NAD ⁺ -dept.) Lactate monooxygenase EC 1.13.12.4	X						CO ₂
	Malate dehydrogenase EC 1.1.1.37						X	
	Nitrite reductase (NAD(P)H) EC 1.6.6.4						X	NH ₃
	Oxalate oxidase EC 1.2.3.4	X						
Penicillin	β -Lactamase penicillase EC 3.5.2.6					X		
	Penicillin amidase EC 3.5.1.11					X		

The selectivity of the glass electrode for NH_3 and CO_2 may be improved over that of pH measurement by inclusion of a gas permeable membrane between the enzyme layer and the pH electrode. At constant solution, pH a defined relation exists between the potential of the glass electrode and the concentration of the gas-forming ions HCO_3^- or NH_4^+ which are formed in the enzyme reaction. Maximum sensitivity of the electrode is reached when the H^+ concentration in the solution is sufficient to ensure maximum conversion of the weak electrolyte into its undissociated form, that is CO_2 or NH_3 . With NH_3 this occurs at $\text{pH} > 10$ and with CO_2 at $\text{pH} > 5$. Generally, these pH values differ substantially from the pH optima of deaminase and decarboxylase enzymes; therefore, for the respective enzyme electrodes a compromise pH has to be found. To obtain optimal conditions for both steps, the enzyme reaction is often separated from the potentiometric indication and a pH change is included between these stages. This setup is termed a *reactor electrode*.

The semipermeable membrane may be replaced by an air gap between the measuring solution and the pH electrode. This increases the measuring rate but affects the electrolyte layer and thus the reproducibility of the measurement.

Other pH-sensing transducers used in biosensors are metal oxide electrodes. Beside the common antimony oxide electrode, palladium oxide and iridium oxide probes have been coupled with immobilized enzymes. These sensors may be miniaturized by using chemical vapor deposition technology. Moreover, they are mechanically more stable than glass electrodes. Unfortunately response of metal

oxide electrodes is affected by redox active substances [3].

Furthermore, the gate area of pH-sensitive ISFET's (ion-sensitive field-effect transistor) has been covered with pH changing enzymes, such as urease and β -lactamase [12]. Furthermore, ATPase, glucose oxidase, and trypsin were used for ATP, glucose, and peptide ENFET's (enzyme-field-effect transistor).

Representative examples of monoenzyme electrodes are presented in Table 3.

13.6

Performance Parameters of Mono-Enzyme Electrodes [13]

13.6.1

Concentration Dependence of the Signal (Measuring Range)

The linear measuring range of enzyme electrodes extends over 2 to 5 decades of concentration. The lower detection limit of simple amperometric enzyme electrodes is about 100 nmol l^{-1} whereas potentiometric sensors may be only applied down to $100 \mu\text{mol l}^{-1}$. This shows that the detection limit is affected not only by the enzyme reaction but also by the transducer.

The measuring signal of the amperometric glucose electrode increases with increasing substrate concentration and reaches a concentration-independent saturation corresponding to the maximum rate. The substrate concentration giving rise to the half-maximum current in air saturated solution is between 0.5 and 1.0 mmol l^{-1} glucose.

The linear range extends to 2 mmol l^{-1} glucose in the measuring cell. At low glucose concentration the cosubstrate

concentration (ca. $200\ \mu\text{mol l}^{-1}$ at air saturation) influences the response only slightly.

13.6.2

pH Dependence

With a high enzyme excess in the membrane, pH variations should have only a minor influence on the measuring process. Therefore the pH profile under diffusion control should be substantially less sharp than those of the respective enzyme in solution. The results obtained with GOD-membranes agree with this assumption.

13.6.3

Temperature Dependence

The rate of enzyme reactions rises with temperature up to a certain optimum. Above that, the effect of the thermal inactivation dominates over that of the increase of the collision frequency.

For immobilized enzymes, frequently an increase of the temperature optimum for substrate conversion is observed. Because enzyme kinetics and diffusion are superimposed, the higher activation energy results in a predominant acceleration of the enzyme reaction with rising temperature.

13.7

Coupled Enzyme Reactions in Electrochemical Enzyme Sensors

The number of substances that can be measured by monoenzymatic approaches in electrochemical biosensors is limited, because in the majority of biocatalytic reactions electrochemically active compounds are not involved. To form readily detectable species, different enzymatic reactions have to be coupled, as is already routine in wet biochemical analysis [13]. This coupling can be accomplished in ways analogous to those present in a living cell. Here, nature provides us a variety of ways of regulating metabolic pathways. Thus, like in nature, catalytic activities of different enzymes can be combined in biosensors either in sequence, competing pathways, or in cycles (Table 4).

In general, enzymes to be used in multienzyme sensors should fulfill the following requirements:

- Their pH optima should be reasonably close to each other.
- They should not be inhibited by cofactors, effectors, or intermediates required for sensing.
- Their cofactors or effectors should not react with each other.

Tab. 4 Coupling principles for design of sensor performance

<i>Principle of coupling</i>	<i>Special cases</i>	<i>Effect on performance</i>
Sequence	— Accumulation Cascade	New analyte specificity Sensitivity specificity New analyte sensitivity
Parallel reaction	Competition elimination, antiinterference	New analyte specificity mutiparameter
Cycle	Multiple cycles nonlinear cycle	Sensitivity

The most effective sensors work in diffusion control with respect to a single reaction.

In conjunction with appropriate measuring regimes not only does a much wider range of analyte species becomes in this way accessible to measurement by the bioelectroanalytical approach also the selectivity and sensitivity of the biosensor may be enhanced through the appropriate choice of the coupling strategy [2, 14].

13.7.1

Sequential Enzyme Reactions

An enzyme sequence electrode is a biosensor, where at least two enzymes metabolize a substrate in consecutive reactions with the formation of a measurable secondary product or consumption of cosubstrate. Obviously, the number of enzymes (E_1 – E_n) in such a reaction chain can be increased as long as recognition of the primary substrate S ends up in a detectable metabolite P^* (Fig. 2). The same is true if a detectable cosubstrate is consumed in the final reaction. On this basis, families of electrodes have been developed, which combine, for example, glucose-, lactate-, and glutamate-generating primary enzyme reactions with the respective oxidases, that is, glucose oxidase, lactate oxidase, and glutamate oxidase (see Sect. 13.5.). The measurement of oxygen consumption of the NAD(P)H oxidation by salicylate hydroxylase (E.C. 1.14.13.1) opened the way to the large group of

dehydrogenase substrates [14]. Enzyme sequence electrodes given in Table 5 show that indicator reaction based on oxidases and dehydrogenases (see Table 3) are coupled with enzymes such as hydrolase, lyases, and transferases. Sensors for oxidase substrates have also been studied using coimmobilized peroxidase for hydrogen peroxide transformation [16]. These electrodes work at lower electrode potential than is necessary for peroxide oxidation and are therefore less affected by electrochemically interfering substances. In principle, all peroxide forming oxidases (E.C. 1.x.3.x) can be combined with peroxide detectors based on peroxidases. Soluble mediators, “electrically wired” enzymes, and mediator-modified electrodes are used. In addition, also the apparent direct electron transfer between electrode and peroxidase that occurs at a favorable low electrode potential is exploited for the indication [14]. Thus, the influence of interfering electrochemical reactions is minimized.

In general, the sensor performance is comparable to those of monoenzyme electrodes. In ideal cases, diffusion limitation is achieved by immobilizing a sufficiently high amount of enzyme [17].

The enzyme sequence sensor approach will be illustrated for the determination of citrate. Here three enzymes are immobilized on an oxygen sensor and the linear reaction sequence is employed:

Citrate lyase:

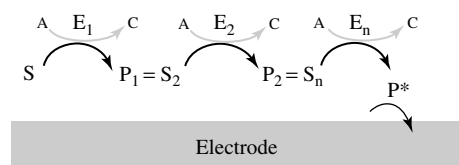


Fig. 2 Scheme of a sequential enzyme sensor. A and C represent coreactants. Up to n enzymes can be used. P^* is electrochemically indicated.

Tab. 5 Enzyme sequence electrodes with oxidase indicator enzyme

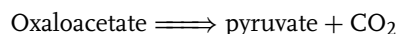
Analyte	Enzyme sequence		Indicator enzyme	
	Auxiliary enzymes	EC number	Enzyme	EC number
Saccharose	Invertase + mutarotase	3.2.1.26 5.1.3.3	Glucose oxidase	1.1.3.4
Lactose	β -galactosidase	3.2.1.23	Glucose oxidase	1.1.3.4
Maltose	Glucoamylase or maltase	3.2.1.3 3.2.1.20	Glucose oxidase	1.1.3.4
Glucosinolate Starch	+ mutarotase	5.1.3.3		
	Myrosinase	3.2.3.1	Glucose oxidase	1.1.3.4
	Alpha-amylase	3.2.1.1	Glucose oxidase	1.1.3.4
Fructose	Glucoamylase	3.2.1.3		
	Glucose isomerase + mutarotase	5.3.1.18 5.1.3.3	Glucose oxidase	1.1.3.4
Glucose	Glucose oxidase	1.1.3.4	Peroxidase	1.11.1.7
	Glucose dehydrogenase + lactate dehydrogenase	1.1.1.47 1.1.1.27	Lactate monooxygenase	1.13.12.4
Pyruvate ADP	Lactate dehydrogenase	1.1.1.27	Lactate monooxygenase	1.13.12.4
	Pyruvate kinase + lactate dehydrogenase	2.7.1.40 1.1.1.27	Lactate monooxygenase	1.13.12.4
Glucose-6-phosphate	Glucose-6-phosphate dehydrogenase + lactate dehydrogenase	1.1.1.49 1.1.1.27	Lactate monooxygenase	1.13.12.4
ATP	Alkaline phosphatase	3.1.3.1	Glucose oxidase	1.1.3.4
	Hexokinase	2.7.1.1	Glucose-6-phosphate dehydrogenase	1.1.1.49
Malate	Malate dehydrogenase, decarboxylating	1.1.1.40	Pyruvate oxidase	1.2.3.3
	Malate dehydrogenase + oxalacetate decarboxylase	1.1.1.37 4.1.1.3	Pyruvate oxidase	1.2.3.3
	Malate dehydrogenase	1.1.1.40	Salicylate hydroxylase	1.14.13.1

(continued overleaf)

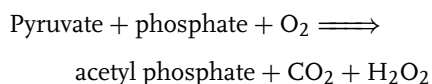
Tab. 5 (continued)

Analyte	Enzyme sequence		Indicator enzyme	
	Auxiliary enzymes	EC number	Enzyme	EC number
Oxalacetate Citrate	oxalacetate decarboxylase	4.1.1.3	Pyruvate oxidase	1.2.3.3
	Citrate lyase	4.1.3.6	Pyruvate oxidase	1.2.3.3
Glycerol	+ oxalacetate decarboxylase	4.1.1.3		
	Glycerol dehydrogenase	1.1.1.6	Diaphorase	1.6.4.3
		1.1.1.72		
Inosine	Nucleoside phosphorylase	2.4.2.1	Xanthine oxidase	1.2.3.2
Acetylcholine	Acetylcholine esterase	3.1.1.7	Choline oxidase	1.1.3.17
Creatine	Creatineamidohydrolase	3.5.3.3	Sarcosine oxidase	1.5.3.1
Creatinine	Creatinine amidohydrolase	3.5.2.10	Sarcosine oxidase	1.5.3.1
	+ creatine	3.5.3.3		
	amidino-hydrolase			
Glutamine	Creatinine amidohydrolase	3.5.2.10	Glutamate dehydrogenase	1.4.1.1/2/3
Ethanol	Glutaminase	3.5.1.2	Glutamate oxidase	1.4.3.11
Cholesterol	Alcohol dehydrogenase	1.1.1.1	hydrogenase	1.12.1.2
Phenylphosphate	Cholesterol esterhydrolase	3.1.1.13	Cholesterol oxidase	1.1.3.6
	Alkaline phosphatase	3.1.3.1	tyrosinase	1.14.18.1
	Nucleoside phosphorylase	2.4.2.1	Xanthine oxidase	1.2.3.2
	Glycogen phosphorylase b	2.4.1.1	Glucose oxidase	1.1.3.4
	+ alkaline phosphatase	3.1.3.1		
	+ mutarotase	5.1.3.3		
AMP	Glycogen phosphorylase a	2.4.1.1	Glucose oxidase	1.1.3.4
	+ alkaline phosphatase	3.1.3.1		
	+ mutarotase	5.1.3.3		

Oxaloacetate decarboxylase:



Pyruvate oxidase:



Citrate conversion by citrate lyase does not yield in a directly detectable species. Therefore the enzymatic decarboxylation of its product oxaloacetate is appended. The product of that secondary reaction is easily measurable by pyruvate oxidase. Hence, the concentration of citrate is related to oxygen consumption (or hydrogen peroxide formation) in the pyruvate oxidase indicator reaction (see Table 3). In addition, carbondioxide formation may be measured potentiometrically.

The main hindrance to practical application of those multienzyme sensors is that they respond to all substrates of the sequence.

However, this may be advantageous if not only the initial substrate is to be measured.

13.7.2

Enzyme Competition

Another coupling principle uses the competitive action of two enzymes on the same substrate, where one of these enzymes produces the electrochemical signal. An example is the ATP-sensor with hexokinase and glucose oxidase coimmobilized

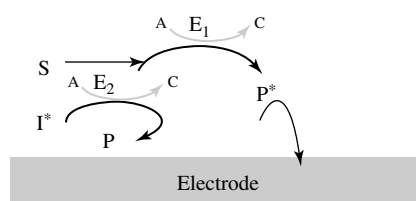
on an oxygen electrode [2]. For in situ and in vivo application, analyte measurements must proceed at concentrations that exceed the measuring range of the sensor. Also here competitive reactions that decrease the amount of analyte are used.

Introduction of an additional (competing) enzyme into the biocatalytic layer capable of filtering chemical signals by eliminating constituents of the sample interfering with either the enzymatic or the electrochemical reaction leads to improved selectivity. In this case a (interfering) substance is completely converted to noninterfering products in the diffusion-controlled enzyme membrane. This is in particular important for the development of sensors well suited for measurement of real samples.

Figure 3 illustrates the basic set-up. Enzyme E_2 is immobilized in the layer to prevent the interfering compound I from reaching the detector surface or the indicator enzyme E_1 that is responsible for analyte conversion. For example, ascorbic acid and acetaminophen, which interfere with the anodic hydrogen peroxide oxidation, can be transformed into inert products by reaction with an eliminator enzyme, for example, ascorbate oxidase [18], laccase [19] or tyrosinase [20] or peroxidase [21].

For the effective elimination of glucose, glucose oxidase, and catalase, but also hexokinase can be used. Other antiinterference systems have been devised to eliminate lactate (with lactate monooxygenase

Fig. 3 Schematic illustration of enzymatic elimination of interfering constituents in biosensors. A and C are coreactants to the indicator enzyme E_1 and the eliminator enzyme E_2 . I^* represents the interfering compound.



in pyruvate measurements), ascorbic acid (with ascorbate oxidase for catecholamine detection at a graphite electrode) [22], ammonia [23] or glutamate (with glutamate dehydrogenase) [24].

13.7.3

Accumulation of Intermediate

The sensitivity of electroanalytical measurements can be enhanced by accumulation of the electrochemically active analyte at the electrode before measurement (stripping analysis) [25]. This principle adapted to enzyme membrane electrodes relies on sequentially acting enzymes with the aim of developing sensitive and selective sensors.

The sensors combine preconcentration of an intermediary product with a biocatalytic indicator system. Oxygen probes as well as chemically modified electrodes are the base sensors. The principle of the measurement is illustrated in Fig. 4. In the first step of the measurement the reaction of the analyte S_1 and a saturating concentration of appropriate cosubstrate A proceeds for a certain time during which an intermediate product I is formed by the generator enzyme E_1 . The intermediate is accumulated in the enzyme membrane, due to its slow diffusion. When this reaction approaches equilibrium, the second step, the actual measurement, is triggered by injection of an excess of substrate (S_2) of the indicator enzyme (E_2), which converts the accumulated intermediate under

formation of an electroactive product P^* . This method yields amplification of the analytical signal between twofold and 60-fold. For example, for the determination of glycerol, glycerol dehydrogenase is used for oxidation of the analyte with formation of NADH [26]. The indicator sequence lactate dehydrogenase/lactate monooxygenase senses NADH with resulting oxygen consumption. Pyruvate acts as initiator substance and reacts with the preconcentrated NADH.

A limit of accumulation is set by the equilibrium of the reaction. Differences in the amplification factors are mainly attributed to the equilibrium constants of the generator enzyme and the diffusion behavior of intermediate and initiator substrate. The largest enhancement due to accumulation is obtained when the intermediate is a large molecule and the initiator a small molecule.

13.7.4

Amplification by Analyte Recycling

Electroanalytical techniques are fairly sensitive and currents as low as 10^{-10} A can be recorded with commercial devices.

The introduction of a layer incorporating the enzyme over the surface of the electrode decreases the sensitivity of the electrode by one to two orders of magnitude, due to the additional diffusion resistance. Therefore, for the measurement of analyte concentrations in the

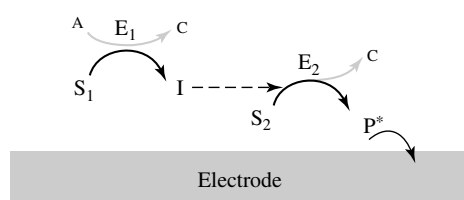


Fig. 4 Scheme of an intermediate accumulating biosensor. A and C represent coreactants; I is the accumulated intermediate, that is stripped after the substrate S_2 is added to initiate enzyme reaction E_2 .

nanomolar range an increase of sensitivity of the enzyme electrode is required. One way to solve this problem is the continuous regeneration of the analyte in cyclic reactions.

The combination of the electrochemical detection principle and the recycling of the analyte can be performed as is illustrated in Fig. 5, the bienzymatic system possessing the potential of the highest amplification rate [14].

13.7.4.1 Enzymatic Recycling

In the bienzymatic approach, the sensitivity enhancement is provided by shuttling the analyte between enzymes acting in cyclic series of reactions accompanied by cosubstrate consumption and accumulation of by-products (Fig. 5a).

The target analyte S can be substrate or coenzyme of the respective enzyme. Assuming a sufficiently high activity of enzyme E_1 in the presence of its cosubstrate C_1 and an analyte at a concentration far below its Michaelis constant, amplification is achieved by turning-on the second enzyme (E_2) through addition of its cosubstrate, C_2 .

By measuring the concentration change of one of these coreactants directly or in an additional analytical step, the recycling system is used as a biochemical amplifier for the analyte ($S = S_1$ or S_2).

13.7.4.1.1 Linear Recycling When one molecule of product is formed per substrate molecule, the total concentration of intermediate substrates ($S_1 + S_2$) remains constant and the concentrations of the coreactants increase or decrease linearly with time. Then the number of cycles in which the substrate is turned over in a given time is a function of the substrate concentration. For this case the amplification factor, G , is under steady state conditions:

$$G = \frac{k_1 k_2 L^2}{2D(k_1 + k_2)}$$

where k_i is the first order rate constant, L the membrane thickness, and D the diffusion coefficient. At high activities of both enzymes immobilized into the enzyme layer with high characteristic diffusion time (L^2/D), the possible amplification is very large.

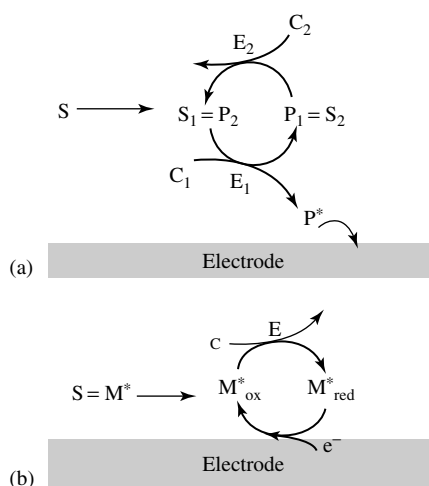


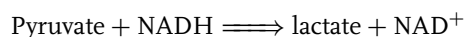
Fig. 5 Illustration of analyte recycling schemes: (a) bienzymatic analyte recycling. C represents cosubstrate of the enzymatic reactions; (b) bioelectrocatalytic analyte regeneration.

This concept of linear enzymatic signal amplification has been realized by coupling dehydrogenases with oxidases or transaminases, or by coupling kinases with each other (Table 6). When oxidases are coupled with their respective dehydrogenases, electrode detectable species are included in the reaction system. Therefore, the change of coreactant concentration can be measured directly at the electrode onto which the recycling enzyme pair is immobilized. In most cases, oxygen consumption has been followed. Production of protons, peroxide, and ammonia have also been monitored.

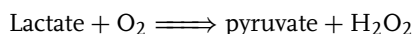
Depending on the enzymes and membrane materials used, amplification by several orders of magnitude has been realized. Detection limits down to 70 pmol l^{-1} have been achieved [27]. When dealing with extremely high amplification one has to bear in mind, however, that the sensor signal becomes highly susceptible to minute amounts of contaminants affecting the enzyme reactions or the diffusion of the reactants.

A well-studied enzymatic recycling pair is lactate oxidase/lactate dehydrogenase.

Lactate dehydrogenase:



Lactate oxidase:

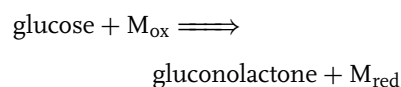


The oxygen consumption in the membrane bearing both enzymes is enhanced in the presence of NADH, yielding an increase in the sensitivity to lactate. The lactate signal can be enhanced by a factor of several thousands and lactate concentrations as low as 1 nmol l^{-1} are measurable [28].

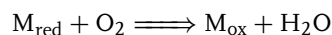
Further examples of recycling enzyme pairs include copper enzymes such as laccase and tyrosinase which oxidizes a wide range of substances including catecholamines, phenols, and redox dyes by dissolved oxygen in combination with flavoenzymes, haem-, and pyrroloquinoline quinone containing (NADH independent) dehydrogenases.

An ultrasensitive biosensor for these phenolic substances and redox dyes has been created with the quinoprotein glucose dehydrogenase and laccase, both of high specific activity coentrapped in a gel matrix in front of a Clark-type oxygen electrode.

(PQQ)glucose dehydrogenase:



Laccase:



The extraordinary efficiency of the amplification sensor is based on the excess of enzyme molecules compared with the concentration of the analyte molecule within the reaction layer. The current density of the membrane-covered sensor is almost three orders of magnitude higher than is the bare electrode with a lower limit of detection as low as 70 pmol l^{-1} [27]. As an alternative to the oxygen sensor the reaction can be followed with an antimony electrode or an ISFET indicating the pH shift during the recycling process [29]. The accumulation of H^+ is not as pronounced as the diminution of the dissolved oxygen concentration. Therefore, the response of the potentiometric sensors is somewhat smaller than that of the amperometric system.

Tab. 6 Enzymatic analyte recycling for signal enhancement in biosensors

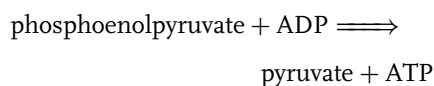
<i>Analyte</i>	<i>Enzyme couple</i>	<i>Transducer</i>
Glucose	Glucose oxidase/glucose dehydrogenase	Oxygen electrode
Lactate	Lactate oxidase/lactate dehydrogenase	Oxygen electrode
Lactate/pyruvate	Cytochrome b ₂ /lactate dehydrogenase	Pt-electrode
NADH/NAD ⁺	Peroxidase/glucose dehydrogenase	Oxygen electrode
	NADH oxidase/alcohol dehydrogenase	Oxygen electrode
	Glycerol dehydrogenase/diaphorase	Oxygen electrode
	p-hydroxybenzoatehydroxylase/glucose-6-phosphate dehydrogenase	Oxygen electrode
Glutamate	Glutamate dehydrogenase/alanine aminotransferase	Modified carbon electrode
	Glutamate oxidase/Glutamate dehydrogenase	Oxygen electrode
	Glutamate oxidase/Alanine aminotransferase	Hydrogen peroxide electrode
L-Leucine	Leucine dehydrogenase/amino acid oxidase	Oxygen electrode
ADP/ATP	Hexokinase/pyruvate kinase	Oxygen electrode with lactate dehydrogenase/lactate mono-oxygenase modified carbon-electrode with glucose-6-phosphate dehydrogenase
ADP	Myokinase/pyruvate kinase	Oxygen electrode with pyruvate oxidase
Ethanol	Alcohol oxidase/alcohol dehydrogenase	Oxygen electrode
Adrenaline	Glucose dehydrogenase/laccase	Oxygen electrode antimony pH electrode
Aminophenol		
Dopamine,	Glucose dehydrogenase/tyrosinase	Oxygen electrode
Ferrocene deriv.	Tyrosinase/diaphorase	Oxygen electrode, with glucose dehydrogenase for NADH-regeneration
	Oligosaccharide dehydrogenase/laccase	Oxygen electrode
Benzoquinone	Fructose dehydrogenase/laccase	Oxygen electrode
Hydroquinone	Cytochrome b ₂ /laccase	Oxygen electrode
Malate/oxalacetate	Malate dehydrogenase/Lactate mono-oxygenase	Oxygen electrode
Phosphate	Nucleoside phosphorylase/alkaline phosphatase	Oxygen electrode with xanthine oxidase
	Maltose phosphorylase/acid phosphatase	Hydrogen peroxide electrode with glucose oxidase

Oligosaccharide: acceptor oxidase (oligosaccharide dehydrogenase), cytochrome b_2 , diaphorase, and fructose dehydrogenase can be employed in place of the above mentioned glucose dehydrogenase and laccase has been replaced by other phenol oxidizing enzymes [30].

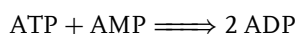
Recycling systems are not necessarily limited to reactions in which electrochemically active compounds are produced. In those cases, the recycling enzyme pair is combined with an indicator enzyme (or sequence) transforming one of the cycle coreactants (mostly a product) into a measurable species (see Table 5).

13.7.4.1.2 Exponential Recycling Enormous signal amplification is expected if in the cycling reaction more than one analyte molecule is regenerated. Here the total amount of intermediates and by-products is increasing exponentially with time. The concentration of any of the cycling intermediates or byproducts at any given time is a linear function of the initial substrate concentration. An example illustrating this principle is the ADP/ATP cycling system myokinase/pyruvate kinase [31]. In a single cycle two molecules of ADP are formed by myokinase per molecule ATP derived from the phosphorylation of ADP by pyruvate kinase.

Pyruvate kinase:



Myokinase:



The amount of ATP and ADP initially present in a very low concentration increases exponentially with cycling time,

when AMP and phosphoenolpyruvate concentrations are high enough to ensure no cosubstrate limitation. The abundance of pyruvate formed in the cycle is manifested by the oxygen consumption in the pyruvate oxidase layer.

13.7.4.2 Bioelectrochemical Recycling

In the bioelectrocatalytic approach the target analyte is recycled between electrode and redox centre of the enzyme, thus mediating the charge transfer to the electrode. Therefore, the enzyme product has to be essentially electroactive (Fig. 5b). In ideal cases sufficient (co)substrate of the enzyme is present, the overpotential required for regeneration is low, and the analyte is stable in both redox states.

Vital for a reaction cycle is the close contact of enzyme and electrode material. Starting from surface immobilization using adsorption, covalent binding, and entrapment of the redox enzyme, bulk modification procedures have been established, the latter appearing to be the most effective way.

The immobilization of PQQ-dependent glucose dehydrogenase onto the surface of a glassy carbon electrode [32] or a thick-film electrode [33] results in a very sensitive detector for various quinoid compounds. Also, tyrosinase-based sensors are used for monitoring a spectrum of mono- and diphenolic compounds that are of particular interest for environmental control [34].

13.7.5

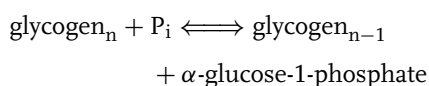
Sequential Activation of Enzymes

An enzymatic reaction cascade can be defined as sequential activation of a series of enzymes triggered, for example, by ligand binding to a receptor and resulting

in a large-scale amplification of the initial step or signal.

Figure 6 illustrates the application of this principle for signal generation in biosensors. The binding of the activator (initiator) transforms the inactive enzyme E_{1i} to its active form E_{1a} . This enzyme activates a second inactive enzyme and so forth. At the end of the cascade an enzyme is activated which produces the product P^* indicated by the transducer.

Phosphorylase *b*:



Muscle glycogen phosphorylase *b* activity is controlled by the concentration of AMP. The effect of AMP is enzyme activation. Therefore, AMP response reflects an amplification of the probe sensitivity, which is considerably higher than that for glucose-1-phosphate. The product of the reaction α -glucose-1-phosphate is indicated in a reaction sequence of alkaline phosphatase, mutarotase, and glucose oxidase [35].

13.8 Application

A relevant aspect in biosensor research is the simplification of operation, the more so as test strips are at present still superior in this respect. The savings of reagents provided by reusable sensors should not be exceeded by the expenses necessary for sensor maintenance. The task is to combine reusability and simple handling.

Whereas in traditional enzymatic analysis spectrophotometric methods dominate, test strips and biospecific electrodes are at the leading edge in the analytical application of immobilized enzymes.

Between 15 and 20 analyzers based on enzyme electrode are on the market worldwide [36]. They are one-parameter instruments for the measurement of glucose, galactose, uric acid, choline, ethanol, lysine, lactate, pesticides, sucrose, lactose, and the activity of α -amylase. They provide for a negligible enzyme consumption of less than 1 μg per sample.

The selective determination of blood glucose is of the utmost importance for the screening and treatment of diabetes. The normal concentration of glucose in

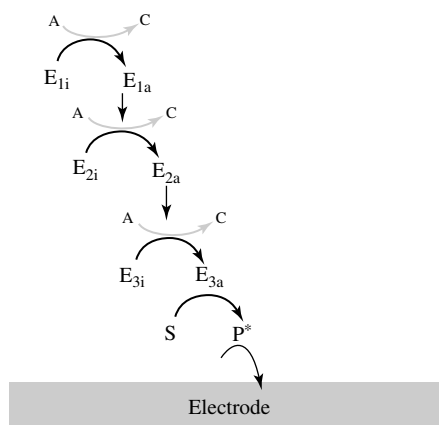


Fig. 6 Schematic illustration of sequential activation of enzymes in biosensors. A and represent coreactants.

blood serum ranges between 4.2 and 5.5 mmol l⁻¹, pathological situations may cause an increase up to more than 30 mmol l⁻¹.

Clinical chemists are interested in auto-analyzers characterized by high measuring frequency as well as in portable bedside-type analytical devices with short lag time between sample withdrawal and availability of the result. Therefore, enzyme electrode-based analytical systems for the application of highly diluted as well as undiluted media have been developed and commercialized.

Glucose analyzers based on enzyme electrodes have been brought onto the market in the United States, Japan, France, Lithuania, and Germany. As compared with the conventional enzymatic analysis, the main advantages of such analyzers are the extremely low enzyme demand (a few milliunits per sample), the simplicity of operation, and the high analytical quality.

The first commercial electrochemical glucose sensor for patient self-monitoring was introduced by Medisense, United Kingdom. There are now a number of systems that measure very rapidly and require less than 1-μl sample (Therasense, USA).

The sensor is based on a ferrocene-modified glucose oxidase electrode strip. For glucose determination, a drop of blood is transferred to a disposable enzyme electrode strip, which is then inserted into a pen-sized readout instrument. The response is more rapid than that of photometric test strips. Venous as well as capillary blood may be used as sample material. There are a number of systems that measure very rapidly and require less than 1-μl sample.

The invasive application of biospecific electrodes for direct analysis of substances

like glucose is one of the most important challenges of biosensor designers. Encouraging results have been obtained for subcutaneous tissue as the sampling site because of the lower risk of infection and blood clotting as compared to that after intravascular implantation.

Nevertheless, no truly reliable implantable sensor has yet reached the market. In the meantime, bedside-type discrete analyzers seem to offer the most economic and reliable means for critical care. In addition, ex vivo on-line analysis based on microdialysis sampling seems to be helpful.

References

1. H. J. Bergmeyer, M. Graßl, *Methods of Enzymatic Analysis*, VCH Verlagsgesellschaft, Weinheim, 1986.
2. F. W. Scheller, F. Schubert, *Biosensor, Techniques and Instrumentation in Analytical Chemistry*, Elsevier, Amsterdam, 1992, Vol. 11.
3. E. A. H. Hall, *Biosensors*, Prentice Hall Advance Reference Series, Engineering, Open University Press, Milton Keynes, England, 1991.
4. M. Dixon, E. C. Webb, (Eds.), *Enzymes*, Longmans, London, 1967.
5. Enzyme nomenclature, *Recommendations (1972) of the International Union of Pure and Applied Chemistry and the International Union of Biochemistry*, Elsevier, Amsterdam, 1973.
6. L. C. Clark, C. Lyons, *Ann. N. Y. Acad. Sci.* **1962**, *102*, 29.
7. K. Mosbach, Immobilized enzymes and cells, in *Methods in Enzymology* (Eds.: S. P. Colowick, N. O. Kaplan), Academic Press, San Diego, 1988, Vol. 137.
8. P. W. Carr, L. D. Bowers in *Immobilized Enzymes in Analytical and Clinical Chemistry, Chemical Analysis, Fundamentals and Applications* (Eds.: P. J. Elving, J. D. Winefordner, I. M. Kolthoff), John Wiley & Sons, New York, 1982, Vol. 56.
9. A. E. G. Cass, Biosensors, in *A Practical Approach*, The Practical Approach Series

- (Eds.: D. Rickwood, B. D. Hames), Oxford University Press, Oxford, 1990.
10. A. Heller, *Acc. Chem. Res.* **1990**, 23, 128–134.
 11. I. Willner, E. Katz, *Angew. Chem., Int. Ed.* **2000**, 39, 1181–1218.
 12. B. W. van der Schoot, P. Bergveld, *Biosensors* **1998**, 3, 161.
 13. A. P. F. Turner, I. Karube, G. S. Wilson, *Biosensors, Fundamentals and Applications*, Oxford University Press, Oxford, 1987.
 14. F. W. Scheller, F. Schubert, J. Fedrowitz, *Frontiers in Biosensorics, I Fundamentals; II Practical Applications*, Birkhäuser Verlag, Basel, 1997.
 15. F. W. Scheller, D. Pfeiffer, F. Lisdat et al., Enzyme biosensors based on oxygen detection, in *Methods in Biotechnology, Enzyme and Microbial Biosensors: Techniques and Protocols* (Eds.: A. Mulchadani, K. R. Rogers), Humana press, Totowa, 1998, Vol. 6.
 16. P. Bartlett, P. Tebutt, R. G. Whitaker, *Prog. React. Kinet.* **1991**, 16, 55.
 17. N. Gajovic, A. Warsinke, F. W. Scheller, *J. Chem. Tech. Biotechnol.* **1995**, 63, 337–344.
 18. J.-I. Anzai, H. Takeshita, Y. Kobayashi et al., *Anal. Chem.* **1998**, 70, 811–817.
 19. U. Wollenberger, F. W. Scheller, D. Pfeiffer, *Anal. Chim. Acta* **1986**, 187, 39–45.
 20. J. Wang, N. Naser, U. Wollenberger, *Anal. Chim. Acta* **1993**, 281, 19–24.
 21. R. Maidan, A. Heller, *Anal. Chem.* **1992**, 64, 23, 2889–2896.
 22. G. Nagy, M. E. Rice, R. N. Adams, *Life Sci.* **1982**, 31, 2611–2616.
 23. K. Kihara, E. Yasukawa, *Anal. Chim. Acta* **1986**, 183, 75–80.
 24. M. B. Madaras, R. B. Spokane, J. M. Johnson et al., *Anal. Chem.* **1997**, 69, 18, 3674–3678.
 25. P. T. Kissinger, W. R. Heineman, *Laboratory Techniques in Electroanalytical Chemistry*, Marcel Dekker, New York, 1996.
 26. F. Schubert, J. Lutter, F. W. Scheller, *Anal. Chim. Acta* **1991**, 243, 17–21.
 27. A. L. Ghindilis, A. Makower, B. G. Bauer et al., *Anal. Chim. Acta* **1995**, 304, 25–31.
 28. U. Wollenberger, F. Schubert, F. W. Scheller et al., *Studia Biophysica* **1987**, 119, 167–170.
 29. A. L. Ghindilis, A. Makower, F. W. Scheller, *Anal. Chim. Acta* **1995**, 304, 25–31.
 30. U. Wollenberger, F. Lisdat, F. W. Scheller in *Frontiers in Biosensorics, I Fundamentals; II Practical Applications* (Eds.: F. W. Scheller, F. Schubert, J. Fedrowitz), Birkhäuser Verlag, Basel, 1997.
 31. D. Pfeiffer, F. W. Scheller, C. McNeil et al., *Biosens. Bioelectron.* **1995**, 10, 169–180.
 32. A. F. Eremenko, A. Makower, W. Jin et al., *Biosens. Bioelectron.* **1995**, 10, 717–722.
 33. A. Rose, F. W. Scheller, U. Wollenberger et al., *Fresenius J. Anal. Chem.* **2001**, 369, 145–152.
 34. F. Ortega, E. Dominuez, G. Jonsson-Pettersson et al., *J. Biotech.* **1993**, 31, 289–300.
 35. U. Wollenberger, F. W. Scheller, *Biosens. Bioelectron.* **1993**, 8, 291–297.
 36. D. Pfeiffer in *Frontiers in Biosensorics, I Fundamentals; II Practical Applications* (Eds.: F. W. Scheller, F. Schubert, J. Fedrowitz), Birkhäuser Verlag, Basel, 1997.

14

Carbon Fiber Microelectrodes for the in vivo Measurement of Neurotransmitters: A Close Up Look at Neurochemical Activity in the Brain

Jennifer L. Peters, Nadezhda V. Kulagina, Hua Yang, and Adrian C. Michael
University of Pittsburgh, Pittsburgh, Pennsylvania

14.1	Introduction	463
14.2	A Mathematical Description of Extracellular Neurochemistry	465
14.3	Histology of Microelectrode and Microdialysis Probe Tracks in vivo	468
14.4	Monitoring Electrically Evoked Dopamine Release with Microelectrodes	469
14.5	In vivo Electrochemistry with Very High Spatial Resolution	471
14.6	Monitoring Spontaneous, as Opposed to Evoked, Dopamine Release	474
14.7	Electrochemical Sensors for in vivo Measurement	478
14.8	Conclusion	481
	References	482

14.1 Introduction

Motivated by the pioneering work of Ralph Adams [1] and his group at the University of Kansas, electroanalytical chemists in several countries have developed a powerful set of microelectrode-based methods that are now making significant contributions to our understanding of the neurochemical activity of the living mammalian brain. Numerous electrochemically detectable substances play important functional roles in the central nervous system, and there is intense interest in obtaining more information about the concentration, lifetime, and regulation of these substances in the extracellular space of the living brain. Although early work in this area focused on the neurotransmitter, dopamine, the list of substances that have now been monitored electrochemically *in vivo* is quite long and still growing. Strategies have been demonstrated for the selective *in vivo* electrochemical detection of dopamine [2–4], norepinephrine [5–7], serotonin [8–10], glutamate [11–13], choline [14–16], nitric oxide [17–19], ascorbic acid (vitamin C) [11], glucose [14, 16], lactate [20, 21], hydrogen peroxide [22], and oxygen [23, 24]. Ultimately, the goal of *in vivo* electrochemical monitoring is to aid in the elucidation of the role

of neurochemistry, not only in normal brain function but also in the numerous pathological conditions that afflict the human brain, such as Parkinson's disease, Alzheimer's disease, schizophrenia, ischemia, traumatic brain injury, and drug abuse. The electroanalytical techniques available for *in vivo* monitoring provide access to unique neurochemical information that is presently inaccessible by other *in vivo* analytical methods, such as microdialysis and spectroscopic imaging [e.g. positron-emission tomography (PET), single-photon-emission computed tomography (SPECT), and magnetic resonance imaging (MRI)]. Taken in combination, electrochemical methods, microdialysis, and spectroscopic imaging comprise a powerful array of tools for unlocking the chemical secrets of the brain.

The electrochemical methods that have evolved for neurochemical applications have several advantages that make them ideally suited to the task for which they are intended: the methods are selective, sensitive, and rapid. Nevertheless, the key advantages that will be highlighted in this chapter are derived from the micrometer physical dimensions of the microelectrodes themselves (Fig. 1). Today, the majority of *in vivo* electrochemistry is conducted in the brain with microelectrodes constructed with individual, or a

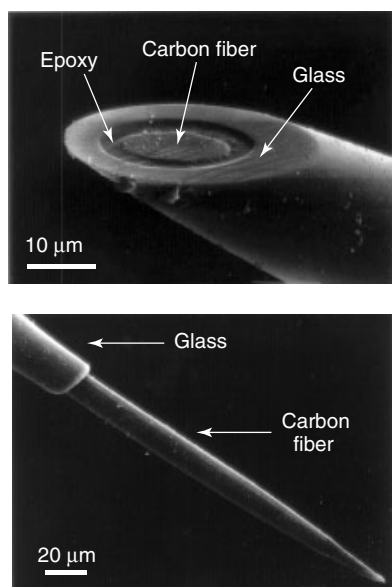


Fig. 1 Electron micrograph of carbon fiber microdisk and microcylinder electrodes.

few, carbon fibers. Carbon fibers with diameters less than 10 μm are readily available; they are quite easy to use for electrode fabrication, and despite their small size are surprisingly robust. The tiny dimensions of these electrodes have two immediate and immensely important consequences for *in vivo* analysis: first, measurements with micrometer spatial resolution are possible [25]; second, the electrodes produce very little physical disruption of the delicate architecture of the brain tissue. The latter point can be qualitatively appreciated just by considering the dimensions of structures found in the brain. For example, the body of most neuronal cells in the mammalian brain is typically on the order of 10 to 20 μm in diameter [26], while blood capillaries in the brain are separated from each other by distances of 20 to 100 μm [27]. Evidence from light and electron microscopy, discussed later in the chapter, confirms that implantation of these tiny electrodes inflicts essentially imperceptible brain injury.

The minimal amount of brain injury that microelectrodes cause renders them uniquely well suited to monitoring ongoing neurochemical events in the brain. Carbon fiber electrodes can be implanted to within a few micrometers of viable nerve terminals, which comprise the loci of the neurochemical events we desire to monitor. The intimate proximity of the electrodes to nerve terminals is of critical importance to the quality of the neurochemical information that is obtained. Most neurotransmitters are rapidly cleared from the extracellular space by either transporter mechanisms or metabolic processes [28]. These clearance events limit the lifetime of neurotransmitters in the extracellular space to the millisecond regime, which provides the neurotransmitter molecules with very limited opportunity to diffuse the necessary distance to reach an implanted sensor. Hence, if the sensor is not extremely close to functional nerve terminals, the sensor may not be capable of providing accurate neurochemical information about events that occur in the immediate vicinity of neuronal terminals. The full significance of this critical point has only recently begun to be fully appreciated.

Although the limited extracellular lifetime of neurotransmitters represents one of the main challenges for *in vivo* neurochemical analysis, it should also be pointed out that information about extracellular neurochemistry is extremely valuable to our understanding of brain function, not to mention dysfunction associated with disease states of the brain. The role of neurotransmitters is to convey messages between neighboring neurons, and that role is fulfilled by diffusion of

neurotransmitter molecules through the extracellular space [29]. Neurotransmitters are stored in neuronal terminals within small organelles called synaptic vesicles. The arrival of an action potential, the electrical signal originating at the cell body, triggers the fusion of synaptic vesicles with the terminal membrane, allowing a small pore to form through which the contents of the vesicle escape to the extracellular space. While in the extracellular space, the neurotransmitter may encounter and bind to a receptor on the surface of a neighboring cell, thereby conveying neuronal information between the releasing and receiving cell (which may be one and the same, by the way). Hence, by monitoring the extracellular concentration of neurotransmitters, as opposed to their intracellular or total tissue concentration, the measurement specifically focuses on the small fraction of the neurotransmitter that is at any one time engaged in neurotransmission. The resolution of information about the active fraction of neurotransmitter is a powerful aspect of methods that specifically monitor extracellular events.

Although electrochemistry is not the only method that has been developed for *in vivo* neurochemical monitoring, the information it provides is highly unique. For example, microdialysis sampling is widely used as another approach [30]. But, the sampling probes available for microdialysis are larger than the microelectrodes available for *in vivo* electrochemistry. Whereas microelectrodes may have diameters of 10 μm or less, the smallest available microdialysis probes have diameters of about 200 μm , and occupy approximately a 100 00-fold greater volume. Because of their size, the implantation of microdialysis probes into the brain inflicts severe injury on the surrounding tissue. A recent study that used electron microscopy to

examine the tissue near a microdialysis probe implantation site found severe loss of neuronal structure in the immediate vicinity of the probe and less severe damage extending as far as 1.4 mm from the probe site [31]. Recently, it has become apparent that many of the differences between results obtained with microdialysis and *in vivo* electrochemistry can be attributed to the differences between the magnitudes of damage that each methodology inflicts on the brain tissue under investigation.

Spectroscopic imaging technologies have also been developed as tools for monitoring ongoing chemical activity of the brain [32, 33]. Because imaging techniques, such as PET and SPECT, for example, involve no implantation of sensing or sampling devices into the brain itself, they completely eliminate brain injury. A powerful aspect of these methods, therefore, is their suitability for use in human patients or volunteers. In contrast, although the use of microdialysis in humans is emerging as a tool for critical patient care, the application of *in vivo* electrochemistry has been limited to date to laboratory animals. But, it should be mentioned that spectroscopic imaging can only be applied to the study of radiolabeled imaging agents and do not provide direct information about the unlabeled endogenous substances that can be monitored with implantable microelectrodes. With this in mind, it is fair to say that spectroscopy and electrochemistry provide complementary information.

14.2

A Mathematical Description of Extracellular Neurochemistry

In the introduction, we qualitatively explained that the proximity of an implanted

sensor to viable neuronal terminals in the brain has a major impact on the ability of the sensor to provide information about neurochemical events occurring in the vicinity of the terminals themselves. Because this issue has enormous impact both on the design of *in vivo* experiments and on the interpretation of their outcome, it is valuable to examine this issue in a somewhat more quantitative fashion before proceeding to describe the actual *in vivo* experiments. Thus, in this section, we present a mathematical discussion of the diffusion processes that deliver substances to implanted electrodes.

The release of neurotransmitters from neuronal terminals in the brain can be viewed as a quantal event. When an action potential arrives at a nerve terminal, a finite number of synaptic vesicles fuse with the terminal membrane and release their contents into the extracellular space. This release event occurs very rapidly: studies of exocytotic events in single isolated cells show that they occur on a sub-millisecond timescale [34, 35]. Furthermore, the event is spatially discrete, since the nerve terminals themselves have dimensions of just a few hundred nanometers [36, 37]. With this description in mind, it is reasonable to regard each nerve terminal as

a small, spatially discrete diffusion source and to regard each release event as an instantaneous activation of that diffusion source, as depicted in Fig. 2. The concentration profile plotted in the bottom portion of Fig. 2 represents a finite initial source of a diffusible substance: the question we wish to address here is how the concentration of that substance evolves in both space and time after the initial release event.

While neurotransmitters diffuse in the extracellular space, they are subject to clearance processes that either transport them back to nerve terminals or metabolize them to inactive products in the extracellular space. For example, the membranes of many nerve terminals are equipped with transporters, which are transmembrane proteins that transport neurotransmitter from the extracellular space into the cytoplasm of the terminal. On the hand, as in the case of acetylcholine, the extracellular space may contain enzymes that rapidly metabolize the neurotransmitter. The impact of these clearance processes on the concentration of the diffusing substance can be considered with an equation of the following type:

$$\frac{\partial C(x, t)}{\partial t} = D \frac{\partial^2 C(x, t)}{\partial x^2} - kC(x, t) \quad (1)$$

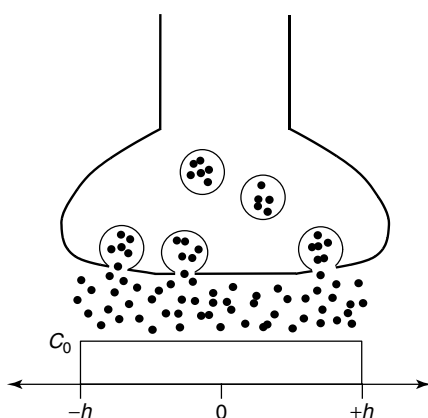


Fig. 2 Schematic representation of a finite diffusion source resulting from neurotransmitter release from a neuronal terminal.

where $C(x, t)$ is the concentration, D is its diffusion coefficient in the extracellular space, k is the rate constant of the clearance process, x is the distance from the center of the initial diffusion source, and t is the time that has elapsed since the initial release event [38]. The first term on the right hand side of Eq. (1) accounts for the impact of diffusion on the concentration of the diffusing substance, while the second term accounts for the impact of the clearance process.

Hence, by solving Eq. (1) we can gain insight into how the combined influence of the diffusion and clearance processes determine the concentration of the diffusing substance that evolves from the initial condition proposed in Fig. 2. With the initial condition of Fig. 2, the solution to Eq. (1) is:

$$C(x, t) = \frac{C_0}{2} \left[\operatorname{erf} \left(\frac{h-x}{2\sqrt{Dt}} \right) + \operatorname{erf} \left(\frac{h+x}{2\sqrt{Dt}} \right) \right] \exp(-kt) \quad (2)$$

where “erf” is the error function [39, 40]. Figure 3 shows plots of Eq. (2) calculated at various times after the initial release event. Figure 3(a) shows plots calculated with a clearance rate constant of zero (no clearance) while Fig. 3(b) shows plots calculated with a rate constant of 10 s^{-1} , which is consistent with the value reported for the pseudo first-order rate constant for the dopamine transporter in the striatal region of the rat brain [41]. The other parameters used to obtain Eq. (3) were also consistent with values for the striatal dopamine system of the rat: the value of h was 100 nm [36, 37] and D was $2.4 \times 10^{-6} \text{ cm}^2 \text{ s}^{-1}$ [42].

Figure 3(a) shows how the substance becomes increasingly diluted with time as it diffuses into an ever-increasing volume of space. In this case, because the

original diffusion source is so small, the dilution effect is quite extreme, even after a relatively short amount of time: after a diffusion time of 50 ms the maximum concentration is less than 2% of the original value, C_0 . Just as importantly, Fig. 3(a) shows that over the time interval considered here, the concentration profile of the diffusing substance does not extend more than a few micrometers in either direction from the diffusion source. This illustrates the point that as the distance between the source and an implanted sensor increases, the measurement is increasingly affected by the dilution phenomenon.

Figure 3(b) shows how the introduction of the clearance process changes the concentration behavior predicted by Eq.(2). The clearance process imposes a finite lifetime on the diffusing substance. Thus, not only is the substance diluted by the diffusion process, it is also lost to the clearance process. After a time corresponding to approximately three times the reaction half-life, the substance has almost completely disappeared. The added contribution of the clearance process limits to an even greater extent the maximum travel distance of the diffusing substance from the source. Figures 3(a) and (b) illustrate how the combined effects of diffusionally induced dilution and the clearance process affect the manner in which concentration varies as function of distance from the diffusion source. If the distance between the diffusion source and a nearby sensor is too great, the sensor will not be able to report concentration events occurring in the vicinity of the source itself.

The most obvious message to be taken from Fig. 3 is that the proximity of an implanted device to viable nerve terminals has a considerable impact on what can be observed with that device. A device that disrupts nearby terminals when it

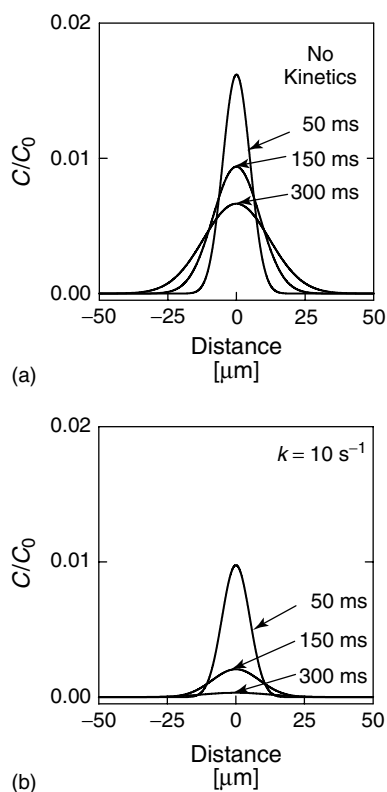


Fig. 3 Theoretical concentration profiles obtained by plotting Eq. (2) at various values of t , as indicated on the figure. Panel A shows the result for the pure diffusion case. Panel B includes the kinetics of a coupled chemical reaction. Values of h , k , and D are discussed in the text.

is introduced into brain tissue, thereby rendering the nearby terminals nonviable, will observe a smaller fraction of the extracellular concentration of substances released by terminals positioned further away from the device. On the other hand, if the device can be introduced without causing disruption, then that device will provide a closer view of events occurring in the vicinity of the viable terminals.

14.3 Histology of Microelectrode and Microdialysis Probe Tracks *in vivo*

The previous section pointed out the critical importance of being able to place a sensor as close as possible to viable

neuronal terminals in order to accurately monitor the release of neurotransmitters from those terminals. This is one of the factors that motivated the use of extremely small electrodes fashioned from carbon fibers for *in vivo* neurochemical measurements. These electrodes, with diameters of less than 10 μm in some cases (Fig. 1), are literally smaller than most of the cells found in the mammalian brain tissue [26]. Recently, we have attempted to use histological methods to directly examine the level of tissue disruption caused by implantation of carbon fiber electrodes into brain tissue [43]. As it turns out, this has been difficult to do because the amount of damage caused by these electrodes is too small to detect.

Carbon fiber microcylinder electrodes (7 μm in diameter and 400 μm in length) were implanted vertically into the brains of anesthetized rats and were used to monitor electrically evoked dopamine release, as described in detail in the next section. After the electrodes were removed from the animal, the brain tissue was collected and thinly sliced in the plane perpendicular to the axis of the electrodes. When we examined the tissue sections through which the carbon fiber passed, we could find no evidence of the electrode track with the light microscope. This shows that the tissue damage caused by the fiber itself is minimal. On the other hand, tracks could be found in tissue sections through which the glass barrel of the electrode had passed because the barrels were tapered and their

diameters were larger than the diameter of the fibers. Tissue sections taken just before the electrode track disappeared were further examined by electron microscopy. The electron micrographs clearly showed the presence of intact axonal terminals within micrometer distances of the electrode barrel. This study confirms that the microelectrodes, by virtue of their ability to penetrate brain tissue without inflicting injury, gain very close proximity to intact axonal terminals once implanted into living brain tissue.

The microscopy of microelectrodes tracks stands in stark contrast to images of tissue in the vicinity of the implantation sites of microdialysis probes, as recently reported by Drew and coworkers [31]. The tissue in the immediate vicinity of the microdialysis probe suffered a severe loss of synaptic junctions. This confirms the general idea that implantation of a larger device leads to further tissue disruption, thereby directly increasing the separation distance between that larger device and viable neuronal terminals. As discussed in further detail in the following section, differences between *in vivo* results obtained with microelectrodes and microdialysis probes can be attributed to differences in this separation distance.

14.4 Monitoring Electrically Evoked Dopamine Release with Microelectrodes

While electron microscopy reveals the presence of intact synaptic terminals in the immediate vicinity of microelectrodes, it does not demonstrate that those terminals are viable. Evidence that the nearby terminals are viable is available in the form of a variety of experimental results. For example, carbon fiber microelectrodes

have been used in numerous laboratories to monitor electrically evoked dopamine release in the rat striatum [2, 44, 45], in addition to several other brain regions of interest [46, 47]. Electrically evoked release of dopamine refers to the release of dopamine upon electrical stimulation of dopaminergic axons that pass through a brain region called the medial forebrain bundle (MFB). For this type of experiment, a bipolar stimulating electrode is positioned just above the MFB and small current pulses are passed between the two poles of the electrode. These current pulses stimulate action potentials that travel along the axons and evoke dopamine release upon reaching the axon terminals in the striatum. The stimulus responses in Fig. 4(a), which were recorded in the striatum with a carbon fiber microcylinder electrode, show that the electrochemical signal essentially changes as soon as the stimulation begins. Usually, the signal changes within the first 100 ms of the stimulation. This confirms that the evoked release takes place very near to the microelectrode, since dopamine can only diffuse a few micrometers in such a short interval of time.

Several lines of evidence have been gathered to confirm that the substance released into the extracellular space during MFB stimulation is in fact dopamine. These have been discussed many times in the literature and so will be mentioned only briefly here. The first line of evidence is electrochemical in nature. The stimulus responses in Fig. 4(a) were obtained by repetitively performing cyclic voltammetry at a sweep rate of 300 V s^{-1} and with an interval of 100 ms. A background subtracted voltammogram of the substance that changed concentration during the stimulation is obtained by taking the difference of the current-potential response recorded during the

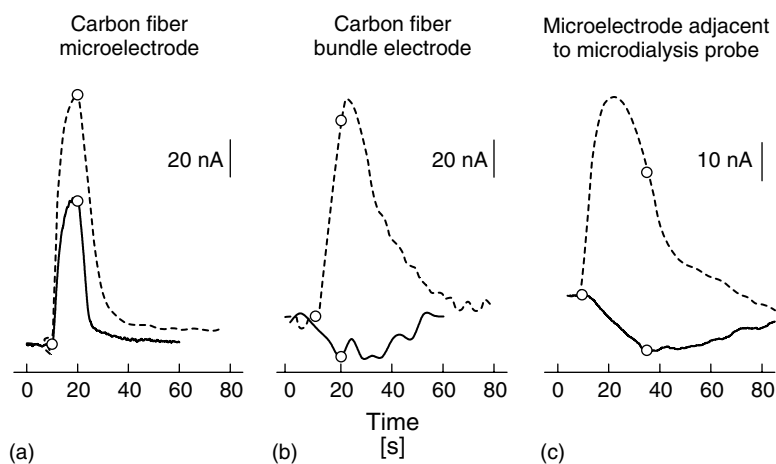


Fig. 4 Stimulated dopamine release measured in striatum by several analytical devices. Stimulation responses were recorded 5 min before (solid lines) and 25 min after (dotted line) the systemic administration of 20 mg kg^{-1} nomifensine. Electrical stimulation was applied to the MFB bundle with the following parameters: 45 Hz, 10 s (a & b) or 25 s (c) and $50 \mu\text{A rms}$. Open circles denote the beginning and end of the electrical stimulation.

stimulation and just before stimulation began. The background-subtracted voltammograms obtained *in vivo* compare very well with those obtained during calibration of the microelectrode in authentic dopamine after removal of the electrode from the animal. Anatomical evidence is also available: both the stimulation and the voltammetric microelectrode must be correctly positioned or no stimulus response will be obtained [46]. Finally, pharmacological evidence exists: the effects of many drugs that interact selectively with dopamine neurons have been shown to exert predictable effects on the amplitude and duration of the stimulus responses [45, 48, 49].

Several times in the discussion presented so far, we have emphasized the importance of the proximity of the sensor to viable axon terminals in the brain. Microdialysis probes, which are considerably larger than carbon fiber microelectrodes, have been confirmed by electron

microscopy to cause severe damage to brain tissue [31]. In a series of experiments that made combined use of voltammetric microelectrodes and microdialysis probes, we investigated the magnitude of the effect of this tissue damage on the neurochemical results obtained by microdialysis [44, 50–52]. In this work, a carbon fiber microelectrode was mounted directly onto the outer surface of a $220\text{-}\mu\text{m}$ diameter microdialysis probe. The combined device was lowered into the striatum of anesthetized rats, where evoked dopamine release has been measured before, as described in the preceding paragraphs. However, when electrical stimulation was applied to the MFB, no evoked dopamine release could be observed at the carbon fiber microelectrode that was mounted onto the microdialysis probe. This result demonstrates that the tissue in the immediate vicinity of the microdialysis probe is devoid of viable dopamine terminals, consistent with electron microscopy findings of Drew

and coworkers [31]. To date, the only way we have been able to observe evoked dopamine release with a microelectrode mounted onto a microdialysis probe has been to make use of a drug, nomifensine, which inhibits the dopamine transporter (Fig. 4b). Consistent with Fig. 3, a drug that decreases the effective rate constant of the transport of dopamine from the extracellular space is expected to increase the distance over which dopamine can diffuse from viable terminals. Blockade of the transporter, however, does not eliminate the diffusionally induced dilution phenomenon, so even after uptake inhibition, we observe smaller signals at the microelectrodes adjacent to the microdialysis probes than at microelectrodes placed themselves into brain tissue.

Consistent with the difficulty we experienced in observing evoked dopamine release in the vicinity of microdialysis probes, we have also recently found that it is similarly difficult to observe evoked dopamine release when a larger-sized electrode is used [53]. Most *in vivo* electrochemistry is conducted with microelectrodes constructed with a single carbon fiber. But, it is also feasible to make larger electrodes by bundling many fibers together. In this work, we constructed electrodes with a bundle of fibers with a diameter of about 100 μm , that is, a diameter approaching that of a microdialysis probe. Although these larger electrodes work just as well as single-fiber electrodes for detecting dopamine in standard solutions, we could not observe evoked dopamine release in the rat striatum without the aid of the dopamine uptake inhibitor, nomifensine (Fig. 4c). Again, this result confirms the importance of the overall size of the device implanted into the brain for neurochemical monitoring. If the device is too large, regardless of whether

it is an electrode or a sampling probe, implantation will lead to tissue damage that increases the distance between the device and viable axon terminals, which in turn significantly impacts the ability of the device to provide information on chemical events taking place in the immediate vicinity of viable terminals.

14.5 In vivo Electrochemistry with Very High Spatial Resolution

Microelectrodes constructed with single carbon fibers come in two basic versions, the microcylinder and the microdisk, as depicted in Fig. 1. All the measurements discussed earlier were performed with microcylinder electrodes, which are small enough in diameter to be implanted with minimal tissue damage. Although these electrodes gain close proximity to viable neuronal terminals, they provide information about extracellular neurotransmitter concentrations as averaged over the length of the cylinder. On the other hand, the microdisk electrodes provide a much higher spatial resolution and provide much more highly localized information. For example, when two microcylinder electrodes are implanted fairly close to each other in the rat striatum, electrical stimulation of the MFB produces very similar responses at each electrode [44]. If instead two microdisk electrodes are implanted, MFB stimulation often produces very different responses [44]. Alternatively, several groups have demonstrated that different stimulus responses are obtained when an individual microdisk electrode is used to record stimulus responses at several locations within the striatal region of the same rat [44, 54]. The contrast between the results obtained at the two styles of electrode

show that the microdisks report local variations in the extracellular response during stimulation, while the microcylinders report the spatial average of that response.

Figure 3, above, explains the origin of the local variations in extracellular dopamine concentrations exhibited in the results obtained with microdisk electrodes. When placed randomly into the tissue, a microdisk electrode sometimes finds itself very near to a site of active dopamine release (a “hot spot”), while on other occasions will find itself in a location where dopamine release does not occur (a “cold spot”). The concept of hot and cold spots is consistent with the known architecture of the striatal region of the brain, which contains numerous bundles of myelinated nerve fibers that do not contain dopamine terminals: if the small electrode were to be implanted in such a bundle, then indeed very little dopamine release would be observed at that location.

Numerous studies have examined the ways in which drugs that selectively act on dopamine neurons alter evoked dopamine responses as measured with microelectrodes [45, 48, 49]. Several drugs are well known to increase the amplitude of the stimulus response, while others decrease the amplitude. Some drugs also affect the time course of the response. At microcylinder electrodes, the effects of drugs on the stimulus responses at different electrodes are generally similar, implying again that these electrodes spatially average out local variations in the response. At microdisk electrodes, however, this may not be the case. For example, in a recent study, we reported that two drugs gave very different responses, depending on whether the microdisk electrode was in a hot spot or a cold spot for dopamine release [25]. In experiments involving the dopamine uptake inhibitor, nomifensine, we found that

the drug had a rather small effect in hot spots, but had a pronounced effect in cold spots. In contrast, when we gave rats a dose of L-DOPA, the biosynthetic precursor of dopamine, we found that the drug had the most pronounced effect in hot spots and a mild effect in cold spots.

We have been interested in understanding the local variations in drug-induced modifications of the stimulus responses because they may be relevant to understanding the mechanisms underlying the functional effects of these drugs. Nomifensine, for example, is a psychoactive drug [55, 56], while L-DOPA is used in the therapy of Parkinson’s disease [57, 58]. Our strategy was to compare the experimentally observed effects of the drugs with predictions obtained by modeling diffusion and clearance processes, in similar fashion to that used to obtain Fig. 3. For this work, however, we modeled the clearance process with Michaelis-Menten kinetics dopamine uptake by the transporter is a saturable process and since nomifensine is a competitive uptake inhibitor:

$$\frac{\partial C(x, t)}{\partial t} = D \frac{\partial^2 C(x, t)}{\partial x^2} - \frac{V_{\max} \cdot C(x, t)}{K_m + C(x, t)} \quad (3)$$

where V_{\max} and K_m are the maximal velocity and the Michaelis constant, respectively. Eq. (3) does not have a simple analytical solution, so a numerical solution method was used. Stimulus responses were simulated by obtaining solutions to Eq. (3) while linearly ramping the concentration at the diffusion source for a finite amount of time. The value of K_m was increased to simulate the effect of competitive uptake inhibition after nomifensine administration, while the rate at which the source concentration was ramped was increased to simulate the effect of increasing

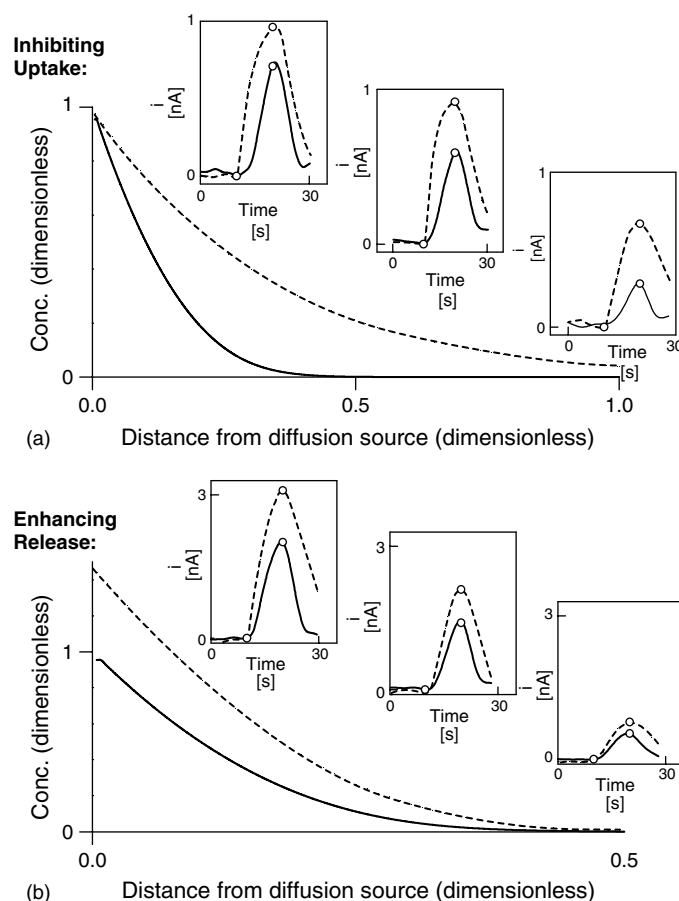


Fig. 5 Theoretical and experimental descriptions of the impact of uptake inhibition (a) and enhancement of release (b) of the responses recorded at microdisk electrodes. Theoretical curves: Numerical solutions of Eq. (3) were used to generate predicted concentration profiles at various times during a simulated period of stimulation. The calculated concentration profiles shown in the main panel of the top and bottom portion of this figure were obtained at the end of the simulated stimulus. The top panel shows how an increase in the Michaelis constant (K_m) changes the concentration profile, while the bottom panel shows the effect of an increase in the magnitude the simulated stimulus (further details can be found in Ref. [25]). Stimulation responses: The inset panels show experimental stimulus responses recorded in the rat brain with microdisk electrodes. Open circles denote the beginning and end of the electrical stimulation. Predrug responses (solid lines) were recorded prior to systemic administration of either 20 mg kg⁻¹ nomifensine (a) or 250 mg kg⁻¹ L-DOPA (b). Postdrug responses (dotted lines) were recorded 25 min after nomifensine administration or 55 min after L-DOPA administration. Note that the trends in the amplitude of the experimental signals correspond very well to those apparent in the theoretical concentration profiles.

the biosynthesis of dopamine after L-DOPA administration. The time course of the simulated change in concentration at locations near the diffusion source was taken to represent the calculated responses in hot spots, while the time course at larger distances from the source was taken to represent the calculated responses in cold spots. Figure 5 shows the correlation between the simulated and the experimentally observed stimulus responses. Hence, the combined actions of diffusion and clearance appear to provide a sound explanation for the local variations in the stimulus response observed with microdisk electrodes, and in drug-induced variations in those responses.

At present, the functional significance of the local variations revealed by these microdisk-based measurements remains to be fully explored. Nevertheless, it is certainly intriguing to speculate that these local variations may be of great functional significance, considering that the mammalian brain contains multiple receptor subtypes for many neurotransmitters, including dopamine. In fact, five genetically distinct dopamine receptors have been identified [59–65]. Most of the dopamine receptors in the striatum, the brain region in which most of our work has been carried out, are of the so-called D₁ and D₂ type. One of the main distinctions between these receptors is their affinity for dopamine. The D₁ receptor has a relatively low affinity for dopamine, with a K_D of 1–5 μ M, while the D₂ receptor has about a 10-fold higher affinity, with a K_D of 100 to 500 nM [66]. Apparently, these two dopamine receptor types are designed to respond to quite different dopamine concentrations: we speculate that the mechanisms giving rise to the local variations in stimulus responses observed at microdisk electrodes, namely, diffusion

and clearance, may also be responsible for producing the different dopamine concentrations for which the D₁ and D₂ receptors are designed.

14.6

Monitoring Spontaneous, as Opposed to Evoked, Dopamine Release

Many of the applications of *in vivo* voltammetry have focused on monitoring the release of dopamine, and other neurotransmitters, as evoked by the electrical stimulation of axons. The use of electrical stimulation is convenient because it evokes dopamine release at a specific and known time. Moreover, the combination of voltammetry and electrical stimulation has revealed a large amount of useful information about the regulation of dopamine release, the kinetics of dopamine uptake, and the diffusion of dopamine in the extracellular space [67]. Nevertheless, the study of evoked dopamine release does not provide information about spontaneous dopamine release, that is, dopamine release triggered by the endogenous neuronal activity of the brain. Such information is also of great interest.

Although some reports on the use of voltammetry to monitor spontaneous dopamine release do exist [68, 69], there is a widely held perception that resting extracellular dopamine levels in the brain are simply too low to be measured with voltammetry. Numerous studies based on microdialysis, for example, suggest that the resting extracellular concentration of dopamine in the rat striatum is in the single-digit nanomolar range [70–72], while the detection limit of voltammetric methods is rarely much below 100 nM. But, there are two problems with the quantitative results

obtained with microdialysis. First, the microdialysis-based estimates of dopamine concentration do not take into account the manner in which diffusion and clearance processes affect that concentration [73, 74]. Considering Fig. 3, it seems reasonable to hypothesize that the concentrations observed by microdialysis are lower than those in closer vicinity to viable axonal terminals, where measurements can be performed with microelectrodes. Second, it is difficult to rationalize the difference between the nanomolar concentrations of dopamine reported by microdialysis and the micromolar dopamine affinity values of the dopamine receptors, as mentioned at the end of the previous section. The D_1 receptor in particular, with its K_D value of 1 to 5 μM [66], would have little chance to play any functional role in the brain if the extracellular dopamine concentration were three orders of magnitude lower than its affinity for dopamine. On the other hand, there is abundant evidence that D_1 receptors do have functional significance in the brain [75], implying that there must be sufficient dopamine in the extracellular space to cause their activation. Hence, there is good reason to expect that resting dopamine levels in the brain are substantially higher than existing estimates, and may even be sufficiently high to detect by voltammetric means.

Nevertheless, reports on the use of voltammetry to measure resting dopamine levels in the brain are scarce. This is mainly because of the large contribution of background currents to the resting voltammetric signal [2]. Especially when fast-scan techniques are used, which are highly selective toward dopamine, background current may comprise the vast majority of the total signal observed in the brain. Furthermore, the background signal recorded in brain tissue might be

quite different from that observed at the same electrode in a calibration buffer. Hence, with the microelectrode implanted in the brain, it is essentially impossible to ascertain what fraction of the resting signal is due to the oxidation of extracellular dopamine. A strategy that has allowed us to at least partially circumvent this problem is to monitor voltammetric signals in the brain under conditions that lead to the suppression of spontaneous dopamine release. The idea in this case is to monitor the decrease in extracellular dopamine levels expected when spontaneous release is suppressed.

The striatal region of the rat brain receives both a dopamine projection from the midbrain and a glutamatergic projection from the cortex. Although it is a matter of some controversy, several lines of evidence suggest that spontaneous release of dopamine in the striatum is regulated by the glutamatergic projection [76–83]. Glutamate is an amino acid neurotransmitter that is recognized by several different receptors found in the brain. Brain glutamate receptors are divided into two main subtypes: the ionotropic and metabotropic glutamate receptors. Kynurenic acid is a naturally occurring substance that acts as a broadly selective antagonist of the ionotropic glutamate receptors: in other words, it blocks those receptors from activation by glutamate. Recently, we conducted a series of experiments in which kynurenic acid was infused directly into brain tissue via a micropipet placed about 100 μm from a carbon fiber microcylinder electrode [84]. The infusion of kynurenic acid caused a sudden and clear decrease in the voltammetric signal at the carbon fiber electrode (Fig. 6), and several lines of supporting evidence were consistent with the idea that this was due to a decrease in the extracellular concentration

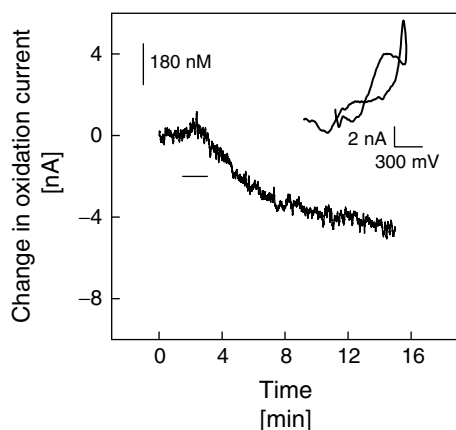


Fig. 6 The effect of local injection of 200 nL of 1 mM kynurenate on the resting dopamine signal measured in striatum with a carbon fiber microelectrode. The kynurenate was delivered via a small pipet placed in the tissue about 100 μm from the electrode. The horizontal bar denotes the duration of the injection. The concentration scale bar was calculated from postcalibration results. Background subtracted voltammogram (inset) was calculated by subtracting the voltammograms collected for 50 s at the beginning of the experiment from the voltammograms collected for 50 s at the end.

of dopamine. According to postcalibration of the microelectrode, the magnitude of the kynurenate-induced decrease in the voltammetric signal corresponded to a 450-nM decrease in the extracellular dopamine concentration. Since we are not certain that the infusion of kynurenic acid into the striatum caused a complete suppression of spontaneous dopamine release, this result allows us to conclude that the resting dopamine concentration in the vicinity of the carbon fiber electrodes is at least 450 nM. Nevertheless, this value, almost fivefold higher than the detection limit of the electrode for dopamine, is approximately two orders of magnitude higher than the concentration estimates obtained by microdialysis, and is consistent with the dopamine affinities of the D₁ and D₂ receptors found in this brain structure.

The results described in the previous paragraph suggest that extracellular dopamine levels in the rat striatum are indeed higher than the detection limits available with carbon fiber electrodes. Under resting conditions, however, the voltammetric signal from dopamine is obscured by a large background current. Nevertheless, this result implies that there may be many more opportunities than we

presently realize for examining changes in spontaneous dopamine release rates. So, we have started to explore this issue in rather more detail than before [85]. We chose to examine the effects of drugs that block the dopamine uptake transporter, which include cocaine, nomifensine, amphetamine, and Ritalin. Interest in the mechanism of action of these drugs is derived from both their illicit and medical uses. Several studies have reported the effects of uptake inhibitors on the voltammetric responses observed during electrical stimulation of dopamine axons in the brain [45, 48], but these reports rarely describe any effect of the drugs on the voltammetric signal recorded in the absence of the electrical stimulation. This has been a point of some confusion for a considerable amount of time, because the actions of these drugs are widely attributed to their ability to increase extracellular dopamine levels [70, 86]. We have been interested in understanding why this expected increase is usually not observed when voltammetric microelectrodes are used.

These so-called uptake inhibitors, it turns out, do not just inhibit uptake. In fact, they indirectly change the rate of

spontaneous dopamine release. This is known from studies in which electrophysiological techniques have been used to monitor the frequency at which dopamine neurons spontaneously generate action potentials, the electrical signal that triggers the release of neurotransmitters from their storage vesicles. After the administration of uptake inhibitors, the frequency at which dopamine neurons spontaneously generate action potentials drops substantially [87, 88]. Thus, these drugs not only decrease the rate of dopamine uptake, they also decrease the rate of spontaneous dopamine release. In essence, this appears to be a homeostatic response designed to regulate the extracellular dopamine concentration. We hypothesized that this homeostatic response is the reason that

dopamine levels, as measured with carbon fiber microelectrodes, have not been observed to increase following pharmacological uptake inhibition.

To test this hypothesis, we administered an uptake inhibitor, nomifensine, to rats that had been pretreated with a drug, sulpiride, which blocks the D_2 dopamine receptor. In animals pretreated with this drug, the uptake inhibitors are less effective at decreasing the action potential frequency in dopamine neurons, strongly implying that the D_2 receptors mediate the homeostatic response by providing negative feedback information to dopamine neurons [85]. In the sulpiride-pretreated rats, an increase in dopamine was observed with carbon fiber microelectrodes immediately after the administration of

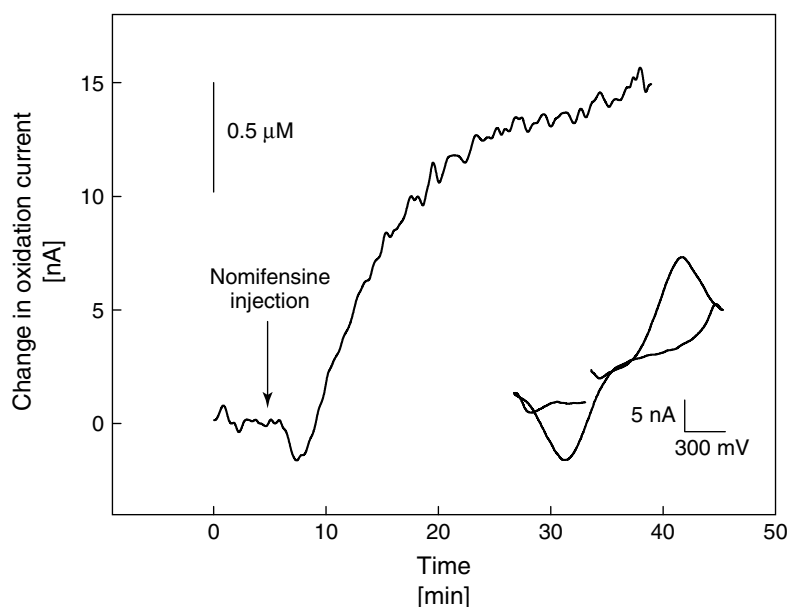


Fig. 7 Change in resting dopamine signal after systemic administration of 20 mg kg^{-1} nomifensine 60 min after administration of 100 mg kg^{-1} sulpiride. The scale bar was determined from postcalibration results. Background subtracted voltammogram (inset) was calculated by subtracting the voltammograms collected for 2 min at the beginning of the experiment from the voltammograms collected for 2 min at the end.

nomifensine (Fig. 7), clearly showing that sulpiride interferes with the homeostatic regulation that would have otherwise prevented the increase in extracellular dopamine.

These results on the change in extracellular dopamine levels following pharmacological manipulations begin to show that microelectrode-based methods for *in vivo* neurochemical analysis have much to offer. These microelectrodes, by virtue of their ability to get so close to viable axonal terminals in the brain, provide a brand new view of neurochemical events in the brain. In comparison to microdialysis, for example, the microelectrode not only provides a totally different estimate of extracellular dopamine levels (as discussed earlier) but also provides new insights into the regulation of those levels. Microdialysis studies, for instance, did not reveal the ability of kynurenic acid to decrease extracellular dopamine levels [89–91]. Microdialysis studies also did not reveal the homeostatic regulation of extracellular dopamine levels by D₂ receptors after the administration of uptake inhibitors. The contrast between the results obtained with microelectrodes and microdialysis probes can generally be attributed to the issue raised previously in this chapter, namely, how close do the devices get to viable axonal terminals in the brain.

14.7

Electrochemical Sensors for *in vivo* Measurement

While much of this chapter has focused on the *in vivo* detection of the neurotransmitter dopamine, which has been the paradigm in this field, there is also a great deal of interest in the development of electrochemical sensors for the

in vivo measurement of other substances of neurochemical interest, including glutamate, choline, and glucose. Such sensors are desirable because they can be fabricated from carbon fiber microelectrodes, affording them the spatial resolution required to measure neurotransmitter release in the vicinity of nerve terminals. There are several important considerations, however, for the development of sensors for *in vivo* use. Care must be taken that the sensors are biocompatible and that they are not susceptible to excessive fouling by the brain. Additionally, *in vivo* electrochemical sensors must respond selectively to the neurotransmitter of interest.

Many different schemes have been used in the design of sensors, several of which make use of the selectivity afforded by the incorporation of enzymes. The majority of enzyme sensors that have been successfully used *in vivo* rely on oxidase enzymes that generate hydrogen peroxide. While hydrogen peroxide can be oxidized directly at the electrode surface, this approach is inconvenient because it requires the use of large positive potentials where many compounds oxidize. The following example demonstrates one way in which these problems can be overcome.

Our group has designed electrochemical sensors for glutamate, choline, and glucose [11, 14–16]. These sensors are constructed by coating carbon fiber microelectrodes ($r = 5 \mu\text{m}$, $l = 300\text{--}400 \mu\text{m}$) with the oxidase enzyme, horseradish peroxidase (HRP) and redox polymer (Fig. 8) containing an $\text{Os}^{2+}/\text{Os}^{3+}$ redox couple, and then applying a cross-linking agent. Ascorbate oxidase (AAox) can also be incorporated to facilitate ascorbate rejection. The sensors are then cured, and a thin layer of Nafion is applied to increase the selectivity for cations over anions. These sensors

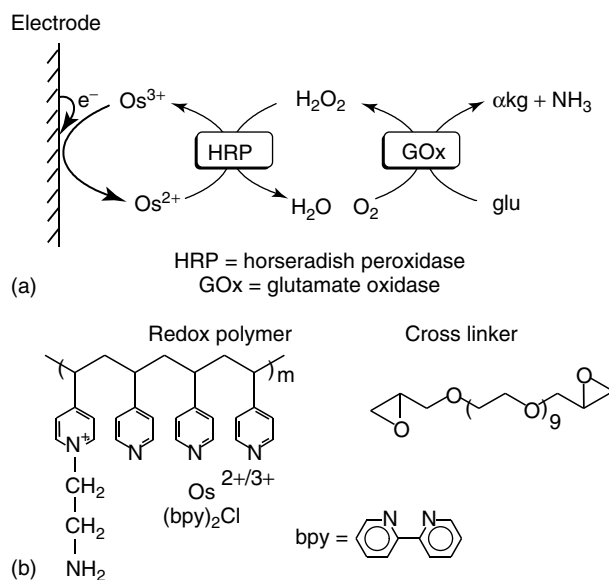


Fig. 8 (a) Scheme for the electrochemical detection of glutamate. (b) Structure of the redox polymer and cross linker.

work according to the following scheme, diagrammed in Fig. 8: the substrate is selectively oxidized by the oxidase enzyme, producing peroxide, which in turn, is reduced by HRP. HRP is reduced by the $\text{Os}^{2+}/\text{Os}^{3+}$ redox couple, which is subsequently reduced at the electrode surface, generating the electrochemical signal. An advantage of this sensor construction is that interference from easily oxidizable compounds, such as ascorbate, are eliminated by operation of the sensor at low potentials (-100 mV vs. Ag/AgCl), inclusion of AAox, and coating with Nafion.

We have recently demonstrated *in vitro* that these sensors respond robustly to the substrate of interest and exhibit no response to, or interference from, a variety of substances present *in vivo*, including ascorbate, dopamine and dihydroxyphenylacetic acid (DOPAC) [11, 14–16]. Furthermore, we have verified pharmacologically that the sensors respond *in vivo* to several

compounds that are expected to alter extracellular levels of the substrate of interest. One such substance that is of particular importance neurochemically is tetrodotoxin (TTX), as will be discussed next.

TTX is a compound that halts the propagation of action potentials and the subsequent release of neurotransmitter by blocking sodium channels. TTX sensitivity has long been recognized as a marker of neuronal activity, and is particularly relevant in the case of glutamate, for which a significant metabolic pool exists. Microdialysis measurements show no changes in extracellular glutamate upon local infusion of TTX, revealing that microdialysis measures only the TTX insensitive, or metabolic pool of glutamate [92–95]. Glutamate sensors, fabricated as described earlier, measure a decrease in extracellular glutamate upon TTX injection (Fig. 9), providing the first reported *in vivo* measurement of the neuronal component

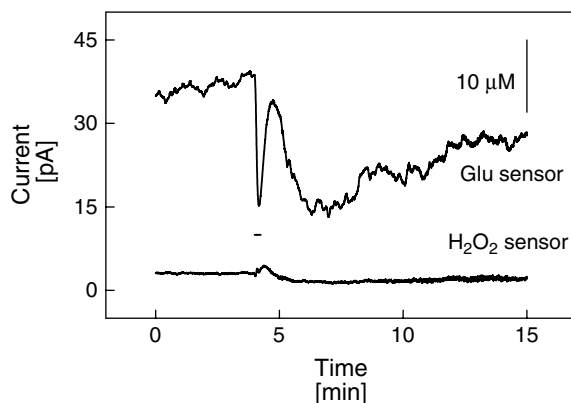


Fig. 9 Signals recorded *in vivo* with glutamate microsensor and glutamate oxide-free background microsensor during the local injection of 200 nL of 100- μ M TTX via a micropipet. The horizontal bar indicates the duration of the injection. The scale bar was calculated based on postcalibration results.

of the extracellular glutamate concentration. This result offers further evidence that microelectrodes provide information about neuronally relevant events because they closely approach synaptic terminals. Local TTX injection was also monitored by glucose and choline sensors, which show no decrease in signal and a modest decrease in signal, respectively, upon TTX injection. These are the expected results: since glucose is not a neurotransmitter, it is not released by an impulse-dependent mechanism. Some component of the extracellular choline concentration results from the metabolism of the neurotransmitter acetylcholine, so it is reasonable that the choline signal be partially TTX dependent. The specificity of the TTX response at these sensors confirms the selectivity of sensors constructed with oxidase enzymes for the substrate of interest.

Glutamate is the major excitatory neurotransmitter used by the brain, making the development of a method that reliably measures the neuronal component of the extracellular glutamate concentration

extremely desirable. Having done so, we are now able to make use of these sensors to address various issues of neurochemical interest. One such question is: what is the basal extracellular glutamate concentration? Our results provide a value in striatum of 30 μ M. This is higher than the values of 1 to 4 μ M provided by microdialysis measurements [92–98], consistent with the idea that microsensors measure close to neuronal terminals where concentrations are highest. Another area of interest is the interaction between glutamate and other brain neurotransmitters. We have just begun to study the interaction effect of dopamine and dopaminergic drugs on extracellular glutamate concentration, and we are able to observe an interaction.

An additional application of sensors based on oxidase enzymes is that they can be modified to respond only to changes in extracellular peroxide, a species of interest in the study of oxidative stress. Many neurodegenerative diseases, including Parkinson's disease, are thought to result at least in part, from oxidative stress, a condition

characterized by the excessive production of reactive oxygen species, including hydrogen peroxide (H_2O_2) [99–105]. Since dopamine is susceptible to autooxidation and to oxidative deamination by monoamine oxidase (MAO) during its metabolism, and both of these oxidative processes lead to the formation of peroxide, an increase in dopamine release may induce an overproduction of peroxide. Therefore, the direct *in vivo* measurements of peroxide would potentially provide insight into the dopaminergic induction of oxidative stress.

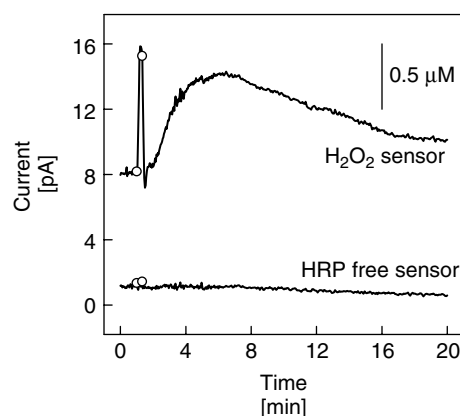
Recently, we have used microsensors selective for peroxide to monitor the *in vivo* formation of peroxide in rat striatum following electrical and pharmacological manipulations of the dopamine system [22]. These studies reveal a biphasic increase in peroxide in striatum upon brief (10 s) electrical stimulation of the MFB (Fig. 10), demonstrating that our sensors are able to monitor the real-time formation of peroxide *in vivo*. The combination of selective and sensitive hydrogen peroxide microsensors with selective axonal stimulation provided a valuable new approach to the investigation of the neurodegenerative mechanisms associated with Parkinson's disease.

14.8

Conclusion

In this chapter, we have tried to illustrate the power of microelectrode-based techniques that have been developed for monitoring ongoing neurochemical events in the living brain. We have not dwelt on the technical details of the electroanalytical methods themselves: these are both well known to the likely readers of a volume such as this and are readily found in the original citations we have provided. Rather, our goal has been to focus attention on the unique capabilities of microelectrode-based measurements, which are mainly derived from the minimal tissue disruption that the electrodes inflict on the brain. The minimal tissue disruption makes it possible to implant these microelectrodes to within micrometer, maybe even sub-micrometer, distances of intact, viable axonal terminals. Hence, microelectrodes allow concentrations of neurochemically active substances to be observed in the most important location within the tissue, namely, right at the site of action of the neurochemicals themselves. To date, no other technique permits monitoring in this prime location.

Fig. 10 Signals recorded *in vivo* with peroxide microsensor and HRP free background sensor during an electrical stimulation of the MFB. Open circles denote the beginning and end of the electrical stimulation. The scale bar was calculated based on postcalibration results.



References

1. P. T. Kissinger, J. B. Hart, R. N. Adams, *Brain Res.* **1973**, 55, 209–213.
2. J. E. Baur, E. W. Kristensen, L. J. May et al., *Anal. Chem.* **1988**, 60, 1268–1272.
3. M. E. Rice, C. Nicholson, *Anal. Chem.* **1989**, 61, 1805–1810.
4. D. J. Wiedemann, K. T. Kawagoe, R. T. Kennedy et al., *Neuroscience* **1988**, 25, 513–524.
5. P. Brun, M. F. Suaud-Chagny, F. Gonon et al., *Eur. J. Pharmacol.* **1993**, 235, 205–210.
6. P. Brun, M. F. Suaud-Chagny, F. Gonon et al., *Neuroscience* **1993**, 52, 961–972.
7. P. Bickford-Wimer, K. Pang, G. M. Rose et al., *Brain Res.* **1991**, 558, 305–311.
8. L. C. Daws, G. A. Gerhardt, A. Frazer, *Neurosci. Lett.* **1999**, 266, 165–168.
9. L. C. Daws, G. M. Toney, G. A. Gerhardt et al., *J. Pharmacol. Exp. Ther.* **1998**, 286, 967–976.
10. J. A. Stamford, Z. L. Kruk, J. Millar, *Brain Res.* **1990**, 515, 173–180.
11. N. V. Kulagina, L. Shankar, A. C. Michael, *Anal. Chem.* **1999**, 71, 5093–5100.
12. Y. Hu, K. M. Mitchell, F. N. Albahadily et al., *Brain Res.* **1994**, 659, 117–125.
13. J. J. Burmeister, G. A. Gerhardt, *Anal. Chem.* **2001**, 73, 1037–1042.
14. J. Cui, N. V. Kulagina, A. C. Michael, *J. Neurosci. Methods* **2001**, 104, 183–189.
15. M. G. Garguilo, A. C. Michael, *Anal. Chem.* **1994**, 66, 2621–2629.
16. M. G. Garguilo, N. Huynh, A. Proctor et al., *Anal. Chem.* **1993**, 65, 523–528.
17. C. Desvignes, F. Robert, C. Vachette et al., *Neuroreport* **1997**, 8, 1321–1325.
18. M. N. Friedemann, S. W. Robinson, G. A. Gerhardt, *Anal. Chem.* **1996**, 68, 2621–2628.
19. H. Tu, J. Xue, X. Cao et al., *Analyst* **2000**, 125, 163–167.
20. C. Meyerhoff, F. Bischof, F. J. Mennel et al., *Biosens. Bioelectron.* **1993**, 8, 409–414.
21. M. Mascini, S. Fortunati, D. Moscone et al., *Clin. Chem.* **1985**, 31, 451–453.
22. N. V. Kulagina, A. C. Michael, unpublished observations.
23. R. T. Kennedy, S. R. Jones, R. M. Wightman, *Neuroscience* **1992**, 47, 603–612.
24. J. B. Zimmerman, R. M. Wightman, *Anal. Chem.* **1991**, 63, 24–28.
25. J. L. Peters, A. C. Michael, *J. Neurochem.* **2000**, 74, 1563–1573.
26. R. J. Preston, G. A. Bishop, S. T. Kitai, *Brain Res.* **1980**, 183, 253–263.
27. J. L. Peters, A. C. Michael, S. R. Sesack, unpublished observations.
28. J. R. Cooper, F. E. Bloom, R. H. Roth, *The Biochemical Basis of Neuropharmacology*, Oxford University Press, Oxford, 1991.
29. K. Fuxe, L. F. Agnati, (Eds.), *Volume Transmission in the Brain*, Raven Press, New York, 1991.
30. T. E. Robinson, J. B. Justice Jr., (Eds.), *Techniques in the Behavioral Neural Sciences*, Elsevier, Amsterdam, 1991, Vol. 7.
31. K. L. Clapp-Lilly, R. C. Roberts, L. K. Duffy et al., *J. Neurosci. Methods* **1999**, 90, 129–142.
32. R. E. Carson, M. E. Daube-Witherspoon, P. Herscovitch, (Eds.), *Quantitative Functional Brain Imaging with Positron Emission Tomography*, Academic Press, San Diego, 1998.
33. M. Laruelle, *J. Cereb. Blood Flow Metab.* **2000**, 20, 423–451.
34. Z. Zhou, S. Misler, *Proc. Natl. Acad. Sci.* **1995**, 92, 6938–6942.
35. G. Y. Chen, P. F. Gavin, G. A. Luo et al., *J. Neurosci.* **1995**, 15, 7747–7755.
36. P. M. Groves, J. C. Linders, S. J. Young, *Neuroscience* **1994**, 58, 593–604.
37. V. M. Pickel, S. C. Beckley, T. K. Joh et al., *Brain Res.* **1981**, 225, 373–385.
38. C. Nicholson, *Biophys. J.* **1995**, 68, 1699–1715.
39. J. Crank, *The Mathematics of Diffusion*, Clarendon, Oxford, 1975.
40. H. Yang, J. L. Peters, C. Allen et al., *Anal. Chem.* **2000**, 9, 2042–2049.
41. K. T. Kawagoe, P. A. Garriss, D. J. Wiedemann et al., *Neuroscience* **1992**, 51, 55–64.
42. C. Nicholson, M. E. Rice in *Volume Transmission in the Brain* (Eds.: K. Fuxe, L. F. Agnati), Raven Press, New York, 1991, pp. 279–294.
43. J. L. Peters, A. C. Michael, S. R. Sesack, unpublished observations.
44. Y. Lu, J. L. Peters, A. C. Michael, *J. Neurochem.* **1998**, 70, 584–593.
45. L. J. May, W. G. Kuhr, R. M. Wightman, *J. Neurochem.* **1988**, 51, 1060–1069.
46. P. A. Garriss, R. M. Wightman, *J. Neurosci.* **1994**, 14, 442–450.
47. S. R. Jones, P. A. Garriss, C. D. Kilts et al., *J. Neurosci.* **1995**, 64, 2581–2589.

48. R. M. Wightman, J. B. Zimmerman, *Brain Res. Rev.* **1990**, 15, 135–144.
49. W. G. Kuhr, J. G. Bigelow, R. M. Wightman, *J. Neurosci.* **1986**, 6, 974–982.
50. H. Yang, A. C. Michael, unpublished observations.
51. H. Yang, J. Qian, A. C. Michael, unpublished observations.
52. H. Yang, J. L. Peters, A. C. Michael, *J. Neurochem.* **1998**, 71, 684–692.
53. C. Allen, J. L. Peters, A. C. Michael, unpublished observations.
54. L. J. May, R. M. Wightman, *Brain Res.* **1989**, 487, 311–320.
55. C. Spyraiki, H. C. Fibiger, *Science* **1981**, 212, 1167, 1168–.
56. S. Fielding, M. R. Szwedczak *J. Clin. Psychiatry* **1984**, 45, 12–20.
57. A. Barbeau, F. H. McDowell, (Eds.), *L-Dopa and Parkinsonism*, F. A. Davis, Philadelphia, 1970.
58. D. B. Calne, M. Sandler, *Nature* **1970**, 226, 21–24.
59. J. R. Bunzow, H. H. M. van Tol, D. K. Grandy et al., *Nature* **1988**, 336, 783–787.
60. A. Dearry, J. A. Gingrich, P. Falardeau et al., *Nature* **1990**, 347, 72–76.
61. F. J. Monsma, L. C. Mahan, L. D. McVittie et al., *Proc. Natl. Acad. Sci. U.S.A.* **1990**, 87, 6723–6727.
62. P. Sokoloff, B. Giros, M. P. Martres et al., *Nature* **1990**, 347, 146–151.
63. R. K. Sunahara, H. C. Guan, B. F. O'Dowd et al., *Nature* **1991**, 350, 614–619.
64. H. H. M. van Tol, J. R. Bunzow, H. C. Guan et al., *Nature* **1991**, 350, 610–614.
65. Q. Y. Zhou, D. K. Grandy, L. Thambi et al., *Nature* **1990**, 347, 76–80.
66. C. Missale, S. R. Nash, S. W. Robinson et al., *Physiol. Rev.* **1998**, 78, 189–225.
67. R. M. Wightman, C. Amatore, R. C. Engstrom et al., *Neuroscience* **1988**, 25, 513–522.
68. A. Gratton, R. Wise, *J. Neurosci.* **1994**, 14, 4130–4144.
69. E. A. Kiyatkin, *Eur. J. Neurosci.* **1993**, 5, 284–291.
70. R. J. Olson, J. B. Justice Jr., *Anal. Chem.* **1993**, 65, 1017–1022.
71. P. M. Sam, J. B. Justice Jr., *Anal. Chem.* **1996**, 68, 724–728.
72. L. H. Parsons, J. B. Justice Jr., *J. Neurochem.* **1992**, 58, 212–218.
73. J. L. Peters, H. Yang, A. C. Michael, *Anal. Chim. Acta* **2000**, 412, 1–12.
74. J. L. Peters, A. C. Michael, *J. Neurochem.* **1998**, 70, 594–603.
75. C. R. Gerfen, T. M. Engber, L. C. Mahan et al., *Science* **1990**, 250, 1429–1432.
76. A. Cheramy, R. Romo, G. Godeheu et al., *Neuroscience* **1986**, 19, 1081–1090.
77. D. W. Clow, K. Jhamandas, *J. Pharmacol. Exp. Ther.* **1988**, 248, 722–728.
78. M. M. Iravani, Z. L. Kruck, *J. Neurochem.* **1996**, 66, 1076–1085.
79. S. Jin, B. B. Fredholm, *Br. J. Pharmacol.* **1997**, 121, 1269–1276.
80. D. Martinez-Fong, M. G. Rosales, J. L. Gongora-Alfaro et al., *Brain Res.* **1992**, 595, 309–315.
81. G. Segovia, A. Del Arco, F. Mora, *J. Neurochem.* **1997**, 69, 1476–1483.
82. Y. Wu, S. M. Pearl, M. J. Zigmond et al., *Neuroscience* **2000**, 96, 65–72.
83. K. D. Youngren, D. A. Daly, B. Moghaddam, *J. Pharmacol. Exp. Ther.* **1993**, 264, 289–293.
84. N. V. Kulagina, M. J. Zigmond, A. C. Michael, *Neuroscience* **2001**, 102, 121–128.
85. H. Yang, A. C. Michael, unpublished observations.
86. A. D. Smith, J. B. Justice Jr., *J. Neurosci. Methods* **1994**, 54, 75–82.
87. N. B. Mercuri, F. Stratta, P. Calabresi et al., *Neurosci. Lett.* **1991**, 131, 145–148.
88. L. C. Einhorn, P. A. Johansen, F. J. White, *J. Neurosci.* **1988**, 8, 100–112.
89. K. A. Keefe, M. J. Zigmond, E. D. Abercrombie, *Neuroscience* **1992**, 47, 325–332.
90. D. W. Miller, E. D. Abercrombie, *Brain Res. Bull.* **1996**, 40, 57–62.
91. B. Moghaddam, R. J. Gruen, *Brain Res.* **1991**, 544, 329, 330.
92. M. W. Lada, T. W. Vickroy, R. T. Kennedy, *J. Neurochem.* **1998**, 70, 617–625.
93. M. Herrera-Marschitz, Z. B. You, M. Gojny et al., *J. Neurochem.* **1996**, 66, 1726–1735.
94. J. Semba, S. Kito, M. Toru, *J. Neural Transm.* **1995**, 100, 39–52.
95. M. Shiraishi, Y. Kamiyama, P. C. Huttemeier et al., *Brain Res.* **1997**, 759, 221–227.
96. E. Zilkha, T. Obrenovitch, A. Koshy et al., *J. Neurosci. Methods* **1995**, 60, 1–9.
97. O. Niwa, K. Torimitsu, M. Morita et al., *Anal. Chem.* **1996**, 68, 1865–1870.
98. M. W. Lada, T. W. Vickroy, R. T. Kennedy, *Anal. Chem.* **1997**, 69, 4560–4565.
99. S. Fahn, G. Cohen, *Ann. Neurol.* **1992**, 32, 804–812.

100. H. S. Maker, C. Weiss, D. J. Silides et al., *J. Neurochem.* **1981**, 36, 589–593.
101. B. Halliwell, *J. Neurochem.* **1992**, 59, 1609–1623.
102. J. T. Coyle, P. Puttfarcken, *Science* **1993**, 262, 689–695.
103. M. E. Gotz, G. Kunig, P. Riederer et al., *Pharmacol. Ther.* **1994**, 63, 37–122.
104. P. Jenner, C. W. Olanow, *Neurology* **1996**, 47, 161S–170S.
105. N. A. Simonian, J. T. Coyle, *Ann. Rev. Pharmacol. Toxicol.* **1996**, 36, 83–106.

15

Potentiometric Measurements of Proteins

Jackson Pellett and Marian Stankovich
Chemistry Department, University of Minnesota, Minneapolis, MN, USA

15.1	Introduction	487
15.1.1	What Electrochemical Studies Can Tell Us	487
15.1.2	Direct versus Indirect Electrochemistry	488
15.2	Materials	490
15.2.1	Mediator Titrant	490
15.2.2	Redox Indicators	491
15.3	Apparatus – Glassware Components for Anaerobiosis	492
15.3.1	Argon Line	492
15.3.2	The Cell Parts: Preparation of Auxiliary, Reference, and Working Electrodes	493
15.4	Methods – Setting up the Mediated Electron Transfer Experiment	497
15.4.1	The Coulometric Titration	497
15.4.2	The Potentiometric Titration	501
15.5	Data Analysis and Sample Systems	503
15.5.1	Coulometric Titration	503
15.5.2	Potentiometric Titration	505
	References	509

15.1

Introduction

Why is the redox potential measurement of enzymes important?

Many enzymes use redox centers to store and transfer electrons during catalysis. These redox centers can be composed of metals such as iron or cobalt, or organic cofactors such as quinones, amino acid radicals, or flavins. In order to fully appreciate the catalytic mechanisms of these enzymes, it is often necessary to determine the free energy required to reduce or oxidize their protein redox centers. This is called the redox potential. The measurement of enzyme redox potentials can be performed by either direct or indirect electrochemical methods. The type of electrochemistry suitable for a particular protein system is simply dictated by the accessibility of its redox center to the electrode surface. Because most reactions catalyzed by enzymes occur within hydrophobic pockets of the protein, the redox sites are often far from the surface of the protein. Unless an electron transfer path exists from the protein surface to the redox center, it is not feasible to use direct electrochemistry to measure the redox potential. Since only a few enzymes (most notably certain heme-containing enzymes) have such electron transferring paths and

are thus amenable to direct electrochemical study, this review will focus primarily on indirect electrochemical methods for studying redox active enzymes. Unless otherwise stated, the potentials determined in this work are reported as formal potentials at pH 7.0 ($E^{\circ'}$) versus the standard hydrogen electrode (SHE). This nomenclature is frequently used by biochemists, as the physiologically relevant pH for biological molecules is generally close to neutral. In reporting a formal potential for a particular protein, we ascertain that it obeys the Nernst equation under a set of very specific conditions of ionic strength, pH, temperature, and protein concentration.

Although the formal potential is reported versus the SHE, the measurements are made using a silver–silver chloride reference electrode that is calibrated versus ferri/ferrocyanide.

Before discussing the specific electrochemical methods used to measure protein redox potentials, we will examine the type of information that an enzymologist can obtain from electrochemical studies.

15.1.1

What Electrochemical Studies Can Tell Us

It is crucial that the redox potentials of enzymes that catalyze reactions involving electron transfer be rigidly controlled.

This is true because the interactions between the protein and redox center enable enzymes to modulate the redox properties of the limited number of metals and cofactors available in nature. This regulation arises from the tighter binding by the apoprotein of one oxidation state of the redox active cofactor relative to the other oxidation state. This is illustrated in Fig. 1 for the noncovalent binding of flavin adenine dinucleotide (FAD) to porcine medium-chain acyl-CoA dehydrogenase (MCAD). As a result of the tighter binding of the two-electron-reduced FAD ($\text{FADH}_{2\text{-red}}$) to MCAD ($K_a = 2 \times 10^6$ vs $K_a = 6 \times 10^8$), the redox potential for the two-electron reduction of FAD is shifted negative by 74 mV upon protein binding [1]. Several factors can account for the preferential binding of one oxidation state of a metal or cofactor over another. These include the formation of covalent and hydrogen bonds as well as electrostatic and solvent interactions with the redox center. Since changes in these interactions can have profound

effects on the redox potentials of the species involved, the redox properties of enzymes can also serve as sensitive probes of the protein environment surrounding the redox center. For instance, changes in the ionization state of amino acids in the vicinity of redox centers may perturb the redox potential of the enzyme. These redox-linked ionizations have been used successfully to assign $\text{p}K_a$ s of certain residues in the active sites of several enzymes [1–3].

15.1.2

Direct versus Indirect Electrochemistry

The electrochemical properties of most of the metals and cofactors used by enzymes can be characterized using standard direct voltammetric electrochemical methods (see Chapter 1 by Fraser Armstrong and Chapter 11 by Katsomi Niki). When free in solution, these species interact well with a variety of different electrodes and usually exhibit Nernstian behavior upon oxidation or reduction. The incorporation

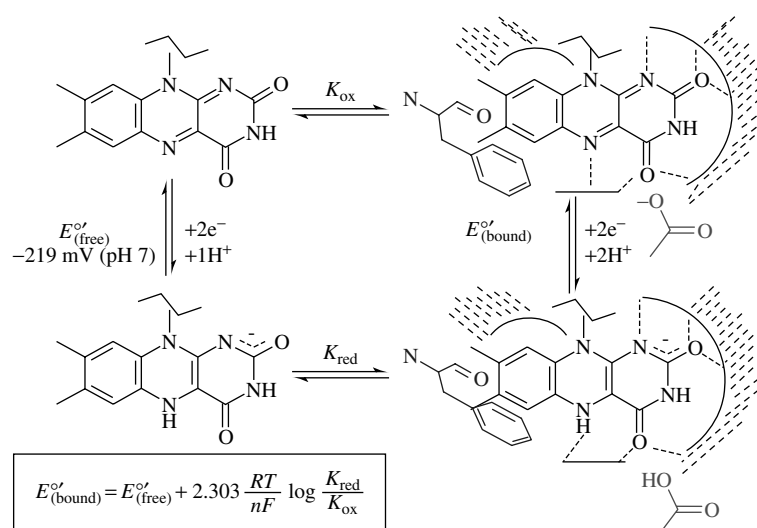


Fig. 1 Regulation of redox potential.

of these species into the protein matrix, however, usually results in unfavorable electron transfer properties between the redox center and most electrodes. In some circumstances, it is possible to construct modified electrode surfaces that do interact well with certain proteins [4, 5].

One advantage of being able to perform the voltammetric analysis of enzymes is that it is possible to obtain information about the kinetics of electron transfer by varying the scan rate. It is crucial, however, that proper control experiments be performed to demonstrate that interactions between the modified electrode and enzyme are not perturbing the electrochemical properties of the enzyme. In the likely event that voltammetric analysis is not feasible for a particular protein system, indirect electrochemical methods are often successful.

An advantage of dynamic techniques such as cyclic voltammetry is that potentials of unstable states can be more readily evaluated. They are most applicable to proteins whose function is to transfer electrons (cytochromes, ferredoxins, etc.) rather than catalyze redox reactions. Flavoproteins and dinuclear iron proteins are in this category: they have the equivalent of very low self-exchange rates, meaning that they cannot readily transfer electrons to each other, and they also do not interact well with electrodes. This is because their active sites are only accessible to small molecules. Accessibility to active sites of enzymes is also a topic that has been addressed by Willner in Chapter 17 in this volume. In our flavoprotein and dinuclear iron cluster work, we will consider only those proteins that have the dual function of transferring electrons and selectively catalyzing reactions.

Four different indirect methods that rely on UV-visible spectroscopy have been

successfully used to determine the redox potentials of proteins. In the first method to be developed, sodium dithionite is used as a reductant in an anaerobic cell, with the spectral changes of enzymes and redox indicator dyes monitored as a function of the amount of reductant added [6–9]. Massey devised a second method, which uses 5-deazaflavin and ethylenediaminetetraacetic acid (EDTA) light to generate the powerful reductant, the deazaflavin radical [10]. Spectral changes are monitored as a function of irradiation time. A third method was later developed by Massey, in which a large amount of xanthine (the reductant) and a small amount of xanthine oxidase (the catalyst) are added initially to a solution of enzyme and redox indicator dye. Note that in contrast to other methods, the reductant is *not* added stepwise but batchwise at the beginning of the experiment. The amount of xanthine oxidase catalyst used is also very small to allow the reduction to proceed relatively slowly, allowing sufficient time for the enzyme and mediator to equilibrate during the entire course of the reduction. Spectra are taken during the course of the reduction. Since both the enzyme and dyes are spectrally active, the position of equilibrium at each point of the reduction is used to calculate the redox potential of the enzyme [11].

The redox potential of the mediator dye–enzyme system is not measured directly using reference and indicator electrodes in any of the methods just described. In contrast, our spectroelectrochemical method [12], which is based on the methods of Kuwana [13] and Wilson [14], is still an indirect method. We use mediator dyes, which are in equilibrium with the enzyme and have the advantage of measuring the potential that is associated with each equilibrium position of the dye and enzyme as both

become reduced in a reductive titration. In order to do this, we have designed an anaerobic cell in which both spectral and electrochemical measurements may be made. All the components – custom made electrodes, reference, auxiliary, and working – are designed to fit into the cell. A spectrophotometer is required, as well as a potentiostat to electrochemically generate a titrant and measure equilibrium redox potentials.

15.2

Materials

This chapter provides the reader with the background necessary to determine the redox potentials of proteins using gold electrodes whose surfaces are unmodified, so that the potential measurements rely on the equilibration of enzymes and redox mediators. The electrodes sense the potential of the mediator dyes, not the enzyme; that is why this is termed an *indirect electrochemical approach*. This indirect method is useful because the active sites of most enzymes are buried and do not interact well with modified or unmodified electrodes. Although this indirect method was originally designed to work on flavoproteins, it has been applied to enzymes containing a variety of redox and spectrally active cofactors. The chemical reduction that takes place is very similar to what we find in a dithionite titration, except that in this case the titrant is generated in situ electrochemically. The titrant then transfers electrons quantitatively to the enzyme. When the potential is measured, a second molecule, a redox indicator is present to equilibrate with the partially reduced enzyme and the electrode, which now acts as a redox sensor. It can now be seen that the working electrode plays two roles

in these experiments: first, its potential is controlled at a negative value to reduce the mediator titrant, and second, when the enzyme and mediator dye are allowed to equilibrate at open circuit, the electrode merely reports the potential achieved at equilibrium.

This method was developed to overcome several disadvantages of the earlier dithionite titration method, the most severe being the complexation of the flavoprotein oxidases by bisulfite, an oxidation product of dithionite [15]. The present method presents additional advantages: it is able to generate many redox titrants in situ without standardization by titration, and has a more flexible experimental design, as indicated in the following section.

15.2.1

Mediator Titrant

On the basis of the work of Szentirmai and Kuwana [13], methyl viologen (MV^{++}) was chosen as the electrogenerated mediator titrant. MV^{++} has a negative redox potential, (-450 mV) and once reduced at the electrode, quantitatively transfers electrons to most flavoproteins and other redox enzymes, with redox potentials in the range of -100 to -350 mV. MV^{++} has other advantages as a mediator titrant (Table 1): (1) its oxidized form does not absorb visible light, so its spectrum does not interfere with that of the enzyme; (2) it reacts quickly with the electrode and is able to transfer electrons quickly and quantitatively to many enzyme active sites, even to those of enzymes that cannot be reduced by dithionite. Methyl viologen's unique reactivity may be due to its aromatic character and the fact that it is positively charged even in the reduced state, in contrast to most other dyes that are negatively charged

Tab. 1 Selected redox potentials of mediator/titrants

$E^{\circ'}$ (mV vs SHE) ^a	Compound	Reference
465	1,1'-bis(hydroxymethyl)ferrocene	13
425	Ferri/ferrocyanide	17
422	Ferrocene	13
92	Phenazine methosulfate	6
60	1,4 naphthoquinone	6
55	Phenazine methosulfate	6
5	Methylene blue	6
0	Duroquinone	6
−3	5-hydroxy-1, 4-naphthoquinone	13
−10, −19	Pyocyanine	6, 13
−46	Indigo-tetrasulfonic acid	6
−116	Indigo-disulfonate	6
−133	2-amino-1,4 naphthoquinone	13
−139	2-hydroxy-1,4-naphthoquinone	6
−150	8-Cl-riboflavin	18
−208	Riboflavin, FAD, FMN ^b	6
−225	Anthraquinone -2-sulfonate	6
−244	Phenosafranin	6
−325	Neutral red	6
−350	Benzyl viologen	6
−446	Methyl viologen	6, 13

^aPotentials measured at pH 7.^bFlavin mononucleotide.

or neutral; (3) it is a good redox indicator for enzymes with negative potentials; and (4) the characteristic spectrum of reduced methyl viologen ($MV^{+•}$) signals the end point of the titration. The advantage of using MV^{++} is that it can be present at high concentrations (0.1 mM) to rapidly transfer electrons to the enzyme (10 μ M). Speed is important in “coulometric titration” where we are counting the number of electrons required to reduce the enzyme in order to minimize the time in which oxygen leaks can occur.

While benzyl viologen is similar in structure to MV^{++} , its potential is more positive ($E^{\circ'} = 350$ mV). It can be used as an alternative mediator titrant for an enzyme if binding to an enzyme by MV^{++} is suspected. A reductive titration with dithionite can be used as a control to test

to see if MV^{++} is binding to the enzyme under study.

Ferrocene is used as an oxidative titrant – its potential is much more positive than those of the enzymes (+0.5 V), so it can be used as a chemically generated oxidant, useful for reversing the reduction reaction.

15.2.2

Redox Indicators

These dyes are spectrally and redox active, and must have redox potentials near that of the enzyme to function as a “redox buffer”. The potential of the enzyme is measured at equilibrium after a certain number of reducing equivalents have been transferred. The dye equilibrates with the partially reduced enzyme at open circuit to

produce partially reduced dye and partially reduced enzyme. The working electrode, acting as an indicator electrode, reports the potential of the dye–enzyme mixture. Since the indicator dye is the link to the electrode in the equilibrium mixture, these dyes *must* (1) be able to equilibrate both with the enzyme active site and the electrode, (2) exhibit reversible electron transfer behavior themselves, and (3) be stable under experimental conditions. They *must not* bind to the enzyme. After equilibrium is reached, more reducing equivalents are added, so that a Nernst plot can be constructed and $E^{\circ'}$ and n can be obtained. (Equilibrium is determined to be the point at which the potential and spectra of enzyme and dye stop changing.)

Extensive lists of redox indicator dyes are given in Clark [6], Kuwana [13], and the *CRC Handbook of Biochemistry* [16]. Some of the best indicator dyes for flavoproteins and dinuclear iron proteins are pyocyanine, indigo disulfonate (IDS), 8-chlororiboflavin, and lumiflavin acetate. Redox indicator dyes must be titrated, and their spectra and potentials determined under conditions of temperature, pH, and buffer identical to those in the enzyme experiments to allow for spectral correction.

15.3

Apparatus – Glassware Components for Anaerobiosis

In order to perform any of these studies, the system has to be made oxygen-free and maintained in this state if quantitative electron transfer to the proteins and mediator system is to occur, making it necessary to install an argon/vacuum line, with scrubbers; special spectroelectrochemical cells are needed as well. This elaborate setup

for oxygen removal and anaerobic maintenance is necessary because the simpler methods of oxygen removal, such as bubbling argon or electrochemical scrubbing, cannot be used with proteins because they lead to denaturation.

Since the system design is driven by the requirement for anaerobiosis, the electrodes must fit inside a spectrophotometric cuvette whose contents have previously been made anaerobic by the procedure described in the following section. The electrodes must also be custom made to fit inside without leaking oxygen, either around the joints or through the tips. They must also be stored anaerobically between experiments (see following section).

15.3.1

Argon Line

Figure 2 illustrates a typical anaerobic train that can be used to remove dissolved oxygen from buffers and protein solution. Pure argon (99.99%) is passed first through an Oxyclear disposable cartridge (Fisher) and then over activated Ridox catalyst (Fisher) to remove all residual oxygen. While the Ridox scrubber can be used at room temperature, unlike some other scrubbers, it is important that it be activated according to the manufacturer's instructions before it is first used. This is done by heating the scrubber to 215 °C while a 10% hydrogen and argon mixture is passed over the Ridox, liberating water. Once activated, the Ridox turns reddish. After the activated Ridox is cooled by flowing argon, the line is ready to run. The pressure is maintained at 5 psi, using a regulator to keep excess pressure from building up in the line. The second side of the nitrogen line is attached to a vacuum pump, making it possible to switch between positive gas pressure and a

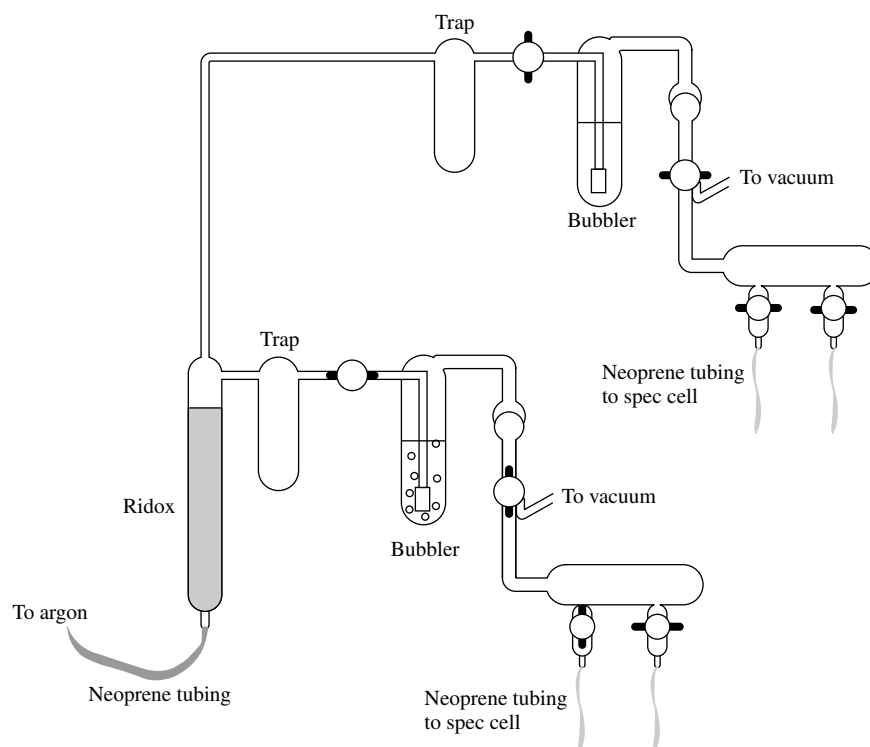


Fig. 2 Argon line.

vacuum by turning the two-way stopcock. This will be necessary when degassing protein solution (see following text). Neoprene rubber tubing is used to connect the cells to the argon line because the oxygen permeability of neoprene is much lower than that of other polymers, for example, Tygon. Once in operation, the argon line can be maintained to give 1-ppm O_2 .

15.3.2

The Cell Parts: Preparation of Auxiliary, Reference, and Working Electrodes

Working, auxiliary, and reference electrodes are custom made to fit individual spectroelectrochemical cells. Three factors should be considered when designing

these electrodes. First, all the electrodes must be long enough to make contact with the protein solution. Second, the tips of the electrodes must be thin enough to fit comfortably inside a 1 cm × 1 cm square cuvette. Third, the electrodes must be capable of being made anaerobic.

The components of a silver–silver chloride *reference electrode* are shown in Fig. 3. First, cleaned silver wire is epoxied into a 7/25 female ground glass joint. A layer of AgCl is then deposited on the silver by dipping the wire into a HCl:HNO₃ (3:1) solution. A small thirsty glass plug (Bioanalytical Systems; BAS) is attached with heat-shrink tubing to the end of the slender glass sleeve (made by the glass blower) that is topped by back-to-back male

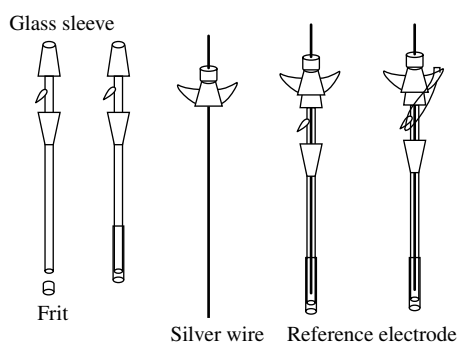
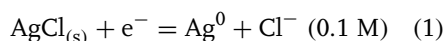


Fig. 3 Reference electrode components and assembly.

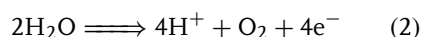
7/25 ground glass joints. This thirsty glass capped sleeve provides electrical contact between the electrode and the solution without allowing the analyte solution to mix with the electrolyte. The sleeve is filled with a 0.10 M KCl solution saturated with AgCl. The silver wire is inserted and the 7/25 ground glass joint is sealed with Apiezon N stopcock grease. The silver–silver chloride reference electrode is now complete. The equation that governs the potential of this reference electrode is:



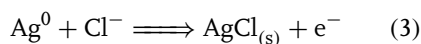
Because the electrode's potential is dependent on the type of crystal structure of the $\text{AgCl}_{(s)}$ that is used, as well as other factors, the potential is standardized by measuring it versus that of standard ferri/ferrocyanide solution, as described below [17]. It remains sealed and is not remade frequently. Since this electrode remains sealed, its potential remains relatively constant. However, its potential is checked before each experiment. The potential difference is about -144 mV , which indicates that the reference electrode is 144 mV more negative than the $+425 \text{ mV}$ of the ferri/ferrocyanide, or $+281 \text{ mV}$ versus SHE. This is close to what one would calculate for a silver–silver chloride electrode with 0.1 M chloride.

The ferri/ferrocyanide system must be kept out of light and free of oxygen in order to be stable. The solution should also be made fresh daily.

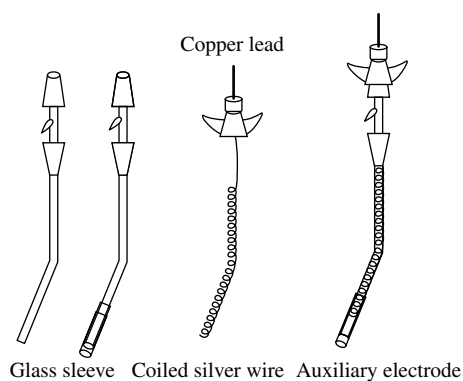
The *auxiliary electrode* has an unusual composition, designed to prevent the generation of oxygen. This is important because most of the reactions taking place at the working electrode are reductions; thus, equal and opposite reactions (oxidation) will be taking place in the auxiliary electrode. If oxygen were generated, it could diffuse into the solution, reoxidizing the enzyme analyte. To prevent oxygen being generated from the water as would occur at a typical auxiliary electrode in an aqueous solution containing a supporting electrolyte, the composition of the auxiliary electrode is modified.



The modified auxiliary electrode is a silver wire in contact with 0.1 M KCl. In this case, since the oxidation described in Reaction (3) is easier to carry out than that described in the oxidation of water (Reaction 2), Reaction (3) would occur preferentially.



To achieve this end, the composition of the auxiliary electrode is very similar

Fig. 4 Auxiliary electrode components and assembly.

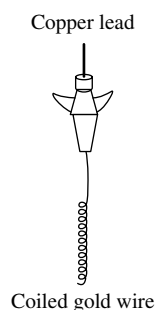
to that of the reference electrode, except the electrode area is much larger, equal to that of the working electrode (Fig. 4). In the auxiliary electrode, silver wire is encased (enclosed) in a glass sleeve tipped with thirsty glass to allow electrical contact with the solution, while preventing the electrode compartment contents from mixing with the solution. This glass sleeve is filled with 0.1 M KCl. Sometimes an oxygen scrubber such as glucose–glucose oxidase is added to the auxiliary electrode. The electrode must be remade before each experiment because, unlike the reference electrode, its composition changes with time as oxidation and reduction occur, and products buildup in the solution.

Finally, the *working electrode* is a coiled gold wire. As shown in Fig. 5, gold wire is

sealed into a female 7/25 ground glass joint with epoxy. The gold wire is then cleaned with a slurry of ethanol and silica before being coiled. The coiled gold electrode is rinsed between experiments.

All three electrodes, the reference, the auxiliary, and the working, are fine-tuned to fit into the cramped spectroelectrochemical cell. None of these electrodes are in the optical path. The current path is not optimized inside the cell because the IR drop is not large in aqueous solutions.

The *electrode storage cell* (Fig. 6) is used to store the reference and auxiliary electrodes anaerobically between experiments to prevent oxygen from being absorbed by the thirsty glass and then diffusing into the solution during experiments. The electrodes are transferred from the storage cell to the degassed spectroelectrochemical cell

**Fig. 5** Working electrode.

Coiled gold wire

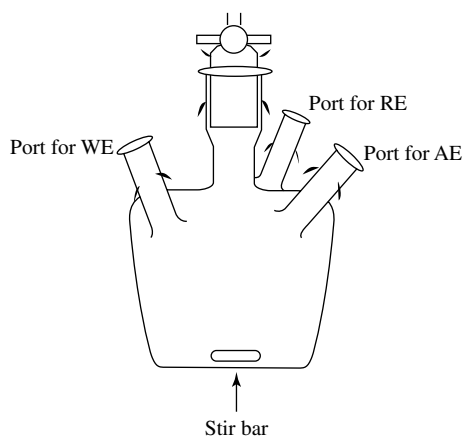
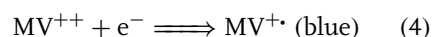


Fig. 6 Storage cell.

under positive argon pressure (see following text).

The storage cell contains MV^{++} in buffer, which has been degassed by 10 min of argon bubbling. The electrodes are placed in the cell under positive Argon pressure. The potential of the working electrode (another gold electrode in the storage cell) is then controlled at a negative value (-550 mV vs SHE) and the MV^{++} solution is reduced until it turns blue. This way the electrodes are stored in reduced

solution.



In Fig. 7, the *spectroelectrochemical cell* and stir bar are shown without electrodes, with ground glass plugs in the 7/25 and 10/25 female joints designed to hold the electrodes. The cell is configured as it would be for anaerobiosis. The cell is made of glass or quartz; and no graded seals that would increase the cell volume are used. The bottom part is a glass cuvette made

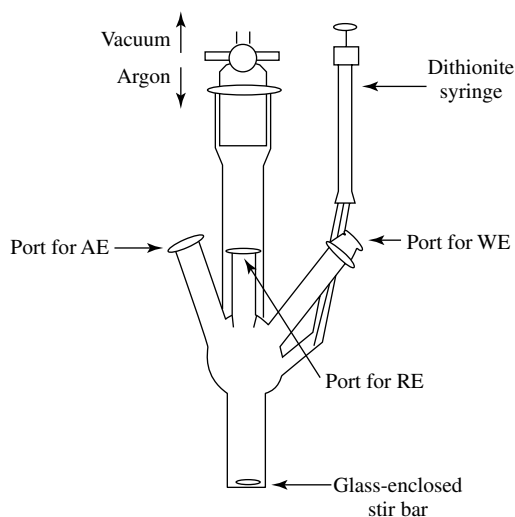


Fig. 7 Spectroelectrochemical cell without electrodes. Ports are sealed using ground glass plugs before anaerobic procedure.

up of square glass tubing, onto which a superstructure is attached: three female ground glass joints or ports for electrodes, and a long glass sidearm (extension) topped by a stopcock and ground glass joint for connection to the argon line. The ports are adjusted for fitting the electrodes. There is a small glass sidearm near the top of the extension (sidearm) that provides the option of adding other reagents after the cell containing the enzyme solution has been made anaerobic. There is a glass-encased stirrer for mixing during electrochemical reduction. Some researchers add scrubbers to the sidearm or to the analyte solution. The cell is optimized so that it will sit in the spectrophotometer to be used in the experiments.

15.4 Methods – Setting up the Mediated Electron Transfer Experiment

Two types of reductive titration experiments, namely, coulometric and potentiometric, will be described. This is because two kinds of experiments are required to completely characterize an enzyme, namely, measurement of n and of $E^{\circ'}$ since mediators and other conditions differ for the two measurements. Even so, the cell used and the anaerobic requirements are the same: in both experiments a bulk electrolytic reduction is performed in a spectrophotometric cell and the spectral changes are monitored as a function of the number of reducing equivalents added.

15.4.1 The Coulometric Titration

First, the enzyme solution is prepared by adding concentrated enzyme solution and

MV⁺⁺ to buffer solution in the open aerobic spectroelectrochemical cell. The buffer also serves as a supporting electrolyte. The stirrer is added. The volume of the enzyme solution is typically 4.3 ml, which is sufficient for immersing the electrodes (which are out of the optical path) and filling the optical path. The enzyme concentration is determined by measuring the absorbance of the enzyme solution in the open spectroelectrochemical cuvette. The enzyme concentration required for the experiment is dictated by the absorbance change desired, about 0.1–0.2 absorbance units during the entire coulometric titration. This requires a solution of about 10 μ M for an enzyme that has a molar absorptivity of about 10 000 M⁻¹ cm⁻¹. The viologen concentration is about 100 μ M. Oxidized MV⁺⁺ does not absorb in the visible region, so it does not interfere with the absorbance reading for the enzyme. A buffer solution is chosen in which the enzyme will be stable, for example, 50 mM phosphate at controlled pH. Additional supporting electrolyte is not added because many ions may bind to enzyme or interfere with the binding of other ligands, which are under investigation. The cell temperature is maintained at a temperature at which the enzyme is most stable. Glycerol can be added to the buffer to stabilize protein, and if necessary, to prevent protein precipitation out of solution, since glycerol does not seem to interfere with electrochemical measurements themselves, although it can influence the slope of Nernst plots. The spectrum of the enzyme solution in the spectroelectrochemical cell is taken before and after degassing in order to establish whether solvent evaporation occurred during degassing, leading to a change in volume and concentration.

After the spectrum is recorded, the cell is made anaerobic as follows:

1. An elaborate procedure is required for degassing protein solutions, because ordinary bubbling of argon through the solution causes bubbling and foaming of the protein, leading to protein denaturation. Since anaerobiosis cannot be induced with the electrodes in place, the electrode ports are sealed by inserting matched ground glass plugs to which Apiezon N grease has been applied (Fig. 7). In order to make a protein solution anaerobic, the lower part of the spectroelectrochemical cell is immersed in an ice bath (to lower the vapor pressure of the solution and to help stabilize the enzyme). The cell is then attached to the argon line via the Neoprene tubing, the stopcock at the top is opened, and a vacuum is applied. As the first bubbles start to form in the enzyme solution, the cell is slowly back-filled with argon. It is then turned, and the solution is tipped into the large sidearm extension of the cell
2. to maximize the surface area of the enzyme solution. Next, the cell is gently rocked to promote gas exchange with the argon of the atmosphere. The cell is rocked for about 5–10 min, reimmersed in the ice bath, held upright, and a vacuum applied again. This cycle is repeated about 10 times over the course of 1.5 h.
3. When anaerobiosis is complete, the spectroelectrochemical cell is clamped in position under positive argon pressure.
4. The auxiliary and reference electrodes are removed from their anaerobic storage cell, the plugs are removed from the spectroelectrochemical cell, and the electrodes are quickly inserted into the spectroelectrochemical cell under positive argon pressure (the reference electrode needs to be standardized against ferri/ferrocyanide, either before the start of the titration or at the end of the experiment, depending on the experiment (see following text)).
5. The gold working electrode does not need to be stored anaerobically, so it

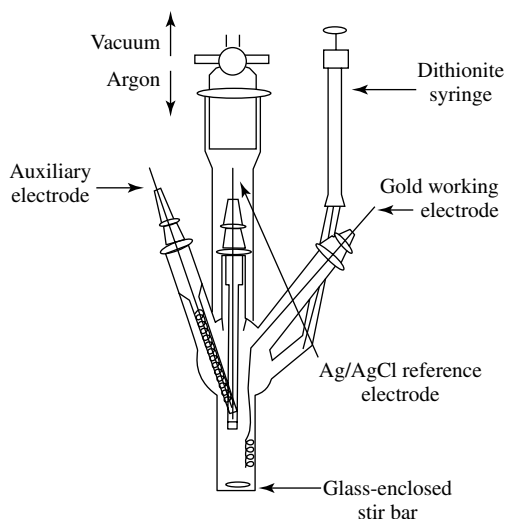


Fig. 8 Spectroelectrochemical cell with electrodes.

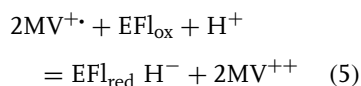
is just greased and inserted into the spectroelectrochemical cell.

5. The spectroelectrochemical cell is sealed by turning the stopcock at the top of the cell, so that the cell is shut off from the argon line. The cell is then removed and placed in the spectrophotometer, which is equipped with a stirrer and a temperature control apparatus. Figure 8 shows the assembled cell.

6. A spectrum is recorded; then appropriate leads from the potentiostat are connected to the reference, working, and auxiliary electrodes. The stirrer is turned on.

Several good potentiostats with current integration and the ability to measure open circuit potentials are available. One is produced by BAS (West Lafayette, IN), the CV-50 W (\$12 000), and two by CH Instruments (Austin, TX), the CHI600A for \$6000, and possibly the CHI1200 for \$2500.

7. In order to perform electrochemical reduction, the potential of the working electrode is set and maintained at a value at least 100 mV more negative than that of the MV^{++} redox potential (-450 mV vs SHE), so that the viologen is reduced to produce $MV^{+\bullet}$ radical, which is highly colored (ϵ at 600 nm is $12\,000\text{ M}^{-1}\text{ cm}^{-1}$). MV^{++} is reduced at the working electrode (as shown in Eq. 4) and transfers electrons quantitatively to the protein (flavoprotein, EFl_{ox}), which is now undergoing a two-electron transfer, as shown below:



The potential of the working electrode should not be controlled at

too negative a value for two reasons. First, a second electron will transfer to $MV^{+\bullet}$, forming MV, an insoluble material. Second, the hydrogen ions may be reduced to hydrogen gas, a process that utilizes electrons, but not for the process of interest. The reversible potential for hydrogen evolution is -420 mV, a value more positive than our controlled potential value. The reaction is negligible at this potential because the gold electrode has a small overpotential for hydrogen evolution, so hydrogen evolution does not occur at the thermodynamic value.

8. The current is monitored and integrated, and the enzyme spectrum monitored at an appropriate wavelength as the reduction proceeds. Since $MV^{+\bullet}$ quantitatively transfers electrons to enzymes with more positive potentials and/or to oxygen in the system, the spectrum of reduced MV does not appear until the end point of the titration.
9. The number of coulombs, namely, the integrated current (Q), expressed as coulombs (C) required to completely reduce the protein, must be calculated so that the appropriate number of points can be taken in the reductive titration:

$$Q = nFM \quad (6)$$

where M is the number of moles of protein in solution, n , the number of electrons required to reduce one mole of enzyme, and F , the Faraday constant. Because of the presence of residual oxygen, 3–5 mC of charge may be consumed before the enzyme spectrum starts to change. Oxygen is reduced, either by the reduced enzyme or by methyl viologen. In most cases, protein reduction does not occur until

after the oxygen has been reduced. After the reduction of the enzyme starts (denoted by spectral changes), the solution may be shaken to scrub the oxygen out of the atmosphere to make sure the oxygen is reduced. (Sometimes the oxygen is removed with an internal scrubber.)

10. After the absorbance becomes stable, the spectrum is recorded, without stirring; the stirring is then restarted and a few millicoulombs of charge are added to generate $MV^{+\bullet}$. The absorbance change at a selected wavelength is monitored. For example, for a flavoprotein at a concentration of 10^{-5} M and a volume of 4.3 mL, 8.3 mC of charge would be required for the full two-electron reduction. On the basis of this number, one should calculate the charge required for 20, 40, 60, and 80% reduction. This incremental addition of reductant will provide a titration with at least six points. The solution should be stirred during the electrochemical reduction. The current should be monitored and integrated. After an appropriate number of millicoulombs are added, for example, at 20% reduction, the reduction is stopped, and when the absorbance at 450 nm stabilizes, stirring is stopped and the UV-visible spectrum is recorded using a double-beam instrument; then the addition of reducing equivalents is continued. The end of the experiment is signaled when the spectrum of $MV^{+\bullet}$ is observed, indicating titrant excess.

The absorbance at 450 nm is plotted as a function of the number of millicoulombs or reduction equivalents (Eq. 6) added to the sample. In the case of a simultaneous two-electron transfer to a flavoprotein, the

A_{450} versus n plot should be linear with an intersection on the x axis at $n = 2$. This wavelength (450 nm) is chosen because the greatest difference in molar absorptivity between the oxidized and reduced form of flavin occurs at this wavelength.

Flavoprotein reduction can alternatively take place in two single-electron steps, resulting in stabilization of a significant amount of the one-electron reduced form, $EFl^{-\bullet}$ ("red" anionic semiquinone) or $EFlH^{\bullet}$ ("blue" neutral semiquinone) during the coulometric reductive titration. These spectra are distinct from each other and from the oxidized and two-electron reduced forms of the flavin. $EFl^{-\bullet}$ has distinctive large absorbances at 530 and 370 nm, whereas $EFlH^{\bullet}$ has a broad absorbance in the range 600–700 nm. If these spectra are seen, the absorbances A_{630} , A_{530} , or A_{370} can be plotted as a function of n . If the potentials of the two-electron transfers are widely separated, that is, if the first electron is easier to transfer and is quantitatively transferred before the second, almost quantitative amounts of semiquinone are stabilized. Under these conditions, the plots of A versus n are linear and maximize at $n = 1$. From the extrapolated portions, the molar absorptivity of semiquinone at that wavelength can be determined. In this case – one reaction is proceeding in the first part of the titration and another at the second – there should be two separate sets of isosbestic points in the first and second halves of the titration. For an enzyme exhibiting such behavior, one would expect that in the potentiometric titration, each electron will be transferred at a separate potential, and potential-pH behavior determined for each electron separately.

In contrast, if less than 50% semiquinone is stabilized, the A versus n plots can be curved, whereas the spectra exhibit no

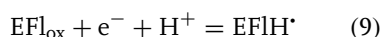
tight isosbestic points because all three oxidation states are present during the majority of the titration. If the molar absorptivity of the particular semiquinone is known, the maximal amount at 50% titration can be determined. From the amount of semiquinone (M), the potential separation of the two electrons can be calculated

$$E_1^{\circ'} - E_2^{\circ'} = \left(4.606 \frac{RT}{F}\right) \log \left[\frac{2M}{1-M} \right] \quad (7)$$

In many cases, the midpoint potential is determined for the two-electron transfer at half reduction (E_m) via the potentiometric titration described later, and the potentials of the individual electrons are calculated from that value and the percent semiquinone. Thus, the individual $E^{\circ'}$ can be determined in this manner by using Eqs. (7 and 8).

$$E_1^{\circ'} - E_2^{\circ'} = 2E_m \quad (8)$$

If semiquinone is stabilized, we can determine its protonation state by noting the spectral properties of the semiquinone, and thus we can determine if the first electron is accompanied by a proton to form EFlH \cdot as indicated below:



Such predictions from spectral changes observed on coulometric titrations must be verified by potential/pH studies using potentiometric titrations (described below) to determine if one or both electron transfers are transferred with a proton and where $\text{p}K_a$ s may occur.

In the case in which no semiquinone is stabilized, the entire process is treated as a two-electron transfer. Therefore, a coulometric titration can predict which will happen in the potentiometric titration.

The two are used together to define the behavior of the enzymes.

Usually, the spectroelectrochemical cell and anaerobic technique are tested before use on an enzyme by reducing an indicator dye alone, making sure reduction is taking place without oxygen leakage. The criteria are that (1) the correct number of reducing equivalents be transferred and (2) the correct potential obtained for the dye, as well as good Nernst plots, namely linear over a wide range and with correct slopes. Because the dyes can react directly with the electrode, one experiment should be enough to provide all this information. It is important to titrate the dyes under the same conditions as for the enzyme.

15.4.2

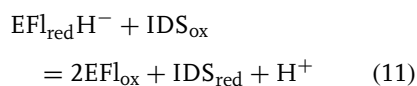
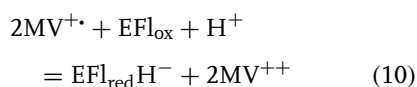
The Potentiometric Titration

The potentiometric titration is performed in a similar way, except that there is an additional mediator or mediators present. The potentiometric titration gives optimal results when performed in the presence of two kinds of mediators, a mediator titrant such as MV^{++} and a redox indicator or indicators. These redox indicators must have redox potentials very near that of the protein, because when in equilibrium with the protein, the redox indicator is poisoning the potential of the indicator (working electrode).

The gold working electrode has two roles in this experiment: first, with its potential controlled at -0.550 mV, it is the cathode at which the MV^{++} is reduced. After transferring an aliquot of charge, which is transferred to the protein and the mediator, the potentiostat is turned off, and the cell is held at open circuit in order for the contents of the cell and the gold electrode to equilibrate at open circuit. The potential of the electrode and the spectrum

are monitored: when both stop changing and are constant for 10 min, equilibrium has been achieved. After equilibrium has been achieved, the electrode acts as an indicator electrode, sensing the potential of the redox indicator couple, which is also the potential of the enzyme and the potential of the system, E_{cell} .

These concepts and procedures are shown in an example in which we assume electrons from $MV^{+\bullet}$ are transferred first to the protein ($E\text{Fl}_{\text{ox}}$) (Eq. 10) and then to the redox indicator indigo disulfonate (IDS_{ox}). As the concentration of the two-electron reduced form of the enzyme $E\text{Fl}_{\text{red}}\text{H}^-$ increases, it equilibrates with the redox indicator, for example, indigo disulfonate (IDS) (Eq. 11)



The titrant of Eq. (10) is chosen so that the position of equilibrium of this reaction is far to the right, whereas for Eq. (11), the mediator is chosen so that there are approximately (within a factor of 10) equal amounts of the two forms of the mediator, IDS_{ox} and IDS_{red} .

At each point in the titration, the system is allowed to equilibrate. Then both the potential and the spectrum of the system are recorded. This gives the measured potential in the following Eq. (12), which represents the equilibrium between the enzyme and the dye, which is communicated to the electrode by the dye.

Equilibration times range from 10 to 30 min, and are considered reached when the potential does not drift more than a millivolt in 10 min. The potential is then measured and the spectrum taken. Several

more aliquots of reducing equivalents are transferred, further reducing the enzyme. A Nernst plot covering as broad a range as possible is constructed from the points of the reductive titration. The range of the Nernst plot may be limited by the potential range of the mediator dye.

The concentrations of all species are calculated from the spectra and the molar absorptivities. $E^{\circ'}$ and n are calculated from the Nernst plot of the E measured versus $\log [\text{ox/red}]$ for the enzyme. The dyes must be titrated under the same conditions as the enzyme, in order to obtain the spectrum of the enzyme alone.

A disadvantage of this method is that it depends on good equilibration, making controls necessary. For example, to minimize the effect of dye binding to the enzyme, the indicator dyes are present in small concentrations (about 3 μM) to prevent binding to the enzyme (10 μM). In order to remove possible effects from dye interaction, the potential of the enzyme is determined in two separate experiments using two different indicator dyes.

The slope and intercept of the Nernst plot are evaluated. It should be 29 or 59 mV at room temperature, and a large range of potentials should be covered. If the slope deviates from these values, this may indicate incomplete equilibration. The experiment can then be rerun using different dyes to alleviate the problem. If the Nernst plot has a good slope, the reaction is judged to be reversible. As a further test of the reversibility, some reoxidative points are obtained in a reductive titration. For example, if 3 mC of reductive equivalents were transferred to obtain a point in the titration, the enzyme will then be reoxidized by 0.5 mC. The potential and spectrum are measured to make sure the data obtained from

reoxidation fits on the same Nernst plot as data obtained in the reductive direction.

The mediator dyes are the limiting factor in making the redox potential measurements. The dyes chosen must have potentials very near the potential of the enzyme; they must also be able to interact with the active site of the enzyme quickly. One problem is that there are few good indicators in the potential range between 0 and -150 mV at pH 7.0, which is the redox potential region for many flavoproteins, so only part of the potential region for the enzyme studied may be covered by the dyes available. Because of the lack of good redox indicators in the potential region of interest, it may not be possible to repeat the potentiometric experiment with dyes with different structures. If this is done and the same potential is obtained, this is a clear indication that the measurement is valid and independent of dye properties.

15.5

Data Analysis and Sample Systems

15.5.1

Coulometric Titration

Several kinds of information can be acquired from this experiment such as the total number of electrons transferred to the enzyme, the confirmation that a spectral intermediate is present along with its quantitation, and finally, an indication of whether the process occurs by two single electron transfers or a simultaneous two-electron transfer. A plot of absorbance at selected wavelengths versus number of electrons transferred can be used to analyze the data. Current efficiency is calculated by comparing the number of

electrons required to reduce the enzyme, once reduction starts, to the theoretical number of reducing equivalents (see earlier text).

Such results are shown in Fig. 9 for a flavoprotein (MCAD) bound to hexadienoyl-CoA (HD-CoA). HD-CoA was designed to be both a Raman active probe and a thermodynamically stable product analog. It was desired to verify that this product analog did not accept electrons from the reduced enzyme, which would destroy its Raman active properties, making it unsuitable to probe the properties of the reduced enzyme. The best way to show that no significant reduction was occurring to HD-CoA was to perform a coulometric reductive titration of the MCAD saturated with HD-CoA and confirm that the enzyme was indeed 100% reduced before the analog started to accept electrons. It was established that the reducing equivalents were transferred to the enzyme first by simultaneously monitoring the number of reducing equivalents transferred to the enzyme–HD-CoA complex and the spectral changes occurring at the enzyme.

The coulometric titration shown in Fig. 9(a) was performed at an HD-CoA concentration such that 95% of the MCAD was complexed. The titration consisted of two reductive events. The absorbance at 456 nm decreased sharply ($\Delta A = -0.20$) during the first part of the titration because the reduction of flavin (see inset). An increase in absorbance at 570 nm accompanied flavin reduction, consistent with the formation of a charge transfer complex between the dienoyl-CoA ligand and the reduced enzyme. The absorbance at 570 nm reached a maximum between $n = 2.6$ and 3 reducing equivalents, with the majority of the 456 nm decrease in absorbance occurring during this part of the titration. From $n = 3$ to 11.8, the absorbance of

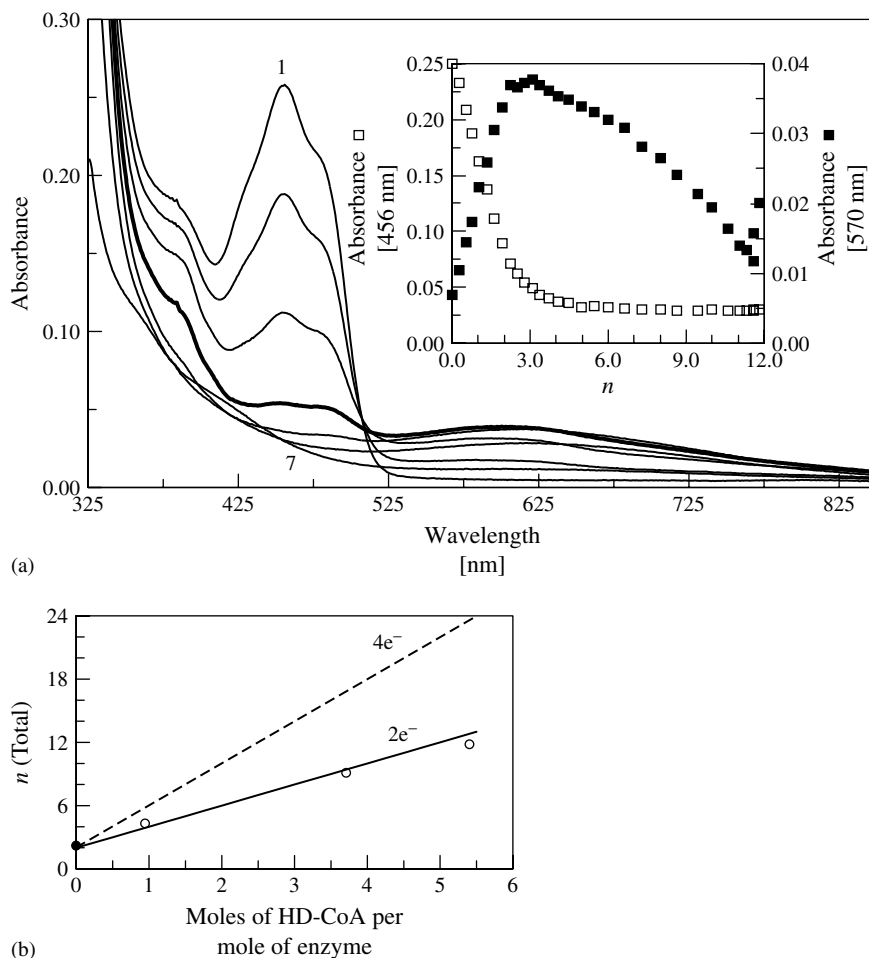


Fig. 9 (a) Coulometric reduction of MCAD (14.7 μM) in the presence of HD-CoA (80 μM) and MV^{++} (100 μM). Titrations were performed under anaerobic conditions at 25 $^{\circ}\text{C}$ in 50 mM potassium phosphate buffer, pH 7.6. Only selected spectra are shown for clarity. Curves 1–7: $n = 0.0, 1.0, 1.8, 2.6$ (bold), 4.7, 8.2, and 11.8, respectively. Inset: plot of absorbance at 456 nm (\square) and 570 nm (\blacksquare) as a function of the number of reducing equivalents (n) added during the titration and (b) correlation between the total number of reducing equivalents (n) and the amount of HD-CoA in solution. Datum at 0 μM HD-CoA (\bullet) was obtained from Ref. [1]. All other data (\circ) were obtained from coulometric titrations in this work. Concentrations of HD-CoA were varied from 14.3 to 80 μM . Enzyme concentrations were kept between 13.8 and 14.8 μM . Theoretical fits are shown for two (—) and four (---) electron reduction of HD-CoA.

the charge transfer band decreased. After 11.8 reducing equivalents had been transferred, reduced methyl viologen was thermodynamically stabilized.

Since more than two reducing equivalents could be added to the system, it became apparent that both the flavin and the HD-CoA were undergoing reduction.

To determine if one or both double bonds of HD were being reduced, coulometric reductions of HD-CoA were performed at several different HD-CoA concentrations. Figure 9(b) clearly indicates that the reduction of HD-CoA is a two-electron process.

It is clear that 85% the MCAD reduces before the HD-CoA, so that the redox potential of the MCAD bound to HD-CoA can be measured. Thus, it should be possible to correlate the Raman signal with the redox potential of the ligand bound to the enzyme.

15.5.2

Potentiometric Titration

The measured potential, relative to the reference electrode employed (E_{cell}), represents the equilibrium position of the enzyme and the dye, and is communicated to the electrode by the dye:

$$\begin{aligned} E_{\text{cell}} &= E_{\text{dye}}^{\circ'} + 0.059 \log \left[\frac{\text{ox}}{\text{red}} \right] \\ &= E_{\text{enzyme}}^{\circ'} + 0.059 \log \left[\frac{\text{ox}}{\text{red}} \right] \quad (12) \end{aligned}$$

The concentrations of all species are calculated from the absorbance spectra and the molar absorptivities. $E^{\circ'}$ and n are calculated from the Nernst plot of the E_{cell} versus $\log [\text{ox/red}]$ for the enzyme. The dyes must be titrated under the same conditions as the enzyme so that their spectra can be subtracted and the spectrum of only enzyme obtained.

Potentiometric titrations can be used to determine three things in addition to basic protein characterization: first, the enzyme is being bound and regulated by regulatory proteins or substrates; and second, protons are being transferred along with the electrons, and the ionization of acidic groups is occurring in the pH region being studied. The case of ligands

that bind to the protein causing a change in its potential will be considered first. However, let us look back at the illustration shown in Fig. 1, in which the potential of the redox-active cofactor, in this case the flavin undergoes a change in redox potential ($E^{\circ'}$) upon binding to apoprotein (ligand). In this case, the redox potential of the flavin at the active site of the enzyme (MCAD) shifts positive because of the ratio of the binding constants (shown in the inset). The new potential is -145 mV. Now we will see that the binding of a ligand (L), substrate or regulatory protein, to MCAD can cause the redox potential of the MCAD enzyme (or the flavin at the active site) to change again. These redox potential shifts present the clearest evidence that binding is occurring. The example used for illustration in Fig. 10 is of HD-CoA, a product analog, L, binding to the enzyme MCAD, designated E. It is assumed that a single ligand binds to a single flavin active site, and that if there is more than one active site per protein molecule, they function independently. This concept of binding coupled to electron transfer is represented in the following series of equations, which can be incorporated into a thermodynamic box in which E_{ox} = free oxidized enzyme, E_{red} = free reduced enzyme, $E_{\text{ox}} \cdot \text{L}$ = oxidized enzyme bound to ligand, $E_{\text{red}} \cdot \text{L}$ = reduced enzyme bound to ligand

$$E_{\text{ox}} + 2e^- = E_{\text{red}} \quad E_1^{\circ'} = -145 \text{ mV} \quad (13)$$

$$E_{\text{ox}} \cdot \text{L} + 2e^- = E_{\text{red}} \cdot \text{L} \quad E_2^{\circ'} = -52 \text{ mV} \quad (14)$$

These values are related by (1) the binding constant of the oxidized enzyme to the ligand, and (2) the binding of the reduced enzyme the reduced enzyme to the ligand:

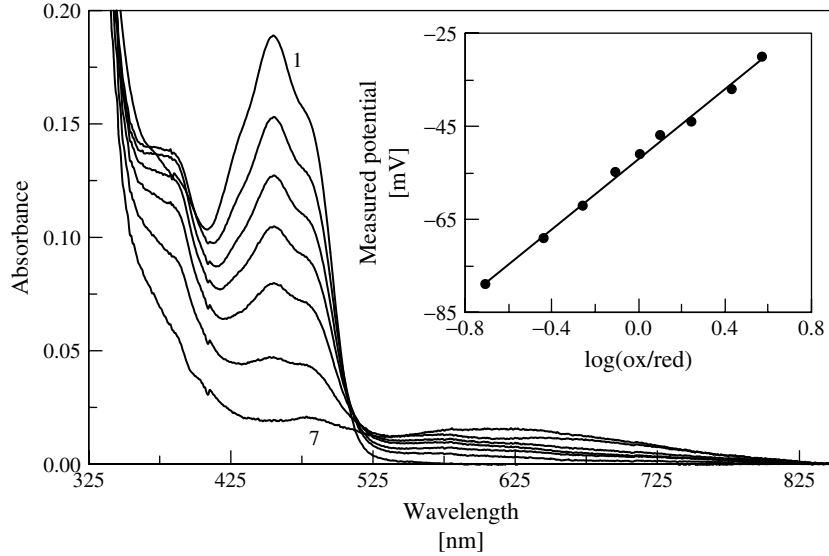
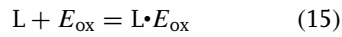
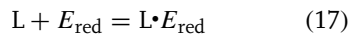


Fig. 10 Potentiometric titration of MCAD (10.7 μM) in the presence of HD-CoA (181 μM). MV^{++} (100 μM) serves as a redox mediator. Redox indicators are pyocyanine (5.0 μM) and indigo disulfonate (2.5 μM). Titration was performed under anaerobic conditions at 25 $^{\circ}\text{C}$ in 50 mM potassium phosphate buffer, pH 7.6. Intermediate spectra have been removed for clarity. The spectrum of the oxidized MCAD•HD-CoA complex is shown by curve 1. Curves 2–6 show the complex at $E = -30$, -44 , -51 , -62 , and -79 mV versus SHE. Curve 7 is the spectrum of the fully reduced MCAD bound to HD-CoA. Inset: Nernst plot indicating an $E^{\circ'} = -0.052$ V and $n = 1.6$.



$$K_{\text{ox}} = \frac{[\text{L} \cdot E_{\text{ox}}]}{[\text{L}][E_{\text{ox}}]} \quad (16)$$



$$K_{\text{red}} = \frac{[\text{L} \cdot E_{\text{red}}]}{[\text{L}][E_{\text{red}}]} \quad (18)$$

$$K_{\text{dox}} = \frac{1}{K_{\text{ox}}} \quad (19)$$

$$K_{\text{red}} = \frac{1}{K_{\text{dred}}} \quad (20)$$

By rearranging these equations and substituting into the Nernst equation for the free enzyme, we can calculate the potential of the bound enzyme:

$$E = E'_{\text{free}} - \frac{0.059}{n} \log \left(\frac{E_{\text{red}}}{E_{\text{ox}}} \right) \quad (21)$$

Rearranging the binding equation:

$$[E_{\text{ox}}] = \frac{[\text{L} \cdot E_{\text{ox}}]}{K_{\text{ox}}[\text{L}]} \quad (22)$$

$$[E_{\text{red}}] = \frac{[\text{L} \cdot E_{\text{red}}]}{K_{\text{red}}[\text{L}]} \quad (23)$$

and substituting these values into the Nernst equation, we obtain for 1 M ligand, and the unit activity of other species:

$$E'_{\text{bound}} = E'_{\text{free}} + 2.303 \frac{RT}{nF} \log \frac{K_{\text{red}}}{K_{\text{ox}}} \quad (24)$$

So the magnitude of the potential shift on binding is related to the ratio of the binding constants. We could modify it using the dissociation constants. Likewise, if we know any three of the thermodynamic

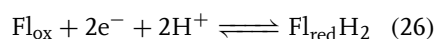
constants, we can calculate the fourth. We can also represent this relationship as a thermodynamic box, as for Fig. 1.

The redox potential of HD-CoA-complexed MCAD was determined at several pH values. A representative potentiometric titration at pH 7.6 is shown in Fig. 10. The midpoint potential is for the oxidized FAD/hydroquinone couple. An $E^{\circ'}$ of -52 mV (inset, Fig. 10) for the MCAD•HD-CoA complex is 93 mV more positive than the midpoint potential of the free MCAD (-145 mV) [1], indicating a significant potential shift in the enzyme upon binding HD-CoA. Equation (24) can be used to calculate a dissociation constant for the analog and reduced enzyme (K_{dred}) of 2.5, a 1400-fold difference between K_{dox} and K_{dred} . Tighter binding of product to the reduced enzyme is consistent with previous work on acyl-CoA dehydrogenases (ACDs).

$$K_{\text{dred}} = 10^{-\left[\frac{(E_{\text{m}(\text{bound})} - E_{\text{m}(\text{free})})nF}{2.303RT}\right]} \times K_{\text{dox}} \quad (25)$$

We can detect whether electron transfer is coupled to the proton transfer reaction by measuring the redox potential over as wide a pH range as enzyme stability allows. If $E^{\circ'}$ is independent of pH, this indicates that there is no proton transfer coupled to the electron transfer reaction, or that the simultaneous ionization of the oxidized and reduced forms offset one another (see below). However, if proton transfer is coupled to electron transfer for a particular redox state, the electron transfer will be dependent on pH. For enzymes, proton transfer usually accompanies electron transfer in order to maintain charge neutrality at the active site. This is illustrated in the simple case of oxidized free flavin, abbreviated (Fl_{ox}). In order to understand how $\text{p}K_a$

values can be determined from redox potential values determined over a broad range of pH, consider the relatively simple example of the following half-reaction that is true for free flavin (at low pH) and the accompanying Nernst equation.



$$E^{\circ'} = E^{\circ} - \frac{0.05916}{2} \log \frac{[\text{Fl}_{\text{red}}\text{H}_2]}{[\text{Fl}_{\text{ox}}][\text{H}^+]^2} \quad (27)$$

$\text{Fl}_{\text{red}}\text{H}_2$ is an acid that can dissociate. We need to express the Nernst equation in such a way that the log term contains the formal concentration of Fl_{ox} and $\text{Fl}_{\text{red}}\text{H}_2$. Fl_{ox} is not an acid or a base, so its formal concentration (F) equals its molar concentration:

$$F_{\text{Fl}_{\text{ox}}} = [\text{Fl}_{\text{ox}}] \quad (28)$$

For the diprotic acid $\text{Fl}_{\text{red}}\text{H}_2$, we use the following equation to express $[\text{Fl}_{\text{red}}\text{H}_2]$ in terms of the formal concentration of $\text{Fl}_{\text{red}}\text{H}_2$. To do this, the fractional composition equation or (α equation) is used to convert the form of an acid or base to its concentration in a particular form:

$$\begin{aligned} [\text{Fl}_{\text{red}}\text{H}_2] &= \alpha_{\text{Fl}_{\text{red}}\text{H}_2} \cdot F_{\text{Fl}_{\text{red}}\text{H}_2} \\ &= \frac{[\text{H}^+]^2 F_{\text{Fl}_{\text{red}}\text{H}_2}}{[\text{H}^+]^2 + [\text{H}^+]K_{a1} + K_{a1}K_{a2}} \end{aligned} \quad (29)$$

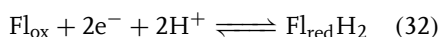
substituting Eqs. (28 and 29) into Eq. (27) we obtain

$$\begin{aligned} E^{\circ'} &= E^{\circ} - \frac{0.05916}{2} \\ &\times \log \frac{[\text{H}^+]^2 F_{\text{Fl}_{\text{red}}\text{H}_2}}{[\text{H}^+]^2 + [\text{H}^+]K_{a1} + K_{a1}K_{a2}} \\ &\quad \frac{F_{\text{Fl}_{\text{ox}}}}{[\text{H}^+]^2} \end{aligned} \quad (30)$$

that can be rearranged to form

$$E = E^\circ - \frac{0.05916}{2} \times \log \frac{1}{\underbrace{[H^+]^2 + [H^+]K_{a1} + K_{a1}K_{a2}}_{E'^{\circ}}} - \frac{0.05916}{2} \log \frac{F_{\text{Fl}_{\text{red}}}\text{H}_2}{F_{\text{Fl}_{\text{ox}}}} \quad (31)$$

This first term is the formal potential. In this case, the potential/pH curve would have three line segments as the pH, which is initially below $\text{p}K_{a1}$, is raised to values higher than all $\text{p}K_a$ s. In the first case, in which pH is lower than $\text{p}K_{a1}$ the reaction that involves a two-electron, two-proton transfer is



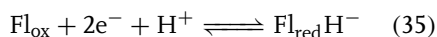
The Nernst equation is

$$E = E^\circ - \frac{0.05916}{n} \log \frac{[\text{Fl}_{\text{red}}\text{H}_2]}{[\text{Fl}_{\text{ox}}][\text{H}^+]^2} \quad (33)$$

If the pH-dependent term is factored out, we can see the potential/pH slope = 59 mV, and thus this pH dependence becomes a part of E'° :

$$E = E^\circ - 0.05916 \log[\text{H}^+] - \frac{0.05916}{n} \times \log \frac{[\text{Fl}_{\text{red}}\text{H}_2]}{[\text{Fl}_{\text{ox}}]} \quad (34)$$

In the second case, in which the pH values are between the two $\text{p}K_a$ values, or $\text{p}K_{a1} < \text{pH} < \text{p}K_{a2}$, the reaction becomes a two-electron, one-proton transfer:



The Nernst equation becomes:

$$E = E^\circ - \frac{0.05916}{n} \log \frac{[\text{Fl}_{\text{red}}\text{H}^-]}{[\text{Fl}_{\text{ox}}][\text{H}^+]} \quad (36)$$

If we separate out the pH dependence, we see that the pH-dependent term has a 0.059/2 factor, giving a 29-mV slope for this part of the pH range.

At $\text{pH} < \text{p}K_{a2}$, there is no pH dependence since no protons are transferred with the electrons. The pH at which the potential/pH slope changes corresponds to $\text{p}K_a$ s for the reduced form.

Obviously if the oxidized flavin is bound to a protein, two things may occur, first, its $\text{p}K_a$ s may be shifted from the free form, so that the redox data become influenced by the $\text{p}K_a$ s of nearby acid residues. For example, there may be a positively charged amino acid side chain that can hydrogen bond to the N(1) position of the flavin. The presence of the positive charge near the flavin may make electron transfer easier, thus causing the redox potential of the flavin to be shifted positive. This positive charge near the flavin may cause the $\text{p}K_a$ s of the flavin group to be shifted so that over much of the pH range, only one proton would need to be transferred to maintain charge neutrality. Second, the $\text{p}K_a$ s of these amino acid groups of the protein part of the enzyme may be influenced by the redox state of the flavin, namely, the $\text{p}K_a$ of the same group could change. Therefore, for the flavoproteins, there may be as many as three or four $\text{p}K_a$ s that can influence redox behavior, typically two from the reduced flavin and two from the protein. By measuring the redox potentials of the enzyme over a wide range of pH values, we may be able to discover the presence of those ionizable amino acid side chains that control the redox potential of the bound flavin and determine the $\text{p}K_a$ values of those ionizable groups. In the more complex cases, the potential/pH behavior must be modeled by fitting the data to a redox-linked ionization model

described by Clark [6] as in Eq. (37):

$$E^{\circ'} = E_0 + 2.303 \frac{RT}{nF} \times \log \left[\frac{[\text{H}^+]^3 + [\text{H}^+]^2 K_{\text{red},1} + [\text{H}^+] K_{\text{red},1} K_{\text{red},2} + K_{\text{red},1} K_{\text{red},2} K_{\text{red},3}}{[\text{H}^+]^3 + [\text{H}^+]^2 K_{\text{ox},1} + [\text{H}^+] K_{\text{ox},1} K_{\text{ox},2} + K_{\text{ox},1} K_{\text{ox},2} K_{\text{ox},3}} \right] \quad (37)$$

where E_0 is an extrapolated value because the potential at $\text{pH} = 0$ cannot be obtained experimentally. In the data whose $\text{p}K_a$ s are established by curve fitting, $E^{\circ'}$ values at a particular pH are determined from the intersection of the Nernst plot in which by definition the $\log[(\text{ox})/(\text{red})]$ term is equal to zero. In this case, three $\text{p}K_a$ s were considered and used to fit the experimental $E^{\circ'}$ data taken at various pH values.

It is important to point out, as Eq. (37) illustrates, the principle that the redox-linked ionizations will not be detected if $K_{\text{ox},1} = K_{\text{red},1}$ and so on, because then the second term of the equation will be zero.

References

1. J. D. Pellett, K. M. Sabaj, A. W. Stephens et al., *Biochemistry* **2000**, 39, 13 982–13 992.
2. G. J. Mancini-Samuelson, V. Kieweg, K. M. Sabaj et al., *Biochemistry* **1998**, 37, 14 605–14 612.
3. L. H. Bradley, R. P. Swenson, *Biochemistry* **1999**, 38, 12 377–12 386.
4. H. A. Heering, J. Hirst, F. A. Armstrong, *J. Phys. Chem. B* **1998**, 102, 6889–6902.
5. J. N. Butt, S. E. J. Fawcett, J. Breton et al., *J. Am. Chem. Soc.* **1997**, 119, 9729–9737.
6. W. M. Clark, *Oxidation-Reduction Potentials of Organic Systems*, Williams & Wilkins, Baltimore, Md., 1960.
7. D. B. Burleigh Jr., G. P. Foust, C. H. Williams Jr., *Anal. Biochem.* **1969**, 27, 536–544.
8. G. P. Foust, D. B. Burleigh Jr., S. G. Mayhew et al., *Anal. Biochem.* **1969**, 27, 530–535.
9. S. G. Mayhew, *Methods in molecular biology in Flavoprotein Protocols* (Eds.: S. K. Chapman, G. A. Reid), Humana Press, Totowa, N.J., 1999, Vol. 131.
10. V. Massey; P. Hemmerich, *Biochemistry* **1978**, 17, 9–16.
11. V. Massey in *Flavins and Flavoproteins*, 1990 (Eds.: B. Curti, S. Ronchi, G. Zanetti), Walter de Gruyther, Berlin, 1991, pp. 59–66.
12. M. T. Stankovich, *Anal. Biochem.* **1980**, 109, 295–308.
13. R. Szentirmay, P. Yeh, T. Kuwana in *Electrochemical Studies of Biological Systems*, ACS Symposium Series 38 (Ed.: D. T. Sawyer), American Chemical Society, Washington, DC, 1977, pp. 143–169.
14. G. S. Wilson, *Methods in Enzymology*, Academic Press, New York, 1978, Vol. 54, pp. 396–410.
15. V. Massey, F. Muller, R. Feldberg et al., *J. Biol. Chem.* **1969**, 244, 3999–4006.
16. G. Fasman, (Ed.), *CRC Handbook of Biochemistry and Molecular Biology*, Physical and Chemical Data Vol. 1, 3rd ed., 1985, Vol. 1, pp. 122–130.
17. J. E. O'Reilly, *Biochim. Biophys. Acta* **1973**, 292, 509–515.
18. J. D. Pellett, D. F. Becker, A. K. Saenger et al., *Biochemistry* **2001**, 40, 7720–7728.

16 Membrane Electrochemistry

H. Ti Tien and Angelica Ottova

Physiology Department, Michigan State University, East Lansing, MI, USA

16.1	Introductory Remarks	513
16.2	Types of Membranes	513
16.2.1	Semipermeable Membranes	513
16.2.2	Ion-exchange Membranes	514
16.2.3	Microporous Membranes	514
16.3	The Lipid Bilayer Principle of Biomembranes	514
16.4	Classification of Biomembranes	515
16.5	Composition, Structure and Function of Biomembranes	517
16.5.1	Composition	517
16.5.2	Structure and Function	517
16.5.3	The Ultrastructure of Biomembranes	518
16.6	The Function of Biomembranes Pertaining to Electrochemistry	518
16.6.1	Basics of Membrane Electrochemistry	519
16.6.1.1	Nernst–Planck Equation	519
16.6.1.2	Thermodynamic Considerations	520
16.6.1.3	Nernst Equation	523
16.6.1.4	Electroneutrality Principle	523
16.6.1.5	Ion Selectivity, Ion Specificity, pH, and Cell Membranes	523
16.6.1.6	The Henderson–Hasselbalch Equation	524
	Ion-selective membranes	525
	The Nicolsky equation	525
16.6.1.7	Origins of Membrane Potentials	525

16.7	The Role of Electrical Double Layers (EDLs) and their Biological Implications	526
16.7.1	Electrokinetic Potential, U_k	527
	The Dorn effect	528
	Streaming potential	528
	Electrophoresis	528
	Electroosmosis	528
16.7.2	Adsorption Potential	529
16.7.3	Distribution Potential	529
16.7.4	Diffusion Potentials	529
16.7.5	The Gibbs–Donnan Potential	530
16.7.6	Phase Boundary Potentials	532
16.7.7	Relationship among Various Potentials	533
16.8	Experimental Membrane Systems	535
16.8.1	Langmuir–Blodgett Films	535
16.8.2	Immiscible Liquid–Liquid (L–L) Interfaces (ITIES)	535
16.8.3	Planar Lipid Bilayers and Liposomes	536
16.9	Bilayer Lipid Membranes	536
16.9.1	Formation Techniques	536
16.9.1.1	Conventional BLM	536
16.9.1.2	BLMs via L–B Technique	537
16.9.1.3	Supported BLMs	537
16.9.2	Methods of Investigation	540
16.9.2.1	Potentiometry	540
16.9.2.2	The Patch-Clamp Technique	541
16.9.2.3	Cyclic Voltammetry	542
16.9.2.4	CV and BLM Experiments	542
16.9.2.5	Modeling of BLM Behavior by Electrochemical Equivalent Circuit	544
16.9.3	Electrochemical Impedance Spectroscopy	545
16.9.4	Photoelectrospectrometry	548
16.10	Electronic and Charge Transfer Processes in Membranes	550
16.10.1	Properties of Iodine–Iodide-containing BLMs	550
16.10.2	Polypyrrole BLMs	551
16.11	Photoelectric Effects in Membranes	551
16.12	Applications	552
	References	556

16.1

Introductory Remarks

There is at least one similarity between electrochemistry and biological membranes (biomembranes); they are both interface science. Electrochemistry is a well-established discipline dealing with electrical phenomena at, as well as across, the interfaces. The study of biomembranes, on the other hand, is a relatively new endeavor, whose investigations involve the use of powerful physicochemical techniques based on electrochemistry. Hence, membrane electrochemistry may be defined as the application of electrochemistry to membrane studies, including both artificial and natural systems. Defined in another way, *Membrane Electrochemistry*, the title of this chapter, is a synonym to the origin of electrophysiology. This brings us immediately to the often-cited story about how Galvani observed the twitching of a frog's leg upon touching by two dissimilar metals. Thus, the electrical properties of membranes, natural and synthetic, have been investigated since Galvani and Volta's time (1737–1798 and 1745–1827, respectively). There are many different types of membranes: semipermeable, ion exchange, microporous, synthetics of all kinds, biomembranes of all sorts, and reconstituted biomembranes (bilayer

lipid membranes or BLMs). Among the unique features of these membranes are their selectivity and specificity; they limit unrestricted hydrodynamic flow. Today, membrane electrochemistry is a mature field of endeavor. Among the aims of membrane electrochemistry are investigating charge generation, separation, and transport in natural and model membrane systems at the molecular level, and using the relevant knowledge thus gained for developing practical devices such as sensors for chemical, biomedical, and environmental applications.

16.2

Types of Membranes

16.2.1

Semipermeable Membranes

Generally speaking, the bilayer lipid membrane (BLM or planar lipid bilayer) is semipermeable, meaning that some molecules are allowed to pass freely (diffuse) through the structure. The lipid bilayer is virtually impermeable to large molecules, relatively impermeable to small ions and polar molecules. Specifically, osmosis, a diffusion phenomenon, can be easily observed in a device called osmometer in which a membrane separating two

aqueous chambers is permeable only to water. When solutions of different concentration are present, water will flow from the dilute chamber into the concentrated one until equilibrium is reached, at which the extra pressure known as the osmotic pressure is produced. Van't Hoff found empirically that the osmotic pressure is directly proportional to the concentration of solute for dilute solutions. In this connection, Pfeffer immersed plant cells of *Chara* in salt solutions of various concentrations and observed that the cells swelled in hypotonic (low salt) solutions and shrank in hypertonic (high salt) solutions. To account for similarities in the osmotic behavior of plant cells and man-made osmometers, Pfeffer, recognizing that the boundary of discontinuity between the protoplasm and its environment must constitute an osmotically semipermeable membrane, postulated the existence of an invisible (under light microscope) plasma membrane in the plant cell.

16.2.2

Ion-exchange Membranes

Synthetic polymers containing fixed charge groups ($-\text{COO}^-$, $-\text{SO}_4^-$, $-\text{PO}_4^{2-}$, etc.) in the form of thin sheets are known as ion-exchange membranes. The equilibrium selectivity coefficients for alkali cations for polymers containing strongly acidic groups follow the Hofmeister series (i.e. Li, Na, K, Rb, Cs), whereas the order is reversed for ion-exchange membranes having weakly acidic groups [1]. The electrical potential difference between two solutions separated by an ion-exchange membrane in the absence of any current flowing through the membrane can be measured. Carboxylated ion-exchange membranes have been used as a substrate for ion sensors.

16.2.3

Microporous Membranes

Polycarbonate membranes, known commercially as microporous NucleoporeTM filters, are outstanding examples. Also included in this type of membranes are cellulose filters. With the former, they contain pores of known density and diameter. A novel BLM system with a longer lifetime, a larger surface area, and a greater stability in the face of chemical and mechanical disturbances has been reported [1]. The polycarbonate-BLM system is supported in such a manner that an aqueous solution could be easily added to both sides. In an ideal situation, this Nucleopore-coated membrane may be visualized as tens of thousands of micro-BLMs simultaneously generated in situ.

16.3

The Lipid Bilayer Principle of Biomembranes

All living beings are made of cells, from simple single-celled bacteria to complex multicelled humans. The conclusion that the fundamental structure of biomembranes is a lipid bilayer is based on three pivotal experimental findings: firstly, the elegant and simple experiment of establishing the orientation of amphipathic molecules at interfaces by Langmuir in 1917. Secondly, using that method Gorter and Grendel in 1925 reported that the extracted lipid molecules from the plasma membrane of red blood cells (RBCs) occupied the area on the surface of a Langmuir trough that was twice that of the original membrane. Thirdly, the lipid bilayer concept, as deduced from the above, was dramatically substantiated in 1961 by

reconstituting a BLM from the lipids extracted from the white matter of cow's brain [1, 2]. Electrical activities of the nerve and light-induced effects in photosynthesis have been elucidated with the aid of experimental planar BLMs and liposomes. In nerves, translocation of ions across protein channels embedded in the lipid bilayer play the pivotal role. In photosynthesis, light absorption by pigments, confined in the lipid bilayer, initiates electronic charge generation and separation, leading eventually to redox reactions on opposite sides of the membrane. Presently, electron and charge transfer processes through the lipid bilayer are being actively investigated, from both theoretical and biotechnological viewpoints. The crucial role played by the lipid bilayer may be summarized as follows. Living organisms are made of cells bound by their membranes. They are self-assembling entities; each is organizing a particular combination of phospholipids in the form of a bilayer with other constituents (e.g. proteins) embedded in it. This lipid bilayer, existing in all biomembranes, is most unique; it serves not merely as a physical barrier but functions as a two-dimensional matrix for reactions. Also, the lipid bilayer acts as a conduit for ion transport, as a framework for antigen–antibody binding, as a bipolar electrode for redox reactions, as a reactor for energy conversion (e.g. light to electric to chemical). Further, a modified lipid bilayer performs as a transducer for signal transduction (i.e. sensing), and numerous other functions as well. All these myriad activities require the ultrathin lipid bilayer. To study BLMs in detail, the task has been a daunting one until a few years ago because a 5-nm BLM is an extremely labile structure with limited lifetime. Planar BLMs can now be formed on various substrates with long-term stability, thereby opening the way for

basic research and development work in the domain such as biotechnology, catalysis, electrochemistry, microelectronics, and membrane biophysics. Today, from all lines of experimental findings, there is little doubt that all biomembranes possess a lipid bilayer structure, thereby underlying the *lipid bilayer principle* of biomembranes. The self-assembled lipid bilayer, the crucial component of most, if not all biomembranes, is in a liquid-crystalline and dynamic state. A functional cell membrane system, based on self-assembled lipid bilayers, proteins, carbohydrates, and their complexes, should be considered in molecular and electronic terms; it is capable of supporting ion or/and electron transport, and is the site of cellular activities in that it functions as a “device” for either energy conversion or signal transduction. Such a system, as we know intuitively, must act as some sort of a transducer capable of gathering information, processing it, and then delivering a response based on this information. All these myriad activities are predicated on the BLM of nanometer thickness, whose electrochemistry is the focus of this chapter (Fig. 1).

16.4

Classification of Biomembranes

Broadly, biomembranes may be divided into two types: plant and animal. Plant cell membranes generally contain little cholesterol. In terms of cells and organelles, the following classification is usually accepted according to their particular functions:

- the plasma membrane (e.g. red blood cells);
- the chloroplast (e.g. thylakoid membranes);

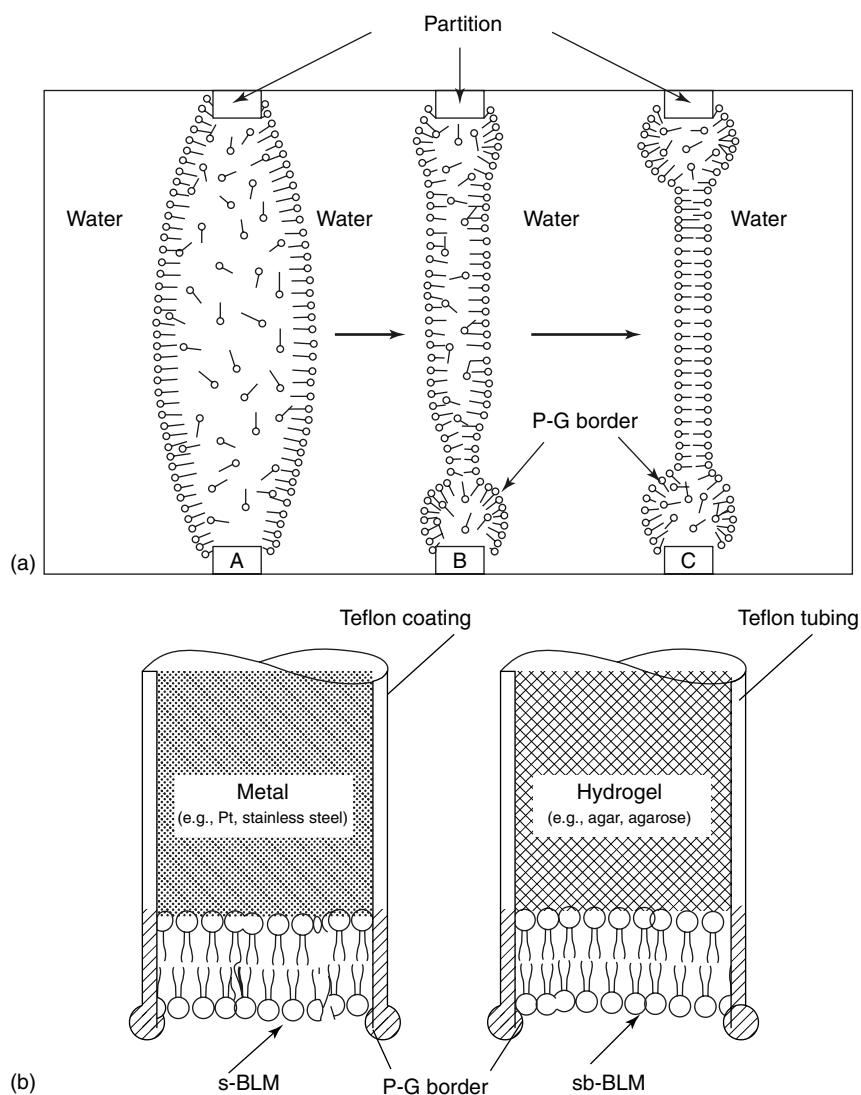


Fig. 1 Two basic types of BLMs (planar lipid bilayers). (a) A conventional BLM separating two aqueous solutions in formation [1] (a short movie illustrating the BLM-forming process) may be seen by visiting the URL: http://www.msu.edu/user/ottova/soap_bubble.html; (b) supported BLMs; (c) a BLM on metal substrate (s-BLM); (d) a salt-bridge supported BLM (sb-BLM). P-G stands for Plateau-Gibbs border that supports the BLM [2, 3].

- the mitochondrion (e.g. cristae membranes);
- the nerve (e.g. axon membranes);
- the eye (e.g. the visual receptor membranes);
- other membrane systems (muscles, microtubules, cytoskeletal elements, etc.).

From the viewpoint of membrane electrochemistry, some of these membranes have been reconstituted and characterized electrochemically via experimental BLMs (or planar lipid bilayer). Monographs and reviews covering many aspects of membrane research are available [1–28].

16.5 Composition, Structure and Function of Biomembranes

16.5.1 Composition

Overall, a cell membrane is a lipid bilayer matrix modified by functional proteins, carbohydrates, and their complexes. Typically, cells are about 90% water. The

rest, on the dry weight basis, is approximately: 50% protein, 15% each for carbohydrate and nucleic acid, 10% lipid, and 10% miscellaneous compounds. More specifically, Table 1 presents the gross composition of biomembranes, along with their functions.

16.5.2 Structure and Function

The general ultrastructure of the biomembrane is that the lipids are in the form of a bilayer providing the framework for embedding proteins, carbohydrates, and other constituents. These membrane constituents are immersed to a varying degree in the lipid bilayer. The lipid bilayer of the membrane is fluidlike and has the consistency of olive oil (viscosity ~ 1 cP). The lipids, proteins, and other constituents are thus perceived to be able to extend freely within the confine of the lipid bilayer. However, the picture is a dynamic one, in that phospholipids and cholesterol form a hydrophobic, fluid bilayer in which functional entities such as receptors, ion channels, pigments, proteins, and so on

Tab. 1 Gross composition and function of some basic types of membranes^a

	<i>Lipids</i>	<i>Proteins</i>	<i>Carbohydrates</i>	<i>Function</i>
Plasma membrane	25–50	50–70	10	Diffusion barrier active transport
(Gram + bacteria)	75	25	10	Antigenic properties
Cristae (mitochondrion)	20–40	60–80	2–4	Energy transduction ATP synthesis
Thylakoid (chloroplast)	40	35–65	6	Sunlight conversion ATP synthesis
Visual (visual receptor)	8% pigments	50	4	Light detection signal transduction
	40			
Nerve (axon)	4–10% pigments	20	3	Conduction of nervous impulse
	80			

^a (Expressed in % of dry weight, taken from p. 38 [3].)

could be embedded. That is, membrane constituents are able to exchange and/or be modified by compounds in contact with the cell membrane. At the molecular level, both lipids and proteins exhibit asymmetry; the composition of the inside of a membrane is different from the outside. Since membrane function and structure are the “two sides” of the same lipid bilayer, this must be so in order to explain the active transport of species across the membrane. Also, active sites of membrane-bound enzymes or immunological determinants are found only on one side of a lipid bilayer.

16.5.3

The Ultrastructure of Biomembranes

A brief account of the molecular structure of biomembranes may be presented from a chronological viewpoint. The recognition of the lipid bilayer as a principal element for all biomembranes dates back only to the second quarter of twentieth century. The origin of the lipid bilayer concept, however, is much older, which is traceable to more than three centuries! It all began with the physicist and inventor Robert Hooke of Hooke’s Law fame, who in 1665 coined the term *cell* to describe the tiny array of a cork slice after observing it with a primitive microscope that he had constructed. By happenstance, the same Robert Hooke, along with Isaac Newton, also studied mundane soap bubbles under the microscope, and described the so-called *black holes* in soap films. Newton estimated the thickness of “blackest” soap films to be $3/8 \times 10^{-6}$ in. When converted into modern units, the thickness is about 6 to 9 nm, which is in excellent agreement with modern measurements [1, 13]. The early investigation of black soap films had a profound influence in the development

of the lipid bilayer concept of biomembranes and its subsequent experimental realization in BLMs (planar lipid bilayers and spherical liposomes).

16.6

The Function of Biomembranes Pertaining to Electrochemistry

At about the time while the lipid bilayer concept was being proposed in the 1920s, Fricke, a physicist, carried out the following electrical measurements on RBCs, in answering the question “*How thick is the plasma membrane of red blood cells (RBC)*”? Using a Wheatstone bridge, the conductivity and capacity of the RBC suspension were measured as a function of frequency. At low frequencies, the impedance of the suspension of RBC is very high, whereas at high frequencies the impedance decreases to a low value. To explain his findings, Fricke proposed a model. That is RBCs are surrounded by a thin layer of low dielectric material electrically equivalent to a resistor (R_m) and a capacitor (C_m) in parallel. Thus, the lines of current flow around the RBC at low frequencies. At very high frequencies, the resistance becomes very low because all the current is shunted through the capacitor. In this connection, it should be pointed out, however, that Hober in 1910 found that suspensions of intact RBCs have a high electrical resistance, while the cytoplasm has a conductivity similar to that of physiological saline. From this fact, Hober concluded that the cell membrane has a high electrical resistance. Using the formula for a parallel plate, Fricke determined the capacitance (C_m) of the RBCs to be $0.81 \mu\text{F cm}^{-2}$. For a parallel-plate condenser, the capacitance is given by

$$C_m = \frac{\epsilon_0 \epsilon_r}{4\pi t_m} \quad (1)$$

where C_m = membrane capacitance ($\mu\text{F cm}^{-2}$), ϵ_r = relative dielectric constant of the membrane, and t_m = membrane thickness. Fricke calculated the thickness of RBC membrane, t_m , to be 3.3 and 11 nm, assuming $\epsilon_r = 3$ and 10, respectively. Indeed, modern measurements on artificial BLMs and biomembranes, fully confirmed Fricke's estimation of the thickness of the basics of membrane plasma membrane [3].

16.6.1

Basics of Membrane Electrochemistry

In membrane electrochemistry, the most useful approach is based on the Nernst–Planck (N–P) equation, as will be discussed in this section. In membranes, transport processes are of paramount

importance. The key concept here is the electrochemical potential ($\tilde{\mu}_i$), a quantity that is related to the chemical potential (μ) and the electrical potential (ϕ). Other electrical parameters of membranes are resistance (R_m), capacitance (C_m), current/voltage (I/V) characteristics, and breakdown voltage (V_b). These electrical properties of membranes are often used in fundamental studies and in practical applications (Fig. 2).

16.6.1.1 Nernst–Planck Equation

Ionic gradients and ion transport are deemed to be the principal processes responsible for the formation and changes of the transmembrane electrical potential, affecting the membrane excitability, enzymatic and immunological activities, and

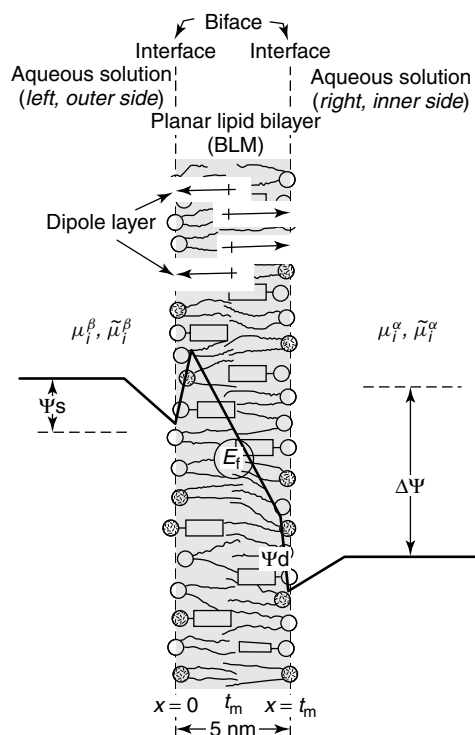


Fig. 2 An ultrathin membrane (e.g. BLM) separating two aqueous solutions. Biface is defined as two interconnecting interfaces where material and energy transport are possible. $E_f = \Delta\Psi/t_m$, Ψ = electrical potential, $\Delta\Psi$ = potential difference across the membrane = E_m , t_m = lipid bilayer thickness (estimate varies from 5 to 6 nm) (see Fig. 1 and text for details).

transducing function. All these phenomena are generally credited with metabolic processes being able to maintain the steady state, nonequilibrium conditions across the biomembranes by generating an active transport of ions or electrons. For instance, in the case of excitable membranes, this transport of ions across biomembranes generates and maintains nonequilibrium ionic concentration gradients, allowing the membrane potential to shift back and forth between the equilibrium potentials of different ionic species. The membrane system under consideration is assumed to be of molecular thickness and of planar configuration, and that transport of charged species (flux = J_i) takes place in one dimension (the x -direction) perpendicularly to the membrane (Fig. 3). Thus, the flux is given by

$$J_i = -kU_i C_i \frac{d\tilde{\mu}_i^\alpha}{dx} \quad (2)$$

where the electrochemical potential, $\tilde{\mu}_i^\alpha$, is defined in terms of chemical potential, μ , and electrical potential, ϕ . That is

$$\tilde{\mu}_i = \mu_i + z_i F \phi = \mu_i^0 + RT \ln a_i + z_i F \phi \quad (3)$$

and $a_i = \gamma_i c_i$, where γ_i is the activity coefficient. We will assume that $a_i \cong C_i$ (i.e. ideal solution) in all further equations of this chapter.

The driving force for moving ionic species across a planar lipid bilayer in the x -direction may be expressed as an electrochemical potential gradient, that is

$$\frac{d\tilde{\mu}_i}{dx} \cong \frac{RT}{dx} \frac{d \ln[C_i]}{dx} + z_i F \frac{d\phi}{dx} \quad (4)$$

The electrochemical potential is a fundamental measure of irreversibility as may be deduced from the second law of thermodynamics in the following manner. From the entropy S and $dS \geq 0$, where dS is the

change in S for the reversible ($\Delta S = 0$) and irreversible processes ($\Delta S > 0$), respectively. With a BLM interposed between two aqueous solutions, it can be shown that, for electrical work (W_{ele}) only,

$$\begin{aligned} T dS &= -\Sigma \mu dn - dW_{\text{ele}} \\ &= -(\tilde{\mu}_i^\alpha - \tilde{\mu}_i^\beta) dn - \{z_i F (\mu_i^\alpha - \mu_i^\beta)\} \\ &= -(\tilde{\mu}_i^\alpha - \tilde{\mu}_i^\beta) dn - \{z F (\mu_i^\alpha - \mu_i^\beta)\} \\ &= -(\tilde{\mu}_i^\alpha - \tilde{\mu}_i^\beta) \\ &= -\Delta \tilde{\mu}_i^{\alpha\beta} \end{aligned} \quad (5)$$

where superscripts α and β denote inside and outside of the membrane, respectively (Fig. 2). From Eq. (4), transport of ions and other species is caused by a force equivalent to $-d\tilde{\mu}/dx$ (Fig. 3).

16.6.1.2 Thermodynamic Considerations

A living cell is most unique in that its plasma membrane separates *two* aqueous solutions, which gives rise to a voltage or an electrical potential difference (PD) on the order of tens of millivolts (mV). This small PD is essential, however, for functioning of the cell. What is the meaning of this observed PD? From the viewpoint of thermodynamics, a cell is an “open system” involving both transport of matter and energy. Thus, the answer to the posed question may be simply answered as follows: the observed PD is a manifestation of electrical activities across the barrier membrane, which in turn is a measure of the Gibbs free energy change (ΔG):

$$\Delta G = -nFE_m \quad (6)$$

where E_m denotes the membrane potential or voltage (PD), n is the number of electrons involved in the reaction, and F is the Faraday constant. From Eq. (6) the following can be obtained:

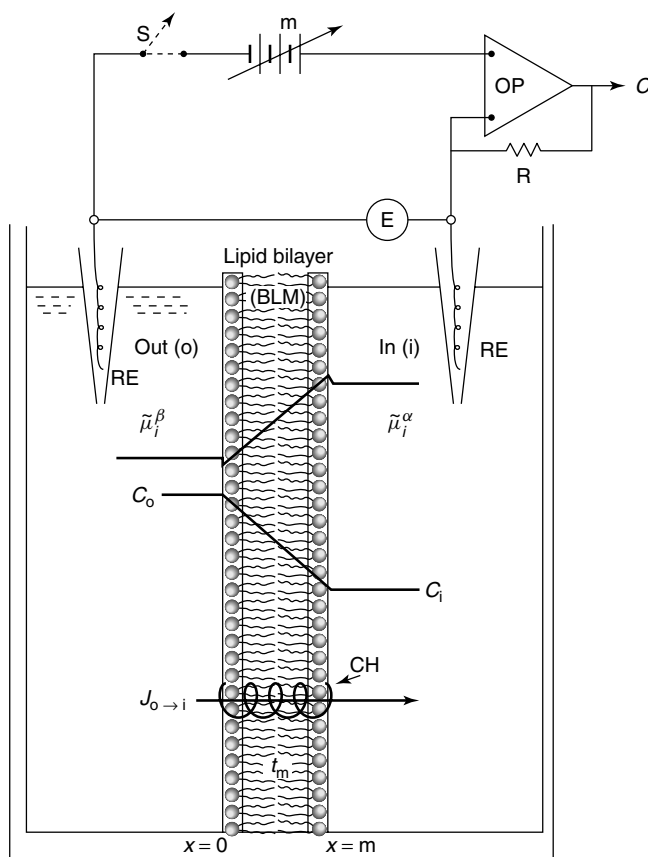


Fig. 3 An ultrathin membrane (e.g. BLM) separating two aqueous solutions. (a) Electrical arrangement for measuring membrane potential and current. S = switch, m = voltage supply, OP = operation amplifier, C = current out, R = resistor ($>10^{10} \Omega$), E = electrometer. (b) Experimental cell showing a BLM interposed between two aqueous solutions. RE = reference electrode (Ag/AgCl or SCE saturated calomel electrode), $\tilde{\mu}_i$ = electrochemical potential, C = concentration, J = flux, CH = channel, t_m = membrane thickness, o and i denote, respectively, outside and inside bathing solution [2, 3].

$$E_m^0 = \frac{RT}{nF} \ln K \quad (7)$$

where E_m^0 is a potential at standard conditions and K is the equilibrium constant of a given reaction. It should be pointed out that, when a pair of reference electrodes is placed across the

cell membrane, one is actually measuring the sum of two half-cells:

$$E_{\text{cell}} = E_m = E_{\text{in}} - E_{\text{out}} \quad (8)$$

where E_{in} and E_{out} denote the inside and the outside of the cell, respectively. By convention, the inside of the cell is taken

as negative. In this connection, the potential developed across the membrane results from a difference in electrochemical potential resulting from the equilibrium of ion, I, partitioned between two phases:



where I^α and I^β represent species I in the inner and outer phase, α and β , respectively. Through the Nernst equation, the values of half-cell potentials can be related to the activities (or concentrations) of the species involved in the solutions bathing the membrane. Then one obtains

$$E_m = E_{\text{cell}} = E^0 + \frac{RT}{nF} \ln \frac{[I^\alpha]}{[I^\beta]} \quad (10)$$

where $[I^\alpha]$ and $[I^\beta]$ are the concentrations of active species, in the two phases. All activity coefficients are taken as unity. On the basis of information given in Fig. 3, a PD of 58–60 mV would be expected for 10-fold difference in concentrations at room temperature ($22 \pm 2^\circ\text{C}$). If the membrane is selective, for example, it prefers cations over anions, then the more concentrated side will be negative. Later, after completing our discussion of the N–P equation, we will return to the experimental methods of monitoring these membrane potentials.

Since the N–P equation is central to membrane biophysics (transport, electrochemistry, and physiology), it is instructive to present more details here. From Eq. (2), the flux (J) across a membrane is equal to velocity times concentration (C), i.e. $J = vC$. The negative sign indicates the direction of decreasing concentration. The flux is also proportional to the mobility (U) and concentration (C), and the driving force of the species involved. In Eq. (4), where k is a constant to be evaluated. For simplicity, we have dropped the subscript

i . By substituting $\tilde{\mu}$ (Eq. 3) into Eq. (2), we can write:

$$J = -kUC \left\{ \frac{RT}{dx} \frac{d(\ln C)}{dx} + zF \frac{d\phi}{dx} \right\} \quad (11)$$

The value of k is found by rewriting the last term of Eq. (11) using for $\mu = v/(-z d\phi/dx)$ because the mobility U of the species is defined as the ratio of the velocity v of the ion and the potential gradient of the field causing the ion's motion. Since vC has the dimension of the flux J , it follows that $k = 1/F$. Eq. (11) can then be rewritten in the following way:

$$J = -\frac{UC}{F} \left\{ RT \frac{d(\ln C)}{dx} + zF \frac{d\phi}{dx} \right\} \quad (12)$$

Equation (12) is the famous *Nernst–Planck flux equation*, upon which all basic equations relevant to membrane electrochemistry and electrophysiology depend! For example, if the species being transported is not charged (i.e. $z = 0$), we have Fick's diffusion equation. Note here that the first term of the right-hand side of the above Eq. (12) describes the diffusion force caused by concentration gradient, while the second term describes the electrical force caused by the electrical gradient developed across the membrane (Fig. 2). In order to integrate Eq. (12), a two-variable differential equation, many attempts have been made. In all cases an a priori assumption has been made, that is, that the independent variable in the resulting solution is the concentration distribution, with potential gradient being its consequence. The first approach was made by Henderson in 1907, who assumed that the concentration gradient is linear within the membrane phase so that potential gradient is nonlinear. This is valid for the liquid junction potentials. However, in the case of biomembranes, and particularly

for BLMs, the lipid core is a barrier with very high energy for charge penetration. Thus, the assumption of a constant concentration gradient is unrealistic. The best known is the second approach by Goldman, who assumed linearity of potential gradient across the membrane phase so that the concentration gradient cannot be linear. It is worth noting that the Henderson equation gives the better results for a system with only one simple electrolyte present in different concentrations on both sides of the membrane. However, for biological systems with various permeant ion species on both sides of the membrane, the Goldman approach usually gives better results.

With the above-mentioned background, it is informative to describe an application of the N–P equation as applied to the nerve axon, which is surrounded by a plasma membrane. One of the main functions of the plasma membrane is to control the passage of ions and molecules into and out of the cell. For most biomembranes, the intracellular $[K^+]_i$ greatly exceeds extracellular $[K^+]_o$, and the opposite is true for the extracellular $[Na^+]_o$ and $[Cl^-]_o$. These concentration differences are due to the active transport system embedded in the lipid bilayer of the plasma membrane [3].

16.6.1.3 Nernst Equation

At equilibrium, there is no net flow of ions across the membrane. Therefore

$$\Delta J = 0; \quad RT \, d \ln C = -zF \, d\phi \quad (13)$$

Upon integration of the above Eq. (13) across the membrane, with $z = 1$ for univalent ions, it gives us

$$E^\alpha - E^\beta = E_m = \frac{RT}{F} \ln \frac{[a_i^\beta]}{[a_i^\alpha]} \quad (14)$$

where E_m is the membrane potential. By substituting appropriate ionic concentrations of the nerve axon, the Nernst potentials $E_m = -88 \text{ mV}$ for K^+ and $E_m = 55 \text{ mV}$ for Na^+ , are obtained.

16.6.1.4 Electroneutrality Principle

In a system consisting of an ultrathin membrane (e.g. a planar BLM or a cell membrane) separating two aqueous solutions, the law of electroneutrality must be obeyed. That is, the sum of positively charged species is equal to the sum of negatively charged species for the system as a whole. However, as pointed out by Guggenheim, charge separation on a microscopic scale may occur at membrane/solution interfaces [7]. For example, to develop a potential difference ($PD = E_m$) of 50 mV across a BLM of 5 nm thickness, the amount of charged species involved is far too small ($\ll 10^{-10} \text{ M}$) to be detected chemically, or by any other means, except electrically. Therefore, the E_m across a modified BLM (or a biomembrane, for that matter) cannot be simply related to the composition of bulk solution concentrations. The pivotal role played by the membrane is implicated, as described in the following section.

16.6.1.5 Ion Selectivity, Ion Specificity, pH, and Cell Membranes

One of the main tasks of biomembrane functions is ion or molecular recognition, which entails selectivity and specificity of the membrane. By selectivity for ions is meant that positively charged species over the negatively charged ones (e.g. Na^+ over Cl^-), whereas ion specificity is defined that one kind of ions over another (e.g. K^+ over Na^+). Thus, understanding the principles that lie behind the structural–functional relationship of biomembranes should help

in providing the insights of much of the cell's membrane electrochemistry.

Let us return to the discussion of the observed membrane potential (E_m) of the cell; the magnitude of which is on the order of millivolts. This brings us immediately to the problem of how to measure and analyze this vital electrical parameter of the cell. Fortunately, electrochemists have provided life scientists with a variety of reference electrodes such as Ag/AgCl and Hg/Hg₂Cl₂. The purpose of a reference electrode is to maintain a constant potential without changing it with respect to time. A good reference electrode should not be easily polarized during a measurement. Further, to prevent contaminations, a salt bridge made of a piece of tubing filled with agar gel (e.g. 0.3 g of agar/15 ml of 3 M KCl) is usually attached to the electrode. For example, "Hg/calomel Hg₂Cl₂/saturated KCl/agar gel" represents a so-called saturated calomel electrode (SCE). The standard potentials for Ag/AgCl and Ag/Hg₂Cl₂ are 0.222 and 0.268 mV, respectively (vs. NHE, normal hydrogen electrode). Thus, when a pair of these reference electrodes are placed across the cell membrane (for that matter across any physical barriers with electrical conductance), the resulting PD observed is owing to the contribution of the membrane and its bathing solutions only, since the reference electrodes themselves are invariant. It is worth remembering that we cannot measure a single potential of an electrode but only the PD. The voltage (V) or the PD of a cell is measured, when nearly zero current is passing through the contacting reference electrodes. Nowadays, it can be easily accomplished. All one needs is a high impedance voltmeter or an electrometer. In this connection, we need to consider the measurement of H₃O⁺ or pH, since ionic species of all

kinds are involved in biomembrane functions. The hydrated H⁺ occupies a most unique place, and its function in membrane electrochemistry deserves a special consideration, as investigated by Henderson and Hasselbach, and by Nicolsky (see following section and Ref. [3]).

16.6.1.6 The Henderson–Hasselbalch Equation

In acid–base physiology, one is concerned with the concentration of hydrogen ions (H₃O⁺) in the bulk phase. The Henderson–Hasselbalch equation of the form given below is of interest:

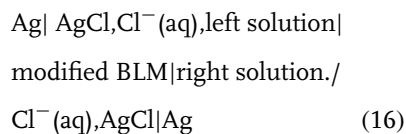
$$\text{pH} = \text{pK} + \log \frac{[\text{HCO}_3^-]}{[\text{H}_2\text{CO}_3]} \quad (15)$$

where pH is defined as $-\log[\alpha_{\text{H}^+}]$, pK = 3.6 for the bicarbonate reaction. For normal healthy people, the pH values of the extracellular and intracellular fluids fall in the range 7.35–7.45. When pH values are outside the range between 7.1 and 7.7 for long periods, the life as we know it is no longer viable. This narrow 0.6 pH unit appears to be small but is actually misleading. From a biophysical viewpoint, the pH values are best expressed in terms of H⁺ ion concentration in moles per liter. Thus, a pH of 7.4 represents a 40 nM of H⁺ ion concentration. A pH of 7.7 is equal to 20 nM of H⁺ ion concentration. Evidently, a change of merely 0.3 pH unit represents a twofold change in H⁺ ion concentration! To better appreciate these numbers, one is reminded of the normal K⁺ ion concentration in the extracellular fluid, which is on the order of 5 mM, and is of crucial importance in nerve functioning, whereas the H⁺ ion concentration is expressed in nM (1 nanomolar = 1×10^{-9} moles per liter). Thus, there is a 1 000 000 times difference in magnitude of these two ion concentrations! Further, the vital role is played

by hydrogen ions in the body fluids, both intracellular and extracellular, in cell functions (e.g. enzyme catalysis, periodontal disease, etc.).

Ion-selective membranes A simple and reliable way to access pH is of evident importance. The problem for accurate pH measurements was solved successfully in the 1930s, using a soft soda-lime glass (made of $\text{SiO}_2:\text{Na}_2\text{O}:\text{CaO} = 72:22:6$ wt.%). Owing to the high impedance of the glass used for pH sensing, an electrometer was necessary. Today, with modern electronics, this presents little problem, as already mentioned above. It is worth noting, however, that a pH glass electrode used today may be thought of as a *thin* membrane separating two aqueous solutions, with ion selectivity and specificity for H_3O^+ . In this sense, certain doped BLMs have been found to behave similarly. Therefore, equations developed for ion-selective membranes are applicable to both cases. We will discuss here only the ion-selective BLM interposed between two solutions.

A typical cell for BLM studies usually consists of two silver–silver chloride (or SCE) reference electrodes arranged as follows:



It is worth stressing that a modified BLM in the above cell arrangement behaves as a bipolar electrode or two working electrodes connected in series. The two reference electrodes depicted in the setup merely facilitate the connection to the measuring instrument. The cell potential

difference (E_m) observed across an ion-selective membrane (e.g. BLM) is called a *membrane potential*. In other words, membrane potentials are responsible for the operation of the cell membranes in living organisms. Electrochemists make use of ion-selective membranes to construct chemical sensors for various ions such as hydrogen, sodium, potassium, calcium, and fluoride ions, to name a few [7–9].

The Nicolsky equation With common pH instruments, the Nernst equation can accurately predict the pH of an unknown solution, over the pH range 2 to 12. At more extreme values of pH, some response to other ionic species in solution begins to become apparent. This is the so-called *salt error*. For example, a valinomycin-doped BLM for K^+ suffers from some interference because of Na^+ . A better equation proposed by Nicolsky should be used. Accordingly,

$$E_m = k + \frac{RT}{z_i F} \ln \left(a_i + \sum K_{ij}^{\text{pot}} a_j^{z_i/z_j} \right) \quad (17)$$

where K_{ij}^{pot} stands for the selectivity coefficient. The slope (RT/F) is measured in millivolts per decade.

16.6.1.7 Origins of Membrane Potentials

By placing a pair of reference electrodes (e.g. SCE) on opposite sides of a biomembrane, a PD (voltage, V) on the order of tens of millivolts (mV) is usually detected. This voltage suggests an unequal distribution of charges across the membrane. These charges may be ions or free charges such as electrons and holes, or they may be dipolar molecules [3]. This charge imbalance across the membrane is a result of charge separation, and may be due to one or a combination of several of the following situations:

- preferential adsorption of ions;
- orientation of dipolar molecules;
- movement of ions from one side to the other;
- deformation of molecules;
- oxidation–reduction (redox) reactions;
- perturbation of the membrane by external sources (light, applied voltage, pressure or temperature difference, and others).

In addition to the membrane voltage (V or E_m), there are other electrical parameters associated with the membrane. Prominent among these are membrane capacitance (C_m), resistance (R_m), current (I_m), and breakdown voltage (V_b). From basic physics, $V \propto q$ (the fundamental charge associated with an electron), one can write

$$q = CV \quad (18)$$

where C is the proportionality constant, termed *capacitance*. Thus, we have the familiar formula:

$$C = \frac{q}{V} \quad (19)$$

The unit for C in membrane electrochemistry is defined in microfarad (μF) per unit area in cm^2 . Recalling Eq. (1), Fricke determined the capacitance (C_m) of the RBC membrane using a parallel-plate condenser formula. It should be noted here that a capacitor can be discharged, and therefore there is a capacitive current (i_c) connected with it, which is given by

$$i_c = \frac{dq}{dt} = C \frac{dV}{dt} \quad (20)$$

and

$$\int dV = V = \frac{1}{C} \int i_c dt \quad (21)$$

This capacitive current, i_c , differs from the current, I , expressed in Ohm's law

($E = IR$). The capacitive current is a displacement of charges on opposite sides of the membrane, and therefore, it does not involve a direct translocation of ions through the membrane. One needs to remember that the electrical current is expressed in amperes (coulombs per second).

16.7

The Role of Electrical Double Layers (EDLs) and their Biological Implications

A separation of charges occurs at almost all interfaces; that is, interfaces are electrified. This leads to the formation of EDLs at the interface. This effect is of particular importance for the systems of well-defined surfaces relative to the volume or thickness of a given phase. This is because the presence of EDL being the primary energy barrier, is the factor governing the properties of such systems [3, 5, 7].

The experimental evidence demonstrates that the EDL model elaborated independently by Gouy and Chapman at the turn of twentieth century can describe adequately the distribution of electrical potential adjacent to a BLM. In the Gouy–Chapman theory, the Poisson equation relates the electrostatic attraction of the counterions to the charged surface and the Boltzmann relation – the tendency of the counterions to diffuse from a region of high concentration. The Gouy–Chapman theory does not account for the discreteness of fixed structural surface charges but considered them to be smeared uniformly over membrane surface. Gouy and Chapman assumed also that the aqueous phase is structureless with a constant electric permittivity coefficient and the ions are point charges. The Gouy–Chapman theory was derived for uniunivalent electrolyte

solutions. Physiological solutions usually are more complicated, containing both monovalent and divalent cations. In this case, the description given by Grahame and others is more correct. Moreover, some ions bind to the surface, producing an electrostatic potential at this surface lower in magnitude than those predicted by Gouy–Chapman theory. The simplest way to include this process was proposed by Stern who introduced the Langmuir adsorption isotherm into the Gouy–Chapman theory. Although the EDL theory for classical electrochemical systems (metal/electrolyte solution) was developed relatively early, it was not until 1935 that Theorell applied it to the membrane processes. He also introduced the idea that the membrane potential is a sum of an electrodiffusion potential across the membrane proper and the effects of two boundary potentials at both membrane–solution interfaces. Since then, there has been a renaissance of activity testing various models of EDL at the membrane–solution interface. The electrochemical behavior of biomembranes and their models is therefore largely affected by the presence of EDL. In the following paragraphs, we will illustrate the origins of various membrane potentials in terms of BLMs (planar lipid bilayers).

The unique aspect of BLM, similar to biomembranes, is the ultrathin lipid bilayer separating two aqueous solutions (Fig. 3). Membranes of these types have two interdependent interfaces (i.e. a *biface*, meaning the two coexisting solution–membrane interfaces, through which material, charge, and energy transfer are possible). The creation of a biface is the result of two immiscible phases with very different relative dielectric constants ($\epsilon_{\text{wr}} = 80$; $\epsilon_{\text{mr}} = 2-5$). At each interface,

as well as across the ultrathin lipid bilayer (~ 5 nm), powerful electric fields may exist, which facilitate charge separation and transport, as discussed later in conjunction with the origins of BLM potentials.

An observed transmembrane PD (E_{m}) in a BLM system may be due to one or a combination of the following potentials [3, 7]:

- diffusion (concentration) potential, ϕ_{d} ;
- adsorption (surface or interfacial) potential, V ;
- distribution (outer) potential, U ;
- Galvanic (inner) potential, $\phi (= V + U)$;
- Gouy (Donnan) potential, U_{G} or ϕ_{Don} ;
- electrokinetic potential, U_{k} ;
- thermoelectric potential, E_{t} ;
- redox (electrostenolytic) potential, E_{RX} ;
- photoelectric potential, E_{hv} .

In the classification given above, redox, thermoelectric, and photoelectric potentials in the BLM are discussed in a later section, whereas a brief summary will be given on the electrokinetic potential relevant to membrane electrochemistry.

16.7.1

Electrokinetic Potential, U_{k}

The electrokinetic potential manifests itself when one phase is in motion relative to the other. This relative movement may be on account of (1) applying mechanical forces acting on the liquid or solid phase, and (2) applying an electric field tangentially to the EDL. To the first group belong two electrokinetic phenomena: the Dorn effect and streaming potential. The second group consists of two other phenomena: electrophoresis and electroosmosis. These are summarized in Table 2.

Tab. 2 Electrokinetic phenomena at interfaces

<i>Phenomena</i>	<i>Stationary phase</i>	<i>Moving phase</i>	<i>Mechanical force</i>	<i>Potential difference</i>
Dorn effect	Electrolyte solution	Suspended particles	Cause	Result
Streaming potential	Walls of capillary	Electrolyte solution	Cause	Result
Electrophoresis	Electrolyte solution	Suspended particles	Result	Cause
Electroosmosis	Wall of capillary	Electrolyte solution	Result	Cause

The Dorn effect It occurs when particles suspended in the electrolyte solution precipitate under the influence of gravity (or centrifugal force), and results in potential difference between the top and bottom of suspension.

Streaming potential When liquid flows along a narrow tube or capillary, or through a porous plug (a bundle of narrow tubes in parallel or channels in BLMs and biomembranes) under a hydrostatic head, a difference of potential is set up between the ends of the capillary or across the porous plug as the case may be.

Electrophoresis This is the migration of large molecules (e.g. proteins, polymers), microscopic aggregates of molecules (e.g. colloidal particles) or cells, or liposomes (e.g. erythrocytes) under the influence of an electric field applied to the medium in which the particles are suspended.

Electroosmosis If a difference of potential is deliberately set up along the axis of narrow tube or across a porous plug, liquid in the tube or plug flows until a hydrostatic head sufficient to prevent continued flow has built-up to the value of the electroosmotic pressure. In all these phenomena, the EDL and potentials are involved as stated above.

Among electrokinetic phenomena, electrophoresis plays a prominent role. In the form of a special technique, it serves for analytical purposes and as a tool in the investigation of cell diseases and membrane phenomena. For analytical purposes, this technique has been used in various forms of paper or gel electrophoresis (two-dimensional electrophoresis, immunoelectrophoresis, isotachoelectrophoresis, and others) for preparative separation and identification of fraction components. Besides this, as a microelectrophoresis, the technique may be used to elucidate the nature, number, and distribution of charge groups in the peripheral zone of biological cells or to separate subpopulations in a mixture of cells, or vesicles (continuous flow electrophoresis, electrofocusing). Microelectrophoresis has been used for diagnostic tests in medicine as well as for investigations of cell diseases and membrane phenomena. It is also a very important method in the investigation of membrane structure and bioelectrochemical phenomena at the cell membrane–electrolyte solution interface.

Under separate headings, the nature and origin of other membrane potentials: diffusion (concentration) potential adsorption (surface or interfacial) potential, distribution (outer) potential, Galvani (inner) potential, and Gouy (Donnan) potential will be considered. These potentials are

best described in the language of interfacial chemistry, and have been treated in detail [3, 6, 7]. In order to apply these concepts relevant to membrane electrochemistry, it is informative, first of all, to define the terms and to summarize some of the general conclusions of these potentials [3, 7].

16.7.2

Adsorption Potential

Also known as surface or interfacial potential (designated by symbol V), it is opposite to that observed with the diffusion potential. For this interfacial potential to appear, a difference in salt concentrations across the BLM is not required; it depends upon the sorbed species and/or the dipoles. With cationic interface-active compounds, such as hexadecyltrimethylammonium bromide (HDTAB) and phosphatidylethanolamine (PE) at low pH, a negative potential results and vice versa with anionic interface-active compounds, such as dodecyl acid phosphate (DAP) and phosphatidylserine (PS). The magnitude of V decreases with increasing of the salt concentration. Two other caveats should be noted about this potential: (1) it may have only transient existence; however, the time for its decay can take a long time and (2) the law of electroneutrality at the interfaces is not obeyed [1].

16.7.3

Distribution Potential

It is also called outer potential, symbolized by U . The potential arises as a result of a differential distribution of the oppositely charged species across the interface, the magnitude of which is influenced by the diffusion of ions and their concentrations,

and increases with increasing salt concentration, but is independent of the nature of the common ion.

The sum of interfacial potential and distribution potential is termed the inner or *Galvani potential*, designated by ϕ . It will be discussed below that the observed transmembrane potential difference, E_m , is due either to ΔV , ΔU , or to ΔV plus ΔU , as defined above. It should be remembered that there are two components of ϕ ($=V + U$). They are concerned with only the distribution potential. If compounds, such as phospholipids and interface-active agents, are preferentially adsorbed at the interface, the so-called adsorption potential (V) may also develop. As shown in Fig. 2, both adsorbed fixed charge species and dipoles may contribute to the observed potential. The nature and origin of the adsorption (or interfacial) potential can be discussed in terms of the classical EDL theory of Gouy–Chapman–Stern–Graham [7, 15–19].

16.7.4

Diffusion Potentials

In general, *diffusion potentials* appear always when an electrolyte diffuses down its concentration gradient. However, one prerequisite condition, namely, both cationic and anionic species must have different mobilities. The magnitude and sign of such potential depends on the difference in mobilities between cation and anion (the greater the mobility difference, the greater the potential difference), with the more dilute region having the same sign as the faster ion. In bulk solution, these potentials are readily disturbed by convection and may be neglected, but if two electrolyte solutions of different concentrations are in contact in a way that avoids

convictional mixing but allows a diffusional flow, the diffusion potentials are stable. Such electrolyte contact may be accomplished either in a direct way or by electrolyte separation by semipermeable membrane. The direct contact of two immiscible solutions leads to the so-called *liquid junction* potentials that are a possible source of error whenever electrodes with salt bridges are used. The electrolyte separation by a permselective membrane is characteristic of biomembrane systems, and has already been discussed above. For the sake of simplicity, all ion fluxes are constant and independent of time (steady state conditions). This requires the stable properties of the membrane and constant concentrations at the membrane. The latter may be achieved in several ways. In the case of experiments with BLMs, the vastness of the two compartments on both sides of the membrane provides practically constant concentrations.

16.7.5

The Gibbs–Donnan Potential

The *Gibbs–Donnan potential* occurs when a nonpermeant ion (for biological systems, usually a polyion such as a protein) is unequally distributed between the two electrolyte solutions separated by a permselective membrane, which allows certain electrolyte ions to move freely between the two solutions. The second law of thermodynamics and the principle of electroneutrality restrict this movement. The first restriction requires that each permeant ion species moves only down its electrochemical potential gradient, the latter requires the sum of all positive charges (cations) to be equal to that of all negative charges (anions) in each solution. When the system reaches its equilibrium, there is no flux of any permeant species i , $J_i = 0$.

Eq. (12) then takes the form

$$z_i F \frac{d\phi}{dx} = -RT \frac{d(\ln C_i)}{dx} \quad (22)$$

Integration of this equation over the whole membrane thickness at the equilibrium conditions leads to the expression for electrical potential difference developed across the membrane, known as *Donnan potential*,

$$\phi^{\text{II}} - \phi^{\text{I}} = {}^{\text{II}}D^{\text{I}}\phi = \frac{RT}{z_i F} \ln \frac{C_i^{\text{I}}}{C_i^{\text{II}}} \quad (23)$$

where superscripts I and II denote the two sides of the membrane. This dependence may also be obtained in another way. The main condition of the equilibrium state is equilibrium of electrochemical potentials of each permeant species on both sides of the membrane

$$\tilde{\mu}_i^{\text{I}} = \tilde{\mu}_i^{\text{II}} \quad (24)$$

which leads immediately to the dependence

$$RT \ln C_i^{\text{I}} + z_i F \phi^{\text{I}} = RT \ln C_i^{\text{II}} + z_i F \phi^{\text{II}}$$

or

$${}^{\text{II}}D^{\text{I}}\phi = \frac{RT}{z_i F} \ln \frac{C_i^{\text{I}}}{C_i^{\text{II}}} \quad (25)$$

being identical with Eq. (25) may be useful in the determination of nonpermeant polyion concentration (see Eq. 13).

An electric potential difference is generally established at a membrane (e.g. a BLM) and adjacent solution interface. There have been two entirely different approaches to describe this potential difference, with respect to location of fixed membrane charges and BLM permeability to ions. When a membrane being permeable to ions contains homogeneously distributed fixed charge groups and is in

equilibrium with a symmetrical electrolyte solution, one can consider the existing potential difference in terms of Donnan equilibrium potential. Donnan, in 1911, studied the electrical potential set up at a semipermeable membrane between two electrolytes, an effect of importance in living cells, known as the Donnan effect. Specifically, when a thin, selectively permeable membrane separates two solutions to small ions (e.g. Na^+ , K^+ , Cl^- , etc.) but not to large ionic species (e.g. proteins). The diffusion of oppositely charged, permeable ions will be in equilibrium as soon as the concentration ratios for the ions have been established. That is, for example, $[\text{Na}^+]_{\text{out}}/[\text{Na}^+]_{\text{in}} = [\text{Cl}^-]_{\text{in}}/[\text{Cl}^-]_{\text{out}} = r_D$, where subscripts “out” and “in” denote, respectively, the outer and inner solution, and r_D is the so-called Donnan equilibrium constant (assuming of course the activity coefficients of respective ions are unity). Owing to the concentration differences of permeable ions, an electrostatic potential difference is established in addition to a difference in osmotic pressure across the membrane. This membrane potential difference, known as the Donnan potential, may be described by the Nernst equation. It should be stressed that the Donnan phenomenon is the result of certain ionic species, either fixed on or not able to, move away from the membrane. Further, the Donnan phenomenon may be discussed in its simplest form. The potential changes discontinuously at the boundary between the two electroneutral phases. However, replacing the assumption of local electroneutrality, used in the classical approach, by the Poisson–Boltzmann equation, under suitable modification of BLM or electrolyte solution with lipophilic probe ions this situation may be improved. If, on the other hand, one assumes that all charges are smeared

uniformly over the surface of impermeable BLM, the potential profile in the EDL is described by the Gouy–Chapman theory. The potential distribution in the proximity of membrane–electrolyte interface may be regarded in fact as the two limiting cases of more general Poisson–Boltzmann equation. This equation may be derived for a model charged membrane, permeable to some extent to ions, in which the fixed charges are uniformly distributed through a layer of finite thickness t . It also includes the possibility of ion binding to the fixed charge sites. By varying the thickness of charged layer, it has been shown that the constant changes of potential profile occur across the membrane interface, which for $t \ll l$ take the form of Gouy–Chapman theory, while for $t > l$ is described by the Donnan theory. Thus, both the Gouy–Chapman theory and the Donnan theory can be considered as special cases of the Poisson–Boltzmann equation. This model assumes the uniform and delocalized distribution of charges for BLMs containing certain amount of charged phospholipids (e.g. PA or PE). For this case, the negative charges of these molecules should be considered as localized, although they may still be distributed homogeneously. Under the influence of external field applied across the BLM, the surface charge density induced by membrane polarization would be considerably high for discrete charges than for “smeared out” ones. This should largely affect the BLM stability and conductance properties. The simplest way to treat the problem of lateral discrete distribution of charges on the membrane surface is to replace the continuous distribution function by the sum over all discrete membrane charges fixed in a regular lattice, usually square. From the solution to the Poisson–Boltzmann equation, the electrostatic

potential at any point in the aqueous phase is calculated to be identical to the lattice sum over the Coulomb potentials because of individual fixed charges. The local potential maxima at all charged sites in the lattice are taken into consideration. As a consequence of such maxima, this model predicts that the discrete nature of the surface charge should manifest itself in the discrete adsorption of ions at the membrane surface. However, the effects of discrete charges have to be considered when charges are buried within the low dielectric interior of the BLM or the lipids have multiple charges in their headgroups [3].

16.7.6

Phase Boundary Potentials

These are also known as *surface potentials*. Phase boundary potentials, appearing at the interfaces between the membrane and adjacent electrolyte solutions, are attributed mainly to fixed charges within or attached to the membrane phase. These fixed charges that originated from ionic groups are part of the membrane structure and, under special conditions, may change their number through the dissociation of weak acidic groups or conversely through association of ions with binding groups. The electric dipoles (e.g. headgroups of lipid matrix) also contribute to these potentials. The phase boundary potentials do not usually directly add to the transmembrane potential difference; however, they do affect the electrical potential profile within the membrane. Therefore, their presence may alter the permeability properties of membrane (e.g. by affecting organization of integral or peripheral proteins), indirectly affecting in this way, the transmembrane potentials. The relationship between fixed charges and phase

boundary potentials can be illustrated by either one of two simplified models. The first model assumes that the fixed charges are adjacent only to both surfaces of a nonpolar membrane interior. This model may represent an artificial BLM. It is also close to a biological membrane. In the second model, an assumption is made that the fixed charges are homogeneously distributed over the whole membrane. An ion-exchange membrane may represent this model.

In the case of an ion-exchange membrane that is the second model mentioned above, an assumption has been made that its fixed, say negative charges, are homogeneously distributed over the membrane phase. In this situation, the appearing phase boundary potentials may be treated as two separate Donnan equilibrium potentials at each interface. The role of impermeable polyion from the previous section is now as the fixed charges from the membrane interior. If at the beginning an initial unequal distribution of permeant ions exists on both sides of such membrane (let us assume that a less concentrated electrolyte solution is on the right side of the membrane), the whole system will proceed toward equilibrium. As a consequence, at equilibrium, the electrochemical potentials must be identical on both sides of each boundary. Since biological membranes do not have a high density of fixed charges in their interior, the effects of Donnan distribution are of smaller magnitude than for ion-exchange membrane. As stated at the beginning of this section, it appears that the permeability and conductance properties of the membrane are strongly influenced by the electrical potential profile. Since the variations of phase boundary potentials may alter the behavior of pores, channels, and ion carriers, they may express themselves

as alterations of current–voltage relationships, giving indirect information about potential distribution within the membrane and at its interfaces. However, the phase boundary potentials are not usually readily measurable with electrodes towing to the thickness of the membrane phase.

16.7.7

Relationship among Various Potentials

Of immediate concern here, we have been discussing the observed membrane potential, E_m , which is the sum of all interfacial potentials and diffusion (concentration) potentials at the interfaces and within the membrane. Thus, we have the appropriate name, the so-called *transmembrane potential*, E_m , which is given by

$$E_m = \Delta\phi + \phi_d \quad (26)$$

or

$$E_m = \Delta V + \Delta U + \phi_d \quad (27)$$

or

$$E_m = \Delta U_G + E_p + \Delta U + \phi_d \quad (28)$$

For most of these individual potentials, the final expression takes the form of the Nernst equation (Eq. 14). Experimental conditions or circumstances can be such, that E_m measures one or a combination of these potentials. Specifically: (1) for a symmetrical BLM, the polarization potential, E_p , is unimportant, (2) for an unmodified BLM, whose interior is liquid-hydrocarbon-like, $\Delta\phi$ is not measured, (3) for BLM with low interfacial charge density (e.g. $\sigma < 1$, net charge per 100 \AA^2), $\Delta\phi_G$ contributes very little, (4) for charged species with substantial solubility in BLM, $\Delta\phi$ may be neglected, and (5) for a BLM with high interfacial charge density

($>1 \text{ e}/100 \text{ \AA}^2$), the diffusion potential, ϕ_d , is inconsequential.

It should be emphasized, however, that the above statements are offered as general guidance only. Even for a relatively simple BLM, the measured transmembrane potential (E_m) could be a result of various potentials. The extent of contributions of these potentials to the overall E_m is dependent upon the nature and properties of BLM-forming constituents, whose charge densities, dipole orientations, and relative permeabilities to ions are some of the factors that should be taken into consideration for a careful analysis of the observed membrane potential [1, 3, 6–11, 29, 30].

In concluding this section, mention should be made concerning the dipoles of membrane constituents in the BLM. The dipole flip-flop could be important for the voltage-dependent conductance in BLM (e.g. alamethicin-modified BLM). Derzhanski et al. have derived an equation for the current as a function of frequencies. Pastushenko and Chizmadzhev have considered the energetic profile of dipole molecules in biomembranes in general, and in BLM in particular. This topic has been reviewed in detail by Shchipunov and Drachev, and by de Levie [3, 15–24].

It is known that the value of dielectric constant is a function of the local electric field. Since the electric field near the interface is not a constant, but a function of distance from it, the further refinement of EDL theory and potential profile at the BLM interface should include this positional dependency of dielectric coefficient. The local value of this coefficient is of course a measure of the influence of uncharged species such as water or lipid molecules on the interaction between charges in their vicinity. The dielectric coefficient of bulk aqueous electrolyte at

293 K is about 80. Its value near the interface is not precisely known; usually it is assumed to be about 2 to 6. However, owing to finite size of ions and water molecules, one may speculate that the value of dielectric coefficient in close proximity of the surface would be about unity. The transition between these two limiting values is obviously continuous in the interfacial region.

Since conventional BLMs are usually formed as a symmetrically oriented double layer of lipid molecules on a hydrophobic support separating two aqueous phases, these closely packed and aligned molecules should generate surface dipoles, hence dipole potentials, at each of the two BLM–solution interfaces. Thus, all the latest interest in evaluation of coherent and precise theory of EDL at the membrane interface should not be underestimated. The electrostatic potentials due to the charges on lipids or proteins are important in membrane functioning. They appear to influence the calcium effect on excitable membranes, channel conductance in membranes, passive ion transport, function and structure of thylakoid membranes, kinetics and catalytic properties of membrane-bound enzymes, electron transfer reactions, and the interaction of some electroactive compounds inside the membrane (e.g. porphyrins) with their electron exchange partners in aqueous phase. This influence may also be because of the simple electrostatic screening effect of membrane surface charge against the coionic substrates. Such simple model of the interfacial region as Gouy–Chapman's can provide the explanation for experiments carried out on conductance of BLMs modified with channel forming ionophore, gramicidin [5–7, 13, 15–19, 29].

All dissolved molecules, including those that can readily pass through lipid

bilayers and those that transverse with difficulty (lipid bilayer–hampered substances), are capable of diffusion. For lipid bilayer–impeded substances, diffusion across cell membranes may nevertheless be highly probable but such diffusion must be facilitated by lipid bilayer spanning proteins. Such proteins and their polypeptides essentially form carriers or channels (pores). In this case, they (1) accept specific lipid bilayer–hampered substances at one side, (2) allow the substance to enter the lipid bilayer without dissolving in it, and (3) then deliver the substance to either side.

In the case of water flow across a semipermeable membrane separating two electrolyte solutions, two electrokinetic phenomena may be demonstrated, namely, electroosmosis and streaming potential. The former associated with J_v , volume flow, is driven by an electric current, I , (because of $\Delta\psi$), whereas the latter is owing to pressure difference (ΔP). In sum, we have

$$J_v = L P \Delta P + L P \psi \Delta \psi \quad (29)$$

and

$$I = L \psi P \Delta P + L \psi \Delta \psi \quad (30)$$

where ψ , $L \psi P$, and $L P \psi$ are, respectively, potential, and phenomenological coefficients. In other words, J_v and I are both driven by ΔP and $\Delta \psi$, where $L \psi P = L P \psi$ (due to Onsager) is the so-called phenomenological (cross) coefficient. The most significant conclusion from the above equations is that the coefficients relate the volume flow and current in a given system. Thus, experimentally one needs only to measure one parameter or the other, which may not be directly determinable [3, 31].

16.8 Experimental Membrane Systems

Owing to complex structural and environmental factors associated with biomembranes, numerous investigators used different techniques and carried out studies on model systems in order to understand the fundamental life processes. These include ion accumulation or active transport, conduction of nerve impulses, energy transduction, protein synthesis, permeability barrier of ions and molecules, immunological reactions, phagocytosis and pinocytosis, and so on, in physical and chemical terms [3]. Under separate headings below, different model systems will be described.

16.8.1

Langmuir–Blodgett Films

In 1917, Langmuir demonstrated in a simple apparatus (now known as the Langmuir trough) that fatty materials including lipids in organic solvents spread in a monomolecular (monolayer) way when they are placed at an air–water interface. From the known quantity of the material used and measured area covered, the dimensions of a molecule may be estimated. Later, the Langmuir–Blodgett (L–B) technique and self-assembly of BLM methods were developed for use in technology. However, in the case of the L–B technique, the “pinhole defects” are difficult to avoid. There is a major difference between the BLM and multilayers formed by the L–B technique. A BLM, formed either by the conventional “painting” method or self-assembled on a substrate (e.g. a freshly cleaved metallic wire or agar gel [2, 3, 32] is a dynamic liquidlike structure that is capable of accommodating a host of modifiers. In contrast, an L–B

multilayer of bimolecular thickness, albeit much more stable than a BLM, usually contains pinholes and is in a solid state. The modifier molecules capable of electron transfer through the film are frequently short-circuited by the pinholes. Until now, however, the above approach seems to be applied only to the UQ10 incorporated in the L–B films at the electrode surface and conducting polymer nuclei deposited in the alkanethiol monolayer modified electrodes [32].

16.8.2

Immiscible Liquid–Liquid (L–L) Interfaces (ITIES)

The interface between two immiscible solutions (e.g. water and nitrobenzene) containing dissolved species is a site of an electric potential. By measuring this potential difference at the aqueous electrolyte/solid electrolyte phase boundary, the phenomena taking place at the interface between two immiscible solutions or the membranes of ion-selective electrode have been studied. Changing the composition of the solutions in contact can alter this potential; or applied current can alter the composition of the solutions. Thus, judicious choice of applied potential or current can be used to study the structure of the interface. Since the interface is “ultrathin” ($\ll 1$ nm), it cannot be observed directly. It can be, however, investigated by electrochemical or optical methods [14, 33]. The knowledge gained on the immiscible liquid interfaces can be applied also to the studies between solution–metal, or solution–membrane interfaces. Further, by controlling the interfacial potential difference between two immiscible solutions rates of interfacial electron and ion transfer may be controlled. In the electron transfer case, the interest is in two-phase reactions

that are important in organic synthesis, whereas in the case of ion transfer, liquid membranes for metal recycling can be successfully carried out. For example, AC impedance studies of the ion transfer have evidenced the transient adsorption of xanthene-type anions and other ions having asymmetric charge distribution at the nitrobenzene/water interface. The phase angle of the charge transfer admittance becomes smaller than unity at the potentials beyond the midpoint potential of the ion transfer. This anomaly does not appreciably depend on the sign of the ionic charge or the location of the midpoint potential, as predicted by the theory proposed recently based on the thermodynamic reasoning of the adsorption and ion partitioning of surface-active ions in electrochemical liquid–liquid two-phase systems [14, 33].

16.8.3

Planar Lipid Bilayers and Liposomes

A good experimental model for biomembranes should possess a lipid bilayer structure, onto as well as into which functional entities can be embedded. Thus, since the 1960s, the two most widely used model membranes have been BLMs, also referred to as planar lipid bilayers and spherical liposomes. Planar BLMs and spherical liposomes are complementary to each other, since both types are derived from common amphipathic lipids and related compounds. Both are excellent model membrane systems, and have been extensively employed for investigations into a variety of physical, chemical, and biological functions. In the remainder of this chapter on membrane electrochemistry, the focus will be mainly on planar BLMs, because they are easily and have been investigated electrochemically (for liposomes, see Refs. [3, 12, 34]). As a result

of experimental BLM studies, we now have a better knowledge in the following areas of biomembranes:

- structural–functional relationship of lipids, proteins, carbohydrates, pigments, and their complexes;
- mechanisms of transport, energy transduction, signal processing; and
- sensory perception such as vision, olfaction, hearing, taste, and touching sensations.

16.9

Bilayer Lipid Membranes

16.9.1

Formation Techniques

16.9.1.1 Conventional BLM

For all conventional BLM experiments, a cell with two chambers is necessary. This is usually accomplished by having a cup made of Teflon (or other highly insulating material) placed in a container made of glass (or some other transparent plastic material) for visualization. The two chambers are electrically isolated from each other apart from a small aperture in the wall of the Teflon cup, onto which the BLM is formed. The process of BLM formation is monitored by measuring the increase in membrane capacitance (C_m) and also by visual observation. The area of a BLM is measured using a graticle placed inside the ocular piece of the microscope. As illustrated in Fig. 3, the usual picture of a BLM interposed between two aqueous solutions consists of a liquid-hydrocarbon phase sandwiched between two hydrophilic regions. The structure of the BLM is considered to be a thin slab of liquid crystals in two dimensions, having a fluid hydrocarbon core about 5 nm thick. This liquid-crystalline structure of BLM

is essentially an excellent insulator. The electrical properties of BLMs have been extensively investigated, which usually entails measuring membrane resistance (R_m or conductance, $G_m = 1/R_m$), capacitance (C_m), potential difference (E_m), dielectric breakdown voltage (V_b), and current/voltage (I/V) characteristics (voltammogram). Unmodified BLMs (i.e. BLMs formed from common phospholipids such as lecithin or oxidized cholesterol dissolved in an *n*-alkane solvent in 0.1 M KCl solution) has typical intrinsic values of R_m greater than 10^8 ohms cm^2 , $C_m \simeq 0.5 \mu\text{F cm}^{-2}$, $E_m \sim 0$, $V_b < 200$ mV, with I/V curves obeying Ohm's law. With a few exceptions, the results of these measurements have been interpreted by treating the BLM electrically, in a system equivalent to that of a resistor connected in parallel with a capacitor Fig. 4.

16.9.1.2 BLMs via L–B Technique

Conventional BLMs can also be formed by the L–B technique, [see Tien, 1974]. Essentially, it is a combination of the monolayer technique and the dipping method. A partition made from a sheet of Teflon (25–500- μm thick) with a hole (0.25–1 mm) at the center is placed between the two halves of a trough, with the hole above the aqueous phase. The trough is first filled with an aqueous solution. After the surface has been cleared, a monolayer of a suitable lipid solution is spread in the surface in the usual manner. After evaporation of the solvent, the Teflon partition is then lowered slowly into the aqueous solution. A BLM is thus formed over the hole (see Fig. 4). Conversely, with the Teflon partition bearing a hole in place, the aqueous solution on either side is covered by a monolayer. Then, the levels of aqueous solutions are raised simultaneously above the

hole thereby forming a BLM from the apposition of the hydrocarbon chains of the two lipid monolayers. Another variation of the monolayer-dipping technique is by having a closed chamber used in the water permeability studies. The closed chamber with an aperture on its side is held in place. The chamber, while immersed in aqueous solution below its aperture, is filled completely with aqueous solution. A few drops of BLM-forming solution (*n*-hexane or *n*-octane as lipid solvent) are introduced to the surface of the outer aqueous solution. After the solvent has evaporated, the level of outer aqueous solution coated with a lipid monolayer is slowly lowered below the aperture and then raised carefully above it, thereby forming a BLM. It should be mentioned, however, that there is a major difference between the BLM and multilayers formed by the L–B technique. A BLM, formed either by the conventional “painting” method or self-assembled on a substrate (e.g. a freshly cleaved metallic wire or agar gel) is a dynamic liquidlike structure that is capable of accommodating a host of modifiers. In this connection, efforts to stabilize BLMs by using polymerizable lipids have been successful. However, the electrochemical properties of these BLMs were greatly compromised [3].

16.9.1.3 Supported BLMs

Figure 5 portrays the two most essential steps of our experimental procedure. In the first step as shown in Fig. 5, the tip of a Teflon-coated wire (platinum, silver, or stainless steel) is cut with a sharp knife under a lipid solution, for example, a 1% glycerol dioleate in squalene. When the nascent metal surface is exposed in a lipid solution, a monolayer of lipid molecules is irreversibly bound onto its surface. The adsorbed lipid monolayer with unattached

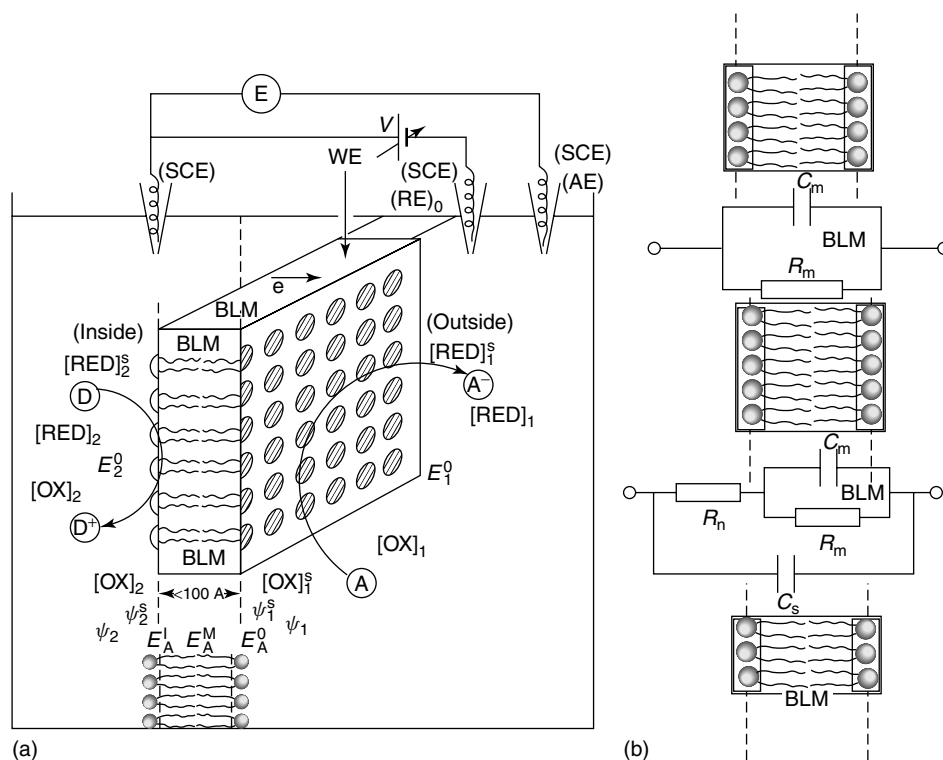


Fig. 4 Cyclic voltammetry of membranes. (a) Experimental details showing a three-dimensional view of a BLM modified with electron mediators (such as TCNQ, TTF, ferrocene, iodine, fullerene C60). A

three-electrode system is illustrated. (b) A usual representation of a BLM separating two aqueous solutions. Electrically, a BLM is shown to be equivalent of a resistor (R_m) and a capacitor (C_m) connected in parallel [1–3, 20–24, 35].

hydrocarbon chains interacts with the hydrophobic chains of other lipid molecules. A brief explanation of the first step is as follows. A freshly cut metallic surface has great affinity for lipid molecules. Amphipathic lipid molecules interact with the nascent metallic surface because they are highly hydrophilic. In the second step of self-assembly process, the lipid-coated metallic wire is immersed into a bathing solution (e.g. 0.1 M KCl). The lipid layer adhering to the metal surface will attenuate to a thin lipid layer under favorable conditions. It is believed that the various forces of interactions among lipid molecules lead

eventually to a spontaneous phase transition to the lowest energetic equilibrium state, that is, a lipid bilayer. The second step is illustrated in Fig. 5, which leads eventually (under favorable conditions) to the spontaneous formation of an exceptionally stable, self-assembled lipid bilayer, as shown in Fig. 5.

The precise arrangement and degree of ordering of the lipid molecules in the final structure shown in Fig. 4 is not known for certain. But it seems highly probable that the bilayer nature of the assembly is a consequence of the thermodynamics of free-energy changes at the metal-lipid

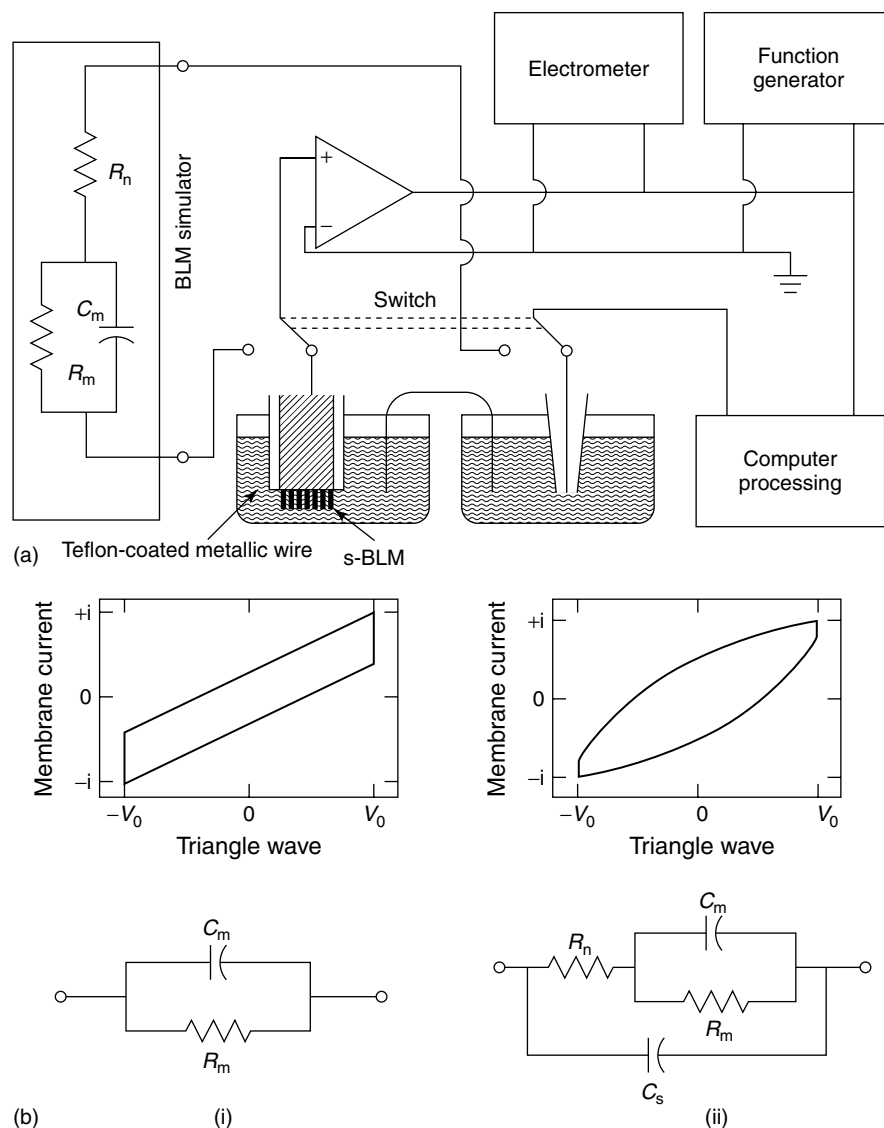


Fig. 5 Experimental setup for investigating supported BLMs. (a) Arrangement in details. (b) (i) scan result and its equivalent circuit and (ii) scan result and its representation [3, 35].

surface and at the lipid–aqueous solution interface. Our measurements of the electrical properties of supported bilayer lipid membranes (s-BLMs) are consistent with those of conventional BLMs and closely related systems.

To further improve both the reproducibility of obtaining s-BLMs with similar electrochemical properties and of forming even longer lifetime of such s-BLMs, a modified version of the original method of s-BLM formation has been developed.

For the best cutting of Pt wire, we constructed a miniature guillotine in which the sharp knife is moved vertically onto the wire placed on the flat base. The wire is then cut while immersed in a drop of lipid solution so that the initial contact of the newly exposed wire surface is with the lipid solution. The newly cut surface is almost perpendicular to the length of wire. This lipid-coated wire is then inserted into a small piece of Teflon tubing, which has been filled with lipid solution. This assembled Teflon-covered Pt wire is transferred into an aqueous bathing solution. This process is shown in Fig. 4(a). We then let the system stand for a few minutes or longer. Supplied by diffusion within the lipid solution, the nascent platinum support surface will attract the polar groups of lipid molecules. In order to promote the process of self-assembling of BLM, one of the following two methods has been used: (1) by removing glycerol dioleate (GDO) solution from teflon (TEF) sleeve simple using capillary forces (Fig. 4b), or (2) by a piston system, which is shown schematically in Fig. 4(c). The final step is self-adjusting thinning and formation of the P-G border (Fig. 4d). During the time of self-adjusting process, the change in capacitance of a layer was monitored. After 5 to 10 min, the capacitance reached a constant value and the bilayer structure. Using these methods we are able to control both, the rate of the BLM formation process and also the ratio of BLM to the P-G border. These simple steps allowed us to produce stable and reproducible s-BLMs.

16.9.2

Methods of Investigation

16.9.2.1 Potentiometry

Up to now, we have used mainly the classical concepts of electrochemistry in

describing the various phenomena associated with membranes, involving only hydrated ions and ions surrounded by other ions (ionic cloud). For ions in the solution, there is ceaseless motion (or random walk). Ions get nowhere by random walk alone (their time average displacement is zero). A net transport of ions is possible by: (1) the presence of an electrical field, and (2) a chemical potential gradient. Thus, a net drift is superimposed on the random walk. When ions reach the interface, properties change abruptly; the anisotropy of the forces compel ions to adopt new configurations unknown in bulk solutions. Here, a variety of phenomena occur such as charge separation, potential gradient, adsorption, and orientation of H₂O dipole, etc. At present modern electrochemistry is focused on the transfer of charges across the interface, in particular, the electrified interface. The involvement of the EDL, therefore, is self-evident.

Of special interest to the above topics is the question: "Experimentally, how does one go about measuring membrane potential such as $\Delta\phi(=E_m)$?" One may place a pair of identical electrodes, such as: (1) Ag/AgCl, (2) K⁺-sensitive glass electrodes, or (3) saturated calomel electrodes (Hg/Hg₂Cl₂) with salt bridges, across the membrane with fixed negative charges. When the concentration ratio of the solutions bathing opposite sides of the membrane is 10:1 (say, 0.1 M KCl on the outside and 0.01 M KCl inside), an E_m of about 116 mV would be measured for case (1), about 0 mV for case (2), and 58 mV for case (3). Evidently, the choice of the kind of electrodes used to measure E_m is of crucial importance. For BLM and most membrane studies, calomel electrodes with saturated KCl bridges have been extensively employed. A pertinent

interpretation to the above data is to liken the membrane as a bipolar electrode rather than merely as a permeating barrier.

16.9.2.2 The Patch-Clamp Technique

To measure what is happening in a single, living cell, researchers use a so-called the patch-clamp technique (PCT), which requires an extremely fine pipette held tightly against the cell membrane. By carefully heating and pulling a small glass capillary tube, a very fine pipette can be formed. When pulled by machine, the tip will be much smaller than a human hair and the opening on the end of the pipette may be only 1 μm in diameter. The impetus for developing the PCT was the realization of the existence of ion channels in biomembranes [3, 4]. In the 1970s, shortly after the single-channel activities were demonstrated in BLMs, the PCT was then developed. Briefly, the PCT involves placing a glass micropipette in contact with a patch of cell membrane so as to isolate one or several ion channels of the same type. The membrane-coated pipette is then used as an electrode to record the flow of ions between the inside of fluid-filled pipette and the other side of the membrane fragment. As in planar BLMs, tiny electrical currents at the picoampere (10^{-9} A) level are measured. The pipette is usually filled with a KCl and pressed against the cell membrane (or BLM or giant liposome). A small suction is then applied so that a tiny patch of the membrane forms a tight seal around the edge of the pipette tip. Thus, any current through the pipette probe must also flow through the patched membrane. The most crucial aspect of the technique is the formation of a tight seal between the pipette and membrane patch, which is usually on the order of gigaohms ($>10^{10} \Omega$). The technique calls for an electronic feedback circuit, which

ensures that the voltage applied across the patched membrane is held at a constant value, so that the monitored currents are proportional to changes in the membrane resistance. If the patched membrane contains an ion channel, a brief pulse of current is observed each time the channel opens. The observed pulses are generally of the same size, monitored as current steps, in a given experiment, suggesting that ion channels are usually either open or closed, although the time for which the channel is open varies from one opening to the next. From the observed current steps, which are on the order of 10^{-12} A, an opened ion channel allows a translocation of a few thousand ions across the membrane per millisecond. It should be pointed out that the openings and closings of channels are random events; they can be predicted only in statistical probabilities. The PCT provides experimenters with a picture at the molecular level how thousands of channels might behave in a given cell membrane. An ion channel consists of a single protein molecule or a complex of molecules, which forms a mutable, water-filled pore through the lipid bilayer of cell membrane. Some of the ion channels are operated by an electrical signal (voltage-gated), whereas others are activated by chemical signal (ligand-gated). The channel allows specific ion species to flood into or out of the cell. It is believed that opening and closing of the channel is achieved by a minute change in the conformation of the channel protein complex. Mention should be made that prior to the PCT, intracellular electrodes used in the voltage-clamp technique (VCT) measure the transmembrane potential across the membrane and through it [3]. The influences of electrical stimuli or of neurotransmitters are described in terms of change in membrane conductance. It has been very successful

in accounting and describing the nerve action potential. However, the VCT approach, as practiced earlier, was incapable of giving direct information at a molecular level. In contrast, the PCT brings membrane biophysics to the molecular level, which enables electrophysiological studies to be done on single channels embedded in BLMs, liposomes, or biomembranes [13].

16.9.2.3 Cyclic Voltammetry

The charges that we are concerned with here are the electronic charges (electrons and holes). For charges of this type to be transported across the interface, electrochemical reactions must take place. In the presence of a membrane that is impermeable to ions, what will happen then? Here, the membrane must serve at least two functions: (1) pathway for electronic charges, and (2) electrode surface for chemical transformation (reduction and oxidation or redox reactions). To probe such a membrane, we will describe a well-established cyclic voltammetry (CV) method of electrochemists, which was applied to the BLM system in 1984 [20–24, 32, 36].

CV is an elegant and simple electrochemical technique for studying redox reactions at the metal electrode–solution interfaces and has become increasingly employed in all fields of chemistry. Until recently, however, the technique has apparently not been applied to any membrane systems including the BLM separating two aqueous solutions.

16.9.2.4 CV and BLM Experiments

Before discussing the results obtained on a BLM system using the powerful CV technique, a brief description of the setup used in this type of experiment is in order (Fig. 4). The Teflon cup will be referred

to as the inside, and the other chamber will be referred to as the outside. We have used a three-electrode system is used for obtaining voltammograms in the following configuration: one calomel electrode (SCE) is placed in the Teflon cup and two other calomel electrodes are on the outside. For membrane CV, that is, by applying the above voltammetric techniques to the BLM system, a Lucite block containing two adjacent 2-cm diameter chambers (8 ml), one of which holds a 10-ml Teflon cup having a hole on its side, is used. This aperture or hole is most simply made by punching into the wall of the Teflon cup. (usually less than 0.5 mm diameter) should be smooth so that the stability of the BLM is enhanced. The Teflon cup is referred to as the inside, and the other chamber is referred to as the outside. The voltammograms of the BLM are obtained using an X-Y recorder fed by a picoammeter and the voltage generator (e.g. CHI Workstation, CH Instruments, Austin, TX). The voltage from the programmer is applied through the potentiometer to the calomel electrode (SCE) immersed in the inside solution. Another SCE immersed in the outside solution is connected to the picoammeter. The important feature of the setup is a very weak dependence of its input voltage on the current being measured.

The significant advantages of the CV technique are, besides its simplicity and the good precision of measurement, the involvement of the lipid bilayer and the capability for future development. Since the electron transfer chain components are known to be closely associated with the lipid bilayer, the values thus determined hitherto by the usual Pt electrode may be quite different from their actual values in the membrane. Conceivably, the

technique described offers a novel approach to the determination of $E^{\circ'}$ of membrane-bound biomolecules such as the cytochromes and other redox enzymes, using modified BLM as the working electrode. Further, this new type of electronically conducting BLMs coupled with the CV technique may be useful in the study of membrane bioenergetics and in the designing of molecular electronic devices based on ultrathin films. For example, to impart electronic properties, an organic semiconductor such as TCNQ (7,7,8,8-tetracyanoquinodimethane) or TTF (tetrathiafulvalene) has been embedded into the BLM, thereby making the lipid bilayer electron conducting.

In order to apply the powerful CV technique to the BLM system, a conceptual effort has to be made, that is to consider one side of the BLM as the working electrode, while the other side is providing the connection to the external circuit. An unmodified BLM behaves essentially as an excellent insulator (specific resistivity $>10^{14} \Omega$) and does not function as a working electrode. However, upon incorporation of TCNQ into the BLM and in the presence of ascorbic acid in the outer solution and equal molar (0.001 and 0.01) $K_3Fe(CN)_6/K_4Fe(CN)_6$ in the other inside, the observed electrical properties are such (R_m decreasing from 10^8 to 10^6 ohms cm^2 , C_m increasing from 0.4 to 0.5 F cm^{-2} , E_m developing to about 180 mV with the ascorbic acid side positive. In the absence of TCNQ in BLM with other experimental conditions the same, the I/V characteristic is linear; it practically coincides with the x -axis on the scale used. In the absence of redox couples in the bathing solution, but with TCNQ in the BLM, the I/V curve remains linear. To show more clearly that the redox reactions are occurring across the TCNQ-containing BLM the following

experiment has been carried out. To one side of a TCNQ-containing BLM, a concentration of equal molar ferri-ferrocyanide solution was added, whereas to the other side, aliquots of ascorbic acid of known concentration were introduced. Concurrently, the membrane potentials (E_m) after each addition of ascorbic acid were measured. It is most interesting to note that the extrapolated value of E_m at the equal molar concentrations of the two redox couples agrees very well with the difference of the two standard redox potentials ($E^{\circ'} \sim 300$ mV). The highly asymmetrical I/V curves are reminiscent of those of a p-n junction diode, which permits an electron current flow in a forward-bias direction only. In the TCNQ-BLM system, oxidation occurs at the membrane-solution interface contacting the ascorbic acid solution and reduction of ferricyanide to ferrocyanide takes place on the other side of the BLM that has a negative polarity. Implicit in this interpretation is the transmembrane movement of electrons via the TCNQ molecules imbedded in the lipid bilayer; that is, the whole system has the properties of a p-n junction with the TCNQ-BLM acting as a rectifier.

To demonstrate that the TCNQ-BLM behaves like a semiconductor electrode (e.g. Pt, which is frequently used in CV), a comparative experiment was carried out, in that cyclic voltammograms of quinhydrone were obtained using either Pt or TCNQ-containing BLM under very similar conditions. In particular, the cathodic portions of the voltammograms are quite alike, thus substantiating that the TCNQ-BLM functioned as a working electrode. In this connection, a cyclic voltammogram of horse-heart ferricytochrome *c* was also obtained. Thus, in order to be consistent with the theory of CV, the TCNQ-BLM

must function as a redox electrode in the usual practice of electrochemistry [20–24].

Under normal physiological conditions, there exists a transmembrane potential difference of about 50 mV, which means that the electrical field is on the order of $100\,000\text{ V cm}^{-1}$, which is close to the critical value and may lead to mechanical rupture of the membrane. In this connection, the effect of magnetic fields on the conductance characteristics of A protein channels embedded in BLMs should be examined in future studies. Thus, a detailed understanding of the electrical parameters of the membrane has great biological significance and is important in a wide scope of applications. Further, the properties of experimental BLMs on the whole, and the interactions between their components, are better understood than those of the more complicated intact biological membranes. For example, studies on membrane transport phenomena in BLMs provide a frame of reference for understanding material transport in biomembranes. As such, biomembranes, including the mitochondrial cristae and photosynthetic thylakoid membranes that efficiently transduce energy into the chemical free energy on which almost all forms of life depend, are far too complex to be understood in physicochemical terms [1–3]. Therefore, the real interest in the conventional BLM system lies in its usefulness for the interpretation of results from biological membranes. Indeed, studies of BLMs facilitate the initial testing of working hypotheses that may generate guidelines for a better choice of appropriate in vivo and reconstituted membrane experiments.

16.9.2.5 Modeling of BLM Behavior by Electrochemical Equivalent Circuit

The possible ionic and electronic mechanisms of charge transfer across the

membrane interior for their I/V characteristics have been investigated. These two types of mechanism give practically identical voltammogram shapes in the presence of the same redox couples in the aqueous phases. However, the ionic model differed from the electronic one in the characteristic potentials of peak currents, which were shifted along the potential axis toward more negative (cathodic peak) and more positive (anodic peak) values, when compared to the corresponding peaks in the electronic model. This is mainly due to the difference in the resistance of the membrane interior in these two models. Moreover, both sides of the membrane separating the two redox couples in aqueous solutions parameters of the membrane has great biological significance and is important in a wide scope of applications. Further, the properties of BLMs on the whole, and the interactions between their components, are better understood than those of the more complicated intact biological membranes. For example, studies on membrane transport phenomena in BLMs provide a frame of reference for understanding material transport in biomembranes. As such, biomembranes, including the mitochondrial cristae and photosynthetic thylakoid membranes that efficiently transduce energy into the chemical free energy on which almost all forms of life depend, are far too complex to be understood in physico-chemical terms. Therefore, the real interest in the BLM system lies in its usefulness for the interpretation of results from biological membranes. Indeed, studies of BLMs facilitate the initial testing of working hypotheses that may generate guidelines for a better choice of appropriate in vivo and reconstituted membrane experiments [1–3, 13].

16.9.3

Electrochemical Impedance Spectroscopy

For the investigation of the properties of BLMs, electrical methods have been applied at the very beginning. In addition to the CV technique, other methods such as electrical impedance spectroscopy (EIS) have been applied. Shortly after the discovery of the BLM system, Hanai and Haydon reported the thickness measurement of a planar lipid bilayer using the impedance technique [1–3]. Their results are in accord with the value obtained on RBC, estimated by Fricke (see Eq. 1). The impedance technique, nowadays also known as EIS, has subsequently used by many others. The basis of the technique is that a small alternating current (AC) of known frequency and amplitude is applied to the system (e.g. a BLM). The resulting amplitude and phase difference that develop across the BLM are monitored. For a BLM of cross-sectional area (A), and thickness t_m , the ability of the BLM to conduct and to store electrical charges are described by the following:

$$G = \frac{\sigma A}{t_m} \quad C = \frac{\varepsilon A}{t_m} \quad (31)$$

where G and C denote, respectively, the conductance and capacitance of the system. σ and ε are constant, representing the electrical conductance and dielectric permittivity, respectively. Note that these two elements, G and C , are connected in parallel. Thus, the impedance (Z) of the system may be expressed as follows:

$$z(f) = \frac{1}{G + C} \quad (32)$$

where f is the frequency. Therefore, a measurement of Z provides estimates of G and C , and is given by

$$G = \frac{1}{Z} \cos \theta \quad \text{and} \quad C = -\frac{1}{fZ} \sin \theta \quad (33)$$

where θ is the phase angle. It can be shown that Z will disperse as a function of frequency, f . The above Eq. (33) reveals that the dispersion becomes most conspicuous for f greater than G/C . Typical plots, known as Bode plots (Z vs f ; θ vs f) are made, from which the first insights of a BLM separating two aqueous solutions concerning its thickness and infrastructure are obtained. Additional comments are given below to illustrate the usefulness of EIS as applied to the BLM system [3, 5, 36, 37].

The BLM system, electrically speaking, has two distinct regions, with particular electrical characteristics. These are: (1) the BLM itself, which behaves as a resistor (R_m) connected in parallel with a capacitor (C_m), and (2) the two contacting BLM–solution interfaces, which can act as an interfacial capacitor (C_i). When an alternating voltage is applied between the two reference electrodes, immersed in the bathing solutions, and across the BLM, ions flow toward and away from the electrodes, depending on their polarity. At low frequency, the time the ions flow (in one direction, before reversing their flow), is long enough to drive the ions through embedded channels, if present, in the BLM, and into the bathing solution on the opposite side. The interfacial capacitance, C_i , may or may not be of consequence; it depends on size when compared with C_m . Here, R_m is the controlling factor. At medium frequency, more ions get a chance to pass through the channels, if present. Once on the other side, the rate of arrival of ions into the BLM–solution interface is slow enough that they can easily disperse away from their entry points at the channel. At medium frequency, the

distinguishing characteristic of the BLM circuit is the membrane resistance (R_m). At high frequency, the movement of ions is most affected by the capacitance (C_m) of the BLM. It is informative to mention here the treatment of data as obtained by EIS, using the Bode plot [3].

In an idealized impedance spectrum (admittance or Z vs f) where admittance is defined as the rate at which charges are stored in the capacitor per cycle. The behavior of a pure capacitor, in a Bode plot, forms a line at 45° , whereas a pure resistor forms a horizontal line. The Bode plot is a graph derived from plotting frequency against the admittance of an electrical current. The Bode plot enables us to track the responses of a diverse electrical system by applying and following a range of frequencies. For example, the phase angle between the electrical excitation and the resultant electrical flow is measured at a range of frequencies. The significance of the phase diagram is that if one plots phase shifts over the same range of frequencies that one uses to generate the Bode plot, one can detect when the different electrical characteristics of the circuit are important. On a phase diagram, the behavior of a pure capacitor shows a 90° phase angle, while the more the circuit behaves as a resistor the more it will show up as approaching 0° phase angle. Thus, if one makes a composite of these graphs, the dip in the phase corresponds to the part of the Bode plot that looks like a resistor trace. From an analysis of impedance data, one may be able to find out specifically the electrical behavior of the BLM, which correlates with the behavior of the modifier (e.g. ion channel) at R_m , and search out specifically changes in the impedance/admittance of the BLM at the point at which the modifier behavior is controlling. The impedance spectra of the base system, as typified by

the so-called Bode plots, including the BLM and its adjacent aqueous solutions exhibited for all tested cations a single capacitive contribution. The corresponding time constant was discussed in terms of a model, which includes a dielectric dispersion in the BLMs. This phenomenon was detected by using either DC or AC voltage perturbations [35, 36]. Data obtained using EIS techniques show two time constants, which can be assigned to the lipid bilayer and to the channel/BLM contributions, respectively. In connection to the liposome study using EIS, Karolis and colleagues have reported low-frequency impedance measurements of pure egg lecithin (PC) BLMs have revealed the presence of four layers that can be attributed to the acyl chain, carbonyl, glycerol bridge, and phosphatidylcholine regions of the lecithin molecule. Measurements on bilayers formed in the presence of unoxidized cholesterol revealed that cholesterol molecules were located in the hydrocarbon region of the bilayer with its hydroxyl groups aligned with the carbonyl region of the lecithin molecules. Measurements of oxidized cholesterol–lecithin BLMs revealed that these molecules protruded less into the hydrocarbon region and their polar hydroxyl group aligned with the glycerol bridge region of the lecithin molecule [13].

Generally, either AC (e.g. EIS) or DC is used for investigating BLMs. Recently, a simple setup for measurements of electrical properties of supported planar lipid bilayers (s-BLMs), using a complementary AC/DC method has been reported [3, 13]. The results obtained demonstrated the usefulness of such an approach for studying BLMs. The frequency dependence of resistance and capacitance makes it possible to compare different published data obtained by AC at different frequencies or DC. In some experiments, capacitance

increases more sharply with the lowering of frequency. As determined, certain s-BLMs modified by anthraquinone-2-sulfonic acid (AQS) or TCNQ can transfer electrons readily from the bathing solution via the BLM to the supporting Pt surface. Concerning the analysis and interpretation of the experiments, certain assumptions are made about the dielectric constant (ϵ) and the thickness of the BLM (t_m). For example, a planar lipid bilayer system *aqueous solution|BLM|aqueous solution*, is represented by the equivalent circuit shown in Fig. 5, in which the capacitance (C_m) has been found to be independent of frequency in the range from DC to AC about 10 MHz, directly proportional to the BLM area, and apparently dependent only on the dielectric constant (ϵ) layer of the hydrophobic interior of the membrane. The C_m of the lipid bilayer, according to the parallel plate condenser equation is followed. Monitoring the BLM formation, thinning, perturbation, and rupture may be achieved by recording a function of membrane impedance using the equivalent circuit shown in Fig. 5. Essentially, a BLM separating two interphases: *(aqueous solution|BLM|aqueous solution or aqueous solution|BLM|metal support, or aqueous solution|BLM|hydrogel substrate*, is represented by three $R_m - C_m$ domains connected in series. Each domain has its own impedance due to a difference in constituents and physical attributes. Thus, the BLM domain, owing to its ultrathinness and low dielectric constant, is predominant over the other two adjacent domains. For example, the contribution of the EDL (the so-called Gouy–Chapman layer), which may be two orders of magnitude higher than the lipid bilayer, may be neglected in a serial arrangement. It is worth noting here that, when modifiers are present, they may affect the R_m/C_m signals differently

as well as selectively, which may be frequency dependent.

In general, it is simpler to use the DC method in assessing the planar lipid bilayer (BLM) properties. However, it causes a transient response, owing to the C_m . The advantage of the EIS method is that it permits observation of fast changes when investigating interactions between the BLM and its modifiers. It should be further pointed out that, in using the EIS method, the applied frequency must be carefully chosen so that the effect of capacitive shunting is minimized. Moreover, the selected frequency must not be close to the line frequency (i.e. 50, 60, or 400 Hz). Some preliminary measurements indicate that a frequency around 350 Hz is a suitable one to use. The other advantage with the EIS method is that membrane/electrode polarization is less likely to occur. Perhaps, a complementary AC–DC mode is a method of choice [3]. Insofar as the technique is concerned, it seems evident, on the basis of experimental findings [3, 37], that it may open new vistas in basic membrane biophysics studies, and offer fresh prospect for biotechnological exploitation (see below on *Applications*).

It is worth pointing out that, although DC measurements have the inherent advantages such as simple instruments and straightforward interpretation, the dynamics of transport processes are not readily accessible. Therefore, AC impedance spectroscopy methods have also been used. For example, a frequency range of 0.2–1000 kHz, a capacitance bridge is coupled to an external oscillator. Sometimes electrical connection to the aqueous solutions is made via two sheet Pt electrodes (1 cm²) coated with Pt black, or Ag/AgCl electrodes. Impedance spectroscopy, also referred to as EIS, is a well-established

technique for investigating the dynamics of membranes including planar lipid bilayers and spherical liposomes. The principle of the EIS technique is based on the choice of an appropriate equivalent circuit, which represents the main features of the membrane system. The instrumentation for AC impedance spectroscopy is a gain/phase analyzer (Solartron Instruments, UK) controlled by a personal computer.

In recent experiments using the EIS technique, for example, a BLM-containing gramicidin-A is reported to exhibit two time constants, one of which can be assigned to the BLM and the other to the channel BLM contributions. Earlier, Yamada et al. have studied electron transfer with three different redox couples through a BLM-containing TCNQ using AC impedance spectroscopy and claimed that the impedance spectroscopy technique can resolve perturbations in the molecular organization of membranes down to 0.1-nm resolution (see Ref. [3]), and may be used to monitor perturbations in the molecular structure due to external influences (e.g. the presence of pharmacologically active molecules in the external environment adjacent to the membrane). This technique is being used to study the dielectric properties of proteins. Also applicable are examinations of the effects of intense electric fields on cells and cell membranes, electro-mechanical properties and stability of biomembranes, electrical breakdown phenomena, and electroporation impedance spectroscopy (EIS), reported the heterogeneous electron transfer rate constants for $\text{Co(phen)}_3^{(2+/3+)}$ and $\text{Fe(CN)}_6^{(4-/3-)}$ in BLMs saturated with TCNQ. Related studies of supported lipid membranes have been reported [13, 36–39].

16.9.4

Photoelectrospectrometry

In view of the sensitivity and sophistication of spectroscopy techniques, and their utility in elucidating certain aspects of the structure and dynamics of membranes, attempts have been made to apply absorption, fluorescence, and impedance spectroscopy to the BLM system [25, 26, 38, 40–42]. Additionally, by combining electrical methods with those of spectroscopy, a photoelectric action spectrum of a pigmented BLM may be obtained. This technique of measuring action spectra of pigmented membranes, termed *photoelectrospectrometry*, is several orders of magnitude more sensitive than conventional absorption spectroscopy. For applications of electrochemical and electro-optical methods, the BLM is a system of choice and has been so employed. For example, pigmented BLMs have been studied by photoelectrospectrometry and shown to be capable of light-induced electron transfer and redox reactions (see Fig. 6). Owing to the importance of dyes, researchers have investigated systematically dye-sensitized BLMs. Redox reactions at the BLM–solution interfaces are most conveniently scrutinized by this technique. Fifty-seven dyes of different chemical groups have thus been studied. From the obtained voltammograms, five types of characteristic curves have been established. Electronic processes in, as well as across, the BLM are considered. In the presence of light of known wavelengths, a number of dye-sensitized BLM have also been investigated by photoelectrospectrometry. Ultra-violet light flashes can also induce voltage transients across BLMs, when aromatic amino acids are absorbed to one side of the membrane. These photoeffects varied with the chromophore structure, the aqueous

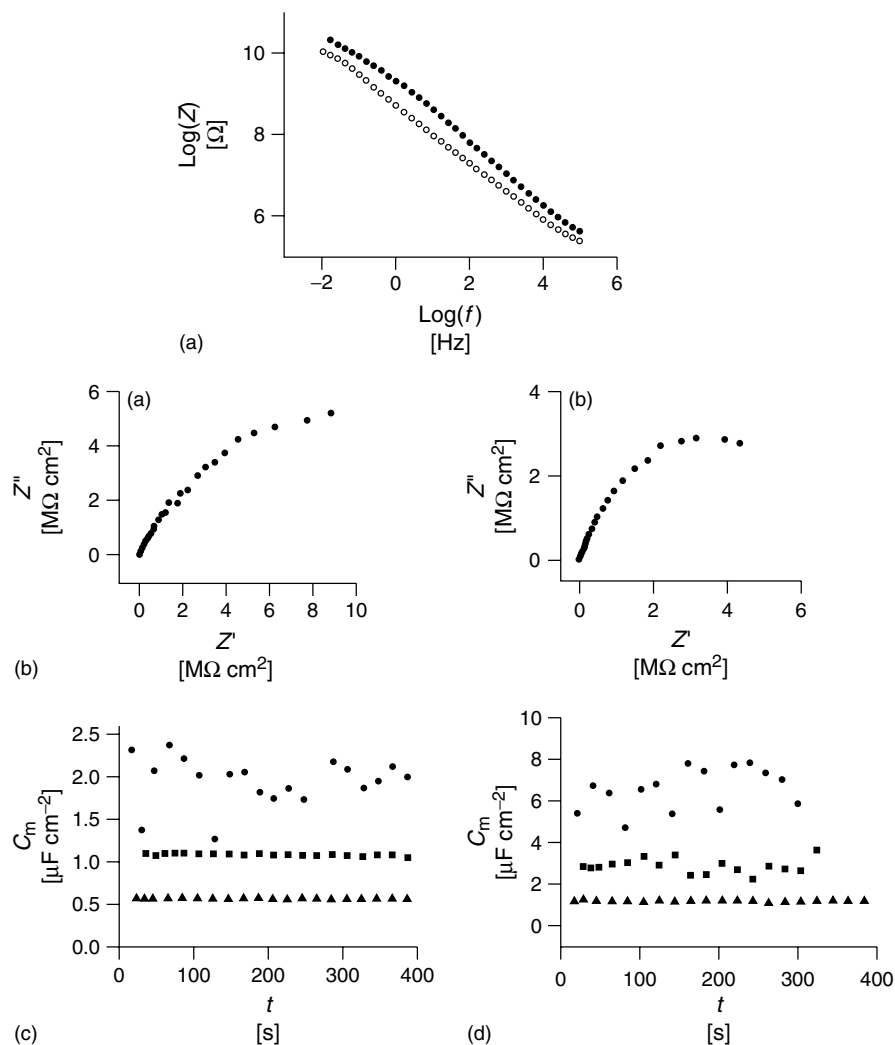


Fig. 6 (a) Bode plots of the impedance for s-BLM (●) and C60 modified s-BLM (○). Impedance was measured in 0.1 M PBS at 0 V DC with respect to open-circuit potential and with AC frequency between 0.01 Hz and 100 kHz. (b) (i) Nyquist complex plane plot for s-BLM and (ii) C60 modified s-BLM. (c) Time course of membrane capacitance C_m of s-BLM under 100 Hz (●), 1 kHz (■), and 10 kHz (▲). (d) Time course of membrane capacitance C_m of C60 modified s-BLM under 100 Hz (●), 10 kHz (■), and 100 kHz (▲).

solution salt concentration, pH, and oxygen partial pressure. These photoeffects are attributed to the migration of electrically charged photochemical intermediates in the BLM, and provide a new method for studying the effect of UV light on

membranes. When a s-BLM doped with Zn-phthalocyanine was excited by light, a voltage and a current were recorded, with the action spectra paralleled closely to that of the absorption spectrum of the photoabsorber [13, 26, 40, 43, 44].

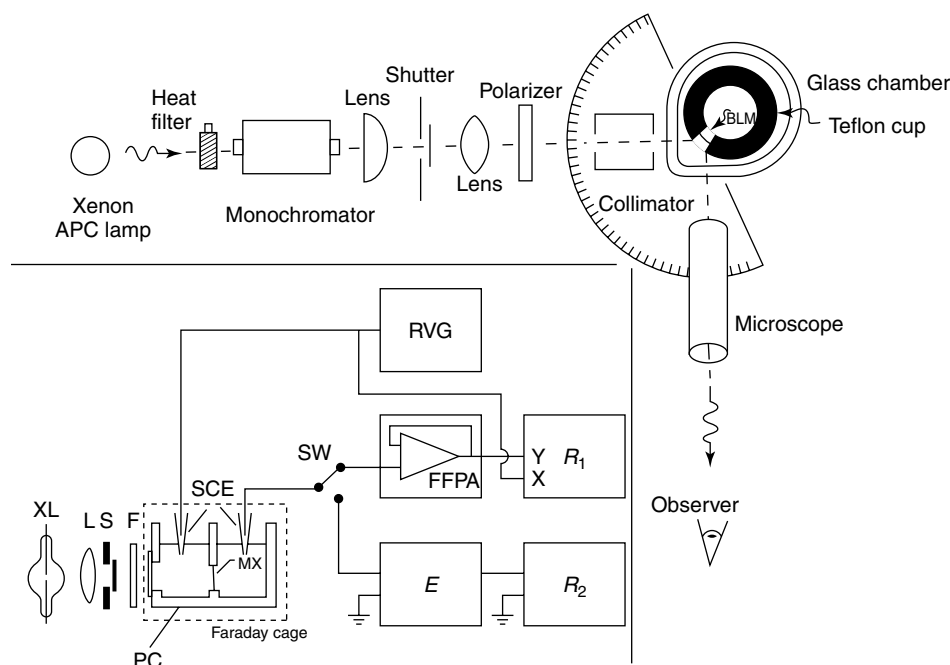


Fig. 7 Setup for studying light-induced effects in p-BLMs. (a) Setup used for obtaining action spectra of BLMs containing pigments or dyes. The setup is also useful for investigating the structure of lipid bilayers [2, 15–19, 40, 41]. (b) Arrangement for studying p-BLMs with redox

species in the bathing solutions XL – xenon lamp, L – lens, SCE – saturated calomel electrode, PC – transparent chamber, SW – switch, FFPA – Amplifier, E – electrometer, and R – recorder [15–19].

16.10

Electronic and Charge Transfer Processes in Membranes

Although unmodified BLMs are excellent insulators, incapable of either ion or electron conduction, a suitable modification makes them ion selective or electron conducting. Presently, it is evident that a variety of compounds can be incorporated into BLMs giving them design types of membrane conductivity. A great deal of experimental work has also been done, which proves that BLMs modified with suitable materials show an electronic conductivity with redox reaction taking place at both interfaces of the membrane.

With these types of BLMs, an oxidation takes place on the side of the membrane facing the negative electrode whereas reduction occurs on the side facing the anode. A transverse movement of electrons occurs across the membrane and the BLM functions essentially as a bipolar redox electrode [1–3, 32].

16.10.1

Properties of Iodine–Iodide-containing BLMs

The conduction properties of bilayer lecithin membranes in iodine-containing solutions have been examined from a potentiodynamic experimental approach.

Voltammetric data obtained by using a variety of forms of iodide ions (derived from charge transfer type interactions) implicated the I_3^- ion as the charge carrier, accounting for the diffusion-limited voltammetric response, whereas the charge transport of I^- seemed to be limited by transmembrane diffusion. The data were used to support one of many proposed mechanisms for the conductance of iodide in membranes.

16.10.2

Polypyrrole BLMs

Studies were performed on oscillations across a polypyrrole-lecithin BLM separating two electrolyte solutions, one containing an electron-acceptor reagent and the other an electron-donor reagent. Systems studied showed sustained oscillations of electrical potential of about 15 mV with an interval of about 40 s. The proposed mechanism of these oscillations was based on the polypyrrole oxidation-doping reduction-doping process. The equivalent electrical circuit of the investigated oscillating system was presented. It was suggested that the mechanism for this phenomenon could be useful in interpretation of some oscillations observed in biological systems [25, 26, 38, 42]. It may be noted that polypyrrole can be synthesized and doped in situ, which has been shown capable of electronic conduction. The possible application of the described system to the development of molecular electronic devices has been also suggested.

16.11

Photoelectric Effects in Membranes

The use of pigmented bilayer lipid membranes (p-BLMs) has yielded a wealth of

information concerning the permeability of the lipid bilayer to ions, electrons and holes. The light-driven transmembrane charge separation and electron transfer processes in pigmented BLMs involving chlorophylls, porphyrins, and their derivatives have been of particular interest to photobiochemistry and photobiophysics. In this connection, mentioned must be made of experiments using lipid vesicles. For example, it has been found that there is a clear difference between transmembrane electron transfer and transmembrane molecular diffusion. The p-BLMs have been investigated since the late 1960s as an experimental model for the photosynthetic thylakoid membrane of the chloroplast and the visual receptor membrane of the eye. For the investigation of light-induced effects in p-BLMs, a technique termed photoelectrospectrometry has been used, as described in the preceding section. The photoactive BLMs transduce the light energy into electron movement across the membrane. Such a model of a molecular photosensors based upon BLM structure has been expanded by using the thermotropic liquid crystal materials as a BLM. In the thermotropic liquid crystal bilayers, the light not only induces both photocurrent and photovoltage, but also the change of a membrane capacitance. In this connection, the various methods for measuring photoelectric effects in p-BLMs have been compared and concluded that, insofar as the two measured parameters, open-circuit voltage (V_{oc}) and V_{fb} , are concerned, both of which result from asymmetrical charge displacements across the BLM following light excitation and can provide kinetic information on membrane reactions. V_{oc} , denoting the photovoltage measured under current clamped conditions, offers advantages of detecting photoeffects from

charge displacements that have long time constants, and producing data that can be used to reconstruct (membrane current) waveforms, which under favorable circumstances can accurately resolve time constants from about 10 ns to 5 s. As shown earlier, I_m with three different time constants can be resolved in single V_{oc} . The resolution of long time constants is limited by the BLM's RC time constants, which can be readily determined on V_{oc} apparatus. It should be mentioned that common difficulties with V_{oc} and V_{fb} are twofold: (1) the use of small diameter BLMs (<0.1 mm), result in increased R_m values, which further limit resolution of photoelectric effect time constants and increase noise, and (2) from a single experimental arrangement, it is not easy to distinguish various types of waveforms. Thus, although no systematic procedure has yet emerged, the more detailed information provided by V_{oc} has proven nonetheless useful.

A p-BLM consists of an ultrathin (~ 5 nm) insulating lipid bilayer with chlorophyll or porphyrin molecules separating two redox solutions. For example, the photopotential of more than 150 mV has been observed across a BLM formed from chloroplast has been depicted that a photoactive BLM is similar to that of a barrier-layer type of photovoltaic cell, and that the observed photoelectric effects have been explained in terms of light-induced redox reactions on opposite sides of the membrane. In other words, the threshold for light absorption is given by the embedded pigment and the excitons (electron-hole pairs) thus produced by light absorption are separated to opposite sides of the BLM owing to the presence of high electric field across the lipid bilayer. The separated excitons, that is, electrons and holes, move to opposite sides of the

BLM effecting reduction and oxidation, respectively. The characteristics of the action spectra (either photovoltage or photocurrent) are determined by its action [1–3, 15–19, 25, 26, 41].

16.12 Applications

The development of conventional BLMs (black lipid membranes, or planar lipid bilayers) and later s-BLMs and sb-BLMs, have made it possible for the first time to study, directly, electrical properties and transport phenomena across a 5-nm ultrathin lamina separating two aqueous solutions. s-BLMs, formed on metallic wires, conducting glasses, and gel substrates, as well as on microchips, possess properties resembling biomembranes. These self-assembled, s-BLMs, have opened research opportunities in studying hitherto unapproachable phenomena at interfaces. As a specific example, in living organisms, the specificity is dictated by the DNA molecule, which carries the organism's genetic master design. Thus, a single-strand of DNA is complementary to its counterpart, thereby forming a double-stranded DNA (dsDNA) – a double helix. It seems that the first report relating DNA and BLM was by Amao and Kumazawa in 1993, who reported the hydrophobic and electrostatic effect of basic polyamino acid–DNA polyion complex in BLMs. Since then, other investigators have carried out many interesting experiments [45].

Some recent findings demonstrate the potential for investigating processes at solid–liquid interfaces. As a result of these studies, biomembranes have now been recognized as the basic structure of Nature's sensors and molecular devices. For example, the plasma membrane

as a result of applications of many disciplines and techniques including interfacial chemistry, electrochemistry, voltage- and PCTs, spectroscopy, and microelectronics. We now know a great deal about the structure of biomembranes, "ion pumps", electroporation, membrane channels, etc. In membrane reconstitution experiments, for example, the evidence is that intracellular signal transduction begins at membrane receptors. It should be reiterated that the research area covered in this paper is highly interdisciplinary. Emphasis has been placed on basic research. The BLM research has been benefited by a cross-fertilization of ideas among various branches of sciences. It seems likely that devices based on "smart" materials may

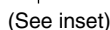


Fig. 8 Experimental setup for investigating s-BLMs. (a) Equivalent circuit and (b) showing an s-BLM on the gate of a FET device [1–3].

be constructed in the form of a hybrid structure, for example, utilizing both inorganic semiconducting nanoparticles and synthetic lipid bilayers. The biomimetic approach to practical applications is unique and full of exciting possibilities. We can glean the design principles from Nature's successful products and apply them to our research and development from which advanced sensors may ultimately depend (Figs. 8, 9, 10).

To date, planar lipid bilayers (s-BLMs) on solid or hydrogel substrates are of great scientific interest and of practical merit due

to their ability to mimic biomembranes. Further, they provide a natural environment for embedding proteins or other compounds under nondenaturing conditions. In respect to practical applications, they permit the preparation of ultrathin, high-resistance films with well-defined orientation on metals or semiconductors, and the incorporation of receptor proteins into these insulating structures for the design of biosensors and bioelectronic devices using electrical methods of detection. It is worth pointing out that, with all other systems the compound of interest is

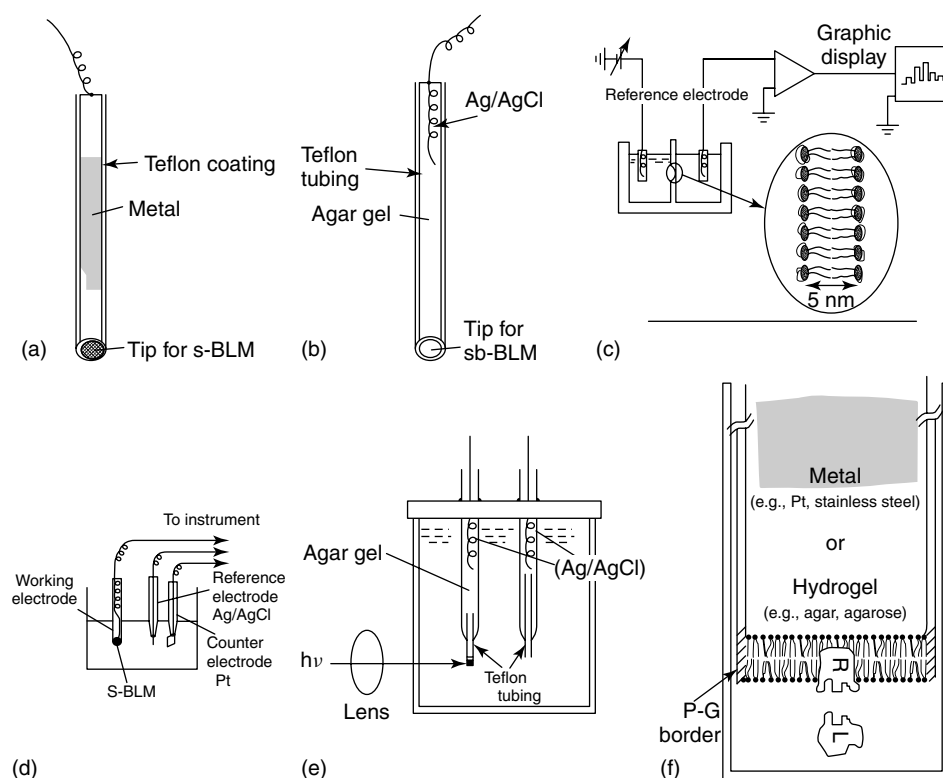


Fig. 9 Experimental arrangements for conventional and supported BLM studies. A and B are probes, respectively, for metal and hydrogel supported BLM experiments; C setup for conventional BLM experiments; D setup for

s-BLM experiment using three-electrode system [45]; E setup for investigating light-induced effects in sb-BLMs; and F illustrating ligand–receptor contact interaction in s-BLMs [1–3].

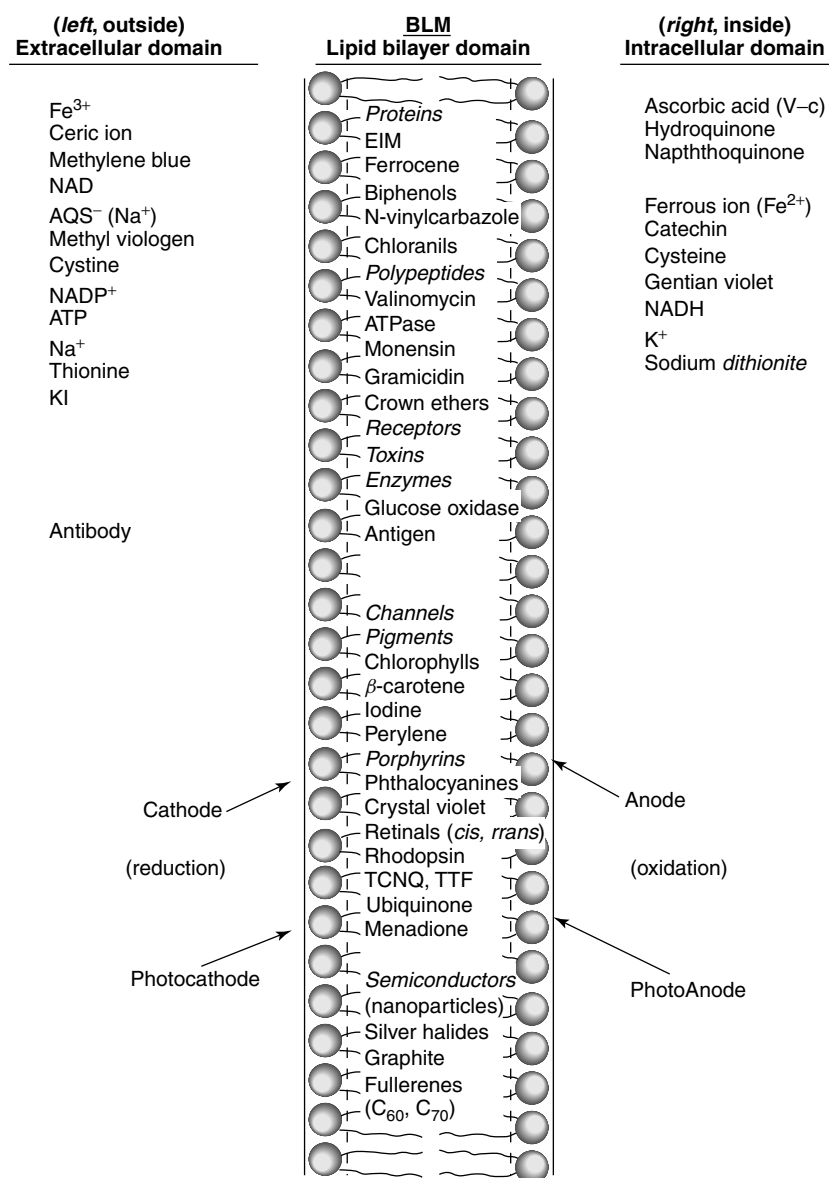


Fig. 10 To elicit desired effects, some of the compounds and materials have been embedded into BLMs (planar lipid bilayers). Also listed are a few of the species in the bathing solutions that have been used in experiments [1–3, 13, 51].

immobilized in a rigid, solid-like structure, whereas in the BLM it is embedded. By embedding is meant that the compound(s) (membrane modifiers such as electron

acceptors, donors, mediators, polypeptides, proteins, etc.) of interest in the lipid bilayer is relatively free to adapt to its surroundings. The functions of lipid bilayers

are mediated via specific modifiers, which assume their active conformations only in a liquid-crystalline environment. Further, the presence of the lipid bilayer greatly reduces the background noise (interference) and effectively excludes hydrophilic electroactive compounds from reaching the detecting surface causing undesired reactions. From specificity, selectivity, and design points of view, a supported planar lipid bilayer (s-BLM) is an ideal natural environment for embedding a host of materials of interest. Hence, the s-BLM system offers a wider opportunity for biosensor development. Many investigators have reported chemical sensing with modified probes that mimic gating at biomembranes, incorporating ion-channel receptors [46–48]. These self-assembled, supported BLMs, not only have overcome the long-term stability problem of conventional planar lipid bilayers, but have also opened a range of possibilities for manipulating interfacial films as well as in developing practical biosensors. It is beyond the scope of this chapter even to mention, let alone to describe any of these new and exciting developments (e.g. in semiconductor–septum electrochemical photovoltaic – SC–SEP-cell). A number of comprehensive reviews as well as some recent publications are available [3, 16, 17, 27, 28, 32, 34, 37, 45–51].

References

1. H. T. Tien, *Bilayer Lipid Membranes (BLM): Theory and Practice*, Marcel Dekker, New York, 1974.
2. A. Ottova-Leitmannova, H. T. Tien, *Prog. Surf. Sci.* **1992**, 41, 337–446.
3. H. T. Tien, A. L. Ottova, *Membrane Biophysics: As Viewed From Experimental Bilayer Lipid Membranes (planar lipid bilayers and spherical iposomes)*, Elsevier, Amsterdam, New York, 2000, p. 648.
4. J. R. Harris, A.-H. Etemadi, (Eds.), *Artificial and Reconstituted Membrane Systems, Subcellular Biochemistry*, Plenum Press, New York, 1989, Chap. 3, Vol. 14.
5. M. Blank, (Ed.), *Electrical Double Layers in Biology*, Plenum Press, New York, 1986.
6. B. Ivanov, (Ed.), *Thin Liquid Films: Fundamentals and Applications*, Marcel Dekker, New York, 1988, Chap. 14, 15.
7. T. Osa, J. L. Atwood, (Eds.), *Inclusion Aspects of Membrane Chemistry*, Reidel Publishing, Boston, Mass., 1991, pp. 191–274.
8. A. A. Marino, (Ed.), *Handbook of Bioelectricity*, Marcel Dekker, New York, 1988, pp. 181–242.
9. M. Blank, E. Findl, (Ed.), *Mechanistic Approaches to Interactions of Electric and Electromagnetic Fields with Living Systems*, Plenum Press, New York, London, 1987.
10. G. Milazzo, (Ed.), *Topics in Bioelectrochemistry and Bioenergetics*, John Wiley and Sons, New York, 1983, pp. 157–224, Vol. 5.
11. G. Dryhurst, K. Niki, (Eds.), *Redox Chemistry and Interfacial Behavior of Biological Molecules*, Plenum Press, New York, 1988, p. 529.
12. A. D. Bangham, *BioEssays* **1995**, 17, 1081.
13. H. T. Tien, A. L. Ottova, *J. Membr. Sci.* **2001**, 189, 83–117.
14. J. Koryta, *Ions, Electrodes and Membranes*, John Wiley and Sons, New York, 1982.
15. S. G. Davison, (Ed.), *Prog. Surf. Sci.* **1985**, 19.
16. S. G. Davison, (Ed.), *Prog. Surf. Sci.* **1986**, 23.
17. S. G. Davison, (Ed.), *Prog. Surf. Sci.* **1989**, 30.
18. S. G. Davison, (Ed.), *Prog. Surf. Sci.* **1992**, 41.
19. S. G. Davison, (Ed.), *Progress in Surface Science*, Pergamon Press, New York, 1985–1992.
20. H. T. Tien, *J. Phys. Chem.* **1984**, 88, 3172.
21. H. T. Tien, *Bioelectrochem. Bioenerg.* **1978**, 5, 318.
22. H. T. Tien, *Bioelectrochem. Bioenerg.* **1982**, 9, 559.
23. H. T. Tien, *Bioelectrochem. Bioenerg.* **1984**, 13, 299.
24. H. T. Tien, *Bioelectrochem. Bioenerg.* **1986**, 15, 19.
25. M. Blank, (Ed.), *Biomembrane Electrochemistry*, Advances in Chemistry Series No. 235, American Chemical Society, Washington, DC, 1994, Chap. 24.
26. A. G. Volkov, D. W. Deamer, D. L. Tanelian et al., *Liquid Interfaces in Chemistry and Biology*, John Wiley and Sons, New York, 1998.

27. F. L. Carter, R. E. Siatkowski, H. Wohltjen, (Eds.), *Molecular electronic devices, Proceedings of Third International Symposium*, North Holland, Amsterdam, 1988.
28. K. L. Mittal, D. O. Shah, (Eds.), *Surfactants in Solution*, Plenum Press, New York, 1991, pp. 133–178, Vol. 11.
29. P. Krysinski, H. T. Tien, *Prog. Surf. Sci.* **1986**, 23, 317.
30. R. Guidelli, G. Aloisi, L. Becucci et al., *J. Electroanal. Chem.* **2001**, 504, 1–28.
31. R. P. Rastogi, R. C. Srivastava, S. N. Singh, *Chem. Rev.* **1993**, 93, 1945–1990.
32. P. Krysinski, H. T. Tien, A. Ottova, *Biotechnol. Prog.* **1999**, 15, 974–990.
33. T. Kakiuchi, *J. Electroanal. Chem.* **2001**, 496, 137.
34. M. Seitz, E. Ter-Ovanesyan, M. Hausch et al., *Langmuir* **2000**, 16, 6067–6070.
35. L.-Q. Gu, L. G. Wang, J. Xun et al., *Bioelectrochem. Bioenerg.* **1996**, 39, 275–283.
36. K. Asaka, A. Ottova, H. T. Tien, *Thin Solid Films* **1999**, 354, 201–207.
37. H. Gao, J. Feng, G.-A. Luo et al., *Electroanalysis* **2001**, 13, 45–53.
38. V. J. Cunnane, D. J. Schiffrin, M. Fleischmann et al., *J. Electroanal. Chem.* **1988**, 243, 455.
39. Y.-F. Cheng, D. J. Schiffrin, *J. Chem. Soc., Faraday Trans.* **1994**, 90, 2517.
40. H. T. Tien, (Ed.), *Photochem. Photobiol.* **1976**, 24, 95–207.
41. G. J. Kavarnos, *Fundamentals of Photoinduced Electron Transfer*, VCH Publishers, New York, 1993.
42. J. O'M. Bockris, F. B. Diniz, *J. Electrochem. Soc.* **1988**, 135, 1947.
43. J. Feng, C. Y. Zhang, A. L. Ottova et al., *Bioelectrochemistry* **2000**, 51, 187–191.
44. H. Gao, G. A. Luo, J. Feng et al., *J. Electroanal. Chem.* **2001**, 496, 158–161.
45. Y. L. Zhang, H. X. Shen, C. X. Zhang et al., *Electrochim. Acta* **2001**, 46, 1251–1257.
46. Y. S. Umezawa, Kihara, K. Suzuki et al., (Eds.), *Anal. Sci.* **1998**, 14, 1.
47. D. Ivnitski, E. Wilkins, H. T. Tien et al., *Electrochem. Commun.* **2000**, 2, 457–460.
48. Y. L. Cheng, R. J. Bushby, S. D. Evans et al., *Langmuir* **2001**, 17, 1240–1242.
49. J.-M. Kauffmann, (Ed.), *Bioelectrochem. Bioenerg.* **1997**, 42, 1–104.
50. C. M. A. Brett, A. M. Oliveira-Brett, (Eds.), *Electrochim. Acta* **1998**, 43.
51. H. T. Tien, A. Ottova, *Current Topics in Biophysics* **2001**, 25(1), 39–60.

17 Mediated Electron-transfer between Redox-enzymes and Electrode Supports

*Eugenii Katz, Andrew N. Shipway, and Itamar Willner
The Hebrew University of Jerusalem, Jerusalem, Israel*

17.1	Introduction	561
17.2	Electron-transfer Provided by Diffusional Mediators	562
17.2.1	Dissolved Enzymes Activated by Diffusional Mediators	563
17.2.2	Monolayer- or Multilayer-enzyme Electrodes Activated by Diffusional Mediators	564
17.2.3	Polymer- or Inorganic Matrix-immobilized Enzymes Activated by Diffusional Mediators	566
17.3	The Electrical Contacting of Dissolved Enzymes at Mediator-Functionalized Electrodes	566
17.4	Chiroselective Electron-transfer-mediated Biotransformations	568
17.4.1	Chiral Diffusional Electron-transfer Mediators	569
17.4.2	Chiral Monolayer-immobilized Electron-transfer Mediators	569
17.5	The Electrical Contacting of Mediator-modified Enzymes	569
17.5.1	Dissolved Redox Enzymes Functionalized with Electron-transfer Mediators	570
17.5.2	Monolayer- and Multilayer-enzyme Assemblies Functionalized with Electron-transfer Mediators	573
17.6	Polymer- and Inorganic Matrix-bound Enzymes Contacted by Coimmobilized Mediators	576
17.6.1	The Electrical Contacting of Enzymes in Mediator-functionalized Polymers	576
17.6.2	The Electrical Contacting of Enzymes in Mediator-functionalized Sol-gel Matrices	580
17.6.3	The Electrical Contacting of Enzymes in Mediator-containing Graphite Paste Composites	582

17.7	The Electrical Contacting of FAD-enzymes by Mediator-functionalized FAD	583
17.7.1	Electrical Contacting of Enzymes by Reconstitution of Apo-flavoenzymes with Relay-FAD Cofactor Units	583
17.7.2	Electrical Contacting of Enzymes by Surface-reconstitution of Apo-flavoenzymes on Relay-FAD-functionalized Electrodes	583
17.8	The Electrical Contacting of NAD(P)⁺-dependent Enzymes	587
17.8.1	The Electrochemical Regeneration of NAD(P) ⁺ -cofactors	587
17.8.2	The Electrochemical Regeneration of NAD(P)H-cofactors	590
17.8.3	The Association of NAD(P) ⁺ -dependent Enzymes with NAD(P) ⁺ Cofactors by Covalent and Entrapment Methods	594
17.8.4	The Integration of NAD(P) ⁺ -dependent Enzymes with Monolayer Arrays of NAD ⁺ -cofactor and Redox-catalysts	597
17.9	Electrical Contacting by Interprotein Electron-transfer	599
17.9.1	Soluble Cytochromes as Electron-transfer Mediators	599
17.9.2	Heme-protein Monolayers as Electron-transfer Mediators	601
17.9.2.1	Microperoxidase-11 Monolayers	603
17.9.2.2	Heme-containing De novo Protein Monolayers	603
17.9.2.3	Cyt c-aligned Monolayers Associated with Cytochrome Oxidase	605
17.10	Applications of Enzymes Electrically Contacted by Mediated Electron-transfer	606
17.10.1	Biosensors Based on Electrically “Wired” Enzyme Electrodes	606
17.10.2	Bioelectrocatalyzed Synthesis by “Wired” Enzyme Assemblies	607
17.10.3	Biofuel Cells Based on “Wired” Enzyme Assemblies	607
17.11	The External Control of the Electron-transfer Process	610
17.11.1	Photochemical Control by Enzyme-bound Photoisomerizable Units	610
17.11.2	Photochemical Control by Electrode-bound Photoisomerizable Units	614
17.11.3	Photochemical Control by Mediator-bound Photoisomerizable Units	616
17.12	Conclusion and Perspectives	617
	Acknowledgment	618
	References	618

17.1 Introduction

The redox-active component of most redox enzymes is encapsulated deep inside the enzyme structure. This spatial isolation from the bulk environment helps in the chemical and electrochemical isolation of the redox-center, allowing it to be out of equilibrium with the protein's surroundings. The imbalances that result facilitate the selective and directed chemical and electrochemical processes that sustain life. In an effort to gain understanding of these processes, the distance dependence of electron-transfer rates in proteins has been extensively studied, both experimentally [1–7] and theoretically [8–14]. According to electron-transfer theory, the electron-transfer rate constant between a donor–acceptor pair is given by Eq. (1), where ΔG° and λ correspond to the free energy and reorganization energy accompanying electron-transfer and d_0 and d are the Van der Waals distance and actual distance separating the donor and acceptor centers. If one views the electrode and the enzyme redox-center as a donor–acceptor pair, it becomes clear that the thick protein layer surrounding the active center provides an effective kinetic barrier to electron-transfer.

$$k_{\text{et}} \propto e^{[-\beta(d-d_0)]} e^{[-(\Delta G^\circ + \lambda)^2 / 4RT\lambda]} \quad (1)$$

The electrochemical insulation of the enzyme-active site by its protein or glycoprotein shell usually precludes the possibility of any direct electron-transfer with bulk electrodes [15]. However, under carefully controlled conditions, some enzymes can exhibit direct, nonmediated electrical communication with electrode supports, and biocatalytic transformations can be driven by these processes [16, 17]. For example, the direct electroreduction of O_2 and H_2O_2 biocatalyzed by laccase [18] and horseradish peroxidase (HRP) [19], respectively, have been demonstrated. This unusually facile electronic contacting is believed to be the consequence of incompletely encapsulated redox centers. When these enzymes are properly orientated at the electrode surface, the electrode-active site distance is short enough for the electron-transfer to proceed relatively unencumbered. Direct electron communication between enzyme-active sites and electrodes may also be facilitated by the nanoscale morphology of the electrode. The modification of electrodes with metal nanoparticles allows the tailoring of surfaces with features that can penetrate close enough to the enzyme active site to make direct electron-transfer possible [20, 21].

The electrical contacting of redox enzymes that defy direct electrical communication with electrodes can be established

by using synthetic or biologically active charge-carriers as intermediates between the redox-center and the electrode. These artificial electron donor or acceptor molecules (in case of reductive or oxidative enzymes, respectively), usually referred to as *electron-transfer mediators*, can be accepted by many redox enzymes in place of their natural oxidants or reductants [22]. They have a wide range of structures, and hence properties, including a range of redox potentials. The redox potential of a suitable mediator should provide an appropriate potential gradient for electron-transfer between an enzyme active site and an electrode. The redox potential of the mediator, $E_M^{\circ'}$, should be more positive or more negative than the redox potential of the enzyme-active site, $E_E^{\circ'}$, in the case of oxidative ($E_M^{\circ'} > E_E^{\circ'}$) and reductive ($E_M^{\circ'} < E_E^{\circ'}$) bioelectrocatalysis, respectively. In the process of shuttling charge between the redox-center and the electrode, the mediator is cycled between its oxidized and reduced states. The mediator should be stable in both the reduced and oxidized forms and any side reactions between the mediator redox states and the enzyme or the environment should be eliminated. To be effective in its role, the mediator must often compete with the enzyme's natural substrate (e.g. molecular oxygen in case of oxidases), effectively and efficiently diverting the flow of electrons to and from the electrode. An efficient mediator should provide rapid reaction with the redox enzyme, effectively oxidizing or reducing the enzyme-active center. A mediator should also exhibit reversible electrochemistry (a large rate constant (k_{et}) for the interfacial electron-transfer at the electrode surface).

The total efficiency of the electron transport provided by mediators depends not only on the mediator properties, but also on the whole system architecture. A

mediator that cannot compete with the natural dioxygen electron acceptor when it is functioning via a diffusional route could be very efficient when it is included into an organized supramolecular assembly and operates in a nondiffusional mode. Several approaches have been developed and many bioelectrochemical systems have been designed to enhance the electrical contacting of redox enzymes at electrode surfaces by the use of electron mediators. These methodologies range from the simple application of soluble enzymes with diffusional electron mediators to systems with very sophisticated biomolecular architectures composed of numerous components. Common to all these systems is the application of a multistep mediated electron-transfer (MET) process, each step of which proceeds over a short distance. The development of these efficient electrical contacting methodologies has resulted in the construction of numerous amperometric biosensors and bioelectrocatalytic systems including bioreactors and biofuel cells. The contacted enzyme may also be used as part of a more complex assembly – the triggering of any electron-transfer step by an external signal (e.g. light) results in the control of the biocatalytic activity.

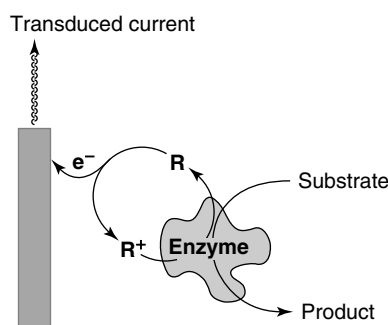
The aim of this paper is to review the various systems in which redox enzymes are electrically contacted via a MET process including those in which the mediating process is triggered by external signals. All potentials in the text and figures are quoted versus saturated calomel electrode (SCE).

17.2

Electron-transfer Provided by Diffusional Mediators

MET can be affected by a diffusional mechanism (Fig. 1) in which the electron

Fig. 1 The electrical “wiring” of an oxidative redox enzyme via a diffusional electron-transfer mediator shuttling between the enzyme active center and the electrode.



relay is either oxidized or reduced at the electrode surface. Diffusional penetration of the oxidized or reduced relay into the protein yields a sufficiently short electron-transfer distance for the electrical activation of the biocatalyst. Penetration of the mediator close to the enzyme-active center inside the protein matrix is controlled by the hydrophobic/hydrophilic properties of the mediator and the enzyme, the size and shape of the mediator, and the electrostatic charge interactions between the mediator and the enzyme. The mediators can diffusively shuttle electrons between the electrode and enzymes in several configurations: soluble, immobilized as monolayers (or multilayers), or incorporated into porous matrices. In all these cases, the medium needs to provide a free diffusion pathway between the conductive support (providing electrochemical regeneration of the mediator) and the enzyme molecules (working as biocatalysts).

17.2.1

Dissolved Enzymes Activated by Diffusional Mediators

Ferrocene derivatives, organic dyes, ferri-cyanide, Ru-complexes, and other electrochemically active substrates have been employed for diffusional MET and the electrical activation of soluble redox enzymes

lacking direct electrical contact with the conductive support [22]. Cyclic voltammetry (CV) allows to assess the effectiveness of a particular enzyme/mediator combination using the theory for the catalytic electrochemical processes. The second-order rate constant for the reaction between the enzyme and the mediator can also be determined [23–25]. Soluble redox enzymes electrically contacted by the use of diffusional electron-transfer mediators with various redox potentials (E_M^0) providing different rate constants of electron-transfer (k_{EM}) have been extensively reviewed [22].

Comparison of the electron-transfer efficiency provided by different mediators in the presence of the same redox enzyme allows the definition of the important parameters of MET. The reaction of glucose oxidase (GOx) has been extensively studied with a number of artificial electron acceptors including organic dyes such as phenazine methosulfate, 2,6-dichlorophenolindophenol, and *N, N, N', N'*-tetramethyl-4-phenylenediamine [26]. However, these mediators have a number of limitations such as poor stability and the pH dependence of their redox potentials. Simple inorganic redox species such as hexacyanoferrate [27], hexacyanoruthenate, and pentaamine pyridine ruthenium [28] do not suffer from these problems. These

inorganic compounds have almost ideal electrochemistry and are more stable than the organic dyes. The application of inorganic mediators has been exemplified with other oxidases such as sarcosine oxidase and lactate oxidase [29]. Inorganic mediators are difficult to “tune” for solubility and electrochemical properties though, as they cannot be modified or derivatized as easily as their organic counterparts.

The majority of these problems have been overcome by the use of ferrocene derivatives as electron acceptors for soluble oxidases (e.g. GOx). Ferrocene derivatives of varying charge and solubility, with redox potentials ($E_M^{\circ'}$) between +0.1 V and +0.4 V, have been shown to accept electrons from GOx [30]. The published values [22] for the second-order rate constant (k_{EM}) for the reaction of the reduced active center of GOx (FADH₂) and an oxidized ferrocene derivative range from 0.26×10^5 to $5.25 \times 10^5 \text{ M}^{-1}\text{s}^{-1}$. There is no simple correlation between k_{EM} and $E_M^{\circ'}$; however, it is clear that positively charged ferrocenes are favored for the mediated electron transport from GOx [31]. This effect originates from the electrostatic attraction between the positively charged oxidized mediator and the negatively charged GOx. Comparison of the mediating efficiency of charged electron relays and charged enzymes should always take electrostatic interactions into account [32–34]. The size of the mediator is also important and it has been shown that ferrocenes inside cyclodextrin cavities do not mediate electron transport from GOx [35]. To improve the contact between electron relay molecules and redox enzymes, micellar systems composed of ferrocene-functionalized surfactants have been applied [36–38]. GOx has been electrically contacted using such redox-active micelles and an advantage in the electron-transfer

efficiency over homogeneous electron-relays was demonstrated.

17.2.2

Monolayer- or Multilayer-enzyme Electrodes Activated by Diffusional Mediators

Monolayers and multilayers of redox enzymes (e.g. GOx [39], bilirubin oxidase [40]) have been organized on electrode surfaces using bifunctional reagents (producing covalent bonding between the layers) [39, 40] or using bioaffinity interactions (for instance, biotin/avidin [41–43] or antigen/antibody [44, 45]). The enzyme content in monolayers is low, however, and electrical contact in the presence of a diffusional mediator does not usually result in a detectable amperometric response. Thus, an increase of the enzyme content is essential to obtain the detectable current when diffusional mediators are applied. The stepwise deposition of a multilayer assembly results in the increase of the enzyme content, leading to a significantly larger current. The deposition of a controllable number of the enzyme layers also allows the “tuning” of the enzyme electrode–amperometric output [46].

The enzyme content of monolayer assemblies may also be increased by the application of rough electrode surfaces. Treatment of Au surfaces with Hg results in a roughening of the conductive support by the generation and dissolution of an Au-amalgam [47]. Typically, Au surfaces with initial roughness factor of 1.2–1.5 can be roughened to exhibit a roughness factor of 15–25. Multilayers of GOx were linked to smooth and rough Au electrodes by coupling to cystamine-functionalized surfaces, and ferrocene monocarboxylic acid was applied as a diffusional mediator to contact the enzymes [46]. The resulting

currents of a four-layer roughened GOx electrode are approximately sixfold greater than those for a smooth electrode.

The organization of ordered enzyme multilayer arrays opens the possibility of assembling multilayers of two or more different enzymes [46], one of which is a redox enzyme electrically contacted via diffusional MET. The other enzyme(s) may turn the analyte substrate into a product that is the substrate for the redox enzyme. The resulting transduced current is therefore proportional to the concentration

of analyte. A multilayer enzyme electrode consisting of choline oxidase (ChO) and acetylcholine esterase (AChE) was tailored according to this concept (Fig. 2a) [46]. The analyte acetylcholine is hydrolyzed to choline in the presence of AChE and the resulting product is bioelectrocatalytically oxidized by ChO to betaine in the presence of 2,6-dichlorophenolindophenol (1) as a diffusional mediator. The current developed by the biocatalytic electrode is proportional to the concentration of the primary substrate acetylcholine (Fig. 2b).

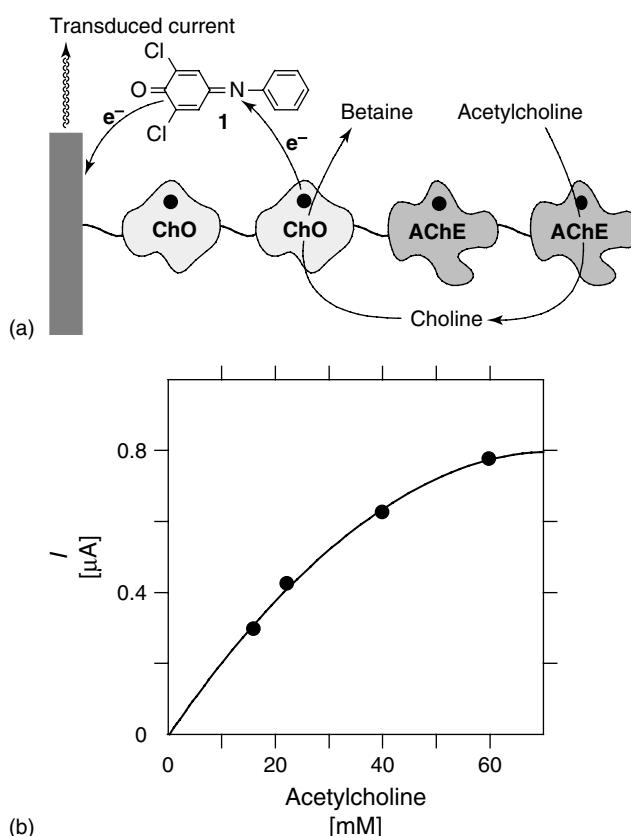


Fig. 2 (a) A bienzymatic network consisting of ChO and AChE for the amperometric detection of acetylcholine; (b) dependence of the electrocatalytic current produced by the assembly on the concentration of acetylcholine. Applied potential 0.3 V, with 40- μM 2,6-dichlorophenolindophenol (1) as the electron mediator.

17.2.3

Polymer- or Inorganic Matrix-immobilized Enzymes Activated by Diffusional Mediators

Redox enzymes may also be electrically contacted with electrode supports by their entrapment in an electropolymerized film [48–52]. One of the original motivations for this approach was the possibility that direct electrical contact with the enzyme by the conducting polymer might be possible, but this question remains unresolved. Although direct oxidation has been claimed in some conductive polymers (e.g. polypyrrole (PPy) [52]), the balance of the evidence indicates that if there is any direct electrical contact, the effect is small. It is possible to enhance the electrical communication using diffusional mediators shuttling electrons between the conductive electrode support and the enzymes incorporated into the polymeric film. *N*-Methyl phenazinium [48], benzoquinone [48, 53], hydroquinonesulfonate [54], and ferrocene monocarboxylic acid [50, 51] have been used for this purpose. The polymer porosity is an important issue for this kind of enzyme electrical “wiring” as it provides the route for the mediator to transport the charge.

The electrical “wiring” of redox enzymes entrapped in inorganic (e.g. sol–gel) matrices can also be achieved by the application of solution-state electron-relays that can penetrate through the matrix. For example, HRP films deposited in carbon paste substrates and then covered with a thin silica sol–gel layer have been used to detect H_2O_2 in aqueous media [55] and organic peroxides in nonaqueous solutions [56] by the use of $[\text{Fe}(\text{CN})_6]^{4-}$ or ferrocene mediators, respectively. The extension of this electrode configuration to other enzymes has led to the development of new amperometric

sensors for glucose [57] and phenolic compounds [58].

It should be noted that all the systems discussed above operate using low molecular weight, soluble, mediators that can leach out the electrode and be lost to the bulk solution. This is a significant disadvantage, particularly for in vivo applications. Practically important systems can be designed using similar immobilization approaches, but with the critically important difference that the mediator molecules are also immobilized in the assembly and provide the electron transport via a nondiffusional route (Sect. 17.6).

17.3

The Electrical Contacting of Dissolved Enzymes at Mediator-Functionalized Electrodes

The electrochemical contacting of solution-state enzymes with surface-immobilized redox-mediators is of interest for studying the interfacial association affinity interactions between enzymes and mediators. The electrochemical kinetics of electrodes functionalized with layers of various mediators (e.g. viologens [59], C_{60} -derivatives [60], microperoxidase-11 [61]) have been studied upon their interaction with diffusional free enzymes. Some relay-functionalized interfaces demonstrate MET without a significant amount of association of the enzyme molecules with the relay-modified surfaces. For example, a C_{60} monolayer-functionalized Au-electrode has been applied to contact soluble GOx (Fig. 3a) [60]. CV revealed an efficient electrocatalytic current developed by the C_{60} -modified electrode in the presence of GOx and glucose (Fig. 3b) [60], dependent on the glucose concentration (Fig. 3b, inset). However, kinetic analysis

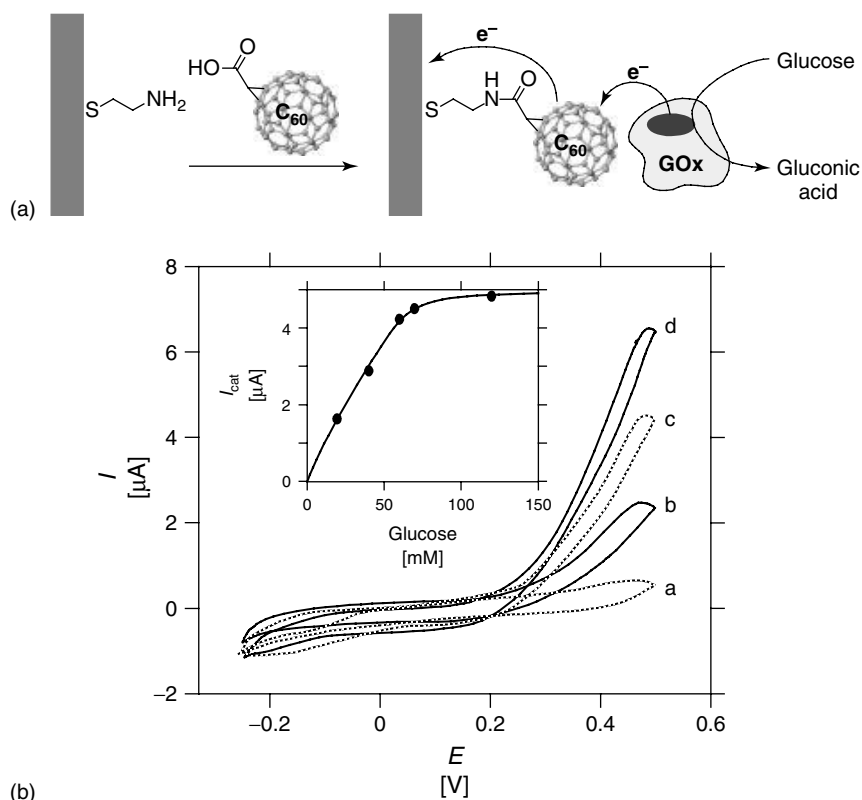


Fig. 3 (a) Assembly of a C_{60} monolayer-functionalized-electrode for the bioelectrocatalysed oxidation of glucose. (b) Voltammograms of the C_{60} monolayer electrode in the presence of GOx (2 mg mL⁻¹) and glucose at (a) 0, (b) 20, (c) 40, and (d) 100 mM. Measurements were performed in 0.1 M-phosphate buffer, pH 7.1, under Ar, at a scan rate of 5 mV s⁻¹. Inset: calibration curve for the concentration dependence of the catalytic current.

performed using a rotating disk electrode modified with the C_{60} -monolayer showed no temporary association of GOx with the relay-modified surface. This observation suggests that the interaction of the enzyme with the relay-interface and the resulting electron-transfer proceeds in a short timescale and it is not the limiting step in the bioelectrocatalytic process.

In the case of surfaces modified with biological mediators such as microperoxidase-11 (MP-11) (2), the temporary association of enzyme molecules to the relay-functionalized electrode surface has

been demonstrated. The MP-11 monolayers can mediate electron-transfer to hemo-proteins (e.g. cytochrome *c* (Cyt *c*), myoglobin (Mb), and hemoglobin (Hb)) by the formation of affinity complexes at the interface [61]. The heme-containing monolayer can also stimulate MET to cytochrome-dependent enzymes. The electrocatalytic reduction of nitrate ions was achieved when the dissolved cytochrome-dependent nitrate reductase (NR) was electrically contacted by a monolayer of MP-11 (Fig. 4a). Figure 4(b) shows the cyclic voltammograms of the MP-11 monolayer-electrode

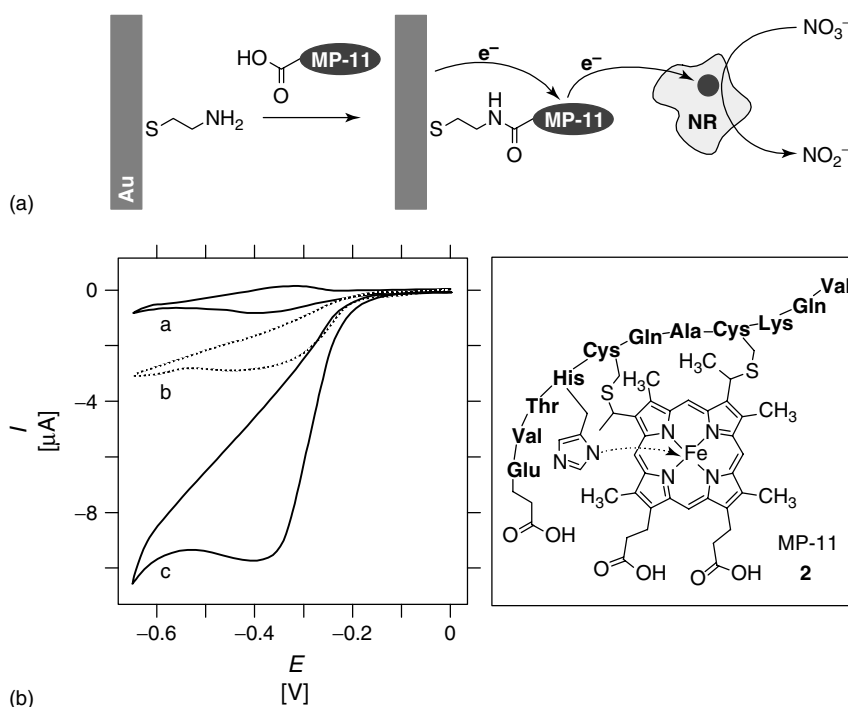


Fig. 4 (a) Bioelectrocatalytic reduction of nitrate by NR mediated by a monolayer immobilized MP-11; (b) cyclic voltammograms of an MP-11-modified electrode (a) in 0.05 M phosphate buffer, pH 7.0, (b) after the addition of NR (24 μM), and (c) after the subsequent addition of KNO₃ (5 mM). Recorded under Ar, potential scan rate 5 mV s⁻¹.

(curve a) and with added NR (curve b). With NR, an electrocatalytic cathodic current is observed indicating the mediated electrochemical reduction of NR. Addition of NO₃⁻ to the system results in a substantial enhancement in the cathodic current (curve c) resulting from the electrochemical reduction of the nitrate biocatalyzed by NR. The Michaelis-Menten analysis of the cathodic electrocatalytic currents developed in the presence of different concentrations of NO₃⁻ results in the conclusion that NR produces a temporary complex with the MP-11-modified interface and the MET proceeds within this complex.

As these systems operate in the presence of soluble enzymes, they have little potential for practical purposes.

However, the study of these systems has revealed temporary affinity association of the enzyme molecules with the mediator-functionalized electrode surfaces (e.g. MP-11). This, in turn, has allowed the development of integrated biocatalytic systems composed of mediators and enzymes by the lateral cross-linking of the enzyme-mediator affinity complex generated at the electrode support (Cf. Sects. 17.8 and 17.9.2).

17.4

Chiroselective Electron-transfer-mediated Biotransformations

The MET process involves the penetration of an electron-relay into a protein matrix to

reach a position close to the enzyme active site. As the protein structure is chiral, it might be expected that the ability of two enantiomeric mediators to reach the active site, affect efficient electron transfer, and exit back into the bulk solution could be significantly different.

17.4.1

Chiral Diffusional Electron-transfer Mediators

Chiroselective MET has been addressed in a series of studies using diffusional chiral electron mediators [62–64]. The enantiomeric electron relays (*S*)- and (*R*)-*N*, *N*-dimethyl-1-ferrocenyl-ethylamine were reported to stimulate chiroselective bioelectrocatalyzed oxidation of glucose in the presence of GOx [62]. The bioelectrocatalyzed oxidation of glucose was approximately twofold enhanced in the presence of the (*S*)-isomer as compared with (*R*)-isomer. Kinetic analysis of the bioelectrocatalyzed oxidation of glucose by the two enantiomeric electron relays performed using a rotating disk electrode suggests that the protein induces chiral discrimination because of diastereoisomeric interactions during the mediator's penetration and dissociation pathways. Chiral discrimination in MET and subsequent bioelectrocatalyzed transformations has also been observed for other diffusional electron relays and enzymes [63, 64].

17.4.2

Chiral Monolayer-immobilized Electron-transfer Mediators

The concept of enantioselective electrical contacting of redox enzymes and electrode surfaces was further developed by the organization of a chiral

electron-transfer mediator as a monolayer on an electrode surface [65]. The (*R*)- and (*S*)-2-Methylferrocene carboxylic acids (**3** and **4**) were assembled as monolayers on Au-electrodes (Fig. 5a). The monolayer-mediated oxidation of glucose in the presence of GOx showed an approximately 1.9-fold enhancement at the electrode functionalized by the (*S*)-enantiomer (**4**) over the electrode functionalized by the (*R*)-enantiomer (**3**) (Fig. 5b). Rotating disk electrode studies revealed that the MET proceeds via the formation of a complex between the mediator monolayer and GOx. The electron-transfer rates within the complex from GOx_{red} to the (**3**) and (**4**) differ substantially, 0.3 s⁻¹ and 0.5 s⁻¹, respectively, whereas the Michaelis-Menten constants characterizing the complex are identical, $K_M = 1.2 \times 10^{-5}$ M. Thus, the affinity for the association of GOx_{red} to the chiral ferrocenyl cation monolayers are similar. However, the diastereoisomeric nature of the complex yields different electron-transfer distances between the oxidized mediator and the reduced flavin sites, thereby stimulating the different electron-transfer rates.

17.5

The Electrical Contacting of Mediator-modified Enzymes

The chemical modification of redox enzymes with electron relay groups can enable nondiffusional MET, often referred to as the electrical *wiring* of the proteins [66–69] (Fig. 6a). The covalent attachment of electron-relay units at the protein periphery and inner sites yields short interrelay electron-transfer distances. Electron “hopping” or tunneling between the periphery and the active site enables electrical communication between

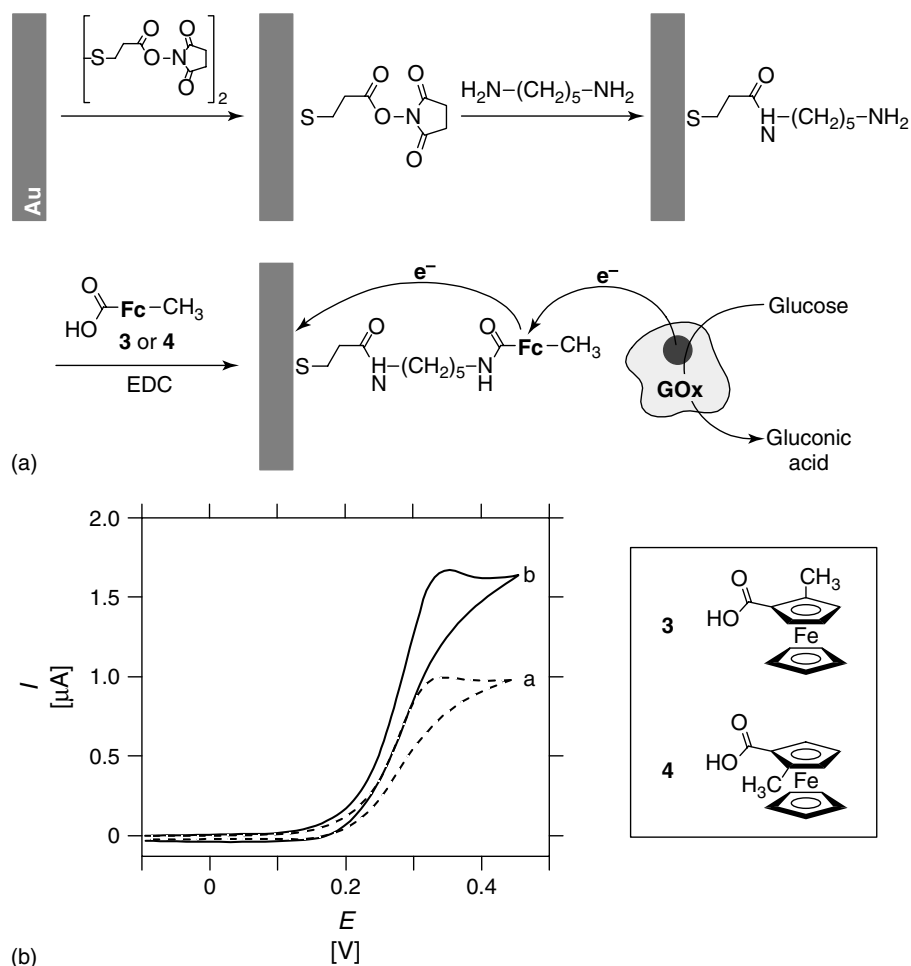


Fig. 5 The enantioselective bioelectrocatalyzed oxidation of glucose by GOx at an electrode modified by a chiral electron-transfer mediator: (a) organization of the chiral ferrocene monolayer-modified Au-electrode and its interaction with soluble GOx. (EDC = 1-(3-dimethylaminopropyl)-3-ethylcarbodiimide hydrochloride); (b) cyclic voltammograms of the ferrocene-modified-electrode (curves a and b for *R*-Fc (**3**) and *S*-Fc (**4**), respectively) in the presence of 1×10^{-5} M GOx and 50 mM glucose. Recorded in 0.1 M phosphate buffer, pH 7.0, under Ar, potential scan rate 5 mV s^{-1} , electrode area 0.26 cm^2 .

the redox enzyme and its environment. The simplest systems of this kind involve electron relay-functionalized enzymes diffusively communicating with electrodes [66, 67], but more complex assemblies include immobilized enzymes on electrodes as integrated assemblies [70].

17.5.1

Dissolved Redox Enzymes Functionalized with Electron-transfer Mediators

GOx has been covalently modified with ferrocene electron-relay groups by the carbodiimide coupling of ferrocene

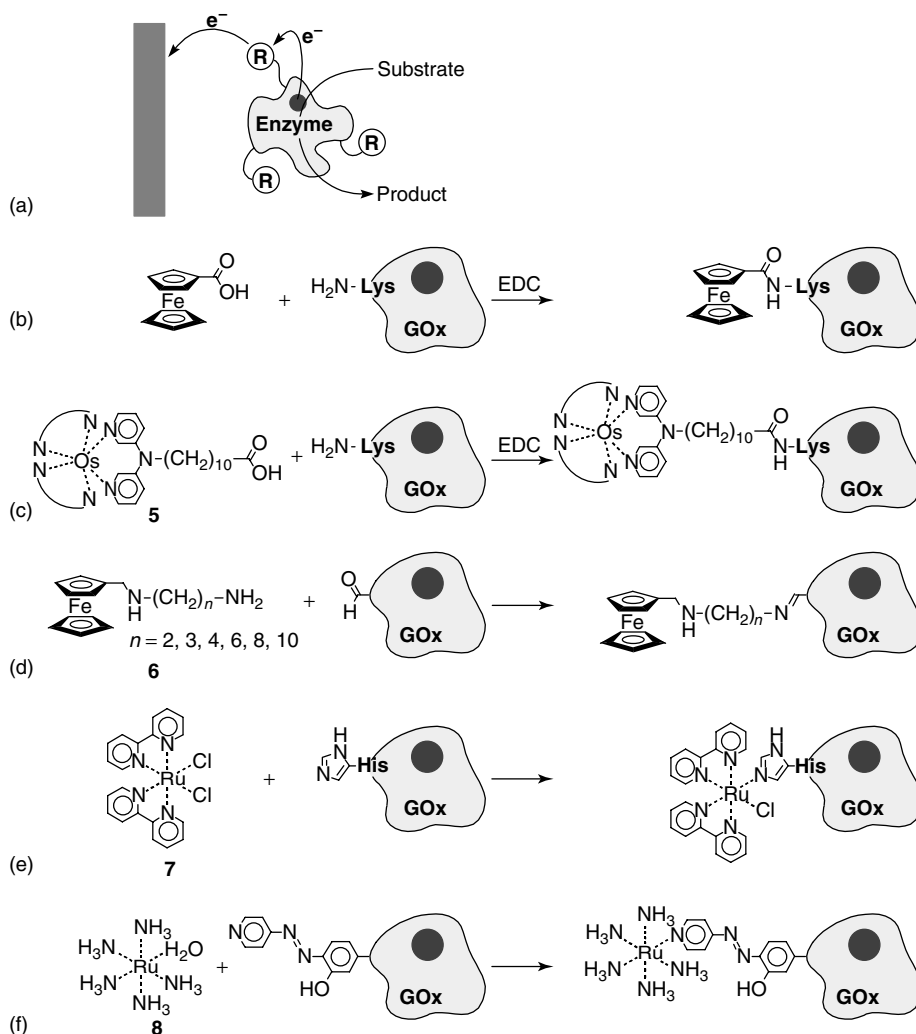


Fig. 6 (a) A soluble enzyme electrically contacted with an electrode surface via redox-mediator groups covalently tethered to the protein backbone. (b)–(f) Different kinds of redox-mediators tethered by different means to the protein backbone; (b) a ferrocene unit linked to a lysine amino group via an amide bond; (c) an Os-complex linked to a lysine amino

group via an amide bond; (d) a ferrocene unit linked via a Schiff-base to an aldehyde group generated on the glycoprotein by oxidation with IO_4^- ; (e) $\text{Ru}(\text{bpy})_2\text{Cl}_2$ linked to histidine residues by the formation of a $\text{Ru}(\text{bpy})_3$ His-complex; (f) a Ru-complex linked to a pyridine group by ligand exchange.

carboxylic acid [66, 67] (Fig. 6b) or osmium (*bis*-4,4'-diaminobutane-*N,N*-bis-2-pyridyl-11-aminoundecanoic acid) (5) [36] (Fig. 6c) to the amino functions of the

protein backbone. Other chemical procedures have also been used to produce relay groups peripherally bound to proteins. For example, carbonyl functions generated

in glycoproteins (e.g. GOx) by oxidation with periodate have been coupled to an amino-functionalized ferrocene (**6**) via Schiff bases (Fig. 6d) [68]. In a different approach, ruthenium complexes (**7**, **8**) were formed on GOx using either natural histidine residues [71] (Fig. 6e) or artificially

introduced pyridine groups [67] (Fig. 6f) in the protein backbone. The randomly distributed ferrocene relay groups provided electrical contact between the GOx redox center and the unmodified electrode surface. It was also demonstrated that longer spacer groups bridging the electron relay

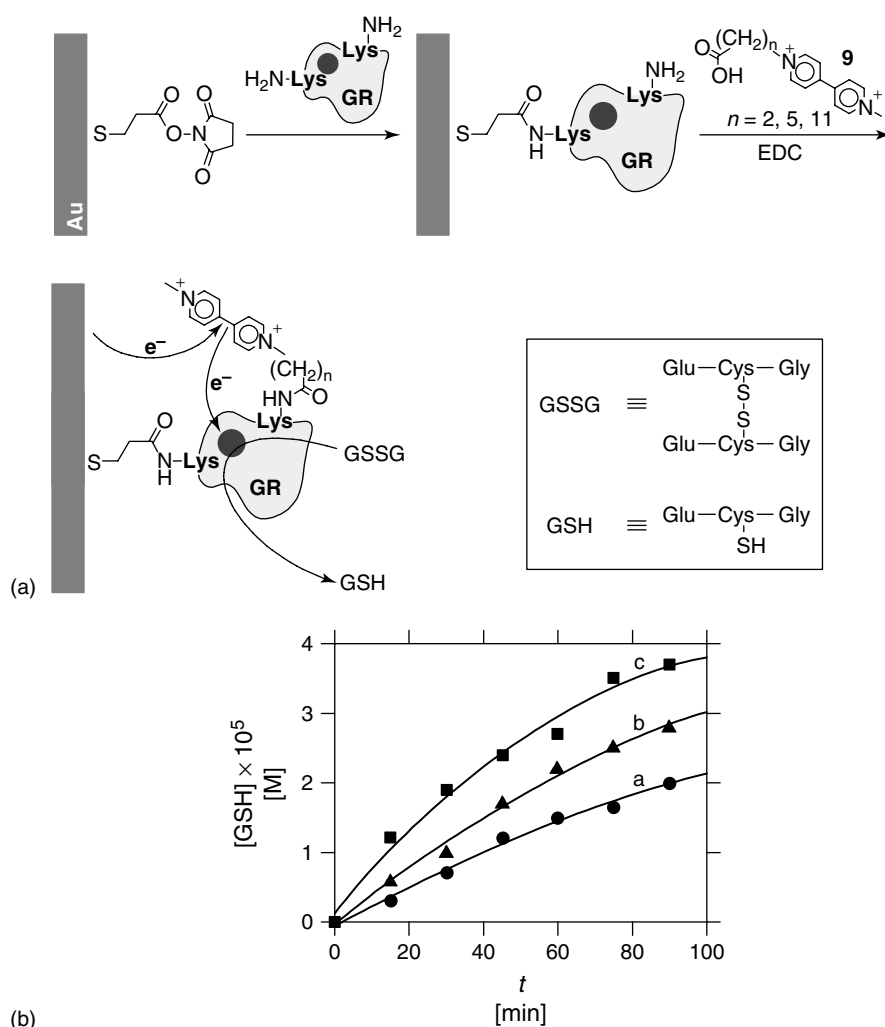


Fig. 7 (a) The assembly of an electrically contacted glutathione reductase monolayer on an electrode; (b) the rate of bioelectrocatalyzed reduction of GSSG by the electrically contacted enzyme-electrode using chain-lengths of (a) $n = 2$, (b) $n = 5$, (c) $n = 11$ and upon the application of a potential corresponding to -0.72 V on the enzyme-electrode in the presence of GSSG (10 mM). The experiments were performed in 0.1 M phosphate buffer, pH 7.2, under Ar.

groups and the enzyme provide higher mobility, shorten the electron-transfer distance, and thus enhance the enzyme's bioelectrocatalytic activity [68]. Partial and reversible unfolding of the enzyme (using urea) during the covalent modification of the protein with the relay is also important as it allows the attachment of the electron mediator to inner positions close to the active site of the enzyme [72].

While an increased loading of an electron mediator on a protein enhances the effectiveness of electrical contacting, the enzyme activity suffers because of changes brought about in its structure. The chemical modification of redox proteins with synthetic electron mediators is always accompanied by this partial denaturing of the native biocatalyst, and so the modification must be carefully controlled to achieve the optimum effect. With GOx modified by ferrocene units, the optimal MET was found at a loading corresponding to 12–13 electron relay units [72]. The rate constant of electron-transfer between the enzyme's flavin adenine dinucleotide (FAD) site and the nearest electron relay group was found to be approximately 0.9 s^{-1} (substantially lower than that for electron-transfer to the native dioxygen electron acceptor of the enzyme, proceeding with a rate constant of ca. $5 \times 10^3 \text{ s}^{-1}$) [72]. Improvements in the efficiency of electrical contact may be possible by the use of protein engineering, genetic manipulation, or relay units placed at optimal positions in the enzyme structure.

17.5.2

Monolayer- and Multilayer-enzyme Assemblies Functionalized with Electron-transfer Mediators

Enzyme monolayers can be electrically contacted by using electron mediators

covalently attached to the protein [73–75].

In this case, electron mediators must be available close enough to both the enzyme active site and the electrode to facilitate an efficient electron-transfer path between them. A glutathione reductase monolayer assembled onto Au-electrodes through a thiolate bridging unit (Fig. 7a) was functionalized with *N*-methyl-*N'*-carboxyalkyl-4,4'-bipyridinium salts (9), where the chain length tethering the electron relay was systematically lengthened [73, 74]. Electroreduction of the bipyridinium unit was found to activate the enzyme for the reduction of oxidized glutathione (GSSG). The effectiveness of GSSG reduction was controlled by the chain length tethering the electron relay to the protein, and longer bridging chains enhanced the electrobiocatalyzed reduction rate (Fig. 7b). This phenomenon was rationalized in terms of shorter electron-transfer distances between the electron-relay sites and the enzyme redox-center for the systems with long-chain tethered bipyridinium units. It was also found that in order to attain electron-transfer communication between the enzyme redox-center and the electrode, it is important to modify the protein with the bipyridinium components in the presence of urea. Added urea partially unfolds the protein and enables the functionalization of inner lysine residues. These inner electron relay units provide a route for electron “hopping” between the electrode and the active redox-center of the protein, and thus contribute to the electrical contacting of the enzyme layer with the electrode [73, 74].

Nonorganized multilayers of mediator-tethered enzymes have been constructed by cross-linking on an electrode surface [76]. A ferrocene-contacted GOx film was assembled on an Au-electrode by the

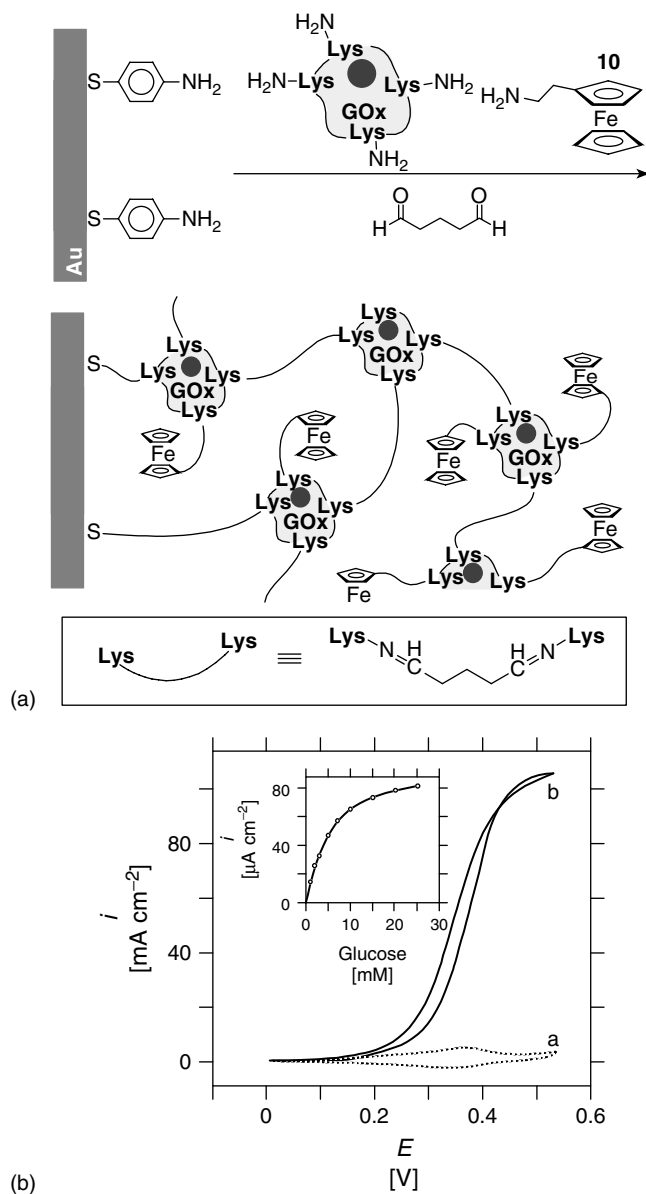


Fig. 8 (a) The preparation of a nonordered polymeric layer of GOx electrically "wired" by ferrocene groups incorporated in the enzyme net; (b) cyclic voltammograms of the GOx/ferrocene-modified electrode in the absence (a) and in the presence (b) of glucose, 30 mM. Performed under argon, in phosphate buffer, pH 7, scan rate 10 mV s⁻¹. Inset: calibration curve for the amperometric response to glucose at 0.35 V. [Adapted from S. Kuwabata, T. Okamoto, Y. Kajiya et al., *Anal. Chem.* **1995**, 67, 1684–1690.]

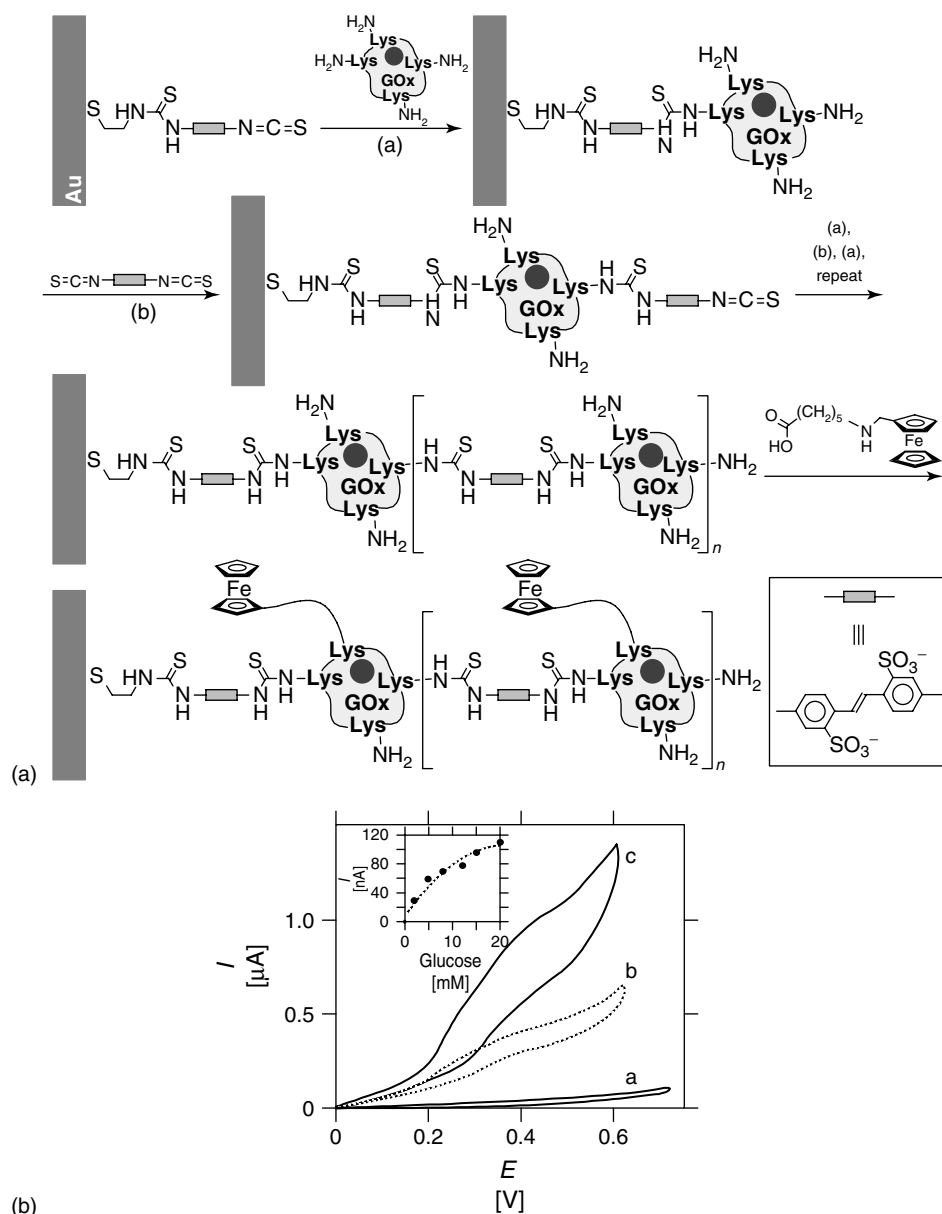


Fig. 9 (a) The stepwise assembly and electrical contacting of a crosslinked organized multilayer array of GOx on an Au-electrode; (b) cyclic voltammograms of the GOx/ferrocene-modified electrode in the presence of glucose (20 mM) in

(a) 1, (b) 4 and (c) 8 layer configurations. Inset: amperometric responses of the 4-layer GOx array at 0.4 V as a function of glucose concentration. Recorded in 0.1 M phosphate buffer, pH 7.3, under argon.

cross-linking of GOx, (2-aminoethyl)ferrocene (**10**), and a monolayer of *p*-mercaptoaniline with glutaric dialdehyde [76] (Fig. 8a). The immobilized enzyme was effectively contacted through the electron-relay groups, providing electron propagation throughout the assembly. A calibration curve (Fig. 8b, inset) for the modified electrode in the presence of glucose was derived from the analysis of CV (Fig. 8b). More controlled superstructures can be constructed in a stepwise manner by the layer-by-layer deposition of enzymes and the covalent attachment of relay units to the enzyme backbone. A multilayer of GOx was modified with (6-ferrocenemethylamino)hexanoic acid (Fig. 9a) [39]. The ferrocene units are oxidized by the electrode, and they in turn oxidize the enzyme redox-sites. The amperometric responses of the layered electrodes were found to be controlled by the number of protein layers, implying that all the enzyme-layers are electrically contacted with the electrode. As the rate-limiting process in the oxidation of glucose is the electron-transfer between the substrate and the enzyme redox-center, the amperometric response of the electrode is dependent on the glucose concentration. This dependence allows the application of the layered enzyme-electrode as a glucose biosensor (Fig. 9b, inset), whose sensitivity is controlled by the number of enzyme layers in the assembly (Fig. 9b).

17.6

Polymer- and Inorganic Matrix-bound Enzymes Contacted by Coimmobilized Mediators

The incorporation of enzymes into organic polymer or inorganic composite matrices provides very convenient and stable

biocatalyst interfaces that have important practical applications. Many cheap and versatile matrices composed of different kinds of polymers (e.g. PPy [48–52]) or inorganic components (e.g. sol–gel [77, 78], graphite paste [79, 80]) impregnated with electron-transfer mediators, cofactors, and other materials have been investigated for biosensor design.

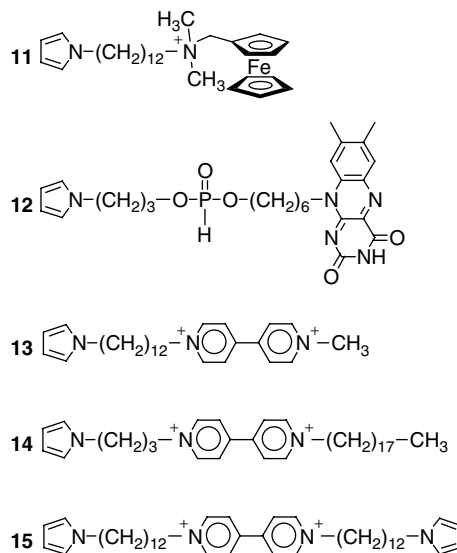
17.6.1

The Electrical Contacting of Enzymes in Mediator-functionalized Polymers

Many examples of bioelectrocatalytic electrodes consisting of polymer-embedded enzymes exist [81–83]. The electrical contacting of enzymes immobilized in polymer matrices is achieved either by virtue of a conducting polymer or by incorporating electron relay groups within the polymer, providing electron hopping between the enzyme and the electrode support. Here, we will focus on the application of electron relay groups introduced into polymer films to provide mediated electrical “wiring” of entrapped enzyme molecules [83].

The simplest way to achieve these assemblies involves the incorporation of ionic redox-groups (e.g. ferrocyanide [84–86]) by the anion-exchange properties of the polymer. Consequently, the coentrapment of enzymes and anionic redox-relays can be employed for electrical “wiring” of the biocatalysts [87, 88]. The anion-exchange properties of regular PPy has been used to incorporate ferrocene carboxylate [50] and pyrroloquinoline quinone (PQQ) [89] for the electrical “wiring” of GOx during the electrogeneration of a PPy film. This approach does not offer, however, covalent binding of the mediator, resulting in its leakage from the polymeric matrix. Biocatalytic electrodes based

Fig. 10 Structures of redox-functionalized pyrrole derivatives applied for electropolymerization and the entrapment of redox enzymes.



on this technology therefore tend to be unstable and cannot be used for in vivo measurements. To stabilize the electron-relays inside the polymeric matrix, new amphiphilic pyrrole derivatives containing redox-units (**11–15**) have been synthesized (Fig. 10) [83, 90–92], allowing the relay to be covalently incorporated into the polymer structure. For example, a ferrocene-containing pyrrole derivative (**11**) has been employed to electrically contact GOx [83] and pyruvate oxidase [93], and a flavin analog-functionalized pyrrole (**12**) to contact flavin reductase [94]. Enzymes operating in reductive pathways (e.g. NR, pyridine-nucleotide oxidoreductase) have been electrically contacted in polymeric matrices by the use of the viologen-functionalized pyrrole derivatives (**13–15**) [90, 95–97]. NR, electrically contacted by the viologen units of a polymer matrix, has been used for the

amperometric detection of nitrate ions (Fig. 11a), leading to the calibration curve given in Fig. 11(b).

Another approach to the electrical contacting of polymer-bound enzymes involves the use of polymers that are functionalized with redox-units [98, 99]. Polyelectrolytes represent the best choice

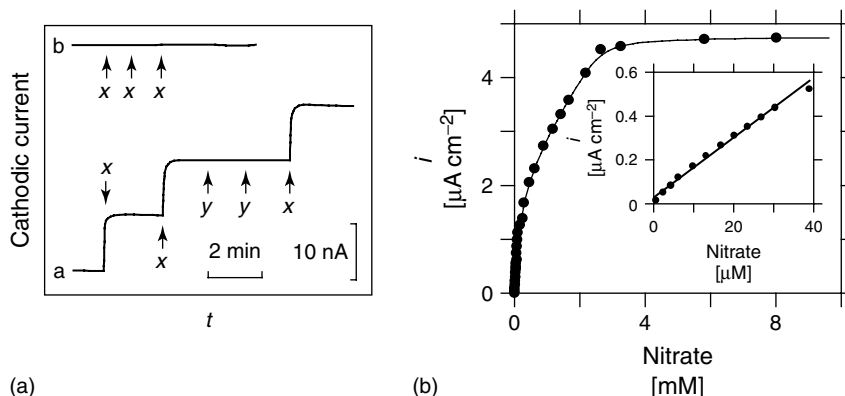


Fig. 11 (a) The amperometric responses of (a) a PPy-viologen-NR electrode, and (b) an identical electrode constructed without the enzyme, in response to injections (x) increasing the nitrate concentration by $3.5 \mu\text{M}$, and (y) of buffer; (b) calibration curves (Inset: smaller concentration range) for the response to nitrate of a PPy-viologen-NR electrode at -0.7 V . [Adapted from S. Cosnier, C. Innocent, Y. Jouanneau, *Anal. Chem.* **1994**, 66, 3198–3201.]

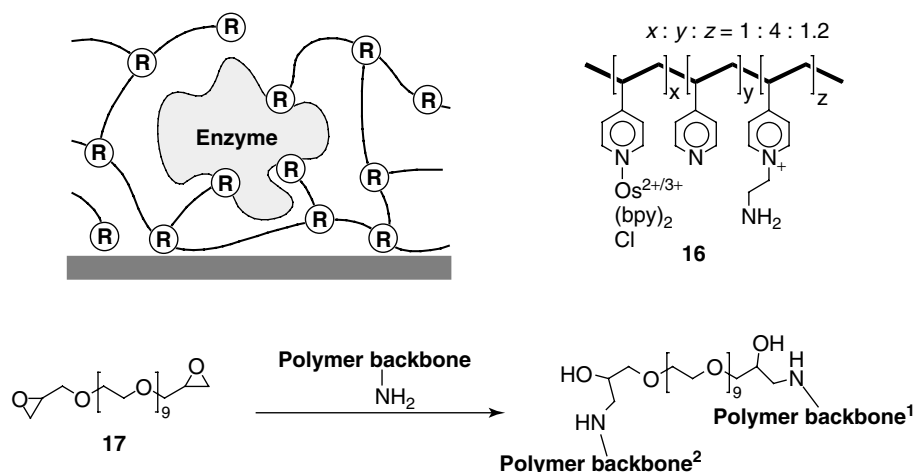


Fig. 12 A redox enzyme electrically “wired” to an electrode surface by flexible polymer chains functionalized with redox-mediator groups and surrounding the enzyme at the electrode surface.

for the optimization of interactions with enzymes and electrodes. Hydrophilic, charged, flexible chains of polyelectrolytes can easily surround protein molecules, and even penetrate inside the protein matrix, providing good contact between the protein structures and polymer backbone (Fig. 12). Each unit of a polyelectrolyte is weakly adsorbed on an electrode surface, but the cooperative effect of the entire polymer chain leads to strong adsorption, while some parts of the chain remain unattached, providing binding domains for protein molecules. Three-dimensional redox polyelectrolyte networks that electrically connect enzyme redox centers to electrodes have been formed in several systems [100–102], of which enzyme “wired” hydrophilic epoxy cements are an excellent example [101, 102]. In this case, the polymeric chain consists of a poly(vinylpyridine) backbone of which approximately one-sixth of the pyridine units are complexed to $[\text{Os}(\text{bpy})_2\text{Cl}]^{2+}$ and about one-fifth of the pyridines have been reacted with 2-bromoethylamine to form

pyridinium-*N*-ethylamine polycationic domains (16). This redox polyelectrolyte interacts with enzymes easily and “wires” their redox centers by penetrating into the protein shell (e.g. of lactate oxidase, glycerol-3-phosphate oxidase, or cellobiose oxidase) [98, 103]. Although negatively charged enzymes can strongly interact with this polycationic polymer even without cross-linking, cross-linking with the water-soluble diepoxide poly(ethylene glycol) diglycidyl ether (17) can further stabilize the system. For example, GOx was incorporated into a cross-linked polymeric matrix containing $\text{Os}(\text{bpy})_2$ units coordinated with the pyridine groups in the protein backbone. This enzyme-modified electrode shows an electrocatalytic anodic current in the presence of glucose (Fig. 13a), leading to the calibration curve given in Fig. 18(a, inset). A similar positively charged copolymer of allylamine and ferrocene-functionalized acrylic acid can interact with negatively charged proteins and be cross-linked with glutaric dialdehyde in the presence of GOx to

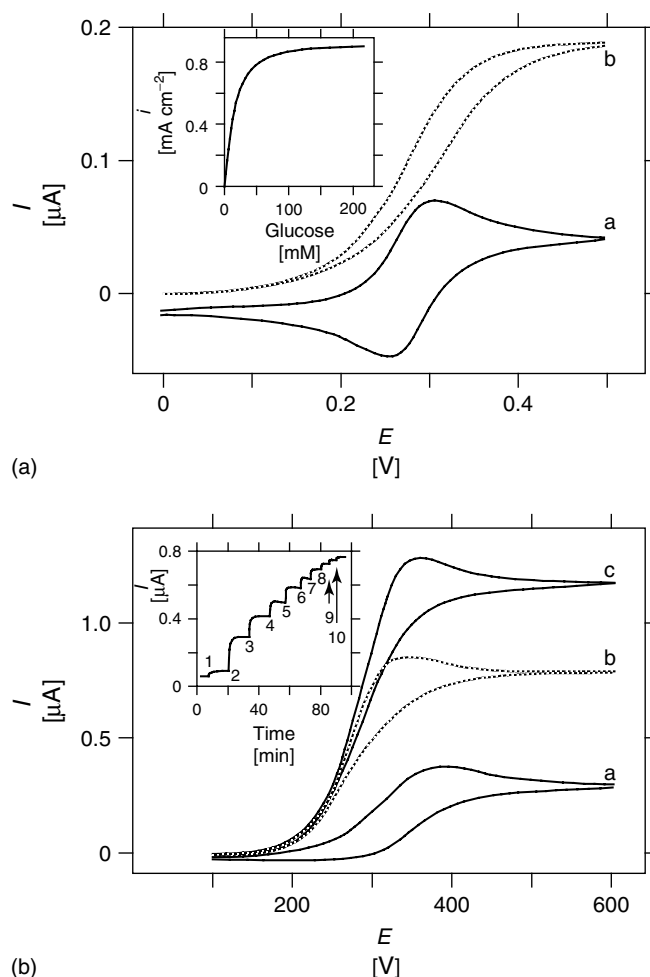


Fig. 13 (a) Cyclic voltammograms of a graphite micro-electrode (7 μm diameter) modified with the Os complex-containing polymer **16**, crosslinked with the bi-epoxy reagent **17** with embedded GOx: (a) in the absence of glucose and (b) with glucose, 5 mM. Potential scan rate 5 mV s^{-1} . Inset: calibration curve for the amperometric determination of glucose at 0.4 V; (b) cyclic voltammograms of the electrode modified with ferrocene-functionalized crosslinked polyallylamine containing GOx in the polymer matrix: (a) in the absence of glucose, (b) with glucose, 1 mM, and (c) with glucose, 3 mM. Potential scan rate 5 mV s^{-1} . Inset: amperometric responses of the enzyme electrode (at 0.6 V) upon successive additions of glucose. Numbers show glucose concentration in mM. [Adapted from A. Heller, *J. Phys. Chem.* **1992**, 96, 3579–3587, S. Koide, K. Yokoyama, *J. Electroanal. Chem.* **1999**, 468, 193–201.]

yield stable electrically “wired” biocatalytic matrices [104, 105]. These enzyme electrodes also demonstrate an electrocatalytic current for glucose oxidation (Fig. 13b). Successive additions of glucose at a fixed oxidative potential result in increases in the current (Fig. 13b, inset). A neutral polyacrylamide chain carrying ferrocene units has been used for the entrapment of GOx molecules without the assistance of electrostatic interactions [99]. Many other polymers functionalized with different redox groups (e.g. quinones [106]) have also been employed for the electrical “wiring” of entrapped redox enzymes. The

free-radical polymerization of redox hydrogels (as an alternative to the electropolymerization process) has also permitted the efficient entrapment of enzymes [107].

17.6.2

The Electrical Contacting of Enzymes in Mediator-functionalized Sol–gel Matrices

Sol–gel matrices are ideal candidates for the construction of enzyme-containing matrices. They are chemically inert, resist swelling, are processed at low temperatures, and have tunable porosity [77]. To date, silicon alkoxide

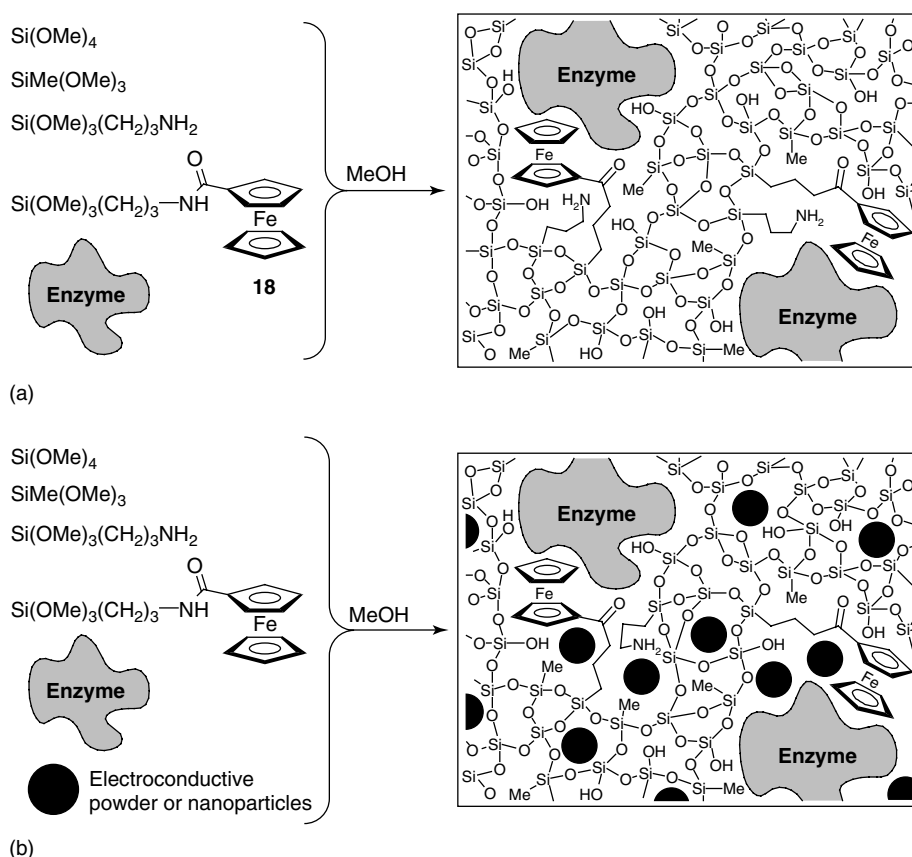


Fig. 14 Encapsulation of enzyme molecules into a sol–gel matrix containing redox-mediator groups (a) and with the addition of conductive graphite (or metal) particles (b).

precursors have been most extensively studied as they are inexpensive and exhibit slow reaction kinetics. With these starting materials, one can readily prepare silica sol–gels that are doped with a wide variety of reagents (e.g. enzymes, electron-transfer mediators, cofactors, promoters, etc.), and the characteristics of the final matrix can be “tuned” by adjusting the processing conditions (pH, precursor ratios, etc.). GOx has been electrically contacted in a sol–gel matrix along with a ferrocene mediator (Fig. 14a) [108]. Over 80% of the GOx remained active in the sol–gel and the amperometric response agreed well with theoretical predictions. The construction of sol–gel/enzyme multilayer matrices has allowed the amperometric sensing of glucose [109] and L-lactate [110] with linear responses within large concentration ranges.

The electrical characteristics of these films can be improved by the incorporation of electroconductive materials such as carbon powder or metal particles into the mixture (Fig. 14b). The electrodes prepared with these additions benefit from the porosity and rigidity of the silica matrix and from the electrical conductivity of the additive [77].

Composite sol–gel electrodes containing GOx and coimmobilized redox mediators have been applied for the preparation of glucose biosensors [111–115]. In these procedures, the redox mediator is either added during the gellification process (resulting in its physical entrapment in the silicate structure) [112] or is chemically bound to the silicate network (e.g. *N*-(3-trimethoxysilylpropyl)ferrocenylacetamide (**18**) may be used as a functionalized comonomer) [114, 115]. The electron relay may also be tethered to the protein backbone prior to the synthesis of the matrix. Relay-functionalized GOx has been entrapped in composite graphite/sol–gel matrices [113, 116]. The presence of the relay facilitates electron hopping between the enzyme-active site and the nearest graphite particle from where the graphite provides conductivity to the electrode. Ferrocene-mediated “wiring” of GOx resulted in an amperometric response of the electrode in the presence of glucose [78] (Fig. 15). Metallic components for the improvement of matrix conductivity are often composed of a graphite core covered with a metal (e.g. palladium or rhodium) shell [117, 118]. More recently,

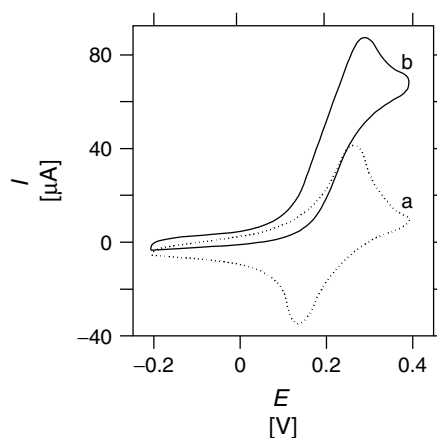


Fig. 15 The electrochemical response of a GOx-ferrocene-sol-gel modified electrode in the presence of glucose: cyclic voltammogram before (a) and after (b) the addition of 10 mM glucose solution; phosphate buffer, pH 5.6; potential scan rate, 10 mV s⁻¹. [Adapted from D. Avnir, S. Braun, O. Lev et al., *Chem. Mater.* **1994**, 6, 1605–1614.]

the carbon particles have been replaced by gold nanoparticles embedded together with the enzyme in the porous silicate matrix [119].

17.6.3

The Electrical Contacting of Enzymes in Mediator-containing Graphite Paste Composites

Amperometric biosensors based on carbon paste electrodes have received a virtual explosion of reports in the last decade [79, 80]. In essence, this approach allows the simple mixing of an enzyme, an electron-relay, and a conductive powder to form a biosensing paste. The modification of an electrode with a thick carbon paste layer allows the regeneration of a deactivated surface by polishing or cutting to expose a new and fully bioactive surface. This feature is certainly attractive compared with thin film-modified electrodes, which have to be discarded or at least remodified after deactivation. The main challenge in the construction of carbon paste biosensors is the establishment of efficient electrical “wiring”. Electron-transfer mediators have been introduced into GOx/graphite pastes, either as conjugates with the particles or enzyme, or simply as free molecules. Examples of mediators include ferrocene derivatives [120–135] (monomeric or polymeric), benzoquinone and benzoquinone-functionalized polymers [136–143], viologen derivatives [144], tetrathiafulvalene (TTF) [145, 146], tetracyanoquinodimethane (TCNQ) [147–149], TTF–TCNQ conducting salts [150], cobalt phthalocyanine [151], Meldola blue [152], methylene green [153], cupric hexacyanoferrate [154], and others [79, 80]. Many other redox enzymes have been incorporated into graphite paste electrodes with appropriate electron-transfer mediators

and used as amperometric biosensors for their respective substrates [80]. It should be noted that low potential redox-relays (particularly viologens [144]) provide effective oxidation of the FADH₂ cofactor under potentials negative enough to prevent the nonspecific oxidation of interferants. Also, the application of NAD⁺-dependent enzymes (e.g. glucose dehydrogenase (GDH) [155], alcohol dehydrogenase (AldH) [156]) requires the incorporation of NAD⁺ cofactor and a redox catalyst for the oxidation of NADH.

Carbon paste electrodes have also been used as supports for multienzyme systems. For example, AChE and ChO have been coimmobilized in carbon pastes, either with monomeric TTF [157] or flexible ferrocene-containing polymers [158] as the electron mediator. The hydrolysis of acetylcholine is biocatalyzed by AChE, and then the choline produced is oxidized by the electrically contacted ChOx giving an analytical amperometric signal corresponding to the acetylcholine concentration.

It should be noted, however, that carbon pastes do not offer a general route to any desired assembly. Some enzymes, for example, fructose dehydrogenase [136, 159] and aldose dehydrogenase [160], have defied all efforts at incorporation into the matrix without loss of activity. It is possible to introduce these enzymes to the surface of preformed carbon paste electrodes while retaining their biocatalytic activity, but this procedure does not exploit the many advantages of the carbon paste technique [79, 80]. The construction and optimization of multicomponent matrices composed of graphite powder, organic oils, enzymes, redox mediators, cofactors, and other materials is still a subject of intensive study.

17.7

The Electrical Contacting of FAD-enzymes by Mediator-functionalized FAD

We have already noted that the random functionalization of the protein backbone with electron relay groups leads to a mixture of products, the average of which is detected electrochemically. In order to accomplish the best possible electron contacting, the mediator should be selectively placed in an optimum position between the redox-center and the enzyme periphery. In the case of surface-confined enzymes, the orientation of the enzyme-mediator assembly with respect to the electrode should also be optimized. These requirements have been addressed by the use of mediators that are covalently attached to the enzyme cofactor or to both the cofactor and to the electrode surface. This specific covalent attachment positions the mediator at exactly the point that is required, leading to much more homogeneous behavior of the many enzyme molecules in a sample.

17.7.1

Electrical Contacting of Enzymes by Reconstitution of Apo-flavoenzymes with Relay-FAD Cofactor Units

A novel means for the establishment of electrical contact between the redox-center of enzymes and their environment based on a reconstitution approach has recently been demonstrated [161, 162]. According to this method (Fig. 16a), the FAD-redox centers of GOx or D-amino acid oxidase (AOx) were removed to yield the respective apo-enzymes. The amino-functionalized semisynthetic *N*⁶-(2-aminoethyl)-FAD (**19**) was covalently linked to (6-ferrocenemethylamino) hexanoic acid, and the bifunctional

redox-active ferrocene-FAD cofactor produced (**20**) was reconstituted into apo-GOx or apo-AOx. The resulting semisynthetic enzymes revealed bioelectrocatalytic features for the oxidation of glucose or D-alanine, respectively. Figure 16(b) shows cyclic voltammograms recorded in a solution of ferrocene-FAD-reconstituted GOx at a cystamine-modified electrode in the presence of different concentrations of glucose. The calibration plot (Fig. 16b, inset) was derived from the respective cyclic voltammograms. The bioelectrocatalytic features of these “electroenzymes” originate from the single ferrocene electron-relay group that electrically contacts the FAD center with the electrode surface.

17.7.2

Electrical Contacting of Enzymes by Surface-reconstitution of Apo-flavoenzymes on Relay-FAD-functionalized Electrodes

The organization of a reconstituted enzyme aligned on a catalyst-FAD monolayer was recently realized by the reconstitution of an apo-enzyme on a surface functionalized with a relay-FAD monolayer (Fig. 17a) [162, 163]. PQQ, (**21**) was covalently linked to a base cystamine monolayer, and *N*⁶-(2-aminoethyl)-FAD (**19**) was then attached to the PQQ redox-relay units. Following the construction of this organized electrode-PQQ-FAD assembly, apo-GOx was reconstituted onto the semisynthetic FAD unit to yield an immobilized biocatalyst on the electrode with a surface coverage of 1.7×10^{-12} mole cm⁻². The resulting reconstituted enzyme reveals bioelectrocatalytic properties. Figure 17(b) shows cyclic voltammograms of the enzyme electrode in the absence and the presence of glucose. When the substrate is present, an electrocatalytic anodic current

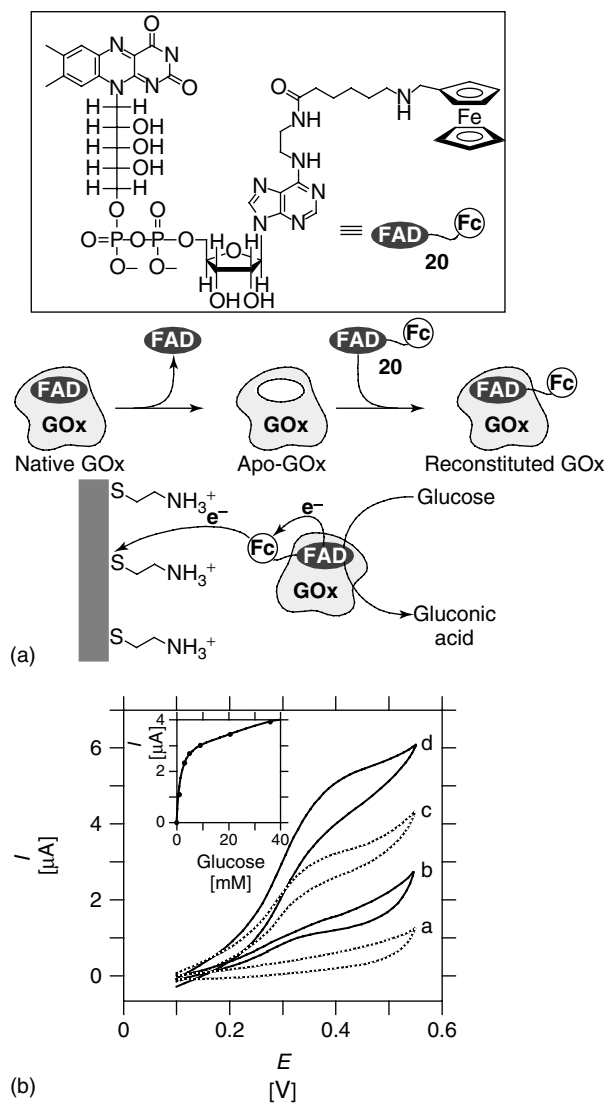


Fig. 16 (a) The preparation of an electrically “wired” enzyme by the reconstitution method, involving the removal of the native FAD cofactor from the enzyme (e.g. GOx) and the incorporation of the artificial FAD-ferrocene dyad into the apo-enzyme; (b) cyclic voltammograms of a system consisting of ferrocene-FAD-reconstituted GOx (1.75 mg mL⁻¹) at various concentrations of glucose: (a) 0, (b) 1, (c) 3, and (d) 20.5 mM. Experiments were performed in 0.1 M phosphate buffer, pH 7.3, at 35 °C, using a cystamine-modified Au-electrode, potential scan rate 2 mV s⁻¹, under argon. Inset: calibration curve of the biocatalytic current (0.5 V) at different glucose concentrations.

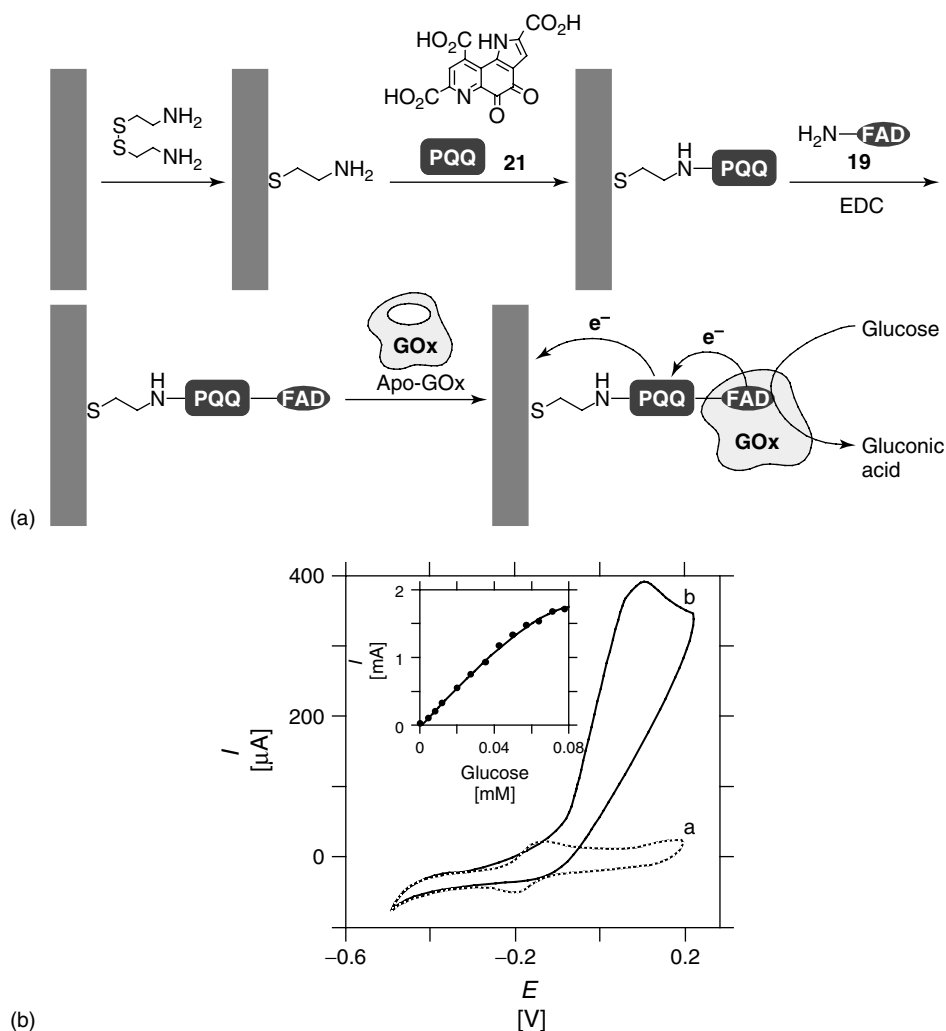


Fig. 17 (a) The surface-reconstitution of apo-GOx on a PQQ-FAD monolayer assembled on an Au-electrode; (b) Cyclic voltammograms of the PQQ-FAD-reconstituted GOx on an Au-electrode. (a) In the absence of glucose. (b) With glucose, 80 mM. Recorded in 0.1 M

phosphate buffer, pH 7.0, under Ar, at 35 °C, scan rate, 5 mV s⁻¹. Inset: Calibration curve corresponding to the amperometric responses (measured by chronoamperometry, $E = 0.2$ V) of the PQQ-FAD reconstituted GOx enzyme-electrode at different concentrations of glucose.

is observed, implying electrical contact between the reconstituted enzyme and the electrode surface. The PQQ site located at the protein periphery is constantly oxidized by the electrode, and the PQQ-mediated oxidation of the FAD center

activates the bioelectrocatalytic oxidation of glucose. The resulting electrical current is controlled by the recycling-rate of the reduced FAD by the substrate. Figure 17(b, inset) shows the derived calibration curve for the amperometric

responses of the reconstituted enzyme electrode at different concentrations of glucose. The resulting current densities are unprecedentedly high ($300 \mu\text{A cm}^{-2}$ at 80 mM of glucose). Control experiments revealed that reconstituted GOx on an electrode-FAD assembly (lacking the PQQ component) does not exhibit direct electron-transfer communication with the electrode surface, demonstrating that the PQQ relay unit is indeed a key component in the process [162, 163].

The electron-transfer turnover rate of GOx with molecular oxygen as the electron acceptor corresponds to ca. 600 s^{-1} at 25°C . Using an activation energy of $7.2 \text{ kcal mole}^{-1}$, the electron-transfer turnover rate of GOx at 35°C is estimated to be ca. 900 s^{-1} [162, 163]. A densely packed monolayer of GOx (ca. $1.7 \times 10^{-12} \text{ mole cm}^{-2}$) that exhibits the theoretical electron-transfer turnover rate is expected to yield an amperometric response of ca. $300 \mu\text{A cm}^{-2}$. This indicates that reconstituted GOx on the PQQ-FAD monolayer exhibits an electron-transfer turnover with the electrode of similar effectiveness to that observed for the enzyme with oxygen as a natural electron acceptor. Besides the high sensitivity of the resulting enzyme-electrode, the impressive efficiency of electrical contact has important consequences in the design of future enzyme-electrodes. Amperometric glucose-sensing electrodes generally suffer from the nonspecific oxidation of various interferants such as ascorbic acid or uric acid. Also, oxygen interferes with current transduction as a result of nonelectrochemical oxidation of the enzyme redox-site. The efficient electrical contact of the biocatalyst suggests that the nonspecific oxidation of the interfering substrates and the reaction of the biocatalyst with oxygen should

have little effect on the resulting current. Indeed, it was found that the transduced amperometric response at a glucose concentration of 5 mM was almost unaffected in the presence of oxygen or other interferants [162, 163]. The resulting selectivity of the reconstituted enzyme electrode and the high current densities achieved have further importance in the application of these electrodes as invasive glucose sensors. These assemblies are sensitive enough to function on microelectrodes at the end of needles thin enough to be of versatile medical use.

The intermediate location of a redox-relay between the electrode surface and the cofactor unit embedded in the enzyme is of key importance for the establishment of electrical contact between the enzyme and the electrode. For example, a PQQ monolayer assembled onto an Au-electrode was employed to reconstitute the PQQ-dependent apo-GDH [164, 165]. In this case, the PQQ plays the role of the embedded cofactor, and since no additional electron-relay was immobilized between PQQ-cofactor and the electrode, the reconstituted enzyme lacks the electrical contact with the electrode. The electrochemical oxidation of glucose by the reconstituted biocatalyst was only stimulated in the presence of a diffusional electron-transfer mediator. In other cases, however, the orientation of the protein with respect to the electrode is sufficient to promote electron-transfer without the need for a mediator. An Fe(III)-protoporphyrin IX complex was assembled as a monolayer on an Au-electrode and apo-Mb was reconstituted with the heme-cofactor monolayer [166]. Although native Mb usually lacks direct electrical communication with electrode supports as a result of insulation of the heme center,

the surface reconstituted Mb revealed electrical contact with the electrode. This property was attributed to the alignment of the heme center on the electrode surface in a structural orientation that facilitates electron-transfer with the electrode.

electrochemical regeneration of its oxidized or reduced form (NAD(P)^+ or NAD(P)H) is vitally important for the electrical contacting of these enzymes. In view of this great importance, electrocatalysts for the oxidation and reduction of $\text{NAD(P)}^+/\text{NAD(P)H}$ have been developed.

17.8

The Electrical Contacting of NAD(P)^+ -dependent Enzymes

The nicotinamide redox cofactors (NAD(P)^+) play important roles in biological electron transport, acting as carriers of two electrons and one proton. It is of prime importance for the functioning of the living systems that these redox cofactors recognize and undergo rapid reaction with their desired redox partners (NAD(P)^+ -dependent enzymes), and at the same time resist thermodynamically favorable side reactions. The two nicotinamide cofactors, nicotinamide adenine dinucleotide (NAD^+) and nicotinamide adenine dinucleotide phosphate (NADP^+), have closely related structures and electrochemical properties. Their oxidation and reduction involves two electrons and a proton, and can formally be considered to be a hydride transfer. In aqueous solution at pH 7.0, the thermodynamic redox potentials (E°) for NAD^+/NADH and $\text{NADP}^+/\text{NADPH}$ redox pairs are -0.561 V and -0.565 V, respectively [167]. Electrochemistry of $\text{NAD(P)}^+/\text{NAD(P)H}$ has been extensively studied at different electrodes (e.g. gold, platinum, and glassy carbon), and it has been demonstrated that the electrochemical oxidation/reduction process is highly irreversible and proceeds with large overpotentials [168, 169]. Dehydrogenases, the vast majority of redox enzymes, require $\text{NAD(P)}^+/\text{NAD(P)H}$ -coenzyme for their operation; thus, the

17.8.1

The Electrochemical Regeneration of NAD(P)^+ -cofactors

The oxidation of NAD(P)H appears to occur as a single-step two-electron process at high overpotentials at bare electrodes [22, 170, 171] (ca. 0.4 V, 0.7 V and 1 V at carbon, Pt, and Au electrodes, respectively [172, 173]), and the electrolysis of NAD(P)H under appropriate conditions can regenerate NAD(P)^+ with almost 100% efficiency [174, 175]. However, strong adsorption of NAD(P)H and NAD(P)^+ (e.g. on platinum, gold, glassy carbon, and pyrolytic graphite) generally poisons the electrode surface and inhibits the oxidation process [172, 173, 176–179]. Furthermore, NAD(P)^+ is an inhibitor of the direct oxidation of NAD(P)H [180], and adsorbed NAD(P)H can be oxidized to unwanted products (probably dimers [170] and/or stable adducts with the electrode surface [181]). The differences in activity of electrode materials and the effects of electrode pretreatment on NAD(P)H oxidation originate from adsorption phenomena. An appropriate choice of electrode material can significantly decrease the overpotential and enhance the process [182] (e.g. the NAD(P)H oxidation proceeds at an Ag electrode at 0.23 V [183]). Special electrode pretreatment (e.g. electrochemical surface oxidation) can decrease the NAD(P)H adsorption and enhance the NAD(P)^+ yield [184–186]. Moreover, oxidative pretreatment of glassy carbon electrodes can

produce quinonoid groups on their surfaces, which act as catalytic sites for NAD(P)H oxidation [186, 187].

For the efficient electrooxidation of NAD(P)H, mediated electrocatalysis is necessary [22, 170, 171], and a wide range of diffusional mediators has been studied [188–193]. Organic compounds that undergo two-electron reduction-oxidation processes and also function as proton acceptors-donors upon their redox transformations (such as *ortho*- and *para*-derivatives of quinones, phenylenediamines and aminophenols) have been found to be ideal for the mediation of NAD(P)H oxidation, although single-electron-transfer mediators (e.g. ferrocene derivatives) are also capable of oxidizing NAD(P)H [190, 191]. Some compounds demonstrate very high rates for the mediated oxidation of NAD(P)H in aqueous solutions [188, 189, 194, 195].

The use of electrode-immobilized mediators [22, 170, 171] (such as *o*-quinones [181, 193, 195–199], *p*-quinones [200, 201], phenazine, phenoxazine and phenothiazine derivatives [202–210], Os-complexes [211], metallophthalocyanines [212], and organic conductive salts [213, 214]) has also been applied for the regeneration of NAD(P)⁺. A great variety of immobilization techniques has been applied for the preparation of these modified electrodes – the mediator molecules have been directly adsorbed onto electrode surfaces [181, 196, 199, 202–205], incorporated into polymer layers [197, 198] or covalently linked to functional groups on electrode surfaces [193, 195, 206, 207]. The covalent coupling of redox mediators to self-assembled monolayers on Au-electrode surfaces has an important advantage for the preparation of multi-component organized systems. For example, PQQ (21) has

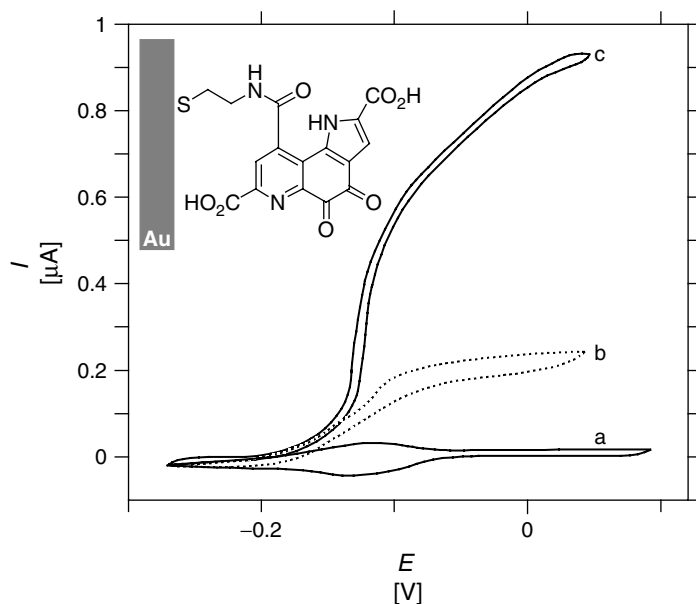


Fig. 18 Cyclic voltammograms of an Au-PQQ electrode with (a) 0.1 M Tris-buffer, pH 7.0, (b) 10 mM NADH and (c) 10 mM NADH and 20 mM Ca²⁺. Recorded at a scan rate of 1 mV s⁻¹.

been covalently attached to amino groups of a cystamine monolayer assembled onto an Au surface, and the structure obtained demonstrated good electrocatalytic activity

for NAD(P)H oxidation, particularly in the presence of Ca^{2+} -cations as promoters (Fig. 18) [215]. The NADP^+ -dependent malic enzyme was covalently linked to

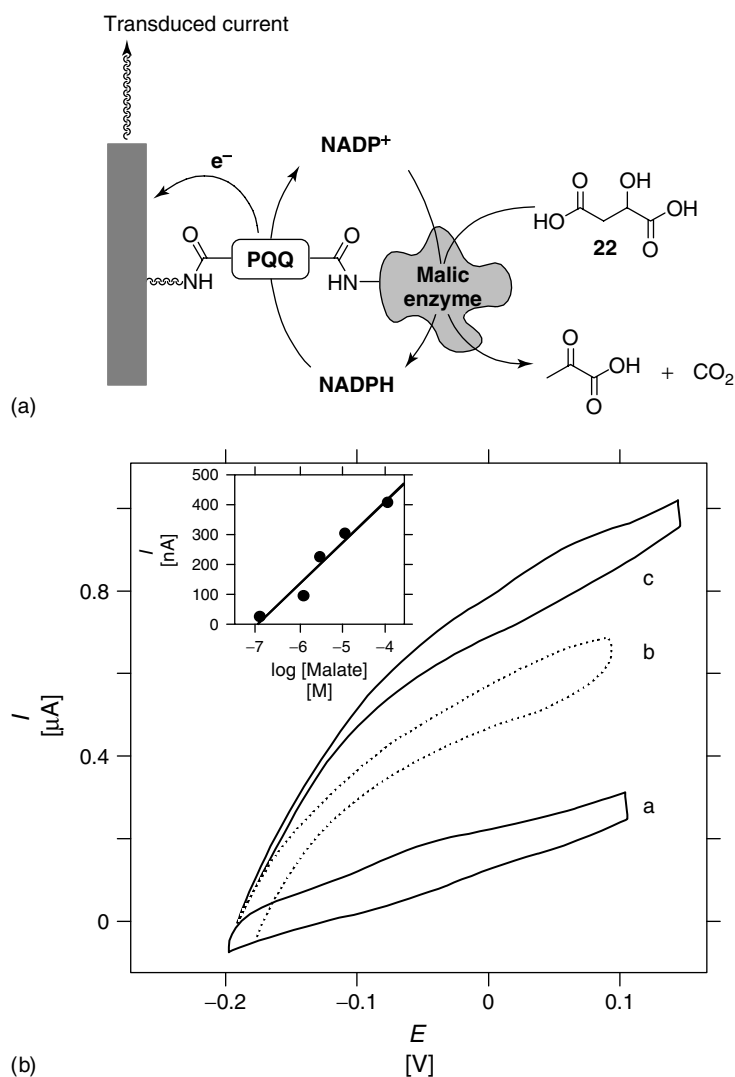


Fig. 19 (a) Amperometric detection of malate by PQQ-malic enzyme monolayer electrode using diffusional NADP^+ electrochemically regenerated by the PQQ catalyst; (b) cyclic voltammograms of the PQQ-malic enzyme electrode in the presence of malic acid at (a) 0, (b) 0.125, (c) 125 and (d) 1250 μM . Inset: calibration curve corresponding to the concentration dependence of the biosensor. Recorded in 0.1 M phosphate buffer, pH 7.2, with 2 mM NADP^+ and a scan rate of 2 mV s^{-1} .

the PQQ monolayer assembled on the Au-electrode [216] (Fig. 19a). In the presence of NADP^+ as diffusional cofactor and malic acid (**22**) as substrate, biocatalyzed oxidation of **22** yields the reduced cofactor, which is electrocatalytically reoxidized by PQQ. The resulting current is controlled by the concentration of NADPH, while the concentration of the reduced cofactor is determined by the analyte malic acid (Fig. 19b). This system is still not fully integrated, however, as the cofactor is in a diffusional configuration.

NAD(P)^+ -dependent enzymes, electrically contacted with electrode surfaces, can provide efficient bioelectrocatalysis for the NAD(P)H oxidation. For example, diaphorase (DI) was applied to oxidize NADH, using a variety of quinone compounds, several kinds of flavins, or viologens as mediators between the enzyme and electrode [217, 218]. The bimolecular reaction rate constants between the enzyme and mediators whose redox potentials are more positive than -0.28 V at pH 8.5 can be as high as $10^8\text{ M}^{-1}\text{ s}^{-1}$, suggesting that the reactions are diffusionally controlled. The high stability of the enzyme GDH has even allowed the bioelectrocatalytic regeneration of NAD(P)^+ on a preparative scale [219].

Electrocatalytically regenerated NAD(P)^+ has been coupled to secondary NAD(P)^+ -dependent enzymes, thus providing recycling of the cofactor for the biocatalytic transformations [220, 221]. For example, L-lactate was converted into D-lactate, with a yield better than 97% using L-lactate dehydrogenase lactic dehydrogenase (LDH), relying on NAD^+ regenerated by an electrocatalytic reaction [222]. The system involves stereospecific catalysis of L-lactate oxidation by the enzyme, with the electrochemical regeneration of NAD^+ at the

anode and electrochemical reduction of pyruvate at the cathode.

Electrocatalytic recycling of NAD(P)^+ has allowed the development of numerous amperometric biosensors based on NAD(P)^+ -dependent hydrogenases [221]. Bioelectrocatalytic regeneration of NAD(P)^+ using electrically contacted DI has been used to drive the biocatalyzed oxidation of methanol to CO_2 , using NAD^+ -dependent dehydrogenases [218], and a methanol/dioxygen biofuel cell has been assembled using these bioreactions in the anode compartment.

17.8.2

The Electrochemical Regeneration of NAD(P)H -cofactors

The electrochemical reduction of NAD(P)^+ has been studied in aqueous [223–225] and nonaqueous solutions [226]. It usually proceeds stepwise at very negative potentials (e.g. in aqueous solution at pH 7.0 and at a mercury electrode, two separated waves [224] are observed at -1.0 V and -1.6 V); thus, the process requires a large overpotential. The first step is a one-electron reduction of NAD(P)^+ , resulting in the neutral radical species NAD(P)^\bullet , which goes on to produce a nonenzymatically active dimer [227]. The second step results in the formation of the enzymatically inactive 1,6-reduction product. Only a small amount of the enzymatically active 1,4-reduction product NAD(P)H can be found in the product mixture, with a yield dependent on the electrolysis conditions. The initial state of the electrode surface and the background electrolyte, as well as the applied potential, strongly affect the mechanism of the NAD(P)^+ reduction and the composition of the product mixture. The electrode material has a dramatic effect on the kinetics of the process and

an appropriate selection of electrode can greatly improve the process efficiency. For example, a bare silver electrode provides a quasi-reversible reduction-oxidation of $\text{NAD(P)}^+/\text{NAD(P)H}$ (i.e. cathodic and anodic peak are observed at potentials 0.12 V and 0.23 V, respectively [183]), although NAD(P)H is usually a minor product of noncatalytic electrochemical processes at bare electrodes [22].

Direct, nonmediated electrochemical reduction of NAD(P)^+ at modified electrode surfaces has been used to produce the enzymatically active NAD(P)H and even to couple the NAD(P)H regeneration process with some biocatalytic reactions [228]. The modifier molecules used for these purposes are not redox active and they do not mediate the electron-transfer process between an electrode and NAD(P)^+ ; however, they can effectively decrease the required overpotential and prevent formation of the nonenzymatically active dimer product [228]. For example, the efficiency of the direct electrochemical regeneration of NADH from NAD^+ was enhanced by the use of a cholesterol-modified gold amalgam electrode that hinders the dimerization of the NAD^+ radicals on its modified-surface [228]. This direct electrochemical NAD^+ reduction process was used favorably to drive an enzymatic reduction of pyruvate to D-lactate in the presence of lactate dehydrogenase. The turnover number for NAD^+ was estimated as 1400 s^{-1} . Other modifiers that enhance formation of the enzymatically active NAD(P)H include L-histidine [229] and benzimidazole [230], immobilized as monolayers on silver electrodes. Cyclic voltammetric experiments demonstrated that these modified electrodes can catalyze the reduction of NAD^+ to enzymatically active NADH at particularly low overpotentials.

The electrocatalysis of NAD(P)H regeneration by the application of either non-biological redox materials or NAD(P)^+ -dependent enzymes can greatly improve the process efficiency and avoid the formation of enzymatically inactive byproducts. Complexes of Rh have been reported to be active for the electrocatalytic reduction of NAD(P)^+ to NAD(P)H [231, 232]. Similar Rh complexes have been utilized in homogeneous catalysis with chemical [233] and photochemical [234–236] activation. The electrocatalytic process includes the regioselective transfer of two electrons and a proton to NAD(P)^+ . In these systems, hydrido-rhodium species are assumed to be the active catalytic moiety. $\text{Tris(bipyridine)rhodium(III)}$ [232, 234], $\text{tris(5-sulfo-2,2'-bipyridine)rhodium(III)}$ [236], $\text{(pentamethylcyclopentadienyl-2,2'-bipyridine-chloro)rhodium(III)}$ [231, 237], and $\text{chlorotris[diphenyl(m-sulfonatophenyl)phosphine]rhodium(I)}$ [235] have been used as homogeneous mediation of electrons to NAD(P)^+ . The catalytic efficiency of a series of Rh-complexes has been studied [238] and it was shown that the catalyst activity decreases in the presence of electron-withdrawing substituents in the 2,2'-bipyridine ligand and increases with electron-donating substituents. Substituents in the 6-position of the ligand slow the catalytic reaction because of steric effects. Structure-activity relationships were found in the mechanism of the regioselective reduction of NAD^+ by Rh-complexes [239]. These examples demonstrate the ability of diffusionally free, catalytically active mediators to transport hydride equivalents to the soluble NAD(P)^+ cofactor. The NADH cofactor, electrochemically regenerated using Rh-complexes, has been used to mediate biocatalytic reactions [231].

Electrode modification with the Rh-complexes catalytically active in hydride transfer (thus for the catalysis of NAD(P)^+ reduction) has brought important improvements in the electrocatalytic regeneration of NAD(P)H [240–243]. Rhodium complexes have been immobilized at electrode surfaces by their incorporation into polymeric films organized on electrode surfaces. Films of substituted PPys were prepared by the oxidative polymerization of the corresponding pyrrole-ligand derivative. Immobilization of Rh-complexes into the polymeric films was achieved by a ligand-exchange reaction of the complex with this ligand-containing polymer-film [243]. Another method includes the immobilization of copolymers of hydrophilic *N*-vinyl-pyrrolidone and polymerizable derivatives of the Rh-complex (pentamethylcyclopentadienyl-2,2'-bipyridine-chloro)rhodium(III). Gamma-irradiation of these mixtures on an electrode surface gives highly permeable redox active polymer films [240]. These films swell easily in water and thus provide a three-dimensional reaction layer, which is advantageous for electrocatalytic processes mediated by the surface-confined rhodium complex. A quinone-modified electrode surface has also been reported to be electrocatalytically active for NAD^+ reduction [244].

The regeneration of NAD(P)H with the participation of mediator-contacted enzymes ensures that NAD(P)^+ reduction proceeds selectively and that only enzymatically active NAD(P)H is produced. Many enzymes have been used in this context to provide the bioelectrocatalytic reduction of NAD(P)^+ , for example, ferredoxin- NADP^+ reductase (FNR) [245–249], lipoamide dehydrogenase [250–254], formate dehydrogenase

(FDH) [252, 255, 256], 2-oxocarboxylate reductase [257], enoate reductase [257, 258], DI [247, 259–262], ALDH [263], and hydrogenase [264, 265]. A variety of low potential electron-transfer mediators have been used to activate the reductive enzymes, for instance, viologen derivatives [246, 248–250, 253, 254, 261, 262], flavins [255, 256, 259, 264], quinones [247], and the redox protein ferredoxin [266]. Some redox enzymes can directly communicate with electrode supports, and thus stimulate the regeneration of the NAD(P)H cofactor. For example, hydrogenases (from *Rhodococcus opacus* and *Atcaligenes eutrophus* H16) have been successfully applied for the bioelectrocatalytic regeneration of NAD^+ , without the application of a redox-mediator [267, 268]. However, the electrocatalytic rates of these systems are generally too slow to produce observable catalytic current on the cyclic voltammetric time scale (notable exceptions include dimethyl viologen (MV^{2+})/DI [253, 254, 261, 262], MV^{2+} /FNR [249], and ferredoxin/FNR [266]). Application of a low potential quinone adriamycin as an electron-transfer mediator to DI or FNR allows highly effective bioelectrocatalytic reduction of NADP^+ , with an electrocatalytic current appearing at potentials more negative than -0.7 V. A high current yield (ca. 97%) was also achieved with soluble ALDH and diffusional acetophenone as an electron mediator [263].

Immobilized low potential electron-transfer mediators (e.g. viologens) are more promising than diffusional mediators for the practical regeneration of NAD(P)H coupled with further biocatalytic reactions. The immobilization of viologens usually results in significant positive potential shift of their redox potential [269–272], which however, badly affects their efficiency. The potential shift

of the immobilized viologen mediator results from dimer formation and interactions with the supporting organic matrices. A special immobilization technique, which includes the cross-linking of long-chain amino-viologen derivatives, FNR, and bovine serum albumin (BSA) with glutaric dialdehyde on an electrode surface, has been developed to prevent such potential shifts, retaining the high reductive capabilities of the viologen mediator [248]. A cyclic voltammogram observed at this viologen/FNR/BSA-modified electrode in the presence of NADP^+ shows high cathodic bioelectrocatalytic current at potentials more negative than -0.45 V. The bioelectrocatalytic regeneration of NAD(P)H with the use of the coimmobilized viologen mediator and DI can proceed with a very high current yield (97.8%) upon the application of a potential of -0.8 V [262]. Therefore, this process was applied for amperometric biosensing of NAD(P)^+ [273]. Sensitivities of 1.4 and $3.5 \text{ mA M}^{-1} \text{ cm}^{-2}$

were recorded for NAD^+ and NADP^+ , respectively.

Bioelectrocatalytically regenerated NAD(P)H has been coupled with further biocatalytic reactions, where the NAD(P)^+ -dependent enzymes utilize the regenerated NAD(P)H and perform the reduction of their respective substrates. For example, the reduction of acetone to 2-propanol has been achieved in the presence of AlcDH upon the biocatalytic regeneration of NADPH in the presence of MV^{2+} and FNR [263] (Fig. 20a). NADH regenerated by directly contacted hydrogenase (from *Alcaligenes eutrophus* H16) has been utilized to drive the transformation of α -ketoglutarate into L-glutamate, catalyzed by an L-glutamate dehydrogenase [274]. Turnover numbers of 450 h^{-1} and 207 h^{-1} were obtained in an electrochemical thin-layer cell and in a preparative scale-batch reactor, respectively. Coimmobilization of two enzymes, one of them catalyzing the regeneration of NAD(P)H and the second

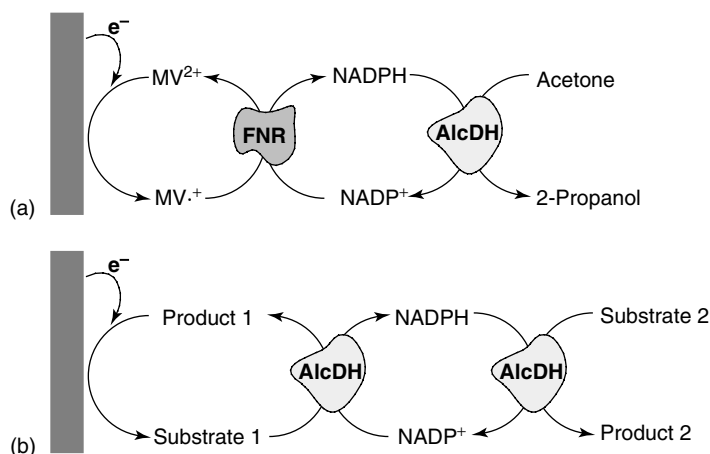


Fig. 20 Bioelectrocatalytic reduction systems using: (a) AlcDH and FNR for the biocatalyzed transformation and the regeneration of NADPH , respectively, and; (b) using AlcDH for both processes, where the biocatalytic cycle Substrate 1/Product 1 performs the mediating function for the NADPH regeneration and the second biocatalytic cycle results in the formation of the aim product 2.

utilizing the NAD(P)H, allows NAD(P)H-driven biocatalytic transformations to be performed in a single biocatalytic matrix in the presence of NAD^+ and a mediator. Glutamate dehydrogenase (GluDH) and FNR coimmobilized on a glassy carbon electrode surface have been shown to stimulate the biocatalytic reduction of α -ketoglutarate in the presence of diffusional NADP^+ and adriamycin [247]. In some cases, single enzymes (e.g. ALDH) can perform both functions: (1) regeneration of NAD(P)H in the presence of a mediator providing electron transport from the electrode and (2) biocatalytic reduction of a ketone to an alcohol [263] (Fig. 20b). Stereoselective biocatalytic reactions performed on a preparative scale with high current yield (ca. 98%) and utilizing bioelectrochemically regenerated NAD(P)H and secondary enzymatic processes have been also reported [275, 276].

17.8.3

The Association of NAD(P)^+ -dependent Enzymes with NAD(P)^+ Cofactors by Covalent and Entrapment Methods

In view of the high cost of NAD(P)^+ / NAD(P)H cofactors, practical applications require their immobilization together with the enzymes. The covalent coupling of natural NAD(P)^+ cofactors to an organic support results, however, in a substantial decrease of their efficiency. Mobility of the cofactor is vital for its efficient interaction with enzymes, so serious attention has been paid to the synthesis of artificial analogs of the NAD(P)^+ cofactors carrying functional groups separated from the bioactive site of the cofactor by spacers [277, 278]. The spacer is usually linked to *N*-6 position of the NAD(P)^+ molecule, and should provide some flexibility for the bioactive part

of the cofactors, allowing them to be associated with the enzyme molecules. Structure/activity relationships of the artificial functionalized NAD(P)^+ -derivatives have been studied with different enzymes, and the possibility to substitute the natural NAD(P)^+ cofactor with these artificial analogs has been demonstrated [277, 279]. The artificial NAD(P)^+ derivatives (e.g. *N*⁶-aminoethyl- NAD^+ , (23)) have been covalently linked to insoluble matrices (e.g. Sepharose [280–282]) or water-soluble polymers (e.g. dextran [283–286], polyethyleneimine [281, 282, 287], polylysine [281], polyethyleneglycol [288–291]). In another study, a NAD^+ derivative carrying a polymerizable acrylamide group was prepared and subjected to radical polymerization to produce NAD^+ -functionalized polymers [292].

All the polymeric NAD(P)^+ -derivatives have been checked for their cofactor activity and compatibility with enzymatic biocatalytic processes. The polymer-linked NAD(P)^+ -derivatives were associated with NAD(P)^+ -dependent enzymes such as ALDH [281, 282, 291, 292], lactate dehydrogenase [286, 292], malate dehydrogenase [288, 292] and aldehyde dehydrogenase [287]. It was found that different NAD(P)^+ -polymers are active as cofactors towards different enzymes. For example, polyethyleneimine and polylysine bound NAD^+ -derivative revealed 60% and 25% activity, respectively, as compared with the native NAD^+ in the presence of rabbit muscle lactate dehydrogenase, but only minute activity (ca. 2–7%) in the presence of alanine dehydrogenase from *Bacillus subtilis* [281]. A comparative study of the cofactor activity with different enzymes is a subject of great interest. Even though several studies [279] attempt to predict the structural/functional relationship for the polymer-bound NAD(P)^+ -derivatives,

most of the NAD(P)⁺-dependent enzymes still have unknown 3-D structures, and their compatibility with the polymeric cofactors can only be tested experimentally.

A polymer-bound NAD⁺-derivative (NAD⁺-alginic acid) was immobilized on an electrode surface. Despite the high molecular weight of the NAD⁺-alginic acid, all NAD⁺-units were reduced electrochemically in the presence of MV²⁺ and DI, providing NADH for coupling with reductive enzymatic reactions [293]. A reagentless ethanol biosensor was developed using a NAD⁺-dextran conjugate [284]. A mixture of ALDH, NADH-oxidase, and NAD⁺-dextran was incorporated into a poly(vinylalcohol) matrix onto an electrode surface. In the presence of ethanol, ALDH reduced the polymer-bound NAD⁺-units, producing NADH. The resulting NADH was then oxidized by the NADH-oxidase in the presence of oxygen, recycling the original NAD⁺ and producing H₂O₂ that was finally detected by the electrode. The system could be improved further if a redox-mediator provided electrical contacting of the NADH-oxidase instead of hydrogen peroxide generation. The biocatalytic systems based on the association between polymer-bound NAD(P)⁺-derivatives and the corresponding enzymes allow the performance of biocatalytic processes, including application in a model enzyme bioreactor [289]. Polyethyleneglycol-bound NAD⁺ has been successfully employed in the continuous production of L-amino acids from the corresponding α -keto acids by stereospecific reductive amination [291]. (S)-1-Phenyl-2-propanol was obtained by reduction of the corresponding ketone using ALDH (from *Rhodococcus erythropolis*) together with a polymer-bound NADH and a total turnover of 8×10^4 was achieved [294].

A different approach to the association of NAD(P)⁺ with enzymes involves the covalent coupling of the functionalized cofactor molecules to the enzyme backbone [295–299] (Cf. coupling of redox-mediators with the enzyme backbone, Chapter 5). For example, ALDH carboxyl groups (aspartic and glutamic residuals) were activated with a carbodiimide and *N*-hydroxysuccinimide and then the active ester groups were reacted with *N*⁶-[*N*-(6-aminohexyl)carbamoylemethyl]-NAD⁺ (24), resulting in an enzyme-cofactor complex [295] (Fig. 21a). This modification technique resulted in the spacially random attachment of NAD⁺-units, with an average loading about 0.3–1.6 NAD⁺ per enzyme. To provide specific attachment, a 44-cysteine residue was introduced on the surface of GDH using site-directed mutagenesis [300]. A synthetic analog of NAD⁺ was site-specifically covalently linked to the mutant by a disulfide bridge at the 44-cysteine residue (Fig. 21b). The enzyme-NAD⁺ complex demonstrated biocatalytic activity that could be explained either by enzyme activation with the NAD⁺ unit linked to the same enzyme (intra-complex activation), or by cross-reaction between the NAD⁺ units and enzymes from different complexes (inter-complex activation). The possibility of the cross-reaction allows the use of two different enzymes with NAD⁺-units linked only to one of them (Fig. 21c). A mixture of the NAD⁺-functionalized GDH with the native nonfunctionalized lactate dehydrogenase allowed the biocatalytic processes of both enzymes, producing L-lactate and gluconic acid from pyruvate and D-glucose [300]. A turnover of 45 cycles per minute for each NAD⁺ molecule and total turnover per cofactor of 1.35×10^5 for the first 2.5 days were found in this system when the reaction was performed in a hollow fiber

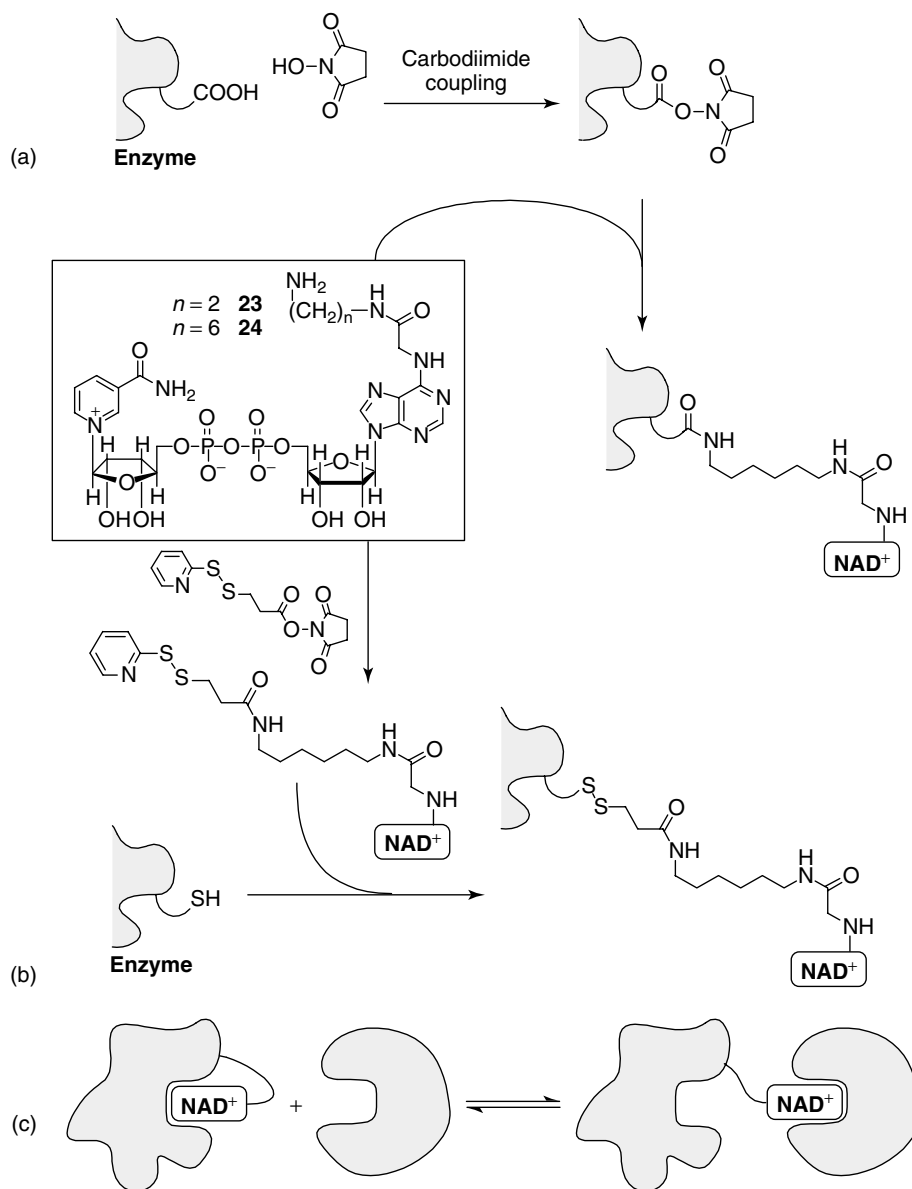


Fig. 21 (a) Preparation of a randomly linked enzyme-NAD⁺ complex by the use of a semisynthetic amino-NAD; (b) preparation of a specifically linked enzyme-NAD⁺ complex by the use of a genetically modified enzyme and

amino-NAD⁺; (c) the biocatalytic functions of two different enzymes activated by NAD⁺ covalently tethered to only one of them via inter- and intra-molecular complexation.

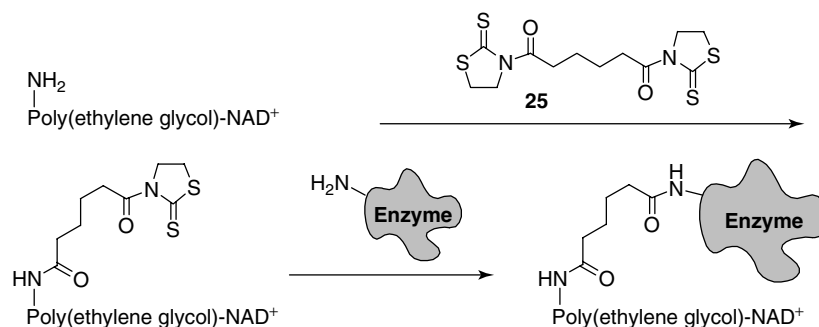


Fig. 22 Preparation of a malate dehydrogenase-polyethylene glycol-NAD complex.

reactor. The recycling of NAD^+ in these systems was achieved either by a diffusional redox-mediator [299], or by a second enzyme utilizing the reduced NADH for a secondary biocatalytic reaction [296] (Cf. Chapter 7.1).

Covalent coupling between synthetic NAD^+ -derivatives, water-soluble polymer matrices, and enzyme molecules has combined both techniques mentioned above. For example, polyethyleneglycol carrying covalently bound NAD^+ -units was activated with a bifunctional reagent (25) and covalently attached to malate [288] or glucose dehydrogenase [290] (Fig. 22).

17.8.4

The Integration of NAD(P)^+ -dependent Enzymes with Monolayer Arrays of NAD^+ -cofactor and Redox-catalysts

Electrodes functionalized with monolayers of enzyme cofactors (e.g. NAD^+ -monolayers) demonstrate the ability to form stable affinity complexes with their respective enzymes [301]. These interfacial complexes can be further cross-linked to produce integrated bioelectrocatalytic matrices consisting of the relay-units, the cofactor, and the enzyme molecules. Electrically contacted biocatalytic electrodes of NAD^+ -dependent enzymes have been

organized by the generation of affinity complexes between a catalyst/ NAD^+ monolayer and the respective enzymes [302]. A PQQ monolayer covalently linked to an amino-functionalized nicotinamide adenine dinucleotide, N^6 -(2-aminoethyl)- NAD^+ (23), was assembled onto an Au-electrode. The resulting monolayer-functionalized electrode binds NAD^+ -dependent enzymes, such as lactate dehydrogenase and ALDH, by affinity interactions between the cofactor and the biocatalyst (Fig. 23a). These enzyme electrodes electrocatalyze the oxidation of their respective substrates (in these cases lactic acid and ethanol). The enzyme electrode reveals only temporary stability and ca. 25% of the biocatalyst dissociates from the monolayer affinity-complex to the electrolyte solution within 30 min. Two-dimensional cross-linking of the enzyme layer associated with the PQQ/ NAD^+ -cofactor monolayer with glutaric dialdehyde generates a stable, integrated, electrically contacted, cofactor-enzyme electrode. The electrical response of a cross-linked layered PQQ/ NAD^+ -LDH electrode in the absence (curve a) and the presence (curve b) of lactate and a calibration curve for the amperometric responses of the integrated LDH layered electrode to lactate are given in Fig. 23(b). This system

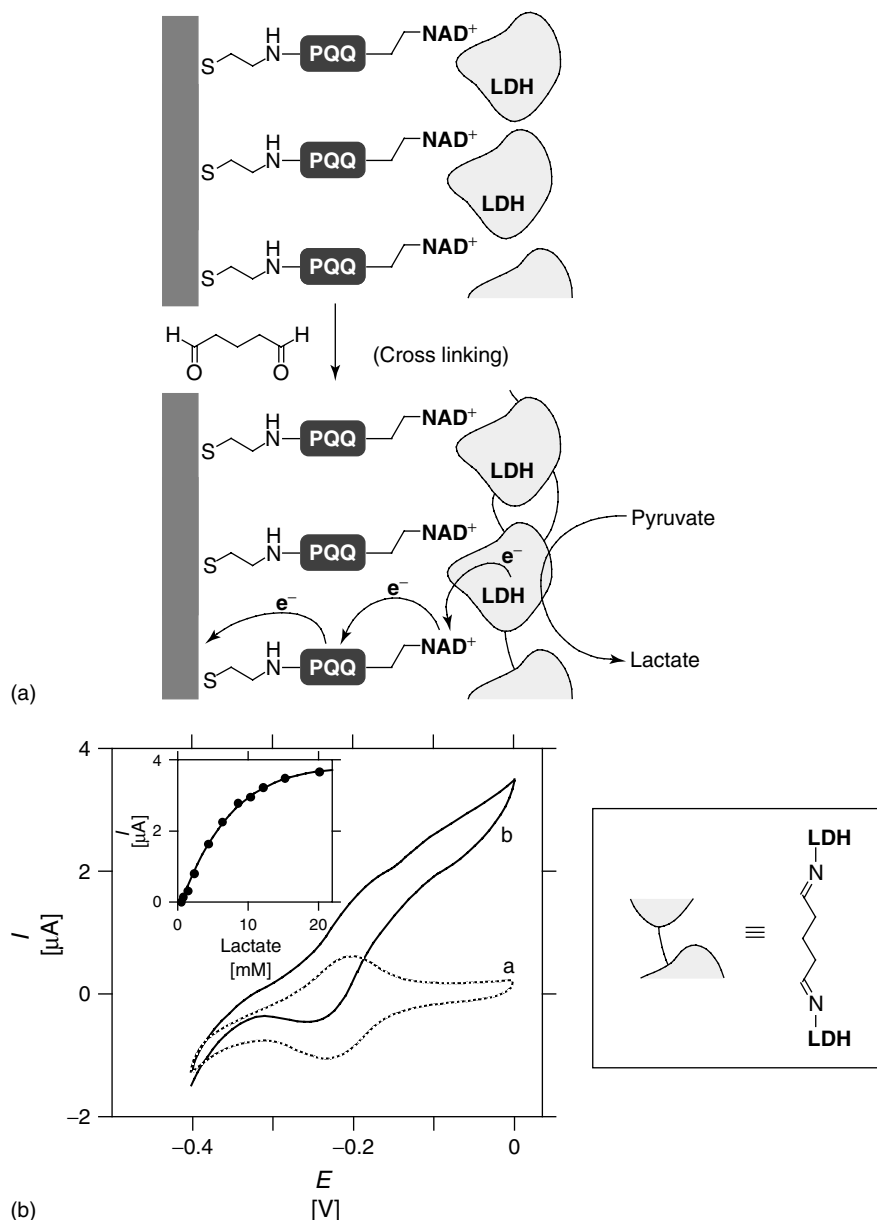


Fig. 23 (a) The assembly of an integrated lactate dehydrogenase monolayer-electrode by the cross-linking of an affinity complex formed between the enzyme and a PQQ-NAD⁺ monolayer-functionalized Au-electrode; (b) cyclic voltammograms of the integrated cross-linked PQQ-NAD⁺/LDH electrode (roughness factor ca. 15): (a) In the absence of lactate. (b) With lactate, 20 mM. Recorded in 0.1 M Tris-buffer, pH 8.0, in the presence of 10 mM CaCl₂, under Ar, scan rate, 2 mV s⁻¹. Inset: amperometric responses of the integrated electrode at different concentrations of lactate upon application of potential 0.1 V.

exemplifies a fully integrated rigid biocatalytic matrix composed of the enzyme, NAD^+ -cofactor, and catalyst. The complex between the NAD^+ -cofactor and LDH aligns the enzyme on the electrode support, thereby enabling the effective electrical communication between the enzyme and the electrode, while the PQQ-catalytic sites provide the electrochemical regeneration of NAD^+ .

17.9

Electrical Contacting by Interprotein Electron-transfer

The electron-transfer cascades utilized by nature (e.g. in the respiratory and photosynthetic schemes) tend to be very high yielding, suffering little loss through unwanted side- and back-reactions. The key to this efficiency lies in the insulating protein shell and the ability of the charge-carriers to form highly selective complexes. Small molecular electron mediators offer little selectivity in their electronic reactions as they can exchange electrons with any appropriate donor or acceptor that can approach them. Proteins, on the other hand, do not allow the close contact of their redox-active site with anything except certain substrates. This allows their use as electron mediators between specific species that form complexes with them, even in the presence of other redox-active molecules. Proteins have been used as electron mediators in artificial systems, ranging from simple diffusional systems to complex immobilized multiprotein assemblies.

17.9.1

Soluble Cytochromes as Electron-transfer Mediators

Cytochromes, particularly cytochrome c (Cyt c), are small heme-containing redox

proteins capable of mediating electron transfer between redox enzymes with great specificity [303]. The electron-transfer event between Cyt c and enzymes occurs specifically in interprotein complexes [304].

Reversible electrochemistry of Cyt c, which includes a partially exposed heme site, has been observed at Au-, Pt-, and Ag-electrodes modified with monolayers of various promoters [305–307]. Generally, these promoters are linked to the electrode by a thiol or disulfide group and include an organic functional unit that interacts with the Cyt c backbone. The promoter monolayer prohibits direct contact between the protein and the metal electrode surface, thus preventing irreversible unfolding of the protein. In addition, interactions between the promoter and the protein molecules can result in the specific alignment of the protein at the electrode surface, providing short electron-transfer distances. The most common promoter for the activation of the interfacial electrochemistry of Cyt c is *bis*(4-pyridyl)disulfide [308–312], but several other thiol and disulfide derivatized molecules are also effective [313]. Amino acid and oligopeptide monolayers have been used as promoters for enhancing the interfacial electrochemistry of Cyt c [314, 315], as well as other cytochromes [316]. Other promoters, such as imidazole [317], thiophene [318], and iodide [319] deposited onto Au or Ag-electrodes have also been used to facilitate Cyt c electrochemistry. Thus, electrochemically contacted at a promoter-modified electrode surface, soluble Cyt c can mediate specific electron transport events between Cyt c-recognizing enzymes and the electrode. Since the electrochemistry of Cyt c is reversible at the promoter-modified electrodes and Cyt c

is able to donate and accept electrons to/from enzymes, both directions (cathodic and anodic) of electron transport are possible.

Reductive biocatalytic transformations mediated by Cyt c have been exemplified in a variety of following systems. Cyt c electrochemically reduced at a promoter-modified electrode surface has mediated the electron-transfer to soluble laccase (from *Coriolus hirsutus*), which biocatalyzed the reduction of O_2 to water [320].

A similar O_2 biocatalytic reduction has been also demonstrated using a longer sequence of inter-protein electron-transfer steps [321] (Fig. 24a). Figure 24(b), curve a, shows a cyclic voltammogram typical for the reversible electrochemistry of Cyt c at an Au-electrode in the presence of a promoter [321]. The addition of cytochrome c_{551} (Cyt c_{551}) and cytochrome oxidase (COx), from *Pseudomonas aeruginosa* under aerobic conditions results in a significant increase in the cathodic current

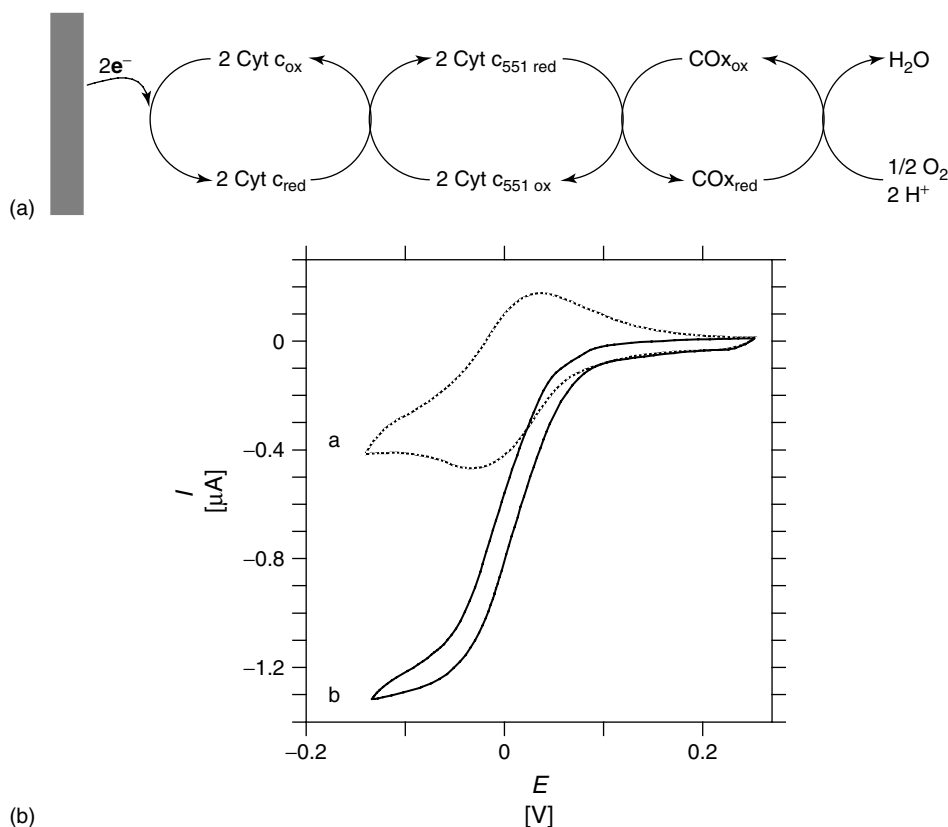


Fig. 24 (a) The bioelectrocatalyzed reduction of dioxygen by COx, mediated by Cyt c and Cyt c_{551} in a multistep electron-transfer process; (b) cyclic voltammograms of a promoter-modified Au electrode (a) in the presence of Cyt c (5.3 mg mL^{-1}), and (b) after the addition of

Cyt c_{551} (0.74 mg mL^{-1}) and COx (770 nM). Recorded in 0.02 M phosphate buffer, pH 7.0, scan rate 1 mV s^{-1} , in the presence of O_2 . [Adapted from D. A. Powis, G. D. Wattus, *FEBS Lett.* **1981**, 126, 282–284.]

(curve b), originating from inter-protein electron-transfer, resulting in the electrocatalytic reduction of O_2 . It should be noted that the addition of either Cyt c_{551} or COx to the Cyt c alone does not yield the electrocatalytic process, nor does the system generate an electrocatalytic current in the absence of O_2 . Thus, considering the sequence of electron transport in natural respiratory chains, one can conclude that this artificial process proceeds in the following steps: (1) the interfacial electrochemical reduction of Cyt c at the electrode, (2) the homogeneous inter-protein electron-transfer from reduced Cyt c to Cyt c_{551} , (3) the electron-transfer from reduced Cyt c_{551} to COx, and finally (4) electron-transfer from COx to O_2 (Fig. 24a). This system illustrates that even under homogeneous conditions directed MET can be achieved by the exploitation of specific electron-transfer events. Application of nitrite reductase, instead of COx, results in a similar system, ultimately reducing NO_2^- to NO [322].

Oxidative biocatalytic processes mediated by Cyt c have been exemplified in several systems. The electrochemical oxidation of Cyt c has been coupled to lactate dehydrogenase, which catalyzes the oxidation of L-lactate [323]. Similar electron transport was also provided by ferrocene monocarboxylic acid mediating the electron-transfer from lactate dehydrogenase to the electrode. Although the rate constants for electron-transfer between lactate dehydrogenase and Cyt c - and ferrocene-mediators are similar ($6.7 \times 10^6 \text{ M}^{-1} \text{ s}^{-1}$ and $5.0 \times 10^6 \text{ M}^{-1} \text{ s}^{-1}$, respectively), the Cyt c mediation process is much more specific and is not affected by any interferant that is not recognized by Cyt c . The specificity of this mediation process can be further utilized to provide regeneration of $NADP^+$, which can be connected

to any $NADP^+$ -dependent enzyme [324]. In this system, NADPH-cytochrome- P_{450} -reductase oxidizes NADPH, and later donates electrons to the oxidized Cyt c , which is finally regenerated at the promoter-modified electrode.

17.9.2

Heme-protein Monolayers as Electron-transfer Mediators

The first step toward the construction of organized multiprotein/enzyme bioelectrocatalytic matrices is the monolayer deposition of the protein that serves as a base, mediating electron-transfer to further enzyme-layers. The positively charged Cyt c molecules have been adsorbed as a monolayer by the electrostatic attraction to negatively charged electrode interfaces produced by the self-assembly of thiol carboxylic acids [324–330]. The specific alignment of nonsymmetrically charged Cyt c can be achieved when the Cyt c adsorption is performed under application of a potential on the electrode [331]. After immobilization, the Cyt c molecules remain free for lateral and spinning movements on the electrode surface, which aids their interaction with secondary enzymes. Covalent binding of Cyt c to self-assembled monolayers [324, 332] usually results in their random orientation, because many functional groups around the Cyt c backbone are involved in the immobilization reaction. In this case, the Cyt c molecules are fixed on the surface and cannot adjust their orientation to communicate with other enzymes. For example, Cyt c adsorbed onto a self-assembled monolayer atop an electrode is capable of mediating electron-transfer from soluble NADPH-cytochrome- P_{450} -reductase to the electrode [324]. Cyt c molecules covalently fixed at the interface did not

exhibit such properties. These results suggest that the electrostatically adsorbed Cyt c has some mobility that allows re-orientation, as required to interact with the electrode and with the enzyme. In

contrast, covalently bonded Cyt c has a permanent, random orientation with respect to the electrode surface and blocks the Cyt c electron mediating process. Thus, alignment of the heme-protein is

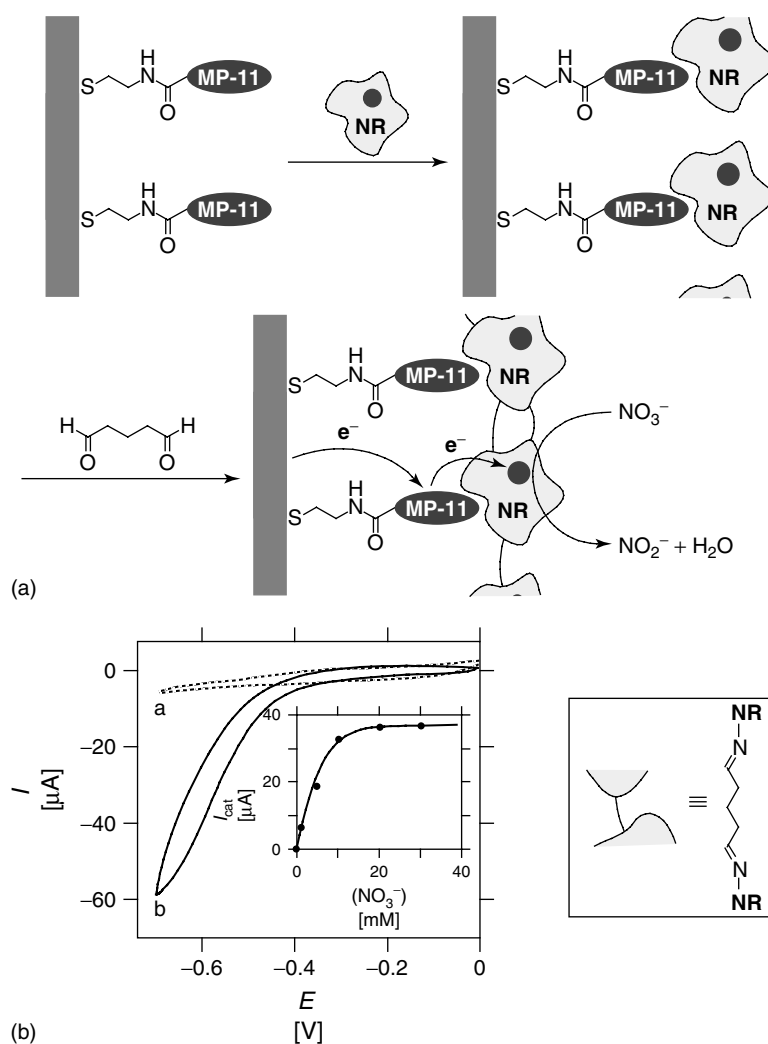


Fig. 25 (a) The assembly of an integrated nitrate sensor electrode by the cross-linking of a microperoxidase-11/NR affinity complex on an Au-electrode; (b) cyclic voltammograms of the integrated MP-11/NR monolayer-modified Au-electrode (roughness factor ca. 15). (a) 0.1 M phosphate buffer, pH 7.0, (b) in the presence of KNO_3 , 20 mM. Potential scan rate 5 mV s^{-1} . Inset: electrocatalytic cathodic currents ($E = -0.6 \text{ V}$) transduced by the modified electrode at different concentrations of KNO_3 . Measurements were performed under argon.

highly important for it to interact with enzymes that require specific binding sites.

17.9.2.1 Microperoxidase-11 Monolayers

Microperoxidase-11 (2) consists of the active-site microenvironment of Cyt c [333, 334], and is obtained by tryptic digestion of the native hemoprotein. Despite the structural similarities between MP-11 and Cyt c, the heme sites of the oligopeptide and the native protein differ substantially in their redox-potentials ($E^\circ = -0.40$ V for MP-11 [335] and $E^\circ = +0.012$ V for Cyt c [305–307, 336]). Microperoxidase-11 assembled [335, 337] as a monolayer on an Au-electrode provides affinity interactions with hemoproteins and cytochrome-dependent enzymes [61]. An MP-11 monolayer was found to yield an affinity complex with the native cytochrome b₅-dependent NR, (from *Escherichia coli*), giving an NR surface coverage estimated at 3.8×10^{-12} mol cm⁻² [337]. The association constant of the MP-11/NR complex was determined by quartz crystal microbalance (QCM) measurements to be $K_a = 3.7 \times 10^3$ M⁻¹. Cross-linking of this affinity complex layer with glutaric dialdehyde generates a stable electrically contacted enzyme electrode that effects the bioelectrocatalyzed reduction of nitrate to nitrite (Fig. 25a). The bioelectrocatalyzed transformation proceeds with a current efficiency of ca. 85%, and the resulting enzyme-electrode can be employed as an amperometric nitrate sensor (Fig. 25b).

Cobalt(II)-protoporphyrin IX-reconstituted Mb has also been found to form an affinity complex with MP-11 monolayer electrodes [338, 339]. The association constant of the affinity complex between the reconstituted Mb and MP-11 corresponds to $K_a = 1.6 \times 10^5$ M⁻¹, and the electron-transfer rate constant in

the resulting supramolecular complex is $k_{et} = 0.3$ s⁻¹. The MP-11 mediates the electrocatalyzed reduction of Co(II)-Mb and the resulting cobalt hydride hydrogenates alkynes (e.g. acetylene dicarboxylic acid to maleic acid). Cross-linking of the Co(II)-reconstituted Mb affinity complex with glutaric dialdehyde generates a stable electrode for the electrocatalytic hydrogenation of acetylene dicarboxylic acid with a current yield of ca. 80%.

17.9.2.2 Heme-containing De novo Protein Monolayers

De novo synthetic proteins containing heme-units and mimicking cytochrome b functions have been assembled on solid supports [340, 341]. The controllable alignment of their structure and redox properties of their heme-units makes them interesting for mediating electrons between enzymes and electrode supports. Recently, de novo synthesized four-helix polypeptides were applied to the mimicking of cytochrome b functions and to tailor layered cross-linked electrocatalytic electrodes. A four-helix bundle de novo protein (14,728 D), which includes histidine units in two of its helices, was assembled onto Au-electrodes (Fig. 26a). Two Fe(III)-protoporphyrin IX molecules were reconstituted into the assembly to yield a system that demonstrates a vectorial electron-transfer cascade [342]. Thus, the application of this artificial heme-containing protein as a mediator in supra-protein/enzyme assembly allows vectorial electron-transfer to the biocatalytic redox enzyme. The de novo-synthesized protein assembly forms affinity complexes with the cytochrome-dependent NR and with Co(II)-protoporphyrin IX-reconstituted Mb [343]. The resulting layered complex of

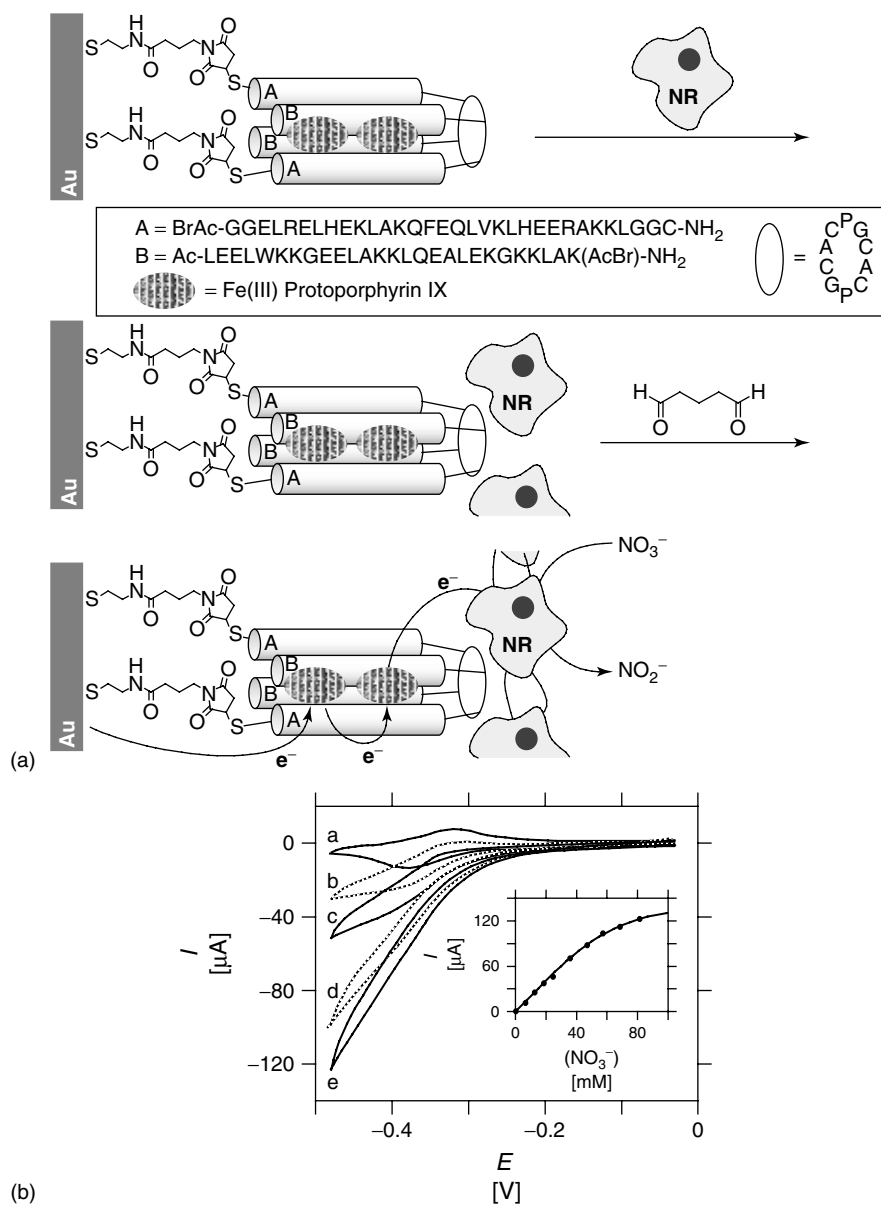


Fig. 26 (a) The assembly of a nitrate sensing electrode by the cross-linking of an affinity complex formed between NR and a Fe(III)-protoporphyrin reconstituted de novo four helix-bundle protein; (b) cyclic voltammograms of the NR/two heme-reconstituted de novo protein-layered Au-electrode at nitrate concentrations of (a) 0, (b) 12, (c) 24, (d) 46 and (e) 68 mM. Inset: calibration curve for the amperometric response of the electrode at different nitrate concentrations (at *E* = -0.48 V). Potential scan rate 5 mV s⁻¹, 0.1 M phosphate buffer, pH 7.0, under argon, electrode roughness factor ca. 20.

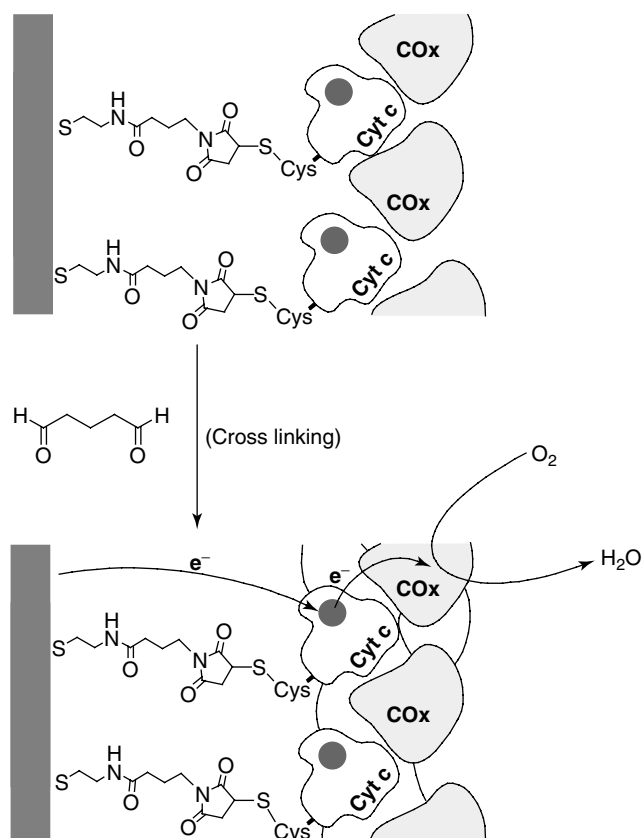


Fig. 27 The cross-linking of COx in an affinity complex with a surface-aligned Cyt c-electrode to form an integrated assembly capable of the bioelectrocatalytic reduction of O₂.

Fe(III)-de novo protein/NR, or Fe(III)-de novo protein/Co(II)-reconstituted Mb were cross-linked with glutaric dialdehyde to yield electrically contacted electrocatalytic electrodes. The Fe(III)-de novo protein/NR-electrode assembly was applied for the electrocatalyzed reduction of NO₃⁻ to NO₂⁻ and acted as an amperometric NO₃⁻ sensor (Fig. 26b), and the Fe(III)-de novo protein/Co(II)-reconstituted Mb integrated electrode stimulated the electrocatalyzed hydrogenation of acetylene dicarboxylic acid to malic acid.

17.9.2.3 Cyt c-aligned Monolayers Associated with Cytochrome Oxidase

Electrical contacting of iso-2-cytochrome c (iso-2-Cyt c, from *Saccharomyces cerevisiae*) can be achieved by the covalent linking of its cysteine residues to an electrode-bound maleimide monolayer [344]. The association constant between the iso-2-Cyt c-monolayer and COx is very high ($K_a = 1.2 \times 10^7 \text{ M}^{-1}$) [301], and an integrated iso-2-Cyt c/COx electrode is, therefore, prepared with relative ease (Fig. 27). The iso-2-Cyt c monolayer electrode was first interacted with COx to generate the

affinity complex on the surface with an almost close-packed surface density (ca. 2×10^{-12} mole cm^{-2}). The resulting layered complex was cross-linked with glutaric dialdehyde to yield the integrated electrically contacted electrode. The specific orientation of the mediator on the surface along with the restrictions placed on the enzyme by its closely packed state lead to a complex that is highly optimized for efficient electron-transfer. Nuncatalyzed electrochemical reduction of O_2 at a bare Au electrode proceeds with an overpotential that is even larger when the electrode is covered with iso-2-Cyt c or COx alone, because of the partial blocking of the electrode surface. Thus, when the electrode surface covered with either iso-2-Cyt c or COx, the electrocatalysis of O_2 reduction is not achieved. For a layered iso-2-Cyt c/COx-cross-linked-electrode in the presence of O_2 , an electrocatalytic O_2 -reduction-wave is observed at potentials more negative than -0.07 V, indicating that the iso-2-Cyt c/COx layer acts as a biocatalytic interface for the reduction of dioxygen. Thus, the effective bioelectrocatalyzed reduction of O_2 by the iso-2-Cyt c/COx interface originates from direct electrical communication from the electrode to iso-2-Cyt c to COx, which acts as an electron storage biocatalyst for the multielectron reduction. Systems providing four-electron transfer mechanisms for the reduction of O_2 are scarce, yet they are of extreme importance for the development of O_2 -based biofuel cells [345].

17.10

Applications of Enzymes Electrically Contacted by Mediated Electron-transfer

Although the study of enzyme electrochemistry is of great value for the

understanding of natural processes, it also opens up interesting prospects for the development of new technologies. In the utilization of redox enzymes for the construction of new devices, the biomolecules may be applied, either for their natural functions (e.g. in biofuel cells and biocatalysis) or for functions that are not performed in nature (e.g. in quantitative sensors).

17.10.1

Biosensors Based on Electrically “Wired” Enzyme Electrodes

The electrochemical activation of enzyme electrodes results in the bioelectrocatalyzed oxidation or reduction of a substrate specific to the biocatalyst. Provided the MET is fast, it is controlled by the substrate concentration. Hence, the mediator-enzyme assemblies provide a basis for the construction of quantitative analytical biosensors [346]. The continuous monitoring of endogenous compounds or drugs by implantable biosensors enables the close surveillance of patients via a rapid return of clinical information [347, 348]. Such real-time measurements are thus highly desired in intensive care units, during surgery and for the management of diabetes, as they offer an early warning of changes in a patient's condition, allowing rapid corrective action to be undertaken. The analysis of blood glucose levels in diabetics is just one example where such cheap and continuous monitoring is particularly desirable [346]. Several other important metabolites can also be readily detected using amperometric biosensors based on electrically “wired” enzymes (e.g. biosensors for lactate [349, 350], bilirubin [40, 351], amino acids [352], and peptides [353] have been developed

using lactate oxidase or lactate dehydrogenase, bilirubin oxidase, amino acid oxidase, and tyrosinase, respectively). Amperometric biosensors for the monitoring of drugs have also received considerable attention (e.g. for assay of theophylline [354] using theophylline oxidase). In addition to medical applications, electrically “wired” redox enzymes have found many uses in food technology and biotechnology (e.g. for analysis of carbohydrates, organic acids, alcohols, additives, pesticides and fish/meat freshness [355, 356]), in environmental monitoring (e.g. for analysis of pollutants, pesticides [357–359]), and in defense applications (e.g. for detection of toxins, pathogenic bacteria [360, 361]).

17.10.2

Bioelectrocatalyzed Synthesis by “Wired” Enzyme Assemblies

The coupling of enzymatic and electrochemical reactions has provided efficient tools, not only for analytical but also for synthetic purposes. In the latter field, the possibilities of enzymatic electrocatalysis, for example, the coupling of glucose oxidation (catalyzed either by GOx or GDH) to the electrochemical regeneration of a co-substrate (benzoquinone or NAD^+) have been demonstrated [362–364]. An electroenzymatic reactor has also been developed [363–364] to demonstrate the production of biochemicals on a laboratory scale. NAD(P)^+ derivatives immobilized by covalent attachment to polymer matrices or protein backbones have been used in enzyme reactors [365, 366]. Another important coenzyme ubiquinone can be regenerated at an electrode [367, 371] and applied to drive secondary enzymatic reactions with the participation of membrane enzymes (e.g. fumarate reductase),

resulting in the production of biologically important compounds [372].

A biosynthetic multienzyme reaction of particular interest involves carbon dioxide fixation with the production of methanol [373, 374]. FDH catalyzes the reduction of carbon dioxide to formate, and methanol dehydrogenase (MDH) catalyzes the reduction of formate to methanol. Both of these enzymes require NAD^+/NADH -cofactor, and in the presence of the reduced dimethyl viologen mediator ($\text{MV}^{\bullet+}$), they can drive a sequence of enzymatic reactions. The cascade of biocatalytic reactions results in the reduction of CO_2 to formate catalyzed by FDH, followed by the reduction of formate to methanol catalyzed by MDH. A more complex system composed of immobilized cells of *Parococcus denitrificans* has been demonstrated for the reduction of nitrate and nitrite [375].

17.10.3

Biofuel Cells Based on “Wired” Enzyme Assemblies

Considering the need to explore energy alternatives, the development of biofuel cells is an extremely attractive application of bioelectrocatalytic electrodes. Biofuel cells utilize biocatalysts for the conversion of abundant raw materials (e.g. methanol, glucose) to electrical energy using molecular oxygen or H_2O_2 as an oxidizer [376–379]. The fact that an electrically “wired” enzyme can catalyze the oxidation or reduction of substrates enables the use of enzyme-modified electrodes as key elements of biofuel cells. With this possibility in mind, a biofuel cell element based on the bioelectrocatalytic oxidation of glucose by H_2O_2 was constructed [380] (Fig. 28a). An electrically contacted GOx monolayer (assembled on

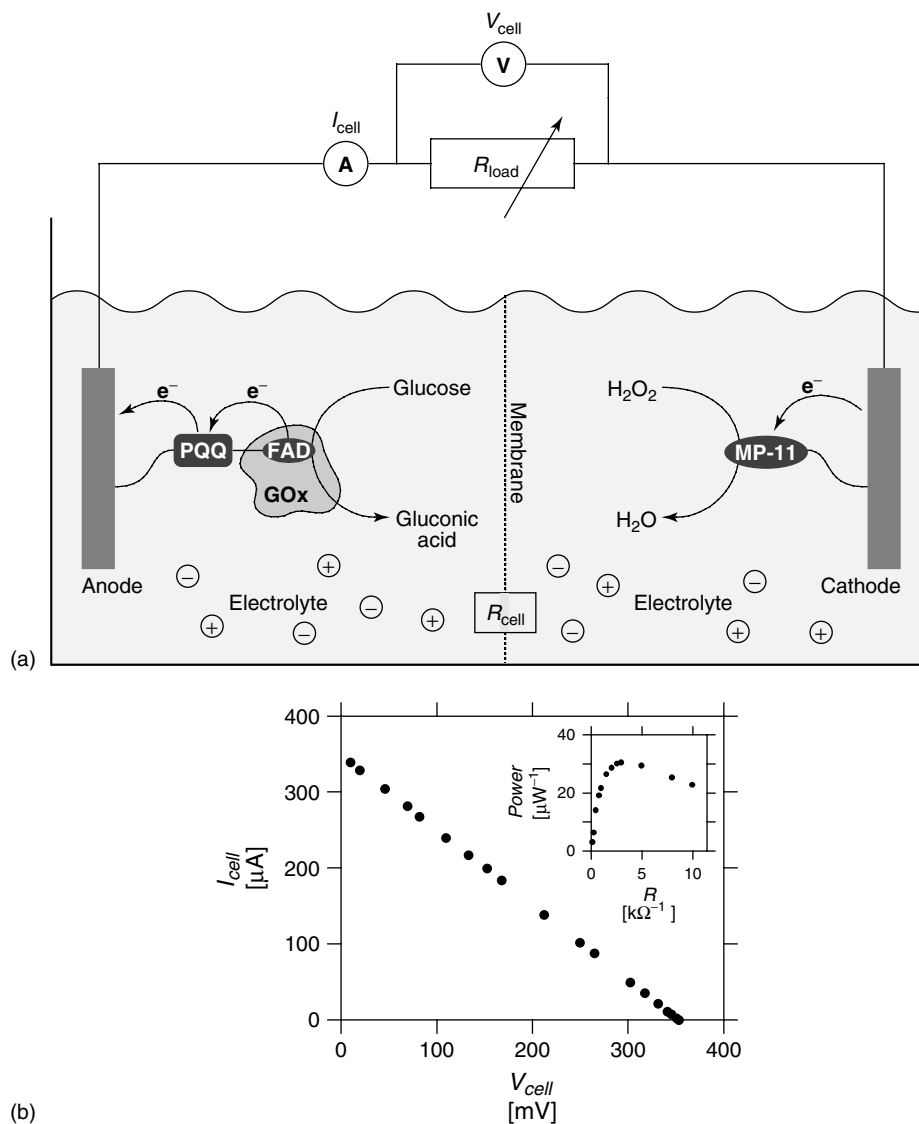


Fig. 28 (a) Schematic configuration of a biofuel cell employing glucose and H_2O_2 as fuel and oxidizer, and using PQQ-FAD/reconstituted GOx and MP-11-functionalized electrodes as biocatalytic anode and cathode, respectively;

(b) current-voltage behavior of the biofuel cell at different external loads. Inset: Electrical power extracted from the biofuel cell at different external loads.

an electrode by the reconstitution of apo-GOx on a PQQ-FAD layer, Fig. 17) was used as the anode, and a microperoxidase-11-functionalized electrode was applied

as the cathode. The bioelectrocatalyzed oxidation of glucose proceeds at the anode, while the MP-11 catalyzed the reduction of H_2O_2 in the catholyte compartment.

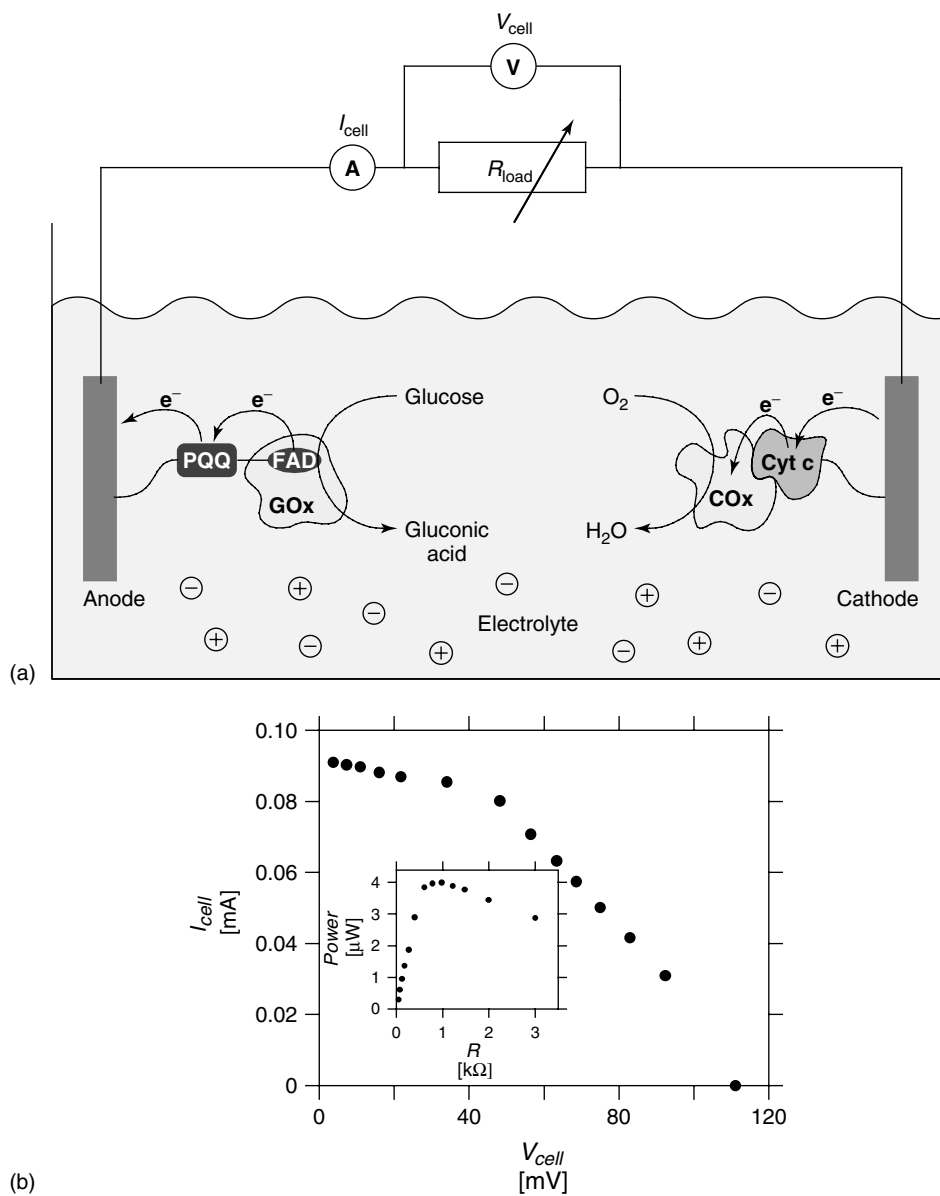


Fig. 29 (a) Schematic configuration of a noncompartmentalized biofuel cell employing glucose and O_2 as fuel and oxidizer, and using PQQ-FAD/GOx- and Cyt c/COx-functionalized electrodes as biocatalytic anode and cathode,

respectively; (b) current-voltage behavior of the biofuel cell at different external loads. Inset: Electrical power extracted from the biofuel cell at different external loads.

The current-voltage behavior of the biofuel cell at different external loads and at optimized concentrations of the oxidizer and fuel substrates are shown in Fig. 28(b). Up to 32 μW could be extracted at an external load of 3 k Ω (Fig. 28b, inset). The configuration of this biofuel cell represents a very general method for the development of future biofuel cell elements as it can be extended to other oxidative enzymes and fuel substrates, such as methanol oxidase or lactate oxidase and the respective alcohol or lactic acid fuel substances.

The next generation of biofuel cells could utilize complex, ordered enzyme or multienzyme systems immobilized at both electrodes, even removing the need for compartmentalization of the anode and the cathode. In a working example, the anode described above (based on the reconstituted GOx), together with a cathode based on an aligned iso-2-Cyt c (from *Saccharomyces cerevisiae*)/COx couple was constructed, providing the reduction of O_2 to water (Cf. Chapter 8.2.3) (Fig. 29a). Since the reconstituted GOx provides extremely efficient biocatalyzed oxidation of glucose that is unaffected by oxygen, the anode can operate in the presence of oxygen. Thus, this biofuel cell uses O_2 as an oxidizer and glucose as a fuel without the need for compartmentalization [345]. The cell operation was studied at different external loads (Fig. 29b), and achieved a fill factor of ca. 40% with a maximum power 4 μW at an external load of 0.9 k Ω .

17.11

The External Control of the Electron-transfer Process

We have seen how the functions of various enzyme and multienzyme systems can be persuaded to operate in synthetic

environments with a knowledge of design considerations and use of electron-transfer mediators. The assemblies that have been discussed are of use, both for fundamental research and for real-world applications, such as biosensors and biofuel cells. What they all lack, however, is the ability to control their activity after they have been put into operation. In some cases, the electrode sensitivity can be “tuned”, for instance, by the number of biocatalyst layers, but the final structure cannot be changed. Assemblies that can be “tuned” or turned on and off during their operation are highly desirable. The use of such interfaces could allow the construction of variable output fuel cells or variable range sensors. It is even possible that architectures with rudimentary information processing abilities could be assembled. For instance, photo-switchable biomaterials open a route to optobioelectronic systems [381].

17.11.1

Photochemical Control by Enzyme-bound Photoisomerizable Units

The activity of biocatalysts is highly dependant on their ability to adopt their natural conformation. We have already seen that enzymes that are functionalized with too many relay groups begin to lose their activity due to the disruption of their correct shape. Photoisomerizable molecules undergo reversible structural changes when exposed to specific energies of light. Their two states often differ considerably, for instance, in their charge, polarization, and shape. If an enzyme molecule is functionalized with photoisomerizable groups, then the local environment of that enzyme will depend on the state of those groups. As the conformation of the enzyme is very sensitive to its environment, the shape and, therefore, the activity of the enzyme may

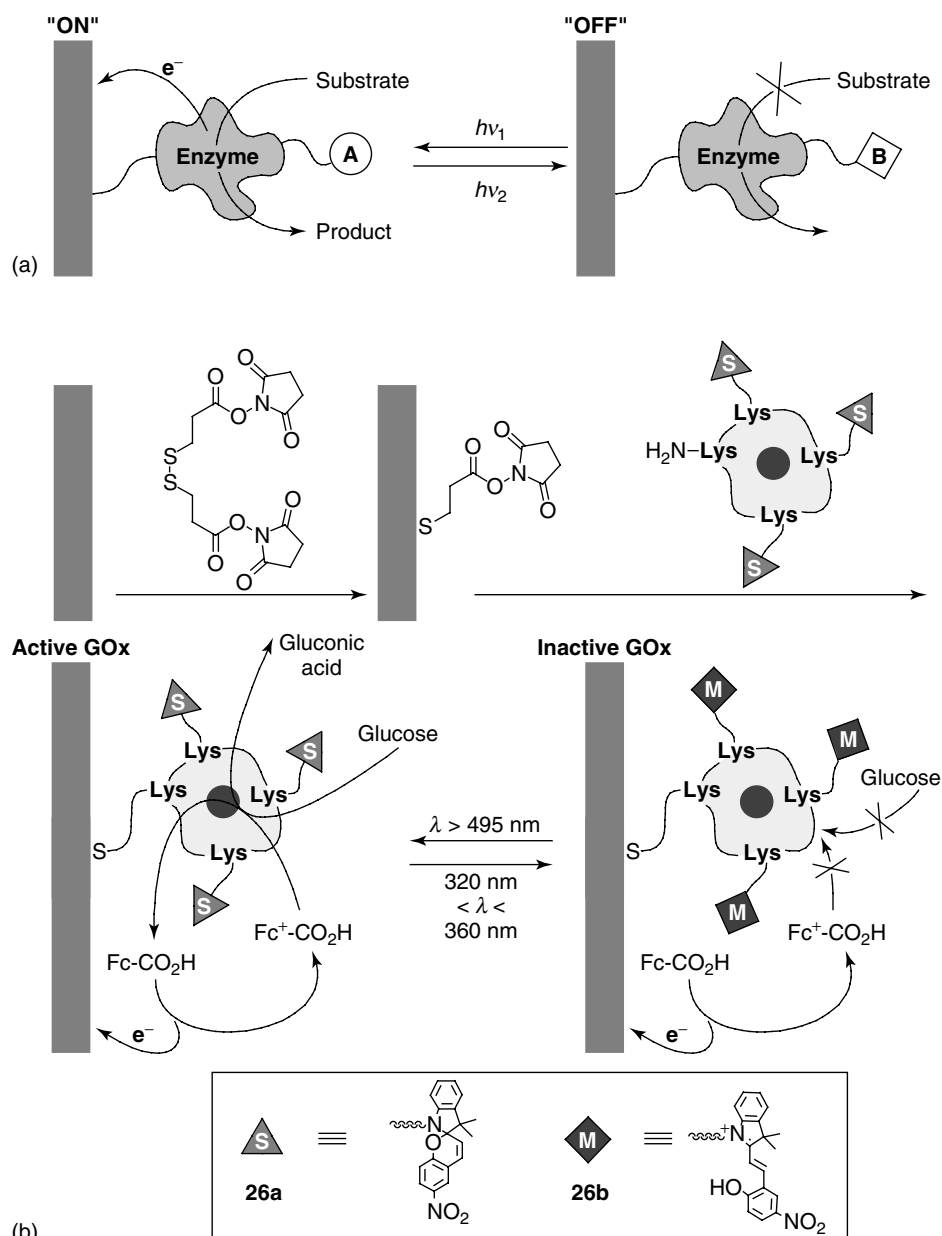


Fig. 30 (a) The assembly of an optobioelectronic system by the immobilization of an enzyme tethered with photoisomerizable units; (b) a nitrospiropyran-functionalized GOx

layer for the photo-controlled oxidation of glucose, with ferrocene carboxylic acid as a diffusional electron mediator.

be controlled by photonic input (Fig. 30a). If the enzyme is electrically contacted by an electron mediator, then there is a possibility that photoisomerization may control the enzyme activity by changing the ability of the mediator to interact with

the redox-center (as opposed to changing the catalytic ability of the enzyme).

The enzyme GOx was transformed into a photoswitchable enzyme by its chemical modification with nitrospiropyran photoisomerizable units [382]. The

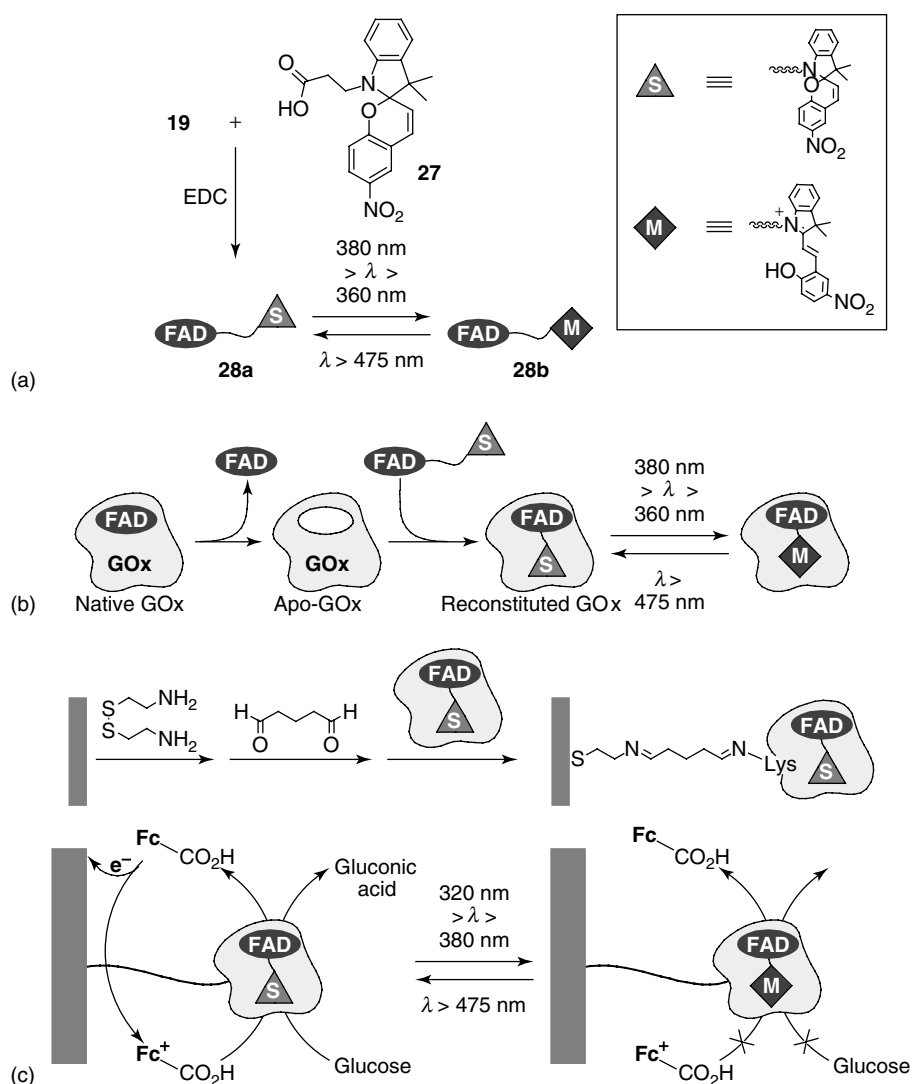


Fig. 31 (a) The synthesis of a photoisomerizable semisynthetic FAD; (b) reconstitution of the semisynthetic FAD into apo-GOx to give a photoisomerizable enzyme; (c) immobilization of the photoisomerizable enzyme to give an assembly with photoswitchable bioelectrocatalytic functions.

nitrospiropyran units (**26a**) are photoisomerized to the protonated merocyanine-state (**26b**) upon irradiation with $360\text{ nm} < \lambda < 400\text{-nm}$ light. The opposite photoisomerization from (**26b**) to (**26a**) proceeds upon illumination with visible light ($\lambda > 475\text{ nm}$). The structurally modified enzyme was assembled as a monolayer on an Au-electrode (Fig. 30b). In the presence of the diffusional electron mediator ferrocene carboxylic acid, the (**26a**)-functionalized GOx was activated for the oxidation of glucose, as evidenced by the high electrocatalytic current resulting from the oxidation of glucose. Photoisomerization of the monolayer to the (**26b**)-state results in a structural distortion of the protein that prevents electrical contact with the electron mediator, and a substantially lower amperometric response. By the cyclic photoisomerization of the enzyme monolayer between the (**26a**) and (**26b**) states, reversible “high” and “low” amperometric responses of the functionalized electrode are transduced. Incomplete “on”-“off” bioelectrocatalytic functions of the enzyme-electrode were observed. This was attributed to the insufficient distortion of the protein by photoisomerizable units attached randomly, far from the active site, thereby, perturbing only to limited extent the biocatalytic activity of the enzyme.

To optimize the photoswitchable bioelectrocatalytic features of redox enzymes, the site-specific functionalization or mutation of the active-site microenvironment is essential. This has been accomplished by a semisynthetic approach, involving the reconstitution of the flavoenzyme GOx with a semisynthetic photoisomerizable FAD-cofactor [383, 384]. Nitrospiropyran carboxylic acid (**27**) was covalently coupled to N^6 -(2-aminoethyl)-FAD (**19**) to yield a photoisomerizable nitrospiropyran-FAD cofactor (**28a**)

(Fig. 31a). The native FAD cofactor was extracted from GOx and the semisynthetic FAD cofactor was reconstituted into the apo-GOx (apo-GOx) (Fig. 31b). This reconstituted enzyme includes a photoisomerizable unit directly attached to the redox center of the enzyme, and hence, the enzyme is predisposed for optimized photoswitchable bioelectrocatalytic properties. The photoisomerizable enzyme was assembled on an Au-electrode as described in Fig. 31(c). The bioelectrocatalytic oxidation of glucose was stimulated in the presence of ferrocene carboxylic acid as a diffusional electron-transfer mediator. The (**28a**)-state of the reconstituted GOx was inactive for the bioelectrocatalytic transformation, whereas photoisomerization of the enzyme to the (**28b**)-state activated the system (Fig. 32). By the cyclic photoisomerization of the enzyme monolayer between (**28a**) and (**28b**) states, the bioelectrocatalyzed oxidation of glucose was cycled between the “off” and “on” states, respectively (Fig. 32, inset). It was also found that the direction of the photobioelectrocatalytic switch of the (**28a/28b**)-FAD-reconstituted GOx is controlled by the electrical properties of the diffusional electron-transfer mediator [385]. With ferrocene dicarboxylic acid as a diffusional electron-transfer mediator, the enzyme in the (**28a**)-state was found to correspond to the switched “off” biocatalyst, while the (**28b**)-state exhibits switched “on” behavior. In the presence of the protonated 1-[1-(dimethylamino)ethyl]ferrocene, the direction of the photobioelectrocatalytic switch is reversed. This control of the photoswitch direction of the photoisomerizable GOx was attributed to electrostatic interactions between the diffusional electron-transfer mediator and the photoisomerizable unit linked to the FAD. The (**28b**)-state attracts the oxidized negatively charged

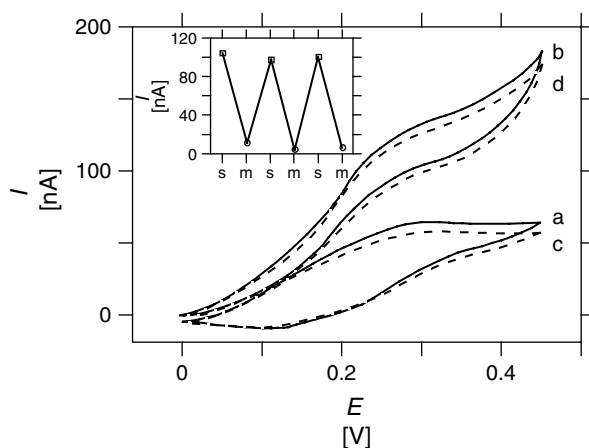


Fig. 32 Cyclic voltammograms of an electrode bearing a monolayer of GOx reconstituted with photoisomerizable dyad **28(a/b)** in the presence of glucose (50 mM), ferrocene carboxylic acid (50 μ M), and with the photoisomerizable units (a, c) in the spiropyran-state (**28a**), and (b, d) in the merocyanine-state (**28b**). Recorded in 0.01 M phosphate buffer, pH 7.3, scan rate 5 mV s^{-1} . Inset: switching behavior of the electrocatalytic current as a function of the state of the photoisomerizable group: “s” and “m” represent the photoisomerizable units in the spiropyran and the merocyanine states, respectively.

electron-transfer mediator, but repels the oxidized positively charged relay. As a result, this photoisomer state of the enzyme is switched “on” in the presence of negatively charged mediator, but exists in the “off” state, using positively charged electron-transfer mediator.

17.11.2

Photochemical Control by Electrode-bound Photoisomerizable Units

Photonic control over electroactivated biocatalytic processes can also be achieved by the use of electrode surfaces that are modified by photoisomerizable units. These interfaces, whose state controls the ability of a substrate to interact with them, are known as “command” surfaces [382, 386–390]. In one example, a

mixed monolayer consisting of pyridine-4-thiol and nitrospiropyran thiol (**29a**) revealed “command” interface properties for Cyt c electrochemistry [386, 388]. On a gold surface, a pyridine-4-thiol monolayer functions as a promoter for the Cyt c electrochemical reduction/oxidation process [305–307]. The monolayer composed of the pyridine-promoter groups and neutral spiropyran units (**29a**) provides efficient reduction and oxidation of Cyt c, allowing enzymatic reactions that require the participation of a Cyt c-dependent enzyme. A biocatalytic cascade of reductive reactions was achieved in the presence of COx and O_2 (Fig. 33a). Oxidative reactions with the participation of lactate dehydrogenase resulted in lactate oxidation (Fig. 33c). When the photoisomerizable groups are transformed into the positively charged

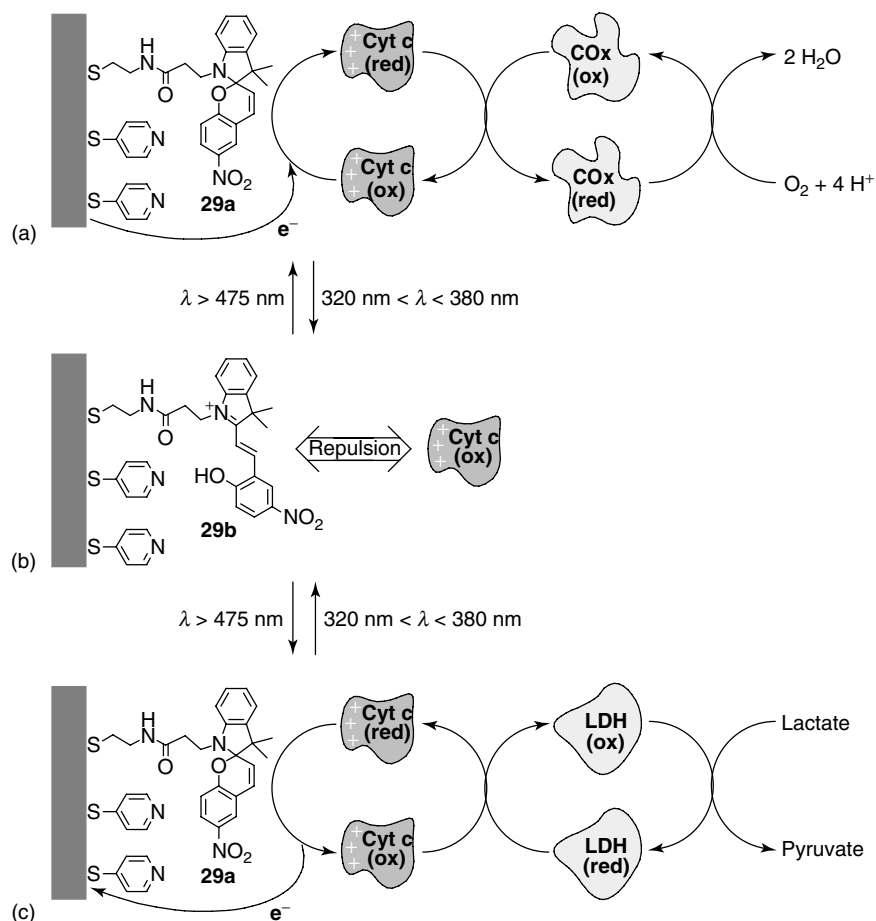


Fig. 33 Coupling of the photoswitchable interactions between Cyt c and a (**29a**)-pyridine mixed monolayer with: (a) the reduction of O_2 by COx and (c) the oxidation of lactate by LDH; (b) when the electrode is in the cationic merocyanine state (**29b**), repulsive interactions disallow the functioning of bioelectrocatalytic processes.

protonated merocyanine state (**29b**), the positively charged Cyt c molecules are repelled from the electrode surface and electrical contact is no longer established (Fig. 33b). In this case, not only Cyt c electrochemistry is inhibited, but also any secondary reactions. Switching between the electrochemically contacted system and the electrochemically inactive system was studied by CV for Cyt c only (Fig. 34a) and in the presence of the secondary enzyme

with the respective substrate (e.g. LDH and lactate) (Fig. 34b). Reversible switching between electrochemically active and inactive states was obtained (Fig. 34a&b, insets). Related photoisomerizable command interfaces have been used to control the biocatalytic activity of GOx [387, 390] and the electrocatalytic regeneration of NAD^+ -cofactor [391]. Command surfaces have also been used to detect various signals (temperature change [392],

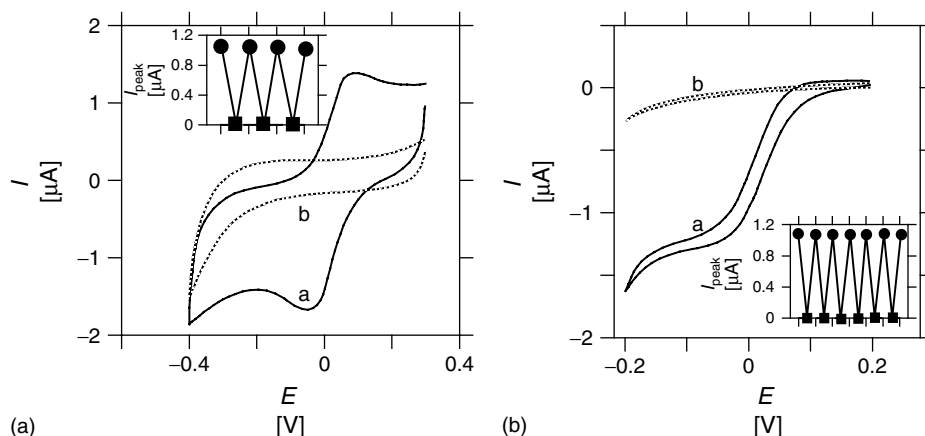


Fig. 34 (a) Cyclic voltammetric response of Cyt c (0.1 mM) at a mixed (29(a/b)) and pyridine monolayer-modified electrode in (a) the neutral spiropyran-state (29a) and (b) the positively charged merocyanine-state (29b), recorded at 50 mV s^{-1} . Inset: switching behaviour of the Cyt c electrochemistry as a function of the state of the photoisomerizable group: circles and squares represent the photoisomerizable units in the spiropyran and the merocyanine states, respectively; (b) cyclic voltammetric response of Cyt c (0.1 mM) with COx ($1 \mu\text{M}$) at a mixed

(29(a/b)) and pyridine monolayer-modified electrode in the presence of O_2 and in (a) the neutral state (29a), and (b) the cationic merocyanine state (29b). Inset: switching behaviour of the electrocatalytic current as a function of the state of the photoisomerizable group: circles and squares represent the photoisomerizable units in the spiropyran and the merocyanine states, respectively. All experiments were performed in 0.1 M phosphate buffer, pH 7.0.

pH change [393]) by the variation of redox cofactor regeneration rates (therefore by the control of enzymatic activity). Thus, they represent examples of biocatalytic switches.

17.11.3

Photochemical Control by Mediator-bound Photoisomerizable Units

Photoswitchable electrical communication between enzymes and electrodes has also been achieved by the application of photoisomerizable electron-transfer mediators [386, 389] (Fig. 35). Diffusional electron mediators (viologen (30) or ferrocene (31) derivatives) were functionalized with photoisomerizable spiropyran/merocyanine units. These mediators can be reversibly photoisomerized from

the spiropyran-state (30a, 31a) to the merocyanine-state (30b, 31b) ($360 < \lambda < 380 \text{ nm}$) and back ($\lambda > 475 \text{ nm}$). An enzyme multilayer array composed of glutathione reductase or GOx was only electrically contacted when the photoactive group linked to the redox relay (viologen or ferrocene derivative, respectively) was in the spiropyran-state (30a, 31a) (Fig. 35a). Cyclic activation/deactivation of the enzyme arrays was achieved upon photochemical isomerization of the electron-transfer mediators between (30a, 31a) and (30b, 31b) states (Fig. 35b). Thus, the application of photoisomerizable redox relays provides a novel means of controlling the electrical communication of redox enzymes with electrode surfaces. The lack of electrical interactions between the respective enzymes and the mediators in the

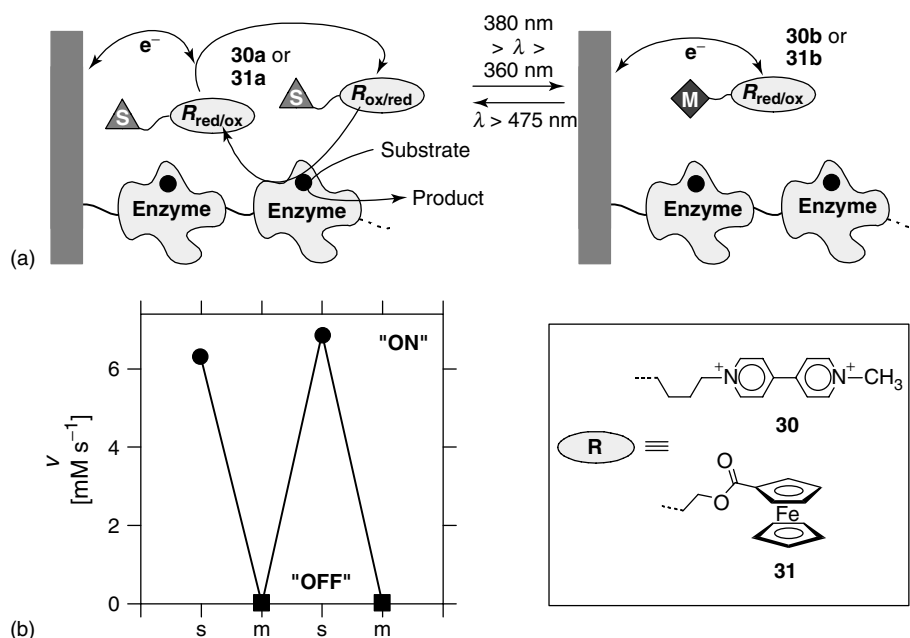


Fig. 35 (a) The electrochemical contacting of a multilayer array consisting of either GOx or GR in the presence of diffusional mediators (ferrocene and viologen, respectively) tethered to photoisomerizable units (**30** and **31**); (b) switching behaviour of the bioelectrocatalytic function

of a multilayer array of GR as a function of the state of a photoisomerizable group attached to a diffusional viologen mediator (**30**): "s" and "m" represent the photoisomerizable units in the spiropyran (**30a**) and the merocyanine (**30b**) states, respectively.

merocyanine state could originate from steric constraints or electrostatic repulsive interactions between the isomers and enzymes, preventing the intimate contact of the mediator and the enzyme redox center required for electron-transfer.

17.12 Conclusion and Perspectives

The electrical contacting of redox enzymes or redox-active proteins with electrodes is a fundamental concept in the rapidly developing field of bioelectronics. Molecular, macromolecular or biomolecular electron-transfer mediators can act as diffusional electron carriers that shuttle

charges between the protein redox-sites and the electrodes. Electron mediators may also act as electrocatalysts that shuttle electrons between cofactors and electrodes (e.g. FADH₂, NAD(P)H) or activate complex multi-enzyme biocatalytic cascades. The integration of electron mediators, redox-proteins, and conductive supports in rigidified assemblies leads to the organization of bioelectronic devices. Nanoengineering of electrodes with electron-relay units or electron-relay-functionalized proteins to yield electrically contacted enzyme electrodes represents a major recent advance in bioelectronics.

The tailoring of electrical contact between redox enzymes and electrodes provides a basis for electrochemical

biosensors. Besides the broad application of electrically contacted enzyme-electrodes for the amperometric analysis of enzyme-substrates, one may apply electrically contacted enzymes as redox labels for the sensing of biorecognition events, such as antigen-antibody [385, 394, 395] or oligonucleotide-DNA [396] complexation. The use of bioelectrocatalytic electrodes as active components of biofuel cells is also appealing. In particular, the development of catalytic electrodes that can drive the reduction of O₂ to water may contribute important interfaces for biological or chemical fuel-cell elements [345].

Future efforts at improving and extending the scope of electron-transfer mediation may take any of several approaches. The design of mediators may be carefully tuned to accomplish ideal redox potentials and specific interactions, and methods of immobilization and coimmobilization that minimize losses in activity may be developed. The modification of the enzymes themselves, either by mutagenesis, de novo synthesis or site-specific reactions may lead to structures with readily accessible active sites or with mediators attached in optimized positions. The construction of carefully integrated multicomponent systems could lead to highly efficient biosensing, biocatalytic, and biofuel devices. The control of electron-transfer events may also see a growth of interest. Photochemical control of bioelectrocatalysts has already been established by the use of photoisomerizable units, photocommand interfaces, and photoactive electron-relays. Other switchable biocatalyzed transformation can be envisaged by the application of magnetic, thermal or pH changes as external triggering signals. These addressable assemblies could even find uses in information storage and processing.

Acknowledgment

This research is supported by the Israeli Ministry of Science, Infrastructure Project of Biomicroelectronics, and the MINERVA German-Israeli Program (DIP).

References

1. J. A. Cowan, H. B. Gray, *Chem. Scr.* **1988**, 28A, 21–26.
2. A. G. Sykes, *Chem. Soc. Rev.* **1985**, 14, 283–321.
3. S. S. Isied, *Prog. Inorg. Chem.* **1984**, 32, 443–517.
4. S. E. Peterson-Kennedy, J. L. McGourty, P. S. Ho et al., *Coord. Chem. Rev.* **1985**, 64, 125–133.
5. G. McLendon, T. Guarr, M. McGuire et al., *Coord. Chem. Rev.* **1985**, 64, 113.
6. T. Tanaka, K. Takehaka, H. Kawamura et al., *J. Biochem. (Tokyo)* **1985**, 99, 833.
7. J. R. Miller in *Antennas and Reaction Centers of Photosynthetic Bacteria* (Ed.: M. E. Michel-Beyerle), Springer-Verlag, Berlin, 1985, p. 234.
8. M. Bixon, J. J. Jortner, *J. Phys. Chem.* **1986**, 90, 3795.
9. R. A. Marcus, N. Sutin, *Biochem. Biophys. Acta* **1985**, 811, 265.
10. D. DeVault, *Quantum Mechanical Tunneling in Biological Systems*, 2nd ed., Cambridge University Press, Cambridge, 1984.
11. A. K. Churg, R. M. Weiss, A. Warshel et al., *J. Phys. Chem.* **1983**, 87, 1683–1694.
12. S. Larson, *J. Chem. Soc., Faraday Trans. 2* **1983**, 79, 1375.
13. J. J. Hopfield, *Proc. Natl. Acad. Sci. U.S.A.* **1974**, 71, 3640–3644.
14. J. N. Onuchic, D. N. Beratan, J. J. Hopfield, *J. Phys. Chem.* **1986**, 90, 3707–3721.
15. A. Heller, *Acc. Chem. Res.* **1990**, 23, 128–134.
16. A. L. Ghindilis, P. Atanasov, E. Wilkins, *Electroanalysis* **1997**, 9, 661–674.
17. W. Schuhmann, *Biosens. Bioelectron.* **1995**, 10, 181–193.
18. I. V. Berezin, V. A. Bogdanovskaya, S. D. Varfolomeev et al., *Dokl. Akad. Nauk SSSR* **1978**, 240, 615–618.
19. A. I. Yaropolov, V. Malovik, S. D. Varfolomeev et al., *Dokl. Akad. Nauk SSSR* **1979**, 249, 1399–1401.

20. J. Zhao, R. Henkens, J. Stonehuerner et al., *J. Electroanal. Chem.* **1992**, 327, 109–119.
21. S. Yabuki, F. Mitzutani, *Electroanalysis* **1997**, 9, 23–25.
22. P. N. Bartlett, P. Tebbutt, R. C. Whitaker, *Prog. React. Kinetics* **1991**, 16, 55–155.
23. G. Davis, *Biosensors* **1985**, 1, 161–178.
24. G. Davis in *Biosensors: Fundamentals and Applications*, (Eds.: A. P. F. Turner, I. Karube, G. S. Wilson), OUP, Oxford, 1987, p. 247.
25. R. S. Nicholson, I. Shain, *Anal. Chem.* **1965**, 37, 178–190.
26. Y. A. Aleksandrovskii, L. V. Bezhikina, Y. V. Rodionov, *Biokhimiya* **1981**, 46, 708–716.
27. J. Mahenc, H. Aussaresses, C. R. *Hebd. Seances. Acad. Sci. Ser. C* **1979**, 289, 357–359.
28. A. L. Crumbliss, H. A. O. Hill, D. J. Page, *J. Electroanal. Chem.* **1986**, 206, 327–331.
29. I. Taniguchi, S. Miyamoto, S. Tomimura et al., *J. Electroanal. Chem.* **1988**, 240, 333–339.
30. A. E. G. Cass, G. Davis, G. D. Francis et al., *Anal. Chem.* **1984**, 56, 667–671.
31. J. E. Frew, H. A. O. Hill, *Philos. Trans. R. Soc. London B* **1987**, 316, 95–106.
32. B. A. Feinberg, M. D. Ryan in *Topics in Bioelectrochemistry and Bioenergetics*, (Ed.: G. Milazzo), John Wiley & Sons, 1981, p. 225, Vol. 4.
33. S. Wherland, H. B. Gray, *Proc. Natl. Acad. Sci. U.S.A.* **1976**, 73, 2950–2954.
34. H. C. Davis, L. Smith, A. R. Wasserman, *Biochim. Biophys. Acta* **1964**, 85, 238–246.
35. A. D. Ryabov, E. M. Tyapochkin, S. D. Varfolomeev et al., *Bioelectrochem. Bioenerg.* **1990**, 24, 257–262.
36. S. M. Zakeeruddin, M. Grätzel, D. M. Fraser, *Biosens. Bioelectron.* **1996**, 11, 305–315.
37. A. D. Ryabov, A. Amon, R. K. Gorbatoeva et al., *J. Phys. Chem.* **1995**, 99, 14 072–14 077.
38. C. Deshaies, J. Chopineau, J. Moiroux et al., *J. Phys. Chem.* **1996**, 100, 5063–5069.
39. I. Willner, A. Riklin, B. Shoham et al., *Adv. Mater.* **1993**, 5, 912–915.
40. B. Shoham, Y. Migron, A. Riklin et al., *Biosens. Bioelectron.* **1995**, 10, 341–352.
41. P. Pantano, T. H. Morton, W. G. Kuhr, *J. Am. Chem. Soc.* **1991**, 113, 1832, 1833.
42. T. Hoshi, H. Takeshita, J. Anzai et al., *Anal. Sci.* **1995**, 11, 311, 312.
43. X. Du, J. Anzai, T. Osa et al., *Electroanalysis* **1996**, 8, 813–816.
44. C. Bourdillon, C. Demaille, J. Guerin et al., *J. Am. Chem. Soc.* **1993**, 115, 12 264–12 269.
45. C. Bourdillon, C. Demaille, J. Moiroux et al., *J. Am. Chem. Soc.* **1994**, 116, 10 328, 10 329.
46. A. Riklin, I. Willner, *Anal. Chem.* **1995**, 67, 4118–4126.
47. E. Katz, D. D. Schlereth, H.-L. Schmidt, *J. Electroanal. Chem.* **1994**, 367, 59–70.
48. N. C. Foulds, C. R. Lowe, *J. Chem. Soc., Faraday Trans. 1* **1986**, 82, 1259–1264.
49. M. Umaña, J. Waller, *Anal. Chem.* **1986**, 58, 2979–2983.
50. C. Iwakura, Y. Kajiya, H. Yoneyama, *J. Chem. Soc., Chem. Commun.* **1988**, 1019, 1020.
51. F. Mizutani, M. Asai, *Bull. Chem. Soc. Jpn.* **1988**, 61, 4458–4460.
52. S.-I. Yabuki, H. Shinohara, M. Aizawa, *J. Chem. Soc., Chem. Commun.* **1989**, 945, 946.
53. P. Janda, J. Weber, *J. Electroanal. Chem.* **1991**, 300, 119–127.
54. Y. Kajiya, H. Sugai, C. Iwakura et al., *Anal. Chem.* **1991**, 63, 49–54.
55. J. Li, S. N. Tan, H. L. Ge, *Anal. Chim. Acta* **1996**, 335, 137–145.
56. J. Li, S. N. Tan, J. T. Oh, *J. Electroanal. Chem.* **1998**, 448, 69–77.
57. J. Li, L. S. Chia, N. K. Goh et al., *Sens. Actuators B* **1997**, 40, 135–141.
58. J. Li, L. S. Chia, N. K. Goh et al., *Anal. Chim. Acta* **1998**, 362, 203–211.
59. V. J. Razumas, A. V. Gudavicius, J. J. Kulys, *J. Electroanal. Chem.* **1986**, 198, 81–87.
60. F. Patolsky, G. Tao, E. Katz et al., *J. Electroanal. Chem.* **1998**, 454, 9–13.
61. A. Narvaez, E. Dominguez, I. Katakis et al., *J. Electroanal. Chem.* **1997**, 430, 217–233.
62. S. Marx-Tibbon, E. Katz, I. Willner, *J. Am. Chem. Soc.* **1995**, 117, 9925, 9926.
63. S. J. Sadeghi, G. Gilardi, G. Nicolosi et al., *Chem. Commun.* **1997**, 517, 518.
64. A. D. Ryabov, Y. N. Firsova, V. N. Gozal et al., *Chem. Eur. J.* **1998**, 4, 806–813.
65. G. Tao, E. Katz, I. Willner, *Chem. Commun.* **1997**, 2073, 2074.
66. Y. Degani, A. Heller, *J. Phys. Chem.* **1987**, 91, 1285–1289.
67. Y. Degani, A. Heller, *J. Am. Chem. Soc.* **1988**, 110, 2615–2620.

68. W. Schuhmann, T. J. Ohara, H.-L. Schmidt et al., *J. Am. Chem. Soc.* **1991**, *113*, 1394–1397.
69. P. N. Bartlett, R. G. Whitaker, M. J. Green et al., *J. Chem. Soc., Chem. Commun.* **1987**, 1603,1604.
70. I. Willner, E. Katz, *Angew. Chem., Int. Ed. Engl.* **2000**, *39*, 1180–1218.
71. E. S. Ryabova, V. N. Goral, E. Csöregi et al., *Angew. Chem. Int. Ed. Engl.* **1999**, *38*, 804–807.
72. A. Badia, R. Carlini, A. Fernandez et al., *J. Am. Chem. Soc.* **1993**, *115*, 7053–7060.
73. I. Willner, E. Katz, A. Riklin et al., *J. Am. Chem. Soc.* **1992**, *114*, 10 965,10 966.
74. I. Willner, N. Lapidot, A. Riklin et al., *J. Am. Chem. Soc.* **1994**, *116*, 1428–1441.
75. E. Katz, A. Riklin, I. Willner, *J. Electroanal. Chem.* **1993**, *354*, 129–144.
76. S. Kuwabata, T. Okamoto, Y. Kajiya et al., *Anal. Chem.* **1995**, *67*, 1684–1690.
77. D. Avnir, S. Braun, O. Lev et al., *Chem. Mater.* **1994**, *6*, 1605–1614.
78. A. Walcarius, *Electroanalysis* **1998**, *10*, 1217–1235.
79. K. Kalcher, J.-M. Kauffmann, J. Wang et al., *Electroanalysis* **1995**, *7*, 5–22.
80. L. Gorton, *Electroanalysis* **1995**, *7*, 23–45.
81. S. Cosnier, *Electroanalysis* **1997**, *9*, 894–902.
82. C. Kranz, H. Wohlschläger, H.-L. Schmidt et al., *Electroanalysis* **1998**, *10*, 546–552.
83. S. Cosnier, *Biosens. Bioelectron.* **1999**, *14*, 443–456.
84. H. Mao, P. G. Pickup, *J. Electroanal. Chem.* **1989**, *265*, 127–142.
85. G. Lian, S. Dong, *J. Electroanal. Chem.* **1989**, *260*, 127–136.
86. S. Dong, G. Lian, *J. Electroanal. Chem.* **1990**, *291*, 23–29.
87. W. Schuhmann, *Mikrochim. Acta* **1995**, *121*, 1–29.
88. S. Yabuki, H. Shinohara, M. Aizawa, *J. Electroanal. Chem.* **1990**, *277*, 179–187.
89. M. G. Loughram, J. M. Hall, A. P. F. Turner, *Electroanalysis* **1996**, *8*, 870–875.
90. S. Cosnier, C. Innocent, Y. Jouanneau, *Anal. Chem.* **1994**, *66*, 3198–3201.
91. S. Cosnier, L. Allien, L. Coche-Guérente et al., *Sens. Mater.* **1996**, *8*, 169–177.
92. S. Cosnier, B. Galland, C. Innocent, *J. Electroanal. Chem.* **1997**, *433*, 113–119.
93. N. Gajovic, K. Habermüller, A. Warsinke et al., *Electroanalysis* **1999**, *11*, 1377–1383.
94. S. Cosnier, J.-L. Décout, M. Fontecave et al., *Electroanalysis* **1998**, *10*, 521–525.
95. T. Parpaleix, J. M. Laval, M. Maida et al., *Anal. Chem.* **1992**, *64*, 641–646.
96. I. Willner, E. Katz, N. Lapidot et al., *Bioelectrochem. Bioenerg.* **1992**, *29*, 29–45.
97. G. Ramsay, S. M. Wolpert, *Anal. Chem.* **1999**, *71*, 504–506.
98. A. Heller, *J. Phys. Chem.* **1992**, *96*, 3579–3587.
99. H. Bu, S. R. Mikkelsen, A. M. English, *Anal. Chem.* **1995**, *67*, 4071–4076.
100. B. A. Gregg, A. Heller, *Anal. Chem.* **1990**, *62*, 258–263.
101. B. A. Gregg, A. Heller, *J. Phys. Chem.* **1991**, *95*, 5970–5975.
102. B. A. Gregg, A. Heller, *J. Phys. Chem.* **1991**, *95*, 5976–5980.
103. I. Katakis, A. Heller, *Anal. Chem.* **1992**, *64*, 1008–1013.
104. E. J. Calvo, C. Danilowicz, L. Diaz, *J. Electroanal. Chem.* **1994**, *369*, 279–282.
105. S. Koide, K. Yokoyama, *J. Electroanal. Chem.* **1999**, *468*, 193–201.
106. G. Arai, M. Masuda, I. Yasumori, *Bull. Chem. Soc. Jpn.* **1994**, *67*, 2962–2966.
107. S. A. Emr, A. M. Yacynych, *Electroanalysis* **1995**, *7*, 913–923.
108. P. Audebert, C. Demaille, C. Sanchez, *Chem. Mater.* **1993**, *5*, 911–913.
109. T.-M. Park, E. I. Iwuoha, M. R. Smith et al., *Anal. Commun.* **1996**, *33*, 271–273.
110. T.-M. Park, E. I. Iwuoha, M. R. Smith et al., *Talanta* **1997**, *44*, 973–978.
111. M. Tsionsky, G. Gun, V. Glezer et al., *Anal. Chem.* **1994**, *66*, 1747–1753.
112. I. Pankratov, O. Lev, *J. Electroanal. Chem.* **1995**, *393*, 35–41.
113. S. Sampath, I. Pankratov, J. Gun et al., *J. Sol.-Gel Sci. Technol.* **1996**, *7*, 123–128.
114. J. Gun, O. Lev, *Anal. Chim. Acta* **1996**, *336*, 95–106.
115. J. Gun, O. Lev, *Anal. Lett.* **1996**, *29*, 1933–1938.
116. S. Sampath, O. Lev, *Electroanalysis* **1996**, *8*, 1112–1116.
117. S. Sampath, O. Lev, *Anal. Chem.* **1996**, *68*, 2015–2021.
118. S. Sampath, O. Lev, *J. Electroanal. Chem.* **1997**, *426*, 131–137.
119. S. Bharathi, O. Lev, *Anal. Commun.* **1998**, *35*, 29–31.
120. B. Gründig, C. Krabisch, *Anal. Chim. Acta* **1989**, *222*, 75–81.

121. H. Gunasingham, C.-H. Tan, T.-C. Aw, *Anal. Chim. Acta* **1990**, 234, 321–330.
122. P. D. Hale, T. Inagaki, H. I. Karan et al., *J. Am. Chem. Soc.* **1989**, 111, 3482–3484.
123. L. Gorton, H. I. Karan, P. D. Hale et al., *Anal. Chim. Acta* **1990**, 228, 23–30.
124. J. Wang, L.-H. Wu, Z. L. Lu et al., *Anal. Chim. Acta* **1990**, 228, 251–257.
125. P. D. Hale, L. I. Boguslavsky, T. Inagaki et al., *Mol. Cryst. Liq. Cryst.* **1990**, 190, 251–258.
126. P. D. Hale, L. I. Boguslavsky, T. Inagaki et al., *Anal. Chem.* **1991**, 63, 677–682.
127. P. D. Hale, H. L. Lan, L. I. Boguslavsky et al., *Anal. Chim. Acta* **1991**, 251, 121–128.
128. A. Amine, J.-M. Kauffmann, G. J. Patriarche, *Talanta* **1991**, 38, 107–110.
129. A. Amine, J.-M. Kauffmann, G. J. Patriarche et al., *Anal. Lett.* **1991**, 24, 1293–1315.
130. F. Mizutani, S. Yabuki, A. Okuda et al., *Bull. Chem. Soc. Jpn.* **1991**, 64, 2849–2851.
131. S. Sakura, R. P. Buck, *Bioelectrochem. Bioenerg.* **1992**, 28, 387–400.
132. P. D. Hale, H. S. Lee, Y. Okamoto, *Anal. Lett.* **1993**, 26, 1–16.
133. A. Amine, J.-M. Kauffmann, G. G. Guilbault et al., *Anal. Lett.* **1993**, 26, 1281–1299.
134. I. Rosen-Margalit, J. Rishpon, *Biosens. Bioelectron.* **1993**, 8, 315–323.
135. J. Wang, N. Naser, *Electroanalysis* **1994**, 6, 571–575.
136. T. Ikeda, *Bull. Electrochem.* **1992**, 8, 145–159.
137. T. Ikeda, I. Katasho, M. Senda, *Anal. Sci.* **1985**, 1, 455–457.
138. T. Ikeda, H. Hamada, K. Miki et al., *Agric. Biol. Chem.* **1985**, 49, 541–543.
139. T. Ikeda, H. Hamada, M. Senda, *Agric. Biol. Chem.* **1986**, 50, 883–890.
140. N. Motta, A. R. Guadalupe, *Anal. Chem.* **1994**, 66, 566–571.
141. T. Inagaki, H. S. Lee, P. D. Hale et al., *Macromolecules* **1989**, 22, 4641–4643.
142. H. I. Karan, P. D. Hale, H. L. Lan et al., *Polym. Adv. Technol.* **1991**, 2, 229–235.
143. T. Kaku, H. I. Karan, Y. Okamoto, *Anal. Chem.* **1994**, 66, 1231–1235.
144. P. D. Hale, L. I. Boguslavsky, H. I. Karan et al., *Anal. Chim. Acta* **1991**, 248, 155–161.
145. H. Gunasingham, C.-H. Tan, *Analyst* **1990**, 115, 35–39.
146. H. Gunasingham, C.-H. Tan, T. C. Aw, *Clin. Chem.* **1990**, 36, 1657–1661.
147. U. Wollenberger, V. Bogdanovskaya, S. Bobrin et al., *Anal. Lett.* **1990**, 23, 1795–1808.
148. T. Tatsuma, T. Watanabe, *J. Electroanal. Chem.* **1993**, 356, 245–253.
149. P. C. Pandey, A. M. Kayastha, V. Pandey, *Appl. Biochem. Biotechnol.* **1992**, 33, 139–144.
150. H. Gunasingham, C.-H. Tan, *Anal. Chim. Acta* **1990**, 229, 83–91.
151. I. Rosen-Margalit, A. Bettelheim, J. Rishpon, *Anal. Chim. Acta* **1993**, 281, 327–333.
152. J. Kulys, H. E. Hansen, T. Buch-Rasmussen et al., *Anal. Chim. Acta* **1994**, 288, 193–196.
153. J. Kulys, L. Wang, H. E. Hansen et al., *Electroanalysis* **1995**, 7, 92–94.
154. J. Wang, X. Zhang, M. Prakash, *Anal. Chim. Acta* **1999**, 395, 11–16.
155. G. Bremle, B. Persson, L. Gorton, *Electroanalysis* **1991**, 3, 77–86.
156. F. Tobalina, F. Pariente, L. Hernández et al., *Anal. Chim. Acta* **1999**, 395, 17–26.
157. P. D. Hale, L. F. Liu, T. A. Skotheim, *Electroanalysis* **1991**, 3, 751–756.
158. L. I. Boguslavsky, P. D. Hale, L. Geng et al., *Solid State Ionics* **1993**, 60, 189–197.
159. T. Ikeda, F. Matsushita, M. Senda, *Biosens. Bioelectron.* **1991**, 6, 299–304.
160. M. Smolander, G. Marko-Varga, L. Gorton, *Anal. Chim. Acta* **1995**, 303, 233–240.
161. A. Riklin, E. Katz, I. Willner et al., *Nature* **1995**, 376, 672–675.
162. E. Katz, A. Riklin, V. Heleg-Shabtai et al., *Anal. Chim. Acta* **1999**, 385, 45–58.
163. I. Willner, V. Heleg-Shabtai, R. Blonder et al., *J. Am. Chem. Soc.* **1996**, 118, 10 321, 10 322.
164. E. Katz, D. D. Schlereth, H.-L. Schmidt et al., *J. Electroanal. Chem.* **1994**, 368, 165–171.
165. H.-L. Schmidt, W. Schuhmann, *Biosens. Bioelectron.* **1996**, 11, 127–135.
166. L.-H. Guo, G. McLendon, H. Razafitrimo et al., *J. Mater. Chem.* **1996**, 6, 369–374.
167. A. L. Lehninger, *Biochemistry*, 2nd ed., Worth, New York, 1975, p. 479.
168. Z. Samec, P. J. Elving, *J. Electroanal. Chem.* **1983**, 144, 217–225.
169. L. Falat, H.-Y. Cheng, *J. Electroanal. Chem.* **1983**, 157, 393–397.
170. I. Katakis, E. Dominguez, *Mikrochim. Acta* **1997**, 126, 11–32.
171. L. Gorton, B. Persson, P. D. Hale et al. in *Biosensors and Chemical Sensors*, (Eds.:

- P. G. Edelman, J. Wang), American Chemical Society, Washington, 1992, pp. 56–83, Chap. 6.
172. W. J. Blaedel, R. A. Jenkins, *Anal. Chem.* **1975**, *47*, 1337–1343.
173. Z. Samec, P. J. Elving, *J. Electroanal. Chem.* **1983**, *144*, 217–234.
174. R. W. Coughlin, M. Aizawa, B. F. Alexander et al., *Biotechnol. Bioeng.* **1975**, *17*, 515–526.
175. H. Jaegfeldt, A. Torstensson, G. Johansson, *Anal. Chim. Acta* **1978**, *97*, 221–228.
176. W. J. Blaedel, R. A. Jenkins, *Anal. Chem.* **1974**, *46*, 1952–1955.
177. R. D. Braun, K. S. V. Santhanam, P. J. Elving, *J. Am. Chem. Soc.* **1975**, *97*, 2591–2598.
178. J. Moiroux, P. J. Elving, *Anal. Chem.* **1978**, *50*, 1056–1062.
179. J. Moiroux, P. J. Elving, *J. Am. Chem. Soc.* **1980**, *102*, 6533–6538.
180. R. L. Blankespoor, L. L. Miller, *J. Electroanal. Chem.* **1984**, *171*, 231–241.
181. H. Jaegfeldt, T. Kuwana, G. Johansson, *J. Am. Chem. Soc.* **1983**, *105*, 1805–1814.
182. A. Silber, C. Bräuchle, N. Hampp, *J. Electroanal. Chem.* **1995**, *390*, 83–89.
183. G. X. Li, J. J. Zhu, H. Q. Fang et al., *J. Electrochem. Soc.* **1996**, *143*, L141, L142.
184. N. Cénas, J. J. Kanapienienė, J. Kulys, *J. Electroanal. Chem.* **1985**, *189*, 163–169.
185. K. Ravichandran, R. P. Baldwin, *Anal. Chem.* **1984**, *56*, 1744–1747.
186. N. Cénas, J. Rozgaite, A. Pocius et al., *J. Electroanal. Chem.* **1983**, *154*, 121–128.
187. W. B. Nowall, W. G. Kuhr, *Anal. Chem.* **1995**, *67*, 3583–3588.
188. A. Kitani, L. L. Miller, *J. Am. Chem. Soc.* **1981**, *103*, 3595–3597.
189. A. Kitani, Y.-H. So, L. L. Miller, *J. Am. Chem. Soc.* **1981**, *103*, 7636–7641.
190. B. W. Carlson, L. L. Miller, *J. Am. Chem. Soc.* **1983**, *105*, 7453–7454.
191. B. W. Carlson, L. L. Miller, P. Neta et al., *J. Am. Chem. Soc.* **1984**, *106*, 7233–7239.
192. B. W. Carlson, L. L. Miller, *J. Am. Chem. Soc.* **1985**, *107*, 479–485.
193. L. L. Miller, J. R. Valentine, *J. Am. Chem. Soc.* **1988**, *110*, 3982–3989.
194. N. Cénas, J. J. Kanapienienė, J. Kulys, *Biochim. Biophys. Acta* **1984**, *767*, 108–112.
195. D. C.-S. Tse, T. Kuwana, *Anal. Chem.* **1978**, *50*, 1315–1318.
196. H. Jaegfeldt, A. Torstensson, L. Gorton et al., *Anal. Chem.* **1981**, *53*, 1979–1982.
197. C. Degrand, L. L. Miller, *J. Am. Chem. Soc.* **1980**, *102*, 5728–5732.
198. M. Fukui, A. Kitani, C. Degrand et al., *J. Am. Chem. Soc.* **1982**, *104*, 28–33.
199. E. Lorenzo, L. Sánchez, F. Pariente et al., *Anal. Chim. Acta* **1995**, *309*, 79–88.
200. C. Ueda, D. C.-S. Tse, T. Kuwana, *Anal. Chem.* **1982**, *54*, 850–856.
201. H. Huck, H.-L. Schmidt, *Angew. Chem., Int. Ed. Engl.* **1981**, *93*, 421, 422.
202. L. Gorton, A. Torstensson, H. Jaegfeldt et al., *J. Electroanal. Chem.* **1984**, *161*, 103–111.
203. A. Torstensson, L. Gorton, *J. Electroanal. Chem.* **1981**, *130*, 199–207.
204. H. Huck, *Fresenius J. Anal. Chem.* **1982**, *313*, 548–552.
205. L. Gorton, *J. Chem. Soc., Faraday Trans. 1* **1986**, *82*, 1245–1258.
206. D. D. Schlereth, E. Katz, H.-L. Schmidt, *Electroanalysis* **1994**, *6*, 725–734.
207. D. D. Schlereth, E. Katz, H.-L. Schmidt, *Electroanalysis* **1995**, *7*, 46–54.
208. L. Gorton, G. Johansson, A. Torstensson, *J. Electroanal. Chem.* **1985**, *196*, 81–92.
209. B. Persson, L. Gorton, *J. Electroanal. Chem.* **1990**, *292*, 115–138.
210. B. Persson, *J. Electroanal. Chem.* **1990**, *287*, 61–80.
211. T. Vering, W. Schuhmann, D. Seiwald et al., *J. Electroanal. Chem.* **1994**, *364*, 277–279.
212. F. Xu, H. Li, S. J. Cross et al., *J. Electroanal. Chem.* **1994**, *368*, 221–225.
213. W. J. Albery, P. N. Bartlett, *J. Chem. Soc., Chem. Commun.* **1984**, 234–236.
214. J. Kulys, *Enzyme Microb. Technol.* **1981**, *3*, 344–349.
215. E. Katz, T. Lötzbeier, D. D. Schlereth et al., *J. Electroanal. Chem.* **1994**, *373*, 189–200.
216. I. Willner, A. Riklin, *Anal. Chem.* **1994**, *66*, 1535–1539.
217. Y. Ogino, K. Takagi, K. Kano et al., *J. Electroanal. Chem.* **1995**, *396*, 517–524.
218. G. T. R. Palmore, H. Bertschy, S. H. Bergens et al., *J. Electroanal. Chem.* **1998**, *443*, 155–161.
219. J. M. Obon, P. Casanova, A. Manjon et al., *Biotechnol. Prog.* **1997**, *13*, 557–561.
220. M. Hedenmo, A. Narvaez, E. Dominguez et al., *Analyst* **1996**, *121*, 1891–1895.
221. M. J. Lobo, A. J. Miranda, P. Tunon, *Electroanalysis* **1997**, *9*, 191–202.
222. A. E. Biade, C. Bourdillon, J. M. Laval et al., *J. Am. Chem. Soc.* **1992**, *114*, 893–897.

223. J. N. Burnett, A. L. Underwood, *Biochemistry* **1975**, 5, 2060–2066.
224. P. J. Elving, W. T. Bresnahan, J. Moiroux et al., *Bioelectrochem. Bioenerg.* **1982**, 9, 365–378.
225. C. O. Schmamel, K. S. V. Santhanam, P. J. Elving, *J. Am. Chem. Soc.* **1975**, 97, 5083–5092.
226. K. S. V. Santhanam, P. J. Elving, *J. Am. Chem. Soc.* **1973**, 95, 5482–5490.
227. A. J. Cunningham, A. L. Underwood, *Biochemistry* **1967**, 6, 266–271.
228. S. H. Baik, C. Kang, I. C. Jeon et al., *Biotechnol. Tech.* **1999**, 13, 1–5.
229. Y. T. Long, H. Y. Chen, *J. Electroanal. Chem.* **1997**, 440, 239–242.
230. G. X. Li, H. Y. Chen, D. X. Zhu, *Chem. J. Chin. Univ.* **1996**, 17, 553,554.
231. R. Ruppert, S. Herrmann, E. Steckhan, *Tetrahedron Lett.* **1987**, 28, 6583–6586.
232. R. Wienkamp, E. Steckhan, *Angew. Chem., Int. Ed. Engl.* **1982**, 21, 782,783.
233. R. Ruppert, S. Herrmann, E. Steckhan, *J. Chem. Soc., Chem. Commun.* **1988**, 1150–1151.
234. R. Wienkamp, E. Steckhan, *Angew. Chem., Int. Ed. Engl.* **1983**, 22, 497.
235. I. Willner, R. Maidan, M. Shapira, *J. Chem. Soc., Perkin Trans. 2* **1990**, 559–564.
236. M. Franke, E. Steckhan, *Angew. Chem., Int. Ed. Engl.* **1988**, 27, 265–267.
237. U. Koelle, A. D. Ryabov, *Mendeleev Commun.* **1995**, 187–189.
238. E. Steckhan, S. Herrmann, R. Ruppert et al., *Organometallics* **1991**, 10, 1568–1577.
239. H. C. Lo, O. Buriez, J. B. Kerr et al., *Angew. Chem., Int. Ed. Engl.* **1999**, 38, 1429–1432.
240. E. Hofer, E. Steckhan, B. Ramos et al., *J. Electroanal. Chem.* **1996**, 402, 115–122.
241. Y. Shimizu, A. Kitani, S. Ito et al., *Denki Kagaku* **1993**, 61, 872,873.
242. Y. Shimizu, A. Kitani, S. Ito et al., *Denki Kagaku* **1994**, 62, 1233,1234.
243. S. Chardonnoblat, S. Cosnier, A. Deronzier et al., *J. Electroanal. Chem.* **1993**, 352, 213–228.
244. H. X. Ju, W. Ma, C. X. Cai et al., *Chem. J. Chin. Univ.* **1995**, 16, 1680–1684.
245. R. J. Day, S. J. Kinsey, E. T. Seo et al., *Trans. N.Y. Acad. Sci.* **1972**, 34, 588–594.
246. M. Ito, T. Kuwana, *J. Electroanal. Chem.* **1971**, 32, 415–425.
247. K. Kano, K. Takagi, Y. Ogino et al., *Chem. Lett.* **1995**, 589,590.
248. A. L. de Lacey, M. T. Bes, C. Gómez-Moreno et al., *J. Electroanal. Chem.* **1995**, 390, 69–76.
249. S. Peguin, P. Soucaille, *Biotechnol. Bioeng.* **1996**, 51, 342–348.
250. R. DiCosimo, C.-H. Wong, L. Daniels et al., *J. Org. Chem.* **1981**, 46, 4622,4623.
251. Z. Shaked, J. J. Barber, G. M. Whitesides, *J. Org. Chem.* **1981**, 46, 4100,4101.
252. S. Chao, M. S. Wrighton, *J. Am. Chem. Soc.* **1987**, 109, 5886–5888.
253. T. Matsue, H.-C. Chang, I. Uchida et al., *Tetrahedron Lett.* **1988**, 29, 1551–1554.
254. H.-C. Chang, T. Matsue, I. Uchida et al., *Chem. Lett.* **1989**, 1119–1122.
255. A. Bergel, M. Comtat, *J. Electroanal. Chem.* **1991**, 302, 219–231.
256. A. Bergel, M. Comtat, *Bioelectrochem. Bioenerg.* **1992**, 27, 495–500.
257. H. Simon, J. Bader, H. Günter et al., *Angew. Chem., Int. Ed. Engl.* **1985**, 24, 539–553.
258. H. Simon, H. Günter, J. Bader et al., *Angew. Chem. Int. Ed. Engl.* **1981**, 20, 861–863.
259. K. Takagi, K. Kano, T. Ikeda, *Chem. Lett.* **1996**, 11,12.
260. K. Takagi, K. Kano, T. Ikeda, *J. Electroanal. Chem.* **1998**, 445, 211–219.
261. S. Kim, S. E. Yun, C. Kang, *J. Electroanal. Chem.* **1999**, 465, 153–159.
262. Y. Kashiwagi, Y. Yanagisawa, N. Shibayama et al., *Chem. Lett.* **1996**, 1093,1094.
263. R. Yuan, S. Kuwabata, H. Yoneyama, *Chem. Lett.* **1996**, 137,138.
264. J. Contet, A. Bergel, M. Comtat, *Bioelectrochem. Bioenerg.* **1992**, 27, 475–486.
265. K. Delecouls, P. Saint-Aguet, C. Zaborosch et al., *J. Electroanal. Chem.* **1999**, 468, 139–149.
266. K. Nishiyama, H. Ishida, I. Taniguchi, *J. Electroanal. Chem.* **1994**, 373, 255–258.
267. P. Gros, C. Zaborosch, H. G. Schlegel et al., *J. Electroanal. Chem.* **1996**, 405, 189–195.
268. J. Cantet, A. Bergel, M. Comtat et al., *J. Mol. Catal.* **1992**, 73, 371–380.
269. K. W. Willman, R. W. Murray, *J. Electroanal. Chem.* **1982**, 133, 211–231.
270. C. Van Dijk, T. Van Eijs, J. W. Van Leeuwen et al., *FEBS Lett.* **1984**, 166, 76–80.
271. Y. S. Obeng, A. Founta, A. J. Bard, *New J. Chem.* **1992**, 16, 121–129.
272. E. Katz, N. Itzhak, I. Willner, *Langmuir* **1993**, 9, 1392–1396.
273. S. Cosnier, K. LeLous, *Talanta* **1996**, 43, 331–337.

274. J. Cantet, A. Bergel, M. Comtat, *Enzyme Microb. Technol.* **1996**, 18, 72–79.
275. N. Takano, K. Matuda, M. Itaya, *Denki Kagaku* **1998**, 66, 86–91.
276. Y. Kashiwagi, Y. Yanagisawa, N. Shibayama et al., *Electrochim. Acta* **1997**, 42, 2267–2270.
277. M. Maurice, J. Souppe, *New J. Chem.* **1990**, 14, 301–304.
278. A. F. Bückmann, V. Wray, *Biotechnol. Biochem.* **1992**, 15, 303–310.
279. J. Hendle, A. F. Bückmann, W. Aehle et al., *Eur. J. Biochem.* **1993**, 213, 947–956.
280. H.-L. Schmidt, G. Grenner, *Eur. J. Biochem.* **1976**, 67, 295–302.
281. P. Zappelli, A. Rossodivita, L. Re, *Eur. J. Biochem.* **1975**, 54, 475–482.
282. P. Zappelli, A. Rossodivita, G. Prosperi et al., *Eur. J. Biochem.* **1976**, 62, 211–215.
283. A. F. Bückmann, *Biocatalysis* **1987**, 1, 173–186.
284. B. Leca, J.-L. Marty, *Biosens. Bioelectron.* **1997**, 12, 1083–1088.
285. B. Leca, J.-L. Marty, *Anal. Chim. Acta* **1997**, 340, 143–148.
286. M. Montagné, J.-L. Marty, *Anal. Chim. Acta* **1995**, 315, 297–302.
287. P. Zappelli, R. Pappa, A. Rossodivita et al., *Eur. J. Biochem.* **1977**, 72, 309–315.
288. T. Eguchi, T. Iizuka, T. Kagotani et al., *Eur. J. Biochem.* **1986**, 155, 415–421.
289. S. Furukawa, N. Katayama, T. Iizuka et al., *FEBS Lett.* **1980**, 121, 239–242.
290. A. Nakamura, I. Urabe, H. Okada, *J. Biol. Chem.* **1986**, 261, 16 792–16 794.
291. S. A. M. Vanhommerig, L. A. A. E. Sluyterman, E. M. Meijer, *Biochim. Biophys. Acta* **1996**, 1295, 125–138.
292. Y. Yamazaki, H. Maeda, *Agric. Biol. Chem.* **1981**, 45, 2277–2288.
293. Y. Nakamura, S. Suye, J. Kira et al., *Biochim. Biophys. Acta* **1996**, 1289, 221–225.
294. U. Kragl, W. Kruse, W. Hummel et al., *Biotechnol. Bioeng.* **1996**, 52, 309–319.
295. M.-O. Månsson, P.-O. Larsson, K. Mosbach, *Eur. J. Biochem.* **1978**, 86, 455–463.
296. M.-O. Månsson, P.-O. Larsson, K. Mosbach, *FEBS Lett.* **1979**, 98, 309–313.
297. C. Woenckhaus, R. Koob, A. Burkhard et al., *Bioorg. Chem.* **1983**, 12, 45–57.
298. J. Kovár, K. Simek, I. Kucera et al., *Eur. J. Biochem.* **1984**, 139, 585–591.
299. P. Goulas, *Eur. J. Biochem.* **1987**, 168, 469–473.
300. M. Persson, M.-O. Månsson, L. Bülow et al., *Biotechnology* **1991**, 9, 280–284.
301. A. B. Kharitonov, L. Alfonta, E. Katz et al., *J. Electroanal. Chem.* **2000**, 487, 133–141.
302. A. Bardea, E. Katz, A. F. Bückmann et al., *J. Am. Chem. Soc.* **1997**, 119, 9114–9119.
303. R. J. P. Williams, *Electron Transfer in Biology and the Solid State*, American Chemical Society, Washington, D. C., 1990, pp. 1–23.
304. M. Brunori, *Biosens. Bioelectron.* **1994**, 9, 633–636.
305. F. A. Armstrong, H. A. O. Hill, N. J. Walton, *Q. Rev. Biophys.* **1986**, 18, 261–322.
306. F. A. Armstrong, H. A. O. Hill, N. J. Walton, *Acc. Chem. Res.* **1988**, 21, 407–413.
307. J. E. Frew, H. A. O. Hill, *Eur. J. Biochem.* **1988**, 172, 261–269.
308. I. Taniguchi, K. Toyosawa, H. Yamaguchi et al., *J. Chem. Soc., Chem. Commun.* **1982**, 1032, 1033.
309. I. Taniguchi, S. Yoshimoto, K. Nishiyama, *Chem. Lett.* **1997**, 353, 354.
310. B. D. Lamp, D. Hobara, M. D. Porter et al., *Langmuir* **1997**, 13, 736–741.
311. H. A. O. Hill, D. J. Page, N. J. Walton, *J. Electroanal. Chem.* **1987**, 217, 141–158.
312. Y. Xie, S. Dong, *Bioelectrochem. Bioenerg.* **1992**, 29, 71–79.
313. P. M. Allen, H. A. O. Hill, N. J. Walton, *J. Electroanal. Chem.* **1984**, 178, 69–86.
314. Z.-X. Huang, M. Feng, Y.-H. Wang et al., *J. Electroanal. Chem.* **1996**, 416, 31–40.
315. R. Santucci, A. Faraoni, L. Campanella et al., *Biochem. J.* **1991**, 273, 783–786.
316. S. Bagby, P. D. Barker, K. DiGleria et al., *Biochem. Soc. Trans.* **1988**, 16, 958, 959.
317. G. Li, H. Chen, D. Zhu, *Anal. Chim. Acta* **1996**, 319, 275, 276.
318. X. Qu, T. Lu, S. Dong et al., *Bioelectrochem. Bioenerg.* **1994**, 34, 153–156.
319. T. Lu, X. Yu, S. Dong et al., *J. Electroanal. Chem.* **1994**, 369, 79–86.
320. W. Jin, U. Wollenberger, F. F. Bier et al., *Bioelectrochem. Bioenerg.* **1996**, 39, 221–225.
321. D. A. Powis, G. D. Wattus, *FEBS Lett.* **1981**, 126, 282–284.
322. H. A. O. Hill, N. J. Walton, *J. Am. Chem. Soc.* **1982**, 104, 6515–6519.
323. A. E. G. Cass, G. Davis, H. A. O. Hill et al., *Biochim. Biophys. Acta* **1985**, 828, 51–57.
324. W. Jin, U. Wollenberger, E. Kärger et al., *J. Electroanal. Chem.* **1997**, 433, 135–139.
325. M. J. Tarlov, E. F. Bowden, *J. Am. Chem. Soc.* **1991**, 113, 1847–1849.

326. D. Hobara, K. Niki, C. Zhou et al., *Colloids Surf., A* **1994**, 93, 241–250.
327. T. M. Nahir, E. F. Bowden, *J. Electroanal. Chem.* **1996**, 410, 9–13.
328. S. Song, R. A. Clark, E. F. Bowden et al., *J. Phys. Chem.* **1993**, 97, 6564–6572.
329. P. N. Bartlett, D. J. Caruana, *Analyst* **1992**, 117, 1287–1292.
330. M. Collinson, E. F. Bowden, M. J. Tarlov, *Langmuir* **1992**, 8, 1247–1250.
331. B. A. Kuznetsov, N. A. Byzova, G. P. Shumakovich, *J. Electroanal. Chem.* **1994**, 371, 85–92.
332. J. M. Cooper, K. R. Greenough, C. J. McNeil, *J. Electroanal. Chem.* **1993**, 347, 267–275.
333. P. A. Adams in *Peroxidases in Chemistry and Biology* (Eds.: J. Everse, K. E. Everse), CRC Press, Boston, 1991, pp. 171–200, Vol. 2, Chap. 7.
334. G. Ranghino, G. Antonini, P. Fantucci, *Israel J. Chem.* **1994**, 34, 239–244.
335. T. Lötzbeyer, W. Schuhmann, E. Katz et al., *J. Electroanal. Chem.* **1994**, 377, 291–294.
336. H. A. O. Hill, N. J. Walton, I. J. Higgins, *FEBS Lett.* **1981**, 126, 282–284.
337. F. Patolsky, E. Katz, V. Heleg-Shabtai et al., *Chem. Eur. J.* **1998**, 4, 1068–1073.
338. V. Heleg-Shabtai, E. Katz, I. Willner, *J. Am. Chem. Soc.* **1997**, 119, 8121–8122.
339. V. Heleg-Shabtai, E. Katz, S. Levi et al., *J. Chem. Soc., Perkin Trans. 2*, **1997**, 2645–2651.
340. A. E. Strong, B. D. Moore, *J. Mater. Chem.* **1999**, 9, 1097–1105.
341. D. L. Pilloud, F. Rabanal, B. R. Gibney et al., *J. Phys. Chem. B* **1998**, 102, 1926–1937.
342. E. Katz, V. Heleg-Shabtai, I. Willner et al., *Angew. Chim.* **1998**, 37, 3253–3256.
343. I. Willner, V. Heleg-Shabtai, E. Katz et al., *J. Am. Chem. Soc.* **1999**, 121, 6455–6468.
344. V. Pardo-Yissar, E. Katz, I. Willner et al., *Faraday Discuss.* **2000**, 116, 119–134.
345. E. Katz, I. Willner, A. B. Kotlyar, *J. Electroanal. Chem.* **1999**, 479, 64–68.
346. J. Wang, *J. Pharm. Biomed. Anal.* **1999**, 19, 47–53.
347. M. E. Collison, M. E. Meyerhoff, *Anal. Chem.* **1990**, 62, 425A.
348. S. A. Jaffari, A. P. F. Turner, *Physiol. Meas.* **1995**, 16, 1–15.
349. M. Kyrolainen, H. Hakanson, R. Ekroth et al., *Anal. Chim. Acta* **1993**, 279, 149–153.
350. C. Meyerhoff, F. Bischof, F. J. Mennel, et al., *Biosens. Bioelectron.* **1993**, 8, 409–414.
351. J. Wang, M. Ozsoz, *Electroanalysis* **1990**, 2, 647–650.
352. V. Kacanicklic, K. Johansson, G. Marko Varga et al., *Electroanalysis*, **1994**, 6, 381–390.
353. H. Bramwell, A. E. G. Cass, P. N. B. Gibbs et al., *Analyst* **1990**, 115, 185–188.
354. J. Wang, E. Dempsey, M. Ozsoz et al., *Analyst* **1991**, 116, 997–999.
355. A. Maines, D. Ashworth, P. Vadgama, *Food Technol. Biotechnol.* **1996**, 34, 31–42.
356. A. S. Bassi, D. Q. Tang, E. Lee et al., *Food Technol. Biotechnol.* **1996**, 34, 9–22.
357. C. Nistor, J. Emneus, *Waste Manage.* **1999**, 19, 147–170.
358. J. L. Marty, B. Leca, T. Noguer, *Analysis* **1998**, 26, M144–M149.
359. M. P. Marco, D. Barcelo, *Measurement Sci. Technol.* **1996**, 7, 1547–1562.
360. D. Ivnitski, I. Abdel-Hamid, P. Atanasov et al., *Biosens. Bioelectron.* **1999**, 14, 599–624.
361. B. M. Paddle, *Biosens. Bioelectron.* **1996**, 11, 1079–1113.
362. C. Bourdillon, J. M. Laval, D. Thomas, *J. Electrochem. Soc.* **1986**, 133, 706–711.
363. C. Bourdillon, R. Lortie, J. M. Laval, *Biotechnol. Bioeng.* **1988**, 31, 553–558.
364. A. Fassouane, J. M. Laval, J. Moiroux et al., *Biotechnol. Bioeng.* **1990**, 35, 935–939.
365. Y. Yamazaki, H. Maeda, *Agric. Biol. Chem.* **1982**, 46, 1571–1581.
366. J. R. Wykes, P. Dunnill, M. D. Lilly, *Biotechnol. Bioeng.* **1975**, 17, 51–68.
367. T. Erabi, H. Hiura, M. Tanaka, *Bull. Chem. Soc. Jpn.* **1975**, 48, 1354–1356.
368. O. S. Ksenzhek, S. A. Petrova, M. V. Kolydzhny, *Bioelectrochem. Bioenerg.* **1982**, 9, 167–174.
369. R. S. Schreiber, A. Arratia, S. Sánchez et al., *Bioelectrochem. Bioenerg.* **1990**, 23, 81–91.
370. K. Takehara, H. Takemura, Y. Ide et al., *J. Electroanal. Chem.* **1991**, 308, 345–350.
371. E. Katz, *Studia Biophysica* **1988**, 125, 211–217.
372. K. T. Kinnear, H. G. Monbouquette, *Biotechnol. Bioeng.* **1993**, 42, 140–144.
373. S. Kuwabata, R. Tsuda, K. Nishida et al., *Chem. Lett.* **1993**, 1631–1634.
374. S. Kuwabata, R. Tsuda, H. Yoneyama, *J. Am. Chem. Soc.* **1994**, 116, 5437–5443.

375. K. Takayama, K. Kano, T. Ikeda, *Chem. Lett.* **1996**, 1009,1010.
376. G. Prentice, *CHEMTECH* **1984**, 14, 684–701.
377. G. Tayhas, R. Palmore, G. M. Whitesides, *Enzymatic Conversion of Biomass for Fuels Production*, ACS Symposium Series No. 566, 1994, pp. 271–290, Chap. 14.
378. K. Kordesch, *Ber. Bunsen-Ges. Phys. Chem.* **1990**, 94, 902–907.
379. C. Van Dijk, C. Laane, C. Veeger, *Recl. Trav. Chim., Pays-Bas* **1985**, 104, 245–249.
380. I. Willner, E. Katz, F. Patolsky et al., *J. Chem. Soc., Perkin Trans. 2* **1998**, 1817–1822.
381. I. Willner, *Acc. Chem. Res.* **1997**, 30, 347–356.
382. M. Lion-Dagan, E. Katz, I. Willner, *J. Am. Chem. Soc.* **1994**, 116, 7913,7914.
383. I. Willner, R. Blonder, E. Katz et al., *J. Am. Chem. Soc.* **1996**, 118, 5310,5311.
384. I. Willner, E. Katz, B. Willner et al., *Biosens. Bioelectron.* **1997**, 12, 337–356.
385. R. Blonder, E. Katz, I. Willner et al., *J. Am. Chem. Soc.* **1997**, 119, 11 747–11 757.
386. I. Willner, M. Lion-Dagan, S. Marx-Tibbon et al., *J. Am. Chem. Soc.* **1995**, 117, 6581–6592.
387. I. Willner, A. Doron, E. Katz et al., *Langmuir* **1996**, 12, 946–954.
388. M. Lion-Dagan, E. Katz, I. Willner, *J. Chem. Soc., Chem. Commun.* **1994**, 2741,2742.
389. M. Lion-Dagan, S. Marx-Tibbon, E. Katz et al., *Angew. Chem., Int. Ed. Engl.* **1995**, 34, 1604–1606.
390. E. Katz, B. Willner, I. Willner, *Biosens. Bioelectron.* **1997**, 12, 703–719.
391. E. Katz, M. Lion-Dagan, I. Willner, *J. Electroanal. Chem.* **1995**, 382, 25–31.
392. E. Katz, I. Willner, *Electroanalysis* **1995**, 7, 417–419.
393. E. Katz, M. Lion-Dagan, I. Willner, *J. Electroanal. Chem.* **1996**, 408, 107–112.
394. R. Blonder, E. Katz, Y. Cohen et al., *Anal. Chem.* **1996**, 68, 3151–3157.
395. F. Patolsky, B. Filanovsky, E. Katz et al., *J. Phys. Chem. B* **1998**, 102, 10 359–10 367.
396. F. Patolsky, E. Katz, A. Bardea et al., *Langmuir* **1999**, 15, 3703–3706.